PROCEEDINGS OF NACOB II
THE SECOND NORTH AMERICAN CONGRESS ON BIOMECHANICS

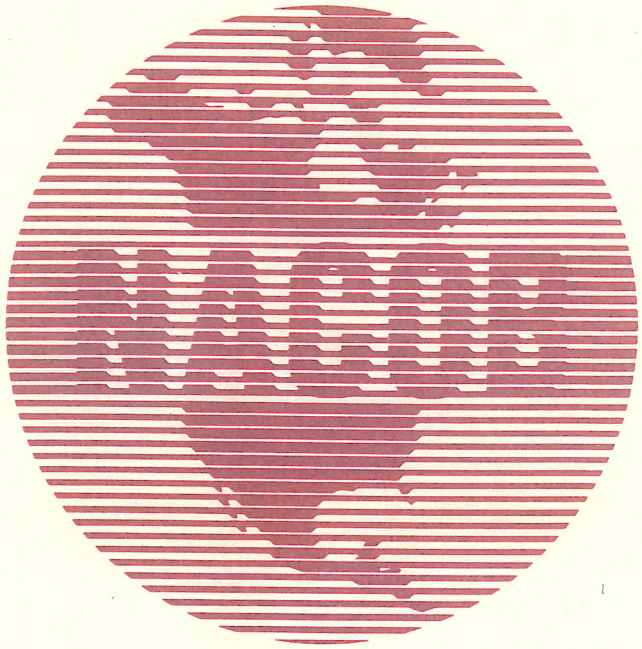

The Sixteenth Annual
Conference of the American
Society of Biomechanics

and

The Seventh Biennial
Conference of the Canadian
Society for Biomechanics/
Société Canadienne de
Biomécanique

McCormick Center Hotel
Chicago, Illinois, USA
August 24th - 28th, 1992



Proceedings of the Second North American Congress on Biomechanics

The Sixteenth Annual Conference of
The American Society of Biomechanics (ASB)

and

The Seventh Biennual Conference of the
Canadian Society for Biomechanics (CSB)/
Société Canadienne de Biomécanique (SCB)
LOCOMOTION VII

Chicago, Ill., USA
Published by the Organizing Committee, August 1992
L. Draganich, R. Wells and J. Bechtold

All rights to this publication reserved.

This book may not be reproduced in any form without permission of the publisher.
The rights to individual papers are held by the authors.

Additional copies may be obtained from:
Secretariat ASB
Melissa G. Gross
Secretary/Treasurer
Dept. of Movement Science
The University of Michigan
401 Washenaw Avenue
Ann Arbor, MI 48109-2214

Secretariat CSB/SCB
School of Physical and Health Education
Queen's University
Kingston, Ontario
K7L 3N6

Price:
$35.00 (U.S.) cheque or money order payable to American Society of Biomechanics to be forwarded to Secretariat ASB.

$45.00 (Can.) cheque or money order payable to Canadian Society for Biomechanics to be forwarded to Secretariat CSB/SCB.



North American Congress on Biomechanics

The Executive Boards which have governed the American Society of Biomechanics (ASB) and the Canadian Society for Biomechanics (CSB/SCB) during the past year comprise the following members:

NACOB
Conference Co-Chairs

Louis F. Draganich
University of Chicago
Orthopaedic Biomechanics

Richard Wells
University of Waterloo
Department of Kinesiology

Joan E. Bechtold
Hennepin County Medical Center
Orthopaedic Biomechanics Laboratory

ASB
1991/1992

Thomas P. Andriacchi
President
Rush-Presbyterian-St. Luke's Med. Ctr

George T. Rab
Past-President
University of California

Ronald Zernicke
President-Elect
University of Calgary

Melissa G. Gross
Secretary/Treasurer
University of Michigan

Louis F. Draganich
Meeting Chairperson
University of Chicago

Joan E. Bechtold
Program Chairperson
Hennepin County Med. Ctr.

Andrew Biewener
Program Chairperson-Elect
University of Chicago

Thomas D. Brown
Membership Committee Chairperson
University of Iowa

Mary M. Rodgers
Education Committee Chairperson
Wright State University

CSB/SCB
1991/1992

Carol Putnam
President
Dalhousie University

Walter Herzog
Secretary-Treasurer
University of Calgary

Tim Bryant
Newsletter Editor & Secretariat
Queen's University

Richard Wells
Conference Chairperson
University of Waterloo

Carol Richards
Past Conference Chairperson
Université Laval



North American
Congress on
Biomechanics

LIST OF EXHIBITORS

ARTMA Biomedical Inc.
12021 Willshire Blvd.
Los Angeles, CA 90025

Advanced Medical Technology, Inc.
151 California Street
Newton, MA 02158

B & L Engineering/Oxford Metrics
P.O. Box 3905
Santa Fe Springs, CA 90670

Computer Functional Testing Corporation
2201 W. Campbell Park Drive, Rm. 215
Chicago, IL 60612-3501

Gideon Ariel Life Systems Inc.
P.O. Box 1169
LaJolla, CA 92038

Greenleaf Medical
2248 Park Blvd.
Palo Alto, CA 94306

Kistler Instrument Corporation
75 John Glen Drive
Amherst, NJ 14120

MTS Systems Corporation
Box 24012
Minneapolis, MN 55424

Motion Analysis Corporation
8001 Frost Street
San Diego, CA 92123

Northern Digital
403 Albert Street
Waterloo, Ontario N2L 3G1

Novel Electronics
511 11th Ave, Suite 266
Minneapolis, MN 55415

Peak Performance Technologies
7388 S. Revere Pkwy., Suite 601
Englewood, CO 80112

Promatek Medical Systems Inc.
1851 Black Road
Joliet, IL 60435

Qualysis Inc.
P.O. Box 117
Glastonbury, CT 06025-0117



North American Congress on Biomechanics

ACKNOWLEDGEMENTS

The Organizing Committee of the Second North American Congress on Biomechanics acknowledges the generous support of the following institutions:

NACOB II, Cosponsors

- University of Chicago
  - *Section of Orthopaedic Surgery and Rehabilitation Medicine*
  - *Department of Surgery*
  - *Department of Organismal Biology and Anatomy*
- University of Waterloo
  - *Faculty of Applied Health Sciences*
  - *Department of Kinesiology*
- Natural Science and Engineering Research Council of Canada
- Biomet, Inc.

ASB Sustaining Members

- *Aircast, Inc.*
- *DePuy, Inc.*
- *DonJoy, Inc.*
- *Electro-Biology, Inc. (EBI)*
- *Howmedica, Inc.*
- *Interpore Orthopaedics, Inc.*
- *Kistler Instrument Corporation*
- *Motion Analysis Corporation*
- *Orthofix, S.R.L.*
- *Orthomet*
- *Protek, Inc.*
- *Zimmer, Inc.*



CONTENTS

North American Congress on Biomechanics

Keynote Address	Podium	1
Soft Tissue	Podium Session 1	5
Tissue Material Properties and Implants	Poster	17
Biomechanics of Throwing	Podium Session 2	49
Development & Aging	Podium Session 3	61
Anthropology	Podium Session 4	71
Anthropometry	Poster	81
Instrumentation and Methodology	Poster	93
ASB Young Scientist Awards	Podium	115
ASB Symposium	Podium	121
Knee Ligament Deficiency	Podium Session 5	131
Posture	Podium Session 6	143
Sport Biomechanics	Podium Session 7	157
Muscle Modelling	Podium Session 8	171
Electromyography: Techniques, Modelling and Muscle Models	Poster	181
Trauma and Impact	Podium Session 9	199
Energy Costs	Podium Session 10	209
Microgravity & Airborne	Podium Session 11	219
Running	Podium Session 12	229
Running, Cycling and Sport	Poster	239
Footwear	Poster	263
CSB Symposium: Locomotion VII	Podium	287
Non-Normal Gait	Podium Session 13	311
Motor Control	Podium Session 14	325
Motor Control	Poster	339
Bone Remodelling	Podium Session 15	353
Normal Gait	Podium Session 16	367
Locomotion and Posture	Poster	381
Ergonomics	Podium Session 17	423
Upper Extremity	Podium Session 18	437
Upper Extremity	Poster	451
Spine	Podium Session 19	461
Spine Models and Implants	Poster	477
Lower Extremity Loading	Podium Session 20	493
Manual Materials Handling	Podium Session 21	509
Manual Materials Handling	Poster	521
Jumping and Landing	Podium Session 22	541
Human Performance	Poster	555
Author Index		579

KEYNOTE ADDRESS

Podium

MOBILITY IMPAIRMENTS IN THE ELDERLY: CHALLENGES FOR BIOMECHANICS RESEARCH

Albert B. Schultz

MEAM Biomechanics Research Laboratory
University of Michigan, Ann Arbor, MI 48109-2125

In 1987, there were 28 million residents of the United States who were 65 or more years old. In 2020, there will be 52 million such residents. In 1987, there were 2.3 million US residents who were 85 or more years old. In 2020, there will be 6.7 million such residents.

In 1987, of the 28 million residents 65 or older, 3.6 million (12.9 percent) had difficulty with performing one or more activities-of-daily-living (ADL) and 2.2 million (7.7 percent) had difficulty with walking. Of the 2.3 million residents 85 or older, 0.8 million (34.5 percent) had difficulty with performing one or more ADL. Among nursing home residents 85 or older, 92 percent need personal assistance in performing one or more ADL.

The public health problem of mobility impairments in the elderly is already staggering. The problem is almost certain to get worse, given the projected sharp increases in the population of the elderly. Whatever the underlying causes of mobility impairments in the elderly are, those impairments ultimately express themselves in the biomechanics of mobility task performances. Biomechanics research faces new and exciting challenges. How can mobility impairments in the elderly be better assessed and better remedied? Can any of them be prevented? Which biomechanical features of a mobility impairment are critical and which are of lesser importance?

This Keynote Address will outline further the magnitude of those challenges, the problems one faces when trying to address them and the current state-of-the-art in the area. Examples of recent studies will illustrate what kind of work needs to be done and what questions need to be answered. The Address will be based on a recent review of the biomechanics of mobility impairments in the elderly (Schultz 1992).

REFERENCES

Schultz, A. B. **J Biomechanics 25**: 519-528, 1992.

SOFT TISSUE

Podium Session 1

A New Methodology for Direct, Non-Contact Determination of *In-situ* Forces in Soft Tissues

H. Fujie, G. A. Livesay, S. Kashiwaguchi, G. Blomstrom and S. L-Y. Woo

Musculoskeletal Research Laboratories
Department of Orthopaedic Surgery
University of Pittsburgh, Pittsburgh PA 15261

INTRODUCTION

A direct, non-contact methodology to examine *in-situ* forces in the soft tissues of a human cadaveric knee joint was developed. The magnitude, direction and point of application of *in-situ* forces are determined through the application of a force transformation technique to the outputs of a universal force sensor. This approach avoids surgical intervention as well as the use of mechanical devices on or near the ligaments of the knee, and requires no geometric assumptions for lines of resultant force in the soft tissues of the knee. One notable advantage of the present approach is that the error associated with the point of application of the external force, when the direction of the *in-situ* force is not perpendicular to the sensor surface, is much smaller than previous methods used with three-dimensional force plates.

A preliminary test revealed that the *in-situ* force developed in the ACL was greater than the applied 100 N anterior tibial load. Additionally, the point of application of the *in-situ* force in the ACL shifted with increased loading. Although only data on the ACL is presented, this methodology can be readily extended to determine the *in-situ* forces in all of the soft tissues at the knee joint under varied loading conditions.

REVIEW AND THEORY

Determination of *in-situ* forces in the soft tissues of the knee is important for better understanding of their normal function and contribution to joint kinematics. Previous studies have addressed the *in-situ* forces developed in the anterior cruciate ligament (ACL) with buckle transducers [Barry *et al*, 1986; Lewis *et al*, 1982] or strain gages affixed near the bony insertions [France *et al*, 1988]. Recently, Markolf et al. measured the resultant forces in the ACL by instrumenting the tibial insertion of the ACL with a load cell [Markolf *et al*, 1990]. Although providing much useful information, these measurements are invasive to the knee joint or require the application of mechanical devices to the ligaments which may alter the ligament load-elongation behavior. The *in-situ* force in the ACL has also been previously addressed in our laboratory using a non-contact, kinematic linkage methodology, however, a geometric assumption for the direction of the force was required [Takai *et al*, 1991].

In this study, a new methodology has been developed to determine *in-situ* forces without any surgical intervention, the application of mechanical devices to the ligaments, or the geometric assumption. Using a universal force-moment sensor (UFS), the magnitude, direction and point of application of the force in the insertion site of the knee soft tissues can be directly determined through a force transformation technique.

Force-Moment Vector

A force-moment vector, ***F***, consisting of three forces and three moments along and about three Cartesian axes in a rigid body, is defined with respect to a Cartesian coordinate system and is measured by the UFS (JR3, California, USA).

Force Transformation

Consider a body that is rigidly attached to the UFS (Fig. 1). An external force applied to the body will be transmitted to the UFS. With the three force components, the magnitude and direction of the external force can be easily determined. Knowing the direction of the external force, the local Cartesian coordinate system is then mathematically rotated so that the z axis of the new system is parallel to the external force. The location of the external force relative to the Cartesian coordinate system can also be determined very easily and precisely, because the external force is now perpendicular to the x-y plane of the new Cartesian coordinate system. After the location of the force is determined with respect to the new Cartesian coordinate system, the coordinate system is mathematically rotated back to its original orientation, thereby determining the point of application of the external force on the rigid body.

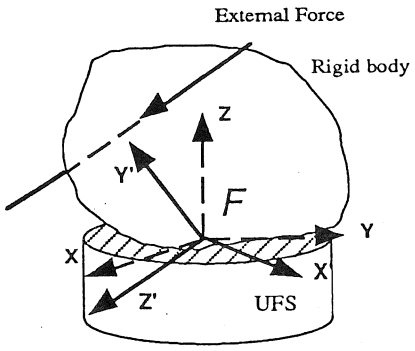

Figure 1. Transmission of the external force to the UFS and rotation of the coordinate system (xyz is the original coordinate system, while x'y'z' is the rotated coordinate system).

Evaluation of Point of Application Error

The measurement error associated with the point of application of the external force determined with the new methodology was compared to that of the three-dimensional force plate, which is primarily utilized in gait analysis. The 3-D force plate is regularly used to determine the location (point of application) of the center of pressure during the stance phase of walking. When the angle between the direction of the external force and sensor surface is close to 90° (or nearly perpendicular), the measurement error is very small for both the new methodology and the three-dimensional force plate (Fig. 2). However, when the angle is close to 0° or 180°, the measurement error associated with the new methodology remains small, but the three dimensional force plate error becomes very large.

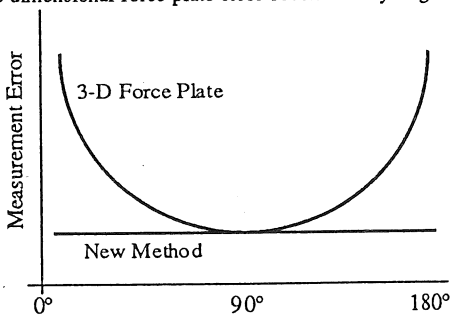

Figure 2. Schematic of easurement error for both methods.

PROCEDURE

Application to Joint Biomechanics

It is possible to replace the rigid body with a human tibia if the tibia is considered to be "rigid" in comparison to the soft tissues at the knee. *In-situ* forces will develop in each of the soft tissues of the knee as a result of external loading or external motion of the knee joint, which are then transmitted through the tibia to the UFS. Using the previously described methodology, the magnitude, direction, and point of application of the *in-situ* forces in the soft tissues can be determined.

Preliminary Experiment

A young human knee joint (34 years) was dissected free of musculature, leaving the joint capsule intact. The tibia and femur were cut to 12 cm in length from the joint line and secured within thick-walled aluminum cylinders with three 6 mm diameter bolts. The femur was rigidly fixed to the base of an Instron testing machine, and the UFS was mounted between the tibial clamp and the crosshead with specially designed clamps. The knee was then fixed in the testing machine at 30° of flexion allowing only anterior-posterior (A-P) translations.

During the application of a 100 N A-P load to the intact knee, force-moment information was measured by the UFS, and the A-P displacement was recorded with a personal computer. After removal of the medial collateral ligament (MCL), the same path of motion of the tibia with respect to the femur was reproduced through position control provided by the Instron while the force-moment information and A-P translation were again measured. Since the difference between the force-moment information measured for the intact and MCL dissected-knee can be attributed to the removed structure, the magnitude, direction, and point of application of the *in-situ* force in the MCL could then be determined though a force transformation technique. Subsequently, the lateral collateral ligament, medial meniscus, lateral meniscus, posterior cruciate ligament, and anterior cruciate ligament were removed, and the same path of tibial motion reproduced at each stage of dissection. This allowed the determination of the *in-situ* force developed in each of these soft tissues during the A-P loading, although only sample data for the ACL is presently reported. The measurement for each state of the joint was repeated three times with 10 minutes between each trial to allow the tissue to equilibrate.

The magnitude of the *in-situ* force in the ACL was examined under 50 and 100 N of anterior tibial loading. The direction of this *in-situ* force was also determined for 100 N of anterior loading, and was expressed with respect to a local ACL coordinate system. The origin of this coordinate system was located at the tibial insertion site of the ligament, and x, y and z-axes of the local coordinate system correspond to the medial-lateral (M-L), proximal-distal (P-D), and anterior-posterior (A-P) directions at the knee joint, respectively. Further, the point of application of the *in-situ* force within the tibial insertion site of the ACL was determined at both 50 and 100 N of anterior loading.

RESULTS

Preliminary Results

The ACL supported *in-situ* forces of 34.4 N and 110.4 N, under 50 N and 100 N of anterior tibial loading, respectively. The direction in the *in-situ* force in the ACL under 100 N of anterior drawer is shown in Figure 3, and is -35.6 (lateral), 73.5 (proximal), and -74.2 (posterior) with respect to the local ACL coordinate system. The point of application of the *in-situ* force in the ACL moved from the medial portion of the tibial insertion site toward the antero-medial portion of the insertion site, as the anterior load increased from 50 to 100 N (Fig. 4)

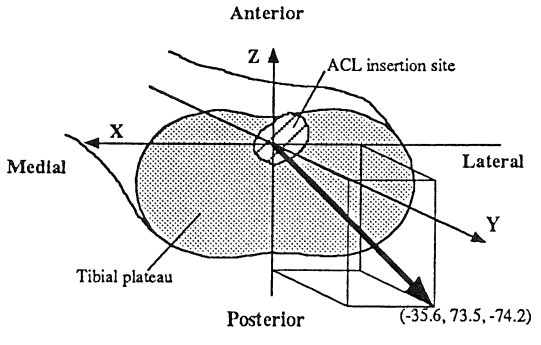

Figure 3. Direction of the *in-situ* forces in the ACL when 100 N of anterior load is applied to the knee joint at 30° of flexion.

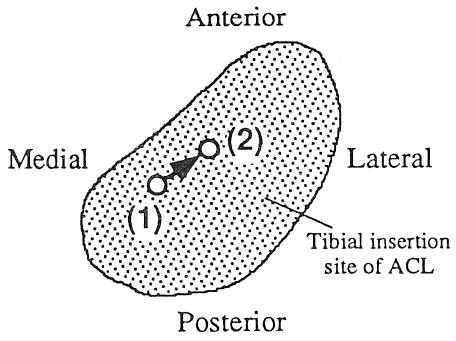

Figure 4. Centroid of point of application of the *in-situ* force in the tibial insertion site of ACL, (1) when 50 N of anterior load, and (2) when 100 N of anterior load were applied to the tibia.

DISCUSSION

A new methodology has been developed to determine the *in-situ* forces in the soft tissues of the knee generated during external loading or motion of the joint. This is accomplished through a force transformation technique applied to the force-moment information measured by the UFS. Additionally, the error associated with the determined point of application of the force in this methodology is not affected by the angle between the direction of the external force and sensor surface. As the directions of loading within the soft tissues of the knee are expected to shift significantly with knee loading, the minimal error associated with this non-contact methodology will allow the determination of the *in-situ* force in the soft tissues of the knee under varied loading conditions.

The *in-situ* force in the ACL was 110 N when 100 N of the anterior load was applied to the knee joint. This value for the *in-situ* force is similar to data obtained previously in our laboratory using a kinematic linkage [Takai *et al*, 1991], and also to that obtained by Markolf *et al*, 1990. Based on the point of application of the *in-situ* force in the ACL, it is surmised that the medial portion of antero-medial portion of the ACL bears the majority of the load in the ACL when anterior load is applied to the joint at 30° of flexion. It has also been determined that with increasing anterior load, the point of application of the *in-situ* force moves from the medial portion to antero-medial portion of the tibial insertion site of the ACL. This may be caused by the fact that each bundle of the ACL has a different length, and the number of "tensed" bundles may increase as the anterior load increases [Hollis *et al*, 1991].

Using this direct, non-contact methodology, the "complicated" roles of the soft tissues of the human knee joint may be explored without disruption of their in-situ geometries . Simulation and testing of more physiologic loading conditions at the knee joint are currently under investigation.

REFERENCES

1) Barry, D et al: *J Biomech Eng* 108: 149-152, 1986.
2) France, PE et al: Prosthetic Ligament Reconstruction of the Knee, 1988.
3) Hollis, MJ et al: *J Biomech Eng* 113:208-214, 1991.
4) Lewis, JL et al: *J Biomech Eng* 104: 125-128, 1982.
5) Markolf, KL et al: *JBJS* 72A: 557-567, 1990.
6) Takai, S et al: *Trans ORS* 16: 235, 1991.

ACKNOWLEDGEMENTS

The authors gratefully acknowledge the support of NIH Grant AR 39683.

Proceedings of NACOB II, The Second North American Congress on Biomechanics, Chicago, August 24th - 28th, 1992

VISCOELASTIC PROPERTIES OF THE HUMAN PATELLAR TENDON: AGE RELATED CHANGES

G. A. Johnson, N. Y. Choi, D. M. Tramaglini, P. J. McMahon and S. L-Y. Woo

Musculoskeletal Research Laboratories
Department of Orthopaedic Surgery
University of Pittsburgh

INTRODUCTION

A portion of the human patellar tendon (PT) is commonly used as a replacement graft for a ruptured anterior cruciate ligament (ACL) primarily because of its strength. Little is known, however, about its time-dependent viscoelastic properties in terms of graft function. The experimental study presented here is intended to measure these properties and determine how they change with donor age. Tensile tests were carried out using specimens from a young age group (15-35 years) and an old age group (60-90 years). Results point to a small decrease in stiffness for the older age group.

REVIEW AND THEORY

Rupture of the anterior cruciate ligament (ACL) is often treated surgically by replacing the injured ligament with a graft. One of the most commonly used graft materials is a portion of a human patellar tendon (PT) (Friedman *et al.* 1985). It is important, for the kinematics and stability of the surgically treated knee, to match the mechanical properties of the graft material to those of the normal ACL as closely a possible. The mechanical properties of the ACL have been extensively studied (Butler, 1989), but relatively little is known about the properties of the PT. Though stiffness and viscoelastic (i.e. time and rate dependent) mechanical properties are of primary importance in determining the tissue's effectiveness as a graft, previous work has focused upon the tensile strength of PT allografts (Noyes *et al.*, 1984).

Limited information is available concerning the effect of age upon the properties of the human PT. Hubbard and Soutas-Little (1984) investigated age dependent changes of the mechanical properties of the human palmaris longus and hallucis longus tendons. It was concluded that subject age had no effect on the tendon modulus and a minimal effect on hysteresis and relaxation. Similar observations were reported by Haut *et al.* (1992) in studying the effect of age on the mechanical properties of the canine PT. No significant age related effect was identified for tensile modulus, failure load, or failure mode. Haut *et al.*(1987) evaluated the effect of age and irradiation on the mechanical and structural properties of the human PT. No significant differences were noted in the mechanical and structural properties of the different age groups.

Despite the results cited above, it is thought that human connective tissue becomes weaker and less stiff with age (Noyes *et al.*, 1976); therefore, the age of the graft donor should be a crucial determinant of the mechanical properties of the graft material. Quantifying these age effects will help the clinician decide upon the maximum acceptable age of an ACL graft donor. The goals of this study are to determine the normal mechanical properties of the human PT and to assess the effects of aging on its mechanical properties.

PROCEDURES

Eight fresh-frozen non-irradiated patella-patellar tendon-tibia preparations were separated into two groups (15-35 yrs. and 60-90 yrs.). In the preliminary phase of this study, the specimens were tested to evaluate the effects of age on the viscoelastic mechanical properties. When completed, the study will include ten specimens in each age group.

Approximately 24 to 48 hours prior to testing, the patellar tendon and its insertions were removed from the patella and tibia, leaving a small block of bone on each end of the PT. The patellar and tibial bone blocks of the specimens were then embedded in PMMA bone cement and fit into specially designed clamps for testing in an Instron materials testing machine. The specimens remained inside a freezer to prevent heat damage during polymer curing. On the day of testing the PT was cut to a cross-section of approximately 15 mm^2. The portion remaining was from the central third of the PT as that is most commonly used for grafts. The cross-sectional area of the specimen was measured using a laser micrometer and dye lines were placed across the length of the tendon to allow strain measurement using a video dimensional analyzer (Woo *et al.*, 1981).

The specimens were tested in a saline bath equilibrated to 37 °C. Each specimen was preconditioning by cyclic loading between zero and 2% elongation. The specimens were preconditioned for 10 cycles at a strain rate of 4% per minute. After preconditioning, the specimens were unloaded and allowed to equilibrate in the saline bath for 30 minutes. Two stress relaxation tests were then performed for the assessment of time-dependent (viscoelastic) properties. For the first stress relaxation test the specimen was loaded rapidly (100 mm/min) to a stress of approximately 1 MPa and held at the resulting elongation for 15 minutes, followed by a 30 minute unloaded, resting period. During the second stress relaxation test the specimen was loaded to an initial stress of approximately 4 MPa and held at the resulting elongation for 15 minutes, followed by a 30 minute resting period. A cyclic test was performed between elongation limits determined from the stress relaxation tests. The specimens were stretched for a total of 15 cycles in 5 minutes. After a rest period of 30 minutes, the specimens were loaded to failure at a rate of 200 mm/min. Load data for all tests were acquired using both a personal computer with a metrabyte A/D board and a strip recorder. Strain was obtained from a videotape of the experiment using a video dimension analyzer to track the distance between dye lines. The data acquired is used to construct a stress-strain curve and a stress relaxation curve for each specimen.

RESULTS AND DISCUSSION

The data for linear stiffness, stress relaxation, and the stress and strain at failure are listed in Tables 1 and 2. Sample stress vs. strain curves for both the young and the old specimens are shown in Figures 1 and 2, respectively. Results obtained indicate a small decrease in stiffness for the older age group. Relaxation tests have also shown that there is a decrease in the time required for stress relaxation in the older group. A statistical evaluation of the data would be premature at this time.

The stability of the knee following ACL reconstruction depends on the mechanical properties of the material used as a replacement, among other factors. Despite the obvious importance of the viscoelastic properties, studies of the mechanical properties of the human patellar tendon have emphasized ultimate strength. Clearly, during normal activity, the graft does not carry loads that would cause it to fail or nearly fail. The most important properties of the tissue are the linear

stiffness and the time-dependent viscoelastic properties which determine its response to cyclic stresses such as those it will experience *in vivo*.

One would expect experimental results to support the proposition that human connective tissue becomes weaker and less stiff with age. More important than this, however, is the question of how much the stiffness tends to decrease with age and how the time-dependent stress-relaxation properties change with age. Will tissue from older donors provide adequate grafts? This study is intended to address these issues and provide quantitative information about how stiffness and time-dependent mechanical properties of the human patellar tendon change with age.

Table I. Preliminary Time-dependent Mechanical Properties for Young Specimens

Specimen	PTN11	PTN14	PTN15	PTN16
Donor Age (yrs.)	34	33	39	34
Modulus* (in linear region)	1043	608	806	989
Ultimate* Strength	67.3	79.2	73.6	70.4
% Strain at Failure	8	19	11	6
Initial stress* (2nd relaxation)	4.52	4.57	4.68	4.74
Final stress* (2nd relaxation)	2.82	2.35	2.66	2.40

* Units are MPa

Table II. Preliminary Time-dependent Mechanical Properties for Old Specimens

Specimen	PTN7	PTN8	PTN14	PTN18
Donor Age (yrs.)	64	77	75	86
Modulus* (in linear region)	761	502	920	404
Ultimate* Strength	66.2	46.9	59.6	18.3
% Strain at Failure	22	13	9	5
Initial stress* (2nd relaxation)	4.31	4.53	4.59	2.72
Final stress* (2nd relaxation)	2.53	2.35	2.68	1.08

* Units are MPa

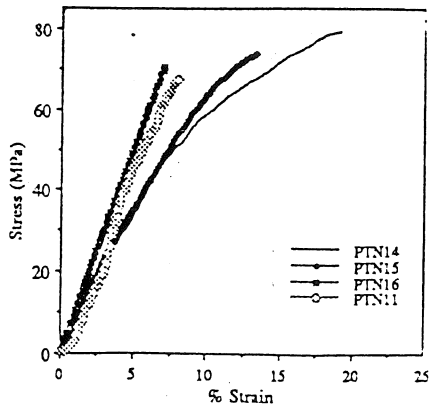

Figure 1. Stress vs. Strain for Young Specimens

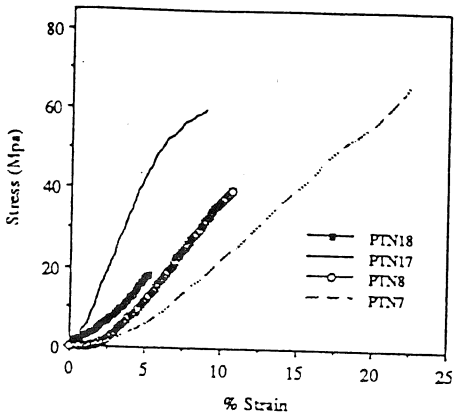

Figure 2. Stress vs. Strain for Old Specimens

ACKNOWLEDGEMENTS

This work is supported by NIH grant AR39638.

REFERENCES

Butler DL, JOR, 7:910-921, 1989.
Friedman MJ, *et al.*., Clin Ortho, 196:9-14, 1985.
Haut RC, *et al.*, J. Biomech, 15:75-78, 1988.
Haut RC, *et al.*, J. Biomech, 25(2):163-173,1992.
Hubbard RP, *et al.*, J. Biomech Eng, 106:144-150,1984.
Noyes FR, *et al.*, JBJS, 58A:1074-1082, 1976.
Noyes FR, *et al.*, JBJS, 66A:344-352, 1984.
Woo SL-Y, *et al.*, J. Biomech Eng, 103:293-298, 1981.

BIOMECHANICAL PROPERTIES OF AN INJURED LIGAMENT TREATED WITH CORTICOSTEROIDS

M. Wiggins[1], P.Fadale[1], H. Barrach[1], H. Sasken[3], D.C. Judge[1], M.Ehrlich[1], W. R. Walsh[1,2]

[1]Dept. of Orthopaedics, Brown University/Rhode Island Hospital , [2]Div. of Engineering, Brown University, [3]Dept. of Pathology, Brown University/Rhode Island Hospital, Providence, Rhode Island

INTRODUCTION

128 skeletally mature New Zealand white rabbits were used to study the effect that a single corticosteroid injection has on the biomechanical, histological , and biochemical properties of ligamentous healing. Two different steroid doses were studied. The first dose was determined from in-vitro cell culture analysis of fibroblasitc protein synthesis after exposure to differing concentrations of the corticosteroid betamethasone. The lowest dose which inhibited [3H] proline uptake (a relative indicator of collagen synthesis) was used as the low dose, and a human equivalent dose was used as the high dose. These two doses and a saline control were injected around a transected medial collateral ligament. At 10 days all groups showed significantly inferior biomechanical properties relative to non-injected controls. By 3 weeks the human equivalent steroid dose group continued to demonstrate significantly inferior properties. Histological and biochemical analysis confirmed the biomechanical results. This implies that a corticosteroid treated injured ligament may not be able to withstand the mechanical loads of early vigorous rehabilitation.

REVIEW AND THEORY

Corticosteroids have been used extensively in the practice of orthopaedics, predominantly for arthritis and chronic overuse injuries. However, in the treatment of acute soft tissue injuries involving tendons and ligaments many physicians have been hesitant to use steroidal injection therapy. Most of this hesitancy originated from isolated case reports of spontaneous tendon/ligament rupture occurring after steroid injection or chronic corticosteroid use. Basic science data consists of scattered reports and conflicting results. Recent studies in the literature, however, report no detrimental effects to a healing/injured tendon or ligament following steroid injection (Campbell et al. 1991, McWhorter et al. 1991).The purpose of this study is to examine the biomechanical, biochemical, and histological properties of an injured ligament when it is exposed to different steroid doses immediately following injury. In-vitro cell culture analysis and the transected rabbit medial collateral ligament (MCL) model were employed in the study.

PROCEDURES

Rabbit skin fibroblasts were isolated and grown in culture. Cells were exposed to differing concentrations of betamethasone followed by [3H] proline incubation. [3H] proline uptake was measured and used as an indication of relative collagen synthesis. The lowest concentration of betamethasone which inhibited collagen synthesis was used as the initial steroid dose.The rabbit medial collateral ligament (MCL) served as the animal model for this experiment (Woo et al. 1986). The medial colllateral ligament (MCL) was exposed through a medial parapatellar skin incision. Fascia was similarly opened and the MCL transected at the joint line. Fascia was closed thus creating a fascial pocket in which to inject the steroid solution. Animals were divided into 5 groups. INJ-1, determined from the in-vitro experiment, in which 5.8x10-5 M betamethasone was injected. INJ-2 in which 1.3x10-3M betamethasone was injected, representing a human equivalent dose. SALINE in which saline was injected. NON-INJ in which no injection was performed and a SHAM group. All injections were made under direct vision. Animals were sacrificed at 10 days and 3 weeks.

Specimens for biomechanical testing were cemented in polymethylmethacrylate Cross sectional area was calculated assuming the MCL to be rectangular shaped, and measurements were made with a microscopic eye piece. The tensile testing protocol was carried out on an MTS model 810 in accordance with previously described methods (Woo et al. 1986). The structural properties were expressed by the load-deformation output. The peak load and stiffness in the linear region and energy at failure were determined from the load deformation curves. Ultimate stress was determined using the cross sectional area and the peak load. Statistical analysis was done using the unpaired Student's t-test.Type I and III collagen ratios were determined by use of cyanogen bromide mapping technique (Amiel et al. 1984) using sodium dodecyl sulfate gel electrophoresis and video densitometric scanning. Specimens for histological analysis were immediately fixed in formalin and stained with hematoxylin-eosin and Masson's trichrome.

RESULTS

A betamethasone concentration of 5.8x10-5 M caused a statistically significant reduction in uptake of radioactive proline at all cell densities examined. This value represents the lowest dose, used in our in-vitro experiments, which inhibited protein synthesis by fibroblasts.and was used as the initial steroid dose, INJ-1.The sham operated group revealed no statistical difference for area, peak load, stiffness or ultimate stress compared to its contralateral control side at 10 days or 3 weeks. The structural and mechanical properties improved with time for the NON-INJ, SALINE, INJ-1, and INJ-2 groups. Structural and mechanical properties of INJ-2 ligaments were consistently lower at 10 days and 3 weeks compared to INJ-1 ligaments. The structural properties (peak load, stiffness and energy to failure) are summarized in figures 1-3. The ultimate stress values are summarized in figure 4. Histological and biochemical analysis in the form of collagen typing supported the biomechanical results.

DISCUSSION

Steroids use is based on their anti-inflammatory properties. Injured tissues incite an inflammatory repsonse leading to local tissue edema, swelling, pain and limited motion. An anti-inflammatory agent can potentially blocks this response, limits pain, allows earlier motion and presumably quicker and adequate healing This theory is both supported and contradicted by authors who have examined steroid's effect on ligament or tendon in the laboratory Steroids are also known to inhibit collagen synthesis. This would lead one to assume that steroids would inhibit ligamentous healing since 70 - 80% of the dry weight of ligament is collagen What is not known about corticosteroids is if the anti-inflammatory properties can be separated from the collagen inhibition properties. If the dose which inhibits inflammation is different than the dose which inhibits collagen synthesis, then steroids could possibly be used to diminish pain and swelling without affecting the healing of injured tissues. However, if

inhibition of collagen synthesis occurs at a dose less than or equal to the anti-inflammatory dose, then it would probably not be wise to administer steroids to injured soft tissues. Additionally, if the inflammatory phase is disturbed or altered by steroids, is wound healing just delayed, or permanently altered.

The biomechanical results obtained in this study indicate that a single corticosteroid injection treatment to a transected MCL significantly effects its structural and mechanical properties. Our in-vitro cell culture results indicated that even the low steroid dose group (INJ-1) slightly inhibited protein synthesis as indicated by [3H] proline uptake. However, biomechanically the INJ-1 group was similar to the saline carrier control. In contrast, the high steroid, human equivalent dose (INJ-2) completed inhibited protein synthesis in-vitro and resulted in marked reductions in the biomechanical properties compared to non-injected and saline controls, and the low dose steroid group (INJ-1). This suggests that in addition to the mere presence of an injected solution in the injury site, a human equivalent steroid dose (INJ-2) dramatically impairs the repair process and compromises the biomechanical properties of the healing FMTC.

The reduction in the structural and mechanical properties continued to exist in the high dose steroid group (INJ-2) at 3 weeks relative to all other groups. The SALINE and INJ-1 groups were similar to controls at 3 weeks. This suggests that the presence of fluid or low dose steroid no longer has an apparent effect at 3 weeks following injury. However, the properties of the INJ-2 group remained markedly reduced compared to all other groups.

The results of this study indicates that a corticosteroid injection into an acute ligamentous injury has significant inhibitory effects on the healing process in the early phases (inflammatory and matrix and cellular proliferation) of ligament healing. This is supported by biomechanical, biochemical, and histological analysis. Even the low dose steroid (1/23 that of a normal human equivalent dose INJ-1) showed inferior biomechanical properties and a higher percentage of type III collagen at 10 days compared to the non-injected. By 3 weeks there was no longer a statistically significant difference, but there remained a less linear collagen fiber arrangement. The higher dose steroid (human equivalent dose, INJ-2) demonstrated a complete inhibition of healing. At 3 weeks the INJ-2 ligaments were still significantly weaker than non-injected ligaments and had not reached the histological maturity seen in even the 10 day INJ-1 specimans. The proportion of type III collagen present (17%) was now similar to low dose steroid and non-injected specimens. Thus corticosteroid, given in a human equivalent dose, significantly impair the healing process of a transected ligament at 10 days following injury. By 3 weeks, these ligaments still had significantly inferior biomechanical properties, which was paralled by an inferior histological organization and a high percentage of type III collagen.

REFERENCES

Amiel, D. et al. J. Orthop. Res. 1:257-265, 1984Campbell, R. et al. Trans. Orthop. Res. Soc. 16:112, 1991McWhorter, J. et al. Am. J. Sports Med. 19:435-439, 1991Woo, SL-Y. et al. J. Orthop. Res. 4: 133-141, 1986

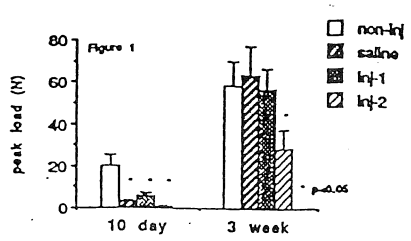

Figure 1: Peak load at failure (mean +/- s.e). At 10 days the SALINE, INJ-1, and INJ-2 are statistically significantly inferior to NON-INJ, $p<0.05$. At 3 weeks the INJ-2 ligaments are signicantly inferior to all other, $p<0.05$.

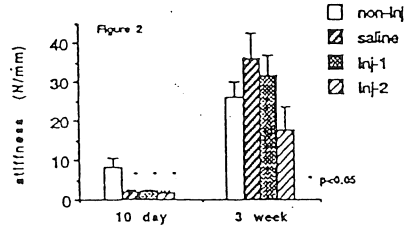

Figure 2: Linear stiffness (mean +/- s.e.). At 10 days the NON-INJ ligaments are significantly superior to all others, $p<0.05$. At 3 weeks no statistical significance exists between the groups.

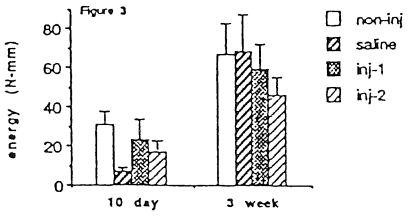

Figure 3: Energy absorbed at failure (mean +/- s.e.) for the 10 day and 3 week groups. No statistical significance exists between the groups at either time point.

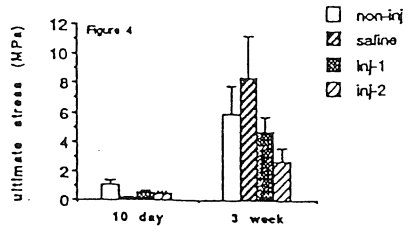

Figure 4: Ultimate stress (mean +/- s.e.). Reductions seen at 10 days and 3 weeks are not statistically significant, although strong trends in the reduction are observed especially the 3 week INJ-2 group

EFFECT OF GROWTH HORMONE ON TENSILE STRENGTH AND THICKNESS OF BLADDER FROM PIGS

J. Vossoughi and T. J. Caperna

Engineering Research Institute
University of the District of Columbia
4250 Connecticut Ave, NW
Washington, DC 20008

and

NANL, US Department of Agriculture
Beltsville, MD 20705

ABSTRACT

Tensile strength of bladder from growth hormone-treated and control pigs was compared. The results indicate that administration of growth hormone was associated with decreased tensile strength of the bladder by as much as 26%. Also growth hormone-treated pigs had approximately 20% thicker bladders compared to control pigs, while the wet weight of this tissue was similar for both groups.

METHODS

A total of 14 castrated male pigs were used in this experiment. Pigs were restrictively fed a common diet such that average feed intake for the experimental period was identical for all pigs. At 30.4 ± 0.1 kg body weight the pigs were divided into two groups of seven each. The experimental group was injected daily intra muscularly with porcine growth hormone (100 μg/kg body weight/day). The control group was injected daily with the same volume of buffer solution. Pigs were sacrificed at 64.2 ± 0.8 kg body weight. The bladders were removed and kept in physiological saline at 4 °C prior to testing. All testing was performed within four hours postmortem. From each bladder 5 mm wide tensile specimens were cut through the thickness of the bladder. From bladders of growth hormone-treated pigs a total of 29 circumferential and 31 longitudinal strips were tested to failure and compared with the tensile strength of 27 circumferential and 26 longitudinal strips from bladders of control pigs. The thickness of each specimen was measured using a technique explained elsewhere [1]. Each specimen was connected to the clamps of an Instron testing machine (model 1011) and after preconditioning stretched to failure. The failure load of each specimen was recorded and later divided by the initial cross-sectional area of each specimen to obtain the tensile strength.

RESULTS

The tensile strength of all the circumferential and longitudinal specimens in both the control and growth hormone

treated groups were separately averaged as shown in Table I. Two types of comparisons were performed by Student's t-test analysis; 1) the tensile strength of circumferential and longitudinal strips within each group were compared to see if the tensile strength of the bladder is different in circumferential and longitudinal directions and 2) the tensile strength of the bladder of control group was compared with that of the growth hormone-treated group separately in circumferential as well as longitudinal directions. The results indicate that the tissue of the bladder is slightly but not statistically significantly stronger in the longitudinal direction compared to the circumferential direction. Comparison of the tensile strength of the bladders of growth hormone-treated pigs with controls indicated that growth hormone treatment was associated with decreased tensile strength of bladder tissue by 26 and 11% in the circumferential and longitudinal directions, respectively. The average value of the thickness of 53 strips from control group was compared with 60 strips of the growth hormone-treated group which indicates that growth hormone administration was associated with a 21% increase in thickness of the bladder. However, the weight of the tissue was found to be similar in both groups.

It should be mentioned that in a separate study it was shown that the tensile strength of diaphragms from growth hormone treated pigs was increased by as much as 25% compared to control group [2].

REFERENCES

[1] Vossoughi, J. 1984. Thickness measurement for soft rubber. Experimental Techniques, Vol.8, No. 9, pp 32-33.

[2] Vossoughi, J.,T. J. Caperna. 1991. Effect of growth hormone on tensile strength of diaphragm. In proceedings of 10-th Southern Biomedical engineering conference, P P176-177.

ACKNOWLEDGEMENTS

Partial support of NSF grant HRD-9104562 is greatly acknowledged.

TABLE I

	Control group	GH group
Thickness [mm]	4.14 ± 0.16	5.00 ± 0.13
Wet weight [g]	47.7 ± 0.5	46.2 ± 0.5
Circ. tensile strength [MPa]	0.455 ± 0.030	0.335 ± 0.020
Long. tensile strength [MPa]	0.467 ± 0.022	0.416 ± 0.024
Average tensile strength [MPa]	0.461 ± 0.019	0.378 ± 0.016

TISSUE MATERIAL PROPERTIES AND IMPLANTS

Poster

EFFECT OF PASTEURIZATION ON THE MECHANICAL PROPERTIES OF HUMAN CANCELLOUS BONE

R. J. Zimmerman, J.E. Bechtold, D.T. Eastlund*, P.T. Bianco

Orthopaedic Biomechanics Laboratory, Hennepin County Medical Center, Minneapolis, MN 55415
***American Red Cross, St. Paul, MN**

INTRODUCTION

The material properties under axial compression, of human cancellous bone sterilized with pasteurization (60C for 10 hours) were compared with fresh frozen controls. Pasteurization caused a 17.5% decrease in ultimate strain, 16.9% decrease in ultimate stress, 4.1% decrease in elastic modulus, and a 34% decrease in the energy absorbed at failure. None of these differences were significant in the nine location and subject matched pairs.

REVIEW AND THEORY

Human bone allografts are being increasingly used in orthopaedic reconstructive surgery. Allograft material may be preserved with freeze-drying; treated with various methods of sterilization such as heat, chemicals, or gamma irradiation;[14] or it may be fresh frozen at temperatures ranging from -20C to liquid nitrogen.[1] The use of fresh frozen allograft may be complicated by infection from the donor[6] and/or from handling[2] as well as by complications due to the host's immunologic response.[17] Freeze dried allograft, with its undetermined risk of transmitted infection, may also be viewed as foreign. Fresh frozen and freeze dried specimens do preserve the bone's material properties,[1] and thus are the most widely used for reconstruction of weight bearing skeletal defects.[10] The problems with sterilized graft are decreased structural integrity,[1,8,9,13,18,22] and the loss of osteogenic capability of devitalized bone.[10] The ideal would be a structurally satisfactory allograft with the biological characteristics of Urist's AAA bone - a chemosterilized, antigen extracted, autodigested allograft.[23,24] This form of bone would have few risks of infection or immunological rejection and an enhanced ability to incorporate.[11] The search for this ideal requires biomechanical and histological investigations into the known methods of allograft procurement, preservation, and sterilization. Boiled bone has been found to be devoid of osteoinductive capability, and inferior to freeze dried and frozen allografts for purposes of transplantation,[3] although it and autoclaved bone have been used in reimplantation.[10,16]

The present study investigates pasteurization, low level heat treatment at 60C for 10 hours, as an alternative to conventional sterilization methods. Pasteurization has been found to effectively inactivate a broad spectrum of viruses, including CMV, Epstein-Barr, Herpes Simplex, Polio, and Vaccinia. The AIDS virus, HTLV III, is rapidly inactivated, becoming nondetectable within 30-60 minutes.[7] We compared the compressive strength, ultimate strain, elastic modulus,[15,20] and energy at failure of human cancellous bone treated with pasteurization to that of fresh frozen controls.

PROCEDURES

18 cancellous bone dowels were drilled from the fresh frozen bones of a human donor using a 12 mm trephine drill,[4,12] at identical locations on right and left bones in the proximal and distal femur and tibia. Controls were alternated systematically between left and right to accommodate any asymmetry in the structural properties of the donor's bones.

The dowels were immediately placed in water in a sealed container and the controls were returned to the freezer[4] while the test specimens were treated at 60C for 10 hours. Following treatment, the test specimens were likewise placed in water and frozen.

On the day of testing, all specimens were thawed in normal saline. The articular cartilage of each dowel was scraped with a sharp chisel and sanded square using a hollow aluminum cylinder and plunger. Each dowel was then placed in a vice equipped with a tool to prevent crushing and was sawed at exactly 15 mm, resulting in a square ended cylindrical dowel of 12 mm diameter and 15 mm length. Each of these dowels was then oriented with the long axis of an MTS servohydraulic materials test machine (MTS Systems, Inc., Minneapolis) and was crushed to failure[5] at a rate of 0.5 mm/sec.[18,19]

Load as a function of axial deformation was recorded. Ultimate stress, ultimate strain, elastic modulus, and energy absorption at failure were calculated.

RESULTS

Data were analyzed for effect of site of dowel harvest and treatment (pasteurization or control), and no effect for location was seen, nor were any of the mechanical properties significantly different in this limited sample of 8 pairs (t test, $p < .05$).

	PASTEURIZATION	CONTROL	%
STRAIN (mm/mm)			
mean	.035	.040	17.5%
sd	.009	.006	
STRESS (N/mm^2)			
mean	11.0	13.3	16.9%
sd	3.4	3.7	
MODULUS of ELASTICITY (N/mm^2)			
mean	424.0	441.7	4.1%
s.d.	95.7	181.7	
ENERGY (N-mm)			
mean	332.2	500.9	33.7%
s.d.	193.7	170.6	

DISCUSSION

The only other reported study in the literature of low level heat sterilization studied the effect of 60C for *20* hours on cancellous bone, and found a decrease in failure stress and elastic modulus, and increase in failure strain, however at *56C* these effects were not seen.[21] In our study, the specimens were exposed to *60C* for *10* hours, and reductions in failure stress and strain of approximately 17% were seen, with no effect on elastic modulus. Energy at failure was decreased with heat treatment, but none of the differences were statistically significant. Further studies, with more subjects, and different pasteurization parameters are currently being undertaken.

REFERENCES

1) Bright R, Burchardt H: The Biomechanical Properties of Preserved Bone Grafts. In Friedlaender G, Mankin H, Sell K (eds.): Osteochondral Allografts - Biology, Banking, and Clinical Applications. Little, Brown and Co, 1983, pp 241-7
2) Bright R, Smarsh J, Gambill V: Sterilization of Human Bone by Irradiation. In Friedlaender G, Mankin H, Sell K (eds.): Osteochondral Allografts - Biology, Banking, and Clinical Applications, Little, Brown and Co, Boston/Toronto, 1983, pp 223-31
3) Burwell GR: The Fate of Bone Grafts. In Apley AG (ed): Recent advances in Orthopaedics. Churchill, London. 1969. pp115-207
4) Carter D, Hayes W: Bone compressive strength: The influence of density and strain rate. Science 194: 1174-5, 1976
5) Carter D, Spengler D: Mechanical properties and composition of cortical bone. Clin Orthop and Rel Res 135: 192-217, 1978
6) Eastlund T: Infectious disease transmission through tissue transplantation: Reducing the tisk through donor selection. J Transplant Coordination 1: 23-30, 1991
7) Hilfenhaus J, Hermann A, Mauler R, Prince AM: Inactivation of the AIDS-causing retrovirus and other human viruses in antihemophilic plasma protein preparations by pasteurization. Vox Sang 50(4): 208-11, 1986
8) Koehler P, Kreicbergs A, Stromberg L: Physical properties of autoclaved bone - Torsion test of rabbit diaphyseal bone. Acta Orthop Scand 57: 141-5, 1986
9) Komender A: Influence of preservation on some mechanical properties of human haversion bone. Materia Medica Polona 1(26) 13-17, 1976
10) Kreicbergs A, Koehler P: Bone Exposed to Heat. In Aebi M, Regazzoni P (eds.): Bone Transplantation. Springer-Verlag, Berlin Heidelberg, 1989, pp 155-61
11) Kreicbergs A, Koehler P: Reconstruction of Large Diaphyseal Defects by Autoclaved Reimplanted Bone: An Experimental Study in the Rabbit. In Aebi M, Regazzoni P (eds.): Bone Transplantation, Springer-Verlag, Berlin Heidelberg, 1989 pp.204-8
12) Lindahl O, Lindgren A: Cortical bone in man III. Variation of compressive strength with age and sex. Acta Orthop Scandinav 39: 129-135, 1968
13) Loty B, Courpied J, et al: Bone allografts sterilized by irradiation - Biological properties, procurement and results of 150 massive allografts. International Orthopaedics (SICOT) 14: 237-42, 1990
14) McCullough J, Eastlund T: Tissue and Organ Preservation and Transplantation. In Rossi E, Simon T, Moss G (eds.): Principles of Transfusion Medicine, Williams and Wilkins, Baltimore, 1991, pp 673-86
15) Odgaard A, Linde F: The underestimation of Young's modulus in compressive testing of cancellous bone specimens. J Biomechanics 24(8): 691-8, 1991
16) Orell S: Surgical bone grafting with os purum, os novum and boiled bone. J Bone Joint Surg 19:837, 1937
17) Pelker R, Friedlaender G: Biomechanical aspects of bone autografts and allografts. Orthopedic Clinics of North America 18(2): 235-9, 1987
18) Pelker R, Friedlaender G, Markham T, Panjabi M, Moen C: Effects of freezing and freeze-drying on the biomechanical properties of rat bone. J Orthop Res 1(4): 405-411, 1984
19) Pelker R, Markham T, Friedlaender G, Moen C, Panjabi M: The Effects of Preservation on Allograft Strength. 28th Annual ORS, New Orleans, Louisiana, Jan 19-21, 1982
20) Reilly D, Burstein A, Frankel V: The elastic modulus for bone. J Biomechanics 7(3): 271-5, 1974
21) Sharkey NA, Hollstien SB, Martin RB: Thermal Inactivation of HIV in Cadaveric Specimens: Biomechanical Effects on Bone, Proceedings, Combined Meeting of the Orthopaedic Research Societies of USA, JAPAN and CANADA, October 21-23, 1991, Banff, pg. 279.
22) Triantafyllou N, Sotiropoulos E, Triantafyllou J: The mechanical properties of the lyophilized and irradiated bone grafts. Acta Orthopaedica Belgica 41, Suppl 1: 35-44, 1975
23) Urist MR, Dawson E: Intertransverse process fusion with the aid of chemosterilized autolyzed antigen-extracted allogeneic (AAA) bone. Clin Orthop and Rel Res 154:97, 1981
24) Urist MR, Mikuliski A, Boyd SD: A chemosterilized antigen extracted autodigested alloimplant for bone banks. Arch Surg 110:416, 1975

ACKNOWLEDGEMENTS

Minnesota Medical Foundation, Minneapolis, MN American Red Cross, St. Paul, MN

COMPRESSIVE STIFFNESS OF THE CANCELLOUS BONE OF THE CANINE PROXIMAL TIBIA

T.L. Willke, D.R. Sumner and T.M. Turner

Department of Orthopedic Surgery
Rush-Presbyterian-St. Luke's Medical Center
Chicago, Illinois 60612

INTRODUCTION

Canine cancellous bone is used as a model for human bone in experimental orthopedic research, including models of total knee arthroplasty (1,2). Extensive information on the mechanical properties of human cancellous bone is available, yet little is known of the properties of the proximal canine tibia. Depth-force measurements produced by small-diameter indentation testing were used to derive the variation of Young's modulus (E) over the transverse cross-sectional surface at three levels within the proximal epiphyseal canine tibia. At the most proximal section the presence of lateral and medial peaks of maximal modulus were found. Modulus averages for the three surfaces revealed a trend of distally decreasing stiffness. Overall, the stiffness values for the canine tibia were two-fold larger than published values for the proximal human tibia (3).

REVIEW AND THEORY

Small diameter surface indentation tests have commonly been employed to derive the spatial heterogeneity of cancellous bone stiffness or strength in the axial direction. Stiffness slopes computed in such a manner can be used to find Young's modulus with an equation of elasticity for a plane boundary of a semi-infinite elastic solid proposed by Timoshenko and Goodier (4) and first implemented for cancellous bone by Finlay et al (3). This equation is applicable when the material is assumed homogeneous and the test surface is semi-infinite relative to the cross-sectional area of the applied indentor. To validate the assumptions needed to calculate Young's modulus for the case of a 2.49 mm diameter cylinder and canine cancellous bone, depth-force slopes produced by the indentor and subsequently transformed using Timoshenko and Goodier's equation were compared with empirically calculated results from 13 non-destructive compression tests on the same samples. The results were found to be to in agreement ($r^2 = 0.94$, $p < 0.05$), validating the use of this equation in our experiment.

A closely spaced 4 x 4 mm quadratic grid pattern of testing was implemented to produce high spatial resolution of the stiffness trend. Trabecular damage from penetration testing is limited to the radius of the indentor (5); thus there should be no effect of testing at one site on each of its neighbors. Tests performed in this manner with an adequate number of preloading cycles and low strain rates (< 5 mm/min) are accurate in describing the properties of the bone at discrete locations.

The purpose of this study was to identify and spatially map the pattern of longitudinal compressive stiffness of cancellous bone in the proximal canine tibia.

PROCEDURES

Six right tibias were obtained from adult male mongrel dogs. The proximal subchondral bone plate was removed with a diamond-tipped blade mounted on a modified surface grinder under constant irrigation. The resection was made parallel to the joint surface to simulate the method employed in experimental canine total knee arthroplasty (1). Three serial sections approximately one centimeter in thickness were produced by making parallel cuts further distally. These are referred to as level one, two, and three, respectively.

Indentation tests were performed using a 2.49 mm flat-headed punch fixed to an Instron Universal 1321 Testing Machine. The cylindrical rod penetrated the trabecular bone at right angles to the resection surface at a constant rate of 2 mm/min. The force of indentation versus position was plotted to a depth of 0.15 mm. The apparent stiffness was calculated from the maximum slope of the initial linear region of the curve. By using the formula originated by Timoshenko and Goodier and empirically verified for the case of canine cancellous bone, the modulus of elasticity was determined. The mechanical tests were carried out in a quadratic pattern over the entire proximal surface at each section level with 4 mm between the center of each indentation. Elements that did not completely overlay cancellous bone were discarded.

RESULTS AND DISCUSSION

For level one, the modulus of elasticity was plotted along a lateral to medial transect beneath the centers of the condyles (Fig. 1). In the coronal plane, a pattern of two peaks with a central minimum was found. With approximately equal magnitudes of 1100 MPa, the peaks are unlike those found in the proximal human tibia which has a medial-to-lateral maximal strength ratio of 1.7:1 (6) and a stiffness ratio of 1.5:1 (3). Typical maximal values for the young adult subchondral proximal human tibia (3) are roughly 50% of those found for dogs in the present study. Resection levels two and three showed a pattern of stiffness with centrally located minima. As with humans (6), there was a gradient of decreasing compressive modulus in the distal direction (Fig. 2). Specifically, the average modulus of the third level was significantly less than that of the two proximal levels ($p < 0.05$).

These data should prove useful for finite element models and interpreting mechanical tests of total knee prosthetic components.

Acknowledgment: NIH Grant AR39827

REFERENCES

1. Turner et al.: J Orthop Res 7:893-901, 1989.
2. Sumner et al.: Trans ORS 17:268, 1992.
3. Finlay et al.: Clin Orthop 247:193-201, 1989.
4. Timoshenko and Goodier: Theory of Elasticity, 3rd ed. New York: McGraw-Hill, 1970, p. 408.
5. Hvid: Mechanical Strength of Trabecular Bone at the Knee. Arhus, Denmark: Laegeforeningens Forlag, 1988.
6. Hvid and Hansen: J Orthop Res 3:464-472, 1985.

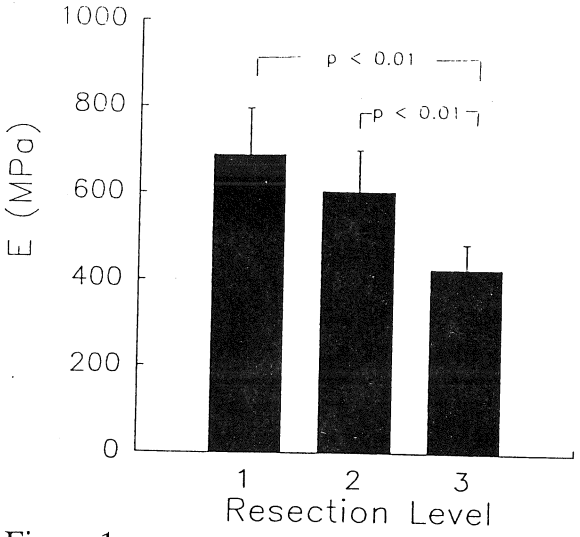

Figure 1.

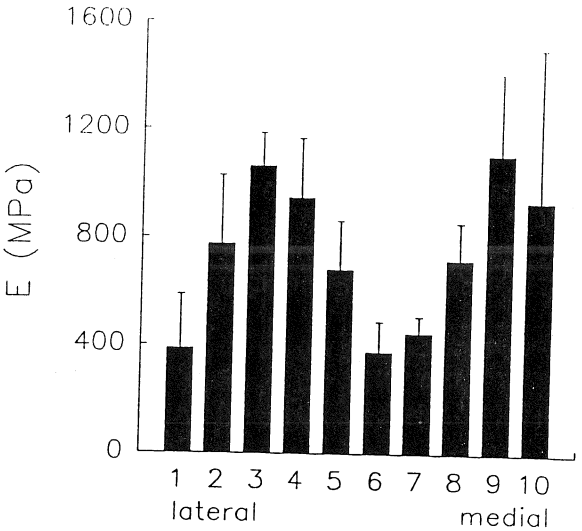

Figure 2.

ULTRASONIC CHARACTERIZATION OF CORTICAL BONE VERSUS POSITION AND ORIENTATION

H. Kim[1], J. Harry[1] and W.R. Walsh[1,2]

[1]Division of Engineering, Brown University, Providence, RI

[2]Department of Orthopaedics, Rhode Island Hospital, Brown University School of Medicine, Providence, RI

INTRODUCTION

The anisotropic nature of bone can be determined ultrasonically by measuring the velocity of transmission through bone and calculating the ultrasonic modulus from velocity and bone density measurements. Ultrasound allows the properties of bone versus position to be determined on a single sample. This study employed an ultrasound transmission technique to examine the mechanical properties of normal cortical bone along the entire length of the diaphysial region of an adult bovine femur in the longitudinal (z), radial (r), and circumferential (theta) directions in each of the four quadrants (anterior, posterior, medial, lateral). The ultrasonic properties vary in each of the four quadrants along the entire length of the femur in all directions.

Characterizing the mechanical properties of normal bone using ultrasound will enable an understanding of positional variations along the length of the femur as well as establish a control for comparison to diseased bone and bone subject to altered forces and remodeling as a result of prosthetic implants.

REVIEW AND THEORY

Ultrasonic techniques have been used to measure the anisotropic elastic properties of bone [1 - 6]. Katz *et al.* (1984) observed anisotropic mechanical properties in both plexiform and Haversian bone, while Ashman *et al.* (1984) and Van Buskirk *et al.* (1981) measured all nine orthotropic elastic constants. More recently, Zimmerman *et al.* (1990) observed bone remodeling around total hip prostheses from changes in mechanical properties as measured from ultrasound velocity. Kholes *et al.* (1992) demonstrated longitudinal velocity variations in normal canine bone.

PROCEDURES

A fresh bovine femur was obtained from a slaughterhouse immediately following sacrifice. The epiphysial ends were cut with a hacksaw. The remaining region of 20cm in length was kept wet throughout the study. The femur was then marked into four quadrants - anterior, posterior, medial, and lateral. After cutting the femur into three segments of equal length, each segment was cut along the previously marked four quadrants. Thirty cubes running from the proximal to the distal end of the femur were obtained from each of the four quadrants. Cancellous bone and marrow was removed. Cubes (5mm) from the central region of each quandrant were cut using a Buehler low speed diamond saw and orientations noted. Each specimen was polished and dimensions measured using a caliper.

The most proximal specimen in each quadrant was labeled as "position 1" and the most distal as "position 30." A total of 120 specimens, 30 from each quadrant, were obtained. Volume was measured on each specimen using Archimedes' Principle and density calculated based on mass/volume relationship.

Cubic specimens of bone were tested in z, r, and theta directions using a 5MHz square wave piezoelectric ultrasonic transducer (Ultran Labs, Inc.) in the pulse-echo mode by placing the transducer on bone and recording the reflections. The reflections were displayed on an IBM PC using Sofrascope (Ultran Labs), a software package for ultrasound analysis. Pulse width of 110ns and amplitude of 200V was employed for optimal reflection detection. In the pulse-echo mode, twice the thickness of bone is divided by the time of flight to obtain the velocity. The ultrasonic elastic modulus, E, can then be calculated by multiplying the square of the velocity by density.

RESULTS AND DISCUSSION

Modulus versus specimen position is plotted for the medial quadrant in Figure 1. Modulus is greatest in the z direction followed by theta and r directions. Modulus in the z direction varied considerably more along the length of the femur than those in the r and theta directions which were relatively constant or had little variability. The modulus in the z direction gradually increased starting from the proximal end of the femur (specimen position 1 in the x-axes), peaked near the midshaft, and then gradually decreased toward the distal end. The variation of modulus in the z direction correlated well with the density variation along the length of the femur as seen in Figure 2. The density peaked near the midshaft of the femur and tapered off towards the two ends.

Medial quadrant data are presented as a representative data. The other quadrants possess similar patterns and values with small variations in their mechanical properties compared to medial. Table 1 presents the average mechanical properties for all four quadrants. Differences in the mechanical properties in z, r, and theta directions as well as in anterior, lateral, medial, and posterior quadrants are noted. These properties demonstrate the anisotropic nature of bone.

Table 1. Average Mechanical Properties of a Bovine Femur

	Velocity (m/s)	Density (g/cc)	E (GPa)
Longitudinal (z)			
Anterior	4274	2.065	37.36
Lateral	4257	2.060	37.41
Medial	4178	2.070	36.18
Posterior	4190	2.059	36.16
Radial (r)			
Anterior	3493	2.065	25.19
Lateral	3439	2.060	24.37
Medial	3478	2.070	25.05
Posterior	3486	2.059	25.03
Circumferential (theta)			
Anterior	3745	2.065	28.95
Lateral	3635	2.060	27.27
Medial	3789	2.070	29.75
Posterior	3690	2.059	28.04

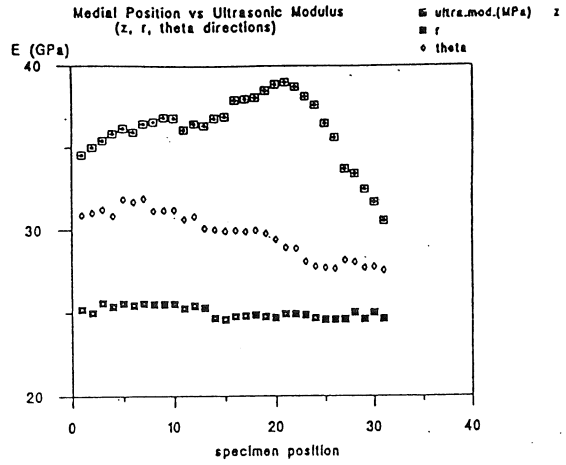

Figure 1. Position vs Ultrasonic Modulus

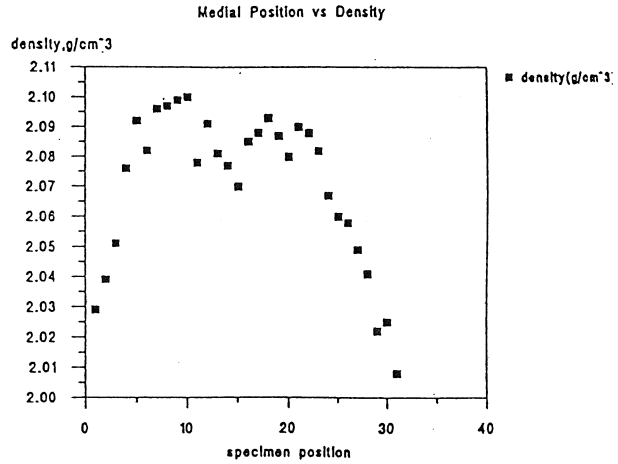

Figure 2. Position vs Density

REFERENCES

1. Van Buskirk, W. et al. *J Biomech Eng*, 8, 143-148, 1986.
2. Ashman, R. et al. *J Biomechanics*,17, 349-361, 1984.
3. Lakes, R. et al. *J Biomed Eng*, 8, 143-148, 1986.
4. Katz, JL. et al. *IEEE Trans Biomed Eng*,31, 878-883, 1984.
5. Zimmerman, M. et al. *IEEE Trans Biomed Eng*,37, 433-441, 1990.
6. Kohles, S. et al. *Transactions of the 38th Annual Meeting: Orthopaedic Research Society*, Washington, DC, (p. 316) 1992.

COMPRESSIVE PROPERTIES OF CORTICAL BONE- THE ROLE OF MINERAL-ORGANIC INTERFACIAL DEBONDING

W.R. Walsh [1,2], D.C. Judge [1] and N.Guzelsu [3]

[1]Department of Orthopaedics, Brown University, Rhode Island Hospital, [2] Division of Engineering, Brown University, Providence, RI and [3] University of Medicine and Dentisty of New Jersey & Rutgers University Biomedical Engineering, Piscataway, NJ

INTRODUCTION

The compressive properties of adult bovine cortical bone were examined following a detergent and ion equilibration protocol. This study was designed to determine the role of bonding interactions between the bone mineral (fiber) and organic matrix constituents (type I collagen and non-collagenous proteins) on the compressive properties of cortical bone. Results indicate that load transmission between the mineral and organic constituents can be modified by altering interfacial bonding interactions through phosphate or fluoride ion treatments. Equilibration in fluoride ion buffers resulted in a reduction in the compressive properties of bone as previously observed in tension (Walsh and Guzelsu, 1990,a,b 1991a). Equilibration in phosphate ion buffer solutions however, resulted in an increase in the compressive properties of cortical bone compared to controls. This differs from our previous results on the effects of phosphate ions on the tensile properties of cortical bone (Walsh et al., 1991). These results suggest that the mechanism of phosphate and fluoride ions in altering mineral-organic interfacial bonding interactions are different. Finally, load transmission through the constituents of bone tissue may not be the same in tension versus compression.

REVIEW AND THEORY

The mechanical properties of composite materials are dependent, in part, upon the individual constituent properties and volume fractions as well as interactions between them. Load transfer and mechanical properties of composites are greatly influenced by the bonding characteristics at the constituent interface . Cortical bone is a naturally occurring calcified composite composed of high modulus inorganic mineral fibers (hydroxyapatite) embedded in a compliant organic matrix (type I collagen and of non-collagenous proteins). Cortical bone mechanical properties have been shown to be dependent upon the mineral content, density and ultrastructure orientation. Interfacial bonding interactions have been hypothesized to be an important factor in the mechanical properties for normal, aged and diseased bone (Bundy, 1985).

Our previous work has demonstrated a statistically significant reduction in the tensile mechanical properties of cortical bone following phosphate or fluoride ion treatment due to an alteration in mineral-organic interfacial bonding (Walsh and Guzelsu, 1990a,b; Walsh et al., 1991; Walsh and Guzelsu, 1991). This work suggests that the mineral and organic phases of bone are linked up through adsorption forces (electrostatic interactions) providing load transfer through the constituents. Based on our experimental results, we hypothesize that load transfer mechanisms in cortical bone in tension and compression may not be the same. In addition, the role of mineral-organic interfacial bonding on the mechanical properties of cortical bone in compression may not be the same as observed in tension. The goal of this study is to examine the effects of mineral-organic interfacial interactions on the mechanical properties of cortical bone in compression and compare these effects to our previous results obtained in tensile testing experiments.

PROCEDURES

Three adult bovine femurs were obtained from a local slaughterhouse immediately following sacrifice. Samples remained wet during all phases of preparation and testing. Samples were prepared from the medial portion of the central diaphysis to minimize biological variability. Forty cube samples (5 mm) were prepared by wet grinding and cutting on a low speed saw. Long bone (z axis) orientation was noted during preparation. All treatment and testing were performed at room temperature. Mineral-organic interfacial bonding interactions were examined using the detergent - ion treatment protocol developed by Walsh and Guzelsu (1991; Walsh et al., 1991). This protocol has been shown to remove the organic barriers to diffusion and allow ions access to the mineralized matrix without demineralizing bone or removing any structural organic material .Samples were treated for 24 hours in 0.1% Nonidet P40 (NP40) followed by ion equilibration for three days (pH7.3). Group 1 was treated for 24 hours in 0.145 M NaCl and tested. Group 2-4 were treated with 0.1% NP40 for 24 hours. Groups 2-4 were then treated with 2.0 M NaCl, 0.66 M Na_2HPO_4 or 2.0 M NaF respectively for 72 hours and tested. Samples were tested submerged on an MTS model 810 at a strain rate of 2.65 x10-3. Sample dimensions were determined prior to testing using a caliper. Sample densities and ash fraction were determined to obtain mineral content of each sample. Student's t-tests were performed on the mean values to ascertain statistical significance.

RESULTS AND DISCUSSION

Density and ash weights did not vary between any of the groups tested. Biochemical characterization of the treatment solutions indicated that samples were not demineralized or deproteinized during ion equilibration consistent with our previous results (Walsh et al., 1991). SDS gel electrophoresis on the NP40 solution indicated that only blood serum products were removed during detergent treatment. Collagen and other structural proteins were not removed during NP40 treatment. SDS gels on the ion

buffer solutions confirmed that organic material was not removed during ion treatments. TABLE1

Sample	Ultimate Stress (MPa)	Modulus (GPa)
Controls	209.2 (6.9)	19.75 (3.09)
NP40 + 2.0 NaCl	207.7 (16.2)	19.00 (1.50)
NP40+ 0.66 M P	225.5 (12.7) *	20.85 (1.78)#
NP40 + NaF	142.0 (30.1) **	11.33 (2.21) ##

(* $p < 0.03$; ** $p < 0.001$; # $p < 0.02$; ## $p < 0.0001$)

The compressive properties found in the present study are in agreement with those of McElhaney (1966) tested at a similar strain rate. The ultimate compressive stresses reported here are substantially greater than the tensile properties of adult cortical bone tested at the same strain rate. However, the elastic modulus for control samples determined in compression do not vary greatly from our tension results (Walsh et al., 1991).

The compressive properties of control samples compared to the NP40 + 2.0 M NaCl treated samples confirm that NP40 alone does not influence the mechanical properties of cortical bone. NP40 removes the organic barrier to diffusion and allows ions access to the mineralized bone matrix (Walsh and Guzelsu, 1991b). In addition, an ionic strength increase of 0.145 to 2.0 M did not influence the compressive properties as found in tension (Walsh et al., 1991).

Phosphate ion treatment resulted in a statistically significant increase in the compressive properties . These phosphate ion results are in direct contrast to our tension results where a reduction in the mechanical properties was observed. Phosphate ion action has been suggested to be due to competition with the negatively charged organic molecules for mineral cationic bonding sites (Bernardi et al, 1972; Walsh et al., 1991). Mineral-organic interfacial debonding results in a significant reduction in the tensile properties. However, the effect of such interfacial debonding under compressive loads are not so easily explained. A possible explanation may be an electrostatic stiffening effect that results due to repulsion of the negatively charged organic phase at pH 7.3 and the negatively charged phosphate adsorbed mineral under compression. This electrostatic condition would lead to an increase in the compressive properties and a reduction in the tensile properties.

Compression testing of fluoride ion treated samples demonstrated a drastic reduction in the ultimate stress and elastic modulus compared to controls, similar to samples tested in tension (Walsh and Guzelsu, 1991a,b). The pH of the fluoride ion solution increased from pH 7.5 to 9.8 as previously noted. The increase in pH is due to an ionic exchange between the mineral hydroxyl (OH) and fluoride ions. Hydroxyl ion release results in a local increase in pH at the interface and a reduction in the mechanical properties. Possible mechanisms for fluoride ions' action may be attributed to the OH exchange that occurs at low fluoride ion concentrations or the precipitation of CaF_2 at higher concentrations (Lin et al., 1981).

The effect of ion treatments (phosphate or fluoride) on the mechanical properties are attributed to ion interaction at the mineral-organic interface. Ionic strength alone does not influence the properties. Samples demineralized in EDTA and treated with similar ion solutions have been shown not to alter the mechanical properties of the organic constituents of bone (Walsh and Guzelsu, 1991c). The action of the phosphate and fluoride ions have been attributed to the mineral-organic interface and not between organic-organic interactions. Finally, density and ash fractions of all sample groups did not vary due to well controlled sampling techniques.

The compressive mechanical data support the hypothesis that the action of phosphate and fluoride ions may be occurring at different bone mineral lattice sites and influencing mineral-organic interactions differently. The fluoride-induced reduction and phosphate-induced stiffening in compressive forces and our tension results (where both ions caused a reduction in the mechanical properties) suggests that load transfer mechanisms between the mineral and organic constituents in tension and compression may not be the same.

The compression results support our three point bending study of cortical bone subjected to the same detergent - ion treatment protocol (Walsh and Guzelsu, 1992). Three point bending data revealed that phosphate ions had no effect on the ultimate stress or elastic modulus. Therefore, the increase observed in compression and the reduction in tension are cancelled out in three point bending. Fluoride ion treated samples tested in three point bending continue to demonstrate a marked reduction in mechanical properties and post-yield deformation. This is consistent with the reduction in the mechanical properties in compression and tension results following fluoride ion treatment. Load transfer can be influenced by alterations in interfacial bonding forces. Mineral-organic interactions play an important role in the mechanical properties of normal cortical bone tissue. The importance of interfacial bonding in the aged and diseased conditions remains to be determined.

REFERENCES

Bernardi et al. *Biochem. Biophys. Acta.* 278, 409-420, 1972. Bundy, *Ann. Biomed. Eng.*13,119-135, 1985. Lin et al., *Colloids and Surfaces* 3,357-370, 1981. McElhaney, *J. Appl. Physiol.* 21,1231-1236, 1966. Walsh and Guzelsu, *American Society Biomechanics,* p21 1990 a. Walsh and Guzelsu, In: Electromagnetics in Biology Medicine, Chapter 9. 1990b. Walsh and Guzelsu, *ORS Transactions* , p492, 1991a. Walsh and Guzelsu, *J. Orthop. Res.* 9, 683-692, 1991b. Walsh and Guzelsu, *ASME-BED* 20,369-372, 1991c Walsh and Guzelsu, *ASME-ESDA* in press, 1992. Walsh et al., submitted *J. Orthop. Res.* 1991.

EFFECT OF CEMENT LINE PROPERTIES ON INTERFACE STRESSES

R. M. V. Pidaparti * , P. A. Naick * , C. H. Turner *,** , and D. B. Burr **,†

* Department of Mechanical Engineering, ** Department of Orthopaedic Surgery, † Department of Anatomy
Biomechanics and Biomaterials Research Center, IUPUI, Indianapolis, IN 46202

INTRODUCTION

Cement lines separate the osteon and the extra-osteonal bone matrix in a compact bone and contribute to the bone's fracture toughness. The functional importance of cement lines lies in their ability to control fatigue and fracture processes, energy absorption and viscous damping (Lakes et al. 1979, Martin et al. 1982, Carter et al. 1977) in compact bone. We hypothesize that variations in cement line properties are significant in controlling interfacial stresses and contribute to the bone's fracture toughness.

The present study deals with an investigation of interface stresses between interstitial bone and cement line, between osteon and cement line and on the Haversian canal wall for an idealized three dimensional model of compact bone consisting of osteon, cement line and interstitial bone matrix (Figure 1). The interface stresses presented illustrate the behavior of cement lines which have either isotropic or transversely isotropic material properties.

MATERIALS AND METHODS

A three component micromechanics model with circular osteon, cement line and interstitial bone matrix of compact bone is developed using a three dimensional (3D) finite element model. Perfect bonding is assumed among osteon, cement line and interstitial bone matrix. The 3D finite element model consisted of 1152, eight node brick elements. It is assumed that the bone is subjected to a pure bending strain of 2000 $\mu\varepsilon$. Finite element simulations were carried out to study the effects of (i) varying the cement line modulus between 60%-90% of E for osteons keeping the interstitial bone matrix and osteons isotropic and (ii) varying the cement line properties from isotropic to transversely isotropic (taken as 80% of osteon properties) and the interstitial bone matrix and osteons as isotropic, transversely isotropic or orthotropic.

The material properties were assumed as follows:
Osteon - isotropic (Ascenzi et al. 1967) and transverse isotropic, (Pidaparti et al. 1992) .
Cement line - isotropic and transversely isotropic with 80% of the properties of osteon.
Interstitial bone matrix - isotropic (Evans et al. 1974), transversely isotropic (Reilly et al. 1974) and orthotropic (Ashman et al. 1984).

The finite element mesh was created using PATRAN software and linear stress analysis was carried out using ABAQUS software.

RESULTS

The Tresca shear stresses at the interface between interstitial bone and cement line, at the interface between osteon and cement line, and on the Haversian canal wall are presented in Figures 2-4 to illustrate the significance of varying cement line properties. Tresca stresses at the interfaces increase by about 50% when the cement line modulus is varied from 60% to 90% of the modulus of the osteon. In contrast, alterations in cement line modulus have no effect on the Haversian canal wall stresses.

When the cement line is considered as an isotropic material, stresses at the cement line-interstitial bone interface increase by about 35% as the bone matrix become more orthotropic (Figure 3). However, stresses at the cement line-osteon interface decrease by about 45% under the same conditions.

When the cement line is considered as transversely isotropic, stresses at interfaces are roughly the same as for the isotropic case, but Haversian canal wall stresses are increased by about 390 %.

DISCUSSION AND CONCLUSION

The present study shows that cement line properties significantly affect both interface stresses

and Haversian canal wall stresses. These data show that stresses on either side of the cement line interface in human osteonal bone, which is transversely isotropic, would be minimized by a cement line with isotropic properties. Cement line isotropy also minimizes Haversian canal wall stresses. This suggests that an isotropic cement line may prevent the initiation of crack growth and afford protection from lamellar debonding that could cause bone to fatigue more quickly. On the other hand, by causing greater interfacial stresses, an anisotropic cement line could provide the locus for crack initiation, thereby increasing bone's fracture toughness.

The actual properties of cement line are unknown. Because this analysis shows that cement line properties are important to the microlevel stress distribution in human bone, it will be important to establish the mechanical properties of cement lines using experimental data.

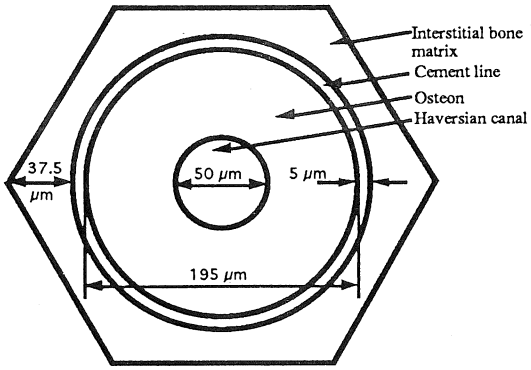

Figure 1. Cross section of an idealized compact bone model used for finite element analysis.

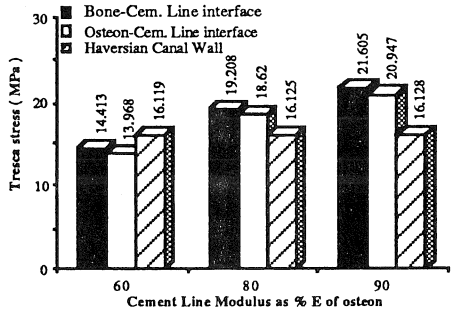

Figure. 2. Interface Tresca stresses for varying cement line properties (isotropic case)

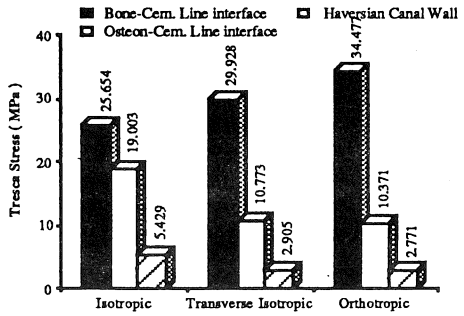

Figure. 3. Interface Tresca stresses for various material properties for interstitial bone and osteon with isotropic properties for cement line.

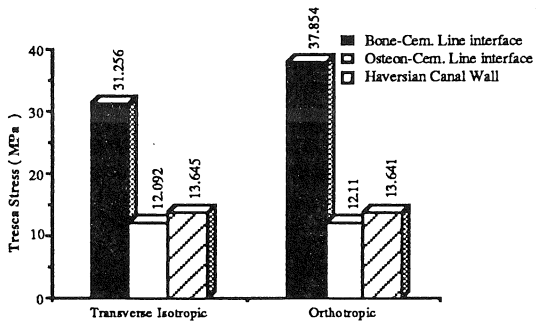

Figure. 4. Interface Tresca stresses for various material properties for interstitial bone and osteon with transverse isotropic properties for cement line.

REFERENCES

ABAQUS users manual (1989)

Ascenzi A. and Bonucci E. (1967) Anat. Rec. 158, pp 375-386

Ashman R.B., Cowin S.C., van Buskrik W.C., Rice J.C. Jr. Biomech (1984) ,17, pp 349-61

Carter D.R. and Hayes W.C. (1977) Jr. of Bone and Joint Surgery 59A, pp 954-962

Evans F.G. and Vincentelli R. (1974) Jr. Biomechanics 7, pp 1-10

Lakes R. and Saha S. (1979) Science 204, pp 501-503

Martin R. B. and Burr D.B.(1982) Jr. of Biomechanics 15, pp 137-139

PATRAN Plus users manual (1989)

Pidaparti R.M.V. and Burr D.B. (1992) Jr. of Biomechanics (in press)

Reilly D.T. and Burstein A. H. Jr. Bone and Joint Surgery (1974) 56A , pp 1001-22

ACKNOWLEDGEMENT

Support for this work was provided by the Whitaker Foundation.

IN VITRO STRAIN MEASUREMENTS IN THE CONDYLAR PROCESS OF THE HUMAN MANDIBLE

G.S. Throckmorton

Department of Cell Biology and Neuroscience,
Southwestern Medical Center, Dallas

INTRODUCTION

The condylar process of the mandible is a common site for fractures. This region is also thought to be an important growth center whose rate of growth may depend upon functional loading. Previous experimental studies used macaques and have been limited to strain measurements from the lateral surface of the condylar process during mastication and biting (Hylander, 1979). Theoretical studies have used finite element analysis to examine strain patterns in the condylar process, but rely on unvalidated theoretical calculations of forces on the condylar head (Hart, et.al., 1992; Koolstra and van Eijden, 1992; Korioth and Hannam, 1990). There have been no previous measurements of strain on the lateral surface of the condylar process with simultaneous force measurements and no measurements at all of strain on the three other surfaces of the condylar process.

PROCEDURES

Rosette strain gages (Model No. WA-06-030WR-120, Micromeasurements Group Inc., Raleigh, NC) were bonded to the anterior, posterior, lateral, and medial surfaces of the right condylar processes of five fresh human cadaver mandibles. The gages were oriented so that the middle element of each gage was aligned parallel to the long axis of the condylar process. Each instrumented mandible was then placed in a special compression tester which allowed a load cell to apply a simulated resultant muscle force of approximately 600 N to the mandible. Three force transducers measured the resultant forces at a selected tooth position (the bite point) and at each condyle. Strain measurements were recorded with five different bite positions (Incisor, right and left premolar, and right and left molar) and with the resultant muscle force at up to nine different positions. Combinations of resultant muscle force and bite position which resulted in no compressive loading of the right condyle were excluded from the analysis.

RESULTS

Within a single experimental setting the variance in principal strain values was considerably higher than the variance in the condylar load values. These results suggest that condylar strain patterns were very sensitive to the seating of the condyle in the apparatus. Absolute principal strain values at each gage differed among mandibles under similar loads and within the same mandible under different loading conditions. Therefore, to determine the effects of muscle position and bite position principal strain values were standardized by dividing the absolute principal strain by the magnitude of the force at the condylar transducer. When the forces on the mandible were relatively symmetrical (for example, during incisor bites with the resultant muscle force in the midline) all gages exhibited compressive strain per unit force which tended to be higher than tensile strain per unit force (Fig. 1). When the forces on the mandible were asymmetrical (For example, a right premolar bite position with the resultant muscle force on the right side) the lateral gage exhibited high tensile strain per unit force and low compressive strain per unit force. At the other gage positions compressive strain per unit of force remained the higher (Fig. 2).

DISCUSSION

The results of this study indicate that strain patterns within the condylar process are quite sensitive to the direction and position of the applied muscle forces and to the direction of the joint reaction forces. Similar conclusions have come from theoretical studies modeling mandibular forces (Hart, et.al.,1992; Koolstra and van Eijden, 1992). The lateral surface of the condylar process appears to be most sensitive to changes in the loading of the mandible. These results suggest that there is little bending of the condylar process under symmetrical loads but that during asymmetric loading of the mandible there was bending of the condylar process toward the medial side.

REFERENCES

Hart, R.T. et.al., J. Biomech. 25, 261-286, 1992.
Hylander, W.L., Am. J. Phys. Anthrop. 51, 433-456, 1979.
Koolstra, J.H. and van Eijden, T.M.G.J., J. Biomech. 25, 175-187.
Korioth, T.W.P. and Hannam, A.G., J. Prosthet. Dent. 64, 62-73.

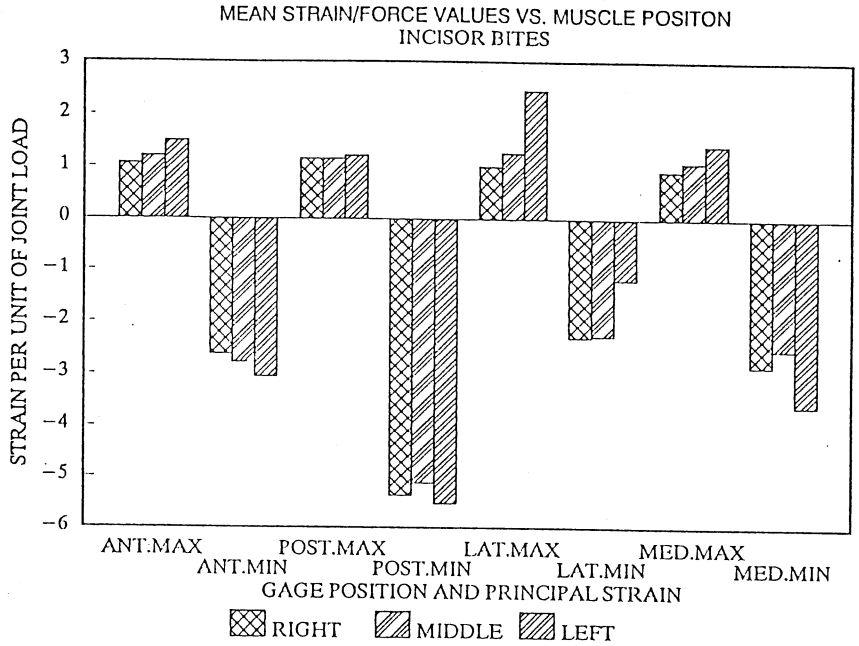

Figure 1. Maximum and minimum prinicipal strain per unit of condylar force for the four strain gage positions during simulated incisor bites. Right, middle, and left represent the position of the load applied to the mandible.

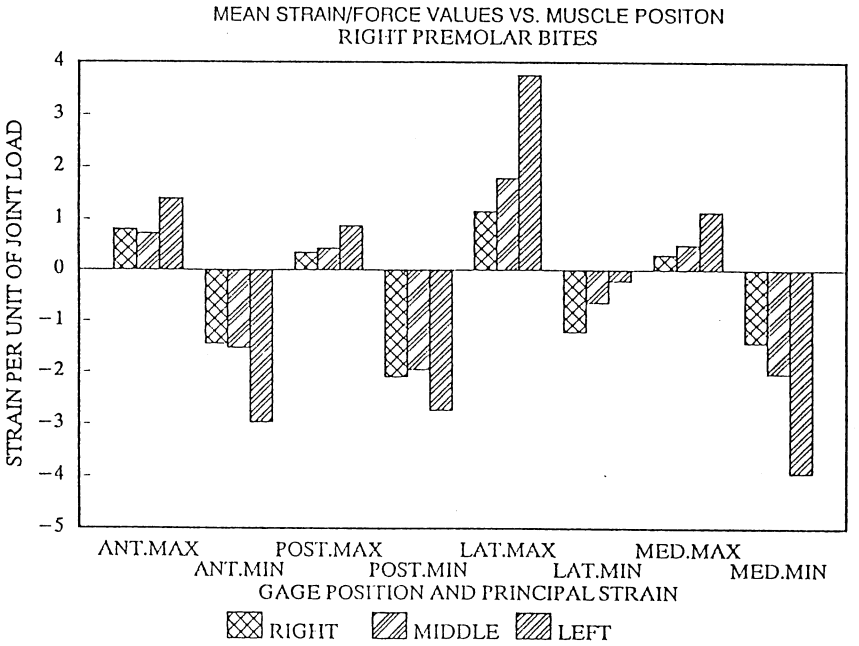

Figure 2. Maximum and minimum principal strain per unit of condylar force for the four strain gage positions during a simulated right premolar bite. Right, middle, and left represent the position of load applied to the mandible.

THE RELATIONSHIP OF CT-APPARENT DENSITY TO PIN PULL-OUT STRENGTH IN THE HUMAN CADAVER RADIUS

M. Baratz†, J. Spaeder†, G. Lam†, J. Ralston‡, D. Anderson‡, and J. Imbriglia†

†Department of Orthopaedic Surgery, Allegheny General Hospital,
‡Biomechanics Research Laboratory, Allegheny-Singer Research Institute,
320 E. North Ave., Pittsburgh, PA

INTRODUCTION

Surgical decisions involving wrist reconstruction often hinge on the degree of osteopenia observed on plain radiographs. This is an imprecise method that can be subject to wide variability from one radiograph to the next. We have correlated computed tomography (CT) scan-derived density measurements of cortical bone in the distal radius with one of its material properties, pin pull-out strength, to evaluate the use of CT as a measure of the suitability of a patient's bone for pin implantation. A modest exponential relationship ($R^2 = 0.66$) was found between CT-apparent density and pin pull-out load in the human cadaver distal radius.

REVIEW AND THEORY

Extra-articular fractures of the distal radius are common injuries. Most can be managed with closed reduction and cast immobilization. A portion of these fractures will prove to be unstable. This instability will permit shortening and rotation of fracture fragments. If untreated, the resulting malunion will produce a loss of wrist motion and grip strength.

If the loss of clinical reduction is recognized early, a variety of fixation methods can be used to reduce and hold the fracture until union occurs. Traditional techniques have included percutaneous pin fixation, pins and plaster, open reduction, internal fixation with a T-plate, or external fixation.

External fixators are usually mounted with pins placed in the metacarpals and in the distal radius (Anderson *et al.* (1944), Cooney *et al.* (1979)), the latter inserted just proximal to the fracture. The frame maintains the reduction through a traction that is applied across the wrist joint. Melendez *et al.* (1989) have described the use of a mini external fixator in which a reduction was maintained by pins placed only in the proximal and distal portions of the fractured radius. With this technique, they successfully treated unstable extra-articular fractures of the distal radius that had failed closed treatment. This method has the advantage of permitting wrist motion while stabilizing the radius fracture. The relative merit of these various treatments depends in large part on the immediate post-operative fixture stability they provide.

Pull-out force is one reliable measure of a pin's ability to secure a fixture to bone. Factors which affect the holding ability of pins and screws include physical properties of the bone (including thickness and bone density – Bechtol *et al.* (1951), Koranyi *et al.* (1970)), size and shape of the fasteners, speed of withdrawal, changes in material after time of insertion (e.g. bone remodeling), damage (both mechanical and thermic) due to insertion (Andrianne *et al.* (1987)), and the nature of prebored lead holes.

Recent experimental work by Ciarelli *et al.* (1991) has demonstrated the capability of CT as a noninvasive method of estimating the local mechanical properties of trabecular bone. In the present study, we have attempted to correlate the pin pull-out properties of the human cadaver distal radius with CT-apparent density, in order to evaluate the usefulness of such measures as a predictor of pin fixation performance.

PROCEDURES

Eight fresh frozen human cadaver radii were stripped of all soft tissue and suspended in a bath of normal saline. CT scans using 2 mm cuts were performed from the tip of the radial styloid to the junction of the middle and proximal third of the radius. Three measurements of CT-apparent density were recorded for the cortex at each level.

Specimens were then mounted in a custom-built holding apparatus (figure 1) which consists of two semi-circular clamps affixed to a plate. The plate has a center hole for pin clearance and allows for variable separation of the clamps. An additional plate, as described by Andrianne *et al.* and Bechtol *et al.*, was mounted with the bone to reduce overt shear failure of the bone and to insure that during pull-out the threads are truly stripped out. 2.5 mm external fixation pins were placed along the radial aspect of the bone (figure 1) according to clinical indication. Each pin was advanced so that the threads fully engaged the opposite cortex.

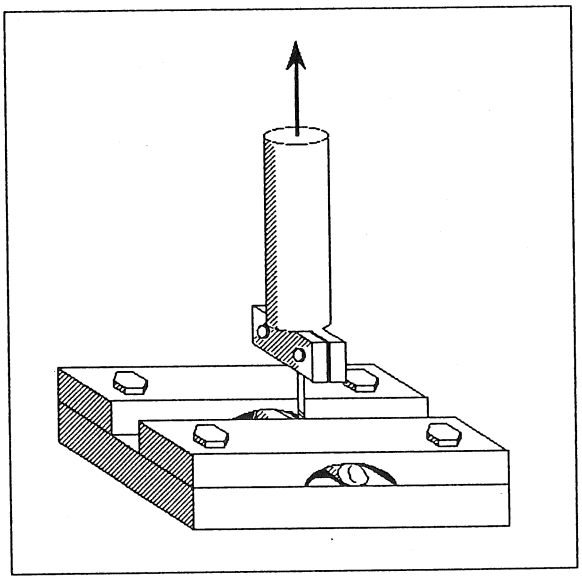

Figure 1. Schematic of pin pull-out fixture.

Uniaxial pull-out tests were performed using an MTS (model 858.20 Bionix) testing machine under displacement control at a pull-out rate of 0.0423 mm/s. Various rates of withdrawal have been reported in the literature on pin pull-out from human bone (Andrianne *et al.*, Daum *et al.* (1988), Seitz *et al.* (1990)). The relative contribution of withdrawal rate to pull-out strength has not been addressed to our knowledge. The ASTM standard D1761 (1977) screw withdrawal test protocol, intended for use in pull-out

testing of wood fasteners, calls for a constant withdrawal rate of 2.54 mm/min. Thus, tests were performed at this rate. An adapter connecting the pins to the MTS (see figure 1) was placed in series with a universal joint to minimize any loading which was not along the axis of pin insertion.

Force versus displacement and peak load were recorded with a digital oscilloscope (Tektronix model 2520). The cortical bone thickness was measured at each pull-out site after the tests were performed, and its relationship to the pull-out strength and toughness was investigated. Measurements of pull-out load to failure and pull-out toughness were also compared to the CT-apparent density of the bone at the location of each pin pull-out.

RESULTS

Sixty-nine uniaxial pull-out tests were run on the eight specimens tested. The average pull-out load was 891.9 ± 349.1 N (mean ± S.D.) and the average toughness was 1023.5 ± 471.3 N·mm.

Cortical thickness was only weakly related to pull-out load for the specimens tested (linear correlation coefficient of 0.27, see figure 2). The trend was toward increased pull-out load with increased cortical thickness, as one might expect. There was no apparent relationship between cortical thickness and pull-out toughness (linear correlation of 0.03).

Plots of CT-apparent density versus pin pull-out load to failure reveal an exponential relationship with a correlation coefficient (R^2 value) of 0.66 (figure 3). (The correlation for an assumed linear relation was 0.61.) The relationship between toughness and CT-apparent density was slightly weaker (R^2 = 0.6 for exponential, 0.52 for linear).

DISCUSSION

Uniaxial pull-out tests are not a totally adequate means for testing the fixation properties of orthopaedic pins. Shear forces acting on the pins *in vivo* as well as the cyclic nature of *in vivo* loading are not considered in such tests. Nevertheless, pin pull-out tests can accurately measure one aspect of a bone's pin-holding capability, and can therefore be useful for assessing the local integrity of a given bone.

The pull-out loads measured are consistent with those published previously in literature. Koranyi *et al.* and Andrianne *et al.* both reported peak pull-out forces from cattle bone in the neighborhood of 800 N. The finding that cortical bone thickness and peak pull-out load were poorly correlated contradicts earlier work which relied on relatively small sample sizes. In general, previous researchers have made only qualitative observations of increased pull-out force associated with increased cortical thickness.

The results correlating CT-inferred density with pull-out force suggest that CT scans may provide valuable information about bone quality that can be used in the pre-operative planning for wrist reconstruction in trauma and joint replacement.

REFERENCES

Anderson, R. et al. *Surg. Gynecol. Obstet.*, **78**, 788-791, 1944.
Andrianne, Y. et al. *Orthopedics*, **10**, 1507-1516, 1987.
Bechtol, C. et al. Metals and Engineering in Bone and Joint Surgery, (pp.158-164), Williams & Wilkins Co., 1959.
Book of ASTM Standards, Part 16, (pp.411-425), American Society for Testing and Materials, 1977.
Cooney, W. et al. *J. Bone Joint Surg.*, **61A**, 840-845, 1979.
Daum, W. et al. *J. Orthop Trauma*, **2**, 229-233, 1988.
Koranyi, E. et al. *Clin. Orthop.*, **72**, 283-286, 1970.
Melendez, E. et al. *J. Hand Surg.*, **14A**, 807-811, 1989.
Seitz, W. et al., *Clin. Orthop.*, **251**, 207-212, 1990.
Ciarelli, M. et al. *J. Orthop. Res.*, **9**, 674-682, 1991.

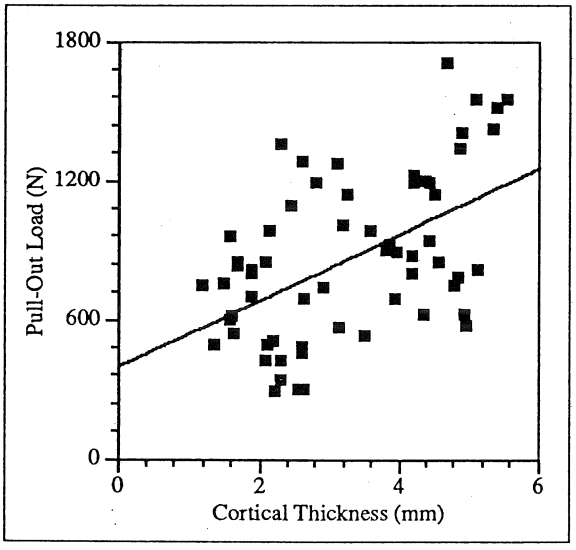

Figure 2. Relationship of pull-out load to cortical thickness.

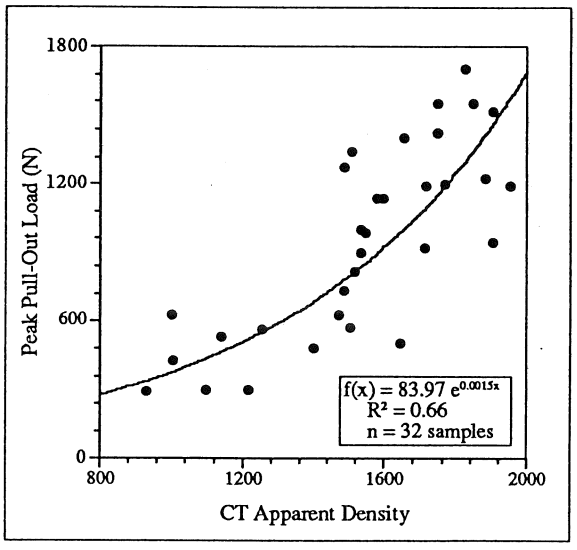

Figure 3. Variation of pin pull-out load with CT-apparent density.

BONE MINERAL MEASUREMENTS IN EXPERIMENTAL BIOMECHANICS

MAHADEVAPPA MAHESH[@], FRANK PINTAR[*], NARAYANAN YOGANANDAN[*@] and CHARLES R. WILSON[@]
[@]Medical Physics Section - Biophysics Program, Dept. of Radiology, Medical College of Wisconsin.
[*]Dept. of Neurosurgery, Medical College of Wisconsin and Veterans Affairs Medical Center,
Milwaukee, WI-53226, USA.

INTRODUCTION

Measurements of bone mineral content have been used in the clinical setting for quantitative assessment of skeletal status. Over the past decade major advances have been made in noninvasive bone mineral measurements (Mazess, et.al, 1989). Techniques with high accuracy and precision are now available to measure the trabecular or cortical components of the axial and the peripheral skeleton (Wilson, et.al, 1990). The major methods in clinical use include : (a) Single photon absorptiometry (SPA), (b) Dual photon absorptiometry (DPA), (c) Quantitative computed tomography (QCT), and (d) Dual energy x-ray absorptiometry (DXA). The biomechanics of biological systems can be greatly enhanced by bone mineral measurements when assessing tissue tolerances and fracture probability.

REVIEW AND THEORY

The introduction of various methods of bone densitometry and the findings of a number of independent studies that bone density is related to fracture incidence and risk constitutes a significant development in this area. SPA developed in the early 70's uses the transmission of a narrow beam of monoenergetic radiation (usually iodine-125). SPA has been used in longitudinal monitoring of bone mineral content (BMC) but is restricted to peripheral sites (eg., distal radius) of the skeleton. Measurement at peripheral sites do not clearly discriminate between patients with crush fracture osteoporosis and controls (Riggs, et.al, 1981, Wasnich, et.al., 1985). In DPA, a dual energy radionuclide source (usually gadolinium-153) is used. This is used extensively in the spine, hip and the total body measurements. Both SPA and DPA are projection techniques (Thorson et.al., 1986). The radiation exposure at the site of measurement is 5-10 millirems for a typical spine scan. The disadvantages of DPA are longer scan time, loss of resolution and higher precesion error (2 to 4%) for measurement of the lumbar spine. QCT can be used to measure the volume density of the spine. Studies have shown however, that there can be a high accuracy error (10-20%) (Mazess, et.al, 1989). The QCT measurements are not as reproducible as DPA and the radiation exposure is between 600-1000 millirems.

The introduction of dual energy x-ray absorptiometry which uses an x-ray tube as a source of dual energy photons has been a significant development in the past four years. The high count rate from the x-ray source permits shorter scan times with improved images and more importantly, precision. Radiation exposure to the patients is comparable to DPA systems. The DXA systems can measure bone mineral content in spine, femur, whole body and other peripheral sites. Accuracy 2-4 percent of bone densitometric systems are typical when assessed by measuring the ash weight. Wahner et,al. (1988) have reported the precision of the DXA instrument as 0.4% in vitro compared to 1.5% for the DPA systems and in vivo precision of 1% as compared to 2%.

The study of fracture risk has focussed on the basic biomechanical properties of bone and the ability of noninvasive bone densitometric techniques to predict the strength of bone. The probability of a fracture depends on the strength of the bone. The risk of vertebral fracture is directly proportional to the density with relative risk increasing two to threefold for each 10% decrease in density (Melton, et.al., 1985). Hansson et.al (1980) measured the bone mineral content (BMC) and ultimate compressive strength on lumbar vertebrae and found that the strength increased linearly with increasing bone mineral content.

EXPERIMENTAL PROCEDURES

The performance of a DXA bone densitometer (XR-26, Norland Corporation, Fort Atkinson, WI) has been studied. A spine phantom was measured for routine quality control over a six month span to evaluate the long term precision of

the instrument. Aluminum blocks of known dimension were scanned to evaluate the accuracy of the area measurements. Accuracy of the bone mineral content was evaluated by measuring the BMC of bone plugs and comparing with the ash weight. Volume of each bone plug was determined by Archimedean displacement method. Ashing was done in an oven (Hotpack Corpn) at 700°C for 18 hours. The total ash weight of each bone sample was measured on a digital balance (Sartorius Universal). Bone mineral content (BMC) is given in grams and bone mineral density (BMD) is BMC divided by the projected area (gm/cm^2).

RESULTS AND DISCUSSIONS

The long term precision error of BMC, BMD and projected area was found to be 0.5%, 0.6% and 0.6% respectively over six months. The area of the aluminum blocks calculated by DXA system correlated highly with the actual area (r^2=1.00). High correlation between the ash weight and the BMC was found (r^2=0.99). The percentage difference between the ash weight and the BMC ranged from 0.2 to 3.7%. Typical spine scan and femur scan is shown in fig 1 & 2.

Understanding the mechanisms of injury and determination of human tissue tolerances with particular reference to fracture threshold is an important step in a clinical diagnosis; it is of value to a safety engineer to develop injury mitigating devices such as helmets and landing platforms, and injury assessment devices such as an anthropomorphic manikin. While mathematical analogues and physical models may appear to offer an alternative to traditional in vivo animal or in vitro human cadaveric experiments, the often needed critical data has to be based on cadaveric material as it is one of the closest surrogates to the living human. Because of the inherent variability in the biological materials, interpretation is often difficult. For example, fracture strength from an older population is lower compared to the younger group. Bone mineral analysis which can be determined with greater precision using DXA technique in addition to its clinical merits such as less radiation, reduced cost, proves to be a promising tool to synergistically synthesize the pathoanatomical and other biomechanics data to solve the above mentioned problems.

REFERENCES

1. Mazess, RB. et al. Ann. Biomed. Eng., 17:177-181, 1989.
2. Wilson, CR. et al. Curr. Opin. Rheum., 2:369-378, 1990.
3. Riggs, BL. et al. J. Clin. Invest., 67:328-335, 1985.
4. Wasnich, RD. et al. Am. J. Obstet, Gynecol., 153:745-751, 1985.
5. Melton, LB. et al. J. Nucl. Med., 26:24, 1985.
6. Thorson, LM. et al. J. Nucl. Med. Tech., 14 (3):163-171, 1986.
7. Wahner, HW. et al. Mayo Clin Proc, 63:1075-1084, 1988.
8. Hansson, T. et al. Spine, 5(1):46-55, 1980.

ACKNOWLEDGEMENTS

This research was supported in parts by Dept. of Veterans Affairs Medical Center Research Funds, PHS CDC Grant R49CCR.703640 and fellowship from Gammex Inc., Charles Lescrenier CEO, Milwaukee.

Fig 1. Spine scan.

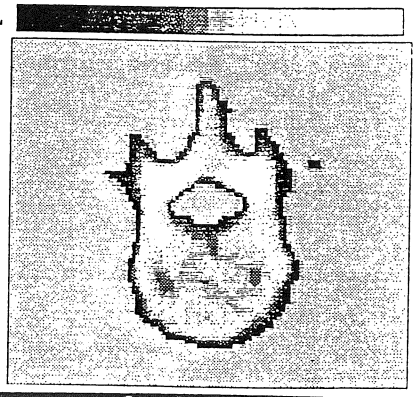

	BMD (g/cm^2)	BMC (gm)	Area (cm^2)
Vertebra	0.465	9.611	20.7

Fig 2. Femur scan.

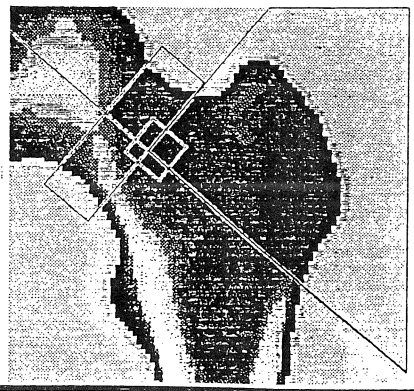

	BMD (g/cm^2)	BMC (gm)	Area (cm^2)
Fem neck	0.809	3.193	3.95
Troch	0.663	7.735	11.67
Wards Tri	0.483	0.483	1.00

EFFECTS OF A LONG-TERM, HIGH FAT-SUCROSE DIET ON MORPHOLOGY AND BIOMECHANICS OF FEMORAL NECK AND LUMBAR VERTEBRA

[1,2]Ronald F. Zernicke, [2]R. James Barnard, [2]George J. Salem, and [2]Eric Schramm

[1]Department of Surgery, University of Calgary, Calgary, Alberta, Canada T2N 4N1
[2]Department of Physiological Science, UCLA, Los Angeles, CA, USA 90024-1568

INTRODUCTION

Exposure to high fat and sucrose (HFS) diets may induce hyperinsulinemia and glucose intolerance, influence calcium and magnesium metabolism, and result in reduced bone mineralization and structural properties. Thus, here, we studied the morphological and structural changes in the rat femoral neck and sixth lumbar vertebra (L6) that may result from a long-term exposure to an HFS diet.

With the HFS diet, vertebrae had significantly smaller cross-sectional area and volume, and HFS femurs were shorter than controls. In the HFS femoral neck the relative contribution of cortical-shell to trabecular-core was significantly reduced. When normalized to body mass, the HFS L6 and FN had lower structural properties. The HFS L6 stress and strain energy density values were also significantly less than controls, and the normal stress of the FN was significantly less than the control values. These results suggest that long-term exposure to a HFS diet can adversely effect bone morphology and mechanics.

REVIEW AND THEORY

The occurrence of femoral neck fractures and vertebral fractures has risen in the past thirty years, and the incidence of these fractures is increasing faster than demographic changes in the population (Nilsson & Obrant, 1978).

Of the several factors that can lead to spontaneous and low-energy traumatic fractures of these bones, nutritional and metabolic factors can have significant effects on bone morphology (Hou *et al.*, 1990; Li *et al.*, 1990; Salem *et al.*, 1992), ash weight (Atteh & Leeson, 1984), and structural properties (Hou *et al.*, 1990; Li *et al.*, 1990; Salem *et al.*, 1992). High fat-sucrose diet (HFS) has been found to be detrimental to the geometric and structural properties of the tibia, metatarsus (Li *et al.*, 1990), femoral neck (Hou *et al.*, 1990), and vertebrae (Salem *et al.*, 1992). The HFS diet has been found to produce hypercalciuria resulting from hyperinsulemia (Lemann *et al.*, 1970) and reduce intestinal calcium absorption (Atteh & Leeson, 1984). Bone studies done, to date, using an HFS diet, however, have been short-term studies with young rats. Thus, we investigated effects of a 2-yr exposure to an HFS diet in the rat.

PROCEDURES

Twenty female Sprague-Dawley rats (8 weeks old) were assigned randomly to an HFS diet group (n=10) or a control diet group (n=10). Throughout the 2-yr study, food and water were provided *ad libitum* to all rats. The rats were fed either a high fat and sucrose (HFS) diet or a low-fat complex-carbohydrate (control) diet (Hou *et al.*, 1990; Li *et al.*, 1990; Salem *et al.*, 1992).

At the conclusion of the 2-yr, the sixth lumbar vertebra (L6) and femurs were dissected. Vertebrae were tested in compression using procedures previously reported by our laboratory (Salem *et al.*, 1989, 1992). The femurs were prepared and tested in cantilever bending using established procedures (Hou *et al.*, 1990).

RESULTS

Average body masses were significantly different between the HFS and control rats. Thus, structural properties were normalized per unit body weight.

L6 Vertebra. L6 height was not significantly different between the two groups. The control L6 had significantly greater cross-sectional area than the HFS L6. The control vertebrae also had a significantly greater volume than the HFS vertebrae.

All mechanical properties of the control vertebrae are greater than those of the HFS vertebrae with the exception of the elastic modulus. L6 loads at the proportional limit and the initial-maximum were significantly greater in the control than HFS group (128% and 133%). L6 energies at the proportional limit and the initial-maximum were significantly greater in the control than HFS group (183% and 126%). The compressional stiffness was also significantly greater (83%) in the control L6 than HFS L6.

Compressional stress at the proportional limit and the initial-maximum load was significantly greater in the control L6 than in the HFS L6 (35% and 38%). Strain energy density at the proportional limit and the initial-maximum load was significantly greater in the control L6 than in the HFS L6 (80% and 103%).

Femoral Neck. The length of the control femurs was significantly greater than HFS femurs, but the cervical-diaphysial angles and fracture surface orientation were not significantly different

between groups. The cortical shell in the control femurs was significantly greater than for the HFS femurs.

All structural properties of femoral necks were significantly greater for the control femurs than HFS femurs. In the control femurs load at the proportional limit was 59% greater and maximum load was 58% greater than HFS femurs. The energy in the control femurs was significantly greater at the proportional limit (57% greater), at maximum (52% greater), and at complete failure (88% greater). The compressional stiffness was significantly (62%) greater in the control femurs.

DISCUSSION

Results of this study indicate that in the female rat a long-term exposure to a high fat-sucrose (HFS) diet substantially reduces femoral neck and lumbar vertebrae structural properties. Despite the significantly greater body weight of the HFS rats, their bones were structurally inferior. In comparison to the results of studies lasting 10 wk (Hou *et al.,* 1990; Li *et al.,* 1990; Salem *et al.,* 1992), the current results indicate that there were no compensatory mechanisms in the adult rat to assist with the metabolic disturbances and diminished bone properties that result from exposure to the HFS diets.

REFERENCES

Nilsson, B.E. and Obrant, K.J. Secular tendencies of the incidence of fracture of the upper end of the femur. *Acta Orthop. Scand.* **49**, 389-391, 1978.

Hou, J.C-H., Zernicke, R.F. and Barnard, R.J. High fat-sucrose diet effects on femoral neck geometry and biomechanics. *Clin. Biomech.* **5**, 162-168, 1990.

Li, K-C., Zernicke, R.F., Barnard, R.J., Li, A-F.Y. Effects of high-fat sucrose diet on cortical bone morphology and biomechanics. *Calcif Tissue Int* **47**, 308-313, 1990.

Salem, G.J., Zernicke, R.F. and Barnard, R.J. Diet-related changes in mechanical properties of rat vertebrae. *Am. J. Physiol. (Reg. Integ. Comp. Physiol.)*, 1992 (in press).

Atteh, J.O. and Leeson, S. Effects of dietary saturated or unsaturated fatty acids and calcium levels on performance and mineral metabolism of broiler chicks. *Poult. Sci.* **63**, 2252-2260, 1984.

Lemann, J., Lennon, E.J., Piering, W.R., Prien, E.L. and Ricanati, E.S. Evidence that glucose ingestion inhibits net renal tubular reabsorption of calcium and magnesium in man. *J. Lab. Clin. Med.* **75**, 578-585, 1970.

Salem, G.J., Zernicke, R.F., Vailas, A.C., Martinez, D.A. Biomechanical and biochemical changes in lumbar vertebrae of rapidly growing rats. *Am. J. Physiol. (Reg. Integ. Comp. Physiol.)* **256**, R259-R263, 1989.

ACKNOWLEDGMENTS

This research was supported in part by grants from the National Institutes of Health (DK 34326), American Diabetes Association (J890725), and the Nathan Pritikin Research Foundation.

NORMAL FORCES ON WRIST STRUCTURES TRANSMITTED BY THE FINGER FLEXOR TENDONS

P.J. Keir and R.P. Wells

Department of Kinesiology, Faculty of Applied Health Sciences, University of Waterloo, Waterloo, Ontario, Canada.

INTRODUCTION

Since the belt-pulley model of Armstrong and Chaffin (1979), very little research has been done on the effects of the radius of tendon curvature in the carpal tunnel on injury. The work of Armstrong and Chaffin has, however, provided a basic model from which an ergonomist can make decisions. The recent advances in medical technology, namely Magnetic Resonance Imaging (MRI), have allowed *in vivo* measurements of tendon geometry in the carpal tunnel. Three-dimensional description of the tendons has been completed and the directional components of the normal force from those tendons have been estimated. These data have been used to ascertain the postures and loading conditions most likely to contribute to carpal tunnel syndrome (CTS), as evidenced by greater load bearing by the median nerve. This paper presents one aspect of a study in which MRI was used to acquire *in vivo* measures of the effects of wrist posture and tendon loading on the load bearing structures of the wrist.

REVIEW AND THEORY

Many methods have been used to determine the nature of the mechanical compression of the median nerve within the carpal tunnel. These methods include pressure measurements in the carpal tunnel (*cf.* Gelberman *et al.*, 1981; Szabo and Chidgey, 1989), as well as pressure recordings from transducers located as the median nerve (Smith *et al.*, 1977). Armstrong and Chaffin (1978) proposed a belt-pulley model in the sagittal model with a constant radius of curvature. The anatomy of the hand/wrist/forearm system would suggest that this radius of curvature is not constant nor restricted to the sagittal plane.

The radius of curvature and force transmission using a belt-pulley model are well described in Armstrong and Chaffin (1979), however, we suggest that the directional component of force transmission is not solely in the sagittal plane. The angle of force transmission is related to the radii of curvature by the equation,

$$\theta = \arctan\left(\frac{1/\rho_y}{1/\rho_x}\right) = \arctan\left(\frac{\rho_x}{\rho_y}\right) \qquad (1)$$

where, ρ_x, ρ_y are the radii of curvature in x (radio-ulnar) and y (palmar-dorsal), respectively.

The purpose of this paper is to present three-dimensional information on radius of curvature measures as they affect the loads on structures of the wrist. In particular, this paper addresses the directional component of the radius of curvature. It was postulated that wrist postures involving flexion would increase the loading on the median nerve, as would loading the extrinsic flexor tendons by using a pinch grip.

PROCEDURES

The subject's wrist was MR scanned in four wrist positions; straight, extended 20°, flexed 20°, and flexed 45°. PVC splints were used to maintain the wrist in each of the postures and minimize out of plane movement. In addition to postural differences, the effect of tendon loading was monitored. Force was applied to a fluid filled rubber tube in a three finger pinch grip at a nominal level (approximately 10 N), maintained via visual feedback.

Due to the maintenance of a static force level, acquisition time of MR data had to be minimized. The scanning procedure which combined good resolution and contrast as well as insuring minimal acquisition times is known as "gradient echo." This represents a combination of T1- and T2- weighting, or t^* weighting. Contiguous four millimetre axial slices were acquired from approximately 2 cm proximal to the distal wrist crease to approximately 2 cm distal to the hook of the hamate. This procedure resulted in twenty to twenty-five cross-sectional slices for digitizing. Scans in coronal and transverse planes were collected for complete posture measurements to monitor the effectiveness of the splints.

MR digitizing software (J. Davis, St. Joseph's Health Centre, London, Ontario) was used to manually digitize each tendon from the MR scans. Each tendon centroid was digitized three times per slice then averaged to reduce random digitization error. The resulting tendon paths were then spatially low pass filtered using a fourth order zero-lag Butterworth filter with a sampling frequency to cut-off frequency ratio of 20. The digitized coordinates were then transformed into an anatomical reference system defined by bony landmarks on the scans. The origin of the anatomical system was the most prominent portion of the hook of the hamate. The z-axis conformed to the progression of the MR slices which were cross-sections of the hand and forearm. The x-axis was defined as the component of the vector from the hook of the hamate to the tubercle of the trapezium that was perpendicular to the z-axis. The tendon centroids from each slice formed a trajectory which was differentiated digitally allowing calculation of its instantaneous radius of curvature.

RESULTS AND DISCUSSION

The normal force transmission lines of action for a flexed posture are demonstrated in Fig. 1. The tendons diverge from the mid-line (the approximate location of the median nerve) as they head toward their respective digits. However, there is a trend that when in a flexed wrist posture the forces are directed towards the palmar surface of the wrist (Table 1). Table 1 reports the angle, Θ, for each of the eight flexor tendons at the level of the hook of the hamate, the distal end of the carpal tunnel.

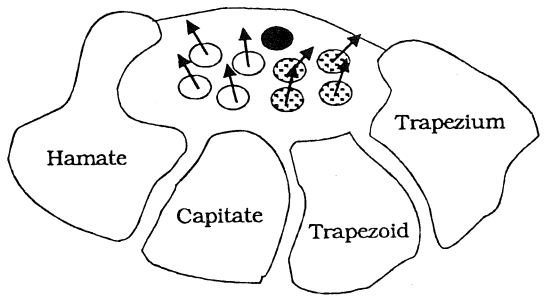

Figure 1. Schematic of the normal forces of the tendons transmitted to wrist structures at the distal end of the carpal tunnel. Shown is the posture of 20° flexion with tendon loading (pinch grip). Only tendons of the flexors digitorum profundus and superficialis are shown. Loaded tendons are shaded and the median nerve is black.

With a few exceptions, the deviation of the normal forces from the sagittal plane for the extended and neutral postures are greater than those for the flexed postures. There is little difference between the two flexed postures indicating that the degree of wrist flexion may not alter the lines of force transmission. Tendon loading (L), ie. the pinch grip conditions, appears to have no effect on the direction of force transmission when compared to the unloaded (U) conditions (Table 1).

The values in Table 1 denoted with an asterisk are curved towards the dorsum of the wrist, that is, they are found only in extended and neutral postures. There is considerable variance in this angular measure, much of it is related to the magnitude of the curvature in the x or radio-ulnar direction. The digital differentiation combined with the large radii of curvature found in the radio-ulnar axis are hypothesized as the sources of this variance.

If flexion tends to increase the normal force of some tendons directed towards the palmar surface of the wrist, then the summed effect of all tendons will be considerably greater in the confined carpal tunnel. Other investigations in our laboratory (Keir and Wells, 1992) indicate that the minimum radius of curvature is smaller with increasing flexion, more so when the tendons are loaded. Thus, a combination of increased normal forces due to smaller radii of curvature and an increase proportion of force borne by the median nerve may be present. It must be noted that the pinch grip used in this study does not load all tendons. The grip used would directly involve only those tendons of the second and third digits (shaded tendons in Fig. 1). These effects, combined with increased transmitted forces in loaded conditions may prove to be injurious. These findings partially support the findings of Smith *et al.* (1977) who found that flexion angle and tendon loading induced greater pressures on the median nerve in cadavers.

Table 1. Direction of the lines of normal force transmission at the distal end of the carpal tunnel. Values represent absolute angular difference from y-axis (in degrees). An asterisk, *, denotes that tendon is curving towards dorsum.

	Ext. 20°		Straight		Flex. 20°		Flex. 45°	
	L	U	L	U	L	U	L	U
FDS 2	38*	51*	83	90	45	65	45	66
3	26*	31*	65*	69*	42	4	17	37
4	12*	4*	74	14	7	17	21	9
5	76	79	59	69	30	33	44	41
FDP 2	50*	43*	85*	72*	18	39	34	51
3	30*	28*	82*	57*	13	19	3	0
4	86	45	71*	12	14	18	22	9
5	81	64	65	58	29	32	31	41

This method may prove invaluable when it is applied to pronated and supinated postures. In these postures, ulnar and radially deviated, or combined postures, the transmitted forces may actually be directed towards the median nerve as evidenced by the altered shape of the median nerve shown by Markison (1990). Evidence of a flattening of the median nerve has been cited by many authors (*cf.* Phalen, 1966), and may be attributable to the force transmitted to the median nerve by tendons.

MRI has allowed us to improve our anatomical knowledge of the wrist and by doing so, we have found that there may be several contributing mechanisms to median nerve compression. The mechanisms include: (i) decreased radii of curvature with increased wrist flexion, (ii) decreased radii of curvature with tendon loading, and (iii) an increased proportion of normal tendon force directed towards the flexor retinaculum in flexion. These mechanisms appear to be multiplicative in their effects and the combination of them may predispose certain individuals to CTS.

REFERENCES

Armstrong, T.J. & Chaffin, D.B. (1979) *J. Biomechanics* **12**, 567-570.
Gelberman, R.H. *et al.* (1981) *J. Bone Joint Surg.* **63-A**, 380-383.
Keir, P.J. and Wells, R.P. (1992) *Advances in Industrial Ergonomics and Safety III* (in press), Taylor and Francis.
Markison, R.E. (1990) *Hand Clinics* **6(3)**, 225-244.
Phalen, G.S. (1966) *J. Bone Joint Surg.* **48-A**, 211-228.
Smith, E.M. *et al.* (1977) *Arch. Phys. Med. Rehab.* **58**, 379-385.
Szabo, R.M. & Chidgey, L.K. (1989) *J. Hand Surgery* **14-A**, 624-627.

ACKNOWLEDGEMENTS

The authors would like to thank the Ontario Workplace Health and Safety Agency and Ministry of Labour and NSERC for support of parts of this research.

ENVIRONMENTAL EFFECTS ON GROWTH PLATE CARTILAGE COMPRESSIVE PROPERTIES

M.J. Ciarelli, J.L. Kuhn, D.J. Mason

Orthopaedic Research Laboratories, Section of Orthopaedic Surgery
The University of Michigan, Ann Arbor, Michigan 48109-0486

INTRODUCTION

Growth plate cartilage specimens were mechanically tested in order to evaluate the effects of freezing and the use of enzymatic inhibitors on their compressive properties. Four groups of specimens were prepared in the following manner: fresh with inhibitors, frozen with inhibitors, fresh with Ringer's, and frozen with Ringer's. Each specimen was tested in uniaxial unconfined compression at a constant strain rate. Based on the results from the stress relaxation tests, we found no significant differences in the measured mechanical properties between the four groups. There was a difference, however, in the percentage of specimens tested from each group. The highest number of specimens came from the group that was prepared fresh with inhibitors, the smallest number came from the groups that were frozen.

REVIEW AND THEORY

Investigation of growth plate cartilage has generally involved whole bone models of simulated clinical conditions. Only recently has growth plate cartilage been studied at a material level, examining the properties of prepared specimens of regular geometry. As is the case with all biological tissues, the testing environment is an important aspect of these mechanical tests. Sedlin (1965) found that environmental factors had significant effects on the mechanical properties of bone while Viidik and Lewin (1966) found differences in tensile characteristics of ligaments due to freezing and other postmortem storage techniques. Past investigations on the storage of articular cartilage have shown both decreased mechanical properties with freezing (Hori *et al.* 1976) as well as no difference due to freezing (Athanasiou *et al.* 1991, Kempson *et al.* 1971). Studies by Lee *et al.* (1985) found no significant difference with freezing in the whole bone failure patterns of rabbit femoral growth plates. To the best of our knowledge, there have been no studies which have examined the effects of freezing and or the use of enzymatic inhibitors on the material properties of growth plate cartilage.

PROCEDURES

Growth plate specimens were obtained from the proximal tibial growth plates of two seven week old male New Zealand White rabbits, identified as rabbits 1 and 2. Inhibitor solution was used for the right and left tibias of rabbit 1 (1R and 1L) while Ringer's solution was used for the right and left tibias of rabbit 2 (2R and 2L). The inhibitor solution has previously been used in the mechanical testing of articular cartilage (Athanasiou *et al.* 1991) and contains enzymatic inhibitors (2 mM EDTA, 5 mM Benzamidine, 10 mM N-Ethylmaleimide, and 1 mM PMSF) in a normal saline solution (0.15 M NaCl). Ringer's solution has also been used by previous investigators for mechanical testing of articular cartilage (Kempson *et al.* 1971, Kwan *et al.* 1992). Both solutions were kept refrigerated at 4° C and the specimen baths were kept cool by storage over ice packs.

Specimens obtained from the right tibias of rabbit 1 (1R) and rabbit 2 (2R) were tested fresh. The specimens were prepared and tested within 36 hours of sacrifice, during which time they were never frozen. Specimens obtained from the left tibias of rabbit 1 (1L) and rabbit 2 (2L) were stored at -20°C. During preparation, these specimens underwent no more than four freeze-thaw cycles. A total of 88 growth plate specimens were tested: 33 from rabbit 1R, 23 from rabbit 1L, 14 from rabbit 2R, and 18 from rabbit 2L.

Cutting guides were used to produce the 1x1 mm prismatic specimens which consisted of an epiphyseal boney cap, growth plate cartilage, and a metaphyseal boney cap (Ciarelli *et al.* 1991). Specimens were excluded from the study if their growth plate angle exceeded 15°, growth plate tears developed during preparation, or they had misaligned boney end caps.

The mechanical tests were performed on each group separately. After the specimens from each group were prepared and ready for testing, they were refrigerated at 4° C. One specimen at a time was then placed in a room temperature bath for at least 15 minutes prior to testing. Each specimen was then mechanically tested at room temperature while immersed in its respective solution.

Unconfined uniaxial compressive stress relaxation tests were conducted at a constant strain rate of 0.02/second. After application of a 0.002 MPa preload, the specimen was loaded to 15% compression. The test was monitored for four minutes to capture the stress relaxation response of the growth plate cartilage. From each test, the following parameters were determined: maximum stress, equilibrium stress, equilibrium modulus (equilibrium stress/equilibrium strain), stress ratio (maximum stress/equilibrium stress), tangent modulus (slope of the loading stress-strain curve at 15% compression), and relaxation time (time for load to relax 63% of total relaxation).

RESULTS

Of the 88 growth plate specimens tested, the most were obtained from rabbit 1R (Inhibitor/Fresh). Approximately 44% of the possible specimens from 1R were prepared and tested successfully. Only 36% of the specimens from rabbit 1L (Inhibitor/Frozen) were tested successfully. The use of Ringer's for rabbit 2L (Ringer's/Frozen) and 2R (Ringer's/Fresh) caused an even larger reduction, with only 23% - 25% of possible specimens successfully tested. This increase in yield with the use of inhibitors resulted from a reduction in the number of specimens which developed tears within the growth plate during preparation. The percentage of specimens excluded from the study due to these growth plate tears were: rabbit 1R (Inhibitor/Fresh) lost 8%, rabbit 1L (Inhibitor/Frozen) lost 19%, rabbit 2R (Ringer's/Fresh) lost 37%, and rabbit 2L (Ringer's/Frozen) lost 40%.

While the specimen preparation called for all specimens to be approximately 1 x 1 mm, a significant difference in the average size of the specimens from the four groups was found. Specimens from rabbit 2R, with average dimensions of 1.29 x 1.20 mm in cross section, were significantly larger than specimens from the other three groups, which were not significantly different from each other. The growth plate height was not significantly different between groups and had an average value of 0.58 mm.

The results of the stress relaxation tests for the four groups are shown in Table I. No significant differences between the four groups were found for the maximum stress, equilibrium stress, equilibrium modulus, stress ratio, or tangent modulus. The overall average values for these parameters were 0.023 MPa, 0.009 MPa, 0.058 MPa, 2.58, and 0.169 MPa, respectively. A significant difference was found in the relaxation times. The specimens from rabbit 2R had an average relaxation time of 8.84 seconds which was significantly longer than the average relaxation time of 6.95 seconds found for specimens from rabbit

1L. The differences between the other groups were not significant.

DISCUSSION

Kempson *et al.* (1971) performed indentation tests of human femoral heads immersed in Ringer's solution. Indentation measurements made within 48 hours of death were found to be within +-5% of those measured after storage at -20° C. Since this difference was equivalent to their repeatability limit, freezing was concluded not to make a significant difference. These findings support the lack of significant differences due to freezing found in the material properties of our growth plate cartilage specimens. The only significant difference found in our mechanical data was between the relaxation times of control groups 1L and 2R, which may be due to the larger dimensions of group 2R. While the other parameters are normalized for specimen size, the relaxation time reflects the time necessary for fluid flow within the matrix. It is not only dependent on the characteristics of the matrix, but also on the amount of matrix. Larger specimens, as seen in group 2R, require longer relaxation times.

The goal of mechanically testing biological tissues is to determine their properties before any significant deterioration has occurred. Therefore we also investigated the effect of matrix autolysis on the mechanical properties of growth plate cartilage. It has been shown that matrix degradation leads to loss of load carrying capabilities for articular cartilage (Kempson *et al.* 1970, 1971). This relationship between matrix integrity and mechanical properties is clearly demonstrated through the use of proteolytic enzymes. Articular cartilage specimens incubated in trypsin were found to have significantly reduced stiffnesses (Harris *et al.* 1972). Kempson *et al.* (1971) repeatedly tested articular cartilage which was bathed in Ringer's solution and determined a 'progressive cartilage softening' after a total of approximately 24 hours at 37°C, indicative of autolysis. The use of enzymatic inhibitors is intended to slow this process of tissue degradation.

The results from our mechanical tests, however, found no significant differences in the material properties due to the use inhibitors. Kempson's data showed significant softening occurring only after 24 hours at 37°C. Our specimens were kept either frozen at -20°C or at 4°C until testing. During specimen preparation, cooled fluids were used to keep the specimens moist and only prior to testing was each specimen, individually, allowed to reach room temperature for any significant period of time. A recent study by Kwan *et al.* (1992) determined that articular cartilage plugs kept at 4°C in culture media had no significant decrease in mechanical properties even after 60 days of storage. Therefore, while any tissue not tested *in vivo* will experience tissue degradation, the rate of that degradation will depend on the environmental conditions of the tests. The inability to detect differences between the various groups in our study indicates that the degree of degradation undergone by the growth plate cartilage during preparation and testing did not significantly affect the mechanical properties measured. Other material properties, however, may have greater sensitivity to the degradation process.

One difference that was noted with the use of inhibitors was a higher yield of specimens. Of the four groups, 1R (Inhibitor/Fresh) had the highest yield of 44%. The reasons for excluding specimens included large growth plate angles, growth plate tears, or misaligned boney end caps. The main reason for the decrease in the yield of specimens produced using Ringer's as opposed to inhibitors, was an increase in the percentage of specimens which tore during the preparation process. This could be indicative of reduced shear properties within the growth plate cartilage. This sensitivity of shear properties to environmental testing conditions was also found in a study by Hori and Mockros (1976).

In conclusion, a series of control tests evaluated the effect of freezing and the use of inhibitors on growth plate compressive material properties. No significant differences in the growth plate cartilage properties were determined for the groups tested, however, a higher yield of testable specimens was obtained when inhibitors were used.

REFERENCES

Athanasiou KA *et al. J Orthop Res,* 9, 330-340, 1991
Ciarelli MJ *et al. Trans of the 37th Orthop Res Soc,* 363, 1991
Harris ED *et al. Arthritis Rheum,* 15(5), 497-503, 1972
Hori RY and Mockros LF *J Biomech,* 9, 259-268, 1976
Kempson GE *et al. Biochim Biophys Acta,* 215, 70-77, 1970
Kempson GE *et al. J Biomech,* 4, 597-609, 1971
Kwan MK *et al. J Biomech Eng,* 114, 149-153, 1992
Lee K and Pelker RR *J Orthop Res,* 3(4), 514-515, 1985
Sedlin ED *Acta Orthop Scand Suppl,* 83, 20-44, 1965
Viidik A and Lewin T *Acta Orthop Scand,* 37, 141-155, 1966

ACKNOWLEDGMENTS

The authors thank Steve Goldstein, Mark Stock, Dennis Kayner, and Kathe Derwin. This work was aided by grants from the Orthopaedic Research and Education Foundation, the Whitaker Foundation, and the Frederick Fischer Endowment.

Table I: Environmental effects on compressive mechanical data for growth plate cartilage. The Overall group contains means for the entire specimen population. The means for each of the four control groups are also shown separately. Four test conditions were tested: Standard deviations are shown in parentheses.

Variable	Overall	1R: Inhibitor/Fresh	1L: Inhibitor/Frozen	2R: Ringer's/Fresh	2L: Ringer's/Frozen
n	88	33	23	14	18
Width, mm*	1.107 (0.182)	1.072 (0.114)	1.097 (0.122)	1.290 (0.261)	1.042 (0.198)
Depth, mm*	1.054 (0.175)	1.040 (0.129)	1.010 (0.122)	1.204 (0.303)	1.019 (0.120)
Height, mm	0.583 (0.056)	0.588 (0.059)	0.572 (0.046)	0.589 (0.057)	0.586 (0.064)
Angle, °	10.36 (2.93)	9.68 (2.99)	10.10 (3.03)	10.50 (3.02)	11.80 (2.28)
Maximum Stress, MPa	0.023 (0.011)	0.025 (0.012)	0.018 (0.007)	0.024 (0.011)	0.023 (0.010)
Equilibrium Stress, MPa	0.009 (0.004)	0.009 (0.004)	0.007 (0.002)	0.010 (0.005)	0.009 (0.003)
Equilibrium Modulus, MPa	0.058 (0.025)	0.061 (0.025)	0.049 (0.015)	0.066 (0.035)	0.060 (0.022)
Stress Ratio	2.58 (0.51)	2.67 (0.47)	2.50 (0.58)	2.47 (0.53)	2.58 (0.48)
Tangent Modulus, MPa	0.169 (0.079)	0.182 (0.091)	0.132 (0.050)	0.187 (0.075)	0.175 (0.078)
Relaxation Time, sec.	7.85 (2.02)	7.92 (2.29)	6.95 (1.33)**	8.84 (0.96)**	8.09 (2.44)

* The specimens from rabbit 2R were significantly larger than specimens from rabbits 1R, 1L, and 2L

** Significant difference between groups ($p < 0.05$)

HIP IMPLANT STABILITY TESTING WITH FUNCTIONAL LOADS

A.Berzins, D.R.Sumner, E.A.Giron and T.P. Andriacchi

Department of Orthopedic Surgery
Rush-Presbyterian-St. Luke's Medical Center, Chicago, Il, USA.

INTRODUCTION

A software program to compute the three-dimensional moment arms and the action lines of muscles crossing the hip joint was developed. Using it with additional data on muscular physiology and kinetic data we designed a mechanical testing system to simulate functional joint reaction and muscular forces of the human hip joint. The system was used to asses the initial stability of the femoral components in total hip arthroplasty. In addition, another setup with smaller joint reaction force and no muscle simulation was used. Data obtained as 6 degree of freedom motion of the implant with respect to the cortical bone indicated a substantially changed pattern of stability due to addition of the muscle forces and increased joint reaction force. Previous studies may have overestimated transverse (torsional) instability, and underestimated longitudinal instability of the implants due to the nonphysiological loading conditions simulated.

REVIEW AND THEORY

In vitro mechanical testing has been widely used to asses the initial stability of different designs of the femoral component in total hip arthroplasty. These studies have led to considerable attention of torsional micromotion induced by high out of plane loading caused by activities such as stair climbing or rising from a chair. However, it could be argued that these studies do not provide a very accurate representation of the types of motion which occur in vivo because the experimental setups lack a realistic axial component of force and incorporate artificial distal constraints.

The goals of the present study were (i) to develop a mechanical testing system to include functional joint reaction and muscular forces of the human hip joint and (ii) to determine if simulation of the muscle forces influenced implant stability.

We developed a software program to compute the three-dimensional moment arms and the action lines of muscles crossing the hip joint as a function of the hip anatomical position. Origin and insertion coordinates of the hip muscles were taken from Brand et al. (1). Based on additional osteometric data (2), the scaled coordinates from Brand et al. (1) were assigned actual metric values. In order to specify angular displacements about orthogonal anatomical axes, corresponding goniometric data were used (3). The force contribution by each muscle was considered to be proportional to its physiologic cross-sectional area (4). Maximum external hip moments were obtained from kinetic data (5). With the moment arms and cross-sectional areas for each abductor and extensor known, we were able to assign moments due to separate muscles. Then, the force generated for each muscle was calculated. For the hip position examined, stair-climbing, only the abductor force exerted by the gluteus medius and the extensor force exerted by the gluteus maximus were modeled because these muscles account for most of the hip moments in the coronal and sagittal planes.

PROCEDURES

A fresh cadaver femur implanted with a straight cementless stem underwent mechanical testing in two modes. First it was tested without muscle simulation then tested with muscle simulation. For the test without muscle simulation the force was applied to the head of the prosthesis by a flat flange and the distal femur was rigidly fixed. The joint reaction force for the system without muscle simulation was chosen as 1 body weight (BW) to avoid failure of the specimen due to high bending moments at the distal femur. For the muscle simulation, a flat plate with 2 universal joints between the actuator and prosthesis and 2 cables to simulate muscles was used. The point of actuator load application and its magnitude were calculated to create appropriate muscular forces, joint reaction force (6) and to provide stability of the horizontal loading plate based on the equilibrium of moments applied. Distally, all rotations of the bone were permitted, and thus, despite a constraint in internal-external rotation between the stem and the actuator, the stem was free to twist with respect to the bone. The actuator load was chosen so that the joint reaction force was 2.5 BW, and the force of the gluteus maximus was 2.25 BW and gluteus medius was 0.9 BW. Components of the joint reaction force with respect to the femur are given in Table 1. The position of the femur was kept the same at simulated stair climbing in both setups. Displacements between the tip of the stem and the cortical bone were sensed by a 6-degree of freedom displacement measuring system (7).

RESULTS AND DISCUSSION

The predominant components of motion were posterior-anterior translation in the system without muscles and superior-inferior translation in the system with muscles simulated (Fig.1a). Transverse rotation was 3 times smaller in the system with muscular support (Fig.1b). The sagittal rotations were of the same magnitude, but differed in direction. The coronal rotation was much greater for the case with muscle simulation.

Thus, there was a substantially changed pattern of initial stability from the simulation without muscles to the system with muscles. All components of the joint reaction force increased in the muscle simulation but these increases were not necessarily followed by increases in the corresponding motions. Specifically, with muscles simulated the AP component of the joint reaction force increased by a factor of 2.2, but the corresponding translation (PA) was greatly reduced, the rotation in the sagittal plane changed direction and the rotation in the transverse plane was greatly increased. The ML component increased by a factor of 7.3, and the corresponding translation (ML) doubled and changed direction while the rotation in the coronal plane increased dramatically and also changed direction. The SI component increased by a factor of 2.6, and the corresponding translation was greatly increased.

The differences in the pattern of initial stability can be attributed to (i) simulation of the out-of-plane load component with a realistic axial load component, (ii) presence of the posteriorly directed component of the gluteus maximus force possibly affecting strain distribution in the proximal femur and (iii) avoidance of nonphysiological bending and torsional moments of the specimen due to a constrained femoral shaft.

We hypothesize that previous studies may have overestimated transverse instability, and underestimated longitudinal instability of the implants due to the nonphysiological loading conditions simulated.

REFERENCES

1. Brand, R.A. et al. JBME, 104, 304-310, 1982.
2. Mikosz, R.P. Ph.D. Thesis, University of Illinois at Chicago, 29-31, 1985.
3. Johnston, R.C. et al. Clin. Orthop., 72, 205-215, 1970.
4. Schumacher, G. and Wolff, E. Anat. Anz., 119, 259-269, 1966.
5. Andriacchi, T.P. et al. JBJS, 62-A, 749-757, 1980.
6. Goldberg, V.M. et al. Non-Cemented Total Hip Arthroplasty, (pp. 251-256), Raven Press, 1988.
7. Berzins, A. et al. Transactions of Combined Meeting of the ORS of USA, Japan and Canada, Banff, Canada, 243, 1991.

SETUP	AP(BW)	ML(BW)	SI(BW)	RESULTANT(BW)
WITHOUT MUSCLES	0.55	0.03	0.83	1.0
WITH MUSCLES	1.20	0.22	2.18	2.5
RATIO	1:2.2	1:7.3	1:2.6	1:2.5

Table 1. Components of joint reaction force in body weights (BW) with respect to the femur, where AP is anterior-posterior, ML is medio-lateral and SI is superior-inferior.

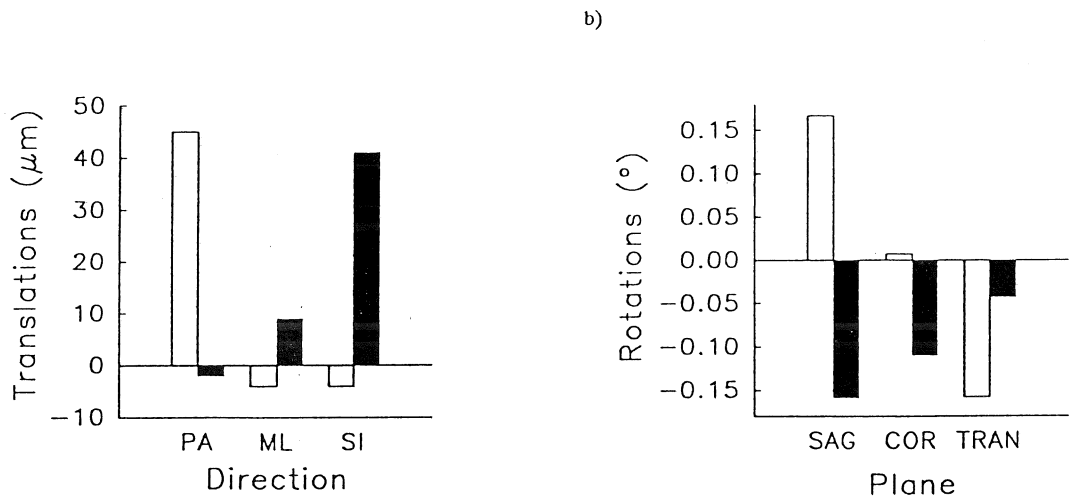

Figure 1. Implant stability. The open bars represent the simulation without muscles and the closed bars represent the simulation with muscles. The pattern of translations (a) and rotations (b) was different in the two experimental setups. Note in (b) that SAG is oration in the sagittal plane, COR is rotation in the coronal plane and TRAN is rotation in the transverse plane.

THE EFFECT OF FEMORAL COMPONENT GEOMETRY ON PROXIMAL FEMORAL STRESS SHIELDING

R.N.Natarajan, D.R. Sumner and T.P.Andriacchi
Department of Orthopedic Surgery
Rush Presbyterian St.luke's Medical Center, Chicago

INTRODUCTION:

Long term advantages of cementless fixation in total joint replacement have led to expanded usage. As a result of stringent requirements, cementless devices are usually bulkier than their cemented counterparts. Clinical reports of follow-ups of these devices have suggested substantial bone remodelling in early periods following surgery with a variety of stems (Engh CA et al. 1987). Many factors can influence the stress shielding in the femur including prosthetic shape, tightness of fit and quality of bone.

Recently Poser et al. (1992) from their in-vitro study on a canine model demonstrated decreased strain restoration in a femur fitted with a straight stem design whereas in the femur with a curved stem design showed a significant strain restoration. So far no analytical studies have been reported in the literature including the effect of femoral component geometry on proximal femoral stress shielding.

In the current study an analytical finite element model was developed and used to study the stresses in proximal femur including the complex phenomenon which account for various interfacial conditions in terms of its stiffness and failure criterion (Natarajan RN.et al. 1991). The goal of the present investigation was to study the stress distribution in the cortex and cancellous bone in a femur implanted with a stem fixed only at the proximal one third region. With the help of this study the relationship between the geometry of the femoral stem and changes in the mechanical enviornment of the proximal femoral cortex and medullary bone following total hip replacement was analyzed. To meet this goal, one specific parameter, change in strain energy density, was used to asses the effect of varying stem geometry.

METHODS:

A standard finite element approach (Zienkiewicz OC et al. 1989) was used to analyze the femur with and without an implant. The finite element model of the proximal femur was developed from serial CAT scans of a human cadaver femur. A three-dimensional finite element model was then assembled using 742 twenty noded three dimensional elements. The interface between bone and the implant was modelled by 168 curved 16 noded bond elements (Beer G ,1985). The approximate value of the interface shear stiffness representing a frictional fit between the porous coated portion of the implant and bone was obtained using a simple beam model (Natarajan RN et al. 1991). The longitudinal and transverse stiffness of 40 MPa/m was used for the shear stiffness of the interface layer representing a frictional fit between the porous coated portion of the implant and bone. The non-porous coated portion was given a shear stiffness of a very small value (4.0 Pa/m) compared to the porous coated surface.

Two proximally porous coated femoral stems were used in the analysis. One of them was a curved collarless anatomic stem (Zimmer, Warsaw) and was modelled such that the centroids and orientation of the principal axes of the stem were alligned with those of the bone at each cross-section. The other was a straight collarless HGP stem and was modelled such that it appropriately fitted the femoral canal. Both these stems were assumed to be made of Ti alloy. The load applied to the femoral head was 1.0 Newton along the axis of the femur and 0.2 Newton directed along the anterior-posterior direction. It was assumed that this load simulated the hip in slightly flexed position. The distal end of the femur was fixed.

The difference between the intact femur and the femur with the implant in place was calculated for 22 mechanical parameters (6 stresses, 6 strains, 2 principal stresses, 2 principal strains, maximum shear stress, maximum shear strain, von mises equivalent stress, mean stress, deviatoric stress and strain energy density) at 368 sites (4 periosteal, 4 endosteal, 4 outer canvcellous, and 4 inner cancellous at each of 23 cross-sections). The description of the effects of prosthetic geometry on the femur's mechanical environment was based on the changes in strain energy density.

RESULTS:

Changes in medial cortex

The changes in strain energy density at the periosteal and endosteal surfaces showed similar trends and were averaged to represent change with in the cortex (Fig. 1). The femur with a curved stem

and the femur with the straight stem both showed a general pattern of reduction in strain energy density with a proximal-to-distal gradient. A substantial reduction in strain energy density was observed near the proximal region of the femur implanted either with curved or straight stem. However there was a much higher reduction in strain energy density in the mid-stem, region of the femur implanted with a straight stem as compared to the femur with a curved stem.

Changes in the medial medullary cavity

In the cancellous bone region, the effects of stem geometry on the change in strain energy density were quite different from those observed in the cortical bone (Fig. 2). The general pattern showed an increase in strain energy density both in the proximal region as well as near the tip of the implant. Proximally the femur with the straight stem showed higher increases in strain energy density than predicted for the femur with an anatomic stem. Near the mid-stem the femur with the curved stem showed an increase in strain energy density whereas the femur with the straight stem showed a decrease in strain energy density. Near the stem tip both the femurs showed an increase in strain energy density.

DISCUSSION :

The largest decreases in strain energy density in the cortex were observed proximally. This is consistent with radiographic and densitometric studies of clinical series and animal experiments (Sumner DR et al. 1992) which have shown that the largest changes in the cortex occur proximally. Interestingly, changing the geometry of the stem from anatomic to straight had only a minor effect on the change in strain energy density at the most proximal level. On the other hand in the mid-stem region more bone resorption would be predicted in the femur with a straight stem.

In the medullary canal, the straight stem showed an increase in the strain energy density in the most proximal region whereas it showed a decrease in strain energy density in the mid-stem region. The anatomic stem showed no decrease in strain energy density along it's length.

Thus, for both the cortex and medullary bone, these analyses would predict less bone loss with a curved stem than with a straight stem.

REFERENCES :

Beer G. Int.J.Num.Methods in Engg., 21:585-600, 1985; Engh CA. et al. JBJS, 69B:45-55, 1987; Natarajan RN et al. Advances in Bioengineering, BED 20: 177- 179, 1991; Poser RD et al. Trans. ORS, 38: 307, 1992; Sumner DR et al. JBJS 74A:239-250, 1992; Zienkiewicz OC et al. Finite element method, Mc Graw Hill, 1989

ACKNOWLEDGEMENTS:

Bristol Meyers Excellence Award, NCSA Grant CUS910001N, NIH Grant AR16485

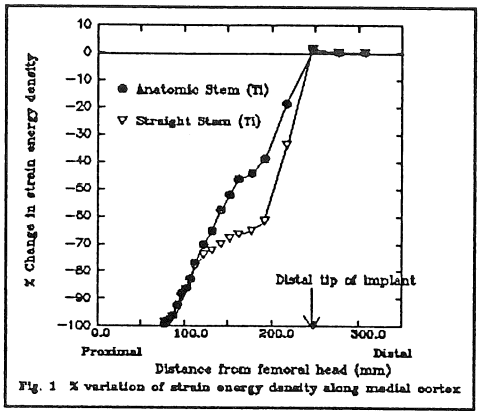

Fig. 1 % variation of strain energy density along medial cortex

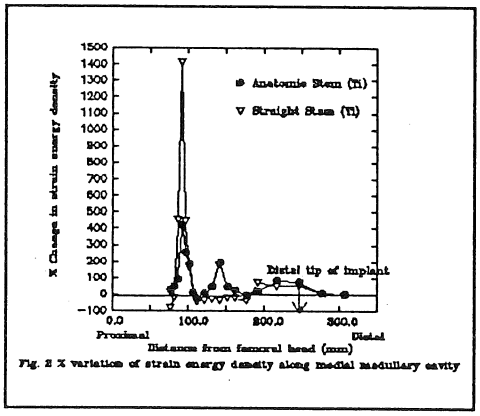

Fig. 2 % variation of strain energy density along medial medullary cavity

INTRAOPERATIVE FEMUR FRACTURE DURING NON-CEMENTED TOTAL HIP ARHTHROPLASTY: THE EFFECT OF CERCLAGE WIRING TECHNIQUE ON MICROMOTION

S.H. Elder, J.J. Callaghan, and T.D. Brown

Orthopaedic Biomechanics Lab, University of Iowa, Iowa City, IA 52242

INTRODUCTION: An initially tight interference fit of the prosthesis in the femoral canal is essential for bone ingrowth. Such a tight fit is accomplished by impaction of rasps and the prosthesis itself into the proximal femur. These procedures sometimes cause intraoperative fracture, the incidence of which may be as high as 6.3% [1]. The most common type of intraoperative fracture is a longitudinally oriented linear fracture of the anteromedial aspect of the proximal femur, which occurs most frequently during insertion of the prosthesis [2]. Such fractures may be untreated intraoperatively, or cerclage wires may be applied. Furthermore, cerclage wiring may be performed with the prosthesis in place, or after prosthesis removal but prior to reinsertion. The present study was undertaken to determine the effect of cerclage wiring on the micromotion associated with a simulated intraoperative fracture, for in-place wiring versus wiring performed with the prosthesis removed prior to reinsertion.

METHODS: Seven fresh frozen femurs from 5 donors (mean age = 50.6 years) were used in the experiment. Radiographs were used to confirm the absence of structural defects and for templating to determine the correct prosthesis size for optimal canal filling. The prosthesis used in this study was an isthmus-filling, straight stem Harris-Galante component (Zimmer U.S.A., Warsaw, Indiana) made from Ti-6Al-4V alloy.Before insertion of the component, a 5 cm longitudinal saw cut, simulating an intraoperative fracture, was made through the anteromedial cortical wall. The cut extended from the osteotomy site to a 3 mm diameter terminus hole. The first treatment alternative, designated as in-place wiring, involved application of a cerclage wire (18 gauge wrought Zimaloy suture wire, Zimmer U.S.A.) without prosthesis removal. This wire passed through a 3 mm diameter hole drilled in the lesser trochanter, in order to standardize wire placement. The second alternative was to remove the prosthesis and wire the fracture shut prior to reinsertion of the component to its original position. For both techniques, a device was used to reproducibly tighten the cerclage wire to a torque of 58 N-cm. The third alternative was to again remove both the wire and the prosthesis, followed by reimpaction of the component to its original position without wiring. For each specimen, the orthogonal components of relative stem/bone displacement at one proximal and one distal location on the prosthesis were measured, as well as the stem's rotation about an axis through these points. These measurements were made using liquid metal strain gages (LMSGs, Parks Medical Electronics, Aloha, Oregon). One end of each gage was affixed to one of two small aluminum cubes attached to the ends of outrigger rods that were tightly screwed into the prosthesis. The other ends of the LMSGs were fastened to rigid extensions of steel rings that had been anchored to cortical bone with pointed screws. The prostheses were loaded through a simulated hemipelvis fixture attached to an

MTS servohydraulic testing machine. Axial load was applied so as to develop a peak (calculated) joint reaction force of 1500 N. LMSG signals were sampled at 100 Hz/channel by a 12-bit A/D converter linked to a personal computer. All specimens were subjected to one loading in each of the three treatment conditions: 1) wired with prosthesis in place, 2) wired before prosthesis reinsertion, and 3) non-wired.

RESULTS AND DISCUSSION: None of the cracks propagated past the terminus hole during prosthesis loading, even when no cerclage wire was applied. The respective components of micromotion at the proximal and distal monitoring points are given in Tables 1 and 2. Three dimensional rigid body motion of the prosthesis relative to bone is reported in Table 3. Vector **A** is a global displacement vector. Θ, Φ, and Ψ designate stem axis rotation, coronal plane rotation, and sagittal plane rotation, respectively. The average proximal component of micromotion was 32 μm, compared to 18 μm distally. This difference was statistically significant as determined by a paired t-test ($p = 0.019$). However, there were no statistically significant differences among treatment options (including the non-wiring option) with respect to displacement components or three dimensional rotations, although both wiring techniques showed a trend of reducing the average micromotion. Therefore it seems that the choice between in-place versus pre-reinsertion cerclage wiring is relatively inconsequential, but that wiring by either technique may important in keeping micromotion below or near the threshold for not inhibiting bone ingrowth. Cerclage wiring probably also serves to discourage further crack propagation, which likely would lead to great increases in micromotion if the crack extends far enough to compromise tight distal fixation. To summarize, cerclage wiring did not have an appreciable effect on the total micromotion. Nor was there any significant difference between the alternative wiring techniques with respect to component stability. There was consistently more micromotion proximally than distally, a phenomenon which seems consistent with the presence of a proximal simulated fracture. Since cerclage wiring had so little effect on the total micromotion, it seemed that a tight distal fit, in and of itself, was sufficient to provide good overall stability. Indeed, this idea is part of the rationale behind the isthmus-filling stem.

Table 1. Mean components of proximal micromotion (μm)

Condition	AP	ML	SI
1	44	29	11
2	49	33	15
3	60	29	18

Table 2. Mean components of distal micromotion (μm)

Condition	AP	ML	SI
1	8	16	10
2	7	33	17
3	5	40	29

Table 3. 3-D micromotion

Condition	A(AP,ML,SI)	Θ°	Φ°	Ψ°
1	38,30,12	.02	.06	.06
2	49,30,17	.02	.05	.06
3	51,18,13	.05	.05	.09

REFERENCES: 1. Fitzgerald, R.H. et al. Clin. Orthop., 235, 61-67, 1988. 2. Mallory, T.H. et al. Orthopedics, 12, 231-239, 1989.

A TECHNIQUE TO MEASURE RELATIVE MOTION BETWEEN TWO RIGID BODIES WITH APPLICATION TO IMPLANTED FEMORAL PROSTHETIC COMPONENTS

Alan S. Litsky, MD, ScD; Andrew W. Ryan, MD;
Thomas N. Hickey, BS*; Douglas N. Mackay, BS
Orthopaedic Biomaterials Laboratory and *Department of Chemistry
The Ohio State University, Columbus, Ohio 43210

INTRODUCTION

A new technique and device are described for measuring the relative motion between two rigid bodies. The first rigid body is affixed to the structure of our measuring device. The mobile second rigid body is connected to a frame apparatus which serves as an antenna to amplify relative motion. As the immobile first body is rigidly fixed in space relative to the measuring device, any relative motion between the two bodies will be detected as motion of the frame. If the spatial dimensions of the mobile body-frame complex are known, then quantified motion of any part on the second body can be easily calculated.

In our first application of this technique, a femoral prosthesis is implanted into a composite artificial femur. The femur is encased in bone cement inside a plastic box which is locked in place to the testing table of a Bionix MTS 858 materials testing system.

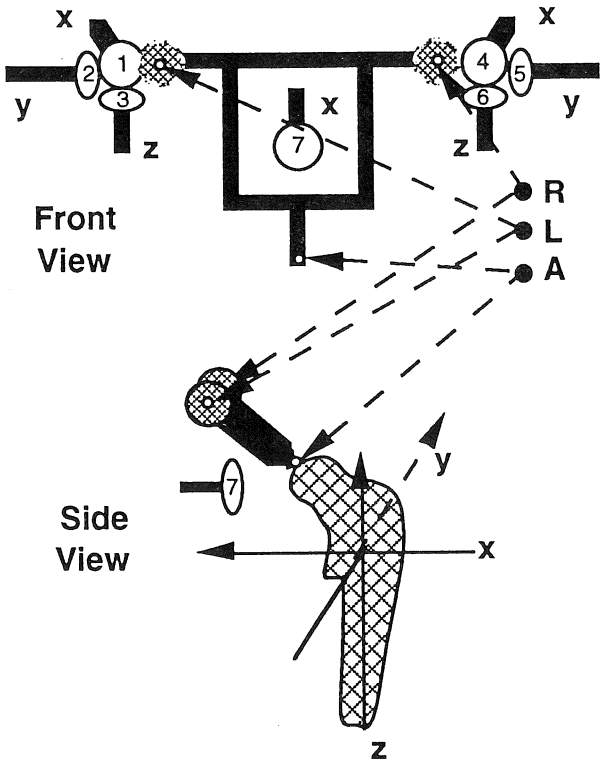

Figure 1. Schematic of the prosthesis-frame, shown with the seven LVDT's in position.

The femoral prosthesis (with prosthetic head) is connected to a triangular frame, with one apex at the femoral head. Seven LVDT's (linear variable differential tranformers) are used to measure the motion of the frame's corners, and the MTS is also used to measure vertical motion of the prosthesis.

A generalized method for translating from the linear data of the frame into three dimensional motion of the mobile second body is also described. This method makes use of a vector coordinate transformation from the global (x,y,z) coordinates of the measuring device to the local coordinates of the prosthetic shaft relative to the femoral head. Both linear and rotational deviations can be calculated using this method.

REVIEW AND THEORY

Many authors have described techniques for measuring the relative motion (aka "interface motion" or "micromotion") which occurs between a femoral prosthesis and the inner layer of the intramedullary canal. Such motion is suspected to play a role in clinical loosening of the prosthesis. Previous techniques have required (1) delicately placed strain gauges in the bone-prosthesis interface region or (2) cortical windowing of the bone and/or cement to measure relative prosthetic motion at a specific level. These techniques all have the drawback that the process of motion detection disrupts the bone-prosthesis interface.

Our technique leaves the bone-prosthesis interface unadulterated. The bone and prosthesis are both treated as rigid bodies. The bone is rigidly fixed within a box filled with bone cement, which is then locked to the testing table. The prosthesis is rigidly connected to a measuring frame. The frame is an isosceles triangle with the apex at the femoral head. Six LVDT's are situated to record deviations of the triangle's base corners along the x,y, and z axes (see figure 1). A seventh LVDT is situated to record the horizontal or "x" deviation of the apex. The MTS actuator is available to measure the vertical or "z" deviation. The lateral or "y" deviation of the apex can be calculated using the other data, or can be calculated from the rotational deviation of the MTS actuator.

The initial positions of the frame's triangular corners are determined in the global (x,y,z) coordinates of the testing system. After applying a physiologic load to the prosthesis, deviations of the triangle are recorded and can be determined by the LVDT's to within about 50 microns. Using a method similar to that described by Panjabi *et al.* (1981), a local coordinate system is constructed. The vector transformation between the local coordinates and the changing global coordinates of the triangle can be used to calculate the absolute motion of any point on the prosthesis. Since the bone is assumed immobile, absolute motion of the prosthesis is also motion of the prosthesis relative to the femur.

PROCEDURES

Let **L** be the position vector of the left hand triangle corner of the frame. Similarly **R** and **A** will be the initial positions of the right hand corner and the apex of the frame (see figure 1). After applying a load, these corners may move to new positions. The old and new positions are known in the global (x,y,z) coordinate system. Let vector **v** be the unit vector along the line from **L** to **R**. Let **w** be the normalized (unit length) vector of the cross product of **v** and the vector from **L** to **A**, i.e., $\mathbf{w} = \mathbf{w}' / |\mathbf{w}'|$, where $\mathbf{w}' = (\mathbf{A}-\mathbf{L}) \times \mathbf{v}$. We now have two normalized and perpendicular vectors **v** and **w**. Let vector **u** be the cross product of **v** and **w**, i.e. $\mathbf{u} = \mathbf{w} \times \mathbf{v}$. Vector **u** is also a normalized vector and is mutually perpendicular to **v** and **w**. These three vectors can be used as basis vectors for a new local coordinate system (see figure 2).

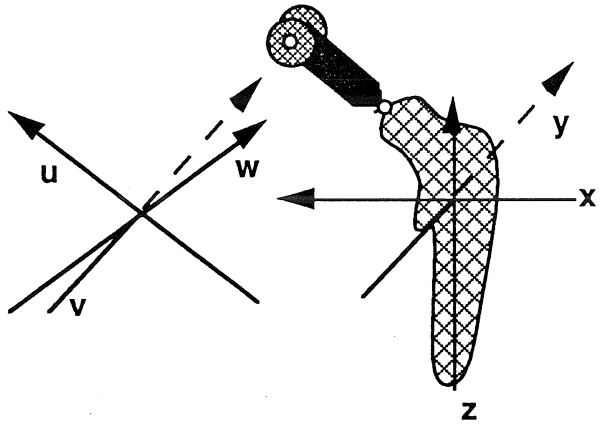

Figure 2. Relative orientation of the x,y and z axes of the global coordinate system and the u,v and w axes of the local coordinate system.

Points of interest on the prosthesis are given coordinates in the local coordinate system which will remain constant. With each new position of the frame, the basis vectors **u**,**v** and **w** will be recalculated in the global coordinates. A simple operator will convert from local to global coordinates: $x_g = {}_gR_l * x_l + T$; where x_l is a point x given in local coordinates; x_g is the same point x given in global coordinates; ${}_gR_l$ is a rotation matrix from local (*l*) to global (g) coordinates whose column vectors are equal to the global coordinates of **u**,**v** and **w**; and **T** is a translation vector which runs from the origin of the local system to the origin of the global system, i.e. **-L**. The initial position x_g is then calculated and compared to the final position x_g'. Thus, motion or "micromotion" of the prosthesis at any point of interest is easily calculated.

DISCUSSION

We have described the theory of a device which we are currently using to measure the relative motion of femoral prostheses to the inner wall of the femur. This technique allows us to measure motion on the order of about 0.050 mm. A distinct advantage, that this technique has over others currently used, is that our technique does not disrupt the integrity of the bone-prosthesis interface. Using the data generated in the manner described above, we can determine motion of any point on the prosthesis in any given direction. When combined with the use of an artificial femur to limit variations at the bone-prosthesis interface, this device will be able to compare the relative motion of different prosthetic devices available to the practicing orthopaedic surgeon.

REFERENCES

Panjabi, M. *et al. J. Biomechanics*, **14**, 447-460, 1981.

ACKNOWLEDGMENTS

We would like to thank Joint Medical Products for their support of this project; and Larry Stern for his technical assistance.

FLOW STUDIES ON ATRIOPULMONARY AND CAVOPULMONARY CONNECTIONS OF THE FONTAN OPERATIONS FOR TRICUSPID ASTRESIA

H T Low, Y T Chew and C N Lee*

Mechanical & Production Engineering Dept., National University of Singapore
***Cardiac Dept., National University Hospital**

INTRODUCTION

Tricuspid atresia is a congenital cardiac anomaly in which an atretic tricuspid-valve severely restricts flow from the right atrium to ventricle. Two main types of surgical procedures, named Fontan operations, are performed as treatment. The atriopulmonary connection (Fig. 1) is performed by anastomising the right atrium with the pulmonary artery, bypassing the right ventricle. In the cavopulmonary connection (Fig. 1), both the superior and inferior vena cavae are anastomised with the pulmonary artery, bypassing the right atrium.

The objective of the present paper is to investigate the pressure and power loss coefficients of in-vitro models of the atriopulmonary and cavopulmonary connections. The study will be conducted at steady flow-rates of 3 to 9 l/m and vessel elasticity will not be modelled.

EXPERIMENTAL PROCEDURE

The experimental models are shown in Fig. 1. The blood analogue fluid used was glycerol solution with a density of 1130 kg/m^3 and dynamic viscosity of 3.5×10^{-3} Pa s. The inlet ducts were connected to constant head reservoirs whilst the outlet discharged to the atmosphere. Upstream valves controlled the inlet flow rates such that 1/3 of the total flow passed through the superior vena cava and 2/3 through the inferior. Similarly, downstream valves ensured that 45% passes through the left pulmonary artery and 55% through the right.

The pressure distribution along the inlet and outlet ducts were determined from pressure tappings mounted, at 30-50 mm spacing, up to 25 diameters away from the test model. These experimental data were then curve-fitted by the Darcy-Weisbach equation with the friction factor obtained from the Moody's chart. By extrapolation of the pressure distribution curve, the pressures at the model were determined with less uncertainties arising from local-flow effects.

RESULTS AND DISCUSSION

The pressure losses of the atriopulmonary and cavopulmonary connections are presented in Figs. 2 and 3, where it has been non dimensionalized by the respective inlet flow velocities to obtain the pressure coefficients.

The pressure-loss coefficients is seen to vary inversely with flow rate up to about 5 l/m, indicating laminar flow. Then the pressure-loss coefficient levels off at a flow rate of about 6 l/m after which it increases slightly, indicating turbulence and increasing flow separation.

It is observed from Figs. 2 and 3 that the pressure loss from the vena cavae to the pulmonary artery is generally much lower in the cavapulmonary connection. For this configuration the main pressure loss occur at the junctions. However for the atriopulmonary connection there are additional presure losses due to the sudden flow-area enlargement at the atrium. The junction loss for the atriopulmonary connection is also expected to be larger due to its larger dynamic pressure.

The overall hydrodynamic loss of the two configurations may be compared in terms of the power loss coefficient which is the net power change non-dimensionalized by the inlet power. The power is defined as the product of the fluid energy (pressure and kinetic) per unit volume and the flow rate. The power loss coefficient in Fig. 4 shows a much lower power loss for the cavopulmonary connection.

It may be concluded that the steady flow losses are much lower for the cavopulmonary connection as compared with the atriopulmonary connection, for flow rates at the normal physiological ranges.

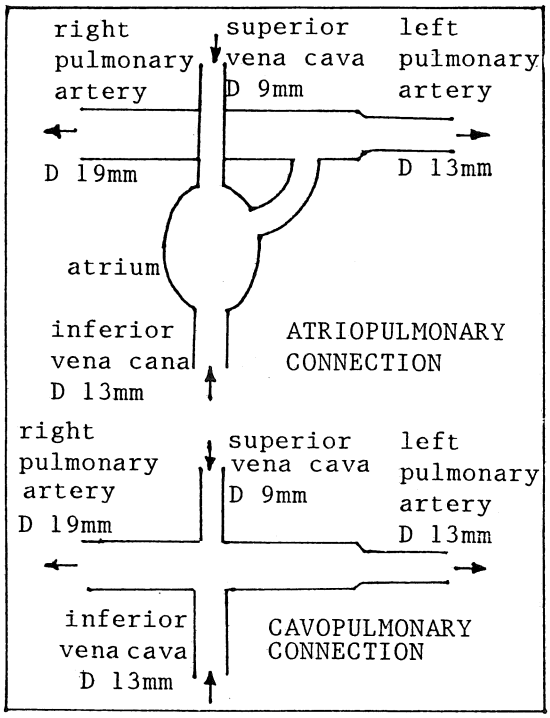

Fig. 1 Models of the atriopulmonary and cavopulmonary connections

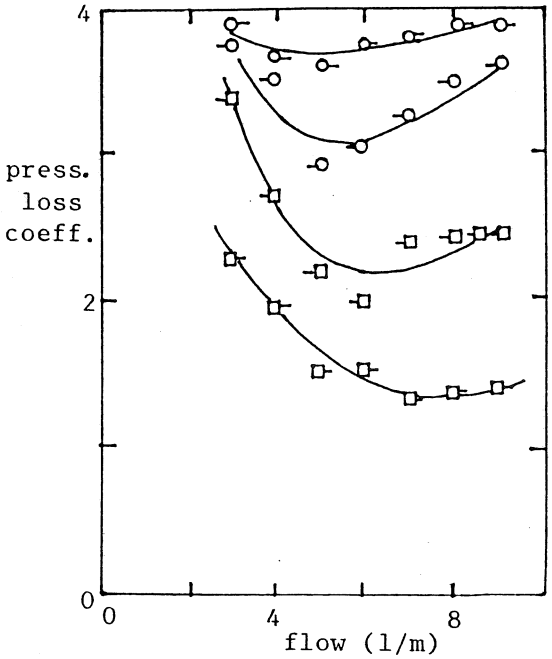

Fig. 3. Pressure loss from inferior vena cava to:
left pulmonary; ○, atriopulmonary
□, cavopulmonary
right pulmonary; ○, atriopulmonary
□, cavopulmonary

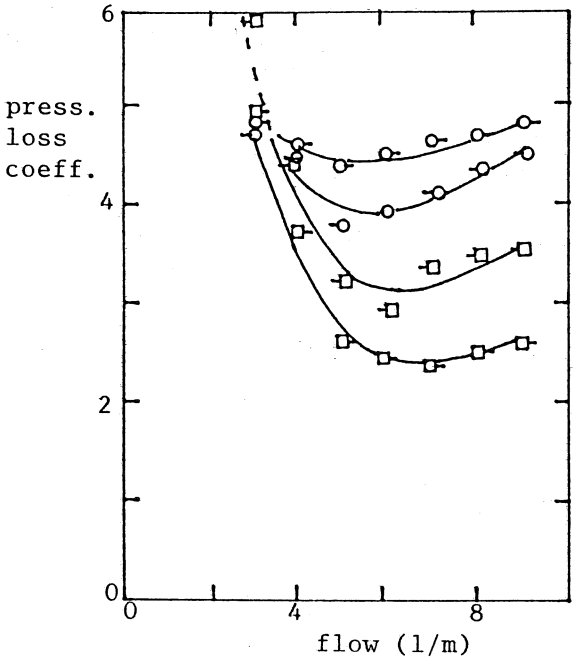

Fig. 2. Pressure loss from superior vena cava to:
left pulmonary; ○, atriopulmonary
□, cavopulmonary
right pulmonary; ○, atriopulmonary
□, cavopulmonary

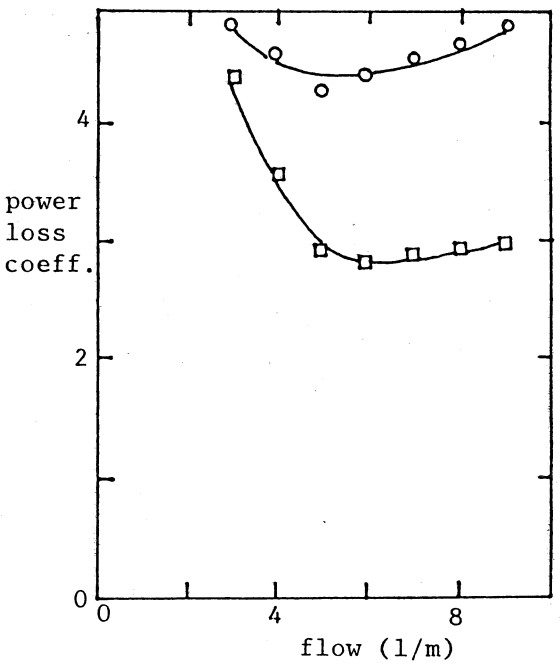

Fig. 4. Power loss of models:
○, atriopulmonary
□, cavopulmonary

BIOMECHANICS OF THROWING

Podium Session 2

THE EFFECTIVENESS OF UPPER LIMB ROTATIONS IN PRODUCING RACKET-HEAD SPEED IN RACKET SPORTS

E. Sprigings[1], R. Marshall[2], B. Elliott[2], L. Jennings[3]

[1]College of Physical Education, University of Saskatchewan, Saskatoon, SK. S7N0W0
[2]Department of Human Movement, and [3]Department of Mathematics
University of Western Australia, Perth WA, Australia

INTRODUCTION

The velocity of departure (Daish, 1972), for a ball or shuttlecock, from a racket can be expressed as:

$$v' = \frac{M[V(1+e) - ev] + mv}{M+m}$$

where: v' = velocity of ball after impact
v = velocity of ball before impact
V = racket-head velocity before impact
M = effective mass of racket
m = mass of ball
e = coefficient of restitution

Of these independent variables, the velocity of the racket-head at impact is of paramount importance, since it is the one parameter that relies strictly on the player's swing mechanics. The racket-head speed at impact results from a series of upper limb segment rotations generated through muscular torque. It should be recognized that the effectiveness of a segment's rotation in generating racket-head speed depends both on the segment's angular velocity, and on the instantaneous position of the racket-head with respect to the segment's axis of rotation.

The purpose of this paper is to outline the results of a technique that permits one to measure the contribution that each of the upper limb segments make to the instantaneous racket-head speed at the moment of ball contact. Such a technique permits a coach or player to evaluate the effectiveness of a player's sequence of segment rotations leading up to ball contact. As well, it would seem reasonable that comparison of the contribution profile obtained by this method with that of an elite player' profile could provide insight into what it is that separates out the skilled swing mechanics from the less skilled. Single examples are shown to illustrate the technique's application to squash and tennis.

REVIEW AND THEORY

A review of the literature reveals that researchers such as Jack, et al. (1979); Elliott et al. (1986); and van Gheluwe et al. (1987); have documented the segment rotations as well as their associated timing patterns during a typical arm-swing in a given racket sport. However, the contribution of the individual segment rotations to the production of racket-head speed at impact has not been examined. The magnitude of the segment's angular velocity at the moment of ball contact is, by itself, not sufficient information to allow one to evaluate a particular anatomical rotation's contribution to racket-head speed. As well, any analytical technique that is going to comment on the relative effectiveness of a given anatomical rotation must be able to remove the influence that another adjoining segment's rotation has on the measured value.

PROCEDURES

The relative angular velocities (3-D) of the three segments of the right upper limb were determined with respect to separate sets of segment fixed orthogonal axes that were constructed to closely approximate the corresponding anatomical axes. This was achieved using standard vector algebra techniques, coupled with 3-D displacement histories of 10 selected markers on the racket and upper limb (Fig. 1). The 3-D displacement histories were gathered using three cine cameras operating at a nominal rate of 300 fps for squash and 200 fps for tennis. The cameras employed 12 factor shutters and were positioned on the racket-arm side in front, beside, and behind the subject at different levels above the floor. A large calibration frame, previously described by Wood, et al, (1986), was used to provide the spatial calibration values for the DLT procedure (Abdel-Aziz et al., 1971). The displacement histories of the 10 digitized markers were filtered using the optimally regularized quintic spline subroutine GCVSPL (Woltring, 1986).

RESULTS AND DISCUSSION

Figure 2 (tennis serve) and figure 3 (squash forehand drive shot) compare the racket speed as measured from film, with that of the calculated speed as determined from the equation:

$$\mathbf{V}_K = \mathbf{V}_G + \{(\mathbf{w}_{1L} + \mathbf{w}_{1FE} + \mathbf{w}_{1AA}) \times \mathbf{r}_{K/G}\} + \{(\mathbf{w}_{2L} + \mathbf{w}_{2FE}) \times \mathbf{r}_{K/D}\} + \{(\mathbf{w}_{3FE} + \mathbf{w}_{3UR}) \times \mathbf{r}_{K/C}\}$$

The calculated results compare favourably with those determined directly from the film. As would be expected, the accuracy of the method is very much dependent on the accuracy of the 3-D displacement histories of the segment landmarks. In a technique such as this that relies on precise knowledge of 3-D coordinates in space, three cameras would appear to be an absolute minimum. A cursory look at the results using only two cameras confirmed this thought. Although the dramatic improvement in results when going from two to three cameras would not be expected to continue undiminished when going to a still higher number of cameras, the addition of at least two more cameras would seem warranted.

Figure 4 shows the individual contributions of the anatomical rotations of the upper limb over the last 18 frames leading up to ball contact. It is evident, that for this particular subject, the greatest contributions to racket-head speed were provided by the internal rotation of the upper arm, and the pronation of the forearm. Figure 5 shows the rotational velocity about the longitudinal axes of the upper arm and forearm for the same 18 frames as shown in Fig. 4. It is evident that the rate of pronation of the forearm is significantly greater than that of the forearm. However, the contribution of the forearm's

pronation to racket-head speed at ball contact is much less than that of the internal rotation of the upper arm (8.5 VS 13 m/s). This is not unexpected, since for forearm pronation, the racket-head is closely aligned with the rotational vector during the period just prior to ball contact.

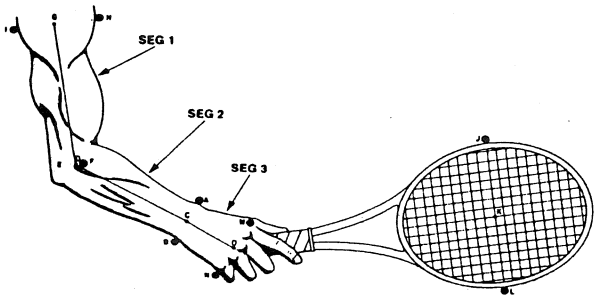

Figure 1. Arrangement of surface markers

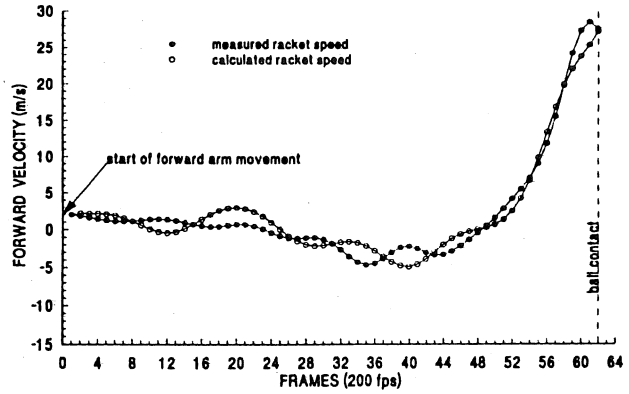

Figure 2. Tennis serve

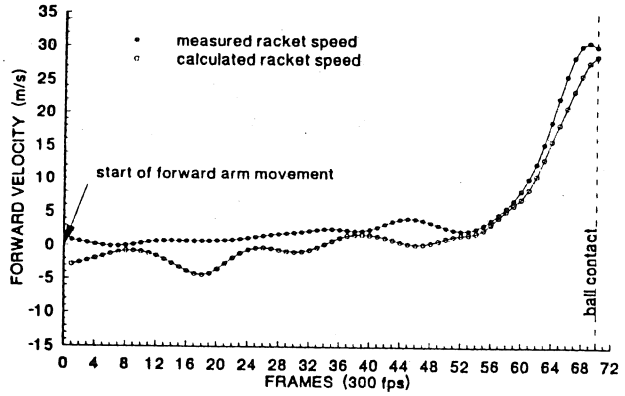

Figure 3. Squash forehand drive shot

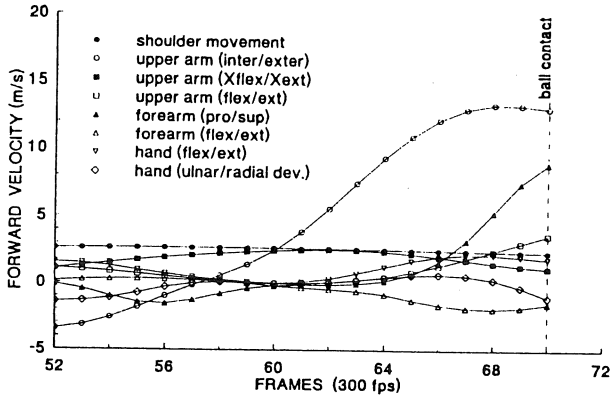

Figure 4. Contributions of the anatomical rotations (squash)

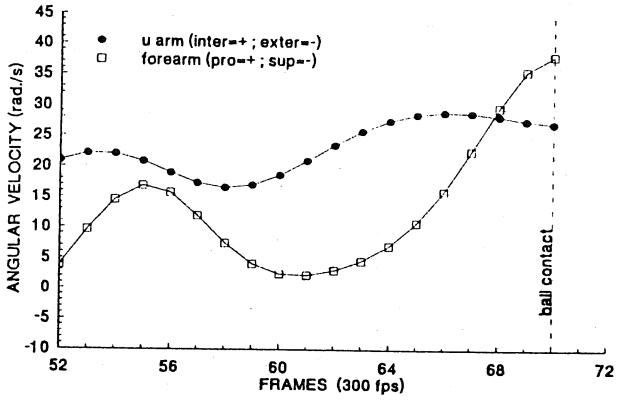

Figure 5. Longitudinal ang. vel. of upper arm and forearm (squash)

REFERENCES

Abdel-Aziz, Y. et al. Proceedings ASP Symposium on Close Range Photo

Daish, C. The Physics of Ball Games, 1972.

Elliott,B. et al. Int. J. Sport Biomech. 2,260-271,1986.

Jack, M. et al. Science in Racket Sports, 1979.

van Gheluwe, B. et al. Biomechanics X-B, 667-672,1987.

Woltring, H. Adv. Engng. Software 8, 104-113,1986.

Wood, G. et al. J. Biomech. 19,781-786,1986.

THREE DIMENSIONAL KINETIC ANALYSIS OF THE THROWING MOTION IN EIGHT ELITE COLLEGE FOOTBALL QUARTERBACKS

Gregory Rash* and Robert Shapiro**

*BIO/MED Research & Consulting, Louisville, KY 40218.
**Biodynamics Laboratory, The University of Kentucky, Lexington, KY 40506.

INTRODUCTION

Very little work has been conducted analyzing the three dimensional forces and moments produced at the shoulder and elbow in the overarm throw. Furthermore, all of the work to date has been with respect to the baseball pitch (Feltner, 1984; Feltner & Dapena, 1986; Horn, 1984; and Kauffman, 1989). The objective of this study was to determine the three dimensional forces and moments at the shoulder and elbow of American football quarterbacks' during a 30 yard pass and compare these results to those previously reported for baseball pitchers.

METHODOLOGY

Eight of the United States top senior college football quarterbacks were video taped while performing a dropback pass into a calibrated area during a practice session for the 1990 and 1991 Senior Bowls in Mobile Alabama. Synchronized 60 Hz video images from two cameras were manually digitized using a Peak Performance system and three dimensional kinetic data were calculated and averaged via a BASIC computer program. Figures 1 and 2 show the forearm and upper arm local coordinate systems respectively. Data were digitally smoothed using a second order Butterworth filter with a cut-off frequency of 6 Hz.

RESULTS & DISCUSSION

Table 1 shows the maximum forces, moments and the time they occurred with respect to release for pitchers and quarterbacks. The values for pitchers are from Feltner & Dapena (1986) and Kauffman (1989). From these finding one can see that there are both similarities and differences between the forces and moments of baseball pitchers and American football quarterbacks. With only a few exceptions at the elbow, the quarterbacks achieved their maximum forces and moments later in the sequence of the throw with smaller magnitudes than that reported for pitchers.

Differences between the throwing mechanics of a pitcher and quarterback may impact not only performance, but injury repair and rehabilitation as well. An understanding of these

differences may allow the quarterback coach, training staff, and medical community to better advise in the treatment and prevention of possible injuries.

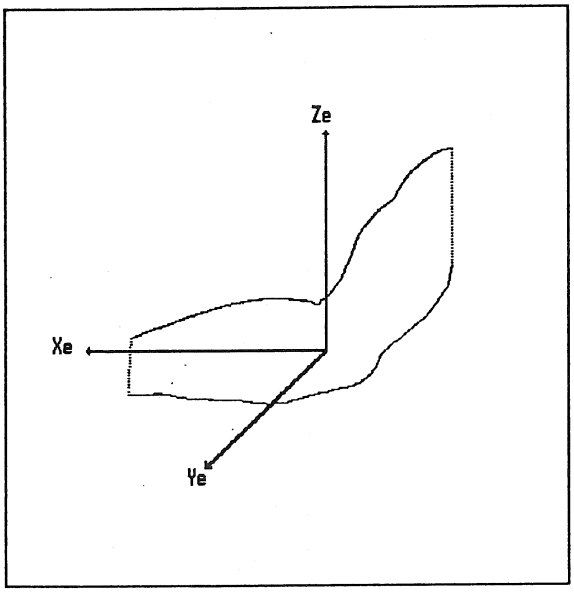

Figure 1. Forearm local coordinate system.

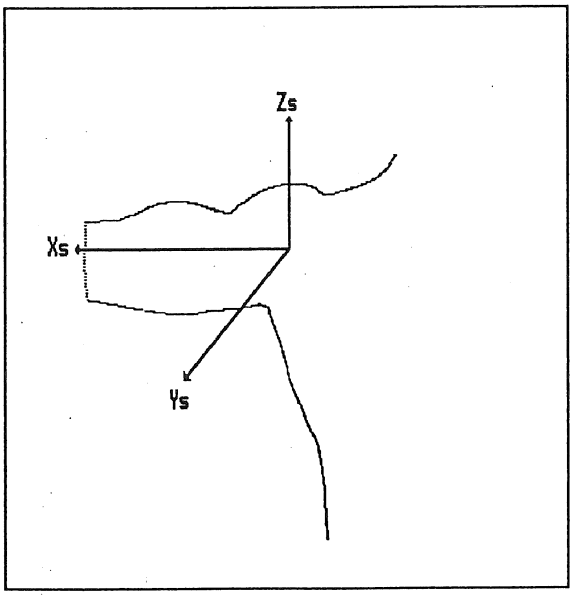

Figure 2. Upper arm local coordinate system.

Table 1

Maximum Kinetics and Time Occurred with Respect to Release

	FELTNER	KAUFFMAN	QUARTERBACKS
Shoulder			
Fxs (N)	- 860(5)	-511 to -866(5 to 20)	-342(33)
Fys (N)	±225*	-600 to 700	223(-133)
Fzs (N)	±250*	±400*	188(-83)
Mxs (Nm)	-90(-46)	-56 to -132(-10 to -25)	-61(-50)
Mys (Nm)	-70(-48)	-65 to -179(-10 to -25)	-39(100)
Mzs (Nm)	110(-60*)	113 to 265(-10 to -40)	55(-17)
Elbow			
Fxe (N)	-830(0)	-953 to -973(10 to 15)	-266(50)
Fye (N)	320(-48)	408 to 583(-15 to -30)	207(-83)
Fze (N)	170(10*)	±200*	101(-33)
Mxe (Nm)	< -10	< -15	-25(117)
Mye (Nm)	-30*(15)	-48(-10 to -15)	19(67)
Mze (Nm)	100(-47)	100(-20)	64(-50)

Time with respect to release in milliseconds are in parentheses. A minus sign for time indicates prior to release. The asterik sign {*} indicates the information is an estimate from a graph. For reference, maximum external rotation for Feltner occurred at -32 ms, Kauffman -34 ms and Quarterbacks -67 ms.

REFERENCES

Feltner, M., (1984). Unpub. Master's thesis, Indiana University.

Feltner, M., & Dapena, J., (1986). IJSB, 2, 235-259.

Horn, T., (1984). Unpub. Master's thesis, Auburn University.

Kauffman, K., (1989). Unpub. Master's the sis, University of Kentucky.

A THREE-DIMENSIONAL, SIX SEGMENT CHAIN ANALYSIS OF FORCEFUL OVERARM THROWING

D. Hong and E. M. Roberts

Motor Coordination Laboratory, Rush Medical College, Chicago
Department of Physical Education and Dance, University of Wisconsin-Madison, Madison

INTRODUCTION

In an effort to understand the mechanical cause-effect relationship and muscular coordination of overarm throwing, a three-dimensional, six segment model was developed to investigate muscular and interaction moments on the upper trunk and both upper extremities, using the angular momentum principle with respect to the proximal end point of each segment. All subjects showed similar muscular coordination patterns for the throwing upper extremity. For the trunk rotation two different muscular activation patterns were observed. Data in this study generally confirmed a proximal-to-distal sequence kinematically but not kineticly. Muscular moments for elbow extension and humerus internal rotation displayed stretch-shortening contraction patterns indicating that this pattern is an important muscular coordination strategy used in throwing. Also, the segment interaction moment on the forearm due to the linear acceleration of the elbow joint center accelerated elbow extension. Unchecked it might cause elbow damage. The humerus internal rotation velocity played an important role in checking the rapid extension thereby helping to prevent injure to the joint.

REVIEW AND THEORY

The overarm throw is one of the fundamental skills in many sport activities which generate high end-point speed. Early insight into the kinematics of the movement were obtained by Atwater (1970). Bullard (1989) measured kinematically in 3D the important rotations of the upper trunk and pelvis about their longitudinal body axes. To reveal the biomechanical mechanisms that produce this movement pattern, Feltner (1986, 1989) investigated the muscle moments and interactions between the forearm and upper arm. In previous kinetic investigations it has not been unusual to apply the angular momentum principle with respect to the mass center of a segment. In the present study the angular momentum principle with respect to the proximal end point was applied, instead. With this approach joint force moments and certain difficulties in their interpretation are avoided. An different moment term (MAP) appears. It is a moment produced by a special "force" equal to the product of the linear acceleration of the proximal end point with reverse sign and the mass of the segment, and is exerted on the center of mass of the segment. This term can reasonably be interpreted as the interaction from the adjacent proximal segment, and is in addition to the muscular moment around this articulation. Under this conceptual framework for a six-segment chain the muscular moments and interactions of not only the throwing arm but also the trunk as well as non-throwing arm were measured to reveal the mechanics and muscular coordination in the motion of a baseball throw.

PROCEDURES

High speed (250 fps) 3D film data were collected for three professional baseball pitchers. They threw in such a manner as to attain maximum ball speed. Five trial were analyzed kinematically and kineticly for each subject. Eulerian angles generated with respect to the inertial reference frame by three successive dextral rotations were defined as the anterior/posterior lean, medial/lateral lean and counterclockwise/clockwise (CCW/CW) rotation angles for the upper trunk and pelvis. The humerus horizontal adduction/abduction (HOR.ADD/ABD), adduction/abduction (ADD/ABD) and external/internal (EXT/INT) rotation angles were also defined by means of three Euler angles but with respect to the upper trunk reference frame for both throwing and non-throwing arms.

RESULT AND DISCUSSION

The sample plots presented here are limited to the time between the instant of stride foot contact (SFC) and the instant of ball release (REL). Four other important events include the beginning of ball deceleration (BDC), the beginning of ball acceleration (BAC), the start of elbow extension (EE) and the start of humerus internal rotation (INT), indicated by the vertical lines. The following abbreviations are used here: M.MUS. - muscular moment, M.JNT. - moment of joint force, P - proximal end point, D - distal end point, R - right shoulder, I.ACC - angular acceleration term of rate of change of angular momentum, I.VEL - angular velocity term of rate change of angular momentum, which is related to angular velocities in directions other than the rotation direction.

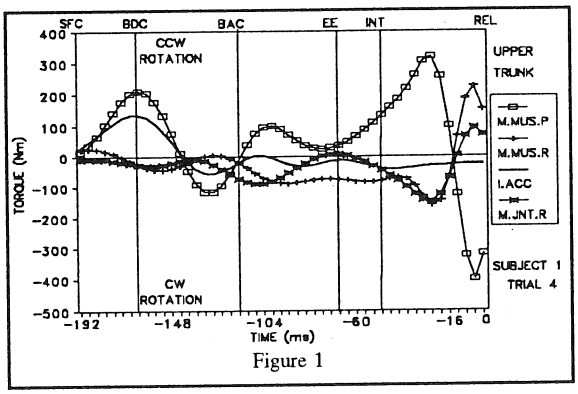

Figure 1

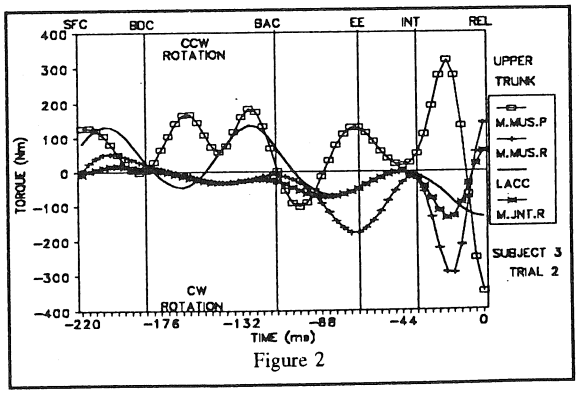

Figure 2

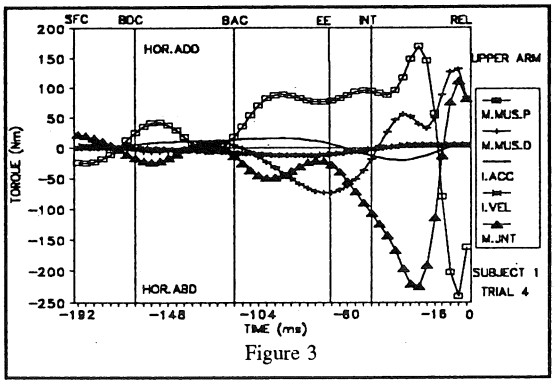

Figure 3

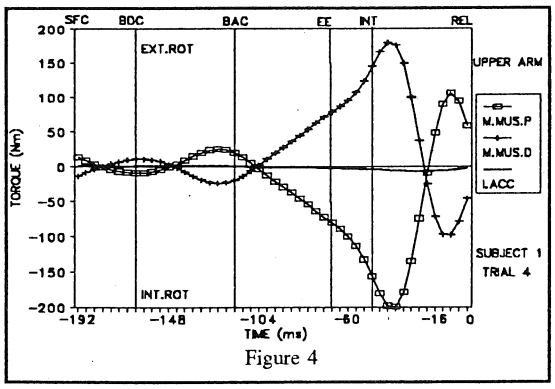

Figure 4

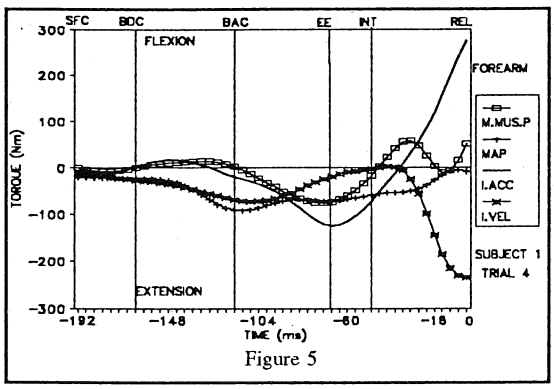

Figure 5

Left arm influences were relatively very small and are not shown here. The trunk rotators were almost the only contributor to the ball acceleration during the early phase from SFC to BDC (Figs.1 and 2). During the first ball acceleration phase from BAC to EE, HOR.ADD velocity continued to increase slightly and the extensor of the forearm started to act forcing elbow flexion to slow down (Fig.5). These actions became an inertial load which was passed to the upper trunk by M.MUS.R and M.JNT.R at the shoulder (Fig.1). The trunk rotators resisted this load by action CCW but not enough in magnitude to maintain the rotation speed, resulting in slight slowing. During the second acceleration phase from EE to INT, the main function of HOR.ADD muscle moment (Fig.3) was to relay the distal inertial load to the trunk. The trunk rotators again resisted this load to prevent too much slowing of the CCW rotation of the whole body.

Although the angular position and angular velocity of trunk CCW/CW rotation showed a certain similarity among the subjects, there were significant differences in the angular acceleration and the moments of the muscles and joint forces between subjects. Two distinct patterns can be observed in the use of trunk rotation to assist the throwing arm achieve a high end velocity (Fig.1 and 2).

The data in this study confirm the proximal-to-distal (P-D) sequence kinematically except for internal rotation of the humerus, but do not agree with the suggestion that temporal onset of the torques is also in a successive P-D sequence (Herring et al, 1989). Substantially, the major muscles involved in the throws, the trunk rotators, the humerus HOR.ADD muscles and internal rotators, as well as the forearm extensors were recruited at almost the same time (BAC) and kept acting until shortly before release (Fig.1 to 5). Also, a suggestion that the P-D sequence is accomplished by reversing muscular moment in a P-D sequence which would enhance the ball velocity was not observed in this investigation. The major muscular activations mentioned above do not reverse until very shortly before release.

For all subjects, shortly after BAC, the internal rotation muscle moment acted eccentrically while the humerus was still rotating externally. By the time external rotation was arrested, the internal muscle moment was near peak value and starting to act concentrically resulting in a dramatic increase of the ball velocity. Similarly, staring at BAC the elbow extension muscle moment acted against forearm flexion, and when extension started had already reached maximum in magnitude which contributed markedly to the high ball acceleration during the second acceleration phase.

The interaction moment MAP from the proximal segments plays an important role in assisting the forearm extensor to slow flexion and produce rapid elbow extension (Fig.5). These data also agree quite well with the nerve block data when the extensor nerve paralyzed (Roberts, 1971). Without elbow extensors the elbow would flex much too far and not extend adequately for throwing. MAP also tends to cause elbow extension to continue as it approaches the end of its range which could damage the joint if unopposed by the elbow flexor initiated after INT. The appropriate role of segment interaction (MAP) may reflect the ideal strategy of muscular coordination of the whole linked system, which was adopted by all subjects.

It is interesting to note that I.ACC is largely balanced by I.VEL shortly after INT in the forearm flexion/extension motion (Fig.5). I.VEL is produced by angular velocities other than that in the flexion/extension direction, and is dominated by the internal rotation velocity in this case. For this reason, only a small flexion muscular moment is needed to produce the large deceleration required to stop rapid extension and prevent possible injury to the joint. This phenomena has not been reported in previous literature. It is reasonable to assume that the central nervous system presets the motion in this manner by knowing the mechanical consequence.

REFERENCES

Atwater,A.*University of Wisconsin-Madison,Ph.D. dissertation,*1970.
Bullard,S.*University of Wisconsin-Madison,Ph.D. dissertation,*1989.
Feltner,M.et al.*Int.J.Sport Biomech.***2**,235-259,1986.
Feltner,M.*Int.J.Sport Biomech.***5**,420-450,1989.
Herring,R.et al.*Proc.13th.Ann.Meeting.of Amer.Soc.Biomech.*Vermont (pp.96-97),1989.
Roberts,E.*Proceedings of the C.I.C. Symposium on Biomechanics*,Chicago,(pp.41-50),1971.

CRITICAL CHARACTERISTICS OF TECHNIQUE IN THROWING THE DISCUS

Bing Yu and James G. Hay

Department of Exercise Science, The University of Iowa
Iowa City, IA 52242

INTRODUCTION

Several investigators have conducted two-dimensional analyses of techniques used in the discus throw. For the most part, however, these have been limited to a few variables measured with doubtful validity. A small number of three-dimensional analyses of the techniques used in the discus throw have also been conducted. While these studies have made useful contributions to our knowledge of discus techniques, there remains a need for a thorough, valid description of the techniques currently used by leading exponents of the event. In addition, none of the previous studies have been expressly directed towards identifying those characteristics of technique that are most closely related to success in the event, those factors that from a technical standpoint may be regarded as determinants of success. And, finally, none of these studies have addressed the controversial practical questions that have for years exercised the minds of athletes and coaches. The purposes of this study were (a) to provide a comprehensive, three-dimensional description of the techniques used by elite male and female athletes in throwing the discus; (b) to identify those characteristics of the techniques used that are most closely related to the distances of the throws recorded; and (c) to address some long-standing questions about techniques used in the discus throw.

PROCEDURES

A theoretical model of a discus throw was developed to identify those characteristics of the athlete's technique that determine the distance of the throw.

The subjects were the 29 competitors in the men's and women's discus throw at the 1990 U.S. Olympic Festival and the 1990 Goodwill Games.

Two video camcorders were used to record the position of a control object and the performances of the subjects, at a sampling frequency of 60 Hz. The trial in which each subject recorded his (or her) best official distance was selected for analysis. Twenty-one body landmarks and the center of the discus were digitized in each frame from each camcorder for each analyzed trial. Three-dimensional coordinate data were computed using the Direct Linear Transformation procedure (Abdel-Aziz, *et al.*, 1971) and then smoothed using a second-order, low-pass, recursive digital filter (Winter, *et al.*, 1974) at the optimum cutoff frequency estimated from the sampling frequency. All variables which were included in the theoretical model and could be quantified were computed from the smoothed coordinate data.

Means and standard deviations were computed for each variable and zero-order correlations were computed between each of the independent variables and the official distance of the throw (the dependent variable). Hierarchical, stepwise, multiple regression analyses were conducted with the factors at each level in the model regressed in turn against d_O (the dependent variable). Where possible, the factors were entered into the regression in the temporal order with which they were associated in the throw. The 0.05 level of confidence was chosen to indicate statistical significance after considering the consequences of Type 1 and Type 2 errors.

RESULTS AND DISCUSSION

The official distance (d_O) is equal to the sum of the distance lost at release (d_L), the distance the discus would travel from release to landing in the absence of air resistance, the theoretical flight distance (d_F), and the distance gained due to the action of aerodynamic forces during the flight (d_G). That is

$$d_O = - d_L + d_F + d_G$$

Mean values for these part distances indicated, as expected, that the flight distance was by far the longest (Table 1). They also revealed that absolute and relative values for the male and female samples were remarkably similar, despite the difference in gender and the differences in the dimensions of the discus thrown.

Table 1. Means for Official Distance and Absolute and Relative Part Distances.

Sex	Distance Lost	Flight Distance	Distance Gained	Official Distance
M	0.38 (0.6%)	51.82 (87.7%)	7.63 (12.9%)	59.07
F	0.43 (0.7%)	49.31 (85.2%)	9.03 (15.6%)	57.90

The flight distance is determined by the speed, angle of height of release of the implement. The means and standard deviations for these variables are shown in Table 2. Here, too, with the exception of the height of release, the values for the male and female subjects were remarkably similar. The difference in the height of release was due almost exclusively to a corresponding difference in the standing heights of the two samples (the mean heights of release, expressed as a fraction of the standing height, were 0.86 and 0.84 for the male and female subjects, respectively).

Critical instances and phases were identified for a discus throw: (a) end of preliminary backswing/start of the first support phase (t_0); (b) right foot up/end of first double support phase/start of first single support phase (t_1); (c) left foot up/end of first single support phase/start of flight phase (t_2); (d) right foot down/end of flight phase/start of second single support phase (t_3); (e) left foot down/end of second single support phase/start of pre-release phase (t_4); (f) release/end of pre-release phase (t_5) (Figure 1). The mean change in the speed of the center of gravity of the discus was computed for each critical phase (Table 3).

These data revealed large gains (31-35% of the speed at release)

during the initial ground support phase (t_0-t_2); small losses in speed during the flight phase (t_2-t_3); a suprising gain in speed for the females during the second single support phase (t_3-t_4), when friction between the support foot and the ground might be expected to retard the athlete's rotation and decrease the speed of the discus; and the expected dramatic change in speed during the final throwing action (t_4-t_5). They also revealed, for the first time, clear differences between the techniques used by the male and female subjects.

Table 2: Means (and Standard Deviations) for the Speed, Angle and Height of Release of the Discus.

Sex	Speed of Release (m/s)	Angle of Release (deg)	Height of Release (m)
M	22.70 (0.91)	35.74 (2.80)	1.66 (0.17)
F	22.10 (1.36)	35.69 (4.49)	1.52 (0.19)

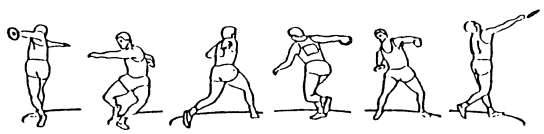

(a) (b) (c) (d) (e) (f)

Figure 1. Critical instants in a discus throw.

Table 3: Average Changes in Speed of Center of Gravity of Discus during Critical Phases in the Throw.

Sex	t_0-t_1	t_1-t_2	t_2-t_3	t_3-t_4	t_4-t_5
M	5.00	3.03	-0.55	0.01	15.22
F	4.77	2.13	-0.43	1.39	14.16

Significant, positive correlations were found for both male and female subjects between the flight distance and the official distance (r = 0.64 and 0.91, respectively); and between the speed of release and the official distance (r = 0.68 and 0.90, respectively). These results were expected. What was not expected was the disparity between the correlation coefficients for the males and females.

Two other significant, positive correlations were found for the female subjects. These were between the height of release and the official distance (r = 0.55); and between the change in speed of the discus during the flight phase of the turn and the official distance (r = 0.75). These too were unexpected. The first of these findings appears to have been due to the close relationships that existed between the height of release and both the speed and angle of release (r = 0.67 and 0.64, respectively). The second of these findings indicated that the greater the change in the speed of the discus during the flight phase the greater the distance of the throw. The change in the speed of the discus during the flight was also significantly related with the speed at release, suggesting that it may have had a causal influence on the latter parameter and thus on the distance of the throw. It is however a surprising candidate for such an influential role.

The results of the multiple regression analyses revealed that d_G accounted for 59% and 14%, and d_F for 36% and 77%, of the explained variance in d_o for the males and females, respectively. These findings suggested that the way in which the discus was flighted is of major importance to elite male throwers (perhaps, in part, because of the implement's large cross-sectional area) and of only minor importance to their female counterparts. They also suggest that d_F is of much less importance to the success of male throwers than is commonly supposed. And even more so than appears here, given that the order in which the variables were entered into the regression (d_F before d_G) meant that the contribution of d_F to the explained variance in d_o was somewhat inflated by it receiving 'credit' for the variance it shared with d_G.

It thus appears that, although the techniques employed by elite male and female discus throwers have much in common, they differ in the factors that exert the dominant influence on the distances they achieve. Variation in the distances recorded by the males depends primarily on how the discus is flighted and only secondarily on the speed at which it is released; variation in the distances recorded by the females depends overwhelmingly on the speed of the discus at release.

REFERENCES

Abdel-Aziz, Y. I., *et al. ASP Symposium on Close Range Photogrammetry*, 1971.

Winter, D. A., *et al. J. Biomechanics*. 7,157-159, 1974.

DEVELOPMENT AND AGING

Podium Session 3

NEUROMUSCULAR ADAPTATIONS DURING STRENGTH TRAINING IN MIDDLE-AGED AND ELDERLY MALES AND FEMALES

K. Häkkinen and A. Häkkinen

Department of Biology of Physical Activity, University of Jyväskylä, Jyväskylä, Finland
Central Hospital of Central Finland, Jyväskylä, Finland

INTRODUCTION

Effects of intensive strength training combined with explosive types of exercises for 12 weeks on electromyographic activity (EMG), muscle cross-sectional area, isometric maximal force and force-time curve of the leg extensor muscles were investigated in middle-aged males (M50 years) and females (F50) as well as in elderly males (M70) and females (F70). Great gradual increases took place in maximal force during the 12-week training period both in M50 (from 2834 $\pm$ 452 to 3941 $\pm$ 772 N; $p<0.001$) and in F50 (from 2627 $\pm$ 725 N to 3488 $\pm$ 1017 N; $p<0.001$) as well as in M70 (from 2591 $\pm$ 736 to 3075 $\pm$ 845 N; $p<0.01$) and in F70 (from 1816 $\pm$ 427 to 2483 $\pm$ 408 N; $p<0.001$). Significant ($p<0.05$ - 0.001) increases occurred also in the maximum integrated EMGs of the trained muscles in all groups primarily during the first 8 weeks of training. Significant ($p<0.01$-0.001) enlargements took place during the 12-week training period in the CSA of the QF muscle in all groups. Significant ($p<0.05$-0.001) changes occurred in all groups in the higher force portions of the force-time curves and in the maximal rate of force production. The present findings suggest that progressive strength training may lead to considerable increases both in maximal and explosive force production of the trained muscle accompanied by adaptations in the nervous system and by muscular hypertrophy not only in middle-aged but also in elderly males and females.

REVIEW AND THEORY

It is rather well known that under normal conditions human muscle strength decreases with increasing age especially after the middle-age at the onset of the sixth decade in both sexes(Larsson et al.1978, Heikkinen et al. 1984, Häkkinen et al. 1991, Narici et al. 1991). The decrease in strength may be related to a great extent to the reduction in muscle mass observable both in men and women especially as aging is often also associated with a decline in normal daily physical activities. The decline in muscle mass may due to both a reduction in the size of individual muscle fibers, especially of fast twitch fibres and a loss of individual muscle fibres (Larsson et al. 1978, Lexell et al. 1983). Therefore, other changes such as worsening in explosive force production as well as lengthening in relaxation time of the activated muscles (Clarkson et al. 1981, Narici et al.1991, Häkkinen et al. 1991) may also take place characterizing further age related overall changes in the neuromuscular system both in males and females. On the other hand, it is known that considerable increases in muscle strength may take place due to the application of progressive strength training even in older subjects resulting from neural adaptations during the early weeks of training, while later strength development takes place primarily due to a gradually increasing contribution of muscle hypertrophy (Frontera et al. 1988, Fiatarone et al. 1990, Charette et al. 1991). However, to minimize overall age related changes on the neuromuscular system strength training combined with modified explosive type exercise could be useful to maintain better the overall functional capacity among elderly people at a sufficient level. The purpose of the present study was therefore to examine neuromuscular adaptations in middle-aged and elderly males and females during a 12-week training period, when heavy resistance and explosive type strength training programmes were simultaneously used.

PROCEDURES

Nine middle-aged males and 9 females in the 50- year age group (M50; range 44-57), (F50; range 43-54), 10 elderly males and 11 females in the 70-year age group (M70; range 64-73), (F70; range 66-73) volunteered as subjects for the study. Full advice was given to the volunteers regarding possible risk and discomfort that might ensue and all subjects gave their written informed consent to participate. The subject were healthy and habitually physically active but they had no background in regular strength training or competitive sports of any kind. In this study the subjects participated in supervised heavy resistance strength training including explosive types of exercises for 12-weeks (with the loads between 30 and 80% of 1RM) 2 times a week during the first 8 weeks and 3 times a week during the last four weeks of training.

Maximal voluntary force and force-time curve of the leg extensor muscles were measured during the isometric bilateral contraction on a dynamometer (Komi 1973). Electromyographic activity was recorded from the vastus lateralis (VL) and vastus medialis (VM) and rectus femoris (RF) muscles by surface electrodes and integrated to obtain maximum voluntary integrated EMG (IEMG) during the maximal force production. The cross-sectional area (CSA) of quadriceps femoris muscle (QF) of the right thigh was measured with an ultrasonic apparatus (Aloka Fansonic, SSD-190).

RESULTS

Great gradual increases took place in maximal force during the course of the 12-week training period both in M50(from 2834 $\pm$ 452

to 3941 ± 772 N; p<0.001) and in F50 (from 2627 ± 725 to 3488 ± 1017 N; p<0.001) as well as in M70 (from 2591 ± 736 to 3075 ± 845 N; p<0.01) and in F70 (from 1816 ± 427 to 2483 ± 408 N; p<0.001) (Fig.1). The relative increases in maximal force during the training didn't differ significantly between the groups but during the last four weeks of training the plateaus observed in strength development were significant in F50 (p<0.05), in M70 (p<0.01) and in F70 (p<0.05) but not in M50. Significant (p<0.05 - 0.001) increases took place also in the maximum IEMGs of the trained muscles in all groups primarily during the first 8 weeks of training (Fig. 2). Significant (p<0.01 - 0.001) enlargements took place during the 12-week training also in the CSA of the QF muscle in all groups (Fig. 3.) but maximal force per CSA of the QF muscle increased (p<0.05 - 0.01) in all groups as well. The training in all groups led also to significant (p<0.05-0.001) changes primarily in the higher force portions of the force-time curves and in the maximal rate of force production.

DISCUSSION

The present findings demonstrated that intensive strength training led to gradual great increases not only in maximal force but also in explosive force characteristics of the trained muscles accompanied by considerable functional and structural adaptations in the neuromuscular system both in the middle-aged and elderly males and females. Significant increases in the voluntary maximum IEMGs of the trained muscles indicate that considerable training- induced adaptation took place in the nervous system, while on the other hand significant gradual enlargements in the CSA of the QF muscle demonstrated that considerable muscular hypertrophy may also occur both in middle-aged as well as in elderly males and females, when the intensity and duration of the training are sufficient (Frontera et al. 1988, Charette et al. 1991, Fiatarone et al. 1991). The magnitudes and time courses of neuromuscular adaptations during the training period didn't differ significantly between the subject groups of different ages and sexes, although these adaptations may become more limited in magnitude due to hormonal factors during more prolonged training especially in females and in older males. The shifts in the shape of the force-time curves of the trained muscles further demonstrate that considerable adaptations may take place in the explosive performance of the neuromuscular system also in older people. This may result both from the increased rapid neural activation of the motor units of the trained muscles and from selective hypertrophy of fast twitch muscle fibres. Since older people may usually be involved more in endurance type of physical activities, one could suggest that to minimize the effects of aging on the neuromuscular system, strength training combined with explosive types of exercises could be recommended as a part of an overall physical training programme to maintain the functional capacity among elderly people at as high a level as possible for as long as possible.

REFERENCES

Charette, S. et al. J. Appl. Physiol. 70, 1912-1916, 1991
Clarkson, P. et al. J. Gerontol. 36, 648-653, 1981
Fiatarone, M. et al. Jama, 263, 3029-3034, 1990
Frontera, W. et al. J. Appl. Physiol. 64, 1038-1044, 1988
Heikkinen, E. et al. Scand.J. Soc. Med. 33,1-93,1984
Häkkinen, K. et al. Eur. J. Appl. Physiol. 62, 410-414, 1991
Komi, P. Int. Sem. Ergom., Berlin, (pp 173-176), 1973
Larsson, L. et al. Acta Physiol. Scand. 103, 31-39, 1978
Lexell, J. et al. Muscle Nerve. 6, 588-595, 1983
Narici, M. et al. J. Appl. Physiol. 71, 1277-1281,1991

ACKNOWLEDGEMENTS

This study was supported in part by a grant from the Ministry of Education, Finland.

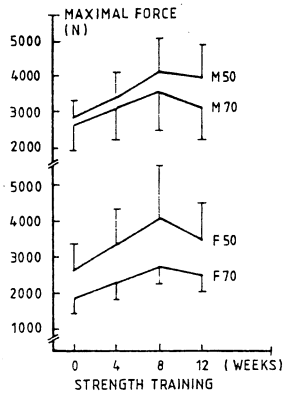

Fig. 1. Maximal force

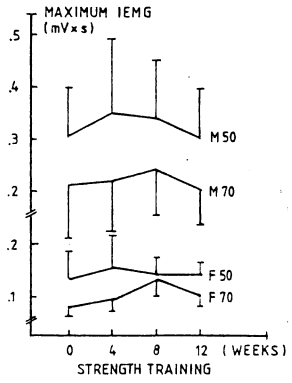

Fig. 2. Maximum IEMG (averaged for VL,VM and RF)

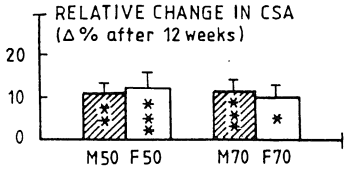

Fig. 3. Relative changes in muscle CSA

AGE DOES NOT IMPAIR THE VOLUNTARY ABILITY TO MAXIMALLY ACTIVATE MUSCLE

R.M. Enoka, A. J. Fuglevand, and P. M. Barreto
Department of Exercise & Sport Sciences, University of Arizona, Tucson, AZ 85721.

INTRODUCTION

The maximal voluntary force that an individual can exert with a muscle depends on the ability to provide a sufficient neural drive to the muscle, the mechanical characteristics of the muscle, and musculoskeletal geometry. Because the force that can be exerted during a maximum voluntary contraction (MVC) declines with age, there has been an interest in determining the role of these factors in the age-related diminution of performance capabilities. We used electrophysiological measurements of voluntary and artificially evoked muscle activity to assess the effect of age on the capability of the nervous system to activate muscle during an MVC. We found that although the quantity of electromyographic activity (EMG) declined with age, this decrease was not due to an impairment of the neural drive to muscle but was probably caused by a reduction in the amplitude of muscle fiber action potentials.

REVIEW AND THEORY

As humans age, there is a decline in both muscle mass and MVC force (Aniansson et al., 1986; Narici et al., 1991) and an associated reduction in the number and size of motor units innervating a muscle, including an apparent reduction in the proportion of fast-twitch muscle fibers (Kanda & Hashizume, 1989). These changes in morphology undoubtedly contribute to the reduction in MVC force with age. In addition, however, aging is associated with a decline in the magnitude of the electrically elicited compound muscle action potential (M wave), which is an index of the electrical excitability of muscle (Hicks et al., 1992; Vandervoort & McComas, 1986). Furthermore, even young subjects are unable to maximally activate muscle during voluntary contractions (Enoka & Fuglevand, 1992). For these reasons, we wondered whether the excitatory drive to muscle during an MVC might decline with age. The purpose of this study was to determine the contribution of age-related changes in neural drive to the reduction in MVC force. We assessed this possibility by comparing the magnitude of the voluntary and artificially evoked EMG (M wave) in young and old subjects.

PROCEDURES

Experiments were performed on older human subjects (58-74 years) and their results were compared to younger adults (18-40 years) who had been tested in the laboratory. The older subjects were carefully screened to eliminate those candidates with a history of neuromuscular deficits, including the use of medication that might impair neuromuscular function. The test muscle was first dorsal interosseus (FDI) of the left hand; FDI is located between the thumb and the index finger and it is the only muscle that abducts the index finger. The hand was placed so that the proximal interphalangeal joint of the index finger was aligned with two force transducers, one that sensed abduction force and another that sensed flexion force. EMG signals were obtained from bipolar surface electrodes (4-mm diameter, silver-silver chloride, 1.2 cm interelectrode distance) placed on the skin overlying FDI and abductor digiti minimi (the abductor of the little finger, which, like FDI, is innervated by the ulnar nerve). Electrical stimulation was applied percutaneously to the ulnar nerve. The supramaximal stimulus, which had a duration of 1.0 ms and was delivered once every 3 seconds, was used to elicit direct motor responses (M waves) in FDI. Concurrent measurement of M waves in abductor digiti minimi assured stability of the stimulating electrode.

The experimental protocol consisted of MVCs that were performed before and after a fatiguing contraction. For the MVCs, subjects performed 2-4 trials in which the abduction force was gradually (2-5 s) increased up to maximum (MVC). The greatest force that was achieved was taken as the MVC and the target force for the fatiguing contraction was set at 35% MVC. Five M waves were elicited before and immediately after the fatiguing contraction, which involved sustaining an isometric abduction force with the index finger to exhaustion. The force and EMG data were stored on FM tape and were replayed and analyzed with Spike2 (CED 1401), an event and waveform data-capture and data-analysis system. For the fatiguing contraction, time was normalized as a percentage of the endurance time. The EMG was rectified and averaged over epochs that represented 10% of the endurance time. In addition, a Fourier transformation of the EMG was performed on each epoch of the fatiguing contraction and of the MVC to obtain the power spectrum from which the mean power frequency was calculated. The M waves, which were generally biphasic, were quantified by the measurement of peak-to-peak amplitude and duration.

RESULTS

A comparison of the initial values for the young and old subjects indicates that both the force and average EMG of the MVC for the FDI muscle declined with age (decreases of 14 and 41%, respectively; Table 1). This reduction in MVC occurred despite the healthy and active lifestyles of the older subjects, whose mean age was 67 years. In parallel with the decline in voluntary EMG, the amplitude of the artificially evoked M wave was smaller in the older subjects (42% reduction). The fatiguing contraction, however, had a similar duration for the two groups of subjects. Although the contraction was associated with comparable increases in average EMG (181 and 189% of initial) and reductions in M-wave amplitude (74 and 68% of initial) for the young and old subjects, respectively, there were significantly different reductions in the mean power frequency for the average EMG during the final MVC (61 and 73% of initial) and at the end of the fatiguing contraction (48 and 62% of initial).

Table 1. Older subjects had a lower MVC and average EMG but less of a change in the mean power frequency as a consequence of the fatiguing contraction.

		Young		Old	
Age (years)		28 ± 6	(31)	67 ± 4*	(18)
MVC force	Initial (N)	36 ± 7	(31)	31 ± 7*	(18)
	After (% initial)	76 ± 6‡	(15)	70 ± 13‡	(14)
MVC average EMG	Initial (mV)	0.78 ± 0.34	(26)	0.46 ± 0.23*	(14)
	After (% MVC)	98 ± 28	(15)	82 ± 31	(14)
MVC mean power frequency	Initial (Hz)	111 ± 20	(26)	126 ± 31*	(14)
	After (% initial)	61 ± 5‡	(15)	73 ± 18‡*	(14)
M wave amplitude	Initial (mV)	13.71 ± 3.29	(22)	8.02 ± 5.65*	(13)
	After (% initial)	74 ± 24‡	(11)	68 ± 19‡	(13)
Endurance time (s)		212 ± 111	(15)	183 ± 81	(14)
Fatigue average EMG	Initial (mV)	0.19 ± 0.08	(15)	0.15 ± 0.11	(14)
	Final (% initial)†	181 ± 57‡	(15)	189 ± 74‡	(14)
Fatigue mean power frequency	Initial (Hz)	129 ± 20	(15)	137 ± 28	(14)
	Final (% initial)†	48 ± 11‡	(15)	62 ± 14‡*	(14)

Values are mean ± SD (n). Significantly different ($p < 0.05$) to the young subjects (*) and to the initial value (‡). † value at the end of the fatiguing contraction.

DISCUSSION

An M wave is elicited by the synchronous activation of muscle with an electrical stimulus. The amplitude of the M wave depends on the amplitude of individual muscle fiber action potentials, the proportion of whole-muscle activity detected by the electrodes, and skin impedance (Hicks et al., 1992). For a given electrode configuration, the variability across subjects and across muscles in the proportion of whole-muscle activity detected by the electrodes is small (Hicks et al., 1992). Furthermore, because the effect of the fatiguing contraction on the mean power frequency for the two groups was different, this suggests that skin impedance is not the dominant factor underlying differences in M-wave amplitude. Consequently, M-wave amplitude represents a reasonable index of the excitability of the muscle fibers for the two groups of subjects.

When the average EMG during the MVC was normalized to M-wave amplitude, the voluntary EMG represented 5.7% of the artificially evoked EMG (M wave) for both the young and old subjects. This indicates that the older subjects provided a comparable neural drive to the muscle during the MVC and that impaired neural drive was not responsible for the decrease in MVC force. These data, therefore, suggest that age does not alter the voluntary ability to maximally activate muscle and that differences in the average EMG during an MVC were due to changes at the muscle fiber level.

REFERENCES

Aniansson A, Hedberg M, Henning G-B, Grimby G: Muscle morphology, enzymatic activity, and muscle strength in elderly men: a follow-up study. *Muscle Nerve* 9: 585-591, 1986.

Enoka RM, Fuglevand AJ: Neuromuscular basis of the maximum voluntary force capacity of muscle. In: Grabiner MD (ed) *Current Issues in Biomechanics: A Prospectus.* Champaign, IL: Human Kinetics, in press.

Hicks AL, Cupido CM, Martin J, Dent J: Muscle excitation in elderly adults: the effects of training. Muscle Nerve 15: 87-93, 1992.

Kanda K, Hashizume K: Changes in properties of the medial gastrocnemius motor units with aging. *J Neurophysiol* 61: 737-746, 1989.

Narici MV, Bordini M, Cerretelli P: Effect of aging on human adductor pollicis muscle function. *J Appl Physiol* 71: 1277-1281, 1991.

Vandervoort AA, McComas AJ: Contractile changes in opposing muscles of the human ankle joint with aging. *J Appl Physiol* 61: 361-367, 1986.

ACKNOWLEDGMENTS

The authors acknowledge the technical assistance of Peter B. Worden. This research was supported by USPHS grants AG 09000, NS 20544, NS 07039 and NS 08634.

BODY SEGMENT GROWTH CURVES DURING INFANCY

H. Sun and R.K. Jensen

Centre for Research in Human Development and School of Human Movement, Laurentian University, Sudbury, Ontario.

INTRODUCTION

Locomotor development depends on not only maturation of the motor cortex, but also many other components, such as anatomical parts and physiological factors (Thelen, Ulrich and Jensen, 1989). Surveys of the anthropometry of infants show that growth affects the size and shape of body segments (Snyder *et al.*, 1977) and rapid growth during infancy causes the greatest changes of body proportion (Malina, 1984). Movement of the body is due to the application of force about the joints producing angular acceleration and the moments of inertia are indicative of resistance to angular acceleration (Newell, 1984). However, segmental parameters of human infants are not available. Therefore, the purpose of this study was to use a mathematical model of the segments to examine changes of mass and moments of inertia during infancy.

Table I Mean regressions for individual antero-posterior axis principal moments Y=A0+A1X

	A0	A1
Segment	MEAN	MEAN
Head	2.41e-03	7.88e-05
Neck	3.10e-05	9.26e-07
U.Trunk	9.66e-04	1.25e-04
L.Trunk	5.15e-03	-2.67e-05
Arm	-1.85e-05	6.37e-06
Forearm	6.57e-05	2.81e-06
Hand	1.54e-05	1.11e-07
Thigh	-1.48e-04	4.10e-05
Shank	9.43e-05	9.59e-06
Foot	2.41e-06	2.11e-06
Body	7.54e-02	5.16e-03

Very few studies using anthropometric models on children have been reported. A sixteen segment model in which the body segments are considered to be composed of elliptical zones 2 cm wide has been used to evaluate the body segment parameters in a mixed-longitudinal study of children aged 4 to 20 (Jensen, 1989; Jensen and Nassas, 1988). Schneider *et al.* (1990) studied limb movement in infants by analyzing the anthropometric parameters of infants' limbs.

These studies establish that growth affects the size and the shape of the segments and consiquently the mass and the moments of inertia. Based on the knowledge that infancy is the period of most rapid growth (Gesell, 1940), it is reasonable to assume that substantial changes of inertia parameters of body segments occur during infancy and these could be crucial for the development of infant locomotion.

PROCEDURES

A mixed longitudinal design was used in the study. Twenty-seven full-term, normal infants aged between two months and nine months at the beginning of the study were chosen as subjects. The subjects were photographed and measured once a month six times.

The data were obtained by tracing the outline of the body by projecting front and side photographic images, then digitizing the outline of the segments. The values of the segment mass and principal moments of inertia were then calculated (Jensen, 1978). Segment densities were considered uniform and as reported by Clauser *et al.* (1969). Polynomial regression (Dixon, 1983) was used to obtain the regression coefficients of the average development curves of segment mass and moments of inertia, and linear regressions were fitted to individual growth curves.

RESULTS

Average regression curves for the upper and lower extremity regions, and the head/trunk, for mass and moments of inertia are shown (Fig.1-5). The means of the individual regressions for segment moments of inertia are shown in Table I.

DISCUSSION

The mean individual growth curves coefficients (Table I) were similar to the coefficients for average development, as shown in the figures. The upper arm mass had the greatest growth velocity for the upper extremity (Fig.1) with the forearm slightly greater than the hand. These differences are also seen in Fig.2 for the antero-posterior and transverse principal moments of inertia. For the lower extremity, the thigh mass had the greatest growth velocity and the foot had the least (Fig.3). This trend is shown more prominently by the longitudinal moment of inertia (Fig.4). These segment development patterns for the upper and lower extremities are consistent with the principle of distal to proximal development (Tanner, 1962).

The relationships between chronological age and segment mass

and segment moments of inertia were linear and significant for most of the regressions. The differences between segments within each region for the mean individual slopes were significant. The growth of the head/trunk region is consistend with cephalocaudal development (Fig.5). However, there are considerable interindividual differences in the intraindividual growth patterns, especially after forty weeks. It is recommended that inertial parameters of body segments be estimated directly rather than by statistical regression with age as the predictor variable.

REFERENCES

Clauser, C. E., et al. AMRL-Technical Report 60-70, Wright-Patterson Air Force Base, OH, 1969.

Dixon, W. J. (1983). *BMDP Statistical Software.* Los Angeles, CA: U. California Press.

Gesell, A., et al. *The First Five Years of Life.* New York: Harper & Row, 1940.

Jensen, R. K. *J. Biomech.*, 11:349-358, 1978.

Jensen, R. K. & Nassas, G. *Med. Science Sports & Exercise*, 20:594-604, 1988.

Jensen, R. K. *J. Biomech.*, 22:529-536, 1989.

Malina, R. M. In Thomas, J. R. (Ed.), *Motor Development During Childhood and Adolescence.* Minneapolis: Burgess, 1984.

Newell, K. M. In Thomas, J. R. (Ed.), *Motor Development During Childhood and Adolescence.* Minneapolis: Burgess, 1984.

Schneider, K., et al. *J. Motor Behavior.* 22:493-520, 1990.

Snyder, R. G., et al. *Anthropometry of Infants, Children and Youths.* Warmendale: Soc. Automotive Engin, 1977.

Tanner, J. M. *Growth at Adolescence.* Oxford: Blackwell, 1962.

Thelen, E., et al. In Woollacott, M. H. & Shumway-Cook, A. (Eds.), *Development of Posture and Gait Across the Life Span.* Columbia: U. S. Carolina Press, 1989.

ACKNOWLEDGMENTS

This research was supported by a research grant from the Natural Sciences and Engineering Research Council of Canada.

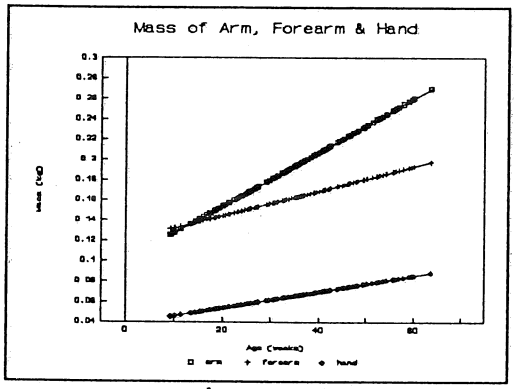

Figure 1

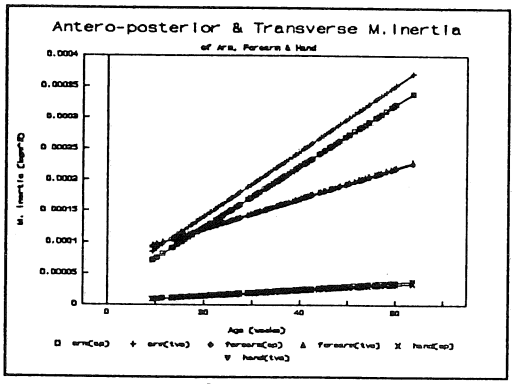

Figure 2

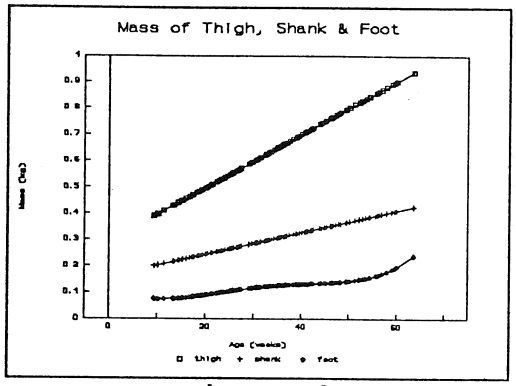

Figure 3

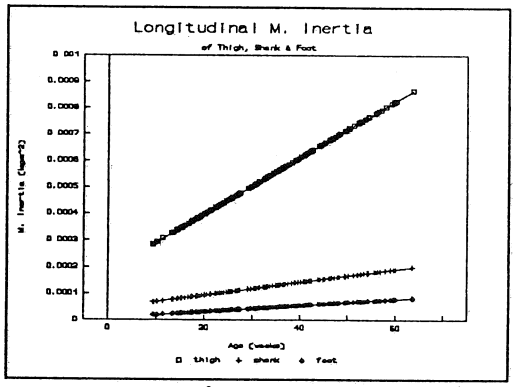

Figure 4

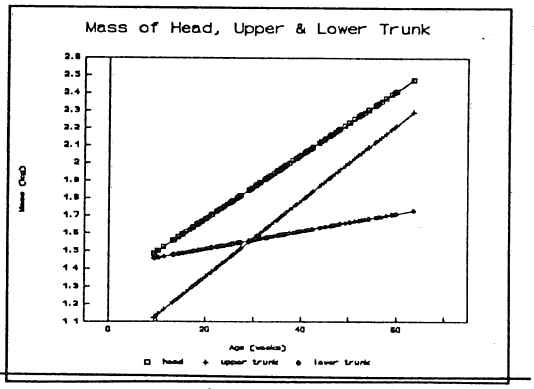

Figure 5

THE EFFECT OF AGE ON THE DYNAMICS OF A CONSTRAINED CHAIR RISE

Margaret Schenkman and Patrick O. Riley

Graduate Program in Physical Therapy, Duke University, Durham, NC
MGH Biomotion Laboratory, Mass General Hospital, Boston, MA

INTRODUCTION

The dynamics of rising from sitting to standing (STS) were compared for 20 healthy older and younger subjects using chairs set at four chair heights relative to the subject's knee height (KH): (115%, 100%, 80%, and 65% KH). Kinematics were determined using a bilateral optoelectronic system integrated with two force plates. There were differences, particularly at lower chair heights, that are indicative of possible alterations in balance control.

REVIEW AND THEORY

Standing up from sitting down is a requirement of daily life that becomes increasingly difficult with age. If one cannot rise to standing independently one cannot accomplish many tasks independently involving and including ambulation. Several investigators. have recently characterized the phases and events of the sit-to-stand activity under a variety of conditions (1-3). Schenkman, Riley, and their colleagues (1,2) have identified four phases of rising from sitting to standing which they named the flexion momentum phase, the momentum transfer phase, the extension phase, and the stabilization phase. The four phase model of STS permits investigators to analyze the stability characteristics of the activity in addition to the body segment displacements that occur and provides a means for quantitative comparisons of balance control of young and elder persons within the context of a functional task. Ikeda et al performed a preliminary comparison of older and younger individuals performing this task from a chair set at 80 % of KH. This analysis indicated that there are subtle differences between the two age groups.

The present study was carried out to further elucidate the differences. The task was made increasingly difficult by decreasing the height of the chair seat relative to each subject's knee height. We hypothesized that as chair height decreased, the maximum head to trunk extension would be significantly decreased in the older subjects and that the maximum extension angular velocity of the trunk, hip, and knee would occur significantly later for the older subjects compared to the younger subjects.

PROCEDURES

Subjects: Twenty one healthy adults were studied: Nine women and two men ages 25 to 36 years (mean age 28.9 +/- 3.0 years, mean height 64.5 +/- 4.0 inches, mean weight 132.4 +/- 25.6 lbs. Four women and six men 61 to 79 years (mean age 67.9 +/- 6.0 years, mean height 67.8 +/- 4.0 inches, mean weight 156.3 +/- 35.0 lbs

Instrumentation: A Selspot II kinematic data acquisition system was used in combination with two Kistler piezoelectric forceplates to simultaneously obtain kinematic and force plate data. Arrays of infrared emitting diodes were anchored to eleven body segments as described previously (1,2). TRACK/NEWTON processing developed at MIT was used to integrate the forceplate and kinematic data. An eleven segment six degree of freedom model developed by Riley et al (1,2) was used as described previously to capture total body motion.

Protocol: Subjects rose in time to a metranome set at 52 bpm from an armless, backless chair as described previously (1). Chair height was varied in relation to each subject's knee height and was set at 115%, 100%, 80%, and 65% of KH.

Data reduction Body segment motions were quantified to identify hip, knee, and ankle excursion; maximum ankle dorsiflexion, head to trunk extension, and trunk flexion; maximum flexion angular velocity of the trunk and extension angular velocity of the trunk, hip, and knee (1) as well as COM and kinetic energy peaks (2). The time at which specific events were achieved was also determined including maximum angles, maximum angular velocities, kinetic energy maxima and minima, and the time at which center of force (COF) and center of mass (COM) first coincided, abbreviated MAZ (2).

Data analysis: The following events, (which occurred in the order noted) were compared by Student's t test: Start of movement, max flexion velocity of the trunk, 1st kinetic energy peak, max trunk flexion, kinetic energy relative minimum, max head extension, max ankle dorsiflexion, MAZ, 2nd kinetic energy peak, max extension velocity of the hip, trunk, and knee respecively, end of movement.

RESULTS

Timing: There were differences of timing of eight of the thirteen events of interest. These differences were generally subtle at the higher chair heights and became increasingly apparent at lower chair heights.(Tab. 1). These differences are analyzed by phase. **Phase I:** the timing of events was the same for young and older subjects at all chair heights. **Phase II:** maximum trunk flexion and MAZ occurred increasingly later for the older compared to younger subjects as chair height decreased. **Phase III:** there were substantial differences in timing of five events, including the second kinetic energy peak, and the maximum extension angular velocities of the trunk, hip, and knee, and the older subjects reached the erect posture slightly earlier at the higher chair heights but at the same time at the lowest chair height. *Excursions, maximum angles achieved*: There were also differences between the young and older subjects with respect to excursions, angles, and angular velocities, and the moment arm between COF and COM

(Tab. 2). At all chair heights knee excursion was decreased for the older subjects, with the greatest decrease seen at 115% KH. The younger subjects continue to reach maximum extension angular velocities of all segments at about the same time, the older subjects show considerable variability in the time at which maximum angular velocities are reached, suggestive of some dissociation of the smooth coordination of the trunk, hip, and knee..

DISCUSSION

As predicted,the differences between the younger and older groups of subjects that were accentuated at the lower chair heights. The differences appear to fall into three groups: Differences in generating maximum angular velocities; differences in control of the COM relative to COP (which may relate to balance control); and differences in segmental excursions and motions (which may also relate to balance control). The task was carried out under controlled conditions, specifically to determine whether older subjects have different dynamic capabilities than do younger subjects. Clearly, in functional situations the older subjects may alter their preferred strategy of standing up from a chair. This and future studies may help to elucidate the differences in dynamic capabilities that necessitate such functional changes.

TABLE 1. Timing of Major Events as a Function of Chair Height and Age (Time in Seconds)

	Phase II						Phase III									
chair Ht as % of KH	max trunk flex		MAZ		max head ext		KEP II		Ext vel trunk		Ext vel hip		Ext vel knee		End vertical ascent	
	y	o	y	o	y	o	y	o	y	o	y	o	y	o	y	o
115	.14	.21	.24	.28	.21	.24	.37	.38	.51	.52	.46	.56	.51	.52	.81	.73
100	.15	.20	.27	.30	.22	.22	.38	.37	.47	.58	.48	.70	.48	.55	.82	.76
80	.19	.24	.19	.28	.29	.38	.44	.45	.57	.64	.53	.59	.56	.56	.92	.87
65	.21	.31	.18	.32	.30	.47	.44	.58	.59	.83	.52	.73	.59	.68	.92	.94

TABLE 2. Angles, excursions, and angular velocities as a function of Chair Height and Age

Chair Height as % KH	Knee excursion in degrees		max head ext. in degrees		ext vel of the trunk /sec		ext vel of the hip /sec		ext vel of the knee /sec	
	y	o	y	o	y	o	y	o	y	o
115%	84	75	33	20	74	71	136	143	121	139
100	91	84	32	16	75	76	149	169	143	157
80	103	96	39	18	86	83	156	188	147	177
65	113	106	29	13	94	103	171	190	163	181

REFERENCES

1. Schenkman, M, Berger R, Riley PO, et al: Whole body movements during rising to standing from sitting. Phys Ther 1990; 6318-648.
2. Riley PO, Schenkman M, Mann RW, et al: Mechanics of a constrained chair rise. J Biomechanics 1991;24:77-85
3. Krajl A, Jaeger RJ, Munih M: Analysis of standing up and sitting down in humans: definitions and normative data presentation. J Biomech 1990; 23: 1123-1138.
4. Ikeda ER, Schenkamn M, Riley PO, et al. Influence of age on dynamics of rising from a chair. Phys Ther 1991;71:473-481

ACKNOWLEDGEMENTS

Supported by grants from the Physical Therapy Foundation and from the US Department of Education, National Institute of Disability and Rehabilitation Research Grants #H133E0024-89 and H13380005.

ANTHROPOLOGY

Podium Session 4

Gait Related Changes in Limb Mechanical Advantage In Humans

A. A. Biewener and J. Chang
Department of Organismal Biology & Anatomy, Univ. of Chicago, Chicago, IL

INTRODUCTION

Considerable attention has been focused on the mechanics of lower limb support in normal human gait. These studies have investigated ground reaction force transmission by the foot and joint moment and muscle force transmission from distal to more proximal joints (e.g. 1,2) largely in an attempt to provide bases for comparing and evaluating abnormal mechanical function associated with various gait pathologies. Accordingly, much of this work has been mainly concerned with the mechanics of walking, rather than running. In addition few, if any, studies have evaluated the mechanics of lower limb support in humans from a comparative locomotor perspective.

In a series of studies, we (3) have shown that changes in locomotor limb posture represent a key mechanism for altering the mechanical advantage of the limb in different sized mammalian species. By running with a more upright posture, larger animals decrease the mass-specific moments developed at limb joints, and hence, the mass-specific forces developed by their limb muscles. In effect, this represents an increase in the (effective) mechanical advantage (EMA= r/R, Fig. 1) of synergistic anti-gravity limb muscles. Given that the cost of locomotion in a variety of quadrupedal mammals appears to depend on the integral of force generated by the limb during support (4), a decrease in muscle force achieved by increased EMA might be expected to result in a decrease in energy cost of locomotion. The erect bipedal posture of humans, which is unique among terrestrial species, therefore, would seem to favor a a comparatively low energy cost of locomotor transport. Empirical data for the energy cost of human bipedalism show, however, that humans have a greater cost of transport compared to quadrupedal mammals of similar size (5).

This study explores this question by testing the hypothesis that the evolution of a fully erect bipedal posture in humans has, in fact, not resulted in a higher mechanical advantage compared to quadrupeds of similar body size. It also examines how mechanical advantage of the limb changes as a function of gait and speed.

METHODS

Four adult male human subjects (body mass range: 67.4 to 80.6 kg) were filmed (100 f/s) in lateral view while they walked or ran over a force platform (Kistler, model 9261A) located midway along a rubber covered runway 40 m in length. Photocells located at 1 m intervals on either side of the force platform provided measurements of velocity at four intervals to establish the eveness of the subject's forward speed. Prior to filming, the joint centers of the hip, knee, ankle and metatarsophalangeal joints were palpated and labelled with dark ink on bright tape markers that were attached to the skin overlying the joint. The subjects wore standard running shoes. Three repeated trials at three walking (slow, preferred and fast) and three running (slow, preferred and fast) speeds

1.

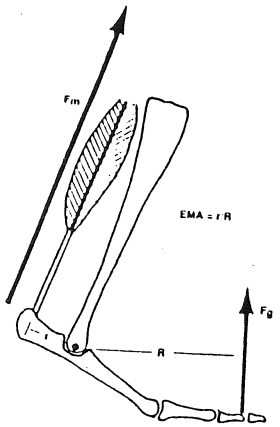

2.

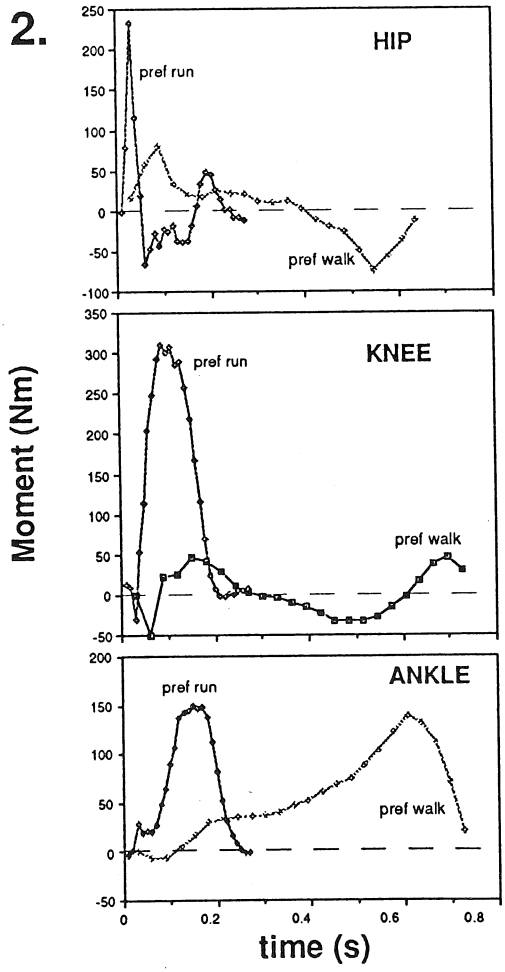

were recorded for each subject. Vertical force outputs from the front and rear of the plate were recorded separately (to establish the center of pressure), together with the horizontal force (fore-aft or 'shear'), photocell output, and a synchronization pulse from the camera's shutter. These signals were sampled at 200 or 500 Hz and entered into a computer for subsequent integration with limb kinematic data and mechanical analysis.

RESULTS & DISCUSSION

Joint moments developed due to external loading of the limb via the ground reaction force (GRF) during a preferred walk and a preferred run are shown in Fig. 2. Inertial moments developed due to segment motion during support were also calculated, but in most cases were quite small (< 5% at ankle; < 15% at knee and hip) compared to those generated by GRF moments. GRF moments, moreover, are those which are most relevant to the question of how limb posture affects muscle mechanical advantage. Although important differences exist at the ankle and hip in terms of the timing of joint moment (and hence, muscle force) development, only at the knee is a significant increase in joint moment observed at a run compared to a walk.

In contrast to its position during walking, in which the knee is fully extended throughout much of support and little power is generated at the joint, during running the knee is held in a flexed position (135 - 144°) during the middle third of support. This greatly decreases the EMA of the quadriceps at the knee (run: 0.33±0.04 vs walk: 0.91±0.18, N=36) at a time when GRF is at its peak, requiring a pronounced increase in extensor muscle force. This also corresponds to the large negative power absorbtion that occurs at this joint in running (1), as the knee flexes and the quadriceps are stretched during weight acceptance. Subsequently, the knee extends as the quadriceps contribute to generate power during push-off of limb support.

Measurements of EMA at each joint as a function of speed (Fig. 3) clearly show the large decrease (3-fold) in knee EMA that occurs as a subject changes gait from walking to running. Hip and ankle EMA's, on the other hand, do not exhibit as great a shift (a 22% decrease in hip EMA vs a 41% increase in ankle EMA). Interestingly, when running, humans have a considerably higher (40%) cost of transport than when walking at their preferred speed (6). This increase in energy cost, therefore, would appear to be at least in part related to the much higher forces that must be generated by the quadriceps to support knee during running.

In comparison to quadrupedal mammals of similar size, the mechanical advantage of the human lower extremity (averaged for the three joints combined) during walking is less than that predicted (Fig. 4 adopted from (3); overall human EMA at a walk: 0.595 vs predicted quadrupedal hindlimb EMA: 0.822), but is within the 95% confidence limit of the regression (0.584). The overall human EMA during running (0.408), however, is significantly less than that predicted for a quadruped of similar size.

The lower EMA of the human lower extremity compared to similar sized quadrupeds is consistent with empirical data showing a greater cost of transport in humans compared to quadrupedal mammals (5). This is particularly the case for

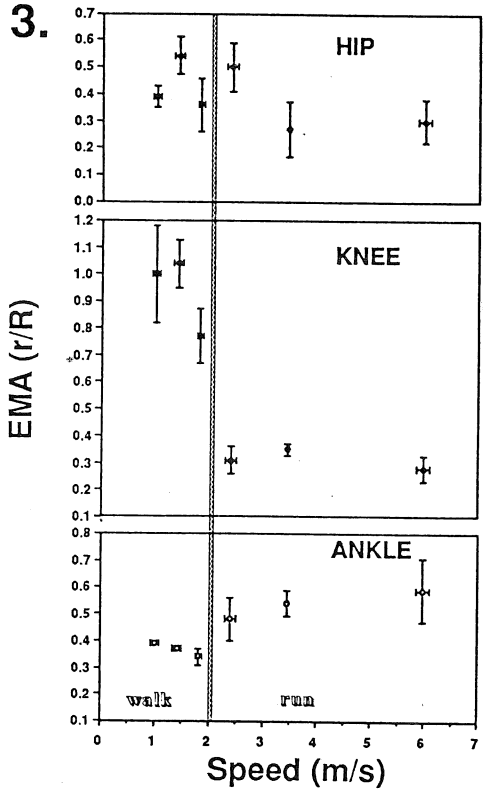

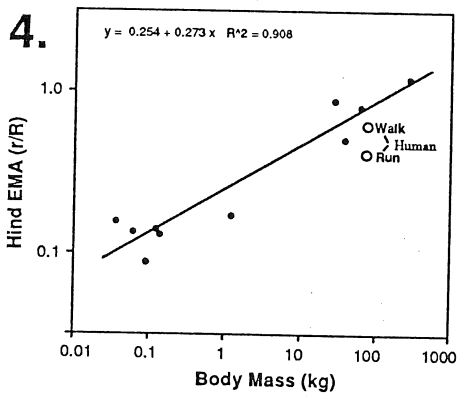

running (for which the cost data were obtained), due primarily to the flexed position of the knee which enables it to absorb and subsequently generate power during the support phase. These data further suggest that there is no energetic savings favored by the evolution of a "fully erect" bipedal gait in humans.

REFERENCES

1. Winter, D.A. (1980). *J. Biomech.* 13: 923.
2. Chao, E.Y. et al. (1983). *J. Biomech.*16: 219.
3. Biewener, A.A. (1989. Science 245: 45.
4. Taylor, C.R. (1985). *J. exp. Biol.* 115: 253.
5. Taylor, C.R. et al. (1970). *Am. J. Physiol.* 219:1104.
6. Farley, C.T. (1991) *Ph.D. Thesis*, Harvard Univesity.
(Supported by NSF grant DCB-9019767)

THE FUNCTIONAL SIGNIFICANCE OF THE FIBULA AS DESCRIBED BY DIFFERENCES IN HUMAN AND CHIMPANZEE

S. McLean, Department of Ex. Sci. and Phys. Ed., Arizona State University, Tempe, AZ.
M. Marzke, Department of Anthropology, Arizona State University, Tempe, AZ.

INTRODUCTION

A portion of the human skeleton receiving little attention with regard for economy of design has been the lower leg, however, the necessity of this two-bone structure has been questioned. Shillingford (1985) suggested that the fibula was not used in weight-bearing but primarily in stabilizing the ankle. Lambert (1971) modelled the lower leg and found that the fibula supported approximately 1/6 of the load transmitted through the tibia. Cavanagh (1980) suggested that a simpler one-bone system could achieve the same functions as the two-bone system.

Goodship *et al.* (1979) investigated the response of simplifying a two-bone system by removing the ulna from the forelimb of pigs. The compressive stress in the radius increased 2-2.5 times in normal walking. The radius functionally remodelled by increasing its cortical thickness to accommodate this increase in stress. This economy of design was present in the horse, ox, and sheep whose fibulae have fused with the larger tibiae.

This trend questions the necessity of the fibula in the human structure. A comparative approach was used to examine differences in the lower extremity between humans and their closest evolutionary relative, the chimpanzee, to determine if any evolutionary changes had occurred. Specifically, the cross-sectional thickness of the fibula was compared to address the functional significance of this bone.

PROCEDURES

15 human and 17 chimpanzee specimens were examined using a GE 9800 series computerized tomography scanner. Seven sites at 5%, 20%, 35%, 50%, 65%, 80%, and 95% of the total bone length were scanned. The cortical thickness on the anterior, posterior, medial and lateral aspects was determined by manually digitizing the CT scans using the Peak Performance Technologies System. Digitizing trials were repeated three times and averaged. Cortical thickness values were normalized to the total length of the bone. A discriminant analysis was used to determine group membership. T-tests were used to follow-up the discriminant analysis to determine significant differences between the human and chimp means.

RESULTS

All aspects, except lateral, showed a strong discrimination between groups (Table 1) for the scan sites between 20% and 80%. Data from the 5% and 95% scan sites were not included because they included trabecular bone. With the exception of the lateral aspect, the chimpanzee had significantly thicker cortical bone than humans (Table 2). The lateral aspect showed significantly thicker cortical bone only at the extreme scan sites.

Table 1 - Structure correlations.

	ANT	POS	MED	LAT
Canonical Corr Coeff	0.8864 (78.6%) *p<0.001*	0.8350 (69.7%) *p<0.001*	0.8895 (79.1%) *p<0.001*	0.8676 (75.3%) *p<0.001*
20%	0.61474	0.28462	0.62573	0.64262
35%	0.68591	0.79211	0.74860	0.16157
50%	0.66178	0.77400	0.47457	0.04381
65%	0.77531	0.58675	0.38136	0.13959
80%	0.84914	0.81914	0.43785	0.57751

Table 2 - Normalized mean cortical thickness (* = $p<0.05$).

	Species	20%	35%	50%	65%	80%
ANT	C	0.062*	0.071*	0.071*	0.075*	0.071*
	H	0.035	0.037	0.037	0.037	0.033
POS	C	0.053	0.074*	0.065*	0.063*	0.061*
	H	0.042	0.049	0.048	0.050	0.040
MED	C	0.056*	0.067*	0.064*	0.063*	0.054*
	H	0.036	0.037	0.041	0.041	0.034
LAT	C	0.068*	0.074	0.069	0.067	0.058*
	H	0.043	0.064	0.067	0.062	0.040

DISCUSSION

The significantly higher normalized cortical thicknesses found in the majority of the sites measured suggested that the fibula was stressed more in the chimpanzee than human. Stress could be applied in various ways but two factors considered here were the forces generated by muscles and weight-bearing functions.

Weight-Bearing

Lambert (1971) modelled the weight-bearing contribution of the fibula in man and found it to be only 1/6 that found in the tibia. However, the chimpanzee fibula appeared to be designed to accommodate a greater vertical load because its distal articular facet had a greater downward inclination (Stern and Susman, 1983). This may have partially explained the larger cortical thickness observed in the chimpanzee.

The stabilizing role of the ankle joint was another factor influencing the stress applied to the fibula. In humans the distal fibula was used as a primary lateral support of the ankle where chimpanzees required less stability from this bone to permit a greater range of motion. The results indicated that the lateral aspect had the least amount of discrimination between the species. This similarity in lateral cortical thickness may have been the result of the increased stabilizing role of the human fibula.

Muscular Influence

In the bipedal locomotion of humans, plantar flexion has been found to be a primary component (Inman *et al.*, 1981). The plantar flexion moment was used both for propulsion through toe-off and control of the foot during heel contact. The primary plantar flexors originating on the fibula (peroneus longus and brevis, and soleus) attached laterally and posteriorly.

In contrast, chimpanzees have combined quadrupedal, suspensory and bipedal modes of locomotion demanding a greater range of motion at the ankle joint. In addition to plantar flexion, the supplementary modes of locomotion required pronation. This has been linked to higher EMG activity for the peroneus longus and brevis (Stern and Susman, 1983). Increased muscle use may have offered the added stimulus needed to maintain a greater cortical thickness.

The higher posterior cortical thickness values exhibited by the chimpanzee may have been linked to the soleus because it attached **only to the posterior fibular head.** The higher anterior cortical thickness could not be easily explained. Further study of the musculature of the lower leg would be necessary to define the exact influence of musculature on the design of the lower leg.

CONCLUSION

The fibula appeared to be a functional bone in our anatomy related to the large dependence on plantar flexion and stability of the ankle joint. This could be related to an economy of design. As human bipedal locomotion has evolved, aspects of the bone have changed from human ancestors related to the weight bearing function of this bone. The decreased muscular dependence on this bone in humans related directly to differences between species in this bone. No evidence has indicated that humans will evolve beyond the need of a two bone system in the lower leg.

REFERENCES

Cavanagh, P.R. The Running Shoe Book, Anderson World Inc., 1980.

Goodship, A.E. *et al. J. Bone Jt. Surg.*, **61A**, 539-546, 1979.

Lambert, L.L. *J. Bone Jt. Surg.*, **53**, 507-513, 1971.

Shillingford, C. Osteology for Radiographers, Blackwell Scientific Publications, 1985.

Stern, J.T. and Susman, R.L. *Am. J. Phys. Anthrop.*, **60**, 279-317, 1983.

Inman, V.T. *et al.*, Human Walking, Williams and Wilkins, (1981).

Swartz, S.M. *Am. J. Phys. Anthrop.*, **83**, 477-498 1990.

ACKNOWLEDGEMENTS

We thank the Primate Foundation of Arizona for providing use of their skeletal primate collection and the Scottsdale Memorial Hospital for use of and technical assistance with their CT scanner.

SUPERQUADRIC MODELING OF CRANIAL ASYMMETRY

T. Y. Shiang, H.J. Sommer, and R.B. Eckhardt

Departments of Mechanical Engineering and Anthropology
The Pennsylvania State University, University Park, PA 16802, USA

INTRODUCTION

Cranial and cerebral asymmetry have been hypothesized as correlates of lateralization of cerebral function, which in turn has been shown to be related to phenomena as diverse as handedness, aphasia, dyslexia, stuttering, autism, and even some disorders of the immune system. Specifically, physical asymmetry of the upper surface of the posterior portion of the left temporal lobe has been related to lateralization of speech function in the left hemisphere for the majority of humans (Geschwind and Galaburda 1987).

A central problem in quantifying cranial and cerebral asymmetry arises from the use of conventional measurement techniques that are diverse, non-comparable, and often imprecise. Consequently, a new method has been developed which fits symmetric superquadric geometric models to three dimensional coordinate measurements from cranial and cerebral surfaces, and models asymmetry as deviation from these symmetric models.

REVIEW AND THEORY

Superquadrics are surface primitives that can be used to model many objects including spheres, ellipsoids, cylinders, cubes, cones, and wedges. A tapered superquadric surface centered on and aligned with local x, y, z axes can be defined using surface coordinates η and ω which correspond respectively to latitude and longitude as shown below. Parameters a_x, a_y, and a_z are principal radii of the superquadric. Parameter e1 is the squareness parameter in planes parallel to the z axis, and e2 is the squareness parameter in planes parallel to the x-y plane. Squareness parameters less than one effectively provide corners on the superquadric. Taper parameters k_x and k_y provide linear taper along the z axis.

$$x = f_x(z)\, a_x\, (\cos\eta)^{e1}\, (\cos\omega)^{e2}$$
$$y = f_y(z)\, a_y\, (\cos\eta)^{e1}\, (\sin\omega)^{e2}$$
$$z = a_z\, (\sin\eta)^{e1}$$
$$f_x(z) = z\, k_x / a_z + 1 \quad \text{for} \quad -1 \le k_x \le 1$$
$$f_y(z) = z\, k_y / a_z + 1 \quad \text{for} \quad -1 \le k_y \le 1$$

Surface points defined in the local superquadric coordinate system can be transformed into global coordinates (X,Y,Z) using position parameters p_x, p_y, and p_z and Euler angle rotation parameters ϕ, θ, and ψ. A global superquadric model with taper can then be defined using 13 parameters (a_x, a_y, a_z, e1, e2, k_x, k_y, p_x, p_y, p_z, ϕ, θ, ψ). Given global coordinates for surface points, the superquadric parameters can be iteratively adjusted to fit a superquadric surface using the implicit inside-out function of Solina and Bacsy (1990).

PROCEDURES

Typically 225 points per skull were digitized over the external cranial vault surfaces of 20 dried adult human skulls, and computationally aligned with Frankfort Horizontal conventions (X superior, Y right, Z anterior). Superquadric models were then determined to provide best fits for each cranial surface data set. Roll ϕ about the anterior-posterior (AP) axis and yaw ψ about the inferior-superior (IS) axis, were constrained to zero to force bilateral symmetry of the superquadric models.

A key conceptual feature of this approach is that superquadrics are inherently symmetric. Consequently, asymmetry in the experimental data was quantified by radial deviations of individual data points from the best fit superquadric model (Sommer and Miller, 1980). These deviations were presented in polar contour form to visualize surface variation as a function of right-left (RL) and AP location. Average deviation contours for all crania were also combined to assess normative asymmetry of the entire specimen set (Sommer and Miller, 1981).

RESULTS

Means of best fit superquadric parameters over all 20 skulls are reported below with single standard deviations in parentheses. The center of the normative superquadric model was 33.76 mm (±5.33 mm) above Frankfort Horizontal, 0.66 mm (±3.70 mm) posterior to the tragions, and in the sagital plane (±2.05 mm). Mean orientation of the largest principal radius was 14.53 degrees

(±6.63 degrees) below Frankfort Horizontal. Mean principal radii were IS 69.71 mm (±5.19 mm), AP 80.23 mm (±4.31 mm), and RL 70.78 mm (±2.05 mm). The mean squareness parameter in sagital/transverse planes was 0.890 (±0.043) and in frontal planes was 0.927 (±0.043). The mean taper parameter in the sagital plane was 0.003 (±0.052) and in the transverse plane was -0.068 (±0.036).

A typical contour plot of asymmetry in the form of radial residuals is shown in Figure 1 using polar coordinates from a superior view. The center of the polar plot is the zenith of the skull. Circles indicate latitude angles of 75, 60, 45, 30, and 15 degrees respectively from the center. The outer circle is Frankfort Horizontal at 0 degrees latitude. The skull shown in Figure 1 demonstrates positive radial residuals in the left inferior posterior region, and is typical of the majority of skulls that were digitized.

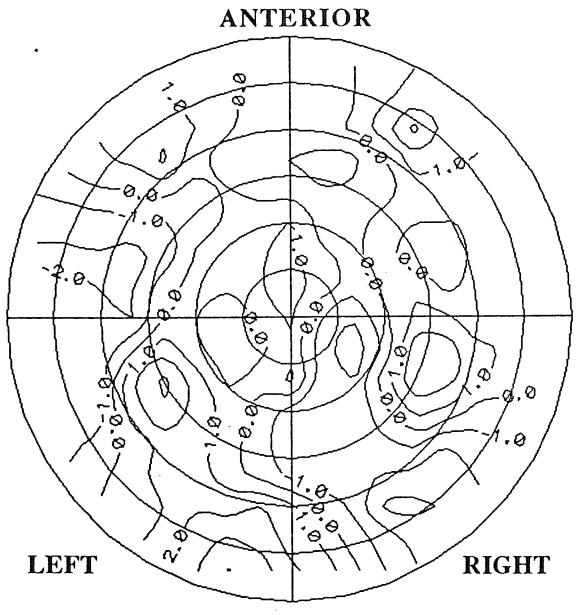

Figure 1. Superior View of Radial Residual Contours of Experimental Surface Data Minus Superquadric Model (Contours in mm, Circles Indicate Latitude Angles)

All skulls showed paired symmetric posterior parietal bulges of 2 to 3 mm at 45 degrees latitude and 25 degrees posterior longitude; and paired symmetric anterior bulges of 1 to 2 mm near the eyebrows at 20 degrees latitude and 50 to 55 degrees anterior longitude. Average residual contours accumulated over all 20 skulls demonstrate these symmetric bulges at the parietal bones and eyebrows with excellent statistical replicability, and are otherwise almost perfectly symmetric except for a positive radial bulge in the left inferior posterior region.

DISCUSSION

Superquadric parameters accurately modeled skull shape variation. Respective superquadric principal radii correlated very well to traditional sliding caliper measurements of skull AP length and RL width. Mean superquadric parameters indicated moderate skull squareness and seven percent mean taper in transverse planes (narrower anterior) with larger variation in taper in the sagital plane. These preliminary findings are particularly important in that they provide bases for quantitative measurements previously not available from simple caliper measurements.

The most striking observation of anatomical variation available from the radial residual contours, is that all skulls demonstrated marked asymmetry in the inferior posterior region. A majority of the skulls measured in this study had positive bulges of 1 to 3 mm in the left inferior posterior region below 30 degrees latitude and within 65 to 80 degrees posterior longitude. In a very preliminary sense, the general tendency for left posterior cranial asymmetry in this limited sample set may be viewed as an inferential correlate of cerebral asymmetry in the left posterior temporal lobe. More importantly, it demonstrates the improved precision in quantifying asymmetry that is provided by this new superquadric surface modelling technique.

REFERENCES

Geschwind, N. and Galaburda, A. *Cerebral Lateralization.*, MIT Press, 1987.

Solina, F. and Bajcsy, R. *IEEE PAMI* 12(12):131-147, 1990.

Sommer, H. J. and Miller, N. R. *ASME Adv. in Bioeng.* pp. 221-223, 1980.

Sommer, H. J. and Miller, N. R. *ASME Biomech. Symp.* AMD-43:229-231, 1981.

Proceedings of NACOB II, The Second North American Congress on Biomechanics, Chicago, August 24th - 28th, 1992

Center of Mass of Trunk Segments relative to the Spine as Determined by Computed Tomography

D.J. Pearsall[a], J.G. Reid[a,b], L.A. Livingston[c]

[a] Department of Anatomy, Queen's University
[b] School of Physical and Health Education, Queen's University
[c] Department of Physical Education, Wilfrid Laurier University

INTRODUCTION

This study employed CT imaging technology to determine *in vivo* the location of the center of mass of discrete segments of the human torso with respect to the three cardinal anatomical planes. Four subjects, two male and two female (ages 46 to 68 yrs), had serial CT scans collected at 1 cm intervals for the full length of the trunk. The grey scale of the scans was correlated to tissue densities, thus, enabling trunk section mass properties to be calculated. The findings of this study did not concur with all previous reports. The center of mass and center of volume of vertebral trunk segments were shown to be coincident except in the mid-thoracic region. With regards to the vertebral centroids of the spine, the respective center of mass was found to coincide along the anteroposterior axis. However, within the sagittal plane, the center of mass locations were found to be anterior to most of the vertebral centroids, contrary to popular belief. The centers of mass of the upper and lower torso segments were found to be similar to volumetric estimation techniques in the transverse plane but varied in the longitudinal direction. Although of limited sample size, this study has provided insight into the mass distribution properties of the human torso that is of significance for use in biomechanical modeling of the trunk and spine.

REVIEW AND THEORY

Predictive models of muscular and joint reactive forces about the vertebral column in addition to postural balance studies require the precise knowledge of segmental mass and inertial parameters to create as true a mechanical representation of the body's structure as possible. However, estimates of these torso properties have been derived from only a few cadaveric studies of limited sample size (Dempster, 1955; Liu and Wickstrom, 1973). Consequently, our restricted knowledge of the mass properties of the trunk remains a limiting factor to the validity of mechanical models of the trunk and spine.

However, recent technological advances permit for better estimates to be made. For instance, from computed tomographic (CT) scans it has been possible to determine tissue densities and discrete segment properties *in vivo*. (Huang and Suarez, 1983; Reid, 1984). Hence, the purpose of the present study was to take advantage of CT imaging technology so as to determine the location of the segmental center of mass of the trunk segment within the three cardinal anatomical planes of live subjects.

METHOD

Four adults, two men and two women, comprised the subject sample (age = 46 - 68 yrs; height = 152.4 -185.3 cm; mass = 62.3 - 75.9 kg). CT images were obtained on a CT/T Continuum scanner using a window size of 250 and a CT number -027. Transverse CT images of the trunk were collected at 1 cm intervals from the superior surface of the symphysis pubis to the level of the first thoracic vertebrae.

Several properties were estimated from the CT scans including mass, volume, and density distribution. The trunk was separated into several segments. Each segment was comprised of several transverse slices derived from CT scans. The segment combinations examined included (a) vertebral trunk segments from T1 to L5, inclusively, (b) the upper trunk segment (T1 to T12), (c) the lower trunk segment (L1 to L5, plus S1 to S5), and (d) the whole trunk segment (T1 to S5).

RESULTS AND DISCUSSION

In the frontal plane, the position of vertebral segment centers of mass (SCM) relative to the vertebral centroids (VC), from the level of the first thoracic to the fifth lumbar vertebrae, were essentially coincident. These results concur with previous findings by Liu and Wickstrom (1973). In both studies, the VC and SCM locations varied slightly to the right of the trunk's geometric midline in the thoracic region. The centers of mass appeared to mimic the vertebral curvature in the frontal plane, thereby suggesting a potential relationship between lateral curvatures of the spine and mass distribution within the trunk segment.

In the sagittal plane, the SCM and SCV were found to coincide while following a slight curvilinear path except for the mid-thoracic region where the SCV tended to lie anterior to SCM by up to a maximum of 0.7 cm at T4 (see Fig. 1). Along the transverse axis, the SCM was situated in very close proximity to the SCV.

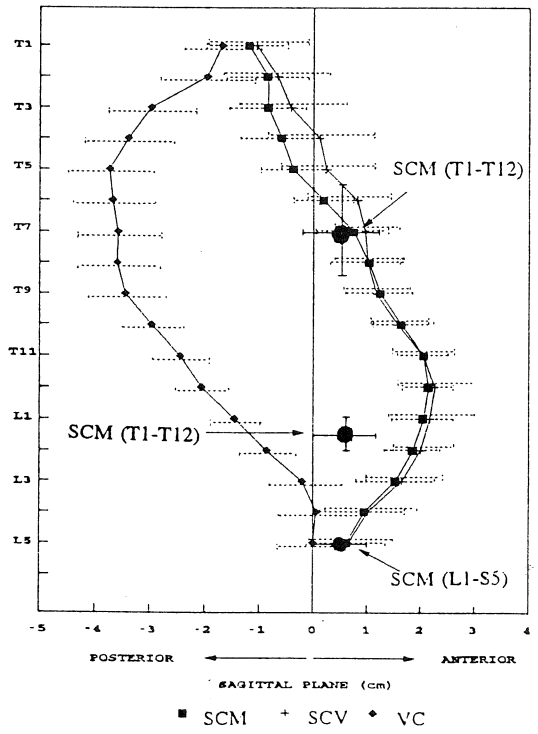

Figure 1. SCM, SCV and VC of trunk segments in the sagittal plane.

The profile of vertebral centroids (VC) was observed to reflected the normal primary (thoracic and sacral) and secondary (lumbar) curvatures of the spinal column within the sagittal plane (see Fig.1). The SCM positions were not found to coincide with the VC profile except at the levels of T1 and L3 to L5 inclusive. The results indicated that the SCM was anterior to its respective VC at most levels. The SCM-VC displacement was greatest in the mid-spine, ranging from 0.6 (0.5) cm at T1 to 4.7 (0.5) cm at T9 to 0.7 (0.7) cm at L5. These findings are similar to those reported by the cadaver study by Liu and Wickstrom (1973) but conflict with the findings of Duval-Beaupère and Robain (1987) gamma-ray scan study. These and previous results appear to contradict the predominant belief that the trunk mass must be centred about the vertebral column for it to effectively support the mass of the erect trunk in the sagittal plane.

The SCM of the upper and lower trunk segments were found to be opposite the T7 and L5 vertebral levels, respectively. The SCM of the total trunk was determined to be at the L1/L2 vertebral level or 52.9% the trunk length. Volume estimation techniques tended to locate SCV one vertebral segment higher than SCM positions. In the transverse plane, the trunk's SCM was located at the approximate geometric center of the trunk segment

The results of this study may have important implications for biomechanical modeling since refinement of future models of human motion will require an enhanced understanding of the discrete segmental properties of the trunk.

REFERENCES

Dempster, W.T. *USAF WADC Technical Report 55-159.* Wright-Patterson Air Force Base, Ohio, 1955.

Duval-Beaupère, G.; Robain, G., *Int. Ortho.* **11**:262-269, 1987.

Huang, H.K., Suarez, F.R. *J. Biomechanics* **16**, 821-832, 1983.

Liu, Y.K.; Wickstrom, J.K. *Perspectives in Biomedical Engineering*, Ed: R.M.Kenedi. University Park Press, 203-213, 1973.

Reid, J.G. *Arch. Phy. Med. Rehab.*, **65**, 246-250, 1984.

ACKNOWLEDGEMENT

This study was supported by the Natural Sciences and Engineering Research Council of Canada (Project A7154)

ANTHROPOMETRY

Poster

CALCULATED FIBER LENGTHS IN CAT GASTROCNEMIUS MUSCLE DURING WALKING

T. Allinger and W. Herzog*

Department of Mechanical Engineering, University of Calgary, Alberta.
* Faculty of Physical Education, University of Calgary, Alberta.

INTRODUCTION

Although data on entire muscle-tendon length of cat medial gastrocnemius muscle during walking are abundant, there is little information on corresponding fiber lengths. A muscle model was developed to calculate fiber lengths of cat gastrocnemius muscle as a function of knee and ankle joint angles and muscular forces. The model also contains non-linear properties of elastic elements in series with the gastrocnemius fibers. Fiber lengths were calculated using a constant muscle width assumption. Because tendon elasticity may be critical in the calculation of muscle fiber lengths, a rigid tendon was compared to a "normal" tendon. Stress-strain properties of this "normal" tendon were obtained experimentally. During the stance phase, gastrocnemius fibers were found to shorten, in general, although periods of lengthening occurred. The rigid tendon produced larger changes in fiber length and on average caused the fibers to be at a less favorable length on the force-length curve during the step cycle than the "normal" tendon. It is hypothesized that with increasing speeds of locomotion, the "normal" tendon will allow muscle fibers to be at a more optimal length/velocity than the rigid tendon.

REVIEW AND THEORY

Information on fiber length and velocity is crucial in assessing the instantaneous contractile conditions of muscle and in determining the maximum possible force that could be developed by a muscle during locomotion. Of particular interest is the behavior of the fiber during active lengthening. For slow walking, the cat medial gastrocnemius muscle-tendon lengthens during the initial stance phase (E2), (Goslow, et al., 1973; Walmsley, et al., 1978). However, corresponding data on fiber lengths were not reported. In order to determine fiber lengths, changes in tendon lengths and angles of pinnation must be considered. Unverified experimental measures indicate that fiber length remains nearly isometric during E2 (Hoffer, et al., 1989). Theoretical predictions of the behavior of muscle fibers during the E2 stance phase are not present in the literature. Since fiber length is partly dependent on tendon properties, the effect of fiber length using a "normal" and a rigid tendon in the muscle model are evaluated. The purpose of this study was to assess the effects of tendon stiffness on fiber lengths for cat gastrocnemius muscle during slow walking.

PROCEDURES

Kinematics of the left hind limb were obtained using high speed cinematography (100 Hz) for one cat (5.0 kg) walking on a motor driven treadmill at a nominal speed of 0.4 m/s. Forces in the soleus, gastrocnemius, and plantaris muscles were measured using E-shaped tendon force transducers (Herzog and Leonard, 1991).

Three "steady state" step cycles were chosen for a frame-by-frame analysis. The greater trochanter, lateral femoral condyle, lateral malleolus, calcaneus, and metatarsal head were manually digitized in each film frame. Knee and ankle joint angles were then calculated from the digitized data. The knee and ankle joint angles of the three selected steps were averaged. Muscle origins and insertions were measured from the cat, posthumous. Muscle-tendon lengths were then determined for each instant in time assuming a straight line from origin to insertion.

Tendon lengths were calculated from a stress-strain relation,

$$\text{strain} = (\ln(\text{stress}) - b) / m$$

where:

stress = tendon force / resting tendon cross sectional area (N/mm^2)

strain = tendon elongation / resting tendon length

b and m were empirical constants.

"Normal" tendon constants were m = 104.68 and b = -0.62, while for the rigid tendon case no strain could occur. Muscle belly length (ML) was calculated as muscle-tendon length minus tendon length (T1+T2).

The muscle was modeled as two tendons on either side of a single fiber (Figure 1). Muscle and tendon properties were assumed to be constant along the length of the muscle, thus the proximal tendon length (T1) plus the distal tendon length (T2) was the same for all fibers in the muscle. If a proximal fiber was examined, the length of T1 would be small while the length of T2 would be large. Likewise, a distal fiber would have a large T1 and a small T2 length. From the instantaneous knee and ankle joint angles and the corresponding tendon forces during walking, gastrocnemius muscle belly lengths (ML), and fiber lengths (FL) were derived, assuming that the muscle width (MW) remained constant. Therefore, during a shortening contraction, the length of the muscle belly decreased and the angle of pinnation (α) increased. Muscle width was calculated from the resting angle of pinnation and fiber length. Thus,

$$FL = \text{sqrt}(MW^2 + ML^2)$$

and

$$\alpha = \arccos(ML / FL)$$

The above analysis was executed on raw data. Results were then filtered using a Butterworth low pass filter with a sample to cut-off frequency ratio of 7.5. Only results for the gastrocnemius muscle are presented.

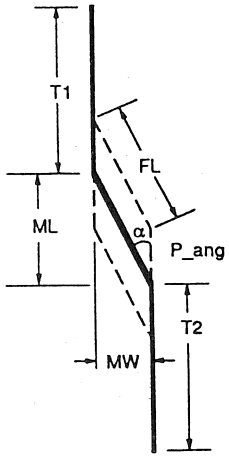

Figure 1. Diagram of pinnate muscle model used to calculate fiber length.

RESULTS

Knee and ankle joint angles were generally in-phase and followed a similar pattern (Figure 2). During the initial stance phase (E2), the knee and ankle joint angles decreased and then increased through the E3 phase until push-off. Following push-off, knee and ankle joint angles decreased during the initial swing phase (F) and then increased again (E1) before touch down.

The muscle-tendon length increased about 1 mm after touch down (during the E2 stance phase) and then generally decreased 6 mm (during the E3 stance phase) until push-off (Figure 2). During the passive swing phase, the muscle-tendon length increased 9 mm (F phase) until it started to decrease (E1 phase) before touch-down. Because of the in-phase behavior of the knee and ankle joint angles, the changes in gastrocnemius muscle-tendon length were less than those of the one-joint, soleus muscle (not shown).

The effective tendon length increased and decreased during the stance phase following the time course of the gastrocnemius force (Figure 2). During the swing phase the gastrocnemius forces were not great enough to cause measurable strain in the tendon. "Normal" tendon properties exhibited a 1.5 mm increase in tendon length during the stance phase.

Changes in fiber length ("normal" tendon model) were similar but smaller in magnitude than changes in gastrocnemius muscle-tendon length with one notable exception. Right after touch down (i.e. at the start of the E2 phase), gastrocnemius muscle-tendon length remained nearly constant, whereas fiber lengths clearly decreased in the "normal" tendon model. Noticeable differences in the fiber length between the "normal" and stiff tendon model occurred only during the stance phase. At the end of the stance phase the two curves merged when the force in the gastrocnemius muscle decreased and the tendon length became the same in both models.

Only results of the phase where the two tendon models differ will follow. The rigid tendon model had fiber lengths slighlty greater than the resting fiber length (23 mm). However, the "normal" tendon model had fiber lengths that fluctuated near the resting fiber length. During the E2 phase, the fiber lengthened more for the stiff tendon model than for the "normal" tendon model. Also, the fiber length of the stiff tendon model fluctuated more in magnitude than the fiber length of the "normal" tendon model.

DISCUSSION

Ankle and knee joint angles exhibited a similar behavior to those reported in the literature (Goslow, et al., 1973; Walmsley, et al., 1978). Muscle-tendon lengths also followed the same trends as those in the literature, except there was more length fluctuation in the E3 period. At faster speeds of locomotion than were analyzed here (0.4m/s) larger increases in muscle-tendon length would be expected in the initial stance phase, E2 (Goslow, et al., 1973).

Hoffer et al. (1989) found experimentally that fiber length of the cat medial gastrocnemius muscle remained nearly constant during the E2 period while the muscle-tendon length increased by 2 mm. The "normal" tendon model used here showed fiber length behavior closer to the experimental data (Hoffer et al., 1989) than did the stiff tendon model. However, the fiber length increased in both tendon models for at least some period during the E2 phase. The differences in the results shown here and those by Hoffer et al. (1989) may be associated with the tremendous difficulty of measuring (or calculating) fiber lengths accurately.

Stiff tendon properties resulted in greater velocities and larger changes in length of fibers in the gastrocnemius muscle than those calculated using "normal" tendon properties. This phenomenon only becomes apparent during periods of high muscular force production. Therefore, tendon properties are likely to become even more important in the determination of fiber kinematics in high intensity movements, such as jumping or galloping than they are in slow walking.

Direct measurements of fiber kinematics in a chronic animal model are not trivial, and theoretical predictions of fiber kinematics lack the possibility of vigorous validation. It will be a challenge in the future to develop accurate and reliable measurements of in-vivo fiber kinematics and to model fiber kinematics in a realistic way.

REFERENCES

Goslow, et al., J. Morph., 141:1-42, 1973.
Herzog, et al., J. Biom., 24(S1):31-39, 1991.
Hoffer, et al., Prog. Brain Res., 80:75-85, 1989.
Walmsley, et al., J. Neurophysiol., 41(5):1203-1216, 1978.

ACKNOWLEDGEMENTS

This study was supported by NSERC of Canada.

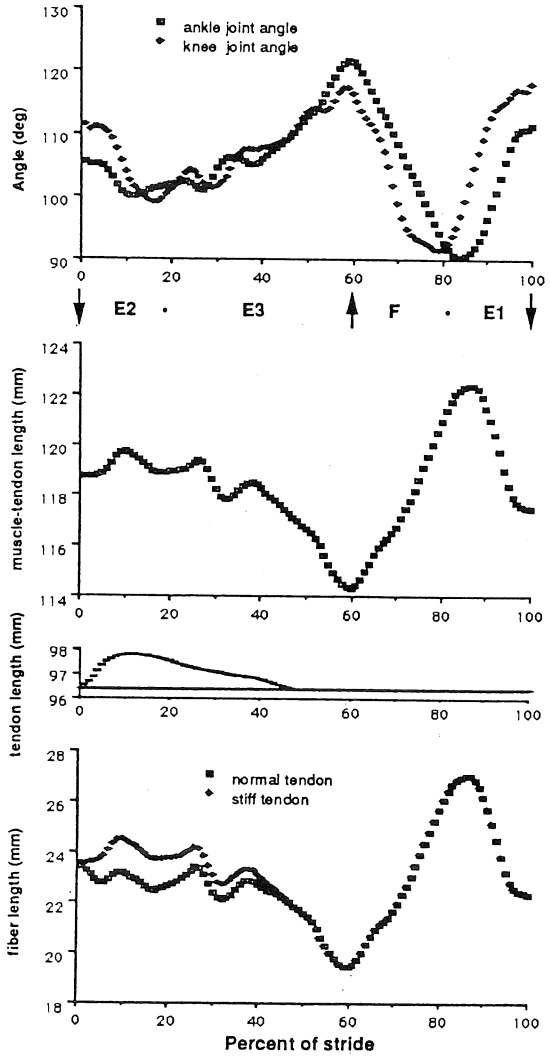

Figure 2. Selected variables as a function of normalized stride time. | indicates touch-down and | indicates lift-off. F, E1, E2, E3 are stride phases described by Goslow et al. (1973).

Proceedings of NACOB II, The Second North American Congress on Biomechanics, Chicago, August 24th - 28th, 1992

DETERMINATION OF FETAL LIMB SEGMENTAL WEIGHTS FROM MEASUREMENTS OBTAINABLE FROM ULTRASOUND IMAGING

C Riegger-Krugh

Division of Physical Therapy CB #7135 Medical School Wing E
University of North Carolina at Chapel Hill Chapel Hill NC 27599-7135

INTRODUCTION

Anthropometric measurements that may be obtainable from the fetal ultrasound image were measured on normal appearing stillborn fetuses. Measurements of segmental length and diameter were used to calculate the volumes of the thigh, leg, foot, arm and forearm modeled as truncated cones and the hand modeled as a sphere. Segmental volumes were multiplied by the specific gravity to determine segmental mass.

REVIEW AND THEORY

Knowledge of segmental weights is required to establish normal body proportion changes throughout fetal development. Segmental weights have been documented mainly for adult white males (1), to a lesser extent for women and children (5), and mostly qualitatively for fetuses (6). This knowledge is also required to estimate net muscle moments during functional movement. Normal and abnormal fetal movement are presently being documented (7).

Of the numerous methods of determining segmental weight, immersion, balance board, gamma scanner, elliptical zone, and direct weighing methods are not suitable for use with viable fetuses. The geometrical modeling method could be used with viable fetuses. The best validation of segmental mass or weight calculation is by direct weighing of the segment, when this in vitro method is possible.

Research hypothesis: Fetal limb segmental masses calculated by multiplying segmental volume calculated from anthropometic measurements, which could be obtained from the fetal ultrasound image, and fetal limb density will not be significantly different from direct segmental weighings.

PROCEDURES

Subjects: 27 normal appearing stillborn fetuses of various ages.

Anthropometric measurements: Lengths and sagittal and frontal plane diameters of the segments were measured with either a tape measure, which was secured to a measurement board, or with skin calipers. Measurements were either defined by Lohman (3) or were operationally defined.

Direct segmental weighings: The segments were dissected at the joints surface and weighed on a balance scale.

Calculations: Segmental volume of segments modeled as truncated cones was $\frac{1(Cp^2 + Cd^2 + CpCd)}{12\ pi}$, where 1 = segmental length and Cp and Cd are the proximal and distal circumferences, respectively, of the segments. The equation was modified to $.26\ 1\ (Dp^2 + Dd^2 + DPDd)$, where 1 = the segmental length and Dp and Dd are the proximal and distal diameters, respectively. Sagittal and frontal plane diameters were averaged for the foot, because the foot shape is markedly noncircular. Sagittal plane

diameters were used for all other segments. Segmental volume of the hand was 4/3 x (Radius of the hand)^3, with the radius of the hand defined as hand length/3. **Density** of each limb segment was assumed to be 1.0 gm/cm3. **Segmental mass** = Segmental volume x density. **Segmental weight** = Segmental mass x 9.81 m/sec^2.

Data analysis: Calculated segmental mass of each segment was compared, by the paired t-test, to the respective segmental mass recorded when the dissected segment was placed on a balance scale. The level of significance was p=.05.

RESULTS

Means, Standard Deviations (SD), and p values of the comparison of direct weighings and calculated segmental masses are listed in **Table I**. Calculated and directly weighed segmental masses were not significantly different for the thigh and the foot. Calculated segmental mass was larger than the direct weighing for the arm, forearm, and hand, and smaller for the leg.

DISCUSSION

The results suggest that, with valid measurement of limb segmental length and diameter from the fetal ultrasound image, fetal thigh and foot segmental weight could be accurately calculated. Operational definitions of segmental length may result in overestimation of segmental volume of the arm and forearm, while hand radius may be overestimated if the hand length is divided by 3. Leg segmental volume may be underestimated, because the proximal diameter does not include the increased circumference of the midcalf.

Fetal femoral segmental lengths have been measured from ultrasound imagings and validated with X-ray (4), indicating the possibility of valid measurement of fetal segmental lengths with appropriate equipment.

REFERENCES

1. Dempster WT. Space Requirements of Seated Operator, (WADCTR 55-159), 1955.
2. Hanavan EP. A Mathematical Model of the Human Body (ARML-TR-64-102), 1964.
3. Lohman T, et al. Anthropometic Standardization Reference Manual, 1988.
4. O'Brien GD et al. Assessment of gestational age... Am J Ob Gyn, 1981.
5. Pheasant S. Bodyspace, 1988.
6. Scammon RE and Calkins LA. Growth in the Fetal Period, U Minn Press, 1929.
7. Sparling JW, Wilhelm IJ, et al. Developing a taxonomy of fetal movement, Phys and Occup Therapy in Pediatrics 10(1), 1990.

TABLE I

Segment	Direct weight gm Mean +/- SD	Calculated weight gm Mean +/- SD	p value
Arm	16.3 =/- 18.5	20.0 =/- 23.9	.01
Forearm	10.6 +/- 12.7	12.7 +/- 16.2	.02
Hand	6.1 +/- 5.76	4.0 +/- 4.1	.0001
Thigh	35.7 +/- 34.1	34.1 +/- 43.6	.40
Leg (calf)	17.1 +/- 21.1	13.8 +/- 15.9	.02
Foot	8.9 +/- 9.3	6.8 +/- 8.9	.003

DETERMINATION OF THE MOMENT OF INERTIA OF HUMAN LOWER LEG USING THE SMALL OSCILLATION TECHNIQUE

Mario Lamontagne[1,2] and Steve McFaull[1]

School of Human Kinetics[1] and Department of Anatomy[2]
University of Ottawa
Ottawa, Ontario, Canada K1N 6N5

INTRODUCTION

For practical considerations, the area biomechanics relies heavily on modelling as a mean of understanding the mechanics of the human body in various situations. Early models of the human system (Bresler and Frankel, 1950) treated the articulations rather simplistically as resistance free, kinematically constrained hinge joints and all segment parameter data were retrieved from cadaverous experimentation. More recent models of the human system (Hatze, 1976) have demanded more accurate and detailed segment and joint data. The mass, centre of mass and moment of inertia of human segments as well as the passive viscoelastic properties of human joints are essential parameters in the development of accurate human joint modelling.

The determination of moment of inertia of *in situ* body segment can be performed by using various known methods such pendulum method (Hill, 1940), calculation method (Hanavan, 1964), and quick release method (Cavanagh and Gregor, 1974) but all these methods present difficulties and weaknesses. The small oscillation method is relatively simple, requires few calculations, and depends upon only a few parameters.

The present investigation consists of the validation of an application of the small damped oscillation method for the determination of the moment of inertia of human lower leg.

THEORETICAL CONSIDERATIONS

Joint consists of two adjacent segments attached with muscles. In a perfectly relaxed condition, the joint is still subjected to passive moment of force when moving in the vertical plane. The nonlinear elastic moment of force $M_e(\theta)$ is due to the elastic structures spanning the joint. The nonlinear viscous moment of force $M_v(\theta,\dot{\theta})$ depends on the viscous components in the joint. The small damped oscillatwn theory (Wells, 1967; Goldstein, 1981) allows a generally non-linear situation to be linearized for sufficiently small intervals of oscillation.

Linearization of $M_e(\theta)$ and $M_v(\theta,\dot{\theta})$

The function $M_e(\theta)$ can be linearized by retaining the first two terms of the Taylor series expansion (Hurley, 1981):

$$M_e(\theta + \theta^*) = M_e(\theta^*) + \theta K_e(\theta^*) \quad (1)$$

where θ^* is the joint angle at about which the small oscillations are taking place and $K_e(\theta)$ is the first derivative (stiffness) of $M_e(\theta)$ with respect to θ.

Over a small interval of oscillation the function $M_v(\theta,\dot{\theta})$ can be linearized by assuming that (Hatze, 1975; Engin, 1984):

$$M_v(\theta,\dot{\theta}) = C_K(\theta)\dot{\theta} \quad (2)$$

where $C_K(\theta)$ is the angular damping coefficient of the joint. It is expected that this function is well behaved and is not strongly dependant on θ or contain singularities (Engin, 1984). Hence for a small oscillation of the leg-foot segment about an equilibrium position θ^*, $C_K(\theta^*)$ can be taken as constant. Thus the function $C_K(\theta)$ can be mapped out over the entire range of knee joint motion by using this piecewise linear approximation technique.

For small oscillations the equation of motion is linear as is given by

$$(I_l + I_a)\ddot{\phi} + [C_K(\theta^*)]\dot{\phi} + [Kd^2 + K_e(\theta^*)]\phi = 0 \quad (3)$$

Equation (3) is a standard second order homogenous linear differential equation with solution (Tierny, 1979)

$$\phi(t) = \phi_o e^{-\zeta\omega_n t}\left[\left(\frac{\zeta\omega_n}{\omega_d}\right)\sin\omega_d t + \cos\omega_d t\right] \quad (4)$$

Analysis of equation (4) leads to the equation for the damping coefficient

$$C_K(\theta^*) = \frac{2\delta(I_l + I_a)}{\tau} \quad (5)$$

where δ is the logarithmic decrement and τ is the time period of the oscillation both of which can be obtained from the output of the load cell of the SOA. The moment of inertia of the segment can be found from the system of equations and substituted into equation (5), where

$$I_l = \left[\frac{\tau^2(Kd^2 + K_e(\theta^*))}{(4\pi^2 + \delta^2)}\right] - m_a d^2 \quad (6)$$

EXPERIMENTAL PROCEDURES

The small oscillation apparatus (SOA) is a custom made device (2.95m height x 1.5 m width). Two frames are hinged and allow various body positions (knee angles) to be attained while keeping the leg horizontal (which is a requirement of the technique)(Figure 1; side view). The subjects leg is fixed in the ankle clamp and the system is displaced by a small amount (less than 8°). The leg will undergo underdamped oscillations under the restoring forces of the linear springs (two custom made springs (Hi-Bek Precision Spring Company Ltd.) and the passive moments.

The validation procedures were carried out using a mass, an aluminum plate, and nylon cylinder (Canus Plastics inc., Ottawa) of known physical properties. The moment of inetia of the nylon cylinder is 0.4768 which are comparable to a human leg. The mass, aluminum plate, and the nylon cylinder are successively and securely positioned in the SOA with the distal clamp. The mass, plate, and cylinder-springs system are displaced by a small amount (less than 8°) and the system undergoes undamped oscillations the amplitude of which is proportional to the load cell output. The analog signal from the load cell was amplified, A\D converted and collected on a Compaq 386 (16 MHz) microcomputer at 100 Hz for later processing. The load cell signal was digitally filtered (dual pass, second order low pass Butterworth

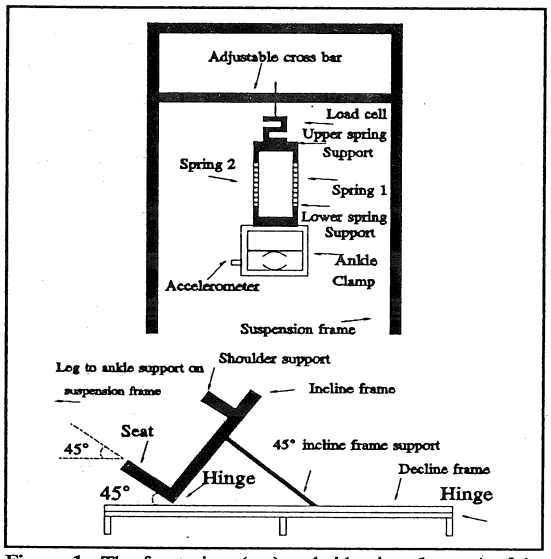

Figure 1. The front view (top) and side view (bottom) of the small oscillation apparatus.

filter at f_c=6Hz. The resulting oscillograms were analyzed to calculate τ and δ .These parameters can then be substituted into equation (6) to yield the moment of inertia of the mass, plate, and nylon cylinder.

RESULTS AND DISCUSSION

A series of five trials was carried out on the mass, plate, and the nylon cylinder. The load cell signal was collected for 10 s at a sampling rate of 500 Hz and subsequently filtered. Finally τ and δ were calculated for each cycle, averaged, and then substituted into equation (6).

Using this method, masses can be predicted with relatively high accuracy. In the best case, the percentage of mass prediction is less 0.4 % for a mass of 8.6 kg. However, it has been noticed that small masses (3.5 and 6.5 kg) had larger percentage of errors 4.0 and 2.0% respectively than a mass of 10.6 kg with an error of around 1.0%.

The absolute percent errors are related to three major factors the spring constant, the distance between the SOA attachment et the rotation axis, and the distal end fixation. The figure 2 depicts the percent errors of the cylinder moment of inertia for the three factors. The percent errors of the measured moment of inertia and the known value for the nylon cylinder vary from 1.4% to 50%. The best result for the prediction of the moment of inertia was for a spring constant of 1000 N/m without the distal end clamped and supported at a distance of 51.8 cm from the rotation axis. This method appears to be valid but very sensitive to the above mentioned three factors and to the time period interval during which a large variation in the moment of inertia is induced.

In this investigation a simple and valid method was presented for the experimental determination of the moment of inertia and the prediction of knee joint damping coefficient. From some improvements made to the protocol, the accuracy and the reliability of this method has been tremendously improved.

This simple method can be used in order to measure the segmental moment of inertia or to predict joint damping coefficient. These human parameters are critical information for the development of human joint model.

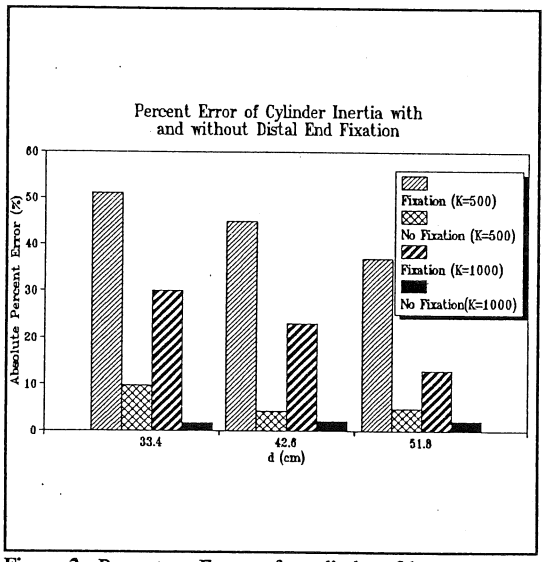

Figure 2. Percentage Errors of a cylinder of known moment of inertia with and without distal end fixation

REFERENCES

Bresler, and Frankel (1950). ASME, 72, 27-36.
Cavanagh and Gregor (1974). Biomechanics IV, 524-530.
Engin (1984) J. of Biomech. Engng, 106, 360-363.
Goldstein (1981) Classical Mechanics. Addison-Wesley, L.A.
Hanavan (1964) AMRL Technical Report 64-102, OH.
Hatze (1975) European J. App. Physiology, 34, 217-226.
Hatze (1976) Mathematical Biosciences, 28, 99-135.
Hill (1940). Proc. Roy. Soc. B., 128, 263-274.
Tierny (1979) Differential Equations. Allyn and Bacon. Boston
Wells (1967) Lagrangian Dynamics, McGraw-Hill Book, N.Y.

ACKNOWLEDGEMENTS

This research project was partly funded by Natural Sciences and Engineering Council and the Research Committee of the University of Ottawa.

SEGMENT INERTIAL PROPORTIONS OF YOUNG FEMALE ATHLETES

S.J. Tupling* and M.R. Pierrynowski

*School of Physical and Health Education
University of Toronto, Toronto.

INTRODUCTION

A downward trend in the age of elite female athletes has been noted during the past two decades. In sports, such as gymnastics, tennis and figure skating, athletes in training are often pre-pubescent. Sport scientists who wish to study the mechanics of these young athletes do not have specific inertial anthropometric data for this athletic age group.

REVIEW AND THEORY

Total body and segment inertial parameters have been estimated for young males between 4 and 15 years using an elliptical zone technique (Jensen, 1986). Regression equations were developed for segment mass proportions and transverse radius of gyration for a 14 segment human body model including the head, trunk, upper arms, lower arms, hands, thighs, legs, and feet. The model assumes symmetry between right and left extremities (i.e. eight unique segments). Other authors have adopted the elliptical zone technique to study male and female Japanese children (Yokoi *et al.*, 1986) and adult females (Finch, 1985). The technique has been modified to measure segment inertial parameters for each limb independently (Tupling *et al.*, 1984).

The purpose of this paper was to report the segment mass and radius of gyration about the centre of mass proportions of young female athletes from four sport areas (tennis [T], modern gymnastics [M], artistic gymnastics [A], figure skating [F]), and to compare these data with those obtained using the age-specific regression equations developed on young males [J] (Jensen, 1986) and cadaver-based adult values [W] (Winter, 1979).

PROCEDURES

Forty-three female athletes (12.0 + 2.1 yr., 37.1 + 9.7 kg, 1.46 + 0.12 m) and their parents consented to participate in this study. Subjects were recruited from the North York - Seneca Sport School, a programme in which an athlete trains for her sport 2-4 hours per weekday while attending school.

A 35 mm photograph was taken of each swimsuit-clad subject standing in the anatomical position. This image captured front, right and left views. Segment endpoints and outlines were manually obtained (HP9874A Digitizer) from two orthogonal views for each segment. Segments were mathematically sectioned into 50 elliptical zones, from which their masses and moments of inertia about the centre of mass were determined (Tupling *et al.*, 1984). Segment mass as a proportion of estimated total body mass (m/M) and radii of gyration about an anterio-posterior axis through the segment's centre of mass as a proportion of segment length (k/L) were determined. In addition, age predicted m/M and k/L values for each subject were calculated using Jensen's regression equations (1986).

Correlation coefficients for the masses of the right and left upper arms (UA), lower arms (LA), thighs (TH), and legs (LG) were calculated. An ANCOVA, with age as the covariant, was performed on the m/M and k/L values determined for the T, M, A, F and J groups. The significance level was set at $p < 0.05$. Post-hoc analyses were performed using Tukey's Test.

RESULTS

The linear regression equation between predicted (y) and measured (x) total body mass of the 43 athletes was $y = 0.988x - 0.080$ (Figure 1) with $r = 0.987$. Correlation coefficients between the mass of the left and right UA, LA, TH, and LG segments ranged from $r = 0.908$ to $r = 0.979$ (Figure 2).

The means and standard deviations of the m/M and k/L values for the T, M, A, F, J and W groups are depicted in Figures 3 and 4. Significant differences were noted between the LA, TH and LG for the 4 sport groups and Jensen's regression values. Post-hoc analyses indicated that for the lower limb m/M the gymnasts [M, A] differed from the T and F groups, while the lower arm m/M differed with gender. For k/L in the lower limb and LA, the M, A and F groups differed from T, except for the LG of the figure skaters. In addition, for LG the m/M and k/L values for the M, A and J groups were similar. In general the adult-calculated m/M and k/L values only differed in the lower limb segments.

DISCUSSION

In this study the differences in mass and radius of gyration proportions among young athletic women participating in four sport groups, young men and cadaver-based adult values were investigated. The similarity between estimated and measured

total body mass and right and left limb segment mass symmetry suggests that the elliptical zone technique is a sensitive and reliable measure of segment inertial proportions.

Mass ratios of the upper limb did not differ among the sport groups, with gender or when compared to adult values. However, m/M of the lower limb of the gymnasts differed from the T and F groups. Radius of gyration proportions for the LA, TH and LG segments of the M, A, and F differed from the tennis players and young males. However, both female and male groups differed from the cadaver-based adult values for the lower limb. These results suggest that sport training, gender and age-specific segment inertia proportions must be considered when biomechanical analysis are performed.

REFERENCES

Finch, C.A. MHK Thesis, U. of Windsor, ON, 1985.
Jensen, R.K. *J. Biomech.*, 22, 529-536, 1986.
Tupling, S.J. et al. *Proceedings of Human Locomotion III (CSB Conference)*, Winnipeg, (pp.69-70), 1984.
Yokoi, T. et al. *Jap. J. Phys. Ed.*, 31, 53-66, 1986.
Winter, D.A. Biomechanics of Human Movement, (p.151), John Wiley & Sons, 1979.

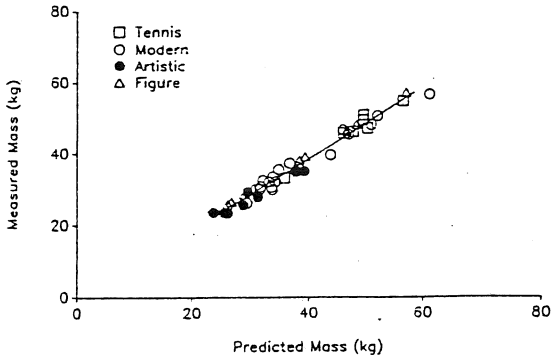

Figure 1 Predicted versus measured mass (kg).

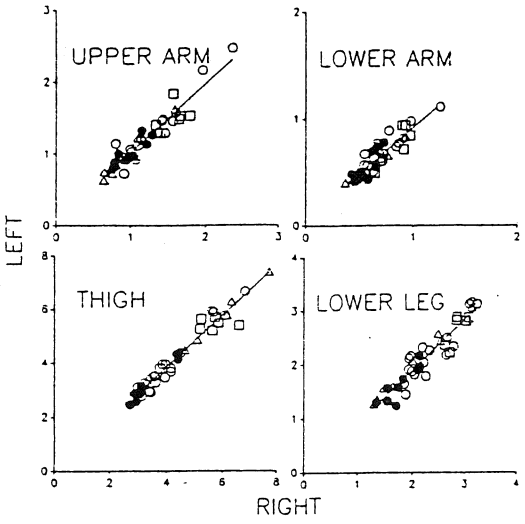

Figure 2 Left segment mass (kg) versus right segment mass (kg) for the upper arm, lower arm, thigh and leg. See Figure 1 for symbol definitions..

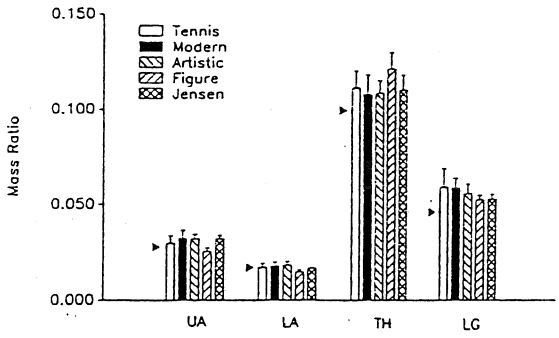

Figure 3 Mass ratios of the UA, LA, TH and LG for the T, M, A, F, and J groups. Horizontal arrows represent cadaver-based m/M values.

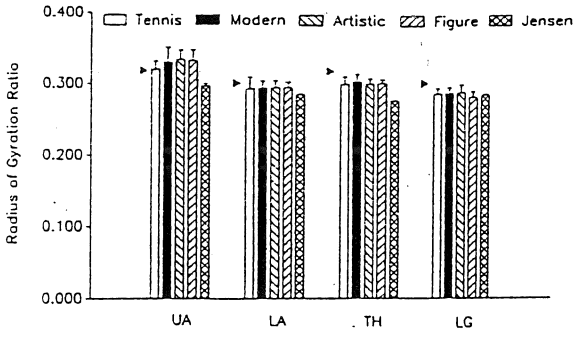

Figure 4 Radius of gyration ratios of the UA, LA, TH and LG for the T, M, A, F, and J groups. Horizontal arrows represent cadaver-based k/L values.

DETERMINING SUBJECT-SPECIFIC MUSCULOSKELETAL GEOMETRIC AND MASS PROPERTIES FROM MAGNETIC RESONANCE IMAGES

Daniel W. Moran and Gary T. Yamaguchi

Department of Chemical, Bio & Materials Engineering
Arizona State University, Tempe, AZ 85287-6006

INTRODUCTION

Dynamic modeling of various musculoskeletal tasks (e.g. ambulation) requires quantitative knowledge of the geometric and mass properties of the systems involved. These properties include masses, lengths, moments of inertia, etc. of the various structures that are represented by the model (e.g. muscles, tendons, bones, etc.) Although there have been many articles in the literature detailing some of these parameters for several types of subjects, the data is not easily scaled to a specific individual. Scaling is even more difficult if the mass properties of the model are to match those of a particular subject with an abnormal and/or asymmetric physique. For instance, modeling the abnormal gait of a cerebral palsied child requires geometric parameters and mass properties that vary significantly from one leg to the other. Therefore, subject-specific dynamic modeling requires a non-invasive method for accurately determining musculoskeletal parameters.

Of the various 3-D imaging modalities, magnetic resonance imaging (MRI) provides the best contrast where soft tissues such as muscles, ligaments, and tendons are concerned while still providing good contrast with bone. Likewise, MRI is one of the safest 3-D imaging techniques available which makes it an ideal source for determining subject-specific musculoskeletal parameters *in vivo*. To this end, this paper will discuss various techniques of extracting musculoskeletal parameters from MRI data.

REVIEW AND THEORY

The literature cites many examples of using MRI to image the musculoskeletal system; however, the goal of most of these articles is the diagnosis of various musculoskeletal diseases. Nevertheless, such articles provide important background as to the technical factors that are used to enhance various features of the musculoskeletal system. These features include the separation and identification of individual muscles, tendons, and bones. Once the desired structures have been isolated within the MRI data set, various geometric properties may be measured.

The MRI data set consists of a 3-D array of voxel information in which each voxel value corresponds to a specific type of tissue. One of the disadvantages of MRI data is that voxel values do not directly correspond to any simple physical quantity. However, the geometric information contained in MRI data is quantifiable. Determining properties such as muscle volumes requires the simple addition of all the individual voxels representing that muscle and multiplying by the unit voxel volume. Likewise, it can be seen that determining muscle lengths would be rather simple provided the data has been properly separated into the individual structures of interest. Mass properties can be indirectly determined from geometric properties by assigning standard densities to individual tissues. For instance, mass moments of inertia for a uniform structure can be calculated by summing the squares of the distances of each voxel to the axis about which the moment is taken and then multiplying this sum by the mass of a single voxel. Therefore, determining geometric and mass properties is a rather simple affair once the MRI data set has been properly segmented into the individual structures of interest.

PROCEDURES

The initial test of this procedure was performed on the lower extremity of a 10 year-old hemiplegic male. The goal of this preliminary test was to measure 3-D muscle origin and insertion sites (*i.e.*, points) relative to segmentally defined coordinate systems. The subject was strapped into a frame which restricted the movement of his legs so as to reduce movement during each of two 12 minute scans. The subject was then scanned in a 1.5 Tesla GE MRI unit. Two successive scans had to be done in order to image the full 1.0 meter length of the subject's lower extremity. The first scan included all the tissues lying between the anterior superior iliac spines and the tibial tuberosities. The second scan enclosed a volume from the femoral condyles to the patient's toes. The overlap was done to enclose in single scans full path information for biarticular muscles crossing the knee. The total data record of the scans produced a 3-D array that was 512 voxels in length, 256 voxels in width and 60 voxels in depth. Each voxel was 2 mm in length, 2 mm in width, and 3 mm in depth yielding a voxel volume of 12 mm^3. The voxel information has a resolution of 12 bits yielding a possible 4096 different values; however, a histogram of the data revealed that almost all the data was contained in the range between 0 and 500.

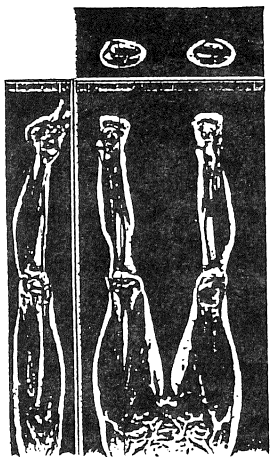

Figure 1. Illustration of three orthogonal views intersecting at the left tibial tuberosity.

TABLE 1
Raw Coordinates of various points in the MRI data set (all units are mm)

	X^{MRI}	Y^{MRI}	Z^{MRI}
right lateral epicondyle	308	482	60
right medial epicondyle	256	486	57
right femoral head center	252	74	72
right med. gastroc. origin	264	444	45
right vast. intermedius origin	284	120	75
right vast. medialis origin	272	124	72

The data set was transferred to a Silicon Graphics Personal IRIS 4D/35GT via magnetic tape for processing. The data was displayed as three orthogonal views corresponding to the frontal, sagittal and transverse planes. Each of the three views could be independently updated to show a different "slice" in their respective planes. The frontal view had a total of 60 separate slices, while the sagittal view contained 256 slices. Each view contained two orthogonal lines depicting the location of the other two planes. Therefore, each view had a set of "cross-hairs" which represented the intersection of the three orthogonal planes. Once aligned on a desired point of interest, these cross-hairs were used to identify the coordinates of muscle origins and insertions as well as bony landmarks within the data set. The visualization software used to display the MRI data set was developed by the authors for the IRIS workstation. An illustration of three orthogonal views aligned to measure the left tibial tuberosity can be seen in Figure 1. (Please note that this illustration was screen captured and dithered into a Postscript format; therefore, the resolution is much poorer than that actually displayed by the graphics workstation.)

The origins and insertions of all the major muscle groups of the lower extremity were measured as well as the bony landmarks that define the segmental reference frames. Three segmental reference frames (pelvis, femur and tibia) were utilized in this study which correspond directly to those defined by Brand *et al.* (1982). The axes of a given segmental frame is defined using bony landmarks. For instance, the femur reference frame has its origin at the midpoint between the medial and lateral epicondyles. The principal vertical axis (Y^F) is defined as the vector connecting the origin with the center of the femoral head. The frontal axis (X^F) is defined as the cross product of the principal vertical axes with the vector connecting the origin with the center of the lateral epicondyle. Finally the sagittal axis (Z^F) is defined as the cross product of the frontal axis with vertical axis. The vectors corresponding to each of these axes are defined relative to the MRI coordinate system. Therefore, by doing a vector dot product of the vector connecting the segmental origin to a desired muscle origin/insertion with each of the segmental axes vectors, the coordinates of the desired muscle origin/insertion relative to the segmental frame is achieved. Therefore, each of the origins and insertions of the muscles measured in this study were converted from the MRI coordinate system to their respective segmental coordinate system.

RESULTS

An example of the results obtained for the right femur can be seen in Table 1. The three bony landmarks that define the femur reference frame relative to the MRI reference frame are listed first. Following this is a list of several muscles which either originate or insert into the femur and their respective coordinates relative to the MRI coordinate system. Table 2 illustrates the normalized principal femoral axes relative to the MRI coordinate system as well as the converted muscle origin/insertions relative to the femoral reference frame.

TABLE 2
Vectorial values of each of the right femoral reference frame axes relative to the MRI reference frame and several muscle origins relative to the right femoral reference frame.

	X^{MRI}	Y^{MRI}	Z^{MRI}
right femoral origin	60.8	-501.2	250.0
right femur frontal axis (X^F)	-0.055	0.037	0.998
right femur vertical axis (Y^F)	-0.073	-0.997	0.033
right femur sagittal axis (Z^F)	0.996	-0.071	0.058
	X^F	Y^F	Z^F
right med. gastroc. origin	-14.0	40.8	-15.9
right vast. intermedius origin	2.9	363.3	28.8
right vast. medialis origin	0.7	360.1	16.4

DISCUSSION

The results of the preliminary case correlated well with the literature; however, it is difficult to ascertain the accuracy of this method due to the fact that there is nothing to directly compare the MRI results to. To this end, the second test of this method will involve the *in vivo* scanning of an anesthetized rhesus monkey's arm at a resolution of 1 mm^3. This resolution is significantly higher than the 12 mm^3 resolution of the preliminary case which, in turn, will yield a much more accurate data set. Also, following the MRI data collection, the monkey will be sacrificed and its arm dissected and electromagnetically digitized in order to directly compare dissection results of musculoskeletal parameters with those generated from the MRI data set. The results targeted for this procedure will be more extensive than the preliminary case and will include tendon and muscle lengths and cross-sectional areas as well as masses, volumes and moments of inertia of muscles, bones and body segments. This procedure is currently scheduled for two weeks following the deadline of this paper.

It is the belief of the authors that this method is a viable technique for determining musculoskeletal geometric and mass properties given an MRI data set with sufficient resolution. Currently obtaining such resolution is very expensive as well as time consuming for the subject and is currently suited only for research purposes.

REFERENCES

Bassett, L. *et al.*, *Clin-Orthop.*, 244, 119-30, 1989.
Brand, R. *et al.*, *J. Biomech. Engrg.*, 104, 304-10, 1982.
Yamaguchi, G. *et al.*, *Multiple Muscle Systems*, (pp. 717-73), Springer-Verlag, 1990.

ACKNOWLEDGMENTS

The authors wish to thank the Whitaker Foundation for its support as well as Jonathan Green for his technical assistance.

KNEE FLEXION MOMENT ARMS OF THE RECTUS FEMORIS AFTER TENDON TRANSFER

Deborah A. Ringwelski, Scott L. Delp, Norris C. Carroll

Departments of Mechanical Engineering, Biomedical Engineering, and Orthopaedics, Northwestern University, and Rehabilitation Institute of Chicago, Chicago, IL

INTRODUCTION

An interactive, graphics-based model of the lower extremity was used to simulate the rectus femoris transfer surgery. This surgery involves transferring the distal end of rectus femoris to one of the following tendon transfer sites: (1) semitendinosus, (2) iliotibial tract, (3) sartorius, (4) gracilis, or (5) semimembranosus. The knee flexion moment arm vs. knee angle curve for each of the five transfer sites was calculated using the model. To test our simulations, we performed tendon transfers on two alcohol-preserved cadavers and measured knee flexion moment arms after the transfer. Both experimental and simulation results showed that rectus femoris has the largest knee flexion moment arm when it is transferred to the semitendinosus. In contrast, when transferred to the iliotibial tract the moment arm is approximately zero. This suggests that semitendinosus is a more effective transfer site for increasing knee flexion moment.

REVIEW AND THEORY

Since its introduction by Perry (1987), the rectus femoris transfer has become widely used in the treatment of "stiff-knee" gait (i.e., decreased knee flexion during swing). In this surgery, the rectus femoris is released from its insertion on the patella and reattached posterior to the knee. The surgery is intended to increase knee flexion during the swing phase of gait and to maintain the rectus femoris as a hip flexor. Although Perry originally suggested transferring the rectus femoris to sartorius or gracilis, the muscle is now commonly attached to semitendinosus, semimembranosus, or the iliotibial tract.

Gait analysis has shown that the increase in knee flexion is greater after rectus femoris transfer than after simply releasing the tendon from its insertion (Gage et al., 1987; Sutherland et al., 1990). However, no studies have evaluated how the various transfer sites affect the capacity of the rectus femoris to produce knee flexion moment. The objective of this study is to quantify differences in the moment arms of the rectus femoris when transferred to the five most common sites.

METHODS

Computer Simulation

A graphics-based model of the lower extremity musculoskeletal system was used to simulate the rectus femoris transfer (Delp et al., 1990). To understand how surgery changes the muscle path, the rectus femoris was transferred to each of the five post surgical sites on one cadaver. The origin-to-insertion path of the rectus femoris was digitized with a three-dimensional optical digitizer and input to the computer model. Since the model characterizes the kinematics of the hip and knee, moment arms of the transferred muscle can be computed at any body position. Knee flexion moment arm vs. knee angle curves were calculated for each of the five transfer sites.

Anatomical Studies

Moment arms were estimated from measurements of tendon displacement as a function of knee angle. On each of two cadavers (one male and one female) the rectus femoris was released from its origin. A wire was sewn to the end of the muscle and fed through a pulley placed at the muscle's origin. The wire was attached to a position transducer, which loaded the muscle with a constant tension of 7.5 N. The distal end of rectus femoris was released from its insertion on the patella and attached to the tendon at each transfer site. For each transfer, the tendon displacement was measured over a range of knee flexion angles.

To control the knee flexion angle during the tendon length measurements, a locking brace was mounted to the leg. A dial at the center of the brace's hinge acted as a goniometer and indicated knee flexion angle. Two pins were drilled through the femur to fix the upper portion of the brace. The lower portion of the brace was loosely strapped to the calf so that normal knee kinematics were not disrupted. The tendon displacement vs. knee joint angle data was fit using quintic splines (Woltring 1986). The knee flexion moment arm vs. knee angle curves were calculated by differentiating the smoothed displacement vs. joint angle data.

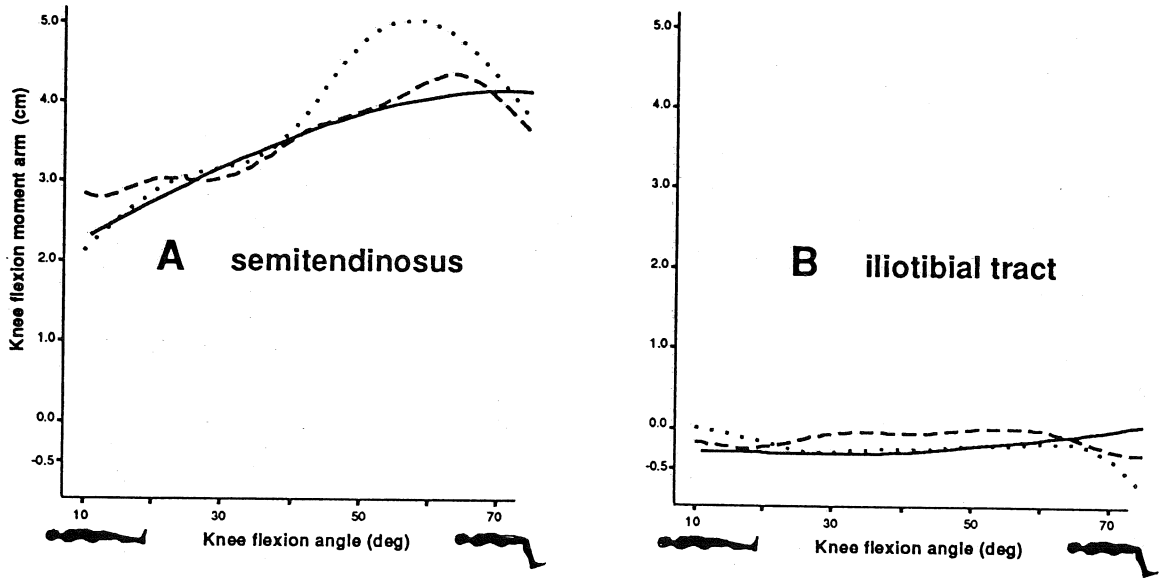

Fig. 1 Knee flexion moment arm vs. knee angle of the rectus femoris for two different transfer sites: A (semitendinosus), B (ilitobial tract). The solid line represents the model estimates. The dashed (dotted) line represent moment arms measured on the male (female) cadaver

RESULTS AND DISCUSSION

We found substantial differences among the surgical techniques. When transferred to semitendinosus, the rectus femoris has a maximum knee flexion moment arm of 4-5 cm at approximately 60° knee flexion (Fig. 1A). In contrast, when the rectus femoris is transferred to the iliotibial tract, it has a very small moment arm (<5 mm, see Fig. 1B). The moment arm vs. joint angle curve for rectus femoris transferred to gracilis and semimembranosus are similar to Fig. 1A, but with a maximum of approximately 4.0 cm. When transferred to sartorius, the rectus femoris moment arm maximum is approximately 2.5 cm at 60° knee flexion.

Our results indicate that transfer of the rectus femoris to the semitendinosus is the most effective means to increase knee flexion moment, since this provides the largest knee flexion moment arm. Transfer of the rectus femoris to the iliotibial tract may increase knee flexion during swing. However, we expect that any increase in knee flexion results from a decrease in knee extension moment, not from an increase in knee flexion moment.

REFERENCES

Delp, S.L. et al. IEEE Transactions on Biomedical Engineering, **37**, 757-767, 1990.
Gage, J.R. et al. Developmental Medicine & Child Neurology, **29**, 159-166, 1987.
Perry, J. Developmental Medicine & Child Neurology, **29**, 153-158, 1987.
Sutherland, D.H. et al. Journal of Pediatric Orthopaedics, **10**, 433-441, 1990.
Woltring, H.J. Advances in Engineering Software **8**, 104-113, 1986.

ACKNOWLEDGEMENTS

Supported by a General Motors Fellowship and The Whitaker Foundation.

INSTRUMENTATION AND METHODOLOGY

Poster

Construction of a High-pass Digital Filter

S.D. Murphy and D.G.E. Robertson
School of Human Kinetics, University of Ottawa, Ontario

Introduction

Low-pass digital filters have been in use for a substantial period of time to remove high frequency noise but nowhere in the biomechanics literature does there exist a high-pass digital filter which removes low frequency noise. Pezzack *et al.* (1977) showed that the process of digitally filtering cinefilm coordinate data to remove high frequency noise and then applying finite differences was an appropriate solution for obtaining segmental kinematics. More detail on the construction of the low-pass filter used by Pezzack *et al.* can be found in Winter (1990).

Low frequency noise is present in EMG, force platforms and temperature sensitive force transducers. To date, there are no documented means in the biomechanics literature of removing this low frequency noise digitally. A high-pass digital filter can be constructed from a low-pass digital filter by means of a transformation. A brief presentation of this derivation as well as an application of the high-pass filter follows.

Theory

The general N-th order digital filter is a recursive equation of the form (Hamming, 1977)

$$y_n=\sum_{k=0}^{N} c_k x_{n-k}+\sum_{k=1}^{N} b_k y_{n-k}$$

Therefore a second order (N = 2) digital filter is

$$y_n=c_0x_n+c_1x_{n-1}+c_2x_{n-2}+b_1y_{n-1}+b_2y_{n-2}$$

Let the *known* low-pass filter have the following transfer function

$$H_{lp}(Z^{-1})=\frac{C_0+C_1Z^{-1}+C_2Z^{-2}}{1-B_1Z^{-1}-B_2Z^{-2}} \qquad (1)$$

To get the corresponding high-pass filter let (Oppenheim and Schafer, 1989)

$$Z^{-1}=-\frac{(z^{-1}+\alpha)}{1+\alpha z^{-1}}$$

where

$$\alpha=-\frac{\cos(\frac{\theta_{lp}T+\omega_{hp}T}{2})}{\cos(\frac{\theta_{lp}T-\omega_{hp}T}{2})} \qquad (2)$$

and

θ_{lp} = angular velocity of low-pass filter in rad/s

ω_{hp} = angular velocity of high-pass filter in rad/s

T = sampling period

After expanding and regrouping the constants into the same form as (1) one gets a high-pass filter

$$H_{hp}(z^{-1})=\frac{c_0+c_1z^{-1}+c_2z^{-2}}{1-b_1z^{-1}-b_2z^{-2}} \qquad (3)$$

with coefficients

$$c_0=\frac{C_0-C_1\alpha+C_2\alpha^2}{\delta} \qquad b_1=\frac{-2\alpha-B_1(1+\alpha^2)+B_2 2\alpha}{\delta}$$

$$c_1=\frac{C_0 2\alpha-C_1(1+\alpha^2)+C_2 2\alpha}{\delta} \qquad b_2=\frac{-\alpha^2-B_1\alpha+B_2}{\delta}$$

$$c_2=\frac{C_0\alpha^2-C_1\alpha+C_2}{\delta} \qquad \delta=1+B_1\alpha-B_2\alpha^2$$

Before the coefficients for the low-pass filter can be calculated a suitable low-pass cutoff frequency must be chosen. Since the high-pass cutoff frequency is given and the low-pass cutoff frequency can be chosen arbitrarily based on α, set $\alpha = 0$ and solve for Θ_{lp}. Choosing $\alpha = 0$ simplifies the calculations of the high-pass filter coefficients (see (3)) and (2) implies that

$$\theta_{lp}T+\omega_{hp}T=\pi$$

Solving for Θ_{lp} gives

$$\theta_{lp}=\frac{\pi-\omega_{hp}T}{T}$$

Since it is typical that the user enters a frequency rather than an angular velocity recall that

$$\omega_{hp}=2\pi f_{hp}$$

Perform a similar substitution for Θ_{lp} and simplify to get

$$f_{lp}=\frac{1}{2T}-f_{hp} \qquad (4)$$

In summary, use the following "easy" steps to build a high-pass filter:

i) Calculate a cutoff frequency, f_{lp}, for the low-pass filter using the given cutoff frequency, f_{hp}, for the high-pass filter and equation (4).

ii) Determine the coefficients (C_i and B_j) of the low-pass filter using the known equations (Winter, 1990) and basing it on the low-pass cutoff frequency, f_{lp}, determined by step i).

iii) By letting $\alpha = 0$ in (3) the new coefficients, c_i and b_j, for the high-pass filter will be given by

$$c_o = C_o,\ c_1 = -C_1,\ c_2 = C_2$$
$$b_1 = -B_1,\ b_2 = B_2$$

where C_i and B_j were the previously calculated coefficients of the low-pass filter in step ii).

Procedures

The high-pass filter was constructed from a Butterworth, critically damped, low-pass filter as described by Winter (1990). A typical EMG signal which had drift present was high-pass filtered in the forward and backward directions (zero phase lag, 4-th order) with cutoff frequencies of 0.2 and 0.5 Hz.

Results and Discussion

In Figure 1, the raw EMG signal is plotted above the high-pass filtered signals with cutoff frequencies of 0.2 and 0.5 Hz. Notice that a cutoff frequency of 0.2 Hz (middle curve) removed the drift from the EMG signal. The cutoff of 0.5 Hz removed both the drift and the bias from the signal without adversely influencing the high frequency components of the signal. These results demonstrate the usefulness of a high-pass filter for removing unwanted low frequency noise from EMG signals.

Figure 2 shows the results of both high and low pass filtering a signal containing 0.1, 1.0 and 10.0 Hz sine waves. The top curve is the raw data, the next curve shows the data high-pass filtered at 0.5 Hz cutoff, the third curve shows the effects of low-pass filtering at 5.0 Hz. The bottom curve shows the effects of cascading the data through a 0.5 Hz high-pass filter and a 5.0 Hz low-pass filter. This band-pass filter successfully recovered the 1.0 Hz sine wave from the raw signal. Notice that these filters do require time to reach their specified operating characteristics. In this case (zero phase lag filters) extra leading and trailing data are required (see Smith, 1989).

References

Hamming, R.W. (1977) Digital filters. Prentice-Hall, Inc.

Oppenheim, A.V. and Schafer, R.W. (1989) Discrete-time signal processing.

Pezzack, J.C. *et al.* (1977) *J. Biomechanics*, 10, 377-382.

Smith, G. (1989) *J. Biomechanics*, 22, 967-972.

Winter, D.A. (1990) Biomechanics and motor control of human movement. John Wiley & Sons.

Acknowledgments

For technical assistance, thanks to Dr. Tyseer Aboulnasr, Dept. Electrical Engineering, U.Ottawa. For use of data, thanks to Dr. Mario Lamontagne, School of Human Kinetics, U. Ottawa.

Figure 1

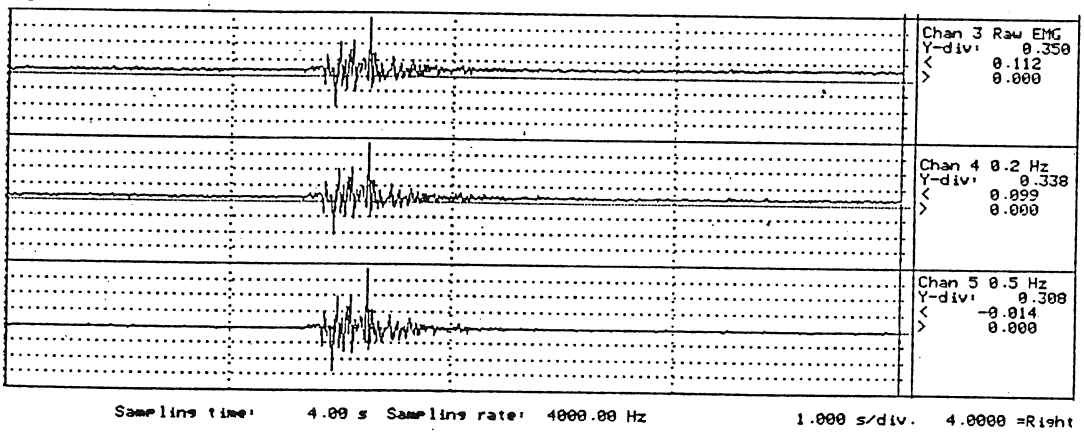

Figure 2

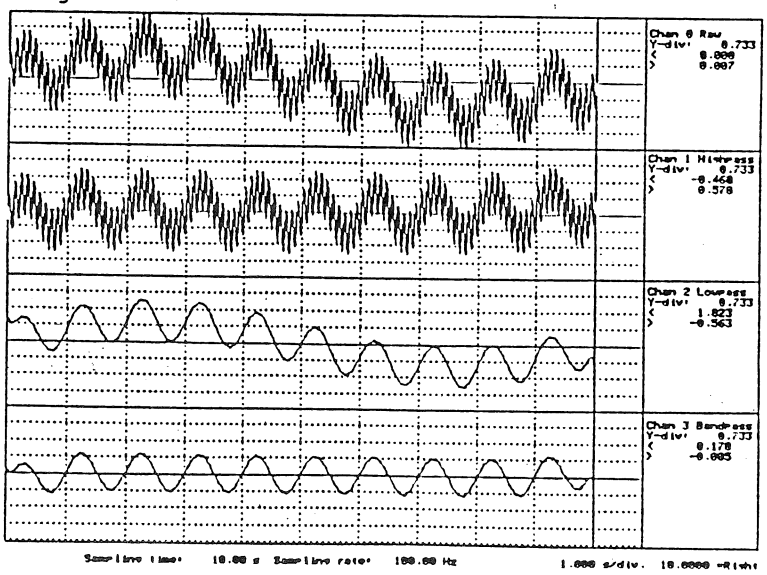

VERY CLOSE RANGE PHOTOGRAMMETRIC TECHNIQUE FOR OBTAINING THREE-DIMENSIONAL COORDINATES OF CRITICAL LANDMARKS ON THE INFANT HEAD

A. Russo, M. Lamontagne, C. Cotton, F. Haman

School of Human Kinetics, University of Ottawa, Ontario

INTRODUCTION

The risk of head injuries to infants and children, during various activities, can be greatly reduced with the use of a properly fitted and protective helmet. In order to construct these helmets extensive impact testing is necessary. Therefore, the development of accurate and representative infant headforms, to be used in the impact testing, is essential. The headforms, presently being used for helmet impact testing are mainly of the adult head. These headforms do not suitably represent the distinct infant and children head shapes. The construction of a appropriate infant headform requires accurate information on the size, shape and geometrical dimensions of the infant head. Schneider et al. (1987) and Snyder et al. (1975,1977), as part of their study on the prevention of infant head entrapment accidents, used standard measurement techniques (anthropometers, callipers and measuring tapes) to obtain data on the size and shape of children heads and necks. Schneider et al. (1987) also used the close range photogrammetric technique known as Direct Linear Transformation (DLT) to identify critical contours and landmarks. Unfortunately the data gathered was not extensive enough. The purpose of this study was to validate a very close range photogrammetric DLT technique for obtaining accurate three-dimensional (3D) geometrical information on the infant head.

REVIEW AND THEORY

The use of standard measurement techniques poses several problems when trying to collect accurate data. Firstly, instrument and technician error must be dealt with. Then there is also the problem of manipulating the instruments to fit the contours of the head. These problems are then compounded by the squirming infant or child. The use of the DLT close range photogrammetric technique (Marzan et al., 1975) can eliminate these problems. The technique involves initially filming or photographing a calibration object, containing known control points, with two or more arbitrarily positioned cameras. The calibration object is then replaced with an "unknown" object so that it occupies the same calibrated space, and without altering the camera setup the filming or photographing is repeated. The 2D coordinates of the points on both the calibration object and the "unknown" object are then digitized and inputted into the DLT algorithm to calculate the 3D coordinates of the markers on the "unknown" object. The control points are used to solve for the DLT parameters which will define camera position and orientation and correct for film deformation and lens distortion errors. The number of control points is not as important as the distribution of these points. Few control points well distributed throughout the object space produce accurate results (Wood et al., 1986). The number of DLT parameters (11,12, 14 or 16) used will depend on the degree of error correction desired. However, it has been shown that use of a greater number of parameters does not significantly improve reconstruction accuracy (Wood et al., 1986; Murphy et al., 1990). The construction and measurement of the calibration object can drastically affect accuracy. As shown by Andre et al. (1990), the use of a well constructed and accurately measured calibration object markedly reduces reconstruction error. Several researchers have reported acceptable reconstruction errors for close range photogrammetric setups (Wood et al., 1986) and for very close range photogrammetric setups (Murphy et al., 1990; Leroux et al., 1990). The accuracy of reconstruction is limited by the digitizing board (± 0.4mm). The use of 35mm film as opposed to 16mm film, may improve the accuracy of digitization due to the larger image and finer grain

PROCEDURES

A calibration object, resembling a cage (38.4cm x 38.4cm x 38.4cm), containing 48 control points was built. This calibration object, big enough to contain an infant head, was placed in the center of a square table, which had four synchronized Minolta 35mm cameras mounted at each corner (Fig 1 and Fig 2).

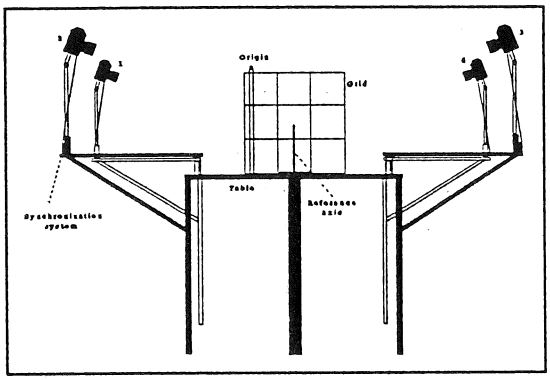

Figure 1 Photographic setup showing table, cameras and calibration object (side view).

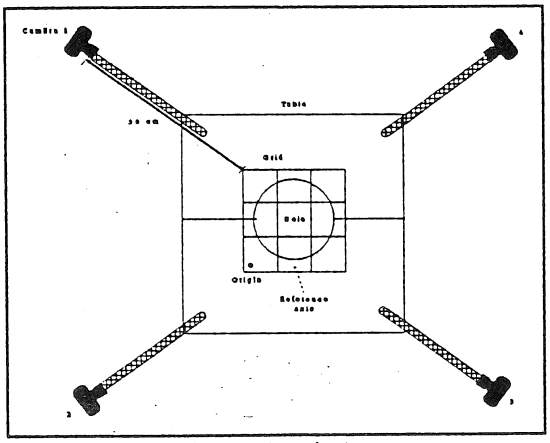

Figure 2 Photographic setup (top view).

The hole at the center of the table allows the infant to place his/her head in the calibrated space. The control points on the calibration

object were measured manually to an accuracy of 0.5 mm. These measurements were then verified with the use of a three-dimensional digitizer. To ascertain the validity of this technique reconstructions of known points were carried out. Three reconstructions were performed: calibration object (all 48 points), two points suspended in the center of the calibration object and four points on a model of an infant head. For the infant head model the calibration object was filmed by itself first, and then removed and replaced by the head model. The film negatives were converted to slides and digitized(Scriptel). All reconstructions were performed using 11 DLT parameters and 8 and 16 control points.

RESULTS AND DISCUSSION

Table 1 presents a summary of the preliminary results. The accuracy and precision (reconstruction errors) were determined for the X, Y and Z coordinates of each reconstructed point. The accuracy and precision range from 1.1 ± 0.9 mm to 4.3 ± 1.4 mm for reconstruction with 8 control points, and from 1.1 ± 0.8 mm to 3.8 ± 0.7 mm for reconstruction using 16 control points. The accuracy and precision is similar for both control point conditions. This is consistent with the results presented by other researchers (Murphy et al., 1990; Wood et al., 1986). The slightly better to markedly better results for reconstruction of the calibration object, compared to the other two reconstructions, is most probably due to a high actual measurement error. The actual measurements of the points on the calibration object were more easily obtainable and therefore more accurate then the other known points. The reconstruction errors for the calibration object are slightly higher than those reported by other researchers using very close range photogrammetry (Leroux et al., 1990; Murphy et al., 1990).

Table 1 Reconstruction error (mm). Standard Dev. ( )

Control points

Reconstruction	8 CP			16 CP		
	X	Y	Z	X	Y	Z
Cage	1.1 (0.9)	1.2 (1.0)	1.6 (0.8)	1.2 (0.9)	1.3 (1.0)	1.1 (0.8)
Center Points	4.3 (1.4)	2.6 (1.8)	1.1 (0.8)	3.8 (0.7)	2.7 (1.0)	1.4 (1.3)
Head Model	2.3 (1.6)	2.4 (1.3)	2.1 (1.9)	1.7 (1.7)	2.8 (1.4)	2.1 (1.7)

This difference is most probably due to the difference in measurement error of the calibration points. Leroux et al. (1990) reports a measurement error of only ± 0.02 mm. However, an error of 1.1 mm in a field of 384 mm is an acceptable error (0.5%). Appropriate camera settings and proper digitizing will also help improve accuracy. A blurred image will hamper digitization and add to the error. Fig. 3 demonstrates a reconstructed image that can be obtained using this very close range photogrammetric DLT technique.

The use of this technique will reduce instrument and technician error inherent in manual measurement. In addition, since the photographs are taken simultaneously, the infant or child need only be still for a few brief seconds. This is more realistic then asking an infant to remain still for longer periods of time.

The proposed, very close range photogrammetry DLT technique will provide accurate 3D information of the infant head which can then be used to construct suitable headforms. For improved accuracy, care should be taken when measuring the actual coordinates of the calibration cage, adjusting the camera settings and digitizing the 2D images.

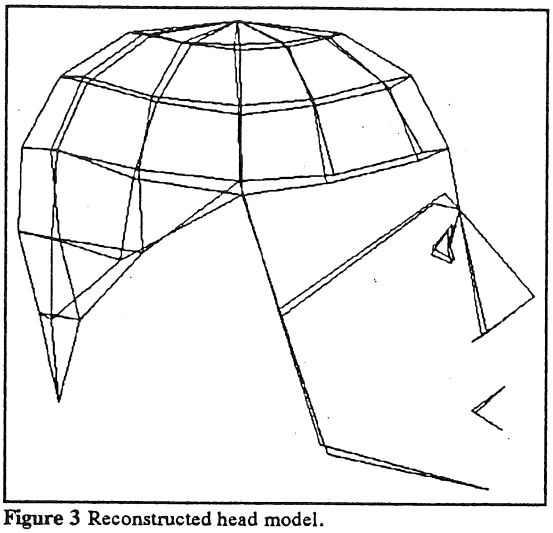

Figure 3 Reconstructed head model.

REFERENCES

Andre et al. *Proc. 14th Meeting of the ASB*, Miami, 89-90,1990
Leroux et al. *Proc. 14th Meet. of the ASB*, Miami, 203-204,1990
Marzan et al. *Symp. Close Range Photogram.* Syst., 420-426,1975
Murphy et al. *Proc. 14th Meet. of the ASB*, Miami, 197-198,1990
Schneider et al. Report to Consum. Prod. Safety Comm, Wash, 1975
Snyder et al. Report to Consum. Prod. Safety Comm, Wash., 1975 and 1977
Wood et al. *J. Biomech.*, 19:781-785, 1986

ACKNOWLEDGEMENTS

This research study was jointly funded by the Research Committee of the University of Ottawa and Biokinetics and Associates Ltd.

Special thanks to Dr. D.G.E. Robertson and Michael Marcoux, School of Human Kinetics, U. Ottawa

TRANSFORMATION FROM LOCATION-TIME DATA OF SURFACE MARKERS TO LOCATION-TIME DATA OF JOINT CENTERS

E.L. Ploeg, and J.R. Engsberg

Department of Mechanical Engineering, University of Calgary, Alberta.
Human Performance Laboratory, University of Calgary, Alberta.

INTRODUCTION

The shift from manual digitization of motion picture film to semi-automatic tracking of video data for kinematic gait analysis has both its advantages and disadvantages. One disadvantage is the use of surface markers to represent the body segment of interest. In the manual digitization method the joint center was estimated directly. Therefore, comparison of data from one subject across sessions and between different subjects was straight forward. Inconsistent marker placement introduces an added complication to the comparison. In addition, inverse dynamics solutions become less relevant without the joint center locations. To overcome these problems a method to transform surface marker locations to joint center locations was developed and tested.

REVIEW AND THEORY

If a body segment is assumed to be a rigid body, the spatial relationship between two points on the segment, with respect two a reference frame on that segment does not change during a movement. Therefore, knowing the spatial relationship between two points at one instant in time and knowing the 3-dimensional location of one of the points during an entire movement allows for the determination of the 3-dimensional location of the other point during the entire movement. The purpose of this investigation was to develop a method of transforming 3-dimensional surface marker coordinates to joint center coordinates.

PROCEDURE

Two 35 mm cameras were used to record the location of the three surface markers on a segment. Manual digitization of the slides was used to obtain the 2-dimensional coordinates of the surface markers and the joint centers. Four video cameras collected location-time data of the surface markers as the subject ran through a calibrated volume. The data were converted to 3-dimensional coordinates through the implementation of the direct linear transformation method (Abdel-Aziz et al., 1971). All coordinates were then converted from a laboratory frame of reference to a segment reference frame. Next a transformation matrix relating a surface marker to a corresponding joint center was determined. The matrix was then used to transform the coordinates of the surface marker during gait to coordinates of the joint center. The result was 3-dimensional location-time data of the joint center for one stride.

RESULTS

Results indicated a good correlation for transformation of the surface marker to the joint center in the vertical and anterior/posterior directions (Figures 1 & 2). The correspondence in the medial/lateral direction was not as favorable (Figure 3).

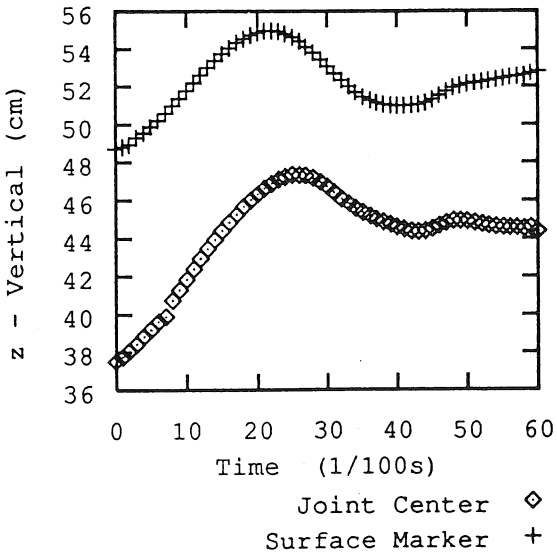

Figure 1. Location-time data of the joint center and the surface marker in the vertical direction.

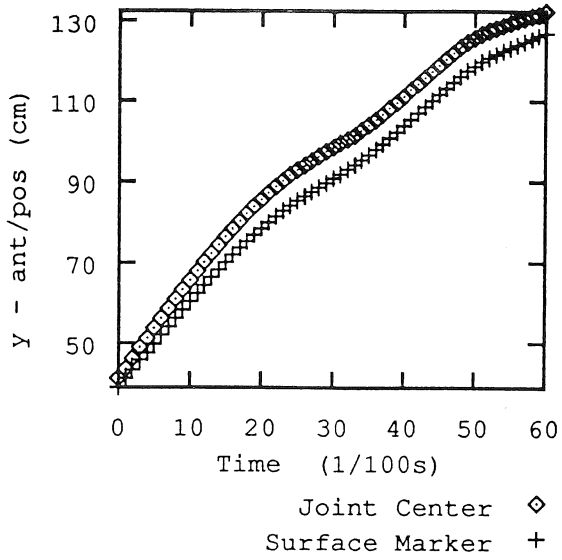

Figure 2. Location-time data of the joint center and the surface marker in the anterior/posterior direction.

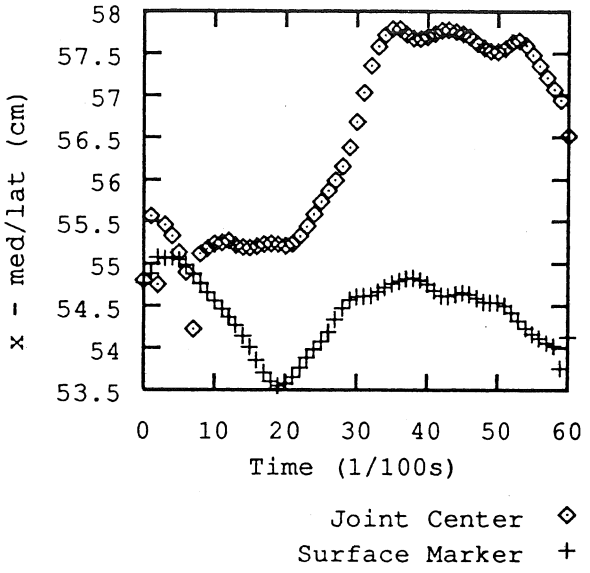

Figure 3. Location-time data of the joint center and the surface marker in the medial/lateral direction.

DISCUSSION

Except for the translation, the path of the joint center should have been identical to that of the surface marker in all directions. However; various sources of error prevented such a result. Two of these sources of error are relative surface marker movement during gait and differences in surface marker location as determined by tracking and digitizing. It is speculated that relative marker movement is the greatest source of error since these movements alter the direction cosine matrix which transforms the surface marker coordinates to the joint center. Evaluation and reduction of these errors is currently being conducted.

The method of transforming location-time data of surface marker coordinates to joint center coordinates as presented here has its advantages and disadvantages. Some of the disadvantages include; 1) manual digitization and 3-dimensional reconstruction of slides, 2) determination of transformations relating surface markers and joint centers, and 3) integration of the procedure into existing software. Advantages of the method include; 1) independent placement of surface markers 2) straight forward comparison between subjects and within subjects for different sessions and 3) relevant solutions when solving the inverse dynamics problem.

REFERENCES

Abdel-Aziz, Y.I. and H.M. Karara, *Proceedings of the ASP/UI Symposium on Close-Range Photogrammetry,* Urbana, Illinois, 1971.

Proceedings of NACOB II, The Second North American Congress on Biomechanics, Chicago, August 24th - 28th, 1992

SKIN MARKER DISPLACEMENT AT THE KNEE JOINT

M.A. Lafortune, C. Lambert and M. Lake

School of Human Biology, University of Guelph, Ontario

INTRODUCTION

Recent studies on the kinematics of the knee joint during locomotor activities have revealed limited angular motion about the secondary axes of the joint (Lafortune et al., 1992; McClay et al., 1991). Most kinematic studies rely upon superficial markers to describe bone motion. The three main sources of error with this technique are inaccuracy of the motion analysis system, positioning of markers over bony landmarks and relative superficial marker displacement (RSMD) over underlying bone. In the present study, the RSMD of an array of superficial markers was quantified using radio-opaque markers and video-fluoroscopy. Seven markers placed over the lateral aspect of the knee were monitored at 60 fields/s during loaded and unloaded cycles of knee flexion/extension. The results indicated substantial movements of the markers relative to the underlying bones. Without correction, the use of superficial markers is likely to introduce notable errors in lower extremity kinematics.

REVIEW OF LITERATURE

RSMD is a vital concern in kinematic analysis of the human lower extremities. Several methods have been suggested to overcome this source of error (Lamoreux, 1991; Ronsky et al., 1991; Whittle, 1991). Yet, little is known about the magnitude of RSMD during dynamic activities. The studies of Macleod et al. (1987) and Ronsky et al. (1991) have demonstrated that RSMD occurs during locomotion but their methods were inadequate to quantify RSMD. Lafortune et al. (1982) using bone and skin markers reported considerable RSMD at foot strike but a quantitative analysis was not undertaken. Maslen et al. (1991) measured RSMD over the foot skeletal structures for a series of static positions.

The purpose of this study was to directly quantify RSMD around the knee joint during dynamic activity of the joint.

METHODOLOGY

Two healthy adult males with no history of knee pathology participated in this study (average 31yr, 75 kg, 1.78 m). Seven lead pellets were glued to the skin overlying the lateral aspect of the knee while the subjects stood with straight legs. Two pellets were aligned approximately over the distal end of the femoral longitudinal axis, two were aligned over the proximal end of the tibial longitudinal axis while the remaining three were located along the joint line (Fig. 1). The kinematics of the tibio-femoral joint and pellets were captured with a videofluoroscopic unit equipped with a 22 cm image intensifier (Apotek Imaging Inc, Model # 300-125CF). The roentgenographic images were downloaded onto video tapes (SVHS) at a rate of 60 fields per second. The following two experimental tasks were performed: three cycles of unloaded (UNL) and three cycles of loaded (LO) knee flexion and extension. For the unloaded condition the femur was held stationary while the tibia was consecutively flexed and extended. Conversely, for the loaded condition the tibia was held vertical while the femur flexed and extended under full body weight. This latter task was similar to a deep knee bend.

The radio opaque markers and bony landmarks were manually digitized (Fig. 1) with a Peak Performance motion analysis system. The data was filtered at 7 Hz with a 4th order digital filter. Movement of the skin markers relative to the underlying bony structures (RSMD) was resolved into displacements along the axes of coordinate systems (CS) fixed onto the femur and tibia. The ordinates of the CS bisected the bones in the sagittal plane. Positive axial RSMD indicated proximal displacements of the markers while positive anterior-posterior (a-p) RSMD indicated posterior displacements of the markers. RSMD were also expressed as functions of knee angle. The knee angle was computed using the digitized bony landmarks coordinates.

RESULTS

Loaded. The results indicated that loaded knee flexion induced posterior and distal RSMD with one exception (Marker C relative to femur, Figure 1). Tibial RSMD were primarily axial while femoral RSMD showed combinations of axial and a-p displacements (Table 1). Among the markers common to both bones (A, B and C), marker A exhibited the smallest tibial RSMD while marker C moved the most. Opposite behaviors were found relative to the femur. In general, the femoral markers displaced twice as much as the tibial markers.

Unloaded. With unloading of the joint, all markers experienced a proximal shift when the knee was near full extension. With joint motion, tibial RSMD displayed a relative increase in the a-p direction while femoral RSMD displayed only small changes with unloading of the knee over the same range of motion. The data presented in Table 1. should be interpreted with caution since the unloaded excursion of the knee was twice as large as its loaded excursion (110 vs 50 deg).

TABLE 1. Average ranges of RSMD (cm).

		TIBIAL		FEMORAL	
PT		LO	UNL	LO	UNL
A	AXIAL	0.90	0.97	2.18	2.52
	A-P	0.97	2.43	4.45	7.00
B	AXIAL	1.37	2.15	1.29	3.41
	A-P	1.07	2.64	3.89	5.56
C	AXIAL	2.10	4.29	1.69	6.32
	A-P	1.08	2.62	3.03	4.31
D	AXIAL	1.23	2.18		
	A-P	0.67	1.61		
E	AXIAL	1.11	2.52		
	A-P	0.67	1.50		
F	AXIAL			1.93	1.25
	A-P			1.69	1.57
G	AXIAL			1.58	1.65
	A-P			2.53	2.97

RSMD were also expressed relative to knee joint angle. The relative displacements of marker B over the tibia and femur for the unloaded condition in one subject are displayed in Figures 2 and 3, respectively. For that marker, the relationship between RSMD and knee angle tended to be linear from maximal extension to 60 deg. of flexion. Some markers displayed a more curvilinear relationships. Loading of the joint caused minor modifications to the relationship. Generally, for a given marker, both subjects exhibited similar RSMD/knee angle relationships and the loading of the joint produced similar changes.

DISCUSSION

As demonstrated by the substantial RSMD measured in the present study, RSMD are a substantial source of error in the study of lower extremity joint kinematics. For instance, the use of marker B to compute maximal knee flexion during the gait cycle would cause a 5 degree underestimation. In the transverse plane (internal/external rotation), the error would exceed 15 degrees.

In general, the proximity of markers to the joint line effected the magnitude of RSMD. Distal marker locations on the tibia and proximal marker locations on the femur displayed the least RSMD. Markers placed along the joint line displaced the most and their RSMD were different relative to the tibia and femur. Thus, the use of a single marker at the knee is not advisable for kinematic studies of the lower limb. Yet, the apparently similar relationships between knee angle and markers RSMD for the loaded and unloaded conditions in both subjects suggests that RSMD could be modelled and accounted for in measuring knee joint motion. The initial period of stance is still problematic, as Lafortune et al. (1982) have reported considerable RSMD at impact due to soft tissues and marker inertiae during running.

REFERENCES

Lafortune, M.A. et al. *Proceedings of Human Locomotion II*, Kingston, (pp.10-11), 1982.
Lafortune, M.A. et al. *J. Biomechanics* (in press), 1992.
Lamoreux, L.W. *Proceedings of the 13th ISB Congress*, Perth, (pp. 372-373), 1991.
Macleod, A. et al. Biomechanics X-B, (pp.1035-1039), Human Kinetics Publishers, 1987.
Maslen, B. M. et al. *Proceedings of the 13th ISB Congress*, Perth, (pp. 377-378), 1991.
McClay, I.S. et al. *Proceedings of the Internationual Symposium on 3-D Analysis of Human Movement*, Montreal, (pp.189-192), 1991.
Ronsky, J. L. et al. *Proceedings of the 13th ISB Congress*, Perth, (pp. 390-392), 1991.
Whittle, M. Gait Analysis: An Introduction, (pp.196-197), Butterworth-Heinemann, 1991.

ACKNOWLEDGEMENTS

The authors would like to thank Dr. J. Ellis for the use of his fluoroscopic unit at the Brampton Chiropractic Clinic.

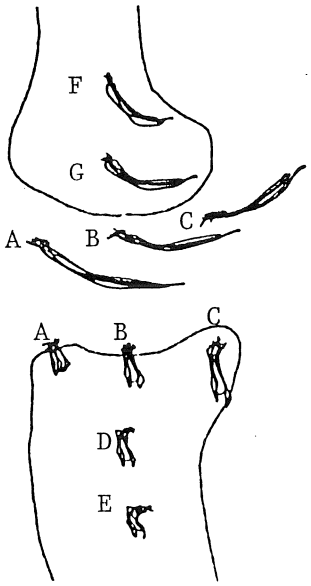

Firgure 1. Typical RSMD for three cycles of loaded knee flexion/extension.

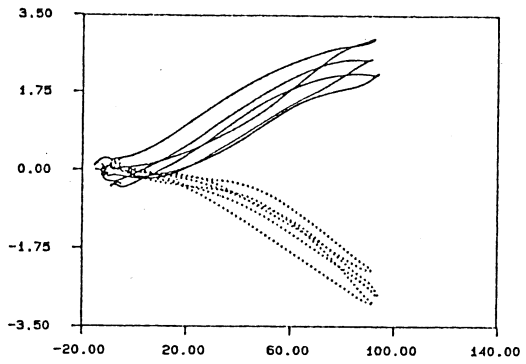

Figure 2. Typical RSMD of marker B relative to the tibia for three unloaded cycles of knee flexion/extension. A-P (—), axial (·····).

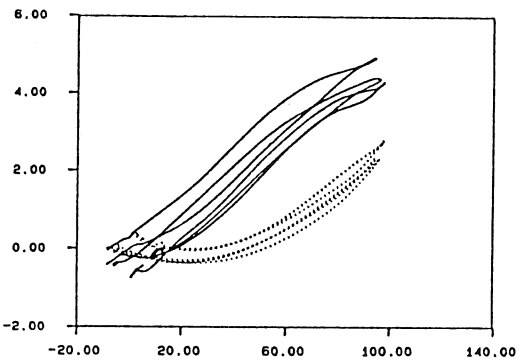

Figure 3. Typical RSMD of marker B relative to the femur for three unloaded cycles of knee flexion/extension. A-P (——), axial (·····).

SKIN AND BONE MOUNTED ACCELERATION SIGNALS

M.A. Lafortune, G.A. Valiant and E. Hennig

School of Human Biology, University of Guelph, Ontario.
Sport Research Laboratory, Nike, Oregon.
Sportmedizine Institut, University of Essen, Germany.

INTRODUCTION

Cushioning properties of athletic footwear prevent overloading of the human body's natural shock absorbers and most likely reduce the risk of injuries associated with repetitive impacts. These properties of footwear are generally evaluated with superficially mounted accelerometers. It is assumed that the latter provide accurate readings of the shock experienced by the lower extremities. In this study, the relationship between bone and skin mounted signals was investigated. The findings have demonstrated that the acceleration signals measured by a superficially mounted transducer were significantly different from those measured with a bone mounted transducer. It was also found that transfer functions allowed the accurate prediction of tibial acceleration from skin mounted transducer signals.

REVIEW OF LITERATURE

Most researchers employed superficially mounted transducers (SMT) to evaluate the shock experienced by the lower extremities during walking (Voloshin et al, 1982) and running (Clarke et al., 1985a & b). In that configuration, the transducer does not benefit from a rigid fixation to the bone. A close examination of the work of Ziegert and Lewis (1979) on accelerometer attachments warrants extreme caution when interpreting signals obtained with SMT. Light et al. (1980) reported that SMT caused time shift and high frequency losses.

Valiant et al. (1987) and, Gross and Nelson (1988) modelled SMT attachments to tibia by spring/damper systems. Both groups reported that surface mounted transduces overestimated tibial axial acceleration. Their predictions of the magnitude of the overestimation ranged between 10 and 25 percent.

The purpose of the present study was to measure superficial and skeletal *in vivo* tibial acceleration during running. An attempt was also made at establishing a relationship between these two signals.

PROCEDURES

Five active male subjects participated in this experiment (28 yr, 1.79 m, 75.5 kg). Two tri-axial accelerometers (Entran EGA3-25-D) were mounted onto their right tibia, one was fixed directly to the bone (BMT) according to Lafortune (1991) while the other was superficially mounted (SMT) using the technique described by Valiant (1987). Briefly, BMT was attached to the free end of a Steinmann pin that was inserted into the proximal tibia under local anesthesia. SMT was fixed to a small piece of balsa wood (2 cm, 2 cm, 0.5 cm) that was itself glued to the anterior face of the tibia midway through its shaft. The latter was further restrained with elastic straps. Precautions were taken to insure uniformity of mounting across subjects.

The subjects ran five times across a force platform in well cushioned running shoes. The analog signals from the accelerometers and force platform were sampled at 1000 Hz for a 2 second duration. While running across the force platform, the subjects were filmed at 200 Hz by 2 phase locked cameras. The combined contribution of segmental angular motion and gravity to the measured acceleration signals were assessed from the film (Lafortune and Hennig, 1991).

Once scaled, filtered (60 Hz low pass) and corrected for angular motion and gravity, the axial tibia acceleration signals were averaged within subject and then across subjects to find the grand average BMT and SMT signals. These signals were subjected to Fast Forward Fourier transformations and the transfer function G(w) was calculated as follows:

$$G(w) = \frac{B(w)}{S(w)} \qquad (1)$$

where B(w) and S(w) were the Fourier coefficients of the bone and surface signals. The merits of G(w) were assessed by using it to predict tibial acceleration from surface mounted sensor signals. For that purpose five additional trials per subjects were used to compute individual average SMT signals in the frequency domain s(w). Predictions of individual bone acceleration signals p(w) were calculated using equation (2).

$$p(w) = G(w) * s(w) \qquad (2)$$

Peak acceleration (PA) and time to peak acceleration

(TPA) were used to compare BMT, SMT and p(w) signals.

RESULTS

The data presented in this section was obtained from the second set of 5 trials recorded for each subject. Typical acceleration signals recorded by BMT and SMT and, prior to correction for angular motion and gravity, are illustrated in Fig 1. The mean absolute difference between the corrected BMT and SMT PA values was 17.5% or 1.52 g. (Individual data in Tables 1 & 2). The mean absolute difference in TPA was 13% or 3.4 ms.

Table 1. Peak Acceleration (g)

	BMT	SMT	p(w)
Sub 1	10.92	9.88	10.76
Sub 2	8.17	7.96	8.16
Sub 3	7.32	9.56	7.58
Sub 4	9.59	13.69	9.77
Sub 5	7.59	7.62	7.82
Means	8.72	9.74	8.82

Table 2. Time to Peak Acceleration (ms)

	BMT	SMT	p(w)
Sub 1	23	22	25
Sub 2	27	27	27
Sub 3	25	33	27
Sub 4	24	29	27
Sub 5	31	34	35
Means	26	29	28.2

The initial attempt at calculating an average transfer function, G(w), produced unsatisfactory results. Deviations between measured and predicted PA and TPA exceeded 5% and 10%, respectively. Careful examination of the corrected SMT signals revealed that the subjects could be divided into two group using peak negative acceleration (Point A in Fig 1) as criterion. Three subjects showed peak values between -0.5 and -1.7 g while the other two subjects showed peak values of -4.4 and -5.4 g. Thus, separate transfer functions were derived for each group. Typical measured and predicted signals (corrected for angular motion and gravity) are shown in Fig 2. Individual results are presented in Tables 1 and 2. The mean absolute differences between measured and predicted PA and TPA were 1.7 % (0.14 g) and 8.5 % (2.2 ms), respectively.

DISCUSSION AND CONCLUSION

The present findings have demonstrated that tibial axial accelerations measured by a superficially mounted transducer (SMT) were significantly different from the measurements obtained with a bone mounted transducer (BMT). On average SMT measured higher acceleration peaks that occurred later than BMT. However, there was considerable individual variability in the results. Thus, the present findings suggest that careful superficial attachments of transducers are insufficient to insure a systematic relationship between BMT and SMT measurements.

Grouping the subjects according to the magnitude of the negative peak acceleration to establish transfer functions between SMT and BMT measurements proved to be a satisfactory approach. The results showed that accurate predictions of tibial axial acceleration could be obtained from surface mounted transducer measurements.

REFERENCES

Clarke, T.E. et al. *J. Sports Sci.* 3, 41-49 ,1985a

Clarke, T.E. et al. Biomechanics IX-B (pp. 101-105), Human Kinetics, 1985b.

Gross, T.S. et al. *Med. Sci. Sp. Ex.*, 20, 506-514, 1988.

Lafortune, M.A. *J. Biomechanics*, 24, 877-886, 1991.

Lafortune, M.A. et al. *Med. Sci. Sp. Ex.*, 23, 360-369, 1991

Light, L.H. et al. *J. Biomechanics*, 13, 477, 480, 1980.

Valiant, G.A. et al. Biomechanics X-B (pp. 937-941), Human Kinetics, 1987.

Voloshin, A.S. et al. *J. Biomechanics*, 15, 21-27, 1982.

Ziegert, J.C. et al. *ASME J. Biomech. Engnr.*, 101, 218-220, 1979.

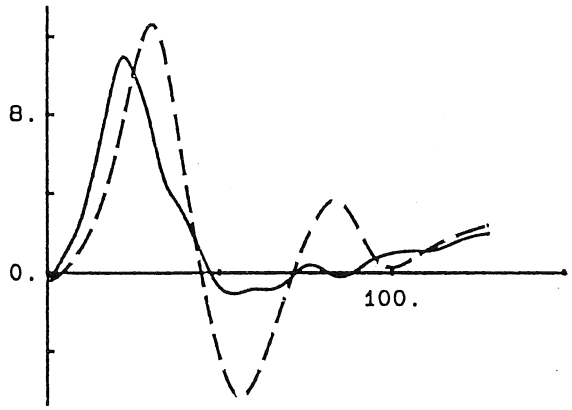

Fig. 1 Typical acceleration signals measured by BMT (- - -) and SMT (----)(*Prior to correction*)

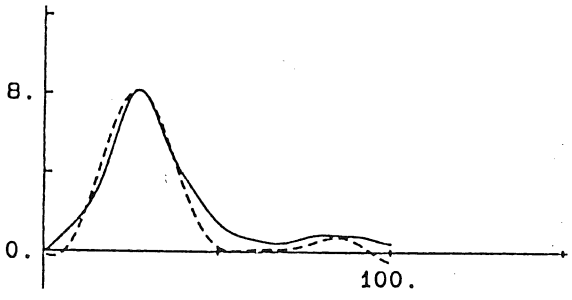

Fig.2 Typical measured (----)and predicted (- - -) acceleration signals (*After correction*).

RESPONSE CHARACTERISTICS OF DIFFERENT BUTTERWORTH LOW-PASS DIGITAL FILTERS

D. Gordon E. Robertson*, John M. Barden* and James Dowling**
***School of Human Kinetics, University of Ottawa, Ontario.**
****Dept. of Physical Education, McMaster Univ., Hamilton, Ontario.**

INTRODUCTION

For many biomechanics investigators, the low-pass Butterworth digital filter is an important tool for the processing of biomechanical data. A variety of digital filtering options exist (e.g., zero lag, damping, order, etc.), which influence the filter's ability to respond to changes in the raw data (Winter, 1990). The purpose of this research was to examine the effects of filtering a known set of data with various combinations of these options.

PROCEDURES

An artificial step function was created, using amplitude values of zero and one. A low-pass Butterworth digital filter (Winter, 1990) was then passed over the data according to the specified trial characteristics. The trial characteristics (or filter options) that were compared examined the effect produced by: critically damping and underdamping, zero lag and nonzero lag, varying cutoff frequency and cascading the filter.

To make a zero lag filter one must pass the data through the filter twice — once in the forward direction and once in reverse. Cascading a filter means to run the data through the filter more than once. Whenever data is run through a filter more than once the effective cutoff frequency of the filter is reduced. Therefore to maintain the correct cutoff when multiple passes of a filter are used you must first adjust the cutoff. The following equations were used to adjust the critically damped and underdamped filters, respectively.

$$f^*_{crit} = \frac{f_{crit}}{[2^{\frac{1}{2*n}} - 1]^{\frac{1}{2}}}$$

$$f^*_{under} = \frac{f_{under}}{[2^{\frac{1}{n}} - 1]^{\frac{1}{4}}}$$

where f_{crit} and f_{under} are the desired cutoff frequencies of the critically damped and underdamped filters, and f^*_{crit} and f^*_{under} are the adjusted cutoff frequencies necessary to produce the requested cutoff, and n is the number of filter passes.

RESULTS AND DISCUSSION

Figure 1.
Critically vs. underdamped filters.

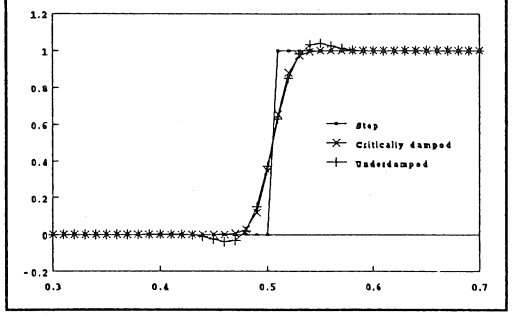

Figure 1 shows the original step function compared to the output from a critically damped and an underdamped filter (both of which are 4th order, zero lag). Sampling rate and cutoff frequency for both filters were set at 100 Hz and 10 Hz, respectively. Notice that, as expected, the critically damped filter does not undershoot or overshoot the data. The underdamped filter does produce an artificial minimum and maximum and takes slightly longer to match up to the original data. It is clear from these results that the critically damped filter is superior to the underdamped filter.

Figure 2
Zero vs. nonzero lag, critically damped

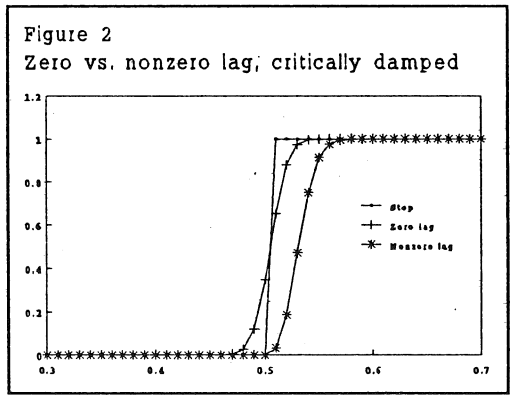

Figure 2 compares the step function to both a zero and a nonzero lag filter. Both filters were critically damped, 4th order and had sampling and cutoff frequencies of 100 Hz and 10 Hz, respectively. A filter which is referred to as zero lag, achieves this by passing over the data twice — once in each direction. This process introduces an equal and opposite phase lag so that the net phase shift will be zero. As is evident here, the nonzero

lag filter significantly lags behind the original data (i.e., is out-of-phase). It should be noted that the zero lag filter begins to respond to the change in the original data before that change actually occurs. It can be said to "anticipate" the data. On the other hand, the nonzero lag filter is not affected until the first change in the original data which, inevitably produces a phase lag in comparison to the original signal. Despite the slight anticipation produced by the zero lag filter, its elimination of phase lag makes it clearly superior to the nonzero lag filter for most purposes.

Figure 3 shows the effects produced by changing the cutoff frequency of a zero lag, critically damped filter. Cutoff frequencies of 1, 2, 4, and 10 Hz were applied assuming a sampling rate of 100 Hz. As was expected, varying the cutoff frequency significantly affected the ability of the filter to follow the original step function. It can be seen that the poorest match

Figure 3.
Effects of varying cutoff frequency.

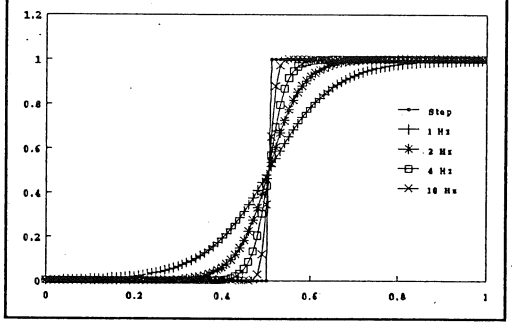

occurs with the filter which had the 1 Hz cutoff frequency. With the addition of more high frequency components, the filter's ability to reproduce accurately the original step function was improved. The cutoff frequency of 1 Hz eliminated almost all of the original harmonics, resulting in a very poor and simplified approximation of the step. Of the four different cutoff frequencies, the best choice for most accurately reproducing the original data was the 10 Hz cutoff. In addition, because of the greater harmonic content, the filter with the highest cutoff frequency is able to get back on track with the original data faster than the filters with lower cutoffs. It should be kept in mind that while producing a better reproduction, a higher cutoff may also be insufficient in eliminating noise from the original data.

Figure 4 shows the affects of "cascading" a 2nd order, nonzero lag, critically damped filter. This has the effect of increasing the rise time and the order of the filter. After adjusting the cutoff frequency for the number of repetitions, the data were filtered 2, 4, 6 and 8 times with the same filter. This produced a 4th, 8th, 12th and 16th order filter. In all cases a sampling rate and cutoff frequency of 100 Hz and 10 Hz, respectively, was used. It can be seen that the lowest order filter has less phase lag compared to the filters of higher order, with the 16th order filter having the greatest amount of lag.

Figure 5 shows the results of cascading a critically damped, zero lag filter 1 and 4 times, producing 4th and 16th order filters. The equivalent 8th and 12th were not plotted since their results were virtually identical to the others. Note that a zero lag filter,

Figure 4.
Cascading nonzero lag, critically damped

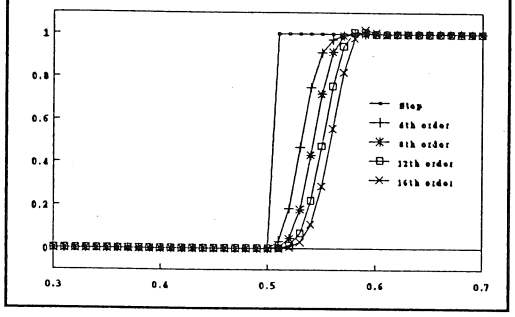

implicitly passes over the data twice — once in each direction. Therefore multiple passes increase the order by four. In Figure 5, it is immediately apparent that there is no difference between the different orders. This result was not expected. What was expected was the pattern shown in Figure 4 for the nonzero lag condition. Increasing the numerical value of the order of the filter should increase its ability to respond to a change in the original data. These results suggest that the order of the filter is irrelevant when it is also zero lag.

Figure 5.
Cascading, zero lag, critically damped.

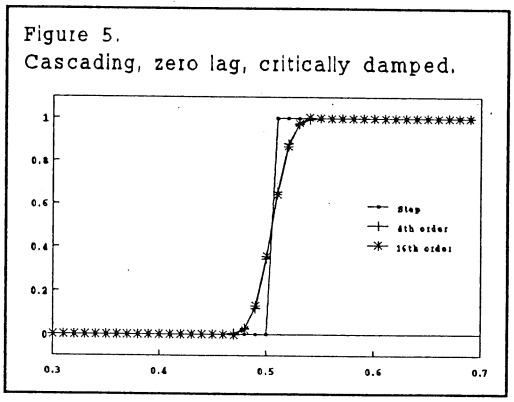

CONCLUSIONS

In this investigation, the effect of several different filtering options on the response characteristics of a low-pass Butterworth digital filter were examined. The results have shown the superiority of using a critically damped and zero lag filter. Furthermore, it was apparent that increasing the order of a zero lag filter has little influence on its ability to respond to changes in the original data. Based on the digital filtering options that were examined in this study, it can be concluded that a critically damped, zero lag filter with a cutoff frequency high enough to include the majority of the harmonic components of the wanted signal, should be the combination used to achieve the best possible data smoothing results.

REFERENCES

Winter, DA, *Biomechanics and Motor Control of Human Movement*, Wiley Interscience, 1990.

Proceedings of NACOB II, The Second North American Congress on Biomechanics, Chicago, August 24th - 28th, 1992

THE EFFECT OF ANKLE TAPING ON GROUND REACTION FORCES DURING DROP LANDINGS

S.T. McCaw & K.M. Johnson

Biomechanics Lab, Dept of HPERD
Illinois State University, Normal, Ill 61761

INTRODUCTION

Ankle taping, routinely used as a prophylactic measure in many sport activities, is intended to maintain the inversion range of motion (ROM) within anatomical limits, preventing a strain of the lateral ankle ligaments. However, standard ankle taping also limits the dorsiflexion ROM (Murray & Gronbeck, 1990), possibly restricting the ability of the ankle to contribute to energy absorption during landing. A paucity of research has quantified the effects of taping on the mechanical loading of the body during landings. The purpose of this pilot study was to evaluate the effect of ankle taping on the magnitude and timing of selected vertical ground reaction force (GRF) variables during controlled landings.

PROCEDURES

Informed consent was obtained from 3 male recreational basketball players. To ensure consistency in landing speed, an adjustable scaffold system was used so that subjects could hang using an overhand grip with the lateral malleolus 60 cm above an AMTI force platform. Subjects were instructed to land with the right foot on the platform using a consistent landing style. GRF data were sampled from the right foot at 1000 Hz. A manual goniometer was used to measure ankle ROM prior to collecting GRF data for each condition. Ten trials were collected for each of 4 conditions: C1) Prior to tape application (Pre-tape); C2) Immediately following ankle taping (Taped); C3) After 12 minutes of running on an indoor 200 m track (Post-Ex); C4) After removal of the tape (Post-tape). For C2, an experienced student athletic trainer taped both ankles using the "Figure 8, Basket weave" technique (Arnheim, 1989). All GRF data were normalized to body mass. Variables describing the maximum forefoot (F1) and rearfoot (F2) impact forces and the times associated with these events (T1 and T2) were measured from the vertical GRF data for each trial (Dufek & Bates, 1991). Ten trial means and standard deviations were calculated for each variable for each subject/condition, and for each condition across subjects. Because of the low power inherent with only 3 subjects, no statistical analyses were conducted on the data. Trends in the data were assessed visually.

RESULTS

Table 1 presents group mean and standard deviation values for the forefoot (F1 and T1) and rearfoot (F2 and T2) GRF variables, and ankle dorsiflexion ROM. There were no obvious trends evident in the group values for either the force or temporal variables. Ankle ROM was reduced during taped conditions (C2 & C3) relative to untaped conditions (C1 & C4).

Although trends were not evident in the group GRF data, individual subjects exhibited a consistent pattern of taping effects on the magnitude and timing of GRF data. Figure 1 graphically presents the forefoot and rearfoot mean GRF data for a single representative subject. No trend was evident in F1 and T1 across the 4 conditions. However, the subjects showed a consistent trend in rear-foot data. F2 values tended to be higher, and T2 values tended to be lower, during the Taped and Post-Ex conditions as compared to the Pre-tape and Post-tape conditions. For the 3 subjects, F2 values increased an average of 4.6%, and T2 values decreased an average of 7.2%, from C1 to C2 (as tape was applied). F2 values decreased an average of 8.8% and T2 values increased an average of 9.3% from C3 to C4, (as tape was removed).

Table 1. Group mean values for GRF and ROM data (n=3; SD below).

	F1	F2	T1	T2	DRSI ROM
C1	14.20	23.36	14.33	63.67	11.2
	1.35	5.20	2.00	9.00	4.6
C2	15.76	24.66	13.33	59.33	5.3
	1.26	4.19	1.00	7.67	0.3
C3	16.38	25.11	14.33	62.33	11.0
	1.75	1.67	5.01	7.00	1.3
C4	15.55	23.17	17.00	68.00	12.7
	1.82	4.16	3.33	8.67	4.3

UNITS
ROM : degrees
F1 & F2: N/kg
T1 & T2: ms

DISCUSSION

Forefoot variables were less affected by ankle taping than were rearfoot variables. Since F1 and T1 reflect the initial collision of the foot with the floor, and landing speed was controlled by the drop height, minimal taping effects on forefoot variables was as expected. The observed trends in F2 and T2 when tape is applied, loosened, or removed suggest that ankle taping disrupts the contribution of the ankle joint to energy absorption during landing. Based on these pilot data, a more extensive study involving the analysis of joint moment of force and mechanical energy profiles appears warranted to indicate how lower extremity joints are differentially loaded when the ankle is taped.

REFERENCES

Arnheim, D. *Modern Principles of Athletic Training*, (pp.324-5),1989.
Dufek, J. & Bates, B. *Med. Sci. Sports & Exer.*, **23**, 1062-67, 1991.
Murray, L. & Gronbeck, C. *Illinois Journal*, **26**, 26-7, 1990.

Supported in part by a Jump Rope for Heart Grant from the Illinois AHPERD.

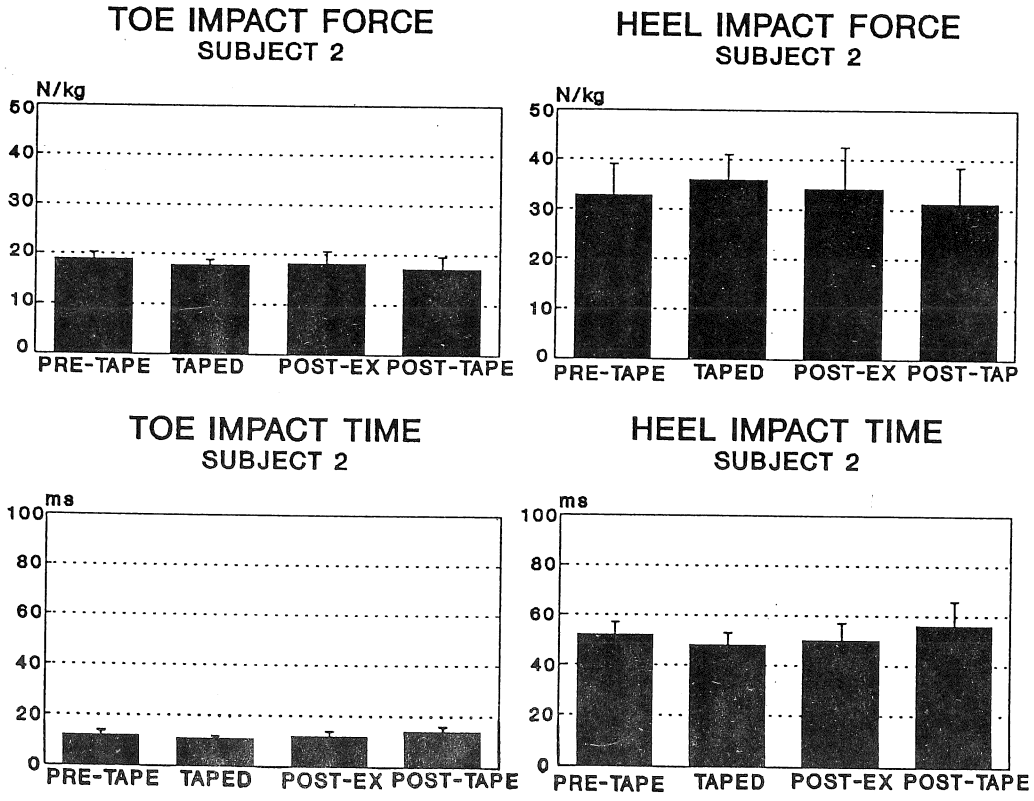

KINEMATIC & GRF ALIGNMENT: TOWARD THE ELIMINATION OF SYNCHRONIZATION ERROR

B.J. O'Connor, H.J. Yack, S.C. White

Biomechanics Laboratory, Department of Physical Therapy & Exercise Science
State University of New York at Buffalo, Buffalo, New York.

INTRODUCTION

Calculation of joint forces, moments and powers requires the combination of ground reaction force (GRF) and kinematic data determined from video tape. The accuracy of these analyses is dependent on the precision with which GRF and kinematic data are aligned in time. This paper presents a synchronization strategy which will greatly reduce errors in these critical biomechanical measures. Utilization of this strategy reduces potential timing errors from 1/60th second (one video field) to 1/1200th second.

REVIEW & THEORY

GRF data are normally acquired via an analog-to-digital (A/D) convertor interfaced with a computer. Typically, these data are sampled at a wide range of rates dependent upon the movement being studied. Conventional video, however, is sampled at a fixed rate of 30 frames per second, with each frame consisting of 2 interlaced fields. Many present video digitizing systems allow for separation of the even and odd fields, thus allowing video data analysis at 60 Hz (60 pictures per second). Additionally, shuttered video systems produce clearer images within each of these fields, by reducing image exposure time to as little as 1/1000th second within the 1/60th second for each field.

To calculate joint forces, moments and powers, GRF and kinematic data must be aligned in time. That is, we must know what GRF values from the force plate record occurred during a particular frame of video data. Alignment can be accomplished by simultaneously marking both the GRF and video data records. Video markings can be made by applying a step voltage to an LED which shows in the video data, while force plate data can be marked by outputting this LED step voltage to an open channel on the A/D input board. By subsequently aligning the point where the step voltage changed on the A/D record with the field from the video where the LED turned on, it is possible to synchronize the data. Using this strategy, if the LED in the video data was turned on after the shuttered image was stored for a particular field, this illumination would not be seen until the next cycle of the shutter (the next field). This delay would cause alignment of the A/D step voltage with the next video picture, resulting in a maximum alignment error of 1/60th second or one field. Figure 1 illustrates this worst-case situation, where force point #1 would be aligned with video picture #2 due to the fact that the LED voltage goes high shortly after video picture #1 is stored. The effect of a one field synchronization error is demonstrated in Figures 2 and 3. Substantial differences in peak values are evident along with a phase shift between curves.

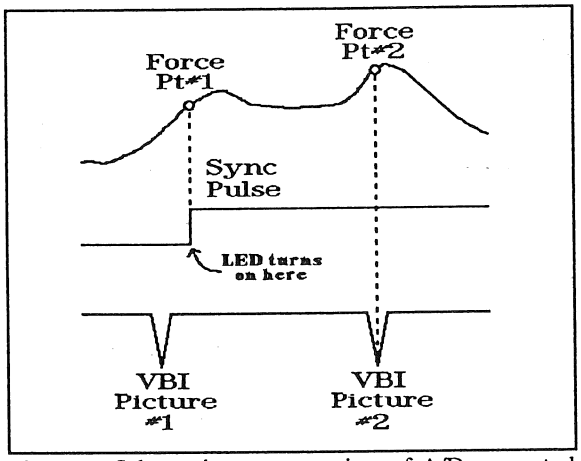

Figure 1: Schematic representation of A/D converted GRF, synchronization and video data. Figure illustrates a worst-case timing situation.

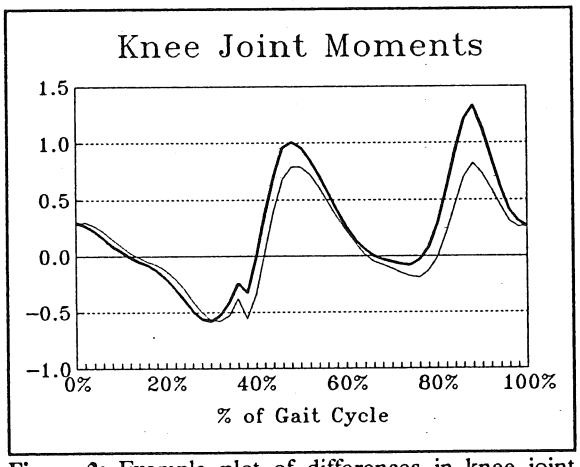

Figure 2: Example plot of differences in knee joint moments due to maximum alignment errors for GRF and kinematic data. Moments are in units of Nm/kg.

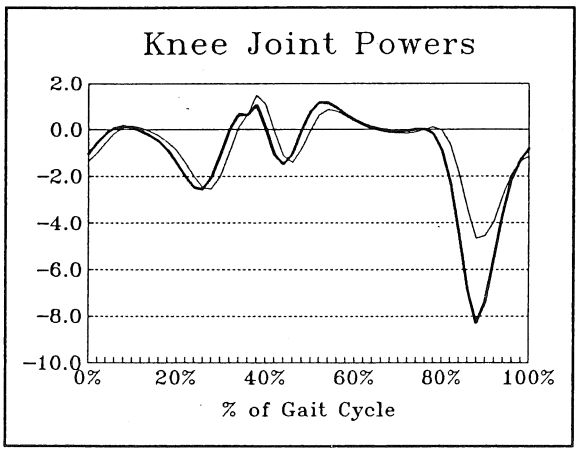

Figure 3: Example plot of differences in knee joint powers due to maximum alignment errors for GRF and kinematic data. Power values are in units of Watts/kg.

METHODS: NEW STRATEGY

Standard video output signals include a series of vertical blanking intervals (VBI ≈ 1.20 msec) which indicate the onset of each new field of image data, along with a more frequent series of very short duration horizontal blanking pulses (HBP ≈ 10 μsec). Figure 4 shows a schematic representation of a standard video voltage signal. When the shuttered video mode is used, images are acquired during a limited period at the initiation of the VBI, equal to the exposure time of the shutter. Identification of this short duration image storage period allows for a more precise knowledge of the timing for the video events, and thus a more precise alignment of GRF data with those video events.

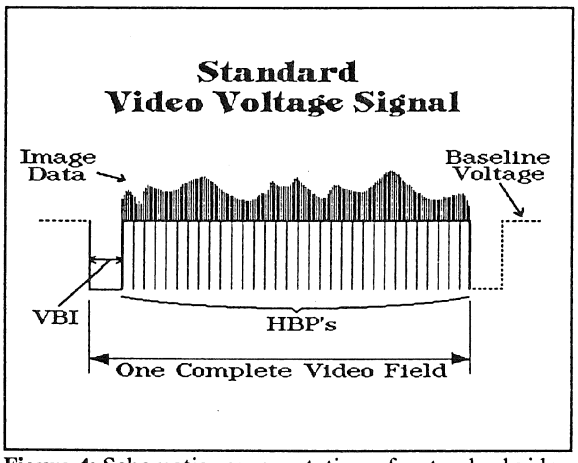

Figure 4: Schematic representation of a standard video voltage signal.

DATA SET-UP: To synchronize GRF and kinematic data more accurately, the video voltage signal must be A/D converted along with the synchronization pulse and force plate data. The sampling rate for these A/D data must be set at a frequency which is **NOT** a multiple of the 60 Hz image sampling frequency. In this case, A/D data were sampled at 598 Hz.

IMAGE PROCESSING ALGORITHM: The image data portion of the output signal maintains voltage levels above some baseline value, as seen in Figure 4 above. Conversely, Figure 4 shows that the VBI and the horizontal blanking pulses maintain voltage levels which fall below that baseline. Although the baseline voltage level is variable between trials, the range from the baseline to the VBI minimum voltage is consistent. By searching the A/D video signal for a minimum value this voltage range can be defined, and thus any A/D video signal values that exist within this range must be either horizontal or vertical blanking pulses.

Using the strategy above, it is possible to identify VBI's and HBP's from the video signal. By using a sampling rate (598 Hz) which is not a multiple of the 60 Hz video sampling, it is possible to distinguish between these two pulses. A/D converting the video signal at 598 hertz equates to just under 10 data points for each video picture. Once an A/D video data point is identified below the baseline voltage, the value which occurred 10 points later (1.0033 pictures) is examined. If this prior point also falls below the baseline voltage, it must be another VBI. (Since the HBP's are of extremely short duration (≈10 μsec.) and repeat at multiples of the 60 Hz sampling rate, this eliminates the possibility that either of the identified data pair are HBP's.)

SUMMARY: Employing the synchronization strategy described above makes it possible to align kinematic and GRF data to within 1/1200th second. This process assures that the force data which occurred precisely when the video image was captured are assigned to that video frame. Using the worst-case situation illustrated in Figure 1, force point #2 would now be aligned with video picture #2, whereas the former strategy had assigned force point #1 to video picture #2. The procedure outlined in this paper will lead to greater precision in calculations of joint forces, moments and powers.

Description of this synchronization strategy was based on specifics of the setup in the University at Buffalo Biomechanics lab, however the process can be adapted to other setups using a wide range of sampling rates.

EFFECT OF UNCERTAINTIES ON JOINT MOMENT ESTIMATION IN CEREBRAL PALSY GAIT

M.P. Kadaba, H.K. Ramakrishnan, M.E.Wootten, D.Jacobs, and J.Burn
Orthopaedic Engineering and Research Center
Helen Hayes Hospital
West Haverstraw, New York-10993

INTRODUCTION:

Joint moments estimated during gait are shown to be useful in clinical decision making (Prodromous, et al., 1985 and Lai, et al., 1988). Kinematic and kinetic data acquired during level walking are used for the calculation of joint moments. The effect of uncertainties in the joint center estimation on joint moments has been previously addressed (Andriacchi, et al.,1985). The accuracy and reliability of estimation of joint moments is also influenced by the errors in the definition of embedded axes (Ramakrishnan, et al.,1991). In this study, we quantify both the effects of uncertainties in the location of joint centers as well as uncertainties in the definition and orientation of embedded axes on the estimation of joint moments during cerebral palsy gait.

MATERIALS AND METHODS:

Kinematic and kinetic data acquired on 15 cerebral palsy patients during level walking at self selected speed formed the basis for this study. Models for computing joint moments and the methods for collecting gait data have been previously described (Ramakrishnan, et al., 1987 and Kadaba, et al., 1990). A computer aided motion analysis system (VICON) was used for acquiring kinematic data and two force platforms (Advanced Mechanical Technologies Inc.) were used for acquiring foot-floor contact forces. Foot-switches(pressure sensitive type) were attached to the heel, first and fifth metatarsal and great toe of each foot and were used to identify the gait events.

Retro-reflective markers were placed on the right and left anterior superior iliac spine (ASIS), greater trochanter, lateral knee, lateral malleolus, and over the space between the second and third metatarsal heads. Three wands, one on the mid thigh, another on the sacrum and a third on the mid shank were used to define the transverse plane rotations. The hip center relative to the ASIS was estimated from an empirical relation (Kadaba, et al., 1990). Knee center was calculated from the lateral knee skin marker by adding a correction to account for the width of knee. Similarly ankle center was obtained from the malleolus marker.

The lower body segments were modelled as rigid bodies connected by pin joints in estimating external joint moments. Embedded coordinates were assigned to the pelvis, thigh, shank and foot segments using the 3-D coordinates of reflective markers. Inertial forces were obtained based on mass center accelerations of different segments. The moments applied on the lower extremity joints were then calculated using ground reaction forces, inertial reactions, and body segment weights. Moments were normalized with respect to body weight and leg length and expressed as a percentage of body weight and leg length.

The first set of sensitivity analysis was performed by displacing hip, knee, and ankle centers by +20mm, +10mm, and +10mm respectively in each of the three coordinate directions. Joint moments were recomputed about these new locations. Hip, knee, and ankle centers were also displaced by -20mm, -10mm, and -10mm respectively from the reference position and the joint moments were recalculated. This analysis was repeated on the data obtained from all 15 cerebral palsy patients.

The second set of sensitivity analysis was performed by perturbing the embedded coordinate axes. The vectorial joint moments were projected onto reference proximal embedded axes to get the flexion/extension and abduction/adduction components. The proximal embedded axes were perturbed by rotating the flexion axis by +15 degrees in the transverse plane. The joint moments were recalculated about this new coordinate system. The procedure was also repeated for -15 degrees of perturbation.

RESULTS :

Figure-1 shows the effect of errors in the estimation of hip center location on hip moments of a representative cerebral palsy patient. The hip flexion/extension moment and adduction moment with the joint centers estimated at reference position are shown as thick lines. The thin solid lines correspond to +20mm(posterior/medial) displacement and dotted lines represent -20mm (anterior/lateral) displacement.

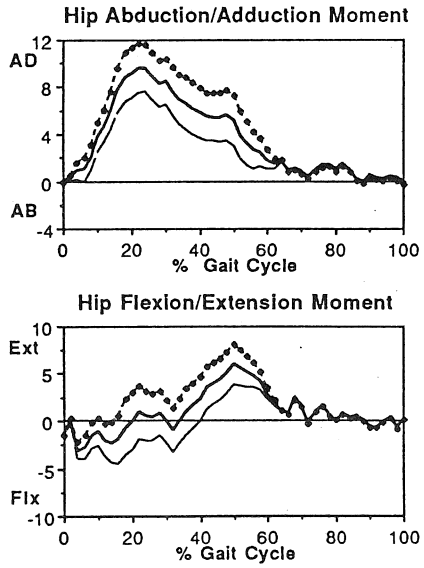

Figure 1. Effect of errors in the estimation of hip center location on hip moments

The percent errors in the magnitude of peak moments averaged over the 15 C.P.subjects are shown in table-1.

TABLE 1 Average percent error in the peak moments due to errors in the location of joint centers

Component of Joint moment	Average error(%)
Hip adduction	39
Knee adduction	38
Hip extension	24
Hip flexion	25
Knee flexion	12
Ankle flexion	11

The effect of perturbing the knee flexion axis in the transverse plane on knee moments of another C.P. patient is shown in figure-2. The solid thick lines in the middle correspond to the data in the reference position. The thin lines correspond to an internal rotation of 15 degrees and the dotted lines represent an external perturbation of 15 degrees with respect to the reference position. The crouch gait of this patient locates the ground reaction force vector behind the knee center throughout the stance phase causing external flexion moment. The force vector passes through the adduction axis at about 50% of gait cycle (zero adduction moment). At this phase of gait cycle, an internal perturbation resulted in ADDUCTION moment but an external perturbation shows ABDUCTION moment. The average percent errors in the magnitude of peak moments obtained from all 15 C.P. patients are listed in table 2.

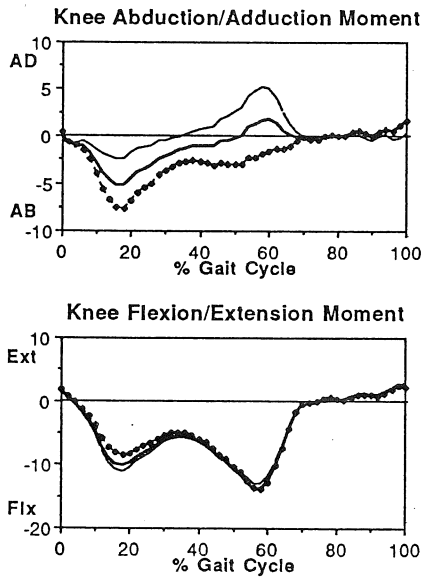

Figure 2. Effect of uncertainties in the definition of flexion axis on knee moments.

Table 2. Average percent errors in the peak moments due to variation in flexion axis

Component of Joint moment	Average error(%)
Hip adduction	19
Knee adduction	50
Hip extension	13
Hip flexion	9
Knee flexion	8
Ankle flexion	6

DISCUSSION:

Finite accuracy of motion analysis systems, skin motion artifacts, and inconsistencies in marker placements can introduce errors of 10 to 20mm in the location of joint centers. Our data show that such errors will result in errors of up to 39% in the peak joint moments.

Joint moment components are derived with respect to an orthogonal embedded coordinate system embedded in the proximal segment reflecting anatomical planes of motion. In most of the gait laboratories, knee flexion axis was defined as a line passing through the medial and lateral femoral condyles and can lead to uncertainty in defining this axis due to finite condylar areas. As seen in figure 2 and Table 2, the uncertainty in defining the flexion axis at knee not only introduces a large error in peak abduction/adduction moment, but also results in a totally different moment pattern. The knee flexion moment was least affected. This is because the resultant force on knee joint acts far behind the flexion axis due to excessive knee flexion seen in cerebral palsy gait. At the same time, the resultant force acts very close to the adduction axis. Thus, a small uncertainty in defining the embedded axes can result in either adduction or abduction moment depending on the direction of flexion axis.

Similar to the knee moments, ankle flexion moment is least affected by errors in embedded axes due to the forefoot walking pattern of cerebral palsy gait, which keeps the resultant force far anterior to the ankle joint.

In summary, pattern of joint moments and magnitude of peak moments are affected by errors in the estimation of joint center location and uncertainties in the definition of embedded axes. Accurate calibration and consistent placement of reflective markers minimize these errors. However, in interpreting joint moment data to make clinical decisions, the extent of these effects must be taken into consideration.

REFERENCES

Andriacchi, T.P. et al. NATO Advanced Science Institute Series, E. No.93, 83-102, 1985.
Kadaba,M.P. et al. J. Ortho. Res.,8, 383-392,1990.
Lai, et al. J. Ped. Ortho 8, 690-695, 1988.
Prodomous, C.C. et al. J.Bone Joint Surg. [Am]67, 1188-1194, 1985.
Ramakrishnan, H.K. et al. Trans. ASME, BED-4/Dsc-7, 87-92, 1987.
Ramakrishnan, H.K. et al. Trans. ASME, AMD-120, 333-339, 1991.

PRESSURE DISTRIBUTION MEASUREMENTS DURING NORMAL GAIT: DEPENDENCY ON MEASUREMENT FREQUENCY AND SENSOR RESOLUTION

M.M. Morlock[2,n] and T.W.F. Mittlmeier[n]

[2]Novel Biomechanics, Munich, Germany, [n]Ludwig Maximilian University, Munich, Germany

INTRODUCTION

Pressure distribution measurements have been established as important contribution to clinical gait analysis (Mittlmeier *et al.*, 1991). One problem, which has only been partly addressed in the literature, is the dependency of measured pressures on measurement frequency and sensor resolution (Cavanagh *et al.* (1991); Schaff *et al.*, 1992). This issue, however, becomes important since the systems, used for pressure distribution measurements, vary greatly with respect to these parameters: the measurement frequency ranges from 20 to 200 Hz (Hennig, 1990; Hennig *et al.*, 1991), the sensor resolution from 0.5 sensor/cm² up to about 9 sensors/cm².

The required size of a sensor is dependent on the size of the anatomical landmark, which causes the pressure during gait. A sensor, which is larger than the actual landmark causes that the measured pressure is lower than the actual pressure: let us assume we have a landmark with an area of 1 cm², which exerts a force of 10N. A sensor with an area of 1 cm² will measure a pressure of 10N/cm²; a sensor with an area of 2 cm², however, will measure a pressure of 5N/cm², since most available systems measure the net force. This is caused by the measurement method, which estimates the pressure from dividing the force by the area of the sensor. The logical conclusion would be to use very small sensors for the measurements. However, the total number of sensors in a measurement device is limited by the available measurement electronics. The size of the measurement platform or the measurement frequency consequently decreases with a decreasing sensor size.

No quantitative data on the influence of different sensor resolutions and measurement frequencies for recorded pressures are available in the literature. The purpose of this study was to estimate practically and theoretically the influence of these two parameters for gait analysis.

METHODOLOGY

Data acquisition: Three EMED pressure distribution platforms with sensor resolutions of 1 sensor/cm², 2 sensors/cm², and 4 sensors/cm² together with an EMED-SF System were used for data acquisition (RESOLUTION CONDITIONS). These platforms were sampled with 100 Hz, 70 Hz, and 50 Hz respectively. Since these 3 measurement conditions varied with respect to resolution and frequency, a second set of measurements was performed with the 2 sensors/cm² EMED platform sampled at 70 Hz, 50 Hz, and 25 Hz (FREQUENCY CONDITIONS). One healthy male subject with no prior foot injuries volunteered for the data acquisition (mass: 85kg, height: 1,78m). Four walking trials for each of the 6 described conditions were performed. The walking speed was controlled to be 4.5 km/h ± 10%.

Calculations: The data of each of the 2 and 4 sensors/cm² platform measurements of the RESOLUTION CONDITION were used to calculate the hypothetical pressures for a smaller sensor resolution (less sensors per cm²). From the 4 sensors/cm² platform data, hypothetical values for 2 sensors/cm² and 1 sensor/cm² resolution were calculated. From the 2 sensors/cm² platform data, hypothetical values for 1 sensor/cm² resolution were calculated (3 CALCULATION CONDITIONS). The algorithm is explained for the calculation of the pressures of a 1 sensor/cm² resolution from the pressures of a 4 sensors/cm² resolution: a quadratic grid with a grid line length of 1 cm was used to average the pressures of 4 adjacent sensors of the 4 sensors/cm² resolution. This was repeated for each of the 4 possible initial locations of the grid, yielding 4 data sets for each original data set.

This procedure yielded a total of 16 data sets for each of the CALCULATION CONDITIONS.

Definition of foot areas: Each foot print was divided into 5 different areas using the MULTIMASK Software package. First the foot axis, defined as a straight line between the center of the heel and the space between the first and second phalangeal was manually identified (adapted from Cavanagh *et al.*, 1987). Then a rectangle, surrounding the foot with its long sides parallel to the foot axis and touching the outline of the foot print on each side as well as anteriorly and posteriorly, was overlaid. The heel was defined from 0%-32% of total foot length, the midfoot as 32%-60%, the forefoot as 60%-100%. The forefoot was further divided into a lateral (0%-32% of foot width), intermediate (32%-64%), and medial (64%-100%) part.

Statistical analysis: The maximum pressure, which occurred at any time of the roll-over-process, was calculated for the whole foot and each defined foot area. The STATGRAPHICS Software package was used to calculate a One-way Analysis of Variance with a Tukey Post Hoc Test for the 9 different conditions. The significance level was set to $\alpha = 0.05$.

Table 1: Maximum pressure during normal gait for the different conditions (means and standard errors).

Measurement Condition	Total		Heel		Midfoot		Lateral Forefoot		Intermed. Forefoot		Medial Forefoot	
	Mean [N/cm²]	S.Err [N/cm²]	Mean [N/cm²]	S.Err [N/cm²]	Mean [N/cm²]	S.Err [N/cm²]	Mean [N/cm²]	S.Err [N/cm²]	Mean [N/cm²]	S.Err [N/cm²]	Mean [N/cm²]	S.Err [N/cm²]
Resolutions												
1/cm²	60.3	5.8	33.5	1.8	7.3	1.1	8.5	1.7	58.5	7.4	45.3	7.7
2/cm²	65.8	6.3	32.8	1.5	7.3	1.6	13.5	4.9	60.0	5.1	55.0	7.8
4/cm²	71.5	2.2	26.5	0.7	5.3	0.3	17.8	2.3	52.5	5.3	69.8	3.6
Calculations												
2/cm²	65.8	6.3	32.8	1.5	7.3	1.6	13.5	4.9	60.0	5.1	55.0	7.8
2 -> 1/cm²	53.1	1.3	31.6	0.7	6.8	0.6	9.0	0.7	52.4	1.4	35.2	2.3
4/cm²	71.5	2.2	26.5	0.7	5.3	0.3	17.8	2.3	52.5	5.3	69.8	3.6
4 -> 2/cm²	59.3	1.0	25.6	0.2	4.4	0.1	14.6	1.1	47.4	2.2	56.5	1.3
4 -> 1/cm²	53.6	2.2	25.6	0.2	4.5	0.2	8.6	1.5	45.9	2.0	47.8	2.7
Frequency												
25 Hz	63.8	4.6	26.0	0.9	5.8	0.8	18.3	5.6	55.5	6.3	56.3	6.2
50 Hz	58.0	4.7	31.0	1.3	6.8	1.4	13.3	2.1	53.8	5.3	50.8	4.2
70 Hz	57.0	2.1	31.0	1.4	7.8	1.2	17.8	0.3	57.0	2.1	47.8	2.4

RESULTS

RESOLUTION CONDITIONS: The maximum pressure of the lateral forefoot and the medial forefoot was significantly lower in the 1 sensor/cm² resolution than in the 4 sensors/cm² resolution (Table 1). The maximum pressure for the total foot showed the same tendency.
The maximum pressure of the heel was significantly lower in the 4 sensors/cm² resolution than in the 1 and 2 sensors/cm² resolution (Figure 1).

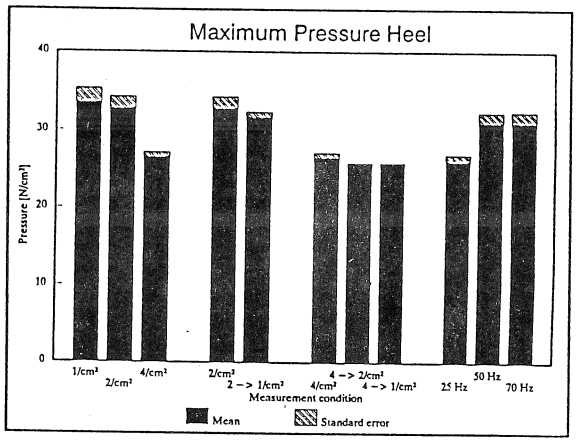

Figure 1: Maximum pressure in the heel area for the different measurement conditions.

FREQUENCY CONDITIONS: The maximum pressure of the heel was significantly lower for the 25 Hz sampling than for the 50 Hz and 70 Hz sampling. The other foot areas showed no significant influence of the sampling frequency.
CALCULATIONS: The calculation of the 1 sensor/cm² resolution from the 4 and the 2 sensors/cm² resolution showed significant lower values for the total foot and the medial forefoot area. The calculation of the 2 sensors/cm² resolution from the 4 sensors/cm² resolution showed no significant differences for any of the foot areas, even so the calculated values were always clearly lower.

DISCUSSION

It should be clearly stated that the presented results are limited due to the evaluation of a single subject and the large standard errors. The study is still ongoing and more subjects will be investigated. Nevertheless, certain tendencies are already visible, which demonstrate the importance of this approach, especially for the heel and forefoot area.
The averaging of adjacent sensors in the heel area showed that the anatomical area, which is responsible for the maximum pressure, is rather large: the calculated 1 sensor/cm² resolution from the 4 sensors/cm² resolution showed values, which were only 0.9 N/cm² lower. This finding can be explained by the thick fat pad underneath the tuberosity of the calcaneus, which distributes high pressures over a rather large area.
The duration of the maximum pressure, however, is short since the maximum value with the 25 Hz sampling is significantly lower than with the 50 Hz and 70 Hz sampling. Furthermore, the finding that the maximum pressure in the heel is the lowest for the highest resolution (4 sensors/cm²) of the resolution conditions supports this speculation, since the 4 sensors/cm² platform has the lowest sampling rate. This finding can be explained by the short duration of the impact peak during walking, which might not be detected at low sampling rates. It is emphasized that the data for the resolution and frequency conditions were collected independently.
The averaging of adjacent sensors in the medial forefoot area showed the opposite tendency than for the heel area: the calculated 1 sensor/cm² resolution from the 4 sensors/cm² resolution yielded values, which were 22 N/cm² lower. The same result was found for the actual measurements using different platform resolutions: the measured maximum pressure with 4 sensors/cm² was 24.5 | 9.7 N/cm² higher than with 1 | 2 sensors/cm² resolution, respectively. These findings can be explained by the thin fat pad and the small size of the sesamoid bones and the bony prominences at the metatarsal heads and phalanges.
The measurement frequency does not seem to influence the magnitude of the measured maximum pressure.

CONCLUSIONS

The investigated sensor resolutions and sampling frequencies represent the range typically used for pressure distribution measurements in the clinical routine. It is not possible to speculate, if the maximum pressure values measured with a resolution of 4 sensors/cm² or a sampling rate of 100 Hz are "accurate" values, represent the actual maximum pressures underneath the foot during walking. It could be that actual maximum pressures are higher but are applied over a smaller area than 0.25 cm² (especially in the forefoot area), or that they only act for such a short period of time that they are not detected with a sampling frequency of 100 Hz, or a combination of the two factors. However, the clinical significance of such values is questionable. Nevertheless, studies have to be conducted to investigate if differences with higher sensor resolutions and/or sampling frequencies can be observed. It has also to be studied, if the reported results are similar for pathologic feed.
It seems justified to speculate that resolutions of 2 or 4 sensors/cm² and measurement frequencies of 50 to 100 Hz are sufficient for clinical measurements.

REFERENCES

Cavanagh, P. et al. *Foot & Ankle*, 5, 262-276, 1987.
Cavanagh, P. The Foot in Diabetes, (pp. 54-70), LEA & FEBIGER, 1991.
Hennig, E. et al. *Foot & Ankle*, 5, 306-311, 1991.
Hennig, E. *Sportverl. Sportschad.*, 4, 109-116, 1990.
Mittlmeier, Th. et al. *Orthopäde*, 20, 22-32, 1991.
Schaff, P. *Orthopädie Technik*, 11, 787-795, 1991.

ASB YOUNG SCIENTIST AWARDS

Podium

THE EFFECT OF QUADRICEPS AND HAMSTRINGS ACTIVITY ON STRAIN IN THE ANTERIOR CRUCIATE LIGAMENT

B. Fleming, B. Beynnon, C. Stankewich, M. Pope
C. Nichols, P. Renstrom, R.J. Johnson
Dept. of Orthopaedics, University of Vermont, Burlington, VT

INTRODUCTION: The anterior cruciate ligament (ACL) is the most frequently totally disrupted ligament in the knee. For the active patient, intra-articular ACL reconstruction using an autogenous graft is the treatment of choice. However, the success rate of these types of procedures is debatable. Many variables influence the success of ACL reconstruction, including the post-operative rehabilitation regime prescribed. Complete immobilization has been shown to hinder the healing process and promote detrimental side effects, while an overly aggressive protocol may stretch out or rupture the healing graft, particularly during the initial 8 weeks when the graft and fixation strength is the lowest. The optimal rehabilitation program remains highly controversial, since it is based on clinical impression and not on scientific data.

The quadriceps and hamstrings are primary muscles which control knee joint motion. Determining the effect that these muscles have on the ACL is important data for the development of rehabilitation programs following ACL injury or reconstruction. The objective of this study was to measure strain of the anteromedial band (AMB) of the normal ACL, *in vivo*, during rehabilitation activities involving the quadriceps and/or hamstrings. Isometric, isotonic and closed kinetic chain activities were investigated. The following five activities were investigated; 1) active flexion-extension with a weight boot, 2) isolated quadriceps contraction, 3) isolated hamstrings contraction, 4) simultaneous quadriceps and hamstrings contraction, and 5) squatting activities. The null hypotheses were; 1) AMB strain during active flexion-extension (AROM) is equal to active flexion-extension with a 45 N weight boot at 20, 40, 60, and 90° of knee flexion (AROM45), 2) AMB strain is equal at 15, 30, 60, and 90° of flexion during an isolated quadriceps contractions (IQ), 3) AMB strain is equal at 15, 30, 60, and 90° during isolated hamstrings contractions (IH), 4) AMB strain is equal at 15, 30, 60 and 90° of flexion during simultaneous quadriceps and hamstrings contraction (SQH), and 5) AMB strain is equal for squatting with and without a resistive elastic cord designed to elevate quadriceps and hamstring activity.

METHODS: Ten patients, between the ages of 18 and 35, participated in the study. All patients were candidates for arthroscopic meniscectomy under local anesthesia. Eight of the 10 patients participated in AROM45 group, 5 participated in the IQ/IH/SQH groups, and 6 participated in the squatting group. A Hall effect strain transducer (HEST) was arthroscopically implanted in the AMB of the ACL. The wounds were closed, and an electrogoniometer was mounted to the leg to measure flexion-extension and axial rotation of the tibia relative to the femur. The patient then sat at the end of the operating room table with femur secured in the horizontal plane and the tibia hanging vertically. Both an anterior-posterior shear test at 30° knee flexion (lachman test) and an AROM test was performed before and after each test group to ensure reproducibility of the HEST measurement. The before/after HEST lengths were compared at 150 N anterior shear load during the lachman, and a flexion angle of 20° during AROM. For the AROM45 group, a 45 N weight boot was secured to the patient's foot. The patient was then instructed to extend and flex the knee four times. AMB strain was compared at 20, 40, 60 and 90°. For the IQ and IH subjects, the distal end of the tibia was strapped against a stationary tension-compression load cell which was attached to a t-bar. The t-bar supported the leg at 15, 30, 60 or 90° of knee flexion. At each flexion angle the patient was instructed to produce a 75% maximal extension effort followed by a maximal flexion effort. The length between the joint line and the load cell was recorded for the calculation of torque. Strain values were compared at -10 Nm, 15 Nm and 30 Nm. After the IQ/IH tests the same patients performed the SQH activities. The patient's leg was supported by the examiner at 15, 30, 60 or 90° flexion. The patient was asked to relax and then simultaneously contract both the hamstrings and quadriceps at maximum effort, while maintaining the specified flexion angle without examiner support. The maximum strain values were compared. The squatting subjects then got off the OR table and performed a normal squat four times. The squats were then repeated using an elastic "Sport Cord" (Sport Cord, Inc., Sandy UT), a commonly prescribed rehabilitation device which was positioned under the foot and pulled up to the waist to increase muscle activity. Strain values were compared at 10, 20, 40, 60, and 90° of knee flexion. For all experiments, engineering strain was calculated from the HEST displacement using a reference length equal to the HEST length at the slack-taut transition

point of the AMB. All tests were repeated four times. The null hypotheses were accepted or rejected using ANOVA coupled with multiple range comparison tests. Each patient served as their own control.

RESULTS: There were no significant differences between the repeated measures Lachman or AROM tests for any of the test groups. The mean AMB strains for AROM and AROM with the weight boot are shown in Fig.1. There were no significant differences at 20, 40, 60, or 90° of knee flexion. The moment versus mean strain results for the four flexion angles are shown in Fig. 2 for isolated quadriceps and hamstrings contraction. At -10 Nm hamstrings contraction, there were no significant differences between flexion angles. At 15 and 30 Nm quadriceps contraction there were significant differences between 60, 30 and 15° ($p<.01$) but not between 60 and 90° flexion. At 60 and 90°, the AMB was not strained. The mean resting and maximum simultaneous contraction strain data are presented in Fig. 3. For isometric simultaneous quadriceps and hamstring contraction, there was a significant difference ($p<.01$) between 15 and 30° at maximal effort. No other statistical differences were found. During squatting, there were no significant differences between the normal squat and squatting with the sport cord at the flexion angles tested (Fig. 4).

DISCUSSION: Although the strain threshold that is detrimental to graft healing and fixation failure remains unknown, it is possible from this data to rank order the different rehabilitation activities involving the quadriceps and hamstrings by maximum AMB strain. For all of the activities investigated, the AMB was not strained as a result of quadriceps or hamstrings activity at flexion angles between 50° and 90°. In this region, quadriceps and hamstrings activity should not place a properly positioned graft at risk to failure or permanent elongation. Isolated isometric hamstrings contraction also did not strain the AMB at any flexion angle whereas isometric quadriceps contraction at 30° (2.8% at 30 Nm) and 15° (5.8% at 30 Nm) knee flexion did strain the AMB. Both squatting and active flexion-extension with a weight boot strained the AMB over 4% towards extension. The strain produced in these latter activities is substantial.

Fig 1: AMB strain during AROM & AROM with a 45 N weight boot.

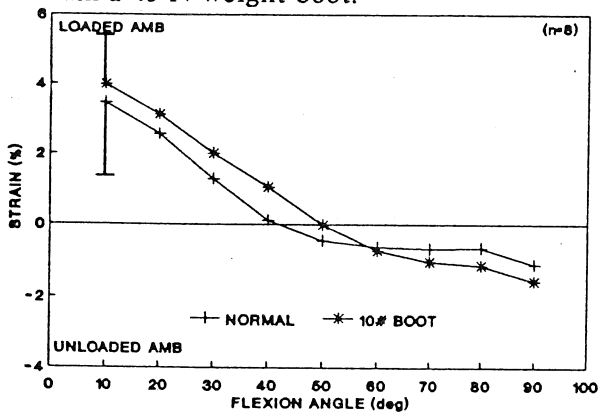

Fig. 2: AMB strain during isolated quads & hams contraction at 15, 30, 60, and 90° flexion.

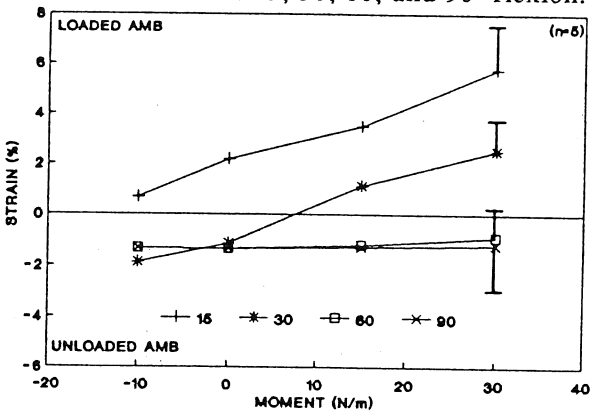

Fig. 3: AMB strain during simultaneous quads/hams contraction.

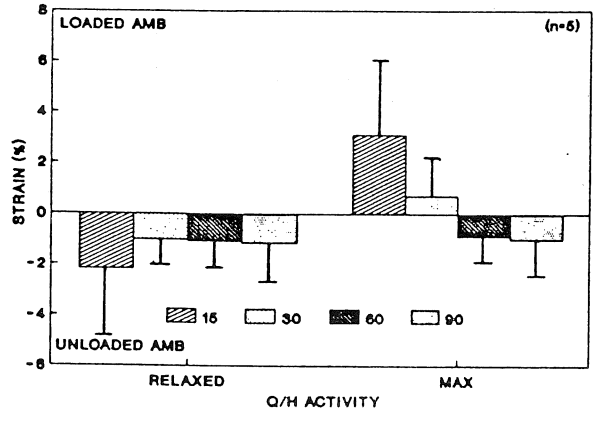

Fig. 4: AMB strain during squatting with and without Sports Cord.

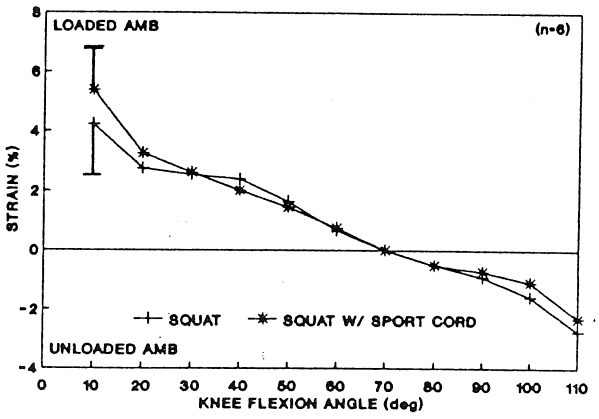

BIOMECHANICAL RELATIONSHIPS OF NORMAL AND DEGENERATIVE HUMAN ANKLE CARTILAGE

K. A. Athanasiou and R.C. Schenck, Jr.

Orthopaedic Biomechanics Laboratory, Department of Orthopaedics
The University of Texas Health Science Center, San Antonio, Texas 78284

INTRODUCTION

In order to elucidate the role of mechanical factors in the etiology or development of articular cartilage afflictions in the ankle, we obtained the topographical variations of the tissue's mechanical properties in 14 human tibiotalar joints. Using the biphasic creep indentation methodology and the automated indentation apparatus, we show that differences in the tissue's intrinsic material properties may contribute to strain mismatches between specific sites in the distal tibia and proximal talus. This disparity of mechanical properties between the articulating surfaces may in turn contribute to an abrasive mechanism which may lead to cartilage degeneration at sites of mismatch. Indeed, these significant variations seem to explain clinically observed cartilage degenerations occurring in specific portions of the joint (e.g., the posteromedial talus), even in the absence of traumatic episodes.

REVIEW AND THEORY

Pathological changes of articular cartilage in the tibiotalar joint, which are less common than those in the knee or hip, are usually associated with transchondral fractures of the talus, osteochondritis dissecans of the talus, and osteoarthritis of tibial and talar surfaces. Osteochondritis dissecans of the ankle is usually manifested in the posteromedial or anterolateral aspects of the talus (O'Farrell and Costello, 1982). Transchondral fractures of the talus result from trauma (Cameron, 1956; Davidson et al., 1967) and occur most frequently in the anterolateral and posteromedial portions of the talus (Berndt et al., 1959). It was postulated that these lesions in the talus result from acute injuries, such as a sprain with ankle inversion. Similarly, localized osteochondritis or avascular necrosis occurs in the medial aspect of the dome of the talus. In this location, inversion stress has been considered a possible etiologic factor but the evidence of trauma is lacking. Ankle osteoarthritis has been related to fracture, malalignment, or even conceivably that of an aging process. In a previous study, we investigated the cartilage biomechanics of the radiocapitellar joint and were able to develop a mechanism for osteochondritis dissecans affecting this joint in the elbow (Schenck et al., 1992).

In this study, we utilized our automated indentation apparatus (Athanasiou et al., 1992) and the biphasic creep indentation methodology (Mak et al., 1987; Mow et al., 1989) to evaluate the material properties of the ankle mortice and talar articulation to look for a possible etiologic mechanism of cartilage degeneration of the ankle when an obvious traumatic episode is not present.

PROCEDURES

We performed creep indentation experiments in 5 sites in the distal tibia, 1 site in the distal fibula, and 8 sites in the proximal talus of 7 pairs of human ankles (4 females and 3 males). The specimens ranged in age from 18 to 82 years (mean of 51 years). Only normal articular surfaces were utilized, as determined with the India ink staining technique (Meachim and Emery, 1973). As shown in Fig. 1, in the talar surface we tested the following sites: anterior lateral (aAL), central lateral (aCL), lateral side (aSL), posterior lateral (aPL), posterior medial (aPM), central medial (aCM), side medial (aSM), anterior medial (aAM). In the tibial surface we tested the following sites: anterior lateral (AL), anterior medial (AM), medial malleolus (Mm), posterior medial (PM), posterior lateral (PL). We also tested the central portion of the fibula (FI). These were labeled in a manner representing the human anatomic position in which the anterior portions of the tibia and talus are in contact. The creep-recovery response of each of these 196 osteochondral specimens under a 1.0 mm dia rigid, porous indenter tip was measured using an automated biphasic creep indenter (Athanasiou et al., 1992). Tare load (0.03N) creep, test load (0.16N) creep, and recovery equilibria were determined using slope criteria. Specifically equilibrium was automatically determined when the slope of the curve became smaller than $1x10^{-6}$ mm/s. The thickness of articular cartilage at each test site was also measured using a needle attached to an LVDT and a force transducer. Articular cartilage was modeled as a biphasic material (Mow et al., 1980), under conditions of creep indentation. This methodology uses the creep indentation solution (Mak et al., 1987) with a corresponding numerical algorithm (Mow et al., 1989). Statistically, results were analyzed using ANOVA, multiple comparisons tests, and Student's t tests at p=0.05.

RESULTS

The material properties and thickness of articular cartilage in the distal tibia and proximal talus are shown in tables 1 and 2 respectively.

Table 1:

TIBIA	H_A (MPa)	ν_s	$kx10^{15}$ (m^4/Ns)	h (mm)
AL n=14	1.20±0.25	.02±.04	1.55±1.79	1.30±0.25
AM n=14	1.34±0.58	.03±.06	1.41±2.23	1.23±0.27
Mm n=14	0.94±0.36	.04±.08	0.93±0.84	0.97±0.16
PM n=14	1.23±0.33	.03±.07	1.79±2.24	1.20±0.29
PL n=14	1.26±0.31	.00±.01	1.56±1.74	1.21±0.25
FI n=14	1.14±0.48	.08±.08	1.32±2.21	0.95±0.17

Table 2:

TALUS	H_A (MPa)	ν_s	$kx10^{15}$ (m^4/Ns)	h (mm)
aAL n=14	1.02±0.36	.06±.08	0.80±0.65	1.01±0.31
aCL n=14	1.21±0.39	.02±.05	0.96±0.51	1.17±0.27
aSL n=14	1.08±0.42	.00±.01	0.98±0.39	1.14±0.23
aPL n=14	0.92±0.33	.00±.00	1.05±0.67	1.45±0.42
aPM n=14	0.92±0.36	.02±.05	1.18±1.39	1.31±0.26
aCM n=14	1.25±0.51	.00±.01	1.17±0.38	1.31±0.33
aSM n=14	1.05±0.29	.02±.05	1.64±2.37	1.18±0.24
aAM n=14	1.01±0.47	.04±.05	0.94±0.62	1.17±0.34

Cartilage in the AM portion of the tibia has the largest aggregate modulus (H_A=1.34MPa). The softest tissue is in the aPL (0.92MPa) and the aPM (0.92MPa) regions of the talus. Overall, tibial cartilage is significantly stiffer than talar and fibular cartilage (1.19MPa vs 1.06MPa). The posterior aspects of the tibia combined together are stiffer than those in the talus (1.25MPa vs 0.92MPa). No statistical differences are shown between the aggregate moduli of male vs female specimens, between left vs right specimens, or between medial vs lateral specimens. The thickest and thinnest tissues are in the aPL ridge of the talus (1.45mm) and the FI (0.95mm), respectively. The largest Poisson's ratio is in the FI (ν_s=0.08). No differences are shown in cartilage permeability among the test sites. Cartilage of all female specimens grouped together is significantly more permeable and has a smaller apparent compressibility than male cartilage; it is also 27% thinner.

As shown in table 3, articular cartilage in the human ankle has material properties and thickness, which differ from those in the elbow (Schenck et al., 1992), hip (Athanasiou et al., 1992), and knee (Athanasiou et al., 1991).

Table 3:

JOINT	H_A (MPa)	ν_s	$kx10^{15}$ (m^4/Ns)	h (mm)
Ankle n=196	1.11±0.40	.03±.05	1.23±1.47	1.18±0.29
Elbow n=132	0.80±0.25	.07±.08	1.29±1.04	1.13±0.31
Hip n=140	1.21±0.61	.05±.06	0.90±0.54	1.34±0.38
Knee n=14	0.60±0.15	.06±.07	1.45±0.61	2.63±1.04

DISCUSSION

In the anatomical position, the significantly softer aPM articulates with the stiffer PM. The significant differences found in the aggregate modulus between aPM and PM, may contribute to initiation of degenerative changes, and agree with the frequently observed pathological changes in the posteromedial aspect of the talus. Our results, however, do not indicate significant stiffness differences between the anterolateral talar and tibial articulation, or the medial talar dome and the mid-portion of the tibia. These findings agree with clinical observations that localized osteochondritis of the medial dome of the talus is probably secondary to avascular necrosis (Berndt and Harty, 1959) and not due to a mechanical mismatch of the articulating cartilages.

Similarly, fractures in the anterolateral portion may be due to inversion and dorsiflexion of the ankle, as described by Berndt and Harty (1959), which brings the lateral aspect of the talus in impact against the articular surface of the fibula.

This study demonstrates significant differences in the mechanical properties of human ankle cartilage, topographically in the tibia and talus, and between these articulating surfaces. This new knowledge seems to explain some clinically observed pathological or traumatic phenomena in ankle cartilege. It may also contribute in designing ankle osteotomies so as to bring in contact articular surfaces with comparable mechanical properties.

REFERENCES

Athanasiou, K. et al., *J. Orthop. Res.*, **9(3)**:330, 1991.
Athanasiou, K. et al.,*J. Bone Jt. Surg.*, in press, 1992.
Cameron, B., *J. Bone Jt. Surg.*, **38A**:857, 1956.
Davidson, C. et al., *J. Trauma*, 7:378, 1967.
Berndt, A. et al., J. Bone Jt. Surg., **41A**:996, 1959.
Mak, A. et al., *J. Biomechanics*, **20**:703, 1987.
Meachim, G. & Emery, I., *J. Anat.*, **116(2)**:161, 1973.
Mow, V. et al., *J Biomech. Eng.*, **102**:73, 1980.
Mow, V. et al., *J. Biomechanics*, **22**:853, 1989.
O'Farrell, T. & Costello, B., *J. Bone Jt. Surg.*, **64B**:494, 1982.
Schenck Jr., R.C. et al.,*Trans. Orthop. Res. Soc.*, **17(1)**, 286, 1992.

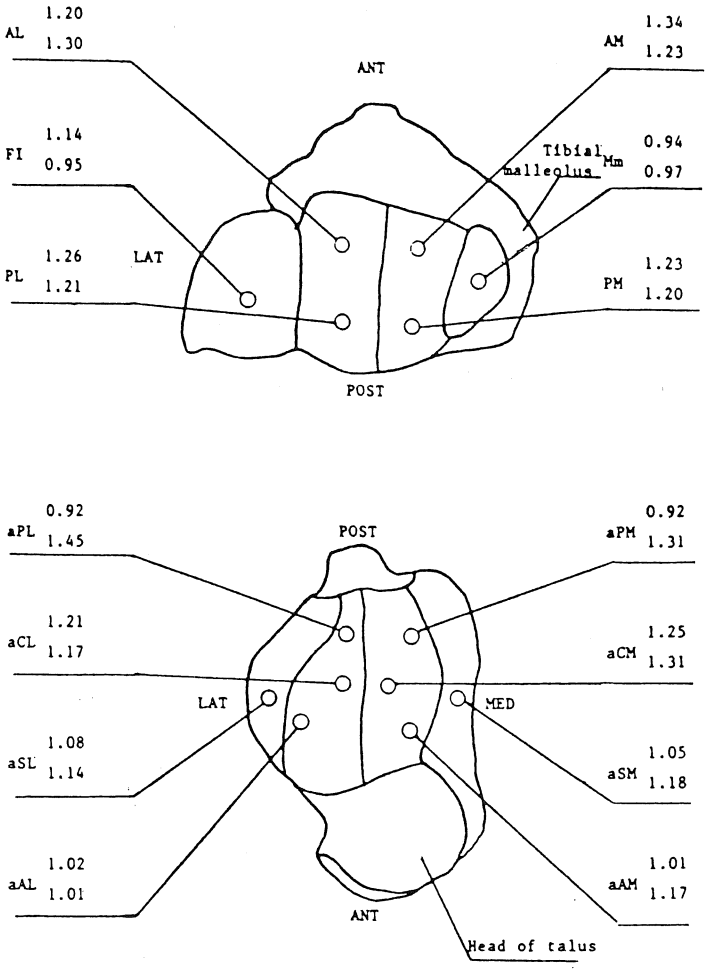

Fig. 1: Six sites were tested in the tibia and fibula, and eight sites were tested in the talus. A, anterior; P, posterior; C, central; S, side; M, medial; L, lateral; a, talus; m, malleolus; FI, fibula. The numbers represent the means of aggregate modulus and thickness, respectively, of each test site(n=14).

ASB SYMPOSIUM

Podium

CARDIOVASCULAR EXPERIMENTATION ON THE SHUTTLE

Drew Gaffney

Professor of Internal Medicine
Director of Clinical Cardiology
Vanderbilt University, Nashville, TN

INTRODUCTION

Microgravity produces almost complete unloading of the musculoskeletal system, in addition to substantial cephalid fluid shifts and changes in cardiovascular and neuroendocrine function. Spacelab Life Sciences 1 provided in-flight as well as pre- and post-flight studies to determine the mechanism of changes noted in previous flights.

RESULTS

This presentation will discuss significant findings of this mission. These findings include:

(1) Marked cephalid fluid shift documented by decrease in leg volume, facial edema and engorgement of veins in the upper body.
(2) Central venous pressure near zero.
(3) Strength was significantly decreased in postural muscles.
(4) Fine and gross motor control was also decreased.
(5) The above changes persisted longer than was previously recognized.

NEUROVESTIBULAR CONSEQUENCES OF MICROGRAVITY

James R. Lackner
Ashton Graybiel Spatial Orientation Laboratory, Bradeis University, Waltham.

INTRODUCTION

The vestibular system of the inner ear has two types of receptor organs. The semicircular canals respond to angular acceleration and the otolith organs to linear acceleration, including gravity. On Earth, the force of gravity continuously stimulates the otolith organs which signal head orientation with respect to gravity. The "pulling" of the body against the ground by gravity also causes asymmetric stimulation of somatosensory receptors and proprioceptive elements of the body that provide information about ongoing body configuration and the direction of 'down". In the microgravity conditions of space flight, the patterns of sensory input associated with orientation and movement are dramatically altered, as are the patterns of muscle activation necessary to produce particular body movements or configurations. The implications of these changes will be discussed for 1) perceived orientation, 2) head movements and motion sickness susceptibility, and 3) sensory-motor reentry effects after prolonged weightlessness.

PERCEIVED ORIENTATION IN MICROGRAVITY

On Earth, if we close our eyes, we continue to feel in the same body orientation. By contrast, in orbital flight or in the weightless phase of parabolic flight maneuvers, eye closure can dramatically affect orientation. Astronauts who are strapped in seats may feel upright when their eyes are open, but on closing them feel as if they are upside down hanging from their seat belt. If they are free floating, eye closure can lead to a loss of apparent orientation. The individual senses the relative configuration of his body and knows consciously his position within the vehicle but he does not feel in any orientation.

If an astronaut is free floating with eyes open, then his apparent orientation is determined by the direction of gaze, the architectural verticals and horizontals of the vehicle, and whether his feet are visible in relation to the features of the vehicle. Depending on body position, simply by changing the direction of gaze an astronaut can go from experiencing one orientation to another, for example, from feeling horizontal in a horizontal vehicle to feeling upside down in a nose down vehicle. Some astronauts over the course of a flight come to feel that wherever their feet are determines their sense of the direction of down.

These observations mean that, in the absence of cues to the vertical provided by the otolith organs, perceived body orientation is determined by patterns of touch and pressure cues, and by a variety of cognitive factors.

CONTROL OF HEAD MOVEMENTS IN MICROGRAVITY: MOTION SICKNESS SUSCEPTIBILITY

In orbital flight, nearly all aspects of movement control are affected. On Earth, rolling and pitching movements of the head are associated with a varying load of the head on the neck and with an altered pattern of otolith activity because of the reorientation of the head with respect to the direction of the gravitational force. In free fall, head movements in roll and pitch are associated with very different patterns of muscular innervation and sensory feedback than on Earth. We have found that pitch head movements compared with yaw or roll head movements are also most evocative of motion sickness in free fall; head stabilization tends to prevent sickness from occurring. However, head movements in free fall - regardless whether they are movements in yaw, pitch, or roll - all tend to bring on symptoms of motion sickness, and more severe symptoms are evoked if the eyes are open.

These findings indicate that motion sickness can occur when the patterns of sensory feedback associated with body movements are no longer normal. In this context, it is interesting that one of the most fascinating findings on space motion sickness concerns the susceptibility of the Skylab astronauts to motion sickness during exposure to Coriolis cross-coupled angular accelerations. Coriolis stimulation of the semicircular canals occurs when a rotating individual makes a head movement out of the plane of his rotation. The intensity of stimulation is dependent on the rotary velocity of the body, the velocity of the head movement out of the plane of rotation, and the angle between the rotation and head movement axes. Coriolis stimulation, when intense, elicits dizziness, nausea, and vomiting. In fact, on Earth it is one of the most provocative forms of stimulation known. Individuals without a functioning vestibular system are totally immune to such stimulation.

The Skylab astronauts were tested both in-flight and pre- and post-flight for their susceptibility to motion sickness during exposure to cross-coupled angular accelerations. When they were tested in-flight on or after mission day 6, each of them was insusceptible even when making head movements at very high velocities of rotation; by contrast, pre-flight every one of them had been quite susceptible. We wondered whether the decreased susceptibility to Coriolis stimulation in orbital flight resulted from some form of adaptation that took place early in the flight and persisted even for some period post-flight, or whether the decreased susceptibility resulted in part from immediate changes in vestibular and sensory-motor function related to being in free fall in orbital flight. We have found in parabolic flight experiments that sensitivity to Coriolis stimulation is highly background force dependent. Susceptibility is immediately decreased on transition into free fall and greatly increased in a 2G background force level relative to 1G terrestrial values. It turns out that the modified susceptibility relates to the altered weight of the head and changed demands on the neck musculature, as well as to the altered otolith signals.

SENSORY-MOTOR REENTRY EFFECTS ON RETURN TO EARTH

After prolonged exposure to microgravity, on return to Earth an astronaut may feel that the ground is not stationary under his feet as he moves about. A related effect occurs in the high force phases of parabolic flight. For example, if an individual lowers his body in a deep knee bend during exposure to a 2G acceleration level, he will feel as if he has moved downward too rapidly and that the aircraft has moved upwards under his feet: he both feels and sees the plane move up several inches. The reverse pattern is experienced when he raises his body.

The occurrence of such illusions indicates that skeletomotor control is normally calibrated to a 1G reference level and that exposure to non-1G acceleration levels affects the execution

and appreciation of voluntary movements. We have been able to show that the illusory effects result from mismatches between the actual and the "expected" movements of the body for particular patterns of alpha and gamma motoneuron innervation. These mismatches arise because of the altered load of the body on the muscles and the decreased otolith-spinal reflexive drive on the antigravity muscles. After an astronaut is in orbital flight for a prolonged period, his sensory-motor control mechanisms recalibrate to the 0G acceleration level. When he returns to the 1G acceleration level of Earth, it is for him like an individual calibrated to 1G being exposed to 2G. These observations show that normal locomotion involves both motor and sensory factors and internal representations of the body's dynamics in a 1G acceleration field.

CONCLUSIONS

The consequences of exposure to unusual force environments that have been described provide insights into the ways our bodies are adapted to the force background of Earth. As we learn more about the nature of this terrestrial adaptation, we gain a better appreciation of the subtlety and complexity of the sensory-motor mechanisms controlling our ability to move and orient. One unexpected consequence of space travel is that it is providing insights into the nature of the spatio-motor adaptations that constitute an essential prerequisite for life in a terrestrial environment. Much of what we take for granted in terms of the perceptual stability of ourselves and our environment is turning out on closer analysis to be the result of highly complex, automatic computations underlying the control of body movement and orientation.

REFERENCES

Lackner JR. Human sensory-motor adaptation to the terrestrial force environments. In: D. Ingle, M. Jeannerod, D. Lee (Eds.) Brain Mechanisms and Spatial Vision, (175-210 Nijhoff, Amsterdam, 1985.

Lackner JR. Sensory-motor adaptation to high force levels in parabolic flight maneuvers. In: M. Jeannerod (Ed.) Attention and Performance, Vol. 13, (527-548) Lawrence Erlbaum Associates, Hillsdale, NJ, 1990.

DiZio P, Lackner JR. Motion sickness susceptibility in parabolic flight and velocity storage activity. Aviation Space and Environmental Medicine, 62, 300-307, 1991.

Lackner JR, DiZio P. Gravitational, inertial and Coriolis force influences on nystagmus, motion sickness, and perceived head trajectory. In: A Berthoz, W. Graf, P.P. Vidal (Eds.) The Head-Neck Sensory-Motor Symposium, (216-222), Oxford University Press, NY, 1992.

NEUROMUSCULAR ADAPTATIONS TO SPACEFLIGHT

V. Reggie Edgerton, Roland R. Roy and John A. Hodgson
Department of Physiological Science and Brain Research Institute, UCLA
Los Angeles, CA 90024-1527

A reasonably complete picture of the general responses of skeletal muscle to spaceflight has been developed from a combination of flights varying in duration (two to three hundred and sixty-six days) and in species studied (humans, Rhesus and rats). Pre- and post-flight comparisons of neuromuscular performance in humans, and some in-flight testing in the early Soviet Union missions, have been made. Muscle biopsies have been obtained from eight astronauts before and after a five-day or an eleven-day flight. In addition, neuromotor performance and muscle tissue analyses have been successfully studied in Rhesus before, during and after a two-week flight on the Cosmos Biosatellite. Finally, biochemical, morphologic and some physiological characteristics from a range of muscles have been obtained from rats flown on the Cosmos Biosatellite or the Space Shuttle for periods ranging from four to twenty-two days. Based on the results derived from these studies, a number of conclusions can be drawn.

It is very clear that extensor muscles of the legs atrophy rapidly. For example, muscle fibers in the soleus, a slow ankle extensor, of rats flown for four days were 25% smaller than in ground-based controls. Fiber size in the soleus was reduced by about 35% after a two-week flight, showing only slightly more atrophy than that observed after one week. Thus, in rats the atrophic process begins early, proceeds rapidly, and appears to stabilize within one to two weeks. In the Rhesus, the adaptations in fiber size associated with spaceflight have not been clearly identified because of confounding variables. First, these studies have been limited by the long period of time at 1G between pre- and post-flight biopsies (up to four months), and thus the results also reflect general body growth. Second, the effects of the Rhesus sitting in a chair (i.e., restrained) during spaceflight have not been separated from the effects of spaceflight alone. Ground-based studies of the effects of chair restraint are needed to address this problem. Analyses of muscle biopsies from astronauts suggest that atrophy can occur rapidly (within five to eleven days) in some individuals. Single muscle fiber analyses in each of the species studied suggest that, at least in short-duration flights, there is not a significant effect on enzyme activities of the oxidative and glycolytic pathways. The type of myosin isoform expressed in some fibers can change, particularly in slow extensor muscles. For example, some fibers that usually express only slow myosin begin to express a fast myosin isoform after only four days of flight, and this adaptation becomes more evident after seven- and fourteen-day flights.

Motor performance also is affected by short, as well as long-duration spaceflight. Decreases in strength, power, motor control and stability of posture have been commonly observed in humans returning to 1G even after flights lasting only a few days. Perturbations also have been observed in specific motor reflexes such as the deep tendon reflex, Hoffman reflex and vibration sensitivity to the sole of the foot. Thus, a complex adaptation syndrome of the neuromotor system that perhaps changes continuously over the duration of a flight seems to be the net result of compensatory events in all components of the nervous and muscular system. The kind and magnitude of the compensatory events appear to be unique to the individual, to the muscle and to the sensorimotor networks that influence those muscles.

Supported by NASA Grant 199-26-12-09.

PATHOPHYSIOLOGY OF MINERAL LOSS DURING SPACE FLIGHT

C.D. Arnaud, C.E. Cann, B.P. Halloran,
M.E. Hammond, D. Matsumoto and S.D. Sanchez

Program in Osteoporosis and Bone Biology, University of California, San Francisco
Department of Psychology, San Francisco State University, San Francisco

INTRODUCTION

Bone loss due to conditions of microgravity could limit the future of manned space exploration.[1] Because the pathogenesis of this bone loss is not known, it has not been possible to develop rational counter-measures to prevent it. We measured serum ionized calcium and calciotropic hormones in four crew members exposed to microgravity during Space Life Sciences 1 (SLS-1), the first NASA space shuttle flight to be completely devoted to life science investigations.

REVIEW AND THEORY

The earth-based paradigm that is thought to most closely mimic microgravity associated bone loss is immobilization osteoporosis. In this disorder, measurements of serum minerals and calciotropic hormones suggest that increased bone resorption is a major factor in its etiology; serum and urine calcium are slightly increased, and serum immunoreactive parathyroid hormone (iPTH) and 1,25 dihydroxyvitamin D are appropriately decreased.[2] The SLS-1 experiment was designed to investigate whether, in response to space flight, there are significant changes in the circulating levels of calciotropic hormones, and whether any changes are primary or in response to a change in skeletal homeostasis.

PROCEDURES

We measured ionized calcium, intact immunoreactive parathyroid hormone (intact PTH), 25 hydroxyvitamin D (250HD) and 1,25 dihydroxyvitamin D [1,25$(OH)_2$D] in the serum of four crew members before, during and after the nine day flight of (SLS-1) in June 1991. The serum compounds were measured using conventional means: ionized calcium by selective ion electrode, intact PTH by a sensitive and specific two-site radioimmunometric assay, and 250HD and 1,25$(OH)^2$D by receptor binding assays.

RESULTS

We expected that among the astronaut crew the biologically normal negative correlation between serum ionized calcium and intact PTH would be exhibited because we expected that any changes due to space flight would be in the normal physiological range of responses. We therefore performed a statistical analysis of the relationship of these variables across all measurements in all subjects. The correlation coefficient for this relationship was negative (0.52) and significant ($p < 0.01$) as expected. Based on this analysis, we concluded that the responses of the crew to perturbations in extracellular calcium homeostasis reflected appropriate physiologic adaptive responses.

Serum ionized calcium increased dramatically on flight day (FD) 2 to levels 30% above control (levels that are normally considered to representative of moderately severe hypercalcemia). By FD 8, serum ionized calcium levels were still 20% above normal, indicating that clinically significant hypercalcemia was maintained throughout the flight. Mean serum intact PTH declined appropriately to about 60% of control throughout the flight, a finding that biologically validates the increase in serum ionized calcium and discounts the possibility that PTH is responsible for the hypercalcemia. Serum ionized calcium returned toward control values one day after the shuttle returned to earth (R + 1) and was no different from control on R + 6. Serum intact PTH returned more slowly to control values. Serum 250HD did not change from baseline values and serum 1,25$(OH)_2$D decreased by FD 8.

We sought cause for the relatively low correlation coefficient between serum ionized calcium and intact PTH by examining the correlation coefficients for these variables in individual subjects. Two of the four subjects fit one pattern with a correlation coefficient of 0.8, while the other two subjects exhibited a much lower correlation

(0.3). On decoding the data, we found that the male crewmembers showed the highest correlation. This is an unexpected finding that deserves further investigation, especially relative to the possible influence of reproductive hormones on calcium metabolism in space flight. There were no significant correlations of serum $1,25(OH)_2D$ with serum ionized calcium or intact PTH.

DISCUSSION

The data suggest that our measurements of serum ionized calcium and intact PTH are biologically valid, that they qualitatively parallel those observed in immobilization osteoporosis except that hypercalcemia is more severe during acute microgravity exposure, and that they are consistent with increased bone resorption playing a major role in the pathogenesis of mineral loss during space flight. Based on these results, antiresorptive drugs could be useful in preventing the bone loss of space flight.

REFERENCES

1. Rambaut, P.C., et al: *Acta Astronaut*, **6**: 1113-1122, 1979.
2. Stewart, A.F., et al: *N. Engl. J. Med.*, **306**:1136-1140, 1982.

KNEE LIGAMENT DEFICIENCY

Podium Session 5

IN VIVO FORCES IN THE ANTERIOR CRUCIATE LIGAMENT DURING WALKING AND TROTTING IN A QUADRUPED

J.P. Holden, D.L. Korvick, E.S. Grood, J.F. Cummings, D.I. Bylski-Austrow

Noyes-Giannestras Biomechanics Laboratories
Department of Aerospace Engineering and Engineering Mechanics, University of Cincinnati

INTRODUCTION

Direct measurements were made of in vivo forces in the anterior cruciate ligament (ACL) in three quadrupeds. The purpose was to determine when and to what levels the ACL is loaded during activity, so as to increase understanding of ACL function in vivo, and to better design and interpret studies of tissue healing and remodeling. The ACL was loaded primarily during the stance phase of gait, indicating that external loading from the ground reaction is an important factor affecting forces in the ACL.

REVIEW AND THEORY

While the structural role of the ACL has been described in vitro, its primary function in vivo remains open to debate (Brand, 1986). Previous estimates of ACL forces during gait have been made using indirect measurements and/or mathematical models of the knee (Collins & O'Connor, 1991; Harrington, 1976; Henning et al., 1985; Morrison, 1970). Transducers such as buckle gages, which are applied to the tissue to measure tissue force, have limited application due to tissue preshortening and impingement with bone (Barry & Ahmed, 1986; Lewis et al., 1982). No direct measurements of in vivo ACL forces during gait have been previously reported. The purposes of this study were to measure in vivo ACL forces during activity, and to test the hypotheses that peak and time-averaged ACL forces are correlated with the speed of gait.

PROCEDURES

A pressure transducer modified to measure tissue force (Holden et al., 1991a) was implanted within the anteromedial band of the ACL in three adult female goats (weight = 587 $\pm$ 73 N). Knee joint flexion angle was measured with a lightweight, flexible electrogoniometer (Penny & Giles Biometrics, U.K.) which was attached to the skin and calibrated using lateral radiographs. Ground reaction forces (GRFs) were measured using a Kistler force platform, and average speed was calculated over a 2.54m distance. Data were collected during a variety of activities performed one (n = 2) or two (n = 1) days after ACL transducer implantation. The transducer output corresponding to zero force was measured with the ACL unloaded in the live, anesthetized animal.

Following animal euthanization, the force transducer was calibrated with respect to total ACL force using anteroposterior (AP) displacement tests at six different flexion angles (Holden et al., 1991b). Calibration data were fit to a single higher-order function of output voltage and flexion angle using a Marquardt-Levenberg least squares algorithm. ACL forces were calculated for 10 trials of level walking or trotting by each animal. The ACL force peaks from the two or three gait cycles per trial were averaged, and a mean ACL force was also calculated for the period during which the instrumented limb was on the force platform. A multivariate regression analysis was used to produce partial correlations, adjusted for the effects of animal subjects, of each of the ACL force variables with speed.

RESULTS

The ACL in the goat was primarily loaded during the stance phase of gait, when the limb was in contact with the ground and under external loading from the ground reaction (Fig. 1). The ACL loading pattern during the stance phase was characterized by two peaks in walking and a single peak in trotting. The peak ACL force occurred during the first 40% of stance, with magnitudes ranging from 63 N to 124 N in walking and 102 N to 150 N in trotting. Forces in the ACL during quiet standing were 30 N to 61 N in the three animals. The time-averaged ACL force during stance ranged from 34 N to 68 N in walking, and 46 N to 69 N in trotting. As a quantitative measure of the animals' use of the limb, the peaks of the vertical GRF (Fz) on the instrumented limb were compared to the Fz peaks on the contralateral limb. These ratios were 71%, 85%, and 109%.

ACL loading occurred during late swing in the animal which showed the greatest knee extension during gait (Fig. 1). This most likely corresponded to the ACL loading observed during passive knee extension in the anesthetized goat. Passive flexion-extension did not cause ACL loading until the knee was extended beyond 40° (i.e., 20° from full extension).

Peak ACL forces had a statistically significant positive correlation with speed of locomotion (Fig. 2). The partial correlation coefficient between peak ACL force and speed, adjusted for the effects of animals, was +.818. This coefficient was significantly different from zero at a level of $p \leq .0001$. Each of the three animals had a statistically significant ($p \leq .05$) correlation between peak ACL force and speed, for that animal alone. Time-averaged ACL forces during stance also had a statistically significant positive correlation with speed. The partial correlation coefficient between mean ACL force and speed, adjusted for the effects of animals, was +.539 ($p = .003$).

Peak and time-averaged vertical ground reaction forces were greater in trotting than in walking. There was no similar increase with trotting, however, in either of the peaks (positive or negative) in the fore-aft ground reaction force.

DISCUSSION

This study is the first report of direct measurement of in vivo forces in the anterior cruciate ligament during activity. The findings demonstrate that the ACL has a structural role in the quadruped during both quiet standing and the stance phase of gait. Peak ACL force showed a positive correlation with speed of locomotion.

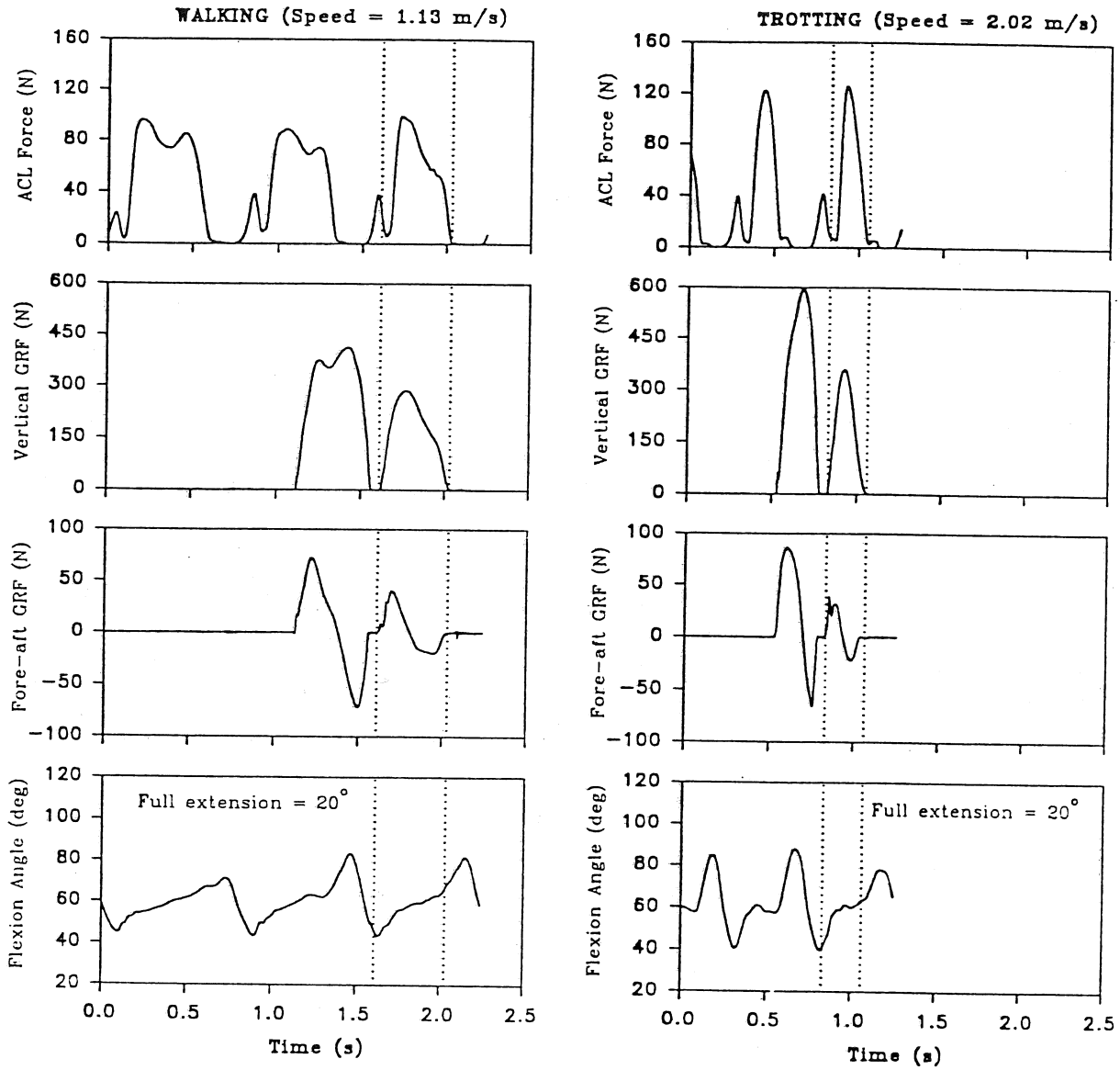

Figure 1. Representative plots of ACL force, ground reaction forces, and flexion angle vs time for walking and trotting by one animal. The period of hindlimb contact on the force platform is indicated by the vertical dashed lines on all graphs.

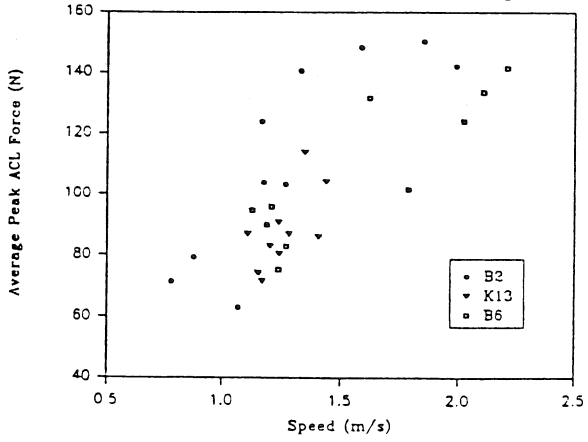

Figure 2. Peak ACL force plotted vs. speed for ten trials by each of the three animals.

REFERENCES

Barry, D. et al. J. Biomech. Engr., **108**, 149-152, 1986.
Brand, R.A. J. Biomech. Engr., **108**, 106-110, 1986.
Collins, J.J. et al. Proc. Instn. Mech. Engrs. **205**, 11-18, 1991.
Harrington, I.J. Biomed. Engr., 167-172, 1976.
Henning, C.E. et al. Amer. J. Sports Med., **13**, 22-26, 1985.
Holden, J.P. et al. Proceedings of the 37th Meeting of the Orthopaedic Research Society, New Orleans, (p. 588), 1991a.
Holden, J.P. et al. Proceedings of the 3rd U.S.A.-China-Japan Conference on Biomechanics, Atlanta, (pp. 127-128), 1991b.
Lewis, J.L. et al. J. Biomech. Engr., **104**, 125-128, 1982.
Morrison, J.B. J. Biomechanics, **3**, 51-61, 1970.

ACKNOWLEDGMENTS

The authors wish to acknowledge Martin Levy, Ph.D., Dept. of Quantitative Analysis and Information Systems, for his assistance with the statistical analysis, and NIH Grant AR39703 for financial support.

A STUDY OF ELECTROMYOGRAPHIC AND KINEMATIC PATTERNS OF NORMAL AND ANTERIOR CRUCIATE LIGAMENT DEFICIENT SUBJECTS DURING LOCOMOTION

L.-Q. Zhang and R. Shiavi

Department of Biomedical Engineering, Vanderbilt University, and
Sensory Motor Performance Program, Rehabilitation Institute of Chicago

INTRODUCTION

The anterior cruciate ligament (ACL) is a critical structure for controlling knee joint stability and movement. The lack of quantitative information on the response of the patient to ACL disruption has diminished our ability to draw conclusions about proper surgical procedures and rehabilitation. The purpose of this investigation is to study the alterations caused by the ACL injury and the muscular compensatory and protective mechanisms used by individuals with ACL deficient knees. Electromyographic (EMG) and kinematic variables, and the relationships between them were studied for this purpose.

REVIEW AND THEORY

Techniques were developed for studying patterns of human EMG and kinematic activity independently during free and fast speed walking. Since the two sets of variables are physiologically related and interact with each other, they were combined into a system and the relationships between them were studied.

In the EMG pattern study it was found that the shapes of the EMG linear envelopes (LE) are mainly determined by their *phase* spectra; their magnitude spectra are much less important [4]. Features were extracted from normalized (in both time and amplitude scales) and averaged EMG LEs with emphasis on their phase spectra. The features were then used in the clustering analysis to investigate the differences of EMG patterns between injured and uninjured subjects.

To study the relationship between EMG activity and limb movement, system identification techniques were applied to the human lower-limb neuromuscular control system. The system was treated as a black box with EMG signals from seven dominant muscles around the knee joint as inputs and the six degrees of freedom (DOF) motion of the tibia with respect to the femur as outputs. Model structure determination, parameter estimation, and various validation techniques were combined to create robust models. Three approaches were tested to identify the system: the multi-input, multi-output (MIMO) linear input-output models, the MIMO linear state-space models, and the nonlinear autoregressive moving average with exogenous inputs (NARMAX) models.

PROCEDURES

In total 57 subjects were involved in the studies, with 49 subjects involved in the clustering analysis of EMG LEs and the other 8 subjects involved in the EMG-Movement relationship study. Twenty-five of them (23 in the clustering analysis) had complete ACL rupture and the other 32 subjects (26 in the clustering analysis) with uninjured knees. None of the injured subjects had had surgical operations. Subjects from the two populations were asked to walk along a 12 meter long track at their regular speed and at faster speed. Data were collected only at the middle 5 meter range to remove the acceleration and deceleration phases. EMG activity was measured from the rectus femoris, vastus lateralis, vastus medialis, biceps femoris (long head), semitendinosus, and the medial and lateral heads of gastrocnemius muscles. Knee kinematics was measured with a six DOF goniometer. The motion was described as three rotations (flexion/extension, abduction/adduction, internal external rotation) and three translations along the x, y, and z axes of the tibial coordinate system.

RESULTS

Clustering analysis of EMG LEs showed the following tendencies exhibited by the ACL injured subjects:

The rectus femoris muscle activity at heel contact is weaker.

The activity peak of quadriceps muscle around mid-stride is smaller or non-existent.

The vastus lateralis muscle showed a narrower activity peak at the beginning of stance phase.

The major activity peak of the semitendinosus muscle was delayed from the end of swing phase

to the beginning of stance phase.

When the EMG and kinematics variables were studied simultaneously, the approaches listed above gave good simulation results under certain conditions. For a MIMO system, the results obtained from linear input-output models are easier to interpret than the state space and NARMAX models, and here we will discuss the linear input-output models only. A linear input-output model performed well across different sets of data from the same task (different runs of free speed walking) and across different but similar tasks (free and fast speed walking). The same model structure with re-estimated parameters performed well for significantly different tasks (free speed walking and leg flexion). For some DOF of motion, models for different subjects could share the same structure with different parameters; for other DOF of motion, different structures as well as different parameters were needed. Different DOF motions had neither the same model structure nor the same parameters. Significant differences (convergent versus divergent simulation results) between the normal and ACL deficient subjects were shown in the model structures. The following characteristics were shown by the ACL injured subjects:

Different model structure had to be used to characterize the relationship between the internal/external rotation and the tibial translation with respect to the femur along the tibial x axis, the lateral direction, as output.

Shorter delay from vastus lateralis muscle activity to the tibial-x translation.

Different model structure had to be used to characterize the relationship between the hamstring muscle activity and the tibial-z translation, the vertical direction, as output.

DISCUSSION

The above differences in characteristics between the two populations were consistent for free and fast speed walking and generally became more evident at the faster walking speed. The characteristics of weaker EMG activity of the quadriceps muscles for ACL injured subjects is consistent with the ``quadriceps avoidance" gait observed by Berchuck et al. in a recent study, although the approach is different [1]. The clustering results showed where in a stride the ACL injured subjects did not activate their quadriceps muscles as the uninjured subjects did.

Previous knee ligament studies on human cadaver knees showed that the ACL experienced the most elongation with internal rotation [2]. This explains why the model structure for normals needed to characterize this tight tibial-x translation and internal rotation relationship. In fact, all uninjured subjects tested can share the same model structure for the tibial-x translation and internal rotation relationship and gave satisfactory simulation results. When the ACL was ruptured, the relationship no longer existed, therefore the same model structure no longer apply. If the same model structure was still used to estimate the model parameters, the resulting model did not represent the true underlying relationship and simulations showed this by giving divergent results.

Similarly, for the tibial-z translation and hamstring EMG relationship, it was shown [3] that stimulation of the ACL directly excited the hamstrings muscles. To characterize such ACL hamstring reflex, a certain model structure is necessary. The same structure determined through optimization worked well for all uninjured subjects. With the ACL ruptured, the direct reflex from ACL to hamstring is probably gone, therefore a different model structure had to be used instead.

REFERENCES

[1.] Berchuck, M. et al. J. Bone \& Joint surg., 72-A, 871--877, 1990.
[2.] Kennedy, J. et al. Clin. Orthorp. & Relat. Res., 129, 225--229, 1977.
[3.] Solomonow, M. et al. Amer. J. Sport Med., 15, 207--213, 1987.
[4.] Zhang, L.-Q. et al. IEEE Trans. Biomed. Eng., 38, 777--784,1991.

DOES CYBEX TESTING INCREASE THE LAXITY OF ANTERIOR CRUCIATE LIGAMENT RECONSTRUCTIONS?

Murray E. Maitland, Ron Lowe, Susan Stewart, Tak Fung, G. Douglas Bell
Sport Medicine Centre and Academic Computing, The University of Calgary

INTRODUCTION

The purpose of this study was to assess whether a Cybex test, without antishear devices, would have an impact on the laxity of anterior cruciate ligament reconstructions (patellar tendon autograft) compared to the affect of a control exercise.

Twenty-four subjects were assessed for changes in anterior tibial translation following a control exercise and following Cybex isokinetic testing. It was found that one episode of Cybex testing did not have a significant effect on the laxity of the ACL reconstruction. However, care must be taken in extrapolating this finding to other populations because of variation in reconstructive technique and interpatient variation. Theoretically, high levels of stress result from isokinetic testing but the impact of this stress on the healing ligament continues to be only conjecture. Consequently, there is a need to more clearly define beneficial and detrimental levels of stress in the diverse classes of healing ACL reconstructions.

REVIEW AND THEORY

ACL reconstruction is intended to provide normal knee joint translation and functional stability over an extended period. This endeavour can be unsuccessful and authors have noted large interpatient variation in the permanence of knee stability measurements. A number of reasons for increased laxity have been suggested: the quality of graft materials, genetic characteristics, surgical technique, rehabilitation techniques and trauma (Noyes et al., 1985; Noyes et al., 1987).

Johnson (1989) states that there is a direct relationship between resistance at the distal leg and increased laxity following reconstructive surgery as a consequence of strain on the ACL caused by quadriceps muscle action. The quadriceps muscle produces various levels of anterior translation of the tibia, resulting in differing ACL strains, depending on the knee joint angle (Grood et al., 1984; Smidt, 1973). A recent cadaver study of ACL strain as a consequence of imitation quadriceps contractions has shown significant increases in strain between 0° to 40° (Draganich et al., 1990). In vivo, Howe et al. (1990) found significant increases in strain during isometric quadriceps contraction at 30° compared to 90° and concluded that this may be detrimental to ACL reconstructions. Consequently, numerous authors have recommended that typical knee extension exercises be avoided (Kaufman et al., 1991; Renstrōm et al., 1986; Yasuda et al., 1987). As an alternative, closed kinetic chain exercises are emphasized in rehabilitation programs in order to decrease presumed anterior shear force.

Questions regarding the clinical relevance of anterior tibial translocation during knee extension exercises are still unanswered due to research design, interpretation, and technical difficulties (Howell, 1990). There does not seem to be any evidence as to the practical importance of the theoretical considerations noted above in the isokinetic testing of ACL reconstruction patients.

Cybex testing has been carried out as early as 5-6 weeks post-operatively with no apparent effects on joint laxity (Shelbourne et al., 1990). Isokinetic training begun in the 14th post-operative week had no effect on stability, joint motion or knee function score (Elmqvist et al., 1988). In addition, Howell (1990) found that instrumented laxity testing produced more anterior tibial translocation than maximal isometric quadriceps contraction at various knee flexion angles.

Whether ACL deficient and reconstructed patients should be tested isokinetically and how early remains unclear.

PROCEDURES

The study population consisted of 24 subjects (14 male, 10 female, mean age 28 years, range 18 to 45 years). Mean time post-surgery was 212 days (approximately 7 months) with a range between 153 and 300 days.

As a control exercise, subjects walked on a level treadmill for 10 min at 5 km/hr. This exercise was chosen because it represents a safe activity and it is of a similar duration to the Cybex testing protocol.

One week later, following a 5 min warm-up on a stationary cycle, subjects performed a maximal isokinetic test using the Cybex 340 dynamometer (Cybex, Ronkonkoma, NY). Standard attachments were used (ie. not the attachments designed to prevent anterior shear force). The protocol consisted of 4 practise repetitions and 4 maximal repetitions at an angular velocity of 60°/sec, 4 practise repetitions and 4 maximal repetitions at an angular velocity of 150°/sec and 4 practise repetitions and 20 maximal repetitions at an angular velocity of 240°/sec.

Nine qualitatively different times were chosen for knee laxity measurements: immediately pre-treadmill, 2) 10 min post-treadmill, 3) one hr post-treadmill 4) 24 hrs post-treadmill, 5) 7 days post-treadmill (immediately pre-cybex), 6) 10 min post-cybex, 7) one hr post-cybex, 8) 24 hrs post-cybex, 9) 7 days post-cybex.

For all measurement sessions, anterior translation of the tibia at 133.5 Newtons was measured from the force/displacement plot produced by the KT2000 knee ligament arthrometer (Medmetric, San Diego) to the nearest 0.25 mm and the average of three measurements at each time period was used.

For reconstructed knees, repeated measures analysis of variance, with two within-subject factors, of eight measurement sessions (excluding the first) was used to test whether there was a significant difference associated with exercise whether treadmill walking or Cybex testing (ie. comparing 10 min post-exercise, measures 2 and 6, 1 hr post-exercise, measures 3 and 7, 24 hrs post-exercise, measures 4 and 8, and 7 days post-exercise, measures 5 and 9). This same analysis of variance was used to test the significance of interaction between time interval and treatment (treadmill or Cybex). Interaction is used to determine if laxity is dependent on the treatment and the time interval in a complex manner. The analysis of variance also tested whether there was a treatment effect: post-treadmill measures and post-Cybex measures.

A separate analysis of variance was used to assess if there was a significant change in the difference between normal and reconstructed knee laxity. The significance of the time interval post-exercise, the interaction between treatment and time interval, and the difference (post-Cybex minus post-treadmill) were assessed in the same manner as for the reconstructed knee alone.

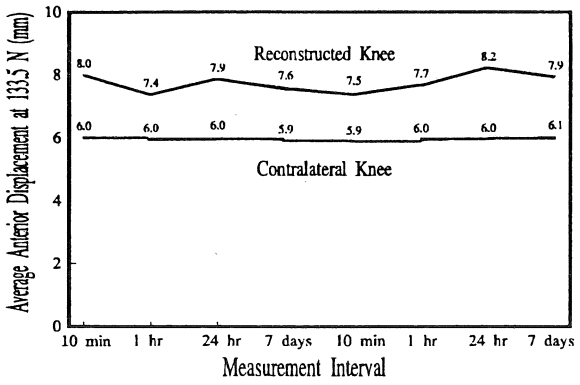

Figure 1. Group means of anterior tibial translation at 133.5 N measured with the KT2000. Cybex testing occurred immediately after the 7 day post-treadmill measurement. There is no apparent trend in these measurement means.

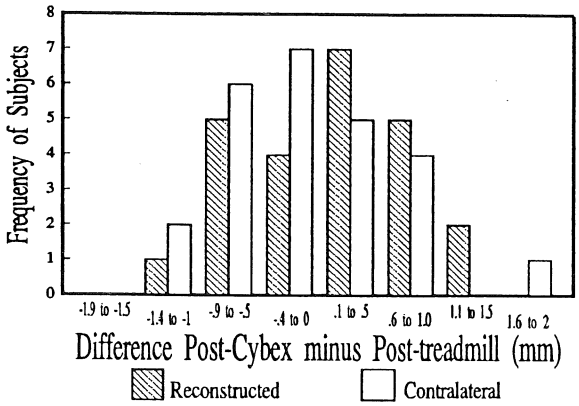

Figure 2. Change in mean anterior tibial translation at 133.5 N (post-Cybex measures minus post-treadmill measures). The mean difference is 0.1mm for both the reconstructed and contralateral knees.

RESULTS

There was no significant effect associated with time intervals after an exercise (p=.14). Also, there was no significant interaction between the effects of treatment (treadmill walking or Cybex testing) and the time interval after testing on knee laxity measurements (p=.15). In addition, there was no significant difference between the knee laxity measurements post-treadmill compared to those post-cybex (p=.43). The average difference between the post-treadmill and post-Cybex measurements was approximately .1 mm (range -1.0 to 1.3)and the 95% confidence limits of this difference are -0.2 to 0.4 mm. Figure 2 presents the frequency of these differences for the reconstructed and normal knees.

The results for the reconstructed and normal knee difference were similar to those of the reconstructed knee alone. This difference had an average change of 0.1 mm with 95% confidence limits of -0.2 to 0.5 mm.

DISCUSSION

This study provides evidence that Cybex testing with the standard testing apparatus, between 6-10 months post-patellar tendon autograft does not cause a demonstrable increase in knee joint laxity. Thus, theoretically harmful effects remain to be confirmed in the clinical environment and the practical importance of ACL strain during quadriceps activity need to be established.

The clinical relevance of the change in laxity is best determined by the 95% confidence limits for the difference pre- and post-Cybex. In this study, the upper limit (0.4 mm) is not clinically significant. In fact, the power of this study to find a 2.0 mm average difference is nearly 1.

The results of this study can not be extrapolated easily to more generalized populations of ACL reconstruction patients. This was not a randomly selected population and so the subjects are likely to be a unique group. Furthermore, the method of surgical reconstruction may be important to mechanical properties of the graft over time. Time post-surgery may also be a critical factor.

The results of the present study emphasize the need to increase our understanding of the reaction of ACL reconstructions to a variety of mechanical stimuli. Anterior shear forces in the tibiofemoral joint during Cybex testing have been estimated to be about 0.3 times body weight and also approximately equivalent to body weight (Kaufman et al., 1991; Nisell et al.,1989). The lower figure for anterior shear during isokinetic testing is comparable to walking. This wide variation in estimates, partly a consequence of assumptions, presents the clinician with the task of determining risk/benefit to the patient. Improvements in theoretical modelling and in vivo measurements may lead to more precise estimates and comparisons to material properties of healing ligament.

The results of this study suggest that isokinetic testing does not pose a significant risk to the integrity of the ACL reconstruction after 6 months post-patellar tendon autograft, and is, therefore, a reasonable approach to quantifying rehabilitation outcomes.

REFERENCES

Draganich, L.F. et al. *J Ortho Res* 8:57-63, 1990.
Elmqvist, L-G. et al. *Am J Sports Med* 16:455-462, 1988.
Grood, E.S. et al. *J Bone Joint Surg* 66A:725-734, 1984.
Howe, J.G. et al. *Arthroscopy* 6:198-204, 1990.
Howell, S.M. *Am J Sports Med* 18:573-578, 1990.
Johnson, D. *J Ortho Sports Phys Ther* 4:23-31, 1989.
Kaufman, K.R. et al. *Am J Sports Med* 19:305-316, 1991.
Nisell, R. et al. *Am J Sports Med* 17:49-54, 1989.
Noyes, F.R. et al. *Clin Ortho Rel Res* 198:61-76, 1985.
Noyes, F.R. et al. *Am J Sports Med* 15:149-160, 1987.
Renstrõm , P. et al. *Am J Sports Med* 14:83-87, 1986.
Shelbourne, K.D. et al. *Am J Sports Med* 18:292-299, 1990.
Smidt, G.L. *J Biomech* 6:79-92, 1973.
Yasuda, K. et al. *Clin Orthop* 220:275-283, 1987.

ACKNOWLEDGEMENT

This study was supported by a grant from The University of Calgary.

GAIT ADAPTATIONS IN PATIENTS WHO HAVE A DEFICIENT POSTERIOR CRUCIATE LIGAMENT

J.C. Otis, J.M. Marzo, T.L. Wickiewicz, S.I. Backus, A.E. Barr, R.F. Warren
Department of Biomechanics, Sports Medicine and Rehabilitation Services, Hospital for Special Surgery
New York, New York

INTRODUCTION

Controversy exists regarding the management of patients with asymptomatic, isolated posterior cruciate ligament (PCL) deficient knees. Gait measurements were obtained and analyzed for compensatory patterns and to assess varus loading. Two patterns were observed, neither of which demonstrated a significant increase in varus loading.

REVIEW AND THEORY

Limited information is available regarding lower extremity function in patients who have a deficient PCL. A previous gait study of patients with PCL deficiency, some of whom were symptomatic, has shown that patients develop functional adaptations during level walking, Tibone et al. (1988). Their findings were a decrease of eight percent in mean free velocity associated with a decreased stride length. They also noted a trend toward less extension and a decreased ground reaction force acting on the affected side during the terminal stance phase. Prolonged electromyographic activity was seen in the quadriceps muscles in terminal stance. The purpose of this study was twofold; 1) to determine if there are consistent gait adaptations among patients with asymptomatic isolated PCL deficiency, and 2) to determine if there is an increase in the varus moment about the asymptomatic PCL deficient knee as compared to the unaffected knee during level walking.

PROCEDURES

Nine subjects with isolated rupture of the PCL documented by clinical exam and arthroscopy or magnetic resonance imaging and who were asymptomatic with regard to pain, swelling and instability served as the study group. All patients were male and averaged 39 $\pm$ 34 months from the time of injury. The mean age was 32 $\pm$ 11 years, ranging from 19 to 50 years. Of the nine PCL deficient knees, five were right and four were left. An objective measure of tibial excursion was obtained using the KT-1000 knee ligament arthrometer (MEDmetric, San Diego, CA). The nine patients underwent isokinetic testing and gait analysis at the time of follow-up examination. Knee flexor and extensor work were measured bilaterally at a constant angular velocity of 90°/second using a LIDO® Active Rehabilitation System (Loredan Biomedical, Davis, CA).

Angular kinematics and ground reaction forces during gait were recorded with a video based Motion Analysis Corporation three-dimensional motion analysis system (60 Hz), Expert Vision™ 3-D and OrthoTrak™ 2.0 software (Motion Analysis Corporation, Santa Rosa, CA), and two Bertec (Bertec, Worthington, OH) force plates (1000 Hz).

Subjects were asked to walk at their freely chosen velocity along a ten meter walkway which was surrounded by six video cameras. For each subject, five trials were collected in which full right and left strides were captured within a calibrated volume and in which distinct sequential stance phases occurred in the two force plates. Joint moments were expressed in Newton-meters (Nm) and were normalized to body mass when grouped. For each subject, ensemble average curves of the stance phase joint moments for each limb were generated and the difference between the affected and unaffected curves was computed. These ensemble average difference curves were then combined by bootstrapping, a statistical curve analysis technique in which a group mean curve with 95% confidence limits is determined.

RESULTS

Figures 1A and B show two typical flexion moment patterns that were demonstrated by the group of PCL deficient subjects studied. Figure 1A illustrates a pattern in which the knee flexion moment on the affected side is greater than the knee flexion moment on the unaffected side. The four subjects who demonstrated this pattern were assigned to the "flexion moment bias group". Figure 1B illustrates a pattern in which the knee flexion moment on the affected side is less than the knee flexion moment on the unaffected side. The five subjects who demonstrated this pattern were assigned to the "extension moment bias group". The bootstrap analysis was applied to the difference curves for the flexion moment bias group and to the difference curves for the extension moment bias group. This yielded the difference curves with their 95 percent confidence limits illustrated in Figures 2A and B. Figure 2A shows that the flexion moment bias group demonstrated a significantly greater flexion moment on the affected side from 45 to 80 percent of the stance phase. For each group, the varus moments on the affected and unaffected sides were determined and compared using the same method of ensemble averaging and bootstrapping. For the flexion moment bias group the varus moments on the affected side were significantly less than the varus moments on the unaffected side from approximately 10 to 80 percent of the stance phase. For the extension moment bias group there was not a significant difference when comparing the affected side varus moment to that of the unaffected side.

Thus, neither group demonstrated a greater varus moment on the affected side.

The KT-1000 anterior-posterior laxity measurements were examined according to group. Three of the four subjects in the flexion moment bias group demonstrated greater than normal laxity, whereas only one of five subjects in the extension moment bias group demonstrated excessive laxity. Isokinetic testing revealed no difference in strength of the extensors or flexors of the affected knee as compared to the unaffected knee.

DISCUSSION

In a previous gait study, significant findings in PCL deficient patients were decreased extension and decreased ground reaction force in the affected knee during the late stances phase of gait, Tibone et al. (1988). These findings are consistent with a decrease in the external extension moment about the knee and were interpreted by the authors to represent an attempt by the patients to increase the internal extension moment generated by the quadriceps muscle. This would tend to hold the tibia forward in a reduced position to compensate for a deficient PCL and relieve stress on the secondary posterior stabilizers of the knee. In support of this, extra activity was observed in the vastus medialis obliques muscle in terminal stance in four out of eight of their patients.

Four of the nine asymptomatic patients in the current study had a greater flexion moment at the knee during the midstance phase of gait during level walking. The subjects in the flexion bias group produce a "quadriceps enhancement", an alteration consistent with an avoidance of posterior displacement of the tibia during walking. The extensor bias group demonstrated a pattern which was not consistent with the mechanisms of quadriceps enhancement for stability. Four of five subjects in this group, however, demonstrated laxity measurements which were not excessive, which is consistent with not requiring additional joint stability through muscular efforts.

There is controversy regarding the occurrence of high medial knee joint loads in individuals with isolated PCL deficiency. Results of the current study indicate that the asymptomatic PCL deficient subjects used in this study have either the same or a decreased varus moment on the affected side as compared to the unaffected side. These results do not support the hypothesis that the PCL deficient knee experiences higher medial joint loads, although higher joint contact pressure may still occur due to changes in contact area.

REFERENCES

Tibone, J.E. et al. Am. J. Sports Med., 16, 217-223, 1988.

ACKNOWLEDGMENTS

The authors gratefully acknowledge the assistance of Dr. Margaret G.E. Peterson.

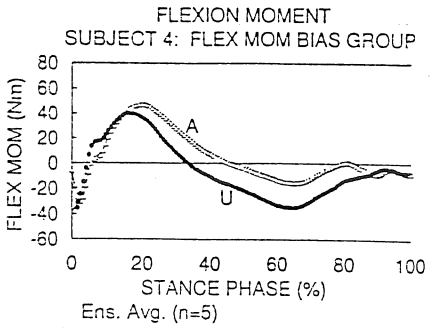

Figure 1A

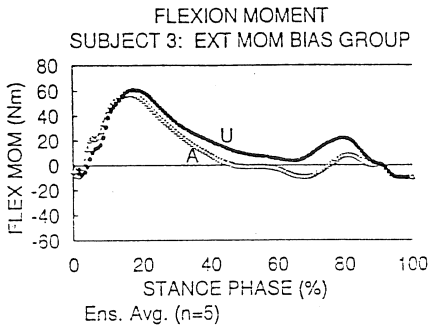

Figure 1B

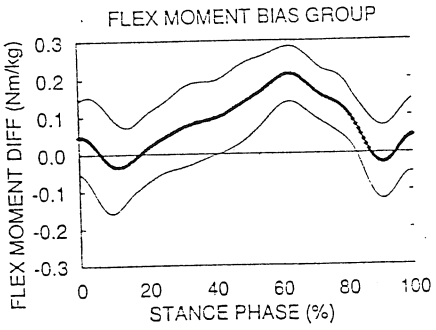

Figure 2A

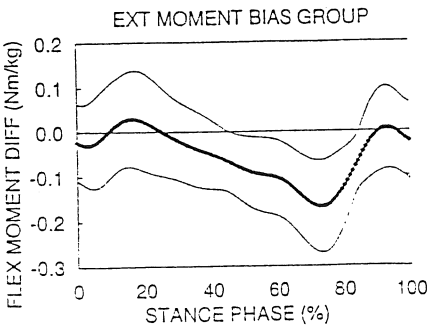

Figure 2B

Proceedings of NACOB II, The Second North American Congress on Biomechanics, Chicago, August 24th - 28th, 1992

THE ROLE OF KNEE JOINT COMPRESSIVE FORCES IN LIMITING ANTERIOR TIBIAL TRANSLATION

H. John Yack & Lisa A. Washco

Department of Physical Therapy & Exercise Science
State University of New York at Buffalo

INTRODUCTION

The role of axial loading of the lower limb in limiting anterior tibial translation (ATT) in anterior cruciate ligament (ACL) deficient knees under various conditions of quadriceps and hamstrings activity was investigated. Having an understanding of the interplay of muscle actions and compressive forces may help explain the paradoxical effects of quadriceps exercises on ATT that has been reported in the literature. Analysis of the no compression (NC) and compression (COMP) conditions revealed significantly less ATT during the laxity test in the COMP condition. Isometric quadriceps activity resulted in significant less ATT than that seen in the laxity test. It was concluded that knee joint compressive forces are a limiting factor in controlling ATT in ACL deficient knees and that the action of an isometric quadriceps contraction may be as effective as external compressive forces in limiting ATT.

REVIEW AND THEORY

An apparent paradox exists in the literature related to how contractions of the quadriceps influence anterior tibial translation (ATT). A number of authors have demonstrated increased ATT with quadriceps contractions (Franklin et al., 1990). They point to models and experimental data which show that during quadriceps contractions the shear forces at the knee increase as the knee approaches full extension (Henning et al., 1985). Other researchers, however, have demonstrated limited ATT during isometric contraction of the quadriceps (Howell, 1990). They point to models and experimental data which document the ability of joint compressive forces to limit ATT as a way of explaining their results (Markolf et al., 1981). Coloring this controversy is the extent to which simultaneous contraction of the hamstrings will limit ATT (Draganich, 1989). The effect of quadriceps contractions on ATT and the consequences these have on stress to the ACL is thus controversial. The purpose of this study was to determine the role of knee joint loading (axial loading) on the fully extended knee in limiting the amount of ATT in ACL deficient knees under regulated conditions of quadriceps and hamstrings activation.

PROCEDURES

Nine subjects, five females and four males participated in the study. Each subject completed an informed consent form and health history questionnaire prior to testing. All subjects had a history of an ACL injury as diagnosed by an orthopedic surgeon, had not undergone any type of ACL surgery, and presented five millimeters or more of ATT as measured by the Knee Signature System (KSS, Acufex Microsurgical, Inc.) with the knee in full extension.

Muscle activation levels of the vastus lateralis and medial hamstring muscles were monitored. The electromyographic (EMG) signals from these muscles were amplified, full wave rectified, and low pass filtered at three Hz. to obtain a linear envelope representation. The EMG data were collected on-line as well as being displayed on an oscilloscope. Maximum activation values (MAV) for each muscle group were recorded. Two target lines representing 30% MAV's levels were set on the oscilloscope.

The KSS was used to measure anterior/posterior tibial translation as the relative movement of the tibia with respect to the patella. The force applicator, that is part of the KSS, was used to apply an calibrated 89 N anterior and posterior force to the leg.

Subjects were seated and stabilized in a reclined position on a chair with the hips in 30 degrees of flexion and the involved leg in full extension. An ankle/foot orthosis was used to maintain the foot in a neutral position during testing. A separate stand with a 2.23 kN load cell and adjustable support rod was aligned with the distal portion of the calcaneus and was used to apply a compressive force to the knee equivalent to 50% of the subject's body weight.

Measurements were taken of ATT in a no compression (NC) condition and a compression (COMP) condition during the following situations: 1) rest; 2) the Laxity test; 3) a 30% MAV quadriceps contraction with the hamstrings relaxed; 4) a 30% MAV hamstrings contraction with the quadriceps relaxed; and 5) a co-activation with equal activation levels. A random sequence of trials was repeated three times with a one minute rest between trials.

A two-way ANOVA with repeated measures ($p < 0.05$) was used to compare the mean ATT calculated over the 3 repeated trials among all trials in the NC and COMP conditions. A Fisher's post-hoc test was used to identify significant differences in the mean ATT within each trial of each condition.

RESULTS

Significantly less ATT occurred during the Laxity test during the COMP condition compared to the NC condition. Table 1 shows the results of the post-hoc testing where significant differences between trials are indicated for COMP and NC conditions.

Table 1. POST-HOC ANALYSIS (* P<.05) FOR NC (TOP, UNSHADED) AND COMP (BOTTOM, SHADED) CONDITIONS. (ATT values () in mm.)

	REST (0)	LAXITY (8.08)	30% QUAD (4.03)	30% HAMS (0.79)	CO-ACT (3.13)
REST	---	*	*		*
LAXITY	*	---	*	*	*
30% QUAD			---	*	
30% HAMS	*	*	*	---	*
CO-ACT	*	*		*	---
	REST (-0.48)	LAXITY (5.23)	30% QUAD (3.71)	30% HAMS (-0.16)	CO-ACT (3.07)

DISCUSSION

The results from this study show that in vivo laxity testing of the ACL deficient knee under axial loading significantly reduces ATT compared to the unloaded condition. These results further demonstrate that, compared to the laxity test, ATT during the quadriceps contractions was significantly reduced. It was further established that with the knee in full extension co-activation of the hamstrings did not affect ATT in either the COMP or NC condition.

EFFECT OF COMPRESSIVE FORCES ON ATT

The finding that ATT is limited by joint compressive forces in ACL deficient knees without the aid of muscular control suggests that joint geometry, in combination with compressive (axial) forces play an important role in maintaining joint stability. Previous cadaver studies support joint geometry as a factor that increases joint stability (Markolf et al., 1981). Likewise, in vivo studies comparing a closed kinetic chain exercise to an open kinetic chain exercise (Yack et al., 1992) have demonstrated significantly less ATT during closed kinetic chain exercises in subjects with ACL deficient knees.

EFFECT OF KNEE EXTENSION FORCES ON ATT

The findings of this study agree with other research that has shown ATT during an isometric contraction to be less than ATT during a conventional Laxity test (Howell, 1990). Knee stability appears to be maintained by joint geometry and compressive forces generated during the quadriceps contraction. The findings of limited ATT, however, differ from other research that has found ATT during knee extension exercises, which did not incorporate a fixed point of resistance, to be equivalent to or greater than that seen during laxity testing (Franklin et al, 1990). The mechanics at the knee are different under the two conditions. During an isometric contraction against a fixed resistance compressive forces, beyond those that are generated by the quadriceps, are developed. Thus, the paradoxical results obtained from knee extensors exercise on ATT may be explained in terms of changing mechanics which effect the magnitude of the compressive forces acting at the knee and ATT.

EFFECT OF CO-ACTIVATION ON ATT

In the present study, there was no significant difference between a 30% MAV quadriceps contraction and a co-activation in both the NC and COMP conditions. Because the angle of insertion of the hamstrings is so acute the forces generated by the hamstrings may act more to compress the tibia to the femur rather than to create a posterior draw force on the tibia during co-activation in full extension. (Draganich et al., 1989; Yasuda et al., 1987)

REFERENCES

Draganich LF et al., J Bone Joint Surg, 71A:1075-81,1989.
Franklin JL et al., J Bone Joint Surg, 73A:365-72,1990.
Henning CE et al., Am J Sports Med, 13:22-26,1985.
Howell SM, AM J Sports Med, 18:573-578,1990.
Markolf KL et al. J Bone Joint Surg, 63A(4):570-585,1981.
Yack HJ et al., Am J Sports Med, in press.
Yasuda K et al., Clin Ortho Rel Res, 220:275-283,1987.

POSTURE

Podium Session 6

BIOMECHANICAL ANALYSIS OF RESPONSE TO A HORIZONTAL PLATFORM PERTURBATION

MA Hughes, JM Chandler, M Schenkman, SA Studenski
Department of Physical Therapy, Duke University, Durham, NC
Durham VA Medical Center, Durham, NC

INTRODUCTION

Current postural control theory is based in part on EMG analysis of unexpected platform perturbation (PP). Patterns of EMG responses have been defined and from these kinematics strategies (ankle and hip) have been assumed[1]. These strategies predict that primary motion occurs at the ankle or hip, consider the knee motionless, and ignore the movements of the upper body. An examination of actual kinematic data of the response to PP reveals the strategies to be more complex, involving 1) knee and upper body motion 2) multisegmental interaction 3) inertial influences of the system[2]. The purpose of this study is to consider the biomechanical effects of perturbing a multisegemented body by relating kinematic and EMG data with platform motion characteristics to construct a better model of response to PP.

METHODS

Sixteen healthy young adults (8 male, 8 female, 20 - 30 yrs.) underwent 10 randomly sequenced forward and backward horizontal PP while standing, arms at the sides, on a motorized force plate. Time to EMG onset (latency) was recorded bilaterally from the tibialis anterior, quadriceps, gastrocnemius and hamstrings at 500 Hz using bipolar surface electrodes. Body segment motion during the first trial was recorded at 60 Hz using the Peak Performance 2D Motion Analysis System. The angular displacement of the ankle, knee, hip, shoulder, and neck were determined. The platform moved 5.08 cm at a velocity of 12.7 cm/s with an acceleration of 76.2 cm/s^2. Analysis included the first trial alone is used for each subject because it most nearly represents an unexpected displacement.

RESULTS

Table 1 gives the relative timing of EMG, kinematic, and platform motion events.
Figure 1 shows a comparison of the mean magnitude of the angular displacement of the ankle, knee, hip, shoulder and neck between the males and females. There were no significant differences between the groups due to gender. Angular displacement at each joint was significantly different than zero. Of particular note were knee flexion ($p<.001$), shoulder flexion ($p<.05$) and neck extension ($p<.05$).

EVENT	TIME
TA LATENCY	141 +/- 8
END OF ACCELERATION	143
QUAD LATENCY	152 +/-20
MAX ANKLE PLANTARFLEX	175 +/-25
BEGIN DECELERATION	400
MAX NECK EXTENSION	409 +/-167
MAX KNEE FLEXION	462 +/-191
MAX HIP EXTENSION	492 +/-180
PLATFORM STOP	543
MAX SHOULDER EXT	619 +/-137

TABLE1. RELATIVE TIMING OF KINEMATIC, EMG AND PLATFORM MOTION EVENTS. TIME +/- 1 STD, IN MS.

The Sixteenth Annual Conference of the American Society of Biomechanics and
The Seventh Biennial Conference of the Canadian Society of Biomechanics/Société Canadienne de Biomécanique

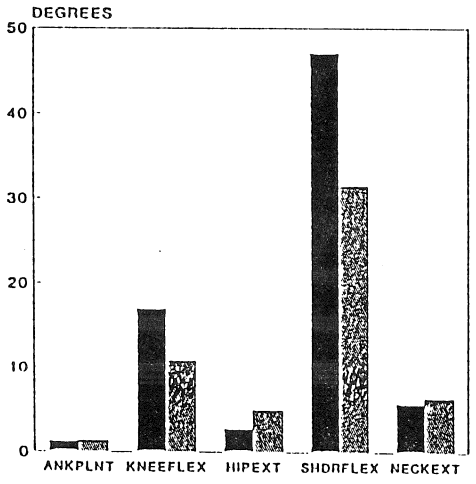

FIGURE 1. COMPARISON OF THE MEAN ANGULAR DISPLACEMENT FOR MEN AND WOMEN

DISCUSSION

The EMG analysis approach to postural control theory is limited because the movements of the body must be inferred. Models based on this theory ignore significant motion of the knee and upper body (see fig. 1). A complete model of responses to unexpected PP must take into account not only the muscular activity but also the kinematics, the perturbation characteristics, and the number of test trials. Only on the first trial is the magnitude and timing of the perturbation truly unknown. Based on the EMG, the kinematics and platform parameters of the first trial of 16 young healthy adults, we propose a model of the response. As the platform accelerates forward, the foot moves forward with the platform away from the shank, which lags behind due to inertia. This effectively produces plantarflexion of the ankle. The TA is activated to prevent further rotation around the ankle. With the ankle motion being checked, the knee is the joint with the greatest torque due to the inertia of the center of mass. This counter-clockwise torque causes knee flexion. The quadriceps is then activated to slow this motion. This progression then continues at the hips, where the inertia of the upper body causes extension which is then checked by muscle activation (see tab. 1). The deceleration of the platform may play a role in reversing the inertial motion of the knee and hip. The onset of platform deceleration would reverse the direction of the inertial force on the knee and hip and assist the musculature in stopping the initial movement (see tab. 1). The knee musculature, in an eccentric contraction, combines with the deceleration of the platform to stabilize the knee. Movement of the arms has been dismissed as a startle reaction[1], but may serve to move mass forward or to pull the shoulders forward. This model may help disentangle the effects of the platform parameters, learning, and age on the response to horizontal perturbations. This model consolidates previous work with our new kinematic and EMG data in a theoretical framework that can be used as the basis of future postural control theory.

REFERENCES

1. Nashner L et al The organization of human postural movements: A formal basis and experimental synthesis. Behav. Brain Sciences 8:135-172, 1985.
2. Isaacs, S et al Relationship of EMG and kinematic responses to platform perturbation. APTA Combined sections, San Francisco CA, Feb. 1992.

REGULATION OF MUSCLE ACTIVITY AT THE ANKLE FOR CONTROLLING BODY SWAY DURING NORMAL STANCE

Jean Woloszko and Robert J. Jaeger

Pritzker Institute of Medical Engineering, IIT, Chicago, IL.

INTRODUCTION

The mechanism by which human posture is regulated in the quiet standing position is controversial. This study was designed to examine the response of postural muscles to shifts in the position of the center of mass of standing subjects.

REVIEW AND THEORY

There is agreement in the literature that small fluctuations in the position of the body segments occur during normal stance. There is less agreement concerning the causal mechanism and role of muscle ankle plantarflexor activity in stance stabilization. Two hypotheses have been advanced: 1) for small deviations from upright posture, corrections are made by the inherent visco-elastic properties of muscles, and not by any reflex activation (Nashner, 1973); 2) normal stance is characterized by continuous minor corrections for position, which are apparently achieved through continuous fine adjustment (Mori, 1972). There is not better agreement on what is (are) the regulated variable(s) during quiet standing, and what are the reflexes actually involved. Body angle (Nashner, 1973), Ycof (Koozekanani *et al.*, 1980) or center of mass (Gohoffer *et al.*, 1985) have been suggested as the regulated variables. If Ycof cannot be the regulated variable for obvious mechanical reasons, there is no published data on the existence of an actual regulation of the position of the center of mass of the body (Ycom). Most of the studies describing the reflex loops involved in postural control used perturbations involving support rotation or translation or body free fall, inducing ankle angular velocities never encountered during daily living activities. From these studies, muscle spindles, vestibular and plantar cutaneous afferents have been suggested as having important roles in postural control. In this study, perturbations generating step transients on the center of mass of the body without generating high angular velocity at the ankle. The body is restrained to behave as a single-link system, so that all the stabilizing activities are done by the ankle muscles.

MATERIAL AND METHOD

Fourteen subjects stood without shoes in a restraining orthosis which limited movement to rotation about the ankle in the anterior and posterior directions. Ground reaction forces, body angle and acceleration were measured. Electromyograms were recorded on the gastrocnemius medialis and lateralis, soleus and tibialis anterior of both legs. There were rectified, combined using a least mean square method and lowpass filtered with a rectangular moving averaging window of 21 ms to obtain an estimate of the Ycof (distance of the projection of the center of force to the ankle axis). Thirty seconds of quiet standing were recorded and EMG, muscle torque were compared using optimal filtering to determine whether there is a modulation of muscle activity and what kind of control loop was involved. Weights of different values (8, 4 and 2 kg) were released from the orthosis by an electromagnet at random times.

RESULTS

Optimal filtering of the Global EMG during quiet standing demonstrated a high level of correlation between EMG and muscle torque, demonstrating an actual modulation of muscle activity during quiet stance.

Male and female subjects reacted differently to the release of the loads. Male subjects tended to keep the position of the center of mass relative to the foot support constant by leaning forward when the load was added, and going back to a smaller angle after the load had been released. Female subjects tended to keep the body angle constant, with little or no regard to the position the center of mass. This behavior was enhanced in subjects who wore high heel shoes, and seems to be a learned behavior.

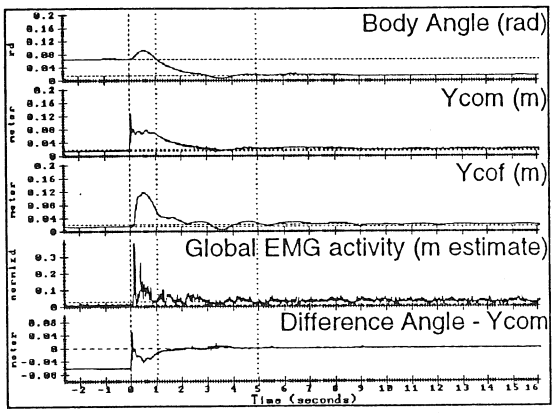

Figure 1. Typical response of a male subject

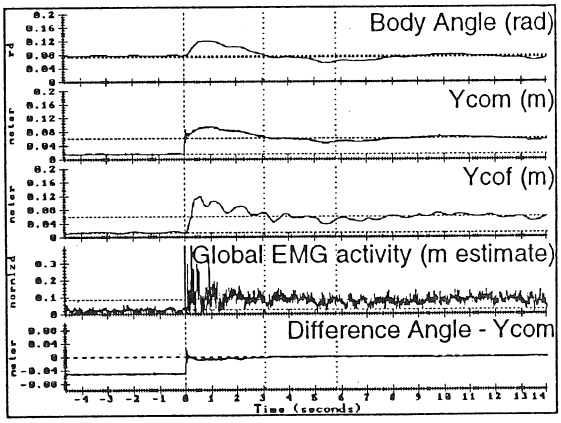

Figure 2. Typical response of a female subject

After load release, the body fell forward until a compensatory reaction in the ankle plantarflexors. Angular velocity for the first 100 ms after release never exceeded 0.15 rad/sec (15°/s). The response of the body to these perturbations is expressed

through modulation of activation of the muscles controlling the ankle joint. It consisted of a series of bursts in the electromyogram in the extensor muscles of the ankle. A first early small and inconsistent burst (P0) with a latency of 37.8 ms (s.d.: 5.6 ms) was attributed to the segmental stretch reflex. The second burst (P1) with a latency of 72.8 ms (s.d.:10.7 ms) seemed to be modulated by the pressure receptors located in the feet plantar skin; the area of P1 was well correlated to the rate of change in Ycof for the first 100 ms after release it was depressed after anesthesia of the plantar sole. The slope of this regression (one representation of the gain of the reflex) was larger in male subject than in female subjects, mainly those subjects who wore high heel shoes and were regulating the body angle. The next responses (P2 and P3) with latencies of 128.9 ms (s.d.: 13.2 ms) and 225 ms (s.d.: 19.5 ms) were attributed to vestibular responses. The first vestibular response P2 was scaled by the averaged angular acceleration of the body for the first 100 ms, as expected from a vestibular reflex. The area of the burst P3 was scaled with the amplitude of the perturbation.

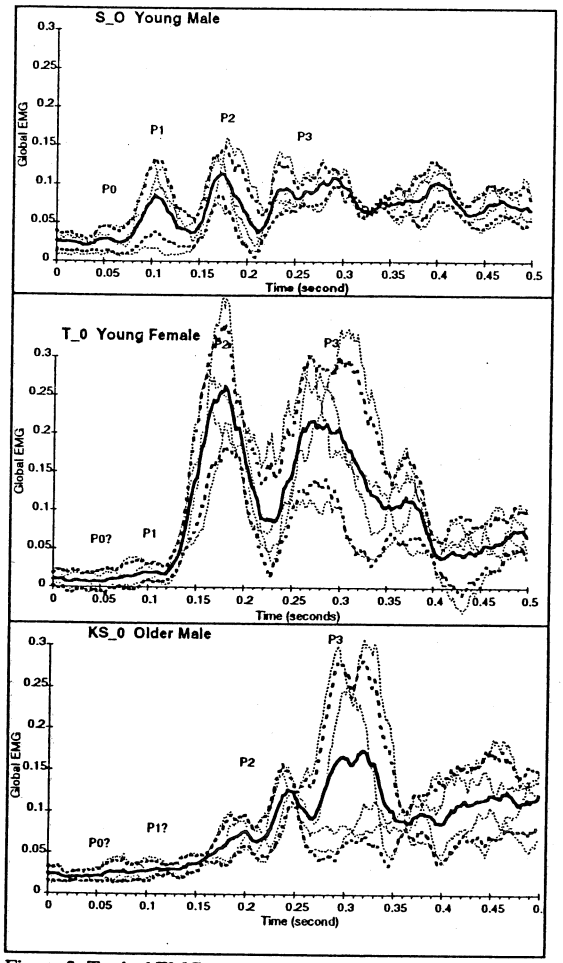

Figure 3. Typical EMG responses for young male, young female and older male subjects.

Older male subjects had lower gain and amplitude for the early responses P1 and P2, and larger amplitude for late responses P3 and for the voluntary contraction for the first body oscillation after load release.

DISCUSSION

This study has demonstrated the presence of an active continuous modulation of muscle activity during quiet stance. It also has shown the there is not one regulated variable, but body angle and/or angle of the center of mass can both be regulated. Male subjects usually regulate the position of the center of mass whereas female subjects regulate the body angle as a learned behavior. They are perfectly able to regulate the position of the center of mass when they are specifically instructed to do so.

In older subjects, the reflex part of the postural regulation was less efficient, then requiring a more important voluntary contraction. This situation enhanced the instability of the system and makes falling more likely to occur.

Cutaneous afferents have been shown to play an important role in this regulating loop, since they are the first mechanically efficient evoked response on the ankle dorsiflexor muscles after a perturbation on the body center of mass. Evaluating the center of mass from plantar cutaneous receptors requires information on the center of pressure and on the shear forces at the ground level or angular acceleration as provided by the vestibular system. The postural control should not be modeled as a one variable controller, but as the integration of the feedback of multiple states provided by many proprioceptive receptors, which have variable weighting factors between subjects, central settings, or posture.

BIBLIOGRAPHY

Gollhofer, A. Horstmann, G.A. Berger, W. Dietz, V. *Neuroscience Letter*, **105**, 73-78, 1985.
Koozekanani, S.H. Stockwell, C.W. McGhee, R.B. Firoozmand, F. *IEEE Trans. Biomed. Eng.*, **BME-27**, 605-609, 1980.
Mori, S. *J. Neurophysiol.*, **36**, 458-471, 1972.
Nashner, L.M. *Control of Posture and Locomotion , (pp.291-308)*, Plenum, 1973.

Proceedings of NACOB II, The Second North American Congress on Biomechanics, Chicago, August 24th - 28th, 1992

EFFECTS OF HAND VIBRATION ON POSTURAL CONTROL AND STABILITY

Bernard J. Martin, Lisa Fletcher and Hee S. Park

Department of Industrial and Operations Engineering, Center For Ergonomics,
The University of Michigan, Ann Arbor, MI 48109-2117

INTRODUCTION

Manipulation of objects or tools requires a steady body reference to achieve accuracy and consistency in performance. However, most industrial tasks requiring the utilization of powered hand-tools or machines are accomplished in vibratory environments. The present work investigated the influence of hand vibration on body balance and attitude. The vibratory stimulus was applied to the hand of subjects maintaining an erect posture on a force platform, eyes closed. The vibrating handle, free in space or fixed to a stationary support, was held in the dominant hand using four different arm positions. The results show that body sways increase significantly during hand vibration exposure when the handle is fixed. Significant shifts of the mean center-of-foot pressure (COP) are elicited in every situation. These shifts are clearly oriented in the direction of the handle when this latter is fixed. The results are interpreted in light of current knowledge of the effects of locally applied vibration on muscle tendons and the contribution of somatosensory information to kinesthesia. The data suggests that hand-arm vibration may contribute to the impairment of postural equilibrium, which constitutes a risk factor in fall accidents

REVIEW AND THEORY

Control of body balance is a complex function for humans which is challenged by reactive forces generated by limb movements. Sensory messages issued from proprioceptive, extero-ceptive, vestibular and visual receptors contribute to the stabilization of equilibrium. Recent studies have demonstrated the high sensitivity of proprioceptive and exteroceptive receptors to a vibratory stimulus (Johansson *et al.* 1982; Vedel *et al.* 1985), and the way in which this stimulus alters the respective sensory messages (Roll *et al.* 1989). This alteration is considered as the source of sensorimotor performance decrement resulting from whole-body or hand vibration exposure (Martin *et al.*1980; Gauthier *et al.* 1981; Martin *et al.* 1991).
Therefore, an alteration of the spatial reference provided by the position of the hand may contribute to the perturbation of postural stability and compromise equilibrium. The aims of the present study were to determine the contribution of vibration-induced alteration of hand proprioceptive feedback to the perturbation of erect standing equilibrium and/or the standing attitude. A second aim was to further the understanding of the elaboration of body representation.

PROCEDURES

Ten Subjects (Ss), age 22 to 35 years, free from any obvious vestibular, neurological or musculoskeletal disorders, participated in the experiment. One S was left handed. A force platform was used to test the postural stability of the Ss (body sway and mean resting posture). Each test consisted of 4 successive posture trials of 30 seconds of erect standing on the platform with eyes closed. The task was simply to remain still around the same trial-to-trial resting position. Successive trials were separated by a 5 s interval during which the subject opened their eyes, while remaining on the platform. Recording was initiated 2-3 s. after closure of the eyes. This allowed transient postural swing resulting from eye closure to dissipate. A vibrating handle, producing a sinusoidal vibration of 150Hz with an acceleration of 60 m/s^2 rms, was held in the dominant hand in eight different situations. Hand vibration was applied during the last two trials of each experimental series.
The subjects were submitted to two groups of four experimental situations :
A) In the first group the vibrating handle, free in space, was held in the dominant hand in the following situations :
1 Arm extended, horizontal in the sagittal plane;
2. Forearm flexed at 90° in the sagittal plane;
3. Arm extended horizontal in the frontal plane;
4. Arm-up vertical in the frontal plane.
B) In the second group, the vibrating handle was attached to a stationary frame. The same experimental situations were used.
Postural stability was evaluated using the length of the posturogram and the mean position of the Center-Of-Foot Pressure (COP). An analysis of variance (ANOVA) was used to ascertain statistical differences related to vibration, handle attachment and hand position.

RESULTS

Application of vibration to the hand induced a significant increase ($p \leq 0.03$) in the length of postural sways only when the handle was fixed in space. Shifts in the mean COP were significant in all eight situations ($p \leq 0.02$). Furthermore, the shift patterns were strongly oriented when the handle was fixed in space. Indeed, a shift of the COP in the direction of the handle was observed for all subjects in situations where the arm was extended in the sagittal or frontal plane. In the latter case, the COP of the left-handed subject shifted to the left. These results are illustrated by the graphs reproduced in Figure 1. The position of the COP before vibration was used as the reference. When the fixed handle was held with the forearm flexed 90° in the sagittal plane, 6 subjects shifted forward, 3 laterally and 1 backward. Neither the arm-up fixed-handle situation nor any of the free-handle situations resulted in a particular shift pattern of the COP.

DISCUSSION

The role of lower limb muscle proprioception in balance control and regulation is well established (Diener *et al.* 1984). However, recent studies (Roll *et al.* 1986,1989) using skeletal and/or extraocular muscle vibration, have indicated that wrist, neck, and eye proprioceptive feedback contribute to the elaboration of body references. Furthermore, the extreme sensitivity of muscle spindle mechanoreceptors to the vibratory stimulus (Burke *et al.* 1976, Vedel *et al.* 1985) is the source of the vibration-induced distortion of the sensory messages issued by these receptors (Roll *et al.* 1989). In the present experiment, alteration of hand proprioceptive cues elicited by hand vibration resulted in a deterioration of balance stability and a change in postural behavior. These detrimental effects confirm the importance of hand proprioception to postural control and spatial orientation.

Free and fixed handle situations resulted in significant differential effects on postural behavior. It appears that the context determines the nature and organization of the behavioral response. The clearly oriented patterns of the postural shifts observed with the stationary handle indicate that the position of the hand is used as an extracorporal spatial reference which

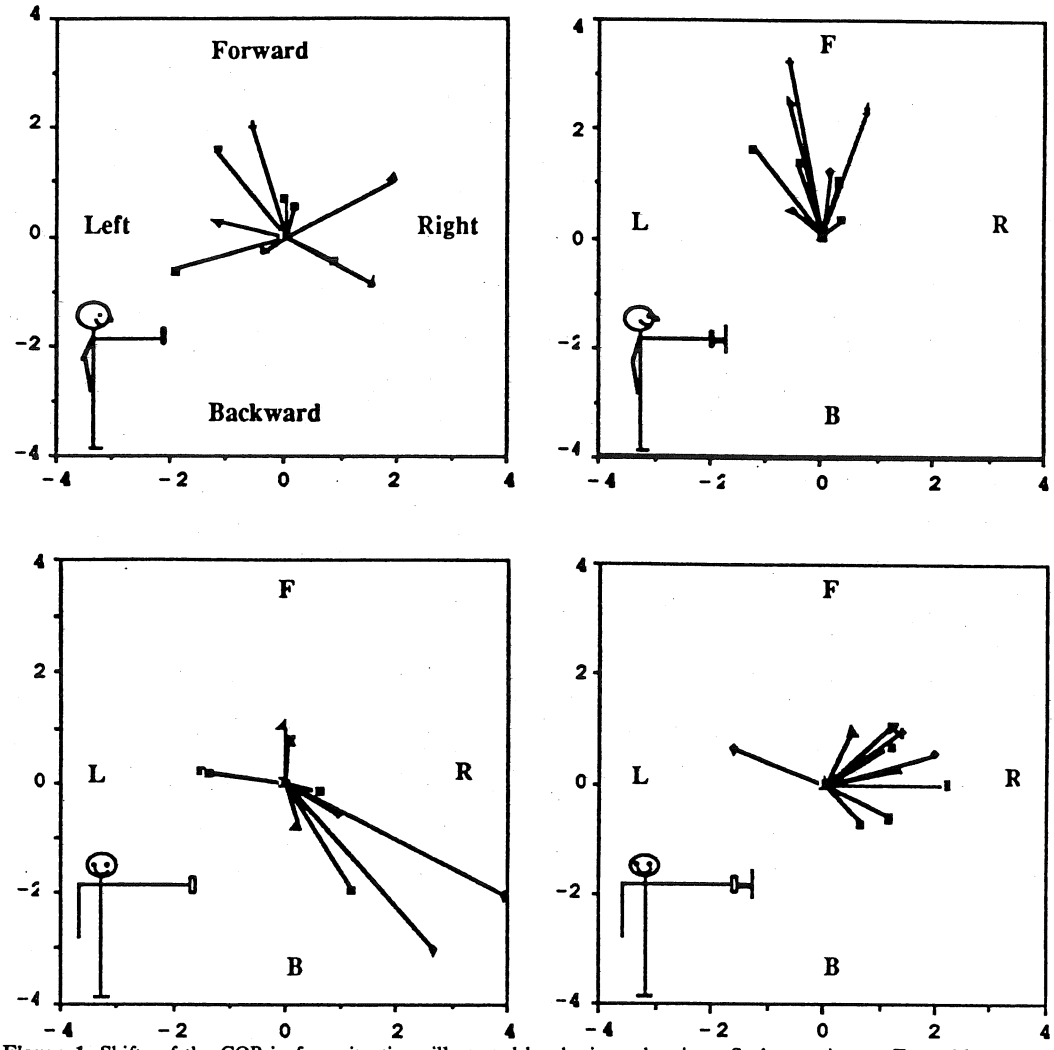

Figure 1. Shifts of the COP in four situations illustrated by the inset drawings. Scales are in cm. Ten subjects are represented. When the handle is fixed (right panels) the shifts occur mainly in the direction of the handle. (♦) left handed subject.

contributes to the control of posture. These shifts can be interpreted in terms of adjustment of the body posture in response to the vibration-modified representation of the whole body. Furthermore, the pseudo-random direction of the shifts elicited when the handle is free in space indicate that in that context the position of the hand may only play a role in the intracorporal coordinate system. These results corroborate previous findings from Roll et al (1986) which suggested that the proprioceptive messages seem to be "interpreted as a function of the postural context in which they occur". Overall, the experimental data presented here suggest that sensory information about the relative and absolute positions of the hand in space contributes to postural control and the elaboration of the body references.

To conclude, these results indicate that hand vibration produced by powered tools may induce postural changes that can put human operator in an "at risk posture control area", which is likely to contribute to slip and fall accidents. In addition, the absence of perception of postural changes leaves the operator unaware of a potential risk. These results are of particular importance for the design of industrial workplaces where hand-held vibrating tools are extensively used. They may provide justification for the enhancement of spatial visual references, which will compensate to some extent for the deficit of other sensory modalities involved in balance control.

REFERENCES

Burke et al. J. Physiol., 261, 673-693, 1976.
Diener et al. Brain Research, 296, 103-109,1984.
Gauthier et al. Aviat. Space Env. Med., 52 (8), 473479, 1981.
Johansson et al. Brain Res., 244, 17-25, 1982.
Martin et al. Aviat. Space and Env. Med., 51, 778-787,1980.
Martin et al. Aviat. Space and Env. Med., 62 (2), 145-152, 1991.
Martin et al. Aviat. Space Env. Med., 55 (1), 8-12, 1984
Roll et al. Sensorimotor plasticity : theoretical, experimental and clinical aspects. (pp.283-304). INSERM. 1986
Roll et al. Progress in brain research, 80, (pp113-123), 1989
Vedel et al. Man under vibration. Second international CISM-IFTOMM Symposium, (pp130-138), 1985.

HOW VARIOUS PHYSICAL CHARACTERISTICS RELATE TO POSTURAL STABILITY IN SUBJECTS WITH AND WITHOUT DIABETIC NEUROPATHY

G. G. Simoneau*, P. R. Cavanagh and J. S. Ulbrecht

Center for Locomotion Studies, Penn State University, University Park, PA

INTRODUCTION

Association between postural stability (PS) and several physical characteristics of 51 subjects between the ages of 40 and 70 was investigated. To determine which physical variables were most closely related to PS, a multidimensional scaling statistical technique enhanced with a factor analysis was used. Based on this data analysis, six factors (accounting for 76.5% of the variance in the original data set) were identified. In agreement with our previous findings that distal sensory neuropathy resulting from diabetes mellitus significantly reduces the ability to maintain a stable stance position (Simoneau 1992), somatosensory functions were the physical characteristics most closely associated with PS.

REVIEW AND THEORY

Several previous investigators have correlated measurements of PS derived from body sway or center of pressure (CoP) signal with various physical attributes of the subjects participating in their studies (Lord et al., 1991, Sheldon et al., 1963). This type of analysis is believed to be helpful in determining the most important physical variables that influence the control of posture. It also offers the possibility, when used in conjunction with regression equations, of predicting PS in a given individual without making a direct posture measurement.

Typically, the level of relationship existing between two variables is expressed as a single correlation coefficient. Therefore, when a large number of variables are included in the experimental design, large tables of correlation coefficients (correlation matrices) are generated, making the results difficult to interpret without extensive scrutiny of the data.

The aim of this research was to determine the physical variables most closely associated with PS. We also proposed the use of a multidimensional scaling technique (Gould 1985) supplemented with a factor analysis to enhance data interpretation.

PROCEDURES

Data were collected on 51 individuals between the ages of 40 and 70. Seventeen subjects were nondiabetic with normal cutaneous sensory function of the plantar surface of both feet, 17 were diabetic with minimal peripheral sensory neuropathy and 17 were diabetic with significant sensory neuropathy. Significant neuropathy was defined as a vibratory perception threshold of the halluces that was greater than two standard deviations above the age-dependent normative values published by Bloom et al. (1984). Except for diabetes, all subjects were considered healthy based on an extensive medical screening. The subjects did not take any medication known to affect PS.

Sensory function was assessed in all subjects using a variety of measurements. The somatosensory function tests included: vibration perception threshold (VPT) measurements of the plantar cutaneous surface of both feet, perception of touch using Semmes-Weinstein monofilaments (SW) of the plantar cutaneous surface of both feet and joint movement perception (JMP) of the ankle.

Visual function was measured with a standard test of visual acuity using the Snellen eye chart and with the assessment of visual contrast sensitivity (VCS) at 4 spatial frequencies corresponding to 1.5 (VCS 1.5), 6.0 (VCS 6.0), 12.0 (VCS 12.0) and 18.0 (VCS 18.0) cycles/degree of visual angle. Vestibular function was tested using the Fukuda test (Fukuda 1959). This test provides a quantitative estimate of vestibular function with three measurements derived from the change of location of the subject after performing 50 "in place" steps with eyes closed.

In addition to these sensory measurements, the following physical characteristics of the subjects were measured: weight, height, strength of the ankle musculature in plantarflexion (PF) and dorsiflexion (DF) and age. Sensory latency response (SLR) of the sural nerve and nerve conduction velocity (NCV) of the peroneal nerve were measured on the diabetic subjects.

PS was measured using the total displacement of the CoP signal obtained from a Kistler force platform over a period of 30 seconds with the subject standing with feet six inches apart and looking ahead. The CoP signal was low-pass-filtered at 5 Hz.

The first step in the analysis of the data consisted of producing a correlation matrix for the 19 variables

being considered. The correlation coefficient values of the matrix were then used to generate a "map," giving a visual representation of the level of relationship among all variables. This map was generated using the multidimensional scaling technique described by Gould (1985). This technique uses a KYST algorithm, which allows one to obtain the best spatial arrangement of all points based on a finite number of iterations. Finally, a factor analysis that grouped the variables into a small number of factors referred to as "spaces" on the map was performed.

RESULTS AND DISCUSSION

The results of the scaling technique and of the factor analysis are presented in figure 1.

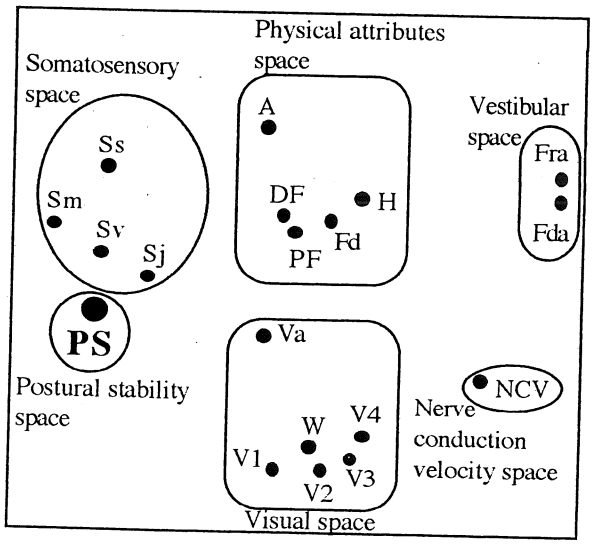

PS = CoP displacement, Sv = VPT, Sm = SW
Sj = JMP, Ss = SLR, Va = Visual acuity,
V1 = VCS 1.5, V2 = VCS 6.0, V3= VCS 12.0,
V4 = VCS 18.0, W = Weight, A = Age,
Fd = Fukuda displacement distance, DF = Ankle DF strength, PF = Ankle PF strength, H = Height,
Fra = Fukuda rotation angle, Fda = Fukuda displacement angle, NCV = NCV

Figure 1. Map of all variables using a multidimensional scaling technique.

The six factors suggested by the factor analysis were given names in a post hoc manner according to the variables included in each factor. These factors accounted for 76.5% of the variance in the original data set. PS was given a space of its own. The second factor, called the somatosensory space, included the four somatosensory measurements performed on the subjects. The proximity of this space to the PS space indicates a high level of relationship between PS and somatosensory function. Within this group (since closeness on the map indicates the level of association between variables), JMP, VPT and SW were more closely related to CoP displacement than SLR (r = .70, .65, .73 and .39, respectively).

The visual space that included all the variables associated with the assessment of visual function pointed to a high level of association among the measurements of VCS at different visual spatial frequencies. It should be noted that the association between the visual acuity variable and the VCS measurements is only moderately strong based on their relative position on the map. Of the seven variables included in this "space," visual acuity appears to be most closely associated with PS (r = .44). Note that, unexpectedly, weight was included in this factor despite its lack of association with VCS measurement.

The fourth space (vestibular space) consisted of two of the three measurements of vestibular function, both giving the results of the Fukuda test in terms of angular values. The large distance between the location of these points and the CoP displacement point coordinates on the map indicates a very poor association between the results of the Fukuda test and PS (r = .01 and .03).

The fifth space (the physical attributes space) included the measurement of age, height, ankle strength and the displacement measured from the Fukuda test. The correlation coefficient values between these variables and PS varied from .46 for age to .08 for height. Finally, NCV was also attributed a space of its own.

We conclude that somatosensory function is most closely associated with PS and that the statistical analysis techniques used for the interpretation of the data allowed a clear visual representation of the levels of association among all variables.

REFERENCES

Bloom, S. et al. *British Med J*, 288, 1793-1795, 1984.
Fukuda T. *Acta Otolaryngologica*, 50, 95-108, 1959.
Gould, P. The Geographer at Work, Rutlidge and Kegan Paul, 1985.
Lord, S. et al. *J Geront:Med Sc*, 46, M69-76, 1991.
Sheldon J. , et al. *Gerontol. Clin.*, 4, 129-138, 1963.
Simoneau G. Ph.D. Dissertation, Penn State University, 1992.

ACKNOWLEDGMENTS

* Dr. Simoneau is currently an assistant professor in the department of physical therapy at Marquette University, Milwaukee, WI. Supported in part by an American Diabetes Association Feasibility Grant.

POSTURAL CONTROL AND THE CLINICAL EVALUATION OF PATIENTS WITH MULTIPLE SCLEROSIS

Victoria Panzer-Decius and Henry McFarland

NeuroCom International, Clackamas, OR
NeuroImmunology Section, NINDS, National Institutes of Health, Bethesda, MD

INTRODUCTION

Dramatic increases in the number of therapeutic treatment trials in multiple sclerosis (MS) have heightened the need for reliable and sensitive methods to evaluate clinical status and disease progression. We measured postural responses to various sensory and motor challenges to determine if these provided information about disease activity and progression required for clinical trials in MS. Nine patients were evaluated monthly with posturography, neurological exam and magnetic resonance imaging (MRI) for at least one year. The concurrence of clinical exacerbations with changes in sensory or motor function as measured by posturography was 59%. Changes in the latency of automatic postural response were associated with 84% of all changes in baseline disease activity by enhanced MRI. Measurement of postural response appears to be a sensitive means to monitor the course of MS and may be useful as a clinical outcome measure.

REVIEW AND THEORY

The postural control system encompasses many of the major CNS areas vulnerable to MS including the brain stem, and dspinal cord as well as, cerebellar, visual, and vestibular pathways. Therefore it seems reasonable that postural measures may provide clinical information relevant to patients with MS.

Tourtellotte (1988) has championed the need for reliable, quantitative measurement in MS, suggesting that clinical trials must employ quantitative measures of clinical outcome. Enhanced MRI is reported to identify lesions in patients with early MS in which no clinical change is evident (Frank et al., 1991). This suggests that clinical examination is less likely to provide a sensitive indicator of change than MRI.

PROCEDURES

Nine patients with clinically definite MS (average age 34.7) were evaluated monthly for at least one year. Monthly examinations included posturography, neurological examination, and magnetic resonance imaging with gadolinium enhancement. Posturography consisted of six conditions of quiet standing (eyes open and closed, sway referenced surface, sway

referenced vision and combinations thereof) and evaluation of motor response latency to forward and backward platform translations. A composite score for patient stability across sensory conditions and a composite of right and left leg motor response latencies across translation types were calculated.

RESULTS

Over a one year period, the total number of clinical exacerbations, bursts of enhancing lesions, instances of increased postural latency, instances of decreased postural stability and the concurrences of these events in the nine patients are detailed in Table 1.

Table 1. THE RELATIONSHIP BETWEEN CLINICAL AND MRI CHANGES AND POSTUROGRAPHY.

Pt.	# of clin. exac.	# bursts enhan. les.	Incr. post. lat.	Con. exac. &les.	Con. les. &lat.	Decr. post. stab.	Con. exac. &stab.	Con. les. &stab.
PA	3	3	2	2	2	3	3	1
HB	0	3	3	0	3	1	0	1
CC	1	0	2	0	0	4	1	0
RF	1	3	3	0	3	3	0	2
DH	3	3	4	3	3	2	2	1
JH	4	4	4	4	4	3	2	2
LJ	1	3	2	0	1	2	1	1
JO	4	3	3	1	3	3	1	1
AZ	0	3	3	0	2	1	0	1
Total	17	25	26	10	21	23	10	10

DISCUSSION

Changes in posturographic measures (stability or latency) were associated with 59% of the observed clinical exacerbations. This proportion is low due to the inclusion of sensory exacerbations unlikely to be related to the systems discussed above; such as tingling in the hands. The relation between stability changes in various sensory conditions and incidences of enhancing lesions was 40%. However, increases in latency of motor response were concurrent with 84% of all bursts of enhancing lesions. It appears that postural response latency is a very sensitive indicator of motor changes in MS, demonstrating disease activity that is not evident clinically. These changes are likely to have the greatest functional significance to the patient and can provide a useful means of monitoring clinical trials.

REFERENCES

Harris, J.O. et al. Ann. Neurol., 29,548-555, 1991.
Tourtelotte, W.W. et al. Neurol.,38(2), 83-86, 1988.

METHOD FOR ESTIMATING FALL POTENTIALS IN CLINICAL, OCCUPATIONAL, AND ENVIRONMENTAL EXPOSURE CASES

Angshuman Bagchee and Amit Bhattacharya

Biomechanics and Ergonomics Research Laboratory
Department of Environmental Health
University of Cincinnati Medical Center, Cincinnati, OHIO 45267-0056

INTRODUCTION

It has been well established that a large number of injuries occur due to falls in all spectrum of population. Postural stability plays a vital role in the phenomena of fall. It has been reported in literature that people with history of falls have higher postural sway (Overstall *et al.*(1977)). However, it is difficult to estimate the exact amount or extent of sway that may be identified with high risk of fall. A method has been developed to superimpose the footprints of a subject on his/her stabilogram. This provides us with a physical dimension to compare the sway pattern. Several clinical, occupational, and environmental exposure case studies have been discussed to illustrate the use of such a method in the prediction of patterns that could be associated with the accident proneness and/or possibility of fall.

REVIEW AND THEORY

The phenomena of fall has been studied in the recent years because of the fact that many injuries occur due to falls. Understanding the role of postural stability is very important in the investigation of the phenomena of fall. The physics of stability dictates that the body can maintain upright posture as long as the vertical projection of one's center of pressure (CP) is maintained within the basal support area or the *stability boundary*. In the case of human body the basal support can be defined by the outer envelope of the footprint (Bagchee *et al.*). The imposition of footprints on the stabilogram offers a physical dimension to compare the amount of sway. In the present study a method for tracing the footprints has been devised to acquire the footprints using a sonic digitizer, that is more efficient for repetitive use.

Fall occurs when the stabilogram (locus of the CP during a test period) of an individual crosses the basal support area or the stability boundary. A combination of intrinsic and extrinsic factors influence the upright balance. Intrinsic factors may include muscle strength, age, gender, fatigue, somatotypic differences etc., while the extrinsic factors may include the environmental factors like lighting, surface conditions, layout, etc. For an individual, the upright balance is influenced by visual input, vestibular system, and proprioception. Any or all of these systems' functional capabilities may be compromised by both intrinsic and extrinsic factors. To illustrate the application of this method, the stabilograms with imposed footprints were compared for subjects of different age and chemical exposure (lead), and other neurological diseases.

PROCEDURES

Movement of the CP of an individual was measured using a strain gauge type force platform (AMTI) capable of measuring forces and moments in the three orthogonal directions. The x-y coordinates are calculated as described in Bhattacharya *et al.*(1987). The data collection for footprints is accomplished in two steps. In step I, the subject is instructed to stand on the force platform, with foot placement as defined by the test protocol. His/her feet patterns are then traced on a paper attached to the top surface of the platform. The subject then performs a series of tests as described by the test protocol, given in Bhattacharya *et al.*(1987). At the end of testing session this paper is stored away with proper identification. Step II involves digitization of the traced footprints. A sonic digitizer (GRAF/BAR GP-7, SAC) is utilized for the purpose. The digitized data is then combined with the stabilogram data in a software developed by the authors. The reproducibility of the footprint digitization is limited by the accuracy of the digitizer (resolution 0.01 cm) and possible human error. The ability of placing the subject's feet on a pre-traced footprint was also investigated, and was found to be less than 2 to 4% of the foot length.

RESULTS AND DISCUSSION

Figures 1-4 show the stabilograms obtained in five different case studies. Figures 1 and 2 illustrate the stabilograms for children with high blood lead (28.3 μg/dL; age: 6 yrs) and low blood lead (5.402 μg/dL; age: 7 yrs) respectively. The CDC criteria for acceptable exposure to environmental Pb is 10 μg/dL. Chronic lead (Pb) poisoning has been shown to affect the higher centers of the nervous system which adversely affects the postural stability (Bhattacharya *et al.*(1987)). It can be observed that the sway appears to be more spread in the high lead child as indicated by previous studies. The superimposed footprints show the difference in sway between the two children when compared to the stability boundary of the individual. In a real life scenario, while performing simple tasks, the child with higher lead levels may show greater proximity of the CP to his/her outer periphery of the footprints (stability boundary) and hence be more susceptible to accidents and eventual fall in the event of even a small perturbation (like a small push).

Figure 3 shows the stabilogram for an 84 year old patient suffering from Alzheimer's Disease and Rheumatoid Arthritis. As can be observed, the stabilogram travels much closer to the boundary of the footprints in this case. During the test period the subject had to be supported by

an assistant several times to prevent an actual fall, especially during the tests requiring the subject to close her eyes. Even simple day to day activity may be detrimental for this subject as the CP could be displaced beyond the stability boundary due to sudden change in extrinsic factors, like lighting. Figure 4 shows the stabilogram for an adult (age: 34 years) who was occupationally exposed to high levels of Pb (109 μg/dL blood Pb level). This person was found to be having difficulty in maintaining upright balance in the eyes-closed condition. Thus, the subject relied heavily on visual system for maintaining balance. The stabilogram shows the proximity to the stability boundary. Even for tasks with available visual cues, a fall may be imminent when the sway lies in the vicinity of the stability boundary. Any undesirable perturbation may cause the sway to cross the stability boundary and result in a fall. Sway pattern for a normal elderly subject with degenerative joint disease shows that although the stabilogram area for a normal elderly patient is much more than that of a young adult, the imposed footprints indicate that the person has better ability to withstand deviations in the CP as compared to the cases discussed in figures 3 and 4.

The present method provides the physical representation required to compare the stabilogram in predicting fall potential. Studies have recently been concluded in this laboratory which have been able to better define the concept of stability boundary and quantitate the proximity of the stabilogram to such a boundary (Bagchee *et al.*(1992)). This method can thus be utilized as a tool for quantification of postural stability, and to provide normative data on fall potential by comparing stabilograms with superimposed footprints for various populations under different intrinsic and extrinsic factors.

NOTE: All dimensions in the following figures are in centimeters. The stability boundary is shown with a dotted line.

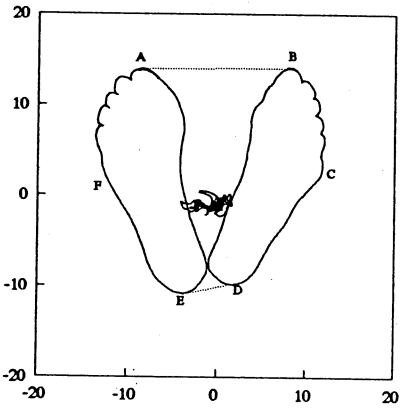

Figure 1. Stabilogram of a high blood lead level child

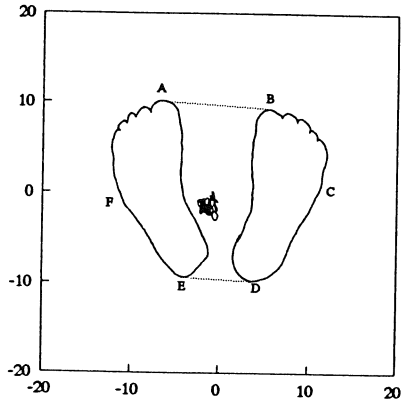

Figure 2. Stabilogram of a low blood lead level child

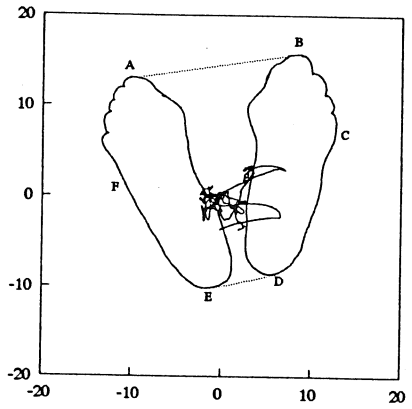

Figure 3. Stabilogram of an 84 year old patient with Alzheimer's Disease and Rheumatoid Arthritis

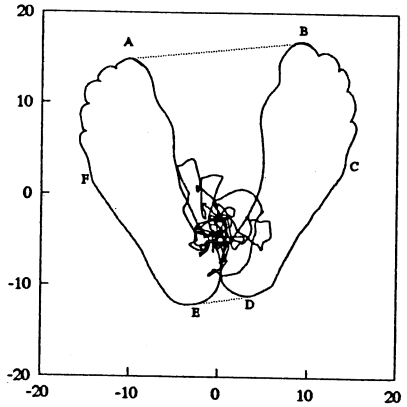

Figure 4. Stabilogram of a worker (occupational lead exposure)

REFERENCES

Bagchee, A. *et al.*, Quantitative Assessment and Functional Implications of Postural Stability Boundary (*In preparation,* 1992).

Bhattacharya, A. *et al.*, Ann. Biomed. Eng., **15**, 533-550,1987.

Overstall, P. W. *et al.*, Brit. Med. J., **1**, 261-, 1977.

SPORT BIOMECHANICS

Podium Session 7

COMPUTER SIMULATION OF THE TAKEOFF PHASE OF THE LONG JUMP

John W. Chow and James G. Hay

Department of Exercise Science, The University of Iowa, Iowa City, IA 52242

INTRODUCTION

The purpose of this study was to investigate the interacting roles played by the approach velocity ($\dot{x}_{TD}$), the explosive strength (represented by the vertical ground reaction force, VGRF), and the change in angular momentum about a transverse axis through the jumper's center of mass (δHzz) during the takeoff phase of the long jump (TOP) using computer simulation. A two-dimensional, two-segment model was used to simulate TOP. The influence of $\dot{x}_{TD}$, VGRF, and body mass (m) on the jump distance (JD) were studied using sensitivity analyses. The major findings were that (1) JD was more sensitive to changes in $\dot{x}_{TD}$ than to changes in VGRF, (2) $\dot{x}_{TD}$ and VGRF seemed to be interdependent factors in maximizing JD, and (3) reducing m could be an effective way to improve performance if muscular strength was not sacrificed.

REVIEW AND THEORY

There is general agreement among coaches and athletes that the jump distance depends upon $\dot{x}_{TD}$ (the horizontal velocity during the flight phase of the last stride), the technique used during the takeoff, and the "explosive strength" of the athlete. Research has shown that both $\dot{x}_{TD}$ and VGRF are significantly correlated with JD. However, conflicting findings have been reported with regard to the relationships among $\dot{x}_{TD}$, VGRF, and JD (Hay, 1986). Because δHzz can be determined by integrating the resultant moment about the jumper's center of mass (CM) with respect to time during TOP (ground reaction force [GRF] x moment arm [MA]), it seems reasonable to expect that there are interactions among $\dot{x}_{TD}$ (which causes changes in the CM location and thus in MA), GRF, and δHzz.

Different approaches have been employed to simulate TOP. Hatze (1981) used a complex musculoskeletal model. Ridka-Drdacka (1986) and Alexander (1990) used single and double inverted pendulum models, respectively, and assumed that GRF was directed through CM. They assumed, therefore, that δHzz was zero. However, Hinrichs et al. (1989) found that δHzz was not zero and the magnitude of δHzz was related to the jumping technique. In order to maximize the validity of the simulation, δHzz was included in our model.

PROCEDURES

In the present model, the jumper is idealized as an inverted pendulum, with mass equal to the mass of the jumper and located at his (or her) CM, connected to a massless rigid foot segment (Fig. 1). The location of the center of pressure (CP) varies throughout TOP. Consequently, the distance between CM and CP – MA for the computation of the resultant moment acting on the jumper – is not constant during TOP. The JD is the sum of the takeoff (x_{TO}), the flight (x_{FL}), and the landing (x_{LD}) distances (Hay, 1985). The mechanical factors that determine these three distances were identified. The inputs to the model include the CM location (x_{TD} and y_{TD}) and the velocity ($\dot{x}_{TD}$ and $\dot{y}_{TD}$) at the instant of touchdown (TD), and GRFs during TOP. Among the outputs of the model (x_{TO}, y_{TO}, $\dot{x}_{TO}$, and $\dot{y}_{TO}$) are the takeoff conditions for a projectile motion that determines x_{FL}. Assuming the CM location at landing (x_{LD} and y_{LD}) is constant, JD is therefore computed.

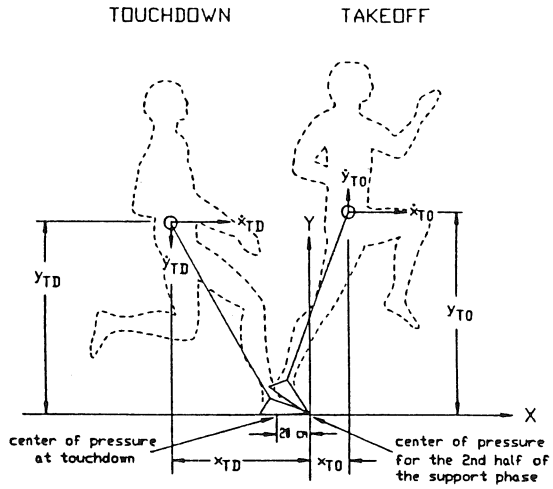

Figure 1. Two-segment model.

Data reported by Bosco *et al.* (1976) for a jump of 6.85 m were used to define a reference jump. The published GRF-time curves for this jump were enlarged and the support phase divided into 98 time intervals of equal duration (δt) [Fig. 2]. The midpoint of the curve segment in a given time interval was taken as the average force during that δt. For a given set of initial conditions, the CM location, the velocity, and the change in angular momentum since TD were updated every δt s. Based on findings reported in the literature, CP was assumed to be 20 cm behind the toe at TD, to move forward uniformly to the toe during the first half of the support phase , and to remain there for the remainder of the support phase (Fig. 1).

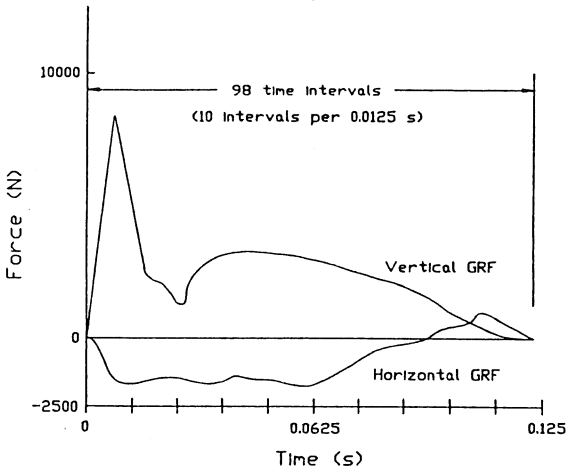

Figure 2. GRFs during the takeoff phase.

Sensitivity analyses (SAs) were conducted to study the influence of $\dot{x}_{TD}$, VGRF, and m upon JD. In each SA, the parameter of interest was increased or decreased from 1% to 10% with steps of 1% and the other two parameters were kept constant. Three constraints were imposed on the model for SAs: (1) δHzz was constrained to values from -15 to 0 kgm^2/s [Hinrichs, 1991], (2) the distance between CM and toe at TO (CT_{TO}) was limited to fall within 99% to 101% of CT_{TO} of the reference jump, and (3) the ratio of CT_{TD} to CT_{TO} was constrained to lie within the range from 0.905 to 1.022 (Hay, unpublished data). In addition, a SA using similar procedures was conducted to determine the influence of increasing both $\dot{x}_{TD}$ and VGRF at the same time.

RESULTS AND DISCUSSION

Although no explicit validation of the model has yet been attempted, it is believed that the model is an acceptable compromise between accuracy and complexity and is detailed enough to capture the gross dynamical characteristics of the TO.

The results of the SA for the effect of changes in $\dot{x}_{TD}$ indicated that both JD and δHzz increased as $\dot{x}_{TD}$ increased. However, there was no simulated jump that satisfied the constraint on δHzz when $\dot{x}_{TD}$ was increased by more than 3%. As $\dot{x}_{TD}$ increased, CM was in a more forward position at TO and the angle of takeoff decreased. It seems that some other parameters must be altered as $\dot{x}_{TD}$ increases if δHzz is to be kept within acceptable limits.

The results of the SA for the effect of changes in VGRF showed that JD increased and δHzz decreased as VGRF increased. The increase in JD was mainly due to an increase in $\dot{y}_{TO}$. The increase in $\dot{y}_{TO}$ caused an increase in both the resultant velocity at TO and in the angle of takeoff. A comparison of the first two SAs suggested that JD is more sensitive to changes in $\dot{x}_{TD}$ than to changes in VGRF. In other words, $\dot{x}_{TD}$ seems to be the more important factor in determining LD. For example, a 3% increase in $\dot{x}_{TD}$ and VGRF yielded 5.2% and 3.7% increases in JD, respectively.

The results of the SA for the effect of changes in m showed that JD increased as m decreased (a 10% decrease in m yielded a 9.3% increase in JD). Changes in δHzz were relatively small when compared with the corresponding changes caused by the other two parameters. Decreases in m were accompanied by increased losses in horizontal velocity during the TO and by an increase in $\dot{y}_{TO}$ (impulse-momentum relationship). The ultimate result of changes in $\dot{x}_{TO}$ and $\dot{y}_{TO}$ was an increase in the angle of takeoff and in JD.

When both $\dot{x}_{TD}$ and VGRF were increased, JD increased to a greater extent than when only one of these parameters was increased. This was attributed to the larger increase in the resultant velocity at TO, which is often regarded at the most important factor in determining the range of a projectile. A relatively small change was observed in δHzz when both x_{TD} and VGRF were increased, suggesting that an increase in one parameter must be accompanied with an increase in the other parameter in order to minimize the change in δHzz. If that happened, maximum improvement in performance could be achieved without significant changes in technique.

The results of the present study, together with the previous findings on the relationship between δHzz and jumping technique (Hinrichs *et al.*, 1989), seem to suggest that a jumper with exceptional running speed should use the hitch-kick technique (associated with a larger δHzz) and a jumper who relies on a strong takeoff should use the hang or sail technique (associated with a smaller δHzz).

REFERENCES

Alexander, R. *Phil. Trans. R. Soc. Lond.*, **329**, 3-10, 1990.

Hatze, H. *J. Biomech.*, **14**, 135-142, 1981.

Hay, J. The Biomechanics of Sports Techniques, (p.422), Prentice-Hall, 1985.

Hay, J. In Pandolf, K. (ed.) Exercise and Sport Sciences Reviews, (pp.401-446), Macmillan Publishing, 1986.

Hinrichs, R. Personal communication, 1991.

Hinrichs, R. et al. Proc. XII Int. Congress Biomech., 1989.

Ridka-Drdacka, E. *Int. J. Sport Biomech.*, **2**, 289-300, 1986.

ACKNOWLEDGMENTS

This study was supported by The Athletics Congress.

Proceedings of NACOB II, The Second North American Congress on Biomechanics, Chicago, August 24th - 28th, 1992

PREDICTION OF OPTIMAL FULCRUM SETTING FOR BACKWARD TAKEOFFS

W.L. Boda and J. Hamill

Department of Exercise Science, University of Massachusetts, Amherst

INTRODUCTION

In springboard diving, it is critical that the diver choose the correct fulcrum setting on the springboard to optimize the flex of the board and achieve maximal height on leaving the board. Maximal height is important because it allows the diver as much time as possible to perform a dive and increases the aesthetic appeal. The purpose of this study was to apply a model of the springboard and diver (Sprigings et al., 1988; Boda and Hamill, 1990) to generate an equation which would predict the optimal fulcrum setting for the diver. The optimal fulcrum setting is defined as that setting at which the diver generates the greatest height.

REVIEW AND THEORY

For this study it was necessary to determine the physical characteristics of the springboard. The springboard used in this study was a Maxi-Flex Model "B" weighing 570.8 N and a center of gravity located 2.3 m from the fixed. The spring characteristics of the diving board were determined by:

$$K = \frac{F}{\Delta y}$$

where F = force imparted to the board and Δy = displacement of the board. The damping coefficient was determined by:

$$b = \frac{\delta^2}{(\delta^2 + 4\pi^2)}$$

where d = ln(x1/x2), x_1 = amplitude of the first positive oscillation, and x_2 = amplitude of the second positive oscillation. Because the damping coefficient was calculated to be less than 0.001, the equation below which does not include damping was used to model the springboard. The equation for the determining the frequency of oscillation using the linear spring with a lumped mass without damping (Beer & Johnston, 1987) is:

$$f = \frac{1}{2}\pi\sqrt{\frac{k}{m_1+m_2}}$$

where m_1 = the effective mass of the board, m_2 = the mass of the added weight, k = the spring constant of the board weight system, π = 3.1416.

PROCEDURES

Subjects : Twenty members (11 males and 9 females) of a college diving team participated as subjects in this study. The subjects ranged in mass from 47.5 to 93.2 kg and in age from 18 to 29 years. All subjects had participated in college diving competitions and could be classified as experienced divers.

Experimental Set-up : A high-speed video camera and recorder was placed 9.14 m sagittal to the springboard and 1.09 m above the pool deck during data collection. Data were sampled at 60 Hz with a shutter speed of 1/250 s. Reflective markers were placed to describe a model that included the arm, head and trunk, thigh, leg, and foot. Markers was also placed 0.5 m apart on the springboard. The video data were digitized using a VP110 video processor interfaced to a SUN minicomputer and were filtered using a low-pass filter with a selective cut-off algorithm.

Protocol : The springboard and diver system were videotaped oscillating at fulcrum settings of 1, 3, 5, 7, and 9. These settings covered the full range of available fulcrum settings. Subjects performed three trials of 10 oscillations followed by a jump from the springboard. Subjects were also videotaped oscillating on the ground both before and after the springboard testing. The mean of three trials was used to determine the oscillation

rate of the diver and the springboard and on the ground. Variables computed included spring energy, vertical velocity, oscillation rate, angle of takeoff, impulse, height of jump from the springboard and anthropometric characteristics.

Statistical Analysis : The condition with the greatest height was used to formulate the prediction equation. A bootstrap method was used to determine a range of regression equations for this sample (Efron and Gong, 1983; Efron and Tibshirani, 1991). Using the bootstrap method, random groups of 15 subjects were employed to formulate a prediction equation and 5 subjects to test the equation. This procedure was repeated 20 times. The average equation resulted in the final regression equation. The ability of the independent variables to predict the optimal fulcrum setting was assessed by cross validation with a hold-out group of 5 divers.

RESULTS

Two sets of regression equations were developed in order to construct a final regression equation. The first set of equations were allowed to pull in any variable in any order with the restriction of an F-ratio of 3.1 which corresponded to $p < 0.05$ for 13 degrees of freedom in the denominator. Of the 20 regression equations, 16 pulled into the equation preferred fulcrums setting, body mass, and oscillation on the ground. The second set of regression equations was based on the first set of equations. This set of regression equations was allowed to pull in only preferred fulcrum setting, body mass, and oscillation rate on the ground.

The final regression equation that was developed was:
$y = 10.46 + 1.24\ B_1 - 4.50\ B_2 - 0.03\ B_3$
where y = predicted fulcrum setting, B_1 = preferred fulcrum setting, B_2 = frequency of oscillation on the ground, and B_3 = mass of the diver. The predicted fulcrum setting for each individual was calculated from the final prediction equation equation. The correlation between the predicted and actual fulcrum setting was $r = 0.90$. The regression equation explained 82% of the common variance.

DISCUSSION

The fulcrum setting at which the divers achieved the greatest height was larger than the fulcrum setting preferred by the divers. This indicates that in general all of the divers were setting the fulcrum too tightly and that they should move the fulcrum back to a looser(higher) setting to achieve more height.

The mean prediction equation is useful because all of the variables in the equation are easily measured by coaches. The final regression equation also indicates that the natural oscillation rate of the diver is a good predictor of height generated on the springboard with faster oscillations tending to result in less height. Body mass also predicts height generated from the springboard. This probably occurs because an individual with more body mass is able to generate more impulse on the springboard. It remains to be seen if this equation can be used for another sample of divers, however, the variables in the equation are logical predictors of jump height.

REFERENCES

Beer, F. & Johnston, E. *Mechanics for engineers - Dynamics (4th edition).* New York: Mcgraw-Hill Book Co., 1987.

Boda, WL and Hamill, J. *Proceedings of VIth CSB Biannual Meeting*, 109-110, 1990.

Efron, B and Gong, G. *The American Statistican*, 37:36-48, 1983.

Efron, B and Tibshirani, R. *Science*, 253:390-395, 1991.

Sprigings, E et al. *Proceedings of Vth CSB Biannual Meeting*, 144-145, 1988.

THE INFLUENCE OF RUN-UP DISTANCE ONTO GROUND REACTION FORCE AND PRESSURE DISTRIBUTION PARAMETERS

E. M. Hennig and G. A. Valiant
Sportmedizinisches Institut, Universität Essen, Germany
Nike Sport Research Laboratory, Portland, Oregon, USA

INTRODUCTION

Most research with force platforms is performed in a laboratory environment. For fast movements, as it is the case for running, limited laboratory space may have an influence on the results of experiments. This study was performed to estimate the necessary space requirements for reliable force platform and pressure distribution measurements in overground running. Three distances from a minimum of three steps towards a free run were chosen for the evaluation of force and pressure parameters.

REVIEW AND THEORY

Cavanagh and Lafortune (1980) reported ground reaction force data for running at a speed of 4.5 m/s. They investigated the magnitude of the vertical and horizontal forces and determined the center of pressure for different running styles. Nigg et al. (1986) found that running velocity has a dominant influence on the impact force peaks as well as the rate of loading. The authors reported also that shoe construction will result in a modification of some GRF parameters. Force and pressure parameters were also found to be valuable for the judgment of shoe performance in comparative shoe tests (Hennig et al., 1990). Although most of the published data on ground reaction force parameters during running is based on experiments in laboratory situations, almost no report includes information on the length of the run-up distance in the laboratory. The present study compared the influence of two relatively short run-up distances towards a free run situation.

PROCEDURES

Fourteen male subjects (71 kg / SD 7.44 kg) volunteered to participate in this study. They performed 8 repetitive running trials (rearfoot strikes) across a 40 cm by 60 cm "Kistler" force platform in each of three run-up distance conditions. The minimum distance was defined by a 3-Step, the medium distance by a 5-Step run-up (figure 1).

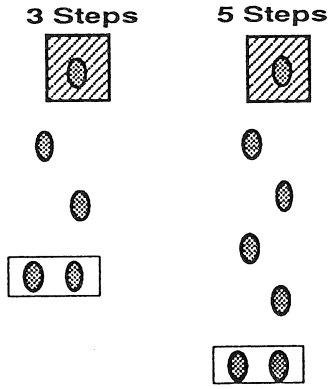

Figure 1: Run-up distances with 3 and 5 steps (right foot)

A free run was chosen as third condition. The experiments took place in a large laboratory facility with more than 15 m of space to both sides of the force platform arrangement. A target velocity of 3.83 m/s (7 min/mile) was chosen for all subjects and conditions. Using two photocells at distances of 1.5 m before and 1.5 m behind the force platform average running velocities across the force platform were determined. Only trials within a range of ± 2% of the target velocity were accepted. The order of the run-up conditions was randomized. The vertical and horizontal ground reaction forces and in-shoe pressure distributions under 8 anatomical locations of the foot were measured. Eight piezoceramic sensors, the properties of which were described by Hennig et al. (1982), were taped onto the plantar surface of the right foot at defined anatomical landmarks. The transducers were placed under the lateral and medial heel, lateral and medial midfoot, under the 1st, 3rd and 5th metatarsal head and the hallux. Data collection was done at a rate of 1 kHz per channel with a resolution of 12 bit. Table 1 lists the chosen GRF parameters for the evaluation of the three run-up conditions. From the pressure distribution data the peak pressures were chosen for comparisons. Prior to further statistical analysis the two most deviant of the 8 repetitive trials were discarded. As a selection criterion the magnitude of the first peak of the vertical GRF was used. A repeated measures ANOVA was used for parameter comparisons.

PVF1	1. Peak of the Vertical Force Curve
TPVF1	Time to 1. Peak
DPVF	Highest Force Rate
PVF2	2. Peak of the Vertical Force Curve
TPVF2	Time to 2. Peak
I-Fz	Integral of the Vertical Force
PHF	Peak Horizontal Propulsion Force
TCT	Total Contact Time
CoV	Coefficient of Variability in %

Table 1: GRF parameters

RESULTS

Table 2 summarizes the GRF parameter value deviations (in percent) between the 3-Step and 5-Step conditions as compared to the Free-Run condition.

Prameter	3 Steps	5 Steps
PVF-1	- 11.6 % **	- 1.0 %
TPVF1	- 5.6 %	- 2.0 %
DPVF	- 4.8 %	+ 3.7 %
PVF-2	- 0.7 %	- 1.4 %
TPVF2	+ 3.0 %	+ 2.1 %
INT-Fz	- 0.4 %	+ 2.0 %
PHF	+ 17.7 % **	+ 4.2 %
TCT	+ 1.5 %	+ 2.9 %

Table 2: Deviations from Free-Run in +% or -%
(* $p<0.05$, ** $p<0.01$)

No significant differences were found for any of the parameter values for the 5-Step condition and the percentile deviations were found to be very small. However, the comparison between the 3-Step and Free-Run conditions revealed highly significantly reduced first vertical and increased peak horizontal force values for the 3-Step condition. The intraindividual coefficient of variability for the first vertical force peak value was significantly less in the 5-Step condition as compared to the Free-Run and the 3-Step.

Parameter	3 Step	5 Step*	Free Run^
PVF1	6.3 % **^	3.6 % ^	5.0 %
PVF2	2.9 %	2.7 %	2.4 %
INT-Fz	2.6 %	2.4 %	2.8 %

Table 3: Coefficients of intraindividual variability (%) (*^ $p<0.05$,**^^ $p<0.01$)

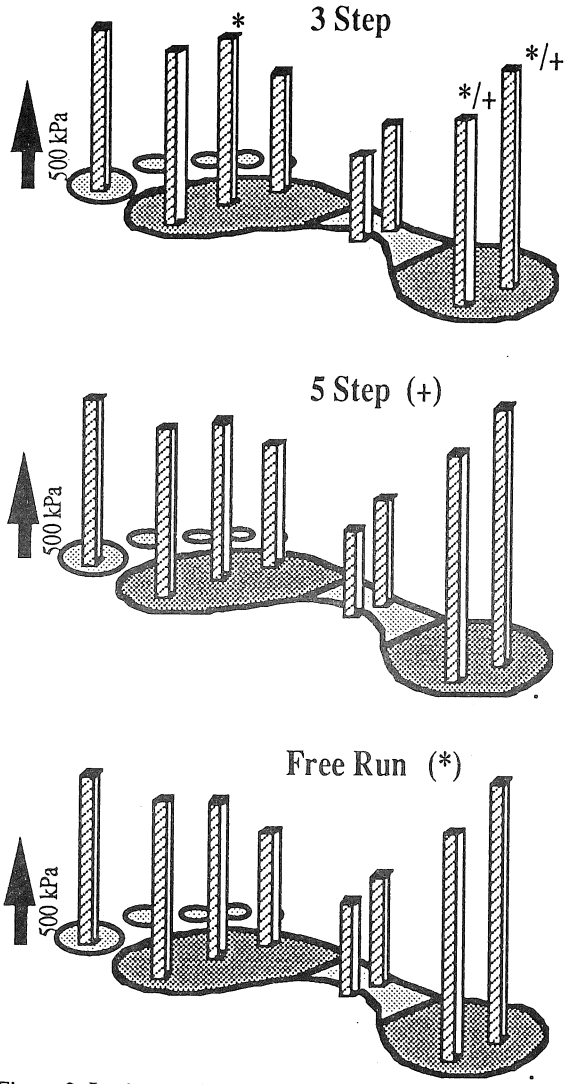

Figure 2: In-shoe peak pressures under the foot for three run-up conditions (*/+ $p<0.05$)

A comparison of the peak pressure distribution of all conditions did not reveal statistical differences in any of the anatomical regions between Free-Run and the 5-Step condition. However, reduced peak pressures were found in the heel region and increased pressures under the 3rd metatarsal head for the 3-Step condition.

DISCUSSION

In the 3-Step conditions the smaller first vertical force peak as well as the lower heel pressures indicate a reduced heel impact. For the 3-Step run-up only a short distance is available, to accelerate the body towards the target velocity of 3.83 m/s. Therefore, it is likely that during contact with the force platform still an overall increase of body velocity takes place. As a consequence, reduced deceleration of the body with lower heel pressures at impact may be present. Similarly, the increased horizontal force PHF during take-off is a probable cause for the increased acceleration to achieve a higher velocity. The second vertical force peak, the vertical force integral and the contact time do not reflect the different behavior at ground contact in the 3-Step condition. The lack of significant differences between the 5-Step and Free-Run conditions in any of the force and pressure parameters suggests that a 5-Step run-up is sufficient for the impact representation of a Free-Run situation. The significantly reduced coefficient of variability for PVF1 in the 5-Step situation suggests that it may even be more advantageous to use a shorter running distance. The lower intraindividual variability is probably a consequence of the small force platform target area on which the subjects are required to land. In a Free-Run situation more adjustments during running may be necessary to achieve the same hitting accuracy as for run-ups with shorter distances. The higher variability in the 3-Step condition is likely to be caused by the necessary acceleration on the platform, to achieve the required target velocity. In this case no steady state velocity has yet been established, thus resulting in increased impact variabilities.

REFERENCES

Cavanagh et al. *J. of Biomechanics*, 13, 397-406, 1980.
Hennig, E.M. et al. J. of Biomed. Eng., 4, 213-222, 1982.
Hennig, E. M. et al. Proc. of the 6th Biennial Conference of the Canadian Society for Biomechanics - Human Locomotion VI, Quebec, Canada, 105-106, 1990.
Nigg, B. M. et al. Biomechanics of Running Shoes, Ed. B. M. Nigg, Human Kinetics, Champaign , 139-160, 1986.

TECHNIQUES USED BY ELITE GYMNASTS IN PERFORMING THE COMPULSORY PARALLEL BAR MOUNT FOR THE 1992 OLYMPIC GAMES

Y. Takei, H. Nohara*, and M. Kamimura*

Department of Physical Education, Northern Illinois University, DeKalb, IL USA
*Department of Physical Education, Kyoto University of Education, Kyoto, Japan

INTRODUCTION

The basket to handstand mount on the parallel bars (Figure 1), a "common denominator" skill that provides an array of carry-over elements for advanced variations and combinations as well as safety, has been chosen as a required skill in compulsory competition during the 1989-1992 Olympic quadrennium. Mastering the skill, therefore, prepares the gymnast not only for the compulsory competition but also for learning more complex mounts and sequences with greater efficiency and safety. Although several authors have studied this maneuver, (Boon, 1977; Grossfeld, 1962; Lascari, 1971; Plagenhoff, 1969), their reports were written long before significant technical advances took place in recent years. There has been no study to analyze the skill under intensely competitive situations involving a large number of elite gymnasts. Furthermore, there is little information concerning the form or body control, an important factor in determining the overall outcome of performance. The purpose of the study was therefore to identify the mechanical factors that are crucial to successful performance, including the aspect of form or body control, of the basket to handstand mount on the parallel bars.

PROCEDURES

Subjects were 25 American and 28 Japanese gymnasts who were competing in their respective 1990 national championships. A 16-mm Locam II DC camera operating at 100 Hz was used to record the performances. All 53 mounts (one per subject) were used in subsequent analysis. The average of the 4 middle scores awarded by 6 judges with international certification was used to arrive at the final score for each mount. The method described by Hay & Reid (1988) was used to develop a deterministic model to identify the mechanical variables that determine the linear and angular motions as well as the aspect of body control or form of the basket to handstand mount. A projection head and a digitizer linked on-line to a microcomputer were used to analyze the films. The x- and y-coordinates of 21 points, defining a 14-segment model of the human body (Clauser et al., 1969), were recorded for each frame analyzed. The data were then smoothed (Hay & Nohara, 1990), the location of the body CG was determined (Clauser et al., 1969), after which the angular momentum was computed (Hay et al., 1977; Whitsett, 1963), and the values for other variables identified in the model were determined. Correlations were obtained between each variable and the judges' score. A value of $p<.05$ was chosen to indicate statistical significance. Use of the Bonferroni procedure (Wilkinson, 1988) to control the potential increase in Type I error rate as a result of performing the serial tests indicated that $r>.43$ ($p<.05/50 = .001$) was required to achieve statistical significance in the correlations. This also meant that 18.5% of the variation in the judges' score could be accounted for by a variable that had a correlation coefficient of .43. It is therefore evident that $r = .43$ ($p = .001$) is both statistically and practically significant.

RESULTS AND DISCUSSION

Significant correlations indicated that (a) large vertical displacement of CG (D_y) from body compression to bar release, (b) large backward horizontal velocity (V_x) at bar release, (c) large backward horizontal displacement of CG (D_x) in flight, (d) large forward angular displacement (AngD) of body rotation, angular velocity (AngV), and angular momentum (H) in flight, (e) large elbow and shoulder angles, large normalized moment of inertia (I), and great height of CG at bar regrasp, (f) large backward D_x and V_x of CG from the bar regrasp to handstand, (g) small D_y of CG and time of support from bar regrasp to handstand, and (h) large normalized I at handstand are important determinants in achieving successful results (Table 1). The conclusions were that focus should therefore be made to achieve (a) a large upward vertical distance of CG from body compression to bar release by forcibly extending the hips and simultaneously exerting an arm pull of long duration till the shoulders are above the bars, (b) the backward D_x of CG and simultaneous forward rotation of the body toward the handstand position while in the air, (c) the great height of CG with large elbow and shoulder angles and full body extension at bar regrasp, (d) the steady backward horizontal motion of CG and simultaneous forward body rotation during the regrasp to handstand, and (e) the fully extended handstand position for successful performance of the basket to handstand mount on the parallel bars.

REFERENCES

Boon, T. Sports Medicine & Physical Fitness, 17, 25-32, 1977.
Clauser, C. et al. AMRL Technical Report, 69-70, 1969.
Hay, J. et al. Anatomy Mechanics & Human Motion (pp 291-301) Prentice-Hall, 1988
Hay, J. et al. J. Biomechanics, 23. 229-239, 1990.
Hay, J. et al. J. Biomechanics, 10, 269-277, 1977.
Lascari, A. Modern Gymnast, 13, 20-21, 1971.
Plagenhoff, S. Modern Gymnast, 11, 19, 1969.
Whitsett, C. AMRL Technical Report, 63-18, 1963.
Wilkinson, L. SYSTAT: The System for Statistics, (pp. 490-491), SYSTAT, Inc., 1988.

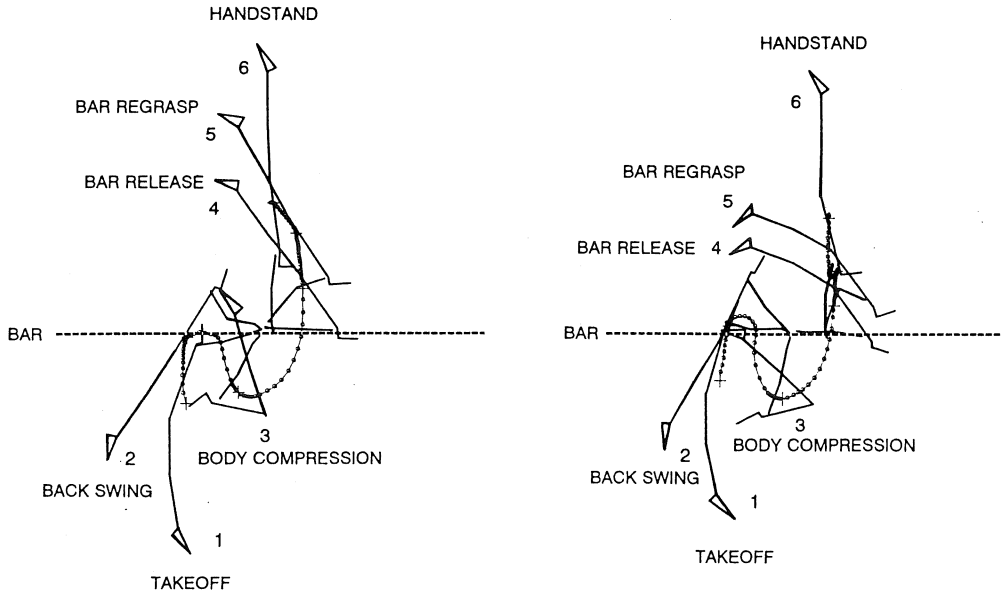

Figure 1. Illustration of highest (9.90, left) and lowest (7.13, right) scored basket to handstand mounts.

Table 1. Descriptive Statistics and r Values With the Judges' Score for the Variables in the Basket to Handstand Mount

VARIABLE	M	SD	MIN	MAX	r
D_y Body Comp. to Bar Release, m	.77	.11	.50	1.05	.43***
V_x at Bar Release, m/s	.00	.33	-.67	.62	-.53***
D_x of Flight, m	.00	.07	-.13	.14	-.54***
AngD of Flight, deg	-2	6	-12	16	-.50***
AngV of Flight, deg/s	-8	28	-58	79	-.47***
H of Flight, kgm^2/s	-1.27	4.59	-9.96	13.03	-.48***
Elbow Angle, Bar Regrasp, deg	112	26	51	170	.59***
Shoulder Angle, Bar Regrasp, deg	67	25	7	117	.45***
Normalized I, Bar Regrasp	.056	.004	.044	.067	.46***
CG Height, Bar Regrasp, m	.63	.10	37	.84	.54***
D_x, Bar Regrasp to Handstand, m	-.07	.09	-.23	.15	-.45***
D_y, Bar Regrasp to Handstand, m	.22	.10	-.01	.49	-.44***
V_x, Bar Regrasp to Handstand, m/s	-.14	.18	-.51	.29	-.46***
Time, Bar Regrasp to Handstand, s	.55	.26	.14	1.34	-.57***
Normalized I, Handstand	.062	.003	.055	.072	.50***

***$p \leq .001$

AN ANALYSIS OF THE BERNOULLI LIFT EFFECT AS A PROPULSIVE COMPONENT OF SWIMMING STROKES

M. Ferrell, J. L. Hendrick* and P. McGinnis*

Department of Health and Physical Education, Syracuse University

*Department of Physical Education, State University of New York at Cortland

INTRODUCTION

Hydrodynamic lift forces as defined by the Bernoulli Principle were introduced in 1970 (Counsilman, 1970) as a means of scientifically identifying the propulsion derived from the observed lateral phases of hand patterns during swimming strokes. Since then, the Bernoulli Lift Effect has become widely accepted as a major contributing component of swimming propulsion (Barthels, 1979; Hay, 1988; Kreighbaum & Barthels, 1990; Maglischo, 1982; Schleihauf, 1979). Upon examination of the Bernoulli Principle, it was found that laminar flow is necessary in order for an airfoil to generate lift forces (Fillingham, 1975; Morgan, 1964; Ross,1973; Tietjens, 1934). The slow-motion and stop-action capabilities of videotape were used in evaluating the data with respect to the proportion of turbulence observed over the back of the small, medium, and large hand models as they were drawn through the water at five different angles of attack from 0 to 40 degrees, and at three speeds ranging from slow to moderate to fast. The observed predominance of turbulent flow suggests that sufficient laminar flow does not exist to support the Bernoulli Lift theory as a propulsive component in swimming strokes.

REVIEW AND THEORY

It is currently reported in most of the literature that two theories combine to identify the scientific rationale for upper body propulsion in swimming - propulsive drag and propulsive lift. According to Hay (1988), the drag theory was the first to be widely accepted by the swimming community. In adherence to this principle, swimmers were taught to maximize effort by pushing the water backwards, in as straight a line as structurally possible, while minimizing any movements that were directed upward, downward, or to the side (ARC, 1968; Counsilman, 1968).

Careful observation and cinematographic analysis of world-class swimmers revealed consistent hand patterns which deviated considerably from the straight line path envisioned by coaches and swimmers (Barthels & Adrian, 1975; Barthels, 1977,1979; Counsilman, 1970; Maglischo et.al., 1989; Schleihauf, 1976). The lateral movements which many coaches considered to be a stroke defect were reviewed from another perspective as Counsilman (1970) attributed the Bernoulli Lift Principle to those observed motions. He suggested that the hand be considered as an airfoil, thereby generating lift on the back of the hand as the hand moves laterally through the water. This concept has become commonly known as the propulsive lift effect and as such, has since become widely accepted by the swimming community as a major propulsive contribution to the movement of the body through the water (Clarys, 1979; Hay, 1988).

Numerous subsequent observations and quite a few research studies have expounded on the relative contribution of the Bernoulli Lift Effect to swimming propulsion (Hay, 1988). Hand motion patterns have been analyzed from the camera perspective of still water (Barthels & Adrian, 1975; Barthels, 1977,1979; Maglischo, 1982; Maglischo et. al.,1989). Results of these observations show the body being propelled with, in some instances, very little backward movement of the hand. Background grids (Maglischo, 1982) show entry and exit positions relative to a fixed point where the hand stays relatively anchored as the body passes over that position. Schleihauf (1976, 1979, 1983, 1988) has conducted and collaborated in many studies analyzing propulsive forces in swimming. In one study, Schleihauf (1979) used castings of hands in a flume in order to quantify the forces at various angles of attack. He suggested that propulsive lift is most effective at an angle of attack of approximately 40 degrees.

In order to accept the possibility of a Bernoulli propulsive lift force as a component of swimming propulsion, one must define the flow characteristics about the hand as an airfoil. The components of shape and angle of attack are critical to the development of lift (Ross, 1973). The Bernoulli principle regarding the lift of an airfoil is not applicable without laminar flow in contact with the lifting surface of the airfoil (Morgan, 1964; Tietjens, 1934; Ross, 1973). Therefore, the existence of laminar flow about the hand must be the primary prerequisite in order to verify the Propulsive Lift Theory as it relates to the Bernoulli Principle. A review of the literature found no studies designed to observe or identify flow characteristics over the back of the hand as it moved through the water. It was hypothesized that the rough contour of the hand is likely to produce boundary layer separation at any angle of attack and flow velocity, severely reducing the lift coefficient.

The attachment of lightweight lengths of material, tufts, to the surface of working sails has been a long established practice of sailors in order to visualize the effects of air flow about their sails (Ross, 1973). Hay and Thayer (1989) incorporated this concept by attaching tufts to the bodies of swimmers in order to visualize water flow characteristics as the swimmers moved through the water. The purpose of this study was to observe the flow characteristics over the back of hand models by means of the distinctive activity of sensitive tufts attached to the hand models as they were drawn through the water.

PROCEDURES

Three fiberglass resin hand models representing the small, medium, and large hands of an intercollegiate swimming team were drawn through the water by the use of a specifically constructed apparatus (Fig. 1). Numerous small, brightly contrasting tufts of yellow latex were attached to the back of the hand models in order to visualize flow characteristics.

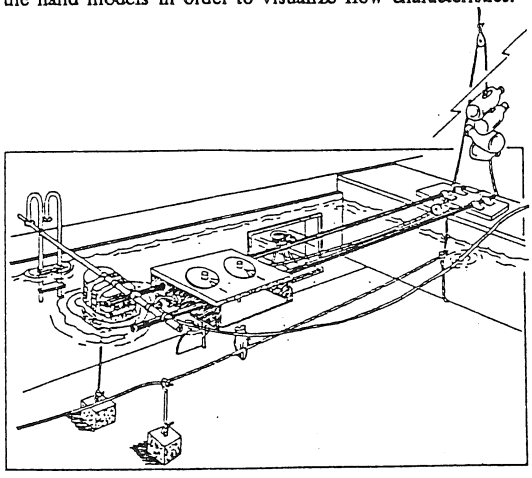

Figure 1. Experimental Apparatus

Each hand model's angle of attack was controlled at 10 degree intervals between 0 and 40 degrees. At each of the different angles of attack, three observations were completed approximating the slow (0.3-0.7 m/s), moderate (1.0-1.5 m/s), and fast (2.0-3.0 m/s) velocities experienced by accomplished competitive swimmers (Pepin, 1983; Schleihauf, et.al., 1988). Each trial was recorded on videotape through an underwater window within the controlled environment of a large volume, indoor swimming facility.

A subjective quantitative analysis of the video data representing the percentage of observed turbulent flow was compiled and used to compare the flow characteristics for the different hand sizes, relative velocities, and angles of attack. A second, independent evaluation was completed following a ten day interval. A rater reliability coefficient of 0.95 was calculated from an Analysis of Variance with repeated measures from the test-retest evaluation of the video data.

RESULTS AND DISCUSSION

The purpose of this study was not to contest the statistical results of previous research, but rather to examine the conclusions that the Bernoulli Principle can be considered a contributing component to the observed forces during the lateral phases of swimming hand patterns. Observation of the videotaped trials revealed some predictable patterns of flow characteristics with regard to the angle of attack and relative hand velocity. The amount of turbulent flow tends to increase with an increase in either the angle of attack (Fig. 2) or the hand velocity. These observations were consistent without

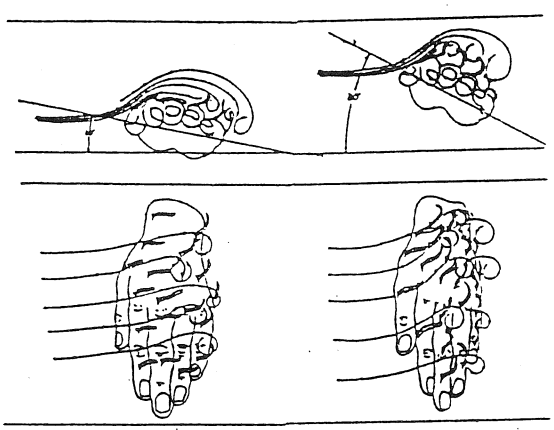

Figure 2. Artistic Enhancement of Water Flow at 10 Degrees and 30 Degrees

respect to hand size variations. Both at higher angles of attack and at higher velocities, the observed flow over the back of the hand was almost entirely turbulent . Even at the smallest angle of attack and the slowest velocity tested, considerable turbulent flow was observed over the back of the hand (Fig. 3).

Due to overwhelming predominance of turbulence, and consequent lack of laminar flow, it appears unlikely that any lift force attributable to the Bernoulli Principle contributes to swimming propulsion. Therefore, the forces generated during the observed lateral arm activity must be based on some other physical principle of motion.

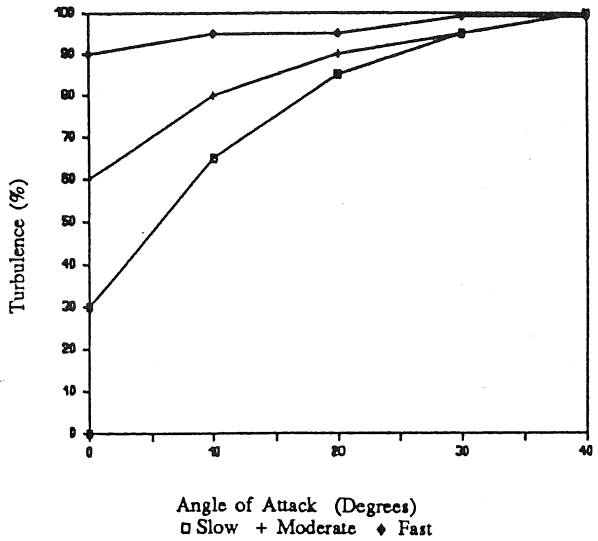

Figure 3. Percent of Turbulence for the Small Hand With Respect to the Five Angles of Attack and Three Hand Velocities

REFERENCES

ARC, *Swimming and Water Safety*, 1968.

Barthels, K. *Swimming III*,(pp.45-54), Terauds and Bedingfield, 1979.

Barthels, K. *Swimming Technique*, 14, 66-70, 1977.

Barthels, K. et al. *Swimming II*,(pp.154-160), Lewillie and Clarys, 1975.

Clarys, J. *Swimming Medicine IV*,(pp.386-394), Erikson and Furberg, 1978.

Clarys, J. *Swimming III*,(pp.3-41), Terauds and Beddingfield, 1979.

Counsilman, J. *First International Symposium on Biomechanics of Swimming*,(pp.59-71), Lewillie and Clarys, 1970.

Counsilman, J. *The Science of Swimming*, 1968.

Fillingham, P. *Basic Guide to Flying*, 1975.

Hay, J. *Swimming Science V*,(pp.3-14), Wilke and Reischle, 1988.

Hay, J. et al. *J. of Biomechanics*, 22, 11-19, 1989.

Kreighbaum, E. et al., *Biomechanics*, 1990.

Maglischo, E. et al., *SOMA: Engineering for the Human Body*, 2, 40-44, 1989.

Maglischo, E. *Swimming Faster*, 1982.

Morgan, J. *Introduction to University Physics*, 1964.

Pepin, R. et al., *The Aquaforum Technical Series* (Videotape), 1983.

Ross, W. *Sail Power*, 1973.

Schleihauf, R. *Swimming Technique*, 12, 100-105, 1976.

Schleihauf, R. *Swimming III*,(pp.70-109), Terauds and Bedingfield, 1979.

Schleihauf, R. et al., *Biomechanics and Medicine in Swimming*,(pp.173-183), Hollander, P. et al., 1983.

Schleihauf, R. et al., *Swimming Science V*,(pp.53-59), Ungerechts, B. et al., 1988.

Tietjens, O. *Applied Hydro- and Aerodynamics*, 1934.

THE TRAJECTORY OF THE SPIKED VOLLEYBALL

S. Kao[α], R. Sellens[β], and J. Stevenson[α]

School of Physical and Health Education[α]
Department of Mechanical Engineering[β]
Queen's University, Kingston, Ontario, Canada K7L 3N6

INTRODUCTION

Since volleyballs are spiked with top spin, the Magnus effect must be taken into account when their trajectories are considered. A wind tunnel test was conducted and the functional relation between the Magnus force M and the angular velocity ω, linear velocity V in case of the spiked volleyball was found. As drag and force of gravity of the spiked volleyball were known, the differential equations of the trajectory were established. By using the Runge-Kutta method, a computer program was written and the equations were solved numerically.

REVIEW AND THEORY

Some experimental studies of spinning spheres have been found in the literature. Almost all of these experiments were conducted to measure the effect of Magnus force and drag on the shape of the sphere's trajectory in many ball games such as tennis, baseball, and golf. Some of papers reported that the Magnus force was proportional to the product of the square of the wind tunnel speed V and the spin rate of the ball ω. But, there is another curious aspect of these results. According to the Kutta-Zhukovskii theorem, it seems reasonable that the Magnus force on a spinning sphere would also depend on ωV rather than on ωV^2. Watts *et al.* (1986) However, these experimental results and theories may not directly apply to volleyball trajectory study, because the size, velocity, spin rate, and the characteristics of the surface of the volleyball are completely different from those balls they studied.

Assuming that the Magnus force and drag respectively are

$$M = C_M\omega^a V^b \quad (1)$$

$$D = 1/2\, C_D\rho S V^2 , \quad (2)$$

(C_M, a, and b to be determined)

we have the following theory. The three forces acting on the ball are shown in Fig 1 and the sums of the their vertical and horizontal components are

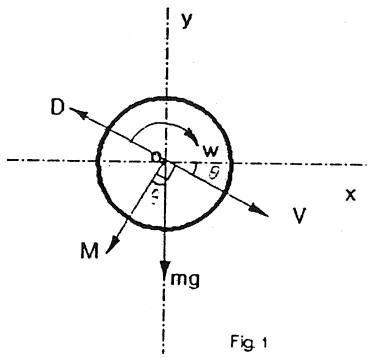

Fig. 1

$$F_x = -C_M\omega^a V^b\sin\theta - 0.5C_D\rho S V^2\cos\theta \quad (3)$$

$$F_y = -mg - C_M\omega^a V^b\cos\theta + 0.5C_D\rho S V^2\sin\theta \quad (4)$$

If the displacement of the spiked volleyball is expressed by the parametric equations

$$X = X(t) \quad (5)$$

$$Y = Y(t) , \quad (6)$$

then we have

$$X' = V\cos\theta \quad (7)$$

$$Y' = -V\sin\theta \quad (8)$$

and

$$V = \sqrt{(X'^2 + Y'^2)}. \quad (9)$$

Therefore, equation 3 & 4 can be substituted by equation 7, 8, & 9 into the derivative expressions. According to Newton's Second Law, the differential equation of the trajectory is eventually obtained as:

$$C_M\omega^a Y'(\sqrt{(X'^2+Y'^2)})^{b-1}/m - 0.5C_D\rho S X'\sqrt{(X'^2+Y'^2)}/m = X'' \quad (10)$$

$$-g - C_M\omega^a X'(\sqrt{(X'^2+Y'^2)})^{b-1}/m - 0.5C_D\rho S Y'\sqrt{(X'^2+Y'^2)}/m = Y'' \quad (11)$$

PROCEDURE

A balancing device for mounting a spinning volleyball in a wind tunnel is shown in Fig. 2, A. Once the motor and the tunnel are turned on, M is able to be detected at point P, which is the same distance as the ball, by loading and unloading weights to keep the whole system in balance.

The motor was started at a given spin rate and a given weight was put at point P. The air flow in the

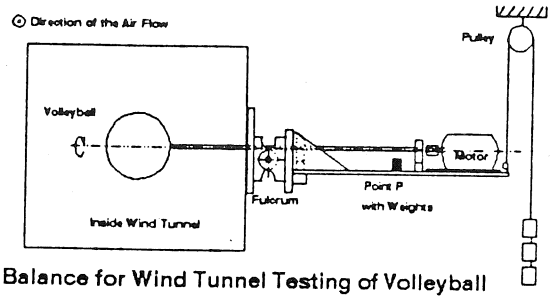

Balance for Wind Tunnel Testing of Volleyball

Fig. 2, A

The Results of Wind Tunnel Test

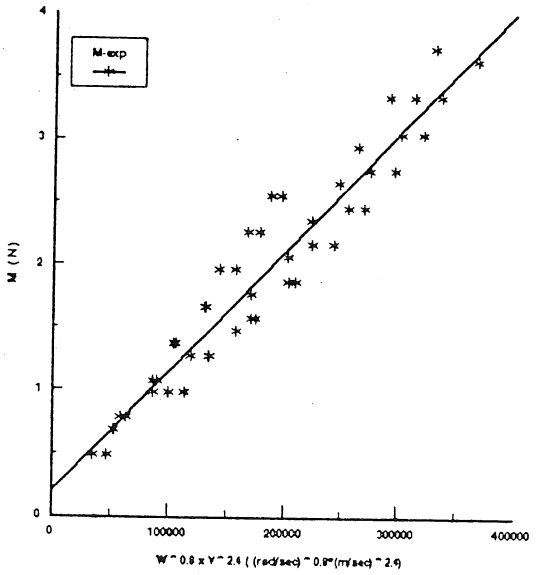

Fig. 2, B

tunnel was increased until the whole system returned to balance again. By recording the readings of the wind tunnel speedometer and the strobe-light tachometer, and the weight, the data for one point was obtained. The weights and rate of spin were changed and more points were obtained.

Data for spin rates between 200 & 400 rpm and flow velocities between 15 and 35 m/sec were obtained. Values of C_M, a, and b were found by minimizing the RMS error in the Magnus force predicted by equation 1.

RESULTS AND DISCUSSION

The functional equation for Magnus force in case of the spiked volleyball was determined

$$M = 0.000041\ \omega^{0.8} V^{2.4} \qquad (12)$$

(M: Newton, ω: rad/sec, V: m/sec)

Fig. 2, B is the plotted results of the wind tunnel test.

The differential equations of the spiked volleyball, therefore, are

$$0.000041\omega^{0.8}Y'(\sqrt{(X'^2+Y'^2)})^{1.4}/m - 0.5C_D\rho SX'\sqrt{(X'^2+Y'^2)}/m = X'' \qquad (13)$$

$$-g-0.000041\omega^{0.8}X'(\sqrt{(X'^2+Y'^2)})^{1.4}/m - 0.5C_D\rho SY'\sqrt{(X'^2+Y'^2)}/m = Y''. \qquad (14)$$

The Runge-Kutta numerical method was used to solve the equations with the initial values shown in Fig. 3, A. Fig. 3, B is the trajectories of the spiked volleyball with various rate of spin.

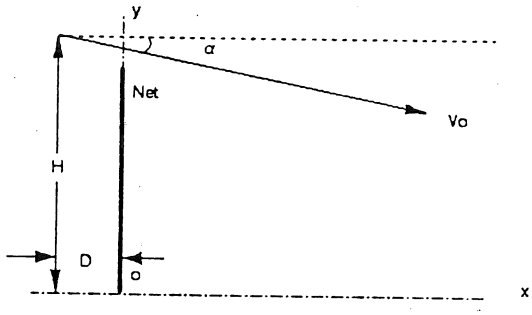

Fig. 3, A

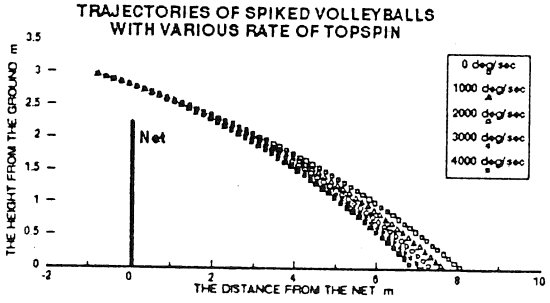

Fig. 3, B

3-D equations have been developed by the same approach. With these equations, the location of the ball in 3-D dimensions may be predicted. A program may be written based on the equations, telling the spikers where and at what angle to hit the ball, such that the possibility of being blocked is the least while the ball still lands within the boundaries. More studies are needed for further applications.

REFERENCE

1. Erlichson, Am. J. Phys. 51, 1983. pp357-363
2. Frohlich, Am. J. Phys. 52, 1984. pp325-334
3. McPhee *et al.* Am. J. Phys. 56,1988, pp933-939
4. Rex, Am. J. Phys. 53, 1985, pp1073-1075
5. Watts *et al.* Am. J. Phys. 55, 1987, pp40-44

MUSCLE MODELLING

Podium Session 8

MODELLING SKELETAL MUSCLE USING A LINEAR, TIME-VARYING MODEL

Jacques Bobet[1] and Richard B. Stein[2]
[1]Department of Physical Education and Sport Studies and [2]Division of Neuroscience, University of Alberta, Edmonton, Alberta, CANADA T6G 2H9.

INTRODUCTION

Most models currently used for the prediction of muscle force are based on the approach used by A.V. Hill. This approach has a number of weaknesses. One is that the resulting models are complex, typically requiring the solution of several simultaneous, non-linear differential equations. A second is that they typically possess a large number of "parameters" (i.e. muscle-specific constants) whose values must be determined before a quantitative prediction is possible. Finally, these models, at least in the past, have been incapable of accomodating any changes in the muscle dynamics such as might occur in fatigue or with potentiation or training. These weaknesses have been most evident when muscle models are incorporated in control systems for functional electrical stimulation (FES). At present, these systems use only a very crude representation of the muscle dynamics (e.g. Crago et al., 1991), since existing muscle models are too nonlinear and too computationally intensive for use in a real-time controller.

In this paper, we present an alternative approach, which considers the muscle as a simple linear system whose parameters vary with time. This approach is computationally simple, can easily accomodate changes due to fatigue or training, and can be implemented in "real-time." Moreover, it provides good fits to muscle force data across a broad range of contraction conditions.

THEORY

Conceptually, the approach used here is to consider the muscle as a system which produces a twitchlike force (a "twitch contribution") in response to each stimulating pulse. The time course of force produced is thus considered as the temporal summation of these contributions. The shape of the contribution is not constant, however, but can vary with time. In the model, the basic twitch contribution shape is obtained from the equation describing a linear, critically-damped second-order system:

$$d^2F/dt^2 + 2\omega\, dF/dt + \omega^2 F = A\omega^2 U$$

where F is a time-varying force (N), ω is the natural frequency (rad/s), A is the low-frequency gain (Mannard and Stein, 1973), and U is the time varying input to the muscle (in this case, a stimulus pulse delivered to the nerve). One set of values of A and ω is assumed to hold for the response to the first pulse in a train (i.e. for the first interpulse interval, the period between the first pulse and the second); a second set is then assumed to hold for the response to the second pulse (the second interpulse interval), and so on.

METHODS

The model was tested with data from a slow (soleus) and fast (plantaris) muscle in the cat. Muscles were stimulated via the nerve and their force recorded. All contractions were isometric, except for one data set in soleus where the muscle was allowed to shorten Pulse trains applied to the nerve contained a mixture of interpulse intervals, in order to cover the entire operating range from a single twitch to a fused tetanus. In the fast muscle, potentiated and fatigued trials were collected, as well as rested ones.

The best fitting values of A and ω for each interpulse interval were obtained using a nonlinear curve-fitting algorithm (Stein et al., 1988). A pure delay was also included in the model to account for the delay between stimulation and the onset of force production.

RESULTS

The model produced very good agreement over all of the data sets tested. A typical result is shown in Figure 1. Other than a small discrepancy around the time of occurrence of each pulse, the predicted and observed traces are virtually overlaid for the entire trial. Gain and natural frequency varied smoothly throughout the trial. As force rose, low-frequency gain fell and natural frequency rose.

Fits were equally good in fast muscle (not shown). Both natural frequency and gain were higher for the fast muscle. In potentiation, gain rose while natural frequency fell, indicating a stronger, slower twitch. In fatigue, both gain and natural frequency decreased, indicating a weaker, slower twitch. Gain and natural frequency varied smoothly in all trials.

To examine whether the model would also hold for non-isometric contractions, one soleus muscle was attached to a servo-motor which simulated an elastic load. This allowed changes in muscle length and velocity as the contraction progressed, although only relatively stiff springs could be simulated. The model still provided very good fits throughout, although there was more variation in A and ω.

In order to determine if the model was fast enough to be used in a practical, "real-time" FES controller, the fitting algorithm was timed in one data set. On a 33-MHz 486-based machine, with the data on disk, the entire 4-second trial in Fig. 1 (about 60 interpulse intervals) was fitted in 1.7 seconds (i.e. about 30 ms per interval). The algorithm can thus "keep up" with a stimulation rate of about 33 Hz, a rate which presumably would be fast enough for applications involving human muscle.

DISCUSSION

This approach could potentially be used to provide a model of the muscle (the "plant") in FES control systems. It is simple and linear, which facilitates control. The algorithm and model are sufficiently fast to be used in real time applications. The model can be used for both slow and fast muscle. It may apply to both isometic and nonisometric contractions, although the data here are limited. Also, it is robust enough to accomodate changes that might occur with fatigue in these patients, or longer-term adaptations to training.

The model may also provide an alternative to high-order, nonlinear models for predicting muscle force during movement. It is simple and linear, and applies across a broad range of contraction conditions. It appears that the gain and natural frequency could be predictable from a knowledge of the stimulation rate, or of the current force, such that the model could be used for a true "prediction" rather than a curve fit. Preliminary dynamic data indicate that the model may also hold when length and velocity are varying. If so, this approach of modelling muscle as a simple time-varying system may lead to models of muscle that are both simpler and more broadly valid than those currently in use. More research is needed to verify this suggestion.

Supported by NSERC (JB) and MRC (RBS).

REFERENCES

Crago, P. et al., IEEE trans BME 38:17-28, 1991.
Mannard, A. and Stein, RB J. Physiol 229:275-296, 1973.
Stein, R.B. et al., Biophys J, 54:705-717, 1988.

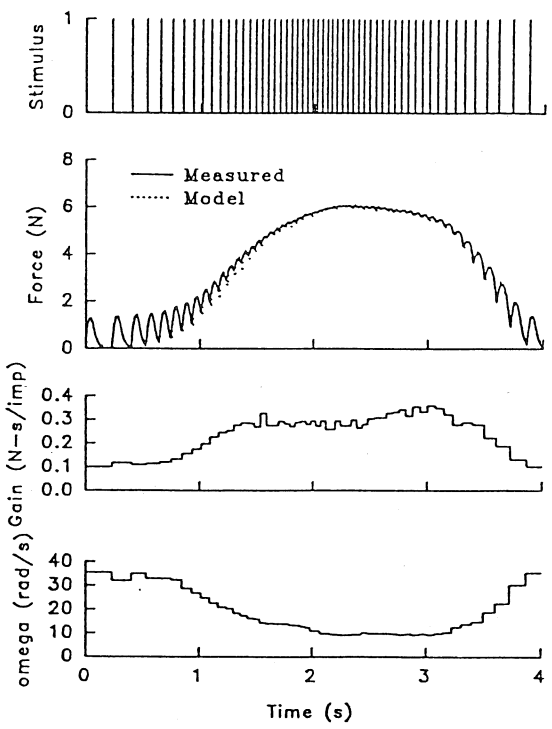

Figure 1: Stimulus, predicted and measured forces, and parameters for rested isometric contraction in the soleus. Predicted force (dashed line) and measured force (solid line) are almost identical over most of the trial.

Proceedings of NACOB II, The Second North American Congress on Biomechanics, Chicago, August 24th - 28th, 1992

EMG-FORCE RELATION OF MAMMALIAN SKELETAL MUSCLE (PART I): RATE MODULATION OF A VENTRAL ROOT FILAMENT CONTAINING SEVERAL MOTOR UNITS

A. Guimaraes, W. Herzog, Y. Zhang *, M. Hulliger +, S. Day +

Faculty of Physical Education
*** Department of Electrical and Computer Engineering**
+ Department of Clinical Neurosciences
The University of Calgary, AB, Canada, T2N 1N4

INTRODUCTION

The relation between the electromyogram (EMG) and force remains controversial. Some experimental evidence indicates that this relation is linear for isometric contractions (e.g. Lippold, 1952) whereas others report that it is not and that EMG increases at a faster rate than force (e.g. Vrendenbregt and Rau, 1973). In addition to these experimental findings, some theoretical models predict that force should increase at a faster rate than EMG (e.g. Person and Libkind, 1970).

It is generally accepted that during non-ballistic contractions, a muscle can increase its force by recruiting additional motor units according to the size principle (Henneman et al. 1965) and by increasing the firing rate of recruited motor units (rate modulation). Thus if one wants to understand the mechanisms underlying the EMG-force relationship, it is necessary to understand the relation between EMG and force (a) for increasing firing rates of a given motor unit (i.e. rate modulation) and (b) for increasing the number of active motor units (i.e. recruitment).

The purpose of this study was to quantify the relation between EMG and force for systematic rate modulation of a ventral root filament containing alpha motor neurons of several motor units of a cat soleus muscle.

REVIEW AND THEORY

Previous investigations typically studied the relation between EMG and force of voluntary contractions using indirect measures of muscular force (e.g. Komi and Viitasalo, 1976). In order to gain a more direct insight into the relation between EMG and force, we believe it is necessary to use methods incorporating direct force and EMG measurments from a single muscle, under conditions where the excitation to the muscle is precisely known, repeatable and physiologic.

PROCEDURES

A male cat was anesthetized and laminectomy was performed to expose the ventral roots of L7 and S1 containing the alpha motor neurons of the soleus muscle. The ventral roots were divided into ten filaments that produced similar tetanic force. Each filament contained axons of several soleus alpha motor neurons but no attempts were made to quantify the precise number of alpha axons. Each filament was in contact with an independent stimulating electrode. The pelvis and left hindlimb were rigidly fixed to a frame. The soleus muscle was exposed. The distal tendon was detached along with part of the calcaneus and tied to the arm of an electromagnetic motor which was instrumented with a force transducer. EMG was recorded using indwelling (wire) and surface electrodes, both in a bipolar configuration. Surface electrodes were sutured directly on the epimysium of the soleus muscle. Blood pressure and body temperature were continuously monitored throughout surgery and data collection. Exposed areas on the back and hindlimb were submerged in a parafin bath that was kept at body temperature.

Ventral root filaments were stimulated in various combinations, using independent stimulation for eight of the ten filaments. Irregular interpulse intervals with a coefficient of variation of 12.5 % were introduced in the stimulation trains. For results reported in this study, single filaments were stimulated at nominal mean rates ranging from 5 to 50 pulses per second (pps) at intervals of 5 pps. Independent constant voltage stimulators were used to stimulate each filament at an intensity approximately twice as high as threshold. Stimulation started 2 to 3 seconds prior to data acquisition to permit recordings under steady state conditions. All experiments were performed under isometric conditions with the soleus muscle at a length corresponding to a 75 degrees ankle joint angle.

EMG and force signals were digitized at 2100 and 350 samples per second, respectively, using an LSI computer and custom built interface boards. EMG signals were quantified by integrating the area under the full wave rectified signal (IEMG) and force values presented here are mean values of the force-time curves calculated over a period of 2 seconds.

RESULTS AND DISCUSSION

IEMG of the the soleus muscle was linearly related to stimulation frequencies applied to a multi-unit ventral root filament (Figure 1). The shape, amplitude and duration of the compound action potentials elicited with each stimulation pulse were approximatelly constant for all stimulation rates, therefore, producing a direct proportional relation between IEMG and frequency of stimulation. The results shown in Figure 1 were obtained using indwelling electrodes, and they are also representative of the results obtained using surface electrodes.

Mean force was non-linearly related to stimulation rate (Figure 2). At frequencies below about 25 pps, mean force increased continuously with increasing frequency of stimulation. At frequencies exceeding about 25 pps, soleus forces increased slowly and tended to become saturated.

Figure 3 shows the curvilinear relation between IEMG and mean force for rate modulation of a single ventral root filament of the cat soleus muscle containing several motor units. This figure may be directly derived from Figures 1 and 2. The general results shown in Figures 1 to 3 were confirmed by results obtained from another filament from the same animal. Based on these results, and assuming that all motor units of a muscle (i.e. cat soleus) show a similar relation between IEMG and mean force as that shown in Figure 3, one would predict that the IEMG-mean force relation over a wide range of stimulation rates for an entire muscle cannot be linear, except possibly for mean rates of stimulation below approximately 25 pps. The relation between IEMG and mean force for the entire cat soleus muscle will be discussed elsewhere.

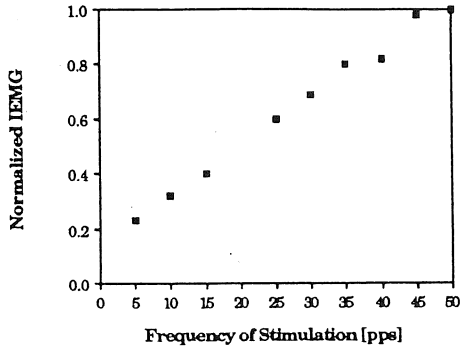

Figure 1. Normalized IEMG response of a cat soleus muscle to a range of stimulation frequencies of a ventral root filament at L7/S1 containing several motor units.

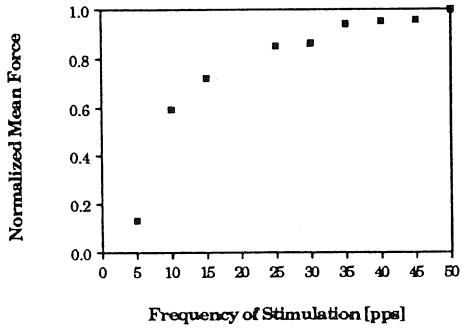

Figure 2. Normalized mean force response of a cat soleus muscle to a range of stimulation frequencies of a ventral root filament at L7/S1 containing several motor units.

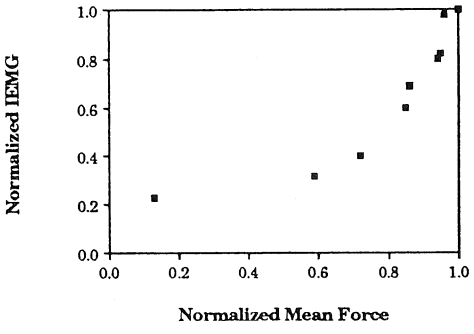

Figure 3. Normalized IEMG-force relation of a cat soleus muscle as a function of rate modulation of a ventral root filament at L7/S1 containing several motor units.

REFERENCES

Person, R.S. and M.S. Libkind. Electroenceph. Clin. Neurophysiol., 28:625-632, 1970.
Henneman, E. et al. J. Neurophysiol., 28:599-620, 1965.
Komi, P.V. and J.H.T. Viitasalo. Acta Physiol. Scand., 96:267-276, 1976.
Lippold, O.C.J. J. Physiol., 117:492-499, 1952.
Vrendenbregt, J. and G. Rau. New Developments in Electromyography and Clinical Neurophysiology, J.E. Desmedt, Karger, Basel, vol. I,(pp.607-622), 1973.

ACKNOWLEDGEMENTS

This study was supported by AHFMR, MRC and NSERC (Canada). A. Guimaraes is supported by CAPES and UFRGS (Brazil).

EMG-FORCE RELATIONSHIP OF ANTERIOR TIBIALIS FOR SURFACE AND INTRAMUSCULAR ELECTRODES

M.E. Wootten, J. Burn, D. Jacobs, M.P. Kadaba
Orthopaedic Engineering and Research Center
Helen Hayes Hospital, W. Haverstraw, N.Y. 10993

Introduction

The relationship of EMG to force has been studied for some muscles under varying conditions. Many studies have shown that the relationship of full wave rectified EMG to force or torque during an isometric contraction is linear or quasi-linear. Other investigators have found a non-linear relationship between EMG and force (1). Woods and Bigland-Ritchie (2) studied factors that could cause the differences in the relationship and found they were due predominantly to physiological and/or anatomical differencs and not due to differences in recording or processing techniques. They concluded that differences in fiber composition within the muscle seems to be the major influence in determining the relationship. This and most studies have been done using surface electrodes, assuming intramuscular electrodes generate too much variability. However in investigating deeper muscles and muscles overlaid by other muscle, it is necessary to use intramuscular electrodes to determine muscle activity. The purpose of this study is to 1. determine the relationship of the Anterior Tibialis to force during isometric contractions; 2. determine if the relationship is consistent across subjects and 3. to determine if the relationship is the same whether one is recording from the surface or from within the muscle.

Methods

Bipolar intramuscular (IM) electrodes (50 μm stainless steel wire with 2mm bared tips) were inserted into the anterior tibialis muscle in the position described by Delagi.(3) Surface electrodes (Iomed Inc.) having 1.2 cm (diameter) stainless steel disks seperated by 2.2 cm were used. The surface electrodes were placed just lateral to this insertion site of the IM electrodes. Intramuscular EMG as well as surface EMG were differential amplified (g=350) with the self-contained electronics of the surface electrodes.

Fourteen normal subjects were investigated. The subjects were seated on a Cybex bench with pelvis and thigh stabilized, hip and knee at 90 degrees. A special unit was built to house a force transducer. The foot was held in placed by straps and the ankle was fixed at 90 degrees during the resisted dorsiflexion. Data from three 100% maximal contraction were acquired first and the average of these contractions was used as the maximum for both the EMG and force data. This level was not the absolute maximum but rather a maximal contraction that could be maintain steadily for 5 seconds. The subject was given seven or eight target force levels between approximately 10% and 90% maximal force. The target force level was set on one channel of an oscilloscope and the feedback from the force transducer was displayed to overlap the targeted force. For each contraction, a steady force level was achieved before data collection commenced. Each trial was for two seconds with rest of approximately 2 minutes between each trial.

EMG signals were filtered 20 to 1000 hz and both emg and force data were acquired at 2400 hz. Emg data were rectified and smoothed with a 64 point moving Hanning window. The average of the rectified smoothed EMG data were used in the analysis. The force data are expressed as a percent of the maximum force level (average of three 100% maximum contractions). The amplitude of data from intramuscular electrodes is roughly twice that of data from the surface electrodes. For this analysis the EMG data were similarly expressed as a percentage of the average maximum data.

Results and Discussion

Figure 1. shows the data from all subjects combined for intramuscular electrodes and for surface electodes. The slope of the regression line for the IM electrodes is 0.99. The 95% confidence interval for the slope is from 0.88 to 1.1. The slope of the surface electrode data is 1.01 (95% CI .94 - 1.13). Coefficient of determination (R^2) for the surface electrode to force data is equal to .80; R^2 for intramuscular electrodes is .75. Data of all subjects combined gives very similar results for surface and intramuscular electrodes indicating that the relationship of EMG to force is similar regardless of the electrode used to detect the activity. Even for intramuscular electrodes 75% of the variance for any subject could be accounted when using this global regression equation.

Figure 2. shows one subject's EMG data from both surface and IM electrodes as it relates to force. For this subject, the correlation coefficient is r=.99 for both types of electrodes. The average difference between the slopes of the intramuscular and surface EMG/force relationship is .09. The average of the correlation coefficients for all subjects is 0.98 for both intramuscular and surface electrodes. The average slope of surface EMG/Force is 1.22 ± .17 (range .93-1.54). Similarly for IM electrode the average slope is 1.3 ± .27 (range .88-1.74). For most subjects the fit to linear is not significantly improved by using higher order regression or by splitting the data into two seperate sections (i.e. 0-30% MVC and 30-100% MVC).

Finally, the relationship of EMG/ force is similar for both electrode types even when the relationship is non-linear. This argues for a uniform distribution of muscle fibers types in this muscles since the electrodes have different pick-up areas.

References

1. Basmajian, JV and DeLuca C.J.: Muscles Alive, Williams and Wilkins, Baltimore MD 1985,p 188.

2. Woods, JJ and Bigland-Ritchie, B: Linear and non-linear surface emg/force relationships in human muscles. Am. J. Phys. Med. 62:6,1983

3. Delagi, EF et al: Anatomic Guide for the Electromyographer. Charles Thomas Publisher, Springfield Ill. 1975.

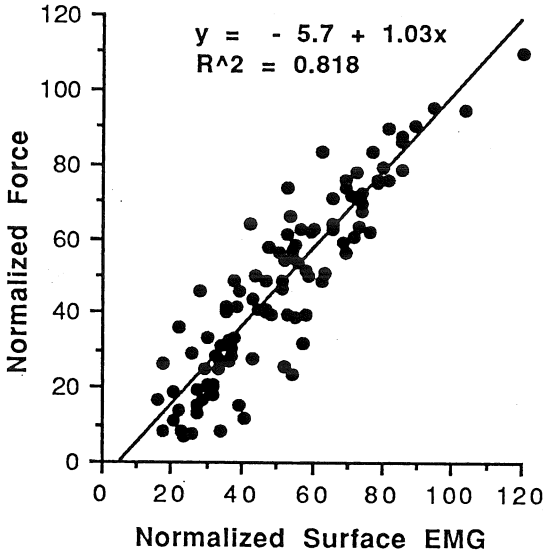

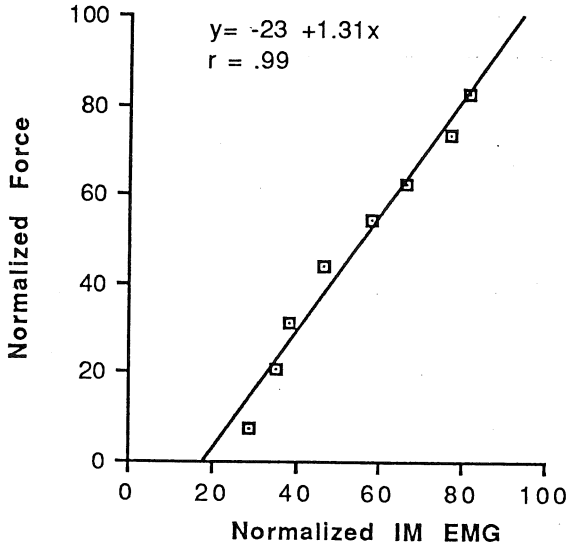

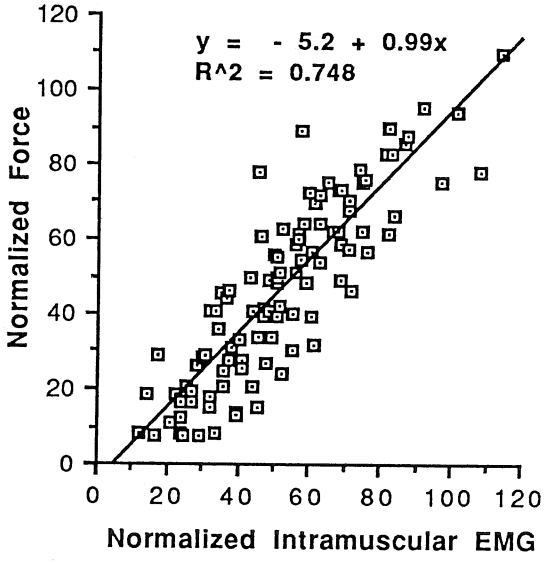

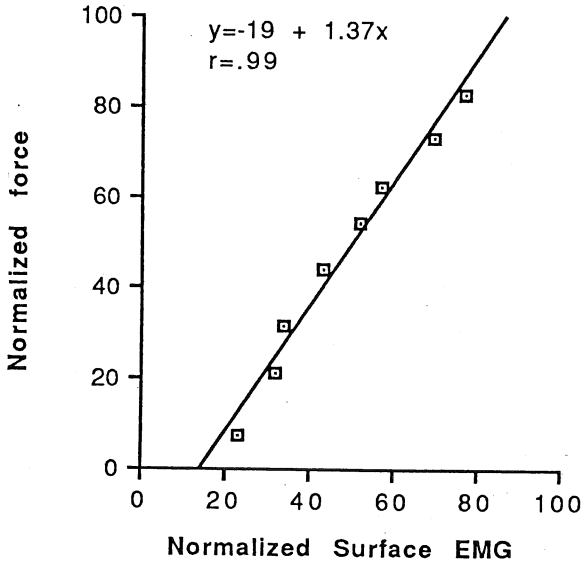

Figure 1. EMG to Force relationship of all subjects (n=14) for the anterior tibialis during isometric contraction. EMG and force are normalized to 100% maximum voluntary contraction.

Figure 2. Relationship of EMG/force of a single subject for both surface and intramuscular electrode.

CONSIDERATIONS IN PREDICTING HAND LOADS FROM EMG USING STATISTICAL AND NEURAL NETWORK METHODS

A. Moore, J. Cholewicki, S. Orr, G. Chen and R. Wells

Department of Kinesiology, University of Waterloo, Ontario.

INTRODUCTION

Measuring the hand grip forces is an essential element in quantifying the loads on the upper limb during repetitive manual tasks. This remains problematic due to the multiple degrees of freedom and the need for minimal encumbrance between the fingers and any object. EMG of the forearm flexors has been used to predict hand grip force as a function of grip type (eg. Armstrong et al, 1979). This study was undertaken to examine the effect of additional factors on the relationship between grip force and EMG. Factors studied included wrist posture (flexion/extension and radial/ulnar deviation), wrist angular velocity, wrist angular acceleration, forearm pronation/supination and an additional extensor side electrode site. Data collected was processed using statistical techniques and neural networks. The results show that grip type is the most important variable, however within grip type the results can be improved using wrist posture and wrist angular velocity in at least the flexion/extension direction. Forearm pronation/supination is important with pinch grips, possibly due to skin movement with respect to the extrinsic muscle mass used. The neural network approach produced comparable results to the statistical methods, however the time required to achieve adequate learning may limit its use in occupational settings.

REVIEW AND THEORY

Force is a recognised risk factor in chronic musculoskeletal problems of the upper limb (Silverstein et al. 1987). The continuous measurement of hand grip forces, therefore, is important in quantifying the loads sustained in repetitive manual work. However, obtaining these measures in a wide range of jobs is problematic. Instrumenting all parts and tools used is expensive and in many cases not possible (eg. a fish during fish processing). Adding force sensors to the hand is currently problematic due to the large number of segments, and the desire to maintain relatively normal interaction between the fingers and the objects. Alternatively, the electromyographic signal (EMG) from the forearm flexor muscles has been used to estimate force (Armstrong et al, 1981, Silverstein et al, 1987, Radwin et al, 1989, Freivelds, 1990, and Titiloye et al, 1990). Most of these studies use the procedure described by Armstrong et al (1979) which uses a linear relationship between submaximal hand force and EMG for different hand grips.

Li et al (1989) showed that surface EMG over the forearm flexors was highly correlated with electrical activity of the two main gripping force producing muscles (FDP and FDS obtained through fine-wire EMG). After windowing out unloaded portions, they also showed a strong linear correlation between grip force and EMG within a speed and posture condition. However, the correlation coefficients differed between speed and posture conditions. This is expected due to the interdependence between muscle tension, activation, velocity (Bigland and Lippold, 1954) and length. The inclusion of factors to account for changes in muscle length and velocity during a dynamic task may improve the accuracy in an industrial setting. Other factors that may improve the accuracy are estimates of co-contraction and postural effects. The purpose of this study was to examine the effect of such additional factors on the relationship between grip force from EMG.

PROCEDURES

Muscle activity was monitored from the forearm wrist and finger flexors (midpoint of a line between the medial epicondyle and the radial styloid), and the forearm wrist and finger extensors (over the extensor muscle mass just distal to the lateral epicondyle). Myoelectric signals were collected using Silver/Silver-Chloride disposable ECG pellet electrodes at a 2 cm spacing. The EMG was collected, amplified and processed on a custom built system. Specifications for the EMG system are: bandwidth 10-1000 Hz, CMRR 80 dB, input impedance 10 MOhm. The signals are full wave rectified and low pass filtered at 2 Hz. Wrist angles were monitored along 2 axes (flexion/extension and radial/ulnar deviation) using a lightweight commercially available goniometer (Penny and Giles, Blackwood, Gwent, UK). Force was collected using a pinch grip dynamometer. All 5 signals were collected using an A/D converter system at 50 Hz/channel and stored.

Two experiments were conducted. The first, designed to look at the effect of wrist posture, involved 3 subjects performing 30 submaximal efforts (between "light" and "strong") at wrist angles within the envelope bounded by extreme flexion/extension and ulnar/radial deviation for each of 6 different grip types (An et al, 1985). The relationship between force and EMG was considered linear, however the calibration factor defining the slope of the line was changed by wrist angle (x=flexion/extension, y=radial/ulnar) and grip type. These effects were modelled by fitting a quadratic function:

$$\frac{force}{EMG} = a + gain_{grip} * (Ax + By + Cx^2 + Dy^2 + Exy + F) * gain_{subj}$$

The second experiment involved one subject. A series of trials covering a range of force, posture and movement conditions were performed using a 2 finger pinch. These trials included static trials with 72 different wrist postures at each of two different forearm postures (pronated and mid), and 3 force conditions (light, medium and heavy). Dynamic trials included 45 conditions: 3 force conditions, 3 forearm postures (supinated, mid, pronated), and 5 movement conditions (smooth, jerky, slow, medium, fast). The dynamic trials were also repeated using a grasp. During each trial the subject attempted to cover most of the range of motion. The angular velocity and acceleration of the wrist was calculated by digitally differentiating the wrist goniometer signals. Data from each trial was sampled and used as input for the analysis. The data was analyzed using a back propagation neural network (McClelland and Rumelhart, 1988) and statistically using a multiple spline regression technique. The results were tested on a separate test file.

RESULTS AND DISCUSSION

The surface defining the relationship between force per unit EMG and wrist angle found in study 1 is shown in Fig. 1. Within a grip posture the wrist flexion/extension angle is important. Between grip types the surface shifts up or down.

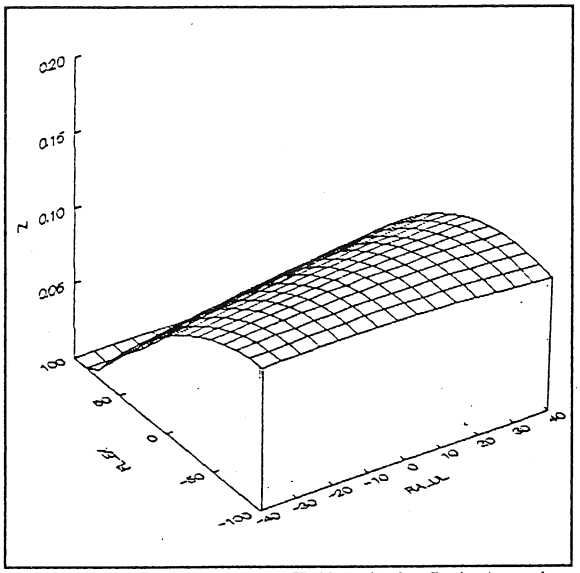

Figure 1 The normalized force/EMG ratio for flexion/extension (deg) and ulnar/radial deviation (deg) for all subjects and grips.

Several different neural networks were tried. The configuration that performed best on the combination of learning and generalization for 8 inputs (EMG, wrist angle, velocity and acceleration) had one hidden layer with 5 units. On the file that it learned on, the neural network performed better than the statistical methods (table 1). However, it was slightly weaker than the non linear regression technique on generalizing to the test file (rms error=.207 vs rms=.198). The processing time involved with the neural network may limit it's use depending on the hardware available.

Table 1 Learning performance of the network and statistical models.

Model	RMS Error	Correlation (R)
8-5-1 Network	.079	.78
EMG only regression	.120	.36
Multiple linear regression	.106	.57
Nonlinear regression	.205	.41

A new method called MARS (Multivariate Adaptive Regression Splines developed by Friedman, 1991) was applied to model the dependence of force on various inputs. This method allows a general continuous relationship to be built and pays special attention to the local changes of the relationship. The modeling was done using an available software package (MARS), and gave similar results as the neural networks with similar constraints. It had the advantage, however, that it lists the relative importance of the variables within the data used. When all data was grouped together, grip type dominated. However, comparing the relative importance of variables between the two grips studied, pronation/supination was much more important during pinch. This could be due to the effect of skin movement with the more localized extrinsic muscle mass used. Wrist posture appeared important with both grasps, as did flexion/extension velocity. However, wrist angular acceleration is important in pinch, possibly due to the relative proportion of extrinsic muscle activity which is used to accelerate the hand. A typical curve matching the predicted and actual values on the test file is shown in figure 2.

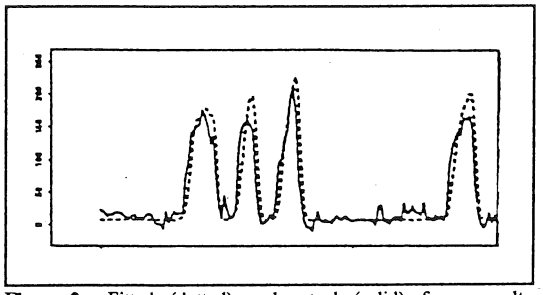

Figure 2 Fitted (dotted) and actual (solid) force results (Newtons) for the test file.

In conclusion grip type appears to be the most important factor affecting the relationship between force and EMG. However, improvements can be obtained by including wrist posture. The use of wide electrodes or multiple electrode sites may reduce the effect of pronation and supination on the force/emg relationship during pinch.

REFERENCES

An et al, *J. Orthop. Res.*, **3**, 202-211, 1985.
Armstrong, T. et al, *J. Biomechanics*, **12**, 131-133, 1979.
Armstrong, T. et al, *Am. Ind. Hygiene Assoc. J.*, **43**, 103-116, 1981.
Bigland, B. and Lippold, *J. Physiol.*, **123**, 214-224, 1954.
Freidman, J.H. *Annals of Statisitics*, **19**, 1-50, 1991.
Freivalds, A. *Int. J. of Ind. Ergonomics*, **6**, 261-266, 1990.
Li, Y. et al, *Proceedings of the International Society of Biomechanics*, Los Angeles, 1989.
McClelland, J. and Rumelhart, Explorations in parallel distributed processing, MIT Press/Bradford Books, 1988.
Radwin, R., et al, Advances in Industrial Ergonomics and Safety, (pp.275-281), Taylor and Francis, 1989.
Silverstein, B. et al, *Am. J. of Ind. Med.*, **11**, 343-358, 1987.
Titiloye, V. et al, *Proceedings of ISEK*, Baltimore, 1990.

ACKNOWLEDGEMENTS

The authors would like to thank the Ontario Workplace Health and Safety Agency and Ministry of Labour and NSERC for support of parts of this research. The statistical contribution of Dr. G. Bennett is gratefully acknowledged.

ELECTROMYOGRAPHY: TECHNIQUES, MODELLING AND MUSCLE MODELS

Poster

STATIONARITY OF EMG SIGNALS OBTAINED ACROSS INCREASING FORCE LEVELS DURING RAMP AND STEP CONTRACTIONS

M. Bilodeau, E.J. de la Barrera, A.B. Arsenault,
D. Gravel, D. Bourbonnais, F. Kemp

School of Rehabilitation, Faculty of Medicine,
University of Montreal and
Research Centre, Montreal Rehabilitation Institute,
Montreal, Quebec, Canada, H3S 2J4

INTRODUCTION

The purpose of this study was to compare the statistical characteristics of EMG signals obtained under ramp and step isometric contraction conditions. Short time windows taken at different force levels of ramp contractions were tested for ergodicity and compared to their respective levels of step contractions. The results suggest that statistical properties of short time windows of EMG signals generated under these two types of contractions are comparable at their respective force level.

REVIEW & THEORY

It has recently been observed that the median frequency of the EMG power spectrum of triceps brachii (TB) and anconeus (AN) increases with force. However, this increase was found to be more pronounced during ramp than during step contractions (Bilodeau *et al.*; 1991).

Power spectral analysis of EMG signals obtained while maintaining steady force levels (step) is most common since these signals are considered to be stationary. However, EMG signals obtained during a progressive increase in the force level (ramp), might not be suited for power spectral analysis due to the fact that changes in the signal associated with the varying force could result in a condition that deviates from stationarity. Thus, analysis of statistical properties of the power spectrum, such as the median frequency, of EMG signals obtained in both ramp and step contractions could be erroneously interpreted if stationarity of the signals is not established.

In order to validate conclusions concerning the different behaviours of the median frequency in ramp and step contractions, a comparison study between the statistical characteristics of EMG signals recorded during both types of contraction was made. More specifically, EMG signals were tested for ergodicity.

The EMG signal is a time and force dependent signal whose amplitude varies in a random nature above and below the zero value. Three conditions guarantee ergodicity of a random process: a) its normal or Gaussian distribution; b) the process is assumed to be stationary; and c) the process has an average value of zero (Basmajian *et al.*; 1975, Bendat & Piersol; 1986).

PROCEDURES

Surface EMG signals from the TB and AN of nine healthy subjects were recorded during both ramp (single contractions with force increasing linearly from 0 to 100% MVC in 5-s) and step (steady contractions maintained at five different force levels (10, 20, 40, 60 and 80% MVC) for 3-s) contractions. These signals were band-pass filtered (16 to 800 Hz) and digitized at a sampling rate of 2000 Hz.

A single data window of 512 points (256-ms) was taken at each of the five above mentioned force levels from the two types of contractions and tested for ergodicity by: a) taking, from each 512 points window, seven 128 points segments overlapping each other by half their length and calculating the ensemble average of the mean value of all segments; b) calculating the mean value (time average) and SD of each 512 points window; and c) estimating the normality of the distribution of the 512 points window and of each of the 128 points segments.

RESULTS

Data from the AN muscle of a typical subject are shown in figures 1 and 2. As can be observed from these figures, the value of the ensemble average of the seven segments and the mean value of the 512 points window are equal. The difference between the two values is, for both types of contraction, always well below 1% of the maximum value of the analyzed window. It can also be seen that both these values are equal to zero (usually below 1% of the maximum value of a given window) in both types of contraction. In addition, the variation in the signal across the seven segments is relatively stable as can be seen by the mean and SD (corresponding to approximately 20% of the maximum value of the segment) which show constant values within a 512 points window, again, for both types of contraction. The distribution of the 512 points taken at a given force level was similar between the two types of contraction. Moreover, the distribution of the points taken from each of the seven 128 points segments of a given window was constant across the different segments and well representative of the distribution of the 512 points window for step as well as ramp contractions. Even though the mean of the majority of the distributions was zero and their shape symmetrical, a Gaussian distribution was not confirmed statistically in most instances for both types of contraction. Identical results were obtained for the TB.

DISCUSSION

The present results, show that EMG signals obtained during a ramp contraction have similar statistical characteristics than that obtained during a contraction performed at a steady force level. This is of importance since EMG signals have to be stationary in order for the Fourier transform to be applied. It thus appears that the results of power spectral analysis performed on EMG signals obtained during ramp contractions can be considered as valid as results obtained from step contractions.

One has to take into account the fact that, in this study, windows of relatively short length were analyzed since they prevent too much force variation. In the present case, a 256-ms window corresponds to approximately 5% of the maximum force in a ramp. Longer window lengths over which force can vary to a greater extent, could bring too much variations in the EMG characteristics

and prevent a valid spectral analysis. On the other hand, a window that is not long enough could degrade the information contained in the EMG signals. The present short windows, however, appear to be sufficiently long to be representative, as was shown previously (Bilodeau *et al.*; 1991).

Consequently, the more pronounced increase in the median frequency of the EMG power spectrum across force levels, observed during ramp as compared to step contractions, seems to be explained by factors others than differences in basic descriptive characteristics of the signals, such as stationarity. Different motor unit activities during the two types of contraction have been suggested to be amongst the factors possibly explaining the varying behaviour of the median frequency across force levels (Bilodeau *et al.*; 1991).

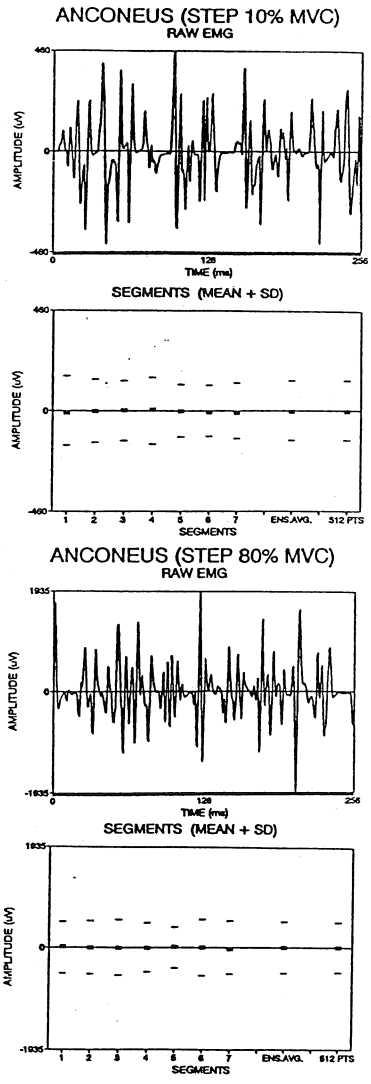

*Figure 1. **STEP:** Graphs showing the raw EMG and the mean amplitude value ± SD of the seven different 128 points segments for the 10 and 80% MVC step windows of a typical subject. The value of the ensemble average (ENS.AVG.) of these seven segments and the overall mean or time average (512 PTS) ± SD of the 512 points window are also shown.*

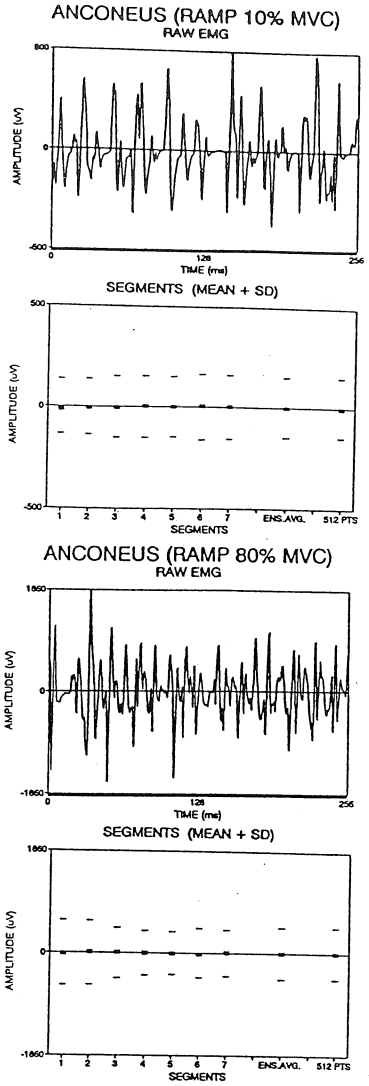

*Figure 2. **RAMP:** Graphs showing the raw EMG and the mean amplitude value ± SD of the seven different 128 points segments for the 10 and 80% MVC ramp windows of a typical subject. The value of the ensemble average (ENS.AVG.) of these seven segments and the overall mean or time average (512 PTS) ± SD of the 512 points window are also shown.*

REFERENCES

Bendat, J.S., Piersol, A.G. Random Data: Analysis and Measurement Procedures, Wiley, 1986.

Bilodeau, M. et al. *Eur. J. Appl. Physiol.*, 63: 24-28, 1991.

Basmajian, J.V. et al. Computers in Electromyography, (pp.47-89), Butterworths, 1975.

ACKNOWLEDGMENTS

Martin Bilodeau is supported by a Ph.D. studentship from the Medical Research Council of Canada.

DISTRIBUTED RANDOM ELECTRICAL NEUROMUSCULAR STIMULATION: DEPENDENCE OF EMG MEDIAN FREQUENCY ON STIMULATION STATISTICS AND MOTOR UNIT ACTION POTENTIALS

Y.T. Zhang[1], W. Herzog[2], P.A. Parker*, M. Hulliger[3], A. Guimaraes[2]

Departments of Electrical & Computer Engineering[1], Biomechanics[2], and Clinical Neurosciences[3], The University of Calgary, Calgary, AB, Canada, T2N 1N4

Department of Electrical Engineering, University of New Brunswick, Fredericton, N.B., Canada, E3B 5A3*

INTRODUCTION

Electromyographic (EMG) signals are widely used to estimate the mechanical output, such as force, and activation state of skeletal muscle (Basmajian, et al. 1985, and DeLuca, 1979). One parameter that has proven useful in EMG signal analysis is the median frequency of the EMG spectrum. In this study, a closed form expression for the EMG spectrum of muscle activated via multiple channels using random stimulation patterns was derived to calculate the median frequency as a function of the shape of compound motor unit action potentials (CMUAP) and stimulation statistics. For a given shape of the CMUAP, the median frequency of the EMG spectrum increases with increasing mean rates of stimulation. However, the rate of increase in the median frequency is inversely related to the magnitude of the coefficient of variation of inter-stimulus intervals (ISI) (in the case of voluntary muscle contraction, ISI represents the inter-spike intervals). For physiologically relevant coefficients of variation (>10%), the median frequency of the EMG spectrum is virtually independent of the mean stimulation rate, but is determined to a large extent by the shape of the CMUAP. These theoretical results are consistent with experimental findings reported previously in the literature.

REVIEW AND THEORY

Physiological activation of motor units of intact skeletal muscle occurs through distributed random excitation that may be approximated using a normal ISI distribution. In contrast, conventional electrical neuromuscular stimulation is typically produced using periodic or near periodic stimulation patterns. The coefficient of variation of the ISI of physiological and periodic activation of muscle is different: a coefficient of about 10% or more for the physiological case and a coefficient of 0% or close to 0% for periodic or near periodic artificial stimulations. It has been reported by DeLuca (1979), Basmajian, et al. (1985), Pan, et al. (1989), Inbar, et al. (1987), and Zhang, et al. (1991) that values of coefficient of ISI variation affect the details of the EMG spectrum. In particular, changes in median frequency of the EMG spectrum of periodically stimulated muscle are typically directly associated with mean stimulation rates, due to the dependence of the spectrum on the coefficient of ISI variation. However, we feel that such an association may not accurately reflect the relation between the median frequency and firing rates in the physiological case. Therefore, the purpose of this study was to test analytically the relation between the median frequency of the EMG spectrum and the mean stimulation rate for varying coefficients of variation of the ISI, and for varying shapes of the compound motor unit action potentials.

PROCEDURES AND RESULTS

a.) A Model of CMUAP

If several motor units are stimulated simultaneously in a ventral root filament, the compound motor unit action potential p(t) results from the summation of the motor unit action potentials elicited in the filament, and will be in-variant in form in a given filaments due to the fixed number of motor units activated and the 'all-or-none' nature of unit potential generation. But p(t) will not be identical to the muscle fiber action potential owing to diameter, endplate and threshold dispersion, and it may not be identical across filaments either, for the reasons above and due to variation in number of motor units in a filament. However, in general the CMUAP could be formed by properly summing the MUAPs activated in a single channel. One expression of a CMUAP that agrees reasonably well with observed data and for which the spectrum could be analytically derived is as follows:

$$p(t) = \sum_{n=1}^{L} h_n(t-\tau_n), \qquad (1)$$

where τ_n is a time shift ($\tau_1 = 0$), L is the number of motor units in a single channel, and h_n is the nth motor unit action potential in the filament which is given by (Parker et al, 1986)

$$h_n(t) = \begin{cases} t(2-b_n t)\exp(-b_n t), & 0 \le t \\ 0, & otherwise. \end{cases} \qquad (2)$$

In this Equation , b_n is a constant determined by the distribution of fiber types in a muscle. It is desirable that one filament corresponding to one simulation channel includes only a single motor unit. In this situation, $\tau_1 = 0$, the amplitude spectrum of the CMUAP can be shown to be

$$|P(f)|^2 = \frac{(2\pi f)^2}{[(2\pi f)^2 + b^2]^3}. \qquad (3)$$

b.) Spectral Expression

In a structural model for the distributed random ENMS, the activation signal (stimulus train) which corresponds to the innervation signal for the fibers of the ith channel is considered, as in the physiological case (DeLuca, 1979, Parker, et al. 1986), as a renewal point process with known activation statistics. For the ideal case where one stimulation channel includes a signal motor unit, the EMG spectrum of the ENMS with uncorrelated channels and Gaussian ISI can be written as:

$$\Phi_{yy}(f) = \sum_{i=1}^{m} \frac{\lambda_i (2\pi f)^2 \sinh[2(\pi f \sigma_{xi})^2]}{\{\cosh[2(\pi f \sigma_{xi})^2] - \cos(2\pi f/\lambda_i)\}\{(2\pi f)^2 + b_i^2\}^3}, \quad f \neq 0 \qquad (4)$$

where m is the number of stimulation channels, λ_i is the stimulus rate in the ith channel, σ_{xi} represents the standard deviation (SD) of the ISI.

c) Effects on Median Frequency

In order to quantify the modification in the EMG spectrum by variation in firing rate λ and standard deviation σ_x of the inter-spike interval, the signal median frequency, f_{med}, was computed numerically from Equation 4 (with m = 1) as a function of λ. The plots of the median frequency against λ are shown in Figure 1 for different values of σ_x.

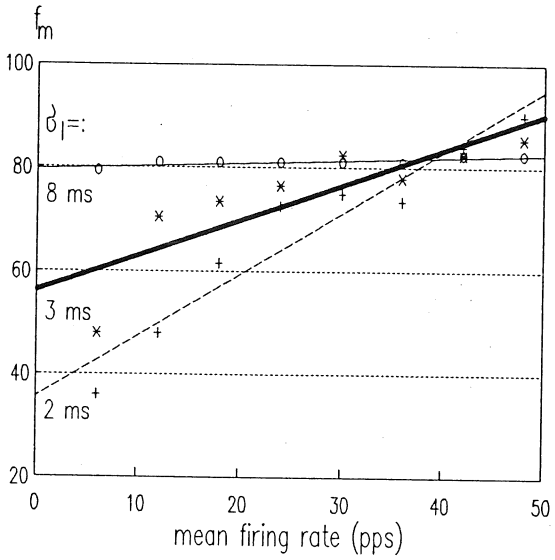

Figure 1. Median frequency of spectrum versus λ for σ_x = 2, 3 and 8 ms (Symbols: the calculated median frequency, Line: fitted regression line).

It is clear that the relationship between the signal median frequency and λ is nonlinear, especially for the cases of small σ_x (Figure 1). This is because of the nonlinear relationship between $\Phi_{yy}(f)$ and λ as indicated in Equation 4. For large values of σ_x, the change of the median frequency with λ becomes small, as seen in Figure 1, where the largest σ_x (8ms) results in the smallest change of the median frequency, nearly independent of stimulation rate λ. This is due to the fact that the dependence of the EMG signal spectrum on λ decreases with increasing σ_x. Nevertheless, in all cases shown in Figure 1 the trend of increasing median frequency with increasing λ is still evident. These data support the experimental results reported by Pan et al. (1989).

DISCUSSION

In general, the median frequency depends on an interaction of the firing (or stimulation) statistics and the MUAP. The results reported here, however, imply that it is possible to use the median frequency as a selective indicator of change of MUAP, namely by increasing the SD of the inter-stimulus interval in distributed random ENMS to sufficient large values (8 ms or higher, see Figure 1). This is particular important when one attempts to determine qualitatively, with random ENMS, the contribution of variation in CMUAP to any change of the median frequency. The median frequency has been used widely to asses muscle fatigue. When muscle fatigue occurs, the median frequency of the EMG signal tends to decrease (Basmajian, 1985). However, it is difficult to determine in voluntary muscle contraction how much change in the median frequency is caused by local muscle properties (reflected in the MUAP) and how much by the decrease in the motor unit firing rate. The distributed random ENMS provides a possibility of separating two main causes of the change in the median frequency with a appropriate choice of the SD of the ISI. These results further strength the argument that distributed random ENMS rather than periodic ENMS should be used in studies of muscle activation.

In summary, the feature distinguishing this study from many previous ENMS investigations is that this work placed significant emphasis on introducing random ISI into ENMS, and on the interactions between MUAP shape and ISI statistics, which strongly influence commonly used EMG frequency parameters such as median frequency. The results of this study confirm observations by Pan et al. (1989), that the median frequency of the EMG spectrum shifts upwards with increase in firing rate, particularly when variations in ISIs are small. Furthermore, our results indicate that the median frequency may become independent of the firing rate (or stimulus rate) when the coefficient of ISI variation is large.

REFERENCE

Basmajian, J. et al. Baltimore Williams and Wilkins, 1985.
DeLuca,C. *IEEE Trans. Biomed. Eng.*, **26**, 313-325, 1979.
Pan, S. et al. *Med. & Biol. Eng. & Comp.*, **27**, 14-18, 1989.
Parker,P. et al. *CRC Critical Reviews in BME.*, **13**, 284-310, 1986.
Inbar, G., et al. *IEEE Trans. on BME.*, **34**, 761-770, 1987.
Zhang,Y., et al. *Proc. of 17th CMBEC.*, Canada, (pp.107-8), 1991

ACKNOWLEDGEMENT

This study was supported by NSERC of Canada. The authors would like to thank Dr. U. Windhorst, at the Department of Clinical Neuroscience, for his contributions to this study.

THE INFLUENCE OF TORQUE PRODUCTION TASK ON EMG FREQUENCY CONTENT

G.E. Caldwell, S. Lee and J.C. Jamison

Department of Kinesiology, University of Maryland, College Park, MD, USA

INTRODUCTION

Frequency characteristics of surface EMG, which have been suggested as indices of motor unit recruitment, were used to study muscular response in different torque production tasks. Torque and EMG data from 14 subjects illustrated task differences for 4 EMG sites among elbow flexors. Possible evidence of task-specific motor units in m. biceps brachii was found, as was support for motor unit task groups. The data provide further support that the concept of muscle equivalence in the elbow flexors does not hold as a general rule.

REVIEW AND THEORY

Studies of motor unit recruitment thresholds have demonstrated the existence of task-specific motor units within the muscles controlling the elbow (ter Haar Romeny *et al.*, 1984; Van Zuylen *et al.*, 1988). Such task specificity is more difficult to detect using amplitude-based surface EMG measures (Caldwell *et al.*, 1991). However, the frequency content of EMG signals has been shown to change under conditions of fatigue and recruitment level (e.g. Komi *et al.*, 1979; Moritani *et al.*, 1987). Recently the possibility of using the median frequency of the power density spectrum to identify recruitment control strategies of muscles has been suggested (Solomonow *et al.*, 1990). Therefore the objective of the present study was to examine the frequency content of the EMG from selected arm muscles during different one- and two-degree-of-freedom (*df*) elbow torque tasks.

PROCEDURES

Torque and EMG activity were examined in 14 male subjects while seated securely in a two-*df* dynamometer system. The subject grasped an instrumented handle which registered elbow torque in two orthogonal directions, i.e. flexion/extension (**FTOR**) and supination/pronation (**SPTOR**). EMG was recorded from electrode pairs located on m. biceps brachii short head (BBSH), m. brachioradialis (BRAD), and lateral (BBLL) and medial (BBLM) sites of m. biceps brachii long head, using miniature Ag/AgCl electrodes connected to Grass PD7 amplifiers. Each subject was seated with his shoulder flexed to 20 degrees, his elbow flexed at 90 degrees, and his forearm in a mid-prone position. Subjects were instructed to perform 4 independent tasks involving maximal effort isometric flexion or supination in conjunction with a second *df* target task. These four tasks were: [i] flexion MVC - supination target torque at 0 Nm (task **F**); [ii] supination MVC - flexion target torque at 0 Nm (**S**); [iii] flexion MVC - supination target at 100 % MVC (**FS**); and [iv] supination MVC - flexion target at 100 % MVC (**SF**).

Torque and EMG signals were collected at 1000 samples per second per channel using an IBM PS/2 microcomputer interfaced with a 12-bit A/D collection board. For each trial steady-state mean torque and EMG measures were calculated over a 512 millisecond time window. The median (**MEDF**) and mean frequency (**MEANF**) of the power density spectrum and the **RMS** amplitude were calculated for each EMG signal.

RESULTS

Torque data for the four tasks are shown in Figure 1. Statistical analysis (ANOVA with Student-Newman-Keuls contrasts) revealed the S task to have less **FTOR**, and the F task to have less **SPTOR**, than the other tasks, as would be expected from task conditions. In addition, the FS task displayed less **FTOR** than either **F** or **SF**.

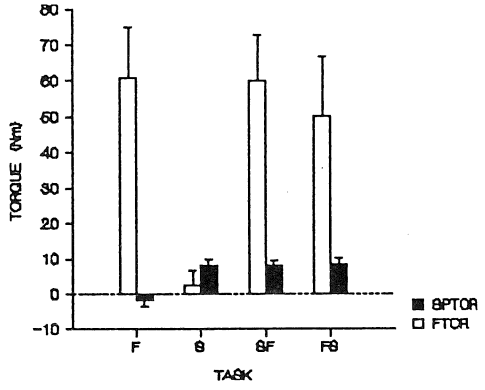

Figure 1: Torque data for each task

The EMG data are displayed in Figure 2. An ANOVA with repeated measures for EMG site showed correlations between the four sites, so subsequent analysis used Greenhouse-Geiser corrections for critical values. The EMG measures were tested using an ANCOVA with the dependant variable value in the F task as covariate. Main task effects were found for **RMS** but not **MEDF** or **MEANF**. Orthogonal contrasts revealed the F and S tasks to have significantly lower **RMS** values than **FS** and **SF**.

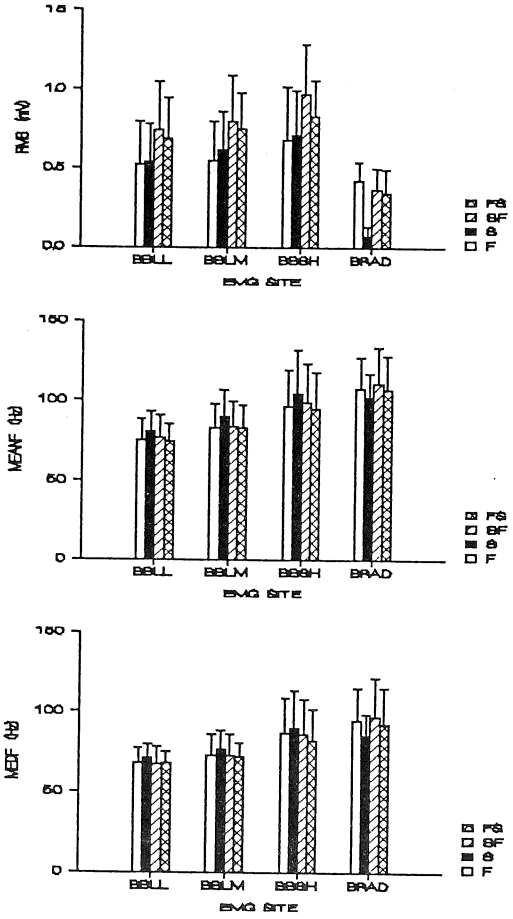

Figure 2: EMG data: *top panel* - **RMS**; *middle* - **MEANF**; *bottom* - **MEDF**.

More differences were found among EMG sites for all EMG variables. BBLL and BBLM **MEANF** values differed, although both **MEDF** and **RMS** were the same. These two BB long head sites were significantly different than BBSH for all three EMG measures. Also, all three BB sites were significantly different than BRAD for **RMS**, **MEDF** and **MEANF**. There was also a significant task by site interaction concerning the tasks **F** and **S**. For all EMG measures the BB sites and BRAD behaved differently with regard to these two tasks.

DISCUSSION

The lower **RMS** values in the **F** and **S** tasks suggest that less CNS stimulation was present compared to the dual MVC **FS** and **SF** tasks. These data may suggest that task-specific motor units are used differentially by the CNS at MVC torque levels, and thus support earlier recruitment studies. This possibility is strengthened by the differences in **MEANF** found between the BBLL and BBLM sites, since task-specific units have been reported to be localized within the long head of BB (ter Haar Romeny *et al.*, 1984).

Further, the fact that no frequency shift was seen across task (while **RMS** values changed) suggests that the normal recruitment order may not occur with the addition of the second df task, and thus may support the concept of task-specific motor pools theorized by Loeb (1985). Orderly recruitment according to the size principle may still occur *within* each task motor pool. However the second *df* MVC would result in additional stimulation (increased **RMS**), but would recruit new units of various sizes from within the second task motor pool, resulting in no change in frequency characteristics.

Finally, differences in the three EMG measures between BBSH and BB long head sites and between BRAD and all BB sites have three possible sources: variation in slow twitch/fast twitch ratios (ST/FT), differences in electrode/motor unit geometry or task-specific stimulation behaviour. While a higher percentage of FT fibers may be the reason for the higher **MEDF** and **MEANF** in BRAD, the task by site interaction indicates a different functional role than BB in the **F** and **S** tasks. These findings refute the generality of the muscle equivalent concept for BB and BRAD proposed by Bouisset (1973).

REFERENCES

Bouisset, S. *In*: New Developments in Electromyography and Clinical Neurophysiology, (pp.547-583), Karger, 1973.
Caldwell, G.E. et al. *EMG clin. Neurophys.*, **31**, 433-445, 1991.
Komi, P.V. et al. *Eur. J. Appl. Physiol.*, **42**, 41-50, 1979.
Loeb, G.E. *J. Exp. Biol.*, **115**, 137-146, 1985.
Moritani, T. et al. *Eur. J. Appl. Physiol.*, **56**, 260-265, 1987.
ter Haar Romeny, B. et al. *Exp. Neurol.*, **85**, 631-650, 1984.
Solomonow, M. et al. *J. Appl. Physiol.*, **68**, 1177-1185, 1990.
van Zuylen, E.J. et al. *J. Neurophysiol.*, **60**, 1523-1548, 1988.

RELIABILITY OF ELECTROMYOGRAPHIC DATA FROM ISOMETRIC CONTRACTIONS

M.E.Wootten, D. Jacobs, J. Burn, M.P. Kadaba

Orthopaedic Engineering and Research Center, Helen Hayes Hospital
W. Haverstraw, N.Y.

INTRODUCTION

Electromyographic data in kinesiological studies are often normalized to a 'standardized' contraction to enable comparisons between different muscles and/or individuals and between retrials on different days. Sometimes data are normalized to the maximum value that occurs during an activity. More often the contraction chosen is a 'maximum voluntary contraction' (MVC). Yang and Winter (4) reported poor reliability of surface EMG data for maximal isometric contractions with significantly better reliability for 50% or 30% maximal contractions. These results suggest the use of submaximal contractions to improve reliability. But a reliable maximal effort is more critical if one is using relative levels of EMG to imply a force level; for example, if one is using dynamic EMG data in a model of muscle force or when one compares agonist/agonist or agonist/antagonist muscle contributions to explain resultant kinematics.

The purpose of this study was to investigate the reliability of data acquired from both surface and intramuscular electrodes during four isometric 'normalizing exercises'.

METHODS

Bipolar intramuscular electrodes (50 micron stainless steel wire with 2mm bared tips) were inserted into the Anterior Tibialis muscle in the position described by Delagi.(1) Surface electrodes (Iomed Inc.) were placed just lateral to this insertion site. Intramuscular EMG as well as surface EMG were differential amplified with the self contained electronics of the Iomed electrodes.

Fourteen normal subjects were investigated. The exercises studied were A) a Manual Muscle Test (MMT)contraction, B) 100% maximal contraction, C) 50% maximal contraction and D) 25% maximal contraction. The MMT contraction was done as described by Kendall et al.(2) with the resistance given by the same person throughout the study. For the remaining exercises, the subject was seated on a Cybex bench, hip and knee were at 90°, with pelvis and thigh stabilized. A special unit was built to house a force transducer and to hold the foot in place during the isometric dorsiflexion. The 100% maximal force level was first determined. This level was not the absolute maximum that could be obtained but rather a maximal contraction that could be maintained steadily for 5 seconds. The subject was then given a target force level (100%, 50% or 25% of maximal) as well as feedback via an oscilloscope. For each contraction, a target force level was achieved before data collection commenced. Each contraction was repeated three times with the order of testing randomized. Each trial was for five seconds with rest of approximately 2 minutes between trials. EMG signals were filtered 20 to 1000 hz and acquired at 2400 hz. EMG data were rectified and smoothed with a 64 point moving Hanning window.

The intraclass correlation coefficient (ICC) was used to measure the reliabilty of both the surface and IM EMG. This coefficient is the ratio of the variance due to the 'true' measure divided by the sum of the variance due to the true scores and the variance due to the mean of the measurement errors. This coefficient estimates the reliabilty of a single measure (r_1) as well as the reliability of the mean of 'k' (r_k) measures. (3). The coefficient of variation (CV) defined as the standard deviation divided by the mean times 100% was also calculated as an additional measure of the variability of the three measures.

RESULTS

Table 1. gives the ICC for a single measure as well as for mean of the three measures. MMT is less reliable than contractions to a targeted force level. There is no significant difference in the reliability of the the 100%, 50% and 25% maximal contraction. During these isometric exercises there is no difference in the reliability of the surface and the intramuscular electrode data.

Table 1.

Exer.	Surface	Intramuscular
MMT	r_1 =.64 r_3=.84	r_1=.61 r_3 =.82
100%	r_1 =.93 r_3=.97	r_1=.96 r_3 =.99
50%	r_1 =.94 r_3=.98	r_1=.86 r_3 =.95
25%	r_1 =.97 r_3=.99	r_1=.93 r_3 =.98

The average coefficient of variation for each electrode type and exercise is given in Table 2. The CV indicates that EMG data acquired during the MMT is more variable than that acquired during the remaining exercises. CV is dependent on the mean as can be seen in the force data.

Table 2.

Exer.	Surface	Intramuscular	Force
MMT	10.5	15.8	--
100%	7.0	6.8	1.2
50%	5.3	11.2	2.3
25%	5.4	9.0	3.4

DISCUSSION

Based on these results, a manually resisted maximal effort contraction is the least reliable of the exercises studied. The fact that targeted 100% contraction is as reliable as the 50% and 25% contraction was unexpected, in light of Yang and Winter's study. This could be due to several factors. Giving feedback undoubtedly decreases the variability. Also, the target level of the 100% contraction was such that the contraction could be maintained for 5 seconds. Finally, the average EMG data from the MMT was greater than from the targeted 100% contraction data. This could indicate a greater effort and/or more co-contraction during these contractions which will add to the variability.

In this controlled set of exercises the reliability of the intramuscular electrode data was very similar to that of surface electrode data. This is important in light of the studies that require a mixture of electrode types to measure the muscle activity.

REFERENCES

1. Delagi, E.F et al: Anatomic Guide for the Electromyographer, Charles Thomas Publisher, Springfield,Ill.,1975.

2. Kendall, H et al: Muscle Testing and Function, Williams and Wilkins, Baltimore,1971.

3. Winer, BJ: Statistical Principles in Experimental Design, McGraw Hill, New York,1971.

4. Yang, J and Winter, D: Electromyographic Reliability in maximal and submaximal isometric contractions. Arch Phys Med Rehabil 64:417-420,1983.

THE EFFECTS OF EMG SAMPLING RATE ON THE POWER SPECTRAL DENSITY UNDER ECCENTRIC CONTRACTIONS OF THE VASTUS LATERALIS

Mario Lamontagne1,2 and Valerie Coulombe1
School of Human Kinetics1 and Department of Anatomy2
University of Ottawa, Ottawa, On., Canada K1N 6N5

INTRODUCTION

The electromyogram (EMG) is a valuable clinical and modelling tool in the area of biomechanics. The relationship of the EMG signal to some physiological (Basmajian, 1967) or mechanical state of the muscle (Petrofsky and Lind, 1980; Perry and Bekey, 1981) has been studied and is still studied extensively. If the EMG signal is to be utilized for a specific purpose in an investigation, it must be properly processed. Early studies investigation (Fugsland-Fredeiksen and Mansson, 1975) used analog techniques (in time domain) such as peak counters, integrators and filter circuits to process the EMG signal. With the advent of high speed digital computers and therefore more sophisticated processing techniques (Blinowska and Verroust, 1967; Zscorlich, 1989) it is possible to extract much more useful information from the EMG signal.

The most commonly used digital signal processing technique is frequency or spectral analysis (Sack, 1978). This technique is particularly attractive since it allows the possibility of identifying a particular muscle (under a given set of conditions) based on the frequency content of its EMG signal. While digital techniques have increased the understanding of EMG signals, they have also added considerable confusion and complexity to the literature database. This situation, of course, has led to further research. Much of this research has focused on the effects of muscles (Gander and Hudgins, 1985), on instrumentation parameters (Chu and Chen, 1985), or on the resulting processed EMG.

One of the main concerns in digital processing is the choice of a proper sampling rate for the analog to digital conversion (A/D). Sampling theory (Sack, 1978) states that the sampling rate must be at least twice as high as the highest frequency in the signal. Given this rule, the investigators must know the frequency band of the specific EMG signal where most of the power is contained in order to choose the appropriate sampling rate. The final choice of sampling frequency in most hardware/software limitations and the sampling theory.

Given the above review, the purpose of this investigation is to study the effects of different sampling rates on the power spectral density and the integrated linear envelop of the raw surface EMG of the vastus lateralis during eccentric contractions at 60 degrees/s.

METHODOLOGY

Six healthy males subjects between 20 and 40 years old with no history of neuromuscular disorders volunteered in this investigation. Each subjects sat on an isokinetic device bench (Kin-Com 500H) with the hip and knee joint at 90*. To insure the alignment of the centre of rotation of the knee joint and the centre of rotation of the device, the subject's right thigh was secured at the isokinetic device seat and the ankle was tied to the lever arm device. The subject was asked to perform, in random order, 5 concentric and eccentric contractions at 30, 60, and 90°/s while the surface EMG of the vastus lateralis was recorded throughout the 90° range of motion.

The vastus lateralis muscle activity was recorded with surface electrodes (MEDI-TRACE, silver-silver chloride electrode) placed 2.5 cm apart, directly over the motor points as described by Zipp (1982) and Delagi (1975). Skin impedance at this site was always below 10 k Ohms. A High input impedance differential bioamplifier (TECA corp.) with a bandwidth frequency of 3.2 Hz to 32 kHz and a gain of 10000 was used to amplify the raw EMG signal. The EMG signal, torque and angular displacement from the isokinetic device were then fed to an A/D converted board (Tecmar, HPGL-40) which was controlled by a micro-computer (Toshiba T5200-100). A custom-made software BIOAD (Lamontagne and al., 1989) was used to collect the raw EMG signal, the torque and angular displacement signal. The EMG signal was collected at 4000 Hz for 4 s and the torque and angular displacement signal were sampled at 100 Hz for 4 s and then stored on magnetic medium for later processing.

Only EMG signals from the eccentric contraction trials (60°/s) (n=30) were processed. A one second window of the largest EMG signal burst was selected for processing. This signal was normalized at 4000, 2000, 10000 and 500 Hz. The normalized signal was digitally filtered with an high-pass filter (Butterworth) at 2 Hz and then the power spectral density (PSD) was obtained using Fast Fourier Transform. From the PSD processing, the median power spectrum of each trial (n=120: 30 trials at 4 different frequencies) was recorded and stored for later statistical analysis. The normalized EMG was also rectified and filtered (critically damped filter) at 6 Hz and then integrated (I LEEMG). The I LEEMG was recorded and stored for later statistical analysis.

Two separated factorial analyses (ANOVA) with repeated measures were performed; the first one using the EMG median power spectrum amplitude as dependant variable and the sampling frequencies as independent variables and the second one using I LEEMG as dependant variable and the sampling frequencies as independent variables.

RESULTS AND DISCUSSION

The sampling time and frequency for collecting raw EMG signal are mainly limited by the instrumentation and the sampling theory. To date, no study has investigated the effects of sampling frequency on the processed EMG signal. A factorial analysis of the median power spectrum frequency amplitude of the raw EMG signal of eccentric contractions (60°/s) and the sampling rate was performed. The preliminary results show that

there is no significant difference ($p < 0.05$) for the median power spectrum frequency amplitude between the sampling frequencies (Table 1). The difference in median power frequency between subjects is larger than between sampling rates. The figure 1 depicts the PSD for the various sampling rates.

Table 1 Factorial analysis with repeated measures ($p < 0.05$) for the EMG Power spectral Density and the sampling rates.

Source	SS	DF	F	Fc
Intersubject	2521.6	5		
Intergroup	318.0	3	0.47	3.29
Errors	3.4	15		

A factorial analysis with repeated measures was performed on the I LEEMG and the sampling rates. No significant difference ($p < 0.05$) was also found for the I LEEMG between the sampling rates (Table 2).

Table 2 Factorial analysis with repeated measures ($p < 0.05$) for the I LEEMG and the sampling rates.

Source	SS	DF	F	Fc
Intersubject	0.362	5		
Intergroup	2×10^{-6}	3	NS	3.29
Errors	1.09	15		

The results of this study suggest that for an eccentric contraction at 60°/s, a sampling rate of 500 Hz is sufficient for collecting reliable raw EMG. This means that the hardware and software limitations can be much more easily overcome. As a result, a larger number of channels can be used simultaneously for data collection and/or sampling time can be increased. Data collection and storage will be limited to the space available on the magnetic medium used.

For a better understanding of the effects of samplinf rates, similar EMG analysis must be done for eccentric and concentric contractions at faster speeds and for different muscles.

REFERENCE

BASMAJIAN (1967). Williams and Wilkins, Baltimore.
BLINOWSKA and VERROUST (1987). Electro. and Clin. Neuro., 27, 349-353.
CHU and CHEN (1985). Arch. of Phys. Med and Rehab., 66, 601-604.
DELAGI, E.F. et al. (1975) C.C. Thomas Publisher, Springfield.
FUGLSANG-FREDEIKSEN and MANSSON (1975). J. of Neurol, Neuros, and Psych., 38, 683-694.
PERRY and BEKEY (1981). CRC Crit. Rev. Biomed. Eng., 7, 1-22.
PETROFSKY and LIND, (1980). Eur. J. of App. Phys., 43, 173-182.
SACK, F.A., (1978). Prentice-Hall,inc. New Jersey.
GANDER and HUDGINS (1985). Electro. and Clin. Neuro., 25, 461-478.
ZIPP, P., (1982). Eur. J. of App. Phys., 50, 41-54.
ZSCHORLICH, V.R., (1989). Electro. and Clin. Neuro., 29, 81-86.

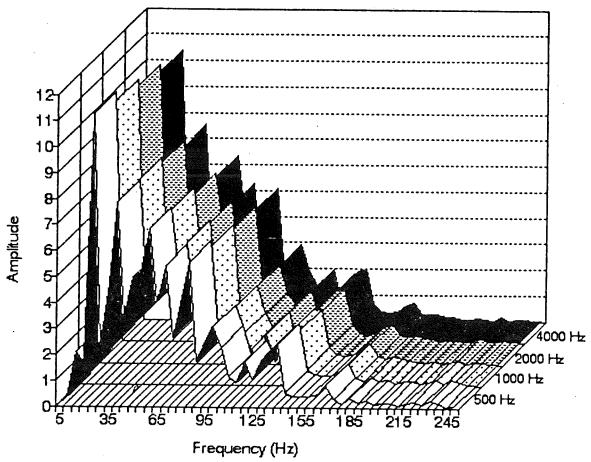

Figure 1. Power spectral Density curves for the 500, 1000, 2000, and 4000 Hz sampling rates.

ACKNOWLEDGEMENTS

This project was partly funded by Natural Sciences and Engineering of Canada. The authors would like to thanks Mr. Andre Russo for his helpful comments.

Proceedings of NACOB II, The Second North American Congress on Biomechanics, Chicago, August 24th - 28th, 1992

EMG-FORCE RELATION OF MAMMALIAN SKELETAL MUSCLE (PART II): EXPERIMENTAL SIMULATION OF RECRUITMENT AND RATE MODULATION USING TEN VENTRAL ROOT FILAMENTS

A. Guimaraes, W. Herzog, M. Hulliger +, Y. Zhang *, S. Day +

Faculty of Physical Education
+ Department of Clinical Neurosciences
*** Department of Electrical and Computer Engineering**
The University of Calgary, AB, Canada, T2N 1N4

INTRODUCTION

We have previously studied the EMG and force response to changing stimulation rates of single ventral root filaments containing alpha motor axons of a cat soleus muscle (Guimaraes et al., 1992). However, under physiological conditions, muscle force is not only determined by rate modulation of motor units but also by the number of active motor units (recruitment) (Burke, 1981). We believe that simulation of the processes of recruitment and rate modulation simultaneously with direct measurments of EMG and force signals from a single muscle may lead to a better understanding of the mechanisms underlying the EMG-force relation. The purpose of this study was to quantify the relation between EMG and force in cat soleus muscle by stimulating a number of ventral root filaments in such a way as to mimick the processes of physiologic recruitment and rate modulation at the same time.

REVIEW AND THEORY

It has been suggested that the force produced by a single muscle may be estimated adequately on the basis of the associated EMG signals and the contractile conditions (e.g. van den Bogert et al., 1988). The precise mechanisms relating EMG to muscular force, however, remain unclear. We are not aware of studies that have used a physiological stimulation protocol of ventral root filaments to study quantitatively the mechanisms that relate EMG to corresponding muscular forces.

PROCEDURES

Two cats were studied. Many aspects of the methods are the same as those presented in the accompanying abstract (Guimaraes et al., 1992). Up to 10 ventral root filaments of the soleus muscle, each containing several motor units, were stimulated in a way to imitate physiological recruitment and rate modulation conditions. Table 1 shows the protocol tested. It contains the order of recruitment of the 10 ventral root filaments (left to right) and the rates at which each filament was stimulated in successive trials (top to bottom). Stimulus pulse trains were irregular (pseudo-random interval distribution with coefficient of variation 12.5 %).

All tests reported here were performed under isometric conditions at a soleus muscle length corresponding to an ankle joint angle of 75 degrees.

RESULTS AND DISCUSSION

The normalized integrated rectified EMG (IEMG) of the soleus muscle obtained during a time interval of 2 seconds for each trial is shown in Figure 1. The rate of increase of IEMG was less pronounced in the initial 2 trials compared to trials 3 to 14. The rate decreased slightly again between trials 15 to 22 and finally reached a plateau. Normalized mean forces were small and increased slowly in the first four trials (Figure 2). From trials 5 to 16, there was a steeper increase in force from one trial to the next. Beyond trial 17 force of the soleus muscle did not increase much, despite significant increases in the stimulation rates of all ten ventral root filaments (Table 1). Figure 3 shows the relation between normalized IEMG and mean force for the cat soleus muscle, using the recruitment protocol shown in Table 1. The results shown were obtained using indwelling (wire) electrodes, and are similar to those obtained using surface electrodes. The results of Figure 3 can be derived from Figures 1 and 2. IEMG increased faster than mean force at low and high force levels. Note that the relation of IEMG and mean force between normalized force levels of approximately 0.08 and 0.8 (Figure 3) may adequately be approximated by a straight line. This result was confirmed in another experiment. The earlier and more pronounced saturation seen for mean force (Figure 2) than for IEMG (Figure 1) explains the curvilinear behaviour at force levels exceeding a normalized value of 0.8. Saturation of force occurs when filaments are stimulated at rates exceeding 25 pps (Guimaraes et al., 1992). In contrast, saturation of IEMG of the soleus muscle does not occur when a single ventral root filament is stimulated. However, when 10 filaments are stimulated at high rates, the IEMG can not be expected to add linearly as action potentials overlap and start to cancel each other. The curvilinear relation between IEMG and mean force at force levels below about 0.08 is not as easily accounted for as that at force levels exceeding 0.8. This particular non-linearity is most likely associated with the protocol adopted in this study, in which filaments were rank ordered according to tetanic force production (i.e. filament 1 was the weakest and recruited first

and filament 10 was the strongest and recruited last). Since IEMG and mean force were not related systematically for individual filaments (most likely due to variations in distance of the motor unit territories in relation to recording electrodes), the non-linearity below force levels of 0.08 could be explained. This problem of non-linearity tends to be reduced when the number of filaments and their respective rates of stimulation increases. Note in Table 1, that trials 1 to 4 contain rates of stimulation that are lower than the rates at which motor units are first recruited during voluntary contractions (Burke, 1981). Thus, the relation between IEMG and mean force could be described as linear or curvilinear depending on the range of force. If trials with frequencies of stimulation below physiological values (i.e. trials 1 to 4) and trials where stimulation rates were so high that forces tended to saturate are excluded (i.e. trials 14 to 27), then the relation between IEMG and mean force becomes virtually linear (r = 0.98).

REFERENCES

Bogert, van den A.J. et al. Biomechanics XI-A, Hollander, Huijing and Schenau, Amsterdan,(pp.68-74), 1988.
Burke, R.E. Handbook of Physiology-The Nervous System II, (pp. 345-422), 1981.
Guimaraes, A. et al. Proceedings of NACOB II, 1992.

ACKNOWLEDGEMENTS

This study was supported by AHFMR, MRC and NSERC (Canada). A. Guimaraes is supported by CAPES and UFRGS (Brazil).

Table 1. Summary of the protocol tested. The rates of stimulation for each filament in each trial is indicated in pps.

Trial	Filament #									
	1	2	3	4	5	6	7	8	9	10
1	3	0	0	0	0	0	0	0	0	0
2	3	3	0	0	0	0	0	0	0	0
3	5	5	3	0	0	0	0	0	0	0
4	5	5	3	3	0	0	0	0	0	0
5	7	7	5	5	3	0	0	0	0	0
6	9	9	7	7	5	3	0	0	0	0
7	11	11	9	9	7	5	3	0	0	0
8	13	13	11	11	9	7	5	3	0	0
9	15	15	13	13	11	9	7	5	3	0
10	17	17	15	15	13	11	9	7	5	3
11	19	19	17	17	15	13	11	9	7	5
12	21	21	19	19	17	15	13	11	9	7
13	23	23	21	21	19	17	15	13	11	9
14	25	25	23	23	21	19	17	15	13	11
15	27	27	25	25	23	21	19	17	15	13
16	29	29	27	27	25	23	21	19	17	15
17	31	31	29	29	27	25	23	21	19	17
18	33	33	31	31	29	27	25	23	21	19
19	35	35	33	33	31	29	27	25	23	21
20	37	37	35	35	33	31	29	27	25	23
21	39	39	37	37	35	33	31	29	27	25
22	41	41	39	39	37	35	33	31	29	27
23	43	43	41	41	39	37	35	33	31	29
24	45	45	43	43	41	39	37	35	33	31
25	47	47	45	45	43	41	39	37	35	33
26	49	49	47	47	45	43	41	39	37	35
27	51	51	49	49	47	45	43	41	39	37

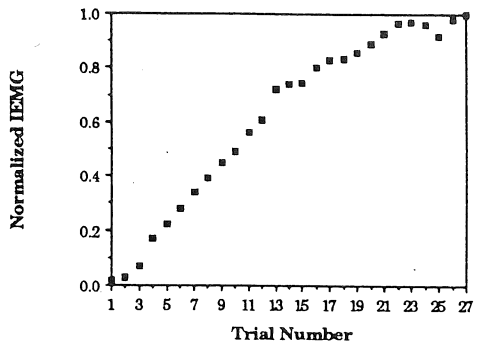

Figure 1. Normalized IEMG response of the cat soleus muscle to a set of trials in which recruitment and rate modulation were implemented by stimulating 10 ventral root filaments.

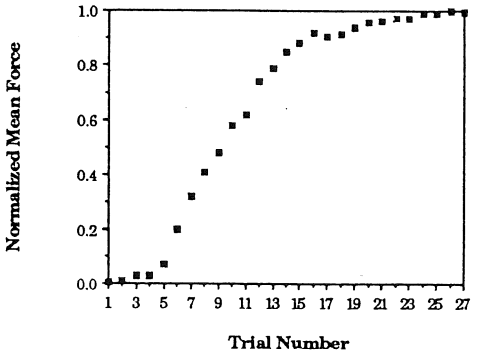

Figure 2. Normalized mean force response of the cat soleus muscle to a set of trials in which recruitment and rate modulation were implemented by stimulating 10 ventral root filaments.

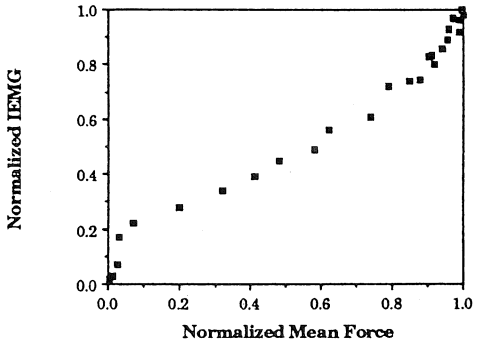

Figure 3. Normalized IEMG-mean force relation of a cat soleus muscle obtained by implementing recruitment and rate modulation of 10 ventral root filaments.

ACCOUNTING FOR ELASTIC RECOVERY IN STRETCH-SHORTENING MOVEMENTS: A MUSCLE MODELLING PERSPECTIVE

Charles S. Lynch and James J. Dowling
Department of Physical Education, McMaster University
Hamilton, Ontario, Canada

INTRODUCTION

A Hill-based muscle model was used to determine the influence of elastic energy recovery in various elbow flexion tasks. The enhanced performance observed in stretch-shortening cycle (SSC) movements could not be accounted for by the same activation-length-velocity relationships which accurately estimated the performance of non-SSC movements. These results suggest that a substantial amount of the enhanced performance resulted from the recovery of strain energy stored in the series elastic component (SEC).

REVIEW AND THEORY

The SSC plays an important role in many human movements. Extensive research has shown that this SSC contributes significantly to enhancing the performance of these activities (Cavagna, 1977). Although this enancement has typically been attributed to the recovery of elastic energy from the muscle's SEC, recent studies have suggested that the enhancement may be largely due to a more effective interaction between muscle lengths, rates of change of length, and activations (Chapman, 1985). The purpose of this study was to establish whether a muscle model, which excludes the abilty to recover elastic energy, is able to accurately estimate the performance of various elbow flexion tasks, with and without a SSC.

PROCEDURES

Eight healthy male subjects performed a variety of elbow flexion and extension tasks. These tasks varied in their range of motion, level of effort and external load. Surface EMG from the biceps and triceps brachii muscles were recorded along with the elbow joint angle and net elbow moment. A Hill-based muscle model was used to estimate the angular impulse generated by the subject in 12 experimental trials: 4 concentric (CO), 4 quick release (QR) and 4 stretch-shortening (SS) contractions. The CO trials started from a relaxed state, the QR trials started from an isometric pre-activation and the SS trials started with an active pre-stretch. The testing procedures were such that the concentric phase of all three conditions began at the same elbow angle. The accuracy of the model's estimates was determined by the RMS error of the angular impulse data over the concentric phase of each trial. The angular impulse generated over the first 100 ms of the concentric phase was used to compare the measured and estimated performance of the 3 types of contractions.

RESULTS

The error of the model's estimates was significantly greater for the SS trials than for either the CO or the QR contractions. These results are summarized in Table 1.

Table I. %RMS error of angular impulse estimates.

	CO	QR	SS
%RMS err	8.3	6.3	14.6

A two-factor ANOVA revealed no significant differences between the measured and estimated angular impulses (at 100 ms) for the CO and QR conditions. However, as can be seen in Figure 1 the model significantly underestimated the true angular impulse in the SS trials.

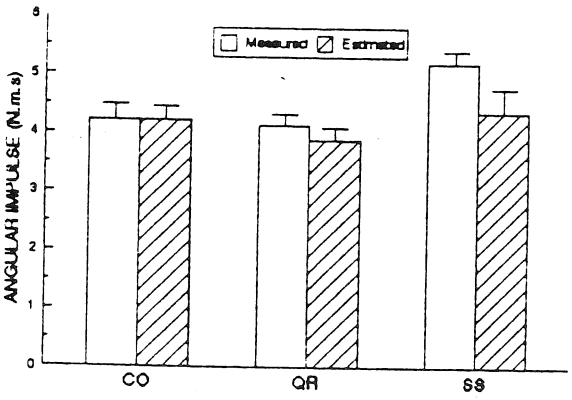

Figure 1. Measured and estimated angular impulses for various types of contractions.

DISCUSSION

The measured values in Figure 1 show that the performance of the SS movements were significantly superior to that of the other conditions. The small %RMS error values listed in Table 1 for the CO and QR conditions show that the muscle model used in this study accurately estimated the angular impulse generated in these types of contractions. The fact that a significant amount of the measured angular impulse was unaccounted for by the model in the SS trials reveals that these contractions most likely exploited a source of angular impulse which was not included in the model. This source was presumed to be strain energy stored in the SEC of the muscle.

The results of this study suggest that the activation-length-velocity relationship of muscle can not completely account for enhanced performance observed in SS movements. Attempts to model muscle should therefore take into consideration the effects of elastic energy recovery. Furthermore, the relative influence of these factors on movement performance seems to be time dependent and probably varies widely between tasks. Finally, attempts to quantify elastic recovery in muscle should also account for the effects of muscle mechanics.

REFERENCES

Cavagna, G.A. Exerc. Sport Sci. Rev. 5:89-127, 1977.

Chapman A.E. et al. in: Multiple Muscle Systems. Springer-Verlag, 1990.

Proceedings of NACOB II, The Second North American Congress on Biomechanics, Chicago, August 24th - 28th, 1992

ELECTRICAL AND MECHANICAL EQUIVALENCE OF HUMAN ELBOW FLEXORS

James J. Dowling, PhD.
Department of Physical Education, McMaster University
Hamilton, Ontario, Canada.

INTRODUCTION

In human movement, the net joint moment generated about most articulations is comprised of the sum of the moments of several individual muscles. The prediction of net joint moments via electromyography (EMG) is simplified if one can assume that one muscle is equivalent to the all other muscles in its functional group. This concept of muscle equivalence was first introduced by Bouisset (1973) were he reported that the elbow joint flexor moment was well represented by the biceps brachii alone. While this finding has been challenged by others (ie. Buchanan, et al. 1989), it is an important concept to muscle modellers and may be better served by a more broad and comprehensive definition of muscle equivalence. In this study, muscle equivalence is defined as the attribution of one or more characteristics of two or more muscles to an individual muscle or smaller group of muscles. Two or more muscles could receive the same neural activation but due to different elements of muscle mechanics (ie. moment arms), produce different moment patterns. Similarity of activation is termed electrical equivalence and similarity of moments is termed mechanical equivalence in this study. The purpose of this study was to examine the electrical and mechanical equivalence of three elbow flexors during static and dynamic elbow flexions and extensions.

METHODS

Smoothed rectified EMG of the biceps brachii (BIC), brachialis (BRA) and brachioradialis (BRD) muscles of three subjects were collected while performing various static elbow flexions and extensions at different joint angles and dynamic flexions and extensions at different speeds and under different inertial loading conditions. Surface EMG was used for BIC and BRD while fine wire EMG was used for BRA. A "Hill type" musculoskeletal model was used to predict the individual muscle moments (Dowling et al. 1987). Time series correlations were performed on the EMGs for electrical equivalence and on the moments for mechanical equivalence.

RESULTS AND DISCUSSION

It was found that overall there was a higher degree of electrical equivalence ($r = 0.869$) than mechanical equivalence ($r=0.824$). The lower mechanical equivalence was due to the different mechanical factors such as moment arms, force-velocity and force-length relationships. On closer examination of the electrical equivalence, it was found that the surface record-

The Sixteenth Annual Conference of the American Society of Biomechanics and
The Seventh Biennial Conference of the Canadian Society of Biomechanics/Société Canadienne de Biomécanique

ings (biceps and brachioradialis) had a greater similarity (r=0.937) than either had with the fine wire recording of brachialis (r=0.841 and r=0.830 for BIC and BRD, respectively). This difference may reflect different activation patterns but is also probably influenced by the much smaller pickup area of the wire recording and possibly not a true measure of the activation of the whole brachialis muscle.

Both electrical and mechanical equivalences were nearly the same during static contractions but a large difference was found during dynamic contractions (r=0.899 and r=0.791 for electrical and mechanical, respectively). Both electrical and mechanical equivalence was higher during rapid movements than during slow movements. This may be an indication that the central nervous system activates the flexors with greater synergy when the movement must be performed quickly. Increasing the task demand by increasing the inertial loading however, decreased the equivalence. Both electrical and mechanical equivalence was higher during unloaded movements than when inertial loads were added.

It was concluded that while activation patterns of the elbow flexors may be quite similar (especially in isometric contractions), caution should be used when considering the mechanical similarities (especially in dynamic movements). The high degree of electrical equivalence (especially between BIC and BRD) may allow muscle modellers to reduce the number of EMG channels that need to be monitored by driving different musculotendon actuators with the same neural drive.

REFERENCES

Bouisset, S. (1973) *New Developments in EMG and Clin. Neurophysiol.* 1:547-583.

Buchanan, T.S., et al. (1989) *J. NEUROPHYSIOLOGY.* 62:1201-1212.

Dowling, J.J. et al. (1987). *BIOMECHANICS XI*: 88-93.

OVERALL	ELECTRICAL	0.869
	MECHANICAL	0.824
OVERALL ELECTRICAL	BIC-BRD	0.937
	BRD-BRA	0.830
	BIC-BRA	0.841
STATIC	ELECTRICAL	0.848
	MECHANICAL	0.856
DYNAMIC	ELECTRICAL	0.899
	MECHANICAL	0.791
UNLOADED	ELECTRICAL	0.917
	MECHANICAL	0.829
LOADED	ELECTRICAL	0.888
	MECHANICAL	0.762
RAPID	ELECTRICAL	0.938
	MECHANICAL	0.834
SLOW	ELECTRICAL	0.790
	MECHANICAL	0.685

TRAUMA AND IMPACT

Podium Session 9

RESPONSE OF THE HUMAN THORAX UNDER DECELERATIVE FORCES

Skrade D, Yoganandan N, Pintar FA, Reinartz J, Sances A, Jr.
Department of Neurosurgery, Medical College of Wisconsin, Milwaukee, WI
Department of Veterans Affairs Medical Center, Milwaukee, WI

INTRODUCTION

While considerable research has been advanced in the past to determine the response of the human thoracic elements under quasistatic and dynamic loading situations, little biomechanical data is available to study the mechanisms of injury and the associated biomechanical parameters under simulated frontal impact conditions with restraint systems. This data is of critical value to the safety engineer due to the advent of seatbelt legislation as well as automatic safety restraints in modern vehicles. Consequently, the present study was conducted to evaluate the dynamic response of the human thorax under decelerations typically encountered in vehicle environments. Dynamic temporal chest deformations, normalized chest compressions, the velocity of chest compression, and the viscous response characteristics (viscous response defined as the product of the velocity and the compression) was derived from data collected using a noninvasive external peripheral instrument for deformation measurement (EPIDM).

REVIEW AND THEORY

Much of the interest in human thoracic response has been driven by the need to understand and mitigate chest injuries in automobile crashes. Initial efforts concentrated on the effects of chest impact on steering wheels, and a great deal of cadaver research was carried out which simulated this (Melvin et al., 1985). With the advent of seat-belts in the 1970's and '80's, newer research needed to be done on thoracic loading due to shoulder belt restraint (Walfisch et al., 1985). Mechanical response under these various loading conditions was quantified in terms of load/deformation, and spinal or sternal accelerations. More recently, there has been interest in quantifying the thoracic response in terms of its viscous characteristics, particularly since the internal viscera are visco-elastic (Viano and Lau, 1988).

One difficult aspect of the research on human thoracic response is to find a reliable technique for measuring this response. The recently developed EPIDM allows for a continuous recording of surface contours representing a transverse cross-section of the thorax during crash simulations (Eppinger, 1989). Previous studies have reported the chest deformation response for the human cadavers under three-point belt restraint in frontal crash simulations (Yoganandan et al., 1991). The present study focuses on the use of the EPIDM to measure thoracic viscous response. The EPIDM is a noninvasive device which can record the discrete peripheral dynamic deformations of the human surrogate thorax. The details of the operational theory, construction, system accuracy, and dynamic response characteristics for the EPIDM are described (Eppinger, 1989). The number of channels or gauges (as often referred to) per chestband varies from 16 to 40. Each gauge (or channel) provides a curvature reading at that particular location of the EPIDM. The curvature values can then be used to derive the contour definition of the thorax at the location of that particular EPIDM.

PROCEDURES

Eight unembalmed human cadavers were procured from the Body Donor Program at the Medical College of Wisconsin. The cadavers were pressurized to approximate *in vivo* conditions in the thoracic vascular and pulmonary systems. The average age of the cadavers was 60 years and the average weight was 74.5 kg. The specimens were instrumented with triaxial accelerometers at the head and at the spinous process location of the first thoracic vertebra. To determine the chest deformation, the external peripheral instrument for deformation measurement (EPIDM) was wrapped around the thorax at the mid-sternum region, approximately at the level of the fourth rib anteriorly. The specimen was placed in the driver's seat of the sled buck and restrained by shoulder and lap belts. Tension in the restraint system was measured by load cells, and an accelerometer on the buck recorded the sled accelerations. A horizontal crash simulator (MTS Systems Corp., Minneapolis, MN) was used to conduct the deceleration sled tests at velocities of approximately 48 kph. The biomechanical data were collected digitally with an onboard data acquisition system with a sampling rate of 12.5 kHz. Data processing included the computation of the temporal thoracic deformation contours based on the EPIDM signals.

Using the EPIDM data analysis routine, contours were computed at 1 ms intervals for the eight human cadaver tests. Software was developed to calculate thoracic compression along the anterior portion of the thorax. This thoracic compression data from the EPIDM was subsequently used to calculate the viscous response according to a previously suggested procedure (Viano and Lau , 1988). Briefly, the compression data was first filtered at 60 Hz, and then differentiated to obtain velocity of compression (V); the velocity data was subsequently filtered at 60 Hz. The viscous response was computed as the product of the V and C, with C the chest compression being normalized by dividing by the surrogate chest depth.

RESULTS

The lap belt forces ranged from 3.5 to 5.2 kN and shoulder belt forces ranged from 6.1 to 8.8 kN. The average peak thoracic compression normalized with respect to chest depth (C_{max}), the peak velocity of compression (V_{max}), and the average peak viscous response (VC_{max}) was 0.33, 3.54 m/s, and 0.98 m/s, respectively. Pathological findings at autopsy revealed bilateral rib fractures in all the specimens. In addition, clavicle fractures and sternum fractures also occurred. The Abbreviated Injury Scale (AIS) rating ranged from 4 to 6 based on autopsy findings. In one case soft tissue injuries occurred; a laceration of the lung pleura at the

left lower lobe and liver laceration in the area of the falciform ligament insertion.

DISCUSSION

The application of the viscous criterion (VC_{max}) is claimed to be a more valid predicator of injury than a compression criterion (C_{max}) when the maximum velocity exceeds 3 m/s (Viano and Lau, 1988). In the present study, average velocity for the cadaver tests was 3.54 m/s suggesting a possible use of the viscous criterion in describing the mechanisms of injury to the human thorax. It should be noted that the compression criterion pertains to injury of the elastic elements of the thorax which are the skeletal parts. In addition, an underlying assumption is that with increased damage to the protective skeleton, the internal soft tissues are more likely to be damaged. However, soft tissues also exhibit rate dependent responses. The viscous criterion was therefore developed to explain the mechanism of soft tissue injuries occurring prior to or even in the absence of skeletal trauma (Viano and Lau, 1988). VC_{max} value of 0.98 m/s found in the present study compares favorably with an earlier study of Cesari and Bouquet (1990) who reported an average VC_{max} of 0.77 m/s and under dynamic seatbelt loading.

It is well known that biological tissues exhibit rate dependent characteristics. Consequently, viscoelastic effects come into play during dynamic loading situations. The traditional procedure of placement of accelerometer and force gauges to document the biomechanical parameters during impact situations in a cadaver often introduces additional constraints on the specimen. The noninvasive EPIDM device, in contrast, provides an alternative method to derive the secondary variables such as normalized chest compression, velocity of compression, and viscous response of the chest by documenting the superficial local chest curvatures as a function of time during the impact event. Our studies have clearly shown the use of this device in deriving the secondary variables which can be used to compute the traditional injury predictors such as the viscous response. These data can be used to understand the mechanism of injury as well as to develop anthropomorphic test devices with improved biofidelity.

REFERENCES

Cesari D, Bouquet R: Proc 34th Stapp Car Crash Conf, Society of Automotive Engineers, Warrendale, PA, 1990, pp 73-81.

Eppinger R: Proc 33rd Stapp Car Crash Conf, Society of Automotive Engineers, Warrendale, PA, 1989, pp 21-28.

Melvin J, et al: Report No. DOT HS 807042, US Dept of Transportation, NHTSA, 1985

Viano D, Lau I: J Biomech 21(5):387-299, 1988.

Walfisch, et al: Proc 29th Stapp Car Crash Conf, Society of Automotive Engineers, Warrendale, PA, 1985, pp 49-68.

Yoganandan N, et al: Proc 35th Stapp Car Crash Conf, Society of Automotive Engineers, Warrendale, PA, 1991, pp 47-67.

ACKNOWLEDGMENT

This research was supported in part by DOT NHTSA Grant DTNH22-89-Z-07305, PHS CDC Grant R499CCR703640, and Department of Veterans Affairs Medical Research Funds.

RESPONSE OF A DYNAMIC MODEL OF HEAD-NECK TO EXTENSION WHIPLASH

H. M. Lankarani, R. Menon and S. Malapati

Mechanical Engineering Department
National Institute for Aviation Research
The Wichita State University
Wichita, KS 67208

INTRODUCTION

There has been a great interest in the mechanisms that cause injuries to the head-neck. This has simulated the development of many different methods, to study the effects of crashes under varying conditions. Field observations of the accidents do not provide enough data for engineers or physicians to determine how the mechanical energy induced by impact cause head injuries. This requires the knowledge of quantitative values such as forces, displacements, and accelerations. Measurements were made on inanimate models (Landkof et al.,1976; Mertz and Patrick,1971), cadavers (Wisemans, 1987; Schneider and Bowman, 1978), animals (Hodgson, 1970). Many different, two and three dimensional models have also been developed (Deng and Goldsmith, 1987; Huston et al.(1976); Reber and Goldsmith (1979); Lankarani et al. (1990). Computer models and simulation methods have lately become the most popular method of determining the cause of injuries. Computer models and methods avoid the necessity of experiments involving cadavers, laboratory animals and anthropomorphic dummies, hence cost efficient, less time consuming and less controversial. They yield substantial and more detailed results quickly, and are capable of simulating many different crash scenarios which may not be feasible, or more still possible, in a laboratory program.

This paper does a study of a multibody model which consists of the head, and the seven vertebrae (C1 through C7) attached to the upper thoracic region (T1) combined with the torso as a rigid base. The joints between the vertebrae allow rotations. The effects of muscles, intervertebral discs, cartilage, and ligaments, cerebrospinal fluids, and other tissues are depicted by nonlinear rotational spring dampers. The aim of this paper was to study the accuracy of the model and its response to extension whiplash conditions. For the purpose of validation, experimental and model simulation results obtained by Huston et al.(1976) was considered. The response of the model seemed to be quite accurate when compared to the experimental and analytical results of Huston et al. With this simple model, a variety of head-neck surges can be simulated and mechanisms of injuries be determined.

DYNAMIC MODELING

Dynamic modeling involves selecting a proper set of coordinate system, defining a kinematic model, proper initial conditions, forces, and the inertia properties of components of the system, formulating and solving the equations of motion that make up the mechanism, and kinematic constraints that act between pairs of bodies. Body-fixed frames must be attached to each body with their origin at the center of mass of the body. As shown in Figure 1, nine bodies were considered, the head, the seven vertebrae elements C1 through C7 which is attached to the upper thoracic region (T1) combined with the torso as a rigid base. All the bodies have reasonably correct proportions, and inertial properties. The joints mimic the kinematic constraints imposed by the upper spinal column, and they allow rotation in all directions within the anatomical limits. The effects of muscles, intervertebral discs, cartilage, and ligaments, cerebrospinal fluids, and other tissues are accounted for by nonlinear translational and rotational springs and dampers. Kinematic information on head and neck elements including the range of rotation in the flexion and extension directions were all taken into consideration. Masses and moments of inertia were taken from Merrill T. et al.(1984),and Tsai (1990).

Once the model of the head-neck is completed a variety of input forcing conditions may be applied to this model, and its behavior under each specific conditions be studied.

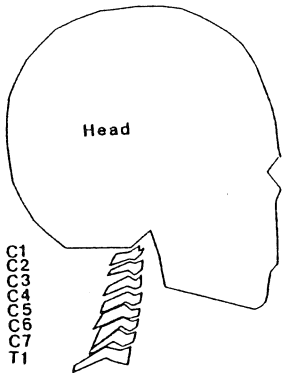

Figure 1. Head-neck model

COMPUTATIONAL PROCEDURES

The response of the model to varying conditions was generated by a dynamic analysis code. A vector of Cartesian coordinates was selected for all the elements in the system. Kinematic relations were developed describing dependency of the coordinates imposed by the revolute joints. The Cartesian coordinates chosen together with the constraint, velocity, and acceleration equations completely describe the geometrical characteristics or the kinematics of the system. A set of Newton-Euler differential equations of motion were constructed for each body in the system. The differential equations were solved using the concept of Lagrange multipliers. In order to damp out the errors in the constraint and velocity equations, the technique of constraint-violation stabilization was used. A variable-step/variable-order multistep algorithm was used as the numerical integrator. The output of the program gave the coordinates, velocities, accelerations, rotational spring damper data, and the reaction forces of each element/body, at different time intervals. A simple post processing graphics program was also developed to draw the configuration of the system at different time intervals.

RESULTS AND DISCUSSION

For the validation of this model a comparison was made with a study done by Huston et al. (1976). Huston et al. presented data from experiments with seated cadavers subjected to pendulum head

impact and a corresponding open-chain type system analysis. The cadavers were confined in a manner so as to allow only head motion during impact. The impact pulse achieved was of a triangular shape. The present model was subjected to a triangular shaped crash force similar to that achieved by the experiment conducted by Huston et al., on the rigid base. The force had a peak of 4000 N and a period of 5 ms. The force was applied in the sagittal-plane, anteriorly at the base to T1. With this force as an input, the response of the model was determined. The configurations of the head-neck system are shown in Figure 2, at some discrete time junctures. From Figure 3, it can be seen that the acceleration of the head in the horizontal (x) direction of the present model agreed well with respect to the shape of the Huston et al. model, whereas the magnitude was lower and closer to that of the experiment. The horizontal velocity component of the present model falls between both the experimental and model velocity components of Huston et al. The horizontal displacements of this model match the Huston et al. model well in the beginning and then tend to match the Huston experiment more. Small discrepancies could occur due to some differences in the modelling techniques, parameters like masses, moments of inertia, stiffness and damping coefficients which for this model were different from the ones used by Huston et al.

In conclusion, the model seems accurate and its responses seem quite fair. This model is much simpler as compared to Huston et al. model, because it considers the effects of all the tissues, muscles, etc combined. A variety of input forcing conditions may now be applied to this model, and its behavior under each specific conditions be studied. These results could indicate whether the displacements, deformations, velocities and accelerations produced were within or beyond the ones which are clinically considered injuries.

REFERENCES

Deng, Y.C., and Goldsmith, W., "Response of a Human Head/Neck/Upper-TorsoReplica to Dynamic Loading - -II. Analytical/Numerical Model," J. Biomechanics, Vol.20,pp.487-497,1987.

Hodgson, V., "In Impact Injury and Crash Protection,"(Edited by Gurdjian, E.S., et. al.), pp.275-307. Thomas, Springfield. 1970.

Huston, J.C., Passerella, C.E. and Huston, R.L. (1976) "Numerical Prediction of Head/Neck Responses to Shock Impact." Measurement and Prediction of Structural and Biodynamic Crash-Impact Responses (Edited by Saczalski, K.J. and Pilkey, W.D.) pp.137-149. ASME, New York.

Landkof, B., Goldsmith, W., and Sackman, J.L., "Impact on a Head-Neck Structure," J. Biomechanics, Vol.9, pp.141-151, 1976.

Lankarani, H.M., Ma, D., and Ermer, G.,"Biodynamic Simulations of an Aircraft Pilot/Passenger in Various Crash Environments," NIAR Report No.90-6,National Institute for Aviation Research, The Wichita State University, April 1990.

Merrill T., Goldsmith W. and Deng Y.C., "Three-Dimensional Response of a Lumped Parameter Head-Neck Model due to Impact and Impulsive Loading," J. Biomechanics, Vol.17, No.2, pp 81-95, 1984.

Mertz, H.J., and Patrick, L.M., "Strength and Response of the Human Head-Neck," Proc.15th Stapp Car Crash Conf., pp.207-255. SAE Paper No. 710955, 1971.

Reber, J.G., and Goldsmith, W.,"Analysis of Large Head- Neck Motions," J. Biomechanics, Vol.12,pp.211-222.

Schneider, L.W., and Bowman, B.M., "Prediction of Head- Neck Dynamic Response of Selected Military Subjects to -G_x Acceleration," Aviation, Space, and Environmental Medicine, Vol.49, No.1, pp.211-223, 1978.

Tsai, D.,"Computer Modeling of the Human Head and Neck to Shaking Motion," M.S. Thesis, University of Arizona, 1990.

Wisemans, J., "Comparison of Human Volunteer and Cadaver Head-Neck Response in Frontal Flexion," Proc.31st Stapp Car Conference, Paper No. 872194, 1987.

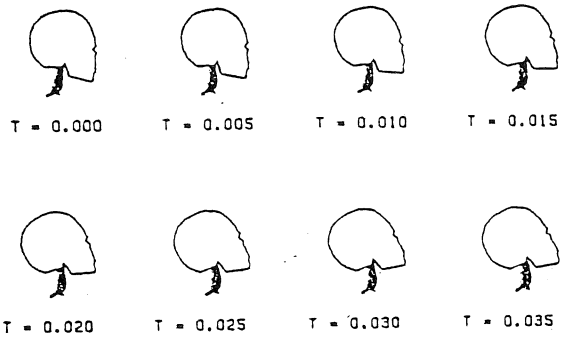

Figure 2. Configuration of the head-neck system to a triangular pulse applied at the base in the anterior direction.

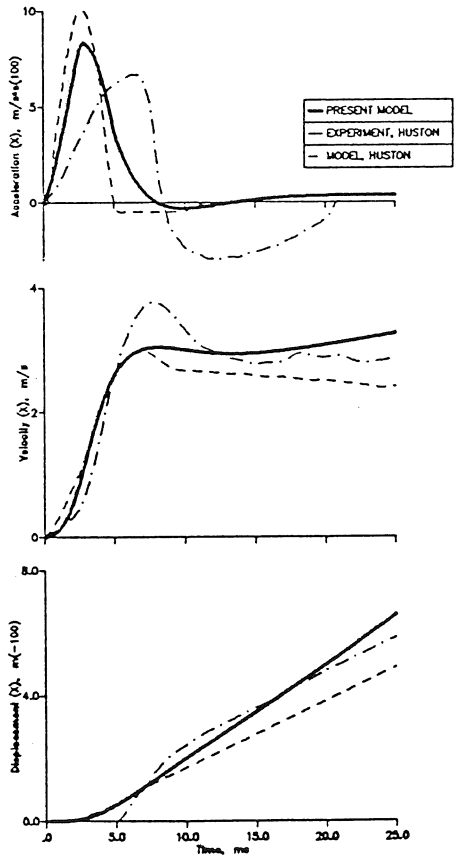

Figure 3. Horizontal components of acceleration, velocity and displacement.

Neck Segment Loading in the Hybrid III Due to Lateral Impacts

Patrick J. Bishop, Weijia Lu
Department of Kinesiology, University of Waterloo, Ontario

Cervical spinal trauma, common in sport pursuits and motor vehicle accidents, is often caused by a head first collision with the neck partially flexed. The head-neck-torso system is brought to rest in stages rather than uniformly (Burstein, et. al., 1982; Bishop, et. al., 1986) so that the neck, trapped between the fixed head and moving torso, is subjected to large compressive forces because it has to manage the very high levels of energy being imparted to it. To reduce these neck loads to tolerable levels (eg 2000 N) would require a minimum thickness for helmet or surface padding of 43 mm (Wells, et. al., 1987). Cadaveric studies showed that extension impacts resulted in injuries to the middle and upper cervical spine levels (Nusholtz, et. al., 1983; Yoganangam, et. al., 1989) while a quasi-static analytical model of the cervical spine in extension predicted that the compressive loads on the cervical spinous processes would exceed failure tolerance by 27% to 52 % in a low velocity, face first impact (Li, 1991) .

One additional strategy for preventing these injuries is that of diverting the axial compressive forces from the cervical spine by means of a glancing blow that would produce lateral bending of the neck (Bishop, et. al., 1990). Using an anthropometric test dummy (ATD) under simulated collision showed that the compression forces recorded at the atlanto-occipital (a-o) junction were substantially reduced depending upon the angle of impact. The present study extends this work and attempts to predict the loads at different segments(S) of the ATD neck in response to glancing blows.

Methods

Several collision simulations were conducted using Hybrid III ATD travelling at 1.8 $m.s^{-1}$. Force and moment data recorded from a transducer located at the a-o junction and position information obtained from an infra-red imaging system were combined with an analytic computer model of the ATD neck under lateral bending (Figure 1) to predict the compressive and shear forces on the individual ATD neck segments. The modelling procedures were similar to those reported elsewhere (Bishop, et. al., 1986; Wells, et. al., 1987) except that the position of each neck segment was obtained from a WATSMAT Infra-red Imaging System (Northern Digital). The relative angle of each segment, defined as shown on Figure 1, was calculated by equation 1. The model outputs include the total compressive and shear forces and bending moments on each segment of the Hybrid III neck.

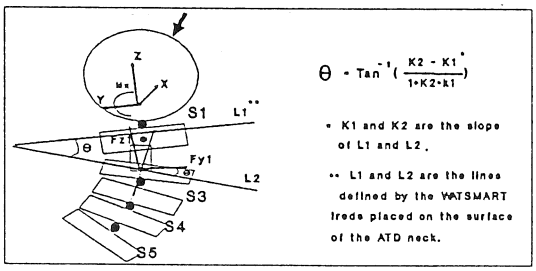

Figure 1. ATD Neck Model and Coordinate System

Three glancing blows were conducted by turning the impact barrier 70° and 50° to the flight of the ATD. The force signals were amplified and digitally converted at a sampling rate of 2300 Hz/channel. Two Watsmat 3-d motion cameras recorded the displacement of eight infra-red diodes (lred) on the surface of the ATD neck. The sampling rate for each lred was 400 Hz and the displacement data were low pass filtered at 40 Hz.

Results

A typical force-time history for each neck segment, predicted by the model , is shown in Figure 2. The neck bending angle at 50° and 70° impacts were 20° and 16°. The total loading at each neck segment is summarized in Table 1. The data were the average of three trials. The outputs from our model indicate that the glancing impact at 70° did not effectively reduce the compressive force

Table 1. Peak shear and axial forces and moment of force at each ATD neck segment. (n=3 ,v=1.8 m/sec)

ATD level:	Axial force 70°/50° (KN)	Shear 70°/50° (N)	Moment 70°/50°(Nm)
A-O	-4.45/-2.18	327/487	89/62
S1	-4.55/-2.19	-365/434	86/53
S2	-4.51/-2.2	-644/396	91/42
S3	-4.52/-2.2	-599/398	103/34
S4	-4.52/-2.2	-577/406	114/26
S5	-4.4/-2.21	-1189/304	127/17

which averaged over 4000 N at each segment. The shear force increased significantly up to S5. The moment of force was 86 Nm. at S1 and then increased to 150 Nm. at S5 level.

When the barrier was turned to 50°, the compressive force at each neck segment was reduced to about 2200 N, a 50% decrease compared to 70° impact. The same situation was found for the shear force, where the

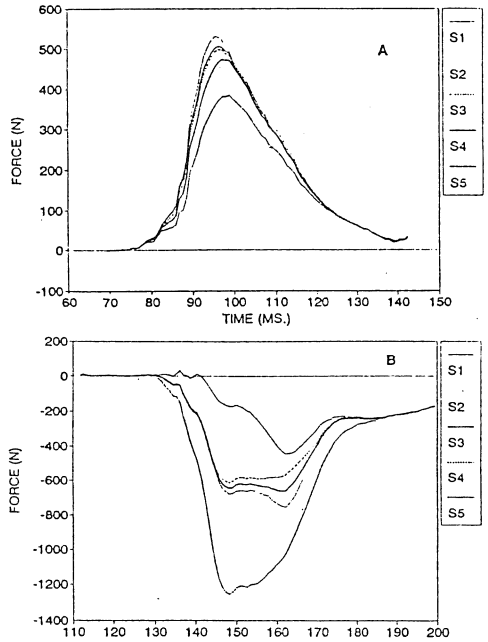

Figure 2. The Shear Forces at Each Neck Segment. A: 50 Deg. Glancing B: 70 Deg. Glancing. Impact Speed=1.8 m/sec.

maximum load at a-o junction was 487 N. and the moments declined from 62 Nm. at a-o junction to -14 Nm. at S5. The results for different trails at the same barrier angle were consistent.

Discussion

Based on numerous cadaver tests (Hodgson, et al. 1980), many failure modes were possible depending on the orientation of neck prior to impact. From Table 1, a change in impact angle from 70° to 50° caused a substantial reduction in ATD neck loading. Estimated compressive failure loads in humans range from 3000 N(Yamada, 1973) to 6000 N (Roaf, 1960). The compressive forces measured here were well below these levels for glancing blows at 50°. Mertz et al. (1971) reported noninjurious neck shear under static load of 190 lb(700 N). Thus, at 50° the increase in lateral shear which accompanied the reduction in Fz, and which was a maximum of 487N, was well below the above tolerance level. However, for the glancing impact at 70°, the shear forces at S5 were much larger than the above limits and are of concern.

Additional observations of these two different glancing angle impacts indicated that at 70°, the head was restrained by the barrier after impact, and the neck was trapped between the fixed head and the still-moving torso. This was similar to the impact posture described by others (Yoganandan, et. al., 1989; Bishop et. al., 1989) for direct axial impact. Moreover, the slightly off-axial impact led to lateral bending at S5 level which caused a large shear load at these locations. Yoganandan et. al.,(1989) studied the mechanism of spinal injuries with sixteen fresh intact human male cadavers and found that the head impact force was much larger with head restrained than when unrestrained. There were also more cervical fractures in the restrained compared to the unrestrained case. For 50° glancing blows the neck displacement observed from the Watsmat Ireds and from high speed film(500 fps) revealed that the head and neck were unrestrained after impact and turned from their starting sagittal plane to move parallel to the barrier plane (which was rotated 50°) for more than 20 cm. before landing. As such, the neck was not trapped between the head and torso.

As well, the high-speed film and the displacement data of the Ireds further showed that in the 50° impact, and neck segments except S1 were bent toward +y as shown in Figure 1. In contrast, the neck was bent to the opposite direction in 70° impact. These facts conform to the outputs of the computer model. Reference to Table 1 and Figure 2 shows that the shear forces were of opposite sign between 70° and 50° impacts which led to increased moments of force for 70° impacts and decreased moments at 50°'s from S1 to S5. In an axial loading study of neck flexion and extension (Wells, et. al., 1987), the high moments were found at S5 level, similar to our 70° impact situation.

The data displayed in Table 1 only show the total loads at each cervical segment and in real life, these loads would have to borne by the vertebral bodies, the facets, the intervertebral disks, the ligaments and muscles (Li, 1991). Whether the loads on the cervical segments would lead to failure of the facets, ligaments or disks require further studies.

In conclusion, model outputs indicated that there was no significant reduction in the compressive and shear forces of the ATD neck at 70° glancing impact. In contrast, at the 50° impact, the compressive forces were reduced by about 50%, and the shear forces were also substantially reduced.

Reference

Bishop, P. et al. Passenger Comfort, Convenience and Safety, SAE Pub.P131, 1986.
Bishop, P.J. et al. Presented at CSB, 1990.
Burstein, et al. Athletic Injuries to the Head, Neck and Face, p139, 1982.
Hodgson V.R. et al. 24th Stapp CCP, SAE, No. 801300, 1980.
Li, Y. M.S Thesis, University of Waterloo, 1991.
McElhaney, J.H. et al. SAE Paper No. 831615. 1983.
Nusholtz, et al. Proc 27th Stapp CCP, SAE, 1983.
Panjabi, M.M. et al. Spine. Vol. 16, No. 8, 1991.
Seemann, M.R. et al. SAE Paper No. 861892. 1986
Wells, R.P. et al. Int. J. of Sport Biomech., pp. 432-442, 3, 1987.
Wells, R.P. et al. Biomech.in Sports, Inst. of Mech. Eng., London, England, 1987
Yamada, H. Strength of Biolo. Materials. Robert E. K., Huntington, N.Y. 1973.
Yoganandan, N. et al. J.Biomech. Eng., Vol.111, pp.250, Aug. 1989.

Proceedings of NACOB II, The Second North American Congress on Biomechanics, Chicago, August 24th - 28th, 1992

RESPONSE OF THE OCCIPITO-ATLANTO-AXIAL (C0-C1-C2) COMPLEX IN RIGHT AXIAL ROTATION AS A FUNCTION OF RATE OF LOADING

V.K.Goel, L.G.Gilbertson, H.Chang, J.M.Wnterbottom, C.R.Clark, and A. Patwardhan*

Departments of Biomedical Engineering and Orthopaedics, University of Iowa, Iowa City, IA 52242
*V. A. Hospital, Hines, Ill 60601

INTRODUCTION

The torque-angular deformation until failure of the ligamentous occipito-atlanto-axial complex subjected to variable loading rate (dynamic) in axial rotation was characterized using a biaxial MTS system. A special fixture and gear box which permitted right axial rotation of the specimen until failure without imposing any additional constraints were used to obtain the data. The specimens were divided into four groups and tested until failure at four different loading rates: 4°/sec, 50°/sec, 100°/sec and 400°/sec. The stiffness of the specimens increased with the increase in the loading rate. The average maximum resistance torque increased from 13.6 Nm at 4°/sec to 27.9 Nm at 100°/sec. The difference between the 100°/sec and 400°/sec values was not significant. The corresponding angular rotation data (65 - 79 degrees), however, did not show any significant variation with loading rate. Post-test dissection of the specimens indicated that the type of injury observed was related to the rate of axial loading imposed on a specimen during testing. The failure mode changed from bony failure in specimens tested at 4°/sec rate to ligamentous rupture at higher rates of loading.

REVIEW AND THEORY

The occipito-atlanto-axial (C0-C1-C2) complex is loosely held together by an intricate arrangement of bony structures and ligaments. Muscular tissue provides the much needed stability. These characteristics make the joint very susceptible to impact-injury. Impact to the head may cause the neck to flex, extend, bend laterally or rotate axially depending upon the direction of the impact. Qualitative clinical data about the role of various structures in providing stability and the structures that may fail is available in the literature. Quantitative data especially under dynamic conditions, however, is sparse. The purpose of this study was to quantify the dynamic response of the C0-C1-C2 complex in axial rotation.

PROCEDURES

Fresh human cadaveric ligamentous cervical spine specimens (skull to C7) were obtained at the time of autopsy. A total of 20 specimens were used in this study. The specimens, prior to testing, were cleaned of extraneous soft tissue. Each specimen was dissected across the C2-C3 or C3-C4 disc and part of the skull was also dissected to obtain a C0-C1-C2 specimen. The C2 (or C2 & C3) vertebra was potted in order to facilitate its fixation within the MTS machine. A loading frame was attached rigidly to C0. The base of the prepared specimen was bolted down to the actuator of a biaxial MTS testing system. The loading frame was attached to the upper cross-head of the MTS via a specially designed fixture. The fixture transmits the torque from the MTS actuator through the loading frame to the specimen, while permitting the specimen to move freely in other

planes/directions. The specimens were twisted until failure and the resulting torque-angular deformation was recorded using a computer. Specimens were divided into four groups and tested at a specified rate of loading: 4°/sec, 50°/sec, 100°/sec, or 400°/sec. Specimens were dissected following tests to examine the mode of failure and the structures that failed.

RESULTS AND DISCUSSION

The shape of the curve (Figure 1), in general, can be divided into four zones: region of least resistance (straight line; OA) -- a transition zone; AB -- region of increasing resistance (straight line; BC) -- and finally the transitional failure zone; CD. The plots clearly indicated that specimens exhibited an increase in stiffness at higher loading rates slope of the straight line regions increased) and that the width of the transitional zones also decreased. Table 1 lists the average values of the torque (Nm) and the corresponding angular rotation for points A, B, C, and D as a function of the loading caseThe failure torque increased from 13.6 Nm at 4°/sec to 27.9 Nm at 100°/sec. The difference between the 100°/sec and 400°/ sec values was not significant. The failure occured at about 70 degrees of axial rotation; angular rotations did not show any significant variation with the rate of loading. Post-test dissection of the specimens revealed that the type of injury observed was related to the rate of loading imposed on a specimen during testing, Table 2. The rupture pattern changed from bony fractures of the odontoid process at 4°/ sec to ligamentous rupture of the alar ligaments at the higher rate of loading. The results indicate that the C0-C1-C2 complex becomes stiffer with the increase in loading rate; however, the angle at which the failure occurs does not show any significant variation. The mode of failure changes from bony avulsion to soft tissue rupture with the increase in loading rate.

ACKNOWLEDGMENTS

Work supported in part by a grant from NIH (AR 40166-01) and grant from V. A. Administration.

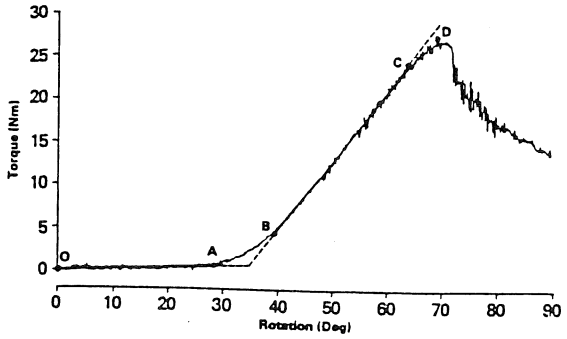

Figure 1

TABLE 1

	Theta (deg)				Torque (Nm)			
Loading rate (°/sec)	4	50	100	400	4	50	100	400
A	20.7	27.7	29.2	30.0	0.5	0.6	1.0	1.5
	(6.5)	(5.8)	(5.1)	(7.1)	(0.6)	(0.2)	(0.4)	(0.6)
B	29.9	37.4	40.1	30.0	2.0	3.0	4.6	1.5
	(11.3)	(5.9)	(6.0)	(7.1)	(1.3)	(0.7)	(1.6)	(0.6)
C	57.8	56.5	65.9	57.8	11.9	13.0	23.7	20.3
	(11.4)	(6.7)	(3.9)	(8.4)	(3.9)	(1.7)	(8.9)	(5.0)
D	68.1	67.8	77.7	64.7	13.6	14.3	27.8	23.2
	(13.1)	(8.8)	(7.5)	(10.9)	(4.5)	(1.4)	(8.9)	(7.8)

( ): S.D.

TABLE 2

Number of cases At Various Loading Rates

Loading rate (deg/sec)	4	50	100	400
Rupture of C1-C2 joint capsule	6	4	5	5
Rupture of posterior C1-C2 ligament	6	4	5	5
Fracture of dens	4	0	0	0
Avulsion of alar ligament at C0	1	1	0	1
Rupture of alar ligament	0	2*	3*	2*

* partial

ENERGY COSTS

Podium Session 10

Proceedings of NACOB II, The Second North American Congress on Biomechanics, Chicago, August 24th - 28th, 1992

MECHANICAL ENERGY MANAGEMENT IN CYCLING: HAMSTRINGS AND GASTROCNEMIUS INTERCOMPENSATE TO BALANCE SYSTEM ENERGY

J.P. Broker and R.J. Gregor
Department of Physiological Science
UCLA, Los Angeles, CA 90024-1568

Introduction

During walking, vertical oscillations of the body center of mass require that mechanical energy be generated at the sources (joints) during one period of the step cycle, only to be absorbed at the sources thereafter. Wells (1988) reported that although some of the energy absorbed at the sources during walking can be transferred to adjacent sources (joints) via actions of two-joint muscles, such energy saving *intercompensations* are limited, and a large fraction of the absorbed energy must be stored in elastic structures and recovered, or degraded to heat within active muscle.

In cycling, energy dissipation to the environment is the task goal. Early attempts to quantify mechanical energy expenditure (MEE) during cycling used a kinematic approach and dramatically overestimated the work performed. More recent investigations suggest that an energy balance can be achieved with only a moderate amount of energy generated in excess of that delivered to the environment (Ingen Schenau et al., 1990). Furthermore, intercompensatory actions of specific two-joint muscles in the lower extremity may uniquely reduce system MEE during cycling to precisely that delivered to the environment This study evaluated the management of mechanical energy during cycling. Energy source characteristics were used to (a) quantify the possible energy savings resulting from appropriate actions of two-joint muscles, and (b) expose probable intercompensatory mechanisms related to two-joint muscle actions during cycling.

Methods

Twelve competitive cyclists rode a racing bicycle on a Velodyne trainer at five conditions of cadence and load. Pedal forces were monitored by piezoelectric transducers within clipless compatible pedals. Joint markers fixed to the right lower limb were tracked by a high speed video camera (Vicon) at 200 fps. Newtonian equations applied to a rigid body system determined hip, knee, and ankle generalized muscle moments (GMMs), reaction forces ($P_{FJ}s$) , joint muscle powers ($P_{MJ}s = GMM_j \cdot \dot{\theta}_{j,}$) and joint reaction force powers ($P_{FJ}s = \bar{F}_J \cdot \bar{V}_J$). Source contributions to system energy were defined as the $P_{MJ}s$ at the hip, knee, and ankle, plus the hip P_{FJ}.

Three MEE models were formulated to characterize the energetic advantage associated with appropriate actions of two-joint muscles during cycling. Two models estimated MEE under hypothetical single-joint muscle (no intercompensation - MEEC) and multi-joint muscle (unlimited intercompensation - MEEFIC) conditions. A third model (MEELIC) used a deterministic algorithm to apportion $P_{MJ}s$ to single- and two-joint muscles and muscle groups in accordance with known two-joint muscle anatomy, appropriate muscle mechanical parameters, and minimum mechanical energy expenditure criteria. Source interactions defined by the MEELIC model were contrasted with the simpler MEEC and MEEFIC models and compared to activation profiles of lower extremity muscles reported for cycling.

Results and Discussion

Mean instantaneous net and summed source powers for the three energy models at 100 RPM/250 W are displayed versus crank angle in Figure 1. Excess power production for the MEEC model is associated with negative P_{MJ} source actions at the ankle during the first quadrant (30 to 70 degrees), at the knee during the second quadrant (125 to 160 degrees), again at the ankle during the third quadrant (180 to 270 degrees), and at the hip throughout recovery (180 to 360 degrees). Under conditions of full intercompensation (MEEFIC), regions of MEEC excess power production during the first half of the pedal cycle are eliminated. Energy absorbed at the ankle (30 to 70 degrees) is fully transferable to the knee. Later in the cycle, energy absorbed at the knee (125 to 160 degrees) is fully transferable to the hip and ankle. During early recovery, energy absorbed at the ankle and hip is mostly transferable to the knee -- where energy was being liberated.

According to the MEELIC algorithm, energy absorbed at the ankle during the first quadrant is not transferable to the adjacent joint (i.e., the knee). GMMs at the ankle and knee at this time are not

consistent with energy transfer mechanics. Between 125 and 160 degrees, energy absorbed at the knee is fully transferable to the ankle (gastrocnemius) and hip (hamstrings). Intercompensations between the hip and knee (hamstrings) and between the ankle and knee (gastrocnemius) attenuated most of the excess power production early in recovery, and a much smaller portion thereafter.

Gastrocnemius and hamstring power profiles derived by the MEELIC model at the 100 RPM/250 W condition are shown in Figures 2 and 3. Total muscle powers are apportioned to the adjacent joints. The gastrocnemius muscle transfers energy from the knee to the ankle during the second quadrant, and from the ankle to the knee during the third. The gastrocnemius never dissipates energy. The hamstring muscles transfer energy from the knee to the hip during the second quadrant, and from the hip to the knee during the third. Between 260 and 310 degrees, the hamstrings are seen to dissipate energy.

Intercompensations primarily involving simultaneous actions of the gastrocnemius and hamstrings muscles reduced the energy dissipated to non-transferable sources during pedalling to less than 6.0 J per limb, and the corresponding MEE associated with single-joint muscle actions alone by up to 14 percent. The energetic advantage of two-joint muscle intercompensations was enhanced at higher bicycle power levels. Furthermore, muscle actions predicted by the MEELIC algorithm agreed remarkably well with reported muscle activation patterns during cycling. Slight differences could be attributed to passive element energetics and energy transport mechanics using antagonist muscle actions. The results were used to suggest that (a) MEE minimization may be achieved during cycling with appropriate actions of two-joint muscles, and (b) stretch-shorten muscle actions may not be necessary to reduce MEE in cycling.

References

Ingen Schenau, G.T. van, et al. *Eur. J. Appl. Physiol,*. **61**, 11-19, 1990.
Wells, R.A. *J. Biomechanics* **21**, 955-964, 1988.

Acknowledgments

The authors thank the U.S. Olympic Committee and the Department of Rehabilitative Services at UCLA.

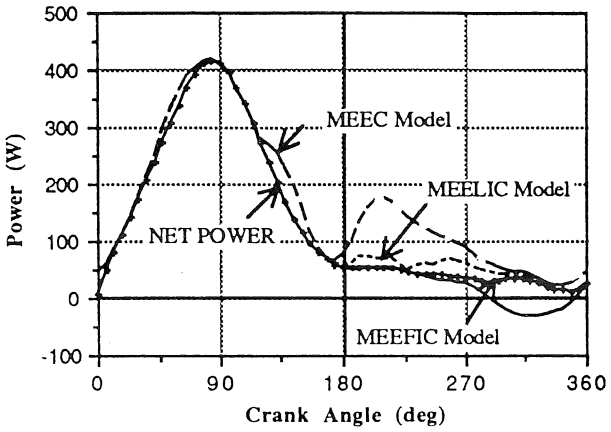

Figure 1. Mean instantaneous net (solid) and summed source powers for the three energy models at 100 RPM, 250 W.

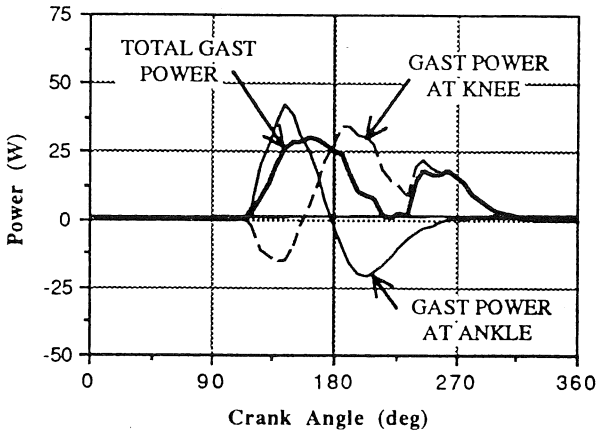

Figure 2. Gastrocnemius power profiles at 100 RPM, 250 W. Total power (thick solid) is apportioned to the knee (dashed) and the ankle (thin solid).

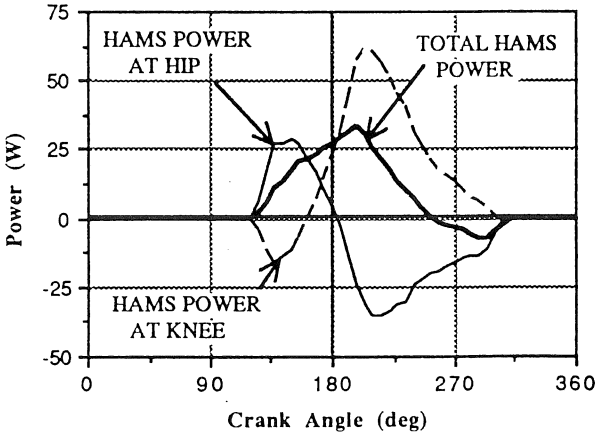

Figure 3. Hamstrings power profiles at 100 RPM, 250 W. Total power (thick solid) is apportioned to the knee (dashed) and the hip (thin solid).

MECHANICAL POWER AND ENERGY EXPENDITURE IN LEVEL TREADMILL RUNNING

Robert A. Hintermeister and Joseph Hamill

Department of Exercise Science, University of Massachusetts, Amherst

INTRODUCTION

Although runners of similar ability display a variety of mechanics, there is little evidence supporting a relationship between running mechanics and energy expenditure (EE). Shorten et al. (1981) reported correlation coefficients of r=0.86 to r=0.92 between EE and mechanical power (MP) in four subjects running at six speeds. However, the results of this study are of questionable value due to the small sample size, and because EE and MP are speed dependent, but were not analyzed independently of speed (Morgan et al., 1989). Williams and Cavanagh (1987) examined the influence of biomechanical parameters on running economy (RE) in 31 trained runners at a relatively slow speed (3.57 $m \cdot s^{-1}$). Net positive power and two measures of angular kinematics were retained in a multiple regression that explained 54% of the variance in RE. These are the only two studies that have examined the relationship between MP and EE in running. The purpose of the present study was to compare the MP and EE of trained distance runners from level treadmill running at different speeds.

REVIEW AND THEORY

Estimates of MP are derived from the work-energy theorem. The mechanical energy of a segment (E_S) equals the sum of potential (PE), translational kinetic (TKE), and rotational kinetic (RKE) energies. The work done by a segment (W_S) is equal to the sum of the changes in these component energies over time and measured in joules.

$$W_S = \Delta E_S = \Delta PE + \Delta TKE + \Delta RKE \quad (J)$$

Total body work in a linked segment model adds the possibility of energy transfer (ETr) between segments and is calculated using variations of the following 3 fundamental assumptions: no transfer, transfer within segments, and transfer within and between segments.

The energy models used in the present study were based on those of Norman et al. (1976), Winter et al. (1979), Pierrynowski et al. (1980), and Williams and Cavanagh (1983). Mean MP was expressed in watts (W) relative to the time required for one complete gait cycle. "P" represents mechanical power and "Pc" denotes the algorithms derived from the Williams and Cavanagh model (1983) that are modified by coefficients and explicitly allowed within segment transfer. The following subscripts define the transfer constraints applied for the "P" models: n = no transfer, w = within segment transfer, wb = within and between segment transfer; and for the "PC" models: s = segment transfer, l = limb transfer, and t = total transfer.

PROCEDURES

Twenty-two competitive male runners (age = 28.9 ± 5.4 yr, mass = 67.8 ± 6.5 kg, stature = 1.80 ± 0.01 m) completed a total of four 10-minute steady-rate (SR) runs at speeds of 3.58 (S1), 3.97 (S2), 4.47 (S3), and 5.11 $m \cdot s^{-1}$ (S4), and one max$\dot{V}O_2$ run over two days. Measures of EE included $\dot{V}O_2$, which was obtained through open-circuit spirometry, and two blood lactate (BLa) samples per SR run, procured via fingertip puncture. Standard high speed video (200 Hz) techniques were used to record sagittal plane kinematics. Five gait cycles were digitized for each subject and processed using a Motion Analysis system. MP was derived from analysis of internal mechanical work using an eleven-segment model and assuming bilateral symmetry of gait (Hintermeister et al., 1991). The relationship between MP and EE was examined using regression analysis for each speed and MP model; a total of 28 (4 x 7) regressions. The bivariate Pearson r and the coefficient of determination (r^2) provided measures of association between MP and EE.

RESULTS

The mean max$\dot{V}O_2$ of 4.68 $l \cdot min^{-1}$ or 69.4 $ml \cdot kg^{-1} \cdot min^{-1}$ reflects the high fitness level of this group of competitive runners. Expressed as a percentage of max$\dot{V}O_2$, mean $\dot{V}O_2$ for the SR runs was 58.5, 65.9, 75.2, and 89.4% for S1 through S4, respectively. A significant increase of 2.4 mmol in mean BLa during S4 resulted in the addition of an oxygen equivalent of 3 ml $O_2 \cdot kg^{-1} \cdot min^{-1}$ per mmol BLa (di Prampero, 1981) to EE values for S4. Mean EE at S4 increased significantly from 4.19 to 4.26 $l \cdot min^{-1}$ with the addition of the oxygen equivalent for BLa.

Means and SD of MP for the seven models at each of the four speeds are presented in Table 1. MP increased with speed and varied widely depending on the ETr constraints of the particular algorithms. MP ranged from a high of 3262.4 W for the Norman model at S4, to a low of 373.3 W for the total transfer model of Williams and Cavanagh at S1. Coefficients of variation ranged from 9% to 13% for the majority of MP algorithms.

Regression analysis revealed that all of the MP models except P_{wb} displayed a significant linear trend with EE. The r^2 and SEE statistics for the 28 regressions are displayed in Table 2 in descending order of explained variance. The greatest amount of variance in EE explained was 56.1% by the Pc_l model at S1, and the least was 6.7% by the P_{wb} model at S3. SEE ranged from 0.185 to 0.395 $l \cdot min^{-1}$.

Table 1. Means and SD for MP (W) of each model at the four SR speeds (N=22). (Means are listed over SD for each model)

	Speed ($m \cdot s^{-1}$)			
Model	3.58	3.97	4.47	5.11
P_n	1813.7	2124.4	2565.2	3262.4
	168.43	226.10	260.23	356.56
P_w	1472.0	1748.6	2147.8	2776.9
	141.24	194.29	227.89	320.66
P_{wb}	510.8	560.9	613.4	696.8
	62.12	75.04	97.21	133.25
Pc_n	686.0	814.5	1000.4	1292.8
	65.65	90.73	106.34	148.32
Pc_s	626.2	733.7	890.5	1134.7
	62.21	84.21	95.26	127.99
Pc_l	496.1	582.8	708.7	907.3
	44.50	60.07	72.44	106.09
Pc_t	373.3	428.8	500.8	616.8
	33.59	47.40	55.97	79.44

Table 2. Coefficients of determination (r^2) and SEE in parenthesis ($l \cdot min^{-1}$) for linear regressions of EE and MP collapsed across subjects (N=22) and grouped by speed.

	Speed ($m \cdot s^{-1}$)			
Model	3.58	3.97	4.47	5.11
Pc_l	0.561	0.465	0.527	0.515
	(0.185)	(0.248)	(0.242)	(0.286)
P_n	0.509	0.426	0.521	0.505
	(0.196)	(0.257)	(0.244)	(0.289)
Pc_s	0.460	0.360	0.474	0.532
	(0.205)	(0.271)	(0.256)	(0.281)
Pc_n	0.428	0.326	0.467	0.454
	(0.211)	(0.278)	(0.257)	(0.303)
P_w	0.417	0.324	0.463	0.451
	(0.213)	(0.278)	(0.258)	(0.304)
Pc_t	0.380	0.237	0.306	0.275
	(0.220)	(0.296)	(0.294)	(0.349)
P_{wb}	0.148	0.090	0.067	0.074
	(0.258)	(0.323)	(0.340)	(0.395)

DISCUSSION

The mean max$\dot{V}O_2$ of 4.68 $l \cdot min^{-1}$, or 69.4 $ml \cdot kg^{-1} \cdot min^{-1}$ indicates that the sample of runners were aerobically very fit and compare favorably with values reported for well trained runners studied by Costill et al. (1973), Conley and Krahenbuhl (1980), and Williams and Cavanagh (1987).

Submaximal measures of $\dot{V}O_2$ expressed as a percentage of max$\dot{V}O_2$, corresponded well with values reported in the literature. For instance, at S1 values were 58.5% (present study) versus 57.9% reported by Williams and Cavanagh (1987). At S2 and S3 percentages were 65.9 versus 62.3, 75.2 versus 70.2 and 72.2, respectively (Conley and Krahenbuhl, 1980; Costill et al., 1973).The significant increase in mean BLa of 2.4 mmol at S4 indicated that BLa production was exceeding removal, and making a greater contribution to the overall energy demand. Thus, an oxygen equivalent for the change in BLa was incorporated into subsequent calculations of EE at S4.

The regressions across subjects and grouped by speed for each MP algorithm were carried out to see what kind of relationship existed between MP and EE. The major finding of this investigation was that all of the MP algorithms except P_{wb} displayed significant linear relationships with EE independent of speed. This provides evidence that changes in MP do influence EE and are not solely due to the effects of speed. The only other study to report a linear relationship between MP and EE was done by Shorten et al. (1981) with four trained runners. However, MP and EE were not analyzed independently of speed, thereby confounding the results since MP and EE are known to increase with speed (Morgan et al., 1989).

The strength of the linear relationships are reflected by the percentage of variance in EE explained by the MP algorithms. Coefficients of determination reported in the present study for the six MP algorithms that displayed linear relationships with EE ranged from 23.7% to 56.1%, and are considerably greater than those reported previously by Williams (14%; 1980). The fact that a large portion of the variance in EE remains unexplained by MP means that other factors influence EE.

In summary, the significant linear relationships reported for six of the algorithms examined in this study indicate that MP does influence EE independently of speed.

REFERENCES

Conley, D.L. and G.S. Krahenbuhl. *Med. and Sci.in Sports and Exer.* 12(5):357-360, 1980.
Costill, D.L., H. Thomason, and E. Roberts. *Med. and Sci. in Sports.* 5(4):248-252, 1973.
di Prampero, P.E. *Reviews of Physiological Biochem. and Pharmacology.* 89:143-222, 1981.
Hintermeister, R.A., J. Hamill and M. Slavin. *Biomechanics in Sports X*, CL Tant et al. (eds), 61-65, 1990.
Morgan, D.W., P.E. Martin, and G.S. Krahenbuhl. *Sports Medicine* 7:310-330, 1989b.
Norman, R.W., M.T. Sharratt, J.C. Pezzack, and E.G. Noble. In *Biomechanics V-B*. P.V. Komi, ed. 1976, pp. 87-93.
Pierrynowski, M.R., D.A. Winter, and R.W. Norman. *Ergon.* 23(2):147-156, 1980.
Shorten, M.R., S.A. Wootton, and C. Williams. *Engin. in Med.* 10(4):213-217, 1981.
Williams, K.R. Ph.D. Dissertation, Penn State University, 1980.
Williams, K.R. and P.R. Cavanagh. *Journal of Biomechanics.* 16(2):115-128, 1983.
Williams, K.R. and P.R. Cavanagh. *J. of Appl. Physiol.* 63(3):1236-1245, 1987.
Winter, D.A. *J. of Appl. Physiol.* 46(1):79-83, 1979.

A COMPARISON OF FIVE MODELS FOR ESTIMATING MECHANICAL WORK WITH ACTUAL METABOLIC COST FOR VARIABLE LOAD RUNNING

V. R. Yingling, S. C. White, F. J. Cerny & H. J. Yack
Department of Exercise Science and Physical Therapy
State University at Buffalo, Buffalo N.Y.

INTRODUCTION

The objective of this study was to compare five models for calculating mechanical work to measures of metabolic cost. Oxygen consumption and mechanical work values were determined for one subject running on a treadmill at a constant speed and stride frequency under various conditions of lower limb loading. The five models all overestimated the work value of the total body but three were found to have percent increases similar to metabolic cost increases over the loading conditions. Work calculated based on motion of the whole body center of mass with the work of moving the limbs included separately, matched the percent change in metabolic cost best. Between segment energy transfers require further investigation before linked segment models become a useful method for mechanical work estimates.

REVIEW AND THEORY

Determining efficiencies for various movements requires realistic estimates of mechanical work. Point mass (PM) and link-segment (LS) models are two approaches commonly used to calculate mechanical work. PM models based on potential and kinetic energies of the body's center of mass (Cavagna et. al. 1964) have been criticized since reciprocal limb motions cancel resulting in underestimations of the work of the whole body motion during locomotion. The PM model was modified by Cavagna et al. (1977) to include estimates of the work required to move the limbs separately, however their approach does not allow energy transfer between the trunk and the limbs. LS models involve the calculation of the energy of each segment separately. The energies are then summed according to different energy transfer assumptions. No transfer of energy within and between segments was assumed by Norman et al. (1976) but their approach is considered to overestimate work. Winter (1979) recognized that segment energies can be conserved and proposed a LS model in which total within and between energy transfers among all segments of the body were allowed. No attempt has been made to validate the various methods of mechanical work estimates against measures of metabolic cost. The purpose of this study was to compare mechanical work estimates from various models, to the metabolic cost of running on a treadmill. Since energy transfer, storage and recovery of elastic strain energy, and the relative cost of muscle contraction affect metabolic cost (Williams et al., 1983), this study was designed to minimize the latter two effects across conditions in order to assess the various energy transfer assumptions. Using this type of experimental protocol, the model which best matches metabolic cost measures was determined.

METHODS

One trained female (24 yr) subject ran at a constant speed (2.38 m/s) and stride frequency (matched to a metronome) for three variable work conditions. The work conditions were achieved by adding various amounts of mass to the lower limb segments (Table 1). Each trial was video taped and oxygen uptake data were acquired during the last 2 minutes of a 7 minute run. Video records were digitized at 60 Hz (Peak Performance) and an 11-member sagittal plane link-segment model was constructed from the cartesian coordinates of anatomical markers. The coordinates were all digitally filtered at 5 Hz (Williams et al., 1983). Mechanical work values were calculated using five modeling approaches:

1. PM1: a PM model assuming within energy transfer (Cavagna et al., 1964).
2. PM2: a PM model including a separate estimate of the work of the limbs (Cavagna et al., 1977).
3. LS1: a LS model ignoring energy transfer (Norman et al., 1976).
4. LS2: a LS model assuming within but no between segment energy transfer.
5. LS3: a LS model assuming within and between segment energy transfer (Winter, 1979).

Metabolic cost was determined using open circuit spirometry and was based on expired air samples collected during two succesive 30 s intervals during the sixth minute of the run. V_{O2} uptake was calculated from expired volume, and the percent O_2 and CO_2 values determined using calibrated Beckman gas analyzers. Both mechanical work and V_{O2} uptake values were converted to power (watts) for comparative purposes.

RESULTS AND DISCUSSION

The power values based on the work estimates were expected to be less than the metabolic cost due to the oxygen cost of muscle stabilization and maintaining function of the vital organs of the body. Of the five models included, LS1 and LS2 are greater than metabolic cost determined for the running trials (Table 2). By converting the two power calculations to efficiency values, an indication of the extent to which the mechanical work models may have overestimated cost can be ascertained. Muscle efficiency has been found to be approximately 30%, (Astrand et al., 1977) therefore, our efficiency calculations should be within that range or lower. The efficiencies of the LS1 and LS2 models were 192% and 149% respectively, suggesting that the absolute values calculated using these models were physiologically unfeasible. The efficiencies of the PM1, PM2 and LS3 models were 65.6%, 83.3% and 58.3%, which are high yet a notable improvement over the LS1 and LS2 models. Efficiency ratios calculated from the mechanical models were higher than muscle efficiency estimates since the recovery of elastic strain energy, and the relative cost of eccentric to concentric work were not accounted for in the calculations. Although the experimental protocol was designed to minimize changes in these factors across conditions, they would have a constant affect on mechanical work estimates for all three trials.

The PM2 model was found to follow the percent change of the metabolic cost between the first and second trials and the first and third trials the best (Figure 1). Comparing the PM1 and PM2 models, it is apparent that the work of moving the limbs

needs to be accounted for separately for any movement involving reciprocal limb motion. The percent changes in LS1 and LS2 matched proportionally the metabolic changes, but as seen in Table 2 these work values overestimate the whole body work of treadmill running. Although the addition of total energy transfer between segments, yielded improvements in the efficiencies relative to the other two LS models, the LS3 percent changes did not match the changes in metabolic cost. Compared to the PM2 models, the major difference in the way work is calculated using the LS3 model, is the assumption of energy transfer between the limbs and the trunk. It is apparent that the assumption of total between segment energy transfer requires further investigation before the linked segment approach becomes a useful model for calculating mechanical work.

REFERENCES

Cavagna, GA. et al., J. Appl. Physiol., 18,1-9, 1964.
Cavagna, GA. et al., J. Physiol., 268,467-481, 1977.
Winter, DA., J. Appl. Physiol., 46,79-83, 1979.
Norman, RW. et al., Biomechanics V-B, 1976.
Williams, KR. et al., J. Biomechanics, 16,115-128, 1983.
Astrand, P. et al., Textbook of Work Physiology. 1977.

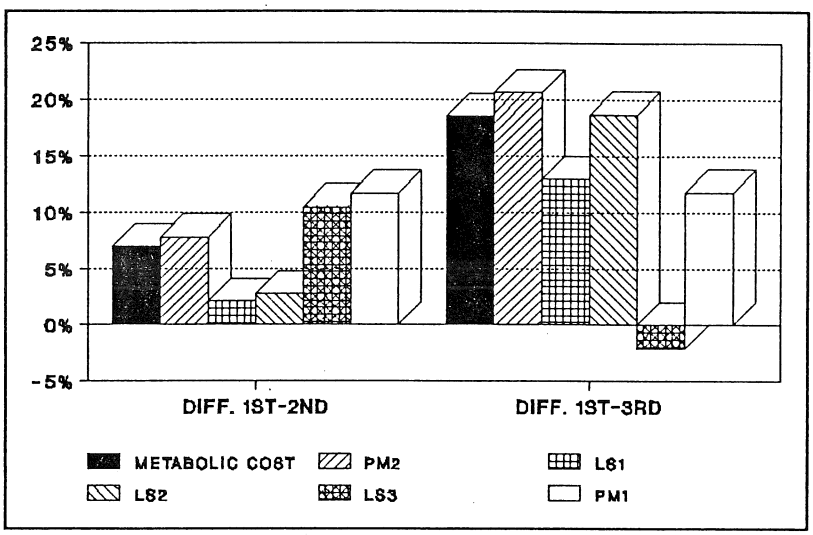

FIGURE 1: PERCENTAGE CHANGES BETWEEN TRIALS FOR VARIOUS MODELING APPROACHES

TABLE 1: LOADING CONDITIONS

TRIAL	THIGH(KG.)	SHANK(KG.)	ANKLE(KG.)
1	0.0	0.0	0.0
2	1.818	0.0	0.0
3	1.818	1.360	0.682

TABLE 2: METABOLIC AND MECHANICAL COSTS EXPRESSED AS POWER

MODEL	VO2 (WATTS)	PM1 (WATTS)	PM2 (WATTS)	LS1 (WATTS)	LS2 (WATTS)	LS3 (WATTS)
WEIGHT 1	482.55	317.78	398.63	947.74	727.68	295.34
WEIGHT 2	516.18	354.35	429.77	967.7	747.79	326.22
WEIGHT 3	571.67	355.38	480.86	1071.83	863.40	289.06

THE MECHANICAL ENERGY REQUIREMENTS DURING THE CANADIAN AEROBIC FITNESS TEST

S. McConnell[1], A. W. Smith[2], S. Thomas[3]

[1]Department of Community Health, University of Toronto, Toronto Ontario
[2]Lyndhurst Spinal Cord Centre, Toronto, Ontario.
[3]Department of Rehabilitation Medicine, University of Toronto, Toronto Ontario

INTRODUCTION

The CAFT (1986) is multistage, cadence-controlled submaximal bench-stepping test used to predict maximal aerobic power ($\dot{V}O_2max$) for people of all ages. The measurement of work done during the test is calculated using only the potential energy component of total mechanical energy. In addition, the regression equation used to predict $\dot{V}O_2max$ assumes that the workload at any given level of the CAFT places equal energy demands for every participant, regardless of age. The purpose of this investigation was to determine whether this is a correct assumption. The amount of mechanical energy and the work done to complete Level 1 of the CAFT protocol was compared between two groups: one group being women under the age of 35 and the other group made up of women over the age of 65. This study found no significant difference in either the total body mechanical energy or work done during Level 1 of the CAFT between the two different age groups.

REVIEW AND THEORY

The CAFT protocol is a widely accepted tool used in clinics, laboratories, and fitness institutions to predict $\dot{V}O_2max$. A regression equation was developed by Jetté *et al*(1976) which allowed $\dot{V}O_2max$ to be predicted from data obtained during the CAFT. The equation assumes that every subject will perform the same amount of mechanical work at each level of the test. Weller *et al.*(in press) investigated the accuracy of the regression equation. The predicted results of the CAFT were compared to maximal oxygen uptake measurements using a treadmill protocol . Weller *et al.* tested men and women ranging in age from 15 to 65 (n=129). It was discovered that the variability between the measured and predicted values of $\dot{V}O_2max$ was large. When the results were separated into different age groups the prediction equation showed that for women between 20 and 30 years and for older subjects the prediction equation underestimated $\dot{V}O_2max$. Thus, the hypothesis of the present study is that for Level 1 of the CAFT, there will be significant differences in actual workload achieved between the two age groups. The rationale for this hypothesis may be as follows: older subjects may produce a greater amount of compensatory movement due to a reduction in stability and strength thereby resulting in a greater amount of total work being done. This extra work would increase oxygen consumption and could explain some of the discrepancy in predicted and measured $\dot{V}O_2max$ values.

The hypothesis of the present study was tested by measuring the amount of mechanical energy expended and total work done during the CAFT protocol within and between the different age groups.

PROCEDURES

Twenty-seven women over 65 and nineteen women under 35 volunteered to participate in this study. Informed consent was obtained in accordance with the policy set forth by the University of Toronto Office of Research Administration. Subjects were required to complete 5 minutes of Level 1 of the CAFT protocol. Each subject was videotaped in the sagittal and frontal plane. The two cameras were synchronized in time and recorded on the same videotape using the split-screen function of a video mixer. A digital video frame counter was used to number each frame of video and was placed in the view of one of the cameras. Using the method outlined by Abraham *et al.* (1987), the videotape was digitized at a rate of 15 Hz. The analysis assumed rigid-body linked mechanics. A different model was used to analyze each of the two planar views. The x,y co-ordinates were digitally filtered (4th-order, Butterworth-type) and used to calculate the amount of energy required to perform one cycle during Level 1 of the CAFT. A complete cycle involves the subject stepping up two 203 mm high steps and back down to floor level. The data were further analyzed to determine the amount of work done. This method of data processing and analysis was derived from Pierrynowski *et al.*(1980).

RESULTS

Mean total body energy curves (normalized to body mass) for each plane and subject group are presented in Figure 1. The data are time-normalized to 100% of the stepping cycle (floor-top stair- floor), with a range of energy values of approximately 10 to 15 J/kg. Figure 2 presents work rate (power) data normalized to body mass as calculated using the method outlined in Pierrynowski *et al.* (1980).

Work rates were calculated using three assumptions: energy transfers within and between segments (Wwb), energy transfers only between segments (Wb) and no energy transfers either within or between segments (Wn). The data in Figure 2 are grouped according to age and shown for each plane.

Statistical analysis of the data included paired t-tests on the work rate data comparing young and old for each of Wwb, Wb and Wn. There were no significant calculated t values ($\alpha = 0.05$).

DISCUSSION

The results of the present study failed to support the authors' hypothesis regarding differences in mechanical work done by females of two different age groups. However, there were some interesting trends evident in the data. First, with respect to Figure 1, it is clear that in either planar analysis, the mean data from the group of younger women showed

higher energy levels to that of the older group. On average, the younger subjects were significantly taller than the older subjects ($p<0.05$) which would result in greater potential energy values for the younger group. The normalization procedure only accounted for differences in mass but did not adjust for height differences.

Second, the application of the work rate analysis method (Pierrynowski *et al.* 1980) to a movement pattern other than level gait has not occurred prior to the present study. With respect to the data in Figure 2, it can be observed that the relative relationships between Wwb, Wb and Wn found by Pierrynowski *et al.* were also consistent in the present study, i.e., Wn being the largest estimate of the work rate, Wwb being the smallest and Wb being intermediate. As well, there was clearly a trend towards lower power output by the younger subjects.

In summary, with respect to mechanical energy, it appears that subject age is not a discriminating factor for performance of Level 1 of the CAFT. Further analysis is required, however, in comparing the metabolic costs of the task to that of the mechanical energy requirements.

REFERENCES

Abraham, L.D. *Biomechanics X-B.* 1107-1110, 1987.
Canadian Standardized Test of Fitness (CSTF) Operations Manual, Third Edition, 1986.
Jetté, M. et al. *Can. J. Pub. Hlth.*, 74, 401-403, 1983.
Pierrynowski, M. et al. *Ergonomics*, 2, 147-156, 1980.
Weller, I et al. *Can. J. Pub. Hlth* (in press).

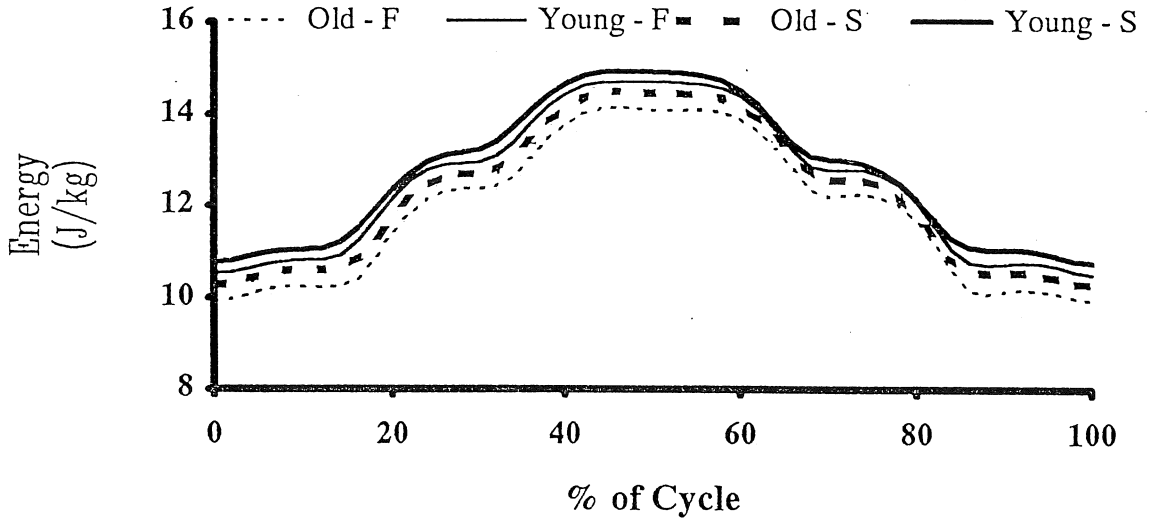

Figure 1: Average normalized total body energy curves for frontal plane (Old - F, Young - F) and sagittal plane (Old - S, Young - S).

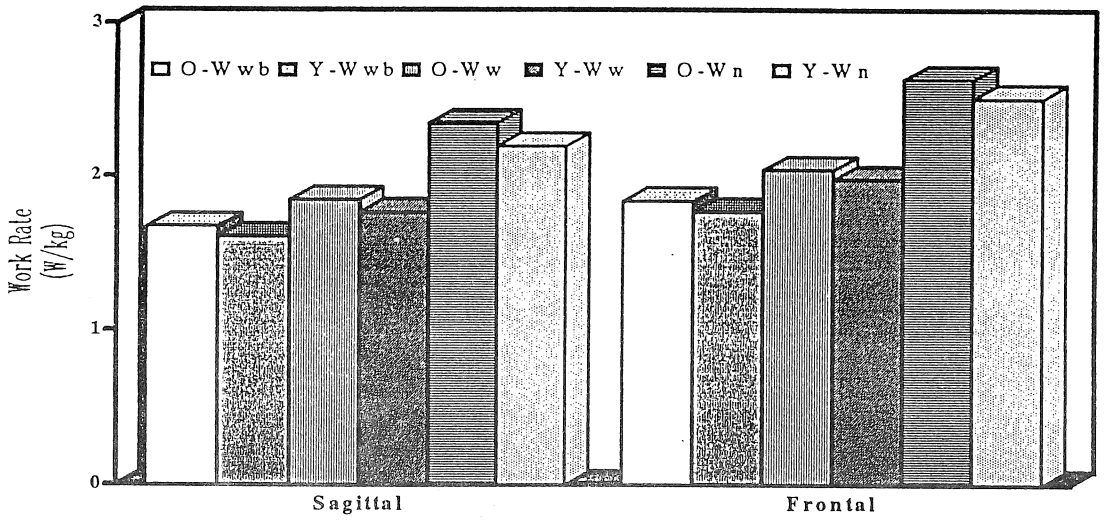

Figure 2: Normalized mean mechanical work rate (power) values for Wwb, Wb, Wn in each of sagittal and frontal planes.

MICROGRAVITY AND AIRBORNE

Podium Session 11

A MODEL OF LOCOMOTION IN A ROTATING SPACE STATION

[1]B.L. Davis, and [2]P.R. Cavanagh
[1]Department of Biomedical Engineering and Applied Therapeutics, Cleveland Clinic Foundation, Cleveland.
[2]Center for Locomotion Studies, Penn State University, University Park.

INTRODUCTION

In the decade prior to the Apollo missions to the moon, concerted efforts were made to investigate locomotion in gravity environments less than 1G (Hewes, 1969, Stone, 1973). Generally these studies focussed on mobility or metabolic issues. In recent years locomotion in reduced gravity has again come under scrutiny. The emphasis now, however, is in combating the losses in bone and muscle mass that are known to occur during periods of weightlessness (Herbison & Talbot, 1985, Zernicke et al., 1990). The underlying hypothesis is that if gravitational effects can be reintroduced (either through the use of springs that tether astronauts to a treadmill, or by creating artificial gravity levels in a centrifuge) then there will still be mechanical loading on the limbs of the astronauts, and presumably less muscle atrophy and bone loss.

REVIEW AND THEORY

The present study focussed on the dynamics of gait in a rotating space station. Some of the unusual features that would be associated with living in such a structure have been discussed by Stone (1973). These include; i) a person's center of gravity would be lower than on earth, ii) hydrostatic pressure differences (e.g., between head and feet) would be less than typically found in 1G, and iii) an object, when dropped, would not land where one would expect it to (due to the fact that, as it falls, it moves into regions with higher velocities). In terms of locomotion, Wiesel (1989) modelled a human body as a point mass and presented an elegant explanation of some of the peculiarities of gait in a rotating space station. He described the origin of "forces" that are perceived by astronauts who mistakenly consider their surroundings to be stationary. (For the remainder of the present discussion both centrifugal and coriolis effects will be treated from the perspective of an astronaut living in a rotating space station, i.e., they will be regarded as actual forces.)

Centrifugal forces are due to the floor constantly preventing the astronaut's motion from following a straight line. During upright stance, the acceleration (A) that is imparted to the feet of the astronaut is given by;

$$A = R(w^2) \qquad (1)$$

where R is the radius of the space station, and "w" is the angular velocity. Coriolis forces occur during motion in a radial direction (e.g., climbing a ladder or lifting/lowering one's feet). They are also due to one mistakenly thinking the surroundings are stationary, and are given by the quantity C, where

$$C = 2(w \times v) \qquad (2)$$

and "v" = the velocity towards the hub of the space station. (C is positive in the anterior direction if the astronaut faces forward in the same direction as the rotation of the space station.)

In the present study, the concepts proposed by Wiesel (1989) were extended to examine specific regions (i.e., the hip and foot segments) during walking and running. It can be expected that, since different regions of the body move with different velocities, the quantity "w" in equation (1) will be modified by an amount w_{limb}, where

$$w_{limb} = (\text{forward limb velocity})/R \qquad (3)$$

Similarly, for coriolis forces, it can be expected that different segments of the body will move with different radial velocities ("v" in equation 2) and thus have different fore/aft forces acting on them.

PROCEDURES

Displacement data (foot and hip markers) for walking at 1.4 m/s and running at 3.8 m/s were obtained from Winter (1979) and Milliron & Cavanagh (1990) respectively. The data was low-pass filtered at 6Hz for walking and 8Hz for running. From the resulting data sets, velocity profiles were calculated using simple finite difference differentiation methods (Winter, 1979). To obtain an indication of the magnitudes of centrifugal and coriolis effects, it was assumed an astronaut walked and ran in a space station (radius 16m) that rotated to achieve an artificial gravity level of 1G at the periphery.

RESULTS AND DISCUSSION

Figure 1 describes the sensations of limb "heaviness" and fore/aft forces that are due to limb motion in the tangential and radial directions respectively. As may be expected, during the stance phases the feet experience a "heaviness" force of 1G and a negligible coriolis force. In contrast, during the swing phases, the "heaviness" effects can result in the foot experiencing peak forces of about 2G (for walking)

and 3G (for running). Although the hip region does not experience the same fluctuations in force magnitudes, it can be observed that there is a "heaviness" effect that always exceeds 1G. (The constancy is due to the fact that during gait the hip moves forward with a velocity that is relatively constant. This velocity results in a continuously elevated centrifugal force.)

Although the coriolis (fore/aft) forces do not attain the same magnitudes as do the centrifugal effects, they could still be a hindrance to locomotion. An example of this can be seen in figure 1b, where there is a braking force of 0.5G acting on the foot at the same time that the foot is sensing a "heaviness" of 3G.

CONCLUSIONS

Despite numerous technical problems associated with designing a rotating space station, it is still thought that such a device would alleviate the problems of muscle atrophy and bone loss that currently pose a threat to long duration space missions. The results of the present analysis show that there are centrifugal and coriolis effects that could hinder one's ability to walk or run in a "natural" way in such an environment. During running at 3.8 m/s, it can be expected that the feet would experience "heaviness" effects that range from 1 to 3G and fore/aft "forces" that range from -0.5 to +0.5G. In contrast, the hip region would sense a relatively constant "heaviness" of just under 2G (which is an increase of about 100% when compared to the situation in quiet stance).

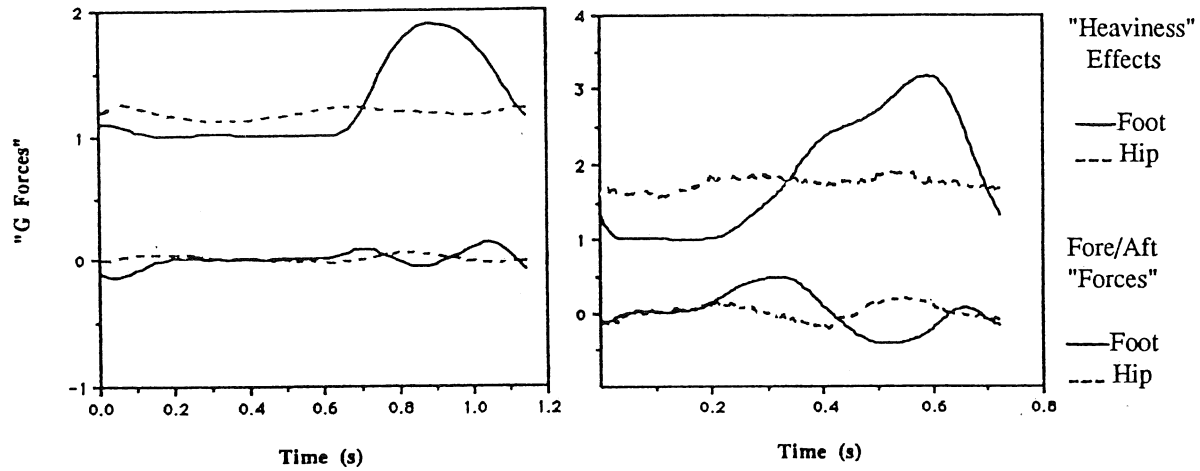

Figure 1. Perceived "forces" on the hip and foot during locomotion in a rotating space station that has a radius of 16m and is rotating at 0.783 rad/s. The subject is (a) walking and (b) running in the same direction in which the space station is rotating. Note that different scales are used in a & b. (Displacement data obtained from Winter, 1979, and Milliron & Cavanagh, 1990.)

REFERENCES

Herbison, G.J., & Talbot, J.M. *The Physiologist*, 28, 6, 520-527, 1985.
Hewes, D.E. *Human Factors*, 11, 5, 419-432, 1969.
Milliron, M.J.,& Cavanagh, P.R. In *Biomechanics of Distance Running* (Ed. P.R. Cavanagh) Human Kinetics Publishers, (pp.65-105), 1990
Stone, R.W. *5th Symp. on the Role of the Vestibular Organs in the Exploration of Space, NASA SP-314*, (pp.23-33), 1973.
Wiesel, W.E. *Spaceflight Dynamics*, McGraw-Hill, New York, 1989.
Winter, D.A. *Biomechanics of Human Movement*, John Wiley, 1979.
Zernicke, R.F. et al. *Exer.& Sport Sci. Rev.* 18, 167-192, 1990.

EFFECTS OF GRAVITY ON JUMPING PERFORMANCE AND COORDINATION

M.E. Loveland*, S. Kim*, M.G. Pandy*, and R.T. Whalen**
**Departments of Kinesiology and Health Education, Biomedical Engineering, and Mechanical Engineering, The University of Texas at Austin, Austin, Texas 78712*
***NASA/Ames Research Center, Code SL:239-17, Moffett Field, California 94035*

Introduction

Although the human body is capable of performing a given task in a number of different ways, commonly observed movements tend to be associated with stereotypic patterns of intermuscular coordination. To better understand muscle coordination of movement, we are currently studying how performance and coordination are altered by changes in both musculoskeletal parameters and environmental constraints. Previously, using a four-segment, eight-muscle, optimal-control model for jumping, Pandy and Zajac [1] studied the dependence of jumping performance and coordination on muscle strength, muscle-fiber speed, and tendon compliance. On the basis of this computational model, we now aim to determine how changes in gravitational acceleration affect the performance and coordination of a maximum-height squat jump. The ability to accurately compute musculoskeletal loading histories and determine changes in performance and coordination under various gravitational fields is of theoretical and practical importance to the space program, where exposure to different loading environments can alter the morphology, biochemistry, and functional properties of muscle and bone tissue.

Methods

The details of our optimal control model for jumping are given in Pandy et al. [2]. The human body is modeled as a four-segment, four degree-of-freedom, planar, articulated linkage, driven by eight musculotendinous units: soleus, other plantarflexors, tibialis anterior, gastrocnemius, vasti, rectus femoris, hamstrings, and gluteus maximus. To investigate how jumping performance and coordination change under various gravitational fields, we varied the value of gravitational acceleration in the model from 0.5 G to 2.5G, where G represents the value of gravitational acceleration on Earth. Because each change made to the nominal musculoskeletal model imposes a new condition on the optimal control problem for jumping, we recomputed the set of neuromuscular excitation signals, muscle activation patterns, body-segmental motions, and muscle forces needed to produce a maximum-height squat jump at each value of gravity.

Results and Discussion

As expected, our model predicts a decrease in jumping performance (i.e., maximum height reached by the body's center of mass above standing) as gravitational acceleration increases (Fig. 1, heavy line). The reason is that increasing gravity causes a decrease in the vertical velocity of the body's center of mass at lift-off, which contributes substantially to overall jump height. Jump height is given by:

$$J = \frac{\dot{y}_{cm}^2}{2g} + y_{cm}$$

where $\dot{y}_{cm}$ and y_{cm} are the vertical velocity and position of the center of mass at liftoff and g is gravitational acceleration. Interestingly, the position of the center of mass at lift-off, which also contributes to total jump height, increases with increasing gravitational acceleration (about 1.5 cm from 0.5G to 2.0G), but this effect is outweighed by a more rapid decrease in the vertical lift-off velocity of the body's center of mass (Fig. 1, light solid line). Note that our model cannot leave the ground at values of gravity above approximately 2.8G, since at this point the vertical velocity of the center of mass at lift-off becomes zero (Fig. 1, light solid line extrapolated to zero velocity). This boundary therefore represents a physical constraint to our model, a constraint which is governed primarily by muscle strength (i.e., at gravitational accelerations of 2.8G and above, our model is not strong enough to jump).

Our optimal control model also predicts that, independent of the value of gravitational acceleration, all uniarticular extensor muscles are activated more-or-less simultaneously during the jump. However, as gravity increases, in general, all muscles, and in particular all uniarticular extensor muscles, are

activated earlier in the jump. Thus, even though total ground contact time for the jump remains almost constant as gravitational acceleration changes, propulsion time for the jump increases with increasing gravity (Fig. 2). Our model suggests, therefore, that increasing gravity changes intermuscular coordination by changing the *timing* rather than the sequence of muscle activation during the jump. That is, optimal jumping performance appears to be relatively insensitive to the mechanism of muscle-force sequencing as gravitational acceleration is altered. We believe this result to be robust, except near the limit of jumping performance in our model (between 2.5G and 3.0G). In this region, gluteus maximus and vasti, the prime movers of the lower extremity, generate forces which approach their peak isometric strength. Consequently, the strategy for muscle coordination changes so that both the sequence and timing of muscle activation become important to the production of an optimal jump.

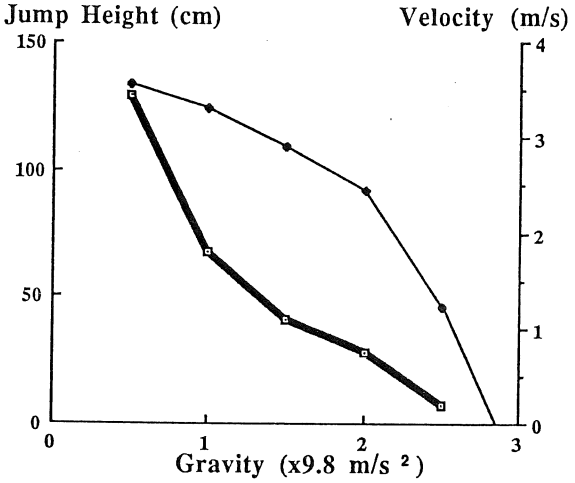

Figure 1: Jump height (heavy solid line) and vertical velocity of the center of mass at liftoff (light solid line) for various levels of gravitational acceleration. Zero jump height signifies the standing level of the center of mass.

To better understand our model's response when gravity becomes very high, we are planning to compute the optimal control solution for jumping at various values of gravity between 2.5G and 3.0G. Our future work also involves conducting jumping experiments in a 17m diameter, human-rated, Centrifuge at NASA/Ames. Collecting kinematic, force-plate, and EMG data simultaneously as humans perform maximum-height squat jumps will enable us to validate the predictions of our optimal control model at 1G and hyper-G.

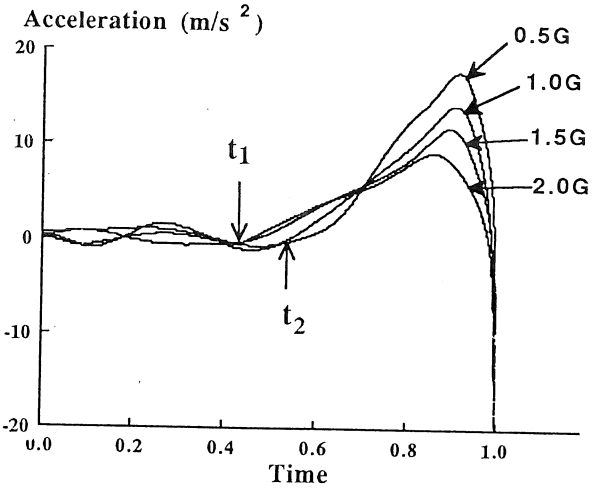

Figure 2: The vertical acceleration of the center of mass vs. time (normalized to liftoff time) for g= 0.5G, 1G, 1.5G and 2G. t1 and t2 indicate the onset of the propulsion phase for jumping at 2.0G and 0.5G respectively. Note that the beginning of the propulsion phase occurs earlier as gravity increases.

Acknowledgements

This work is supported by NASA/Ames Research Center, Grant #NCA2-532. Financial support provided to M.E. Loveland through a National Science Foundation Fellowship is also gratefully acknowledged.

References

[1] Pandy, M.G. and Zajac, F.E. (1991) J. Biomechanics 24(1):1-10

[2] Pandy, M.G., Zajac F.E., Sim, E., and Levine, W.S. (1990). J. of Biomechanics 23(12):1185-1198.

SIMULATION BASED PROGRESSIONS FOR LEARNING AERIAL MOVEMENTS

M.R. Yeadon

Sports Biomechanics Laboratory, Loughborough University, Loughborough, U.K.
Human Performance Laboratory, University of Calgary, Calgary, Canada.

INTRODUCTION

A computer simulation model was used to produce simulations of a half twisting somersault and a 1 1/2 twisting somersault in which the initiation of the twist was identical. These simulations were used as a basis for developing learning progressions for 1 1/2 twisting single and double somersaults with straight arms. The progressions were evaluated using seven trampolinists, all of whom were successful in learning the required movement within a short time period.

REVIEW AND THEORY

In recent years it has become more common for elite trampolinists to twist with their arms fully extended rather than flexed at the elbows. This has produced a need for methods of coaching this style of twisting. Coaching progressions for learning a trampoline skill take the form of a sequence of skills of increasing complexity which lead up to the skill (Yeadon et al., 1991). A progression which employs the same twisting technique in all the lead-up skills is likely to result in more rapid learning than a progression which uses lead-up skills with diverse twisting techniques.

Twist may be initiated during contact with the trampoline or may be produced during the aerial phase. For movements such as a rudi-out fliffus, in which there is no twist during the first somersault and 1 1/2 twists during the second somersault, it may be expected that the contact contribution will be minimal. It has been shown that aerial twist may be produced by asymmetrical movements of the arms or hips (Yeadon, 1986) and that both these techniques are used by divers (Yeadon et al., 1987) and trampolinists (Yeadon, 1988). It was the purpose in this study to develop coaching progressions for both single and double forward somersaults with 1 1/2 twists using trampoline skills which employed the same straight arm aerial twisting technique.

PROCEDURE

It was decided to use asymmetrical hip movement to produce aerial twist since this method is less noticeable and is more aesthetically pleasing. In this technique the body makes a hula movement from a forward flexed configuration through a side arch before extending. This sequence of movements produces tilt of the longitudinal axis away from the vertical somersault plane and results in a twisting somersault (Yeadon et al., 1985). The twist rate is approximately proportional to the angle of tilt which will be large if the arms are abducted prior to the hip movement. Thus, in the learning stages, it will be an advantage to employ wide arms prior to the initiation of twist so that sufficient tilt will be produced to enable the 1 1/2 twists to be completed easily. In addition, it will be of benefit if the production of tilt can be learned in less complex movements prior to attempting the hip movement in a 1 1/2 twisting somersault. Ideally the same hip movement should be used to produce the same amount of tilt before advancing to the 1 1/2 twists. This may be achieved by using a suitably wide arm position during both the production of tilt and the twisting phase in a half twisting movement. By modifying the arm movement so that the arms are adducted in the middle phase the half twisting movement may be transformed into a 1 1/2 twisting movement.

The computer simulation model of Yeadon et al. (1990) was used to produce a simulation of a half twisting forward somersault with arms abducted at 60° using asymmetrical movement of the hips. With a wide arm position the tilt angle increases until the quarter twist position is reached and so it is an advantage to delay the arm adduction until this time (Yeadon, 1986). The arm movement was modified by adducting the arms at around the quarter twist position and another simulation was produced in which more than 1 1/2 twists were produced. The arm movement was further modified by abducting the arms again after 1 1/4 twists had been reached so that a 1 1/2 twisting somersault was produced. In each simulation the timing of the hip and arm movements were adjusted until the required result was obtained.

The two simulations were used as a basis for generating a sequence of trampoline skills of increasing complexity in which just one aspect was changed between adjacent stages. The coaching progressions were evaluated at a coaching clinic using competitive trampolinists.

RESULTS

Figure 1 shows the simulation of the half twisting forward somersault with wide arms. The upper sequence shows the body configuration changes and their effect when there is no somersault. It can be seen that the arms are lowered from an initial abduction angle of 120° to an angle of 60°, as shown in the first three body configurations, and then remain fixed in this position. The tilt and twist produced in the upper sequence are minimal. In the lower sequence the configurational changes are made when somersault is present. In this case the tilt produced by the asymmetrical hip movement is 10° and this is sufficient to produce a half twist even with the arms at angles of 60°.

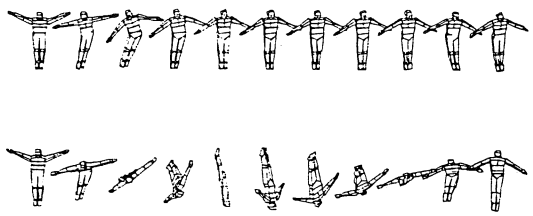

Figure 1. Simulation of a somersault with half twist

The result of adducting the arms in the middle phase can be seen in Figure 2 in which a forward somersault with 1 1/2 twists is produced. In each simulation 10° of tilt is produced by the same hip movement. The simulation with 1 1/2 twists requires 2% less somersault momentum since the transverse moment of inertia is smaller when the arms are adducted.

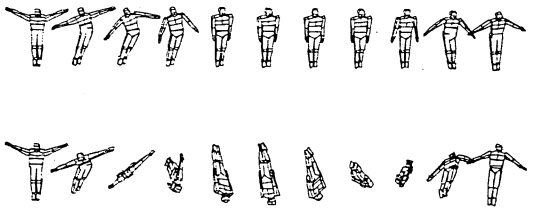

Figure 2. Simulation of a somersault with 1 1/2 twists

The simplest movement in which the asymmetrical hip technique may be used is a half somersault with a half twist from back drop to back drop. Using this as a starting point, a sequence leading to 1 1/2 twists may be devised. The coaching progression comprises:

(a) back drop half twist to back drop
(b) same movement with wide arms throughout
(c) same start and then adduct arms for 1 1/2 twists

In (a) it is essential that the twist be produced by asymmetrical hip movement during the aerial phase rather than being initiated during contact with the trampoline bed. This may be effected by requiring no twist to occur until a signal from the coach is given in mid-flight. The transition from (a) to (b) requires that more tilt be produced by the asymmetrical hip movement to enable wide arms to be used throughout the twist. In order to produce sufficient tilt it is necessary that the arm abduction and the hip flexion be large during the partial hula movement. Once the production of tilt is sufficient this will be indicated by the ability to complete a half twist with wide arms and by the tilt of the body away from the centre line of the trampoline upon landing.

At this stage all that is necessary is to adduct the arms as the quarter twist position is reached. If the arms are adducted upon a signal from the coach during flight this will ensure that exactly the same movements are made to initiate the twist. This may be necessary since any attempt to adduct the arms early will result in less tilt and insufficient twist. Since the angular momentum requirements of (b) and (c) differ by only 2% there is no need to make an adjustment to the somersault produced during the take off.

A progression has been developed using:

(1) forward half somersaults from the back

Corresponding progressions may be used with:

(2) forward somersaults from feet to feet
(3) 1 1/4 forward somersaults from back to feet
(4) Forward double somersaults from feet to feet

The progression for a 1 1/2 twisting forward somersault with straight arms was used at a coaching clinic with five competitive athletes who each learned the skill in less than 10 minutes of practice. All four progressions were used with two international competitors who wished to learn a 1 1/2 twisting forward double somersault with straight arms. Both trampolinists learned the skill in less than two hours of practice.

DISCUSSION

In this paper coaching progressions have been developed using the results of computer simulations. The advantage of such a procedure is that it is possible to obtain progressions in which just one element of technique needs to be changed when progressing from one skill to the next. The method has great potential for developing learning sequences which can shorten the time necessary for mastering these complex skills.

REFERENCES

Yeadon, M.R. *Proceedings of the North American Conference on Biomechanics*, Montreal, (pp.33-34), 1986.

Yeadon, M.R. Biomechanics XI, (pp.740-743), Free University of Amsterdam, 1988.

Yeadon, M.R. et al. Biomechanics IX, (pp.395-400), Human Kinetics, 1985.

Yeadon, M.R. et al. *Proceedings of the 11th Annual Meeting of the American Society of Biomechanics*, Davis, (pp.161-162), 1987.

Yeadon, M.R. et al. *J. Biomech.* 23, 85-89, 1990.

Yeadon, M.R. et al. Trampoline Level 3 Coaching Manual, Canadian Gymnastics Federation, 1990.

BONE LOADING DURING FLIGHT: AN *IN VIVO* STRAIN ANALYSIS OF LARGE FRUIT BATS

S.M. Swartz[1], and M. B. Bennett[2], D. R. Carrier[1]

[1] Program in Ecology And Evolutionary Biology, Brown University, Providence, RI, USA
[2]Department of Anatomy, University of Queensland, Brisbane, Australia.

INTRODUCTION

To what extent does the structural design of animal skeletons reflect the mechanical demands placed upon the skeleton by locomotor performance? One way in which we can determine the broad outlines of an answer is by analysis of species in which the evolution of novel locomotor modes may have drastically altered the mechanics of bone loading. In flight, the forelimb skeleton must clearly experience locomotor forces that differ radically from those engendered by terrestrial locomotion. Forces are imposed on long, slender bones by contractions of wing muscles and by pressure gradients applied by the wing membranes during the generation of lift and thrust. This complex distribution changes dynamically, with pressure magnitudes varying throughout the wingstroke cycle. This contrasts with walking, running and jumping, producing repetitive impacts with forces closely aligned to the limb's axis. We propose that the study of bone loading and structural design in relation to bat flight presents a suitable model for the analysis of bony adaptation in extreme mechanical environments.

REVIEW AND THEORY

For decades, biologists and engineers have worked to establish the rules through which bone form is regulated by mechanical loading. Many recent theories have focused on the role of strain magnitude or orientation in dictating remodeling activities (*e.g.*. Rubin and Lanyon, 1982, 1984; Biewener and Taylor, 1986). One way to explore the robusticity of these ideas is to take advantage of natural experiments in the alteration of the mechanical environment of bones. Animals that use their limbs in mechanically distinctive ways must display compensatory modifications of bone geometry and/or material characteristics in order to maintain strain distributions that will be appropriate for dictating normal bone remodeling. If, for example, the aerodynamic forces exerted on wing bones during flight are large, then bat bones would require a specialized geometry to maintain strain levels within limits seen in other mammals.

We predicted that forces exerted on bat wing bones would differ significantly from those imposed on other mammalian limbs, and that bending and torsion might be particularly important loading modes. Bending is expected to play a large role in the mechanics of wing bones due to their great elongation. Torsional stresses can be expected to arise when the center of pressure of the aerodynamic forces exerted on the wing is located caudal to the center of mass of the stiff structural elements; the force exerted on the wing membrane caudal to the bones will therefore thend to twist the bone in a pronating fashion. Geometrical modifications of the basic mammalian bone design might produce net strain patterns similar to those seen in other mammals.

PROCEDURES

Our subjects were four wild caught gray headed flying foxes (*Pteropus poliocephalus*; 400-750g). Following capture, we trained the animals to fly the length of a 30 m cage without stopping. We attached three rosette strain gauges or two rosette and one single element gauge to the dorsal, ventral, and medial or dorsolateral midshafts of the humerus and radius; surgical procedures were similar to those described in Lanyon (1976) and Biewener *at al.* (1983). We simultaneously recorded wing kinematics on videotape and 6-10 channels of bone strain data via computer during flights along the cage. Raw data from each rosette element were used to calculate principal strain magnitudes and orientations. Bone stresses were calculated using a transversely isotropic model for the material characteristics of bone (Carter, 1978) and assuming that bat wing bones are similar to those of terrestrial mammals.

RESULTS

Within each wingbeat there are three peaks in strain magnitude; this triphasic pattern is unique among vertebrates studied to date. The largest peak occurs at the middle of the downstroke, and it is followed by a second, somewhat smaller peak at the bottom of the downstroke and a third smaller peak at the top of the upstroke. Strain values for each wingbeat reach their maximum values at approximately the middle of the upstroke and near the beginning of the downstroke (Figure 1). The strain magnitudes we observed were comparable to previous recordings from vertebrate limbs, with mean peak strain magnitudes not exceeding 2000 $\mu\varepsilon$ in the humerus and -2200 $\mu\varepsilon$ on the radius (Figure 2) . Principle strain orientations (means for all recording sites between 30 and 38° to the bone's long axis) indicate that torsion is an important element in the normal loading regime of these bones. This torsional loading is also apparent in the pattern of principal stresses: shear stresses are higher than those recorded from any other vertebrate locomotor activity, both in absolute magnitude and relative to the magnitude of longitudinal and transverse stresses (Figure 3).

DISCUSSION

The mechanism producing torsional stress in bat wing bones is probably one that is common to all flying vertebrates. This loading pattern appears to relate directly to structural features of bat wing bones. Despite the widely-held view that bats have slender bones, our comparative allometric analysis shows that some bat wing bones have larger diameters than would be predicted by body size alone. Furthermore, proximal wing elements (humerus and radius) have much thinner bone cortices than is typical for mammals, closely mimicking the pattern seen in birds and pterosaurs. Both of these features directly improve the ability of bat bones to resist torsional stresses, and suggest that thin

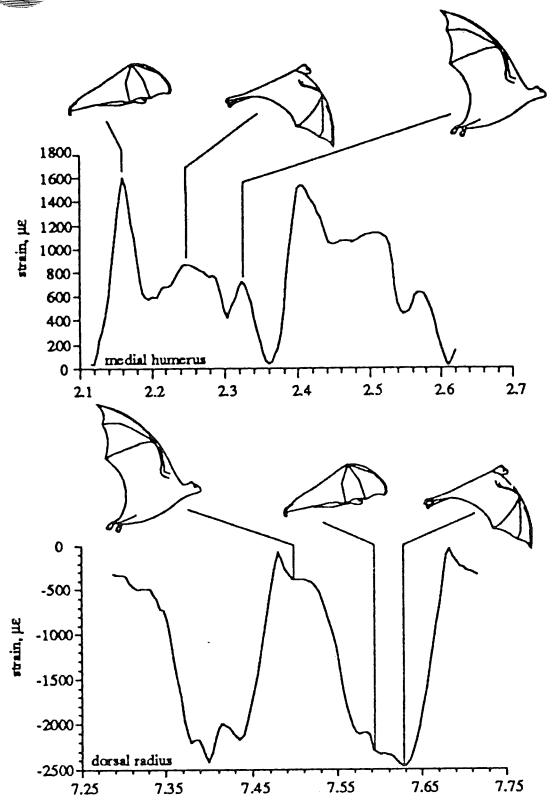

Figure 1. Representative plots of maximum principal strains for two recording sites. Bat schematics indicate the point in the locomotor cycle that corresponds to the stress levels depicted.

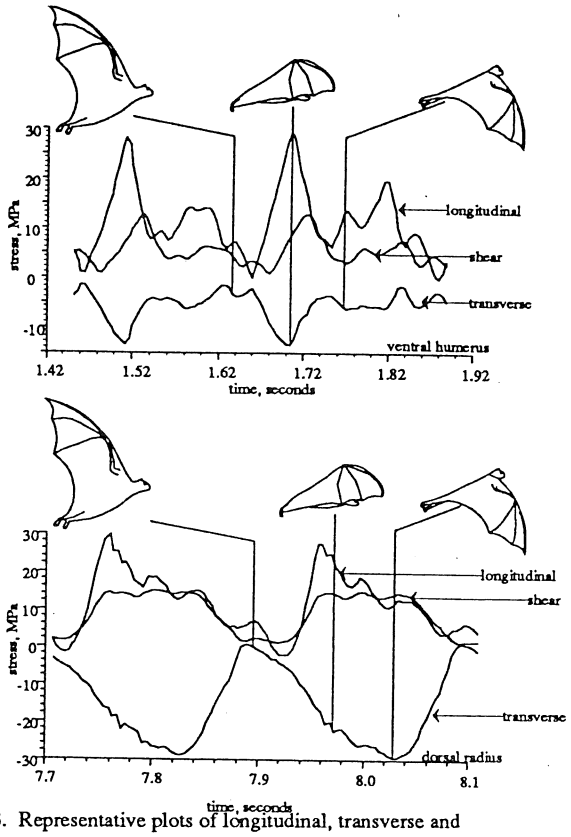

Figure 3. Representative plots of longitudinal, transverse and shear stresses from two wingbeat cycles. Both bones show high magnitude shear stresses (>15 MPa) and the radius displays large transverse stresses.

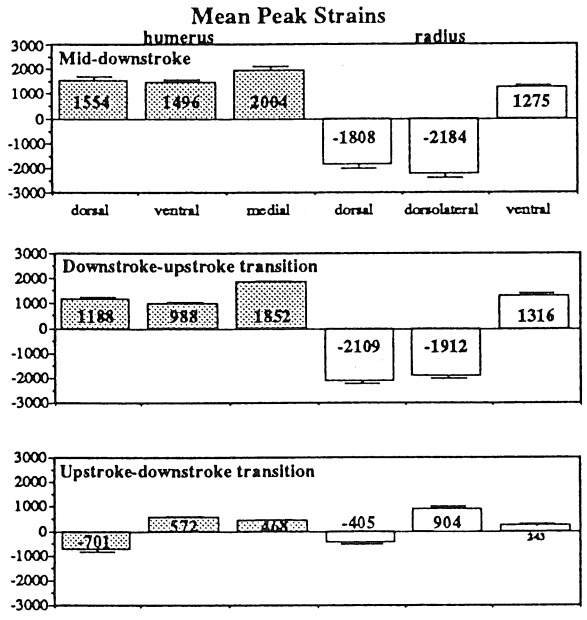

Figure 2. Mean peak principal strain magnitudes for the three recording sites studied in each bone; each mean represents 40-120 wingbeats from 2-3 animals and error bars indicate standard errors.

cortical bone in wings may be as much an adaptation to resist torsional stress as to reduce weight. These results also demonstrate that despite similarities in peak tensile and compressive strain magnitudes among flying and running vertebrates, flight imposes very complex strains on bones. Remodeling responses may thus be mediated in novel ways in wing bones; alternatively, these results may suggest a need to reconsider the role of strains in dictating bone form.

REFERENCES

Biewener, A. A. et al. *J. Biomech.* **16**, 565-576, 1983.
Biewener, A. A. & C. R. Taylor, *J. Exp. Biol.* 123, 383-400, 1986.
Carter, D. R. *J. Biomech.* **11**,199-202, 1978.
Lanyon, L. E. *Acta orthop. belg.* **42**, 98-108, 1976.
Rubin, C. T. & L. E. Lanyon, *J. Theor. Biol.* 107, 321-327, 1984.
Rubin, C. T. &L. E. Lanyon, *J. Bone Jt. Surg.* 66A, 397-402, 1984.

ACKNOWLEDGMENTS

The authors thank Steve Lacy, with help from Jason Harry, for providing crucial programming and data acquisition services. We are also grateful to Ted Goslow, Ron Myers, and Don Wilson for support of this project, and to the Department of Anatomy, The University of Queensland, in particular, Dr. Les Hall. This work is supported by the NSF (IBN-9119143) to SMS and a grant from the Australian Research Council to MBB.

RUNNING

Podium Session 12

THE EFFECT OF 12WEEK SPECIFIC STRENTH TRAINING ON SPEED PARAMETERS IN MIDDLE-DISTANCE-RUNNING.

Dietmar Lüchtenberg and Hartmut Riehle
Fg Sportwissenschaft, University of Konstanz, Germany

INTRODUCTION:

Running is the fundamental ability of human locomotion and essential for all events in track-and-field. The topic of this investigation is if middle-distance-running time can be optimized under simulated competitive conditions.
The starting point of this study is the result of a previous investigation (LÜCHTENBERG/RIEHLE 1987), that stride length is a strong performance predictor for qualified runners. Therefor it is suggested, that specific strength training for increased stride length, lower running time and reduced risk of injuries may be beneficial for middle-distance-runners.

REVIEW AND THEORY:

Not all track-and-field events coaches and athletes accept the necessity of specific strength training. Especially middle and long-distance runners are not used to do a specific strength training. At the beginning of the 80's opinions seem to have changed and some authors (WAGNER 1981, VERCHOSHANSKIJ 1984) begin to point out the necessity of strength training for middle-distance-running. As a result of specific strength training these authors supposed that intensity and capacity of anaerobic endurance would increase. Besides this discussion of the necessity of strength training, some authors discussed which muscles have to be strengthend for middle-distance-running. They focused their controversal discussions on biomechanical and physiological parameters which affect running technique in different running events. Some authors refered to the ability of runners to increase running velocity by fast hip extension instead of fast knee extension. But it is difficult to decide only on the basis of electromyographical and kinnematographical findings which group of muscles are more or less responsible for the accellaration of the center of gravity. Therefore the muscle activity of all body segments has to be estimated as a complex which cannot be studied in isolation. The principle of agonistic and antagonistic muscle movement has to be pointed to as an important principle of specific strength training for runners. Following ZARCIORSKIJ (1987) one cannot give an overall solution of the optimal relationship between stride length and stride frequency for all runners. It seems to be obvious that better qualified runners have a longer stride length than weaker athletes. DILLMANN (1975) theorized that the difference between better qualified and less qualified runners would be shown by the ability of the better runners to control their submaximum speed by increasing stride length, while increasing stride frequency is saved for reaching maximum speed.

PROCEDURES:

30 male subjects of average and less skilled performance levels were involved in this study. The subjects were divided into two randomized groups of 15 athletes. One group which was called the training-group (TG), did a specific strength training for runners twice a week besides their typical middle-distance-running workouts. The other group, called control-group (KG), performed only the typical middle-distance-running workouts. Between the two groups there were no significant differences in personal data like age, body height, body weight and leg length. Before and after the training period speed variables and data on vertical and horizontal jumping were collected. Following results were be found:

RESULTS:

Middle-distance-running training supplemented by specific strength training will influence the speed parameters stride length and stride frequence and with that running time.
It was found:
- that speed changed and running time was lowered.
- that the ability of knee and hip extension muscles to push off in the vertical and horizontal directions increased.
- that only horizontal leg-drive showed a significant correlation to running time.
- that stride length influences running time more than stride frequency.

DISCUSSION:

That there are significant improvements in horizontal and vertical jumping only for the training group suggests an important influence of specific strength training on performance level. Further, the fact that there is a significant correlation only between horizontal jumping ability and running time supposes a priority of this ability for efficiency in running training. This result is supported by VERCHOSHANSKIJ (1984), PÖHLITZ (1984) and SCHMIDT (1988), who stipulate, that specific strength training has to fit the specific demands of running technique. Following WIEMANN (1989) it may be useful to prefer the horizontal component of jumping ability.
Jumping ability only influences the speed parameter stride length, while there is no significant correlation between stride frequency and jumping ability. The influence of specific strength training on increasing stride length is shown in figure 1. This result supports HÖGBERG'S 1952 thesis, that "the power of leg drive is of greatest importance for the length of stride".

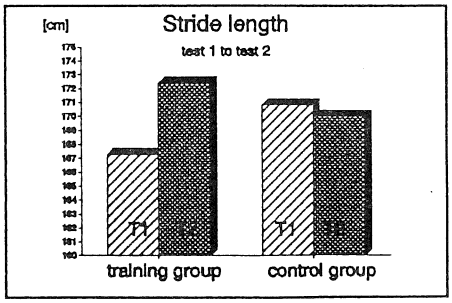

Fig. 1: *The change of stride length from test 1 to test 2 in both groups.*

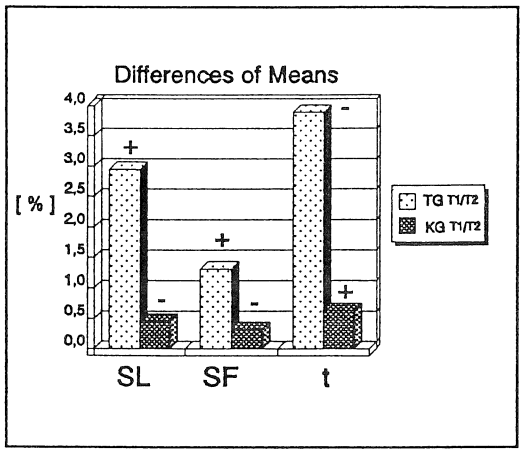

Fig. 2: *Comparison of the differences in mean: stride length (SL), stride frequency (SF) and running time (t) for both groups.*

It is remarkable that, although the parameter stride frequency showed a highly significant increase of 1.3 % in the training group. There was no change in stride frequency in the control group from test 1 to test 2. Thereforem it is unclear what effect specific strength training has on speed parameters.
The differences of means help in ascertaining the primary effect of strength training (Fig.2).
A relation of 2.3 to 1 in favor of stride length to stride frequency in the training group reveals this primary effect. This result can be explained by the fact, that the two groups are running near to their maximum stride frequency. An increase in stride frequency may be useful only, if stride length is increased.
"Optimal stride length" and "freely chosen stride length" (KRAM/CAVANAGH/KERNS 1986) are not fixed. They vary from minute to minute and from step to step. If specific strength training is used to increase leg power, the variations in running economy will still occur, but on a higher performance level.
As a matter of fact, ZACIORSKIJ (1987) inferred, that fatigue may affect the contraction power of leg muscles by the way of lowering leg drive and reducing stride length. Therefore not only a constant stride length over the whole race, but in addition an optimal stride length related to the stage of fatigue will affect speed development and performance level. Accordingly specific strength training will lead to a fatigue-adapted stride length on a higher performance level. The reasons for changing speed parameters in response to fatigue may be caused by a decrease in muscle stiffness. GOLLHOFER et al. (1989) postulated, that the runners impact after a fatiguing race is not answered by the elastic components of the tendomusculataneus system. In spite of using the energy of the stretch-shortening-cycle the muscles have to do an activly contract to produce constant running velocity. This theory could explain on one side variations in speed parameters, on the other side one could estimate the effect of specific strength training as an increase of muscle power and therefor an increase of muscle stiffness.
What are the consequences for training praxis in middle-distance running? First specific strength training in addition to typical running workouts will help to optimize running time. An increased muscle force is shown in better muscle coordination, an increase in muscle stiffness and therefore better anaerobic performance. Also important is the reduced risk of injuries. The question of specific strength training workouts, which are neccesary for middle-distance runners, cannot be answered directly. Following the theory of WIEMANN (1989) it is necessary to strengthen the muscles responsible for hip extension, as the harmstrings and the gluteal muscles. The best workouts to fit the typical demands of running technique, as e.g. horizontal jumping. To the extend that we lack precise physiological data on the efficiency of special strength training workouts, one has to assume that the structure of movement in training workouts must correspond to the structure of movement in running competitons.

REFERENCES:

DILLMANN, C.J. (1975). Kinematic analysis of running. In: J.Wilmore (Hrsg.): Exercise and Sport Sciences reviews (Vol.3). New York: Academic Press.
GOLLHOFER, A.; KOMI, P.V.; HYVÄRINEN, T. (1989). Auswirkungen eines Marathonlaufes auf die Leistungscharakteristik und das Innervationsverhalten der Beinstreckmuskulatur. In: Deutsche Zeitschrift für Sportmedizin 10/1989.
HÖGBERG, P. (1952). Length of stride, stride frequency, flight period, and maximum distance between the feet during running with different speeds. Arbeitsphysiologie 14.
KRAM, R.; CAVANAGH, P.R.; KERNS, M.M. (1986). Stride length changes with fatigue in Distance running. Biomechanics Laboraty, Pennsylvania State University. (unpub).
LÜCHTENBERG, D.; Riehle, H. (1987). Analysis of speed parameters in middle-distance running. In: de Groot/ Hollaender/Huijing/Schenau (ed.): Biomechanics XI-B. Amsterdam.
PÖHLITZ, L. (1984). Kraft - eine wichtige Ausbildungskomponente für Mittelstrecklerinnen. In: Lehrbeilage des Leichtathletik-Magazines 98.
SCHMIDT, P. (1988). Spezifisches Krafttraining für den Mittelstreckenlauf. In: Leistungssport 1/1988.
VERCHOSHANSKIJ, J.W. (1984). Das Krafttraining von Mittelstrecklern. In: Lehrbeilage des Leichtathletik Magazines 97.
WAGNER; P. (1981). Trainingsplanung im Mittelstreckenlauf der Frauen. In: Augustin/Müller (ed.). Leichtathletiktraining. Niedernhausen.
WIEMANN; K. (1989). Die ischiocruralen Muskeln beim Sprint. In: Die Lehre der Leichtathletik 27/1989 und 28/1989, Zschrft. Leichtathletik 25 und 26.
ZACIORSKIJ, V.M. (1987). Biomechanische Grundlagen der Ausdauer. Berlin.

EFFECTS OF ARCH HEIGHT OF THE FOOT ON ANGULAR MOTION OF THE LOWER EXTREMITIES IN RUNNING

B.M. Nigg, W. Nachbauer † and G.K. Cole

Human Performance Laboratory, University of Calgary, AB, Canada.
† Department of Sport Sciences, University of Innsbruck, Austria.

INTRODUCTION

It has been suggested that a relationship exists between the height of the medial longitudinal arch of the foot and injuries to the lower extremities. In attempts to determine this relationship, researchers have examined the influence of arch height on angular motion of the foot and leg. The results of these studies have been conflicting, and the relationship is still not well understood. The goal of this study was to quantify eversion movement of the foot and axial rotation of the leg for subjects with different arch heights. 31 subjects were classified into groups of low, normal, and high arch foot. The 3D kinematics of the lower extremities were measured during running for each subject, and a joint coordinate system was used to calculate 3D angular motion at the ankle joint complex. No significant differences were found between arch groups for the angular variables calculated. However, the transfer of eversion motion to internal leg rotation was found to be significantly greater for the high arch group than the normal and low arch groups.

REVIEW AND THEORY

The medial longitudinal arch of the foot has been proposed as an important constructional feature of the foot in relation to injuries. It has been suggested that subjects with low arched feet are predisposed to injuries of the lower extremities (Nike, 1990). In contrast, an increase in activity related injuries with increasing arch height has been reported in army recruits (Cowan et al., 1989).

Excessive motion in the ankle joint complex has been associated with injuries in running (James et al., 1978), in particular injuries to the knee joint (Bahlsen, 1988). Foot movement has been frequently discussed in connection with foot arch types. The results of these studies have been conflicting. For example, Subotnick (1985) observed greater subtalar range of motion in subjects with flat feet than subjects with cavus feet, whereas Kernozek and Ricard (1990) reported that maximal eversion of the foot was not affected by arch height.

It may be speculated that the occurence of selected knee injuries is associated with the relative rotation of the tibia to the femur and that the rotation of the tibia is related to in-eversion movement of the foot (Bahlsen, 1988). It is proposed that the transfer of movement from the foot to the leg is subject specific and depends on the constructional features of the individual foot, one of these being the medial arch height. The purpose of this study is to quantify the relationship between the eversion movement of the foot and the axial rotation of the leg for subjects with different foot arch heights during heel-toe running.

PROCEDURES

31 subjects were chosen for the study to include a wide variety of foot types. Arch height was measured with a caliper during standing as described by Hawes and Sovak (1992). Subjects were placed into three groups according to arch height: low arch (n=6), normal arch (n=17), and high arch (n=8). The low arch group included the first quartile, the normal arch group the interquartile range, and the high arch group the fourth quartile of the frequency distribution of the measured arch heights. Subjects were required to complete two running trials across a force plate at 4.0 ± 0.4 m/s using a heel-toe movement. The 3D spatial positions of six light reflective markers, three each placed on the subject's foot and leg, were collected for each running trial using a Motion Analysis System and four high speed video cameras sampling at 200 Hz. The vertical ground reaction force was used to determine touchdown and takeoff of each stance phase.

Each subject was placed standing in a calibration fixture to define segment coordinate systems (SCS) in the foot and leg. All coordinate systems were arbitrarily assigned the orientation of the frame of the fixture (X axis medio-lateral, Y axis antero-posterior, Z axis vertical) so that angles between body segments were zero in this position. The relationship between the orientation of the SCS and the positions of the three markers was then determined for each segment.

The orientation of each SCS relative to a laboratory reference system was determined for the stance phase of each running trial. A joint coordinate system (Grood and Suntay, 1983) was used to calculate the 3D components of orientation at the ankle joint complex. In-eversion was calculated as a rotation of the foot relative to the leg about the Y axis of the foot SCS (β), and axial leg rotation as a rotation of the leg relative to the foot about the Z axis of the leg SCS (ρ). The following variables were then determined and averaged over the two trials for each subject: maximal inverted position of the foot during the first 50% of stance (β_{min}), maximal everted position of the foot during the final 50% of stance (β_{max}), initial rotated position of the leg (ρ_0), and the position of maximal internal leg rotation (ρ_{max}). Maximal eversion movement ($\Delta\beta_{max}$) was calculated as the difference between β_{max} and β_{min}. Maximal internal leg rotation ($\Delta\rho_{max}$) was calculated as the difference between ρ_{max} and ρ_0. A transfer coefficient representing the coupling of in-eversion to axial leg rotation through the ankle joint complex was calculated as the ratio $T_{fl} = \Delta\rho_{max}/\Delta\beta_{max}$.

All variables were averaged for each subject, and group means were calculated and statistically analysed. Single factor analyses of variance (ANOVA) were conducted to determine overall differences among arch groups. If overall F-tests were significant, Scheffe's F-test was used to identify differences between groups. The significance level was set at $p < 0.05$.

RESULTS

Figure 1 shows the mean curves of in-eversion (β) and axial leg rotation (ρ) for the normal arch group. At heel strike, the foot is inverted and the leg almost neutral in axial rotation. The foot then everts and the leg internally rotates until both variables reach a maximum slightly after 50% of stance. The foot then inverts and the leg externally rotates until toeoff.

The results presented in Table 1 show that the arch groups differed somewhat in the maximal eversion movement ($\Delta\beta_{max}$): low arch group 27.8°, normal arch group 29.4°, and high arch group 31.6°. However, these differences were not significant due to large interindividual variability. There were no significant differences in the remaining in-eversion variables between arch groups. Table 1 also shows that the internal rotation of the leg from initial position to maximal internally rotated position was significantly greater for the high arch group (29.3 °) than the normal arch group (20.3 °) and the low arch group (13.7 °). There were no significant differences in the remaining leg rotation variables.

The mean transfer coefficients for the three arch groups are shown in Table 1. The mean transfer coefficient T_{fl} was -0.62

for the low, -0.68 for the normal, and -0.96 for the high arch group. The differences in transfer coefficients between the low and the high arch groups and between the normal and high arch groups were significant.

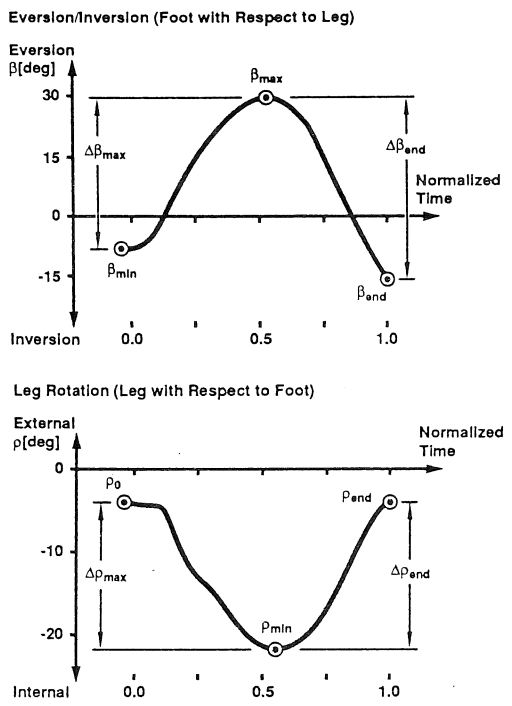

FIGURE 1: Mean curves of in-eversion and leg rotation for the normal arch group normalized to stance time.

TABLE 1: Means, standard deviations ( ), and ANOVA results of ankle joint in-eversion (β) and leg rotation (ρ) variables and the transfer of in-eversion to axial leg rotation (T_{fl}) for the three arch groups. All means and standard deviations are presented in degrees.

Variable	Low n=6	Normal n=17	High n=8	ANOVA p	Comment
β_{min}	-8.6 (8.1)	-7.3 (7.0)	-5.1 (8.9)	0.77	
β_{max}	19.2 (7.2)	22.1 (10.5)	26.6 (11.2)	0.39	
$\Delta\beta_{max}$	27.8 (7.3)	29.4 (9.7)	31.6 (11.7)	0.76	
ρ_0	-7.3 (7.7)	-3.9 (8.8)	-1.4 (9.7)	0.48	
ρ_{min}	-21.0 (8.0)	-24.2 (13.1)	-30.6 (12.3)	0.31	
$\Delta\rho_{max}$	-13.7 (7.8)	-20.3 (9.3)	-29.3 (10.8)	0.02	high>low
T_{fl}	-0.62 (0.19)	-0.68 (0.17)	-0.96 (0.17)	0.002	high>low,norm

DISCUSSION

The shape of the curves for in-eversion in this study were similar to those published previously, although the eversion motion observed ($\Delta\beta_{max}$) was somewhat larger (Nigg, 1986). The shape of the curves for axial leg rotation in this study, as well as the magnitude of internal leg rotation ($\Delta\rho_{max}$), compared favorably to published data (Levens et al., 1948). Values of angular positions are influenced by the definition of the neutral position and by the method of representation of 3D joint orientation. Therefore, it is suggested that emphasis in this study be given to the comparison of results between arch type groups and that the absolute magnitude of the studied variables may be of less importance.

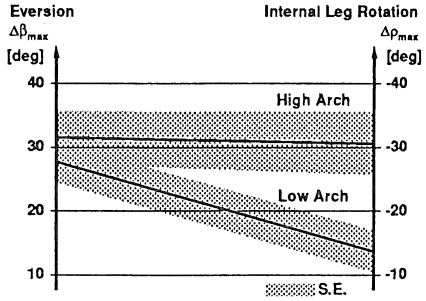

FIGURE 2: Mean maximal eversion of the foot ($\Delta\beta_{max}$) and mean maximal internal rotation of the leg ($\Delta\rho_{max}$) for the low arch (n=6) and high arch (n=8) groups.

Figure 2 shows that a given amount of foot eversion resulted in more internal leg rotation for the high arch group than the low arch group. This result was also indicated by the transfer coefficient T_{fl} which was significantly greater for the high arch group than the low arch group. Functionally, it has been suggested that the coupling of foot in-eversion to tibial rotation is determined primarily through the inclination of the subtalar joint axis in a sagittal plane (Inman, 1976) and increases as the axis becomes more vertical. From the results of this study, it can be speculated that the average inclination of the subtalar joint axis in a sagittal plane is low (more horizontal) for the low arch group and high (more vertical) for the high arch group. It has been shown that the average value of this inclination is 42° and can range from 20.5° to 68.5° (Inman, 1976). Based on the previously observed variation in joint axis inclination, the intersubject variation in the transfer of movement between the foot and the leg seen in this study was not surprising.

It has been suggested that selected cases of anterior knee pain are caused by excessive tibial rotation at the knee joint, which in turn is a result of excessive pronation and the transfer of eversion to tibial rotation through the subtalar joint (Bahlsen, 1988). If this hypothesis is accepted, subjects with high arch feet may be predisposed to anterior knee pain. Furthermore, it may be speculated that a combination of excessive eversion and a subtalar joint axis that is highly inclined in a sagittal plane (high arch feet) may be critical to the incidence of knee injuries to a runner.

REFERENCES

Bahlsen, A. *PhD. Thesis*, The University of Calgary, 1988.
Cowan, D. et al. *Med. Sci. Sports Exerc.*, **21**, S60, 1989.
Grood, E. and Suntay, W. *J. Biomech. Eng.*, **105**, 136-144, 1983.
Hawes, M. and Sovak, D. *Ergonomics*, accepted, 1992.
Inman, V. The Joints of the Ankle, Williams & Wilkins, 1976.
James, S. et al. *Am. J. Sports Med.*, **6**, 40-50, 1978.
Kernozek, T. and Ricard, M. *Arch. Phys. Med. Rehabil.*, **71**, 988-991, 1990.
Levens, A. et al. *J. Bone Jt. Surg.*, **30-A**, 859-872, 1948.
Nigg, B. *Biomechanics of Running Shoes*, Human Kinetics, 1986.
Nike, *Nike Sport Research Review*, **Aug./Nov.**, 1990.
Subotnick, S. *Sports Medicine*, **2**, 144-153, 1985.

ACKNOWLEDGEMENTS

This study was supported in part by an NSERC research grant, by RCL ADIDAS, by an Erwin-SCHROEDINGER grant (Austria), and by the AHFMR.

ANGULAR ORIENTATIONS OF THE ANKLE JOINT COMPLEX DURING RUNNING COMPARED WITH A TOTAL RANGE OF MOTION IN OVERPRONATING AND NORMAL RUNNERS

P. A. Estabrooks, E. L. Ploeg, B. E. Hagel,and J. R. Engsberg

Human Performance Laboratory, University of Calgary,
Calgary, Alberta, Canada

INTRODUCTION

It would be desirable to reduce chronic injuries to distance runners which may be the result of excessive pronation. A step in this regard is to understand the relationships between the angular orientations of the ankle joint complex (AJC) during running and a total active range of motion (ROM) for both normal and overpronating runners. Results quantifying these relationships generally indicated that an overpronating runner had greater angular orientations of the AJC during running and a greater active ROM of the AJC than a normal runner.

REVIEW AND THEORY

In a prospective study monitoring the rates and types of injuries in distance runners , Bahlsen (1989) reported that 50% of the injuries which occurred were related to excessive pronation. Quantifying the angular orientations of the AJC during support has been investigated in both two and three dimensions (Nigg et al., 1986; Engsberg & Andrews, 1987). However no investigations have quantified the 3-D angular orientations of the AJC during running relative to the total active range of motion of the AJC.The purpose of this pilot investigation was to quantify the angular orientations of the AJC during running support relative to a total ROM of the AJC in a normal and overpronating runner.

PROCEDURES

One normal and one overpronating runner, logging a minimum of 20km per week had three reflective surface markers each placed on their right shoe and a sandsplint exoskeleton covering their lower leg (Ronsky & Nigg, 1991). Motion Analysis video system and Kintrak software were used to obtain 3-D coordinates of the these surface markers during five running trials at 3m/s +- 10%. The Coordinates were then used to calculate three Euler angles describing the angular orientations of the AJC during support (Engsberg and Andrews, 1987). In addition an AJC ROM fixture (Allinger and Engsberg, 1991) was used to collect an active ROM for the two runners. The Motion Analysis equipment with associated software was again used to determine the 3-D coordinates of 3 surface markers on both the leg and foot as the subject moved within the fixture. Thirty ab/adduction ROM data points were determined from 15 fixed dorsi-plantarflexion and ev-inversion orientations for the subjects.

RESULTS

Figures 1 and 2 display the 2-D angular orientation and active ROM results for dorsi-plantarflexion and ev-inversion from the running and the from fixture for the normal and overpronating runners, respectively. It can be observed that; 1) the ROM collected from the fixture was greater for the overpronating runner than for the normal runner, 2) except for the final phase of support the angular orientations during running remained within the confines of the fixture ROM, and 3) the maximum angular orientations during running were greater for the overpronator for dorsiflexion, plantarflexion, and inversion, but not for eversion.

DISCUSSION

The purpose of this study was to quantify the angular orientations of the AJC during running support relative to a total ROM of the AJC in a normal and overpronating runner. Such quantitative information has heretofore not been presented. With the presentation of results from only one subject from each group it is impossible to predict any relationships which might exist. However, with additional subjects, relationships may be developed that will provide insight towards understanding how AJC movement could be associated with chronic injuries to distance runners.

REFERENCES

Allinger, T. L. & Engsberg, J. R., **Proceeding of the ISB**, (PP. 326-327),1991.

Bahlsen, A. **The etiology of running injuries: a longitudinal, prospective study.** Doctoral dissertation, University of Calgary, 1989.
Engsberg, J. R. & Andrews J. G., **Med Sci Sport Exer,** 19, 275-284, 1987.
Nigg, B. M., **Med Sci Sport Exer,** 23, 22-29, 1986.
Ronsky, J. L. & Nigg, B. M., **Proceeding of the ISB,** (pp. 390-392), 1991.

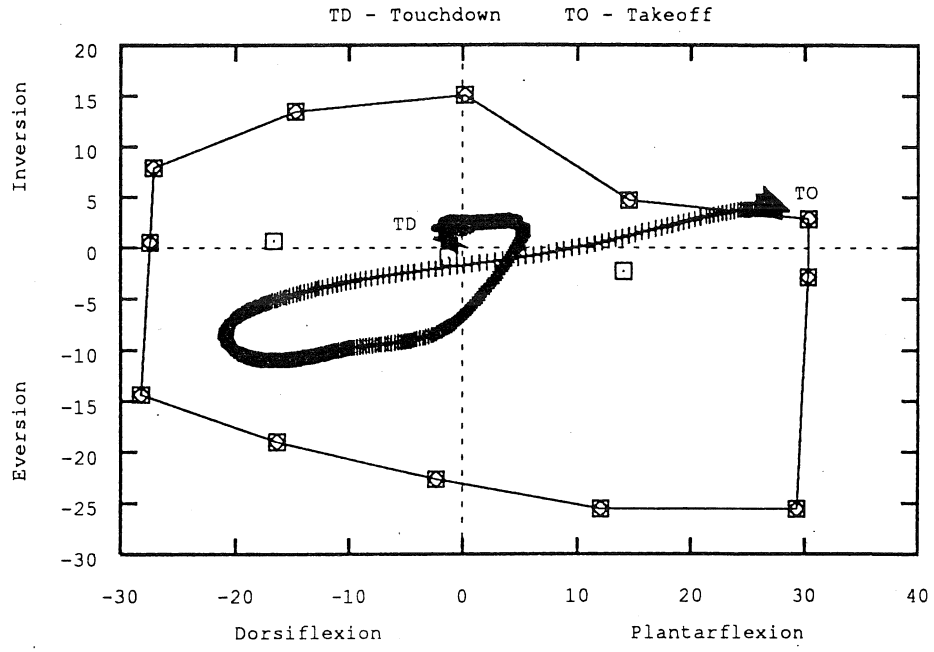

Figure 1: Total ROM and angular orientations during running of the AJC for a normal runner.

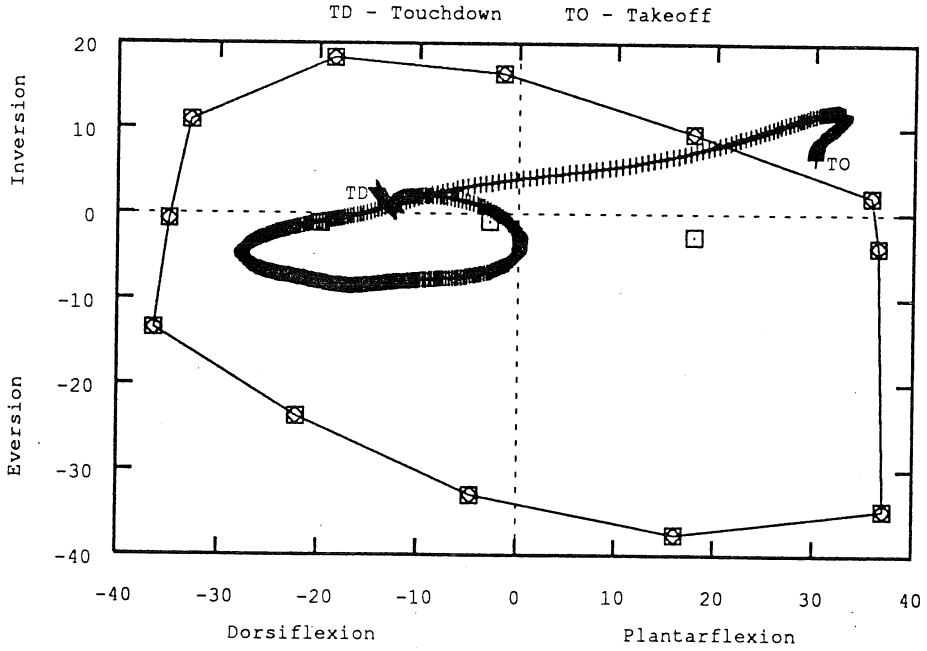

Figure 2: Total ROM and angular orientations during running of the AJC for an overpronating runner.

RANGE OF MOTION OF THE ANKLE JOINT COMPLEX IN NORMAL AND OVERPRONATING RUNNERS

B.E. Hagel, E.L. Pleog, P.A. Estabrooks and J.R. Engsberg
Human Performance Laboratory, University of Calgary, Calgary, Alberta, Canada.

INTRODUCTION

The purpose of this investigation was to compare a range of motion (ROM) for the ankle joint complex (AJC) for normal and overpronating runners. A six degree of freedom (DOF) fixture was used to measure the ROM of the AJC. This ROM included dorsi/plantarflexion, eversion/inversion, and ab/adduction. Results indicated a trend towards a larger ROM in the overpronating runners when compared with the normals.

REVIEW AND THEORY

Insufficient or excessive AJC motion has generally been implicated as a potential injury mechanism for distance runners (James et al., 1978). Investigations using cadaveric material provided initial information for ROM of the AJC (Seigler et al., 1988) yet the application of in vitro data to the in vivo situation has its limitations. A six DOF fixture used to measure ROM of the AJC has recently been developed (Allinger & Engsberg, 1991) and tested. It can be hypothesized that a total ROM of the AJC may provide insight towards understanding the injury mechanisms related to AJC motion. The purpose of this investigation was to compare a total ROM of the AJC for normal and overpronating runners.

PROCEDURES

A 6 degree of freedom fixture (Allinger & Engsberg, 1991) was used to collect a ROM for 7 overpronating and 8 normal runners. Video equipment with associated software determined the 3-D coordinates of 3 surface markers on both the leg and foot as the subject moved within the fixture. Thirty ab/adduction ROM data points (i.e., 15 for abduction and 15 for adduction) were determined from 15 fixed dorsi/plantarflexion and eversion/inversion orientations for the subjects. These 15 orientations were determined from combinations of 5 dorsi/plantarflexion positions and 3 eversion/inversion positions. A student's T-test was used to test for significant differences of the means for the ROM values from a neutral position ($p<0.05$).

RESULTS

The results indicated a trend for the overpronators to have a greater overall ROM than the normals (Table 1). The results for eversion and abduction as well as eversion/inversion indicated a significant difference. Figure 1 presents the mean ROM values for dorsi/plantarflexion and eversion/inversion for a normal and overpronating runner.

DISCUSSION

Excessive AJC motion has been implicated as a potential injury mechanism for distance runners. This investigation displayed a trend towards a greater total ROM of the AJC for overpronator runners when compared to normal runners. The greater ROM could be due to the joint surface geometry, muscle tendon complex, ligament and other soft tissue constraints in the joint neighborhood. Further work appears warranted in at least two areas. The first is to determine the quantitative influence of each of the anatomical structures on the ROM of the AJC. The second area is to determine how the angular orientations of the AJC during running corresponds to the total ROM measured in this investigation.

REFERENCES

Allinger, T.L., & Engsberg, J.R. *Proceedings of the ISB* (pp.326-327), 1991.
James, S. et al. *Sports Med.*, **6**, 40-50, 1978.
Seigler, S. et al. *J. Biom. Eng.*, **110**, 364-373, 1988.

Table 1 Means and standard deviations for AJC orientations of normal and overpronating runners.

Subjects	DF (deg)	PF (deg)	DP (deg)	EV (deg)	IN (deg)	EI (deg)	AB (deg)	AD (deg)	AA (deg)
Normals	23.22	35.05	58.27	12.71	29.09	41.80	32.20	47.23	79.43
SD	4.67	9.29	9.31	3.02	7.48	7.21	6.71	9.01	4.71
Overpronators	25.01	40.75	62.63	17.39*	34.91	52.30*	44.00*	53.66	90.95
SD	7.48	7.02	12.99	5.23	6.01	8.81	10.30	3.16	25.85

DF=dorsiflexion PF=plantarflexion DP=dorsi/plantarflexion EV=eversion IN=inversion
EI=eversion/inversion AB=abduction AD=adduction AA=ab/aduction
* Significantly different from normal ($p<0.05$)

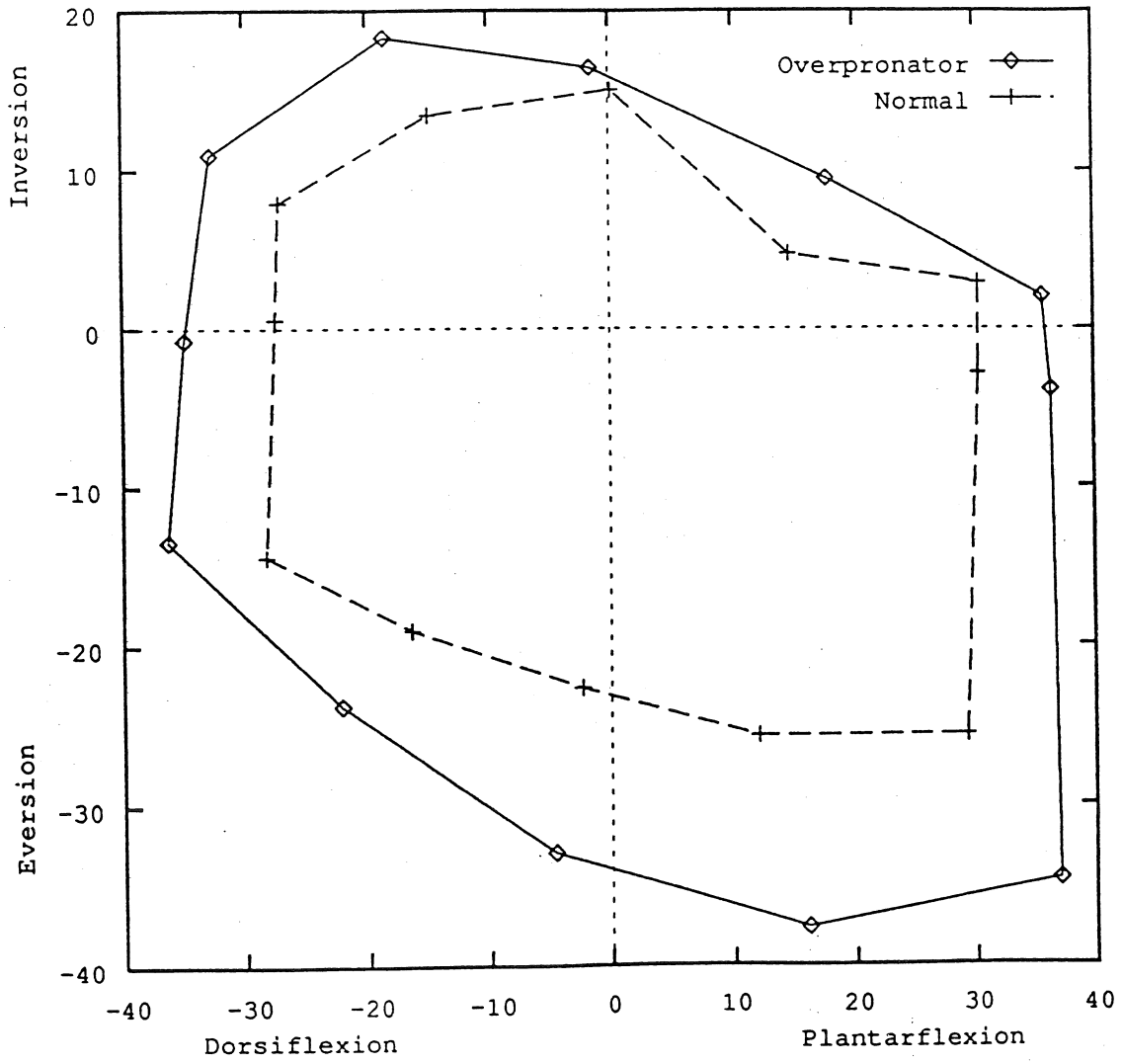

Figure 1 Mean ROM values for dorsi/plantarflexion and eversion/inversion for a normal and overpronating runner.

RUNNING, CYCLING AND SPORT

Poster

BIOMECHANICAL ANALYSIS OF EXPERT TAEKWONDO AX KICKING

S. Lee and S.J. Phillips

Department of Kinesiology, University of Maryland, College Park, MD, USA

INTRODUCTION

Taekwondo (TKD), while remaining a traditional martial art, has been developed as a world-wide sport over two decades. The basic patterns of hip and knee angular kinematics and kinetics for the TKD Ax kick were used to investigate the roles of proximal-to-distal (P-D) sequential patterns of joint actions. The Ax kick in TKD competition is mainly used to attack the high section of the body including the facial area. Filmed records (203hz) of the kicking performed by a former world TKD champion were analyzed using the methods of inverse dynamics. The P-D sequence of joint angular velocity was observed in the lifting phase. The P-D sequence of the stretch followed by shortening cycle (SSC) in the strike phase was found using muscular power analysis, but no P-D sequence of the hip extensor torque and the knee flexor torque was observed. The P-D sequence of SSC was simply parallel to the P-D sequence of joint angular velocity. The P-D sequence of SSC in the Ax kick does not support the principle of summation of force while the P-D sequence of joint angular velocity in the Ax kick supports the principle of summation of velocity.

REVIEW AND THEORY

The joint action patterns in the Ax kicking are similar to those found in throwing, soccer kicking, hitting, running, and walking. What has been typically observed is the involvement of joint actions from proximal to distal during those activities. Putnam (1991) examined the movement-dependent interaction between the adjacent lower extremity segments during the actions of kicking and the swing phases of running and walking. The proximal-to-distal (P-D) sequential pattern for all three activities was observed. Support was found for the principle of summation of segment speeds, whereas no support was found for the principle of summation of force or for general information of negative thigh angular acceleration on positive shank angular acceleration. Herring and Chapman (1989) attempted to understand why the P-D sequential motion pattern appears best. A three-segment, sagittal-plane, overarm throwing task was simulated using constant joint torques. Both ball velocity and range were maximized only if the sequence of onset of torques came from proximal to distal. From this work it was concluded that the P-D is desirable simply because of the linked segmental nature of the model (limb). Also, Chapman (1988) suggested the advantage of use of the stretch followed by shortening cycle (SSC) in P-D sequence in throwing, kicking, and hitting.

The Ax kick has the following features: (1) it is one of the most powerful TKD kicking techniques and frequently results in a knock out; (2) it consists of lifting, strike, and recovery phases on sagittal plane of motion; (3) it has a large range of motion and the knee of the kicking limb is usually fully extended at the maximum hip angular position; and (4) it has the impact moment during the down-phase of the kick. The first part of the task involved placing the kicking foot above the head as quick as possible. The second part is swinging the kicking limb forward and down to transfer as much impulse as possible to the target via the kicking foot. Therefore, the major goal of the Ax kick performer is coordinate the joint actions of the kicking limb such that the minimum time of lifting phase and maximal kicking foot power are obtained. Both minimum time and maximal power relate to velocity. However, the Ax kick has different range of motion, initial conditions, and objectives than other movements. The effect of such difference on the timing of joint or segment actions in a coordinated movement patterns is not certain (Putnam, 1991). The purpose of this study was find the basic patterns of kinematics and kinetics of the Ax kick and investigate the roles of P-D sequential patterns of joint actions.

PROCEDURES

A former world Taekwondo champion in welter weight division was filmed during execution of the Ax kick. The subject, a sixth degree Black Belt, still had excellent techniques with good flexibility. Target distance was 1.04m horizontally and 1.55m vertically from the foot of the supporting leg. This target distance was realistic and comfortable for the subject to perform the most powerful kick. A multi-purpose commercial kicking target was held by a person without resistance. This would be the most realistic striking situation. Joint markers were placed on the shoulder joint, the greater trochanter of the femur, the lateral side of the knee and the malleolus, and the fifth metatarsophalangeal joint (mp) of the kicking leg of the subject. A Photosonic 16mm high-speed camera was used to film the subject. The camera was placed with the lens optical axis at right angle to the sagittal plane of the subject. Actual filming rate for each selected trial was 203 frames per second.

Digitization started twenty frames before toe-off (TO) and ended twenty frames after the target contact. The second order, zero lag, recursive Butterworth filter was used to smooth the data. Cut-off frequency of 15Hz was chosen by residual analysis. The displacement data of shoulder, hip, knee, ankle, and mp were differentiated twice to obtain angular velocity and acceleration data. Kinetic variables were calculated by using inverse dynamics based on the 4-segment model consisting of trunk, thigh, shank, and foot. Dempster's (1955) anthropometric parameters were used to calculate the mass, center of mass, and moment of inertia of each segment of the subject. Time histories of kinematic (joint angular velocity) and kinetic variables (muscular torque and power) were obtained.

RESULTS AND DISCUSSION

Angular velocity-time curves for the hip and the knee are presented in Figure 1-a. At the time of TO the hip was flexing (upward rotation) while the knee was flexing. The kick had a single maximum hip flexion velocity and two peak knee extension velocities during the course of the kicking. The kicking time between TO and the contact moment of the kicking foot with the target was 0.384s (100 %kt). The second peak knee extension velocity (5.5 pi/s) was higher than the maximum hip flexion velocity (4.5 pi/s). The P-D sequential pattern of angular velocity in the Ax kick shown in Figure 1-a is similar to those for soccer kicking and running (Putnam, 1991). The maximum hip flexion velocity is followed temporally by the second peak knee extension

velocity. The maximum hip flexion velocity occurs when the knee extension velocity is near zero (56 %kt). The second peak knee extension velocity occurs when the hip flexion stops (76 %kt). When the hip flexion starts to slow down, the knee starts to speed up in the direction of extension. At this time the knee may pick up the energy released from slowing down of hip flexion and quickly approach peak knee extension velocity. This happens due to large hip extensor torques and knee flexor torques shown in the torque-time graph (Figure 1-b). Their peak torques were 399 Nm and 202 Nm for the hip extensor and the knee extensor, respectively. One of the differences in features of the Ax kick from other coordinated movements of the limb is the large range of motion of hip and knee of the kicking limb for the Ax kick. Therefore, there is progressive increase in hip extensor torque during the lifting phase of the Ax kick is seen in Figure 1-b. Near the initial impact (94 %kt) the knee flexion velocity decreased to zero while the hip extension velocity kept increasing. These joint actions contributed more to forward foot velocity (perpendicular to the face of target) rather than downward foot velocity.

Muscular power-time curves for the hip and the knee are presented in Figure 1-c. These display the P-D sequence pattern of SSC involved in the Ax kick. The Ax kick had a negative peak hip power temporally followed by a positive peak knee power. The negative peak hip power is due to the large hip extensor torque (eccentric, 346 Nm) during slowing the hip flexion near the end of the lifting phase. Thus in the strike phase the hip extensor contracts concentrically when it is highly activated. This conversion of the power absorption (eccentric contraction) to the power generation (concentric contraction) occurs at the maximum hip angular position. This demonstrates occurrence of SSC at hip. The negative peak knee power is due to the large knee flexor torque (eccentric, 197 Nm) during the knee extension right after the end of the lifting phase (or the beginning of the strike phase). The power absorption converts to power generation at the maximum knee angular position during strike phase. This demonstrates occurrence of SSC at knee. The onset of SSC at hip was followed by that at knee with the time delays of 11 %kt. This time delay originated from the time delay of the sequential occurrence of peak angular velocity at hip and knee (20 %kt). The positive maximum hip power coincides the zero knee power at the maximum knee angular position. The positive knee power rises and adds onto the maximum hip power in the manner that enhances forward rotation of the kicking limb at the highest foot position.

The P-D sequence of SSC as seen in muscular power is parallel to the P-D sequence of angular velocity. There is not a P-D sequence of the hip extensor torque and the knee flexor torque. The P-D sequence of angular velocity may simply keep the protagonist (hamstring) on a favorable part of force-velocity relationship. Therefore, the P-D sequence of SSC in the Ax kick does not support the principle of summation of force while the P-D sequence of angular velocity in the Ax kick supports the principle of summation of velocity.

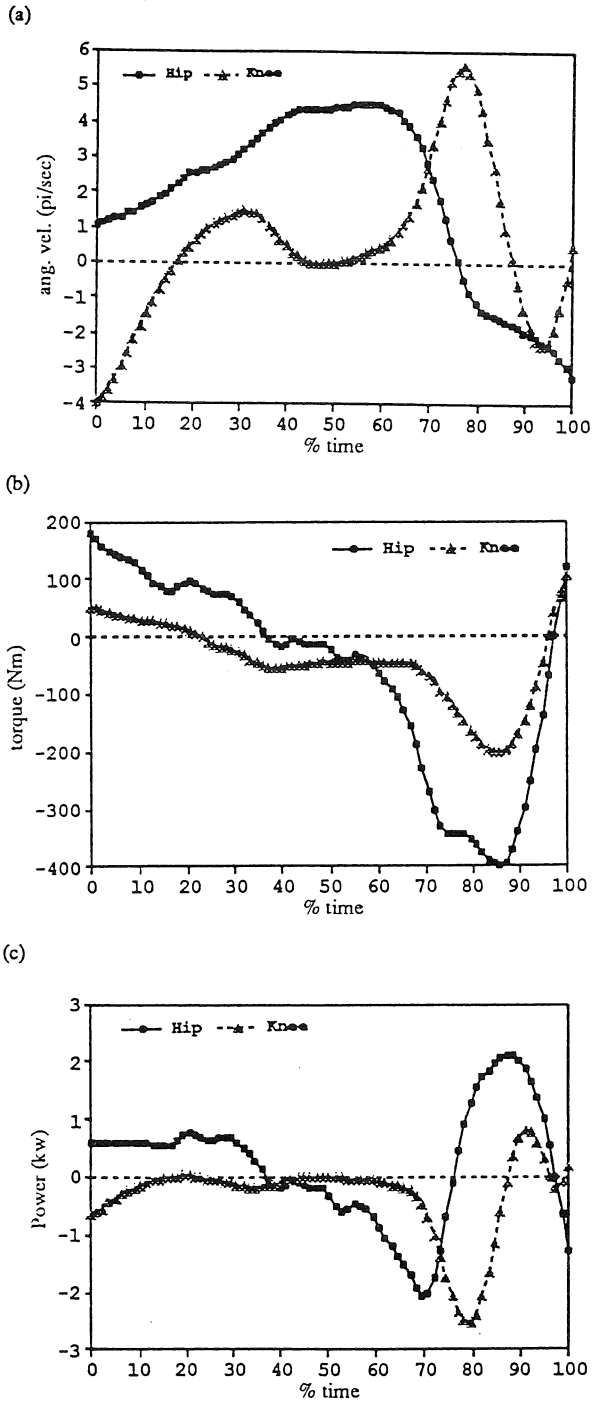

Figure 1: Kinematic and kinetic data of hip and knee.
(a) angular velocity; (b) muscular torque; (c) muscular power.

REFERENCE

Chapman, A. Proc. 5th. Biennial Conf. Can. Soc. Biomechanics, pp.2-4, Spodym publishers, London, Ontario, 1988.
Dempster, W. WADC Technical report, 55-159, Wright-Patterson Air Force Base, Ohio, 1955.
Herring, R. et al. Proc. 13th. Ann. Meeting of Amer. Soc. Biomechanics, Vermont, pp.96-97, 1989.
Putnam, C. Med. Sci in Sports Exer., 23, 130-144,1991.

SURFACE AND SHOE EFFECTS ON LOWER EXTREMITY IMPACT CHARACTERISTICS

B.T. Bates*, J. Hamill#, H.P. Davis*, and N. Stergiou*

*Department of Exercise and Movement Science
University of Oregon, Eugene, Oregon 97403, USA.

#Department of Exercise Science
University of Massachusetts-Amherst, Amherst, Massachusetts 01003, USA.

INTRODUCTION

Impact is a well documented cause of running injuries (James, et al., 1978; Nigg, 1985; Perry, 1983). Numerous researchers have investigated the effects of shoes on impact force characteristics (Bates, et al., 1983; Clarke, et al., 1983; Nigg, et al., 1988; Nigg, et al., 1987). Less research has been undertaken on surface and surface-shoe interaction characteristics (Nigg, et al., 1983). The purpose of this study was to evaluate the interactive effects of different treadmill surfaces and shoes on lower extremity kinematics and impact characteristics. Mean group differences between surface and shoe conditions were generally significant with 82% of the individual performances consistent with the group results.

PROCEDURES

Data were collected for eight runners performing at a self-selected pace. An accelerometer was attached to the subjects' right tibial tuberosity with a tight elastic strap. Twelve foot falls of accelerometer data were collected for each of six conditions while simultaneous high speed video (200 Hz) records of the right lower extremity were obtained to calculate selected joint kinematic and ankle deceleration characteristics. The six conditions evaluated included the three settings (firm, medium and soft) for an adjustable lower impact treadmill (Precor Model 9.3) in combination with a soft and firm shoe. Condition order was randomized. Group data were evaluated using a two factor repeated measures ANOVA (Surface x Shoe x Subject) with planned comparisons between all adjacent conditions ($p < 0.05$). Individual subject data were examined for consistency with the group results. Only the accelerometer data are presented.

RESULTS AND DISCUSSION

Table 1 contains the mean accelerometer values for all conditions along with the percentage differences between conditions. Individual subject mean values ranged from 1.27 to 3.86 g's compared to group minimum and maximum values of 2.07 and 3.08 g's, respectively. The statistical analysis indicated a significant main effect among surfaces but not between shoes in the absence of a significant interaction. The reduction in impact force from the firm to medium surface was 12.0% with an additional reduction of 18.6% between the medium and soft surfaces. Individual subject performances were consistent with the group results in 28 of the 32 comparisons. Three of the four shoe comparisons within surface resulted in significant reductions in impact force (23.0, 14.3 and 16.0%). The 7.9% reduction between the medium and firm surfaces for the soft shoe was not significant. The overall difference between shoes across surfaces was 7.2% with the smallest difference (1.1%) being observed for the medium surface. The soft and hard surface differences were 11.2 and 9.9%, respectively, but only the hard surface value was significant. Individual subject mean values for the soft shoe were less than the corresponding observed values for the hard shoe in 18 of 24 cases with most inconsistent values occurring for the medium surface.

Lafortune and Hennig (1991) indicated that accelerometer values during running typically underestimate the magnitude of tibial acceleration due to impact presenting a mean value of 4 g's for a running speed of 4.5 m/s. The average running pace in the present study was slower suggesting a correction of about 3 g's which would produce a true overall mean value of approximately 5.7 g's for the present study.

Since both impact and stability are associated with various running injuries, future data analysis will focus on ankle deceleration along with knee joint an pronation kinematics computed from the video data.

In summary, mean differences between surface and shoe conditions were significant for five of the seven comparisons with 82% of the individual performances consistent with the group results.

REFERENCES

Bates, B.T. et al. Jrl. Biomech., 16, 181-191, 1983.
Clarke, T.E. et al. Biomechanical aspects of sport shoes and playing surfaces, 25-33, 1983.
James, S.L. et al. Am. Jrl. Spts. Med., 6, 40-50, 1978.
Lafortune, M.A. et al. Med. Sci. Spts. Exerc., 23(3), 360-363, 1991.
Nigg, B.M. Biomechanics of running shoes, 1986.
Nigg, B.M. Spts. Med., 2, 367-379, 1985.
Nigg, B.M. et al. Intl. Jrl. Spt. Biomech., 4, 205-219, 1988.
Nigg, B.M. et al. Jrl. Biomech., 20, 951-959, 1987.
Nigg, B.M. et al. Biomech. VIII-B, 1041-1052, 1983.
Perry, J. Clin. Orthopedics, 177, 9-15, 1983.

Table 1. Mean accelerometer values for all conditions and differences between conditions.

Shoes	Surfaces					Mean
	Soft	Diff	Medium	Diff	Firm	
Soft	2.07 (0.47)	23.0*	2.69 (0.47)	7.9	2.92 (0.43)	2.56 (0.57)
Diff	11.20*		1.10		9.90*	7.20
Firm	2.33 (0.55)	14.3*	2.73 (0.54)	16.0*	3.24 (0.53)	2.77 (0.64)
Mean	2.20 (0.51)	18.6*	2.71 (0.49)	12.0*	3.08 (0.49)	2.66 (0.61)

Note: Condition values in g's; Differences in % reduction from greater value.
* indicates significant differences ($p < 0.05$)

EFFECTIVENESS OF FORCE APPLICATION IN CYCLING

A. H. Black, D.J. Sanderson and E.M. Hennig

UBC Biomechanics laboratory, University of British Columbia, Vancouver, Canada
Sportsmedizinisches Institut, Universität Essen, Essen, Germany

INTRODUCTION

The present study compares the index of effectiveness of two groups of cyclists riding at different cadences and power outputs. Each group of subjects, 17 recreational and 12 competitive cyclists, rode on a stationary bicycle ergometer at three cadences; 60, 80, and 100 rpm and at four power outputs; 100, 200, 300, and 400 watts. Two piezo-electric triaxial force transducers mounted in the right pedal measured components of the resultant force which were recorded through computer interface and then averaged across 12 pedal cycles for each subject. Indices of Effectiveness (IEFF) were then computed for the averages of each cadence/power output combination. The data show three important effects; (1) as power output increases for a given cadence, the IEFF increases; (2) as cadence increases for a given power output the IEFF decreases; and (3) between the two groups there are differences in the IEFF at the low cadence high power output conditions.

REVIEW AND THEORY

To compare the pattern of force application across subjects and between power outputs and cadences it is necessary to have a common scale. One scale that has been proposed is the Index of Effectiveness which has been used by Lafortune and Cavanagh (1983) and subsequently by Sanderson (1991). This index is the ratio of the component impulse applied perpendicular to the crank as compared to the total impulse applied to the pedal. This ratio reflects the percentage of force that contributes to maintaining crank revolutions.

PROCEDURES

The subjects were volunteers with a range of cycling experience. There were 17 recreational riders and 12 competitive riders which were CCA licensed racers or competitive triathletes. All subjects signed an informed consent form before the test. The subjects rode an instrumented bicycle which was mounted on a Schwinn Velodyne, an electronically braked cycle ergometer that simulates inertial characteristics of road riding and can modulate given power outputs based on cadence. The bicycle was equipped with two triaxial piezo- electric force transducers mounted in the right pedal, a continuous output potentiometer to measure pedal angle, and two optical sensors; one to locate crank position and one to indicate top dead centre (TDC). Force data were collected at 15° intervals for 600 msec at a rate of 1 KHz. Cadence and power output were presented randomly to each subject. Force data were collected for 12 pedal cycles. The Index of Effectiveness was then calculated using the integral of the effective force, the portion of the force that is perpendicular to the crank, divided by the total force applied to the pedal. Single factor analyses of variance were used to determine statistical significance between cadences, power outputs and the two groups of cyclists. Significance was set at $p<0.05$.

RESULTS AND DISCUSSION

Cadence/Power Effects. One aim of this study was to investigate the ways in which the Index of Effectiveness (IEFF) changes across levels of power output and cadence and between two groups of cyclists. In Table 1 the summary data for all conditions of each group are presented. Statistical analysis revealed that there was both a significant power and a significant cadence effect. For both groups, as cadence increased there was a decrease in the IEFF for any given power output. whereas, as the power output increased at any given cadence there was an increase in the IEFF .Similar results have been reported by Sanderson(1991) and Patterson et al. (1983), however, this study extends the results to higher power outputs.

rpm	60		80		100	
Recreational group.						
100W	.45	*(.42)*	.37	*(.34)*	.34	*(.29)*
200W	.60		.52		.45	
(235W)		*(.63)*		*(.55)*		*(.46)*
300W	.67		.61		.56	
400W	.68		.65		.60	
Competitive group						
100W	.52	*(.40)*	.38	*(.32)*	.39	*(.27)*
200W	.67		.60		.48	
(235W)		*(.65)*		*(.56)*		*(.45)*
300W	.73		.66		.59	
400W	.74		.71		.64	

Table 1: The mean of the Index of Effectiveness for both the recreational group and the competitive group over the entire pedalling cycle for all conditions. The values in parentheses are data adapted from Sanderson (1991).

In Figure 1 plots of the effective components as a function of crank angle for 100 watts and 400 watts at 80 rpm for the competitive group are presented. These data show that in response to increased power output the riders increase the force overall and increase the effectiveness of its application. With regard to effectiveness, it is clear that the major improvements are in the second half of the pedalling cycle. The increase in effectiveness in both groups is caused by a change in the strategy of force application such that a propulsive impulse is applied over a greater range of crank motion. In fact, as shown in Figures 2, the effective force is positive throughout the pedalling cycle. This indicates that the riders are actively pulling up on the crank during the second 180° of crank rotation.

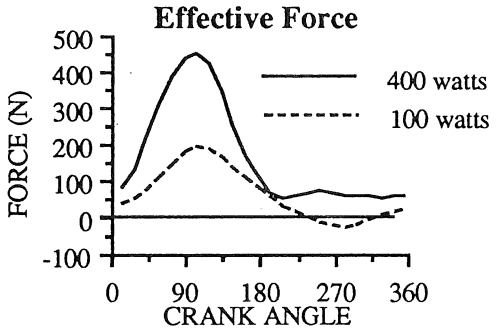

Figure 1: Effective force of the 400 watt and 100 watt trials at 80 rpm, averaged across 12 pedal cycles for the competitive group.

Group Effects. The data in Table 1 show that both groups respond in a similar fashion to the experimental variables. The comparison showed that there were significant differences between groups at the 60 rpm/300W, 60 rpm/400W, and 80 rpm/400W trials but there were no significant differences among the remaining cadence/power output combinations. However, in terms of effectiveness, the competitive group was always more effective than the recreational group. The data displayed in Figure 2 indicate that the major difference between the groups appears in the second half of the pedalling cycle.

The competitive cyclist improves the IEFF by pulling up more effectively in the second half of the pedal cycle. This is clearly evident between crank angles of 225 and 360° where the competitive group has a larger positive effective force. Sanderson (1991) saw no differences between the competitive group and the recreational group because in that study the power outputs were low. If the cyclist is presented with a low cadence, 60 RPM, and a high power output demand, 400 W, then there is a large change in pedal force application in order to overcome the load. An experienced cyclist not only increases the amount of force applied to the pedal, but also changes the way the forces are applied to the pedal when the load becomes difficult to push.

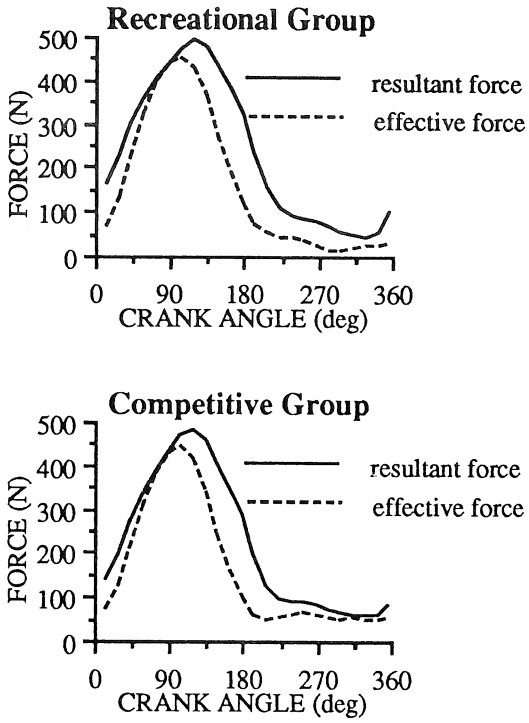

Figures 2: Resultant and effective force averaged over 12 pedal cycles for competitive and recreational groups at 400 Watts and 80 rpm.

This study has shown that there is a difference between competitive and recreational cyclists in terms of index of effectiveness. Furthermore, there are different pedalling strategies depending upon the cyclist's experience and the load that is presented to the athlete.

REFERENCES

Sanderson, D.J. *Journal of Sports Sciences*, **9**, 191-203, 1991.

Lafortune, M.A., P.R. Cavanagh , In *Biomechanics VIII-B: International Series on Biomechanics*. (ed. H.K. Matsui and K. Kobayashi), (pp.928-36.). Champaign, Ill.: Human Kinetics, 1983.

Patterson, R.P et al.. Ergonomics 26, 659-668, 1983.

IN-SHOE PRESSURE DISTRIBUTION IN CYCLING AND RUNNING SHOES DURING STEADY-RATE CYCLING

D.J. Sanderson and E.M. Hennig
UBC Biomechanics Lab, Vancouver BC, Canada
Sportmedizinisches Institut, Universität Essen, Essen, Germany

INTRODUCTION

The aim of this study was to compare the in-shoe pressure distribution between cycling and running shoes during steady-rate cycling. The subjects (n=29) rode a stationary ergometer at a power output of 400 watts and a cadence of 80 rpm in each of the two shoe conditions. Pressure transducers (12), fixed to the plantar surface of the subject's foot were used to record the pressures within the shoe throughout the pedaling cycle. The data indicate that there is a shift in pressure from the toes to the metatarsal region when running shoes are worn.

REVIEW AND THEORY

There is a considerable difference between the characteristics of a cycling shoe and a running shoe. These differences have evolved along with the continuing development of footwear. Sanderson and Cavanagh (1987) compared the distribution of force on the plantar surface of the foot while subjects rode in a cycling shoe and in a running shoe. Their pressure transducer was a 256 element insole. They were able to show, in a small group of subjects, that the important areas of loading were on the medial side of the foot with a consistent decrease to the lateral side of the foot. The aim of the present study was to examine these shoe differences in a larger group of subjects and using single transducers placed over the toes, metatarsal heads, midfoot, and heel regions.

PROCEDURES

Twenty-nine subjects (23 male, 6 female) between 18 and 35 years of age were volunteers. The subjects exhibited a range of experience from CCA license category 1 to recreational. The footwear consisted of a conventional cycling shoe with a molded composite sole and a low-density foam insert.

A pressure distribution unit (PD-16, Halm, Frankfurt / Germany) with 12 individual piezoceramic transducers was used to measure the pressures under the central heel, lateral midfoot, each of the metatarsal heads and all toes. The transducers have an active measuring area of 3 mm * 3 mm with a thickness of 2 mm. Each subject's foot was palpated and the transducers were individually positioned and fastened under specific anatomical regions. This method has previously been used for the measurement of in-shoe pressures during various sports activities (Hennig et al., 1989). A Schwinn Velodyne bicycle simulator was used to create a constant workload resistance. The power on the Velodyne was adjusted to 400 watts. A constant pedaling rate of 80 rpm was chosen for all conditions. Following a warm up period, the two shoe conditions were randomly presented to the riders. Data collection (12 bit resolution) occurred at a rate of 1 kHz per channel for a duration of twelve revolutions. The mean value across the twelve consecutive repetitions were calculated prior to further statistical analysis. A relative load was calculated as a percentage of the relative pressure integral for a full revolution of single transducers towards the total integral across all sensors. A more detailed description of this variable is given in Hennig et al. (1991).

RESULTS AND DISCUSSION

Figure 1 is a graphical representation of the pressure distribution over the foot for each shoe condition. The dominant sites of loading are similar for both types of footwear, namely the 1st metatarsal and the hallux. Of interest are the higher values in the lateral portion of the foot and in the rear and midfoot regions.

These pressures are the relative loads computed over the complete pedaling cycle and are indicative of an overall loading pattern of the foot. There are similarities and differences between these and the data presented by Sanderson and Cavanagh. Among the similarities is the dominant loading of the medial side of the foot and among the differences is the absence of a dominant peak over the fifth metatarsal and the attenuated pressures in the data of Sanderson and Cavanagh. That the peak pressures reported by the latter are smaller than from the present study is most likely the consequence of their smoothing and the possibility that the rubber sheath around the insole acted as a by-pass of some pressures. However, as the transducers in the present study are are of a certain thickness (2 mm) there may be some overestimation of the localized pressure.

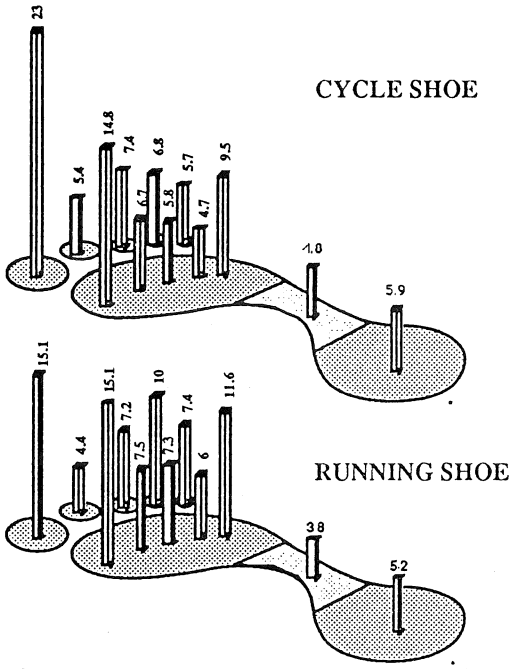

Figure 1: Relative loads for each shoe condition.

Figures 2, 3 and 4 present the mean relative loads over each of the regions for both conditions. The shoe effect is quite different for each region as indicated in the figures. The sum of all the toe loads for the cycling shoe is 48.3% and in the running shoe it is 44.1% whereas for the metatarsal region the total in the cycling shoe is 41.5% and the running shoe is 47.5%. Thus, the overall effect of wearing a running shoe is to shift the dominant area of loading to the metatarsal region and away from the toes. This shift results in a concomitant decrease in the mid and rearfoot loads.

This effect is consistent with the observation by Hennig and Sanderson (1992) that when using a cycling shoe riders generate a moment about the pedal spindle via force from the toe region. To counter this, a moment is generated in the mid and rearfoot regions. In the running shoe, this effect is reduced by virtue of the softer sole. The rider uses the metatarsal region because it lies over the pedal. Consequently, there is general increase in the metatarsal region and decrease in the toes, mid, and rearfoot areas. This may explain why cycling shoes are preferred by competitive cyclists. The nature of the rigid sole enables force to be applied directly to the pedal by more areas of the foot whereas in the running shoe the load bearing is more concentrated across the metatarsal heads. Thus, the added effect of these loads is reduced.

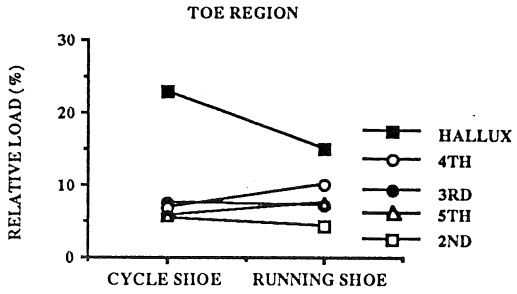

Figure 2. Relative loads on each toe for the two shoe conditions.

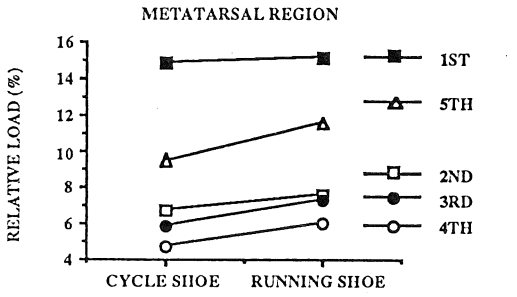

Figure 3. Relative loads on each metatarsal head for the two shoe conditions.

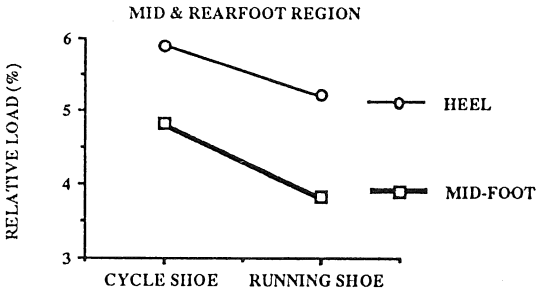

Figure 4. Relative loads on midfoot and heel for the two shoe conditions.

REFERENCES

Hennig, E. M. et al. *Proceedings of the I. Sports World Congress*, Colorado Springs, (pp. 183-184), 1989.

Hennig, E.M. et al. Foot & Ankle, 11, 5, 306-311, 1991

Sanderson, D.J. et al. Biomechanics 10-B, Ed. B. Jonsson, Human Kinetics, Champaign, 903-907, 1987.

IN-SHOE PRESSURE DISTRIBUTION FOR CYCLING AT DIFFERENT CADENCES

A.T. Amoroso, E.M. Hennig and D.J. Sanderson
UBC Biomechanics Lab, University of British Columbia, Vancouver BC, Canada
Sportmedizinisches Institut, Universität Essen, Essen, Germany

INTRODUCTION

The purpose of the present study was to measure the changes in pressure distribution of the foot during cycling at various cadences. Twenty-nine healthy subjects pedalled a conventional bicycle, mounted on a stationary ergometer, at a power output of 400 watts at three cadences; 60, 80 and 100 rpm. Plantar pressure distribution was measured with 12 individual pressure transducers. The results showed large differences in foot pressures between cadences, with lower pressures found at higher cadences. The areas of the foot that experienced the greatest pressures were the hallux and the first metatarsal head, regardless of cadence. There were also relatively high pressures under the fifth metatarsal head, which were consistent across the three cadences. The relative loads under the foot structures were also calculated and showed a large reduction under the first ray as cadence increased whereas the remaining structures were unchanged or increased slightly.

REVIEW AND THEORY

Sanderson and Cavanagh (1987) used a 256-element pressure transducer mat to measure plantar peak pressures at 45 and 90 rpm, while the power output was held constant at 400 watts. A limitation of this study was the inability to associate loads with specific anatomical locations within the foot. The present study utilizes individual pressure transducers located under specific anatomical landmarks of the foot and provides data on the loading patterns of these structures.

PROCEDURES

Twenty-nine subjects (23 male, 6 female) between the ages of 18 and 35 volunteered. The subjects exhibited a range of experience from CCA license category 1 to recreational. The footwear consisted of a conventional cycling shoe with a molded composite sole and a low-density foam insert.

A pressure distribution unit (PD-16, Halm, Frankfurt / Germany) with 12 individual piezoceramic transducers was used to measure the pressures under the central heel, lateral midfoot, each of the metatarsal heads and toes. The transducers have an active measuring area of 3 mm x 3 mm with a thickness of 2 mm. After palpation of the plantar foot area, the single transducers were individually fastened under the specific anatomical regions. This method has previously been used for the measurement of in-shoe pressures during various sports activities (Hennig et al., 1989). A Schwinn Velodyne bicycle simulator was used to create a constant workload resistance. The right pedal was instrumented with two "Kistler" triaxial load cells for the measurement of the normal and shear components of the applied forces. Using potentiometers, crank and pedal angles were determined.

The subjects rode at a constant power output of 400 watts at three cadences; 60, 80, and 100 rpm. Following a warm-up period, the three conditions were randomly presented to the riders. Data collection (12 bit resolution) occurred at a rate of 1 kHz per channel for a duration of twelve revolutions. The mean values across twelve pedalling cycles were calculated prior to further analysis. For a comparison of the pressure patterns, the data at a crank angle of 90 degrees after top dead center (TDC) were evaluated. A relative load was also calculated as a percentage of the relative pressure integral for a full revolution of single transducers towards the total integral across all sensors. A more detailed description of this parameter is given in Hennig et al. (1991).

RESULTS AND DISCUSSION

Figure 1 provides a pictorial representation of the pressures under the different areas of the foot for three cadences at a crank angle of 90 degrees after TDC. For all cadences, the dominant region of loading was under the hallux and first metatarsal head. For the 80 and 100 rpm conditions the next highest load was under the fifth metatarsal head, with less loading on the four remaining toes and middle metatarsal heads. This suggests that riders did not use the middle portion of the forefoot as the main path of force transmission. At the 60 rpm trial however, a different pattern emerged. The pressures were more evenly distributed between the remaining toes and metatarsal heads. The higher pressures were found under the third and fourth toes and the second and fifth metatarsal heads. This difference in pressure distribution can be explained in terms of force production. If the forces that the foot must produce are great enough, as is the case with the 60 rpm condition, a greater area of the forefoot takes on the load.

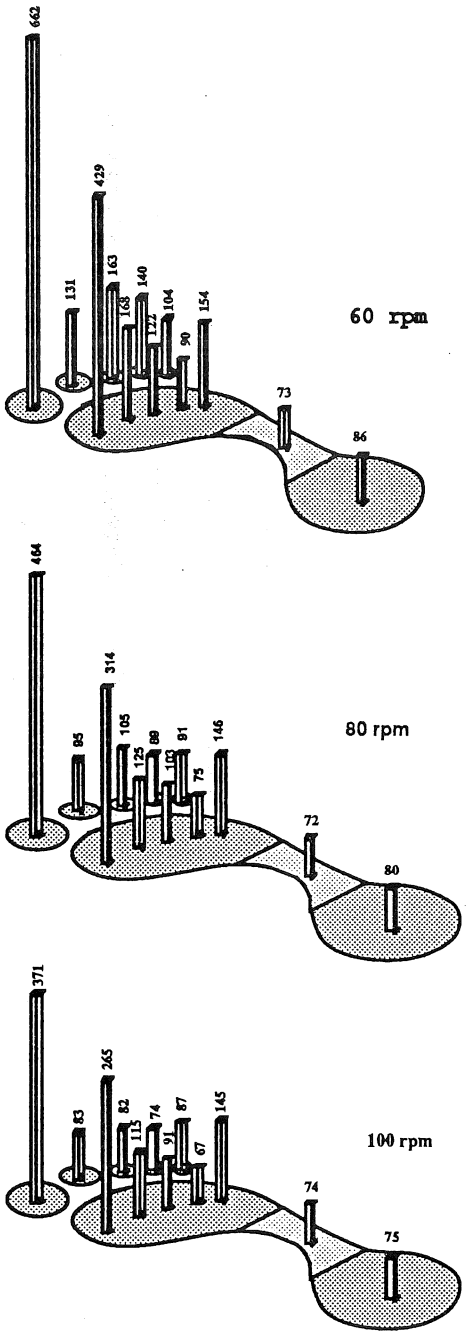

Figure 1: Pressures for the three cadence conditions at 90 degree crank angle.

It has been shown that at a constant power output an increase in cadence results in a decrease in the resultant pedal force (Sanderson, 1991). In this study, the resultant pedal forces for 60, 80 and 100 rpm at 90° crank angle were 541, 445, and 406 newtons, respectively. There was a concomitant decrease in the pressures in all regions except the midfoot. The decreases in pressure were not equal in all regions.

The relative loads on the foot are presented graphically in Figure 2. This analysis reveals that as the pedal force is reduced there is a reduction in the load under the first ray but a gradual increase in the load under the remaining structures. Another view of this response can be seen if the cadence data are reverse: that is, view the rider's response to decreasing cadence. In this case, the response is to increase the loading on the first ray. This observation is consistent with the data presented by Hennig and Sanderson at this conference (1992).

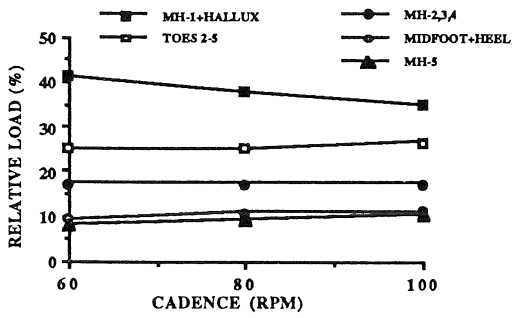

Figure 2: Relative loads (%) under the foot structures with increasing cadence.

REFERENCES

Cavanagh, P.R. et al. Science of Cycling, Ed. E.R. Burke, Human Kinetics, Champaign, 91-122, 1986.

Hennig, E. M. et al. *Proceedings of the I. Sports World Congress*, Colorado Springs, (pp. 183-184), 1989.

Hennig, E.M. et al. Foot & Ankle, 11, 5, 306-311, 1991.

Sanderson, D.J. et al. Biomechanics 10-B, Ed. B. Jonsson, Human Kinetics, Champaign, 903-907, 1987.

IN-SHOE PRESSURE DISTRIBUTION FOR CYCLING AT DIFFERENT POWER OUTPUTS

E. M. Hennig and D. J. Sanderson

Sportmedizinisches Institut, Universität Essen, Essen, Germany
UBC Biomechanics Laboratory, University of British Columbia, Vancouver, Canada

INTRODUCTION

The present study investigated the changes of in-shoe pressure distribution patterns during cycling at various power outputs. Pressures at twelve locations under the foot were examined during steady-rate riding at 4 power conditions. Pressure and relative load analyses were performed to gain insight into the mechanical behavior of the foot in bicycling.

REVIEW AND THEORY

Using instrumented pedals, various researchers have investigated the forces that are applied to the pedal during bicycle riding. Only little information has been presented to date about the distribution of pressures under the foot inside bicycle shoes. Sanderson and Cavanagh (1987) compared the peak pressures inside a conventional cycling shoe with those in a running shoe. They examined 5 subjects at a power output of 400 watts and pedaling rates of 45 and 90 rpm with a 256 element transducer array.

PROCEDURES

Twenty-nine subjects (23 male, 6 female) between 18 and 35 years of age were volunteers. The subjects exhibited a range of experience from CCA license category 1 to recreational. The footwear consisted of a conventional cycling shoe with a molded composite sole and a low-density foam insert.

A pressure distribution unit (PD-16, Halm, Frankfurt / Germany) with 12 individual piezoceramic transducers was used to measure the pressures under the central heel, lateral midfoot, each of the metatarsal heads and all toes. The transducers have an active measuring area of 3 mm * 3 mm with a thickness of 2 mm. After palpation of the plantar foot area the single transducers can individually be fastened for each subject under the specific anatomical regions. This method has previously been used for the measurement of in-shoe pressures during various sports activities (Hennig et al., 1989). A Schwinn Velodyne bicycle simulator was used to create a constant workload resistance. The right bicycle pedal was instrumented with two "Kistler" triaxial load cells for the measurement of the normal and anterior-posterior components of the applied forces. Using potentiometers, crank and pedal angles were determined. In four different conditions the power on the Velodyne was adjusted to 100, 200, 300 and 400 watts. A constant pedaling rate of 80 rpm was chosen for all conditions. Following a warm up period, the four power output conditions were randomly presented to the riders. Data collection (12 bit resolution) occurred at a rate of 1 kHz per channel for a duration of twelve revolutions. The mean values across the twelve consecutive repetitions were calculated prior to further statistical analysis. For a comparison of the pressure patterns the data at a crank angle position of 90 degrees from top dead center (TDC) were evaluated. A relative load was also calculated as a percentage of the relative pressure integral for a full revolution of single transducers towards the total integral across all sensors. A more detailed description of this parameter is given in Hennig et al . (1991).

RESULTS AND DISCUSSION

Assuming symmetry between both legs, the power could be calculated using the pedal forces, crank angle, and pedal angle data (Cavanagh et al., 1986). At the chosen pedaling rate of 80 rpm the calculated powers from all subjects were found to be close to the power settings on the Velodyne simulator (Table 1).

V	100 W	200 W	300 W	400 W
C	99 W	198 W	291 W	390 W
R	175 N	265 N	355 N	445 N
Z	163 N	252 N	347 N	440 N

Table 1: Velodyne Power Setting (V), Calculated Power (C), Result. (R) and Normal Force (Z) at 90 °

Although the transducers have a thickness of only 2 mm, the placement of a discrete transducer underneath the foot will overestimate the local pressures. Furthermore, the pressure transducers only cover 12 chosen locations under the foot. To estimate the value of the pressure measurements, with regard to their ability to describe the interaction between foot and pedal, a linear regression analysis was carried out. For the four power conditions the mean pressures across all 12 pressure transducers were compared to the normal force component on the pedal at 90 degrees (Figure 1). The highly linear relationship suggests that the transducer arrangement

under the foot is well suited for the analysis of the load transfer from the foot to the pedal.

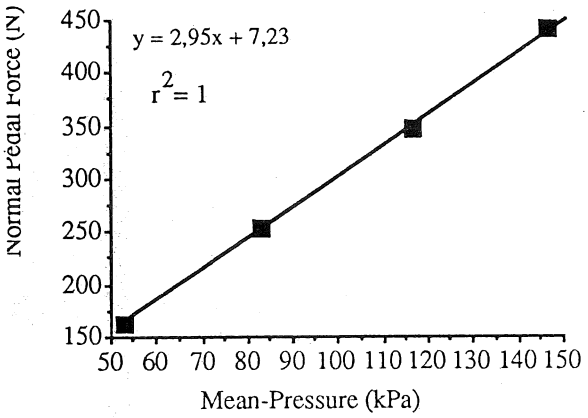

Figure 1: Comparison of mean pressures and pedal forces at 90 degree crank angle.

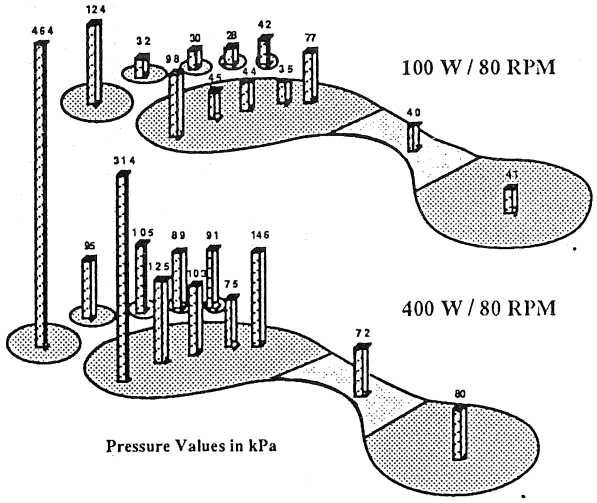

Figure 2: Pressures for 100 W and 400 W at 90 degree crank angle.

Due to the difference in the pedal forces between 100 W and 400 W, the magnitudes of the pressures are also very different (Figure 2). However, similarities in the pressure patterns can be recognized. The pressures under the metatarsal heads I and V are substantially higher than those of the other metatarsal heads. The high pressures under the hallux and the 1st metatarsal head identify the first ray as the dominant structure for the force application onto the pedal. Surprisingly high pressure values are also found under the lesser toes, the heel and the midfoot. This indicates that not only the region on top of the pedal axis (mainly the metatarsal heads) contribute to the applied force, but that the whole plantar surface of the foot is involved in the generation of the pedal forces. Since the large contribution of the toe pressures will create a substantial turning moment around the pedal axis, this moment has to be counterbalanced by midfoot and heel pressures. At the same time the two counterbalancing forces will create an additional force onto the pedal axis (Figure 3).

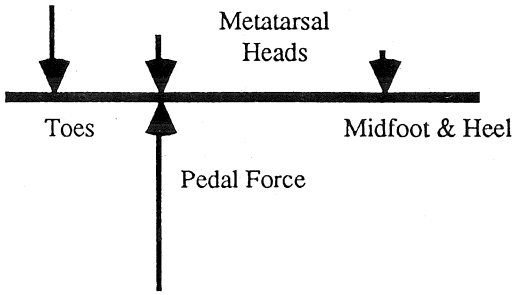

Figure 3: Resultant Pedal Force

The relative load analysis reveals a shift between the contributions of the different anatomical structures with an increase of the load (Figure 4). Whereas there are only minor fluctuations in the relative contributions of the lesser toes (2-5) and the middle metatarsal heads (2-4) a continuous reduction of the relative load in the heel and the 5th metatarsal head is contrasted by a substantial increase of the relative load of the first ray. With an increased demand on force production an anterior and medial shift of the load on the foot occurs, making the dominance of the first ray even more pronounced.

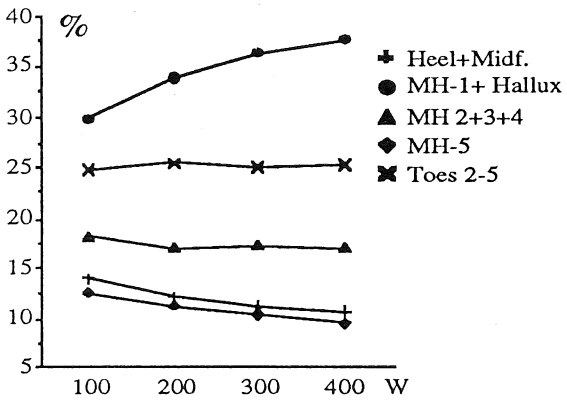

Figure 4: Relative loads (%) under the footstructures with increasing power output (W)

REFERENCES

Cavanagh, P.R. et al. Science of Cycling, Ed. E.R. Burke, Human Kinetics, Champaign, 91-122, 1986.

Hennig, E. M. et al. *Proceedings of the I. Sports World Congress,* Colorado Springs, (pp. 183-184), 1989.

Hennig, E.M. et al. Foot & Ankle, 11, 5, 306-311, 1991

Sanderson, D.J. et al. Biomechanics 10-B, Ed. B. Jonsson, Human Kinetics, Champaign, 903-907, 1987.

THE EFFECT OF EXTENSION-HANDLEBARS ON SELECTED UPPER BODY MECHANICS OF THE CYCLIST: A PRELIMINARY INVESTIGATION

J.A. Miller, Jr., L.P. Laflamme, G.R. Vail, J.G. Reid

School of Physical and Health Education, Queen's University, Kingston, Ontario.

INTRODUCTION

Extension-handlebars are a recent technological advance that have permitted triathletes and cycling time-trialists to significantly reduce their event times. The extension-handlebars allow the rider to adopt a more extended and narrower upper body position than is possible using conventional drop-handlebars, and thereby can increase the aerodynamic efficiency of the rider plus bicycle system (Scott USA, 1991).

Anecdotal information from several triathletes with performance levels ranging from recreational to world-class indicated that there is no general consensus as to how to achieve the optimal upper body position when using extension-handlebars. In many instances, the aerodynamic posture adopted by the rider comes at the expense of enduring pain and discomfort in the shoulder and/or lower back regions. This pain and discomfort may have implications in both short- and long-term riding performance and injuries associated with the upper body.

A cyclist's optimal set-up position is generally determined using a subjective, qualitative process. The set-up position is based initially on opinions from technicians, coaches and/or other cyclists, and then is refined by the cyclist using trial and error experimentation. A set-up procedure individualized to each athlete which identified a group of body positions with approximately equal aerodynamic efficiency, for example, would provide the athlete with alternative positions of equivalent performance potential. The best position might then be selected from the group based on some criterion, e.g., joint loading in each position. We undertook this investigation as an initial step toward developing an individualized set-up procedure.

The purposes of this investigation were (1) to develop a basic, planar model of the upper body of a cyclist and using the model, (2) to determine the effect of variations in extension-handlebars position on selected mechanics of the upper body.

PROCEDURES

A simplified, planar link-segment model of the upper body was developed for this study (Fig.1). The upper body was composed of rigid segments representing the trunk (TR), head and helmet (HH), upper arm (UA), forearm (FA) and hand (HA). The segments were connected by frictionless hinge joints at the hip (H), shoulder (S), elbow (E) and wrist (W). Three angles associated with the upper body were of interest: (1) Θ_{LB} -- the angle between the lower back and the horizontal; (2) Θ_S -- the angle between the trunk and the upper arm; and (3) Θ_E -- the interior angle between the upper arm and the forearm. The angle between HH and the horizontal was set at 40° for all positions.

The center of mass of the upper body with respect to the rear wheel axle (0,0) was determined using the segmentation method (Hay, 1985). For the center of mass calculation, the right and left upper extremities were assumed to be in identical positions, and all segments were oriented in the mid-sagittal plane. The anthropometric data required for the calculations included the subject's segment lengths, and total body mass (Fig.1). In addition, two bicycle dimensions relative to the rear wheel axle were needed: (1) the front of the seat; and (2) the top of the handlebars stem-tube (SO).

Four factors influencing upper body position were varied for this study in the computer program: (1) length of extension-handlebars (LEN: SH = 25 cm; LG = 37 cm); (2) height of handlebars relative to the top of the stem-tube (HGT: LO = 0; HI = 24 cm); (3) position of hip relative to the front of the seat (HIP: FR = 0; BK = -21 cm); and (4) inclination of handlebars relative to horizontal (Θ_{HB}: 0 to 45° in 5° increments); the extreme angles (0°, 45°) as well as the angle closest to the subject's riding position, 15°, have been presented in Table 1. Eight basic set-up positions (POS: a-h; Table 1) combining LEN, HGT and HIP were considered. A link-segment model and its associated mechanics were generated for each Θ_{HB} value at each position (Fig.2).

RESULTS

The center of mass of the upper body ranged from 50.1 cm to 74.8 cm in the horizontal direction, and from 74.1 cm to 98.5 cm in the vertical direction (Fig.2).

The minimum and maximum angles attained overall for Θ_{LB}, Θ_S, and Θ_E were respectively, 8° and 55°, 61° and 146°, and 42° and 170° (Table 1).

The change in Θ_{LB}, as Θ_{HB} varied, ranged by position from 2° to 8° ($\bar{x}$=4.9°). For each Θ_{HB}, the variation in Θ_{LB} across all positions was from 39° to 47° ($\bar{x}$=43.3°). Similarly, the change in Θ_S ranged from 1° to 10° ($\bar{x}$ =4.5°) as Θ_{HB} varied in each position, and from 78° to 85° ($\bar{x}$=82.0°) when considering each Θ_{HB} across all positions. Finally, the change in Θ_E ranged from 35° to 48° ($\bar{x}$=44.4°) across Θ_{HB} in each position, and from 83° to 86° ($\bar{x}$=84.0°) for each Θ_{HB} across all positions.

DISCUSSION

We limited our investigation to a sagittal plane model of the upper body of a cyclist using extension-handlebars,

and examined the effects of changes in the length, height and angle of the handlebars, and hip position on selected mechanics of the upper body.

The height of the handlebars, and the position of the hip influenced the location of the center of mass of the upper body (hereafter, center of mass) the most of the four independent variables considered. As expected, the center of mass shifted in the same direction as the change in the variable, e.g., moving the hip back on the seat caused the center of mass to shift backwards.

Changing the length or the angle of the handlebars (Θ_{HB}) resulted in relatively small movements of the center of mass. An interesting result was found, however, in comparing the patterns of movement of the center of mass using the short and the long handlebars. In the positions using the long handlebars (Fig.2: a,b,c,d), the center of mass shifted back and up as Θ_{HB} increased. In contrast, the center of mass moved down and forward as Θ_{HB} increased in the cases using the short handlebars (Fig.2: e,f,g,h). The relative location between the elbow (lower arm) and the axis of rotation of the handlebars may explain these seemingly contradictory results.

In the first case, with the elbows located equal to or in front of the axis of rotation of the handlebars, an increase in Θ_{HB} causes the elbows to move back and up. The upper arm and trunk remain essentially in the same orientation as shown by average Θ_{LB} and Θ_S values of 2.5° (Table 1: a-d). Thus, the center of mass shifts slightly back and up primarily in response to the displacement of the lower arms. In the second case, when the elbow is located behind the axis of rotation, an increase in Θ_{HB} causes the elbow to move down and forward. This movement tends to pull the upper arms and trunk down and forward, causing a decrease in Θ_{LB}, and an increase in Θ_S. An average decrease of 7.3° in Θ_{LB} and an average increase of 6.5° in Θ_S in our study supported this analysis (Table 1: e-h). The center of mass would then move down and forward in response to the shift in the upper arm and trunk segments. Thus, modifications to an cyclist's set-up which change the position of the elbow relative to the axis of rotation of the handlebars, e.g., placement of the hands along the handlebars, can affect the mechanics of the upper body in different ways.

In summary, changes in length, height and angle of the handlebars, and the position of the hip on the seat can influence to varying degrees the center of mass location and joint angles at the lower back, shoulder and elbow of a cyclist using extension-handlebars. These variables, in addition to the relative position of the elbows with respect to the axis of rotation of the handlebars, should be considered in developing an individualized set-up procedure designed to determine an optimal riding position for the competitive cyclist using extension-handlebars.

REFERENCES

Hay, J.G. The Biomechanics of Sports Techniques, (pp.132-139), Prentice Hall, 1985.
Scott USA. Strategic Gear Technical Manual, 1991.

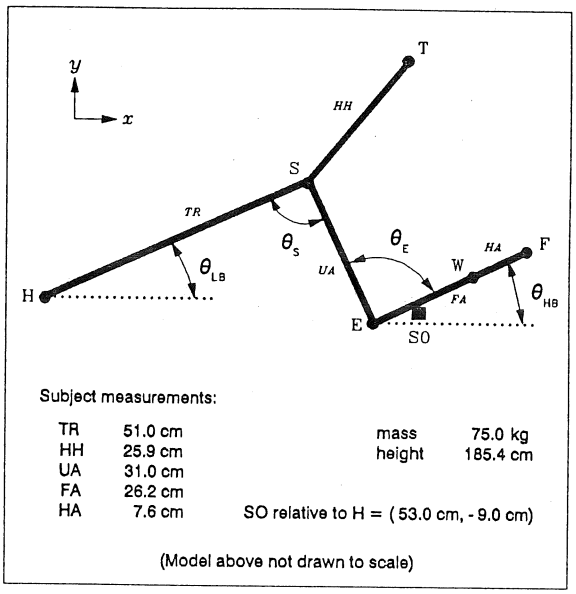

Figure 1. Link-segment model of upper body of cyclist

Table 1. Joint angles for θ_{HB} of 0 , 15 and 45 degrees

Set-up Options				θ_{LB}			θ_S			θ_E		
POS	LEN	HGT	HIP	0	15	45	0	15	45	0	15	45
a	LG	LO	FR	24	25	26	84	84	82	108	93	63
b	LG	LO	BK	8	9	11	142	141	137	149	134	103
c	LG	HI	FR	47	48	50	87	87	86	120	104	72
d	LG	HI	BK	24	24	26	146	146	144	170	156	125
e	SH	LO	FR	25	23	18	61	63	69	87	70	42
f	SH	LO	BK	19	17	11	104	106	114	123	108	80
g	SH	HI	FR	55	53	47	64	63	66	89	76	54
h	SH	HI	BK	39	37	33	107	106	111	146	129	98

* Note: Labels explained in text

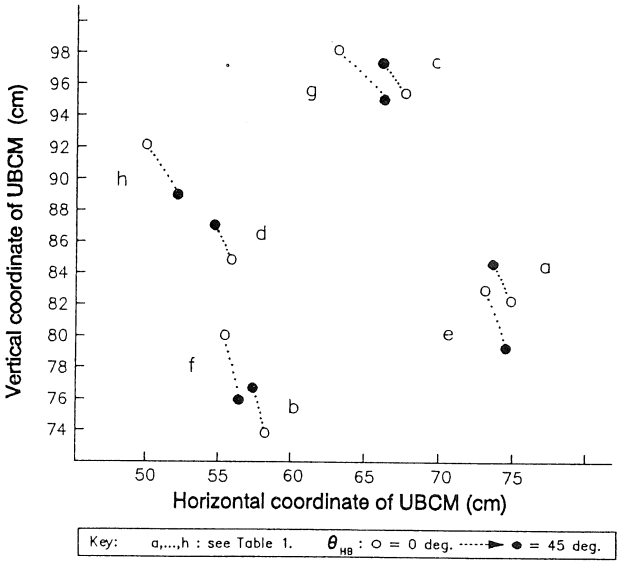

Fig. 2. Effects of variation in length, height and inclination of extension-handlebars, and hip position on upper body center of mass (UBCM).

Proceedings of NACOB II, The Second North American Congress on Biomechanics, Chicago, August 24th - 28th, 1992

THE RELATIONSHIP BETWEEN CADENCE, $\dot{V}O_2$ AND iEMG IN A GROUP OF CYCLISTS AND NON-CYCLISTS

Anthony P. Marsh and Philip E. Martin

Department of Exercise Science and Physical Education
Arizona State University, Tempe AZ 85287-0404.

INTRODUCTION

In order to determine the influence of pedalling cadence on aerobic demand and iEMG of selected lower extremity muscles, trained cyclists (C, n=8) and aerobically trained non-cyclists (NC, n=8) pedalled under 6 cadence conditions (50, 65, 80, 95, 110 rpm as well as a freely chosen (FC) cadence at a 200 W power output. The C and NC did not differ on $\dot{V}O_2$ max or FC cadence and the FC cadence was significantly higher than the most economical cadence in both groups. There were no cadence effects observed in the iEMG data except for the gastrocnemius muscle whose average level of activity increased with cadence.

REVIEW AND THEORY

It has been documented that elite cyclists tend to choose a cadence between 80-100 rpm during steady state riding on level ground. However, the majority of studies of cycling have reported cadences between 20-80 rpm as the most efficient or economical (Dickinson, 1929; Garry and Wishart, 1931; Gaesser and Brooks, 1975; Seabury *et al.* 1977; Croisant and Boileau, 1984; Coast and Welch, 1985). In one of the few studies to use elite cyclists and high power outputs (Hagberg *et al.* 1981), the most economical cadence was 91 rpm. The reasons for these equivocal results remain unclear but maximal aerobic capacity and cycling experience of subjects and procedural factors such as ergometer setup and level of power output are potential contributors.

Lack of agreement between observed FC cadences and experimentally recorded optimal cadences has lead researchers to examine other factors which may influence the selection of a FC cadence. Goto *et al.* (1976) and Reimer *et al.* (1989) assessed the relationship between cadence, iEMG and $\dot{V}O_2$ with varied results. Essentially these studies attempted to determine whether iEMG displayed a minimum at or near the higher cadences used by trained cyclists. At the present time there are no studies that have systematically examined the effect of cycling experience on $\dot{V}O_2$ and iEMG responses to cadence manipulation at a high power output.

This study tested the hypotheses that: 1) the FC cadence of experienced cyclists is higher than that of aerobically trained non-cyclists; 2) the most economical cadence corresponds to the FC cadence in C and NC; 3) average and peak iEMG of lower limb muscles is indicative of a criterion for the selection of the FC cadence.

PROCEDURES

Eight cyclists (C) and eight non-cyclists (NC) were selected based on previous training history and a bike $\dot{V}O_2$max test. Only individuals who achieved $\geq$ 60 $ml \cdot kg^{-1} \cdot min^{-1}$ were selected as subjects. The aim of the initial screening was to identify two distinctly different groups in terms of cycling experience, but similar in maximal aerobic capacity since it was desired to use a power output typical of skilled cyclists for both groups.

Subjects completed two further tests on a bike set up to the dimensions of their own bike or according to generally accepted bike fitting methods. A Velodyne Trainer (Schwinn Corp.) was used to simulate the inertial and non-inertial loading of riding on the road. Steady-state $\dot{V}O_2$ was quantified as subjects pedalled under 6 cadence conditions (50, 65, 80, 95 and 110 rpm as well as their FC cadence) at 200 W. Tests at each condition were separated by 8 min. rest intervals or until such time as the heart rate was below 70 bpm. In a separate session EMG of vastus lateralis (VL), rectus femoris (RF), biceps femoris (BF), soleus (SOL) and medial gastrocnemius (GAST) were collected at 502 Hz using Ag-AgCl electrodes with built-in preamplifiers positioned over the distal half of the muscle belly. A GCS 67 multichannel amplifier was used to further amplify the raw signal. An optical encoder was used to synchronize EMG data with crank angle. Eight cycles of raw EMG were corrected for DC bias, full-wave rectified and integrated over each cycle, then normalized with respect to time and a maximal voluntary isometric action. Further, EMG was integrated in 30° periods to determine peak muscle activation. T-tests and a repeated measures ANOVA were used to test for significant effects associated with training group and cadence factors.

RESULTS

The C and NC did not differ with respect to $\dot{V}O_2$max (67.8 vs 66.2 $ml \cdot kg^{-1} \cdot min^{-1}$, respectively). Further, FC cadence was not significantly different between the two groups (85.2 vs 91.6 rpm). The cyclists FC cadence was similar to that reported by Hagberg *et al.* (1981). In

addition the gross $\dot{V}O_2$ at 200 W was not significantly different between C and NC. The data clearly showed that the most economical cadence (50 rpm for C; 65 rpm for NC) did not correspond to the FC cadence. Neither average nor peak iEMG showed any significant trends which might explain why subjects selected a cadence with an increased oxygen cost as their FC cadence. Only the iEMG of the GAST changed appreciably with cadence but this change did not display a minimum at the FC cadence as was hypothesized. The trends in the peak iEMG data were similar to those seen in the average iEMG values. Peak iEMG activity in GAST increased with cadence while the other muscles showed little change in activity with increases in cadence.

Cadence (rpm)	50	65	80	95	110
$\dot{V}O_2$	40.9	40.4	41.5	43.8	46.8
($ml \cdot kg^{-1} \cdot min^{-1}$)	4.6	4.3	4.4	4.9	4.7
Vast. Lateralis	20.3	19.9	20.8	20.7	22.3
(%max)	10.3	11.4	12.3	11.2	11.8
Rectus Femoris	12.0	11.2	10.6	10.2	11.5
(%max)	5.5	6.0	5.7	5.2	6.0
Biceps Femoris	16.5	16.6	15.9	13.9	14.9
(%max)	11.8	10.5	9.6	7.3	6.7
Soleus	19.3	18.6	19.6	19.7	22.4
(%max)	8.2	8.6	8.9	9.0	10.5
Gastrocnemius	18.3	19.9	22.7	26.6	30.0
(%max)	8.8	8.1	8.0	8.3	8.9

Table 1. Aerobic demand and average iEMG per cycle. Data are means and standard deviations.

DISCUSSION

Previous research has generally reported "optimal" cadences below the range commonly observed during cycling on the road (80-100 rpm). Based on the criterion of minimum oxygen cost, we too would conclude that the most economical cadence was significantly lower than this range. However, the C chose a FC cadence that resulted in a significantly greater oxygen cost. A significant finding of this study was that the NC also chose a FC cadence that was not significantly different from the C and also resulted in a significantly greater oxygen cost. This result was contrary to our hypothesis, that cyclists' FC cadence is higher than that non-cyclists. Comparison with previous research on non-cyclists is difficult due to the dissimilarities between the power output used in this study and those used previously. Other factors such as use of a flywheel ergometer, toe-clips and the aerobic capacity of previous subjects may also invalidate any such comparisons. The gross oxygen consumption data did not display the extreme parabolic trends shown by Coast and Welch (1985). However, the data were in close agreement with those reported by Reimer *et al.* (1989) who also showed that $\dot{V}O_2$ and iEMG (of VL) did not display a minimum value near the higher cadences. It should be noted that both C and NC reported that they felt more comfortable at the higher cadences during the 200 W power output.

The GAST was the only muscle whose average iEMG mirrored the changes seen in the $\dot{V}O_2$ data. Although we had no biopsy data, it is generally accepted that GAST contains a high proportion of fast twitch fibers. It has been shown that at the higher cadences these fast twitch fibers are preferentially recruited (Suzuki, 1979). However, this same line of thought does not apply to the soleus muscle (predominantly slow twitch) or the other muscles (mixed fiber type) examined in this study, whose average iEMG did not change appreciably with increases in cadence. Previous research using force pedals has clearly shown that the peak normal forces on the pedals decrease with increases in cadence (McLean, 1991). However, the peak iEMG did not decrease with increases in cadence as we had anticipated. In general, the changes in the peak values were similar to the changes in the average values.

In summary, these data suggested that cycling experience did not influence the selection of a FC cadence. Further, the FC cadence was not associated with a minimum oxygen cost, average iEMG, or peak iEMG. The data clearly showed that not all muscles behaved in a similar fashion when cadence was manipulated. It is speculated that the iEMG of the muscle may reflect differences in recruitment strategies for muscles of different fiber type composition as the contraction velocity changes.

REFERENCES

Coast, J.R. and Welch, H.G. (1985) *Eur. J. Appl. Physiol.* 53:339-342.
Croisant, P.T. and Boileau, R.A. (1984) *Ergonomics* 27:691-700.
Dickinson, S. (1929) *J. Physiol.* 67:242-255.
Gaesser, G.A. and Brooks, G.A. (1975) *J. Appl. Physiol.* 38:1132-1139.
Garry, R.C. and Wishart, G.M. (1931) *J. Physiol.* 72:425-437.
Goto, s. et al. (1976) *Biomechanics V-A*, 246-252.
Hagberg et al. (1981) *J. Appl. Physiol.* 51:447-451.
McLean, B.D. (1991) *Proceedings of the 13th Meeting of the International Society of Biomechanics, Perth.*
Reimer et al. (1989) *Proceedings of the 12th Meeting of the International Society of Biomechanics, Los Angeles.*
Seabury, J.J. et al. (1977) *Ergonomics* 20:491-498.
Suzuki, Y. (1979) *J. Appl. Physiol. Respirat. Environ. Exerc. Physiol.* 47:263-267.

ACKNOWLEDGMENTS

Partially supported by a grant from the Cycling Research Association.

SEGMENT VELOCITY PRIOR TO CONTACT IN NORMAL AND SOFTER THAN NORMAL LANDINGS

Barry A. Munkasy and Jill L. McNitt-Gray
USC Biomechanics Research Laboratory, Department of Exercise Sciences
University of Southern California, Los Angeles, CA. USA 90089-0652.

INTRODUCTION

The biomechanics of landing from a jump or a fall is important for both performance and safety reasons. Research on this topic has often concentrated on investigation of kinetic, kinematic, and electromyographic (EMG) data from first contact to the end of the landing phase. In addition, researchers have observed that EMG activity in flexor and extensor muscles of the leg occurs prior to contact (Fukada *et al.* (1987), Melvill-Jones *et al.* (1971)). Because large forces occur so soon after contact (before one can react), critical actions for force attenuation must occur prior to contact (Lees (1981), Melvill-Jones *et al.* (1971), Viitasalo *et al.* (1987)). Pre-programmed muscle activity is thought to regulate muscle stiffness at contact and affect the level of impact ground reaction force (Denoth (1986), Mizrahi *et al.* (1982), Stacoff *et al.* (1988), Viitasalo *et al.* (1987)).

Little research has been conducted concerning kinematics prior to contact. Lees (1981) noted that each segment was approximately vertical at contact. Previous researchers studying soft and stiff landings have noted a relationship between the amount of joint flexion used throughout the landing and the magnitude of the peak ground reaction force (Lees (1981), Ozguven et al., (1988)). Since maximum joint flexion occurs well after peak ground reaction force, the amount of joint flexion can only be a consequence of the actions taken prior to the time of peak force. Recently, Devita et al., 1992 have presented results pertaining to moment patterns prior to contact and segment orientation at contact in landings performed with soft and stiff landing strategies differentiated by minimum knee angle. They found that hip extensor moment and knee flexor moment prior to contact differed with respect to the strategy used and subjects at contact were in a more flexed position for soft strategy landings.

The purpose of this study was to further examine segment kinematics prior to contact from a fall. Specifically the velocity of the legs prior to contact in normal and softer than normal landings was investigated.

PROCEDURES

Six healthy male collegiate gymnasts volunteered to serve as subjects. During data collection each subject successfully landed three drop landings using a normal strategy and three drop landings using a freely chosen, softer than normal strategy. All drops were initiated from a height of 0.72 m above the top surface of two 0.12 m thick regulation gymnastics mats (.4 m x .6 m; 100 ILD). The mats were fully supported by two Kistler force plates (.4 m x .6 m). The reaction forces at the mat-plate interface were quantified for each foot using a sampling frequency of 800 Hz. Simultaneously, segment kinematics were recorded at 200 Hz. (NAC Motion Analysis System). Specific data analyzed were velocity of the body center of mass (BCM) and segment velocities of the leg with respect to the BCM, thigh with respect to the BCM, shank with respect to the thigh, and foot with respect to the shank just prior to contact (5 ms), and the peak ground reaction force found during the landing. Data were statistically analyzed using a within subject analysis of variance design ($p < .05$).

RESULTS AND DISCUSSION

As expected, no statistically significant differences were found for the BCM velocity prior to contact. There was, however, a statistically significant difference between peak ground reaction forces for normal (higher) and softer than normal (lower) landings.

In all cases (normal and softer than normal) the lower extremity was found to be falling at a slower rate than the BCM (see Fig. 1). Relative leg, thigh, and foot velocities produced no significant differences between the two landing strategies. However, relative shank velocity was found to be significantly different for softer than normal as compared to normal landings. In a softer than normal landing the shank was found to be falling slower with respect to the thigh than in a normal landing (see Fig. 2). Although not directly investigated, lower segment velocities compared to BCM velocity may be observed from the data of Fukada *et al.* for ankle dorsiflexion prior to contact and Devita et al. (1992) with respect to the hip, knee, and ankle prior to contact.

Leg movement in the air may help to explain the disparity between predications of center of mass velocity at contact using Newtonian mechanics and those actually observed during falls. By retracting the legs prior to contact a faller would increase their time in the air and also increase their center of mass velocity prior to contact.

Future studies may want to explore the relationship between kinematic actions prior to contact and ground reactions forces present during landing.

REFERENCES

Denoth. *Biomechanics of Running Shoes*, (pp. 63-116), 1986.
Devita et al. *Med Sci Sport & Exerc.*, **24**, 108-115, 1992.
Fukada et al. *Biomechanics X-A*, (pp.301-305), 1987.

Lees. *Eng. Med.* **10**, 204-211, 1981.
Melvill-Jones et al. *J. Physiol.*, **219**, 709-727, 1971.
Mizrahi et al. *Eng. Med.* **11**, 141-147, 1982.
Ozguven et al. *J. Biomech.*, **21**, 1061-1066, 1988.
Stacoff et al. *Biomechanics XI-B*, (pp.694-700), 1988.
Viitasalo et al. *Biomechanics X-B*, (pp.695-700), 1987.

ACKNOWLEDGEMENTS

The authors wish to acknowlege the support of the US Olympic Committee, UCLA gymnastics, and the work of members of the USC Biomechanics Lab.

Fig. 1 - Comparison of Body Center of Mass Velocity and the Velocity of the Leg Prior to Contact from a 0.72 m Drop

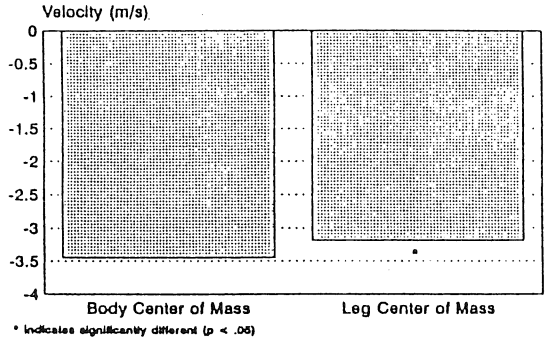

Fig. 2 - Comparison of Shank Velocity with respect to the Thigh in Normal and Softer than Normal Landings

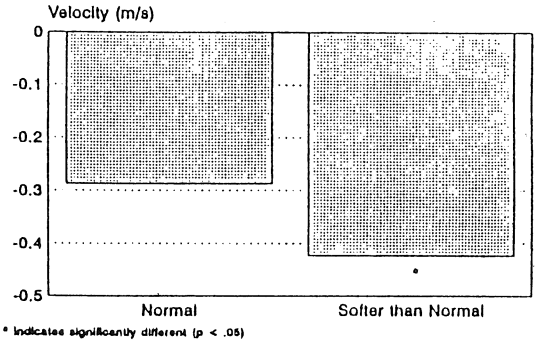

THE MOMENTUM GENERATED BY SEGMENTS DURING DROP LANDINGS

Jill L. McNitt-Gray and Takshi Yokoi
Biomechanics Research Lab, Department of Exercise Sciences
University of Southern California, Los Angeles, CA 90089-0652, USA.

INTRODUCTION

In this study, the adjustments in landing strategies preferred by gymnasts and recreational athletes in response to increases in impact velocity were systematically examined by quantifying and comparing the changes in generated momentum of each segment during drop landings from three heights. Generated momentum, as proposed by Ae et al. (1983), was used to identify the contribution of each segment to the total body momentum during landing. The relative changes in generated momentum by segments across velocities were examined to identify preferred multisegment coordination strategies for dissipation of progressively larger vertical forces experienced during landings.

METHODS

Six male collegiate gymnasts and six male recreational athletes, matched in height, weight, and age, served as subjects. Standardized two foot landings were performed by each subject by stepping off one of three platforms (0.32 m, 0.72 m, 1.28 m) in a randomized order. The segmental movement patterns demonstrated during the landing preferred by each subject at each height were recorded on high speed film at a rate of 202.4 frames per second. The external forces applied to the body at the foot-ground interface were quantified simultaneously using a force plate at a data collection frequency of 1000 Hz. A Butterworth Digital Recursive Filter (Saito & Yokoi, 1982) was used for filtering the random noise introduced during the digitizing process. The residual mean square (RMS) method of Jackson (1979) determined the cut-off frequency for each horizontal and vertical coordinate of the 15 points digitized. The cut-off frequencies used ranged from 5.7 to 12.6 Hz. The second central difference differentiation method was used to determine velocities (Miller & Nelson, 1973) . The landing phase, defined as the time from contact to the minimum vertical position of the TBCG, was selected as the primary interval of interest for this study.

The 15 points digitized formulated an 11-segment model of the human body from which the location of the TBCG was determined (Zatsiorsky & Seluyanov, 1983). The 11-segment model was later reduced to a 5-segment model comprised of segment systems representing the arms, trunk and head, thighs, shanks, and feet. The generated momentum by each segment was determined by using the velocities of the segments and the velocities of the group of segments relative to the velocity of the joint in common (Ae et al., 1983). These absolute and relative velocities were then combined and weighted by the appropriate masses to determine the generated momentum by each segment (1).

$$(1)\quad GM_{\text{distal segment}} = \left(\sum \text{mass}_{\text{segments proximal to distal segment}}\right) \times V_{\text{distal/proximal joint}} + m_{\text{distal segment}} \times V_{\text{distal segment CG/distal joint}}$$

The generated momentum values presented were normalized across individuals by dividing by total body mass and presented in metric units of meter per second.

RESULTS AND DISCUSSION

The peak (local minima) momentum generated by each segment became more negative for all subjects as the magnitude of impact velocity increased (Figure 1). Negative generated momenta indicates that the segments applied a negative vertical impulse on the supported segments acting to encourage downward motion of the segments. The foot and thigh segments consistently reached the largest negative magnitudes, followed by the shanks, head and torso, and arms, respectively. Statistically significant differences in mean peak generated momentum for all segments were noted across impact velocity conditions, however, no significant differences were observed between groups (Figure 2).

From the time of contact, the magnitude of the negative generated momentum of the foot segment steadily declined towards zero during the first 15-20 % of the landing phase. Around the time of heel contact, the generated momentum by the feet shifted from negative to positive. Positive generated momentum indicates that the feet now exert a positive vertical impulse on the supported segments acting to stop the downward motion of the more proximal segments. During this same period of the landing phase, the momentum generated by the shanks, thigh, and head/torso segments become progressively more negative, thus, creating a reduction, or unweighting effect, in the vertical joint force. The similar downward slope in generated momentum demonstrated by the shank and thigh segments indicate both have a similar unweighting effect. The downward slope of the head/torso segment is more gradual thus providing less of an unweighting effect. As the generated momentum of the feet switches signs, the momentum generated by the shanks reaches a local peak and then becomes

less negative. In contrast, the generated momentum of the thighs continues to become more negative, thereby, contributing to greater unweighting perhaps to negate the positive generated momentum of the feet. Examination of generated momentum during landings of more complicated skills or the performance of non-preferred strategies may assist in identifying deviations in preferred multisegment coordination strategies.

REFERENCES

Ae, M., Shibukawa, K., Tada, S., & Hashihara, Y. (1983). A biomechanical analysis of the segmental contribution to the take-off of the one-leg running jump for height. In H. Matsui & K. Kobayashi (Eds.). Biomechanics VIII-B, 737-745. Human Kinetics, Champaign, IL.

Jackson, K.M. (1979) Fitting of mathematical functions to biomechanical data. IEEE Transactions on Biomedical Engineering, 26, 122-124.

McNitt-Gray, J.L. (1991). Kinematics and impulse characteristics of drop landings from three heights. International Journal of Sport Biomechanics, 7, 201-224.

Miller, D. I., & Nelson, R.C. (1973). Biomechanics of Sport. Philadelphia: Lea & Febiger.

Saito, S., & Yokoi, T.(1982). Basic programs of cubic spline smoothing and digital filtering. Bulletin of Health and Sports Science, University of Tsukuba, 5, 201-206

Zatsiorsky, V. & Seluyanov, V. (1983). The mass and intertia characteristics of the main segments of the human body. In H. Matsui & K. Kobayashi (Eds.) Biomechanics VIII-B, 1152-1159. Human Kinetics, Champaign, IL.

The authors would like to acknowledge Richard Nelson, Peter Cavanagh, Jean Landa Pytel, Robert Christina, Carl Millward, Joe Johnstonbaugh, Carolyn Barbieri, Anne Hofmeister, the US Olympic Committee, the Penn State Gymnastics Team, and the USC research team for their contributions to this project.

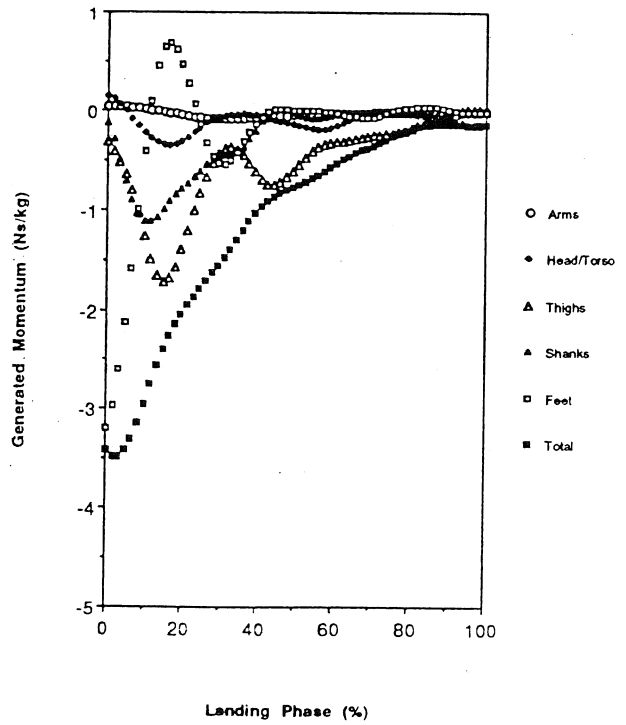

Figure 1. Momentum generated by segments during a drop landing (.72 m) by a gymnast.

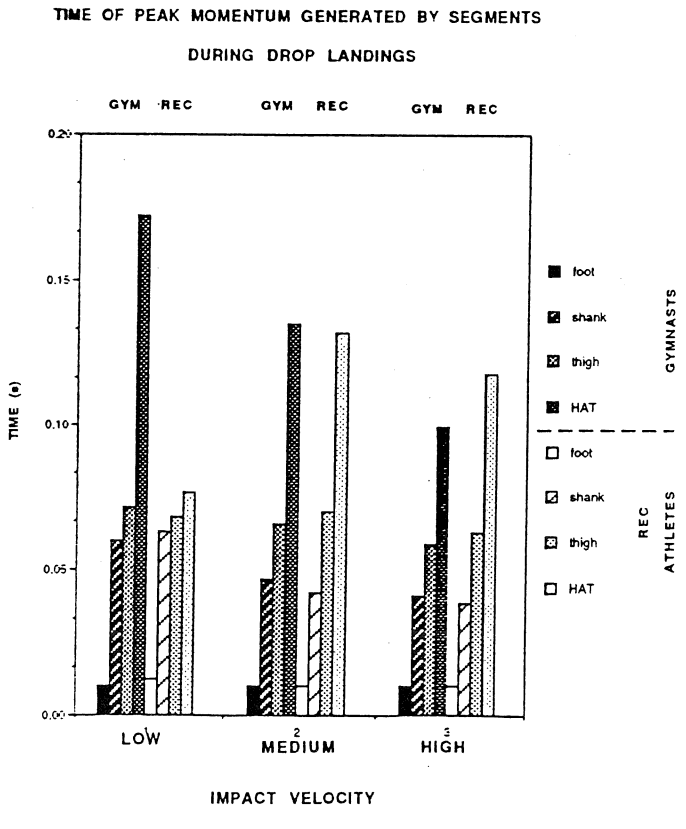

Figure 2. Mean peak generated momentum for gymnasts and recreational athletes during drop landings from three heights.

ADJUSTMENTS IN MUSCLE ACTIVATION PATTERNS DURING LANDINGS OF LOW AND HIGH PEAK VERTICAL FORCES

Michelle D. Welch, Jill L. McNitt-Gray, Dawn M.E.Irvine, and Carolyn Barbieri
Biomechanics Research Lab, Department of Exercise Sciences
University of Southern California, Los Angeles, CA 90089-0652, USA.

INTRODUCTION

The large reaction forces experienced during foot first impacts have been associated with the high incidence of acute and overuse injuries to the lower extremities of athletes. The characteristic of the impulse which has received the greatest attention is the large initial peak in the vertical reaction force (impact peak) corresponding to heel contact. Impact peak magnitudes experienced by a single foot may range from 2 to 4 times body weight (BW) during jumping (Valiant & Cavanagh, 1983; Gross & Nelson, 1987) to as high as 18 BW when landing a double back somersault in gymnastics (Panzer, 1987).

Landing techniques favoring a greater than normal degree of lower extremity joint flexion (soft) have produced reductions in the peak magnitude of the vertical reaction forces experienced during landings (Lees, 1981; Ozguven, & Berme, 1988). However, the mechanisms producing a softer than normal landing are not well understood. An examination of the muscle activity controlling joint motion has not been investigated. The pupose of ths study is to quantify and compare the muscle activation patterns during landings which produce low and high peak vertical forces.

METHODS

Ten male recreational athletes performed nine drop landings using normal, softer than normal, and stiffer than normal landing strategies. Each landing was performed by stepping from a stationary platform positioned 0.72 meters above the force plates. The reaction forces applied to each foot were quantified using two force plates (800 Hz). Segment kinematics were recorded simultaneously using high speed film (100 fps). The muscle activation patterns of seven lower extremity muscles, Vastus Lateralis (VL), Vastus Medialis (VM), Rectus Femoris (RF), Biceps Femoris (BF), Medial Gastrocnemius (MG), Soleus (SO), and Tibialis Anterior (TA), prior to and during the landing were quantified using surface electromyography (1600 Hz; Beckman Silver-Silver Chloride electrodes; Differential Amps, Data, Inc.). The reaction forces, kinematics, and EMG were synchronized at the time of contact. Markers positioned on the body of the subjects were manually digitized using a video based data acquisition system (Peak Performance, Inc.). Each coordinate of the digitized body landmarks (Zatsiorsky & Selyanov, 1982) were digitally filtered independently using a second order Butterworth Filter (Saito & Yokoi, 1983) with a cut-off frequency derived by the method of Jackson (1979). The EMG signals from each muscle were processed using a high and low pass filter (30-800 Hz) , rectified, and integrated during intervals prior to and during the landing phase (SNIP, 1988, Digital Dynamics, Inc.). The interval of interest, identified as the landing phase, was defined as the time required to bring the vertical velocity of the total body center of mass to zero. The temporal and IEMG characteristics of the muscle activity were determined during two separate phases: from contact to time of vertical impact peak force (c-pk), and from contact to the end of the landing phase (c-e). The most extreme landings performed by each subject were then identified based the magnitudes of the vertical impact peak forces (HIGH landings- highest peak vertical forces; LOW landings- lowest peak vertical forces). By comparing the IEMG during landings producing the lowest peak vertical force with respect to IEMG during landings with the highest peak vertical forces, relative adjustments in muscle activity may be observed. Ratios of IEMG (LOW/HIGH) greater than one indicate a relative increase in muscle activity.

RESULTS AND DISCUSSION

Subjects were able to reduce the peak vertical force applied to a leg by an average of 3 BW (Figure 1).

During the interval from contact to time of peak force, 8 of 10 subjects experienced relatively higher levels of plantar flexor and knee extensor muscle activity during LOW as compared to HIGH landings. Examination of relative increases in IEMG within subject exposed three patterns of muscle activity. Subjects (Group A) experiencing the lowest peak and the smallest range of peak vertical forces had relatively larger activity in all muscles monitored in LOW landings. Group B demonstrated increases IEMG in both the plantar flexors and dorsiflexors during LOW landings. Subjects (Group C) failing to reduce peak vertical forces to less than 4.0 BW had relatively larger activity for RF and MG during LOW landings as compared to HIGH landings. These differences in IEMG, however, were negated by relatively longer times to peak force observed for the LOW landings as compared to the HIGH landings. During the interval from contact to the end of the landing phase, relative decreases in average EMG of the knee extensors were observed during the LOW as compared HIGH landings. In conclusion, reductions in external peak vertical forces may be accompanied by changes in IEMG and average EMG. The benefits of each requires further study.

REFERENCES

Gross, T. S., et al. Converse, Inc.,1987.
Jackson, K.M., IEEE Trans Bio Engin 26:122-124, 1979.
Lees, A. , Eng Med 10:207-211, 1981.
McNitt-Gray, J.L. IJSB, 1991.
Ozguven et al. J of Biomech 21,1061-1066, 1988.
Panzer, V.P., Doc. Dissert, U of Oregon, 1987.
Saito, S. et al., B Hlth Sprts Sci, U of Tsukuba, 5:201-206, 1982.

Valiant, G. A. et al., Biomechanics VIII-A, 112-116,1983.
Zatsiorsky, V. et al., Biomechanics VIII-B, 1152-1159,1983.
Acknowledgements: USC Faculty Research and Innovation Fund and USC Biomechanics Research Team.

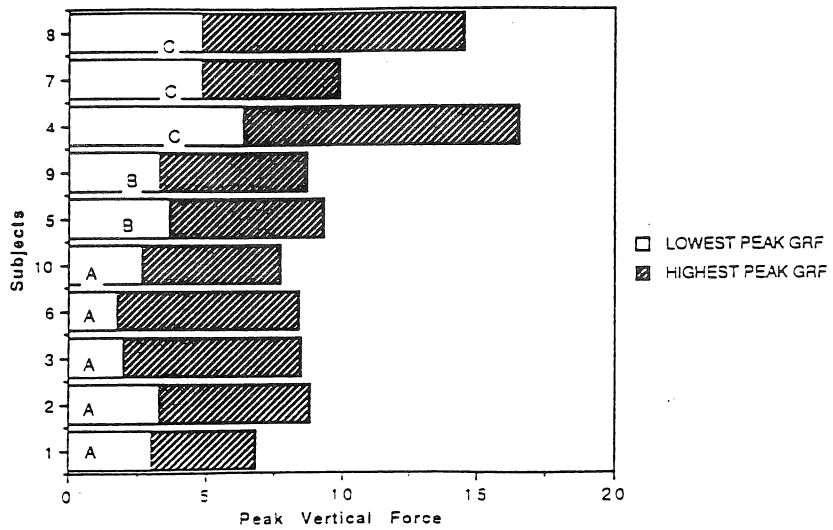

Figure 1. Ranges in peak vertical ground reaction force (GRF) for all subjects during a drop landing.

FOOTWEAR

Poster

Proceedings of NACOB II, The Second North American Congress on Biomechanics, Chicago, August 24th - 28th, 1992

Finite Element Analysis of the Midsole of a Running Shoe

Michael D'Agati, Zvi Ladin
Biomedical Engineering Department and NeuroMuscular Research Center, Boston University, Boston, MA 02215

INTRODUCTION

Over the past 20 years, running has become one of the most popular forms of exercise. As of 1980, there were over 20 million runners in the United States alone and two out of three had been injured once a year [1]. One common cause of injury is over pronation which is believed to be linked to several types of injuries in running.

Studies have shown that pronation can be controlled in part, by shoe design. The goal of this study is to obtain a finite element model of the shoe midsole and find the stress strain relationship in the midsole. This information will be used in a second model to predict ankle rotations and study the effect that the distribution of materials in the midsole has on pronation.

REVIEW AND THEORY

Running is an activity which cyclically subjects the body to large impulsive forces. Repetitive, impulsive loading such as that experienced during running, is suspected of causing injuries such as shin splints, tendon and cartilage damage. Radin et al. [2] have shown that repeated impact loading of the joints equivalent to the animal's body weight for one hour a day, produces microfractures in the bone and degenerative changes in the articular cartilage.

Pronation is one of the methods the body uses to control the impact forces associated with heel strike. It allows an extension of the time over which heel strike occurs, decreasing the peak forces experienced by the body following heel strike. Excessive pronation, however, has been shown to cause additional stresses on the bones and soft tissue and has been linked to various injuries of the hip, knee, achilles tendon and the foot [3].

Numerous researchers have proposed and shown that the shoe has the ability to alter the interaction between the foot and the ground. Clarke [3] has shown that a soft midsole allows significantly more pronation and total rearfoot movement than shoes with medium and hard insoles. Nigg [4] has shown that the stiffness of the midsole does not significantly reduce the impact forces associated with heel strike, but does change the location of the ground reaction forces acting on the foot, therefore, the change in midsole stiffness redistributes the load and does not cushion the foot. These findings suggest that shoe design has the ability to alter the kinematics of the foot in both a beneficial and detrimental way.

Several models of the midsole and its response to loadings have been proposed. Shorten and Winslow [5] modeled the shoe as a set of parallel, non-linear, viscoelastic elements described by simple constitutive equations. The model was solved numerically and the solutions yielded the kinematics of the midsole surface and the energy quantities in the midsole. Another model, proposed by Li and Ladin [6] modeled the midsole as an elastic interface with a linear distribution of vertical compression springs. Li and Ladin also included a model of the foot and shank. They examined the effect of combining two different density foams on pronation, and found both theoretically and experimentally that there was an optimal distribution of foam under the foot which minimizes pronation in a static trial.

The purpose of this study was to use the finite element method (FEM) to analyze the deformations and stresses of the midsole. Over the past 20 years, the FEM, due to its ability to analyze the stresses in structures of complex shape, loading and material behavior, has become an extremely popular method of solving complex structural mechanics problems [7]. Using the FEM, it is possible to better understand how the shoe, and more specifically, the midsole behaves during running. By identifying the stress strain relationships occurring during running, it will be easier to tailor the design of shoes to a variety of runners.

PROCEDURES

A running shoe midsole was digitized and entered into I-DEAS, a finite element package, and a three dimensional model of the midsole was created (figure 1). It consists of approximately 7000 nodes and 4000 solid parabolic tetrahedral elements. The size of the elements was varied with the thickness of the midsole, and optimal element sizes were selected to minimize FEM solution time.

The material of the midsole was modeled as a uniform, linear, elastic, isotropic ethyl vinyl acetate (EVA) foam with a constant modulus of elasticity. The material properties were provided by the research and development department of Reebok Inc.

Pressure distributions measured between the foot and insole during running were used to load the model. The area of the sensors was on the order of 0.5 mm. A total of twenty pressure distributions were obtained from a single step. Ten pressure distributions were used to load ten models at times ranging from heel strike to toe-off. The assumption was made that shear forces are small compared to the normal forces and were negligible.

Two sets of boundary conditions were used for each solution. The first set, which was common to all ten solutions, consisted of restraints of the nodes along the upper edge of the midsole in the X and Y directions. This represented the upper of the shoe. The second set of restraints were on the bottom surface of the sole and were unique to each solution. These restraints represented the contact of the sole with the ground. The boundary conditions are assumed constant with respect to time, and no movement of the restrained nodes can occur during a solution. Displacement, stresses and strains were obtained for each of the paired loadings and boundary conditions. These results will be used in a model to predict ankle rotation.

RESULTS

The solutions obtained for the model are displacements, stresses and strains. The stresses are used to confirm that the midsole is staying within the tested range of the material. EVA's behavior is fairly linear within the range of stresses found, however, hysteresis is still a concern. Solutions of displacements and strains are also obtained. Figure 1 shows displacement results at heel strike and halfway through the stance phase. At heel strike, the displacements of the midsole are concentrated along the lateral side of the shoe. This corresponds to the foot landing in a supinated position, which is what typically occurs at heel strike. An interesting result is that the displacement during heel strike is not as great as one would expect, only 0.2 mm, and is localized to the heel region. At mid stance, however, the maximum displacement is 0.6 mm and is spread out along a line corresponding to the pronated position that the foot is in. The stress values correspond to the displacement values, as would be expected in a linear model. At heel strike, a maximum compressive stress of $6x10^4$ Pa was found, while at mid-stance, a maximum compressive stress of $3.7x10^5$ Pa was found. The displacements and stresses correspond to the pressure distribution. Typically, the foot rolls into a pronated position just after heel strike, which is the time when the most damage can occur to tendons and ligaments. Stabilizing the foot is necessary to avoid over-pronating. Reducing the stiffness of the materials on the lateral side, while increasing the stiffness of the material on the medial side may allow the foot to become more stable. Several investigators have previously suggested this type of distribution, however, a finite element analysis allows specific material properties to be chosen, rather than using a trial and error approach.

REFERENCES

[1] Nigg, B. M., *Biomechanics of Running Shoes.* Human Kinetics Publishers, Inc. Champaign, IL, 1986

[2] Radin, E. L., et. al. Response of joints to impact loading-III. *J. Biomechanics*, 6, 51-57, 1973

[3] Clarke, T. E., Frederick, E. C., Hamill, C. L., *Medicine and Science in Sports and Exercise*, 15(5), 376-381, 1983

[4] Nigg, B. M., Hahlsen, H. A., Luethi, S. M., Stokes, S., *J. Biomechanics.* 20(10), 951-959 1987

[5] Shorten, M. R., Darcy, S. W., Abstract from Thirteenth Annual Meeting of American Society of Biomechanics, *J. Biomechanics.* 23(7), 721, 1990

[6] Li, P., Ladin, Z., In Press, *J. Biomechanics*, 1992

[7] Huiskes, R., Chao, E. Y. S., *J. Biomechanics*, 16(6), 385-409, 1983

ACKNOWLEDGEMENTS

Partial funding for this project was provided by Reebok International Ltd.

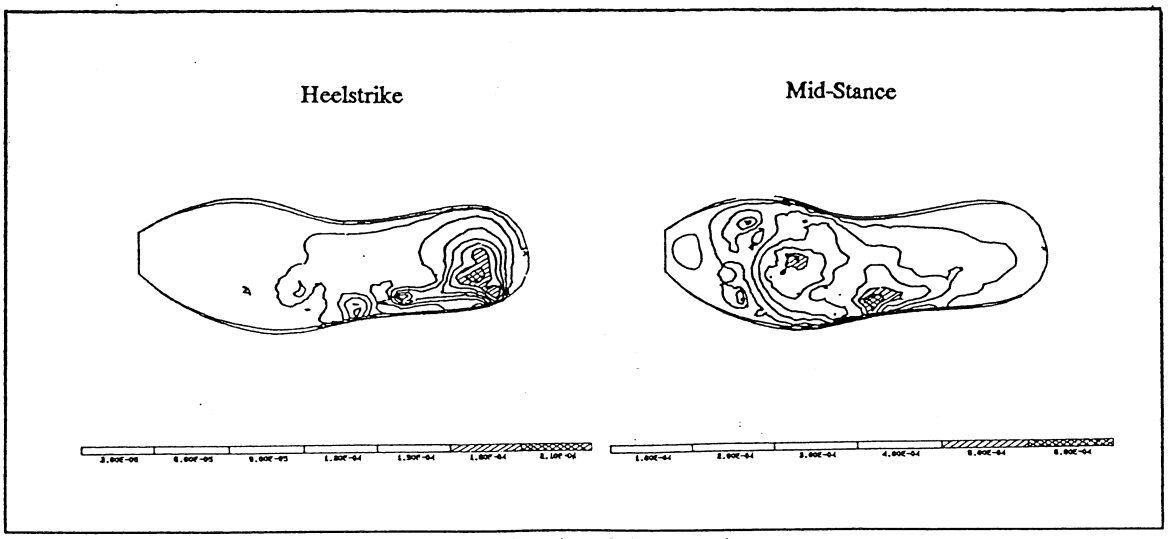

Figure 1 Displacements of midsole at heelstrike and halfway through the stance phase

GROUND AND IN-SHOE REACTION FORCES DURING WALKING

Timothy R. Derrick and Joseph Hamill
Biomechanics Laboratory, Department of Exercise Science
University of Massachusetts, Amherst, MA 01003

INTRODUCTION

The primary function of the midsole in a running shoe is usually considered to be a reduction in the forces experienced by the body. The vertical ground reaction force (VGRF) has been generally accepted as the best reflection of these forces but a more meaningful measurement may be the in-shoe reaction force (ISRF). This investigation was undertaken to compare the VGRF to the ISRF during walking in three conditions: no midsole, hard midsole (50-55 shore A scale) and soft midsole (25-30 shore A scale).

REVIEW AND THEORY

Mechanical material testing devices show decreased impact forces with a softer midsole material. If the body were a completely mechanical system the magnitude of the VGRF curves would decrease when a midsole is added. It is hypothesized that the body detects a reduction in injury potential when midsole cushioning is added and then adjusts kinematics to optimize some unknown factor. Likely mechanisms for this adjustment are the knee angle at contact or the knee velocity at contact (Frederick, 1986). It has been shown that greater knee flexion occurs during contact while walking barefoot than while walking in shoes (Cavanagh et al., 1981). It is unlikely that the controlling factor is the VGRF's because the body cannot directly detect these forces. A more likely candidate is the in-shoe reaction forces (ISRF) or the in-shoe pressures between the foot and the shoe.

PROCEDURES

Five male volunteer subjects performed five walking trials in each of three conditions within 5% of their preferred velocity. Vertical ground reaction force data were collected with an AMTI force platform (100 Hz) and in-shoe pressure data were collected with Tekscan foot sensors (100 Hz). In-shoe reaction force curves were constructed by multiplying the pressure value of each cell in the sensor by its area (5.1 mm^2) and then summing over all the cells. Calibration of the foot sensors was accomplished using two trials performed before each condition and two trials afterward. These trials were collected without a midsole so that both devices were measuring the same force. The period of time that the foot was in contact with the ground (stance) was determined for each pair of curves and this portion of both curves was normalized to 100 points. The ratio of the force platform value to the foot sensor value was then computed for each point of all four calibration trials. The four curves were then averaged so that 100 values representing the calibration factor for each 1% of stance could be used to calibrate the foot sensors for each condition.

Both the VGRF and ISRF curves exhibit a peak value during weight acceptance followed by a valley. Another peak value occurs during the push-off phase. Analysis of the VGRF and the ISRF curves was accomplished by determining the magnitudes of the curves during the peak weight acceptance (F1) and peak push-off (F2) for each condition. This abstract will concentrate on F1.

RESULTS AND DISCUSSION

Since the two measurement devices are in direct contact during the no midsole condition, the values obtained from these methods should be the same (Fig. 1). This condition was used to verify the calibration procedure. The mean difference between the two methods for F1 was .8 Newtons, while the mean difference during F2 was 40 Newtons.

The maximum weight acceptance VGRF values did not change when a midsole was introduced. The no midsole conditon mean was 913 Newtons while the hard midsole condition mean was 894 Newtons and the soft midsole condition mean was 912 Newtons. This result is consistent with studies that have found no increases in VGRF values when midsole hardness has been changed (Frederick, 1986). The ISRF values during weight acceptance increased for four of the five subjects when the hard midsole was added (Fig. 2). A mean value of 914 Newtons was measured during the no midsole condition and 1097 Newtons for the hard midsole condition. During the soft midsole condition (illustrated in Fig. 3) all five of the subjects had greater mean maximum weight acceptance values (1061 Newtons) compared to the no midsole condition. These results indicate that providing a softer midsole does not necessarily decrease VGRF's and actually tends to increase ISRF's. The large differences between the VGRF and the ISRF values suggest that calculations using the former may

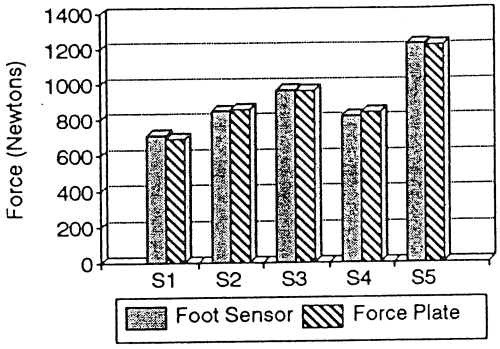

Figure 1. Peak weight acceptance, no midsole.

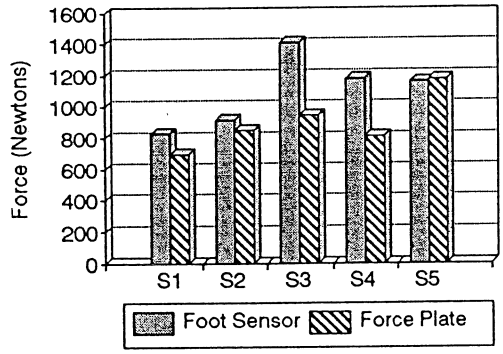

Figure 2. Peak weight acceptance, hard midsole.

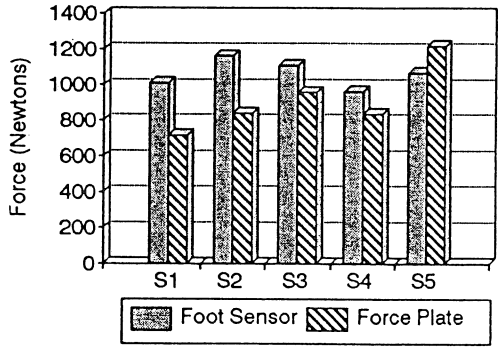

Figure 3. Peak weight acceptance, soft midsole.

underestimate the actual forces experienced by the body.

A possible benefit to increasing the softness of a midsole may be to spread the in-shoe forces over a greater area. In-shoe pressures should be looked at to test this theory.

REFERENCES

Cavanagh, P. Biomechanics VII-B, (pp. 151-156), University Park Press, 1981.

Frederick, E. J. of Spt. Sci., 4, 169-184, 1986.

THE EFFECTS OF MIDSOLE HARDNESS ON SHOE CUSHIONING

N. Stergiou, B.T. Bates, and H.P. Davis

Department of Exercise and Movement Science
University of Oregon, Eugene 97403, USA

INTRODUCTION

Two methods have been identified for evaluating the shock attenuating properties of various shoe designs: 1) material tests using impact testing equipment and 2) evaluation of subjects using a force platform (Clarke et al, 1983; Luethi et al, 1987; Nigg et al , 1987). An unexpected lack of correlation between the two methods has been reported and theories have been forwarded to explain this lack of relationship. The results of this study, however, revealed a strong relationship between in-vivo estimates of ground reaction forces and in-vitro measurements of shoe cushioning.

REVIEW AND THEORY

Protection of the body from excessive impact forces is a primary function of sport shoes. Several cushioning systems have been used to diminish these impact forces. In-vitro impact testing methods are able to distinguish between different cushioning systems (Frederick et al, 1984), however, when impact test values have been correlated with in-vivo results obtained from ground reaction forces, a lack of correlation has been observed (Clarke et al, 1983; Luethi et al, 1987; Nigg et al, 1987). This lack of correlation has generally been attributed to kinematic adjustments resulting in changing ground reaction force (GRF) patterns. This hypothesis was evaluated in the present study by comparing in-vivo and in-vitro results obtained using a more rigorous experimental protocol.

PROCEDURES

Two pairs of shoes were evaluated in each of three test sessions, for a total of six shoes. The shoes were high quality running shoes from reputable manufacturers. Each session incorporated six male runners performing 25 trials for each shoe condition. The subjects ran at their preferred training pace (±5%) while being monitored using a timing light system. Sagittal and rear view kinematic data were collected using a two camera automated tracking system (Motion Analysis Corp., 200 Hz). Reflective markers were attached at the hip, knee and ankle joint centers to monitor sagittal plane knee joint motion and on the heel portion of the shoe and achilles tendon to monitor rear foot motion. GRF data were collected using an AMTI force platform (1000 Hz). In addition, all shoes were tested using an Impact Testing System (Exeter Research Inc.) in accordance with ASTM recommended procedures. The two shoes evaluated in each session were compared and classified as hard or soft based upon the impact test parameter results for peak acceleration (PG), peak press (PP), and time to PG (TG) (Table 1). Lesser values for PG and PP along with greater values for TG, indicated a softer shoe. Pearson correlation coefficients were calculated between hard and soft shoe parameters using mean subject values (n = 18) for the first maximum force (F1), the time to F1 (T1), the second maximum force (F2), the time to F2 (T2), maximum knee angle (K), the time to K (TK), maximum pronation angle (P) and the time to P (TP).

RESULTS AND DISCUSSION

Significant ($p<0.01$) correlations were found for all variables evaluated (Table 2). Explained variance ranged from 49% (T1) to 97% (K) with four values greater than 85% (F1, F2, K, and TP). F1 and F2 increased while T1 and T2 decreased for the harder shoe. The slopes of the regression lines for all the GRF parameters (F1, T1, F2, T2) and TK were significantly different ($p<0.01$) from 1.0 indicating unequal results for these parameters. K, P and TP slopes were not significantly different than 1.0 indicating no performance differences for these parameters. These results are contradictory with results reported in the literature indicating that changes in shoe hardness do not result in changes in impact force peaks. Nigg et al (1987) characterized their results as "surprising and contradictory to common sense". The lack of correlation has been attributed to adjustments in

kinematics. Subjects in the present study did not change their kinematic performances for the variables evaluated (K and P) suggesting that the GRF differences (F1, T1, F2, T2) resulted from shoe differences. In a previous study, Bates et al. (1983) indicated that fewer than 20 trials are inadequate for detecting shoe differences. Therefore a possible explanation for these different results could be unreliable subject data due to too few trials per subject condition in other studies (Nigg et al used 3 trials, Luethi et al 2 trials, and Clarke et al 5 trials versus 25 trials for the present study). Error due to intra-individual variability is a major problem that must be taken into account if subtle differences are to be detected. In summary, the results of the study revealed a strong relationship between in-vivo estimates of ground reaction forces and in-vitro measurements of shoe cushioning.

REFERENCES

Bates, B.T. et al. Proceedings of the International symposium on Biomechanical Aspects of Sport Shoes and Playing Surfaces, Calgary, (pp. 191-198), 1983.
Clarke et al. Proceedings of the International symposium on Biomechanical Aspects of Sport Shoes and Playing Surfaces, Calgary, (pp. 25-33), 1983.
Frederick et al. In Frederick (Ed.) Sport Shoes and Playing Surfaces, 190-198, 1984.
Luethi et al. In Jonsson (Ed.) Biomechanics X-B, 931-936, 1987.
Nigg et al. Journal of Biomechanics, 20, 951-959, 1987.

Table 1. Impact Testing Results for the Six Shoes.

	Session 1		Session 2		Session 3	
	Sh1	Sh2	Sh3	Sh4	Sh5	Sh6
PG (g)	18.49	17.08	16.23	15.99	22.31	20.69
PP (kPa)	969.10	895.40	850.40	838.10	962.90	892.90
TP (ms)	12.62	14.04	13.76	14.50	13.33	15.26
	Hard	Soft	Hard	Soft	Hard	Soft

Table 2. Pearson Correlation Coefficients/Regression Slopes for Hard and Soft Shoe Conditions (n = 18).

F1	T1	F2	T2
0.922*/0.742*	0.701*/1.274*	0.982*/0.869*	0.854*/1.134*
K	**TK**	**P**	**TP**
0.984*/1.010	0.724*/0.687*	0.791*/0.990	0.927*/1.030

* $p < 0.01$ (df = 17)

EVALUATING BASKETBALL SHOE DESIGN WITH GROUND REACTION FORCES

G.A. Valiant and K.B. Eden

NIKE Sport Research Lab, Beaverton, Oregon

INTRODUCTION

Kinetics of running and jumping have been thoroughly described and applied to footwear design. However, little attention has focussed on the implications of the kinetics of lateral movement on footwear design. In this study, ground reaction forces (GRF) developed during cutting, shuffling, and rapid stopping were measured. The findings revealed times when forefoot stability needs of basketball shoes were high, provided minimum outsole traction requirements, and indicated that basketball shoe cushioning requirements can be as important during lateral movements as during running or jumping.

REVIEW AND THEORY

Basketball players perform many different types of movements, including straight-line running, jumping, dribbling, shooting, cutting, rapid stopping and starting, shuffling sideways. GRF during running have been studied extensively (Cavanagh *et al.*, 1980). Magnitudes of the vertical GRF developed during jump landing have been used to quantify the cushioning needs of shoes (Valiant *et al.*, 1985) or to indicate the potential for injury (Cavanagh *et al.*, 1990). The latter authors also recorded high mediolateral GRF during shuffling and implied that extreme foot position during lateral movements may be related to the high incidence of lower extremity fractures in professional basketball players.

Since running and jumping activities have received considerable attention in the past, the purpose of this study was to measure GRF developed during lateral movements and to apply the results to design and evaluation of stability, traction, and cushioning requirements of basketball shoes.

PROCEDURES

Thirteen subjects made 90° cuts around a 1.22 m tall post with the change in running direction occurring on a painted plywood covered force measuring platform, shuffled across the force platform, and performed straight-line runs, rapidly stopping with the right foot on the force platform. Infrared light emitting diodes on the right shoe and on the force platform surface were tracked at 200 Hz, synchronized in time with 12 bit conversion of GRF, sampled at 600 Hz. Forces were expressed relative to medio-lateral, anteroposterior, and normal shoe axes.

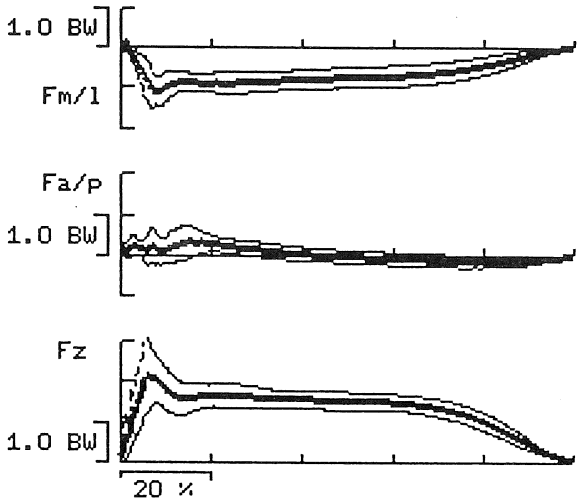

Figure 1. Mean (solid) +/- 1 SD (thin) force components, normalized to body weight, developed during 90° cutting. Mean time of support = 390 ms. Note the attenuation when averaging curves whose peaks do not occur at exactly the same time. (n = 13 subjects)

RESULTS

Mean mediolateral ($F_{m/l}$), anteroposterior ($F_{a/p}$), and vertical (F_z) GRF components developed during the 90° cutting movement are plotted in Figure 1. Horizontal forces are developed primarily in a lateral direction because, in preparation for making the cut, subjects internally rotated their foot or leg.

The force ratios obtained by dividing $F_{m/l}$ and $F_{a/p}$ by F_z provide information about the minimum coefficient of friction necessary for completion of different movements without slipping. Plotted in Figure 2 are the mean F_z

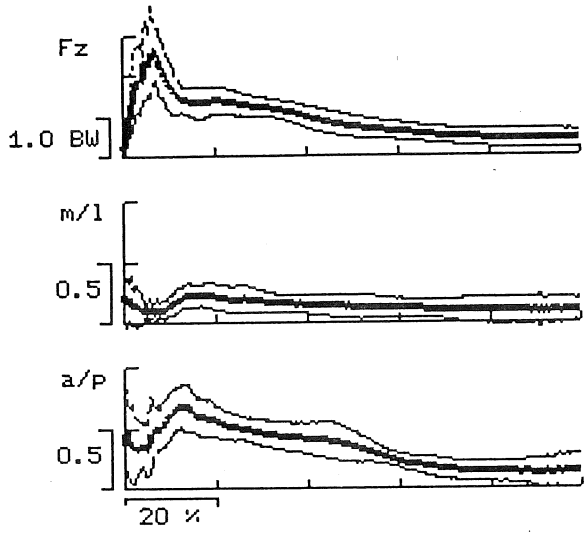

Figure 2. Mean (solid) +/- 1 SD (thin) translational traction coefficients during rapid stopping. Data was averaged for the first 500 ms of support. (n = 13 subjects)

and the absolute value of the mean mediolateral and anteroposterior force ratios developed during the rapid stopping movement.

Table 1. Mean peak GRF normalized to body weight and absolute value of mean peak force ratios for three basketball movements. (n = 13 subjects)

	$F_{m/l}$	$F_{a/p}$	F_z	m/l	a/p
cut	-1.37	0.62	2.57	0.72	0.66
shuffle	-0.66	0.43	1.99	0.58	0.50
stop	-0.61	1.89	3.31	0.41	0.85

DISCUSSION

The mean peak forces for the cutting and stopping movement agree with similar data collected on a group of subjects performing lateral soccer movements (Valiant, 1988).

One may expect the lateral stability needs of the shoe upper and bottom to be greatest when the laterally directed shear forces are greatest. For the cutting movement, these forces peak at a mean of 9% of the total support time. At this time both the rear and fore parts of the shoe are supporting the vertical load, and the torsional stiffness provided by the length of outsole/midsole spanning rearfoot to forefoot sections may contribute to stability. When the rear foot is unloading during the propulsive phase mediolateral stiffness in the forefoot region plays a greater stability role. However, the laterally directed forces which forefoot stability features must resist during the propulsive phase of the cutting movement average only 56% of the mean peak forces during the impact phase.

The greatest translational traction coefficient was measured along an a/p axis during rapid stopping. The mean minimum coefficient of 0.85 exceeds the mean minimum required along an m/l axis during cutting. Generally, traction needs during the initial impact phase are greater than during the propulsive phase. Outsoles coefficients of friction exceeding 1.0 are generally all that are necessary to prevent slip during high intensity basketball activities.

The mean peak anteriorly directed forces of 1.89 BW developed during the rapid stopping movement are at least three times greater than those developed during cutting, shuffling, straight-line running, and more than double those developed when landing from a jump. These magnitudes imply that outsole frictional needs are high during this movement. They also indicate that the tips of basketball shoes must be designed to withstand the very high shear forces that can be developed during stopping, and certain designs and lightweight mesh materials may not be appropriate for basketball shoes.

Mean vertical GRF component peaks were 2 BW or greater for all movements. Thus, in addition to forces developed during jumping and straight-line running, the vertical stresses developed during lateral movements must be considered when evaluating cushioning needs of basketball shoes, especially since the number of stops or the number of cuts performed by some players in a game may exceed the number of jumps.

REFERENCES

Cavanagh, P.R. et al. *J. Biomechanics*, **13**, 397-406, 1980.
Cavanagh, P.R. et al. *Med. Science Sport and Ex.* **22** Suppl, S104, 1990.
Valiant, G.A. Science and Football, (pp. 406-415), Reilly, Lees, et al., 1987.
Valiant, G.A. et al. Biomechanics IX-B, (pp. 117-122), Winter, Norman, Wells, et al., 1985.

Proceedings of NACOB II, The Second North American Congress on Biomechanics, Chicago, August 24th - 28th, 1992

EFFECTS OF FOOTWEAR ON TIBIAL ROTATION

Stephen D. Perry and M.A. Lafortune

Biomechanics Laboratory, School of Human Biology, University of Guelph, Guelph, Ontario, Canada.

INTRODUCTION

Different types of footwear have been shown to affect the shock attenuation at impact with the ground. The mechanism of pronation at heel strike has also been reported to play an important role in the dissipation of impact loading. Yet, excessive pronation appears to be the main cause of athletic knee injuries. In the present study tibial motion was recorded with the use of skin-mounted markers fastened to the tibia of eight subjects walking on a treadmill. Three-dimensional kinematic analysis of tibial angular motion was performed over three different footwear conditions. Imposed eversion and inversion of the foot was achieved with wedged inserts in the shoe midsoles. For the entire stance phase, internal tibial rotation (ITR) was decreased from the normal condition by the varus shoe condition. Conversely, the valgus soled shoes induced a relative increase in ITR that was restricted to the first half of stance. A comparison of modified footwear responses reveal similarly contoured ITR patterns separated by 5 deg.

REVIEW AND THEORY

At the time of initial impact, one mechanism by which the body helps to absorbs the shock is pronation of the foot. As pronation occurs, the eversion of the subtalar joint causes an obligatory internal rotation of the tibia (Close et al., 1967). The inter-relationship of the foot and leg leads to the conclusion that the greater the pronation or eversion, the greater the internal rotation of the tibia. Areblad et al, (1990),and Clarke et al., (1983) have shown that footwear affect rearfoot angle (foot eversion).

Rubin (1971) studied tibial rotation, for that purpose he modeled the subtalar joint as a mitered hinge. When the foot was dorsiflexed he noted an internal rotation of the tibia and external tibial rotation was observed with plantar flexion Wright et al. (1964) recorded subtalar joint motion when a subject walked a sidehill slope (9.5 deg). As the foot was everted and inverted depending on direction of walking on the sidehill, the tibia either externally or internally rotated. Lundberg (1989) did not find a strong coupling between foot rotation in the frontal plane and tibial rotation in the transverse plane. Lafortune (1984) determined the knee rotation during walking using intracortical pins and three-dimensional cinematography. In relation to regular midsole shoes, he found that valgus or varus midsole wedge shoes caused only minimal internal–external rotation of the tibio–femoral joint. Eng et al. (1989) reported similar results with the use of orthotics for walking and running. These latter results suggest that either the knee ligamentous and muscular structures were able to maintain the integrity of the joint or the inversion/eversion of the foot during dynamic activities does not effect lower leg rotation. The purpose of the present study was to investigate the kinematic coupling between foot inversion/eversion and tibial rotation during walking.

PROCEDURES

Eight injury and symptom-free subjects were used. They were male University students averaging 1.79 m and 70 kg. Seven non-coplanar spherical markers were fixed on the front of their left shank. This provided redundant information to solve for the spatial orientation of the lower leg segment. The subjects were photographed in the frontal and sagittal planes while standing in a set position. These photographs were used to estimate the position of each marker relative to a frame of reference fixed into the tibia. All subjects had a five minute walking warm up on the treadmill before data collection. Three shoe conditions were employed; normal, varus wedge and valgus wedge (10 degrees). The subject walked at a speed of 2.0 m/s. After two minutes of walking, two genlocked video cameras recorded fifteen contact phases of the left foot.

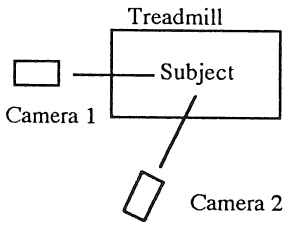

Figure 1: Experimental Setup.

The shank markers for three randomly selected foot contacts were digitized with a Peak Performance motion analysis system. X and Y coordinates of each marker were low pass filtered at 7 Hz. The DLT algorithms were used to determine individual marker three-dimensional coordinates. A series of four by four matrix operations was used to determine the

rotational components of tibial motion during the stance phase of the gait cycle. Internal-external rotation, ab/adduction and flexion/extension were computed.

RESULTS

Tibial rotation was measured across three shod conditions from eight subjects. All three footwear conditions caused internal rotation of the tibia from heel strike to midstance, the tibia then externally rotated until toe off. Different amount of internal tibial rotation (ITR) were observed at foot strike. The varus condition started with the least ITR (1.2 deg), next was the normal with 2.5 degrees and the valgus caused the tibia to be internally rotated by 4.5 deg initially. With respect to the normal shoes, the valgus shoes showed an increased amount of maximal internal tibial rotation during the initial portion of the stance. Conversely, following foot strike there was less internal rotation with the varus shoe than the normal shoe. The pattern of external rotation following maximum internal rotation was similar for all three footwear conditions. The valgus condition showed a 5 degree shift (in the external direction) of a similar pattern as compared to the varus condition. The values for the maximum internal rotation for the normal shoes was 8 degrees, varus shoes 6.5 degrees and the valgus shoes 9.5 degrees as in figure 2.

DISCUSSION

Pronation of the foot involves dorsiflexion, eversion and external rotation. In a closed kinematic chain, it is generally agreed that eversion and inversion are causative of pronation and supination. In the present study, the varus shoes inverted the foot and the valgus shoe everted the foot relative to its normal position. Thus, they likely increased or decreased the normal amount of pronation for each subject.

The results of this study support the idea of coupling between foot and leg kinematics. By controlling pronation/supination, it was found that the rotational components experienced by the shank were altered. The effects of the varus shoes were more pronounced than the effects of the valgus shoes. They reduced internal rotation by almost 4 degrees. The valgus shoes increased internal rotation by less than 2 degrees. It would suggest that in normal footwear, the foot almost reached its pronatory limits. In addition, the magnitude of the changes (5 deg.) effected by the modified footwear (20 deg.), indicates that the coupling ratio between foot and leg motions is imperfect (25 %).

The tibial rotational changes induced by the wedged footwear were larger than the effects produced by similarly modified footwear upon knee rotation (Lafortune et al., 1992). This would suggest that the muscular and ligamentous structures of the knee play an important role in transferring tibial rotation to the femur. The implication of this statement is that the foot positions may effect the torsional strain applied to knee structures.

While pronation has been reported to be a primary cause of knee injuries, it is also regarded as an important shock absorber for locomotor impacts. Ideally, a thorough understanding of segmental kinematic and kinetic couplings is needed in the development of a strategic balance between shock attenuation and pronation control.

REFERENCES

Clarke et al. *Med. Sports Sci. Exerc.*15:376-381, 1985

Close, J.R. et al. *Clinical Orthopaedics and Related Research*, Num. 50 pg. 159-179, 1967.

Eng et al. Proceedings of the XII Congress of Biomechanics, Los Angeles, Abst. 14,1989.

Lungberg, A. *Acta Orthop Scand* ; 60:Suppl.233, 1989.

Lafortune, M.A. Unpublished Ph.D. Dissertation, 1984.

Lafortune, M.A. et al. J. Biomech. (In Press), 1992.

Rubin, Gustav *Bulletin of Prosthetics Research*, Spring 1971: 95-101.

Wright, D.G. et al. *The Journal of Bone and Joint Surgery*, Vol 46-A(2): 361-382, 1964.

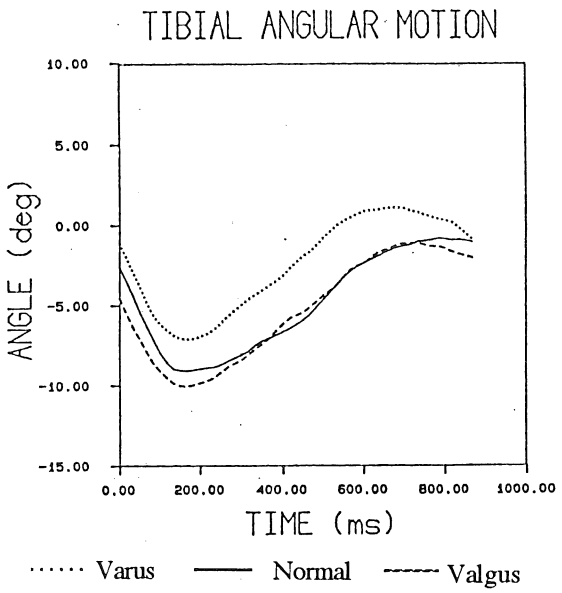

Figure 2: External / internal rotation of the tibia in the three different footwear conditions.

A MULTI-DIMENSIONAL ASSESSMENT OF THE FUNCTIONALITY OF CROSS TRAINING ATHLETIC FOOTWEAR

Brian L. Caster[a], Barry T. Bates[b] and Janet S. Dufek[b]

[a]Montana State University, Bozeman, MT 59717
[b]University of Oregon, Eugene, OR 97403

INTRODUCTION

The effectiveness of cross training (CT) athletic footwear in meeting the demands of running and landing activities were assessed using a multi-dimensional experimental protocol. Comparisons were made with top-of-line running (R) and basketball (BB) shoes from reputable manufacturers. The vertical ground reaction force (VGRF) produced during a drop landing activity was used to evaluate impact force attenuation in comparison with the BB shoes, with the VGRF and rear view kinematics used to assess both force attenuation and pronation control in comparison with the running shoes. Results demonstrated the tendency of the CT footwear to allow larger maximum VGRF values and greater absolute pronation magnitudes compared to the running shoes. Landing results showed that for forefoot contact, the CT footwear allowed for larger peak VGRF values, though the BB footwear produced larger values associated with rearfoot impact. In addition, a materials test supported the dynamic evaluations.

REVIEW AND THEORY

The effects that shoe design have on performance of athletic movements has been widely investigated with respect to running (Bates, 1985; Caster et al., 1991). Dufek and Bates (1991) have identified the need for adequate performance evaluations of footwear other than running shoes. With the advent of cross training athletic footwear, there exists not only the need for evaluation of this relatively new shoe type, but a method of evaluation involving the variety of movements for which the shoe is designed and promoted. A method of evaluation involving performance in both running and landing activities was therefore selected, with comparisons to sport specific shoes conducted. Since load related injuries have been associated with shoe design in relation to both running (Nigg, et al., 1981) and landing (Adrian and Laughlin, 1983) activities, the evaluation of impact force attenuation was a primary focus of this study. Furthermore, as an increasing body of literature is developing related to excessive and prolonged pronation (James and Jones, 1990) and relationships between shoe design and pronation (Caster et al., 1991), an evaluation of pronation control was carried out in the comparison with the running shoes. A materials test was performed on all shoes to identify any possible discrepancy between the purely mechanical function of the force attenuating materials and the dynamic function of the shoes in performance of the activity for which they were intended.

PROCEDURES

Three sets of data are presented in this analysis. In Study 1, 6 male subjects performed in top-of-line CT and running shoes, both from a single manufacturer (M1). Subjects performed 20 trials for each shoe condition, running at their preferred training pace (mean: 7 min/mile), while being monitored by a timing light system (+/- 3% target pace). Right side VGRF data were collected using a force platform system (AMTI, 1000Hz), while rear view kinematic data were acquired using an automated tracking system (Motion Analysis Corp., 200Hz). The pronation angle was defined by reflective markers placed over the posterior tibial segment and on the heel portion of the shoe. Stance phase events used in the analysis included first (F1) and second (F2) maximum VGRF and times of occurrence (T1, T2), and maximum angle of pronation (PRON). Since grouped data has been shown to effectivley mask important within subject differences in running activities (Bates, 1989), shoe condition differences were evaluated using a single subject analysis of variance technique. Of the six running subjects, four (S1-S4) also performed in a drop landing protocol, in addition to three new subjects (S7-S9). Subjects landed from a 50cm drop height onto a dual force platform system (AMTI, 1000Hz), performing 25 trials for the CT and BB conditions. Right side VGRF data were used in the landing analysis, with event selection including fore- (F1) and rearfoot (F2) impact forces and times of occurrence. In order to allow for greater application of results, a second group of subjects (Study 2) was asked to perform the running protocol, with the addition of a CT and running shoe from a second manufacturer (M2). Comparisons were made within subject and manufacturer. The third data set comprises the results of a materials test of rearfoot impact attenuation characteristics of the isolated shoe systems. A gravity driven impact testing system (Exeter Research) was employed. Two shoes sizes (9.5, 10.5) were tested, with results averaged across the two sizes for each shoe type and manufacturer. In accordance with ASTM guidelines, 5J of impact energy was used to simulate related impacts, and 10J to simulate landing impacts.

RESULTS AND DISCUSSION

Running and landing protocol results for Study 1 are presented in Tables 1 and 2, respectively. Values represent condition differences for the single subject analyses. Force units are N/kg body mass, pronation angles are in degrees, and times of force event occurrence are in %Stance time for running and seconds for landing. In the running analysis, 4 of 6 subjects exhibited significantly larger F2 forces for the CT condition, while 2 of 6 were significantly larger in rearfoot impact (F1) for the CT shoe. This suggests that the CT may be less effective in minimizing both the general loading force and rearfoot impact in heel-toe running, though a degree of between subject variability is apparent. In addition, force events occurred at a significantly earlier time for the CT shoe in nearly all comparisons, suggesting a greater loading rate. The rearfoot motion assessment identified a greater ability of the running shoe to control rearfoot motion during stance. In comparing the CT to the BB shoe during landing

(Table 2), forefoot impact forces (F1) were significantly larger for the CT shoe for 4 of 6 subjects. In the rearfoot force (F2) analysis, however, the CT shoe performed equal to or better than the BB shoe. The addition of a shoe from a second manufacturer in Study 2 (Table 3) generally supported the CT shoe assessment with respect to running force attenuation. The greater number of subjects exhibiting larger significant F1 forces in Study 2 is again an indication that between subject variability exists, demonstrating the need for individual subject analyses. The pronation results were not as clear as in Study 1. The fact that 3 of 6 subjects exhibited greater pronation values for the M2 running shoe is an indication that motion controlling characteristics of running and/or CT shoes differ across manufacturers. The materials test results (Table 4) support the dynamic assessments of rearfoot force attenuation for both the running and landing protocols. Greater peak forces were observed for both M1 and M2 CT shoes compared to their running counterparts, whereas greater CT force attenuation was apparent in comparision with the BB shoes from both manufacturers.

Table 1. Cross Trainer vs. Running Shoe (Study 1)
GRF and Pronation Differences

	F1	F2	T1	T2	Pron
S1	**0.70**	**1.30**	**-2.6**	**-2.7**	**2.05**
S2	**4.34**	**0.50**	**-2.2**	-1.0	**4.85**
S3	0.59	**1.32**	**-1.6**	**-2.7**	**5.50**
S4	-0.47	**0.50**	**-2.6**	**-2.9**	**6.63**
S5	0.74	-0.19	**-2.7**	**-2.2**	**3.05**
S6	-0.31	-0.14	-0.5	**-1.1**	**3.99**
Group	0.86	0.53	-2.0	-2.0	4.32

Bold and Underline: $p < 0.01$; Neg. (-): Running shoe value larger

Table 2. Cross Trainer vs. Basketball Shoe (Study 1)
GRF Differences

	F1	F2	T1	T2
S1	**0.87**	2.83	.003	.003
S2	1.38	-2.81	.001	.002
S3	**3.80**	**-2.66**	**-.002**	-.001
S4	1.18	**-4.92**	.000	.003
S7	**2.26**	2.29	**.001**	-.002
S8	0.68	-0.02	**.003**	.001
S9	**3.90**	-2.82	**.002**	**.004**
Group	2.02	-1.16	.002	.002

Bold and underline: $p < 0.01$; Neg. (-): Basketball shoe values larger

Table 3. Cross Trainer vs. Running Shoe (Study 2)
GRF and Pronation Differences

	F1		F2		T1		T2		Pron	
	M1	M2	M1	M2	M1	M2	M1	M2	M1	M2
S1	**1.51**	**1.04**	**1.03**	**1.32**	-1.5	**-2.3**	**-3.5**	-0.5	-0.20	**-3.93**
S2	-0.29	**-1.07**	0.15	0.10	**-1.4**	0.4	0.0	0.8	**1.13**	0.59
S3	**2.06**	**1.17**	0.04	-0.17	**-2.4**	-0.9	**-3.7**	-0.7	0.99	0.40
S4	**1.27**	0.26	0.76	0.28	**-4.5**	**-1.6**	**-1.6**	0.5	**-1.45**	**-4.25**
S5	**2.62**	**1.43**	**1.50**	0.36	**-1.6**	**-3.0**	**-2.2**	**-1.1**	-0.10	**-2.09**
S6	**1.31**	**1.29**	**1.26**	**0.65**	**-3.2**	**-1.2**	**-2.6**	-0.3	**1.27**	-0.69
Group	1.41	0.26	0.79	0.43	-2.4	-1.5	-2.2	-0.1	0.27	-1.72

Bold and underline: $p < 0.01$; Neg. (-): Running shoe value larger

Table 4. Impact Test Results

	CT_R		R		CT_L		BB	
	M1	M2	M1	M2	M1	M2	M1	M2
Peak Force (g)	18.49	17.08	17.89	16.28	19.46	17.80	22.72	19.13

CT_R, R: Cross Trainer and Running Shoes tested with running protocol (5J of Impact Energy)
CT_L, BB: Cross Trainer and Basketball shoes tested with landing protocol (10J of Impact Energy)

REFERENCES

Adrian and Laughlin. Biomechanics VIII-B, (pp.903-914), Human Kinetics, 1983.
Bates. *Journal of Biomechanics*, 22, 693-695, 1989.
Bates (1985). Biomechanics IX-B, (pp.903-914), Human Kinetics, 1985.
Caster, et al. *Proceed. of the Am. Soc. of Biomechanics, 15th Ann. Meeting*, Tempe, Arizona, (pp.150-151), 1991.
Dufek and Bates. *Medicine and Science in Sport and Exercise*, 23(9), 1062-1067, 1991.
James and Jones. Biomechanics of Distance Running, (pp.249-269), Human Kinetics, 1990.
Nigg. Biomechanics VII-B, (pp.88-99), Human Kinetics, 1981.
Valiant, et al. Biomechanics IX-B, (pp.117-122), Human Kinetics, 1985.

HEEL VERSUS SHOE MOVEMENT DURING A LATERAL SIDE STEP

Ch. Reinschmidt, A. Stacoff, E. Stüssi
Biomechanics Laboratory, ETH Zurich, Zurich, Switzerland.

INTRODUCTION

In/eversion is assumed to be an indicator for injuries to the structures in and around the ankle joint. In/eversion of the shoe has been quantified in the attempt to describe the movement of the foot inside the shoe during a lateral movement (Luethi *et al.* 1986, Stacoff *et al.* 1989). In the past, many (e.g. Edington *et al.* 1990) questioned whether markers on the shoe could give an accurate representation of the heel movement inside the shoe.

REVIEW AND THEORY

Stacoff *et al.* (1992) found systematic and relatively small differences (>3°) between the shoe and the movement of the heel inside the shoe during running. To date, no studies have investigated the difference between the heel and the shoe position during a lateral movement.

The purposes of this study were (a) to compare the shoe movement with the heel movement inside the shoe, and (b) to compare heel movement between barefoot and shod trials.

PROCEDURES

Fifteen subjects (male, average age: 24 years, well trained in sports with frequent lateral movements) participated in the study. They were asked to move as fast as possible from a standing start to their left using two or three steps; to stop by placing the left foot perpendicular to the running direction, and to run back to the starting point. A LOCAM camera (150 Hz) was used to film the lateral stopping movement from a posterior view. Three different shoe conditions per subject (shoe A, shoe B, and barefoot) were tested. Shoe A was a standard court shoe (ADIDAS Red Star) with no alteration, shoe B had two windows at the upper and lower part of the heel counter in order to locate skin markers on the heel. One valid trial per subject and shoe condition was filmed, digitized, and then analyzed.
The variables of interest were:

- shoe in/eversion (β_S): angle between the marker pairs on the shoe and on the Achilles-tendon (Fig. 1).
- heel in/eversion (β_H): angle between the marker pairs on the heel and on the Achilles-tendon (Fig. 1).
- maximum change in in/eversion ($\Delta\beta_{Smax}$, $\Delta\beta_{Hmax}$) during the first 100 ms after touchdown.

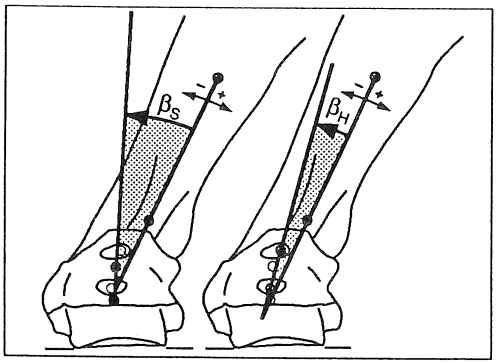

Figure 1: The definition of angles: shoe in/eversion (β_S) and heel in/eversion (β_H).

Due to projection errors and a decreased visibility of the markers on the heel at take-off, the study was confined to the first 100 ms after touchdown. Nonparametric statistics (Wilcoxon test, $p \leq 0.01$) were used to detect differences between the maximum change in heel ($\Delta\beta_{Hmax}$) and shoe angles ($\Delta\beta_{Smax}$).

RESULTS

The maximum change in shoe inversion (Table 1) was not significantly different between the shoe without windows (shoe A) and the shoe with windows (shoe B). The mean curves of shoe in/eversion for both shoes were similar (Fig. 2). Thus, it can be concluded that the windows had a negligible influence on the movement.

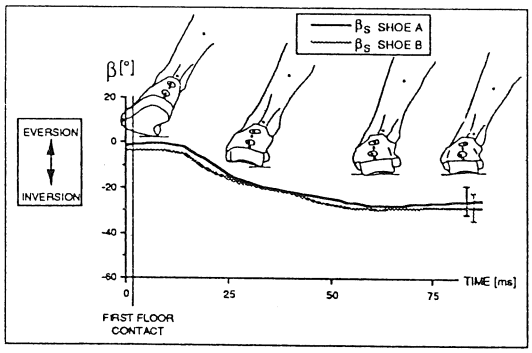

Figure 2: Mean in/eversion of the shoe with no alteration (shoe A), and of the shoe with heel-counter windows (shoe B).

The maximum changes in inversion determined from markers on the shoe and from markers on the heel inside the shoe were significantly different. The difference was in the average more than 15° (Table 1). For all subjects, maximum inversion of the shoe, $\Delta\beta_{Smax}$, was greater than that of the heel, $\Delta\beta_{Hmax}$. In the first 50 ms the difference between heel and shoe inversion increased monotonically. After 50 ms the difference between shoe and heel position remains more or less constant (Fig. 3).

SHOE CONDITION	$\Delta\beta_{Smax}$	$\Delta\beta_{Hmax}$
Shoe A	32.2° ± 6.6°	N/A
Shoe B	30.7° ± 6.2°	13.3° ± 3.8°
Barefoot	N/A	10.1° ± 3.0°

Table 1: $\Delta\beta_{max}$ values for the different shoe conditions.

The comparison between barefoot and shod conditions showed that the in/eversion determined with skin markers through the

heel-counter windows was similar to the in/eversion of the barefoot trials (Fig. 3). The maximum inversion for the barefoot condition was about 3° less than the maximum heel inversion for the shoe condition (Table 1). This difference, however, was not significant at the 1% level.

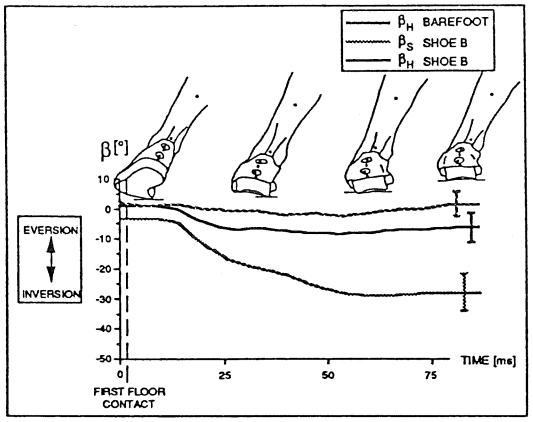

Figure 3: Shoe in/eversion (β_S), heel in/eversion (β_H), and heel in/eversion (β_H) of the barefoot condition.

DISCUSSION

The differences in in/eversion angles between markers on the shoe and on the heel were significant and substantial An appropriate method to estimate the loading in internal structures of the foot and the lower leg would include information about the relative position of the relevant bony structures. Markers on the shoe do not, in general, provide that information for the side-stepping movement analyzed in this study.

Skin markers as used in this study are commonly used to assess heel in/eversion, (or more precisely calcaneus in/eversion) non-invasively. Only speculations, supported by experimental evidence, are available to discuss the relevance of skin markers in the assessment of the actual position of the calcaneus. The comparison between the results for the skin markers in the barefoot condition and the shoe condition provided some insight into this question. Because the skin-marker movements in the shoe condition and in the barefoot condition were similar (Fig. 3), the calcaneus movement can be assumed to be similar for the two conditions. Skin markers may be used in such a situation to represent the movement of the calcaneus. The current experimental set-up, however, did not allow any conclusions to be made as to whether skin markers behave in the same way for shoes with different heel constructions (e.g., stiffer, tighter, or softer). Further research is needed to test these hypotheses and to study the influence of different heel-counter constructions on the movement of the shoe and of the heel inside the shoe.

Differences between shoe- and skin-marker positions and the variables calculated from them were reported earlier for running movements (Clarke *et al.* 1984, Nigg 1986, Stacoff *et al.* 1992). The calculated differences for the in/eversion angle in running were much smaller (<3°) than the differences for the sideways movements reported in this study. In general, markers on the shoe may represent the position of the calcaneus with sufficient accuracy for movements that are predominantly in the anterior-posterior direction, but shoe markers do not provide accurate representation of calcaneal position for predominantly medio-lateral movements. The differences between external marker positions and calcaneal positions may increase with increasing speed of the movement. Further studies, however, are needed to provide more insight into this aspect of the marker position problem.

The relative movement between the heel and the shoe, β_H-β_S, may quantify the stiffness of a shoe in the heel counter region, and the fit of the shoe to the foot. Stiff and tight heel-counter constructions may only allow small relative movements, while loose heel-counter constructions may allow large relative movements between the shoe and the heel, but these ideas need to be specifically tested.

This study showed that markers on the shoe and markers on the skin of the heel provide significantly different information. Skin markers on the heel as observed through windows in the shoe give a better indication of the actual position of the calcaneus than do markers placed directly on the shoe.

REFERENCES

Luethi, S.M. et al. Influence of shoe construction on lower kinematics and load during lateral movements in tennis. *J. Sports Biomech.*, 166-174, 1986.

Clarke, E.T. et al. The study of rearfoot movement in running. In: Sport shoes and playing surface. Champaign, Il: Human Kinetics, (pp. 166-189), 1984.

Edington, J. et al. Rearfoot motion in distance running. In: Biomechanics of distance running. Champaign, Il: Human Kinetics, (pp. 135-164), 1990.

Nigg, B.M. Experimental technique used in running shoe research. In: Biomechanics of running shoes. Champaign, Il: Human Kinetics, (pp. 27-61), 1986.

Stacoff et al. The movement of the heel within a running shoe. *Med. Sci. Sports Exerc.*, in press, 1992.

ACKNOWLEDGMENTS

This work was supported by the Swiss Federal Commission of Sports ESK (Eidgenössische Sportkommission), Ausbildungsförderung des Kantons Aargau Switzerland, and by ADIDAS Germany.

Proceedings of NACOB II, The Second North American Congress on Biomechanics, Chicago, August 24th - 28th, 1992

APPROACHES TO FINITE ELEMENT ANALYSIS OF THE FOOT-SHOE INTERFACE IN DIABETIC PATIENTS

Peter R. Cavanagh and Tzyy-Yuang Shiang

Center for Locomotion Studies and Department of Mechanical Engineering, Penn State University, University Park, PA 16802, USA.

INTRODUCTION

The interface between the foot and shoe is often the critical determinant in the maintenance of lesion-free feet in patients who have lost protective sensation as a result of diabetic peripheral neuropathy. It is well established that elevated plantar pressure during gait in the presence of neuropathy is the principal etiological factor in diabetic plantar ulceration (Boulton 1990). This study is part of a larger effort, which includes both theoretical and experimental approaches, to understand the underlying causes of elevated plantar pressure.

In order to understand the interaction of the biological tissue with a shoe material, the mechanical properties of both components must be well characterized. However, data for such important properties as modulus of elasticity and Poisson's ratio are not readily available for either the soft tissue of the foot or for the materials typically used in therapeutic footwear. The present paper concentrates on the later issue and examines various approaches to modeling the deformation in footwear material under conditions of known stress. An example of a more complete model where forces are applied to an isolated rearfoot segment is also presented.

REVIEW AND THEORY

Crowninshield and Nakamura (1981) proposed a rather complete non-linear two dimensional Finite Element (FE) model of the foot and shoe which was apparently not further developed. Goodman and Hull (1987) have performed 2 and 3 dimensional analyses of athletic shoe midsoles using linear elements from the ANSYS finite element (FE) package. In previous work (Cavanagh et. al 1990) we have also used ANSYS with both linear and non-linear hyperelastic elements. Further analysis using this approach has suggested that the complex mechanical behavior of polymeric materials typically used in footwear applications was not adequately modeled by either of the above methods. The purpose of the present study was, therefore, to compare 3 different approaches to the modeling of footwear materials.

PROCEDURES

Typical stresses imposed by the foot on the shoe were measured using a Mikro EMED in-shoe pressure device. Two values for peak plantar pressure were used (550kPa and 1.08 MPa for the medium and high stress conditions respectively.) Techniques were developed to superimpose an entire pressure distribution over a shoe model, such that nodal forces or element face pressures could be added as input to the model. The shoe component (polyurethane-PU) was modeled by 3 different approaches:

a. A linear FE analysis using ANSYS 4.0 3D eight node brick element "STIF45".

b. A first order non-linear hyperelastic FE analysis using ANSYS 4.0 3D element "STIF86" together with the Blatz-Ko strain energy function.

c. A second order non-linear FE method using ABAQUS in which the relevant region of the stress-strain curve for the material is provided as input to the program also using Blatz-Ko.

The various approaches were first compared using a progressively increasing force input applied to a single element cube model in order to compare the resulting stress-strain curves with the known curve derived from Instron testing. Next, the maximum deformation of a larger model of the entire rearpart of the shoe was examined under the imposed medium and high stress conditions.

RESULTS AND DISCUSSION

The stress-strain curve obtained from Instron testing of the shoe material is shown in figure 1a. Note that the curve is markedly non-linear, becoming stiffer as strain increases. When a series of force values were input to the single cube FE model of the material, the results shown in figure 1b were obtained. It is apparent that there are considerable deviations from the known behavior of the material using either the linear or first order non-linear approaches.

To investigate the functional significance of the differences shown in figure 1b, a large model of the shoe rearpart was solved for both stress conditions using all three approaches to the FE analysis. The results, shown in table 1, reveal differences in the predicted strains of the materials

under both high and medium stress conditions. These differences were of the order of 25% and 15% of total thickness in the medium and high stress conditions respectively. It must be recalled that linear analysis has no allowance for large deflections (which certainly occur) and thus the erorrs due to incorrect geometry will be considerable.

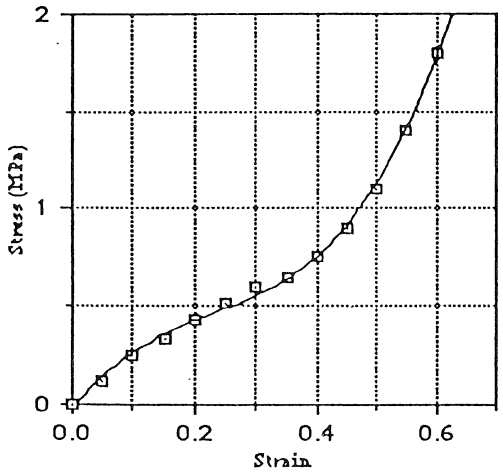

Figure 1a. Experimental stress-strain curve for PU footwear material obtained from Instron testing.

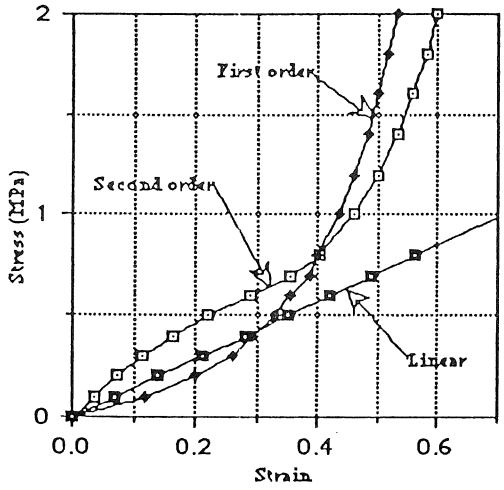

Figure 1b. Stress-strain curves derived from three different finite element models of a single cube of the same material. See text for further details.

Although no experimental data for observed strains in the footwear material are presently available, the obvious discrepancy between known and predicted behavior for the small cube models suggests that neither linear or 1st order hyperelastic analyses are adequate to accurately model the materials typically used in therapeutic footwear.

Table 1: Predicted peak vertical strain ε_z(dimensionless) in 3 different FE models of shoe materials subjected to the same stresses.

	Linear	1st order non-linear	2nd order non-linear
Medium Stress	-0.264	-0.389	-0.138
High Stress	-0.791	-0.715	-0.638

Our current extensions of this work, shown in figure 2, attempt to model the entire bone, soft tissue, and footwear composite using the 2nd order non-linear technique. With this model, the effects of different geometry , mechanical properties of the tissue (which may be affected by diabetes) configuration, and composition of therapeutic footwear on stress in the plantar tissue can be examined. The rearfoot provides a well defined and relatively homogeneous region for modeling but, since the majority of plantar ulcers occur under the metatarsal heads, it is important that future models attempt to examine the effects of different footwear interventions on this region of the foot.

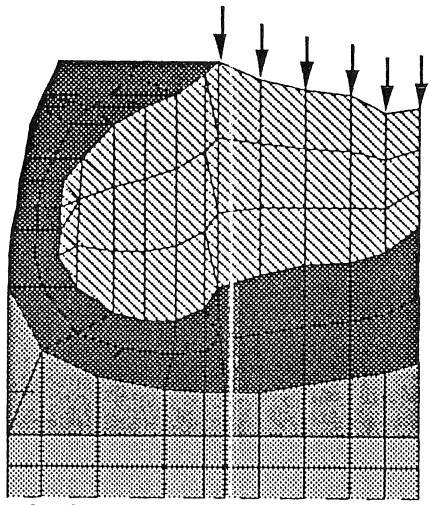

Figure 2. 2-D FE representation of the rearfoot Different shading indicates different material properties used in the model (from top to bottom - calcaneus, heel pad and skin, insole, midsole.)

REFERENCES

Boulton, AJM. *Diabetic Med.*, 7, 852-858, 1990.

Cavanagh, PR et al. *Med. Sci. Spt. Ex.* 23(7) S140, 1991.

Crowninshield, RD and Nakamura, S. *J. Biomech* 14(7), 492, 1981.

Goodman, ED and Hull, AJ. *1987 ANSYS Conference Proceedings*, Houston PA (pp.4.1-4.18), 1987.

The Reliability of Selected Gait Variables onto a Non-Slippery and Slippery Surface

T. J. Eng, R. O. Andres, and D. D. O'Connor

NIKE Sport Research Laboratory, Beaverton, OR
Ergonomic Engineering Associates, Pelham, MA
Isotechnologies, Inc., Hillsborough, NC

INTRODUCTION

Accidents resulting from slips are often injurious and sometimes fatal. Past research into slip prevention has focused on the environmental factors at the shoe-floor interface. Although there have been some investigations concerning gait modifications people make when they knowingly walk onto a slippery surface, there is little reported information regarding the reliability of these modifications. Therefore, the purpose of this study was to establish the reliability of selected gait variables onto both a non-slippery and a slippery surface.

REVIEW AND THEORY

Researchers have examined human locomotion on and onto slippery surfaces attempting:

(1) to validate slip-resistance measuring devices (Perkins et al., 1983, Lanshammar et al., 1985, and Tisserand, 1985),
(2) to validate variables estimating available friction while walking (Lanshammar et al., 1985, and Strandberg et al., 1985), and
(3) to examine motions immediately surrounding the slip event (Carlsöö, 1962, Strandberg, 1983, and Tisserand, 1985).

Other investigators have focused on using slip resistance measures to design shoes and floors to reduce the risk of slipping (Barnbrook, 1985, Manning et al., 1985, and Wilson et al., 1985).

The instability of bipedal gait has also contributed to the problem of human locomotion on and onto slippery surfaces. Perkins et al. (1983), suggested that forward slips of the foot at heel contact were likely to be more dangerous than backward slips during propulsion because the forward momentum of the body might continue to apply the weight of the body to the sliding foot. Since humans are very prone to slipping at heel strike, the available kinematic information on locomotion onto slippery surfaces was limited to the velocity of the foot at heel contact (Perkins et al., 1983, and Strandberg, 1983) and the foot angle at heel contact (Strandberg, 1983). The reliability of this information has not previously been reported.

PROCEDURES

High-speed videography recorded the movements of twelve healthy male volunteers walking down a linoleum-covered runway. They knowingly encountered a rectangular patch which was either non-slippery (dry) or slippery (coated with glycerin). Subjects were instructed to make any gait adjustments within the preceding stride to safely complete the subsequent toe-off from the rectangular patch.

Selected gait variables were compared between two days, the two floor conditions, and among twenty trials. Lower limb angular kinematics included angular velocities of the body angle (see Figure 1) and angle of incidence of the foot (see Figure 2) at heel strike onto the rectangle. Temporal and distance kinematic comparisons over the preceding stride included right and left step lengths and step periods, peak to peak vertical displacement (Sy) of the head, arms, and trunk segment (HAT) center of mass (COM), average horizontal velocity of the HAT COM (Vx HAT) and heel (Vx Heel), and the mean lower limb angular positions (body, hip, knee, ankle, and incidence angles) of the right heel strike onto the designated rectangle. Controlled variables within subjects included footwear, shoe-floor interface, and walking pace up to, but not including the preceding strike onto the rectangle.

A balanced (Days * Trials * Subjects) ANOVA model provided an estimate of stability between days while a completely nested ANOVA with subjects, days within subjects, and trials within days and subjects provided information necessary to calculate an intraclass reliability coefficient (R) according to procedures outlined by Feldt et al. (1958).

RESULTS

Step lengths and periods, body angle, angular velocity of the body angle, Vx HAT, and the peak to peak vertical displacement of the HAT COM were reliable

for both the non-slippery and slippery conditions (see Table 1). The hip and knee angle, angular velocity of the incidence angle, and VxHeel were reliable for the non-slippery condition, but not for the slippery condition. The angular measurements met the stability criteria, but failed to meet the consistency criteria. The VxHeel was not stable or consistent for the slippery condition. Both the ankle and incidence angle were not reliable for either condition. Intraclass coefficients ranged from 0.99 to 0.74.

Table 1. Intraclass Reliability Coefficients

Variable	R Non-Slip	R Slip
L. Step Length	*.99	*.92
R. Step Length	*.98	*.98
L. Step Period	*.98	*.94
R. Step Period	*.97	*.91
Body Ang.	*.95	*.98
Hip Ang.	*.91	.87
Knee Ang.	*.96	.86
Ankle Ang.	.74	.85
Incid. Ang.	.80	.81
Ang. Vel. of Body Ang.	*.97	*.91
Ang. Vel. of Incid. Ang.	*.91	.83
Vx HAT COM	*.98	*.91
Vx Heel	*.94	.75
Sy HAT COM	*.98	*.94

Note: * R*R > 0.80. Ang. = Angle.

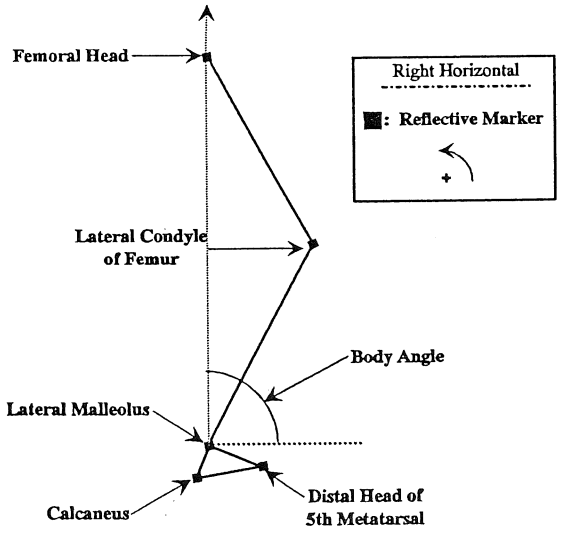

Fig. 1 Body Angle

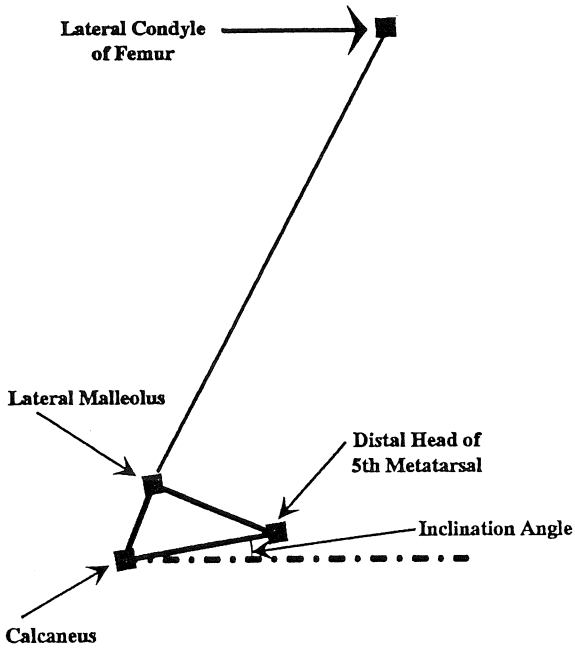

Fig. 2 Inclination Angle

DISCUSSION

Results showed that certain gait variables were reliably measured for the non-slippery and slippery conditions while the consistency of other variables needs to be improved, especially for the slippery condition. These findings provide future gait researchers with an example of the stability, consistency, and the scope of the potential adaptations concerning investigations of human walking onto a variety of surfaces.

REFERENCES

Barnbook, G. et al. *Ergo.*, **28**, 1021-1025, 1985.
Carlsöö, S. *Ergo.*, **5**, 271-274, 1962.
Feldt, L. S. et al. *R. Q.*, **29**, 279-293, 1958.
Lanshammar, H. et al. In Winter et al. (eds.), Biomechanics IX-A, (pp.72-75), Human Kinetics, 1985.
Manning, D. et al. *Ergo.*, **28**, 1011-1019, 1985.
Perkins, P. J. et al. *Ergo.*, **26**, 73-82, 1983.
Strandberg, L. *Ergo.*, **26**, 11-32, 1983.
Strandberg, L. et al. In Winter et al. (eds.), Biomechanics IX-A, (pp.76-81), Human Kinetics, 1985.
Wilson M. P. et al. *Ergo.*, **28**, 1081-1085, 1985.

ACKNOWLEDGMENTS

We wish to acknowledge the contributions of Marguerite Wrona, Steve Smith, and Wanda Boda.

RELATIONSHIP BETWEEN MECHANICAL PROPERTIES OF CARPET AND COMFORT IN WALKING

M.W. Whittle*, T.A. Orofino* and K. Miller†

*** University of Tennessee at Chattanooga**
† Dow Chemical U.S.A., Dalton, Georgia

INTRODUCTION

A study has been made of the relationship between the mechanical properties of carpeting and the subjective comfort of walking on it. Members of a user panel walked on samples of four types of carpet, and ranked them for comfort. Two different mechanical tests were applied to the same samples: an impact test, designed to simulate the heelstrike transient, and measurement of the compression modulus at a low rate of deformation. There was general agreement among the subjects as to which carpet was the least comfortable and which was the most comfortable. These observations corresponded to the carpets giving the highest and the lowest values, respectively, for peak deceleration in impact testing. The other two carpets were intermediate in both user response and impact testing. Of these two, the majority of users preferred the carpet which had the lower compression modulus when measured by slow deformation.

REVIEW AND THEORY

Since the development of accurate methods to study the kinetics and kinematics of walking, a large number of studies have been made of the detailed biomechanics of foot/floor interaction (e.g. Pedotti, 1977). Studies have also been made of the energy attenuation of impact by athletic playing surfaces (Orofino & Hamner, 1988), and of the use of energy absorbing insoles (Johnson, 1988). However, two aspects of foot/floor interaction appear to have been largely neglected in the literature. These are a) the ways in which foot/floor forces may be modified by the mechanical properties of the walking surface, and b) the subjective perception of comfort (or the lack of it) when walking on particular surfaces. The present paper is a preliminary attempt to examine these two topics, especially the second.

It seems likely that two aspects of foot/floor interaction can be perceived subjectively: a) the pressure distribution across the sole of the foot; and b) the forces exerted between the foot and the supporting surface during particular activities. It further seems likely that during quiet standing, only the pressure distribution will be apparent, whereas during activities which involve movement of the foot, both pressure distribution and force magnitude will be noticeable. The present study examines only the latter, the force magnitudes. The proposed hypothesis is that the subjective perception of comfort in a walking surface depends in some way on the readily measurable physical properties of that surface. When a moving limb is arrested by contact with the supporting surface, the surface deflects and the momentum of the leg gives rise to an impulse (the integral of force and time). If a greater deflection occurs, the force will take longer to develop, and the peak force will be correspondingly lower. We suggest that this reduced force is apparent to the subject, and is interpreted as greater "comfort" in the walking surface.

The physical characteristics of the walking surface will only be noticeable while the foot is moving relative to that surface. During walking, the ground reaction force vector varies in both magnitude and direction, although the major component of force is always vertical. Figure 1 shows the vertical component of the ground reaction force during the stance phase of gait for the left foot of a normal male subject, weight 657N, wearing outdoor shoes, and walking on a hard surface. The first part of the stance phase is known as weight acceptance, when the ground reaction force rises rapidly from zero to something greater than body weight. This is usually followed by a "dip" in the ground reaction force, at mid stance. The final part of the stance phase, known as weight release, involves a smooth, continuous unloading of the limb. The heelstrike transient occurs as a discontinuity at the beginning of the weight acceptance phase (Collins & Whittle, 1989). Figure 2 shows the rate of change of ground reaction force, obtained by differentiating the curve in figure 1, without the application of smoothing. In this individual, the highest rate of change of force, both positive and

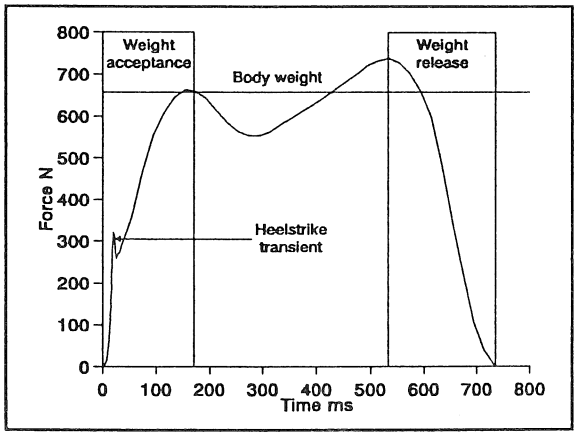

Figure 1: Vertical component of ground reaction force

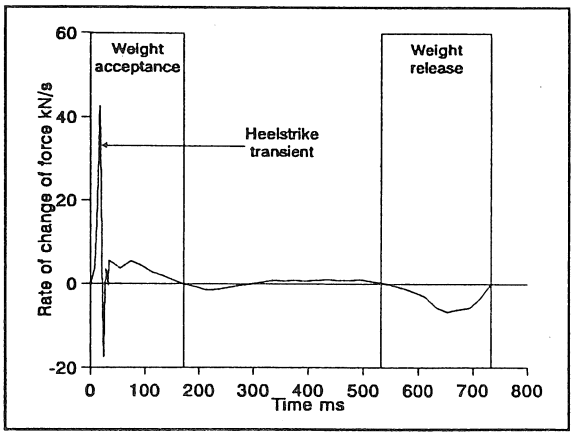

Figure 2: Rate of change of ground reaction force

negative, occurred during the heelstrike transient. Much smaller rates of change were observed during the remainder of the weight acceptance phase and during the weight release phase.

PROCEDURES

The results from subjective user assessments of carpet comfort were compared with objective tests of the carpets' mechanical properties. Four different types of carpet were used, three of which included a cushion underlay. Measurements of mechanical properties were made by two methods, one at a high strain rate, to simulate the heelstrike transient, and one at a much lower strain rate, to simulate weight acceptance and weight release.

Subjective rating of carpet comfort

Forty three adult volunteers (15 women, 28 men) were asked to walk across four carpet samples, and to rank them in order of comfort. They wore their own shoes, and walked at their own comfortable pace. The order of the carpet samples was varied from one subject to another, to reduce the possibility of bias from this source. Appropriate non-parametric statistics were used to analyze the ordinal data from this assessment.

Impact testing

The ability of the carpet samples to attenuate a sudden impact was measured using a Clegg soil tester. This consists of a flat-faced cylindrical missile of 2.27kg mass and 1935mm^2 cross-sectional area, incorporating an accelerometer sensitive to vertical accelerations. The missile was dropped from a predetermined height onto the sample, and a record was made of the peak deceleration (in multiples of "g", the acceleration due to gravity).

The height from which to drop the Clegg tester, to simulate the heelstrike transient, was determined empirically. Five normal adult subjects, of both sexes and covering a range of shoe sizes, made seven normal walks across a sand pit. The sand was wetted and compacted prior to each test. The Clegg tester was then impacted into the sand several times, using different drop heights, in the vicinity of the heel impression. Measurements were made of the maximum depths in the sand of the imprints of both the heel and the Clegg tester. The drop height which was equivalent to each heelstrike impression was determined by statistical regression. A drop height of 178mm was chosen for measuring the carpet samples, this being in the upper half of the range of values obtained.

Compression modulus

The compression modulus was determined from the force required to compress the sample to 75% of its original thickness, using a compression testing machine and a compression rate of 25.4mm per minute.

RESULTS

Subjective rating of carpet comfort

Analysis of the results of the subjective rating of comfort provided the following observations, which were statistically highly significant ($p < 0.001$), using the chi-square test with one degree of freedom:

a) The most comfortable carpet was D.
b) The least comfortable carpet was B.
c) Carpet A was more comfortable than carpet C.

Impact testing and compression modulus

The results for the measurements of impact testing and compression modulus for the four carpet samples are given in Table 1.

Table 1: Results of mechanical testing of carpet samples.

Compression Surface	Type	Impact deceleration g	modulus kPa
A	Carpet and cushion	105	78
B	Carpet alone	308	*
C	Carpet and cushion	100	151
D	Carpet and cushion	54	125

* = not appropriate for carpet without cushion

DISCUSSION

The four carpets provided essentially three levels of impact attenuation by the deceleration test: around 50g (carpet D), around 100g (carpets A and C) and around 300g (carpet B). These three groups corresponded closely with the subjective opinions of comfort provided by the user panel: carpet D was the most comfortable, A and C were intermediate, and carpet B was the least comfortable. This lends strong support to the suggestion that subjective comfort relates to the response of a carpet to transient forces.

Between carpets A and C there was negligible difference in impact deceleration, but the user panel preferred carpet A. This may relate to compression modulus at a lower strain rate, which was less for carpet A than for the other three carpets.

By choosing only four carpet samples, covering a wide range of mechanical properties, it was possible to get a clear, statistically significant, differentiation between comfort ratings from the user panel. The results suggested a probable relationship between perceived comfort and the results of mechanical testing. However, since the number of different types of carpet was so small, it was not possible to confirm this relationship, which will be examined in further studies.

Subjective evaluations of comfort are notoriously difficult to interpret. What is "comfortable" to some people may be "uncomfortable" to others, based on their personal preferences and what they have become accustomed to. However, there may be a real relationship between perceived comfort and certain measurable parameters. It is interesting to speculate on how the "comfort" of a walking surface may relate to the forces being generated in the joints, muscles and ligaments. Comfort may also relate to the energy being used in walking, or to the presence (or absence) of microtrauma in particular joints and associated structures.

REFERENCES

Collins, J.J. & Whittle, M.W. *Clin. Biomech.*, 4, 179-187, 1989.
Johnson, G.R. *Prosthet. Orthot. Intl.*, 12, 91-95, 1988.
Orofino, T.A. & Hamner, W.F. *Encyclopedia of Polymer Science and Engineering*, 14, 245-260, 1988.
Pedotti, A. *IEEE Trans. Biomed. Eng.*, 24, 456-461, 1977.

IN-SHOE PRESSURE DISTRIBUTION IN THE TRIPLE JUMP

T. L. Milani and E. M. Hennig
Sportmedizinisches Institut, Universität Essen, Germany

INTRODUCTION

Extreme loads as they occur in different sports disciplines bear a considerable risk of injuries. Concerning injury prevention as well as to optimize the performance of athletes, the knowledge of local pressures under the foot is an important information for therapists as well as coaches. The present study investigated the loads beneath the foot in triple jumps by in-shoe pressure distribution measurements.

REVIEW AND THEORY

Ramey & Williams (1985) investigated the ground reaction forces in triple jump. The authors found peak force values of 7- to 12-times body weight. An analysis of 4 high performance triple jump athletes (Milani & Hennig, 1990) showed high pressure values and large interindividual differences of pressures under the foot. Since many of the frequent injuries in triple jumpers are likely to be related to overloads in certain foot regions, the authors investigated the effect of individual built orthotics for the prevention of injuries.

PROCEDURES

Ten healthy male subjects (mean age: 19,6 years [SD: 3,7]; height: 182,3 cm [SD: 6,2]; weight: 745 N [SD: 5,3]) volunteered to participate in this study. Ten piezoceramic sensors, the properties of which were described by Hennig et al. (1982), were taped onto the plantar surface of the right foot at defined anatomical landmarks. The pressures were determined under the following structures: the lateral (LH) and medial (MH) heel, the lateral (LM) and medial (MM) midfoot, the heads of the five metatarsal heads (I. - V. M) and the hallux (H). The dimensions of the transducers were 4 by 4 mm with a thickness of less than 2 mm. According to subjects' judgment the transducers were barely felt under the foot during the jumps. At a rate of 750 Hz per channel and a resolution of 12 bit, measurements were performed with a portable, battery operated data acquisition system (total weight 12 N). Using a radio-transmitter, data collection was triggered shortly before the athletes' take off. After the experiment the data were transferred to a host computer for storage and evaluation. Signal evaluation was done for the landing phases prior to the hop and step. From five jumping trials the mean peak pressures, impulses and contact times under the foot were determined. For the duration of the contact the integrated local forces resulted in eight local impulses. Relative loads were determined by dividing each single impulse by the sum of all impulse values. The relative load, expressed as a percentage of the total load, allows insight into the weight bearing contribution of each anatomical region.

RESULTS

The data evaluation showed for both impacts prior to the hop and the step high peak pressures in various regions of the foot (figures 1 & 2). Clear differences in the peak pressure pattern are obvious between both ground contacts. The relative load images (figures 3 & 4) show different patterns. The importance of the first ray (MI + Hallux) can clearly be identified. Peak pressure images show the highest pressures, as they occur at any time throughout the ground contact. The relative load image, however, is based on the integrated pressure values of the total time of contact with the ground. The difference in appearance of the peak pressure and the relative load images can be attributed to the variation in loading duration of the various anatomical regions.

DISCUSSION

The high pressure values under the foot may explain why triple jump athletes have a high incidence of lower extremity injuries. The high pressure values under the first

metatarsus and the hallux in the hop and the step demonstrate the important function of the first ray to propel the body at take off. High pressure values in the heel region seem to be the effect of high deceleration forces for both ground contacts. As compared to the step higher medial heel and midfoot pressures were recorded from the hop.

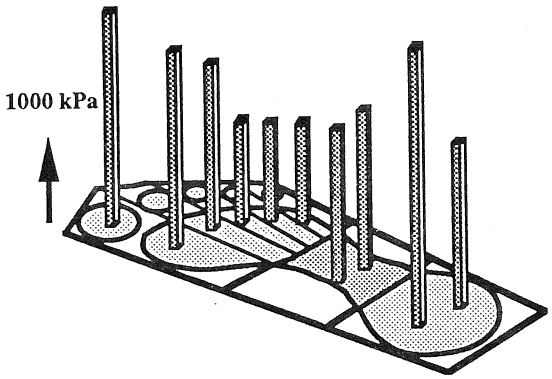

Figure 1: Peak Pressures (kPa) - HOP

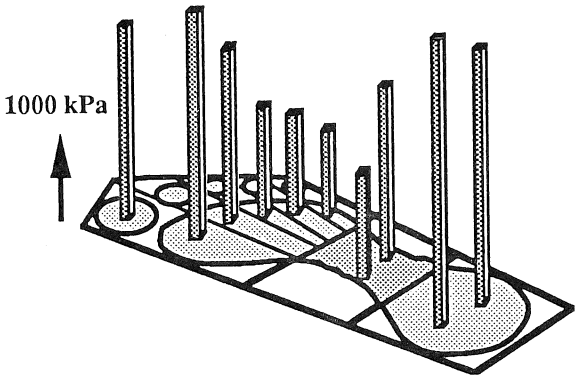

Figure 2: Peak Pressures (kPa) - STEP

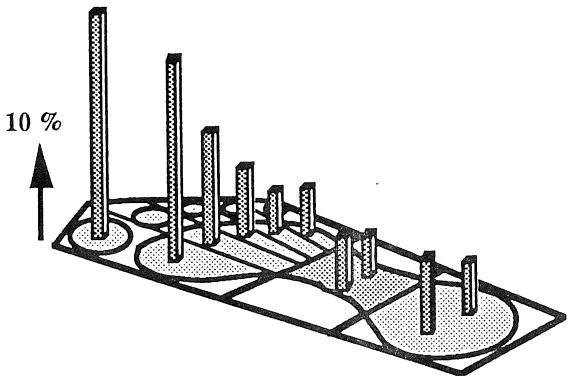

Figure 3: Relative loads (%) - HOP

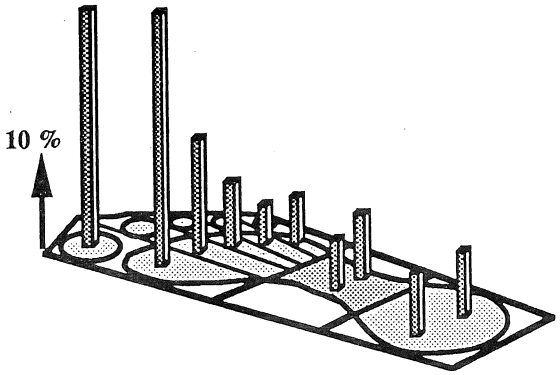

Figure 4: Relative loads (%) - STEP

Eversion of the rearfoot during the pronation at impact may be responsible for the medial shift of the load in the rear- and midfoot. The pressure distribution at the landing for the step is characterized by high pressures in the lateral region of the foot. During the step the jumper lands with a much higher vertical velocity component, causing more of a full foot contact rather than a pronatory movement of the rearfoot. Caused by high vertical load and the limited roll off lateral structures seem to be loaded with higher pressures. The peak pressure distributions of the hop as well as the step demonstrate a distinct difference between the three lateral and the two medial metatarsal heads. The Lisfranc´ joint line shows a peg-shaped link of the 2nd Metatarsus in the joint to the Os cuneiform II. Sammarco (1980) revealed that this connection limits the mobility of the second ray. The reduced mobility results in a pronounced shift of the load onto the II. metatarsus in walking. A similarly phenomenon can be observed under the forefoot in triple jumps. Considering the anatomical dimension of the metatarsal bones the relative load distribution under the 5th metatarsal head appears high. This may be a reason for the frequent occurence of 5th metatarsal bone stress fractures in track and field athletes.

REFERENCES

Hennig, E.M. et al. J. of Biomed. Eng., 4, 213-222, 1982.
Milani, T.L. et al *Techniques in Athletics - I. Int. Conference, Köln*, pp. 753-760, 1990.
Ramey, M. R. et al. Int. J. of Biom., 233-239, 1985.
Sammarco, J. Basic biomechanics of the skeletal system, Eds. V. Frankel & M. Nordin, Lea u. Febiger, Philadelphia, 1980.

CSB SYMPOSIUM: LOCOMOTION

Podium

CLINICAL GAIT AND BALANCE ASSESSMENTS: MILLIONS OF BITS OF DATA, BUT WHERE IS THE CLINICAL INFORMATION?

David A. Winter

Department of Kinesiology, University of Waterloo, Ontario Canada

INTRODUCTION

There is no doubt that clinical gait assessments are one of the most challenging and frustrating of all clinical assessments. There are three major reasons for this: the inherent complexity and plasticity of a multi-segment neuromuscular system; the complexity and volume of data collection, processing and interpretation; the lack of accepted standards in reporting. The situation was so clouded that it even prompted some researchers who were starting to use clinical gait assessments to throw-up their arms in defeat and comment that gait labs had no diagnostic function (Brand & Crowninshield, 1983). Fortunately, there were a number of laboratories who did not give in and forged ahead to solve the many technical & diagnostic problems. What we wish to do to-day is to focus on how many of us have met that challenge in a wide area of pathologies: cerebral palsy, hemiplegia, amputees, balance disorders, joint degeneration. We hope we can demonstrate how we reduced our data to yield our final clinical decisions: surgery, therapy, bracing, drugs, etc.

WHAT IS DATA AND WHAT IS INFORMATION?

As a start I made a crude estimate of the number of bits of data collected during one stride (1 1/2 seconds) of a patient walking over two force platforms while being tracked with 4 cameras and while 8 EMG signals were being recorded. Assuming that 4 seconds of EMG and force plate data need to be collected (to ensure a capture of the middle 1 1/2 seconds) and that only 1 1/2 seconds of the video data are digitized the total data approaches 46 million bytes of which 45 million is video. These numbers do not include any calibrations nor any repeat trials that might be necessary.

The question now put to our panel of experts is how are these data reduced and analyzed to yield those variables that have the information to make our clinical decisions. Can we generalize our diagnostic protocols as has been suggested in the past (Winter, 1985) or do we need specific protocols for each pathology? At the outset we should comment about the word information. I have reviewed half a dozen communications and signal processing texts and their definitions of information, and they all quote Shannon's Theorem

$$I \sim \log \frac{1}{P}$$

where: I is information received from the knowledge of occurrence of an event
P is the probability of occurrence of the event.

Unfortunately, in our clinical assessments we do not yet know what is the event or events we are looking for. Also, we should not be overly influenced by the probability of a given pathological event in the manner inferred by Shannon. Just because a certain pathological event is more or less probable should not influence the final diagnosis. A surgical decision in a less common pathology has the same information content for that patient as a surgical decision in a more common pathology. About the only thing we can benefit from this theory is that it suggests we focus on the lesser likely events (pathological patterns) rather than the more likely events (normal patterns).

As a functional and clinical definition of information I would suggest the following: any measure or pattern which does influence your management of the patient or could influence it in the future. The word "could" is specifically included because some well-identified atypical patterns may be altered by new technology (ie. localized spasticity reducing agents) and should not be dismissed just because we do not yet have the means to alter them. Also included in this information are adaptations that the patient is making to compensate a loss of function elsewhere. For example, a loss of knee extensor function during stance is often compensated for by increased hip or ankle extensor activity. Thus, this information would influence a surgeon by telling him/her where not to consider surgery, or to a therapist where to strengthen and retrain.

A final clarification is necessary regarding the global versus the custom nature of the gait assessments. Until now I have inferred that we were dealing with personalized assessments where each patient is assessed prior to a clinical decision. There is another group of gait analyses that yield clinical information and these are selected population groups where more global treatments are the decision. Examples of such are the physical therapy management of the hemiplegic population where gait assessments could be used to compare drastically different therapy protocols. In such situations it is important to identify those gait measures that influenced the final decision as to the preferred protocol. Also, such information may be valuable in assisting us to speculate about the mechanisms behind the improved rehabilitation.

REFERENCES

Brand, R.A., Crowninshield, R.D. Comment on criterion for patient evaluation tools. *J. Biomech.* 16:655, 1983.
Winter, D.A. Concerning the scientific basis for the diagnosis of pathological gait and for rehabilitation protocols. *Physiotherapy Canada*, 37: 245-252, 1985.

Millions of Bits of Data: How Can We Use It To Treat Cerebral Palsy ?

by
James R. Gage, M.D.

Professor of Orthopaedics, University of Minnesota
Medical Director, Gillette Children's Hospital

WHY IS GAIT ANALYSIS IMPORTANT FOR CLINICAL USE ?

Gait analysis is simply a measurement system which allows us to monitor how well the activity of locomotion is being accomplished. There are three major reasons why an investigator might wish to evaluate gait:

1. To gain better understanding of how the system operates, i.e., investigative research.
2. To optimize an activity which is already at a high level, e.g., to maximize performance in an elite athlete.
3. To bring suboptimal performance up to a more normal standard, e.g., to determine treatment in a child with cerebral palsy.

The parameters &/or constraints of the analysis system used will vary depending on the task at hand. For example, if one wishes to investigate the gait of a child with cerebral palsy the equipment attached to the patient must not be so encumbering that it modifies their usual gait pattern and the atmosphere should be quiet and subdued to minimize distraction &/or excitability which modifies their tone. In such a case, frame speed and field of view would not be critical. However, for the high performance athlete, a different set of criteria apply which might involve a much higher sampling rate, a wider field of view, and relatively portable equipment which could be moved out onto the athletic field.

Although building a gait analysis facility with maximum flexibility is desirable, with today's technology it is still necessary to target the design of the facility to the specific need for which it is intended.

Although gait analysis has applications for amputee gait, stroke, head or spinal cord injury, myelomeningocele, and/or muscle disease, the major use of the kinesiology laboratory at Gillette Children's Hospital is the evaluation and treatment of children with cerebral palsy.

Cerebral palsy is a disorder which affects the motor control system in the brain. The result of the brain injury is a partial loss of control of the locomotor process which manifests itself in the following ways:

1. Abnormal muscle tone which varies with position &/or movement
2. In a growing child, a propensity to develop muscle contractures
3. Loss of selective control of muscles
4. The necessity to use primitive reflexes to accomplish ambulation
5. Difficulty with balance

HOW DO WE APPLY GAIT ANALYSIS TO THE TREATMENT OF CEREBRAL PALSY ?

Children with spastic diplegia and/or hemiplegia nearly always walk. In the past, however, I feel we have done these children a serious disservice with our orthopaedic treatments. We are in the process of trying to prove that many of the children who were treated without the benefit of gait analysis were actually injured by their surgery. Currently, we are monitoring oxygen consumption pre- and post-operatively. What we are finding is that many of the children who have had surgery without the benefit of prior gait analysis actually have much higher oxygen consumption than you would expect, given their degree of neurological involvement. Thus, it is becoming apparent that unless one is very careful about surgical decision-making, the treatment may actually increase, rather than decrease, the energy requirements of walking.

Pre-operative Assessment

For optimal treatment of gait problems, three levels of decision-making are necessary. The first is the

clinical examination and observation of gait, which we have been doing for years. However, secondly, we also have to look at these patients dynamically. Fortunately, with gait analysis we now have the tools to see precisely what is going on in dynamic terms, i.e., kinematics, kinetics (moments and powers), and dynamic EMG. The third level of decision-making is the examination under anesthesia, because only anesthesia can you finally differentiate spastic contracture from true shortening of the muscles.

Pre-operative gait analysis is also essential if one wants to do simultaneous lengthening of all muscles without fear of error, and wants to treat the patient's specific orthopaedic problems in order to avoid "cookbook solutions." Basically, these children have two sources of abnormal gait: 1) the primary problems of neuromuscular control which are emanating from the central nervous system injury, and 2) the "coping responses," i.e., the compensation mechanisms which they are using to circumvent the primary problems of gait. For example, if, as a result of a central nervous system injury, a child is left with co-spasticity between his rectus femoris and hamstrings, he will have difficulty bending his knee during the swing phase of gait, which in turn will lead to difficulties in foot clearance. As a result of this, the child may vault, circumduct, or hyperflex his hip. Therefore, in this scenario, the co-spasticity is the primary problem and the mechanism, for example the vaulting, is the coping response. However, if I, as an orthopaedist, focus on the vaulting and lengthen the child's heelcord I have not done my patient a significant favor. Rather, I have inflicted iatrogenic damage which has the effect of compounding his gait problems. It is my personal feeling that this sort of thing has been the rule rather than the exception in the past, because we as orthopaedists really can't separate the primary problems of gait from the coping responses without dynamic gait analysis. Furthermore, the more surgery we do at one sitting, the more likely we are to introduce error. Thus, it is critical that if we are to correct all of a child's deformities at one surgical sitting, that we do a complete and comprehensive examination prior to the surgical intervention.

Once these three exams (static clinical examination, dynamic gait analysis, and examination under anesthesia) have been completed, one is in a position to formulate a surgical plan which is based upon the true underlying pathology of the condition. In general, this orthopaedic treatment must address five major areas of deficit to improve ambulation. These are:

1. Restoration of stance phase stability.
2. Improvement of clearance on the swing side.
3. Appropriate pre-positioning of the foot in terminal swing.
4. Enablement of an adequate step length.
5. The reduction of energy expenditure.

AN EXAMPLE

In the symposium we will present photos and data of a child with type III hemiplegia. [Winters, T. et. al. 1987] Prior to surgery he had stance phase instability, i.e., he couldn't get his right foot down flat on the floor. In addition he had co-spasticity of his rectus femoris and hamstrings on the affected side so that he had difficulties clearing his foot in swing. He had a shortened stride and poor pre-position of his foot in terminal swing. And, finally, he had excessive energy consumption.

A year after surgery, he walks at the same speed with excellent stance phase stability and good swing phase clearance. He has a longer stride length; good pre-position of his foot in terminal swing (which is provided by a leaf-spring ankle-foot orthosis), and his energy consumption has been reduced by half.

Post-operative Assessment

Post-operative gait analysis enables us to analyze outcomes with precision, to discover treatment errors, to study results collectively, and to gain additional insight into pathology and the results of treatment. Here is normal kinetic, sagittal plane data on the ankle in which the solid line represents the mean and the dotted lines one standard deviation from the mean.(**figure 1**) Compare this to our subject's preoperative (dotted line) and postoperative (solid line) data.(**figure 2**) I'm not going to give you a course in gait analysis, but I think you can see that the solid line much more closely mirrors the normal. In addition, you can see exactly what we have accomplished at the ankle. By inte-

grating the area under the power curves, you can even estimate the work of the plantarflexors pre- and postoperatively.

Summary

Gait analysis really allows practical application of the scientific method which is the accumulation of facts, organization of these facts into principles or laws, postulation of hypotheses to account for the facts and laws, and comparison of the hypothetical deduction with the experimental result. Before we had this tool we would start with a spastic child who walked abnormally and end with a spastic child who walked differently, but it was very difficult to tell exactly what our surgery had accomplished. Now we can critique our surgery. We have been doing this for eleven years at Newington and for five years at Gillette. Because of gait analysis, I think children with cerebral palsy have a brighter future, since we now can learn from the past and so will not perpetuate errors into the future. In the past few years, I have finally reached the point when, after performing gait analysis, I can sit down with the parents; demonstrate their child's gait abnormalities with the data; and then show them the pre- and postoperative videotape of a child who was affected similarly. Following this I can say, "This is what you have a right to expect." It took us a long time to get this far, but it was well worth the effort.

WHAT ABOUT THE FUTURE ?

The technology of gait analysis is moving rapidly, it is largely physician attitudes which need to change. There is still a wide spread perception among orthopaedic surgeons that clinical examination and observational gait analysis are adequate to determine treatment. Human gait is very complex and a thorough understanding of it demands some familiarity with the technology used to measure it and the basic principles of biomechanics. Some of the reluctance may be due to the commitment of time and effort necessary to accomplish this and the necessity for teamwork between the disciplines involved. Other technological advances in medicine such as MRI and/or CAT scans did not require such a significant effort on the part of those who merely wished to use the technology. However, I am certain that, given the steady advance of technology and our continued efforts to document the benefits of that technology and to teach it to our colleagues, gait analysis will soon be a routine part of the evaluation of both the elite athlete and the handicapped adult or child.

FIGURE 1

Sagittal Plane Kinematics :

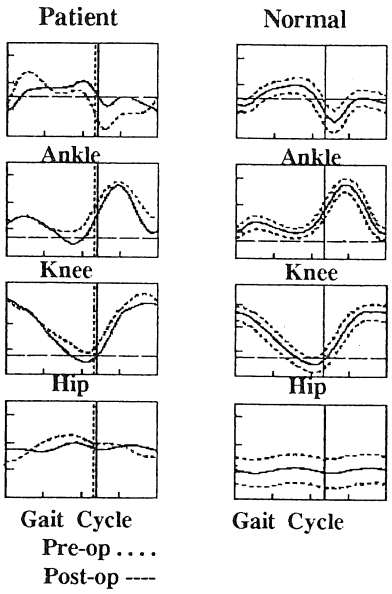

An illustration of the patient's sagittal plane kinematics pre- and post-operatively compared to a normal file (mean and one standard deviation). Notice that post-operatively (the solid line on the left), all graphs more closely resemble the normal.

FIGURE 2

Sagittal Plane Ankle Kinetics:

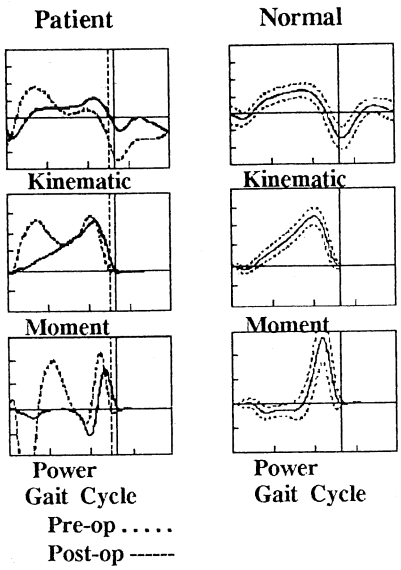

An illustration of the patient's sagittal plane ankle kinetics (pre- and post-operatively) compared to a normal file (mean and one standard deviation). Notice that post-operatively (the solid line on the left), all graphs more closely resemble the normal and the abnormal pre-operative power burst (dotted line in lower left hand graph) has been eliminated.

BIBLIOGRAPHY:

Winters, T. et. al. 1987 Winters, T.F.; Hicks, R., and Gage, J.R.: 'Gait patterns in spastic hemiplegia in Children and Young Adults'. Journal of Bone and Joint Surgery **69-A:** pp 437-441, 1987.

CLINICAL APPLICATIONS OF GAIT ANALYSIS

Thomas P. Andriacchi, Ph.D.
Department of Orthopedic Surgery
Rush-Presbyterian-St. Luke's Medical Center
Chicago, Illinois 60612

INTRODUCTION

Impairment to ambulatory function can be caused by disease or injury. Loss of ambulatory function causes significant handicap and greatly diminishes the overall quality of life. There are numerous treatment modalities (surgical and non-surgical) designed to improve ambulatory function. Gait analysis could provide unique information to aid in the evaluation of the numerous treatments used to improve ambulatory function. Objective measures are extremely relevant to today's current environment where there is a need to evaluate the outcome of treatment. Yet, gait analysis has not been widely accepted as a clinical test and the value of the information generated from gait analysis is often questioned for its value, uniqueness and cost effectiveness(4). The purpose of this presentation is to examine the clinical applications of quantitative gait analysis. Specific clinical applications of gait analysis to the treatment planning for high tibial osteotomy and anterior cruciate ligament reconstruction will be used to demonstrate several concepts related to the clinical applications of gait analysis.

METHODOLOGY

The fundamental approaches to gait analysis is not new. The kinematic and kinetic principles utilized today were used more than one hundred years ago by Braune and Fischer (5). They were able, using rather crude [by today's standards] optical techniques and instrumentation, to do kinematic and kinetic analysis of the body during locomotion. The instrumentation to acquire these measurements has improved automation, resolution and accuracy. However, the increase in resolution and accuracy of the current systems has done little to enhance the clinical relevance of the type of measurements provided. There are a number of highly automated optoelectronic systems that can provide computerized acquisition of motion and force data with more than sufficient resolution to provide meaningful measurements. Gait analysis has not been accepted as a clinical tool because of a lack of instrumentation. The automated instrumentation has been available for the past twenty years, yet it has not been generally applied clinically. What is needed at this is not more accurate systems, or more automated systems or even cheaper systems; what is needed is an understanding to the fundamental approach to obtaining clinical information from quantitative biomechanical testing. Therefore, the future research should not be on instrumentation and methodology but on issues related to setting up an appropriate clinical testing protocol that can obtain information relative to treatment planning and evaluation.

CLINICAL RELEVANCE

1) *Unique Information:* This information must be unattainable through other simpler less costly tests typically conducted during a routine clinical examination. For example, in cerebral palsy patients, the ambulatory deficits only manifest themselves during walking. Thus, applications which quantify these walking abnormalities which cannot be obtained through simple clinical exam would be extremely important.

2) *The Potential to Improve Treatment*: In many cases, the description that gait is either normal or abnormal does not provide information that is useful in improving treatment planning. For example, there may be some characteristics of adaptive gait (which appear abnormal on quantification) which are actually of benefit to specific treatment modalities. This point will be illustrated further in the example of the high tibial osteotomy.

3) *Cost to Benefit Ratio:* It is important to demonstrate that information generated from functional biomechanical testing can increase the probability of improved outcome and, thus, reduce further medical expense for further treatment. This is especially relevant to treatment planning for a number of surgical procedures and will also be illustrated in both of the examples in this paper.

How does one set up a clinical gait analysis to address the above criteria for clinical relevancy. There are some common features which can be identified. These features apply to the clinical use of gait analysis (6,7,8) which include, first, asking an appropriate and *relevant question* of gait analysis; secondly, selecting the protocol which can address that question and, thirdly, having the availability of expertise to provide an appropriate *interpretation* of the gait measurements. Underlying each of these elements is the selection of parameters that reflect the physical aspects of the problem. For example, in the CP applications, the direct measurements of offending muscles were particularly pertinent to the selection of surgical planning to improve the gait associated with the abnormal.

CLINICAL EXAMPLE: HIGH TIBIAL OSTEOTOMY

High tibial osteotomy is a common treatment for varus gonarthrosis. The fundamental premise of the procedure is that realignment of the varus deformity of the limb will reduce the stress on the medial compartment of the knee and, thus, halt or reverse the degenerative changes and reduce or eliminate symptoms associated with the degenerative portion of the medial compartment of the knee. The procedure is attractive since it is more conservative than a total knee arthroplasty and can be used for younger and more active patients. Results are somewhat variable clinically and it is not clear, on the basis of either clinical exam or static alignment based on x-rays, which patients will do well with the high tibial osteotomy. Gait analysis allows for a dynamic measurement of the loads related to the medial compartment load at the knee during walking. The loads are substantially higher than level walking and, thus, it is likely that they are associated with the symptoms as well as the progression of the degenerative changes.

An analysis of patients with varus gonarthrosis (7,8) indicated that patients walk with both low and high adduction moments preoperatively in spite of their

varus deformity. The presence of a low adduction moment would not be predictable from static alignment of the limb since the varus deformity would always suggest a higher adduction moment. However, the gait analysis indicated that some patients with varus knees adapt producing a normal or lower than normal adduction moment (Figure 1). A long-term clinical followup demonstrated that patients who walk with a lower adduction moment preoperatively had substantially better results than those patients with the higher adduction moment. Thus, clinical outcome was directly related to a gait measurement which provided information that could not be obtained through standard clinical examination.

The question, protocol and interpretation were all directly related to the physical characteristics of the clinical pathology and, thus, provided a very relevant clinical application of gait analysis. It is important to note that this application was based on extensive research and nearly eight years of followup on these patients to identify the relationship between the adduction moment and clinical outcome. This extensive research and database have permitted one to use a deductive approach to future interpretations of patients with high tibial osteotomy. However, this does not mean that each clinical application necessarily requires an extensive long-term followup to demonstrate relevance. One can employ an inductive approach if the selection of the variables measured have direct physical meaning. The next example will demonstrate this approach.

CLINICAL EXAMPLE: ANTERIOR CRUCIATE LIGAMENT DEFICIENCY

Injury or rupture to the anterior cruciate ligament (ACL) is one of the most frequently occurring injuries to the knee joint. Some patients do well with only rehabilitation following ACL rupture while others require reconstructive surgery. It was hypothesized that those patients who do well have learned to adapt their function through

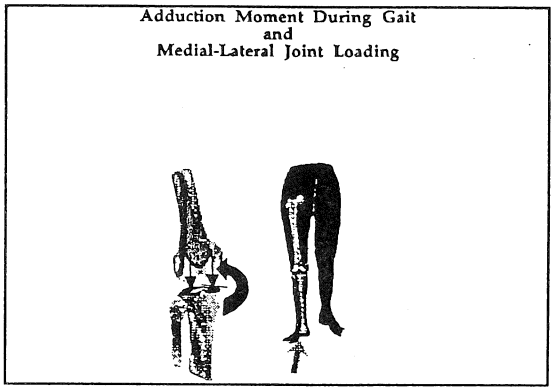

Figure 1. The adduction moment during gait influences the load on the medial compartment of the knee.

the use of dynamic muscular substitution during more stressful activities such as running and cutting or running and stopping.

Hamstring substitution was quantified through an analysis of the flexion-extension moment at the knee while patients are performing these activities in the Gait Laboratory (2,3). Thus, the question of the gait analysis was: "Do patients with ACL deficiency compensate with higher hamstring moments during activities of pivoting and stopping?" The analysis assumed that if the patients have a higher moment than normal while conducting these activities, they were compensating for ACL deficiency.

A test of patients with ACL deficiency demonstrated (Figure 2.) an increased hamstring moment during the running and cutting activities. Further, a group of patients following ACL reconstruction and the reestablishment of anterior stability to the knee demonstrated a return to normal or near normal hamstring moment.

Gait analysis can identify and quantify adaptive mechanisms associated with muscular substitution which can be

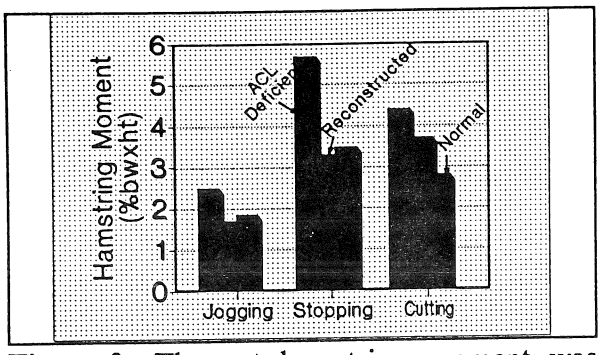

Figure 2. The net hamstring moment was higher the normal in ACL deficient knees and was not different than normal following ACL reconstuction.

beneficial to patients with ACL deficiency. Thus, through the selection of a variable that directly relates to the physical characteristics of the pathology, one can obtain clinically relevant information without a long-term clinical study of each application.

CONCLUSION

Gait analysis can provide unique information which has the potential to improve treatment and can be demonstrated to have an effective cost to benefit ratio. There is a need to carefully plan gait analysis to address specific questions related to the pathological question with an approach that is feasible in a clinical setting. Through the selection of the appropriate question, adequate protocols and the ability to interpret measurements with clinical relevance, gait analysis can meet in many applications the criteria for relevance. There is, however, a need for increased expertise in both the planning and interpretation of gait tests. A simple question of whether the patient is normal or abnormal in most cases is not relevant and is not of sufficient value for clinical applications.

REFERENCES

1. Andriacchi, T.P.: Biomechanics and orthopedic problems: A quantitative approach. In: *Future Directions in Exercise/Sport Research.* J.S. Skinner, C.b. Corbin, D.M. Landers, P.E. Martin and C.L. Wells (eds), pp 45-56, 1989.
2. Andriacchi, T.P.,et al The biomechanics of running and knee injuries. In: *American Academy of Orthopaedic Surgeons, Symposium on Sport Medicine, The Knee*, Mosby, pp 23-32, 1985.
3. Berchuck, M., Andriacchi, T.P.,et al Gait adaptations by patients who have a deficient anterior cruciate ligament. *J Bone Joint Surg* 72A(6):871-77, 1990.
4. Brand, R.A. and Crowninshield, R.D.: Comment on criteria patient evaluation. *J Biomechanics*, 14:655, 1980.
5. Braune, W. and Fischer, O.: *Der Gang Des Menschen*, I. Teil (1895); II. Teil (1899); III. Teil (1900), Lepzig, Bei B.G. Teubner.
6. Perry, J., et al Gait analysis of the triceps surae in cerebral palsy. A preoperative and postoperative clinical and electromyographic study. *J Bone Joint Surg*, 56A(3):511-520, 1974.
7. Prodromos, C.C., Andriacchi, T.P., and Galante, J.O.: A relationship between knee joint loads and clinical changes following high tibial osteotomy. *J Bone Joint Surg*, 67A(8):1188-1194, 1985.
8. Wang, J-W., Kuo, K.N., and Andriacchi, T.P.: The influence of walking mechanics and time on the results of proximal tibial osteotomy. *J Bone Joint Surg*, 72A(6):905-913, 1990

THE RELATIONSHIP OF GAIT SPEED TO CLINICAL MEASURES OF FUNCTION AND MUSCLE ACTIVATIONS DURING RECOVERY POST-STROKE

C.L. Richards, F. Malouin, F. Dumas and S. Wood-Dauphinee
Physiotherapy Department and Neurobiology Research Centre
Laval University, Quebec City, Quebec.
School of Physical and Occupational Therapy, McGill University, Montreal, Quebec.

INTRODUCTION

Although extensive biomechanical gait analyses generate an enormous amount of data, relatively few outcome measures have been defined and validated. If a gait variable is to be used as an outcome measure for stroke patients, it must be possible to measure it reliably and it should reflect motor recovery in groups of patients. For example, gait speed has been shown to be related to motor recovery (Brandstater *et al.* 1983, Wade *et al.* 1987), to strength (Bohannon 1986) but not to the degree of spasticity of knee muscles (Norton *et al.* 1975). When evaluating the effects of therapy, it can thus be assumed that gait velocity will provide a global measure of change that reflects motor recovery but will not, however, reflect qualitative changes in the movement, moment or muscle activation profiles during the gait cycle. On the otherhand, such profiles essential for the understanding of individual motor patterns, (Knutsson and Richards 1979, Winter 1987, Olney *et al.* 1991) are difficult to use as group outcome measures. Because of the unique nature of the brain lesion, patients can be expected to develop different motor strategies as they recover. Furthermore, little is known about the relationship of muscle activations to gait speed or to recovery post-stroke. The purpose of this study is to examine the interaction between gait speed and activations of the ankle muscles and their relationships to clinical measures (Fugl-Meyer *et al.* 1975, Mahoney and Barthel 1954) during recovery post-stroke.

SUBJECTS AND METHODS

Patients with an infarct of the middle cerebral artery, confirmed by CT scan were recruited within one week of stroke onset. The recovery of twenty-seven patients, 14 women and 13 men, ranging in age from 40 to 75 yrs (16 left-sided hemiplegics) was followed from stroke onset to 18 months post-stroke. In the first six weeks post-stroke they participated in a randomized controlled clinical pilot trial designed to evaluate the effects of three physical therapy regimes on the gait outcome (Malouin *et al.* 1992). After the trial was completed, follow-up evaluations were made at 3, 6, 12 and 18 months post-stroke. For this preliminary study, results in all the patients who had completed the evaluations up to 18 months post-stroke were pooled (to ensure an n=14, the results of the 12 and 18 month evaluations were combined). The results of the gait evaluations were compared to data from healthy elderly (n=10) subjects obtained in a prior study using the same methods (Richards *et al.* 1990).

Clinical measures of function were made one week post-stroke (baseline) using the Fugl-Meyer *et al.* (1975) and Barthel (Mahoney and Barthel, 1954) scales. These measures were repeated at 6 weeks and at 3, 6, 12 and 18 months post-stroke when the gait was also analyzed. Gait movements were recorded with a TRIAX electrogoniometer (Isacson *et al.* 1986). Activations (the EMG signals were rectified and time averaged with a time constant = 0.2s and visualized on a Grass polygraph) of the triceps surae (TS) and tibialis anterior (TA) muscles (surface electrodes) were synchronized to footswitch signals as the subjects walked (with manual assistance if necessary) across an 8M walkway. Angle, EMG and footswitch signals were fed to an IBM PC compatible computer for recording and analysis. Changes in the different variables over time were compared by means of an analysis of variance for repeated measures followed by a post-hoc analysis (Scheffe or Tukey test).

RESULTS

Figures 1 and 2 illustrate a typical recovery profile over time of muscle activations and spatiotemporal variables in a 62 yr old woman with left-sided hemiplegia. In Figure 2A, note how the speed increased gradually over time to reach a speed less than 50% of normal. This speed increase was mainly due to a faster cadence. To further examine the changes in muscle activations over time, the area under the activation profiles for specific segments (TS: 20-50% of the gait cycle; TA1: 0-16%, TA2: 60-80% and TA3: 84-100% of the gait cycle, as illustrated in Figure 1) was compared. The size increment of the TS activation burst shown in Figure 1, however, represents only a small proportion of the normal activation level (Fig. 2B). Recovery is more marked in the TA, particularly in the late swing activation burst that attains normal levels 18 months post-stroke. These activation changes are related to the more than three-fold increase in speed and improved ankle movements throughout the gait cycle at 18 months. Clinically, this patient's Fugl-Meyer leg score increased from 5 (maximum = 34) at baseline to 24 at 6 weeks and 28 at 18 months.

Table 1 Pearson Correlation Coefficients Between Muscle Activation Bursts (see Figure 1) and Spatiotemporal Variables 6 weeks post-stroke.

	TS	TA1	TA2	TA3
Speed	.64*	.70**	.84**	.47
Cadence	.46	.56*	.76**	.30
Stride l.	.60*	.64*	.69**	.48

* p<.05, ** p<.01, n=14, l.=length

To probe the relative changes in the size of the activation bursts over time and the relationship of these changes with gait velocity, Pearson correlation coefficients were calculated for the group of patients 6 weeks post-stroke (Table 1). This analysis revealed the stance-swing transition TA burst (TA2: 60-80%) to be the most highly correlated (.84**) to speed, cadence and stride length while the late swing TA burst (TA3: 84-100%) to be the least correlated. As expected, the TS was also significantly correlated (.64*) to speed but its effect was more closely linked to an increase in stride length. Thus it appears that while the TA acts on the foot position in early stance and helps initiate the swing phase, a longer stride length needs to be powered by a larger TS "push-off" activation burst (Winter 1987).

Figure 3 displays the recovery profile for the spatiotemporal variables, the Fugl-Meyer leg score and the Barthel ambulation subscore in the group of patients. Gait speed increases over time as expected and is related to increases in both the stride length and cadence. Furthermore, gait speed is sensitive to change up to 12-18 months post-stroke. In contrast, both clinical scores plateau early, indicating that they are less sensitive to change over time when scores approach maximum values at 6 weeks for the Fugl-Meyer scale (max.=34 and at 3 months for the Barthel subscore (max.=47). This suggests that gait velocity, a continuous quantitative variable, is more sensitive to the small changes that occur after 6 weeks post-stroke than scores that reflect achievement of motor tasks. Figure 4 further examines the relationship between motor performance of the leg as measured by the Fugl-Meyer leg score and gait velocity. The scatter plot suggests that a threshold of at least 25 on the Fugl-Meyer leg score is necessary to achieve higher velocity levels.

The recovery profiles for gait speed and the activations of the ankle muscles over time are shown in Figure 5 in comparison to normal values. The gradual increase in gait speed (Figure 5A) is accompanied by a parallel increase in the size of the muscle activations (Figure 5B). In the group of patients, the mean recovery of the TA activation burst was about 10% better than that in the TS over time and this change was significantly different from baseline values only for the TA (see Figure 6). Since it is important to understand if the time course of recovery in the TS and the TA is similar or if one is predictive of the other, correlation coefficients were calculated between selected variables (Table 2). As shown, the recovery of the TA and TS bursts are highly correlated at 6 weeks post-stroke and these bursts in turn are correlated to recovery at 12-18 months post-stroke.

Table 2 Pearson Correlation Coefficients (r) Between the Tibialis Anterior and Triceps Surae Activation Bursts

	TS 6W	TS 12-18M	TA2 12-18M
TS 6W	1	.81**	.65*
TA2 6W	.79**	.72**	.69**

** p<.01, * p<.05, n=14, TS: triceps surae, TA2: tibialis anterior (60-80%), w: weeks, m: months

DISCUSSION

These results describing recovery after stroke confirm and extend the results of earlier clinical studies that have reported most of the motor recovery occurring within the first 3 months post-stroke (Twitchell, 1951; Skilbeck *et al.* 1983) and plateauing at 6 months. This study further showed that most of the recovery occurred within 6 weeks when active rehabilitation procedures supplemented natural recovery processes. Moreover, the Fugl-Meyer leg score (Brandstater *et al.* 1983, Dettmann *et al.* 1987) and the Barthel total score (Dettmann *et al.* 1987) have been shown to be correlated to gait speed in groups of hemiplegic patients examined transversely in different stages of recovery. This is the first longitudinal study that describes the correlation of these variables over time during recovery from stroke onset in a group of patients with a lesion of the same artery. Both the Barthel and Fugl-Meyer scores, that represent the achievement of specific tasks, plateau early during recovery (Skilbeck *et al.* 1983) and are less sensitive than gait speed to change after 3 months post-stroke. New data were also provided on the recovery of the activation capacity of the ankle muscles during gait and their relationship to gait velocity. In general, the mean level of recovery of the gait speed and muscle activations attained less than 50% of normal values by 12-18 months post-stroke. The slow gait speed can in part be explained by the poor recovery of the TS "push-off" activation burst that generates much of the propulsive force (Winter, 1987; Olney *et al,* 1991) but as shown in this study, recovery of the TA is also important for recovery of gait speed. A surprising result, because of the characteristic lack of dorsiflexion in early stance and swing phases during gait in hemiplegic patients, was the superior recovery of the TA as compared to the TS. The coupling of the recovery profiles of the TS and TA over time, however, confirmed the functional interrelation of these two muscles for the control of ankle movements.

REFERENCES

Bohannon, R.W. *Physiother. Can.*, **34**, 204-206, 1986.
Brandstater, M. et al. *Arch.Phys.Med. Rehab.*, **64**, 583-587, 1983.
Dettmann, M.A. et al. *Am.J.Phys.Med.*, **66**, 77-90, 1987.
Fugl-Meyer, A.R. et al. *Scand.J.Rehab. Med.*, **7**, 13-31, 1975.
Isacson et al. *J. Biomech.* **19**, 627-635, 1986.
Knutsson, E. and Richards, C. *Brain* **102**, 405-430, 1979.
Mahoney, F.D. and Barthel, B.W. *Arch.Phys. Med.Rehab.*, **35**, 359-362, 1954.
Malouin, F. et al. *Posture and Gait*: Control Mechanisms Vol II, Portland, (pp. 407-410), 1992.
Norton et al. *Phys.Ther.*, **55**, 355-359, 1975.
Olney, S. et al. *Arch.Phys.Med.Rehab.*, **72**, 309-314, 1991.
Richards, C.L. et al. *Human Locomotion VI*, Quebec City, (199-202), 1990.
Skilbeck, C.E. et al. *J. Neurol. Neurosurg. Psychiatry*, **46**, 5-8, 1983.
Twitchell, T.E. *Brain*, **74**, 443-480, 1951.
Wade, D.T., et al. *Scand.J.Rehab.Med.*, **19**, 25-30, 1987.
Winter, D. The Biomechanics of Motor Control of Human Gait, Waterloo, 1987.

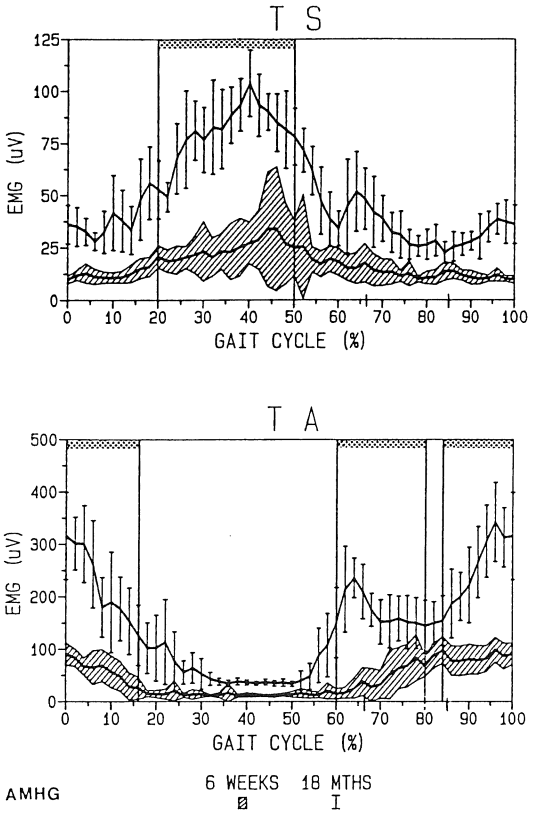

Figure 1. Comparison of activation profiles (mean ± 1SD, n=10 gait cycles) of the triceps surae (TS) and tibialis anterior (TA) of one hemiplegic patient (62 year old woman) 6 weeks and 18 months post-stroke. Vertical lines outline segments of gait cycle submitted to statistical analysis.

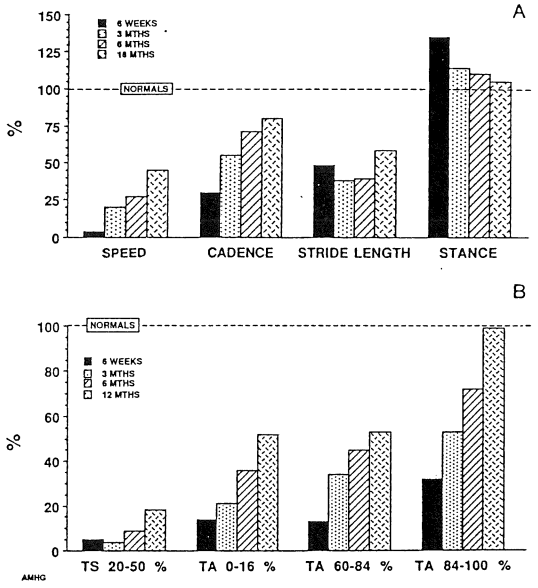

Figure 2. Mean (n=14) recovery profiles of spatiotemporal and muscle activation variables of a hemiplegic patient (same as in Figure 1) over time in comparison to normal values.

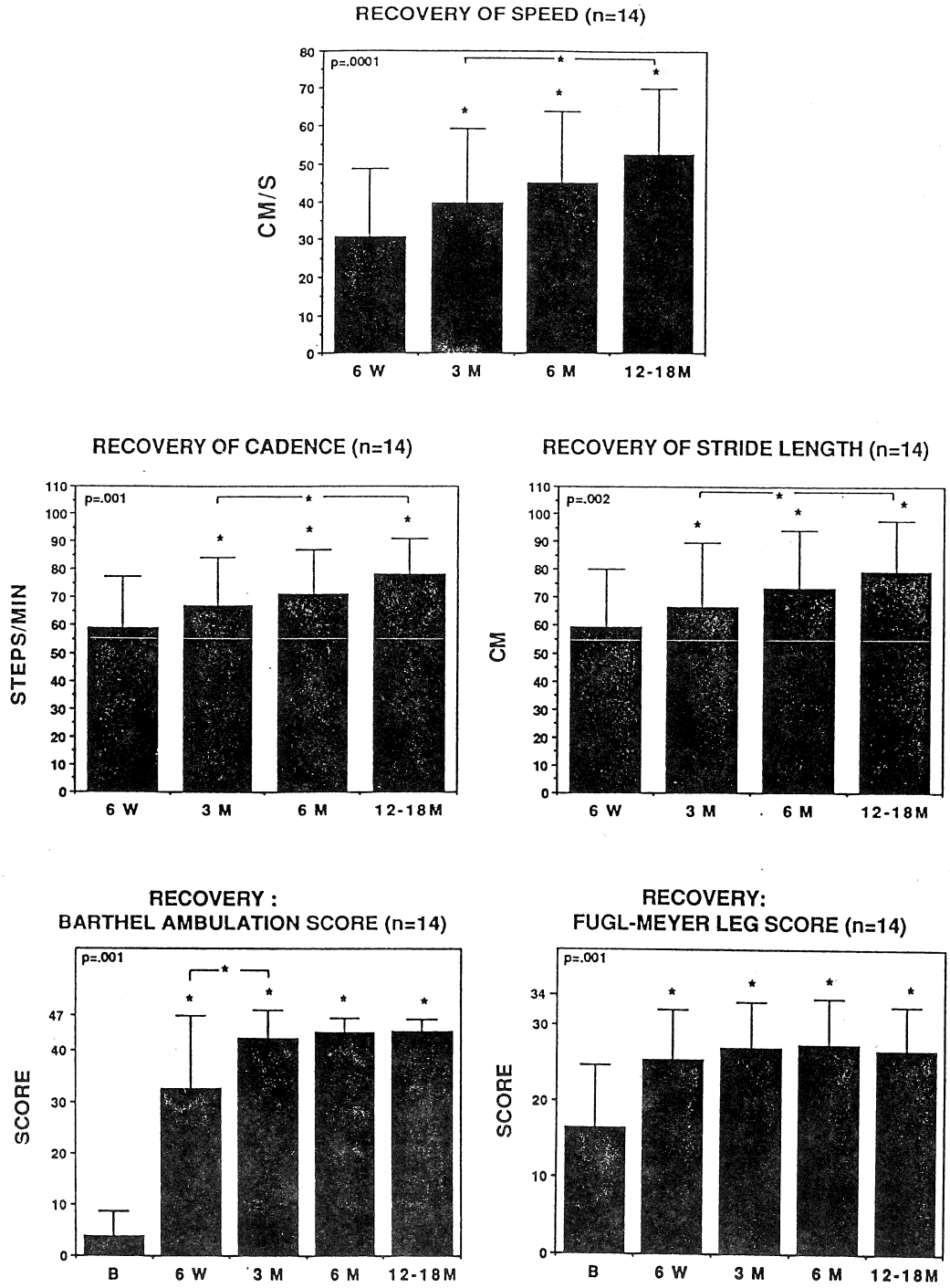

Figure 3. Mean (+1SD) recovery profiles over time (w=weeks, m=months) of the spatiotemporal variables and clinical measures in the group of hemiplegic patients. Significant changes (analysis of variance for repeated measures) from baseline (B) or 6 week evaluations indicated by asterisk. Changes between other times indicated by horizontal line with asterisk.

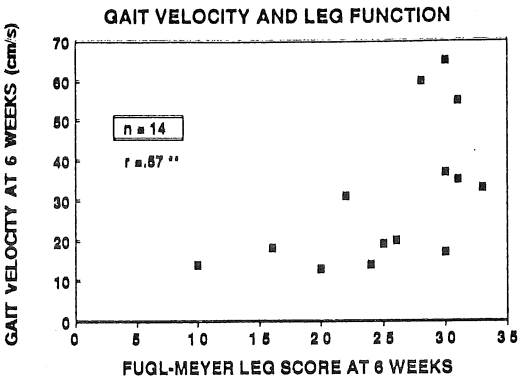

Figure 4. Correlation between gait velocity and the Fugl-Meyer leg score in the group of hemiplegic patients at 6 weeks post-stroke.

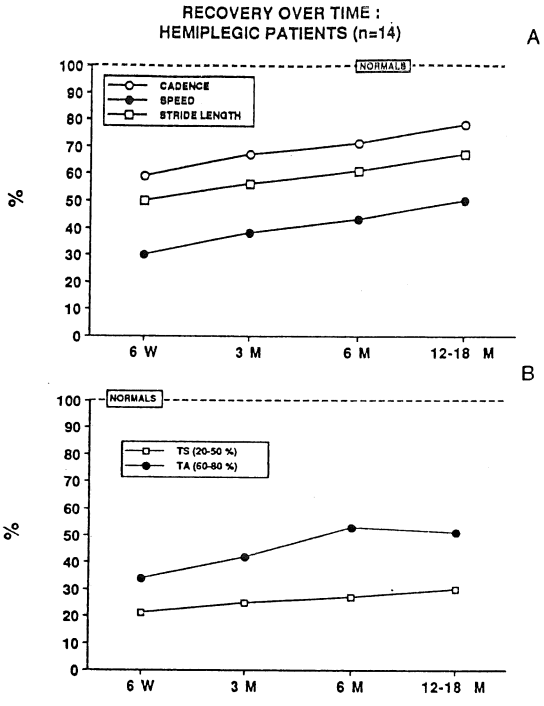

Figure 5. Mean (n=14) recovery profiles over time (w=weeks, m=months) of the spatiotemporal variables and muscle activations in the group of hemiplegic patients in relation to mean normal values (dotted line).

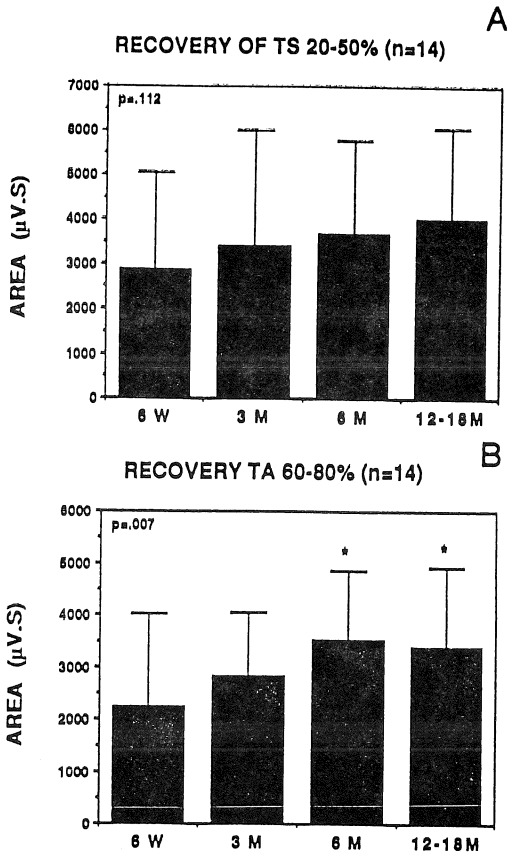

Figure 6. Recovery over time (w=weeks, m=months) of the triceps surae (TS) and tibialis anterior (TA) activation bursts in the group of hemiplegic patients (mean, +1SD). Asterisks indicate statistical (analysis of variance for repeated measures) differences between a given time and 6 weeks.

ACKNOWLEDGEMENTS

This work was supported by grants from the National Health Research and Development Program and Laval University.

CLINICAL INFORMATION IN GAIT ANALYSIS

S. J. Olney

School of Rehabilitation Therapy, Queen's University
Kingston, Ontario K7L 3N6

INTRODUCTION

There have been strong and conflicting opinions arising from gait analysis. It is fair to say that it has met overall clinical acceptance only in applications to cerebral palsy surgery.

The question posed is how gait analysis data can be reduced and analyzed to yield the variables that contain information to make clinical decisions either now or in the future. These clinical decisions may be specific to an individual or to a patient group. To make clinical decisions, however, we are asking for a very high level of knowledge - prediction - not description or explanation.

Accordingly, in clinical gait analysis, the biomechanist is consciously or unconsciously making observation, forming hypotheses and building theory of gait performance, frequently at several different levels of understanding. I urge biomechanists to acknowledge this process and to systematically attempt to reduce the unknowns in the theory of gait performance. In doing this, clinically important variables will be identified.

Some of the typical scientific methods of theory development are not possible in gait research. I will suggest some that we have used in patient groups, I believe, productively.

CHARACTERIZING GOOD PERFORMANCE

In each of the following methods it is necessary that one be able to identify at least one performance variable that is an indicator of overall good performance. While one will necessarily characterize "bad" performance in these methods, I have adopted a positive approach.

1. Descriptive approach

At the least sophisticated level, one can examine the data of the "worst" subjects and compare it with the "best" subjects, and attempt to identify the characteristics associated consistently with each. I believe that many of the initial hypotheses are generated in this manner. For example, in adult stroke subjects, we have used the self-selected speed of walking as a marker of general gait competence (Bohannon, 1987) though one might equally well justify other measures. Further, we pay particular attention to kinetic variables, hoping to remain closer to causative data. In a comparison of groups of high and low performers (Olney et al, 1991), it was clear that members of the fastest group were generating more than three times the positive work with their affected ankle plantarflexors at push-off than were the slowest group (Figure 1). These trends were similar, though less marked, for the unaffected side.

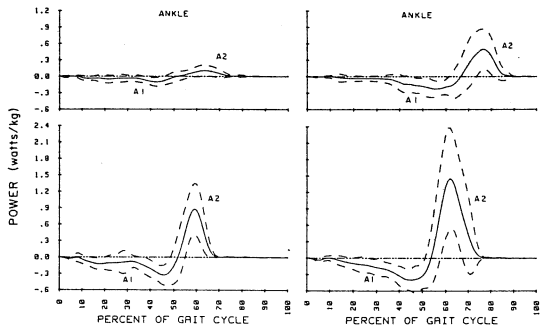

Figure 1. Means and standard deviations of ankle joint power profiles for ten subjects with stroke walking at fast speed (mean .64 m/s) and at slow speed (mean .25 m/s).

The clinical application resulting from these findings (and others in the same data) led to the hypothesis that if one could increase the power generation of the ankle plantarflexors at the appropriate time in the gait cycle, the gait performance would be improved. This was an important objective to define, as little attention has been paid to this aspect of rehabilitation. Therapists are fearful of causing generalized overactivity in a muscle that frequently develops spasticity.

It was, however, inappropriate use of this approach that misled clinicians when they attempted to determine treatment objectives by applying the results of able-bodied subjects to those with pathologies. The application was particularly likely to be misleading when the variables receiving attention were kinematic, and a step removed from causation. To identify clinically important variables it is necessary to develop an understanding of each pathology as well as able-bodied gait.

2. Correlational Approach

A second approach to determining what variables are important in specific gait pathologies is to identify likely candidates and find which of them are consistently associated with good performance. Again, a measure that one can accept as an indicator of performance is needed. By examining the variables that are related, a picture of good performance emerges.

We have used this approach in a study of hemiplegic cerebral palsied children. Using a 2-D kinematic and kinetic analysis of several strides from each side of the body, and normalizing data, we identified important incidents in the profiles. For example, from kinematic profiles we identified the angle of maximum dorsiflexion, maximum plantarflexion, and foot segment plantarflexion; in moment profiles we used the maxima, minima and ranges of the ankle, knee and hip for both sides of the body; among work and power variables we selected normalized maxima and minima as well as certain important work totals. A selection of results are shown in Table 1.

From timing information, the proportion of the time spent in double support with the affected foot behind the unaffected one was consistently related to speed. The joint angles and segment angles were unremarkable, though the highest relationship was found with the maximum hip flexion angle on the affected side. A number of the moment variables of the affected side were significantly related to the normalized velocity chosen by the child. Notable were the peak hip moment variables - the minimum and maximum hip moments as well as the range. Furthermore, the maximum hip power and the positive work of the hip were significantly related.

Table 1. Correlations between gait velocity per leg length and selected variables for hemiplegic cerebral palsied subjects.

Variable	Affected	Unaffected
double support	-0.62**	-0.35
max dorsiflexion, deg	0.27	0.31
max plantarflexion, deg	0.23	-0.06
max hip flexion, deg	0.45	0.28
max hip extension, deg	-0.14	-0.17
max ankle moment, N.m/kg	0.43	-0.09
min ankle moment, N.m/kg	-0.10	-0.08
range ankle moment, N.m/kg	0.47*	-0.04
max knee moment, N.m/kg	0.51*	0.41
min knee moment, N.m/kg	-0.07	0.07
max hip moment, N.m/kg	0.46*	0.03
min hip moment, N.m/kg	-0.67**	-0.34
range hip moment, N.m/kg	0.75**	0.27
max ankle power, W/kg	0.43	0.32
max hip power, W/kg	0.61**	0.46*
hip positive work, J/kg	0.58**	0.05

* $p < 0.05$, ** $p < 0.01$

The composite picture indicated that hip kinematics and kinetics are important in these children. From data on able-bodied subjects, we know that while the major power generators are the ankle plantarflexors during push-off the action of the hip flexors during pull-off is next in importance. The close relationship of normalized velocity with the joint position, the flexor moment, power and work, suggests that better performers use this strategy. For a child making poor use of this strategy, a therapeutic objective would be identified: increase the pull-off action.

Note the limitation of this method: only variables having a consistent relationship to the performance measure can be identified. If, for example, there are two alternative strategies to compensating for a deficit that result in the selection of high values for one variable and low values for the other, simple correlations will not indicate a close relationship with either one.

3. Regression Approach

The problem of identifying groups of variables which, when taken together, contribute to a desirable outcome, can be explored using a regression approach. Again one must be able to identify a variable indicative of good performance. In the case I will describe here, we used a type of stepwise regression to identify the variables most useful in predicting stride velocity in stroke patients. A maximum R-squared method was used which has some important advantages over more familiar methods. Using temporal, kinematic and kinetic variables of the sort listed in Table 1, the gait data from the affected and unaffected sides of the body for 32 stroke subjects were analyzed. Unfortunately separate data collection trials had to be carried out on each side of the body.

The following models, predicting velocity from data of the affected and unaffected sides77, respectively, accounted for 94.1% and 92.1% of the variability, with P values that were 0.0005 or less for each of the variables in the equation:

Affected side:
Velocity = 0.35 - 0.45 min hip moment
+ 0.24 ankle moment range
- 0.24 knee moment range
- 0.007 double support

Unaffected side:
Velocity = 1.34 - 0.015 stance proportion
+ 0.09 max ankle power
+ 0.25 max hip power

The picture from the data on the affected side is that of a person with a large hip flexor moment at the end of stance phase (usually this means a long step with the unaffected limb), a large range between dorsiflexor and plantarflexor moments at the ankle, a small range of knee moments, and a short double support period when the affected foot is placed behind the unaffected. The picture from the unaffected side is of a person with a short period of weight bearing (stance), substantial ankle plantarflexion at push-off, as well as a strong pull-off by hip flexors.

Now variables have been identified that are important when grouped together. As large contributors to the work of walking, it seems reasonable that ankle and hip power complement each other.

One could further restrict the selection of variables according to a particular theory one might build.

4. Principal Component Approach

In dealing with the data using the methods above, it is difficult to see how the variables relate to each other. This is an ideal circumstance in which to determine the principal components that are present. Unfortunately, usually one has had to deal with the information in other ways until there are sufficient numbers of subjects to make these analyses possible.

We have found it helpful to subject the same data described in method 3, above, to principal components analysis for the affected and unaffected sides separately. The analysis for each side showed that approximately 55% of the total variability was retained in the first three principal components. The first principal component of both sides had many power and work variables. When values for principal component one (affected side) were plotted against principal component one (unaffected side), there was a strong correlation, indicating the component was much the same. The first component could be termed the velocity and power component. A plot of the second component (largely unrelated to the first) revealed scatter, indicating that the component was not the same for both sides. By comparing subjects, it was found that the second component encompassed the affected knee strategies - a low score meant the subject tended to hyperextend the knee in stance, have a knee flexor moment, and high hip extension in stance.

This analysis was helpful in that it indicated that the knee hyperextension pattern of the affected side was independent of the work and power variables. Again, clear hypotheses relating to specific variables can be formulated from these findings.

CONFIRMING PREDICTIONS

1. Exploiting Natural Perturbations

In the final analysis, one can be sure that one has picked the right variables for making clinical judgements only when they have been perturbed in a known manner and the results are as expected. This occurs naturally in many clinical circumstances, but surgery provides a unique opportunity for verification.

J.M. is a hemiplegic child with cerebral palsy (CP) who received a heel cord lengthening at the age of six. Based upon what we knew about gait, we hypothesized that, if the biomechanical effects of the primary pathology were to be reduced, compensations evident in other variables would be reduced post-surgically. The primary variable of interest was positive ankle power, and secondary variables included those powers indicating compensatory strategies. Figure 2 confirmed the importance not only of the primary variable, but also those involved in compensatory strategies. Pre-surgically, compensations of the unaffected side for diminished ankle power on the affected side are evident in above normal hip extensor and knee extensor generation in stance, and in hip flexor generation at pull-off. Post-surgically, not only was there drastic improvement in the primary variable, ankle generation, but there was also concomitant reduction in the compensatory measures, confirming their clinical importance, and providing a small contribution to the development of the theory relating to CP gait performance.

2. Imposing Perturbations - The Clinical Trial

The notion of confirming the clinical importance of variables identified by the methods described in the first section is logically extended to the true clinical trial. By manipulating one or more treatment variables in an experimental manner, results will indicate the importance of the selected variables. Though cost and complexity tend to restrict such trials, I believe these will provide final confirmation of variable importance.

REFERENCES

Bohannon, R.W. Arch. Phys. Med. Rehabil. 68,777-781,1987.

Olney, S.J, et al. Arch. Phys. Med. Rehabil 72,309-314,1991.

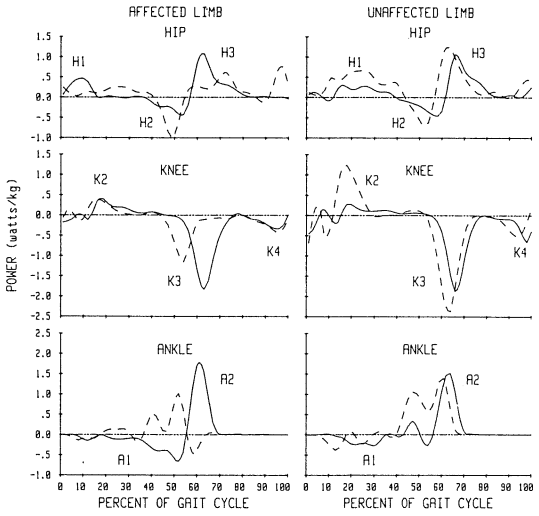

Figure 2. Joint power profiles for the hip, knee and ankle of hemiplegic CP child before (dashed line) and after (solid line) surgery.

IDENTIFYING AND INTERPRETING AGE-RELATED CHANGES IN BALANCE CONTROL SYSTEM

Aftab E. Patla, James S. Frank, and David A. Winter
Department of Kinesiology
University of Waterloo
Waterloo, Canada
N2L 3G1

Falls in the Elderly: A Major Health Issue

The higher incidence of falls in the elderly has been reported by many researchers (cf. Baker & Harvey, 1985). There is no specific age threshold over which the frequency of falls suddenly increase: Rather there is a steady increase as we age (Patla, Frank & Winter, 1990). Cummings, et.al. (1988) have documented fall outcomes in a group of community dwelling elderly. Their results showed that 55% of this group had suffered falls, with 24% of the falls resulting in injury. The injuries ranged from minor bruises or swelling (51%) to fractures (4%). Some of these falls cause health complications leading to premature institutionalization and even death.

Even though the elderly recover from minor injuries caused due to falls, there is a tremendous impact on their lifestyle and ultimately their health. Tineti & Powell (1991) have reported that 48% of the individuals over 75 years of age who had an injurious fall admitted a fear of falling and 26% of these individuals acknowledged avoiding activities that would challenge their balance control system. For people over 65 years of age it is expected that they will have a life expectancy with disability of 8.4 years out of a total life expectancy of 17.2 years (Statistics Canada Health Reports, 1990). It is clear that falls is a major health issue facing this increasingly large segment of our population.

Causes of Falls

Falls clearly represent the failure of the balance control system in taking appropriate proactive and/or reactive action when perturbation is encountered during the execution of various tasks. The important question that follows is: Why did the balance control system fail? Researchers have tried to categorize the causes or types of falls in order to address this question. Rubenstein et al (1988) reviewed eight retrospective studies on primary causes of falls. They listed the causes of falls under nine categories ranging from accident/environment related (36.9%), weakness, balance and gait disorders (12.3%) to drop attacks (11.4%). These categories as the authors point out represent a mixture of presenting symptom complex (e.g., drop attack), precipitating mechanisms (e.g., postural hypotension, environmental hazard, and underlying risk factors (e.g., decreased vision). It appears from this review that there are two broad categories of causes of falls: First category includes problems in other body systems such as cardiovascular or endocrinological which indirectly affects the functioning of the balance control system, and second covers direct problems with subsystems which constitute the balance control system.

Environmental hazards such a slippery surfaces, loose rugs, objects on the floor, poor lighting challenge the elderly to a far greater extent than younger individuals, more often resulting in falls. It is relatively easy to make simple changes in the home and institution setting that can lead to a reduction in falls. Nevertheless it has to be recognized that ultimately it is the inability of the balance control system to cope with these environments that results in falls.

Therefore, documenting the age related changes in balance control system is critical before any intervention programs to improve balance in the elderly can be developed. It is not enough to identify differences in performance compared to a younger population: these differences have to be reliably interpreted as being either detrimental hence increasing the risks of falls, or adaptive changes to cope with deficits in the components of the balance control system. In this paper we discuss how these objectives can be achieved. This is primarily based on the work done at the University of Waterloo.

Assessment of Balance Control System: Characterising Age Related Deterioration and Adaptive Changes

Balance is a critical component and a prerequisite for most movements. Failure to regulate balance results in a fall. But unlike pathologies such as cerebral palsy which affect the movement performance on a continuous basis, falls even among the fall-prone elderly occur only sporadically. This poses a unique problem. To best understand why a fall occurs we should simulate a fall and study it. But ethical and safety consideration limit us to testing the performance of the balance control system at safe subthreshold levels, and making inferences about levels of risk.

At the University of Waterloo we have chosen a series of protocols that challenge the balance control system. These protocols use three tasks: maintaining a upright posture, initiation of stepping, and skilled locomotor behaviour. To assess stability during the performance of these tasks, we have used four types of perturbation: random disturbance, sensory deterioration, controlled expected and unexpected disturbance (Patla, et.al., 1992). The results obtained from these studies are summarised in three sets of figures classified according to the three tasks. Identification of differences between the young and the elderly is the easy part. Interpreting the significance of these differences is considerably more difficult. We have to go beyond statistical significance and determine the functional significance of these differences. This is discussed for each task studied.

Maintaining Upright Posture

The majority of current clinical assessment of balance rely on evaluating the performance while subjects maintain upright posture under different support configuration with their eyes open or closed. The perturbation to the system besides sensory deterioration and alteration in support surface are the small random oscillation of the body. Center of pressure (CoP) recordings are commonly used as performance measures and are often mistakenly referred to sway even though they represent the signal controlling body sway (Winter, Patla, & Frank, 1990). Because the CoP signal is random, statistical measures are used to quantify this signal. Both time and frequency domain analyses are used. Even though the protocol and measures are favoured by many clinicians and researchers, the interpretation of the data is controversial. Consider first the magnitude of CoP signal whose increase is often thought to reflect poorer performance even though this rarely approaches the voluntary limits of stability. As Figure 1a shows age appears to have minimal impact on the magnitude of CoP signal. It seems inappropriate to make inferences about stability when CoP excursions in these protocols range between 2 to 10% of stability limits on the average. Frequency domain analyses have been used to infer which sensory system is dominant in the control of upright posture. Nashner, Shupert, Horak, & Black (1990) have tried to define the operational range of frequencies for different sensory modalities. It is generally agreed that the visual system because of its inherent delays is more suited to control the low frequency oscillation of the body. Low power ratio is one way of quantifying this hypothesis. If vision is dominant and working well one would expect the power in the low frequency range of the CoP signal to be lower. This is what was observed as we age (Figure 1a). However, we should be aware that agreement on the exact values of the ranges is by no means unanimous.

A more common research protocol for assessment of balance control has been to apply controlled short duration perturbation and observe the responses. Because the stimulus (perturbation) is well defined, and the initial conditions controlled, the response by default is also well defined. The organization of this response has received considerable attention and is used to infer whether or not the response is automatic (latency of muscle activation less than reaction time), and whether the different muscles are recruited as a unit (latency between muscles fixed). When the perturbation is unexpected, the response naturally follows this stimulus, whereas if the perturbation is expected (e.g. generated by movements of the upper limb freely or interacting with another object such as door handle) the response precedes the stimulus. It is evident from Figure 1b that age has minimal impact on reactive or proactive response of the balance control system during maintenance of upright posture. The differences noted in Figure 1b can be attributed to smaller perturbation generated by the elderly compared to the younger subjects. In summary control of upright posture is fairly

well maintained as we age.

Initiation of Stepping

Stepping movements are often recruited to maintain stability when the perturbation to the upright posture is too large or to avoid collision with another moving object or as a precursor to walking (Patla, et.al., 1992). Therefore, postural adjustments that precede these stepping movements are important to study. Our results (Figure 2) show that the elderly not only have delayed onset of response selection (reaction time), but also take longer to transfer their weight towards the stance limb prior to stepping. These represent adaptive changes since a rapid transfer of weight would be more destabilizing. But clearly there could be undesirable consequence if the slower response to ensure stability during the execution of this task results in a collision for example.

Skilled Locomotor Behaviour

Consider first the changes in gait parameters while the subject is on a straight level path (Figure 2A). The muscle activity patterns show less variability. Locomotor patterns are a combination of stereotypical patterns generated by the central nervous system and modulations of these patterns based on supraspinal and peripheral feedback (Patla, 1991a). Therefore, one can attribute less variability to reduced online modulation of the stereotypical patterns. Variability in motor patterns is probably a desirable feature incorporated by the control system to minimize injury due to repetition of similar stress patterns (Patla, 1991c). Reduced covariance between the hip and knee joint which regulates balance in the plane of progression and collapse in the vertical direction, suggests deterioration in balance control (Winter, 1987) resulting in higher head accelerations as observed. It is interesting to observe a reduced pushoff energy which is destablising along with increased energy absorption at the knee to control and prevent collapse. Clearly there are adaptive changes: Elderly use different muscle groups for propulsion, with the reduced step length probably a byproduct of these modifications. Increased heel contact velocity is undesirable from safety perspective. Elderly subjects maintained higher cadence with a shorter steplength. This will result in larger limb accelerations followed by decelerations. Higher heel contact velocity suggests subjects had difficulty controlling the limb extension prior to foot contact.

Adapting these normal locomotor patterns for different terrains is a hallmark of legged locomotion (Patla, 1991b). Step length regulation and obstacle avoidance are common visually guided proactive modulation of the normal locomotor patterns. It is clear from the differences observed (Figures 3b & 3c), that elderly subjects could not implement these adaptations within a step cycle. This suggests that the elderly have to plan their adjustments earlier: They are unable to make quick proactive changes in locomotor patterns and therefore would have to rely on the reactive system to respond to a perturbation such as stepping on a undesirable surface or hitting an obstacle. The obstacle, avoidance study revealed interesting adaptive changes. Elderly subjects cleared the obstacle by a larger safety margin. They also increased the toe clearance as a function of obstacle height. Higher limb elevation may also be due to poor judgement of height rather than safety guided response.

It is clear that proactive responses in elderly subjects are compromised. Since proactive adaptations are the first line of defense against potential threat to stability, this greatly increases their risk of falling. Exercises designed to improve their balance therefore have to focus on retuning the proactive system.

References

Baker, S.P. & Harvey, A.H. (1985).In Falls in the Elderly, 501-502.

Cummings, S.R. et.al.(1988).J.Am. Geriatr.Soc., 36: 613-616.

Nashner, L.M. et.al. (1990).In Progress in Brain Res., 801.

Patla, A.E. (1991a,b,c).In Adaptability of Human Gait. Elsevier Publishers.

Patla, A.E. et.al. (1992). Can.J.Pub.Hlth, in press.

Patla, A.E. et.al. (1992). Clin.Biomech. (under review).

Patla, A.E. et.al. (1990). Physio.Can.42(2): 89-97.

Rubenstein, L.Z. et.al. (1988). J. Am. Geriatr.Soc., 36: 266-278.

Tineti, M.C. & Powell,L. (1991). Am. Soc. for Gerontology Mtg.

Winter, D.A. (1991). Biomechanics & Motor Control of Human Gait, U. of Waterloo.

Winter, D.A. et.al.(1990). Med.Prog.Thru. Technology, 16: 31-51.

Supported by grants - NHRDP, NSERC & MRC.

Upright Posture: Random Perturbation / Sensory Deterioration / Different Base of Support

Center of Pressure	Elderly vs. Young
CP, t	⇧ Amplitude (RMS) (M-L Direction / Normal Stance)
Power, MPF $= \left[\frac{\Sigma f \cdot P(f)}{\Sigma P(f)}\right]$, Low power ratio = power in 0-0.1 Hz / total power, 0, 0.1, 3.0 freq	⇧ MPF (A-P & M-L Direction / One Leg & Tandem Stance) ⇩ Low power ratio (A-P & M-L Direction)

Figure 1a

Upright Posture: Expected/Unexpected Controlled Perturbation

EMG Measures	Elderly vs. Young
MG, TA, BF, RF, t	• Onset unaffected • Sequencing of muscle activation unaffected • Magnitude of muscle activation smaller
Center of Pressure	
CP, onset, pk, t	• Onset unaffected • Rate of ↑ in CP is slower • Peak CP is smaller

Figure 1b

Normal Level Gait

Gait Measures	Elderly vs. Young
EMG, SL	⇩ Stride length ⇩ Variability in muscle activity pattern
COVAR	⇩ Covariance between hip & knee joint moment
ACC'N	⇧ Head horizontal acceleration
PO	⇩ Pushoff energy generation at ankle ⇧ Energy absorption at knee during pushoff
HC VEL.	⇧ Heel contact velocity

Figure 3a

Initiation of Forward/Backward/Sideways Stepping

Vertical Force Profile	Elderly vs. Young
%BW, F_{pk}, TTP, 0, RT, WT	⇧ Reaction time ⇧ Weight transfer time ⇩ Peak force & Time to Peak

Figure 2

Obstacle Avoidance During Walking

Measures	Elderly vs. Young
Vx(toe), Toe Clearance	⇧ Toe Clearance Scaling of Toe Clearance as a Function of Obstacle Height ⇧ Toe Horizontal Velocity

Figure 3b

Step Length Adjustment During Walking

Protocol	Elderly vs. Young
short, normal, long	⇩ Success rates (within same step cycle) ⇧ Ratio of horizontal to vertical impulse change

Figure 3c

NON-NORMAL GAIT

Podium Session 13

HOW GAIT CHANGES IN PREOPERATIVE AND POSTOPERATIVE PATIENTS WITH TOTAL HIP REPLACEMENTS

Hurwitz, D.E.[1], Chertack, C.C[2], Andriacchi, T.P.[1]

[1]Rush-Presbyterian-St. Luke's Medical Center, Department of Orthopedic Surgery, Chicago Illinois 60612
[2]Williamsville Orthopedic Surgery, Williamsville New York 14221

INTRODUCTION

Previous studies (1) of patients with total hip replacements (THRs) have reported some abnormalities in the hip motion during gait. The abnormalities appear as an irregularity or bump in the hip flexion/extension motion during gait and are present even in patients with excellent clinical postoperative results. The underlying causes and benefits of this adaptation are not clearly understood at this time. This adaptation may be a response to the prosthesis or it may be a learned response from an adaptation that was present in the preoperative condition. To gain insight into adaptations of patients with THRs we investigated the gait of a group of patients preoperatively as well as a separate group of patients postoperatively.

METHODS

The preoperative group consisted of 15 subjects and the postoperative group of 22 subjects with a HGP cementless prosthesis. The postoperative patients were evaluated at 33$\pm$15 months after surgery. A control group of 20 normals with no history of joint disease were also evaluated. The average age of the three groups was 60$\pm$8 years. Both preoperative and postoperative groups had no other significant joint involvement. All preoperative and postoperative subjects had primary degenerative joint disease (DJD) except for one preoperative and two postoperative subjects with aseptic necrosis, and two postoperative subjects with traumatic arthritis. All postoperative patients were an excellent clinical result with no perceptible limp or any clinical or radiographic evidence of loosening. The clinical status and passive motion of both preoperative and postoperative groups were evaluated using the Harris Hip form. The average Harris score was 57$\pm$7 for the preoperative group and 98$\pm$2 for the postoperative group.

Subjects were asked to walk at three self selected speeds corresponding to slow, normal and fast. The time distance parameters and relative rotational angles at the hip, knee and ankle were determined using a three-dimensional optoelectronic system. When analyzing the angular motion the trial with a velocity closest to 1 m/sec. was chosen.

Comparisons between groups were done with either a oneway analysis of variance and a modified least squares difference or a Chi square analysis. Relationships between velocity and other gait parameters were checked with a linear regression model. A significance level of $p<.05$ was used throughout.

RESULTS

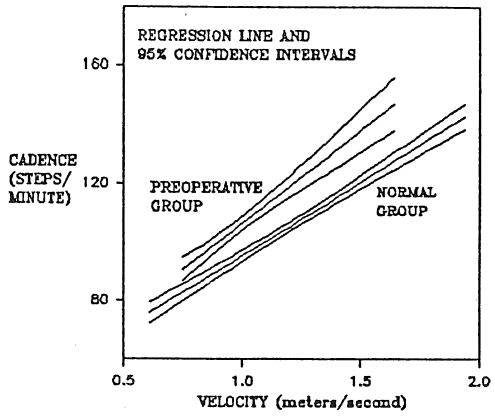

Figure 1: Cadence vs Velocity.

The preoperative group walked slower than normal at all three self selected speeds ($p<.025$). Throughout the range of velocities tested the preoperative patients walked with a decreased stride length and an increased cadence as compared to the normal group (Figures 1 and 2).

The average Hip range of motion during gait (maximum flexion minus maximum extension) was significantly less on the affected side of the preoperative group as compared to both the postoperative group and normal ($p<.000$) (Figure 3). In spite of the fact that the postoperative group was an excellent clinical result the HROM (hip range of motion) was still significantly less than normal

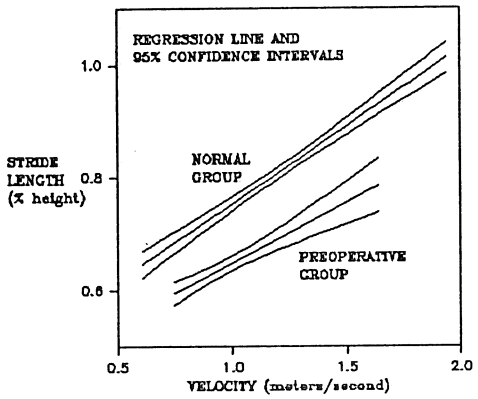

Figure 2: Stride Length vs Velocity.

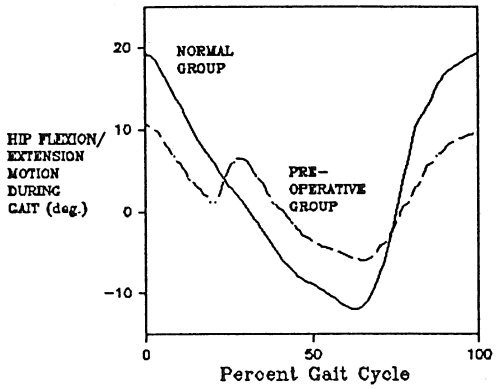

Figure 4: Hip motion during gait.

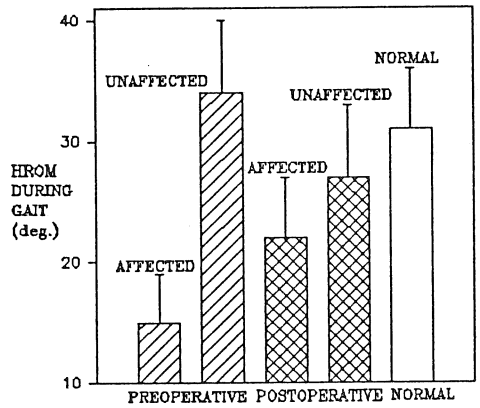

Figure 3: HROM for affected and unaffected sides.

($p < .000$). The HROM of the contralateral sides of both study groups was significantly different from the affected side ($p < .000$) and was not statistically different from normal.

Both the preoperative and postoperative group displayed an irregularity or "bump" in the Hip motion during gait (Figure 4). 94% of the preoperative patients and 55% of the postoperative patients displayed an abnormality or "bump" during the hip motion of gait as compared to only 20% of the normals ($p < .001$). Only 6% and 23% of the pre and postoperative groups displayed this abnormality on the contralateral side.

The knee range of motion (maximum flexion minus minimum flexion) of the preoperative affected side was significantly less than the affected side of the postoperative group ($p < .024$) but was not statistically less than normal. The Knee range of motion (KROM) for the affected sides of the preoperative and postoperative groups and normals were $53 \pm 10°$, $60 \pm 6°$ and $59 \pm 5°$. The KROMs on the contralateral sides of the pre and postoperative groups were not statistically different from normal.

DISCUSSION

The decreased stride length and HROM on the affected side of preoperative group supported the findings of Murray (2). The decreased HROM only occurred on the affected side of both pre and postoperative groups. The irregularity found in the hip motion of the postoperative patients was found in a group of preoperative patients. The preoperative presence of the irregularity in the hip motion during gait may be an attempt to reduce the force and unload the joint. Possibly it is related to the location of the lesion on the femoral head.

Even though all postoperative patients were an excellent clinical result and walked without a perceptible limp their HROM during gait was still less than normal. The abnormality in the shape of the hip motion postoperatively may be a learned pattern of gait from the preoperative adaptation. It is also possible that the adaptations is an attempt to reduce the out of plane force and subsequent rotational forces.

REFERENCES

1. Hurwitz, D.E. et al. (1989). ASME Biomechanics Symposium AMD vol 98:339-42.
2. Murray et al. (1971). JBJS 53A(2):259-74.

ACKNOWLEDGMENTS

NIAMS GRANT #AR39239

PARAPLEGIC GAIT: A QUANTITATIVE EVALUATION OF THE HIP GUIDANCE ORTHOSIS

R. Davis[1], K. Bell[1], J. Fezio[2], P. DeLuca[1], and J. Banta[1]
[1]Department of Orthopaedics, [2]Department of Orthotics and Prosthetics,
Newington Children's Hospital, Newington, Connecticut

INTRODUCTION

The high level paraplegic is afforded the opportunity for reciprocal gait via one of two orthotic alternatives: the reciprocating gait orthosis (RGO), or the hip guidance orthosis, commonly referred to as the Parawalker. The RGO, an evolutionary derivative of the conventional hip-knee-ankle-foot orthosis, is normally a flexor-driven hip extension orthosis (Yngve et al., 1984). High level paraplegics use trunk extension (with support provided by a walker) to produce hip flexion in the swing limb while using the RGO. The Parawalker is also an extension of the conventional long leg brace in that it is comprised of rigid lower extremity braces interfaced to a rigid trunk/pelvic structure by low resistance hip joints (Butler et al., 1984). The strength of the design is the rigid trunk extension which affords the user greater mechanical advantage (than the RGO) to provide control of the orthosis in combination with fixed abduction of the lower extremities for swing limb clearance.

To date, the majority of the effort to assess these two different orthotic modalities has focused on either the qualitative evaluation of functionality (Yngve et al., 1984) or the quantification of the energy cost associated with their use either with direct measurement devices (Banta et al., 1991) or through a correlation to walking speed and pulse rate, i.e., the Physiologic Cost Index (Butler et al., 1984, McCall et al., 1986).

Aside from fundamental stride and temporal parameters, the literature which documents the biomechanical aspects of RGO or Parawalker performance is quite limited. Mazur et al. (1990) collected three dimensional gait data associated with the use of the RGO by three subjects and found that the reciprocating gait approach offered a greater dynamic range of motion at the hip than the swing through pattern. Whittle et al. (1989) compared the application of both devices by twelve subjects and found that orthoses were comparable with the exception of maximum dynamic hip extension where the RGO and Parawalker demonstrated a mean of 25.8° and 20.5°, respectively. While this study provides useful comparative data, it failed to document particular fundamental features of subjects' gait, such as trunk displacement and crutch use.

The purpose of this preliminary investigation was to quantitatively assess the gait kinematics specific to the appliction of the Parawalker by one subject. As described in the paper by Butler et al. (1984), the key aspects of proper Parawalker gait pertain to trunk orientation and crutch placement which facilitate proper load transfer between the lower extremities. This paper documents these characteristics through the detailed examination of one wearer.

PROCEDURES

One paraplegic subject employed the Parawalker to traverse a straight, level walkway while wearing passive reflective markers attached to both the subject and brace and aligned with specific bony landmarks or brace reference points. Markers were also placed on the subject's crutches to assess crutch orientation. The video based motion assessment system described in Davis et al. (1991) was used to collect the marker images. Segment (body/brace) fixed coordinate systems were computed from the three dimensional marker trajectories, which in turn, lead to the absolute and relative angle results presented below.

The subject for this examination was a 29 year old male with a thoracic level (T-4) paraplegia. This subject was qualified as proficient with the Parawalker by the orthotic team after extensive training and experience, i.e., eight months of use. The 62 kg subject was 1.85 m tall.

RESULTS AND DISCUSSION

The essential features of Parawalker gait are illustrated in Figure 1 where the kinematics of the subject's trunk and hips are shown and in Figure 2 where the orientation of both crutches is illustrated. It is important to note that with respect to the brace, a three segment model was employed, i.e., two rigid lower extremities attached to a rigid trunk segment. In this way, hip joint motion referred to the movement of the associated lower extremity relative to the trunk. The principle propulsive dynamics occurred during the two periods of single limb stance. During the first single support period (from 32 to 50% of the gait cycle) on the right side, a force couple associated with a posterior crutch (left) tip force and corresponding shoulder girdle reaction on the left side produced a backward rotation of the trunk in the sagittal plane. This drove the pelvis forward and right hip into extension during midstance. At the same time, the force couple from the vertical component of the left crutch ground reaction force and the right lateral pad of the Parawalker resulted in the rotation (coronal plane) of the orthosis to the right. During this process, the left crutch was tilted backward towards the subject (approximately 20°) and moving from neutral into abduction in the coronal plane. This motion provided a vehicle for the load transfer from left to right side as well as the proper orientation of the brace for clearance of the left foot during swing. That is, as the subject's center of gravity shifted to the right, thereby fully transferring his load to his right foot, the unloaded left limb was lifted off of the ground and the forward movement of the subject's left hip (and gravity) pulled the left limb forward, resulting in flexion of the left hip. During the second single support

period (from 80 to 100% of the gait cycle), the subject again used sagittal plane rotation of the trunk (backward) and coronal plane rotation (to the left) to facilitate extension of the left hip, flexion of the right hip, and clearance for the right foot during swing.

In a comparison of this subject's results to those found in the literature, he employs the same fundamental technique as described by Butler et al. (1984). Relative to Butler's idealized description, the subject realized a greater overall anterior trunk rotation with a mean of 17° (±4°). Moreover, his hip flexion/extension range of motion (right: 23°, left: 18°) fell short of that allowed by the brace (29°) and that reported by Whittle et al. (1989). The lower extremity brace rigidity was relatively good as reflected by the hip ab/adduction range of motion (right: 5°, left: 5°). This is encouraging because of the implications related to adequate foot clearance.

In summary, this paper presented the first detailed, quantitative description of the kinematics associated with one subject's application of the Parawalker. The results were found to be consistent with the qualitative descriptions and the limited quantitative data found in the literature.

REFERENCES

Banta, J et al. Eur J Pediatr Surg 1, Suppl I:7-10, 1991.

Butler, P et al. Pros Orthotics Inter, 8:33-38, 1984.

Butler, P et al. Dev Med Child Neurol 26:607-612, 1984.

Davis, R et al. Human Move Sci, 10(5):575-587, 1991.

Mazur, J et al. Z Kindercir 43, Suppl 1:23-25, 1990.

McCall, R et al. J Pediatr Ortho, 6:157-161, 1986.

Whittle, M et al. National Health Service Procurement Directorate, Her Majesty's Stationary Office, 1989.

Yngve, D et al. J Pediatr Ortho, 4:304-310, 1984.

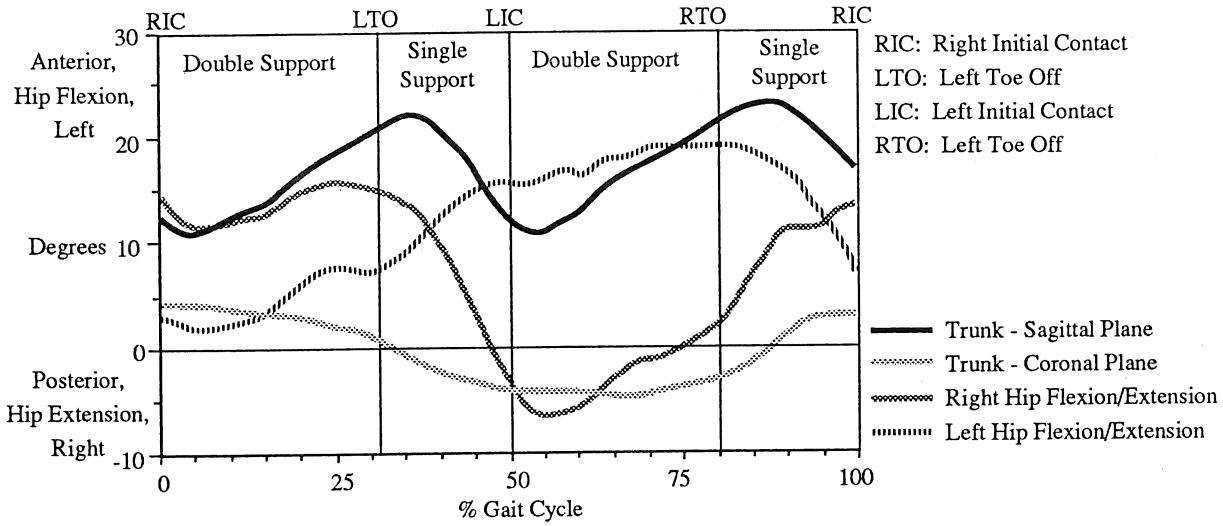

Figure 1. Trunk and hip kinematics, right gait cycle.

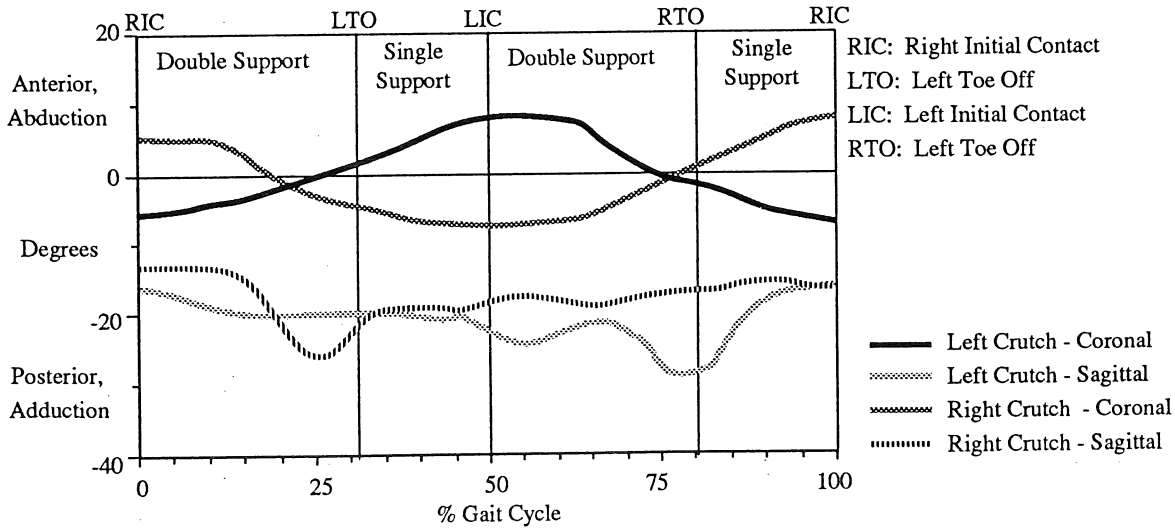

Figure 2. Crutch orientation, right gait cycle.

LEG POSTURE CHARACTERISTICS IN CHILDREN WITH CEREBRAL PALSY DURING WALKING AND RUNNING

P. Luhtanen, E. Mälkiä, J. Huhtinen, P. Rintala and S. Clark

Research Institute for Olympic Sports, Jyväskylä, Finland.
Department of Health Sciences, University of Jyväskylä, Finland.

INTRODUCTION

Six children with cerebral palsy served as subjects in the study where the postural characteristics of the lower legs were investigated with video analysis in walking and running. The comparisons were done between the action of the normal and abnormal leg in the stepping pattern, flexion/extension of the knee and hip and dorsi-/plantar flexion of the ankle. The steps executed from the normal leg were on the average 3 cm longer than the steps from the abnormal leg in walking and 14 cm longer in running, respectively. In walking, the knee of the abnormal leg was on the average 7 degrees more extended in the phase of the heel strike, 8 degrees in the single middle stance and 23 degrees in the toe-off phases. In running, the differences were on the average 7, 12 and 8 degrees, respectively. During the swing phase the minimum angle of the knee in the abnormal leg was 14 degrees more extended than the knee of the normal leg. The differences in the action of the ankle and hip joints between the abnormal and normal leg were less than in the action of the knee.

REVIEW AND THEORY

A clinical diagnosis is the basis for any rehabilitation program for patients with cerebral palsy. The diagnosis can be done using a qualitative or quantitative biomechanical analysis. There is a definite need to expand research into the biomechanical gait analysis of walking and running with persons who have cerebral palsy (e.g. Beuter *et al.*, 1985). Cerebral palsy is a disorder caused by damage or lack of development of the parts of the brain that control voluntary muscle movements. It is a permanent condition characterized by motor involvement such as awkward or involuntary movement, poor balance, irregular gait or spasticity of muscles (Ingram, 1966). Training to achieve a functionally efficient and smooth pattern of gait is a high priority in the rehabilitation of children with cerebral palsy (Seeger *et al.*, 1981). The purpose of this study was to compare the action of the abnormal leg with the action of the normal leg in walking and running in children with cerebral palsy.

PROCEDURES

Six children (four girls and two boys) with cerebral palsy (two monoplegia, four hemiplegia, aged 12.7±3.1 years, (body mass: 40.7±10.4 kg, height: 147±15 cm), served as subjects in the study where the postural characteristics of the lower legs were investigated in walking and running. Each walk and run was recorded with two Magnasonic camcorders at frame rate of 30 Hz. A 3-D kinematic analysis of each performance was completed with APAS performance analysis system package. The comparisons were done between the action of the normal and abnormal leg in the stepping pattern, flexion/extension of the knee and hip and dorsi-/plantar flexion of the ankle.

RESULTS

The average speeds were in walking 2.5±0.3 m x s^{-1} and in running 4.7±0.6 m x s^{-1}. The average stride lengths were in walking 1.13±0.19 m and in running 1.52±0.19 m. The steps executed from the normal leg were in walking 3 cm longer than the steps from the abnormal leg and in running 14 cm, respectively. The average function of the knee and hip both in walking and running and in the normal and abnormal leg during the stride cycle is shown in Figure 1.

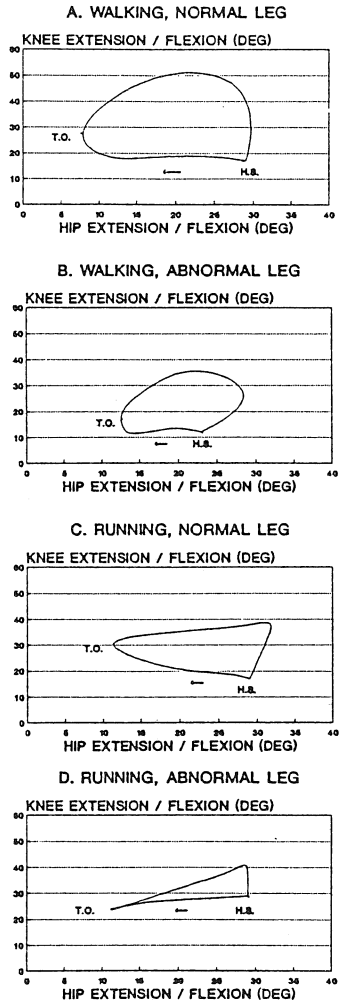

Figure 1. The average function of knee and hip joints in six children with cerebral palsy (T.O. = toe-off, H.S. = heel strike, -> = direction of the cycle)

DISCUSSION

The results indicated a clear limitation in the action of the abnormal leg. This was most remarkable in the knee. The gait analysis and training poses special problems for the therapist in terms of complexity of the skill. The descriptive biomechanical research can benifit therapists and others working in rehabilitation and, thus, help improve the functional capacity of children and adults with cerebral palsy.

REFERENCES

Beuter, A. et al. *Adap. Phys. Act. Quar.*, **2**, 214-227, 1985.
Ingram, T. *Arch. Dis. Child.*, **41**, 337-357, 1966.
Seeger, B. et al. *Arch. Phys. Med. Rehabil.*, **62**, 364-368, 1981.

JOINT TORQUES AND CO-CONTRACTION DURING GAIT FOR NORMAL AND CEREBRAL PALSY CHILDREN

Kristen A. Bowsher, Diane L. Damiano, Christopher L. Vaughan

Motion Analysis Laboratory, Departments of Biomedical Engineering and Orthopaedics
University of Virginia, Charlottesville, VA 22903

INTRODUCTION

The impairment of voluntary motor control is the most clinically obvious functional deficit observed in children with cerebral palsy. Decreasing spasticity alone has been found to be insufficient in alleviating the motor dysfunction (Sahrmann *et al.*, 1977) and alternative explanations need to be explored. Excessive co-contraction and inadequate force production are frequently present in children with spastic cerebral palsy during functional activities (Berger *et al.*, 1982). Co-contraction is an effective control strategy in some tasks requiring increased precision or joint stability despite the fact that it is a mechanically inefficient method for producing force (Winter, 1990). It only becomes problematic in children with cerebral palsy when it is employed in tasks where it is *not* part of a normal control strategy (Campbell, 1991). Although co-contraction can be directly related to muscle force, these two parameters can also vary independently (Smith, 1981). The overall goal of this research was to assess the degree of co-contraction at the hip and knee joint during the swing phase of gait in children with cerebral palsy and in normal children. A co-contraction index (CCI), weighted by the net torque produced at the hip and knee joints, was developed to quantify the degree of co-contraction at each joint at each instant in time.

METHODS

The subjects consisted of ten normal healthy children and six cerebral palsy children with a confirmed diagnosis of spastic diplegia. The normal group consisted of 6 girls and 4 boys between the ages of 5 and 14, while the cerebral palsy group consisted of 5 girls and 1 boy between the ages of 4 and 14. Each subject performed three walking trials at a "normal" or freely-selected pace and three trials at a much faster pace, for a total of six walking trials. The intent of the trials at the higher speed was to try and elicit a spastic response from the cerebral palsy children. All subjects walked barefoot on a level walkway.

The displacement data were captured at 60 Hz for 3 seconds using a 3D ExpertVision System and a body surface marker set developed by Kadaba *et al.* (1990). The EMG signals were captured using surface electrodes and an 8-channel telemetry unit which meant that the subject was not encumbered with trailing wires. The EMG electrodes were placed over both the right and left quadriceps and hamstring muscle groups.

In order to calculate body segment parameters (e.g. segment masses and moments of inertia) and estimate joint centers, anthropometric measurements were taken (Vaughan *et al.*, 1992). The 3D displacement data of the external markers were read into a program developed by Vaughan *et al.* (1992), and published with their book *Dynamics of Human Gait*. This program combined the kinematics with body segment parameters in a Newtonian formulation to produce joint torques (focusing on the swing phase of the gait cycle where the knee undergoes its greatest range of motion). Torques were normalized for weight and leg length.

The EMG data were processed using a program which performed full-wave rectification, low pass filtering with a cut-off frequency of 3 Hz (Winter, 1990), and based on the various gains and the characteristics of the A/D converter, converted into microvolts. Because the displacement data were collected at 60 Hz while the EMG data were collected at 1000 Hz, the EMG data were interpolated to synchronize the two data sets.

CO-CONTRACTION INDEX

In order to contrast the level of muscle activity of the quadriceps with that of the hamstrings and relate it to the torque generated by the hip and the knee at each instant of time, we developed a co-contraction index (CCI). Because it is not possible to compare the actual EMG values (in microvolts) of the quadriceps and hamstrings (dictated by many factors such as electrode placement, skin resistance, subcutaneous fat, fiber type, and skin temperature), the EMG values were thus normalized to values between 0 and 1. The formulae used to calculate the CCI were:

$$\textit{activation level of } H_t = \frac{H_t}{H_{max}} \quad (1)$$

$$\textit{activation level of } Q_t = \frac{Q_t}{Q_{max}} \quad (2)$$

$$X_t = 1 - \left|(\textit{activation level of } H_t) - (\textit{activation level of } Q_t)\right| \quad (3)$$

$$CCI_t = 0.5\left(X_t + ANT_t(X_t)\right) \quad (4)$$

where:

H_t	=	value of hamstrings EMG for data point t,
Q_t	=	value of quadriceps EMG for data point t,
H_{max}, Q_{max}	=	maximum EMG recording for all trials within a subject for the hamstrings and quadriceps,
ANT_t	=	antagonist muscle activity level where the antagonist muscle is determined from the torque curve,
CCI_t	=	co-contraction index for point t.

A CCI of 1 means a maximum level of co-contraction while a CCI of 0 means a minimum level of co-contraction. This index differs from others (*e.g.* Falconer and Winter, 1985) which do not distinguish between low and high muscle activity levels and are not expressed at each instant in time.

RESULTS AND DISCUSSION

For the normal subjects walking at their freely-chosen pace, the EMG levels for quadriceps (hip flexor and knee extensor) and hamstrings (hip extensor and knee flexor) were relatively low. For this reason the CCI has a flat profile. There is also very little difference between the hip and knee CCI values since the torques at the two joints appear to act reciprocally during swing phase. When normals walk at their fast pace, a general strategy emerges: Qt exhibits high activity in early swing while Ht is almost quiescent; Qt then falls off slightly in mid-swing while Ht buils up; and finally in late swing both muscles are at a high level in anticipation of heel-strike. The CCI values therefore start off low and rapidly increase to mid-swing, maintaining this value until heel-strike. The children with cerebral palsy had a flat, but slightly elevated, CCI profile at both the free and fast speeds, suggesting that the increased speed was accomplished without utilizing a change in their co-contraction strategy.

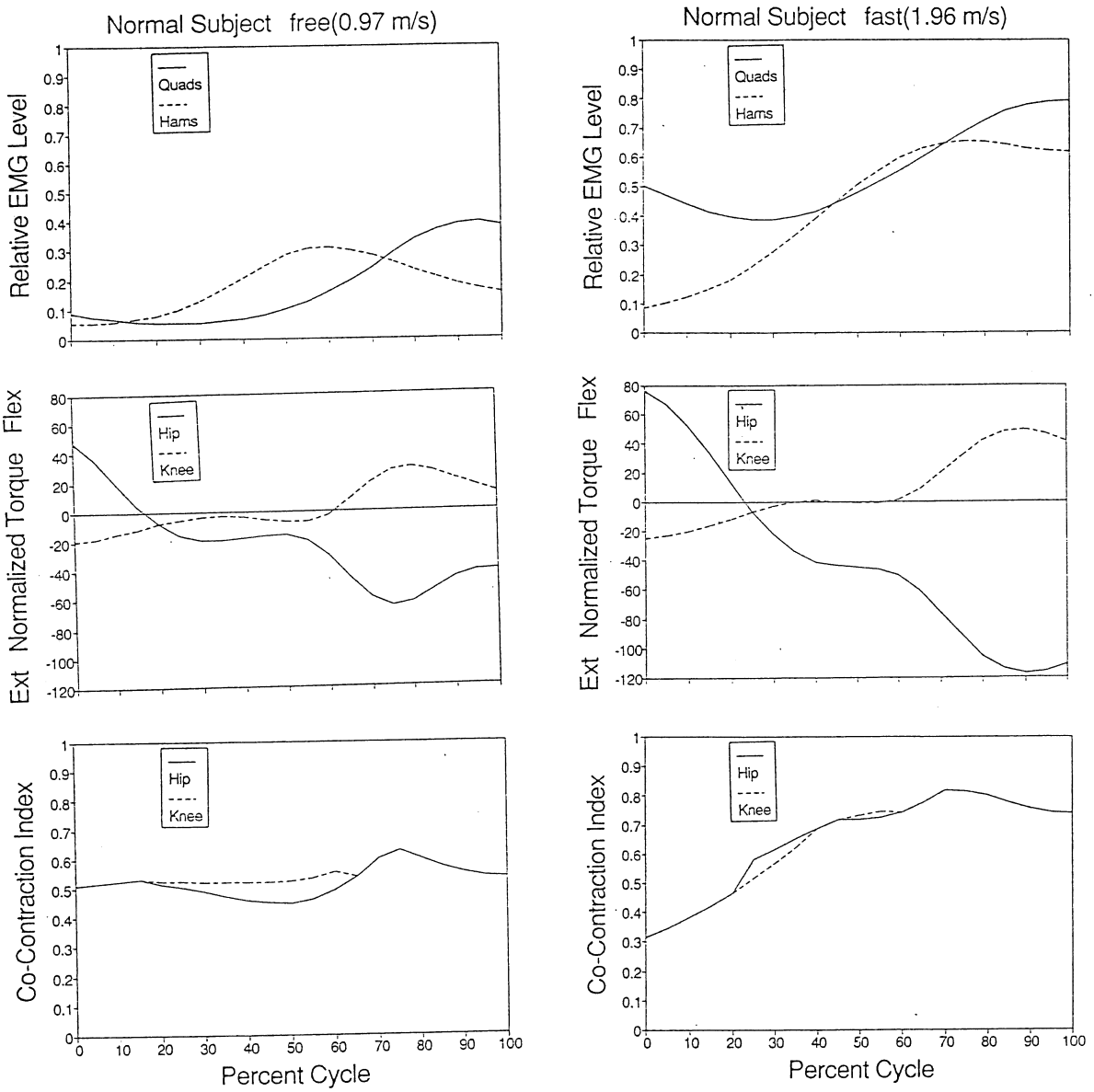

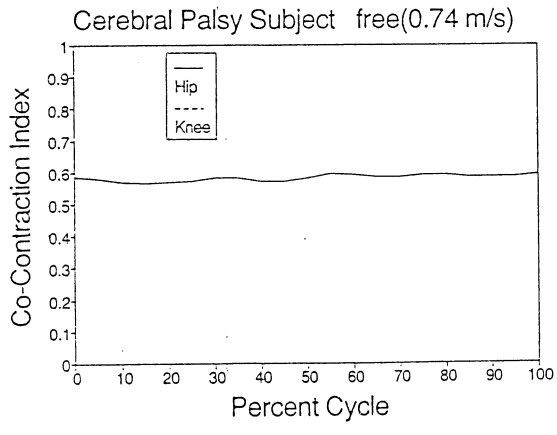

REFERENCES

Berger, W. et al., *Electroenceph. Clin. Neurophys. 53*:538-548, 1982

Campbell, S., In *Contemporary Management of Motor Control Problems,* 1991.

Falconer, K., Winter, D., *Electromyogr. Clin. Neurophys.*, 25:135-149, 1985.

Kadaba, M. et al., *J. Orthop. Research,* 7:849-860, 1990

Sahrmann, S. et al., *Ann Neurol* 2:460-465, 1977

Smith, A., *Can. J. Physiol. Pharmocol. 59*:733-734, 1981.

Vaughan, C.L. et al., *Dynamics of Human Gait,* Human Kinetics, 1992.

Winter, D., *Biomechanics and Motor Control of Human Movement,* 1990.

GAIT ANALYSIS OF AN ADOLESCENT WITH CEREBRAL PALSY BEFORE AND AFTER SELECTIVE POSTERIOR RHIZOTOMY

D.J. Simpson*+#, J.R. Engsberg*, M. McNeil+, A. Chiu+, G.N. Kiefer

* Human Performance Laboratory, University of Calgary, Alberta.
\+ Department of Physiotherapy, Alberta Children's Hospital, Calgary.
\# Department of Physiotherapy, University of Alberta, Edmonton.
Department of Orthopaedics, Alberta Children's Hospital, Calgary.

INTRODUCTION

A paucity of ground reaction force data has been reported for children with cerebral palsy who have received selective posterior rhizotomy (SPR) surgery. Kinetic data were collected from an adolescent male with spastic diplegic cerebral palsy prior to, and after, SPR surgery. Examination of his pre-operative ground reaction force records indicated an asymmetrical gait including toe drag during the final stages of support. Several changes were seen in his ground reaction forces after surgery, yet many asymmetries remained.

REVIEW OF THE LITERATURE

In recent years SPR surgery has been used to reduce spasticity in children with cerebral palsy. Two dimensional kinematic analysis of the gait of children with spastic diplegic cerebral palsy before and after SPR has demonstrated 1) increased hip, thigh, and knee range of motion in the sagittal plane (Vaughan et al. 1992, 1988), 2) improved ankle mobility, and 3) change from forefoot contact, to foot flat or heel contact, at the onset of the stance phase (Cahan et al. 1990). Electromyographic (EMG) analysis showed a decrease in the amplitude, and prolonged activity usually seen in spastic muscles during walking (Cahan et al. 1990; Boscario et al. 1990). Few investigations relating to ground reaction forces of cerebral palsy children before and after SPR exist. The purpose of this pilot study was to determine changes in the ground reaction forces of a cerebral palsy child before, and after, SPR.

METHODS

Kinetic data were collected from a fourteen-year-old male prior to SPR surgery and at 9, 14, and 24 months post-surgery. The subject walked, unaided, along a walkway at his normal walking pace and force data were collected from two adjacent force plates. The data of three force components (X, Y, Z), with respect to time, were stored on a computer. Means and standard deviations of the maximum and minimum forces, and the impulses, were calculated (Engsberg et al. 1991). Force data were normalized to a ratio of body weight, and time was normalized to two consecutive periods of support (Engsberg et al. 1991).

RESULTS

The first peak (Zmax1) of the vertical ground reaction force time-curve was greater on the right than on the left pre-operatively, and this pattern was unchanged after surgery (Table 1). The second peak (Zmax2) was similar in both legs and remained unchanged after surgery. The total impulse was greater on the right than on the left pre-operatively, but varied post-operatively.

In the anterior-posterior force data (Table 2) the anterior (retarding) force maximum increased post-operatively for both left and right legs. The posterior (propulsive) force maximum increased post-operatively on the left, but generally remained unchanged on the right. There was a marked asymmetry between the legs in the retarding and propulsive impulses pre-operatively. The retarding impulse was greater than the propulsive impulse on the right leg, while the propulsive impulsive was greater than the retarding impulse on the left leg. The pattern of asymmetry remained unchanged after SPR surgery but the magnitude increased on the right leg.

An aberrant retarding force which was produced by toe dragging, occurred at the end of the support phase (Table 2). The toe drag impulse, which was greater on the right than on the left, became negligible on both the left and right after SPR surgery on all assessments (Figure 1), except for the 24-month assessment of the right leg. The reappearance of the toe drag on the right leg at the 24-month assessment may have been related to a period of rapid growth.

Considerable variation occurred in the subject's medial-lateral forces postoperatively (Table 3). However, no trends were apparent.

DISCUSSION

Asymmetries existed prior to, and also after, surgery. Patterns which remained asymmetrical post-operatively included a greater first peak on the right leg than on the left for the vertical force curve, and asymmetries in the anterior and posterior impulses for both legs. This is consistent with work by Cahan et al. (1990), who found that the primitive muscle timing patterns seen on EMG were unchanged in children after SPR surgery. However, the total impulse from the vertical force curve did show similarities between the legs post-operatively, but this did not occur until the 14- and 24-month assessments. Toe drag became negligible directly after SPR surgery, suggesting that the reduction of spasticity made foot clearance possible during the transition from swing to stance. However, it recurred on the right after a period of rapid growth.

Table 1

Means and standard deviations for first (Zmax1) and second peak (Zmax2) forces and total impulse (Total Imp) for left (L) and right (R) legs.

		Pre-op	9 months	14 months	24 months
Zmax1	L	1.14 ± .08	1.16 ± .13	1.20 ± .17	1.12 ± .15
	R	1.38 ± .23	1.43 ± .14	1.37 ± .17	1.32 ± .26
Zmax2	L	0.99 ± .08	1.02 ± .09	1.11 ± .10	1.18 ± .07
	R	1.07 ± .05	1.02 ± .06	0.96 ± .11	1.04 ± .06
Total Imp	L	0.34 ± .05	0.37 ± .12	0.43 ± .03	0.44 ± .01
	R	0.43 ± .02	0.44 ± .01	0.42 ± .03	0.41 ± .02

Table 2

Means and standard deviations for the anterior maximum (Ant Max), posterior maximum (Post Max), anterior impulse (Ant Imp), posterior impulse (Post Imp), toe drag impulse (Toe Drag Imp) for left (L) and right (R) legs.

		Pre-op	9 months	14 months	24 months
Ant Max	L	0.08 ± .01	0.15 ± .06	0.22 ± .05	0.15 ± .04
	R	0.16 ± .01	0.28 ± .05	0.27 ± .04	0.25 ± .09
Post max	L	0.10 ± .01	0.15 ± .04	0.17 ± .05	0.18 ± .05
	R	0.07 ± .01	0.09 ± .002	0.09 ± .04	0.06 ± .02
Ant Imp	L	0.005 ± .001	0.014 ± .005	0.02 ± .005	0.012 ± .003
	R	0.013 ± .001	0.026 ± .001	0.026 ± .004	0.025 ± .008
Post Imp	L	0.019 ± .005	0.035 ± .007	0.034 ± .01	0.035 ± .005
	R	0.011 ± .002	0.012 ± .002	0.013 ± .004	0.005 ± .003
Toe drag Imp	L	0.001 ± .001	0.00 ± .00	0.00 ± .00	0.00 ± .00
	R	0.005 ± .003	0.00 ± .00	0.00 ± .00	0.003 ± .002

Table 3

Means and standard deviations for medial maximum (Med Max), lateral maximum (Lat Max), medial impulse (Med Imp), lateral impulse (Lat Imp) and toe drag impulse (Toe Drag Imp) for left (L) and right (R) legs.

		Pre-op	9 months	14 months	24 months
Med Max	L	0.14 ± .06	0.28 ± .06	0.14 ± .05	0.19 ± .03
	R	0.16 ± .15	0.19 ± .06	0.08 ± .05	0.10 ± .05
Lat Max	L	0.13 ± .02	0.08 ± .02	0.11 ± .04	0.09 ± .03
	R	0.14 ± .04	0.18 ± .10	0.15 ± .04	0.11 ± .05
Med Imp	L	0.002 ± .001	0.003 ± .001	0.004 ± .003	0.00 ± .001
	R	0.007 ± .009	0.001 ± .00	0.001 ± .001	0.002 ± .001
Lat Imp	L	0.026 ± .004	0.022 ± .01	0.03 ± .012	0.021 ± .011
	R	0.027 ± .019	0.034 ± .014	0.033 ± .009	0.019 ± .007
Toe drag Imp	L	0.002 ± .001	0.001 ± .00	0.00 ± .00	0.00 ± .00
	R	0.007 ± .007	0.00 ± .001	0.00 ± .00	0.00 ± .00

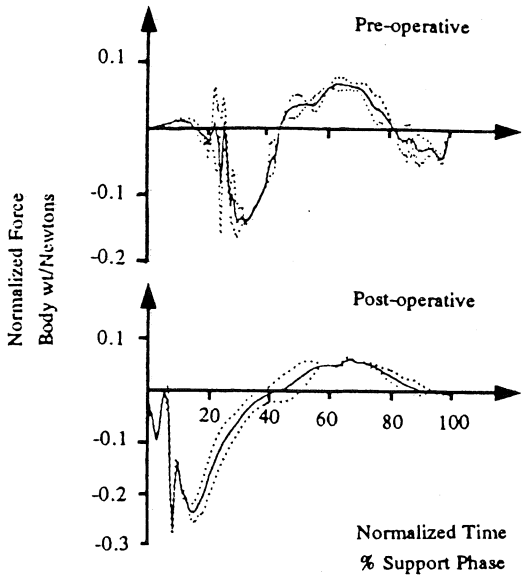

Figure 1. Pre-operative (top) and 14 month post-operative (bottom) records of anterior-posterior forces. Anterior forces are negative, posterior forces are positive.

REFERENCES

Boscario, L. et al. C.S.B. Proc. Human Locomotion VI, Quebec, Canada, 1991.

Cahan, L. et al. *Develop. Med. Child Neurol.* 32, 1037-1043, 1990.

Engsberg, J. et al. *Arch. Phys. Rehab. Med.*, 72, 657-661, 1991.

Vaughan, C. et al. *J. Neurosurg.*, 74, 178-184, 1991.

Vaughan, C. et al. *Pediatr. Neurosci.*, 14, 297-300, 1989.

THE EFFECTS OF ORTHOTICS ON GAIT IN CHILDREN WITH LOW LEVEL MYELOMENINGOCELE

S. Õunpuu, R. Davis, J. Banta and P. DeLuca

Gait Analysis Laboratory, Department of Orthopaedics
Newington Children's Hospital, Newington, Connecticut

INTRODUCTION

Lower extremity bracing is commonly used in children with myelomeningocele (ML) to improve standing stability and gait and to help prevent deformity (Carroll, 1974). Lower level bracing including ankle-foot orthoses (AFO's) and knee-ankle-foot orthoses (KAFO's), in this patient population has seen a long evolution in design with minimal objective documentation. Computerized gait analysis has only been used by Mazur et al. (1990) to describe the effects of higher level bracing including the hip-ankle-foot-orthosis and reciprocating gait orthosis and by Thomas et al. (1989) to describe the effects of the AFO, but these studies have been limited to a sagittal plane analysis only. It is the purpose of this study to evaluate the effects of orthotics on gait using three dimensional joint kinematics and kinetics. Clinical issues, including the necessity to brace above the knee in children with a knee "valgus thrust" during weight acceptance, will also be evaluated.

PROCEDURES

Eighteen children with a diagnosis of ML were selected for the study. Spinal involvement ranged from the S2 to L3 level with 15 children capable of ambulating with out aids. Each child received a complete gait analysis procedure while ambulating barefoot (BF) and with their prescribed AFO's (n=22 sides) and/or KAFO's (n=12 sides). Multiple trials with force plate data were collected on 16 children in both the BF and brace conditions. A detailed description of the data collection system used has been previously described by Davis et al. (1991). Changes in the joint kinematic and kinetic patterns for the ankle, knee, hip and pelvis (kinematics only) in all three planes of motion were evaluated and compared to a normal pediatric data-base previously developed by Õunpuu et al. (1991).

RESULTS AND DISCUSSION

Comparisons of the BF and brace conditions revealed improvements in selected parameters when wearing either AFO's or KAFO's. All subjects showed a statistically significant increase in velocity, step and stride lengths in both the braced conditions versus BF walking (table 1). Improved stance phase stability and ability to weight bear on the forefoot with the braces explain these differences. No significant differences were found in the stance/swing ratio, cadence and cycle time. The stance/swing phase ratio did show a shift to more normal values in the brace conditions, i.e., a reduction in stance from 65 to 64% of the gait cycle with the AFO's and a reduction of 66 to 64% of the gait cycle with the KAFO's. This also suggests improved stance phase stability in the brace conditions. Cadence and cycle time parameters were close to normal limits during barefoot walking.

Table 1 Comparison of the mean temporal and stride parameters .

	velocity (cm/s)	cadence (steps/min)	step (cm)	stride (cm)
barefoot	76	112	40	82
AFO	91	115	47	96
probability	.0047	.3687	.0001	.0019
barefoot	74	106	40	83
KAFO	97	111	49	105
probability	.0169	.2191	.0005	.0001

Sagittal plane joint kinematics showed similar changes in AFO's and KAFO's as compared to the BF condition. Statistically significant improvements ($p<0.001$) in ankle motion with a reduction in the excessive dorsiflexion in stance and plantarflexion in swing were found with the braces. Improvements in sagittal plane extension were noted at the knee (figure 1) and hip when comparing the BF to brace conditions. These differences, however, were not statistically different. Pelvic tilt showed minimal a minimal change between BF and AFO conditions with a mean tilt of 18 and 19 degrees, respectively. Comparing the BF to the KAFO condition there was a significant ($p<.0002$) increase in anterior pelvic tilt from a mean of 21 degrees (AFO's) to 25 degrees (KAFO's). In the transverse plane, foot progression showed significant ($p<0.0115$) improvements with AFO's, which corrected the abducted valgus foot, as compared to BF. Large pelvic rotations (excessive internal rotation at initial contact and external rotation at toe-off) and corresponding hip motion (excessive external rotation at initial contact to internal rotation at toe-off) were present in the BF and braced conditions. In the coronal plane, bilateral pelvic drop and excessive hip adduction in stance occurred in both the BF and braced conditions. These abnormalities about the hip and pelvis may be explained by weakness in the hip extensors and abductors which is not addressed by the braces.

Statistically significant improvements of the ankle muscle moments were seen in the braced versus BF condition (table 2). With braces, a greater plantarflexor moment in stance is possible as the brace allows for increased weight bearing on the forefoot (figure 1). This was not possible when BF because of ankle plantarflexor paralysis in this patient population. Examination of a typical foot force plot shows a comparison of the path of the center of pressure and the resultant ground reaction force in the BF and AFO's (figure 2). When braced the path of the center of pressure is more normal and provides for a smoother transition during stance and more stability which ultimately increases step length (table 1). The AFO also provides enough

support for the shank and reduces knee flexion, specifically in terminal stance and subsequently reduces the excessive knee extensor moment found in the BF condition (figure 1). These differences, however, were not statistically significant.

Table 2 Comparison of mean peak angles and muscle moments among BF, AFO and KAFO's.

	ankle dor.flex. stance (degrees)	ankle pl.flex. swing (degrees)	ankle pl.flexor stance (N.m/kg)	knee extensor stance (N.m/kg)
barefoot	23	8	.66	.6
AFO	13	0	.87	.52
probability	.0001	.0017	.0049	.0681
barefoot	33	22	.371	.643
KAFO	11	1	.786	.571
probability	.0001	.0003	.0045	.5087

Children with ML are often braced above the knee with KAFO's as a result of an apparent visual "valgus thrust" at the knee during weight acceptance (Carroll, 1982). Evaluation of the coronal plane kinetics when barefoot revealed that 4 of 20 knees showed a net adductor muscle moment with the remaining 16 knees demonstrating abductor muscle moments within normal limits. This would suggest that the prescription of AFO's in certain cases would be sufficient as protection of the medial aspect of the knee is not necessary. The visual knee "valgus thrust" appears to be a misinterpretation confounded by the combination of excessive internal rotation of the pelvis, progressive knee flexion and a flail foot, which is externally rotated, all during weight acceptance. Evaluation of the coronal plane knee moments revealed no significant differences between the coronal plane moments at the knee when BF versus when wearing AFO's (figure 3). The gait data, therefore, provides useful information for the clinician to help determine if bracing above the knee is actually required. Visual assessment only of the knee may be misleading in some cases.

In conclusion, sagittal plane kinematics and kinetics are improved with the application of AFO's in children with low level ML. In the coronal plane, the data suggests that a more critical evaluation of knee function than visual observation only is needed to determine if bracing above the knee with KAFO's is necessary. A longitudinal evaluation of knee function with gait analysis would also be useful to determine if the knee function in the coronal plane remains the same during growth. Therefore, three dimensional gait analysis is an appropriate tool for the routine documentation and evaluation of brace function in children with ML.

REFERENCES

Carroll, N. et al. Pros. Orth. Int., 6, 27-34, 1982.
Carroll, N. Clin. Ortho. Rel. Res., 102, 108-114, 1974.
Davis, R. et al. Hum. Move. Sci., 10, 575-587, 1991.
Mazur, J. et al. Z Kinderchir, 45, 23-25, 1990.
Õunpuu, S. et al. J. Pediatr. Orthop., 11, 341-349, 1991.
Thomas, S. et al. Z Kinderchir, 44, 38-40, 1989.

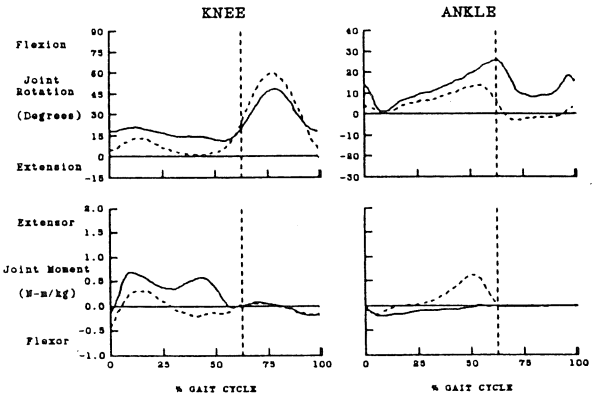

Figure 1. Example of ankle and knee sagittal plane kinematics and moments for BF (solid) and AFO (dashed) in one subject.

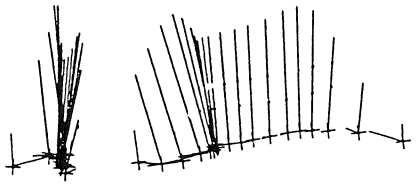

Figure 2. Resultant ground reaction force patterns for BF (left) and AFO (right) in one subject.

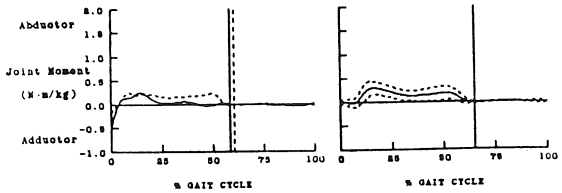

Figure 3. Example of knee coronal plane moments for BF (solid) and AFO (dashed) in one subject (left) and a normal knee moment (right).

MOTOR CONTROL

Podium Session 14

ANTAGONISM vs MUSCULAR EFFICIENCY: THEORETICAL CONSIDERATIONS

W. Herzog, P. Binding

Human Performance Laboratory, University of Calgary, Alberta
Department of Mathematics and Statistics, University of Calgary, Alberta

INTRODUCTION

Static, non-linear optimization approaches based on efficiency criteria such as the minimization of muscular stresses have been claimed to not be able to predict antagonistic muscular activity or co-contraction of pairs of antagonistic muscles (e.g. Hughes and Chaffin, 1988; Zajac and Gordon, 1989). Most recently, it has been shown analytically that antagonistic muscular activity can be predicted using such algorithms (Herzog and Binding, in press), however, the issue of co-contraction of pairs of antagonistic muscles was not resolved.

Here, we used a two-segment, two-joint, six muscles, two-dimensional model (figure 1) to investigate analytically the possibility of co-contraction of pairs of antagonistic muscles using static, non-linear optimization based on a minimum stress criteria (Crowninshield and Brand, 1981). It was found that co-contraction of one-joint pairs of antagonistic muscles cannot be predicted, however there is a set of general solutions predicting co-contraction of two-joint pairs of antagonistic muscles.

REVIEW AND THEORY

Using a static optimization approach based on minimizing muscular stresses, Davy and Audu (1987) showed results of co-contraction of a pair of one-joint antagonistic muscles (soleus and tibialis anterior, figure 10). Zajac and Gordon(1989) stated that such co-contraction cannot be predicted with the algorithm used by Davy and Audu (1987). Since neither of the two references offered an analytical proof of their results (statements), it was not obvious which of the statements was correct. The purpose of this study was to investigate analytically the possibility of co-contraction of pairs of antagonistic muscles using the static, non-linear optimization approach introduced by Crowninshield and Brand (1981).

PROCEDURES

The theoretical, musculoskeletal model used for this investigation consisted of a two-segment, two-joint, six muscles, two-dimensional system (figure 1). Pairs of antagonistic muscles were defined as muscles crossing the same joint(s) and producing opposite moments about each of the joint(s) they cross. In this model, antagonistic pairs are made up of muscles 1 and 2, muscles 3 and 4, and muscles 5 and 6. Numerical solutions were obtained using standard search procedures. Analytical solutions were calculated using the Karush-Kuhn-Tucker conditions which were necessary and sufficient since the objective function is strictly convex for $\alpha>1$ and $F_j \geq 0$ and $PSCA_j>0$, and the moment constraint equations are componentwise linear. Here, α is the power of the objective function (=3), and F_j and $PCSA_j$ are the muscular forces and corresponding physiological cross-sectional areas, respectively. All solutions were calculated by imposing an external force on the distal segment of the model that produced moments at the proximal (M1) and the distal joints (M2) of the system. Muscular forces were determined for static equilibrium conditions and assuming frictionless hinge joints. Moment arms and physiological cross-sectional areas of all muscles were initially taken to be 1 arbitrary unit. Deviations of these parameters from unity are mentioned specifically.

RESULTS

Co-contraction of one-joint antagonistic muscles is not possible using the optimization approach proposed by Crowninshield and Brand (1981). However, co-contraction of two-joint antagonistic muscles is possible and constitutes a set of general solutions. Figure 2 shows such co-contraction for muscles 5 and 6, for conditions requiring moments of M1=-3 and M2=1 at the proximal and distal joints respectively. All $PCSA_j$ and moment arms were 1 unit for these calculations except for the moment arm of muscle 6 about the proximal joint that was varied systematically from 0 to 1.0 at increments of 0.1 (figure 2). Co-contraction of muscles 5 and 6 exists for a range of moment arm values of muscle 6 about the proximal joint of 0-0.8. At moment arm lengths of 0.9 and 1.0, muscle 6 becomes silent. It should be noted that muscle 6 effectively becomes a one-joint muscle when setting its moment arm to 0 at the proximal joint. In this situation, muscle 6 is equivalent to muscle 4, and the forces predicted in muscles 4 and 6 are identical.

When changing the moment arm value of muscle 6 about the proximal joint from 0 to 1.0, the cost encountered (i.e. the sum of the cubed muscle stresses) becomes increasingly larger (figure 3). This result may appear somewhat counter-intuitive, because it implies, for the particular situation at hand, that cost is lowest when co-contraction of muscle 6 (with muscle 5) is high and that cost increases with a decrease of antagonistic force in muscle 6. This result is further surprising, since an increase in moment arm (in this case the moment arm of muscle 6 about the proximal joint) is typically associated with a decrease in force for a given moment requirement, and thus a decrease in the corresponding cost. However, figure 3 shows that the opposite is correct for this case, indicating that the ratios of moment arms of two-joint antagonistic pairs of muscles may affect cost function values substantially and in surprising ways.

DISCUSSION

Co-contraction of one-joint antagonistic pairs of muscles is not possible using the static, non-linear optimization approach of Crowninshield and Brand (1981). However, co-contraction of two-joint antagonistic pairs of muscles is possible and an example of this is shown in figure 2. These findings are in contradiction with statements of Zajac and Gordon (1989) and results shown by Davy and Audu (1987). If one accepts that the cost function of Crowninshield and Brand (1981), minimization of the cubed sum of all muscular stresses, may represent a measure of muscular efficiency, then the results of this study show that antagonistic muscular activity in general, and co-contraction of antagonistic pairs of muscles specifically, constitute a mechanism that may improve efficiency of specific motor tasks.

REFERENCES

Crowninshield, R. D. et al. J. Biom. 14, 793-802, 1981.
Davy, D. T. et al. J. Biom. 20, 187-201, 1987.
Herzog, W. et al. Math Biosci. (in press)
Hughes, R. E. et al. Proceedings ASB, 69-70, 1988.
Zajac, F. E. et al. Ex. Sports Sci. Rev. 17, 187-230, 1989.

ACKNOWLEDGEMENTS

This study was supported by grants from NSERC of Canada.

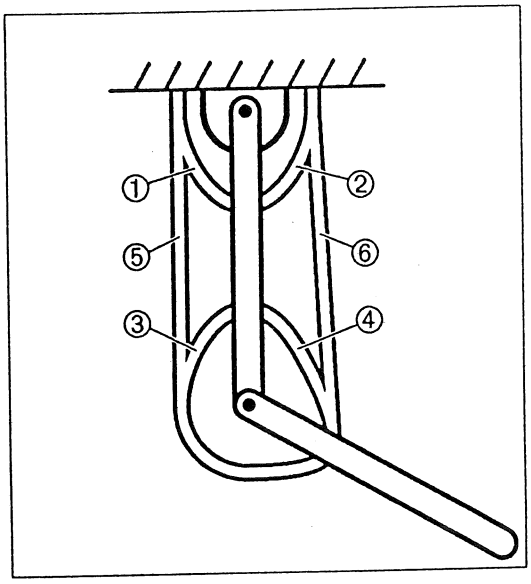

Figure 1. Musculoskeletal model used for all calculations

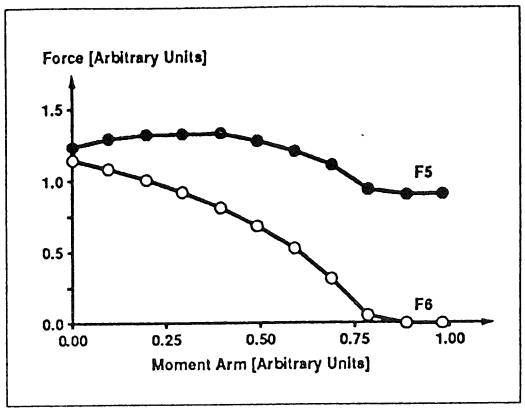

Figure 2. Forces in muscles 5 and 6 as a function of changing moment arm of muscle 6 about the proximal joint.

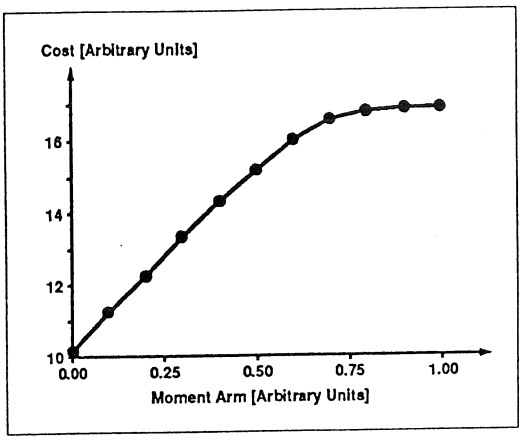

Figure 3. Cost function values as a function of changing moment arm of muscle 6 about the proximal joint.

PREDICTION OF BALLISTIC ELBOW FLEXION MOVEMENT TIME BY AGONIST/ANTAGONIST MUSCLE ACTIVATION PATTERNS

D.A. Gabriel[1], J.P. Boucher[2] and T.B. Hoshizaki[1]

[1]Department of Physical Education, McGill University, Montreal
[2]Department of Kinanthropology, University of Quebec at Montreal, Montreal

INTRODUCTION

This study examined the prediction of movement time [MT] for ballistic elbow flexion by agonist/antagonist muscle activation. Eighteen male subjects performed over four days a total of 400 ballistic elbow flexion trials to a target on a manipulandum in the horizontal plane. A potentiometer and eccentric cams at the elbow axis of rotation of the manipulandum recorded angular displacement and movement time. Beckman Ag/AgCl surface electrodes monitored the electromyographic [EMG] activity of the biceps brachii [BB] and triceps brachii [TB]. As practice improved the speed of ballistic elbow flexion, agonist/antagonist burst duration was found to scale with MT. The decrease in movement time associated with practice was accomplished by an increase in the slope of the agonist/antagonist EMG bursts and other measures of recruitment detailed below. When maximum speed of movement to a target is the task objective, the difference between skilled and novice performance is the level of muscle recruitment and not the temporal innervation pattern.

REVIEW AND THEORY

Muscle coordination for skilled ballistic arm movement has been described by the electromechanical delay, burst durations, slopes, and intermuscle latency [IML] for the agonist/antagonist musculature. The IML is the difference in time between the onset of the first agonist burst [AG1] and the onset of antagonist reciprocal burst [ANT-R]. Empirical observations (Lagassé, 1979; Solomonow et al., 1988) and computer modelling (Kilmer et al., 1982) has shown that a delay in the onset of ANT-R allows AG1 to accelerate the limb unimpeded and decrease MT. However, quantification of agonist/antagonist EMG temporal measures is not without certain difficulties.

Investigators have observed that the antagonist burst can be divided into two components (Gottlieb et al., 1989; Cooke & Brown, 1990). The first component is small and immediately precedes the sharp increase in antagonist muscle activity, termed ANT-R. Gottlieb et al. (1989) noticed that the first component is not always distinguishable in some subjects but if it is present, it is invariant across movement conditions and the main portion of ANT-R shows a strong relationship with movement time.

Lagassé (1979) and Kilmer et al. (1982) associated the early antagonist component with a cocontraction period that can act to slow limb movement. With practice, these authors cite a reduction in cocontraction that can improve MT. In contrast, Darling and Cooke (1987) showed that ANT-R actually begins earlier in well practiced fast elbow flexion. It is clear that the definition of ANT-R can be a confounding factor. Moreover, the studies referenced above did not normalize the EMG recordings with respect to MT. This may produce spurious relationships when making comparisons across subjects and movement conditions. There is then a definite need to reevaluate learning induced modifications to normalized agonist/antagonist patterns.

PROCEDURES

Eighteen college age male subjects completed 4 days of testing; 24 hours separated Days 1 and 2 and Days 3 and 4, with a one week interval between Days 2 and 3. On each test day, subjects performed ballistic elbow flexion on a manipulandum in the horizontal plane to a 90° target until 100 successful trials were completed. A potentiometer at the elbow axis of rotation recorded angular displacement. Microswitches activated by eccentric cams attached to the axis of rotation established MT, target achievement, and error. The tolerance level for error was 15° before target and if the target was overshot the trial was discarded.

The EMG activity of the BB (long head) and TB (lateral head) was recorded with surface electrodes (Beckman Ag/AgCl) placed 3 cm apart, in line with the muscle relative to the estimated motor point (Warfel, 1985). To maintain consistency across subjects skin electrode impedance was monitored and kept below 5 kΩ. The signals were amplified by a Grass P-511 with a band pass of 3 Hz-3 kHz and CMRR of 10,000:1 at 100 Hz. The EMG activity was digitized (MDAS 7000 A/D with an Amiga at 2000 Hz/channel) and then numerically rectified and low pass filtered (10 Hz cut off). To compare across subjects and days the EMG bursts were normalized both in amplitude and in time. Amplitude normalization was accomplished relative to the peak of the signal for a given trial. Time normalization was done using a quadratic fit in order to present trial data over 175 points [pts]: 50 pts before onset of movement, 100 pts for MT, and 25 pts past the reaching of the target. Figure 1 shows the measures extracted from the signal of a normalized trial. The dependent variables presented in order are: (1) AG1 burst duration [AG1BD]; (2) AG1 burst slope [AG1S]; (3) AG1 electromechanical delay [AG1EMD]; (4) AG1-to-ANT-R inter-muscle latency [IML]; (5) ANT-R burst slope [ANTRS]; (6) ANT-R burst duration [ANTRBD]; (7) ANT-R delay to target [ANTRDT]; (8) slope of the angular displacement curve [DISPS]; (9) target error [ERROR]; and (10) end of AG1 [AG1END].

RESULTS AND DISCUSSION

The means and standard deviations of the measurements are presented in Table 1. A repeated measures ANOVA (REANOVA) showed that MT decreased significantly ($p<.05$) from 159 ms on Day 1 to 127 ms on Day 4. Of the 9 EMG parameters subjected to the REANOVA, only AG1EMD and AG1S were found to change. Over the four days of testing, AG1EMD decreased monotonically ($p<.05$) from 26.83 to 24.44 pts whereas AG1S increased ($p<.05$) from 3.00 to 3.95.

At first, these observations would appear to conflict with the fact that AG1BD remained stable. If a second portion of AG1 is considered, from onset of movement to the end of the burst, the results can be explained (see 10 in figure 1). Subsequent analysis showed that this component of AG1 lengthened ($p<.05$) from 68.34 to 78.94 pts by Day 4. This is consistent with Boucher and Flieger (1985) who also demonstrated that AG1 could be functionally

partitioned. AG1EMD was seen as representing a static portion (i.e., before onset of movement) and AG1END a dynamic portion (i.e., during movement). These two divisions of the first agonist burst had different mean power frequencies suggesting dissimilar patterns of motor unit recruitment.

TABLE 1. MEANS (M) AND STANDARD DEVIATIONS (SD) OF THE DEPENDENT VARIABLES ACROSS ALL DAYS.

VARIABLES		DAY 1	DAY 2	DAY 3	DAY 4
MT	M	159	144	135	127
	SD	23	25	21	16
AG1BD	M	96	100	102	104
	SD	13.04	14.97	11.37	15.94
AG1S	M	3.00	3.33	3.43	3.95
	SD	1.12	1.41	1.30	1.30
AG1EMD	M	26.56	24.94	26.72	24.89
	SD	3.76	4.05	2.80	3.54
IML	M	24.44	17.66	19.17	20.06
	SD	32.69	29.09	78.00	20.57
ANTRS	M	1.35	1.10	0.95	1.11
	SD	0.88	0.68	0.36	0.79
ANTRBD	M	112.22	123.83	123.83	121.50
	SD	36.20	29.89	30.50	29.97
ANTRDT	M	95.66	107.00	108.00	105.00
	SD	33.32	29.28	29.83	30.92
DISPS	M	1.10	1.12	1.10	1.11
	SD	0.05	0.07	0.05	0.05
ERROR	M	15.06	14.41	14.23	14.40
	SD	3.94	3.02	2.86	3.71
AG1END	M	68.39	74.89	75.33	78.94
	SD	12.10	15.03	13.67	12.30

The most interesting aspect of the present study was the finding that, although the two different components of AG1 underwent modification, the entire burst remained stable. This is consistent with the Impulse Timing theory (Wallace, 1981), which posits that MT is primordial in the determination of burst duration. This suggests that certain events must occurr in the motor apparatus to scale burst duration to MT. If burst duration is to occupy the same proportion of MT, as revealed by the present study, then the increase in energy put into the system, required to improve speed, must be derived by intensity modulation. The increased AG1S concurrent with a decreased AG1EMD leads to this conclusion. Moreover, the same observation suggests that this intensity modulation occurrs mainly within AG1EMD.

Further, a linear multiple regression equation consisting of AG1S and ANTRS resulted in a multiple R^2 of .42 on Day 1 and went up to .71 ($p<.05$) for Day 4. The addition of the average velocity, as represented by DISPS, in the regression produced only a small (6.7%) increase in the ability to account for the variance in MT. The increasing ability of AG1S and ANTRS to predict MT suggests that intensity modulation is associated with the reduction in MT of ballistic movements due to practice.

FIGURE 1. SAMPLE EMG AND DISPLACEMENT RECORD

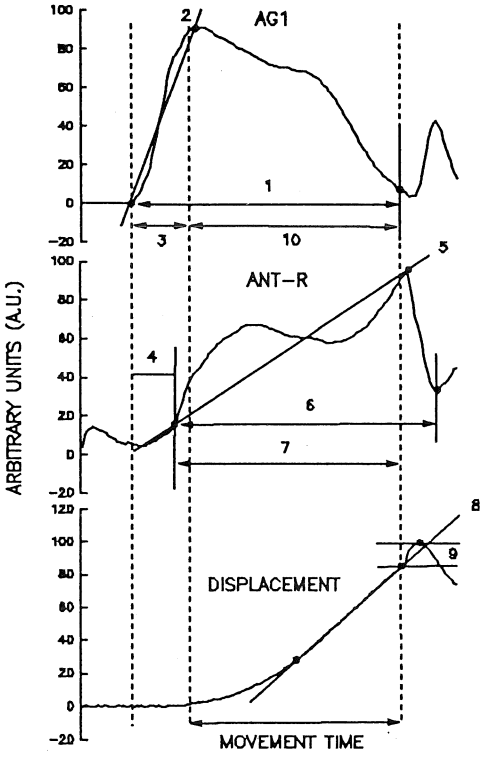

These findings suggest that caution must be applied when making conclusions about modifications to agonist/antagonist EMG bursts without normalizing. Schneider et al. (1989) studied upward and downward arm trajectories around a barrier between two endpoints and quantified the practice effects upon intralimb dynamics and corresponding agonist/antagonist EMG activity. After practice, agonist/antagonist EMG activity became more discrete, the speed of limb movement improved, and changes in muscle recruitment patterns were found to parallel alterations in intralimb dynamics. If the EMG activity was normalized with respect to MT, the bursts may not appear more "discrete". Rather, they would most likely occupy the same percentage of movement time. The modification in AG1 would be reflected in AG1EMD and AG1END and not in the burst duration.

REFERENCES

Boucher, J.P. et al. Biomechanics IX-A, D.A. Winter (Ed), Champaign: Human Kinetics Publishers, Inc, 1985, pp 297-301.
Darling, W.G. et al. Journal of Motor Behavior 19:311-331, 1987.
Gottlieb, G.L. et al. Journal of Neurophysiology 62:342-357, 1989.
Kilmer, W. et al. Biological Cybernetics 44:17-26, 1982.
Lagassé, P.P. Perceptual Motor Skills 49;151-161, 1979.
Schneider, K. et al. Journal of Biomechanics 22:805-817, 1989.
Solomonow, M. et al. Electrophysiological Kinesiology, Amsterdam: Elsevier Science Publishers (Biomedical Division), 1988, pp. 19-23.
Warfel, J.H. The extremities, Philadelphia: Lea & Febiger, 1985.

NET JOINT POWER PATTERNS AS A MEANS OF DOCUMENTING COORDINATION DISABILITIES IN PARKINSON'S DISEASE.

V.Hatzitaki and T.B. Hoshizaki

Department of Physical Education, McGill University, Montreal

INTRODUCTION

The purpose of the study was to investigate the effectiveness of the joint power analysis and the subsequent phase breakdown in identifying coordination disabilities observed in Parkinson's disease. Four(4) non-impaired individuals and three(3) Parkinson's patients were filmed while performing two upper limb tasks of different complexity. Movement was reflected in a series of functional phases describing the dynamic characteristics of the muscle activity around the joint.

The results revealed phase breakdown as a sensitive tool for describing movement deficiencies. Similar muscle phenomena were reflected through the functional phases of both groups. The statistical comparison of selected kinematic and kinetic parameters revealed a significant disturbance in movement patterns of Parkinson's patients.

REVIEW AND THEORY

The ability of the scientist to accurately evaluate movement patterns in Parkinson's disease is an important aspect of any treatment program. Inconsistency exists among the clinical methods used to evaluate the degree of the motor disability as the information they provide is often inaccurate and subjective. Recently, research involving the interpretation of both kinematic and myoelectric information has identified some functional aspects of the disability observed during dynamic activity (Benecke et al.,1987; Berardelli et al.,1986; Crenna et al.,1990; Montgomery et al.,1990). These studies provided further insight into the problem of Parkinson's disease by quantifying the characteristics of the abnormal movement. However, such kinematic analysis cannot explain how movement about a joint is produced or controlled by muscle activity, joint constraints or intersegmental interactions. The phase breakdown proposed in the present investigation relates the processes of movement production with the musculoskeletal responses at the joint(Robertson & Winter,1980; Hoshizaki & Vardaxis,1988). According to the latter, movement is partitioned into functional phases based on the interpretation of the net joint power patterns. The study was designed to test the applicability of such a model in the investigation of movement deficiencies.

PROCEDURES

Four(4) non-impaired individuals and three(3) patients afflicted with Parkinson's disease were required to perform two upper limb tasks of different complexity. The first one required a simultaneous, multijoint elbow extension and shoulder abduction, while the second one required the sequential execution of the same actions. Both actions were restricted to the horizontal plane. A high-speed camera operating at 200fps was used to film the experimental movements. The digitized coordinates were filtered and subjected to differentiation for the calculation of the joint kinematics. The application of inverse Newtonian solutions to kinematic data along the use of anthropometric information (Dempster, 1955) allowed the determination of the joint and segmental kinetic characteristics. Functional movement phases were identified at the elbow and shoulder joints based on information provided by the joint and segmental angular velocities, net joint torques and net joint powers. The analysis involved: i) the description of the joint musculoskeletal responses based on the identification of the functional movement phases, and ii) the statistical comparison of selected time and peak amplitude joint parameters.

RESULTS

The consistency of the net joint power patterns as expressed by the mean coefficient of variation(CV) ranged from 18.9% to 51.5% for the able-bodied group and from 35.3% to 70.3% for the patient group. Parkinson's patients showed less consistent movement profiles.

Similar functional phases were identified in the movement profiles of both ability groups. For the simultaneous task, muscle activity was reflected in two consistently appearing phases (Figure 1); a)energy generation and transfer to the forearm (CETF) and b) energy absorption and transfer to the upperarm (EETU). An additional phase of energy generation and transfer to the upperarm(CFTU) was noted near the end of the able bodied movement, indicating a reversal in joint direction. In the sequential task, the number of phases increased as a function of the additional constraints imposed to the movement. Considerable elbow activity was observed during active shoulder abduction and it was reflected in a variant and subject specific number of phases. The variation in the number of phases was greater in the Parkinson's group. Similar phenomena described the activity of the shoulder during the active elbow extension.

When the relative durations of the basic building phases were compared across groups, only the first phase of energy generation and transfer to the forearm was found to be significantly longer for the Parkinson's patients. The statistical comparison of joint angular velocities,joint torques and net joint powers revealed significantly higher peaks ($p<0.05$) for the able bodied group.

DISCUSSION

The phase breakdown of the movement pattern was found to be a sensitive tool for describing the musculoskeletal responses of different ability groups to movements of different complexity. Similar muscle phenomena were reflected through the functional phases of both groups. The only difference was a third joint "reversal" phase observed near the end of elbow extension in the

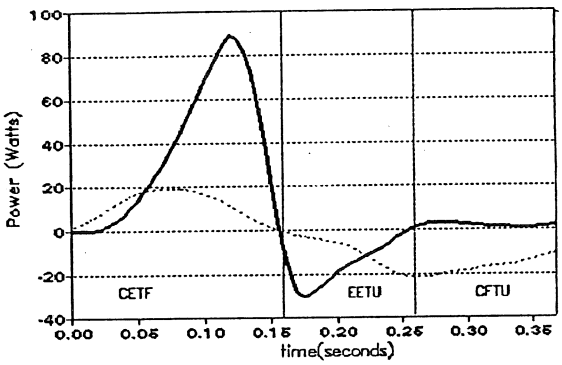

Figure 1:Example of a phase breakdown for the simultaneous task (able-bodied)

able-bodied profile. This phase was attributed to the development of antagonistic activity to prevent collision as a consequence of the restricted joint geometry. Parkinson's patients did not experience such joint reversals because their segmental velocities were quite low to necessitate collision phenomena. In the sequential task, both groups experienced considerable elbow activity during the abduction of the shoulder, as it was reflected through a variant number of functional phases. Many researchers have noticed that the control of movements involving more than one segment must take into account the mechanical interactions between them (Bizzi & Abend,1982; Schneider et al.1990). These interjoint interactions are attributed to the inertial and geometrical properties of the limbs. The partitioning of the movement pattern into functional phases was also found to be in close agreement with electromyographic studies describing muscle recruitment phenomena in Parkinson's disease (Accornero et al.,1984; Benecke et al.,1986).

The statistical comparison of kinematic and dynamic peak amplitude characteristics confirmed some of the functional movement abnormalities found by previous researchers (Hallet & Marsden, 1981; Sheridan et al.,1987). In addition, the comparative analysis showed that individuals suffering from Parkinson's disease lose the ability to produce sufficient energy at the joint that will enable the execution of ballistic functional movements. Based on the evidence provided by the present study, net joint power patterns were found to be a useful tool for describing movement deficiencies at the musculoskeletal level of observation. The extent to which such deficiencies are related to central motor dysfunctions remains to be investigated.

REFERENCES

Accornero, N. et al. Neurosc. Letters, 46, 91-95, 1984
Benecke, R. et al. J. Neur. Neursg. & Psyc.,50,296-303, 1987.
Berardelli, A. et al. J. Neur. Neursg. & Psyc, 49, 1146-1149, 1986.
Bizzi,E. et al. Motor control mechanisms in health and disease, (p.31-45),Raven, 1983
Crenna, P. et al. Motor Disturbances II, (p.161-173), Academic Press, 1990
Montgomery, E. et al. Neurology, 40, 269-272, 1990
Hallet, M. et al. Progress in Clinical Neurophysiology, Vol.9, Karger, 1981.
Hollerbach J. et al. Biol. Cybernetics, 44, 67-77, 1982
Hoshizaki,B. et al. Proccedings of the Fifth Biennial Conference in Biomechanics, Ottawa, 1988.
Robertson, D. & Winter, D.J. Biomechanics, 13, 845-854, 1980
Sheridan, M. et al. Brain, 110, 1247-1271, 1987
Schneider, K. et al. J. Motor Behav., 22(4), 493-520, 1990

Proceedings of NACOB II, The Second North American Congress on Biomechanics, Chicago, August 24th - 28th, 1992

ASYMMETRIC KINETIC INTERFERENCE IN NON-IMPAIRED AND PARKINSONIAN SUBJECTS DURING BIMANUAL TASKS OF DISPARATE DIFFICULTY

K. Manal & B. Hoshizaki
Department of Physical Education, McGill University

Movement times (MT) of 3 different horizontal arm tasks were recorded to investigate whether Parkinsonian individuals exhibit temporal assimilation during intended high velocity bi-lateral movements. The assimilatory phenomenon may reflect an organizational strategy in which the motor system's degrees of freedom are reduced. Simultaneous bilateral movements are expected to be severely compromised in Parkinson's disease (PD). However, if the assimilatory mechanism is intact, movements of differing complexity may actually facilitate simultaneous performance in PD.

The subjects (4 non-impaired of 4 PD's) performed a series of 3 different task protocols. The movements were classified as 1) "easy" individual, 2) "difficult" individual and 3) a simultaneous "mixed" condition of the easy-difficult tasks. Temporal assimilations were elicited by the non-impaired individuals and were characterized by MT increases of the "easy" limb in the "mixed" limb condition. Three of the four Parkinsonians failed to demonstrate the assimilatory response. MT's of the "difficult" limb remained unchanged across conditions for all of the non-impaired subjects and for 3 of the 4 Parkinsonians.

REVIEW

When bi-lateral movements of differing difficulty are performed as rapidly as possible the "easy" limb slows down and is attracted to the temporal structure of the more difficult movement. Kelso, Southard & Goodman, (1979,83) attribute this assimilatory effect to a restructuring of the movements metrical prescriptions in which the system's degrees of freedom are reduced. This strategy decreases the coordinative demands of performing 2 different movements at the same time by constraining groups of muscles to act as a single functional unit. In this model, timing becomes an essential variable that remains unchanged between the 2 movements of the mixed limb condition. Non-essential variables such as force are therefore free to vary and maintain the temporal structure of the 2 limbs.

Marteniuk & Mackenzie's (1980) model of temporal assimilation is quite different than Kelso et al's, and is based on neural cross talk theory. Their model suggests that a significant percentage of the motor commands destined for one limb do not decussate and continue ipsilaterally resulting in a contralateral limb influence. They contend that bi-lateral movements are programmed independently and that facilitative or inhibitive affects are due to neural crosstalk between the motor commands.

Individuals suffering from PD experience a gradual deterioration of their motor faculties. Perhaps the most graphic illustration of these motor difficulties arises when two discrete tasks are attempted simultaneously. The Parkinsonian individual adopts a sequential strategy rather than executing the movements in the same time frame (Schwab, Chafez & Walker, 1954; Benecke, Rothwwell, Dick, Day & Marsden, 1986, 87).

It was the purpose of this paper to investigate whether Parkinsonians elicit temporal assimilation, in the belief that an assimilatory effect may facilitate simultaneous bi-lateral control in PD.

PROCEDURE

Four Parkinsonian subjects (male) participated in the study and were all of the same clinical disability (Gr. II). The subjects were "ON" medication and well within their optimal window of motor ability. Four age matched males with no known motor impairments served as control subjects. The subjects performed a series of 3 horizontal arm movements of differing difficulty. The "easy" task involved a complete extension of the elbow from an initial flexed position of 90 degrees. The subjects performed a series of 3 horizontal arm movements of differing difficulty. The "easy" task involved a complete extension of the elbow from an initial flexed position of 90 degrees. The subjects were instructed to maintain the upper arm at a perpendicular angle with the frontal plane of their torso. The "difficult" task was performed with the subject's preferred limb and involved a maximal abduction of the upperarm while actively extending the elbow. The movement was initiated from the same starting orientation as the "easy" task. The "mixed" limb condition was a combination of the "easy" and "difficult" movements performed simultaneously. The subjects were explicitly instructed to perform the 3 experimental protocols as rapidly as possibly. Immediately following a practice session during which knowledge of results were provided, the subjects performed a minimum of three trials per movement condition. The position-time records were recorded with high speed cinematography at a film speed of 200 fps. A modified version of BIOMECH was used to calculate the horizontal kinematics and kinetics of the smoothed X-Z coordinates.

RESULTS & DISCUSSION

Non-Impaired: A significant slowing down of the "easy" limb was observed in 3 of the 4 subjects during the "mixed" limb condition. This observation was consistent with previous studies (Kelso et al., 1979,83; Marteniuk et al., 1980,84; Walter et al., 1990; Sherwood, 1991). Movement duration of the "difficult" limb remained unchanged across movement conditions. Although a goal of the elbow extension task was to maintain the upperarm stationary, it was inevitably pulled along by the forearm due to their mechanical linkage. However, upperarm velocity increased during the "mixed" limb condition.

Table 1

Mean Upper Arm Velocities ("Easy" Limb)

Subject	Ind	Mixed	p (1 tail)
1	2.016 (.166)	2.968 (.640)	.0162
2	3.413 (.904)	5.016 (.275)	.0167
3	1.570 (.365)	2.898 (.261)	.0005
4	2.571 (.153)	2.167 (.293)	.1110

Mean upperarm velocities (rads/s) of the "easy" limb across movement conditions. SD's reported in parenthesis.

Clearly, the shoulder joint of the "easy" limb underwent metrical changes during the mixed limb trials. This is convincingly illustrated in Fig. 1. The metrical structure of the limb was influenced by the contralateral shoulder activity requisite of the upperarm abduction task. Table 2 reports the normalized torque values (N-m) at the shoulder for the "difficult" limb during the mixed limb condition. Mean torque values are reported for the control and Parkinsonian subjects. Notice that subject #3 failed to generate comparable torque values recorded for the other non-impaired individuals ($p < 0.000$). #3 was the only control subject not to demonstrate a temporal attraction. These data suggest that #3 did not generate sufficient contralateral shoulder torque to elicit the assimilatory response. Marteniuk et al.'s neural crosstalk model compliments these data nicely. It appears that the assimilatory response is elicited only when sufficient contralateral shoulder torque is generated.

Figure 1

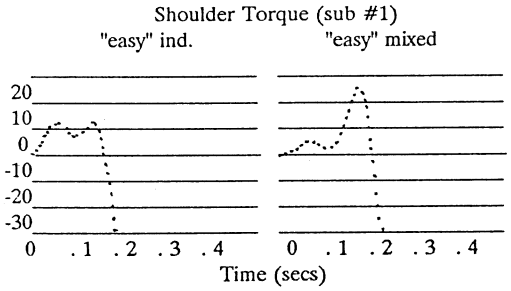

Table 2
Mean Shoulder Torques
(difficult mixed condition)

Subject	Mean	SD
C1	9.54	(.14)
C2	9.88	(.52)
C3	6.25	(.18)
C4	8.60	(.12)
P5	4.00	(.56)
P6	3.74	(.91)
P7	0.95	(.37)
P8	6.43	(.10)

C=control
P=parkinsonians
SD=standard deviations

Parkinsonians: As expected, the Parkinsonians demonstrated significantly greater movement durations across the 3 tasks. Of the 4 Parkinsonian patients, #8 was the only subject to demonstrate a temporal attraction of the "easy" limb. Interestingly, #8 generated similar forces as the control subjects at the shoulder during the contralateral abduction movement (Table 2).

Heightened MT's of the "easy" limb during the mixed limb condition resulted from an associated movement due to neural crosstalk between the motor commands destined for each limb. The data clearly demonstrate that Parkinsonians endure a pure physiological deficiency in generating sufficient force to elicit temporal assimilations. Parkinsonians seemingly experience cognitive-motor impairments in light of simultaneous bi-lateral movements.

The results of this study suggest that temporal assimilations are not a coordinative strategy practiced in movements of this nature, but rather the result of interlimb motor command interference.

REFERENCES

Benecke R, et al. Brain. 1986;109: 739-757.

Benecke R, et al. Journal of Neurology, Neurosurgery & Psychiatry. 1987;50: 296-303.

Kelso JAS, et al., Journal of Experimental Psychology: Perception and Performance. 1979;5:229-238.

Kelso JAS, et al. Quarterly Journal of Experimental Psychology. 1983;35A: 347-375.

Marteniuk RG, et al. Tutorials in Motor Behavior (pp. 185-197). Amsterdam; North-Holland, 1980.

Marteniuk RG, et al., Quarterly Journal of Experimental Psychology. 1984;34A: 335-365.

Schwab RS, et al., Archives of Neurology and Psychiatry. 1954;72: 591-598.

Sherwood DE, Research Quarterly for Exercise and Sport. 1991;62: 302-308.

Walter CB, et al., Brain and Cognition, 1990;14:185-200.

MECHANISMS OF CONTROL OF CAT SOLEUS MUSCLE DURING UNRESTRAINED LOCOMOTION

W. Herzog

Human Performance Laboratory, University of Calgary, Alberta

INTRODUCTION

Peak forces of cat soleus muscle were found to remain nearly constant for a variety of different intensities of locomotion. This result was independent of how intensity of locomotion was altered; either by modifying speed or by keeping speed constant but changing external resistance by varying the slope of the walking surface. From these findings, it appears that peak soleus forces are not limited by contractile (peripheral) conditions of the muscle, but may be constrained through neural control mechanisms. If neural pathways are limiting peak soleus output, they must depend on the intensity rather than just the speed of movement.

REVIEW AND THEORY

The cat ankle extensor muscles have been the preferred model for studying mechanisms of neuromuscular control. Various researchers found that gastrocnemius and plantaris forces increase with increasing speeds of locomotion, as one would expect (e.g. Walmsley et al., 1978; Hodgson, 1983; Whiting et al., 1984; Gregor et al., 1988; Herzog and Leonard, 1991). However, peak soleus forces have been found to remain nearly constant independent of the speed of locomotion (e.g. Walmsley et al., 1978). Hodgson (1983) speculated that peak force production of cat soleus muscle was constrained by cutaneous and rubrospinal pathways that had an increasing inhibitory effect on soleus motor units with increasing speeds of locomotion; whereas Walmsley et al. (1978) suggested that excitation of the soleus muscle actually increased with increasing speeds of locomotion, however, peripheral phenomena were limiting soleus force production. If the argument of Walmsley et al. (1978) was correct, one would expect an increase in soleus forces for constant speeds of locomotion but increasing external resistance (i.e. increased demands of ankle extensor moments). Furthermore, if the inhibitory pathways were only speed dependent (Hodgson, 1983), one would again expect an increase in soleus force for a given speed of locomotion but changing external resistance. Therefore, the purpose of this study was to measure soleus forces for a constant nominal speed of walking of 0.7 m/s on a level, 10° uphill, and 10° downhill slope. It was expected, and later verified, that external resistance (i.e. the moment produced by the triceps surae and plantaris muscles about the ankle joint) increased from the downhill to the level and from the level to the uphill walking condition.

PROCEDURES

Force measurements from ten cats were obtained simultaneously from soleus, gastrocnemius and plantaris muscles for walking at nominal speeds of 0.4 m/s, 0.7 m/s, 1.2 m/s and trotting at the fastest speed the animals would tolerate (~2.4 m/s), as well as for walking at 0.7 m/s on a level, 10° uphill and 10° downhill slope. Measurements were obtained using homemade, "E"-shaped tendon force transducers (Herzog and Leonard, 1991) from a minimum of ten carefully selected, consecutive steps. Selections of steps were made from a precise lateral video record using subjective and objective selection criteria.

RESULTS

Figures 1 and 2 show mean force-time histories of soleus and gastrocnemius muscles from one representative animal walking at speeds of 0.4 m/s, 0.7 m/s, 1.2 m/s and trotting at a speed of 2.4 m/s. Mean peak forces of the soleus muscle are within a range of about 3 N for all speeds, whereas corresponding gastrocnemius forces increase from about 13 N (0.4 m/s) to well over 70 N (2.4 m/s). As expected, peak gastrocnemius forces also increase from the downhill (~15 N), to the level (~22 N), to the uphill walking condition (~ 40 N) (figure 4). However, as for the increase in intensity through increasing speed of locomotion, peak soleus forces remained similar for the level, uphill and downhill conditions (figure 3).

DISCUSSION

Walmsley et al. (1978) argued that peak soleus forces may not increase at increasing speeds of locomotion, because the time to build up a full active state at high speeds of locomotion becomes too short. However, this argument must be questioned when studying the results of figure 3. The time from first paw contact to attainment of peak force in the uphill walking condition is about 100 ms and the stride cycle time is 750 ms on average. This is a slow movement with enough time to build up a full active state, especially when comparing the uphill condition to the trotting condition (figure 1, 2.4 m/s), where the peak soleus force reached similar peak force levels with much less time available; i.e. about 60 ms from paw contact to peak force, and 400 ms for the entire stride cycle. Furthermore, contractile properties of soleus in the downhill, level and uphill walking conditions are similar, therefore, it appears that peripheral factors are not limiting force production in these situations. Thus, it may be hypothesized that the lack of increase of soleus force with increasing movement intensity is associated with central mechanisms. Inhibitory pathways to the motor units of the cat soleus muscle have been proposed (Hodgson, 1983), however, these pathways were only associated with speed of locomotion. The results of this study suggest that such inhibitory pathways (if existent) must be "intensity" sensitive, rather than just speed sensitive. Other possible pathways may include inhibitory signals from golgi tendon organs. If soleus force production is really limited by central pathways, this may be tested experimentally by stimulating the

soleus muscle supramaximally at various instants during the stride cycle.

REFERENCES

Gregor, R. J. et al. J. Biom. 21, 721-732, 1988.
Herzog, W. et al. J. Biom. 24 (1), 31-39, 1991.
Hodgson, J. A. J. Physiol. 337, 553-562, 1983.
Walmsley, B. et al. J. Neurophysiol. 41, 1203-1216, 1978.
Whiting, W. C. et al. J. Biom. 17, 685-694, 1984.

ACKNOWLEDGEMENTS

This study was supported by NSERC of Canada.

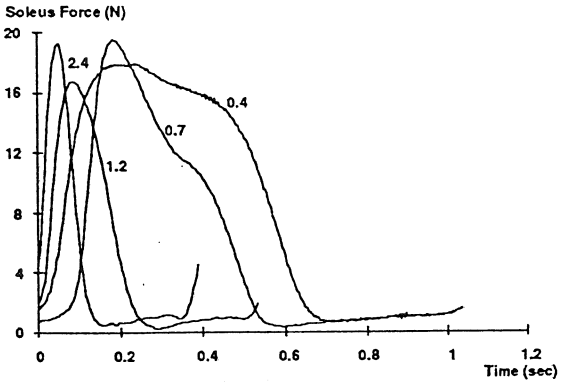

Figure 1. Mean force-time histories of cat soleus muscle for walking speeds of 0.4 m/s (0.4), 0.7 m/s (0.7), 1.2 m/s (1.2) and a trotting speed of 2.4 m/s (2.4)

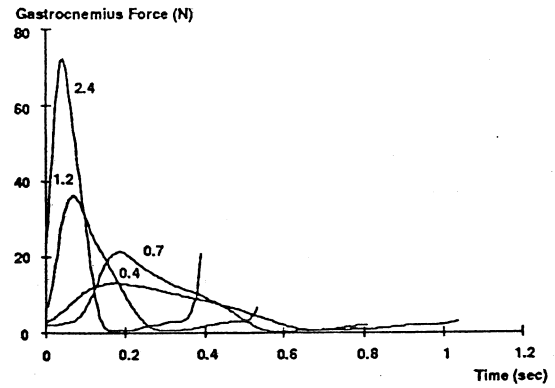

Figure 2. Mean force-time histories of cat gastrocnemius muscle for walking speeds of 0.4 m/s (0.4), 0.7 m/s (0.7), 1.2 m/s (1.2) and a trotting speed of 2.4 m/s (2.4)

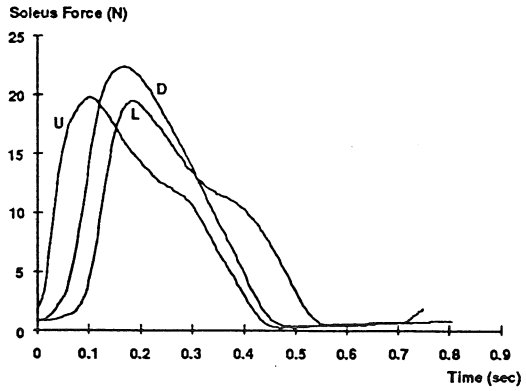

Figure 3. Mean force-time histories of cat soleus muscle for walking at a constant nominal speed (0.7 m/s) on a 10° downhill (D), a level (L), and a 10° uphill (U) slope.

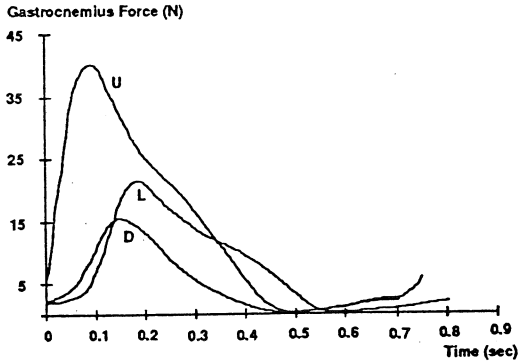

Figure 4. Mean force-time histories of cat gastrocnemius muscle for walking at a constant nominal speed (0.7 m/s) on a 10° downhill (D), a level (L), and a 10° uphill (U) slope.

THE NEURAL CONTROL OF RUNNING: IS THE STEP CYCLE PROGRAMMED INDEPENDENTLY?

Shirley Rietdyk and Aftab E. Patla

Neural Control Lab, Department of Kinesiology, University of Waterloo, Waterloo, Ontario, Canada.

INTRODUCTION

Prospective adaptations to the environment are integral to purposeful locomotion. Attention has only recently been focused in this area, however the studies consider adjustments within one step cycle. When action is geared to the environment, typically more than one step cycle will be adapted. This study compares transient step length (SL) adjustments (either one step or two subsequent steps) during overground running. If the subsequent step is also altered (either an increase or decrease), it dictates the manner in which the first SL change was achieved. The results of this study provide evidence for complex, task-specific modulation and indicate that the individual step cycle is not programmed independently of other step cycles.

REVIEW & THEORY

The literature provides evidence that the modulation of movement parameters depends on the task requirements. Lee, Lishman & Thomson (1982) demonstrate that long-jumpers adopt different adaptation strategies during the strides prior to striking the board depending on the subsequent task, whether a jump or a "run-through" (a practice jump where the athlete did not actually jump). Similar results have been found in arm movement studies where the precision requirements of the task altered the velocity of the arm trajectory (Marteniuk, Mackenzie, Jeannerod, Athenes & Dugas, 1987). Patla (1989) has found that the modulation of gait parameters during single SL adjustments is complex and task-specific.

The purpose of this study is two-fold. First, to ascertain the 'determinants' of SL change during running, and second, to determine if each step cycle is programmed independently, based on the task requirement.

METHODOLOGY

Six healthy, experienced distance runners (three male, three female) participated in the study. The subjects ran across a 13m runway (See Fig. 1). Based on the subject's predetermined SL, green 'targets' were placed along the runway such that the subject landed on the force plate (AMTI) with the contralateral foot. Cue lights were placed along the runway, corresponding to one-third and two-thirds of the SL, providing the subject with a visual cue for foot placement. EMG was collected bilaterally from the rectus femoris (RF), biceps femoris (BF) and the soleus (SO). Kinematics were collected at 60 Hz and shuttered at 1/1000 sec. with reflective markers placed on the ipsilateral shoulder, hip, knee, ankle, heel and toe.

Subjects were instructed to run at a self-selected pace, landing on the cued target when required. Four conditions were presented in random order: (1) a long step with the ipsilateral limb, with no constraints on the subsequent step (LX), (2) a long ipsilateral step followed by a short contralateral step (LS), (3) a long step followed by another long step (LL) and (4) two normal steps (NN). The NN condition accounted for 50% of the trials to prevent anticipation.

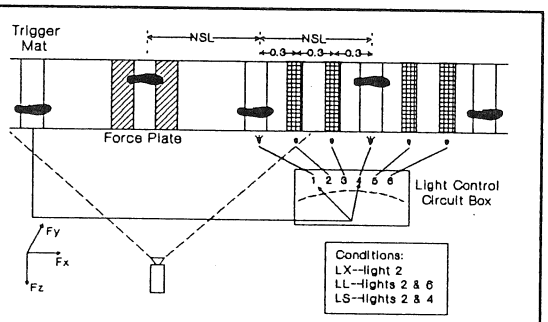

Figure 1: Schematic set-up.

RESULTS AND DISCUSSION

A repeated measures, within subject ANOVA was performed on the kinematic, kinetic and EMG measures. Two separate ANOVAs were run, the first comparing NN and LX to discover the determinants of transient SL change. The second compared LX, LS and LL to determine the effects of subsequent SL requirements on the first step. The significantly different kinematic and kinetic parameters and the EMG measures that are consistent with these changes will be discussed. The NN verses LX results will be considered first.

The 'Determinants' of Step Length

Significant changes were found in several kinetic, kinematic and EMG parameters. The changes in parameters will be discussed as they occur sequentially in the step cycle, from ipsilateral toe-off (ITO) to the following ipsilateral foot contact (IFC).

Kinematic and EMG measures were not significant at ITO and the following free flight phase. The impulse measures of the contralateral foot show less deceleration during the braking phase and an increased acceleration during push-off in both the horizontal and vertical directions for LX (see Fig. 2). The greater push-off is caused by elevated stance limb SO activity. The RF is eccentrically active in this phase to prevent an overly rapid knee flexion prior to toe-off. There is also increased pull-off generated by the elevated RF activity.

Significant changes were seen at IHC and the preceding free flight (FF) phase. The peak vertical hip position increased as a result of the increased push-off vertical impulse. Both the distance travelled by the centre of mass (CM) and the reach increased significantly, demonstrating that subjects were altering their foot placement not only by the change in impulse but also by altering the ipsilateral limb configuration. This is indicated by the trend of increased RF activity, pulling both the thigh and leg forward. The angles at IHC demonstrate a change in body configuration consistent with the increased reach.

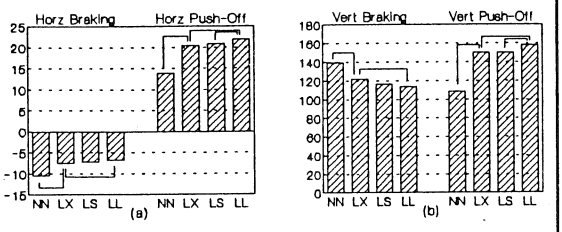

Figure 2: The horizontal (a) and vertical (b) impulse values (N.s).

The velocity data are summarized in Figure 3. An increase in hip horizontal velocity (Vx-hip) during FF and at IHC result from the horizontal impulse increase during the contralateral push-off phase. The hip and foot vertical velocities (Vy-hip and Vy-foot) both increase at IHC, resulting from the increase in vertical impulse. The horizontal foot velocity (Vx-foot) decreases, even though Vx-hip is increasing at this point, due to an increase in ipsilateral BF during FF. Because the subject is reaching further, the foot lands with less surface area (greater absolute foot angle). To prevent slipping, the subject must compensate for this by decreasing the horizontal landing velocity. This is consistent with Winter (1983) who found a positive power phase at the knee just prior to heel contact to decelerate the foot and leg. Patla et al. (1989) did not find elevated BF activity for increased SL even though the muscle was active in this phase. This could be due to the lack of accuracy requirement in the design (instructions were to increase SL, without an actual target). Following IHC, the ipsilateral limb shows increased RF activity during the weight acceptance phase to control the amount of knee flexion following the increased vertical landing velocity.

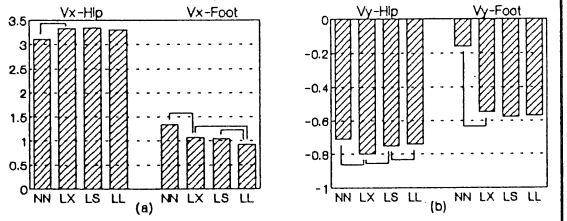

Figure 3: The horizontal (a) and vertical (b) velocities (m/s) of the hip and foot at ipsilateral heel contact.

The above measures indicate that SL is being controlled by ankle push-off, eccentric knee extension at push-off to prevent an overly rapid knee flexion prior to toe-off, hip pull-off and knee extension prior to foot contact. This is consistent with results found by Winter (1992) when speed was varied during steady state walking, and a by-product of the change in speed was a change in SL.

The Effect of Subsequent Step Length Requirements

In the second part of the study, the LX condition was compared against two subsequent SL changes (LS and LL). The kinetic, kinematic and EMG parameters showed significant changes during the first step, even though the foot placement requirement of the first step is identical in the conditions.

The impulse (Fig. 2) showed less deceleration and greater acceleration for the LL step, resulting partially from an increase in SO. The EMG trends indicate less rotational control of the leg during the braking phase, and significantly elevated levels during the push-off phase.

The SL was significantly shorter for the LS condition, and the CM distance also decreased. However, reach was greatest for LS. When the difference between LX and LS of the three measures are compared it appears that reach and CM distances covary (see Fig. 4). The reach is greater to ensure that the CM of the body is farther back relative to foot placement, enabling the deceleration required by the subsequent SL. In this case, balance constrains the available modifications.

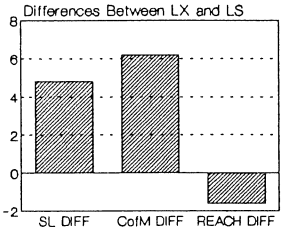

Figure 4: Differences (cm) between LX and LS for the distance measures of SL, CM and reach.

The velocity data (Fig. 3) at IFC showed the Vy-foot and Vx-hip are not significantly different. The Vx-foot decreases significantly for the LL condition, probably to prevent anticipated slipping and the increased accuracy requirement of the task. The Vy-hip decreases for LS, and shows an even greater decrease for LL, returning close to the NN value. In the LX condition, the subject is able to compensate for the Vy increase in subsequent steps because the SL is not constrained. However, when the subject is constrained to a specific SL in the subsequent step, the subject cannot compensate. Prospective modifications in the first step must account for this.

CONCLUSION

Altering the SL during running is a complex task which is under the multisegmental motor control of both the stance and swing limbs. When foot placement is constrained in the subsequent step, the gait parameters show significantly different modifications in both limbs during the first step, even though the requirements for the first step are the same. These adaptive tasks highlight how the task, stability and safety requirements during travel over uneven terrains.

REFERENCES

Lee, DN, et al. J Exp Psych: Human Perc & Perf. 8:448-459, 1982.
Marteniuk, RG, et al. Cdn J Psych. 41(3):365-378, 1987.
Patla, AE. J Exp Psych: Human Perc & Perf. 15(3):624-628, 1989.
Patla, AE, et al. Human Movement Sci. 8:45-66, 1989.
Winter, DA. J Biomech. 16(1):91-97, 1983.
Winter, DA. J Phys Therapy. 72(1):45-53, 1992.

MOTOR CONTROL

Poster

VARIABILITY IN FORCE OUTPUT WITH VARIATIONS IN CHARACTERISTICS OF FORCE PRODUCTION

Les G. Carlton, Y.-T. Liu, and K. M. Newell

Department of Kinesiology,
University of Illinois, Urbana, IL 61801, USA.

INTRODUCTION

Motor activities often require the participant to consistently produce a desired motor outcome over many trials. As an example, sport activities such as target archery assess skill based on the deviation of outcomes from a target. The importance of variability in motor actions extends beyond sport performance and is critical for many fundamental activities. in locomotion stride to stride variations in stride length, stride rate, or height of the swing leg as it passes over the ground can lead to inefficient locomotion or even falls.

The reported experiments examined how the characteristics force production associated with isometric muscle contractions influence the consistency with which forces can be produced. Recent evidence suggests that variability in force production is a function of both the level of force and the rate of force production . The present experiment focused on impulse variability, as well as variability in discrete force production variables such as peak force. Two experiments were conducted which systematically manipulated the characteristics of the required force output.
The results indicated that changes in the to-be-produced force-time curve brought about systematic changes in impulse variability and this effect was more pronounced for larger impulse conditions. The inability of existing theoretical formulations to account for the variability findings led to the generation of a new predicted force variability function. The proposed function accounts for changes in the standard deviation and coefficient of variation of peak force, impulse, and rate of force over a range of force-time conditions.

REVIEW AND THEORY

Over the years a variety of theories and models have been developed to account for variability in the motor system. Initial experimentation on motor variability was designed to test the validity of Weber's Law for perception in the movement domain. As such, it was an initial measure of the psychophysics of the motor system. Subsequent models of motor variability have used information processing, error detection processes, and biomechanical approaches (Schmidt et al., 1979) as the basis for movement outcome predictions.

Recent models have assumed a linear relation between the amount of force produced and variability in producing that force (e.g. Meyer et al., 1982, Schmidt et al., 1979). This assumption has been made for discrete force parameters such as peak force and also for the aggregate of force or impulse. Based on this as well as other assumptions, force variability models have been used to predict trade-offs between speed and accuracy of movement.

There is accumulating evidence, however, that this assumption only holds over small ranges of force level. Nonlinear variability functions for force production parameters such as peak force and impulse size over a large range of force conditions have been linked to the rate of force production (Newell & Carlton, 1988). Increasing the rate of force production in an isometric force task by reducing the criterion time to a given constant peak force, leads to increases in peak force variability (Newell & Carlton, 1988, Experiment 4).

In the present experiments force production characteristics were manipulated to allow for a direct examination of rate of force production while controlling peak force and impulse size. The manipulations also produced conditions with equal impulse size but different durations and peak forces. These manipulations allowed an examination of the influence of rate of force on the variability of force production parameters, and provided a direct test of the assumptions generated by the impulse variability model (Schmidt et al., 1979). It was anticipated, based on previous experiments (e.g. Carlton & Newell, 1985; Newell & Carlton, 1985, 1988), that impulse size alone would not adequately predict impulse variability and that the level of peak force and the rate of force production are strong determiners of impulse variability.

Procedures

The two experiments were nearly identical in procedure. Subjects were required to produce isometric force responses against a force transducer using elbow flexion. The elbow angle was constant at 90 degrees, and the force was generated in the horizontal plane. The subjects task was to consistently produce a template force-time function. This function was displayed on a graphics terminal after each response along with the force time curve produced by the subject for that trial. The force-time characteristics of the conditions are displayed in Figure 1. The subject was given 80 consecutive trials with a specific force-time requirement.

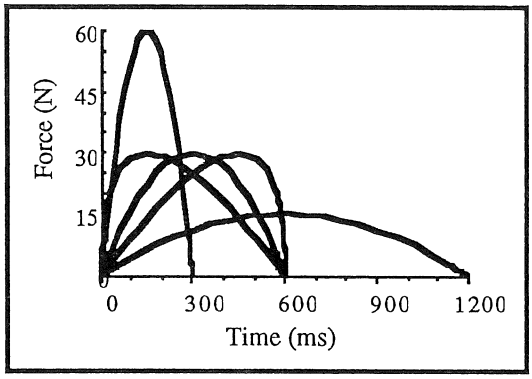

Figure 1. Criterion force-time conditions for Experiment 1

Subjects performed in each of the five conditions. The criterion curves were standard Sandborg-Shaw parabolas. Each of the force-time curves had equal impulse but different peak force, times to peak force, and rates of force production. As can be seen in Figure 1, two of the force-time templates were skewed allowing for three conditions with equal peak force and impulse, but different rates of force production. In Experiment 1 the peak force - time to peak force - force duration combinations were: 60N-150ms-300ms; 30N-300ms-600ms; 30N-150ms-600ms; 30N-450ms-600ms, and 15N-600ms-1200ms. The criterion impulse was identical across conditions at 12 N·s. In experiment 2 the force values were doubled.

Data analysis was performed over the last 50 trials in each condition so that a relatively stable estimate of performance was obtained. The dependent variables included the mean peak force, time to peak force, impulse duration, impulse, and maximum rate of force. The means were computed from Trials 31-80. In addition, within-subject standard deviations from the same trials (i. e., trials 31-80) were calculated along with the coefficient of variation (standard deviation of a distribution of scores divided by the mean of the distribution). If variability in peak force and impulse is proportional to the size of the peak force and impulse,

respectively, the coefficient of variation should remain constant across conditions.

Results and Discussion

The results for the two experiments are combined. Variability in both impulse and discrete force characteristics including peak force and peak rate of force changed significantly as a function of the experimental conditions. Variability in impulse was greatest for the positively skewed force-time curves and the low force level conditions in both experiments. The variability of peak forces was larger for conditions with high peak force values, however, there was not a linear relation between peak force level and peak force variability. This was seen in statistically significant changes in the coefficient of variation of peak force. The greatest relative variability occurred for low force levels. Changing the initial rate of force production while maintaining equal peak forces also significantly influenced peak force variability. The standard deviation of peak force was greatest for the condition with the highest initial rate of force production.

These findings are consistent with a nonlinear force variability description (Newell et al., 1984). Increasing peak force results in an increase in peak force variability but in a less than proportional manner. In addition, increases in time to peak force at the same force level reduces force variability. Based upon these findings an equation was generated to predict the variability of peak force based upon the level of force produced and the time of force production. The proposed equation is:

$$SD_{(Peak\ Force)} \propto (PF^{1/2} / T_{pf}^{1/2})$$

and, therefore,

$$CofV_{(PF)} \propto 1 / (PF^{1/2} * T_{pf}^{1/2}).$$

Based on these predictions and under the assumption that there is no variability over trials in the time of force production, predictions were made for variability of impulse and variability of rate of force production. While the standard deviation equations changed for the different dependent variables, the coefficient of variation remained identical.

The coefficients of variation for peak force, peak rate of force production, and impulse were examined with respect to this predictive equation. The results are presented in Figure 2. As can be seen, there was a close correspondence between the predicted equation and the data for each dependent variable.
The data from this experiment were also examined with respect to the linear and proportional model (Schmidt et al. 1979). The correlation between the coefficient of variation of peak force and peak force was very large (r = -.83). The prediction from the linear and proportional model, however, is that the coefficient of variation should be zero.

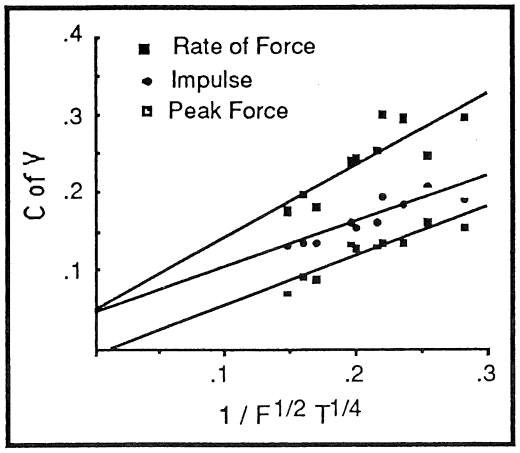

Figure 2. The relation between the CofV and force characteristics

In summary, our findings show that the single discrete impulse parameter of impulse size is not sufficient to predict impulse variability, just as a single discrete force value is not sufficient to predict peak force variability (Newell & Carlton, 1988). The specific force-time properties of impulse production influence the consistency with which impulses can be generated. Variability in space and time in movement tasks will be influenced by impulse variability associated with the required force-time properties of force production as well as variations in the shape of the impulse. Our ongoing work examines the degree to which various physical and neuromuscular models of movement and isometric variability match the coherent description provided here of impulse variability.

Carlton, L. , & Newell, K. (1985). Force variability in isometric tasks. *Biomechanics IX* (pp. 128-132). Winter et al.
Meyer, D. et al. (1988). Optimality in human motor performance: Ideal control of rapid aimed movements. *Psych. Review, 95*, 340-370.
Meyer, D. et al. (1982). Models for the speed and accuracy of aimed movements. *Psych. Rev., 89*, 449-482.
Newell, K., & Carlton, L. (1985). On the relationship between peak force and peak force variability in isometric tasks. J. Motor Behav., *17*, 230-241.
Newell, K. M., & Carlton, L. G. (1988). Force variability in isometric responses. *J. Exp. Psych., 14*, 37-44.
Schmidt, R. et al. (1979). Motor-output variability: A theory for the accuracy of rapid motor acts. *Psychological Review, 86*, 415-441.

LEG KINEMATICS OF CEREBRAL PALSY CYCLISTS: A DYNAMICAL SYSTEM APPROACH

R. Bahamonde and J. Moon

Biomechanics Laboratory, Ball State University, Muncie, IN

INTRODUCTION

Four cerebral palsy cyclists from the United States Elite Cerebral Palsy Camp and one normal competitive cyclist were used to study and compare leg kinematics during cycling. A qualitative dynamics approach was used to evaluate the angular kinematics of the leg. A video camera operating at 60 hz was used to collect the motions of the right leg. The Peak Performance Motion Analysis System was used to digitize and to obtain the joint angular data. Angle-angle plots indicated normal intersegmental coordination patterns between the hip and knee joint, but very erratic patterns between the ankle and knee joints. Phase plots of the knee and hip exhibited a higher degree of joint coupling, contrary to the ankle joint which showed a limited range of motion and a lack of control.

REVIEW AND THEORY

Over the past years many cycling studies have used able-bodied athletes (Gregor, 1976; Nordeen et al., 1975, Pons et al., 1989). However, the increased participation of disabled athletes in competitive sports (over 5,000 athletes in the 1992 Disable Olympic Games) point to a need to also study this population. Cerebral Palsy (CP) athletes participate in a variety of events, including cycling. These athletes must adjust their movement patterns to compensate for abnormal reflexes, muscle spasticity and other coordination problems associated with their condition.

A dynamical system approach was used to analyze and compare the movement patterns of CP cyclists. The area of qualitative dynamics uses topology (shape of graphs) to study the output of a complex dynamical system, in this case a cyclist. This technique has been used by other investigators to compare limb movements (Beuter & Garfinkel, 1985, Winstein & Garfinkel, 1989) of normal and cerebral palsy subjects, and normal and elderly subjects (Beuter, 1984).

PROCEDURES

The sagittal plane of the subjects was videotaped while they rode on a modified bicycle ergometer (toe clips and racing seat). A Peak Performance Motion Analysis System was used to define the joint angles and to obtain the angular velocity data. The raw angular data was smoothed using digital filtering techniques with 6 hz cutoff frequency. Two types of plots were created, phase plane plots and angle-angle plots. The phase plane plots linked the segment velocity with its position, which provided a representation of the control mechanism used by the subjects. The angle-angle plots gave an insight into the intersegmental coordination (Winstein & Garfinkel, 1989).

RESULTS

The results of this study are presented in figures 1-5.

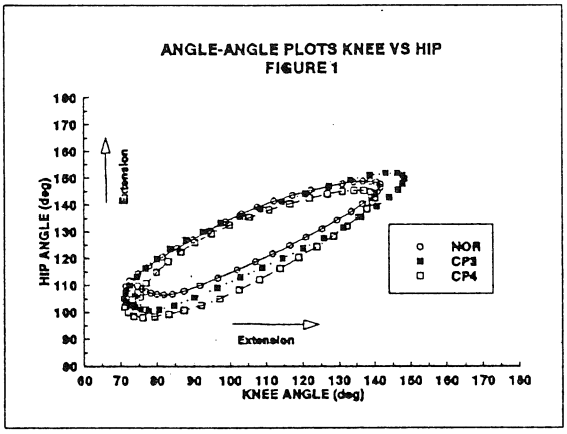

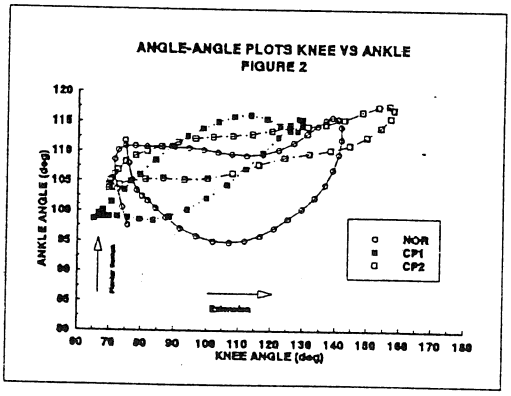

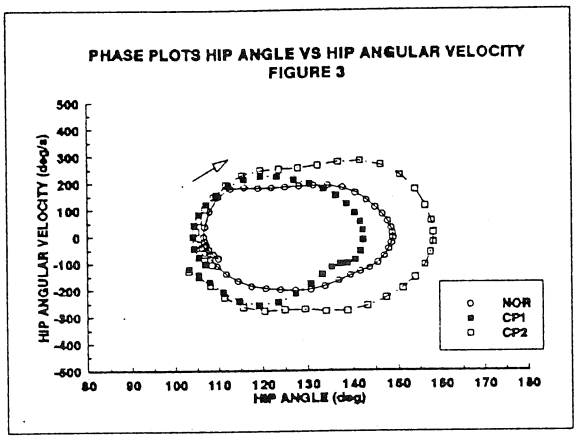

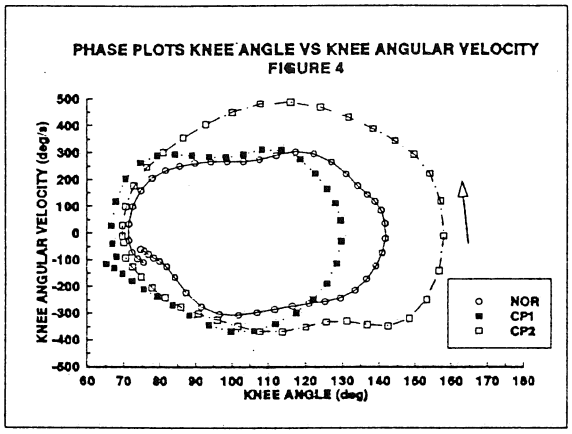

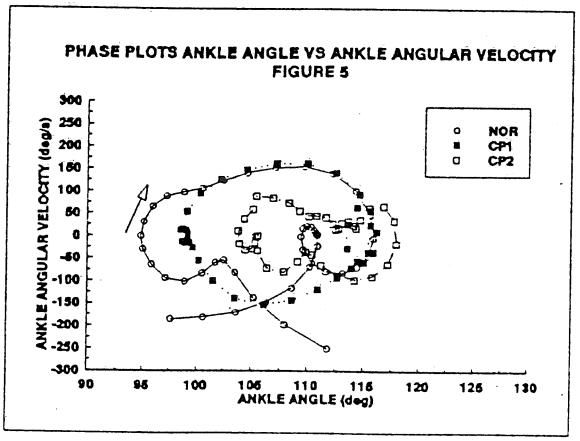

DISCUSSION

Angle-angle plots of the knee vs hip (Figure 1) showed a normal pattern of intersegmental coordination. Both joints extended simultaneously, reaching the turning point synchronization in the angle-angle plots at around BDC (bottom-dead-center of the cycle). From this point, the joints began to simultaneously flex until TDC (top-dead-center).

The knee-ankle plots (Figure 2) of the experienced cyclist demonstrated a normal coordinated pattern. The patterns of the CP cyclist were very erratic, showing a lack of control at the ankle joint, thus preventing them from plantar flexing the ankle joint during the period between TDC and BDC.

Phase plots of the knee and hip joints (Figures 3 & 4) were represented by smooth rounded patterns. This type of patterns is associated with the presence of restoring forces that vary smoothly with position. Each of the ankle phase plots showed different patterns. The CP patterns were characterized by sharp changes in the ankle angular velocity over a a limited range of motion. These alterations indicate abrupt changes of the ankle motion and the lack of proper synchronization of the control mechanism of the joint.

Movement patterns during cycling are highly constrained by the geometry of the cycle, which may force the hip and knee joints of CP athletes to produce smooth joint patterns. Of the three joints of the leg link system the ankle joint is the least constrained. This would explain the erratic patterns found in the CP cyclist.

REFERENCES

Beuter, A., APAQ, 1, 105-111, 1984.
Beuter, et al. APAQ, 2, 214-227, 1985
Gregor, et al., Science of Cycling, 1986.
Pons, et al., Mechanics of Cycling, Biomechanics of Sport., 289-315, 1989.
Winstein, et al. Journal of Motor Behavior, 21, 373-391, 1989.

THE FORCE LOCKED GEAR MECHANISM OF THE KNEE AND ITS SENSORIAL CONTROL SYSTEM.

D. Kubein-Meesenburg, H. Nägerl and J. Fanghänel

Department of Orthodontics, Univ. Göttingen,
Department of Physics, Univ. Göttingen, Germany.
Institute of Anatomy, Univ. Greifswald, Germany.

INTRODUCTION

In order to describe the mechanical structure of the entire knee one cannot merely look at the function of the tibiofemoral joint. The articulating function of the patellar tendon and the patellofemoral joint have to be taken into account, too, because the biomechanical function of the knee is given by the static, kinematic, and dynamic interaction of *three* rigid bodies (tibia, patella, and femur) and with that by three joints: the patellar tendon "joint", the patellofemoral joint and the tibio femoral joint. They are linked up to a gear network with force locked constraint as already described (Kubein-Meesenburg *et al.*(1991)). The patellar tendon joint is always loaded by *tension*. It represents, therefore, a straight dimeric link chain. The patellofemoral joint can be modelled by two overlapped dimeric link chains. These two joints steers the tibiofemoral joint that plays the key role in knee function. It is a force locked, kinematically constrained link quadrangle that is statically stable in all functional positions of the adjacent limbs.

A dominant role of the cruciate ligaments in terms of guidance, as frequently assumed, cannot exist in a force-locked knee for physical reasons. Human beings are able to walk and run with defunct cruciate ligaments. The force transferring structures - the articular surfaces - determine under the terms of the acting force system the relative position of the connected limbs. The articular surfaces are dominant in terms of guidance.

REVIEW AND THEORETICAL IMPLICATIONS

The guidance of the tibiofemoral joint is usually modelled by a four-bar-chain given by the cruciate ligaments. This conception has no physical evidence. The guidance is given by the force transferring structures which take over the acting compressive forces: the articular surfaces. Their differential geometrical structures are the key for the evaluation of the joint's mechanism. For that purpose one has above all to analyse the curvatures of the interacting articular surfaces in antero-posterior, the main functional direction. The guiding structures can be modelled and replaced by dimeric link chains. Their linkage yield a basic gear mechanism which is force locked and mechanically stable. We use the term "stability" as defined in physics. A body, e.g. a lower leg, is in a position of ***stable*** balance if the sum of the acting forces and the sum of the acting torques equal zero (the criteria for balance) ***and*** if a small shift of the body out of its state of balance produces a counteracting force system (criterion for stability).

ANATOMICAL ANALYSIS

In antero-posterior direction both femoral condyles possess convex curvatures, whereas the tibial "plateau" is medially concavely and laterally convexly curved. These two force locked articulating contacts of tibia and femur represent an overlapped and a straight dimeric link chain which transfer the interacting compressive forces and control the kinematics of the joint. By the bony structures, the tibia and the femur, the two chains are linked up to a constrained four-bar-chain (fig. 1). This device has the following properties:

a. In extension the vertical compressing force results in a stable state of the joint: one can stand without muscular balancing or ligamenteous control.
b. The tibia can exclusively rotate backwards. A hyperextension is ruled out by this gear system.
c. Due to the constraint the line (but not the value) of the resultant force loading the joint (muscle tonus) determines the actual relative position of tibia and femur.
d. The tibial positions are normally mechanically stable. A small positional deviation produces a counteracting torque.

DISCUSSION

The traced lines (fig. 1) show the functional four-bar-chain of the tibiofemoral joint in initial position (extension). The lateral centers of curvature (rotational axes) M_{FL} (femoral) and M_{TL} (tibial) represent the lateral straight dimeric link chain. R_L is its pivoting rod. The medial centers of curvature M_{FM} (femoral)and M_{TM} (tibial) define the medial overlapped dimeric link chain. R_M = pivoting rod. The line F (support) is rigidly attached to the femur and T (couple) to the tibia. On principle, this four-bar-chain has two branches of movement. Each one leads to a bending of the knee, to a posterior swinging of the tibia T. Branch p: out of the initial position M_{TL} and M_{TM} move backwards, M_{TL} faster than M_{TM}. After reaching the posterior dead position M_{TM} turns forwards (p_1, p_2). Branch a: M_{TM} only moves forwards (a_1). Which branch is used is determined by the entire gear network of the knee and the acting force system.

Fig. 2 shows the two corresponding fixed centrodes: *p* and *a*. The arrows indicate the migration of the momentary

rotational center while the tibia pivots backwards. T_1 and T_{11} are the momentary centers of the two dead positions of the tibia. The assumed force line f_1 cuts the centrode *a* in A_1. The tibia is then balanced, when its momentary center coincides with A_1. This balance is mechanically stable, when f_1 is cranially directed: a differential small swing of the tibia backwards produces a migration of the momentary center upwards. Consequently, f_1 produces a counteracting torque, which compensates this backward movement. f_2 produces the same balanced position of the tibia. Since f_2 cuts the centrode from the opposite side, the tibial position is now mechanically unstable. The intersection between force and centrode define the balanced tibial position and the angle of intersection the degree of stability. When f_1 coincides with the tangent of *a* in A_1, the tibia is in a neutral equilibrium. Although the muscle tone is working the tibia can be moved without effort and accelerated by small torques. f_1 balances the tibia in the points A_2 and P_1, too. But these equilibria are unstable. In order to stabilize the position P_1 the force line has to be pivoted in P_1 anticlockwise to f_3. Since the resultant applied on the tibia is always cranially directed the tibial positions whose rotational centers lie on *a* between the points M_{FL} and M_{FM} are always unstable: But such great knee bendings are probably not carried out.

Conclusion: Stability is not only a product of the value of musular strength but also a product of its direction. The muscular apparatus can control the extend of stability by pivoting the force line around the momentary rotational center of the tibia with the value of the resultant force remaining unaltered.

The cruciate ligaments function as position monitors and load controlling device: Pacini- and Ruffini-elements are attached to single fibers. They must be stretched like strain gauges in order to function. The number of the extended fibers depends on flexion, the value and the direction of the resultant force. Since the geometrical arrangement of the sensorial elements looks like a measuring bridge, the sensor system is able to record the degree of flexion and the value and the *direction* of joint's load. For instance, one can derive that the difference between the extended fibers in the PCL minus those in the ACL is a function of the bending angle and the direction of force only. Because of the important role that the force direction plays for stability of the joint (as discussed above) the monitoring of the force direction is a crucial point for the joint's functioning. The afferents affect the fusimotor system (Johansson *et al.* (1991)). Thus, the force line and the value of F, and with that the position of the joint is controlled: A compressive force always acts. Guidance by the articular surfaces is guaranteed and stability is controlled. A replacement of the cruciate ligaments does not restore but destroys the sensor system and - physically seeing - does not make any sense.

Final remark: The mechanical contemplations can easily be confirmed by experiments on anatomical models.

REFERENCES

Johansson H., Sjölander P., and P. Sojka: A sensory role for the cruciate ligaments. *Clin Orthop* 268, 161-178, 1991.

Kubein-Meesenburg D., Nägerl H. and J. Fanghänel: Elements of a general theory of joints. 5. Basic mechanics of the knee. *Anat Anz* 173, 131-142, 1991.

FIGURES

Fig. 1: The four-bar-chain of the tibiofemoral joint given by the force-locked guidances of the articular surfaces, details in the text.

Fig. 2: The interaction of fixed centrode and joint load, details in the text..

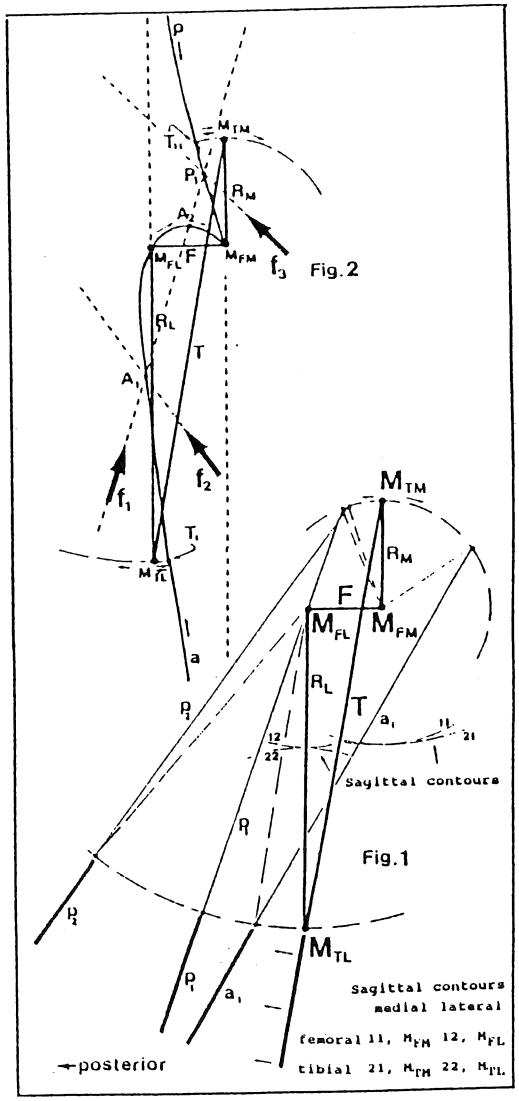

A GENERAL PARADIGMA OF THE KINEMATICS OF LIMBS: THE MOVEMENTS OF THE HUMAN MANDIBLE. MEASUREMENTS AND THEORY.

H. Nägerl, D. Kubein-Meesenburg and J. Fanghänel

Department of Physics, Univ. Göttingen,
Department of Orthodontics, Univ. Göttingen, Germany.
Institute of Anatomy, Univ. Greifswald, Germany.

INTRODUCTION

Corresponding to its dominant guidance the mandible has two different kinds of movement. In cranial border function the mandible is guided by the TMJ and the teeth: It kinematically represents a link quadrangle (Kubein-Meesenburg *et al.* (1988)). TMJ and teeth transfer forces from the mandible to the maxilla. In "free" movements the mandible is guided by the muscular apparatus. The TMJ allows the condyle a certain space of motion: Because of the absence of a compressive joint load the condyle has the possibility to migrate a little bit perpendicularly to the surface of the os temporale. For ergonomic and economical reasons we supposed that the mandibular "free" movements of sound stomatognathic systems obey the Jakobi-Hamilton principle of least action: The set of mandibular movements should be mapped onto a set of geodetic lines in a suitable orthogonal vector space. This implies that the neuromuscular guiding system must anticipate the point aimed at and proceed from the starting point with the correct direction (Nägerl *et al.* (1991). The presented in-vivo-measurements indicate that the mandible of patients with no functional distubances in fact moves along geodetic lines (fig. 1a). This is not the case in patients with disturbances (fig. 1b).

PROCEDURES

The in-vivo-measurements are carried out by means of a very light (=30g) ultrasonic system that is able to detect all six degrees of freedom. Class-I-patients were asked to move their mandible in the sagittal plane along the borders of the space of motion and from centric occlusion to full mouth aperture, and to carry out lateral movements. The fixed and the moved momentary helical axes were determined.

RESULTS

For all types of movement we can state that sound patients do not carry out screw motions: the screw displacement is actually zero. In general the mandible performs spherical movements or, in particular, plane movements parallel to the sagittal plane. Beyond that analyses yield that both the spherical and the plane movements are limited to *two* degrees of freedom. That means: At least one mandibular point exists whose path remains identical in all typs of movement. Consequently, we have a mandibularly fixed rotational axis C_s that moves - sideways looking - along the same path s in all sagittal plane movements (fig. 2). The other mandibular points (e.g. C_e or E) carry out loops and show hystereses. C_s is of no apparent anatomical significance. It is positioned at or beyond the upper margin of the anatomical structures of the TMJ. This neuromuscular guided movable axis C_s is in no way identical to the so called "hinge axis" that does demonstrably not exist. Since the paths can be approximated by a circle, the neuromuscular guidance is structurally identical to that of a maxillarily fixed rotational axis B and an mandibularly fixed rotational axis C_s. C_s moves on a cylinder (plane movements) or a cone shaped jacket (spherical movements) around B. We say: The mandible is guided by a ***neuromuscular dimeric link chain.*** Its rod R_2 is the structural constant of all mandibular movements. The momentary mandibular movement is determined by the two angular velocities $d\mu/dt$ and $d\delta/dt$. Thereby suitable orthogonal variables are found for describing the mandible's position. We use the angles μ and $\alpha = \mu + \delta$ (fig. 1).

DISCUSSION AND THEORY

Figs. 1a and 1b show the plane border movements and additionally the free mouth aperture. The mandible starts in centric occlusion $\delta = \alpha = 0$. The individual types of movement can be clearly distinguished:
I = freely guided mouth aperture,
II = mouth aperture after maximal cranial border protrusion,
III = mouth aperture after maximal "prerotation",
IV = posterior prerotation,
V = protrusive cranial boreder movement.
The data of the sound patient yield practically straight paths of the mandible's movement (fig. 1a). For every kinematical function the derivative

$$d\alpha/d\mu = \text{const.}$$

Because of

$$d\alpha/d\mu = (d\alpha/dt)/(d\mu/dt) = \Omega_\alpha / \Omega_\mu$$

follows that straight paths in this orthogonal (α,μ)-presentation involve a constant quotient of the two angular velocities Ω_α and Ω_ν or $\Omega_\alpha - \Omega_\mu$ and Ω_μ When Ω_μ is positively

signed, Ω_δ is always negative, since $\Omega_\mu > \Omega_\alpha$. The mandible simultaneously carries out two rotations with opposite directions. It revolves at the velocity Ω_μ around B and at Ω_δ around C_s. From plane kinematics of rigid bodies we can conclude that the momentary rotational axis P of the mandible lies on the prolonging of the link R_2 of the neuromuscular dimeric link chain. For the distances l_μ (between B and P) and l_δ (between C_s and P) the formula

$$l_\mu / l_\delta = - \Omega_\delta / \Omega_\mu$$

holds true. Patients with sound neuromuscular guidance show plane movements of the mandible whose ***fixed and movable centrodes are circles.*** Their centers coincide with the fixed or the movable axis of the neuromuscular dimeric link chain, resp. The plane mandibular movement is structurally identical to the unrolling of a smaller circular cylinder within a greater one. The difference of their radii $l_\mu - l_\delta = R_2$ is the constant of all plane movements. Consequently, the paths of the single mandibular points are hypocycloids. Additionally, the data reveals that lateral spherical movements show the same features: A smaller circular cone unrolls within a greater one.

Patients with neuromuscular disorders do not bear these characteristics. E.g. a patient who was operated on an abnormal facial development (fig. 1b) uses a constant quotient $\Omega_\delta / \Omega_\mu$ only for the partial movement "mouth aperture after pre-rotation". Free mouth aperture and mouth aperture after maximal cranial protrusion drastically deviates from a straight line: The mandible does no longer run along a geodetic line. The neuromuscular guidance of the mandible does not anticipate the point aimed at. The mandible starts with a wrong quotient $\Omega_\delta / \Omega_\mu$ that means: towards a wrong direction. In order to reach the desired position the neuromuscular feedback system has to counteract. A distinct feedback oscillation occurs. Its amplitude can be interpreted as a measure of functional disorder.

REFERENCES

Kubein-Meesenburg D., Nägerl H. and B. Klamt: The biomechanical relation between incisal and condylar guidance in man. *J. Biomechanics*, 12, 997-1009, 1988.

Nägerl H., Kubein-Meesenburg D., J. Fanghänel, K.M. Thieme, B. Klamt and R. Schwestka-Polly: Elements of a general theory of joints. 6. General structure of mandibular movements. *Anat. Anz.*, 173, 249-264, 1991.

FIGURES

Fig. 1a: (α,μ)-diagram of plane mandibular movements. Patient with undisturbed neuromuscular guidance. The partial movements I_1, I_2, II, III, IV can be approximated by straight lines. The constancy of inclination indicates a constant ratio of the angular velocities around the two axes of the neuromuscular dimeric link chain. I, II, III, IV have negative slopes: the two rotations are opposite. V, the force transferring cranial border movement possesses two poles of the derivative function. This is an expression of guidance by the bony structures.

Fig. 1b: (α,μ)-diagram of plane mandibular movements. Patient with disturbed neuromuscular guidance.

Fig. 2: Paths of three mandibular points at plane movements of the mandible. Modelling the neuromuscular guidance by a neuromuscular dimeric link chain.

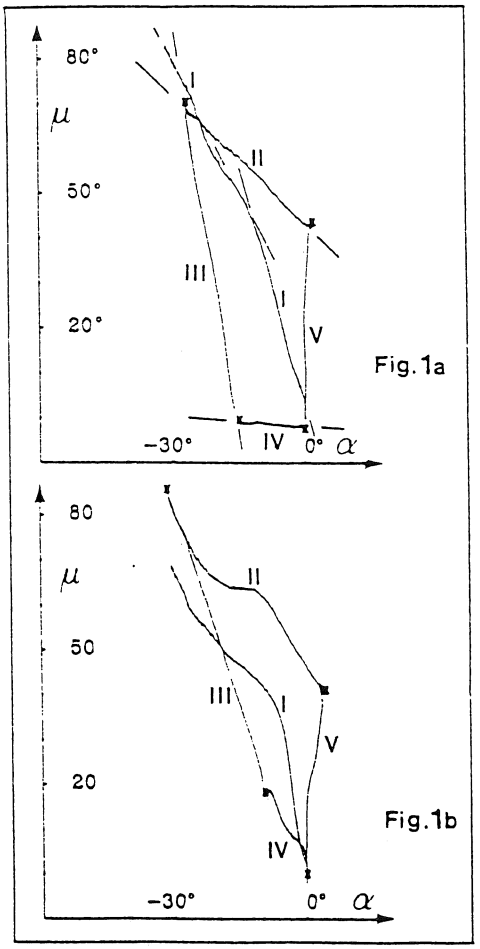

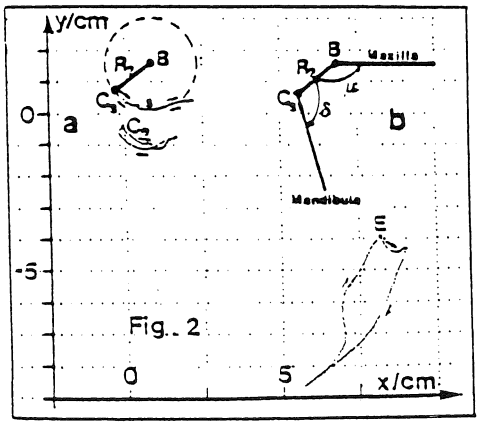

THE EFFECT OF TWO BIOMECHANICAL MANIPULATIONS ON MOTOR TIME / ELECTROMECHANICAL DELAY

Philip K. Schot, Jolene A. Dart, Susan R. Griffin, & Barbara A. Hart
Department of Human Kinetics, University of Wisconsin - Milwaukee

INTRODUCTION

The time elapsed between the sequential events of a simple reaction time task (stimulus presentation, muscle activation, and movement initiation) delineate central (premotor time: PMT) and peripheral (motor time: MT) neuromuscular activity. The peripheral component is also known as electromechanical delay (EMD). The PMT is dependent upon cognitive and neural transmission processes and independent of the MT/EMD (Schmidt & Stull, 1970). The duration of the MT/EMD has been shown to be mediated by factors such as fiber type, rate of tension development and maximum tension capability (Viitasalo & Komi, 1981) and the stretch-state of the series elastic component (SEC) (Norman & Komi, 1979).

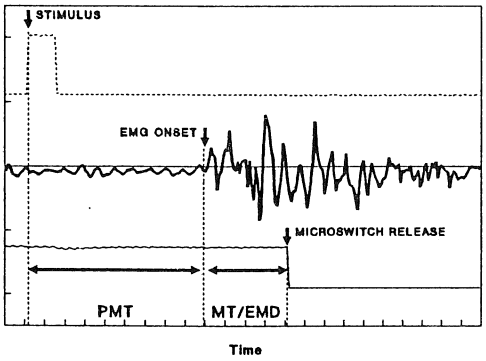

Figure 1. Determination of MT/EMD.

While many of the MT/EMD determinants are neurological or physiological in nature, the SEC factor may be characterized as biomechanical. The role of the SEC has been identified as the primary MT/EMD determinant in at least one study (Norman & Komi, 1979). The elastic nature of muscle interacts with the inertia of the segment to which tension is transmitted to determine the load dependent length at which movement occurs. Initiating movement from varied relative joint angles is assumed to affect gross muscle length and the stretch-status of the SEC, but studies examining MT/EMD responses to this manipulation report inconsistent findings (Furubayashi & Kasai, 1990; Grabiner, 1986; Norman & Komi, 1979). Studies examining the effect of resistance (Kamen, Kroll, Clarkson, & Zigon, 1981) and fatigue (Kroll, 1973) on MT/EMD have also demonstrated inconsistencies. In a relative sense, added resistance or induced fatigue might be akin to varying the segment moment of inertia.

The purpose of this study was to examine the effects of two biomechanical factors on MT/EMD, specifically segment moment of inertia and initial joint position. It was hypothesized that 1) increasing the distal segment moment of inertia and 2) initiating motion from a joint angle that reduces gross agonist muscle length (implied SEC stretch) would each increase MT/EMD.

METHODS

Four adult (2 males and 2 females) volunteers served as subjects for this study. The movement activity used to observe the MT/EMD response was elbow extension using a simple reaction time task. Two test conditions were examined in which the gross agonist muscle length (ML) or the distal segment moment of inertia (SI) was manipulated. For all conditions the dominant arm was positioned in 90° of abduction and full forearm pronation supported on a smooth testing surface while grasping a tennis ball. The upper arm was stabilized to prevent extraneous movement. For the control condition (CC) the relative elbow angle was 55° (full extension = 180°) with an unweighted ball. For SI the elbow angle was 55° and a weighted tennis ball (additional 5.9 N) was grasped. For ML the elbow angle was 125° using an unweighted ball.

Subjects were instructed to place the hand against a microswitch and remove the hand from the switch via elbow extension as quickly as possible after perceiving the stimulus presentation. When the switch was closed, a red warning light was illuminated. After a randomly selected interval of 1.5, 2.0 or 2.5 s the green stimulus light was presented. The warning and stimulus presentations were computer controlled using a specifically developed data acquisition system (DAS-416, Technology Resources). Each subject performed 15 trials under each of the three conditions.

EMG recordings were obtained from the belly of the medial head of the triceps brachii. Surface electrodes were placed 2 cm apart after standard skin preparation. The stimulus light, microswitch, and EMG signals were digitally sampled at 2000 Hz using the DAS-416 and stored on hard disk for subsequent processing. EMG onset and microswitch release events were manually marked for each trial with MT/EMD quantified as the time between these events. Group and individual subject statistical tests were conducted for each biomechanical perturbation separately using the Model Statistic technique (Dufek & Bates, 1991) at $p \leq .05$.

RESULTS

Moment of Inertia Manipulation: Use of the weighted ball resulted in an average increase of the moment of inertia by 106% Significant group effects were observed for the SI manipulation. As a group, when SI was increased MT/EMD increased by approximately 7 ms. The single subject analysis indicated inter-

individual response variability. Two subjects (S1,S3) demonstrated significant SI responses with a mean MT/EMD increase of 11.5 ms while two subjects exhibited non-significant SI effects.

Table 1. Effects of Inertial Manipulation.

Subject	Sex	I_c	I_x	Increase
S1	F	0.045	0.103	129%
S2	F	0.056	0.122	118%
S3	M	0.085	0.159	87%
S4	M	0.091	0.174	91%

Note: I = $kg \cdot m^2$, I_c=control, I_x=experimental

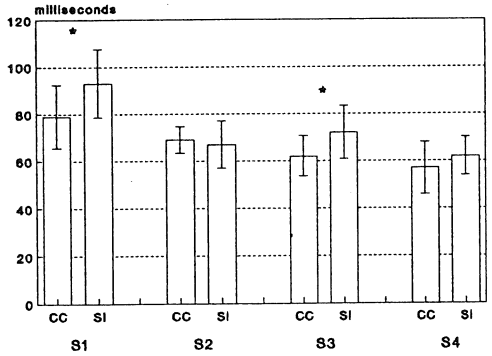

Figure 2. Single subject mean and standard deviations of MT/EMD for SI manipulation.

Gross Muscle Length Manipulation: Group and individual subject ML response patterns were similar to those of the SI results. Initiating motion from ML, the less stretched condition, lead to an average MT/EMD increase of 7.5 ms. The same two individual subjects demonstrated significant responses to the manipulation (mean MT/EMD increase of 19 ms) while S2 and S4 demonstrated no significant ML effects.

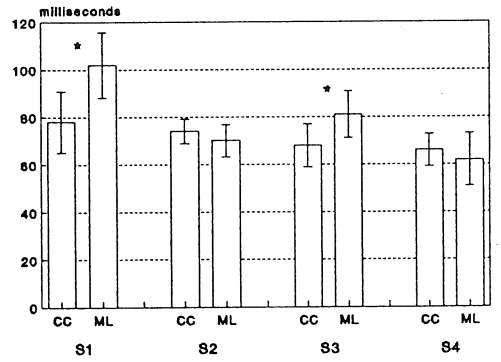

Figure 3. Single subject mean and standard deviation of MT/EMD for ML manipulation.

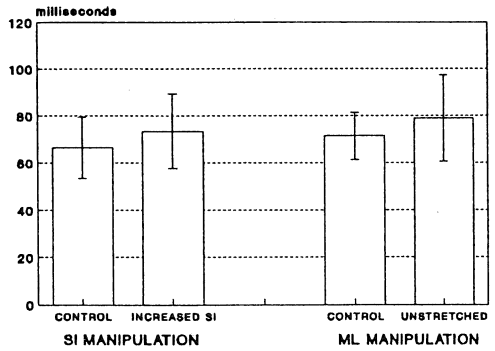

Figure 4. Group mean and standard deviation of MT/EMD for SI and ML manipulations.

DISCUSSION

The results demonstrated inter-subject response variability. Two subjects exhibited significant SI and ML effects and two did not. The relative increase in the SI does not appear to explain this observation; the two subjects demonstrating SI effects experienced the greatest and the least relative SI changes. MT/EMD responses were also split equally across gender. Strength tests and muscle fiber typing were not conducted. These characteristics may contribute to the observed inter-subject variation.

The results of this study carry methodological implications. The non-significant findings by Furubayashi & Kasai (1990) might be attributable to the interaction of the SEC and SI. Movement in their study apparently occurred in the vertical plane such that in the unstretched position, the limb was self supported. If so, the SEC would have been stretched under both test conditions, confounding ML effects.

When efforts are directed toward establishing normative standards, or comparing neuromuscular characteristics of specific populations, methodologies must be consistent. Using a horizontal manipulandum may control for gravitational effects, but the increased inertia of the system can influence results. The position from which movement is initiated may also impact results. Unless equivalent protocols are applied cross study comparisons may be invalid.

REFERENCES

Dufek, J., et al, 1991. Med.Sci.Sport.Ex., 23: 1062-1067.
Furubayashi, T., et al, 1990. Hum.Mov.Sci., 9: 583-598.
Grabiner, M., 1986. Med.Sci.Sport.Ex., 18: 37-43.
Kamen, G., et al, 1981. J.Mot.Behav., 13: 117-129.
Kroll, W., 1973. J.Mot.Behav., 5: 81-93.
Norman, R., et al, 1979. Acta.Physiol.Scand., 106: 241-248.
Schmidt, R., et al, 1970. J.Mot.Behav., 2: 96-110.
Viitasalo, J., et al, 1981. Acta.Physiol.Scand., 111: 97-103.

A 3D PASSIVE MECHANICAL MODEL OF THE HUMAN FOOT FOR USE IN LOCOMOTION SYNTHESIS

D. Meglan and †N. Berme
Orthopaedic Biomechanics Lab, Mayo Clinic, Rochester, MN
†Department of Mechanical Engineering, The Ohio State University, Columbus, Ohio

INTRODUCTION

A key element of any model attempting to synthesize mathematically human locomotive activities (walking, running, stair as/descending) is the interface or contact conditions between the feet and the ground. Proper modeling entails not only inclusion of frictional conditions but also the geometry of the foot sole and the material property characteristics of the foot and ground as well. To accomplish this a passive dynamic model of the foot has been developed which can reproduce experimentally measured distributions of forces as well as overall ground reaction resultant loads (vertical and shearing forces as well as torsion normal to the ground) under the foot during general human locomotion.

REVIEW

A number of sophisticated human locomotion models have been developed in which less effort was exerted upon the foot/ground representation than was focused upon the rest of the body elements [Hatze (1981), Pandy et al. (1988)]. Other locomotion synthesis models have included more detailed representations of the foot [Hemami et al. (1987), Yamaguchi et al. (1989)]. These models have been two dimensional and have not included the toes which have been shown to be critical to proper walking [Mann et al. (1979)]. The methods by which the models have been mathematically constructed and evaluated have limited their generality. More general three dimensional foot/ground models that can be applied to various locomotive tasks involving dynamic conditions ranging from quasistatic to high velocity impact are necessary if the foot model is to be part of a generalized human locomotion synthesis, full body model.

Some studies have focused exclusively upon modeling the foot rather than making it a part of a larger simulation. The foot has been modeled with varying complexity from a single flexible structure [Kofman et al. (1987)] to a multiple segment body connected by ligaments and joint surfaces and driven by muscles [Morlock (1989)]. In most models, no mechanical properties of the foot sole were included and the focus was toward analysis of foot muscle and structure function rather than synthesis of foot motion and load distribution.

The model developed here is a compromise between mathematical complexity and fidelity of the model to represent the actual structures of the foot.. The objective was to estimate the center of pressure (CP) and normal and shear force as well as torque normal to the ground using a model with a minimum of components.

PROCEDURES

A 3D foot model consisting of a rigid frame to which is attached nonlinear, viscoelastic deformable spheres representing the foot sole and rigid toes connected by revolute joints was developed. The number of balls and toes, their size, and their exact placement could easily be modified so that several models of varying complexity were created. The foot geometry, including the ankle joint, was defined relative to a foot local coordinate system (LCS) located at the foot center of mass whose location as well as the mass, inertia, and principal axes of inertia were determined from anthropometric data. An example of the foot geometry can be seen in figure 1. The ground was represented by a general, frictional plane and a mathematical technique was derived to determine the 3D foot contact. Shearing force was modeled with coulomb friction with adjustments for small velocity conditions. Whole foot ground reaction load (GRL) and center of pressure (CP) were determined by summing the ball and toe forces as calculated from their kinematic contact conditions.

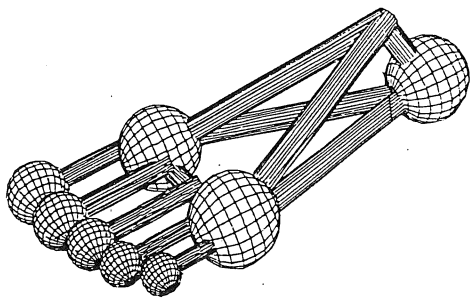

Figure 1. Example of a foot model geometry with three balls and five toes

The material properties of the spheres were estimated from published *in vivo* human heel pad impact response data [Valiant et al. (1990)]. The load-deformation curves show a behavior that, using only passive

mechanical elements, must be described by a system consisting of both nonlinear stiffness and damping. Beginning with an equation based upon the Theory of Elasticity, an optimization procedure was carried out to determine the form of the equation that best reflected the measured heel deformation.

Two foot geometries (one with only 3 balls and the other with 7 balls and 5 toes), derived from a single subject, were tested using two different methods applied to a single set of measured 3D motion/force gait data. One method, called the kinematically (KIN) driven case, consisted of moving the foot along its kinematic trajectory and computing the foot GRL and CP. The other, the dynamically (DYN) driven case, involved applying the ankle resultant joint loads, computed from the gait data, along with the GRL, computed from the model -ground contact conditions, to the dynamic equations of the foot and numerically integrating the resulting foot accelerations combined with initial foot kinematics to obtain an estimate of the foot kinematic trajectory and GRL's during the observed gait cycle.

RESULTS

The simulated impact response, in terms of the deformation and force time histories, for the foot sole spheres properties as determined via optimization reproduced the published data very well. The property equations were used for all spheres in the foot models.

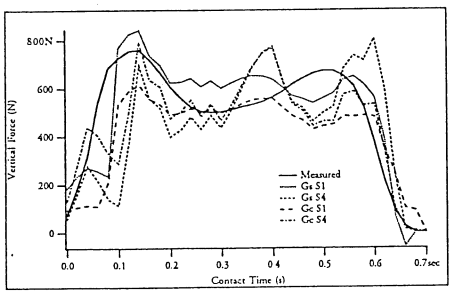

Figure 2. Effect of model complexity upon normal GRL for kinematically driven simulation

The KIN case generated normal force time histories similar to those measured using both foot geometries. The shear forces had similar patterns to the measured forces while the magnitudes of the model forces were several times greater than those measured. The CP path corresponded well with that measured. The DYN simulation yielded GRL patterns which were closer to the experimentally measured data than in the KIN case. The magnitude of both the normal and shear forces corresponded well with the measured though several spikes were observed in the model estimated forces. The model CP path was within 10mm of the measured CP path but oscillated during the foot contact time. It was found that the more complex model geometry produced CP's and GRL's which more closely approximated the measured data but the difference between models was small.

DISCUSSION

The inconsistencies between the model estimated ground reaction shear forces in the KIN case and those measured were traced to inaccuracies in the measured foot kinematics. The motion measurement system resolution for the gait volume used was approximately 4mm and such an uncertainty was sufficient to cause the observed variations between model and actual forces. These errors can be improved by using a smaller measurement volume to increase the resolution of the measured kinematics.

The DYN simulation was difficult to implement. A number of factors were found to make the computer model numerically ill-conditioned. The differential equations describing the foot dynamics were stiff due in part to the nonlinear behavior of the materials in the model. In addition, the model stability was sensitive to the foot mass and inertia. The spiking in the GRF and oscillation in the CP path of the model were the result of the foot rocking while it was in contact with the ground. The spikes occurred when a foot sole sphere struck the ground. The foot motion resulted from the unstable nature of the dynamic equations.

The difficulties encountered in both the KIN and DYN simulations are the result of the simulation approaches and not the foot model itself. The simulation results showed that the model behaved satisfactorily. The foot model has been successfully included in a dynamic simulation of full body locomotion involving 13 body segments. The minimal differences observed here between different foot model geometries was obscured by the difficulties in the simulation approaches. Future improvements of the foot model should further focus upon the tradeoff between model complexity and accuracy. In addition, the specificity of the foot model to individual subjects should be examined.

REFERENCES

Hatze, H., *J Biomech* 14:135-142, 1981.
Hemami, H. et al. *Math Biosci* 61:163-189, 1982.
Kofman, J., et al. *XI Int Cong Biomech*, 166, 1987.
Mann, R.A. et al. *Clin Ortho Rel Res* 142:24-9, 1979.
Morlock, M.M. *XII Int Cong Biomech*, 192, 1989
Pandy, M.G. et al. *J Biomech* 21:1043-1052, 1988.
Valiant, G.A. et al. *The Biomechanics of Distance Running*, 225-248, 1990.
Yamaguchi, G.T. et al. *XII Int Cong Biomech*, 166, 1989.

BONE REMODELLING

Podium Session 15

MECHANICAL BEHAVIOR OF A NEW SUBSTRATUM FOR STRAIN-MEDIATED CELL CULTURE EXPERIMENTS

D.R. Pedersen, T.D. Brown, and A.J. Banes*
Department of Orthopaedic Surgery, University of Iowa, Iowa City Iowa
*Department of Surgery, University of North Carolina, Chapel Hill

INTRODUCTION: Mechanical stimuli play a crucial role in the regulation of a wide variety of cellular activities, including migration, contraction, 2d messenger production, cell division, and matrix production. For studying such relationships, cell culture systems offer an attractive alternative to the complexities of the in vivo environment. Initially, these efforts focused on highly specialized in-house systems targeting narrow ranges of applications. More recently, general purpose turn-key systems have proven increasingly attractive, one design (the Flexercell system [1]) having been adopted by well over fifty laboratories since being made commercially available in 1988.

A common limitation of current culture stimulus systems is the spatial inhomogeneity of their mechanical input. For the case of Flexercell, which involves a rubber diaphragm (currently 25 mm diameter, 2.2 mm thick) induced to deform by vacuum applied to its undersurface, both the radial and the circumferential components of strain at the upper diaphragm surface are strong functions of distance from the center [2]. The need for increased homogeneity has recently prompted the development of a new, much thinner (0.5 mm) diaphragm, for which static quasilinear finite element calculations suggest nearly uniform radial strains over about 70% of the surface area [3]. However, because of the low elastic stiffness of the new diaphragm design, gravitational and inertial effects within the diaphragm itself and in the overlying layer of culture nutrient medium may lead to surface strain distributions less homogeneous than those predicted by quasistatic analysis. A parametric finite element analysis was therefore undertaken to study diaphragm dynamics across a range of input frequencies attainable by the Flexercell vacuum control system.

METHOD: An experimental diaphragm, made of cured silicone elastomer, was modelled as an incompressible, isotropic hyperelastic continuum. The governing strain energy potential was of the form

$$U = C_{10} (I_1 - 3) + C_{01} (I_2 - 3),$$

where I_1 and I_2 are deviatoric strain invariants, and C_{10} and C_{01} are classical Mooney-Rivlin constitutive coefficients. An axisymmetric finite element formulation was adopted (Fig 1), using 8-node nonlinear (i.e., large deformation) elements. The diaphragm per se was zoned into four layers, each having 56 elements radially. An overlying 12 mm deep layer of culture medium was modelled as an extremely compliant (i.e., fluid-like) hyperelastic continuum, using a fifth layer (not shown) of 56 elements. The diaphragm was assumed to be rigidly tethered peripherally by upper and lower confinement of its integral O-ring, and deformations were induced by variations of the undersurface vacuum. Densities of the

elastomer and culture medium were taken as 1.13 and 1.0 g/cc, respectively. This dynamic, nonlinear problem was solved using the Abaqus finite element program running on a VAXStation 4000-60, with typical execution times on the order of 30 minutes.

RESULTS AND DISCUSSION: Evolution of time-variant diaphragm upper surface radial strain distributions is compared in Figure 2 at several driving vacuum levels, for a quasistatic case in which membrane weight and nutrient medium are neglected, versus for a typical dynamic (1 Hz) case that includes membrane and nutient mass effects. The relatively simple displacement history and nearly homogeneous radial strains prevalent quasistatically are appreciably complicated dynamically, by superimposed deformation waves initially propagating inwardly from the O-ring. Depending upon the driving frequency, the time history of strain experienced by a given point on the diaphragm was highly site-specific (indeed, often non-monotonic), even though the maximum radial strains were reasonably uniform. These data indicate that the new diaphragm appears to achieve its main design goal of increased peak strain homogeneity. However, stimulus protocols involving rapidly oscillatory pressure inputs will certainly develop very complex local strain histories, potentially meriting attention as a factor confounding the biologic response attributable to the peak strain levels per se.

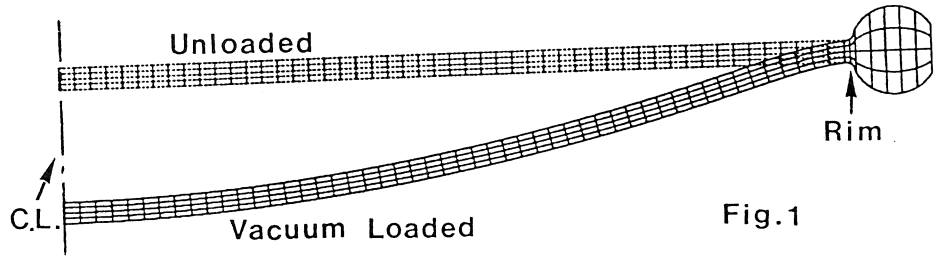

Fig.1

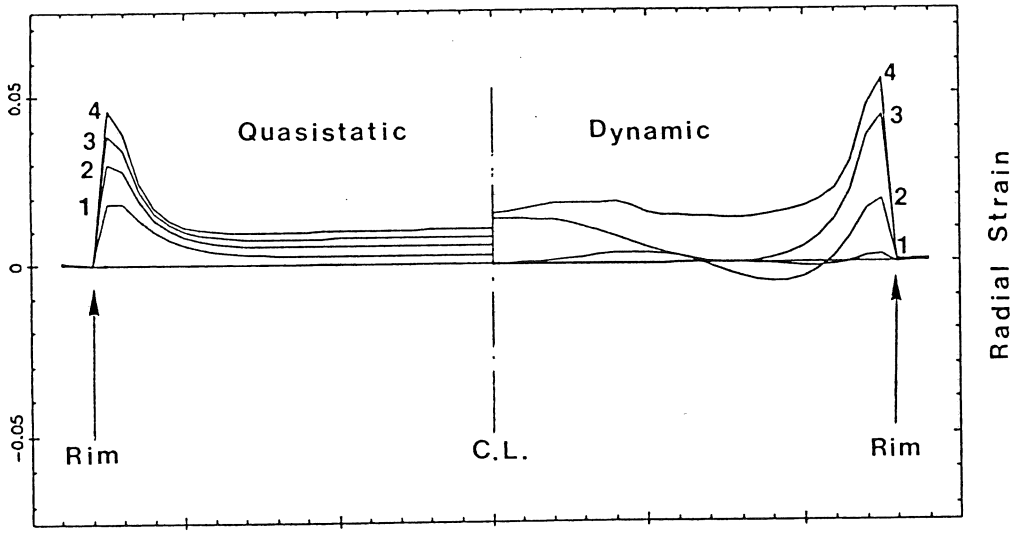

REFERENCES: (1) Banes et al, J. Cell Sci. 75:35-42, 1985; (2) Gilbert et al, Exptl. Tech. 43-45, Oct 1990; (3) Gilbert, personal comm., 1992.
ACKNOWLEDGEMENT: NIH AR-38121

THE DEVELOPMENT OF MICROSTRUCTURE IN CANCELLOUS BONE

N.L.Fazzalari*, D.P.Fyhrie, T.E.Wenzel, M.B.Schaffler

Breech Research Laboratory, Bone and Joint Center
Henry Ford Hospital, Detroit MI 48202 USA
* Visiting from: Institute of Medical and Veterinary Science, Adelaide AUSTRALIA

INTRODUCTION: Formation of cancellous bone from a growth plate is critical in the development of the metaphyses of long bones and of the centra of the vertebral bodies. The resorption of growth plate cartilage, and its replacement by, first, calcified cartilage, and subsequently, primary and secondary cancellous bone is a complex process which may strongly determine adult trabecular morphology. The purpose of this study was to quantify the morphological changes occuring during this growth process. It was shown that the microstructure of the secondary cancellous bone in the metaphysis of rapidly growing rabbits is directly related to the primary calcified cartilage model formed from the hypertrophic zone of the growth plate. Distal from the growth plate, the number of trabeculae declines in a predictable way as the calcified cartilage structure is replaced by bone and then remodeled into secondary lamellar trabecular bone. The endpoint of this growth process certainly determines the number density of trabeculae in the metaphysis. It may also determine the degree to which the secondary trabecular bone can adaptively remodel its microstructure in response to changes in stress and strain throughout life, even after metaphyseal growth has ceased.

METHODS: The proximal tibiae of seven cage-raised female New Zealand white rabbits, 6 to 7 weeks old, were retrieved at necropsy and immersion fixed in neutral buffered formalin. The specimens were decalcified in EDTA, embedded in methylmethacrylate and sectioned using a microtome to a thickness of 3 micrometers. The sections were stained with Safranin-O and fast green to differentiate the calcified cartilage from the primary and secondary bony trabeculae. One section was chosen randomly for stereological evaluation from a set of five sections spaced 10 micrometers apart. The evaluation consisted of measuring stereological point count data that are related to the number of trabeculae per mm (N_l) and to the amount of hard tissue in the crossection (BA/TA). The data collected were: 1) The number of intersections which a grid of parallel lines makes with the bone surface per total length of grid lines ($P_l=2N_l$) and, 2), The number of grid test points on bone per total number of grid test points (P_p=BA/TA) (1). Quantitation was started at the hypertrophic zone in the growth plate and continued distally through the primary trabecular elements down to the secondary lamellar trabecular structure (Fig.1). Trabecular structure was sampled systematically, parallel to the growth plate, at 0.24mm intervals to a depth of 3.12mm. Data were plotted as P_l and P_p versus distance (D) into the metaphysis from the hypertrophic zone of the growth plate.

RESULTS: This study showed that the number of trabeculae (as measured by P_l) is inversely related to the distance from the growth plate ($P_l=21.68*D^{-0.85}$, $R^2=0.811$ Fig.2) and that the bone volume fraction (measured by P_p) is not related to distance from the growth plate (Fig. 3). The inverse relationship between number (P_l) and distance (D) shows a rapid decrease in the number of trabeculae with distance from the the large number of elements created by calcification of the cartilage down to the smaller number of trabeculae of the secondary cancellous structure.

This decrease in trabecular number with distance from the growth plate can be modeled as a decimation process where trabeculae are eliminated as a function of a characteristic length from the calcification front. If every other trabecula is eliminated for some characteristic length from the growth plate, then the mathematical expression for this decimation of structure is: $P_l=50.65*2^{-D/1.05}$, $R^2=0.75$ where D=1.05mm is the characteristic distance from the growth plate in which P_l falls to half the original value, Fig.2.

DISCUSSION: The ability of cancellous bone to adapt from one microstructure to another, and its ability to sustain a loss of trabecular elements during osteoporosis may be limited by

The Sixteenth Annual Conference of the American Society of Biomechanics and
The Seventh Biennial Conference of the Canadian Society of Biomechanics/Société Canadienne de Biomécanique

the initial state of the structure. Therefore, the origin of metaphyseal and vertebral trabecular patterns is of fundamental importance. From a quantitative examination of human autopsy specimens, Johnson (1966), proposed that a halving of the number of metaphyseal trabeculae occurs over some characteristic distance from the growth plate. Our rabbit data strongly support this hypothesis, indicating that the biological process of metaphyseal cancellous bone formation is quantitatively similar between the two species. Current studies are underway to determine whether the relationship is similar for other species over a large size range (rodentia to bovidae).

Abnormal cancellous bone development may be a sensitive early indicator for age related bone and joint conditions. For example, the data of Fazzalari et al (1985) indicate that cancellous bone from the femoral neck of osteoarthrotic patients has only about half as many trabeculae as does cancellous bone from the neck of either normal or osteoporotic people. Whether this difference in trabecular number is due to changes that occur in adult life or to differences in growth pattern is not currently known. However, if the difference is growth related, the potential for early diagnosis of a tendency towards osteoarthrosis is significant. The recent development of new radiological methods applicable to the in vivo characterization of cancellous bone morphology (Reimann et al, 1992) now makes it possible to test this hypothesis.

REFERENCES: 1) Whitehouse WJ, J. Microscopy 101:153-168,1974. 2) Johnson LC, Birth Defects 2:66-142,1966. 3) Fazzalari NL, et al. Bone 6:125-133,1985. 4) Reimann D, Fyhrie D, Fazzalari N, Schaffler M, Trans 38th Mtg ORS, 561, 1992. **Acknowledgments:** The Whitaker Foundation and NIH AR40776.

Fig. 1)



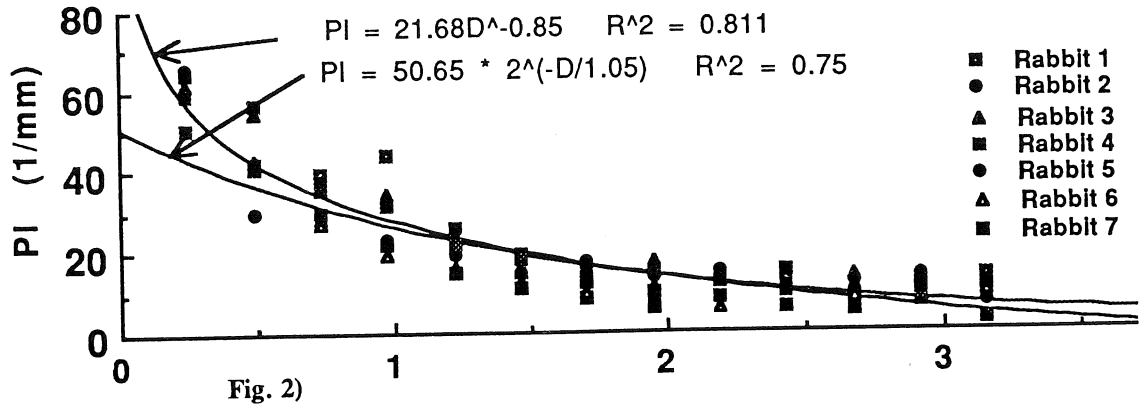

Fig. 2)

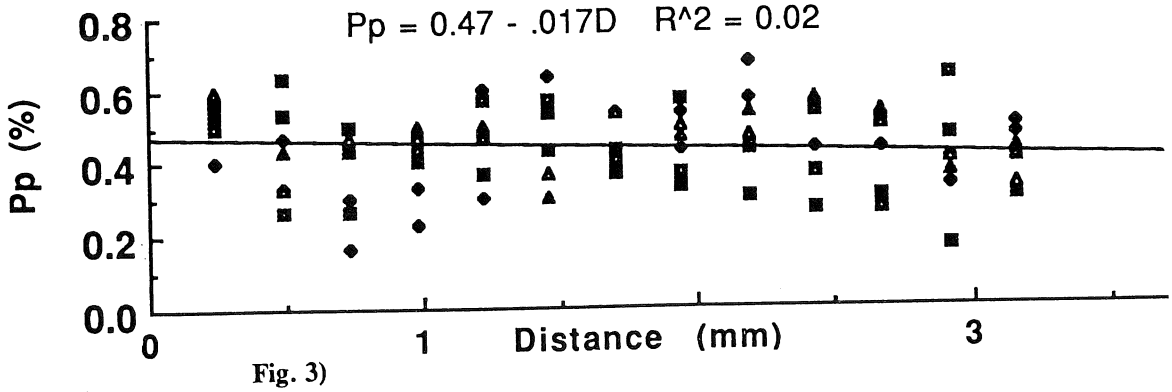

Fig. 3)

CORRELATING LOCAL ADAPTATION OF THE SKELETON TO SPECIFIC MECHANICAL STIMULI

Ted S. Gross and Clinton T. Rubin
Musculo-Skeletal Research Laboratory, Department of Orthopaedics
State University of New York @ Stony Brook, Stony Brook, NY 11794

INTRODUCTION

Specific parameters of the mechanical milieu such as the strain tensor (1), strain energy density (2,3) and a mechanical intensity scalar (4) have been proposed as the controlling stimulus for skeletal adaptation. *In vivo* validation of these postulations has proven difficult, however, as adaptation must be related to a well defined and controlled mechanical stimulus. In this study, we isolate the radius of an adult animal from its normal daily physical stimuli, substitute an exogenous mechanical stimulus physiologic in magnitude, and attempt to relate sites of adaptation to specific components of the applied mechanical stimulus. By correlating adaptive activity at specific sites with the mechanical environment engendered at those sites, we seek to more closely define the relationship between physical stimuli and skeletal adaptation.

METHODS

Under a general halothane anesthesia, the right radius of four adult male turkeys were functionally isolated via the following procedure. Small incisions (2cm) were made above the distal and proximal metaphyses, and the diaphyseal shaft was isolated from functional loading via parallel metaphyseal osteotomies. The exposed bone ends were covered with methacrylate filled stainless steel caps, and Steinman pins (3mm diameter) were passed through mating holes drilled in the radius and in the caps. The muscles, vascular supply, and innervation of the diaphysis were left undisturbed. The pins extended 2cm above and below the wing, and were clamped with external fixators to prevent accidental loading of the bone. The left radius of each animal served as an intact, contralateral control.

The animals underwent a four week daily loading regimen in which the fixators were removed, and external loads applied to the pins using a pneumatic cylinder with custom mating sleeves. The regimen placed the bone primarily in bending (with a small component (< 5%) of axial tension), and consisted of 100 cycles per day of a trapezoidal waveform (2.5s period) calibrated to induce peak longitudinal normal strains of 2000με. The orientation of the transcutaneous pins were such that peak tensile strains were engendered in the dorsal/cranial cortex, and the peak compressive strains were located in the ventral/caudal cortex. Upon completion of the four week loading protocol, the animals were sacrificed and matching 250 micron sections extracted from the mid-diaphysis of the control and experimental radii. The sections were ground to 100 microns, microradiographed, enlarged (x5), and scanned at 600dpi. The resulting binary images were processed to determine the areal properties of the control and experimental sections. Site-specific adaptation was assessed by aligning the experimental section upon the control section, dividing the cross-sections into 8 equal angle pie sectors through the control centroid, and assessing areal properties within each sector (fig 1).

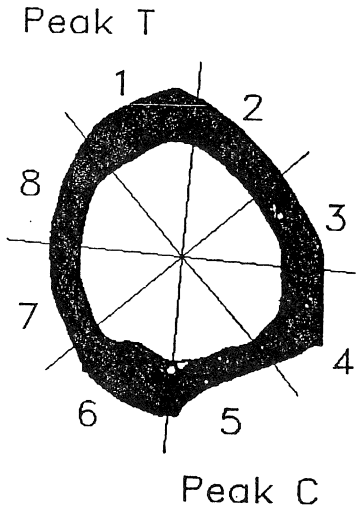

Fig. 1. Control radius with areal sectors and sites of peak engendered tension and compression.

Local area changes within the sectors were correlated to candidate stress and strain parameters generated by a 3-D isotropic (E=17Gpa, ν=0.3), finite element model consisting of 1152 20-node isoparametric bricks. The mesh was constructed from scanned microradiographs of a right radius from an age and weight matched animal. Boundary conditions were resolved using a strain gaged isolated radius preparation. Candidate parameters considered as potential correlates included longitudinal normal strain, strain energy, von Mises stress, minimum and maximum principal stress, and maximal shear stress.

The absolute magnitude, the radial gradient, and the circumferential gradient of each parameter within each sector was then correlated to the magnitude of the adaptive response within that sector. Correlations were first performed upon the averaged areal data, with subsequent analyses performed on each turkey independently.

RESULTS

The four week loading regimen induced a mean 9.1% increase in bone area, with the gain in bone area achieved by expansion of the mean (± S.D.) periosteal envelope in the experimental (48.6 ± 4.7mm^2) vs control (45.3 ± 1.7mm^2) radius. Areal changes within the 8 sectors were highly non-uniform, with means ranging between -5.5% to 40.4% (fig 2). The strongest sector specific correlations to the inter-animal adaptive response included strain energy (r=0.7), von Mises stress (r=0.6), maximum shear stress (r=0.6), the longitudinal normal strain radial gradient (r=0.7), and the strain energy radial gradient (0.6). The most powerful intra-animal correlate was the longitudinal normal strain radial gradient (r=0.9). Each animal demonstrated at least one correlation of r=0.5 (strain energy, maximum shear stress, longitudinal normal strain radial gradient, von Mises circumferential gradient). Of thirty possible correlations, absolute and radial gradient parameters had eight and nine correlates of at least r=0.5, while circumferential gradient parameters only demonstrated one correlation of at least r=0.5.

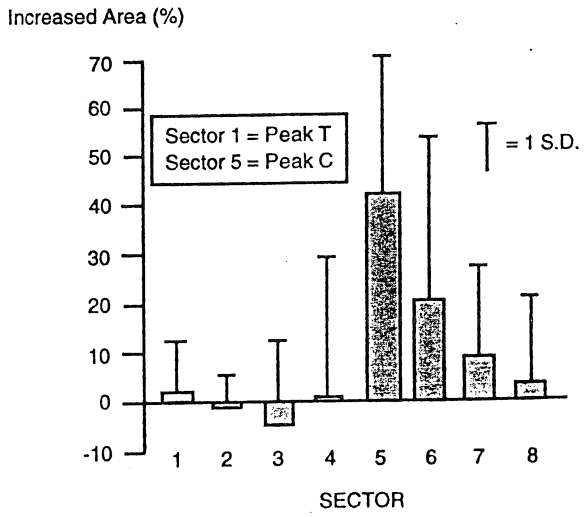

Fig. 2. Mean (S.D.) areal changes within each sector versus control.

DISCUSSION

The experimental loading regimen stimulated an overall increase in bone mass, but the variable nature of the response within a given cross-section (i.e. periosteal and endosteal new bone formation, endosteal erosion) indicates that formative and resorptive activity at specific sites, rather than gross measures of areal changes, must be considered when relating mechanical stimuli to adaptation. Despite the variability between animals and the generic isotropic finite element model, several mechanical parameters emerged as potential correlates to sites of skeletal adaptation. Of these, the radial gradient of longitudinal normal strain (i.e. the difference between periosteal and endosteal values along a fixed angle) was the most consistent correlate (r=0.9 in one animal, r=0.5 in two of the remaining three animals). The strong correlation between remodeling and the radial strain gradient is attractive as these results could be anticipated via the mechano-electric coupling inherent to streaming potentials. Interestingly, the second most consistent correlate, strain energy density, was also a strong correlate of the adaptation engendered in the *ulna* of this animal under different load conditions (5). Although longitudinal normal strain radial gradient was not originally considered in the ulna study, a first order calculation suggests it may also strongly correlate to sites of adaptation. Future efforts will include more rigorous modeling (orthotropic material formulation, meshes constructed from the control bone of each animal) in an effort to improve correlations, and the subsequent validation of the candidate parameters by their ability to predict adaptation under alternative loading conditions in this model.

This work supported by NIH AR40411 and AR39278

REFERENCES

1. Cowin, et al., (1985), J. Biom., 18:665-684.
2. Carter, et al., (1987), J. Biom., 20:785-794.
3. Huiskes, et al., (1987), J. Biom., 20:1135-1150.
4. Hart, R.T. et al., (1992), J. Biom., 25:261-286.
5. Brown, et al., (1990), J. Biom., 23:893-905.

COMPARISON OF STRUCTURAL MODEL PREDICTIONS WITH CLINICAL OUTCOME IN FEMORAL HEAD OSTEONECROSIS

K.J. Baker*, T.D. Brown, and R.A. Brand

Orthopaedic Biomechanics Lab, University of Iowa, Iowa City, IA 52242
*Texas Scottish Rite Hospital for Children, Dallas, TX 75219

INTRODUCTION: In femoral head osteonecrosis, the probability of eventual head collapse is high. However, various therapeutic interventions (osteotomy, core decompression, bone grafting, electrical stimulation) have been advocated to reduce the tendency for structural collapse. Lesion geometry appears to be very important to surgical success, suggesting that infarct configuration and location sensitively influence femoral head stress. If individual lesions are realistically modelled, the mechanical aspects of untreated and surgically treated lesions could be mimicked in order to assess structural competence and identify an optimal clinical strategy on an individual basis. In this study, for the first time, the apparent structural integrity of individual MRI-delineated patient lesions is compared with actual patient outcome parameters.

METHODS: A semi-automated method was developed to map patient lesion geometry from individual MRI scans to our existing finite element model (FEM). The model (13,197 d.o.f.) includes load distributions and magnitudes, isotropic material properties, and necrotic stiffness deficits, inferred from experimental data. Serial MRI scans were available from clinical evaluations of nine patients (ten hips) seen at our institution. All ten lesions were mapped onto the FEM mesh, producing ten individualized FEM models differing only in their specific lesion involvement pattern. The tendency for structural failure or collapse was indexed by the local ratio of compressive stress to yield strength (stress to strength ratio, SSR). Six patients had complete clinical histories in that we were able to determine the final status of their necrotic hip(s) from radiographic and written medical records (five of the six having collapsed). The severity of clinical collapse was evaluated by the depth of femoral head flattening, the percent of articular surface involvement, the rate of head collapse, and the presence of symptoms (i.e. pain and/or poor ambulation). Several SSR-based parameters (peak SSR, mean SSR, volume of bone having high SSR, etc.) were compared with clinical collapse indicators (severity score, depth, extent, rate) using parametric and non-parametric statistical methods (Pearson's product moment correlation and Spearman's rank correlation, respectively). Appropriate scaling factors were introduced for patient weight, use of walking aids (inferring percent resultant loads from experimental data), and core decompression (using results from a current FEM coring study), in order to account for quantifiable clinical factors that could influence FEM results.

RESULTS AND DISCUSSION: Statistically significant correlations (Tables 1, 2) were obtained between peak SSR and collapse rate, when scaled for weight (r_s=0.886, P<0.05; r=0.873, P<0.05) or weight plus coring (r_s=0.943, P<0.05; r=0.929, P<0.01). Moreover, locations directly below collapse sites corresponded spatially to locations of peak SSR in the FEM mesh for the collapsed lesions (Figure 1).

Table 1. Spearman correlation coefficients for comparison between peak SSR and collapse severity indicators, for raw and scaled SSR data.

Scaling	Score	Depth	Extent	Rate
None	0.543	(<0.4)	0.429	0.543
Weight (W)	0.886*	0.486	0.771	0.886*
W. Aids (A)	0.543	(<0.4)	(<0.4)	0.543
Coring (C)	0.600	(<0.4)	(<0.4)	0.600
W + A	0.486	(<0.4)	(<0.4)	0.486
W + C	0.943*	0.600	0.714	0.943*
A + C	0.829	(<0.4)	0.600	0.829
W + A + C	0.829	0.486	0.486	0.829

* P<0.05 (n=6, r_s > 0.886)

Table 2. Pearson correlation coefficients for comparisons between peak SSR and continuous collapse indicators, for raw and scaled SSR data.

Scaling	Depth	Extent	Rate
None	(<0.5)	0.589	(<0.5)
Weight (W)	(<0.5)	0.798	0.873*
W. Aids (A)	(<0.5)	(<0.5)	(<0.5)
Coring (C)	0.654	0.625	0.673
W + A	(<0.5)	(<0.5)	0.642
W + C	0.731	0.746	0.929**
A + C	(<0.5)	0.570	0.756
W + A + C	(<0.5)	0.610	0.850*

* P<0.05 (n=6, r > 0.811)
** P<0.01 (n=6, r > 0.917)

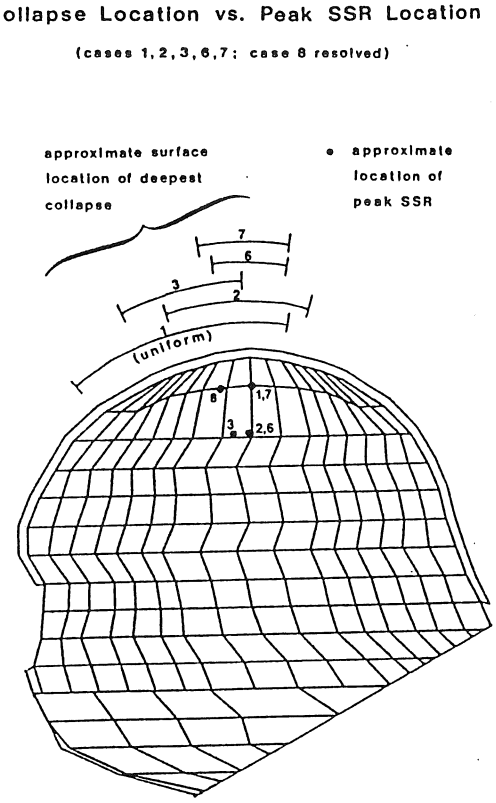

Figure 1. Comparison of location of surface collapse and location of peak SSR in the FEM model, projected onto the coronal midsection.

This series represents the first instance in which patient-specific finite element models have been used to successfully predict the outcome of directly corresponding clinical cases of osteonecrosis. While these preliminary results are very encouraging, a larger series is needed to definitively establish model validity. Eventually, individual FEM analyses could be used to evaluate various surgical treatment options in terms of their ability to reduce collapse propensity.

ACKNOWLEDGEMENTS: The authors appreciate the assistance of Dr. Cami Whitten and Dr. Howard Popp, and financial support from NIH (grant AR35788).

Prediction of Proximal Femoral Architecture Using the Isotropic Strain Criterion

C. H. Turner, V. Anne, and R. M. V. Pidaparti
Biomechanics and Biomaterials Research Center
Department of Mechanical Engineering
Indiana University/Purdue University at Indianapolis
Indianapolis, IN 46202

Introduction - The relationship between function and structure in the proximal femur has been a focus of scientific interest for over a century. Wolff proclaimed that the femur's internal structure was determined by static stresses through objective mathematical laws [1]. More recently, computer models have been used to predict trabecular architecture in the proximal femur using a state of uniform strain energy density as a remodeling objective [2,3]. These models tend to be overdriven, i.e. they drive density predictions to either very high or very low values. This result is consistent with that from a single element positive feedback system in which the high and low density values are attractor states. In the present study we took a different approach - we assumed homeostatic regulation of the bone structure with the remodeling objective of establishing isotropic and uniform peak strains [4]. Our approach implies negative feedback control of remodeling such that apparent density converges to a continuous spectrum of values between 0 and 2.00 g/cc.

Methods - A two-dimensional finite element model was developed using the PATRAN preprocessor. The mesh consisted of 1509 eight-noded, quadratic elements. Accuracy of the model was assured by a convergence study. Initial material properties were assumed to be linearly isotropic (E=1000 MPa, ν=0.3). Applied forces were calculated by static analysis of single-legged stance. Orthotropic Young's moduli then were calculated from the FEA results such that the magnitude of all principal strains took on the value of 2500 μstrain. Apparent densities were calculated from the predicted Young's moduli using a cubic relationship between Young's modulus and density [5] and a "J-curve" relationship [6,7] (Fig 1). Normalized fabric constants were calculated as the cube root of principal stresses [4].

Results - Predicted trabecular trajectories, expressed as normalized fabric constants, are shown in Fig 2. Figures 3 and 4 show the predicted apparent density contours using the cubic and J-curve relationships.

Discussion - The predicted trabecular trajectories corresponded in orientation with the classic architecture of the proximal femur (Fig 2), yet we were unable to find data in the literature with which to make quantitative comparisons. Predicted apparent densities using the J-curve compared well with measured density values from [6] (Fig 4), furthermore familiar structures such as the tensile and compressive trajectories and Ward's triangle were visible. Predicted apparent densities using the cubic relationship tended to be to great in the central regions and provided less resolution of the internal structures.

Acknowledgments - This work was supported by grants from the Whitaker Foundation and Osteonics.

References

1. Wolff J (1892) Das Gesetz der Transformation der Knochen. Verlag, Berlin.
2. Carter DR, et al. (1989) *J Biomechanics* **22**: 231-244.
3. Weinans H, et al. (1992) *J Biomechanics*, in press.
4. Turner CH (1992) *J Biomechanics* **25**: 1-9.
5. Carter DR and Hayes WC (1977) *J Bone Jt Surg* **59-A**: 954-962.
6. Rho J-Y (1991) Ph.D. Thesis, University of Texas Southwestern Medical Center, Dallas, TX.
7. Schaffler MB and Burr DB (1988) *J Biomechanics* **21**: 13-16.

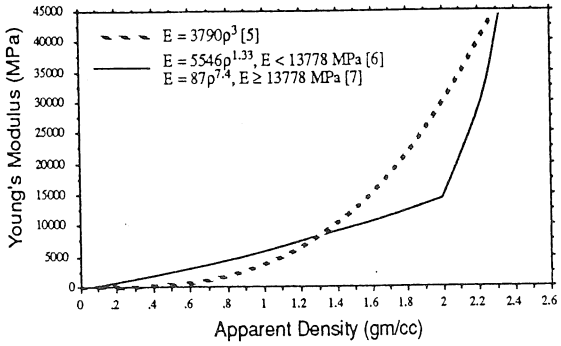

Figure 1. Relationships between Young's modulus and density. The dotted line is the cubic relationship from [5] and the solid line is a discontinuous relationship (J-curve) with data for trabecular bone coming from [6] and data for cortical bone from [7].

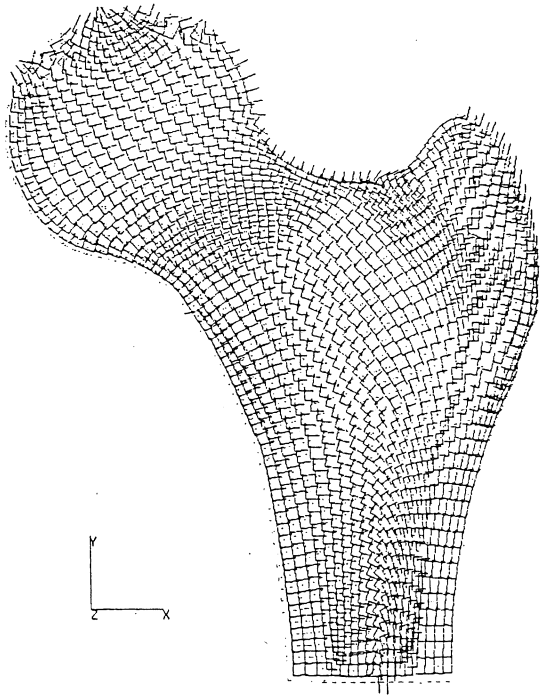

Figure 2. Predicted trabecular trajectories from the isotropic strain criterion expressed as normalized fabric constants.

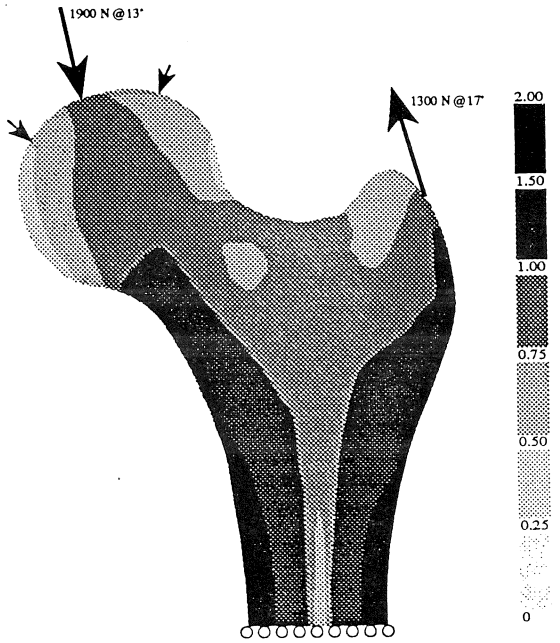

Figure 3. Predicted apparent densities from the isotropic strain criterion using a cubic relationship between apparent density and Young's modulus.

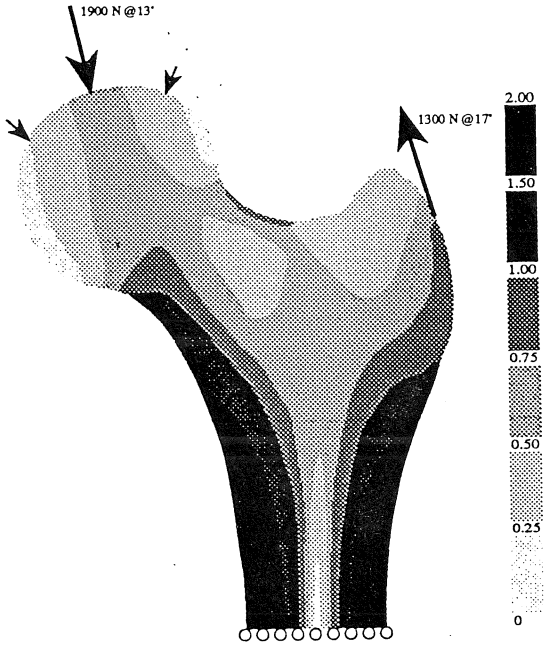

Figure 4. Predicted apparent densities from the isotropic strain criterion using a J-curve relationship between apparent density and Young's modulus.

NECESSARY AND SUFFICIENT CONDITIONS FOR THE STABILITY OF FINITE ELEMENT SIMULATIONS OF BONE REMODELLING

Timothy P. Harrigan Sc. D., James J. Hamilton, M. D.
Department of Orthopedic Surgery, University of Missouri at Kansas City
2301 Holmes St., Kansas City, MO 64108

Bone remodelling simulations using finite element methods have been attempted by many investigators, yielding important information on the reaction of bone tissue to stress in the natural state and in the presence of joint prostheses. The results of these models and the convergence characteristics of these models have been studied using numerical experiments and by assessing many different remodelling rules. Using the methods of Lyapunov, we have derived conditions for these simulations which are necessary and sufficient for stability, using the discretization procedures common in displacement-based finite element analyses.

METHODS:

We assume a material poisson ratio which is independent of density, and a power law relationship between density and elastic modulus. This results in a material property matrix [C] (Bathe, 1982) which can be expressed as

$$[C]=\phi^n[C_o] \quad (1)$$

with ϕ the volumetric density, n the material exponent, and $[C_o]$ the material property matrix for unit volumetric density. Using this matrix in a standard finite element formulation for element stiffness matrices yields

$$[K]_e=\phi^n[K_o]_e \quad (2)$$

with the subscript e denoting which element is used, and $[K_o]$ the element stiffness matrix for unit density. The average strain energy density within the element, for a given displacement solution U is

$$E_e=(\phi^n U^T[K_o]_e U)/2V_e \quad (3)$$

with V_e the element volume. If the tissue stimulus is $E^t_e=E_e/\phi^m$, and an overall remodelling rate equation is

$$d_e' = E^t_e - E_o \quad (4)$$

(with time scaled so that the rate coefficient is unity) the overall rate equation is

$$\phi_e'= (\phi^{n-m} U^T[K_o]_e U)/2V_e - E_o \quad (5)$$

The finite element equations to be solved are $[K]U=R$, with [K], the overall stiffness matrix, formed by a sum of the element stiffness matrices. Taking perturbations of this equation gives

$$[K]\Delta U= -[\Delta K]U \quad (6)$$

with $[\Delta K]$ the change in stiffness for a perturbation in density. This Matrix can be written as

$$[\Delta K]=\Sigma_e\, n\, \phi_e^{n-1}\, [K_o]_e\, \Delta\phi_e \quad (7)$$

with Δd_e the change in density. Perturbations in the rate equation, assuming a converged state, can be written as

$$(\Delta\phi_e)' = \{ (\phi_e^{n-m} +(n-m)\phi_e^{n-m-1}\, \Delta\phi_e)$$

$$*(U^T[K_o]_e U +2U^T[K_o]_e\Delta U +\Delta U^T[K_o]_e\Delta U) \} /2V_e$$

$$- E_o \quad (8)$$

Cancelling terms, neglecting higher order terms in perturbations, and substituting for ΔU gives

$$(\Delta\phi_e)' = M_{es}\, \Delta\phi_s + D_{es}\, \Delta\phi_s \quad (9)$$

with

$$M_{es} = -n(\phi_e^{n-m}\, \phi_s^{n-1}\, U^T[K_o]_e\, [K]^{-1}\, [K_o]_s\, U)/V^e \quad (10)$$

and

$$D_{es} = \delta_{es}\,(n\text{-}m)\phi_e^{\,n-m-1}\,U^T[K_o]_e U \quad (11)$$

with δ_{es} equal to 1 if e=s, and zero otherwise.

Based on a solution which is an exponential in time, the solutions of equation (9) will decay with time, and the equilibrium state arrived at will be stable, if the matrix $M_{es} + D_{es}$ is negative definite. A matrix is negative definite if all the eigenvalues of the matrix have negative real parts. Since the matrix derived here is non-symmetric, techniques from linear algebra were used to test for stability. [1,2]

RESULTS:

A finite element application has been written and run to time step the equations for density changes, using and Euler backward time stepping method. [3] In a number of simulation runs with n<m, the stability of the final distribution arrived at was tested, and the simulations were found to be stable. The results of this simulation method converged to a smooth distribution as the finite element mesh was refined, and thus no element-by-element averaging procedure was needed.

The stability of three time stepping algorithms was investigated using this remodelling theory: Euler forward, Euler Backward, and a modified Euler Backward method in which the diagonal part of M_{es} as defined above was used [3]. The Euler forward method was stable in some cases, but led to a hunting behavior in many cases. The modified Euler backward method was stable where the Euler forward method was unstable, but some cases were encountered in which this modified Euler backward method was unstable. The full Euler backward method has yielded stable results in all test thus far. Stability tests have been applied to all the results arrived at thus far, and the matrix derived above has been shown to be stable in all cases.

DISCUSSION:

The equation in the perturbations is linear, and linear superposition can be applied to investigate D_{es} and M_{es} separately. The equation derived here shows that a negative value for (n-m) is necessary for stability, since the matrix D_{es} is diagonal and every term multiplying (n-m) is positive. This is in agreement with a companion analytic study. Also the diagonal character of D_{es} agrees with the point-wise instabilities seen analytically with n>m. In contrast to the simple conditions necessary for stability, the conditions which are sufficient for stability are complicated, and seem to depend on the particular structure analyzed. We have been unable to prove negative definiteness in general for this equation.

The finite element simulation results for the Euler backward method are encouraging, but the computational cost for these simulations is substantial. As with other bone remodelling simulations, the validity of the simulations must be checked by comparing predictions to experiment. However, since our results converge to very close tolerances and our distributions are smooth and stable, we feel we are close to predicting the natural distribution of bone density.

REFERENCES:

1. Strang, G., Introduction to Applied Mathematics, Wellesley-Cambridge Press, Welleseley, MA, 1986.
2. Lancaster, P., Tismenetsky, M., The Theory of Matrices, Academic Press, Orlando, FL, 1985.
3. Harrigan, T. P., Hamilton, J. J., Finite Element Simulation of Adaptive Bone Remodelling: A Stability Criterion and A Time Stepping Method, submitted, International Journal of Numerical Methods in Engineering, 1991.

NORMAL GAIT

Podium Session 16

CLINICAL ROTATION, FORCE AND MOMENT ANALYSIS OF THE KNEE JOINT DURING WALKING.

U.P. Wyss, T.D.V. Cooke, P.A. Costigan, L. Kamibayashi, J. Li, S.J. Olney, Clinical Mechanics Group, Queen's University, Kingston, Ontario, K7L 2V7.

INTRODUCTION

Orthopaedic surgeons and therapists require a better understanding of the way we walk, what kind of rotations, forces and moments occur within joints, and how these parameters change with age, disease and treatment. This paper shows that the combination of kinematic, radiographic and anthropometric data results in more accurate individual gait assessments. This will be beneficial for a better acceptance of gait studies in a clinical environment.

REVIEW OF THEORY

Many researchers have studied clinical gait in the past (Andriacchi et al., 1982; Wyss et al., 1986; Mikosz et al., 1990). These studies have been useful, but there is still a controversy about the worth of costly gait assessments. A more accurate individual analysis is required in order to make gait assessments more acceptable. It is also clear that three-dimensional assessment is crucial (Kadaba et al., 1990), especially when assessing pathological gait.

PROCEDURES

Gait of 35 young healthy subjects (A) and 12 patients one week before surgery (B) was assessed, using a calibrated three-dimensional motion assessment system (Costigan et al., 1992). The subject specific data of the two groups is summarized in Table One. For each subject, kinematic, x-ray, anthropometric data and EMG data was collected. Characteristic data points are extracted from normalized curves (average of five trials) and stored in a multi-level data base for easy extraction.

Table 1 Characteristic subject data

	Group A		Group B	
	Mean	S.D.	Mean	S.D.
Height (cm)	171.8	10.1	166.2	9.5
Weight (kg)	64.1	12.8	84.1	11.4
Age (-)	24.4	3.2	67.5	8.9
Velocity (m/s)	1.2	0.2	0.8	0.2

RESULTS

The mean and standard deviations of the ranges of the three rotations, three net forces acting on the tibial plateau and three net moments are shown for the two populations in Table Two.

Table 2 Characteristic data of two subject populations

	Group A		Group B	
	Mean	S.D.	Mean	S.D.
TP PA (N/kg)	3.60	0.64	2.87	0.68
TP LM (N/kg)	1.41	0.53	1.38	0.48
TP DP (N/kg)	11.39	0.55	9.63	0.54
A Add (deg)	10.65	5.83	6.77	1.68
A Flex (deg)	62.02	4.96	44.46	10.64
A Irot (deg)	11.57	4.17	9.89	3.52
M PA (Nm/kg)	0.53	0.22	0.57	0.16
M LM (Nm/kg)	0.73	0.15	0.48	0.19
M DP (Nm/kg)	0.18	0.10	0.16	0.06

Tibial plateau (TP) forces normalized in N/kg body mass; angles (A) in degrees; moments (M) normalized in Nm/kg body mass. Posterior to anterior (PA) direction (+) for forces, and axis for moments; lateral to medial (LM) direction (+) for forces, and axis for moments; distal to proximal (DP) direction (+) for forces, and axis for moments. Adduction (Add), flexion (Flex) and internal rotation (Irot) indicates the positive direction of the rotations.

DISCUSSION

It is obvious from Table Two that comparing mean values between normal and pathological groups is problematic. There are some clear differences, especially in the DP direction and a substantially reduced range of flexion/extension is also noticeable. This is further illustrated in Figure One, which also indicates the problems of a detailed parameterization of the curve due to the change of the shapes. It is possible to compare the patient curves to a normal younger or age matched older group before and after surgery. This should help in the assessment of the functional outcome of surgical and therapeutical treatment. Another advantage of an improved individual assessment lies in the possibility of the analysis of irregularities observed in the clinic. The inclusion of muscle forces (with and without co-contraction) and the patellofemoral forces will still be required for a more complete analysis of gait data in the future.

REFERENCES

1. Andriacchi, T.P. et al., J. Bone Joint Surgery 64(A): 1328-1335, 1982.
2. Costigan, P.A. et al., J. Med. & Biol. Eng. & Comp., in press, 1992.
3. Kadaba, M.P. et al., J. Orthopaedic Research. 8: 383-392, 1990.
4. Mikosz, R.P. et al., 36th Annual Meeting, ORS, 283, 1990.
5. Wyss, U.P. et al., North American Congress on Biomechanics, Montreal, 281, 1986.

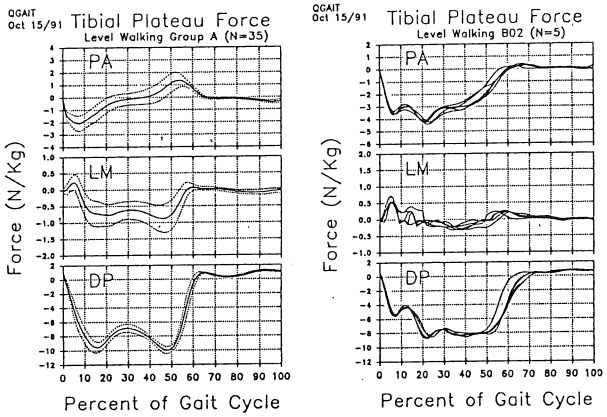

Figure 1 shows the tibial plateau forces for the young healthy population (mean and standard deviation) and five trials of one subject one week before surgery.

RELATIONSHIPS BETWEEN ALIGNMENT AND KINETIC MEASURES OF THE KNEE OF NORMAL ELDERLY SUBJECTS IN LEVEL WALKING

H. Wang and S.J. Olney
School of Rehabilitation Therapy, Queen's University, Ontario.

INTRODUCTION

Static alignment measures of the knee with standing radiographs have been used to evaluate alignment and geometry and to estimate force loading at the knee, providing critical information for clinical treatment. However, the relationships between static alignment and dynamic force and moment of force at the knee remain equivocal. In this study, twelve normal elderly subjects were tested to analyze these relationships in gait. The results showed that the static lower limb alignment measures did not closely correlate with the kinetic measures of the knee in gait. Instead, several dynamic knee angular (DKA) measures were found repeatedly and significantly associated with the forces and moments of force in the corresponding motion planes at probability levels between $P<.05$ and .001. The results of this study indicate that static alignment measures alone may not be sufficient to predict the dynamic knee joint forces for people with intact knees. Instead, attention should be paid to the significant relationships between DKA and dynamic kinetic measures at the knee. Further study using a larger sample size is also suggested since several static alignment measures were significantly related to some of the DKA measures and may be useful in predicting dynamic variables of the knee in gait.

REVIEW AND THEORY

It is recognized that interrelationships must exist among lower limb alignment and geometry, force loading at the knee, and knee joint disorders. However, Prodromos et al. (1985) was unable to show significant correlations between static varus deformity and dynamic adduction moment in patients with varus but intact knees. These results were in contrast to those of Brugioni et al. (1990). The purpose of this study was to determine the relationships between static and dynamic alignment measures and kinetic performance of the knee joint of normal elderly subjects in level walking.

PROCEDURES

Twelve subjects over 60 years of age with no history of lower limb problems took part in the study. The data collection began with the taking of the standard Questor Precision Radiograph (QPR) (Siu et al., 1991). Lead shots were taped over hip, knee and ankle marker positions prior to the x-ray, permitting subsequent application of a correction vector to kinematic data to move each surface marker into a joint rotation centre. A two-camera 3D WATSMART optoelectric system and an AMTI force platform were used for collecting gait data (Costigan et al., 1990). Each limb was described using a fixed body coordinate system

and the difference between x-ray and a computed reference position angle was used as offset to correct calculated knee angles for walking trials. Of the 11 QPR angular parameters, 8 were in the coronal plane, 2 in the sagittal plane and 1 in the transverse plane. Dynamic gait variables, maximum and minimum force, moment and angular measures of the knee in 3 motion planes, were extracted and normalized by gait cycle. Pearson's correlation coefficients were calculated between QPR static angular measures and dynamic gait variables, as well as DKA and kinetic measures in the corresponding motion planes.

RESULTS AND DISCUSSION

QPR angular parameters were not significantly correlated with dynamic joint forces at the knee. Two coronal plane QPR measures, femoral shaft-transcondylar angle (FSXC) and capito midcondylar-transcondylar angle (CMXC) , were significantly correlated with the maximum abduction moment; more valgus static alignment was associated with external abduction moments of the knee in gait. These two coronal plane QPR angular measures were also found to be significantly associated with several DKA measures in gait: the range of DKA in the coronal plane, the range of DKA in stance phase in the sagittal plane and the range of DKA in the transverse plane. Several DKA measures were found repeatedly and significantly correlated with the dynamic force and moment measures at the knee in gait in the corresponding motion plane (table 1). The absence of significant correlations between static alignment measures and dynamic kinetic measures is consistent with the possibility that subjects with intact proprioception can alter their dynamic weight bearing through motor control.

Table 1. Significant Correlations Existing between DKA and Kinetic variables

	Correlated Variables	P Level
Coronal Plane	Range of KA with:	
	- Max Medial F in Early St	<.001
	- Max Medial F in Early Sw	<.05
	- Max Abd M in St	<.05
Sagittal Plane	Max Flex KA in St with:	
	- Vertical F in St	<.05
	- Max Ext M in St	<.05
	Max Flex KA in Sw with:	
	- Vertical F in St	<.05
	- Ext M in St	<.05
	Min Flex KA in Late Sw with:	
	- Ext M in St	<.01

Abd=Abduction; Ext=Extension; Flex=Flexion; KA=Knee Angle; F=Force; M=Moment; St=Stance; Sw=Swing

REFERENCES

Brugioni, D.J. et al. J. Arthroplasty, 5, 173-190, 1990.
Costigan, P.A. et al., Proceedings Sixth Biennial Conference of the CSB, Quebec, 1990.
Prodromos, C.C. et al., J. Bone Jt. Surg., 67A, 1188-1194, 1985.
Siu, D. et al, Invest. Radiol., 26, 71-77, 1991.

ONLY THREE PARAMETERS SUFFICE TO ADEQUATELY DESCRIBE THE SYMMETRIC ASPECTS OF GAIT

Alan CROWE, Piet SCHIERECK and Wim KEESSEN

Department of Medical and Physiological Physics,
Department of Medical Physiology,
Department of Orthopaedics, Wilhelmina Children's Hospital,
State University of Utrecht, The Netherlands.

INTRODUCTION

When regarded from a purely physical point of view, the object of walking is to displace the body centre of mass (BCM) from one position to another. When walking in a straight horizontal line at a steady mean velocity V the BCM undergoes oscillations in the fore-aft, lateral and vertical directions (Saunders, 1953). This motion is the combined result of all the complicated physiological processes and mechanical actions involved in walking and any attempts to characterise and quantify gait patterns should initially be directed to an analysis of the BCM motion. Abnormalities of gait would be revealed by studying these three oscillations.

Oscillations of the BCM have been determined by Cavagna et al (1963, 1985) by doubly integrating data from a set of accelerometers strapped to the subject's belt near the estimated BCM position, or by doubly integrating ground reaction forces (GRF's). It is seen that the lateral oscillation is a rather reasonable approximation to a sinewave with a fundamental frequency equal to that of the walking cycle, and the vertical oscillation approximates to a sinewave with fundamental frequency twice the walking frequency. The fore-aft motion has also a frequency at twice the walking frequency, but in this case the sinewave is less pure. The oscillations have distinct phase relationships. When the gait is reasonably symmetric, the lateral oscillation is zero at the moment when the fore-aft oscillation is zero with positive slope and when the vertical motion is at the trough. Thus, if we analyzed the BCM movement and determined the amplitudes of these fundamental oscillations, we would have a fairly complete description of the symmetric oscillatory motion of the BCM. It would be characterised by just three parameters each having a definite and easily understandable physical meaning. These three components are called the fundamental intrinsic harmonics (FIH's).

Even the best gaits contain asymmetries to a certain extent, and the three parameters suggested above do not indicate them. The fundamental component of asymmetry in the vertical or fore-aft oscillation will have a frequency equal to the walking cycle frequency, and in the lateral oscillation it will have a frequency twice the walking cycle frequency. These fundamental asymmetry components, the fundamental extrinsic harmonics (FEH's) will provide sufficient parameters (amplitude and phase) to adequately describe the asymmetry provided components at the higher frequencies can be neglected.

It is the object of this paper to show that each of the three oscillations of the BCM can to a good approximation be represented by an FIH and an FEH.

MATERIALS AND METHODS

Apparatus. Two Kistler force platforms were installed in a walkway covered with carpet to prevent the subject from seeing the plates and adjusting his walking pattern to plant his feet centrally on them. GRF's in the vertical, lateral and fore-aft directions were sampled at 2ms intervals. Times of four successive heel strikes were also recorded together with the mean walking speed V over a distance of 3.5m.

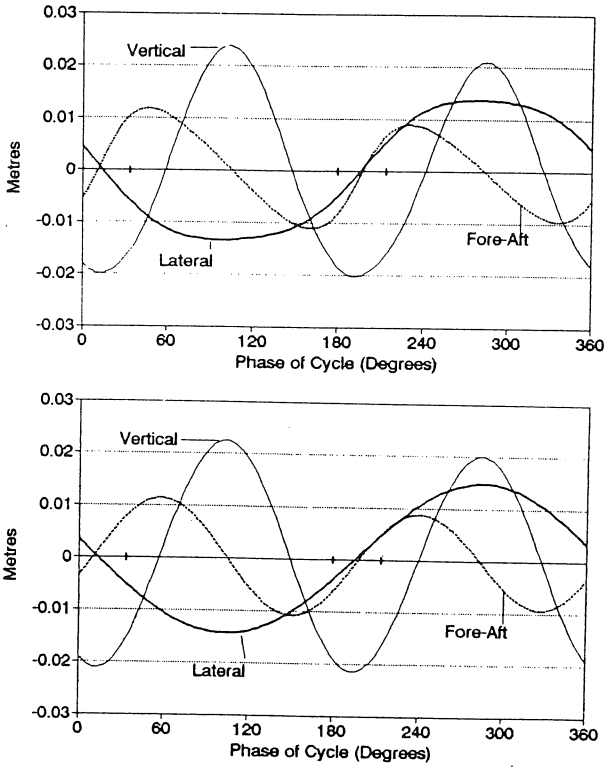

Fig. 1 Upper), BCM oscillations. Lower), Approximate BCM oscillations using the FIH's and FEH's.

Subjects and Protocol. Healthy young adult females walked barefoot at preferred walking speed. Several trials were recorded for each of four conditions a) without load, b) carrying a weight equal to 15% body weight (BW) in the left hand, c) with the weight in the right hand, d) with a weight in each hand.

Data Analysis. Equations of motion were set up incorporating gravitational forces for the vertical direction and zero external forces for the lateral direction. The mean for-eaft force over the walking cycle is always positive and represents the force needed to maintain the steady walking speed against external (air) resistance. Forces were normalised to the walking cycle and the means of several trials under each of the four conditions were obtained. Cyclic BCM oscillations were obtained by solving the equations of motion and analysed to determine the FIH's and FEH's.

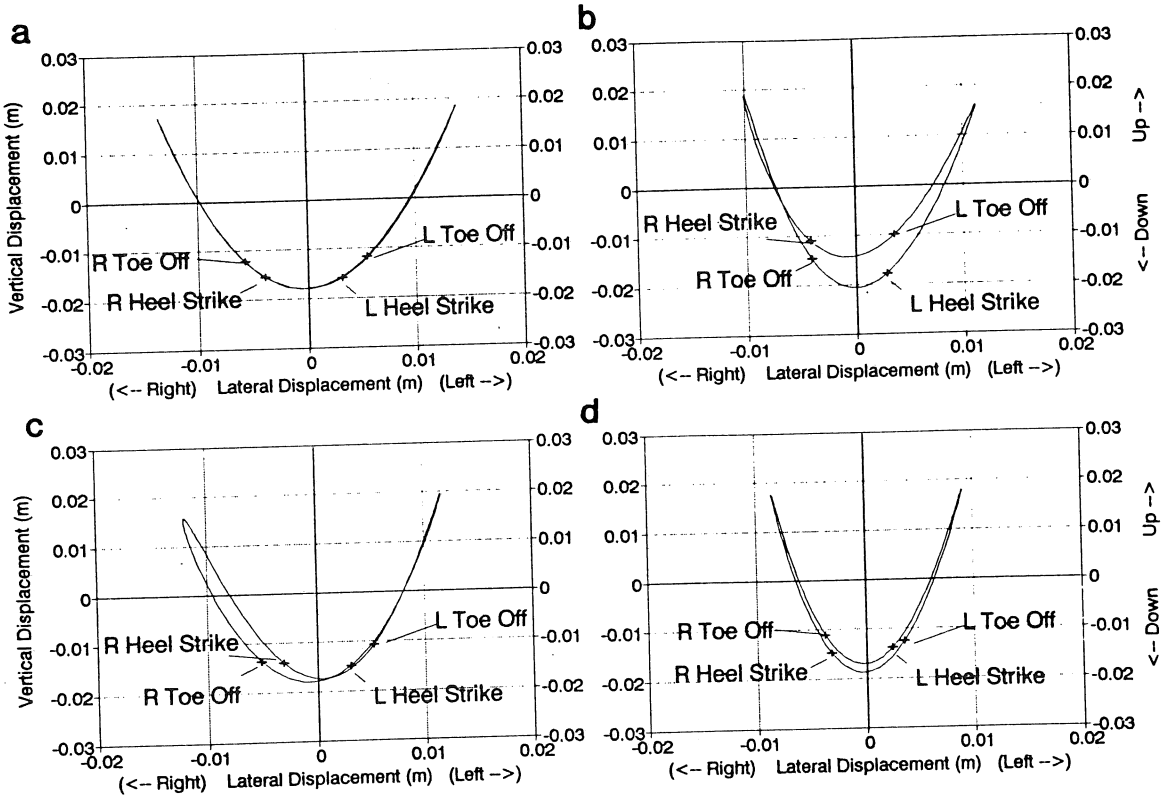

Fig. 2. BCM oscillations in the frontal plane derived from FIH's and FEH's. a) walking without load, b) load in left hand, c) load in right hand, d) load in each hand.

RESULTS

Fig. 1 (upper) shows a typical set of BCM oscillations from a subject walking without load, and Fig. 1 (lower) shows the corresponding oscillations obtained if only the FIH and FEH are used for the oscillations is each direction. Differences between the two sets of curves are small. This justifies our use of the fundamental harmonics to represent the BCM oscillations.

Fig. 2 shows for another subject BCM oscillations in the frontal plane to show effects of carrying loads. In this subject the oscillations without load are very symmetric as seen by the absence of a loop in the curve of Fig. 2a. An asymmetric BCM movement is produced by carrying the load in the left hand (Fig. 2b), the lateral excursion is greater to the left and the height of the vertical oscillation is reduced. The opposite effect is seen when the load is carried in the right hand (Fig. 2c). When 15% BW is carried in each hand, symmetry is largely restored, but the lateral movement is reduced (Fig. 2d).

TABLE 1
Amplitudes of the FIH's and FEH's (cm) and mean speed V (m/s) for subject walking with loads.

	Fore-Aft		Lateral		Vertical		
	FIH	FEH	FIH	FEH	FIH	FEH	V
No load	0.97	0.29	1.37	0.02	1.80	0.06	1.52
In left hand	0.84	0.06	1.07	0.07	1.74	0.34	1.54
In right hand	0.86	0.39	1.18	0.04	1.76	0.19	1.54
In each hand	0.80	0.19	0.88	0.03	1.78	0.09	1.53

The results for this particular subject are summarised in Table 1.

DISCUSSION

We have shown that it is possible to describe gait by a small number of parameters if we restrict ourselves to study of the oscillations of the BCM. The method yields results which are comparable to those produced using other techniques (Cavagna et al, 1963). The methods described permit the accurate measurement of oscillations of the BCM to enable comparison of groups or individuals, to assess the effects of walking under various specified conditions, or to test the effectiveness of orthoses or surgical interventions.

REFERENCES

Saunders, J.B. J. Bone and Joint Surg., **35**, 543-548, 1953
Cavagna et al, J. Appl. Physiol., **18**, 1-9, 1963
Cavagna, A. C. J. Appl. Physiol., **39**, 174-179, 1985

ACKNOWLEDGEMENTS

Substantial financial assistance has been given by the Dutch organisation **Het Zieke Kind in Beweging.**

PREDICTING THE KINEMATICS AND KINETICS OF GAIT BASED ON OPTIMUM TRAJECTORY OF THE SWING LEG

L. S. Chou, S. M. Song*, and L. F Draganich
The University of Chicago, Section of Orthopaedic Surgery and Rehabilitation Medicine, Department of Surgery, Chicago, Illinois
* The University of Illinois at Chicago, Department of Mechanical Engineering, Chicago, Illinois

INTRODUCTION

It has been generally accepted that the motion of the human body during locomotion is controlled in such a way as to minimize the amount of mechanical energy required. Thus, several researchers have modelled human gait based on optimal performance criteria.[1,4]

The swing phase of walking has been of interest from both a biomechanical and clinical standpoint, and is important not only to understanding pathological gait but also for prescribing treatments.[6] Thus, it is important to understand the motion of the swing limb and its effect on gait. The purpose of this study was to develop a mathematical model of human gait based on predicting the minimum energy consumption trajectory of the swing limb.

METHOD

Our motion analysis laboratory includes a 9.5 m walkway. Parameters of force were measured with a multicomponent force platform (Advanced Mechanical Technology, Inc.) in the center of the walkway. The kinematic parameters were measured with the Watsmart (Northern Digital) optical electronic three-dimensional digitizing system (accuracy < 3mm in our laboratory). Biotrack (Osteokinetics) software was used for kinematic analysis of the foot, shank, and thigh, which were modelled as rigid links, each having six degrees of freedom. A segment of either six or eight infrared light emitting diodes was attached to each link of the right extremity of a test subject. An additional segment was attached to the torso at the level of the center of mass of the head, arms, and trunk (HAT). The kinematic and force parameters were sampled at a rate of 130 samples (frames) per second. Gait analysis was performed on a 43 year old normal male subject who walked barefoot at a comfortable self-selected velocity. The parameters of gait as well as anthropometric measurements[5] (shank and thigh lengths, etc.) for the subject were used for input into the model (described below) and comparsion with the model's predictions.

Mathematical Model

The lower extremities during the single support phase of gait were modelled as a planar four-link open-chain (Figure 1). Four simple revolute joints represented the ankle and knee of the stance limb, and hip (common to both the stance and swing limbs), and knee of the swing leg. The moment of the hip of the swing limb was decoupled from the motion of the hip of the stance limb. The motion of the HAT was modelled as an independent inverted single pendulum attached to the hip joint. Using the anthropometric data and flexion angles experimentally obtained for the ankle and knee of the stance limb, we computed the position of the hip.

A two-dimensional search space was defined, large enough to include that which might be traversed by the swing leg. The space was discretized into vertical increments of 1 cm. The number of horizontal increments was computed as the distance between toe-off and heel-strike of the swing limb of the test subject (experimentally measured) divided by the number of samples over the time. Then, all of the flexion angles of the hip and knee of the swing limb potentially possible in this space were computed for each sampling frame. This was achieved by locating the ankle joint of the swing leg at each discrete point and computing the corresponding swing hip and knee joint angles given the experimentally measured location of the hip during stance and given the lengths of the shank and thigh.

The angular velocity and acceleration at toe-off found for the test subject were input as initial conditions into the model. For the rest of the swing period, angular velocities and accelerations were predicted based on the assumption of constant angular acceleration of the hip and knee joints as the ankle traversed between adjacent points in the discretized space for the increment of sampling time (1/130Hz).

Using the predicted kinematic data for each link of the swing limb and the experimentally obtained data for the stance limb, the recursive Newton-Euler method was used to compute all of the links' linear accelerations as well as all of the joints' forces and moments and the ground reaction forces (vertical and horizontal).

Trajectory Generation Using Dynamic Programming

The multistage optimization method, dynamic programming, was adopted to predict the optimum trajectory for the swing leg. We used the experimentally measured toe-off and heel-strike positions for input into the model. We also used those positions to define a search space (described above). The X-coordinate was discretized into stages between the toe-off and heel-strike positions. For every stage we defined a number of states or increments of vertical distance of the search space.

Beginning with the toe-off position (stage 0), we searched for the adjacent point (state) which would lead to the most energy efficient path between the two stages. Then, taking that point as the current position, the procedure was repeated until the swing ankle attained the heel-strike position. In this way, the optimum trajectory, based on the specified objective function, between the given toe-off and heel-strike positions was discovered.

We selected the minimum consumed energy as the objective function. Applying Bellman's optimality principle[2], the recursive cost relationship[3] for the problem can be expressed as:

$$\Phi_{(i+1)j}(k) = \Delta\Phi_{kj} + \Phi^*_{ik}$$

where $\Phi_{(i+1)j}(k)$ is the function value for state j in stage i+1, k is the number which varies from 1 to the number of states in stage i, Φ_{ij}^* is the optimal value for state j of stage i, and $\Delta\Phi_{kj}$ is the cost from state k of stage i to state j of stage i+1.

RESULTS

The optimal knee and hip flexion angles predicted for the swing limb are qualitatively similar to those measured for the subject

tested (Figure 2). They are, however higher in magnitude. The ground reaction forces compared favorably with those measured, oscillating about the experimentally measured magnitudes (Figure 3). The moments predicted for the knee, ankle and hip joints compared favorably with those predicted by a 7-segment three-dimensional model[7] (Figure 4).

DISCUSSION

The large differences at the beginning and ending of the time periods investigated are typical of problems related to the start up and termination of recursive procedures. Differences in the magnitudes between the predicted and measured values are likely the result of the simplified two-dimensional model and system measurement errors. Including a link for the foot in order to account for the changing contact point of the ground reaction forces, a link for the pelvis, and three-dimensional joints should greatly enhance the results of our predictions. Nevertheless, the results of this simple model support the hypothesis that human gait is based on minimum energy consumption.

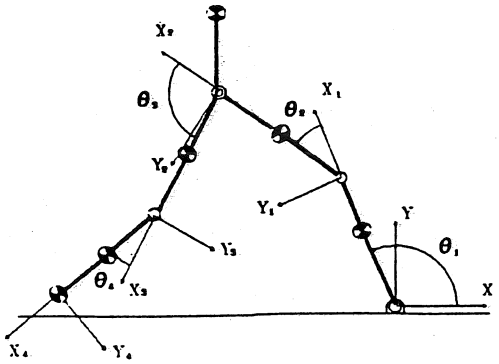

Figure 1. Schematic representation of the model for the single support phase of gait.

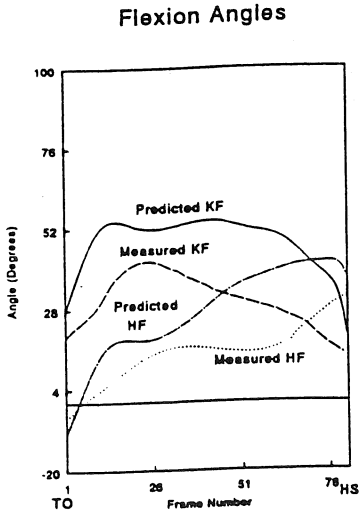

Figure 2. Predicted and Measured hip and knee flexion angles. KF: knee flexion angle, HF: hip flexion angle.

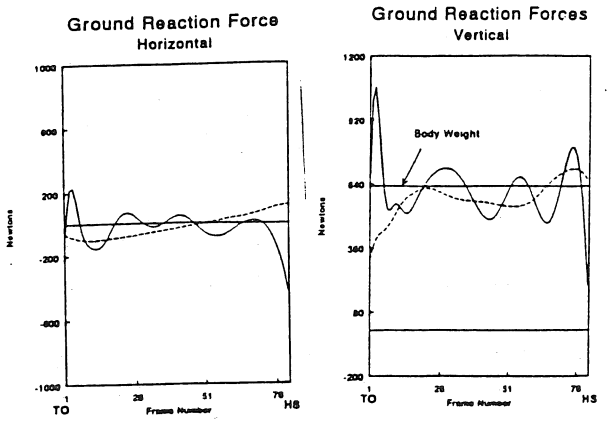

Figure 3. The ground reaction forces for predicted and measured values are indicated by solid and dashed lines, respectively. TO to HS represents the time period for the swing limb.

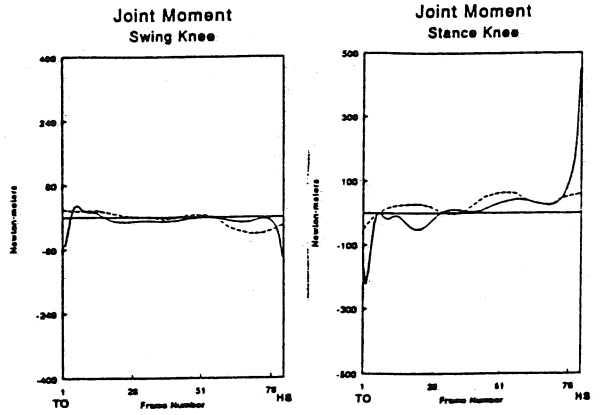

Figure 4. The predicted joint moments (solid line) are compared with the results from Zarrugh (dashed line) (1981). TO to HS represents the time period for the swing limb.

REFERENCES

1. Beckett, R. and Chang, K., Journal of Biomechanics, Vol. 1, pp. 147-159, 1968.
2. Bellman, R.,Dynamic Programming, Princeton University Press, Princeton, New Jersey, 1957.
3. Chou, L.S., Geometric Work of Manipulators and Path Planning Based on Minimum Energy Consumption, M.S. Thesis, University of Illinois at Chicago, Summer, 1990.
4. Chow, C.K. and Jacobson, D.H., Mathematical Biosciences 10, pp.239-306, 1971.
5. Dempster, W.T., Biomechanical Studies of the Musculoskeletal System, Springfield, IL, Charles C Thomas, 1961.
6. Mena, D., et al., Journal of Biomechanics, Vol. 14, pp. 823-832, 1981.
7. Zarrugh, M. Y., Journal of Biomechanics, Vol. 14, pp. 713-725, 1981.

ANGULAR HEAD MOVEMENT DURING GAIT: INFLUENCE OF SPEED AND VISION

Mark S. Redfern, Lori Mitchell Mc Mahon, and Timothy Schumann
Motion Analysis Laboratory, Eye & Ear Institute, University of Pittsburgh

INTRODUCTION

Kinematics of the human head during locomotion is one component of gait analysis that has drawn little attention, even though control of head movement is necessary to stabilize the visual field (Grossman and Leigh, 1990) and maintain balance. Head motions are reduced through feedback from the vestibular system (vestibulo-collic reflex), neck (cervico-collic reflex), and vision (Guitton, et al.,1986). The vestibulo-ocular reflex (VOR) is used to stabilize gaze during locomotion by compensating for head movements (Grossman et al., 1989); if the frequency content of these head movements is too high, however, the VOR cannot effectively stabilize the eyes, thus leading to oscillopsia (Takahashi et al, 1988; Grossman and Leigh, 1990). Many kinematic gait studies have combined the head with the trunk (Thorstensson et al., 1984; Winter, 1987) while some studies have investigated movement of the head as an independent segment and described head translations (Waters, et al., 1971; Capozzo, 1981) and two-dimensional sagittal rotations (Pozzo, et al; 1990).

While these studies have investigated a number of specific aspects of head position during gait, particularly as related to visual stability, no study to date has determined the full three-dimensional kinematics of the head. The purpose of this study was to quantify angular head movement in three dimensions during gait, and to determine the effects of vision and speed on these head movements.

METHODS

Eleven normal subjects (3 male / 8 female, range 19-44 years, mean=34 years), participated in the study. All subjects presented with negative histories for neurologic, orthopedic, and vestibular disease. Small spherical reflective markers were placed on the subjects' limbs, trunk and head. Lower extremity markers were placed bilaterally at lateral malleoli, lateral femoral epicondyles, and greater trochanters. Upper extremity markers were placed at the acromions, lateral humeral epicondyles, and midway between the ulnar and radial styloid processes. Trunk markers were located at the sternal notch, umbilicus, right and left anterior superior iliac spines (ASIS), and midway between the posterior superior iliac spines (PSIS). Head markers were affixed to an adjustable plastic frame that fit snugly around the subjects' heads. Three markers were attached to the frame: one above the auditory meatus of each ear and one centered on the top of the head.

Four high shutter speed video cameras were used to acquire motion data at 60 Hz while subjects walked at a constant speed. Three full steps of gait data were collected for each trial. Three walking speeds were tested: free paced, slow (56 steps per minute), and fast (112 steps per minute). Trials were collected with and without vision (eyes closed). A full factorial design was used with 3 repeats per condition. The trials were blocked on walking speed with the free paced trials always collected first. The speed of the slow and fast trials was controlled by presenting a metronome pulse tone during practice trials. The metronome was not used during actual data collection.

The video data was analyzed with a Peak Performance motion analysis system using a discrete linear transformation matrix to calculate three dimensional coordinates, as well as custom software. The accuracy of the measurement system for the recording window (3mx3mx3m) was approximately 3mm for linear displacements, translating to an angular measurement error for the head of approximately 1.5 degrees.

The angles calculated were: head flexion (pitch) with respect to vertical (θ_W), trunk flexion wrt vertical (ϕ_W), lateral flexion (roll) with respect to horizontal (λ_W), transverse rotation (yaw) with respect to the world axis perpendicular to the line of progression (β_W), and transverse rotation with respect to the shoulders(β_t).

RESULTS

Figure 1 shows plots of head (θ_W) and trunk (ϕ_W) flexion angles for slow/vision and slow/no-vision trials. There was little or no periodicity to these angles for all trials. Means and ranges of all angles were calculated and two types of analysis were performed. In the first analysis, a 2-way ANOVA was performed for each subject on the means and ranges of the calculated angles to determine the effects of vision and speed. Speed was found to be significant ($p<.05$) for the mean of θ_W in 8 of the 11 subjects, and vision in 9 of the 11 subjects. For ϕ_W, speed was found to be significant for the means in 6 subjects, and vision in 5. The means of the remaining angles did not show consistent significance for the eleven subjects. ANOVAs performed on the ranges revealed a significant speed effect for ϕ_W in 6 subjects. Vision effects were found in less than 2 subjects for all five angle ranges.

A second analysis was performed by calculating the differences between vision and no-vision at each speed, thus normalizing across subjects. T-tests for each speed were then performed including data from all subjects. This analysis found vision had a significant effect ($p<.05$) on mean θ_W, mean λ_W, and mean ϕ_W. Only β_t during the free speed trials showed a statistically significant difference in the range. Values for these differences are presented in Table 1. There were relatively large differences between vision and no vision in mean θ_W showing an increase in flexion with no-vision; however very small differences existed in the other angles. Even though the mean ϕ_W and λ_W differences revealed statistical significance, the difference values were extremely small. Note also the small standard deviations in all angles except θ_W, indicating little variability across subjects.

DISCUSSION AND CONCLUSIONS

This study begins to establish normative information regarding the kinematics of the head during gait. Speed and vision have an effect on mean head flexion (θ_w), but little or no effect on other aspects of head angular movement. One surprising finding was the small standard deviations reported in Table 1. Such values indicate consistent mean and range angular differences across subjects. The small mean angle values suggest that head position is controlled without the use of vision during locomotion. Head stability in space, as quantified by the calculated angle ranges, also does not appear to be affected by vision. These results are somewhat contrary to the theory that head control and stability during locomotion is determined by gaze (Berthoz and Pozzo, 1988), except in head flexion control.

REFERENCES

Cappozzo A J Biom. 14(6), 411-425, 1981.
Grossman, GE, et al. J Neurophys 62(1),264-272, 1989.
Grossman, GE, and Leigh, RJ Ann. Neurol, 27:528-532, 1990.
Guitton, D. et al. Exp. Brain Res 64: 59-69, 1986.
Pozzo, T et al. Exp. Brain Res. 82:97-106, 1990.
Takahashi M et al. Acta Otolaryngol (Stockh) 106:348-353, 1988.
Thorstensson A et al. Acta Phys. Scand. 121,9-22, 1984.
Waters, RL, et al. J. Biomechanics 6:167-172, 1973.
Winter, D.A Biomechanics and Motor Control of Human Gait. Unversity of Waterloo Press, 1987.

ACKNOWLEDGEMENTS

This research was supported by a grant from the Whitaker Foundation.

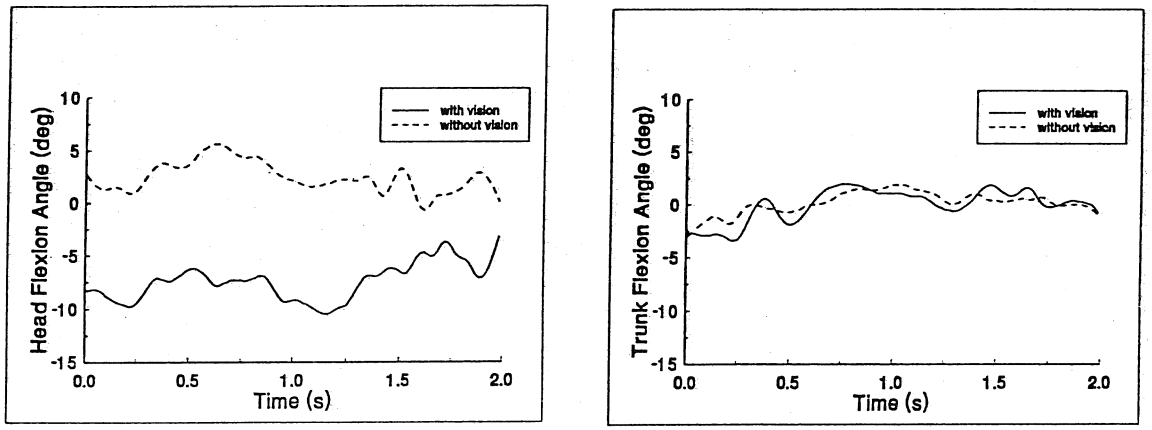

Figure 1: Flexion angle changes (subject S06) during a slow paced trial: a. Head (θ_w); b. Trunk (ϕ_w).

Table 1: Differences (+/- S.D.) in the means and ranges between vision and no-vision for the three speeds pooling all subjects.(* = p<.05)

	θ_w	λ_w	β_t	β_w	ϕ_w
Mean Angles Differences					
Slow:	11.5(8.4)*	-0.7(0.9)*	0.1(2.2)	-0.6(2.8)	-0.2(0.9)
Free:	7.1(7.0)*	0.1(1.0)	1.2(1.8)	-0.6(1.5)	-0.9(0.8)*
Fast:	7.6(6.7)*	-0.9(1.2)*	0.5(1.3)	-0.8(1.8)	-1.0(0.8)*
Range Differences					
Slow:	0.1(2.4)	-0.4(1.3)	-0.1(2.7)	1.5(2.3)	-0.3(1.4)
Free	-0.9(1.66)	-0.3(1.4)	*-1.5(1.8)	-0.7(2.4)	-0.1(1.2)
Fast	-0.3(2.5)	-1.8(1.9)	-1.3(2.1)	-0.3(1.9)	-0.1(0.8)

A NEW METHOD FOR EXAMINING COUPLED JOINT MOTION IN THE LOWER BACK AND THE ROLE OF THE SPINE IN HUMAN LOCOMOTION

P. Roozmon, S.A. Gracovetsky, G.J. Gouw and N. Newman.

Diagnospine Research Incorporated, Montreal, Quebec.
Departments of Electrical and Mechanical Engineering, Concordia University, Montreal, Quebec
Department of Orthopaedic Surgery, Hotel-Dieu Hospital, Montreal, Quebec.

INTRODUCTION

Typical studies of human gait tend to focus upon the role of the upper and lower exremities. Some hypotheses regarding the contribution of the spine and the back muscles in human locomotion are examined here. As a prelude to verifying aspects of these theories in later studies, a new method is introduced for analysing coupled joint motion in the lower back. This method is derived from a similar system developed by the authors to analyse coupled motion in the cervical spine. Both techniques treat data obtained from a high resolution opto-electronic device used to track skin markers. The new treatment of the data is found to consistently and accurately quantify coupled joint motion in lower back movements. It is expected to be useful in further investigations designed to verify the role of the spine and of back muscles in human locomotion.

REVIEW AND THEORY

Analyses of human locomotion typically focus on the arms and the portion of the body from the pelvis down. In particular, a popular approach to gait analysis is to use systems which track skin markers that are located primarily on the lower extremities, hips, and arms. Emphasis is placed on such factors as stride length and cadence, or stance and swing relationships.

For example, Davis (1988) provided an almost comprehensive review of clinical gait analysis techniques. However, no mention was made of the role of the back in locomotion. In the literature, illustrations chosen to show sample configurations for locomotion analysis systems typically do not indicate any markers located on the spine.

For people suffering from neurological disorders, numerous systems have been developed to artificially produce locomotion through functional neuromuscular stimulation (FNS). Several of these are described by Kralj et al. (1989). It may seem natural that these systems also tend to concentrate on the leg muscles. In this case, the focus is on stimulating those muscles which remain viable following spinal cord injuries involving upper motor neurons.

However, relatively little attention has been given to the lower back muscles, which are also often affected. Since lower motor neuron injuries usually result in muscle atrophy, such pathologies unfortunately tend to rule out FNS treatment. This dilemma is explained by Schneider (1990), as well as by Kralj (1989). Therefore, candidates for FNS typically experience paralysis in the low back muscles, as well as in their legs.

In the 1980's, a pioneer in considering the role of back muscles in FNS was Jerrold Petrofsky. Elements of his work are decribed in Petrofsky et al. (1986). However, even in this case, the purpose of back muscle stimulation was primarily to maintain an erect posture. This would, of course, help prevent patients from falling forward while walking. Nevertheless, little emphasis was given to the contribution made by back muscles towards driving the locomotion itself.

Conversely, some researchers have also looked at how the spine and the lower back muscles may actually be essential in attaining "normal" gait. Thortstensson et al. (1984) specifically examined these factors. They found that the back muscles showed two main periods of activation during each step cycle. However, their results involved only frontal and lateral mtion, since they were not equipped to measure axial rotation.

A hypothesis to explain the behaviour of the spine in locomotion was proposed by Gracovetsky (1985). Contrary to popular opinion, he suggested that the spine does not serve only as a static vehicle for transmitting forces to the legs. He speculated that it acts instead as a dynamic "engine", which stores and produces some of the energy required in walking.

This argument was based partly upon an analysis of how the central nervous system controls the appendages to produce locomotion. Thorstensson et al. (1985), on the other hand, considered motor control of the trunk in standing, rather than walking. This is particularly relevant to the procedure we use in this study, as described below.

Another factor which concerns us here is how the spine tends to move simultaneously in various directions. Cotsaftis and Vibet (1988) considered such coupled motion during gait. In particular, they examined the decoupling which must occur as the shoulders and pelvis rotate in opposite directions. They showed that a method known as "direct nonlinear decoupling" could be used to explain this phenomenon.

PROCEDURES

As a precursor to examining the validity of the above results in future studies, we introduce here a new method for analysing coupled joint motion in the lower back. This approach was adapted from a technique developed by Roozmon (1991) for analysing coupled motion in the cervical portion of the spine.

An intermediate step in verifying the role of the spine in locomotion is to examine the coupled motion which occurs for various movements of the lower back while the subject is standing. The kinematic data for this study is obtained from clinical examinations, using an existing non-invasive system designed for lumbar motion analysis.

Subjects are asked to perform a series of movements involving flexion/extension and lateral bending, as part of a standard protocol. Test subjects include both "normal" (ie. asymptomatic) individuals, as well as those experiencing low back pain.

Discrete motion samples are acquired by a high resolution opto-electronic device. This system uses cameras to track sixteen infrared emitting diodes attached to the subject's skin. Samples are recorded at a frequency of 180 frames per second.

A total of twelve markers are placed along the spine. One is situated at C7, with three more located at T6, T8, and T10, respectively. The remaining spinal markers are evenly distributed along the lower back, between T12 and S2. Another diode is also placed above each of the iliac crests and the scapulae, as well as two more on the ankles.

In addition, two EMG electrodes are normally placed in the lower lumbar area to monitor multifidus activity. The configuration of the device is shown in figure 1. In this case, markers are also shown on the shoulders, behind the knees, and on the elbows. The upper spinal IREDs are placed higher on the thoracic spine than indicated above, and some extra EMG electrodes are shown. This alternative configuration will be used for later gait analyses, as explained below.

After the data obtained by the system is filtered to reduce noise, it is subsequently processed by a computer. Specialized algorithms automatically determine lordosis, inter-segemental mobility, and other parameters normally of interest in low back examinations. A nearly linear relationship between the motion of the markers and the underlying spine is used to correlate data for the two. The results are then shown on a colour monitor which displays the data to the user in the form of curves and tables.

As a supplement to this procedure, coupled motion in the spine is characterized by a series of plots showing principal versus secondary motion. These are derived from virtual vectors defined to be perpendicular to the plane made by markers on the hips and the spine.

The motion of the vectors is represented in terms of direction angles corresponding to their projections in the mid-sagittal, transverse, and horizontal planes. Movement of the spine is then derived from that of the virtual vectors, usimg the known relationship between the skin markers and underlying vertebrae. Both motion with respect to the fixed calibration frame, shown in figure 1, and that of the markers relative to one another are considered.

RESULTS AND DISCUSSION

The method described above is found to produce consistent results for the analysis of coupled joint motion in the lower back. In particular, the direction angles derived from the kinematic data appear to accurately describe simultaneous motion of the spine in the three principal orthogonal planes.

These planes are usually defined to correspond to frontal, lateral, and axial rotation movements. This technique is equally valid for all three cases. Hence, it may be used to complement the work of Thorstensson et al. (1984), whose results did not include axial rotation.

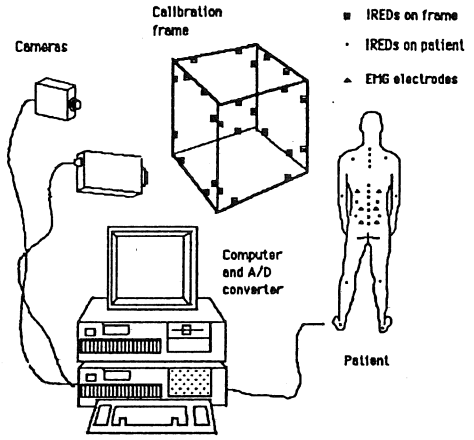

Fig 1: Overview of the motion analysis system used to obtain kinematic data for studying coupled motion in the lower back.

Coupled joint motion is typical of any movements of the spine, and must therefore be corrrectly measured in order to verify its role during locomotion. It is thus expected that this technique will be further adapted to provide analogous information on coupled motion for subjects walking on a tread mill.

The instrumentation and treatment of data will be similar, except that extra diodes will be added on the legs, arms and shoulders. However, the number of markers located on the spine will be maintained. It should therefore be possible to focus upon verifying the contribution of the spine and the back muscles in driving human gait.

REFERENCES

Cotsaftis, M. et al. *IEEE Eng. Med. Biol.*,7, 41-45, 1988.
Davis, B. *IEEE Eng. Med. Biol.*, 7, 35-40,1988.
Gracovetsky, S. *J. Biomed. Eng.*, 7, 205-216, 1985.
Kralj, A.R.et al. Functional Elecrical Stimulation: Standing and Walking After Spinal Cord Injury, (pp.1-9), CRC Press, 1989.
Petrofsky, S. et al. Spinal Cord Injury Medical Engineering, (pp.393-438), Charles C. Thomas, 1986.
Schneider, F.J. Neurological Rehabilitation, (pp. 423-483), C.V. Mosby Company, 1990.
Roozmon, P. Enhancement of the Display and Diagnostic Capabilities of an Opto-Electronic Instrument ... , Master's thesis, Concordia University, Montreal, Quebec, 1991.
Thorstensson, A. et al. *Acta. Physiol. Scand.*, 121, 10-22, 1984.
Thorstensson, A. et al. *Acta. Physiol. Scand.*, 125, 309-321, 1985.

LOCOMOTION AND POSTURE

Poster

Proceedings of NACOB II, The Second North American Congress on Biomechanics, Chicago, August 24th - 28th, 1992

QUANTITATIVE EVALUATION OF THE QUASI-STATIC ANALYSIS OF HUMAN LOCOMOTION

Ge Wu and Zvi Ladin

Biomedical Engineering Department and NeuroMuscular Research Center
Boston University, Boston, MA 02215

Introduction

Joint forces and moments exerted on the lower limb during locomotion are sometimes estimated by a quasi-static analysis, based on the measurements of ground reaction forces and moments [1]. This paper examines the limitations of this quasi-static approach based on a series of human locomotion studies, in which three dimensional body segmental kinematics of the lower limb were measured using the Integrated Kinematic Sensors (IKS) and joint forces and moments in the lower limb were estimated using both the quasi-static and the inverse dynamics approaches.

Methodology

Three healthy young male subjects were tested. Three IKSs, comprised of a rigid fixture that includes one triaxial linear accelerometer, one angular rate sensor, and an array of markers for determining the position and orientation (using the MIT developed TRACK© software) in order to dynamically calibrate the accelerometer's output [2], were attached to the foot, shank, and thigh of the lower right limb, respectively. The WATSMART optoelectronic system with two cameras and an AMTI force plate were utilized for the position and ground reaction load measurements. All the subjects walked along the 15m run way with bare feet. The speeds were varied from slow walking to running and were monitored by a digital timer. All the kinematic variables were low pass filtered at 100Hz and digitized at 200Hz.

The static joint force and moment were calculated based on the ground reaction load measurement, the distal body segmental weight and the orientation of the distal body segments with respect to the Global Coordinate System (GCS). The 'real' joint force and moment were the vector summation of the static components and the components resulting from the dynamic contributions of the distal body segments, which included the segmental accelerations.

Results and Discussion

The differences between the `real' and the static forces were calculated and expressed along three orthogonal directions in the GCS, defined as medial-lateral (m-l), anterior-posterior (a-p) and up-down (u-d) directions. The errors in the force estimates remained generally at similar levels from slow (1.1m/s) to fast (2.0m/s) walking. However, the magnitudes of these errors increased significantly in running (typical speed of 4.1m/s). Also, it was observed that the errors in the m-l and a-p directions were larger than those in the u-d direction, and the errors at the proximal joint (e.g. hip joint) were larger than those at the distal joint (e.g. knee and ankle joints). Table 1 describes the percentage of the errors as a fraction of the peak magnitudes of the `real' joint forces during walking and running.

It is clear that the quasi-static force estimates were reasonable approximations to the `real' joint forces only in the vertical direction or for the total magnitude, in the ankle or the knee joints during walking. This approach could introduce large errors to the force estimates in the m-l and a-p directions in all

	Normal Walking ($1.4m/s$)			
	m-l	a-p	d-p	total
ankle	63%	30%	5%	9%
knee	38%	48%	10%	15%
hip	100%	100%	29%	50%
	Running ($4.1m/s$)			
ankle	100%	67%	17%	22%
knee	86%	80%	20%	29%
hip	133%	100%	45%	60%

Table 1: Relative error between the `real' and static forces in walking and running

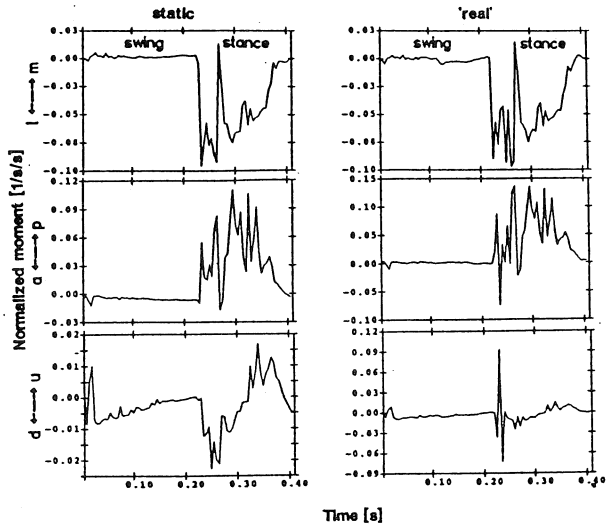

Figure 1. Ankle joint moment in running

quasi-static force estimates were prone to larger errors. The maximal error was observed in the hip joint, in running, and along m-l direction, that reached up to 133%.

The `real' and the static joint moments were also compared. The results showed that the quasi-static approach could be used to obtain fairly good approximations of joint moments in the lower limb during walking. The errors in the m-l and a-p directions were smaller than those in the vertical direction although they were all negligible. As the speed of the movement increases, such as from normal to fast walking, the errors increased slightly. However, a dramatic increase was clearly observed during running, especially in the a-p and vertical directions. In fact, both the ankle and knee moments in the vertical direction showed little resemblance to the quasi-static approximations. Fig. 1 shows a sample of the ankle moments of both `real' values and static approximations during running. Therefore, the quasi-static approach might not be sufficient in the situations in which the speed of the movement is high or the joint moment components other than the m-l direction are of interest.

Conclusion

The IKS approach provided complete three dimensional segmental kinematics measurements and joint force and moment estimates through the inverse dynamics approach. These estimates were compared to the quasi-static approximations of joint forces and moments at various speeds. The results indicated that the static estimations might be reasonable approximations for walking and for distal joints of the lower limb.

References

[1] A Cappozzo, T Loe and SS Cortesi (1980): A polycentric knee-ankle mechanism for above knee prostheses. J. Biomech. 13(3):231-239

[2] G Wu (1991): Dynamic estimation of human joint loading during locomotion. Doctoral dissertation, Boston University, Boston, Mass.

Acknowledgement

This work was supported by a National Science Foundation Grant No. EET-8809060 and by a grant from the Whitaker Foundation.

A MODEL FOR THE ANALYSIS OF FOOT PLACEMENT DURING GAIT.

Mark S. Redfern and Timothy Schumann
Motion Analysis Laboratory, Eye & Ear Institute, University of Pittsburgh

INTRODUCTION

Kinematic analyses of walking have included descriptions of joint angles (Crowninsheild et al, 1978, Apkarian, et al., 1989), and linear displacements (Thorstensson, et al., 1984). In the analysis of swing phase, parameters such as stride length, swing time, toe clearance and heel contact velocity (Winter, 1992; Redfern, et al., 1992;Strandberg and Lanshammer, 1981) have been reported. In all these descriptions, however, the *control* of foot trajectory and placement has not been addressed. Winter (1992) studied the trajectory of the foot during swing along with the associated electromyographic (EMG) activity of major muscle groups in the legs. He found that both toe clearance and joint angles during swing phase had very low variability, indicating that foot trajectory and placement is a precisely controlled task. Further, this control is multisegmental; probably including muscles in both the swing and stance leg. The question of *how* foot trajectory is controlled has received little attention. The objective of this research is to develop a method of analyzing swing trajectories of the foot which may prove useful in this investigation. A hypothesis of swing phase control is also presented and demonstrated.

MODEL

Foot trajectories are traditionally described in reference to the world coordinate system. In order to investigate the control of foot trajectories, a new coordinate system was developed which is aligned with the pelvis. Figure 1 shows a diagram of this coordinate system. The X axis is defined as parallel to the line passing through the two anterior superior iliac spines (ASIS). The Y axis is perpendicular to X and in the plane defined by the ASIS and posterior superior iliac spines (PSIS). The Z axis is perpendicular to X and Y. The origin of this system is placed at the greater trochanter. This Cartesian coordinate system is fixed to the pelvis and other body points are referenced to it.

Foot trajectories are initially calculated first in Cartesian coordinates as a vector(V) with X,Y,Z components, then transformed into polar coordinates. The polar coordinates are defined as the length of V (R), the angle from the X axis to the projection of V onto the XZ plane (Θ), and the rotational angle from V to the Y axis (Φ). The equations for these transformations are:

$$R^2 = X^2 + Y^2 + Z^2 \qquad \Theta = \tan^{-1}(Z/X) \qquad \Phi = \cos^{-1}(Y/R)$$

These Pelvic Polar Coordinates (PPC) provide an efficient method for describing movement of the foot relative to the pelvis during walking. They are related to angles at each joint such that he angle Θ corresponds to hip abduction from the pelvis, and Φ is a combination of hip flexion and transverse rotation from the pelvis. The magnitude R is directly related to knee flexion.

PROPOSED FOOT TRAJECTORY CONTROL

A hypothesis of trajectory control during level support surface walking was developed based on PPCs. The proposed control objective function is the minimization of the sum of the right and left angles at heel contact. This is imposed on both Θ and Φ. Thus, the sums at heel contact should be 0 for both Θ and Φ. This control strategy would provide maintainance of a stable base of support at heel contact, with the center of mass of the body being approximately at the mid-point between the two feet in double support phase. The required feedback sensory information to use PPCs in this control require hip and knee proprioception.

EXPERIMENTAL METHODS

Eight normal subjects participated in the study. All subjects presented with negative histories for neurologic, orthopedic, and vestibular disease. Small spherical reflective markers were placed on the subjects' limbs, trunk and head. Lower extremity markers were placed bilaterally at lateral malleoli, lateral femoral epicondyles, and greater trochanters. Upper extremity markers were placed at the acromions, lateral humeral epicondyles, and midway between the ulnar and radial styloid processes. Trunk markers were located at the sternal notch, umbilicus, right and left ASIS, and midway between the PSIS. Head markers were affixed to an adjustable plastic frame that fit snugly around the subjects' heads. The leg and pelvic markers were the focus of this study.

Four high shutter speed video cameras were used to acquire motion data at 60 Hz while subjects walked at a constant speed. Three full steps of gait data were collected for each trial. Three walking speeds were tested: free paced, slow (56 steps per minute), and fast (112 steps per minute) The trials were blocked on walking speed with the free paced trials always collected first. The speed of the slow and fast trials was controlled by presenting a metronome pulse tone during practice trials. Three repeats per condition were performed. The metronome was not used during actual data collection. The video data was analyzed with a Peak Performance motion analysis system using a discrete linear transformation matrix to calculate three dimensional coordinates, as well as custom software. The accuracy of the measurement system for the recording window (3mx3mx3m) was approximately 3mm for linear displacements.

RESULTS

The PPCs (R,Θ, and Φ) were computed for each leg over the full trial for all the subjects. Figure 2 shows a representative plot of this data for one gait trial. The sum of Θ and Φ between the right and left legs over time is also plotted. The shapes of these curves were similar for all subjects both with and without vision. Note in figure 2 that the curves representing the sum of the right and left leg were close to zero at heel contact for both Θ and Φ. The lengths (R) were approximately equal at heel contact.

Values of the Θ and Φ sum curves (solid lines in figure 2) at heel contact were extracted for all subjects. The means of these values for both right and left heel contact were calculated. The means were very close to zero for both Θ and Φ. Mean Θ values ranged from 0.5 degrees for free paced walking to 3.6 degrees for slow walking. Φ means ranged from 1.0 degrees for free paced walking to 1.5 degrees for slow walking. The standard deviations of these differences ranged from 4.7 to 9.6 degrees for Θ and 5.8 to 13.7 degrees for Φ. Thus, the proposed hypothesis of minimizing sums in Θ and Φ at heel contact is supported by the data in the mean, however there is some variability in the results. This variability was due to slight temporal variations between the zero crossing of the sum curves and the heel contact events. The zero crossing of the sum curve sometimes occurred slightly before or after heel contact. A small change in the temporal relationship caused variations in the sum values at heel contact.

DISCUSSION AND CONCLUSIONS

Foot trajectory control is an end-point control process requiring the foot to be essentially stopped with respect to the floor just prior to heel contact (Winter, 1992). The only sensory information available to the central nervous system to determine the position of the swing foot relative to the floor is proprioception from the hip, knees, ankles, and possibly vision. We believe that since the PPCs represent coordinates which relate to proprioceptive signals at the hip and knee, the method holds great promise for investigations of foot trajectory control. The hypothesis regarding control expressed here incorporates these coordinates into a simple, yet effective, closed loop end point control system for foot placement. The variability in zero crossing of the sum curves seen in the experimental data are believed to be due to some subject differences and limits in precision of the control system. While only tested in steady state gait, the control model may be applicable for other gait tasks such as turning or walking on a graded surface, possibly requiring modifications to the end point objective.

Finally, the model may be useful for investiging various gait disorders resulting in ataxia. In particular, we are interested in the role of foot placement control in balance during walking. Is foot placement affected by balance disorders? If so, how is the control of foot placement different? These are questions currently being addressed using the pelvic polar coordinate analysis.

REFERENCES

Apkarian, et al. J. Biomech. 22(2):143-155, 1989.
Crowninsheild, et al. Clin. Orth & Rel. Res. 132:140-144,1978.
Redfern, et al. Ergonomics (In Press), 1992.
Strandberg and Lanshammer J. Occup. Accidents 4:153-162, 1981
Thorsstensson, et al. Acta Phys. Scanda. 121:9-22, 1984.
Winter, DA Physical Therapy 72(1), 45-53, 1992.

ACKNOWLEDGEMENTS

This research was supported by a grant from the Whitaker Foundation.

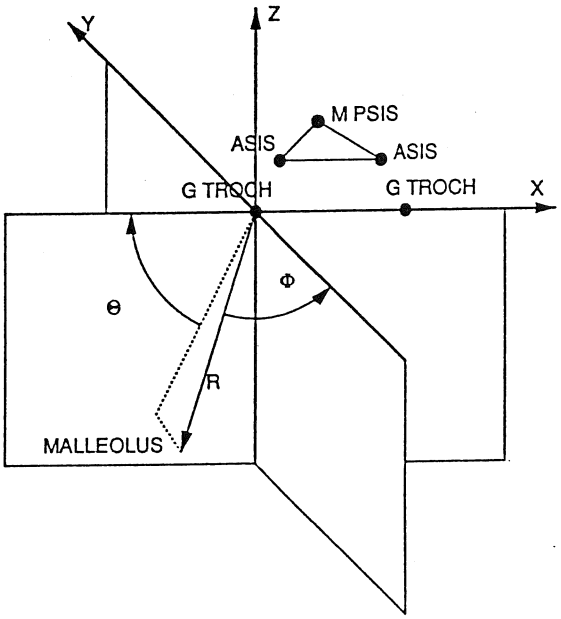

Figure 1: Diagram of the coordinate system used to analyze foot trajectories. The X-Y-Z axes are fixed with respect to the pelvis with the origin at the greater trochantor. A polar coordinate transformation into R, Θ, and Φ is then made.

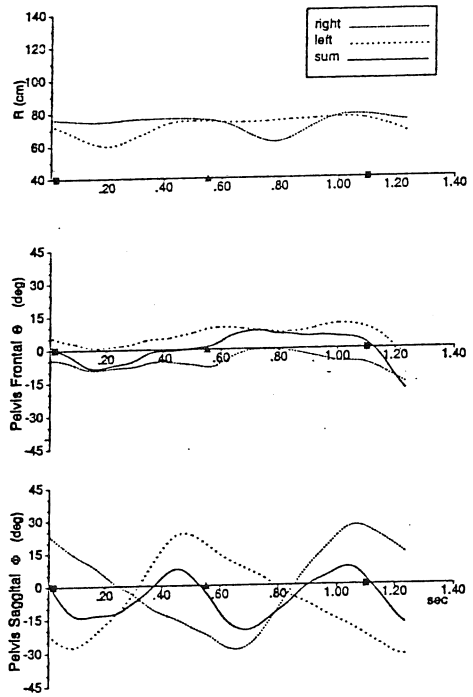

Figure 2: Representative pelvic polar coordinate data from one gait trial at free speed with vision. The squares and triangles represent right and left heel contact time, respectively.

GEOMETRIC TECHNIQUES FOR THE ASSESSMENT OF HUMAN WALKING

B.J. McFadyen

Dép. de Kinanthropologie, UQAM, Montréal, Québec.

INTRODUCTION

The present work combines phase plane analysis with a recently developed power plane technique for gait assessment.

REVIEW AND THEORY

Phase plots present a cartesian product of a system's position and velocity (the state variables), providing geometric solutions to the equations of motion (Spiegel, 1981). Such techniques are established in motor control research (Clark et al. 1990), and have even been applied to clinical gait analysis (Winstein & Garfinkel, 1989). However, phase plots lack direct causal information related to their trajectory evolution. The "power plane" presents a cartesian product of the factors of muscle mechanical power (joint moment and angular velocity) on a single plot (McFadyen, 1990), thus providing such causal data in a geometric form with the plot quadrants uniquely defined as generation or absorption by the flexors or extensors. Combining the two planes provides a more complete graphical account of system dynamics, and the resulting dynamic volume (geometrically dependant on complex biomechanical cause/effect relationships) provides unique access to biomechanical data.

PROCEDURES

For the purposes of this work, hip and knee data of natural, level walking from 10 normal (5 ♂; 5 ♀) subjects where compared to one male subject having suffered right lower limb trauma. Sagittal plane video recordings of all subjects (60 Hz.) were digitized, filtered (0 lag; 6 Hz) and synchronized to a Kistler force plate. Classical link segment analysis was performed and joint moments were normalized to body mass. Power and phase plane curves, as well as complete 3D volumes, were plotted for single stride data of each normal subject and 2 trials for the trauma subject.

RESULTS

Figures 1a & 1b show the dynamic volumes and constituent power and phase planes for the knee and hip respectively. Notable geometric changes are evident for the trauma subject's power plane curves at both joints. The first stance phase loop within the knee power plane is displaced towards absorption by the flexors, while the second knee loop around toe-off (TO), and the hip trajectories in early and late stance, are exaggerated.

DISCUSSION

The first knee power loop is associated with the combined control of power bursts K1 and K2 from time-series plots as presented by Winter (1991) and is coincident with the small loop in the phase plane. As the phase plot shows no abnormality, this suggests the need for hip extensors to maintain knee extension, which is verified by the increased hip power curve in early stance. The larger TO loop within the absorption by the knee flexors quadrant is to control the tendency towards an increased flexor velocity shown in the phase plot. The hip then pulls off with greater generation by the flexors (3rd quadrant of the power plane). Thus, greater stance control is given to the hip joint to maintain support, and initiate swing.

Any analysis technique takes time to become accustom to. Although both the need of appropriately equipped laboratories and interpretive skills are not removed, energetic, kinetic and kinematic data are combined to provide visual access to their coordinated nature. Power and phase plane loops along with the quality of different trajectories can act as "fingerprint" comparisons to assess biomechanical function. Having already found their niche in motor control research, perhaps geometric presentations of complex dynamical behaviour will prove useful for the dissemination of information in

clinical practice.

REFERENCES

Clark, J.E., et al. Sensory-Motor Organizations and Development in Infancy and Early Childhood. (pp. 363-378), Netherlands: Kluwer Academic Pub. 1990.

McFadyen, B.J. Proceedings of the 6th Biennial Conference of the Canadian Society for Biomechanics, Québec, (pp. 141-142), 1990.

Spiegel, M. Applied Differential Equations, Prentice-Hall, 1981.

Winstein, C.J. & Garfinkel, A. *Journal of Motor Behavior*, 21, 373-391, 1989.

Winter, D.A. The Biomechanics and Motor Control of Human Gait. U. of Waterloo Press.

ACKNOWLEDGEMENTS

I acknowledge financial support of NSERC (Canada), and the technical support of Mr. Magnon and Mme. Roy.

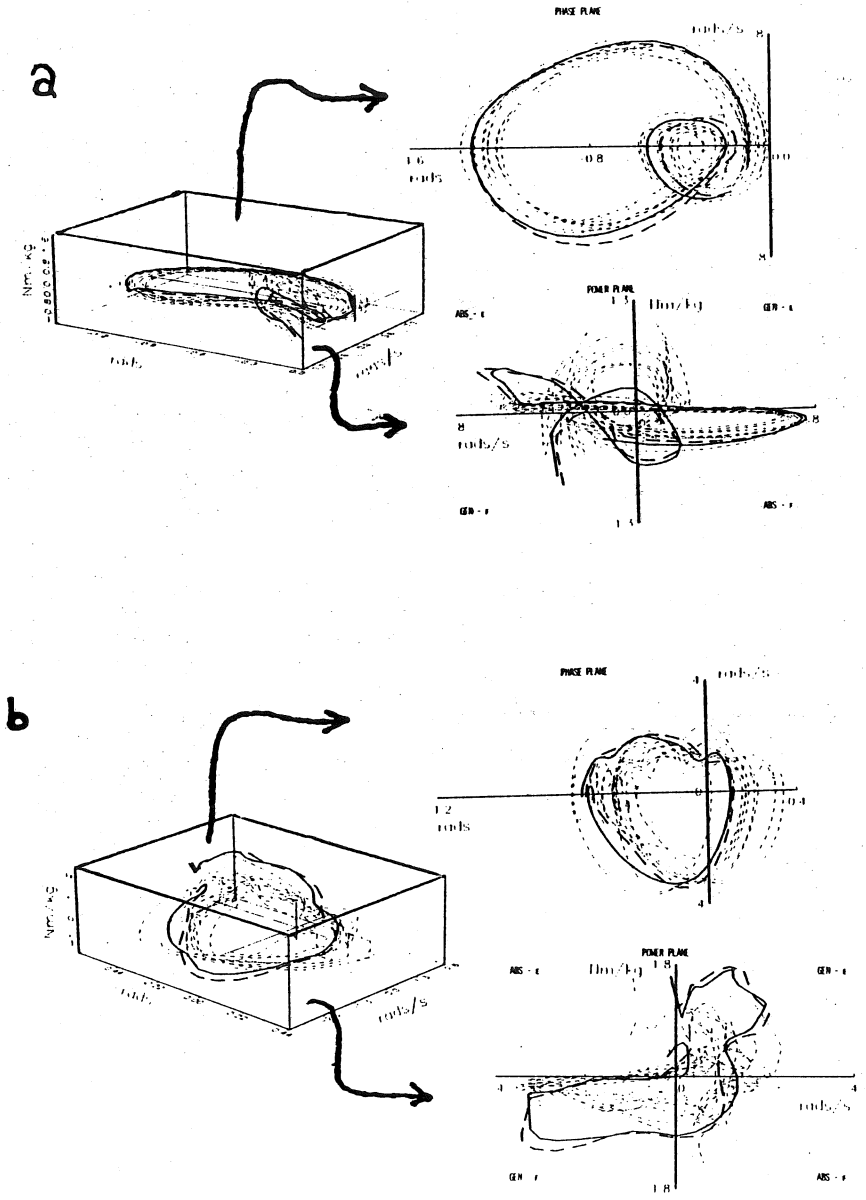

Figure 1. Dynamic volumes and constituent power and phase planes for the knee (a) and hip (b).

TERMINATION OF HUMAN GAIT: A DESCRIPTIVE STUDY

P. Vanitchatchavan[1,2] and R. J. Jaeger[1,3,4]

[1]Pritzker Institute of Medical Engineering, Illinois Institute of Technology, Chicago, IL
[2]Department of Computer Science, Illinois Institute of Technology, Chicago, IL
[3]Department of Rehabilitation Medicine, Northwestern University, Chicago, IL
[4]Section Orthopaedics and Rehabilitation Medicine, University of Chicago, Chicago, IL

INTRODUCTION

This is a descriptive study of termination of rhythmic movements using human gait as an experimental model. This study focused on the transition of human gait from a steady-state gait to a quiet standing posture. The transition from a standing posture to steady-state gait (e.g. Carlsoo (1965)) (which is referred to as the initiation of gait) and steady-state gait (e.g. Winter (1983)) have been thoroughly described in the literature. However, gait termination has not been extensively studied and defined.

METHODS

Series of experiments were performed on a pool of 12 healthy subjects. These experiments focused on the activities of the lower extremity during the termination of gait. Foot-floor contact, ground reaction forces, muscle activity, and joint angles. The foot switches determined the foot-floor contact timing pattern, defined as the sequence and duration between two major events (heel contact and toe-off). The force plate measured the ground reaction forces; and attention was focused on Fy (antero-posterior shear force) and Fz (vertical force). A detailed analysis of the ground reaction forces has been presented elsewhere (Jaeger and Vanitchatchavan (1992)). EMG activities were recorded bilaterally from the following muscles: tibialis anterior, gastrocnemius-soleus, quadriceps, and hamstrings. Joint angles were bilaterally measured using goniometers for hip, knee, and ankle.

Subjects walked along an 8.5 meter walkway. At random times during selected walking trials, an audible command to stop walking was issued. This command was triggered by heel contact.

RESULTS

The results are schematically summarized in Figure 1. The stick figure at the top illustrates the position of the subject at various time during gait termination. Foot-floor contact patterns indicate stance and swing phase. The ground reaction forces (R and L measured in two separate trials) have typical peak values indicated by dotted lines. Joint angles are for the left knee, hip and ankle. EMG activities are for the left leg. For EMG and joint angles, templates from steady-state gait are shown as dashed lines. The following events were observed in Figure 1: a reduction in the push-off of the plantaflexors (GS), denoted by ❶, leads to a lower Fy and Fz at push-off, denoted by ①; an increased activity in the quadriceps, denoted by ❷, and an increase in Fy and Fz, denoted by ②, are needed for body stabilization at the last heel contact; an increased activity in the hamstrings, denoted by ③, suggests that they function as hip extensors to prevent the trunk from excessive swaying and falling forward; an increased activity in TA, denoted by ❹, is still unexplained. Although there is no dorsiflexion of the ankle (at ④), this increased activity exists.

DISCUSSION

There is a critical segment in the gait cycle during which a decision must be made in order to either continue or terminate gait. The results from experiments suggested that at least two mechanism were employed, which occurred very close together in time: first, reduction of the push-off in the step prior to termination, and second, increase of the braking force applied in the final stance phase. An attempt to initiate a gait termination in this region in the gait cycle or failure to employ these termination mechanisms may result in difficulty stopping or even a poorly controlled stop.

The potential applications of this work include identification of elderly people at risk of falling, studying patients with gait deficits, programming the gait sequences of paraplegic individuals walking by electrical stimulation, and the programming of legged robotic vehicles.

REFERENCES

1) Carlsoo, S. *Acta Anat* 65, 1-9, 1965.

2) Jaeger, R. J. and Vanitchatchavan, P. Ground Reaction Forces during Termination of Human Gait. *Journal of Biomechanics*, in press.

3) Winter, D. A. *Journal of Motor Behavior* 4, 302-310, 1983.

ACKNOWLEDGMENT

P. Vanitchatchavan was supported by the Study Abroad Division, Civil Service Commission, the Royal Thai Government.

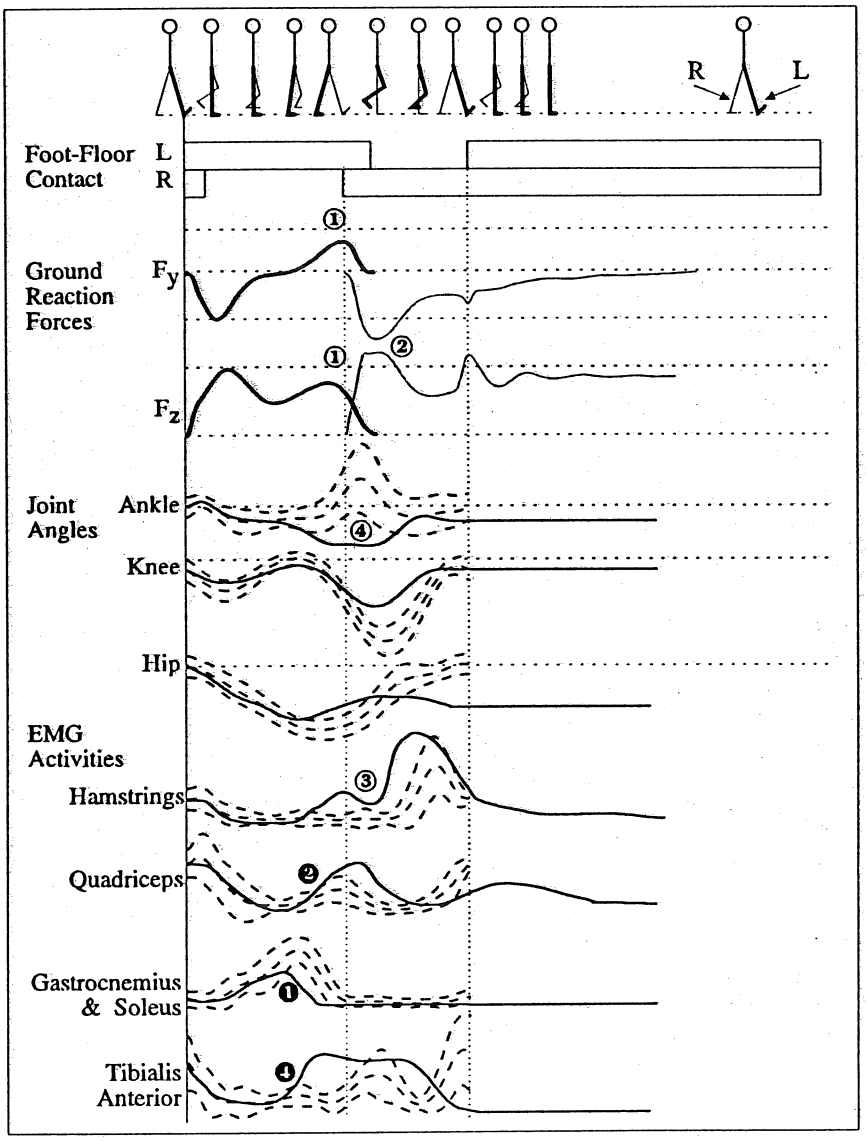

Figure 1. Events during Termination of Human Gait

EFFECTS OF LOAD CARRIAGE SPEED ON MUSCLE TORQUES ABOUT THE ANKLE, KNEE AND HIP

Everett Harman, Ki-Hoon Han, Peter Frykman,
Michael Johnson, Franklin Russell and Michael Rosenstein

U.S. Army Research Institute of Environmental Medicine
Natick, MA 01760-5007, U.S.A.

INTRODUCTION

Walking with loads on the back remains an essential, life-sustaining activity among major segments of the world's population. Even in technologically sophisticated societies, large numbers of soldiers and recreational hikers regularly carry backpack loads, which frequently exceed 50% of bodyweight. The speeds at which loads are carried varies considerably according to the individual and circumstances. Enhanced understanding of the effects of speed on the mechanics of load carriage could lead to the development of various innovations for lessening medical risk and improving performance.

REVIEW AND THEORY

Through the use of high-speed filming and force platform analysis, the effects of walking speed on the net torques produced by muscles about lower extremity joints have been calculated (1). However, such information has not been reported for subjects carrying loads. The purpose of our study was to calculate and compare net muscle torques about the ankle, knee and hip produced while walking at slow and fast speeds while carrying a relatively heavy backpack load.

PROCEDURES

While carrying a backpack loaded with 33 kg across a force platform at 1.1 and 1.5 m/s, in balanced order, 16 normal adult males were filmed at 60 Hz from the right side with a Locam 16 mm movie camera. Their walking speeds were visually cued using a custom-designed device. Resulting film images were rear-projected onto an Altek digitizing table, where the major body joints as well as two points on the pack were hand digitized. After digital filtering, the film and force platform data were processed, using the link segment approach (2), to produce time histories of joint torques about the ankle, knee and hip.

RESULTS

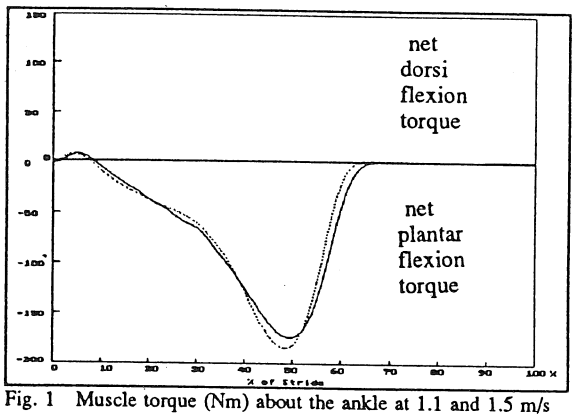

Fig. 1 Muscle torque (Nm) about the ankle at 1.1 and 1.5 m/s
_____ = 1.1 m/s _ _ _ _ _ = 1.5 m/s

Film analysis showed that the subjects actually walked at 1.16±.06 m/s under the slow condition and 1.50±.05 m/s under the fast condition. Figures 1, 2 and 3 respectively show net muscle torque about the right ankle, knee and hip under each speed condition as a function of percent of stride (0% and 100% = right heelstrike), where each point on each curve represents the mean of all subjects. From a right-side point of view, positive torque values indicate counterclockwise, and negative values clockwise torque exerted by the muscles on the body segment distal to the joint indicated.

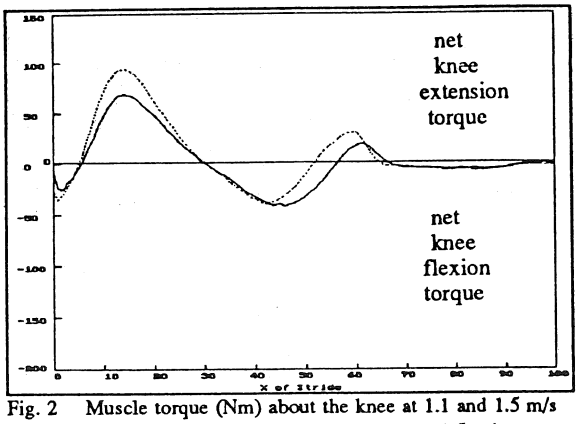

Fig. 2 Muscle torque (Nm) about the knee at 1.1 and 1.5 m/s
_____ = 1.1 m/s _ _ _ _ _ = 1.5 m/s

Muscle torques about all three joints clearly increased with walking speed. Negative peak torque about the ankle, positive peak torque about the knee, and both positive and negative peak torque about the hip increased significantly ($p<.05$) with load carriage speed.

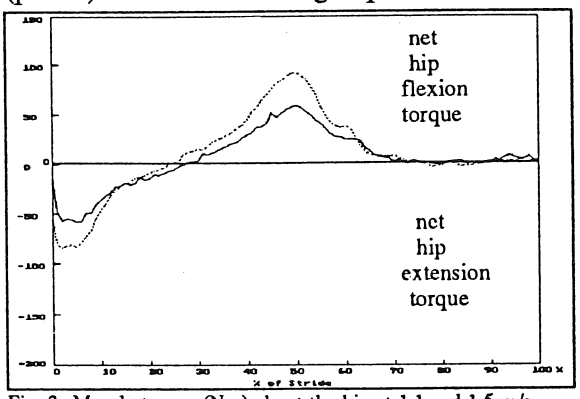

Fig. 3 Muscle torque (Nm) about the hip at 1.1 and 1.5 m/s
_____ = 1.1 m/s _ _ _ _ _ = 1.5 m/s

Table 1 shows the percentage increases in walking pace and peak torques about the ankle, knee, and hip as load carriage pace increased. It can be seen that for the ankle, peak torque increased less than the percent change in walking pace. Knee torque increased somewhat more than pace, while hip torque increased considerably more than pace.

Timing of torque application may be affected by locomotion speed. The following events appear to have occurred

Table 1. Increase in actual walking speed and peak torques as nominal pace increased from 1.1 to 1.5 m/s.

mean magnitude change			
actual walking speed	ankle peak torque	knee peak torque	hip peak torque
+29%	+6%	+37%	+51%

at lower percentages of stride for the faster than the slower load carriage pace.

- peak negative torque about the ankle and its subsequent return to zero.
- peak negative torque about the knee.
- 2nd peak positive torque about the knee.

DISCUSSION

It was expected that joint torques about the ankle, knee and hip would be greater when carrying loads at a faster than a slower pace. However, the degree to which the torques increased around the various lower body joints differed. The greatest increase in torque occurred about the hip, and the least about the ankle, indicating that the muscles producing torque about the hip were most involved in increasing load carriage speed and those producing torque about the ankle were least involved. This is consistent with our previous finding (3) that increase in load carriage speed is effected much more through increasing horizontal force than vertical force. Given the position of the leg and foot during pushoff, torque about the ankle produces mainly vertical force, while torque about the hip produces mainly horizontal force.

REFERENCES

1. Cavanagh, P. and R. Gregor. J. Biomechanics, 8:337-344, 1975.
2. Winter, D. Biomechanics of Human Movement, Wiley, NY, 1979.
3. Han et al. Med. Sci. Sports Exerc. 24(5) 1992 (Abstract in Press).

EFFECTS OF EXERCISE ON GAIT CHARACTERISTICS IN THE ELDERLY

Spiros Prassas and Alina Rominger
Department of Exercise and Sport Science, Colorado State University,
Fort Collins, CO 80523, U.S.A.

INTRODUCTION

It has been suggested that physical activity might delay age-related psychophysical deterioration. Although the relationship between exercise and physiological and psychological parameters on elderly, sedentary populations has been addressed by a plethora of studies (Blumenthal et al., 1989; Kent, 1982; Ryan, 1982; Sager, 1983), the effect of exercise on the mechanics of their gait is not well documented. It was, thus, the purpose of this study to examine the effects of exercise on kinematic gait characteristics in the elderly.

METHODS

Twenty-two healthy, sedentary subjects, randomly divided into exercise (N=12; mean age: 72 yrs, SD: 1.7 yrs), and control (N=10; mean age: 74.4 yrs, SD: 1.41yrs) groups participated in this study. The exercise group was engaged in an eight week moderate, supervised exercise program. All subjects were videotaped initially and at the conclusion of the exercise program with a 60 Hz videocamera while walking at a normal self-selected speed. For each subject, a pre- and post-test full walking cycle from heel strike (HS) to HS of the same foot was digitized. The raw data was digitally filtered with a cutoff frequency of 6 Hz before being submitted to further analysis. Two-way analysis of variance (ANOVA) with repeated measures was used to compare kinematic differences among groups and trials ($p<0.05$).

RESULTS AND DISCUSSION

Table one presents the results of the study. Swing time (ST) was defined as the time of the (swinging) limb from toe-off to HS, stance time (ST) was the time of the supporting limb from HS to toe-off (including single and double-support time), stride length (SL) was the distance from HS to HS of the same foot expressed as a percentage of height, hip and knee joint range of motion (ROM) was the difference in minimum and maximum hip and knee joint angles of the swinging extremity, center of mass (CM) velocity was the average velocity of the CM in the horizontal direction, and CM vertical displacement was the difference between its maximum and minimum vertical position. The results indicate that a short-term exercise program of moderate intensity had no significant effect on SL, hip and knee joint ROM, CM vertical displacement and horizontal velocity and temporal parameters of gait in an elderly, sedentary group of subjects when compared to similar controls. However, data trends suggest the possibility that exercise might invoke positive changes in mechanical gait patterns in the elderly population. In the present study, the duration of the exercise program and/or small sample size may

have been the limiting factors for the failure to demonstrate significant improvements in the gait parameters examined.

Table 1: Comparison of Selected Kinematic Variables of Gait in the Elderly.

		Exercise Group (N=12)		Control Group (N=10)	
VARIABLE		Mean	S.E.	Mean	S.E.
Swing Time (SW) (sec)	+	0.349	0.010	0.350	0.009
	++	0.332	0.008	0.320	0.007
Stance Time (ST)	+	66.300	0.797	66.230	0.612
(% of total)	++	65.720	0.645	66.960	0.874
Stride Length (SL)	+	78.000	0.025	75.600	0.022
	++	84.100*	0.270	78.800	0.024
Hip Joint ROM (degrees)	+	40.900	3.050	40.900	3.030
	++	38.070	1.660	37.600	1.900
Knee Joint ROM (degrees)	+	61.900	1.470	62.300	1.200
	++	61.300	1.330	61.900	1.640
CM velocity (m/sec)	+	1.270	0.056	1.100	0.038
	++	1.450*	0.059	1.310	0.066
CM vertical displac. (m)	+	0.055	0.007	0.051	0.003
	++	0.053	0.003	0.057	0.004

+=Pre-test; ++=Post-test.
*=Significant differences between tests ($p \leq 0.05$).

REFERENCES

Blumenthal, J.A., et al. (1989). *Journal of Gerontology* **44** (5) 147-157.
Kent, S. (1982). *Geriatrics* **37** (6) 132-135.
Ryan, A. (1982). *Physician and Sports Medicine* **10** 45.
Sager, K. (1983). *Physician and Sports Medicine* **11** 31-34.

LOADING OF CONTACT LEG IN SUBMAXIMAL AND MAXIMAL RUNNING IN CHILDREN WITH CEREBRAL PALSY

P. Luhtanen, E. Mälkiä, J. Huhtinen and P. Hanski

Research Institute for Olympic Sports, Jyväskylä, Finland.
Department of Health Sciences, University of Jyväskylä, Finland.

INTRODUCTION

A two dimensional biomechanical model of the lower limb was developed in order to estimate loading of the support leg during running at submaximal speed 2.40 - 2.90 m x s^{-1} and maximal speed 3.70 - 4.04 m x s^{-1}. Data were collected from a girl and boy with cerebral palsy (age 15 and 13 year) using a force platform and film camera. At the maximal speed in the braking phase the average resultant ground reaction forces were higher in the abnormal leg than in the normal leg. In the propulsion phase at the maximal speed the resultant ground reaction forces were higher in the normal leg than in the abnormal leg. The same was observed at the submaximal running speed. The highest maximal joint forces were found at the maximal speed during impact phase in the ankle of the abnormal leg. The highest extending torques at maximal speeds were in the ankle and knee joint of the normal leg. The high loading of the abnormal leg in the braking phase at maximal speed was due to the over extended knee joint in the abnormal leg.

REVIEW AND THEORY

The significance of high muscle forces and joint moments acting in and around the ankle and knee joints are appreciated when monitoring the injuries of athletes. Athletic activity has been increasing in children with hemiplegical cerebral palsy. The major injury sites of running-related injuries is the knee (Orava, 1980). Knee injuries have been found to occur most frequently (39 %), in running. A detailed analysis of muscle and joint forces is important in understanding the history of running related injuries. These forces are affected mainly by the running speed, style, surface and shoes. The purpose of this research was to estimate selected muscle and joint forces concerned using 2-D methods in film and force platform analysis.

PROCEDURES

A two dimensional biomechanical model of the lower limb was developed in order to estimate loading of the support leg during running at submaximal speed 2.40 - 2.90 m x s^{-1} and maximal speed 3.70 - 4.04 m x s^{-1} (Luhtanen and Mero, 1991). Data were collected from a girl (G) and boy (B) with hemiplegical cerebral palsy (age 15 and 13 year, mass 57.3 and 51.0 kg and height 165 and 156 cm, respectively).

Each run was performed on the force platform which was six meters long. The horizontal and vertical force signals were amplified and stored in a Racal Store 7 magnetic tape recorder and processed with HP 21 MX computer.

Each run was filmed for every trial using a Canon Scoopic 16 mm camera operating 64 Hz. For cinematographic analysis the joint markers were digitized using a Vanguard film analyser and Summagraphics digital board and transferred to a HP 1000 A computer. The kinematic data was smoothed using the polynomial curve fitting of the 9th degree. For the kinetic analysis of the joint forces and muscle torques, Newton's second law in translator and rotational motion was applied.

RESULTS

At the maximal speed in the braking phase the average resultant ground reaction forces were higher in the abnormal leg (G: 3.1 BW; B: 2.3 BW) than in the normal leg (G: 3.0 BW; B: 2.0 BW). At the submaximal speed the higher forces were found in the normal leg. In the propulsion phase at the maximal speed the resultant ground reaction forces were higher in the normal leg (G: 2.3 BW; B: 2.0 BW) than in the abnormal leg (G: 2.0 BW; B: 2.0 BW). The same was observed at the submaximal running speed. The highest maximal joint forces were found at the maximal speed during impact phase in the ankle of the abnormal leg (G: 3.1 BW). The highest extending torques at maximal speeds were in the ankle and knee joint of the normal leg G: 173 Nm, B: 133 Nm; G: 194 Nm, B: 239 Nm, respectively.

DISCUSSION

In this study the highest ground reaction and joint forces were developed at maximal running speed in the abnormal leg. At submaximal speed during the ground phase the higher forces were obtained in the normal leg. In normal athletes the high loading in the area of knee and ankle are related to the frequency of sport injuries in knee and ankle. In the children with Cerebral Palsy the probability of injuries may increase in or round the ankle and knee during the impact phase in the maximal running, if the ankle and knee are extended too much and the neuromuscular control impaired.

In the propulsion phase at maximal speed it was observed that the normal leg produced higher force to maintain the maximal speed, than the abnormal leg. This might mean that the failure in the neuromuscular control of the abnormal leg limited both the force production in the muscles and the range of joint movement in the abnormal leg as compared to the normal leg. The muscular training of the abnormal leg should be directed progressively to the eccentric and concentric excercises of the knee extensors and coordination.

REFERENCES

Luhtanen, P. et al. *Akademia Wychowania Fizycnego w Poznaniu. Seria: Monografie*, 271, 81-92, 1991.

Orava, S. Exertion Injuries Due to the Sports and Physical Exercise, (pp. 17-33), Österbottningen, 1980.

EXTERNAL LOADING FOR BELOW-KNEE-AMPUTEE AND ABLE-BODIED CHILDREN DURING RUNNING

J.R. Engsberg, A.G. Lee, B.E. Hagel, J.A. Harder*

Human Performance Laboratory, University of Calgary
*Alberta Children's Hospital, Calgary, Alberta, Canada

INTRODUCTION

Our long term goal is to enable below-knee-amputee (BKA) children to walk and run the same as able-bodied (AB) children. To accomplish this goal it is first necessary to understand how BKA and AB children walk and run. A step in this regard is to establish normative data for relevant variables for both activities based upon relatively large numbers of subjects. Ground reaction force variables for the prosthetic, nonprosthetic and intact limbs of BKA and AB children were compared during running. Results generally indicated greater external loading on the nonprosthetic limbs when compared to the prosthetic limb or limbs of AB children.

REVIEW AND THEORY

Engsberg et al. (1991a,b) have evaluated external force data for BKA and AB children during walking. Prince et al. (1990) have reported similar information for BKA adults during running. Information regarding BKA children during running has not been reported. The purpose of this investigation was to evaluate the external loading patterns of BKA and AB children by testing relatively large groups of both children while running at a fixed speed.

PROCEDURES

Twenty-two BKA (mean age, 10.4 years, range 6-16) and 200 AB (mean age, 9.4 years, range 7-12) children ran across a force platform at 2.2 m/s (± 10%). Force data were normalized by dividing by subject weight and support time were normalized to a value of 1. Local forces, impulses, slopes and times were obtained from the force-time data. One-way ANOVA with a TukeyB Post Hoc test determined any significant differences ($p<0.05$) between the right, left, nonprosthetic and prosthetic legs of the children (Engsberg et al. 1991b).

RESULTS

No significant differences were found between right and left legs of the able-bodied children. However, comparisons among the three leg types (able-bodied, nonprosthetic and prosthetic) indicated significant differences for some of the variables (Table 1).

DISCUSSION

Prince et al. (1990) have reported that the first and second impact peaks and the total impulse for the vertical ground reaction force-time curves were significantly greater for nonprosthetic limb when compared to the prosthetic limb for 7 BKA adults. Further, they have reported that the retarding and propulsive maximum values and impulses were also significantly greater in the anterior-posterior force-time curve for the nonprosthetic limb. These results were generally in agreement with those reported for BKA children during walking (Engsberg et al. 1991a,b). The results of the present investigation indicate that the maximum propulsive force was

two leg types for the BKA children; yet other maximum values were not. However, the total impulse in the vertical direction and the propulsive impulse in the anterior-posterior directions were significantly different and similar to the finding of the Prince et al. (1990) investigation. Variation in methods such as running speed, sample size and age could account for the differences of the two investigations. The present study indicated the rate of loading (Slope), the amount of unweighting (ZMin), and time events (SlopeTim, PMaxTim) were significantly different between some of the leg types. These data provide additional information describing gait asymmetry of BKA children and gait differences between BKA and AB children. It is believed that these variables can be used as indicators of improved prosthetic designs which will eventually allow BKA children to walk and run the same as AB children.

REFERENCES

Engsberg, J.R. et al. **Proceeding of the ISB**, (pp.170-171),1991a.
Engsberg, J.R. et al. **Arch Phys Med Rehab**, 72,657-661,1991b.
Prince, F. et al. **Proceeding of the ASB**, (pp.115-116),1990.

ACKNOWLEDGMENT

Funding by the Hospital for Sick Children Foundation (Toronto) and the Variety Club of Southern Alberta Tent-61 through the Alberta Children's Hospital.

Table 1: Means and standard deviations for selected Force-Time Variables for able-bodied (AB), nonprosthetic (NP) and prosthetic (P) limbs #

Leg	Slope BW/Ntim	ZMin BW	ZImpTo BW*Ntim	SlopeTim Ntim	PMax BW	PMaxTim Ntim	PImp BW*Ntim
AB (N=200)	17.1 (7.6)	1.34 (0.37)	1.37 (0.20)	0.12 (0.04)	0.27 (0.06)	0.70 (0.06)	0.08 (0.02)
NP (N=22)	20.9 + (10.0)	1.57 + (0.39)	1.47 + (0.15)	0.12 (0.06)	0.36 + (0.16)	0.70 (0.24)	0.09 + (0.04)
P (N=22)	15.1 * (12.3)	1.77 + (0.65)	1.43 (0.22)	0.15 + (0.07)	0.29 * (0.33)	0.57 (0.31)	0.06 +* (0.04)

BW = body weight, Ntim = support time normalized to 1, Slope = slope of line from touchdown to first local maximum, ZMin = local minimimum on vertical force-time curve, ZImpTo = total area under vertical force-time curve, SlopeTim = normalized time to first local maximum, PMax = Maximum propulsive force on the anterior-posterior force-time curve, PMaxTim = Normalized time to PMax, PImp = Area under the propulsive aspect of the anterior-posterior force-time curve;
+ Significantly different from able-bodied ($p<0.05$);
* Significantly different from nonprosthetic ($p<0.05$)

DEVELOPMENT OF A SUBJECT-SPECIFIC, DYNAMIC MODEL OF PATHOLOGICAL GAIT

Gary T. Yamaguchi, Jonathan I. Green, and Daniel W. Moran

Department of Chemical, Bio & Materials Engineering
Arizona State University, Tempe, AZ 85287-6006

INTRODUCTION

As part of a long-term study to determine the feasibility of predicting the post-surgical gaits of cerebral-palsied children via digital computer simulations, we developed a complex, 16 degree-of-freedom (DOF) walking model. This model is musculotendon-actuated, dynamic, in that it responds to the actions of forces and torques, and furthermore is bilaterally asymmetric, so that the separate but dynamically-coupled right and left legs can be configured with different dimensions, inertial properties, and musculotendon parameters.

These features will allow us to match, inasmuch as possible with our model, the features specific to a particular individual. It is hoped that such "subject-specific models", in conjunction with pre- and post-surgical 3-D gait analysis, will enable us to correlate changes to the musculotendon actuators imposed during surgery with alterations in the gait patterns. This paper describes our progress to date, and focuses upon the development of the model and our initial efforts to use lower-extremity MRI scans to determine model scaling parameters.

REVIEW AND THEORY

Musculoskeletal models of human ambulation have traditionally been configured to represent average body sizes and muscular strengths (Onyshko *et al.*, 1980; Yen *et al.*, 1987; Ju *et al.*, 1988; Pandy *et al.*; Yamaguchi *et al.*, 1990). Most of these models were, for reasons of simplicity, limited by earlier computing restrictions to planar movements and/or were bilaterally symmetric in nature.

With recent advances in imaging technology and computing power, the opportunity to construct 3-D, dynamic, musculoskeletal models that have *clinical relevance* is at hand. Magnetic resonance imaging (MRI) has been used to estimate body segment inertial properties (Martin *et al.*, 1989) and to measure muscle moment arms *in vivo* (Spoor *et al.*, 1992; Rugg *et al.*, 1990). A musculoskeletal model also requires the origin and insertion sites of individual muscles, and would benefit from information describing muscle-tendon pathways, fibre orientations, and resting fibre lengths.

PROCEDURES

Model Development. In order to choose which of the many degrees of freedom to include in the model, the DOF were prioritized according to the scheme specified in Yamaguchi (1989), which basically outlines a method for choosing the DOF most likely to contribute to the six determinants of gait (Saunders *et al.*, 1953). One DOF is in evidence at each knee, while two DOF are at each ankle and three DOF are at each hip joint. One DOF orients the foot, which has a curved plantar surface (Ju *et al.*, 1988), and one DOF each is evident in the trunk segment to account for lateral trunk bending, trunk flexion-extension, and axial rotation of the upper torso with respect to the pelvis (Figure 1).

Kane's method was utilized to derive the dynamic equations of motion (Kane *et al.*, 1985). The resulting FORTRAN dynamic simulation code was tested for accuracy with an energy test before adding energy-storage elements (nonlinear joint torques due to passive ligamentous structures) or energy sources and dissipators (musculotendon actuator models). The dimensionless musculotendon model (Zajac, 1989) includes simple first-order activation dynamics as a first order response to a step function representing "neural" control. Though this does not include the effects of recruitment or firing rate, it does achieve muscular forces of approximately the correct magnitude.

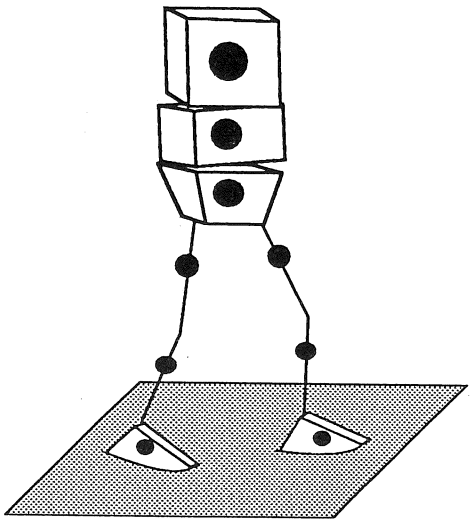

Figure 1. The 16-DOF pathological gait model. A sacrolumbar joint allows lateral trunk bending and flexion-extension. Another joint centered at T7 rotates the upper trunk about the axis of the spine.

MRI. The entire lower extremity 10-year old hemiplegic was imaged in two scans overlapping at the knee joint. Details of the volume acquisition are contained in a related proceedings article. 2mm x 2mm x 3 mm voxels were used to limit the acquisition time (and expense) of the overall scan. A finer scan utilizing 1mm x 1mm x 1mm voxels is planned to more accurately image the region in which surgery was performed.

Muscle volumes were computed by integrating the muscle cross-sectional areas of adjacent slices. Differentiation of muscles from one another was enhanced by displaying the muscle concurrently in the frontal, sagittal, and coronal planes.

RESULTS

The acquisition of musculoskeletal parameters via MRI was found to be difficult using 2x2x3 mm voxels unless muscles were relatively large and isolated. This was because muscles lying atop of one another, separated by a thin layer of fascia, can appear with incomplete boundaries in every view. Tendons were extremely faint relative to muscle tissue, and therefore obtaining origin and insertion sites without referring to secondary sources of information (*e.g.* bony landmarks and anatomy books) was all but impossible.

Even with these limitations, some marked differences were noted in muscle volumes between the right and left legs.

Forward-dynamic simulations of motion are currently underway to match the limb trajectories of the model to the limb trajectories measured via gait analysis. Preliminary results with this model and with a related, bilaterally asymmetric jumping model, indicate a high degree of sensitivity to the presence of slight asymmetries in the model.

DISCUSSION

An Argument for Increasing Model Complexity. The complexity with which we can model specific biomechanical movements might prompt one to ask whether it is indeed appropriate to continue the development of models with ever-increasing complexity. After all, simple models were valued initially because they could illustrate the mechanical principles of physiological movement with extreme clarity. Current forward-dynamic models typically include 10 coupled DOF or more, and are fast becoming "uninterpretable" and uncontrollable with present means. So why the push to greater and greater levels of complexity?

We have chosen to develop models of increasing complexity for several philosophical reasons. The first reason is to encourage the development of models that have relevance in medical practice. We and others aim to develop methods of predicting how surgeries will affect the physical capabilities of specific patients, which requires that our models be asymmetric, three-dimensional, and have sufficient DOF to model pathological ambulation. We also aim to develop methods of predicting how the patients' central nervous (control) systems will respond to the mechanical changes imposed by orthopaedic surgeries. As experience with an earlier 8-DOF gait model has shown (Yamaguchi *et al.*, 1990, 1991), the lack of sufficient DOF leads one to control solutions that may be optimal for the model but erroneous for actual human patients. For this reason, we believe that control solutions for more complex models more adequately represent control solutions utilized by the central nervous system to obtain the desired movement.

If this hypothesis is correct, adding DOF to a dynamic model can actually *decrease* the difficulty of obtaining optimal controls, because muscle electromyographic activity can be used to develop a good initial guess for an iterative optimal control routine. Though the EMG cannot reliably indicate muscle activation levels, EMG does indicate periods of relative activity and inactivity, which is information that can be put to good use in optimal control schemes as long as the model itself adequately matches the physiological system.

REFERENCES

Ju, M.-S. *et al.*, *J. Biomech. Engrg.*, **110**, 223-229, 1988.

Kane, T. *et al.*, *Dynamics: Theory and Applications*, McGraw-Hill, 1985.

Martin, P. *et al.*, *J. Biomechanics*, **22**, 367-376, 1989.

Onyshko, S. *et al.*, *J. Biomechanics*, **13**, 361-368, 1980.

Pandy, M. *et al.*, *J. Biomechanics*, **21**, 1043-1060, 1988ab.

Rugg, S. *et al.*, *J. Biomechanics*, **23**, 495-501, 1990.

Saunders J. *et al.*, *J. Bone Jt. Surg.*, **35-A**, 543-559, 1953.

Spoor, C. *et al.*, *J. Biomechanics*, **25**, 201-206, 1992.

Yamaguchi, G., *Ph.D. Thesis*, Stanford University, 50-55, 1989.

Yamaguchi, G. *et al.*, *IEEE Trans. Biomed. Engrg.*, **37**, 886-902, 1990.

Yamaguchi, G. *et al.*, *Adaptability of Human Gait*, Elsevier, 205-240, 1991.

Yen, V. *et al.*, *Biomechanics of Normal and Prosthetic Gait*, ASME, 1987.

Zajac, F., *CRC Critical Reviews in Biomedical Engineering*, 1989.

ACKNOWLEDGEMENTS

The authors wish to thank the Whitaker Foundation for its past and present support.

QUANTIFYING INTERFACE PRESSURES IN BELOW-KNEE AMPUTEE SOCKETS

M.J.N. Springer and J.R. Engsberg
Department of Mechanical Engineering and Human Performance Laboratory
University of Calgary, Alberta, CANADA.

INTRODUCTION

It is of vital importance that an amputees prosthetic socket fit comfortably. In order to consistently obtain a satisfactory fit it would be beneficial to devise a quantitative method of designing the shape of the socket. One aspect in this regard is to measure the pressure between the socket and the residual limb. In this pilot study, thin pressure sensors were used to measure the socket/residual limb interface pressures of two below-knee amputees during walking. High and low pressure regions were detected and were similar to those previously reported.

REVIEW AND THEORY

A socket for a below-knee amputee (BKA) must have a shape which accounts for the nonhomogeneity of the residual limb surface to tolerate loads. If loads are not properly distributed to the surface of the residual limb, sores develop and the socket is uncomfortable. There is currently no quantitative and repeatable means of ensuring comfortably fitting sockets for below-knee amputees. However, it has been proposed that there is a correlation between socket/residual limb interface pressures and socket comfort, Krouskop et al. (1987).

Steege et al. (1987) reported pressures at the interface during standing of 80 kPa at high pressure locations and 0 to 60 kPa for low pressure regions. Sanders (1991) reported peak normal pressures, during the stance phase of walking, ranging from 23 kPa to 184 kPa. These investigations had two limitations with respect to the present investigation. The first was that each pressure sensor only recorded pressure in a small localized region, not over a broad area. Secondly, special prostheses had to be fabricated for data collection. The purpose of this pilot study was to measure the pressures between the residual limb and the socket during walking using thin pressure sensors.

PROCEDURES

One 30 year old male BKA adult (Subject 1) and one 10 year old male BKA child (Subject 2) volunteered for this pilot study. The adult had been fit with a new prosthesis four days prior to testing, and the child had had his socket for two months. The subjects had both become amputees as a result of trauma, and each had a different prosthetist. In addition each amputee believed that he was wearing a comfortable socket. A nylon stocking was placed on the residual limb of the subject, and sensors (1 mm thin) were taped to four different limb locations (anterior, posterior, medial, and lateral). Bony prominences determined by a prosthetist to be areas of low pressure and soft tissue locations determined to be areas of high pressure were marked on the sensors. For example,in loading the residual limb, the tibial crest has been identified as an area of low pressure while the patellar ligament has been identified as an area of high pressure. The normal socket was placed over the residual limb and sensors and the remainder of the prosthesis was placed on the subject in the usual manner. Pressure data were collected with the subject walking along a short walkway. Two trials from each sensor were collected for each subject.

RESULTS

Three high pressure sites are presented for each of the two subjects 1) the patellar ligament (tendon bar) 2) the posteror wall, and 3) the posterior aspect of the calf (Figures 1,2). Two low pressure sites are also presented 1) the tibial crest, and 2) the lateral tibial condyle (Figures 3,4). The results for walking displayed a change in pressure throughout the support phase of the gait cycle for both the low and high pressure regions. Subject 1 had the greatest peak pressures on the posterior wall (105 kPa) while subject 2 had the greatest peak pressure on the patellar ligament (120 kPa). Both of these peak pressures occurred during the latter portion of support. The low pressure cycle for the region of the lateral tibial condyle peaked at the beginning of the cycle (10 kPa) for Subject 1, but peaked at the end of the cycle (24 kPa) for Subject 2. In the region of the tibial crest the waveform also varied between subjects. For Subject 1 the pressure on the tibial crest remained close to its maximum value for the majority of the cycle and peaked at about mid-cycle (15 kPa). For Subject 2 the peak pressure on the tibial crest (32 kPa) occurred at the beginning of the cycle (just after heal strike) and then dropped drastically (8 kPa) for the remainder of the cycle.

DISCUSSION

The different results between subjects could be due to subject age, socket age, anatomical characteristics of the residual limb, or the different characteristics of the prosthetists' in fabricating the socket. Nevertheless both subjects believed that they had comfortable sockets. This supports the conjecture by Krouskop et al. (1987) that a pressure range exists for fitting comfortable sockets.

The results for the three high pressure sites are slightly greater than those reported by Steege and Childress (1987) (80 kPa) and for the two low pressure sights, results are within their reported range (0-60 kPa). In comparison of results reported by Sanders (1991) for peak pressures during stance phase (23 kPa to 184 kPa), peak high pressures for both subjects, and peak low pressures for Subject 2 fall into this range. However, for Subject 1 (the adult male) peak low pressures fall short of this reported range. Further investigations should consider establishing and confirming these pressure ranges by gathering data on many subjects and systematically altering the socket shape to determine the resulting pressure changes.

REFERENCES

Krouskop T. et al. Arch. of Phys. Med. and Rehab.,68,(pp.713-714), 1987c.
Steege J. et al. ASME Symp. on Biomech. of Normal and Prosthetic Gait,BED-vol 4 , (pp.39-43), 1987b.
Sanders J : Ph.D. Thesis, University of Washington, 1991.

ACKNOWLEDGMENTS

The authors would like to acknowledge funding provided by Clynch Prosthetic and Orthotic Laboratory and Workers' Compensation Board - Alberta.

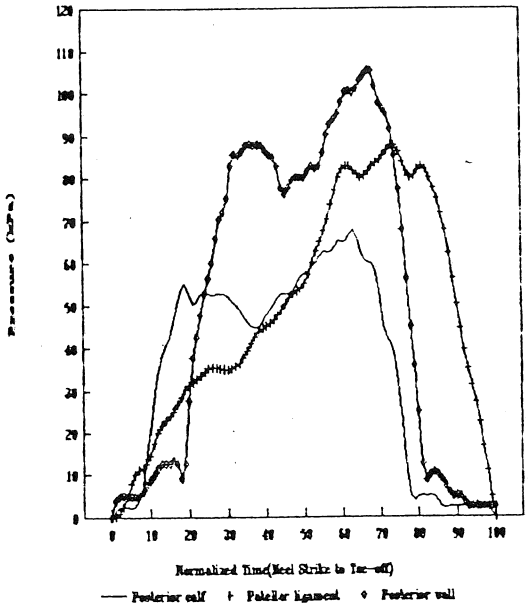

Figure 1. Residual Limb High Pressure Areas For Walking (Subject 1)

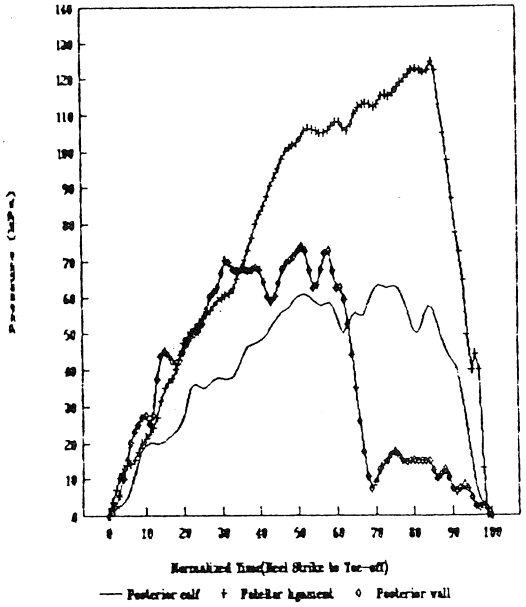

Figure 2. Residual Limb High Pressure Areas For Walking (Subject 2)

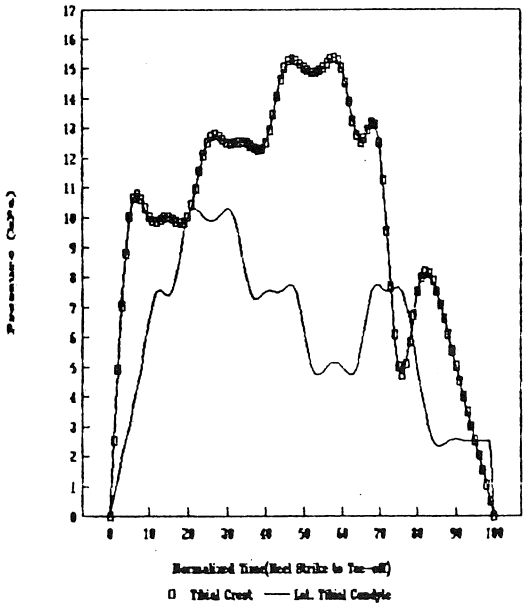

Figure 3. Residual Limb Low Pressure Areas For Walking (SubJect1)

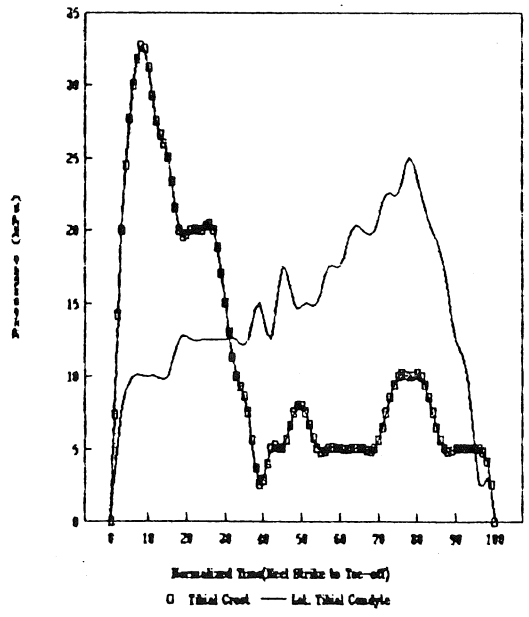

Figure 4. Residual Limb Low Pressure Areas For Walking (Subject 2)

THE INFLUENCE OF LUMBAR DISK HERNIATIONS ON GAIT

O.D. Schipplein, G.B.J. Andersson, M. Hickey and T.P. Andriacchi

Department of Orthopedic Surgery
Rush-Presbyterian-St. Luke's Medical Center, 1653 W. Congress Pkwy, Chicago, Il 60612

INTRODUCTION

One of the major problems in care of patients with spinal disorders is the diagnosis. Clinical history and examination, coupled with structural examinations such as CT, MRI and X-rays are helpful, but only allow a definitive diagnosis in some 20% of all patients. Further in that group, the sensitivity and specificity of individual test does not always permit definitive diagnoses to be made even in disease entities such as spinal stenosis and disc herniations. The purpose of this study was to test the hypothesis that a dynamic functional test would allow determination of deficits which, together with clinical examinations and imaging studies, will provide a more accurate diagnosis.

MATERIALS AND METHODS

Subjects scheduled for surgery because of a herniated nucleus pulposus were studied. The average age, height and weight was 36yrs (range 24 - 47), 181cm (range 171 - 185) and 88kg (range 71 - 113) respectively. Each subject was asked to walk a ten meter walkway. Ground reaction forces were obtained with a force plate and motion data was obtained with an optoelectronic system. Passive reflector markers were placed at the anterior aspect of the iliac spine, the greater trochanter, the center of the knee joint, the ankle and the fifth metatarsal. Moments were predicted at the hip, knee and ankle with a dynamic rigid link model. It was hypothesized that the subjects would walk with a style of gait that would reduce the moments at the joints whose primary muscle group was innervated by the nerve supplied by the irritated nerve root. Table 1 indicates the nerve involvement associated with a particular disk level herniation and the primary muscle group and joint effected by the nerve root irritation. The affected side was compared to the unaffected side for each subject. All subjects had both a physical examination and imaging studies performed to make the preoperative diagnoses. Clinical findings at surgery were used as the gold standard. The herniations were at the L5/S1, L4/5 and L3/4 levels.

RESULTS

Patients with herniations at the L5/S1 level avoided the use of the knee flexors on the affected side and walked with a reduced plantar flexion moment at the ankle compared to the unaffected side. Subjects with herniations at the L4/5 level walked with a style of gait that avoided the use of the flexors on the affected side as

compared to the unaffected side. The plantar flexion moment at the ankle was relatively uninvolved with only a small reduction in the moment compared to the unaffected side. Subjects with L3/4 herniations avoided the use of the extensors at the knee. The unaffected side had normal biphasic knee moments. The ankle plantar flexion moment was relatively uninvolved with a small reduction in moment when compared to the unaffected side.

DISCUSSION

This data, while preliminary, indicates that a daily activity such as walking is sensitive enough to indicate the side of a herniation or whether the herniation is medialized and not causing nerve root irritation. Subjects with a herniation at the L5/S1 level avoid the use of the knee flexors on the affected side and walked with greatly reduced ankle plantar flexor moments. Herniations at the L4/5 level results in walking with reduced involvement of the knee flexors and the ankle plantar flexors. The difference in the moments at the ankle could be explained by a slight difference in walking speed and not a result of the herniation. Subjects with L3/4 herniations walk with a style that avoids the net use of the quadriceps.

This data indicates the potential use of gait analysis as a low stress functional activity that could aid in the preoperative diagnoses of disk herniations.

TABLE 1

Level	L3/4	L4/5	L5/S1
Principal Cord Segment	L4	L5	S1
Primary Joint/Muscle			
Knee:			
Extensors	X		
Flexors		X	X
Ankle:			
Dorsi Flex.	X	X	
Plantar Flex.			X

THE EFFECTS OF KNEE IMMOBILIZATION ON CONTRALATERAL LOWER LIMB GAIT KINETICS

K.J. Lage, S.C. White, H.J. Yack

Department of Physical Therapy and Exercise Science
State University of New York at Buffalo, Buffalo.

INTRODUCTION

Non-operative treatment of acute knee injury typically includes joint immobilization for up to six weeks. Full weight-bearing ambulation with an immobilized knee places increased demands on uninvolved joints to compensate for lost knee function. A bilateral, sagittal-plane kinetic analysis was undertaken to identify changes in contralateral joint contributions to forward ambulation. Comparisons were made between kinetic measures of normal gait and braced gait with the knee fixed at three different angles: 0, 10, or 20 degrees. Significant changes were noted in the uninvolved limb joints, predominantly in the early stance phase of the gait cycle. There were no significant differences between brace angles; however, immobilization at 10 degrees resulted in the fewest variables differing significantly from normal.

REVIEW AND THEORY

The effect of immobilization on soft-tissue healing is well documented (Jenkins, 1986); however, bracing effects on the mechanics of walking has not been addressed. Immobilizing the knee of one limb will require compensatory walking strategies which have the potential to cause secondary problems at other joints, particulary joints of the uninvolved limb. In theory, immobilizing the knee at an angle approaching a normal flexion angle in stance should have less compromising effects on uninvolved joint mechanics. This study therefore proposed to 1) identify the effects knee immobilization has on contralateral lower limb joint kinetic measures, and 2) examine the effect of immobilization angle (0, 10, or 20 degrees of flexion).

PROCEDURES

For seven healthy subjects, three trials of normal gait, followed by five trials of braced gait (0, 10, or 20 degrees, assigned randomly) were videotaped on three separate days. Cadence was controlled with a metronome set to a pilot-determined 90% of each subject's natural preferred cadence. Reflective markers were affixed to six lower extremity anatomical landmarks, which were permanently marked to ensure consistent marker placement over the three test days. Normal trials preceded the application of the brace, which was size-normalized to leg length. Subjects were given a familiarization period prior to data collection such that the 90% cadence was comfortably achieved. Cartesian coordinates for the anatomical markers were determined by digitization of the video records (Peak Performance), and were digitally filtered using a fourth-order zero-lag Butterworth filter (Winter, 1990). A bilateral, sagittal-plane kinetic analysis was completed using an inverse dynamics approach (Winter, 1990), combining marker-defined segment kinematic and anthropometric data, and ground reaction force records (Kistler). Joint moments, powers, and work values were normalized to body mass (kg), time-normalized to 100% stride and averaged at 2% intervals. A one-way repeated measures ANOVA with post-hoc comparisons was used to test specific kinematic and kinetic measures for significant ($p < .05$) immobilization effects.

RESULTS AND DISCUSSION

Five of thirty-one kinetic measures selected for statistical analysis proved to be significantly different from normal under at least one braced condition (Table 1). Increased ankle generation power through toe-off was present with braced gait at 0 (B0) and 20 (B20) degrees of knee flexion, indicating greater contribution of the ankle plantarflexors to forward progression. The hip extensor moment in early stance was greater for the three braced conditions, although only B0 and B20 were significantly different. As a consequence of the increased extensor involvement, generation work at the hip in early stance was significantly greater for all braced

conditions. It is during this stage of support transition that the hip extensors are involved in trunk stabilization as weight is transferred to the support limb during the late stages of propulsion by the braced limb. An increase in knee generation power in early stance was present, but only during the B0 condition, perhaps as a result of the knee having to maintain an extended position to allow clearance of the foot of the braced limb at toe-off. In the braced gait at B0 and B20 there was a reduced knee extensor moment in early stance, indicating changes in extensor muscle activation and walking strategy. While no significant differences were present between bracing conditions, the least number of significant deviations from normal gait kinetics were evident for the B10 condition.

In summary, it was shown that weight-bearing ambulation with knee immobilization results in significant changes in joint kinetics of the contralateral lower limb. In light of the decreased ability of the braced limb to function normally, the contralateral joints were called upon to contribute most notably to forward propulsion and stabilization during support. These alterations in gait strategies have the propensity to cause secondary problems and as such, may need to be addressed in gait training and rehabilitation when employing immobilization treatment. Where joint immobilization is indicated, 10 degrees of knee flexion may be recommended based on our findings that there are fewer significant changes in gait mechanics.

Table 1. Significant Results from Selected Kinetic Measures

Dependent Measure	Condition	0°	10°	20°
Ankle Generation Power	Normal	2.358	2.551	2.600
(W/kg)	Braced	2.737*	2.658	2.879*
Knee Extensor Moment Early Stance	Normal	0.262	0.246	0.285
(Nm/kg)	Braced	0.137*	0.157	0.130*
Knee Generation Power Early Stance	Normal	0.549	0.490	0.552
(W/kg)	Braced	0.787*	0.620	0.666
Hip Extensor Moment Early Stance	Normal	0.704	0.713	0.727
(Nm/kg)	Braced	0.891*	0.817	0.865*
Hip Generation Work Early Stance	Normal	1.758	2.089	1.907
(J/kg)	Braced	4.527*	3.747*	4.543*

* denotes statistical significance between normal and braced condition measures ($p < .05$)

REFERENCES

1. Jenkins, DJ (1986) Ligament Injuries and Their Treatment. Aspen Publ., Rockville, MD.
2. Winter, DA (1990) Biomechanics and Motor Control of Human Movement, 2nd Ed. Wiley-Interscience, Toronto.

ACKNOWLEDGEMENTS

This study was supported by InCare Medical Products and a grant from the Mark Diamond Research Fund.

EXTERNAL LOADING OF INTACT AND ANTERIOR CRUCIATE LIGAMENT DEFICIENT CAT HINDLIMBS

J. G. Brooks, W. Herzog, T. R. Leonard

Human Performance Laboratory, University of Calgary, Alberta

INTRODUCTION

Onset and development of osteoarthritis has been associated with changes in the loading of joints (e.g. Moskowitz et al., 1979; Insall et al, 1972; Maquet, 1979; Bandi, 1972). Such changes in loading have presumably been produced in many animal models of osteoarthritis by transection of the anterior cruciate ligament (ACL), (e.g. Williams et al., 1982; Pond, 1973; McDevitt et al., 1977). However, quantitative and systematic determination of changes in joint loading has not been done in such situations. The purpose of this study was to determine the external loading of ACL transected hindlimbs in the cat, and to gather preliminary information that will allow quantification of joint loading in a second phase of this project. Vertical ground reaction forces were measured in five cats all having one intact and one ACL deficient hindlimb. Ground reaction forces were similar for the intact and ACL deficient hindlimbs before surgical transection of the ACL and were similar again after about 90-120 days post surgery. From the day of surgery to about 90 days past ACL transection, vertical ground reaction forces in the ACL deficient hindlimb were smaller than those in the intact hindlimb. Also, muscle mass of the triceps surae and plantaris muscles was reduced four and twelve weeks post ACL transection in the ACL deficient compared to the intact hindlimb, suggesting a disuse atrophy and/or training effect of the ACL transected and the intact hindlimb, respectively.

REVIEW AND THEORY

Tearing of the anterior cruciate ligament, for example due to a sports accident, may result in changes of articular joint contact forces due to changes in muscular forces, joint kinematics, and external forces. All three of these mechanical factors must be considered when trying to relate ACL tears to onset and development of osteoarthritis. In this study, one of these aspects, namely the changes in vertical ground reaction forces, associated with a surgically induced ACL transection, was investigated.

PROCEDURES

The anterior cruciate ligament was surgically transected in the left knee joint of six deeply anaesthetized cats under strictly sterile conditions. Vertical ground reaction force measurements were obtained from each animal before ACL transection and also after ACL transection for four weeks (one animal) twelve weeks (two animals), and seventeen weeks (two animals) at intervals of about two weeks. Ground reaction forces were measured while the two hindlimbs of the animals were supported by either two 75 by 150 mm force-platforms (AMTI) or a pressure platform (EMED) during feeding. In each session, three to five consecutive measurements were taken for each animal. Each measurement was made over a period of 1.5 s or longer while the animals were standing "quietly". Forces for each animal were averaged over the 1.5 s time period of measurement and over all trials in a given session. Following that, the mean vertical ground reaction forces on the left and right hindlimbs were expressed as a percentage of the total force on the two hindlimbs. Masses of the triceps surae and plantaris muscles were determined for the left and right hindlimbs in a terminal experiment at four and twelve weeks post ACL transection for two animals at each time.

RESULTS

Figures 1 and 2 show the distribution of relative weight between the left and right hindlimbs of the two "seventeen-week" cats. Day zero indicates the date of surgery; the corresponding data point was obtained before transection of the left ACL. Vertical ground reaction forces were almost identical on day zero for cat 1 (figure 1), whereas in cat 2 the left leg dominated the right leg by a ratio of about 60:40 (figure 2). Both animals then show a substantial unloading of the left hindlimb that continues for two to four weeks. After about four weeks, vertical ground reaction forces of the left hindlimb began to increase and approached (or even exceeded) those of the right hindlimb by 90-120 days, post surgery.

Table 1 shows the mean mass of the triceps surae and plantaris muscle group of the left and right hindlimbs for four animals, two animals at four weeks and two animals at twelve weeks post ACL transection. Muscle mass of the left hindlimbs was substantially reduced in comparison to that of the right hindlimbs, indicating disuse atrophy of the left hindlimb muscles, training of the right hindlimb muscles, or a combination of the two. This result supports the findings of figures 1 and 2 which suggest that the right hindlimb was loaded more than the left hindlimb during the first 12 weeks following ACL transection.

DISCUSSION

After ACL transection, cats tend to unload the injured hindlimb. This is consistent with data obtained from ACL deficient dogs (Visco, et al. 1990) and rabbits (unpublished findings). However, the time-history of unloading of the ACL deficient hindlimb in rabbits never reaches the extreme values found for the cats in weeks two and four, and does not recover after about 12 to 14 weeks as recorded for the cats (figures 1, 2). These results suggest that different animal models of osteoarthritis, even if produced using an identical procedure such as transection of the anterior cruciate ligament, may produce different mechanical responses depending on the animal. Differences in absolute and

relative mass of the triceps surae and plantaris muscles of the right and left hindlimbs were larger at four weeks than twelve weeks post ACL transection (table 1). This result parallels that of the external loading (figures 1 and 2) in that the differences in muscle mass are larger after periods of pronounced unloading of the injured hindlimb, (two to four weeks), compared to differences that occurred after a phase of increased loading of the ACL deficient hindlimb. It is hypothesized that muscle mass of the left and right hindlimbs will be about equal again a short time after vertical ground reaction forces have become equal (i.e. 14-18 weeks post ACL transection).

Morphological examination of the left and right hindlimbs of each of two cats four and twelve weeks post ACL transection showed clear signs of onset of osteoarthritis in the ACL transected joints. The injured knee joints had increased fluid contents, showed areas of additional bone growth, and had substantially increased thickness and mass of the articular joint cartilage. These results in conjunction with those obtained on external loading of the hindlimbs suggest that onset of osteoarthritis may be triggered by an unloading of the structures comprising a joint. However, before such a hypothesis may be stated firmly, the internal loading of the cat knee joint in an ACL deficient model must be assessed carefully.

Table 1 Masses of triceps surae and plantaris muscles of the left (ACL transected) and right hindlimbs at four and twelve weeks post ACL transection.

	4 weeks	12 weeks
Left	26.4 g	19.2 g
Right	31.3 g	22.2 g

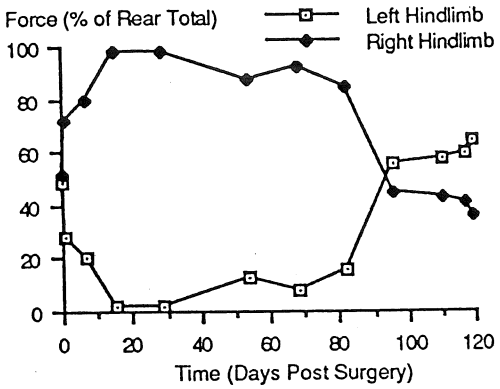

Figure 1. Loading of hindlimbs following ACL transection (Cat 1)

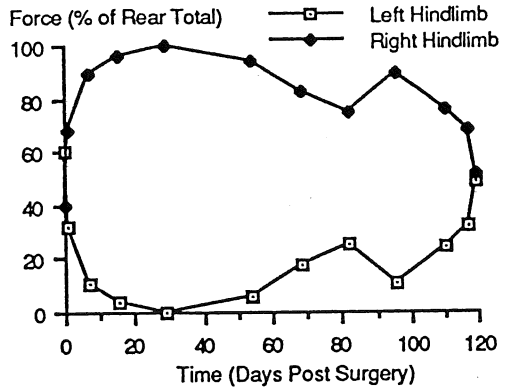

Figure 2. Loading of hindlimbs following ACL transection (Cat 2)

REFERENCES

Bandi, W. Helv. Chir. Acta. Suppl. 11, 3-70, 1972.
Insall, J. et al. Clin. Orthop. 88, 67-69, 1972.
Maquet, P. Clin. Orthop. 110, 177-196, 1979.
McDevitt, C. A., et al. J. Bone Jt. Surg. 59, 24-35, 1977.
Moskowitz, R.W. et al. Arthritis Rheum. 22: 155, 1979.
Pond, M. J. Ann, Rheum. Dis. 32, 38, 1973.
Visco, D. M. et al. Abstr., ORS Meeting, 36, 559, 1990.
Williams, J.M. et al. J. Anat. 134, 103-109, 1982.

ACKNOWLEDGEMENTS

This study was supported by grants from the Arthritis Society and NSERC of Canada and a scholarship from the University of Calgary.

MEASUREMENT OF PASSIVE TIBIAL TRANSLATION IN THE ACL INTACT AND ACL DEFICIENT CAT

Murray E. Maitland, Tim Leonard and Walter Herzog

Joint Injuries and Diseases Research Group, The University of Calgary, Calgary, Alberta

INTRODUCTION

The purpose of this study was to measure changes in passive knee joint range of motion associated with transection of the ACL in the anaesthetized cat. It was found that anterior tibial translation post-ACL transection was approximately double the pre-transection values. Under passive conditions the constraints to anterior drawer and Lachman testing are severely impaired by ACL transection. Therefore, experimental ACL transection in the cat causes significant knee joint laxity. This finding is relevant to the ACL deficient cat model for the study of osteoarthritis.

REVIEW AND THEORY

The clinical measurement of passive tibial translation in humans is considered to be important for the diagnosis of ACL injury, for determining the success of surgical outcomes, and to estimate a patient's disability as a consequence of ACL disruption (Daniel et al., 1985; Stäubli et al., 1991). Scientific studies of the tibiofemoral joint including cadaver studies, in vivo experiments and biomechanical modelling have been used to determine the function of the ACL as well as the implications of ACL deficiency.

Animal models, such as the dog, have been used to increase our understanding of the onset and development of osteoarthritis which is well known in the human ACL deficient patient (Pond, 1973). In human patients it has also been noted that there are alterations in muscular coordination and joint mechanics (McNair et al., 1989; Andriacchi, 1990; Kålund et al., 1990). Therefore, recently, the cat has been used for studies of ACL insufficiency because of its historical importance in neuromuscular and motion studies.

Jackson et al. (1991) have described methods to measure tibiofemoral motion in the goat. However, we are not aware of any studies of the effect of ACL transection on passive tibiofemoral joint range of motion in the cat. This information seems important for comparing study results across species and also for the interpretation of experimental findings regarding joint biomechanics in the freely moving cat.

The method described here was used in the acute setting to describe alterations in tibial translation following ACL transection. The method is also applicable to long-term cross-sectional studies and will be adapted for chronic, longitudinal studies.

PROCEDURES

Skeletally mature mongrel cats were anesthetized with a mixture of Halothane, oxygen and nitrous oxide. Incisions exposed the medial and lateral femoral condyles, the anterior tibial tubercle (distal to the insertion of the patellar ligament), and also the medial and lateral tibial plateaus. A 3mm drill hole, perpendicular to the long axis of the bone, was placed in each of these locations. Stainless steel insert nuts (Aircraft Fasterners, SanDiego) with an external diameter of 4mm were threaded into each drill hole (Figure 1).

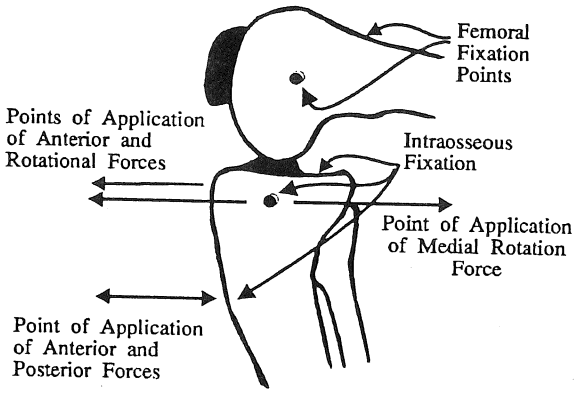

Figure 1. Placement of intraosseous insert nuts.

Dissection continued with an anterolateral incision at the knee joint, separation of the joint capsule and exposure of the ACL. This procedure was carried out prior to any measurements in order to ensure that any changes in joint mechanics were directly associated with transection of the ACL.

The femur was then firmly attached to an external frame by bolts and secured with opposing nuts. The ankle was supported by the same external frame. Rotation was allowed at the ankle joint in the plane of tibiofemoral motion but not translation.

Anterior, posterior, medial and lateral tibial translation, in addition to medial and lateral rotation were tested at 90° of knee flexion. Anterior and posterior tibial translation were also tested at 30° of knee flexion.

Resistive strain gauges (Micro-Measurements, Raleigh, NC) affixed to stainless steel elements, were mounted to the tibia in line with the applied force (Figure 2). One gauge was mounted to both tibial plateaus via cables and a spreader for measurement of anterior translation. Alternatively, a single gauge was used for anterior-posterior translation and was mounted to the anterior tibial tubercle by treaded rod. Two gauges were used to apply a moment to the tibial plateaus, with the forces directed in opposite directions, for both medial and lateral rotation. Force measurements were sampled at 200 Hz for each of the two gauges.

Concurrently, the passive motion of the knee was recorded at a frequency of 60 Hz using a video system (Motion Analysis, Sta. Rosa, CA). Reflective markers were used to facilitate digitization. A video camera was placed with its optical axis perpendicular to the plane of movement, superior to the tibiofemoral joint, for all tests at 90°. For anterior-posterior motion at 90° and 30° the camera was also placed on the lateral side with its optical axis perpendicular to the plane of motion.

Force data were smoothed by moving average of samples, offset, calibrated and synchronized to the digitized motion data. Digitized motion data were also smoothed, and calibrated before being combined with the force information.

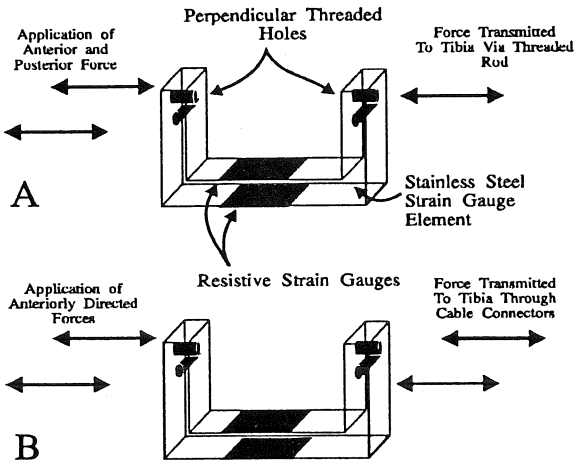

Figure 2. Force gauge orientation. A. In application of anterior and posterior forces directed along an axis parallel to the tibiofemoral joint through the anterior tibial tubercle. B. In application of anterior and medial and lateral rotations through the tibial plateaus.

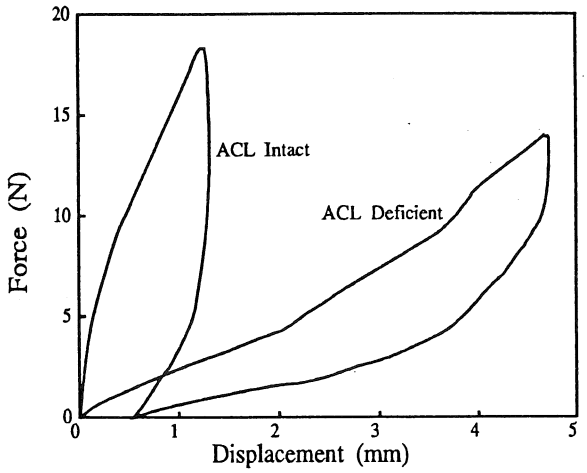

Figure 3. Force-displacement curve of the ACL intact and ACL deficient cat knee. Two single trials of anterior displacement at 30° immediately prior to and immediately after ACL transection.

Error in measurement of the motion analysis system was estimated by the maximum displacement of the femoral bone markers.

RESULTS

Anterior displacement of the tibia was significantly increased at both 90° and 30° of knee flexion. Figure 3 illustrates a typical force-displacement curve for anterior displacement before and after ACL transection. At 30° of knee flexion the average diplacement for three trials for this same animal was 1.6 mm at peak force. Following ACL transection this was increased to 4.1 mm.

Errors in determining centroids of markers during motion analysis and movement of the femoral bone markers accounted for .25 mm of apparent displacement.

DISCUSSION

Mechanisms reponsible for the onset and development of osteoarthritis in the ACL deficient knee have yet to be determined. Increased anterior drawer in knee extension past about 50° (in humans) is believed to cause increased shear forces within the ACL deficient knee (Grood et al., 1984). These shear forces may alter the distribution, magnitude and direction of the resultant loads on the tibiofemoral joint. It has been hypothesized that it is the changes in knee joint loads which result in articular cartilage disease. In this study, relatively low levels of force directed anteriorly through the tibial tubercle at both 30° and 90° produced significant anterior translation. However, in normal gait, the cat rarely achieves less than 60° of knee flexion and relationships between anterior shear forces and joint position are not known for the cat.

It is interesting to note that at 90° of knee flexion, anterior drawer is significantly reduced in humans (Torzilli et al., 1984). Proprioceptive feedback, action of the hamstring muscles and atrophy of the quadriceps muscles are believed to decrease the translation of the tibia on the femur during functional activity (Solomon et al., 1987; Kâlund et al., 1990). In addition, clinical and experimental observation seem to indicate that weightbearing is decreased during the acute stages of injury. Therefore, little is known about the functional consequences of increased anterior instability.

We concluded from this study that the effect of ACL transection on the passive motion of the tibiofemoral joint was similar to the effect of ACL injury on the biomechanics of the human tibiofemoral joint.

REFERENCES

Andriacchi, T.P. *J Biomechanics* 23:99-105, 1990.
Daniel D.M. et al. *J Bone J Surg* 67A:720-726, 1985.
Grood, E.S. et al. *J Bone Joint Surg* 66A:725-734 ,1984.
Jackson, D.W. et al. *J Bone Joint Surg* 73A:201-213, 1991.
Kâlund et al. *Am J Sports Med* 18:245-399, 1990.
McNair, P.J. et al. *Clin Biomechanics* 4:243-248, 1989.
Pond, M.J. *Ann Rheum Dis* 32:387, 1973.
Stäubli, H-U. et al. *Am J Sports Med* 19:172-177, 1991.
Solomon, M. et al. *Am J Sports Med* 15:207-213, 1987.
Torzilli, P. et al. *J Bone Joint Surg* 66A:1438-1442, 1984.

ACKNOWLEDGEMENT

This study was supported by a grant from the Canadian Arthritis Society

MODEL INTERPRETATION OF FUNCTIONAL ADAPTATIONS IN THE ACL-DEFICIENT PATIENT

R.P. Mikosz, C.D. Wu*, and T.P. Andriacchi
Department of Orthopedic Surgery
Rush-Presbyterian-St. Luke's Medical Center, Chicago Illinois
*Department of Orthopedic Surgery, Provincial Tao-Yuan Hospital
Tao-Yuan, Taiwan

INTRODUCTION

Changes in gait have been shown to exist in patients following rupture of the anterior cruciate ligament (ACL)[1]. These changes were characterized by an avoidance or reduction in the magnitude of the net moment tending to extend the joint generated by the quadriceps and hamstring muscles. These adaptive changes were shown to occur and increase with time[2]. The purpose of this study was to test the hypothesis that functional adaptations to an ACL deficient knee decrease the loading on the secondary restraints during activities of level walking and jogging.

METHODS

A three dimensional mathematical model[3] of the knee joint was used. The model included a mathematical representation of the menisci, ligaments, joint capsule, osseous structures, patellar mechanism and hamstring muscles.

Level walking and jogging were simulated by considering that the maximum moment tending to extend the knee occurs at a knee flexion angle of 20 degrees for level walking (midstance) and at 40 degrees for jogging. Cocontraction of quadriceps and hamstrings were simulated to produce a net quadriceps moment or a net hamstring moment where a ratio of 2 to 1 (agonist/antagonist) was assumed.

Forces in the secondary restraints were predicted for the two loading conditions. All forces were normalized to the magnitude of the force in the quadriceps and hamstring muscles and reported as a percentage.

RESULTS

The model predicted a force of 12 % in the capsule (Fig 1) during level walking for normal gait with the ACL and a force of 19 % for the ACL deficient knee. For the ACL deficient knee with a quadriceps avoidance gait the force in the capsule decreased to 10 %. The force in the menisci predicted by the model was 29 % for normal gait with the ACL and increased to 42 % for the ACL deficient knee. For the ACL deficient knee with quadriceps avoidance gait the force in the menisci decreased to 22 %.

The model predicted a force of 25 % in the capsule (Fig 2) for normal jogging with the ACL and 43 % for the ACL deficient knee. The force in the capsule decreased to 36 % for the ACL deficient knee with a reduced quadriceps moment. The force in the menisci for normal jogging with the ACL was 34 % and increased to 52 % for the ACL deficient knee. The force in the

menisci decreased to 43 % for the ACL deficient knee for a reduced quadriceps moment. There was no force in the MCL for normal jogging with the ACL. For the ACL deficient knee for normal jogging the force in the MCL was 11 % and increased to 13 % for a reduced quadriceps moment. There was a force of 1 % in the LCL for normal jogging with the ACL which increased to 21 % for the ACL deficient knee. In the ACL deficient knee with a reduced quadriceps moment the force in the LCL decreased to 20 %.

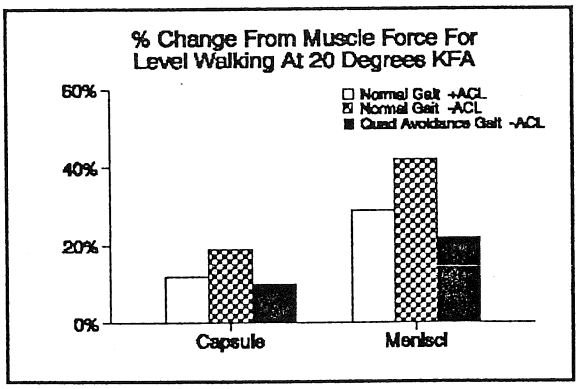

Figure 1 % change in force for level walking at 20 degrees knee flexion angle (KFA).

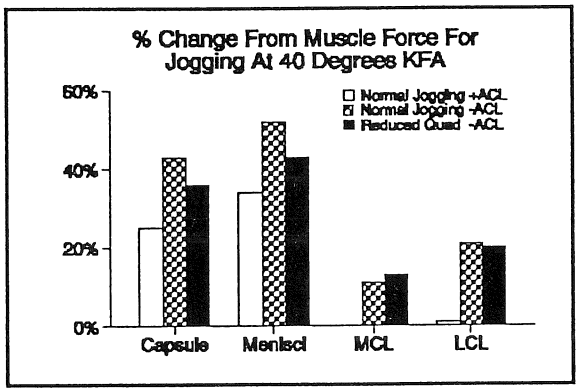

Figure 2 % change in force for jogging at 40 degrees knee flexion angle (KFA).

DISCUSSION

The results of the study suggest that during level walking, patients with an ACL deficient knee increase the force present in the secondary restraints with normal gait. However when patients have the quadriceps avoidance gait the forces in the secondary restraints decreases below that of a normal knee.

During normal jogging a net quadriceps moment is present for the normal knee with a reduced net quadriceps moment for the ACL deficient knee. Forces in the secondary restraints were increased for the ACL deficient knee for both a net extensional quadriceps moment of normal magnitude and one of reduced magnitude. Thus, in jogging it appears that patients cannot adapt sufficiently to reduce the secondary restraint forces to normal levels. These functional adaptations in the ACL deficient patient suggest a mechanism for protecting the secondary restraints.

REFERENCES

1. Berchuk, M., et al.: Gait Adaptations by Patients Who Have a Deficient Anterior Cruciate Ligament, JBJS 72-A(6):871-877, 1990.
2. Birac, D.A., et al.: Time Related Changes Following ACL Rupture, 37th Ann Meet Orthop Res Soc 16:231, 1991
3. Andriacchi, T.P., et al.: Model Studies of The Stiffness Characteristics of the Human Knee Joint, J Biomech 16(1):23-9, 1983.

ACKNOWLEDGEMENT

NIH Grant: AR39421

MOVEMENT ARTIFACT IN FORCE PLATE MEASUREMENT OF POSTURAL SWAY

D. Wisleder and B. Mclean

Biomechanics Lab Australian Institute of Sport, Canberra

INTRODUCTION

During a recent experiment on postural sway in archers, movement of the center of pressure (COP) was quantified for one second prior to arrow release. Center of Pressure movement did not relate to shooting accuracy or precision; however, a significant negative correlation between body-weight and COP movement indicated a possible artifact in the data. This study investigated the presence of an artifact in the determination of COP movement and its relationship to the weight on the force platform.

REVIEW AND THEORY

During force plate data sampling, it is common to sum the horizontal force signals into force couples and to amplify each vertical signal independently. This allows subsequent calculation of the COP (the point of application of the resultant ground-reaction force). Center of pressure is required for joint-reaction force and joint torque calculations (Winter 1979), but COP data is useful in its own right. The COP path has been reported for locomotion and other dynamic activities (Cavanagh et al. 1985; Mason 1991). In addition, COP movement has been quantified for a number of static postural activities (Mason et al. 1986; Niinimaa et al. 1983; Zernicke et al. 1982). There are potential problems with artifact, however, in the measurement of COP movement during static postural activities.

METHODS

A series of thirteen weights (200-1085 N) were placed motionless on a Kistler force platform and force data were sampled for 1 second at 250 hz (Mason et al. 1986). Full-scale force amplification was set at 1000 newtons/vertical channel and 500 newtons/horizontal channel. Raw data were smoothed with a 20 hz butterworth filter, and 3 measures of COP movement (Mason et al. 1986) were calculated separately for the x and y directions. Total excursion, range, and standard deviation of the COP in both the x and y directions were plotted against weight. A line of best fit was calculated for each of the six relationships. The regressions were tested for significance at the level p=.05.

RESULTS

Non-zero values for total excursion, range and standard deviation of the COP indicated movement of the weights. The magnitudes were greater along the long (y) axis of the force plate than along the short (x) axis. Maximal values were:

2.91 and 5.66 cm total excursion on the x and y axes respectively, .37 and .51 cm range, and .068 and .092 cm standard deviation. All 6 parameters were negatively correlated to mass by quadratic functions. The minimum apex of each regression was at or very close to 1000 newtons; though, the values were essentially constant above 800 N of vertical force. The data point above 1 kN was below the increasing quadratic regression line in all six of the graphs.

DISCUSSION

Center of pressure measurements of motionless weights had movement artifact related to the vertical-ground-reaction force. This interfered with comparisons of postural stability between subjects of different weight. The slope of the COP movement curves was zero above 800 newtons; however, most eligible subjects for postural study weighed less than 800 N. The authors believe that rounding error in analog to digital conversion caused the artifact. All three parameters were affected, but the artifact was cumulative for COP excursion. The artifact was negatively related to weight because vertical force was the divisor in the COP algorithm. Filtering raw force data at 20hz reduced the artifact significantly, but the remaining artifact was similar in magnitude to our previous measures of postural sway. In addition, the movement artifact was substantial compared to COP movement during standing (Zernicke et al. 1982) and shooting (Mason et al. 1986; Niinimaa et al. 1983).

Perhaps the COP movement curves will shift favourably if the amplification settings are reduced. This would reduce the force value of a charge unit; therefore, rounding error in the analog to digital conversion would decrease. In addition, the movement artifact might become constant at a lower weight which would facilitate comparison between subjects. Force-plate amplifier settings of 500 N vertical and 200 N horizontal would allow testing on a wide range of subjects provided the body weight is distributed close to the center of the plate and dynamic loading is avoided. Further testing is indicated to determine the level of movement artifact at these reduced amplifier scales. If the artifact magnitude remains significant after reducing the amplifier scales, it might necessitate the use of analogue data to measure postural sway.

REFERENCES

Cavanagh, P. et al. Int. J. Sport Biomech., 1, 36-62, 1985.
Mason, B. et al. Proceedings of the 13th International Congress on Biomechanics, Perth, Australia, (pp.97-99), 1991.
Mason, B. et al. Excel, 3(2), 17-20, 1986.
Niinimaa, V. et al. Can. J. App. Sci., 8(1), 30-34, 1983.
Winter, D. Biomechanics of Human Movement, (pp.65-82), John Wiley & Sons, 1979.
Zernicke, R. et al. J. Hum. Mov. Stud., 8, 1-13, 1982.

EFFECT OF AIRCAST APPLICATION AND ANKLE LIGAMENT ANESTHESIA ON ANKLE JOINT PROPRIOCEPTION

Jon W. Feuerbach[1], Mark D. Grabiner[1], Timothy J. Koh[1] and Garron G. Weiker[2]

[1]Department of Biomedical Engineering and Applied Therapeutics
[2]Department of Orthopaedic Surgery
The Cleveland Clinic Foundation, Cleveland, OH 44195

INTRODUCTION

Ankle sprains are one of the most common injuries among physically active people, most frequently affecting the lateral ligamentous complex. Trauma to lateral ligament mechanoreceptors has been hypothesized as producing a proprioceptive deficit in the ankle (Freeman *et al.*, 1965). Such loss in joint position sense may produce chronic abnormal ankle function (Glencross and Thornton, 1981).

The high incidence of ankle injuries has led to the design of various ankle orthotic supports such as the Aircast Air-Stirrup. The objective of this support system is to restrict undesirable ankle joint motion while providing minimal hindrance to normal joint mechanics. Although ankle bracing has been shown to reduce inversion-eversion (Gross *et al.*, 1991), no data exist which describe the effect of ankle bracing on ankle joint proprioception.

The first purpose of this study was to determine the contribution of the lateral ankle ligaments to ankle joint proprioception. This was accomplished by comparing the ability to match criterion ankle joint positions before and after anesthetizing these ligaments. The second purpose of this study was to determine the effect of Aircast application on ankle joint proprioception. It was hypothesized that: (1) anesthetizing the anterior talofibular ligament would produce a proprioceptive deficit greater than that of the non-anesthetized condition;
(2) anesthetizing both the anterior talofibular ligament and the calcaneofibular ligament would produce a greater proprioceptive deficit than anesthetizing the anterior talofibular ligament alone; and (3) application of the Aircast would reduce the proprioceptive deficit in the non-anesthetized and anesthetized conditions.

METHODS

Ten non-injured subjects performed a perceptual matching paradigm with their eyes closed. Each subject was seated in a chair that allowed his/her right foot to rest freely without touching the floor. The foot was manually placed in a criterion ankle position by the experimenter. After the investigator manually moved the foot back to the resting position the subject was instructed to match the criterion ankle position. A four camera Motion Analysis system was used to record the positions of four reflective markers placed on the shoe (two medial, two lateral) and four markers placed on the shank (two medial, two lateral) for each criterion and match position. The subjects attempted to match nine different criterion ankle positions that were distributed throughout the ankle's functional range of motion. The protocol was performed with and without Aircast application. The order of Aircast application (with or without) was randomized. This protocol was then repeated following anesthesia of the anterior talofibular ligament (Group I, n=5) or anesthesia of both the anterior talofibular and calcaneofibular ligament (Group II, n=5).

The orientation of the foot relative to the shank was determined from the corresponding marker sets and was specified by cardan angles of the following order: plantar-dorsiflexion, inversion-eversion, and forefoot abduction-adduction. These angles were calculated for each criterion and match position. The absolute error in the subjects ability to match the criterion position was calculated by subtracting the match angles from the criterion angles. A 2 by 2 by 2 ANOVA (Group I or II; with or without Aircast; anesthetized or non-anesthetized) was used to test for significant differences in the absolute error in matching the nine criterion ankle positions.

RESULTS AND DISCUSSION

No significant differences in matching the criterion positions were seen between Group I (one ligament anesthetized) and Group II (two ligaments anesthetized). Thus the data was pooled across the two groups (Table 1).

Table 1. Mean (SD) of the absolute error in matching the criterion positions (expressed in degrees).

	NON-ANESTHETIZED		ANESTHETIZED	
angle	NO AIRCAST	AIRCAST	NO AIRCAST	AIRCAST
pf-df	4.5(3.4)	2.3(2.1)*	4.6(3.8)	2.1(1.6)*
in-ev	3.4(2.3)	1.7(1.5)*	3.5(3.0)	1.9(1.4)*
ab-ad	2.4(2.2)	1.3(1.3)*	2.3(2.5)	1.4(1.0)*

pf-df: plantar-dorsiflexion angle
in-ev: inversion-eversion angle
ab-ad: forefoot abduction-adduction angle
* significantly different from no Aircast condition ($p<0.01$)

No significant differences were seen between the non-anesthetized and anesthetized conditions in matching the criterion positions. Thus, these results do not support the first two hypotheses which state that anesthetizing a lateral ankle ligament produces a proprioceptive deficit, and anesthetizing two lateral ankle ligaments produces a greater proprioceptive deficit than anesthetizing only one lateral ankle ligament. These results are in agreement with those of Barrack *et al.* (1983), who concluded that knee anesthesia had no effect on knee joint position sense. Location of a limb in space, in the absence of visual information, must be detected by kinesthetic receptors in the joints, skin and muscles. Possibly, the deafferentiation of some of the ligament mechanoreceptors by anesthesia is not enough to offset afferent feedback from skin, muscle and other joint receptors.

Significant differences in matching the criterion positions were seen between the Aircast and no Aircast conditions. This result supports the third hypothesis which states that Aircast application would reduce the proprioceptive deficit in matching the criterion position. Aircast application may increase the afferent feedback from cutaneous receptors which may in turn lead to an improved ankle joint position sense. Also, there is some evidence that ankle joint position is more difficult to perceive for large ranges of motion compared to small ranges of motion (Glencross and Thornton, 1981). Since the Aircast constrains ankle range of motion, these difficult to perceive ankle joint orientations may not be accessible, and the errors in matching a prescribed ankle position may be reduced compared to the no Aircast condition.

In conclusion, anesthetizing the lateral ligaments of the ankle seemed to have little effect on ankle joint proprioception. In contrast, Aircast application seemed to facilitate ankle joint proprioception.

REFERENCES

Barrack RL, *et al.* Am J Sports Med 11(4):258-261, 1983.
Freeman MAR, *et al.* J Bone Joint Surg [Br] 47:678-685, 1965.
Glencross D, Thornton E J Sports Med 21:23-27, 1981.
Gross MT, *et al.* J Orthop Sports Phys Ther 13(1): 11-19, 1991.

This work was supported by a grant from the Aircast, Corporation.

PHASE PLANE ANALYSIS OF POSTURAL STABILITY

Patrick O. Riley, David E. Krebs and Brian Benda

Biomotion Laboratory, Massachusetts General Hospital, Boston 02114

INTRODUCTION

We analyze the standing balance control of subjects with bilateral vestibular hypofunction using phase plane plots. Two different phase plane (velocity verses displacement) plots are used, one based on estimated center of gravity movement and one based on measured center of pressure displacement. Center of gravity kinematics are estimated using an 11 segment whole body model and kinematic data obtained using a SELSPOT/TRACK motion analysis system. The center of pressure displacements are measured using force plates. Stability is varied by altering the base of support and visual input. Three different foot placements are used; feet 30 cm. apart, feet together (side by side), and semi tandem stance. The subjects stand with the feet together with eyes open and with eyes closed. Both types of phase plane plots reveal decreases in stability as base of support is altered or visual input is removed. Phase plane plots based on center of gravity are different from phase plane plots based on center of pressure due to dynamics. However, both types of plots appear to be informative.

REVIEW AND THEORY

Vestibular function testing is commonly done using force plates and some measure of center of pressure (CoP) movement referred to as postural sway. A number of different parameters are used to quantify postural sway; linear measures such as mean sway path (Kantner *et al* ,1991), area measures; e.g. sway area and velocity measures as mean sway velocity (Enbom *et al*, 1991).

We hypothesize that maintaining postural stability requires not only control of the center of gravity (CG) position but also control of the center of gravity momentum. CoP position is an indicator of CG position. In fact, the two are often treated as synonymous. CoP displacement is identical to CG displacement only when the displacement velocity is infinitesimally small. When CG velocity is not insignificant, when dynamics must be taken into account, the CoP displacement and the CG displacements are different. The fact that CoP displacement is a function of CG velocity and acceleration as well as CG displacement may well account for its usefulness as a measure of postural stability.

We present here a more direct approach to postural sway analysis. Phase plane plots provide a means of examining the CG kinematics that characterizes both CG displacements and CG velocity, as well as their interrelationship. A phase plane plot is developed by plotting the derivative of a parameter against that parameter. Because we believe that postural stability is achieved by controlling both CG displacement and momentum, we expect that phase plane plots of CG velocity (proportional to momentum) against CG displacement will be useful. Also, while CG kinematics is of interest on purely theoretical grounds, CoP displacements are easier to measure. Hence, we also present here phase plane plots based on CoP displacements.

PROCEDURES

The CG displacements are estimated from whole body kinematic data. Kinematic data was acquired using a four camera SELSPOT II/TRACK kinematic data acquisition system, sampled at 153 Hz. This data and subject specific anthropometric data were incorporated into our 11-segment whole body model, Riley *et al.*, (1990) to estimate the body CG kinematics.

The CoP was measured using two force plates (Kistler 9280?). The subject stood with one foot on each force plate. The combined CoP was calculated from the individual force plate CoP's and the known force plate positions. Force plate data was obtained at 153 Hz in synchrony with the kinematic data. Both the kinematic and force plate data sets were 7 seconds long.

The subjects were told to stand as still as possible. The base of support was varied by controlling foot placement. The baseline wide base of support was obtained by placing the feet approximately 30 cm. (**30 cm**) apart. One foot was placed on each force plate. The narrow base of support was obtained by placing the feet side by side, but not touching. The subjects stand with the feet together with eyes open (**eo**) and with eyes closed (**ec**). For semi-tandem (**st**)

stance the feet were the same distance apart as for the narrow base of support. The heel of the forward dominant foot was even with the toe tips of the hind foot. In each case the feet were parallel to each other and to the anterior posterior (AP) plane.

Six subjects for this pilot study were selected from a group of patients with bilateral vestibular hypofunction (BVH) being evaluated in the as part of a study of the effectiveness of vestibular physical therapy. The BVH diagnosed was based on the results of sinusoidal rotation tests and electronystagmography performed at the Jenks Vestibular Laboratory at the Massachusetts Eye and Ear Infirmary.

RESULTS

Figure 1 shows a set of CG phase plane plots representing ten standing trials from a test session of a BVH patient. In addition to the standard test, this subject was also able to perform semi-tandem eyes closed (st ec), tandem eyes open (t eo) and eyes closed (t ec) stance. The plots show the lateral CG velocity plotted against the lateral CG displacement. Lateral CG kinematics was selected for analysis because the manipulation of foot position primarily effected the lateral base of support. The small pattern of Plot 7 indicates relative stability of the **30cm** condition. The larger patterns of plots 1 and 2 indicate that the feet together **eo** condition is less stable than **30cm** support. Plots 5 and 6 indicate that **st** stance is less stable. A further decrement in stability is seen with the **t eo** condition (plot 8). Postural stability is somewhat less for eyes closed (plots 3, 4, 7 and 9) than the corresponding eyes open condition.

The corresponding CoP phase plane plots (Figure 2, note change in scale) for the same data set indicate the same relative stability progression throughout the different stance conditions. The relative stability progression shown is typical but variations are seen. For example, the effect of removing visual input is not always apparent in patients with milder vestibulopathy.

DISCUSSION

On the basis of our pilot study it appears that the CG and CoP phase plane plots are indicative of relative postural stability. CoP phase plane plots, which are easier to obtain, appear to be at least as informative as CG phase plane plots. The sensitivity of postural stability to alterations is base of support and visual input is readily apparent. Studies of normals, additional BVH patients and other balance impaired patients are needed.

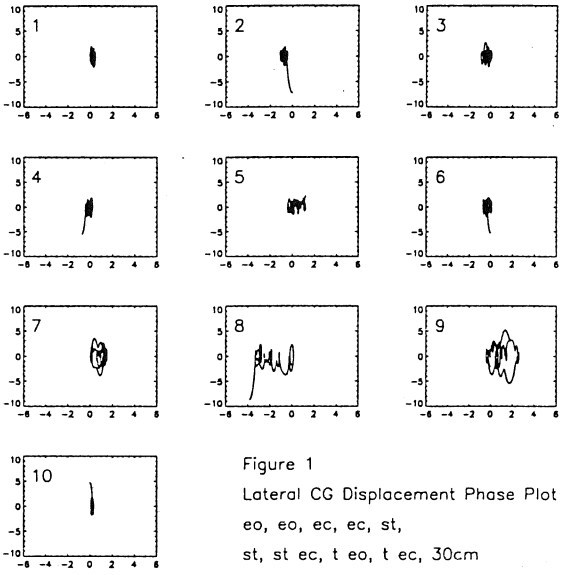

Figure 1
Lateral CG Displacement Phase Plot
eo, eo, ec, ec, st,
st, st ec, t eo, t ec, 30cm

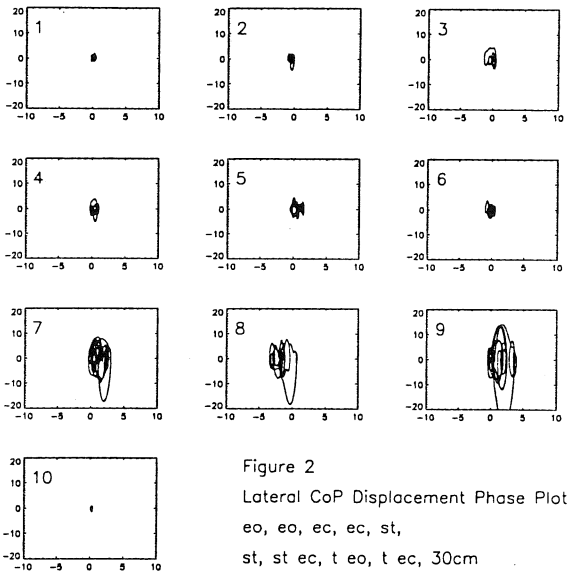

Figure 2
Lateral CoP Displacement Phase Plot
eo, eo, ec, ec, st,
st, st ec, t eo, t ec, 30cm

REFERENCES

Enbom et al, Ann Otl Rhinol Laryngol,**100**,472-8,1991.

Kantner et al, Am J Otolaryngol, **12**,196-204,1991.

Riley et al, J Biomech.,**23**,503-505,1990.

ACKNOWLEDGMENTS

This work was supported by a grant from the Whitaker Foundation and by NIDRR Grants H133G0025-91 and H133E00024.

BIOMECHANICAL ANALYSIS OF THE POSTURAL CONTROL OF VOLUNTARY ARM RAISES: EXPERIMENTAL AND SIMULATED MODELS

J.J. Eng, D.A. Winter, A.E. Patla and C.D. MacKinnon

Department of Kinesiology, University of Waterloo, Ontario, Canada.

INTRODUCTION

Voluntary arm movements during the upright human stance position impose a perturbation to an already unstable posture characterized by a high centre of mass (COM) located over a narrow base of support. Two effects of the perturbation must be opposed: reactive moments created by the arm movement, and the displacement of the arms which alters the COM position of the total system. Kinematic and kinetic analyses, as well as model simulations were used to gain insight into the postural control during this task. The centre of mass regulation was found to be inextricably linked to the reactive moments created by the focal (arm) movement.

REVIEW AND THEORY

The postural activity of the trunk and lower extremities during voluntary arm movements has been documented using electromyography, accelerometry and kinematic imaging techniques (Bouisset *et al.*, 1987; Friedli *et al.*, 1988, Lee et *al.*, 1987). The underlying mechanical causes of the observed kinematics are the moments of force which are representative of the final common mechanical pathway of the neuromuscular system. The lower limb postural moments must not only counteract the focal moment but also generate kinematics to maintain the COM within the base of support. In the past, the centre of pressure or a marker on the trunk has been used to approximate the COM position of the whole body, but a complete kinematic analyses which accounts for all body segments is necessary for valid results.

Simulations of the upright stance posture have potential for increasing the understanding of postural control strategies (Yang *et al.* 1990). The model in this study examines the response to an input perturbation (focal moment) under different conditions of postural stabilization. The biomechanical demands of the task can be assessed through an examination of these effects on the COM and reactive moments.

PROCEDURES

Six subjects stood on a forceplate grasping a light rod between the two hands and were instructed to move their arms from the vertical position up to the horizontal as rapidly as possible with full elbow extension. The movement was self-initiated and assumed symmetrical. Reflective markers fixed to the right side of the subject were recorded by a charge-coupled device video camera at 60 Hz. The video system was interfaced with a frame grabber which produced coordinates with less than .3 cm RMS error. The digitized marker coordinates and forceplate data were filtered with a critically damped, zero-lag filter at 3-7 Hz and 30 Hz, respectively, and used as input into an inverse dynamic model (fourteen segments comprising feet, legs, thighs, pelvis, abdomen, thorax, head-neck, upper arms, and forearms-hands). Moments were calculated in the sagittal plane. The horizontal COM displacements were defined such that the arm COM = the arm, forearm and hands, postural COM = the body excluding the arms, and the net COM = all body segments.

The simulation model comprised the same anthropometrics used in the inverse model for one representative subject except that the ankle joint was pinned to the inertial reference frame and the trunk (pelvis, abdomen and thorax) was represented as one rigid segment. A multibody dynamic simulation tool was used (Automatic Dynamic Analysis of Mechanical Systems) which incorporates Lagrangian techniques to derive the equations of motion once the model components are defined. The equations are then solved using a Newton-Raphson procedure and integrated by a Gear integration algorithm (Ryan, 1990). The input to the simulation was the shoulder moment-time history recorded from the representative subject (Figure 1). The model output consisted of the kinematics of each segment from which the net COM was calculated. The first model simulated the arm movement with complete and instantaneous stabilization of the postural joints such that no motion of the body took place. The second model repeated the simulation of the arm movement but without any postural stabilization, thus there was no attempt to counteract the reactive moments.

RESULTS

In all six subjects, the positive shoulder flexor moment was counteracted by negative moments of the lower limbs (hip extensor, knee flexor and ankle plantarflexor moments) (Figure 1). These results are in agreement with Weiss *et al.* (1979) who reported counteractive moments of the lower extremity joints in response to shoulder flexion. The peak shoulder moment was at least 20 ms prior to the virtually simultaneous peaks of the ankle, knee and hip moments. The peak hip-knee moment ratio was relatively fixed (1.9 ± .5, N=6) while the peak knee-ankle moment ratio was highly variable. The moments generated kinematics which resulted in a posterior movement of the lower limbs and a slight forward flexion of the trunk. The overall motion constituted a posterior postural COM displacement which countered the anterior arm COM displacement and effected a gradual increase of the net anterior COM displacement over time (1.1 ± .4 cm, N=6) (Figure 2).

In the first simulation with complete and instantaneous postural stabilization, the input shoulder moment caused the arm to overshoot the horizontal position and then settle to the horizontal position as observed in the experimental trials. The simulated net COM displacement was initially posterior because the subject underwent a slight shoulder extensor countermovement prior to the flexor movement. The net COM was then rapidly displaced in an anterior direction (2.3 cm) and was a direct result of the arm displacement (Figure 3). Thus, the net COM displacement was approximately double that of the experimental trials which incorporated postural movement. In the second simulation, the shoulder

flexor moment applied an extensor moment to the upper end of the trunk. In the absence of joint stabilization, the lower end of the trunk rotated away from the arm segment. This then caused the trunk to rotate forward, the knees to flex, and finally the body to collapse. Initially, the arm COM displacement is countered by the posterior displacement of the lower end of the trunk such that the net COM displacement gradually increases over time as in the experimental trial. But, as the trunk rotates forward, an exponential increase in the net anterior COM displacement takes place (Figure 3).

DISCUSSION

The collapse of the model in the absence of postural stabilization emphasizes the importance of the postural moments in maintaining the upright posture. A stabilizing moment must be applied to the lower end of the trunk to counter the reactive moment imposed on the upper trunk. In turn this stabilizing moment applies a reactive moment to the adjacent distal segment which results in a destabilization to the proximal thigh segment. The sequence of destabilization/stabilization continues until the most distal segment (ie., the foot) is encountered. Thus, the destabilizing/stabilizing effects must be virtually simultaneous in order for the large hip moment to be effective in directly controlling the large inertial characteristics of the trunk and to minimize subsequent postural adjustments to regain equilibrium. It is possible that since the sequence of destabilization/stabilization commences at the upper trunk and its effects are translated distally, the ankle joint may exert the final fine tuning control if stabilization is not completely established by the fixed hip/knee moment relation. As the postural moments peak slightly after the shoulder moment, a slight initial destabilization of the trunk segment may facilitate the posterior displacement of the lower limbs and forward flexion of the trunk observed in the experimental trials.

The kinematics of the system demonstrate the precise control of the net COM displacement as the arm COM displacement is almost completely offset by the postural COM displacement. In the experimental trials, the postural movement reduces the displacement and rate of change of the net COM over the model condition with complete postural stabilization but no postural movement. Although two extreme conditions of postural stabilization were modelled, the experimental results suggest that the actual postural strategy is a compromise between joint stabilization and COM regulation. The regulation of the net COM displacement and the simultaneous postural moments are two strategies with effects which are not independent of each other. These results demonstrate the temporal and spatial coordination of the postural and focal activity at the kinetic level.

REFERENCES

Bouisset, S. et al. *J. Biomech.*, **20**, 735-742, 1987.

Friedli, W. et al. *J. Neurol. Neurosurg. Psychiatry*, **51**, 232-243, 1988.

Lee, W. et al. *Exp. Brain Res.*, **66**, 257-270, 1987.

Ryan, R.R. (1990) In: Multibody Systems Handbook, W. Schiehlen (ed), (pp.361-402), Springer-Verlag, 1990.

Weiss, P. et al. *Proceedings of the 4th Congress of ISEK*, Boston, (pp.40-41), 1979.

Yang, J.F. et al. *Biol. Cybernetics*, **62**, 309-320, 1990.

ACKNOWLEDGEMENTS

The authors acknowledge the financial support of MRC MT4343 and a NSERC fellowship to J. Eng, and the technical assistance of Mr. P. Guy and Mr. M. Ishac.

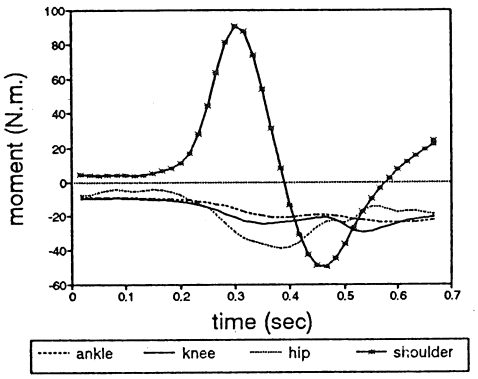

Figure 1. Experimental moments for a representative subject (+ moment = shoulder flexor, hip flexor, knee extensor and ankle dorsiflexor)

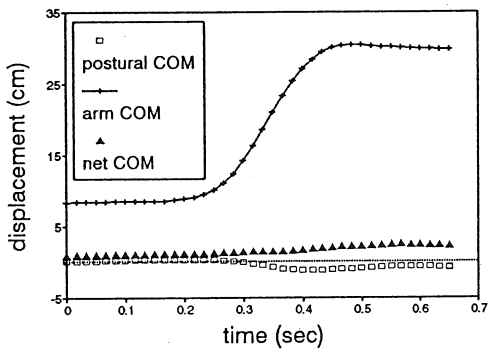

Figure 2. Postural, arm and net centre of mass (COM) displacements for a representative subject (+ = anterior displacement).

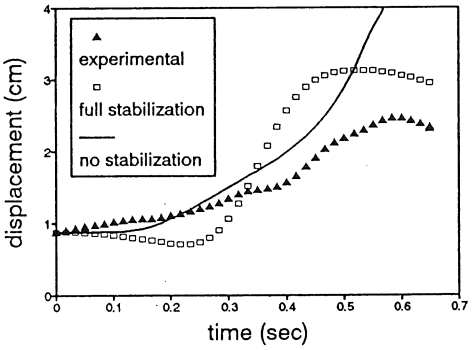

Figure 3. Net centre of mass displacement for the experimental (one representative subject) and model simulations (+ = anterior displacement).

UNPERTURBED FOOT BEHAVIOR DURING PREDICTABLE WALKING INSTABILITY CONDITIONS.

Michel A. Leroux and Paul Allard

Pediatric Research Centre, Sainte Justine Hospital, Montreal CANADA H3C 3J7
Departement of Physical Education, University of Montreal, CANADA H3T 1C5

INTRODUCTION

Locomotion has been well described in term of propulsion mechanisms but balance and joint stabilization were studied at a less extend. Predictable perturbations were used to produce instability during walking gait. The contralateral limb showed more dorsiflexion during push-off and less plantarflexion at toe-off resulting in a longer flat foot period. This stabilization mechanism is assited by higher coactivation of tibialis anterior and peronneus longus and a faster leg movement during early swing. Balance and joint stabilization control may be consider as a major limitation of locomotion even if propulsive resources are present.

REVIEW AND THEORY

Locomotion has been well described in term of propulsion mechanisms involving energy, work and power. Even though propulsion is the major goal, bipodal gait cannot be achieved without balance and joint stabilization. Propulsion and stabilization mechanisms are intimately related during normal walking gait. The best way to study stabilization is to insert perturbation during normal gait and described the adjustments that take place in this condition of instability. In most of these studies,unpredictable perturbations were used to quantify the reflex and voluntary reaction components of stabilization processes (Brunt et al.,1990; Dietz et al.,1987).

However, gait is a well controled cyclic activity witch is highly predictable as most of instability situations such as stairs or holes. Then the contralateral leg may be used to maintain balance since it can adjust itself during the late stance to modify the fallowing stance phase dynamics (Dietz et al.,1989). The contralateral foot would be the most affected segment since it is the first mobile link with the ground. It participates actively to propulsion and adapts itself to the ground surface allowing normal hip and knee movements (Kesner et al.,1988; Nashner,1980).

The object of this study is to describe unperturbed foot behavior modifications during predictable instability situations.

PROCEDURES

Ten subjects with no orthopaedic problems or falling history participated to this project. There was five testing conditions including normal gait. Instability conditions consisted of a 15° forward slope inducing pronounced plantarflexion (PF) and a 15° medio-laterally inclined plane inducing inversion (INV) of the foot. Both perturbations might be fixed or mobile. Anatomical literature suggests ankle instability in exaggerated PF and subtalar joint instability in inversion. In mobile conditions, the horizontal plate under the foot rotate of 15° at the contact of the heel to produce a movement in PF or INV. Mobile conditions were considered as more unstable. The subjects always knew exact features of the perturbation during a trial.

Foot kinematics, ground reaction forces (GRF) and EMG of the contralateral tibialis anterior (TA), peroneus longus (PL) and

gastrocnemius (G) were collected for each of five trials.

RESULTS

Stance phase duration and GRF were not affected by the presence of the perturbations. However, PF/DF movement patterns were highly modified during perturbed conditions (Figure 1). There was larger DF of the foot (4-8°) with mobile perturbations and smaller PF at toe-off (6-15°) in all conditions. This behavior produces a longer flat-foot period (50-75 ms) allowing a good base of support for the heel contact of the perturbed limb. The early swing phase was also different in instability condition. The contralateral leg is brought close to the other leg faster allowing the possibility of a more efficient response to an inadequate behaviour of the perturbed leg.

EVER/INV movements were not affected by the perturbations but muscles acting at the subtalar joint, TA and PL seems to coactivate, increasing joint stiffness and stability during late stance (Figure 2).

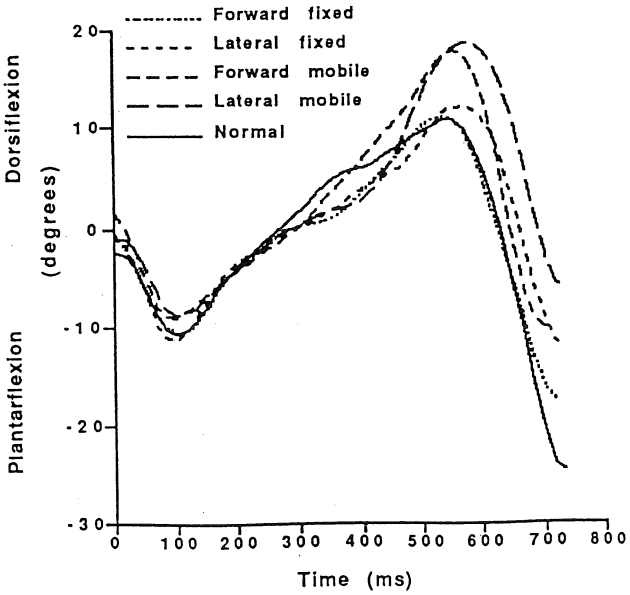

Figure 1

DISCUSSION

The muscular and kinematic behaviors of the contralateral leg during predictable instability conditions were used to enlarge support base and increase rearfoot stiffness and stability. These mechanisms assisted the perturbed leg to maintain balance allowing efficient propulsion and gait. Unpredictable perturbations would not allow this stabilization process to take place, falls and injuries will occur more easily.

The deficiency of the stabilization mechanisms may be consider as a major limitation of locomotion even if propulsive resources are present. This may be the case for different patients such as amputes, blind, elders or hemiplegic.

What if the inefficiency of pathological gait depends on a lack of stabilization in place of propulsion mechanisms deficiency.

REFERENCES

Brunt et al.,*Arch. Phys Med Rehab*,**71**, 473- ,1990.
Charteris et al., Ergonomics, 32, 1539- , 1989.
Dietz et al., *J. Neurophys.*, **62**, 841- , 1989.
Dietz et al., *J. Physiol.*, **386**, 149- , 1987.
Keshner et al., *Exp. Br. Res.*, **71**, 455- ,1988
Nashner, *J. Neurophys.*, 44, 650- , 1980.

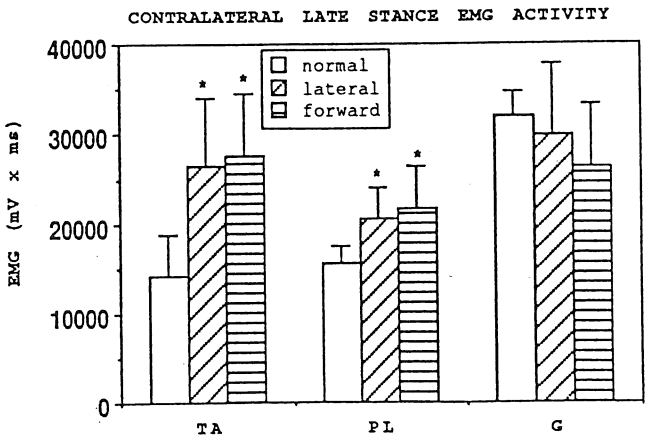

Figure 2

ERGONOMICS

Podium Session 17

FINGERTIP IMPACT LOADING DURING KEYBOARD USE

D. Rempel, J.T. Dennerlein, C.D. Mote, Jr., and T. Armstrong

Ergonomics Laboratory, Division of Occupational Medicine, University of California at San Francisco
Department of Mechanical Engineering, University of California at Berkeley
Department of Industrial Engineering, University of Michigan

ABSTRACT

A new method is presented for measuring fingertip force during a keystroke while subjects type on a computer keyboard. A piezoelectric load cell is mounted in a keycap. Force histories, collected on four touch typist demonstrate three distinct phases: key switch compression, finger impact, and fingertip pulp compression. Each keystroke contained two maximum occurring during finger impact and pulp compression. Finger tip velocities ranged from 0.28 to 0.66 m/s.

INTRODUCTION

Chronic musculoskeletal disorders, such as carpal tunnel syndrome, muscle pain syndromes, wrist tenosynovitis, and epicondylitis have been linked, in cross-sectional epidemiologic studies, to prolonged use of computer keyboards (Sauter 1991, Smith 1981, Burt 1990). In other occupational settings, these disorders have been associated with activities ainvolving prolonged, repetitive and forceful hand activities (Silverstein 1987, Rempel 1992). Finger movements during computer keyboard work are repetitive, and can be as high as 200,000 keystrokes per day. The characteristics of finger force while using a keyboard; however, are unknown. As a first step to developing a biomechanical model of keying, accurate methods are needed for assessing fingertip impact force. In this study a keyboard was instrumented to measure the vertical fingertip force applied by a finger during a typical typing task.

METHODS

The "h" key of a standard Apple Extended II keyboard (ssn) was instrumented with a piezoelectric load cell above the key switch mechanism to measure the direct vertical force applied by the fingertip. Output from the load cell was amplified, sampled at 0.1 ms intervals and stored on magnetic media. A trigger delay was incorporated to initiate data storage 20 ms before the key was struck; data was collected for 400 ms per keystroke. After subjects typed for several minutes keystroke force data was collected on six "h" keystrokes for each subject.

The piezoelectric load cells were calibrated using standard weights (accuracy ± 0.5%). Linearity of the system measured over 250 grams was ± 2% at full scale. Piezoelectric cell output was sensitive to strike position on the key cap (20%). Because the keystrike is near the center of the key this was judged not to be as significant source of error.

The static force-displacement characteristic of the key switch was measured by incrementally depressing the switch and collecting force values using a Chatillon Universal Electronics Tester Model ET1100 (displacement accuracy of ±0.1 mm) and a low-range load cell (±2% accuracy). A minimum of 63 grams was required to activate the switch (Figure 1).

Four male touch typists typed alphanumeric sentences for approximately 5 minutes. The chair and keyboard height were adjusted for each subject so that the thighs and forearms were approximately level (ANSI, 1988). No support was provided for the subjects' palms, wrists or forearms.

Fingertip motion was recorded for one subject using a Kodak SP2000 high speed motion analysis system capturing images at 1000 frames per second. The field of view was 6 x 6 mm region at the key with a vertical resolution of ± 0.04 mm. The distal edge of the volar surface of the right index fingernail was marked.

RESULTS

A typical keystroke force-time curve and the corresponding vertical fingertip displacement-time curve are presented in Figure 2. Keystrokes of the four subjects exhibited the double-peaked force pattern. For each keystroke, three distinct phases were identified: keyswitch compression (I), finger impact (II), and fingertip pulp compression and release (III). The mean keystroke duration was 77.2 ms (s.d. 11.2 ms). On average, the keyswitch compression (I) accounted for 12 % (s.d. 3 %) of the keystroke duration, finger impact (II) 11 % (s.d. 3 %), and fingertip pulp compression (III) 77 % (s.d. 4 %). Mean forces for the three phases are presented in Table 1.

The keyswitch compression phase (I) begins when the fingertip first contacts the keycap at the beginning of the keystroke and ends when the keyswitch has been fully depressed (end of key travel). It is of note that the fingernail velocity is constant throughout this phase. The mean fingertip forces are approximately those required to overcome the keyswitch spring mechanism presented in Figure 1.

The finger impact phase (II) occurs at the end of key travel when the fingertip decelerates and the force of impact is transmitted to the keycap by the fingertip. The highest forces were recorded during this phase. The maximum force ranged from 250.5 grams in one subject to 712.4 grams in another subject.

After the impact phase a second maximum of lower amplitude but longer duration occurs (fingertip pulp compression III). During this phase, the fingernail moves an additional 0.34 mm downward after the keyswitch is already fully compressed and the keycap is stationary. This additional motion is associated with compression of the fingertip subcutaneous fat and pulp septae. This second peak corresponds to maximum nail displacement (Figure 2). The maximum amplitude of this phase was always less than the impact force maximum. The ratio of the mean maximum force of phase III to the mean maximum force of phase II ranged from 0.46 to 0.88.

DISCUSSION

In this study each keystroke fingertip force history contained three characteristic phases: (I) keyswitch compression, (II) finger impact, and (III) fingertip pulp compression and release. These phases were observed for each keystroke for each of the four subjects tested and have been observed in subjects subsequently studied. During the first phase the finger contacts the surface of the key, compresses the switch spring and triggers the switch mechanism. The force measured at the fingertip is approximately the same as the static switch activation force. Based on fingertip motion analysis there is no apparent decline in fingertip velocity when the tip first contacts the keycap until the switch is fully compressed.

The fingertip impact force history was observed to be double peaked. Based on simultaneous high-speed video motion analysis, the first peak (phase II) occurs at the moment that the switch is first fully compressed, before the fingertip pulp is compressed. The second peak (phase III) occurs approximately 20 milliseconds later after the fingertip pulp is fully compressed. The peak amplitude of the phase II impact force appears to be related to the fingertip velocity; the higher the velocity, the higher the peak force during phase II.

The mean peak fingertip force applied by subjects (304 grams) exceeded the static requirements to activate the switch (62 grams) by a factor of five. This characteristic, that

subjects apply a much larger force than is required to activate a switch, was also observed in a study of fingertip force among 10 typists when sampling under the keyboard (Rempel 1991). The fingertip force actually applied during 8,000 keystrokes was always greater than the force at total key travel; on every keystroke the switch bottomed.

The observations that there is no fingertip velocity change until full switch compression, that all keystrokes "bottom-out", and that the impact force is high, indicates a ballistic process of finger motion during typing. That is, the flexor digitorum or lumbricle muscles initiate finger motion around the metacarpophalangeal joint and the mechanical stop in the switch halts finger motion.

The purpose of this study is to gather data that will eventually lead to estimating the loads transmitted to the finger flexor tendons during a keystroke. There is currently no model for translating fingertip impact force to the physiologically significant measures of tendon tensile force. Static loading models would predict flexor tendon tensile force 2 to 4 times larger than the force applied at the fingertip (Schuind, 1992). However, the dampening inherent in the fingertip pulp, flexor tendon pulley system, and intraarticular structures will cause a delay and filtering of the impact force as experienced by the flexor tendons. The delay may be similar to that observed in the achilles tendon during gait (Komi, 1990).

Instrumenting individual keys on a keyboard to assess fingertip force has several advantages over previously reported methods of measuring force by placing the keyboard on a force platform (Rempel 1991). First, by instrumenting individual keys, the keystroke force profile is accurately reproduced and in this study has identified three characteristic phases of a keystroke; phases that have not been observed by using a force platform under the keyboard. When sampling under the keyboard, the switch mechanism, circuit board and keyboard frame lie between the fingertip and the load cell adding complex dynamics to the transducer output. Other erroneous forces may also be added to the force transducer such as the weight of fingers resting on the keyboard.

The disadvantages of instrumenting individual keys are that the system is complicated and expensive. First, the number of transducers is much higher; 32 compared to two. Second, instrumenting individual keys does not lend itself well for comparing different keyboard designs. Key cap and switch post designs differ between keyboards hence the transducer design would differ. Third, the system of instrumenting individual keys limits force measurements to the dedicated keyboard making it difficult for field use. However, it may eventually be possible to characterize an individual's fingertip force history by measuring force at a single key.

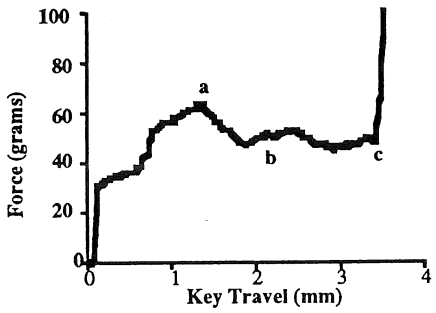

Figure 1. Static Force-displacement curve for "h" key on Apple Extended II keyboard with Alps KCM QSIII switches. The force of activation (a) is 63 grams. The switch electrical make point (b) occurs at 2 mm and full key travel (c) is 3.5 mm.

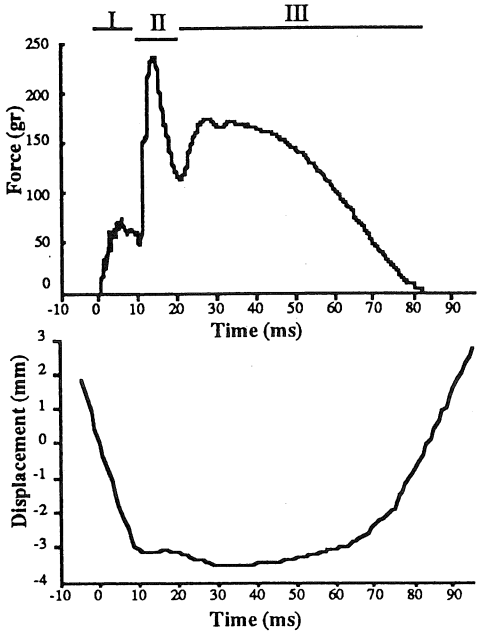

Figure 2. Typical fingertip force history and fingernail displacement during a single keystroke. Phases: (I) Key switch Compression, (II) Impact. & (III) Follow Through.

Subject	Phase I Mean Force gm	Phase II Mean Peak Force gm	Phase III Mean Peak Force gm	Fingertip Velocity (m/s)
1	45.9 (6.9)	167.3 (42.5)	147.6 (32.0)	0.28
2	42.8 (10.3)	178.6 (41.8)	146.4 (33.0)	0.34
3	66.0 (9.9)	329.3 (37.0)	187.6 (14.6)	0.42
4	80.9 (11.8)	542.3 (129.5)	251.1 (39.5)	0.66

Table 1. Comparison of subject mean fingertip forces during 6 "h" keystrokes for 4 subjects. Value standard deviation is in parenthesis().

REFERENCES

ANSI. Human Factors of VDT Workstations. No. 100-1988.
Burt S, et al. ,HETA 89-250-2046*NIOSH*, Cincinnati, Ohio, 1990
Schuind, F. et al. *J Hand Surg* **17A**, 291-298,1992.
Komi PV, *J Biomechanics* **23**(Suppl 1), 23-34, 1990.
Sauter SL, et al. *Human Fact*, **33**, 151-167, 1991.
Smith MJ, et al. *Human Fact*, **23**, 387-400, 1981
Silverstein BA, et al. *Am J Ind Med* **11**, 343-358, 1987.
Rempel D. et al. *JAMA* **267**(6), 838-842, 1992.
Rempel D. et al. *Proceedings of Human Fact*, San Francisco, 1991

ACKNOWLEDGEMENTS

Apple Computer Corporation for partial funding.

WRIST MOTION ANALYSIS IN ELITE WHEELCHAIR RACERS: IMPLICATIONS FOR FOREARM MUSCLE INJURY

J.R. Blackwell and K.A. Ladd

Department of Kinesiology, University of Illinois

INTRODUCTION

The development of humeral epicondylitis is not limited to tennis players, as the term, "tennis elbow" implies. Persons performing repetitive wrist movements, and not necessarily with high forces, appear to be at the greatest risk for the disorder. Wheelchair athletes logically fall into the category of those at risk. However, biomechanical analyses of wheelchair propulsion have typically been aimed at the whole upper body and have not concentrated on the position of the hand, relative to the forearm. Thus, little research exists concerning the wrist motion and how possible mechanisms of injury for epicondylitis are facilitated by the wheelchair athlete.

The present study centered on wrist angular positions and angular velocities during wheelchair propulsion and how these patterns relate to the development of epicondylitis.

Results indicate that wheelchair athletes perform wrist motion patterns which subscribe to the mechanisms for possible injury.

REVIEW AND THEORY

Epicondylitis is a soft-tissue injury associated with pain at the epicondylar regions. Tennis players make up only a small percentage of those persons who develop this injury. Typists, pianists, assembly-line workers, potato pickers, dentists and meat-cutters are just a few of the groups of individuals who are susceptible to epicondylitis (Bernhang, 1979; Cooney III, 1984; Cyriax, 1936; Klimek, 1984; Roto et al., 1984).

Research concerned with injuries to wheelchair athletes has many times identified disability-related injuries (e.g., pressure sores, urinary tract infections). However, recent epidemiological data suggest that muscle strains, tendinitis, epicondylitis, and general neuromuscular injuries occur in this population as well (Curtis et al., 1985; Ferrara et al., 1990; McCormack et al., 1991; Nilsen et al., 1985). Unfortunately, discussion of the mechanisms for muscular injuries is limited.

Injury to the muscle may sometimes occur when forces are higher than the force the muscle can sustain during a single contraction, but injury is also possible during repetitive muscular contractions which are not necessarily at the levels needed for injury on a single exposure (McCully et al., 1985). It may be that this type of repetitive muscle contraction leads to muscular injury in the wheelchair athlete. Additionally, the type of contraction must be considered. For someone who flexes the wrist rapidly, the wrist extensor muscles are at risk. If the fingers are clenched, or holding an object (e.g., tennis racket, wheelchair handrim), the problem increases due to the biomechanical link between the finger flexors, the wrist extensors and wrist stabilization (Snijders et al., 1987).

The purpose of this study was to describe the wrist motion exhibited by elite wheelchair racers while performing at race pace. Additionally, observed patterns are discussed in terms of the possible mechanisms for forearm muscle injury.

PROCEDURES

Three (M=2, F=1) elite wheelchair marathon racers performed at 50%, 75% and 100% of their maximum sprinting abilities. They all agreed that 75% was representative of their race pace. All trials were performed on indoor rollers which allowed each subject to use his/her own chair.

Handrim contact and release timing points were transduced via piezo film which was inserted under the glove and taped to the fingers over the point of contact. Wrist angular motion data were transduced via a twin axis goniometer (Penny & Giles). All data were collected on an FM tape recorder (Vetter) and later analyzed at 400 Hz.

RESULTS AND DISCUSSION

Figure 1 illustrates a typical pattern for three consecutive strokes from the middle of a 45 second trial. It is evident that maximum extension occurs at the point of contact after which the wrist flexes rapidly to a maximum flexion coinciding with the release point. The maximum flexion angular velocity occurs at the release point as well as the maximum ulnar deviation angular velocity. These maximum velocities are typically quite large (flexion=29 rad/s, ulnar=17 rad/s). If these velocity signals occurred clearly after the release, the high values might be explained by a quick-release type mechanism as the load on the hand reaches zero. It is not clear, however, that this is the case. It may be that the high velocity values are reached at a point when the subject reaches the end of the stroking excursion and the wheel and hand are still in contact. In this case, it is possible that the wheel pushes the hand into maximum flexion and ulnar deviation. This idea has severe implications for injury to the wrist extensors because the contraction is a forced eccentric contraction. This relates well with previous work by Blackwell (1991) who found the same forced eccentric contraction pattern as a tennis ball hits the racket during a backhand stroke performed by an unskilled player.

A goal of this research is to offer information that may aid

wheelchair racers in the reduction of forearm muscle injury. A possible mechanism for forearm muscle injury, specifically the wrist extensors, which originate at the lateral epicondyle, is that high muscle forces occur repeatedly due to the rapid wrist flexion while the hand grips the handrim of the wheel. It is suggested, therefore, that to reduce the chance of injury, the wrist motion should be limited and the hand should not grip the wheel. One way this is being accomplished is through the use of a specialized glove (model Harness). This glove forces the fingers over the palm of the hand by means of velcro, while also keeping the thumb close to the fingers. This promotes contact with the wheel on the dorsal side of the fingers, which does not allow the hand to grip the rim. This stroke is currently being developed at the University of Illinois Rehabilitation Education Center. Future research plans are to investigate the wrist kinematics as well as performance variables associated with this new stroke.

REFERENCES

Bernhang, A. *N.Y. State J. Med.*, **Aug.**, 1363-1366.
Blackwell J. Unpub. doctoral dissertation, U. of Iowa
Cooney III, W. *Sports Injuries*, **76**, 45-50.
Curtis, K. et al. *Paraplegia*, **23**, 170-175.
Cyriax, J. *J. Bone Jt. Surg.*, **18**, 921-940.
Ferrara, M. et al. *Paraplegia*, **28**, 335-341.
Klimek, E. *Can. Med. Ass. J.*, **130**, 106.
McCormack, D. et al. *Clin. J. Sports Med.*, **1**, 35-40.
McCully, et al. J. Applied Phys., **59**, 119-126.
Nilsen, R. et al. *Paraplegia*, **23**, 152-158.
Roto et al. *Scand. J. Work & Environ. Health*, **10**, 203-205.
Snijders, C. et al. *Med. Sci. Sports Exer.*, **19**, 518-523.

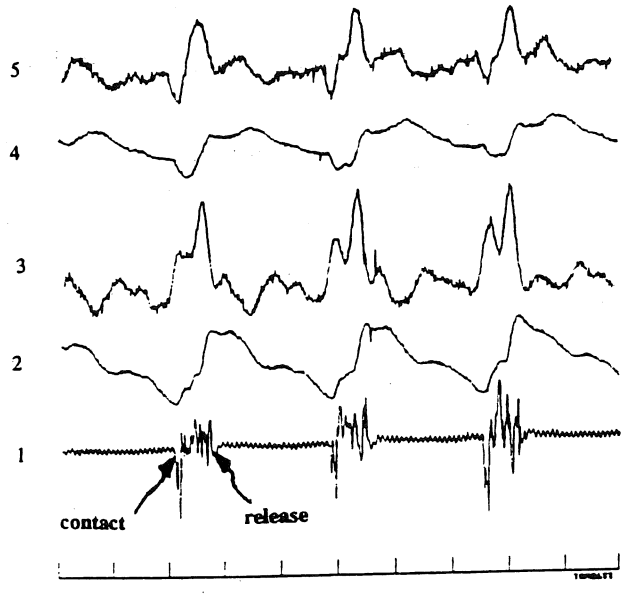

Figure 1. Representative pattern for three consecutive strokes during 75% maximum sprinting trial. From bottom to top, signals are: 1) piezo film; 2) flexion/extension position (flexion is directed up); 3) flexion/extension angular velocity; 4) radial/ulnar position (ulnar deviation is directed up; 5) radial/ulnar angular velocity. The time scale is 0.2 sec/div.

THE EFFECT OF SUBJECT GROUPING ON THE KINEMATIC ASSESSMENT OF WHEELCHAIR PROPULSION

J.H. Bednarczyk and D.J. Sanderson
UBC Biomechanics Lab, University of British Columbia, Vancouver, B.C., Canada

INTRODUCTION

Within and between subject variability has been studied in human locomotion (Winter, 1987) but this issue has not been addressed in wheelchair propulsion. Ensemble averages are performed on grouped subject populations based on either diagnostic categories (ie. amputation, spinal cord injury) or neurological level. The purpose of the present study was to assess how different methods of grouping subjects with disability effects the kinematic evaluation of wheeling. The results demonstrate that the "traditional" method of grouping persons with disability according to neurological level may not be appropriate in wheelchair propulsion studies.

REVIEW AND THEORY

Sanderson (1985), Van der Woude (1991) and Su et al. (1991) identified large between subject variability in the kinematics of wheelchair propulsion in a small population of athletic, paraplegic subjects. Lehman et al. (1974) noted large between subject variability in a group of 12 people with quadriplegia. These studies used subjects with spinal cord injury who presumably had discrete neurological function. However, no mention was made of the type of residual motor ability in the subjects (incomplete vs complete injuries) or the methods used to classify disability. From a clinical perspective, one would expect that subjects with high cervical quadriplegia, who do not have the voluntary use of hand muscles, elbow extensors or trunk muscles, would perform differently when propelling a wheelchair than people with low lumbar paraplegia who had only to compensate for the loss of voluntary leg control.

PROCEDURES

Sixteen subjects volunteered for the study. Inclusion criteria were the presence of a traumatic spinal cord injury (of greater than one year duration) with resultant motor and sensory loss (either complete or incomplete), the dependence on the use of a manual wheelchair for primary mobility, and the absence of any regular sports training. After neurological assessment, subjects were classified according to the American Spinal Injury Association (ASIA) system. This is a 100 point scale based on manual muscle testing (grades 0-5) of selected muscles from each myotome in which a score of 100 corresponds to an intact neurological system. The subjects wheeled in their own wheelchairs over a 5 meter level, overground course (low pile carpet). Two video cameras recorded (60 Hz) the movement of light reflective markers placed on the subject's right shoulder, elbow, wrist, and on the chair wheel rim and center. After several practice trials, each subject wheeled for three trials at two different speeds. Visual feedback of wheeling speed was provided by a cycle computer attached to the right, rear wheel. A small electronic switch was placed on the subject's right hand to signal when hand contact (grab) and release occurred. A single wheeling cycle, from the central portion of each wheeling trial, was selected for analysis. The images were digitized using software from Peak Performance Technologies and after direct linear transformation, the resulting 3D coordinate data were used to compute elbow angles. Before computing the average angular change over three trials, each wheeling cycle was time-normalized to a percentage score with 0% being the first grab and 100% being the next grab. The time spent in contact with the wheel (the propulsive phase) was determined to be 35% of the wheeling cycle for all subjects at the 1 m/s rate of wheeling.

RESULTS AND DISCUSSION

The subjects had a broad range of residual neurological ability as reflected by their ASIA scores from 20 to 66. The subject ages were 21-51 years and mass ranges were 53 to 99 kg. The subjects were grouped according to the frequently used "paraplegic" (para) and "quadriplegic" (quad) categories as well as into four subcategories based on the ASIA scores: para 1 (ASIA score 54-66; n=5); para 2 (ASIA score 41-52; n=4); quad 1 (ASIA score 28-40; n=4) and quad 2 (ASIA score 20; n=3). Figure 1 shows the elbow angular changes over a normalized wheeling cycle for the para and quad groups wheeling at a measured speed of 1 m/s. The differences between the elbow angular patterns for the para and the quadr groups are small during the initial flexion phase of propulsion but become larger between

larger between 20-50% of the wheeling cycle.

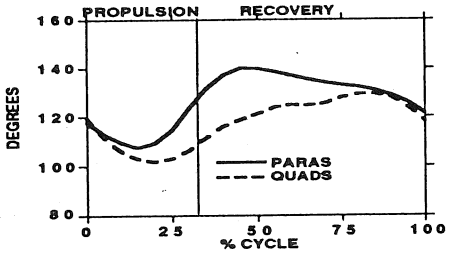

Figure 1: Elbow angle changes over a normalized wheeling cycle for subjects with paraplegia (n=9) and quadriplegia (n=7) wheeling overground at 1 m/s. An elbow angle of 180 degrees corresponds to full elbow extension.

A 2-way (groups x time) repeated measures (time) ANOVA of the elbow angle changes over the propulsive phase of wheeling showed that the para group angular changes were significantly (p=0.04) different from the quad group. In addition, there was a significant groups x time effect (p=0.007). The quad group showed less angular excursion, particularly at the latter half of the propulsive phase, than the para group. This could be as a result of the lack of active elbow extensors in the quad group. These results support the clinical perception that it is inappropriate to group subjects with paraplegia and quadriplegia together.

To assess whether all paraplegics and all quadriplegics could be grouped together, the subjects were divided into four subgroups according to ASIA score. Figure 2 shows the elbow angle excursion over a normalized wheeling cycle for the groups. The differences, especially between the two most clinically divergent groups (quad 1 and para 2), become large in the propulsive as well as the recovery portions of the wheeling cycle. The differences between the two para groups are large during the first 20% of the wheeling cycle

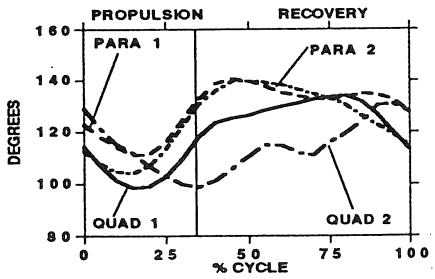

Figure 2: Elbow angle changes over a normalized wheeling cycle for the four subgroups of subjects wheeling at a speed of 1 m/s.

A 2-way repeated measures ANOVA on these data showed no significant difference between the four subgroups (p=0.24) or between the two para groups (p=0.35). This was surprising because the elbow angles at grab, the excursion of maximum elbow flexion, and the time of the flexion phase of propulsion are clearly different between the four groups. The quad 2 group, who had a residual neurological ability closer to the para group, showed kinematic elbow angle changes which were similar to the pattern seen in the two para groups.

When the elbow angle changes were examined by subgroups at a wheeling speed of 2.6 m/s (Figure 3), the differences between the groups were greater than were seen at the slower wheeling speed and were significantly different (p=0.025).

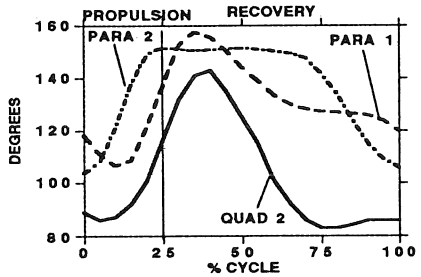

Figure 3: Elbow angle changes over a normalized wheeling cycle for 3 subgroups of subjects. Only two subjects from the quad 2 group and no subjects from the quad 1 group were able to wheel at this speed (2.6 m/s).

CONCLUSIONS

The results of this study illustrate the need to consider the functional residual ability when using people with spinal cord injuries in wheelchair propulsion studies. The differences within even the para group at high load wheeling situations are significant and need to be considered in future studies.

REFERENCES

Lehman, J.F. et al. Arch Phy Med 55:183-6, 1974.
Sanderson, D.J. et al. J Biomechanics, 18:423-429, 1985.
Su, F.C. et al. Proceedings of the XIII International Society of Biomechanics, Australia (pp.198-9), 1991.
Van der Woude, L.H.V. et al. Proceedings of the XIII International Society of Biomechanics, Australia (pp. 203-4), 1991.
Winter, D.H. et al EEG and Clin Neurophys 67:402-411, 1987.

THE OPTIMAL PLACEMENT OF BOXES ON THE SHELVES OF A FOOD WAREHOUSE

Gilmen Smyth*† and Micheline Gagnon†
*CUSLM, Université de Moncton, Edmundston, N.B. E3V 2S8, Canada
†Department of Physical Education, Université de Montréal, Montréal, QC. H3C 3J7, Canada

INTRODUCTION

An experimental study was undertaken to optimize the placement of boxes on the shelves in a food warehouse by minimizing the joint loadings on the shoulders and on the lower back as criteria. A dynamic sagittal plane model was used to estimate net muscular moments on the shoulders and a model of internal forces was used to estimate the compression forces on the L5/S1 vertebral disk. Regression methods were used to estimate joint loadings for each product at each working height and for each task (lifting and lowering). The results revealed that a reduction of the compression forces on the lower back could be achieved by placing the heavier boxes on the top shelf and the lighter ones on the bottom shelf for a two-shelves rack. However, the minimization of loadings at the shoulders indicated that this variable was not sensitive to different placements of the boxes on the shelves. For the two-shelves racks, the integration of all the results suggested to limit the height of placement at the shoulder level and to place the heavier boxes between waist and shoulder height. For the three-shelves racks, the storage of food products with the heavier boxes stored on the middle shelf appeared to be the best method to minimize the lower back loadings.

REVIEW AND THEORY

Although there is an increased mechanization of the work tasks in the industries, the manual materials handling of various objects is still an important activity and a significant source of injuries to the lower back. In the province of Québec, Gervais *et al.* (1987) have indicated that back problems accounted for almost one fourth of all compensated injuries in 1981. On the other hand, a study by Lamonde (1987) on the profile of accidents to workers in a transport company has demonstrated that one third of all the accidents were musculoskeletal injuries and that they mainly affected the back (69%) and the shoulders (17%).

The configuration of the workplace plays an important role to facilitate the task of the worker and to minimize the loadings on their musculoskeletal structures. Snook (1978) has developed a series of tables that suggest the maximum acceptable weight of loads to be handled depending on the frequency of handling, the sex of the worker, the size of the box in the sagittal plane, and the vertical displacement of the box for lifting and lowering. In another study, Ayoub (1982) suggested to avoid the placement of massive boxes close to the floor or at heights above the shoulders when placing boxes on the shelves in warehouses. However, his recommendation was mostly subjective; no objective study relating to a method for the optimal position of products on the shelves in a warehouse has been reported.

Linear programming methods have been used in biomechanics to solve problems of indeterminate nature for the computation of muscular forces (Herzog *et al.*, 1991; Penrod *et al.*, 1974; Schultz *et al.*, 1981). However, these methods have not been used to minimize forces on body joints during manual materials handling tasks.

The objective of this study was to optimize the placement of boxes in a warehouse specialized in the distribution of food products. Given a certain number of products to be stored on the shelves in the warehouse, the objective was to determine the position of each product that would minimize the loadings on a specific body structure. It was hypothesized that a placement of boxes on the shelves that would minimize joint loadings would be different from the actual placement and would result in a decrease of joint loadings for the workers.

METHODS

About 150 products were surveyed in a food product warehouse for the optimization process. Only the products that were stored on two- or three-shelves racks were recorded. Products that were not stored in racks were not examined. Due to the substantial quantity of products and positions for which to estimate joint loadings, a solution based on regression methods was used to estimate these loadings. Five boxes whose mass (3.3, 6.4, 11.6, 16.4, and 22.0 kg) and dimensions were representative of the products in the warehouse were defined. They were lifted to or lowered from five different shelves (15, 61, 109, 147 and 185 cm). These conditions were typical of the company under study. Eight experienced workers from the food product warehouse (age: 23-46 years; mass: 58-82 kg; height: 156-174 cm; experience: 1-18 years) were used as subjects. Each subject performed 2 trials for 50 treatments (2 tasks x 5 loads x 5 heights). Twelve additional trials were performed to estimate the intra-subject variation.

The measurement techniques consisted of cinematography and force platforms. A 16 mm Locam camera operating at 50 frames/s was used to record the subject's segmental positions during the movement. The films were digitized every other frame with a NAC motion analyzer and linked to a PDP 11/23 mini-computer. The coordinates of the joints' centers were smoothed with a second order zero phase recursive filter with a cut-off frequency of 3 Hz for the metatarsals, ankles, knees, and hips and 6,5 Hz for the other coordinates. Differentiation procedures were then applied using finite differences to obtain velocity and acceleration data. Two AMTI force platforms were used to record the external forces under each foot. Synchronization of film sequences and force data was accomplished by means of an electrical pulse recorded on a specific channel of the computer and the simultaneous activation of a light emitting diode (LED) that appeared in the foreground of the film frames.

The kinematic and kinetic data were used as input in a sagittal plane dynamic model including a single muscle equivalent to represent either the flexors or the extensors of the trunk. This model was described by Gagnon *et al.* (1988). The dependent variables included the compression forces on L5/S1 and the maximum net muscular moments at each body joint. The mean and standard deviation were calculated for the eight subjects, for each treatment.

The variables selected for the optimization process were the peak loadings on L5/S1 (COMPMAX) and the net muscular moment on the shoulders (MOMSH). For each variable, the data from the 2 trials and the 8 subjects were grouped resulting in 50 data per variable (2 tasks, 5 masses, and 5 heights). The joint loadings for each product were predicted using the type of task, the mass of boxes, and their height of placement as independent variables. The equations used were tested with the analysis of the residuals and they were also validated. The minimization of joint loadings was performed using linear programming methods described by Dantzig (1963). Post optimal analyses were performed on the results.

RESULTS

The results include the optimized placement of the products on a two-shelves rack with the mass of each product, their original position, and their position using the minimization of loadings on the lower back and on the shoulders (Table 1). The optimal placement of boxes with either variable was different from the original position of the products and the placement resulting from the optimization process was also different for each variable. This difference between the results of the two variables was due to the different pattern of loadings on the joints depending of the height of placement. For the lower back, the loadings were higher for their handling on the bottom shelves while for the shoulders, the loadings were highest for the handling of boxes on the top shelves. There did not seem to exist any pattern of placement when it was examined according

to selected characteristics of the products such as their mass, the length of boxes, their width, their volume, or their density.

To estimate if the minimization process had an important effect on joint loadings, the minimal objective function computed for each variable and for each rack was compared to the objective function calculated for the original placement of the boxes. These comparisons showed that, on the average, the decrease was larger for the lower back than it was for the shoulders; differences were less than 4% for the shoulders but exceeded 10% for the lower back for some of the racks. The decrease for each variable and for each rack is reported in table 2.

For the loadings on the lower back, a comparison was also made between the minimal objective function and the calculated objective function when the heavier boxes were placed on the top shelf. The resulting objective function was intermediate between the optimal placement and the original placement of boxes. The same was done with the net moments on the shoulders but by placing the heavier boxes on the bottom shelves. For this variable there was no difference for some of the racks, an indication of the lack of sensitivity of the shoulders' moments to the different placements of the products.

The minimization of loadings was also applied to a three-shelves rack. The decrease of loadings on the lower back as compared to the original placement was 14%, and on the shoulders, the decrease was 3%. Similarly to the two-shelves racks, there did not seem to exist any pattern of placement when it was examined according to selected characteristics of the products. For the loadings on the lower back, a comparison was made between the minimal objective function and the calculated objective function when the heavier boxes were placed on the top shelf or on the middle shelf in order to avoid excessive loadings on that joint. The reductions of overall loadings were respectively 5% and 4%.

The sensitivity to changes in the coefficients of the objective function, which were the loadings on the joints, was estimated using post optimal analysis. The variation allowed on the coefficients was 1% or less while variation of the original data was around 6% for loadings on the lower back and 12% for loadings on the shoulders. These analyses showed that the results were very sensitive to changes in the objective coefficients.

DISCUSSION

Certain limitations regarding this study must be emphasized in addition to those related to the biomechanical model and the regression methods. Joint loadings resulting from pushing or pulling movements during the handling of boxes on the shelves were not analyzed. The handling of boxes at heights above 166 cm was considered to be performed always at a height of 166 cm relative to the worker, with the worker stepping on a ladder for those placements. Finally, the variation present in the original data affected the sensitivity of the optimal solution for each variable and for each rack; the results must then be interpreted with caution.

It was not surprising to observe that the optimal placement of the products on the shelves for each variable was different from the original placement. The only criterion for the original placement of the products on the shelves was the grouping of all boxes of a product on the same shelf, this criterion being respected during the optimization process. The minimization of joint loadings rationalized the placement of boxes by taking into account forces on specific body joints. This reduction of loadings was particularly important on the lower back. Though the method of placement of boxes according to their mass was inferior to the optimal method for the minimization of loadings on the lower back, this method had the definite advantage of eliminating the higher loadings that can cause injuries to the lower back. Without having to measure compression forces on the lower back, the loadings on this joint could thus be notably reduced.

The results with the net muscular moments on the shoulders were not very sensitive to different placements on the shelves, but the data of muscular utilization ratio on the shoulders have shown that relatively high loadings can exist on those joints when lifting massive boxes at heights above the shoulders (Gagnon *et al.*, 1991). It would thus be judicious to limit the height of placement to the shoulder level as has been suggested by Ayoub (1982).

The results have shown that joint loadings on the lower back can be decreased by rationalizing the placement of boxes on the shelves in a warehouse. Because of a lack of sensitivity of the maximum net muscular moments on the shoulders, the results were not conclusive for this variable. The placement of heavy boxes on the top shelf of two-shelves rack appears important in order to avoid excessive loadings on the lower back. On the other hand, it appears also important to limit the height of placement to the shoulder level in order to limit large loadings on the shoulders. For the three-shelves rack, the placement of the heavier boxes on the middle shelf was an acceptable solution.

Table 1. Original position of the products on the shelves of one rack and their position after optimization.

		Placement		
Product	Mass (kg)	Original	COMPMAX	MOMSH
1	18,0	Bottom	Top	Bottom
2	18,0	Bottom	Top	Bottom
3	12,0	Bottom	Bottom	Top
4	9,0	Bottom	Top	Bottom
5	9,0	Bottom	Top	Bottom
6	9,0	Top	Bottom	Top
7	9,0	Top	Bottom	Top
8	5,0	Top	Bottom	Top
9	5,0	Top	Bottom	Top
10	5,0	Top	Top	Bottom
11	5,0	Top	Top	Bottom
12	5,0	Top	Top	Bottom
13	4,5	Top	Top	Top
14	4,5	Top	Top	Bottom

Table 2. Decrease of the objective function after optimization as compared to the original placement.

	Racks					
Variables	1	2	3	4	5	6
COMPMAX	15%	12%	8%	7%	5%	3%
MOMSH	4%	3%	2%	2%	1%	2%

REFERENCES

Ayoub, M.A., *J. Occup. Med.*, 24, 668-676, 1982.
Dantzig, G.B., Linear Programming and Extensions, 1963.
Gagnon, M. et al., *Int. J. Indust. Erg.*, 3, 29-40, 1988.
Gagnon, M. et al., *J. Biom.*, 24, 190-203, 1991.
Gervais, M. et al., *IRSST*, 1987.
Herzog, E. et al., *J. Biom.*, 24, Supp. 1, 31-39, 1991
Lamonde, F., Master's thesis, École Polytechnique, Montréal, 1987.
Penrod, D.D. et al., *J. Biom.*, 7, 123-129, 1974.
Schultz, A.B. et al., *Spine*, 6, 76-82, 1981.
Snook, S.H., *Ergonomics*, 21, 963-985, 1978.

ACKNOWLEDGMENT

This study was supported with grants from the Institut de Recherche en Santé et en Sécurité au Travail du Québec (N/D RS-87-11) and the Natural Sciences and Engineering Research Council of Canada (OGP0020812).

Assessment Of Four Different Mail Carriage Systems

G.G. Weames and D.G.E. Robertson
School of Human Kinetics, University of Ottawa, Ontario

INTRODUCTION

Since the introduction of the letter carrier the basic side satchel and shoulder strap design of the Canada Post mailbag has gone virtually unchanged. Recently, due to the potentially harmful effects of asymmetrical loading, new letter carrier satchels have been developed or existing models have been modified.

The Biggs Bag (BB), carries the load in two side pouches. A hip belt and shoulder yoke distribute the load to the pelvis and upper girdle. The Front Pack (FP) (Ashton, 1985), situates the load anteriorly on the trunk, superior to the level of the pelvis. The FP is fastened via a hip belt, two shoulder straps that cross posteriorly, and a horizontal strap to keep the FP close to the thorax. The Trap Strap (TS) is a hip belt modifying the existing shoulder slung Side Satchel (SS) (Murray, 1984).

Hip belt utilization removes a major portion of the load from the shoulder girdle by distributing it to the pelvis decreasing shoulder and back discomfort (Centre for Ergonomics, 1984; Vernon and Laufer, 1982). As the load is secured more inferiorly, the lower limbs become more subject to the effects of asymmetrical loading during gait (Vernon and Laufer, 1982).

The purpose of this study was to investigate the responses from carrying four different modes of mail carriage systems during fast, level walking.

METHODOLOGY

Nine healthy males and six healthy females, unfamiliar with mail carriage tasks, volunteered and signed forms for consent. Each subject wore Greb Kodiac #557 ankle boots. A brisk walking cadence was established for each subject using a Seiko Quartz metronome. Repeated practice trials were performed in time with the metronome to establish a set distance to be covered. Six trials of each condition were performed. Normal walking data were collected first with the remaining load carrying conditions (FP, BB, SSTS, and SS) being ordered randomly.

Electromyographs of the right and left m. erector spinae at the L4/L5 level were collected using disposable surface electrodes with an interelectrode distance of 3 cm. A foot switch was attached to the left shoe to identify the stride cycle. The signals were carried by cable to a customized bioamplifier (gain 2000, impedance 10 megohm, >110 dB CMRR). The raw EMG signals were band-passed filtered (10-700 Hz), to remove movement and high frequency artifacts, and then full-wave rectified and low-pass filtered (6 Hz) to obtain a linear envelope signal. The EMG and foot-switch signals were sampled at 50 Hz by A/D converters and stored on flexible disk.

The first ten clean linear enveloped EMG signals for each m. erector spinae were selected from the middle portions of all the trials. These curves were integrated using Simpson's method and averaged for each subject and each condition. A one-way repeated measures analysis of variance (α=0.05) was then performed on these data to determine whether there were significant differences across the five conditions for either (left or right) EMG. Duncan's Multiple Range Test analysis was used to determine which conditions were significantly different. Mediolateral force, normalized to body weight, were measured using a force platform (Kistler) inlaid in a raised wooden walkway. The subjects crossed the force platform at the midpoint of their walking trial while forces were sampled at 50 Hz by the analogue-to-digital converters of a mini-computer (Data General, S/20 micro-Eclipse).

Ensemble averages and ensemble standard deviations were obtained for five mediolateral force curves, and ten right and left m. erector spinae curves, for each subject condition (Winter, 1986). The subject ensemble averages and standard deviations were then averaged to obtain grand male and female ensemble averages for each condition.

RESULTS

Integrated values of the ensemble averaged EMG profiles for the right and left, male and female m. erector spinae are shown in Table 1. Conditions are ordered from smallest to largest values. Significant differences (α=0.05) between conditions within each m. erector spinae are indicated in italics.

Table I. Duncan's Multiple Range Test for significance.

m.ES	Conditions				
F. L	*N*	*SSTS*	*SW*	*BB*	*FP*
F. R	BB	N	*SSTS*	*FP*	*SW*
M. L	*N*	*SW*	SSTS	BB	*FP*
M. R	*N*	*SW*	SSTS	BB	FP

Male and female, bilateral m. erector spinae ensemble averaged EMGs for SS and FP are compared to the standard deviation bars of normal walking in Figures 1 and 2, respectively.

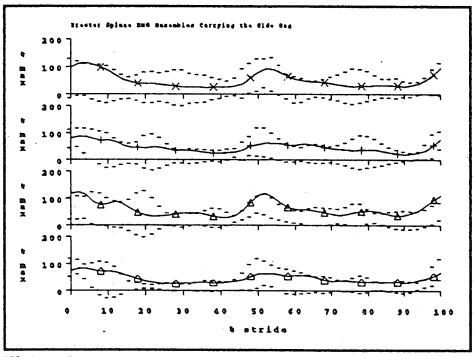

Figure 1. SW grand ensemble means for female right, female left, male right and male left EMGs are ordered from the top to the bottom partitions respectively.

Areas of significantly different muscle activity lie outside the standard deviation bars.The mediolateral ensemble averaged force curves for males and females are shown in Figures 3 and 4. Conditional ensemble averaged force curves are indicated by a solid line and can be compared to the normal standard deviation bars for significant differences. Medial forces are in the positive y-axis and lateral forces are in the negative y-axis.

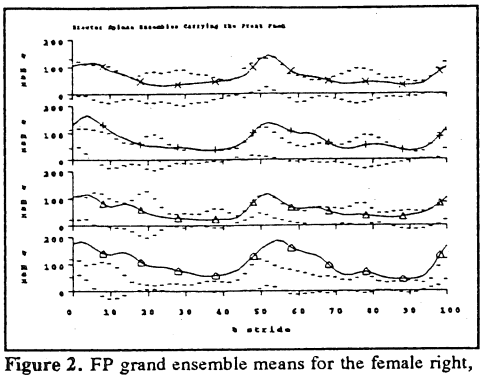

Figure 2. FP grand ensemble means for the female right, female left, male right and male left EMGs are ordered from the top to the bottom partitions respectively.

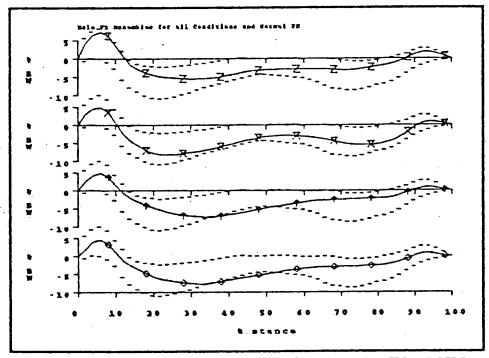

Figure 3. Grand ensemble means for the BB, FP, SSTS and SS are ordered from the top to the bottom partitions respectively.

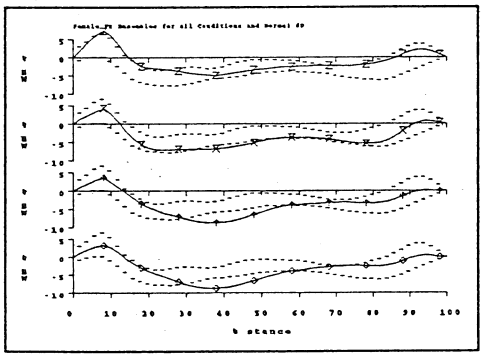

Figure 4. Grand ensemble means for the BB, FP, SSTS and SS are ordered from the top to the bottom partitions respectively.

The mean standard deviation for subject cadence was 3.5 strides/min with a subject mean cadence of 113 strides/min.

DISCUSSION

The conditions involving lateral loading of the subject caused a significant change in the mediolateral force pattern. Closer inspection of the data showed the discrepancies to lie between 30% and 60% of stance phase for both the SS and the SSTS conditions. Similarity between the two side satchel situations suggests that the use of the TS with the SS posed no improvement over the SS condition with regards to mediolateral loading to the lower limb. Since the FP and the BB conditions show no significant change compared to the normal condition, the differences in the force curves were not entirely the result of added weight to the subject, but were also a function of load placement.

There was a larger discrepancy for females between the unloaded and loaded conditions for the SSTS and SS. The load carried represented a mean of 21% body weight for males and a mean of 25% body weight for females. It is interesting to note that the discrepancy was only apparent within areas where a significant difference existed between the normal and loaded force curves. This discrepancy did not appear to manifest itself in nonsignificant force curve graphs suggesting that body weight was less likely a factor in symmetrically loaded situations.

The results of the m. erector spinae are not easily interpreted. There was a significantly greater cost in muscle activity when carrying the FP for males and females compared to most other conditions. Generally, the m. erector spinae FP profiles followed the same phasic pattern as the normal profile but at an increased magnitude. For females, the SW and BB conditions resulted in the most asymmetrical m. erector spinae activity based on the integrated EMG values. However, for males, all conditions showed symmetry of bilateral m. erector spinae activity with the SW condition producing the lowest activity compared to all other conditions. This inconsistency is cause for suspicion that there are differences in load carrying techniques between sexes, although, a more thorough investigation would be needed to isolate those differences.

CONCLUSIONS

Throughout this study, the assumption was made that deviation of mediolateral force from a normal, unloaded walking situation and elevated and/or asymmetrical m. erector spinae EMG activity, had the potential to cause harm to the letter carrier. Based on mediolateral force measures, the SS and SSTS conditions represented potentially harmful methods of mail carriage especially for those individuals of lesser body mass. The force profiles of the FP and BB more closely represented a normal unloaded force curve even for females. However, integrated m. erector spinae results indicated a significantly larger m. erector spinae activity for both males and females in most cases. In this assessment, one measurement parameter would not have adequately determined the most favourable letter carriage method.

REFERENCES

A Biomechanical Comparison of Current Mailbag Designs *Centre for Ergonomics*, University of Michigan, 1984.
Ashton, N.A. *Proceedings of the 29th Meeting of the Human Factors Society* (pp.991-994), 1985.
Murray G.W. et al. *Proceedings of the 1984 International Conference on Occupational Ergonomics* (pp.559-562), 1984.
Vernon, H. et al. The Trap Strap: a Study of its Efficiency, Canadian Memorial Chiropractic College, 1982.
Winter, D. *Arch Phys Med Rehabil*, 69:393-398, 1986.

ACKNOWLEDGEMENTS

The authors wish to thank Doug Scullion for his assistance during the project, Don Lord, Manager of Occupational Health and Safety, CPC, for his initiative and to Canada Post Corporation for their financial assistance in making this study possible.

AN INVESTIGATION OF RETINAL DETACHMENT AND NECK EXERCISE

Rory A. Cooper, James F. Ster III
Department of Biomedical Engineering
California State University, Sacramento, CA 95819-6019, USA

ABSTRACT

The purpose of this study was to investigate the possible onset or aggravation of retinal detachment through head and neck exercise. Three experiments were conducted on a Nautilus Four Way Neck Machine (NFWNM) to determine the maximal accelerations and forces exerted upon or about the eyes. Three quartz accelerometers (PCB piezotronics, series 308B) were mounted to the center of the face pad, six inches to the left of center of the face pad, and to the top weight. The accelerometers were wired through amplifier/power units (PCB Model 480D06) to a high speed strip chart recorder (Gould , RS3400). Each subject had resistive force sensors (Interlink Electronics, Model 151 and 152) attached to their left and right forehead centered above the eyes, and on the eyelids. Each sensor was connected to a simple voltage divider network which was powered by a d.c. power supply (Tektronix CPS 250). Two subjects participated in this study. Each subject was requested to make at least three complete cycles of the machine with 10 pounds , during which the accelerations and forces were measured. The peak face pad accelerations were 3.0$\pm$.0 g (backward rotations) and 2.1 $\pm$ .1 g(forward rotations) for subject one, and 2.0 $\pm$ .9 g (backward rotations) and 1.3 $\pm$ .2 g (forward rotations) for subject two. The continuous face pad accelerations were 5.3$\pm$.6 g (backward rotations) and 4.9 $\pm$ .6 g(forward rotation) for subject one, and 2.7 $\pm$ .8 g (backward rotations) and 3.7 $\pm$ .9 g (forward rotations) for subject two. The facial forces for each of the subjects were 0.0 + 0.0 for the right and left eye of subject one, and 254 + 31 and 136 + 88 grams for subject two's left and right eye, respectfully. The forces were 114+17 and 118+9 grams (subject #1), and 118+2 and 161+ 2 grams (subject #2) for the left and right forehead, respectfully. For all of the trials the maximal accelerations and facial forces occurred at the end of the forward cycle. Forces may be exerted on the eyes which could cause damaging deformation of the globe for individuals predisposed to retinal detachment.

INTRODUCTION

A nonpenetrating injury to the globe may tear the retina or it may indirectly damage the retina as a result of fracturing Bruch's membrane, which loosely adheres the retina to the pigment epithelium (Vaughan et al, 1989).

The causes of retinal separation are many. Movement of the eye (shock) or trauma may cause retinal detachment. The trauma may be quite trivial, when an individual is predisposed to retinal detachment (Allen, 1986).

The history is quite typical. The individual notices flashes of light in part of the visual filed due to the adherent vitreous pulling on the retina during movement.

Eye injuries are rather common sports injuries (Erie, 1991). Several authors have reported that weight lifting can cause retinal detachment (Peyresblanques, 1976). Moderate trauma (stooping, lifting weights) may precipitate retinal detachment in a predisposed eye (Allen, 1986). Pivovarov (1977) and his colleagues found weightlifting to be a significant cause of retinal detachment.

PROCEDURES

Three tests were performed on a Nautilus Four Way Neck Machine to investigate the accelerations (shock) and facial forces developed during use. Three quartz accelerometers (PCB piezotronics, series 308B) were mounted to the center of the face pad (used for measuring when the machine rotates backwards), six inches to the left of center on the face pad (used for measuring when the machine rotates forwards, and to the top weight. The accelerometers wired through amplifier/power units (PCB, Model 480D06) to a high speed strip chart recorder (Gould, RS3400).

Each subject had resistive force sensors (Interlink Electronics, #151 & #152) mounted to their left and right eye and forehead above each eye. Each sensor was connected to a voltage divider circuit with a 15K ohm resistor. The circuit was powered by a d.c. power supply (Tektronix, CPS250). The voltage across the 15K ohm resistor was recorded by the strip chart recorder.

Experiment 1: It was desired to get an estimate of the magnitude of the accelerations that one might observe during typical use. Our subjects were incapable of lifting the full range of weights on this machine. Thus a person centered at the front of the machine simulated the motion by operating the device with his arms. The motion was repeated three times for each weight from 10 to 60 pounds.

Experiment 2: Each subject was positioned in the NFWNM as described in the manual. Each subject performed the complete motion of the machine with 10 pounds a minimum of three times. The accelerations were recorded.

Experiment 3: Each subject was positioned in the NFWNM as described in the manual. Each subject performed the complete motion of the machine with 10 pounds a minimum of three times. The facial forces were recorded.

Data Reduction and Analysis

The data were transcribed from the strip chart recordings and entered into a DOS compatible personal computer. The data were analyzed using the mathematical software package MATLAB. The mean and standard deviations were calculated for the peak and steady-state accelerations, and for the maximum force on each sensor.

RESULTS

Results from experiment 1 showed the peak accelerations of the face pad to be more than twice the maximum continuous accelerations. The peak impulse accelerations of the face pad are on the order of 5g whereas the maximum continuous accelerations are about 2g.

Experiment two showed that the continuous accelerations and maximum peak accelerations for the face pad were similar to those measured in experiment one for subject one. The results of subject two were notably lower (Table 1). The peak impulse accelerations is about twice the continuous value during forward rotation.

Table 1. Accelerations while using NFNM with 10 pounds (g).

Subject	Reverse		Forward		Weights	
	Imp.	S.S.	Imp.	S.S.	Imp.	S.S.
1	5.3+.6	3.0+.0	4.9+.6	2.1+.1	10.5+.2	0+0
2	2.7+.6	2.0+.9	3.7+.9	1.3+.2	10.6+.0	0+0

The results of experiment three show that this machine can exert force on the eye globe of some individuals (Table 2). This force may be substantial. The force varies as the individual rotates the machine. Based upon these subjects, the force shifts from the bottom of the face to the top as the machine rotates forward. The maximal force on the eye region coincides with the end of the forward motion.

Table 2. Facial forces while using NFNM with 10 pounds (grams).

Subject	Eye		Forehead	
	Lt.	Rt.	Lt.	Rt.
1	0.0+.0	0.0+.0	114+17	118+9
2	254+31	136+88	118+2	161+2

DISCUSSION

For all or the experiments the maximal acceleration of the face pad , and the maximal force upon the eyes (or the region surrounding the eyes) appears to occur at the end of the forward cycle. Thus is appears that the machine is about ninety degrees out of phase. Typically one would expect the maximal acceleration to occur while the machine was in the middle of its cycle (when the weights are halfway between their resting and uppermost position). The acceleration should be at or near zero at the end of the forward of reverse motion. to minimize shock or impact and risk of injury. Especially with respect to retinal detachment.

A dampening mechanism which is activated at the ends of the forward and reverse cycle would help to ameliorate some of this problem. The cam could also be redesigned . The face pad needs redesign as excessive, for those individuals predisposed to retinal detachment, force may be exerted on or about the eyes.

The forces recorded during this investigation could cause similar deformation to the globe as that described by Maguire and Benson (1986). This would indicate a risk of retinal detachment for the predisposed.

The use of weights for the load may result in cervical spinal injuries (although this would have to be investigated). A generator or electromagnetic brake would be a more suitable source of resistance for this application, because no force is exerted when there is no motion.

REFERENCES

Allen, J.H., May's Diseases of the Eye, 24th edition, 1986.
Erie, J.C., Eye Injuries: Prevention, Evaluation and Treatment, Phys. & Sportsmedicine, 19(11):108-122, 1991.
Maguire, J.I. & Benson, W.E., Retinal Injury and Detachment in Boxers, JAMA, 255(18):2451-2453, 1986.
Peyresblanques, J., Eye and sports, Archives d'Ophtalmologie, 36(1):81-90, 1976.
Pivovarov, N.N., Malakhove, L.A., Bagdasarova, T.A., & Chetvertukhin, A.P., Role of Weight Lifting in the Development of Retinal Detachment, Vestnik Oftalmolgie, 6:50-53, 1977.

UPPER EXTREMITY

Podium Session 18

DEVELOPMENT OF A GRAPHICS-BASED MODEL OF THE HUMAN ELBOW: MOMENT ARM CALCULATION ISSUES

Wendy M. Murray, Scott L. Delp, Thomas S. Buchanan

Department of Biomedical Engineering, Northwestern University, and
Sensory Motor Performance Program, Rehabilitation Institute of Chicago, Chicago, Illinois

INTRODUCTION

We are developing a computer model of the human elbow to characterize the isometric moment-generating properties of the muscles. The model consists of three-dimensional representations of the bones, line segment approximations of muscle paths, kinematic descriptions of elbow flexion-extension and pronation-supination, and Hill-type models of the isometric force-generating properties of eight muscles. We have found that the isometric moment vs. joint angle curves of the elbow flexors are sensitive to the variation of muscle moment arms with joint angle. Also, we have found that calculated moment arm curves are sensitive to the modeling of the muscle path. This abstract compares the moment arm of the biceps calculated with our three-dimensional model to the experimentally measured moment arms and previously reported data.

REVIEW AND THEORY

Moment arm data of the elbow muscles have been reported by Amis, et al. (1979) and An, et al. (1981). Although these studies provide data that are helpful for testing our musculoskeletal model, neither provides enough data to fully understand how muscle lengths and moment arms change as a function of flexion-extension and pronation-supination angles. Since moment arms reported by An, et al. (1981) were measured from arm cross sections at specific joint angles, moment arms could only be reported for a few discrete elbow/forearm positions. Amis, et al. (1979) computed elbow flexion moment arms over a full range of flexion angles, but the study does not take into account the effects of pronation-supination. Since joint moments calculated with our model are sensitive to the magnitude and shape of the muscles' moment arm vs. joint angle curves, it is necessary to have moment arm estimates for many combinations of flexion-extension and pronation-supination angles. The purpose of our current work is to obtain experimental data that is sufficient to test our calculated moment arms in many body positions.

PROCEDURES

Computer Modeling. The model was implemented using a software system that allows one to create computer graphics models of many different musculoskeletal structures (Delp et al., 1990). The model displays the surfaces of the ribs, scapula, clavicle, humerus, radius, and ulna (Fig. 1). For elbow angles between 35°-130° flexion, the elbow is represented as a uniaxial hinge joint with its axis passing through the centers of the capitellum and the trochlear sulcus (London, 1981). However, to allow for the sliding that occurs between the humerus and the ulna near full extension (London, 1981), the elbow axis translates approximately 3 mm anteriorly and inferiorly from 35° flexion to full extension (0° flexion). In our model of pronation-supination, the ulna remains stationary while the radius rotates about an axis that passes through the centers of the radial head and the distal ulna. The paths of the biceps (short and long heads), brachialis, brachioradialis, triceps (long, lateral, and medial heads), anconeus, pronator teres, pronator quadratus, and supinator, consist of a series of points that are connected by line segments. The moment arms of these muscles can be computed for any combination of elbow flexion and pronation-supination angles.

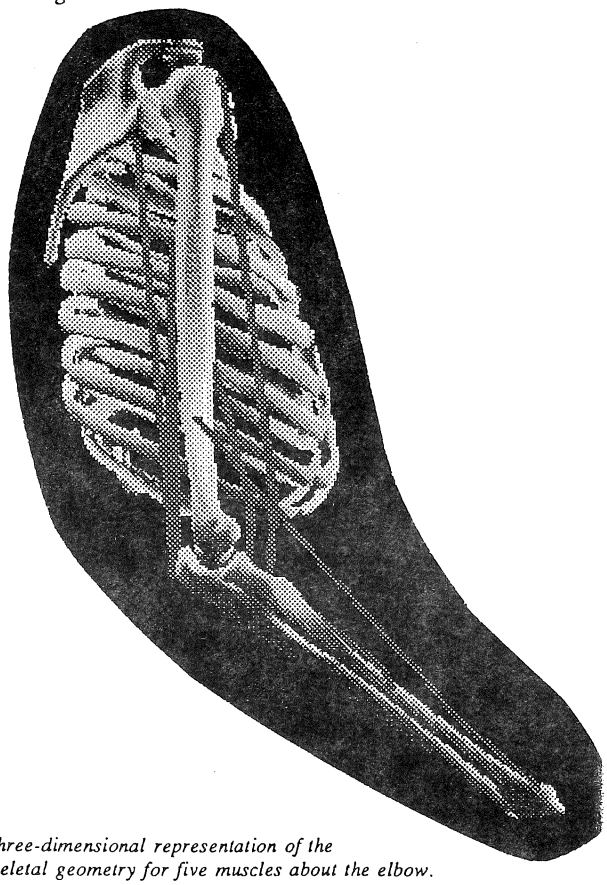

Fig. 1. Three-dimensional representation of the musculoskeletal geometry for five muscles about the elbow.

Preliminary Anatomic Measurements. Moment arms were estimated from measurements of tendon displacement over a range of elbow angles. An alcohol-preserved cadaver arm was disarticulated at the shoulder joint and mounted on a horizontal Plexiglass sheet. The humerus was fixed to the Plexiglass, but the forearm remained free. The Plexiglass was etched with 5° angle increments so that the elbow angle could be measured by aligning a pointer attached to the wrist with the etchings on the Plexiglass. The carrying angle was allowed to vary so that the normal joint kinematics were not disrupted. The tendon of the long head of the biceps was attached to a length transducer that loaded the muscle with a constant tension of 7.5N. As the elbow was extended from full flexion, tendon displacement was recorded at 5° increments over a 115° range of motion. Tendon displacements measured in seven trials were averaged. The average tendon excursion vs. elbow angle was fit by a quintic spline using Woltring's Generalized Cross Validation Software (Woltring, 1986). Moment arms were calculated by differentiating the quintic spline fit of average tendon excursion vs. joint angle, i.e. $ma = \partial l/\partial \emptyset$ (An, et al, 1984).

RESULTS AND DISCUSSION

Our preliminary results show that the moment arm computed for the long head of the biceps is consistent with our measured moment arms and with the data reported by An, et al. (1981) (cf. solid curve, dotted curve, and large dots in Fig. 2). However, there is a large difference between our moment arms and those reported by Amis et al. (1979) for flexion angles greater than 50°. The difference in magnitude of our computed moment arm and the moment arm calculated by Amis, et al. can be explained by the differences in the method of modeling the muscle path. For flexion angles greater than 35°, Amis, et al. represented the muscle line of action with a single line segment that directly connected the muscle origin and insertion. When we approximated the muscle path in this manner, we obtained a moment arm curve similar to the dashed curve in Fig. 2. However, by placing a constraining point in the area of the joint capsule that prevents the muscle path from "bowstringing" away from the humerus, the calculated moment arm more closely corresponds to the experimental data. The magnitudes of our computed curve, our experimentally measured moment arm, and An's data emphasize the need to take into consideration the constraints that the skin and fascia impose on muscle excursion when modeling muscle paths.

Additional anatomic studies are planned to test variation of biceps elbow-flexion moment arm with forearm position, and to measure biceps pronation-supination moment arm.

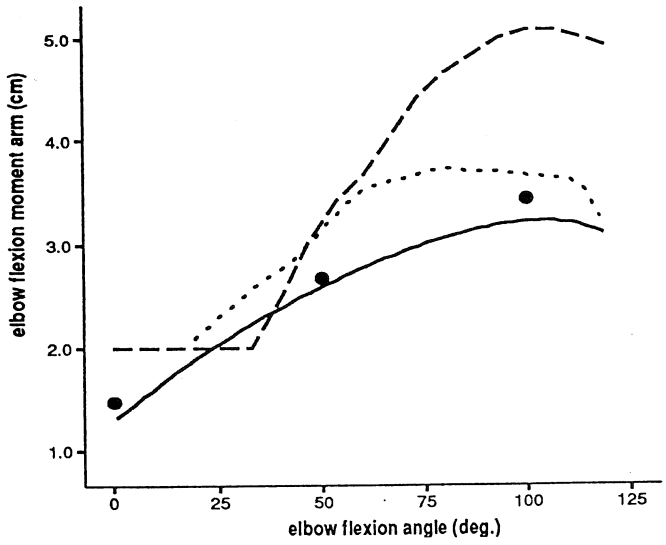

Fig. 2.
Elbow flexion moment arm vs. elbow angle reported by Amis et al. (dashed line) and An et al. (3 dots) compared to moment arms measured in the current study (dotted line) and computed with our computer model (solid line). 0° is full extension. The forearm is in neutral pronation-supination.

REFERENCES
An, K.N., et al. J. Biomechanics, **14** (10), 659-69, 1981.
An, K.N., et al. J. Biomechanical Engng, **106**, 280-2, 1984.
Amis, A.A., et al. Engng Med., **8** (1), 41-48, 1979.
Delp, S.L., et al. IEEE Trans. on Biomed.Eng. **37** (8), 757-67, 1990.
London, J.T., J. Bone and Jt. Surg., **63-A** (4), 1981.
Woltring, H.J. Advances in Engineering Software **8** (2), 104-113, 1986.

Supported by NIH grant AR R29-40408 and the Baxter Foundation

A BIOMECHANICAL STUDY OF THE RADIAL-SIDED STABILIZERS OF THE THUMB MCP JOINT

T. Loebig†, D. Anderson†, M. Baratz§, M. Herron§, A. Zoppi§, and J. Imbriglia§

†Biomechanics Research Laboratory, Allegheny-Singer Research Institute,
§Department of Orthopaedic Surgery, Allegheny General Hospital,
320 E. North Avenue, Pittsburgh, PA 15212

INTRODUCTION

Radial instability of the thumb metacarpophalangeal joint (MPJ) occurs with approximately 10 to 30% of the frequency of ulnar-sided instability; the so called "game-keeper's" thumb. This injury involves variable degrees of disruption of the radial collateral ligament complex, dorsal capsule, and volar plate. Appropriate treatment requires a clear understanding of the anatomy and of the mechanical contributions of the joint's stabilizing ligaments. A cadaver study was conducted to examine the contributions of four structures to radial-sided stability of the thumb MPJ: the dorsal capsule (DC), radial collateral ligament (RCL), accessory collateral ligament (ACL), and volar plate (VP). Two parameters were evaluated: %-decrease in gross MPJ stiffness and the angle of joint opening.

REVIEW AND THEORY

Instability of the thumb metacarpophalangeal joint is a common and often disabling condition. Palmer *et al.* (1978) described the ligamentous stabilizers of the ulnar side of the joint, as well as the effect of disrupting each of these structures. The anatomical pathology as well as the results of treatment for ulnar-sided instability of the thumb MPJ are well documented.

Radial-sided instability has received less attention in the clinical literature. Camp *et al.* (1980) treated nine thumbs for chronic radial instability and found disruption of the RCL at its insertion on the proximal phalanx, in the midsubstance of the ligament or at the metacarpal origin. Ganos *et al.* (1991) reported on the operative treatment of both acute and chronic injuries. They observed some degree of injury to the dorsal capsule in addition to disruption of the RCL that had previously been described. Coonrad *et al.* (1968) noted that partial instability resulted following division of the abductor pollicis aponeurosis (APA) and RCL. The remaining stability was shown to be provided by the volar plate. We know of no formal biomechanical study that has examined the role of static ligamentous restraints to radial stability. Our goals were to assess the relative contributions to the MPJ gross stiffness of the DC (which included the APA), RCL, ACL, and VP; and to compute the angle of joint opening produced by applying a controlled amount of force to the ulnar aspect of the MPJ via a four-point bending device.

PROCEDURES

Twenty-four fresh frozen human cadaver thumbs were dissected free of skin, subcutaneous tissue, muscles, and the flexor tendons. The extensor tendons were transected distally and proximally of the MPJ, but left attached to the dorsal hood, to which they are intrinsically connected. Other investigators treated the APA as a separate structure whereas we regarded it as an intrinsic part of the DC.

The specimens were tested in an MTS Bionix 858.20 servo-hydraulic testing machine using a specially constructed four-point bending fixture to apply a radially-directed load to the MPJ. Specimens were positioned to produce symmetrical deflections of the proximal phalanx and the metacarpal which simulated a spring-loaded, center-hinged beam. Guides on the fixture were used to set the angle of flexion/extension and to prevent any rotation of the specimen. A preload of 3-5 N was then applied. Sub-failure loading was applied to the MPJ for several consecutive paired runs. Each loading run consisted of two segments. The first was a cyclic preconditioning segment using a 1 Hz haversine function to 75 N followed by a 60 s hold at preload. A 150 N/s ramp to 75 N was then applied, returning to zero load at 1500 N/s. Each test pair involved two identical loadings to establish reproducibility of gross response characteristics.

Following preliminary testing of the intact case, serial sectioning of three out of the four ligaments was performed in three different sequences, providing 8 specimens for each sequence. Each configuration was tested in 0° (full extension) and 30° flexion. Decreased peak loads were used when failure was expected. System response to the loading described was characterized by recordings of load uptake versus displacement, which provides a measure of gross joint stiffness. Secant stiffness values were calculated at various load values

RESULTS AND DISCUSSION

Results from two different sequences (#1 and #3) show that the RCL maintained 75% and 85% of the intact stiffness with the thumb at 0° and 30° flexion, respectively. Transection of the RCL alone (Sequence #2) did not cause total instability of the MPJ, with the RCL deficient thumb averaging a decrease in stiffness of $21.3 \pm 13.2\%$ at 0° flexion and $3.9 \pm 3.3\%$ at 30° flexion. Release of both the RCL and ACL resulted in decrease in stiffness of $53.0 \pm 11.5\%$ in extension and $50.6 \pm 12.4\%$ at 30° flexion. These last values, however, were obtained at reduced load levels for the specimens that could not endure the entire loading procedure. Figure 2 shows the values of the normalized gross joint stiffness (N/mm / N/mm).

Coupled with qualitative observations, the data indicates that the RCL/ACL complex is the primary restraint to lateral deviation of the MPJ. After release of the dorsal capsule, joint stability was completely compromised, particularly in flexion. Of the tests able to be completed, the volar plate could maintain only 35% and 25% of the intact stiffness at respective flexion angles of 0° and 30°. Release of the ACL first showed a significant ($p \leq 0.01$) drop of $18.2 \pm 6.2\%$ in extension stiffness compared to $5.3 \pm 6.4\%$ in flexion. The accompanying angle of joint opening was over 6° more in extension than in flexion($p \leq 0.01$).

The angle of joint opening of all intact specimens averaged $24 \pm 6°$ (Fig. 1) at extension and $25 \pm 7°$ at 30° flexion. When the RCL was cut first (Sequence #2), the angle increased to $31 \pm 4°$ at extension and $33 \pm 6°$ at 30° flexion. The difference between extension and flexion was not significant. Further transection of the ACL resulted in angles of $46 \pm 5°$ and $53 \pm 8°$ at extension and flexion, respectively. Once again, these values are due to reduced peak loads and the actual values may be higher. The final cut in

sequence #2, dorsal capsule, resulted in total instability and angles greater than 90°.

Isolation of the RCL, sequences #1 and #3, resulted a maximum decrease in stiffness of only 20% and angles of 31 ± 3° and 28 ± 7° at 0° and 30 ° flexion, respectively. Cutting the ACL first resulted in a joint opening angle of 32 ± 6° at extension, for an increase of 5°, but only a 1° increase at 30° flexion. Similar changes also occured when the ACL was cut last, leaving only the RCL. Changes due to transection of the other ligaments was not significant. Loss of only the DC and VP caused a decrease in stiffness of 7.5% and an increase in joint opening angle of 2.5° at 0° flexion while slightly larger changes, 10 to 15% decrease in stiffness and 3° increase in angle, were noticed at 30° flexion. Thus, the difference between the final extension and flexion angles indicate that the ACL aids stability slightly more in extension than flexion.

The dorsal capsule, as noted earlier, tends to influence stability at higher flexion angles, while the volar plate exerts more stiffness at extension. In the presence of the RCL and ACL, the DC and VP play very minor roles, however, when the RCL and ACL were cut, there was an increased tendency towards volar subluxation of the proximal phalanx. This volar subluxation may be an important part of the injury mechanism, which would place high stress on both the RCL and DC. While the ACL deficient thumb showed a higher joint opening angle at extension than at 30° flexion (5° difference), the loss of the RCL was not as remarkable, showing only a 1° difference.

The RCL/ACL complex appears to be the primary restraint to ulnar loading at the MPJ, with the ACL enhancing extension stiffness. Our results suggest that with disruption of both the RCL/ACL complex and the dorsal capsule, joint opening on a stress radiograph should be at least 45° in both extension and flexion. Qualitative laboratory observations indicate that both the dorsal capsule and volar plate/capsule provide substantial resistance to volar subluxation of the proximal phalanx. Although the clinically observed case of RCL/DC rupture was not tested, this concern is to be addressed in a second part of this study in which complete thumbs, including extraneous tissue and tendons, will be stressed to failure attempting to simulate the injury.

REFERENCES

Coonrad, R. et al. *J Bone Joint Surg [Am]* **50**, 439-451, 1968.
Camp, R. et al. *J Hand Surg [Am]* **5**, 221-225, 1980.
Palmer, A. et al. *J Hand Surg [Am]* **3**, 542-546, 1978.
Ganos, D. et al. *Proceedings of the American Society for Surgery of the Hand.* (pp. 3-25), 1991.

ACKNOWLEDGMENTS

The authors would like to acknowledge that funding for this project was provided by the Albert B. Ferguson, Jr., M.D. Orthopaedic Foundation.

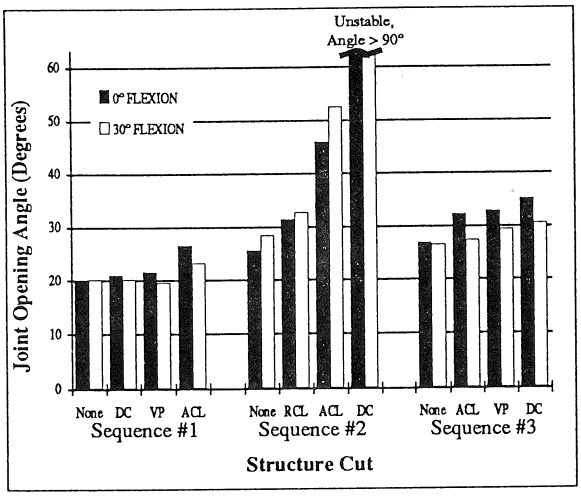

Fig. 1: Joint Opening Angle (Degrees) vs. Structures Cut, in the order of actual cutting and grouped by sequence.

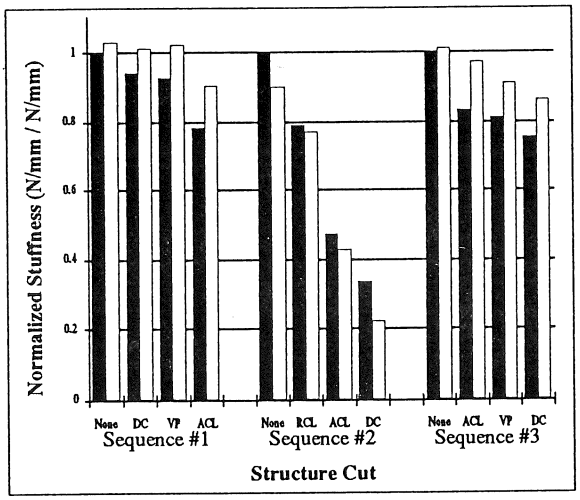

Fig. 2: Normalized Sttiffness (N/mm/N/mm) vs. Structures Cut, in the order of actual cutting and grouped by sequence.

INTERACTION TORQUES CAN ASSIST IN PRODUCTION OF SOME TYPES OF INDEX FINGER MOVEMENTS.

W.G. Darling and K.J. Cole.

Dept. of Exercise Science, University of Iowa, Iowa City, IA

INTRODUCTION

It was shown previously that torques arising from inertial interactions among the moving index finger segments are significant in index finger movements. That is, such torques must be overcome by muscular torques to produce desired motion at a finger joint, and prevent unwanted motions at other index finger joints. However, it is possible for such inertial interactions to assist in movements when the adjacent joints simultaneously move in different directions. The purpose of the present investigation was to determine whether such torques can assist in production of index finger movements as indicated by reductions in muscular activity and joint torques associated with such movements.

Bipolar EMGs were recorded from 6 or 7 index finger muscles using indwelling wires. Subjects produced movements involving (1) simultaneous flexion of all 3 index finger joints, (2) extension of these joints, and (3) oppositely directed movements of the metacarpophalangeal (MCP) and interphalangeal (IP) joints. Movements were recorded optoelectronically. Analysis of the EMG patterns showed that during oppositely directed movements of the MCP and IP joints there were large reductions in activities of the muscles that produce the motions at the IP joints in comparison to movements in which all joints moved in the same direction.

REVIEW AND THEORY

The majority of studies of index finger motion control have considered only slow movements or static postures (e.g., Landsmeer 1955, Landsmeer and Long 1965). Recently, faster motions have been considered (Darling and Cole 1990) but movements were restricted to the MCP and proximal IP (PIP) joints. It was shown that during such fast movements the torques arising from inertial interactions among the finger segments were large in relation to the muscular (joint) torques and must be compensated both in producing movement and in maintaining joint posture during motion at other joints. Recent work in this laboratory has extended this to the kinematics and kinetics of 3 joint index finger movement while simultaneously recording EMGs from 6 or 7 index finger muscles. The purpose of the present work was to determine whether interaction torques can be used to assist in production of index finger movements specifically when the MCP and IP joints move in opposite directions.

PROCEDURES

Six college aged subjects participated in these experiments. EMGs were recorded using indwelling hooked wire electrodes inserted into 6 or 7 muscles of the index finger (in some studies extensor indicis activity was not recorded). Muscle activation levels were quantified by computing the average activity over the interval from 20 ms prior to movement onset to movement terminations. Movements were recorded optoelectronically with infrared emitting diodes (IREDs) placed over the base of the 2nd metacarpal and the centers of the MCP, PIP and DIP joints. Subjects performed 4 different types of discrete motions in the horizontal plane as described in the INTRODUCTION at two instructed speeds: (1) very fast and (2) smooth, natural speed. Joint angles were computed from the recorded IRED positions, joint torques were computed using inverse dynamics and were separated into muscular torques and interaction torques using procedures similar to those described by Hoy and Zernicke (1986).

RESULTS

Flexion movements were produced primarily by activation of extrinsic flexors (FDS, FDP) and the first dorsal interosseus (DIO) muscle (Fig. 1, upper left). When IP flexion movements were coupled with MCP extension, rather than MCP flexion, there was a dramatic decrease in FDP, FDS activity in spite of the fact that the IP joints showed greater and faster flexion movements (Fig. 1, upper right). Substantial reductions in FDS, FDP and DIO activity were observed in all subjects for these movements. Examination of torque records showed that extension of the MP joint produced an initial flexor torque at the PIP and DIP joints that presumably assisted in IP flexion, thereby reducing the need for strong flexor muscle activity.

Extension movements were produced by activation of the extrinsic extensors (EXD, EI) as well as the intrinsic muscles (DIO and first lumbrical - LUM) (Fig. 1, lower left). When IP extension movements were coupled with MCP flexion, large decreases in the activity of EXD and EI were observed, however increased activation of the intrinsic muscles was observed (Fig. 1, lower right). IP motions were larger in amplitude and faster than during all joint extension movements even though activation of the extrinsic extensors was substantially reduced.

DISCUSSION

The results of these experiments show clearly that interaction torques arising from motion of the index finger segments can assist in production of index finger movements. This is further evidence that the nervous system takes account of the dynamics of index finger movements in controlling the activation of the index finger musculature. Although in most normal movements of the index finger the interaction torques are detrimental to movement production (i.e., flexion and extension movements or IP movements in which the MCP

joint posture is maintained), these results clearly show that such torques can assist the muscles in causing motion and thereby reduce muscular effort.

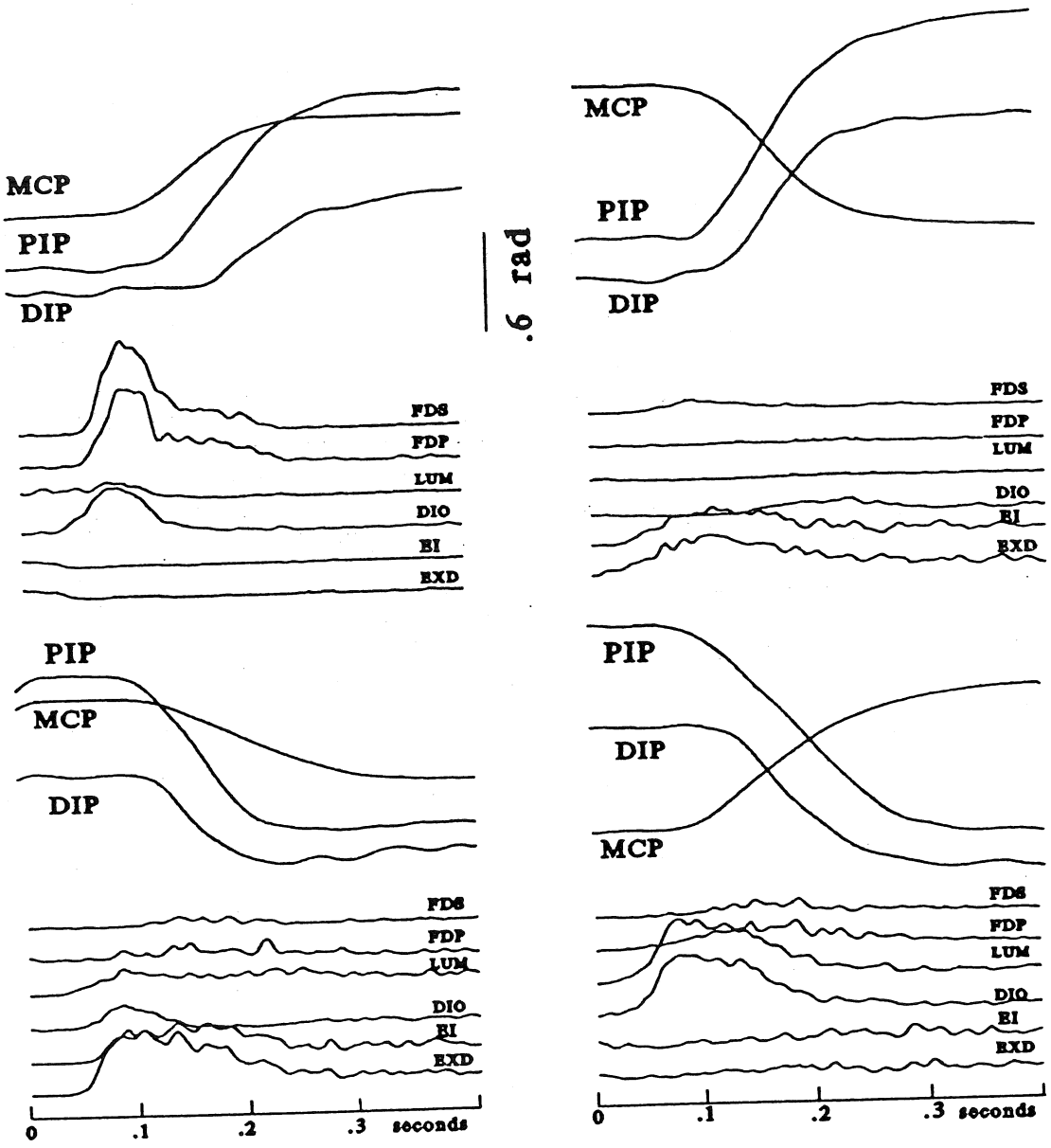

Figure 1. Averaged kinematic and EMG records from all joint flexion (upper left), all joint extension (lower left), MCP flexion - IP extension (lower right) and MCP extension - IP flexion movements (upper right).

REFERENCES

Darling, W.G., Cole, K.J. J. Neurophysiol., 63, 1098-1108, 1990.
Landsmeer, J.M.F. Acta Anat 25, Suppl. 24, 1-69, 1955.
Hoy, M.G., Zernicke, R.F. J. Biomech. 19, 867-877, 1986.

THUMB FORCE ANALYSIS

David J. Giurintano and Anne M. Hollister

Paul W. Brand Biomechanics Laboratory, GWLHDC, Carville, LA
Department of Surgery, Harbor - UCLA Medical Center, Torrance, CA

INTRODUCTION

The mechanics of the thumb has been investigated by many researchers. Most have modeled the Carpometacarpal (CMC) joint as a spherical joint, the Metacarpophalangeal (MP) joint as a universal joint, and the Interphalangeal joint (IP) as a hinge joint. The thumb is modeled as a five link manipulator with the links connected by hinge joints - one for each degree of freedom. The locations of the axes of rotation of the thumb come from the anatomic work of Hollister *et al.* (1992) and the computer simulation work of Buford *et al.* (1990). Four static positions of hand function are analyzed - key pinch, tip pinch, screwdriver hold, and wide grasp.

BACKGROUND

Cooney *et al.* (1981), A. Fick (1854), R. Fick (1908), and Kapandji (1981) postulated CMC joint motion to occur about two axes of rotation, perpendicular to each other and to the metacarpal because of the joint's saddle shape. They modeled the CMC joint as a simple universal joint, with the axes perpendicular to each other and to the bones. Rudolph Fick (1908) and Kapandji (1981) postulated a third longitudinal axis to account for pronation and supination.

Hollister *et al.* (1992) determined the location of the axes of the joints of the thumb. The flexion-extension (F-E) axis of the CMC joint is located in the trapezium, and the abduction-adduction (A-A) axis is near the base of the metacarpal. The axes do not intersect and are not perpendicular to each other or the trapezium or the metacarpal. The F-E and A-A axes of the MCP joint are located near the distal surface of the metacarpal. Likewise, these axes do not intersect and are not perpendicular to each other or the metacarpal. The axis of the IP joint runs parallel to the flexion crease of the joint and is not perpendicular to the phalanx.

Chao (1976) and Cooney (1977) analyzed the tendon forces and joint reactions in the fingers and the thumb and reduced the number of unknowns by assuming that the Extensor Pollicis Brevis and Extensor Pollicis Longus did not carry large loads for pinch and grasp. The Flexor Pollicis Brevis and the Opponens Pollicis were assumed to act as one muscle because of electromyogram studies.

Chao and An (1978) analyzed the hand for postures of grasp and key pinch. To reduce the number of unknowns, they used observations of the functional anatomy of the muscles. Linear programming was implemented to solve the system. The objective function was the minimization of joint torque and maximization of tendon force.

MATH MODEL

In the Five-Link Manipulator Thumb Model, the thumb is composed of five links, connected by hinge joints, unlike the physical system which is composed of three links. The axes of motion of the hinges are not perpendicular to the links (Figure 1). The motion of the bone segments is linked to the anatomic axes as determined by Hollister *et al.* (1992). The two most proximal virtual links simulate the F-E and A-A axes of the CMC joint. The two intermediate virtual links simulate the F-E and A-A axes of the MP joint, and the most distal virtual link simulates the F-E axis of the IP joint. Homogeneous matrix transformations are used to move the bones from their resting posture to the four functional positions investigated - key pinch, tip pinch, screwdriver hold, and wide grasp.

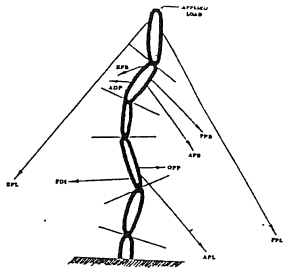

Figure 1. Virtual five-link manipulator model with the lines of action of the muscles and the applied load represented.

Thompson and Giurintano (1989) used a building block approach to construct tendon models for the long flexors of the hand. From that work, building block $\mathcal{A}$, simulating a tendon traveling in a straight line, and building block $\mathcal{B}$, simulating a tendon traveling in a circular path as it crosses a joint were used. Two additional building blocks were developed. Building block $\mathcal{E}$, simulating an extensor tendon's dorsal travel over a joint in a circular arc with the radius of the arc equal to 1.3 times the distance between the two points on the circle and building block $\mathcal{F}$, simulating an extensor tendon's dorsal travel over a joint in an arc modeled as a fourth order polynomial with first derivative continuity at both the proximal and distal segments, were created. Each muscle's line of action was constructed using building blocks $\mathcal{A}$, $\mathcal{B}$, $\mathcal{E}$, and $\mathcal{F}$. The Flexor Pollicis Longus (FPL)'s pattern is $\mathcal{A}\,\mathcal{B}\,\mathcal{A}\,\mathcal{F}$; the Extensor Pollicis Longus (EPL)'s is $\mathcal{E}\,\mathcal{A}\,\mathcal{F}\,\mathcal{A}\,\mathcal{F}$; the Extensor Pollicis Brevis (EPB)'s is $\mathcal{E}\,\mathcal{A}\,\mathcal{F}\,\mathcal{A}$, and the Flexor Pollicis Brevis (FPB), Opponens Pollicis (OPP), the Adductor Pollicis (ADP), the Abductor Pollicis Longus (APL), the Abductor Pollicis Brevis (APB), and the First Dorsal Interosseous (FDI) are $\mathcal{A}$. The information generated from the locations of the control points of the motors of the thumb is used to determine the lines of action of the forces generated by the motors.

Optimization techniques must be used to resolve the distribution of forces generated by the motors of the thumb and determine the joint reactions at the joints. The redundancy problem occurs from the attempt to solve the system of thirty equations with thirty-four unknowns. This system is solved by using non-linear optimization techniques developed by McPhate (1975) after Powell (1964). The routine uses the conjugate gradient method without calculating derivatives. The formal definition of the force analysis of the Five-Link

Manipulator Thumb Model is

$$\left.\begin{array}{ll} \textit{minimize} & \sum \sigma_i^2 \\ \textit{subject to} & \sum M_{\textit{hinge axis}} = 0 \\ & f_i \geq 0 \end{array}\right\} \quad (1)$$

where the muscle stress of the *ith* muscle is defined as the force of the *ith* muscle divided by its physiologic cross-sectional area. The physiologic cross-sectional area for the muscles were determined by Brand *et al.* (1981). From the virtual model (Figure 1), free body diagrams were constructed from initially the most distal link, then the two most distal links, until five free bodies were created. From these free body diagrams, the equations of static equilibrium were generated. Soft tissue effects were neglected. Disease states can be modeled with the five-link manipulator by modifying the location and orientation of the axes. The orientation of the applied load for the four functional positions modeled are: Key Pinch - up on the pulp, Screwdriver hold - at a 60 degree angle to the DP's tip, Tip Pinch - tip pinch orientation, and Wide Grasp - on the ulnar side of the DP.

The use of non-linear optimization techniques does not guarantee that the final solution is a global minimum to the problem. However, because the cost function is convex, global convergence is guaranteed. The tension fractions for the muscles are from Brand *et al.* (1981). With the muscle forces generated from the optimized solution, the forces and moments on the distal surface of proximal phalanx, metacarpal, and the trapezium are solved for using static force analysis.

RESULTS AND DISCUSSION

Tables 1, 2, and 3 list the muscle forces, and the forces and moments at the joint surfaces for the four positions with an applied load of 147 N.

Table 1. Muscle forces(N).

Muscle	Key	Screw	Tip	Wide
FPL	980.0	980.1	357.5	0.0
FPB	624.5	782.6	0.0	0.0
EPL	0.0	213.9	1.0	1.7
EPB	762.9	934.3	68.9	223.5
OPP	-0.1	-0.1	2.1	980.0
ADP	-1.9	-1.9	213.3	505.4
APL	445.5	0.0	376.5	0.0
APB	55.0	0.3	0.0	0.0
FDI	-1.2	-1.2	202.2	132.4

Table 2. Joint forces(N).

Joint	Key	Screw	Tip	Wide
CMC force	2628.9	2859.3	885.2	1703.6
MP force	2258.9	2848.9	490.4	690.3
IP force	941.0	1259.2	275.7	157.7

Table 3. Joint Moments(N-mm).

Joint	Key	Screw	Tip	Wide
CMC moment	7815.3	5521.7	6945.1	22001.0
MP moment	12769.3	14758.6	4116.4	5655.9
IP moment	3294.4	3255.2	2408.5	2967.7

In key pinch, the flexors and the EPB and APL balance the applied load. As expected no adductors are needed since the thumb is in the plane of the palm. For the screwdriver hold, the extrinsics are used with FPB to stabilize the thumb. For tip pinch, the adductors and the FPL and APL balance the thumb, and for wide grasp, the EPB, ADP and OPP balance the thumb. Cooney *et al* (1985) used EMG's to determine which muscles fired during various pinches and grasp. The Virtual Five-Link Thumb Model predicted similar recruitment patterns. The force applied to the surface of the trapezium as a result of the thumb motors firing to balance an applied load is between six and twenty-three times the applied load depending on the posture. Previous results published by Cooney and Chao (1977) predicted forces applied to the trapezium of twelve times the applied load. For key pinch and screwdriver hold the Virtual Five-Link Thumb Model predicted loads of sixty-five percent greater magnitude.

REFERENCES

Brand, PW, *et al.* Relative Tension and Potential Excursion of Muscles in the Forearm and Hand, *J Hand Surg*, **6**(3), 209-219, 1981.

Buford, WL, *et al.* Three Dimesional Computer Simulation of Thumb Carpometacarpal Joint Kinematics, **Abstracts of the First World Congress of Biomechanics, II**, 161, 1990.

Chao, EY, *et al.* Three Dimensional Force Analysis of Finger Joints in Selected Isometric Hand Function, *J Biom.* **19**(6), 387-396, 1976.

Chao, EY and An, KN, Determination of Internal Forces in Human Hand, *J Engr Mech Div ASCE*, **104** No. EM1, 225-272 1978.

Cooney, WP and Chao, EY, Biomechanical Analysis of Static Forces in the Thumb During Hand Function, *J. Bone and Joint Surgery*, **59-A**(1), 27-36, 1977.

Cooney WP, *et al.* The Kinesiology of the Thumb Trapeziometacarpal Joint, *JBJS*, **63-A**, 1371-1381, 1981.

Cooney WP, *et al.* Electromyographic Analysis of the thumb: A Study of Isometric Forces in Pinch and Grasp, *J Hand Surgery*, **10**(2), 202-210, 1985.

Fick A **Die Gelenke mit sattelformigen Flachen. Zeitschrift fur Rationelle Medicin**. Heidelberg, Akademische Verlagshandlung von C. F. Winter, 314-21, 1854.

Fick R *Handbuch der Anatomie und Mechanik der Gelenke unter Berucksichtigung der bewegenden Muskeln*, Jena, Verlag von Gustav Fisher, **II** 1908.

Hollister A, *et al.* The Axes of Rotation of the Thumb Carpometacarpal Joint, *J Ortho Res*, (in press).

Hollister A, *et al.* Axes of Rotation of the Thumb Interphalangeal and Metacarpophalangeal Joints, *J Ortho Res*, (submitted)

Kapandji IA, (1981) Biomechanics of the Thumb, **The Hand I**,(pp.404-422), WB Saunders, 1981.

McPhate, AJ, Mechanical Design Using Nonderivative Search and Quadraric Penalty Functions, Oklahoma State Applied Mechanics Conference, paper 18. 1975.

Powell, MJD, An Efficient Method for finding the Minimum of a Function of several Variables without Calculating Derivatives, *Comput Jour*, **7** pp. 155-162, 1964.

Thompson, DE and Giurintano, DJ, A Kinematic Model of the Flexor Tendons of the Hand, *J Biom*, **22**(4), 327-334, 1989.

LOAD DEPENDENCE OF CARPAL KINEMATICS IN WRIST FLEXION

F. J. Valero-Cuevas and C. F. Small
Mechanical Engineering Department, Design Division, Stanford University, Stanford, CA, U.S.A.
Clinical Mechanics Group, Queen's University, Kingston, Ontario, Canada.

INTRODUCTION

An apparatus, with a movable handle, constrained hand motion to the flexion-extension plane with the forearm fixed, and exerted a torque opposing the motion. By recording the location and orientation of the handle, the finite centre of rotation and radius of curvature of the handle were calculated throughout the motion. Ten normal subjects were tested at no-load and two levels of wrist torque. The radius of curvature magnitude was characterized over the range of motion by five or six fluctuations, whose amplitude depended on wrist torque magnitude ($F[18,2]$, $p<0.0007$), which implies that the centre of rotation of the wrist moves as the flexion motion progresses. This represents the most convincing evidence yet that the wrist joint does not function like a pin joint, and that wrist kinematics depend on the magnitude of joint forces at the wrist. We postulate that wrist flexion consists of a sequence of carpal bone configurations, resulting in metacarpal (hand) motion that alternates between sliding and rotation. By using this relationship between wrist kinematics and load, further development may lead to methods of estimating joint integrity through task-oriented tests.

REVIEW AND THEORY

Sets of kinematic parameters have been used to describe and evaluate the two and three-dimensional characteristics of both normal and abnormal wrist joints to permit an objective determination of the degree of kinematic dysfunction in pathological joints (Youm & Yoon, 1979;Hamas, 1979;Erdman *et al.*, 1979;Brumbaugh *et al.*, 1982). However, the wrist joint does not lend itself to simple kinematic models because of its large range of motion and its complex anatomy, resulting in significant functional interdependence between its osseous, ligamentous and muscular structures (De Lange, 1985). In such a complex joint internal joint forces are resisted and guided by bone and cartilage geometry, ligament structures, and synergistic muscle activation. Hence, the kinematic function of the wrist joint is the result of the balanced interaction between several anatomical structures with different physical reactions to load (compression, stretching, deformation, bone rearrangement). This leads us to expect that the kinematic function of the whole wrist depends on the magnitude of the joint forces at the wrist. This experiment sought to determine if the location of the centre of rotation of the wrist changed with increasing wrist torque magnitudes.

METHOD

The apparatus consisted of a movable, custom molded handle for each subject, which constrained hand motion to the flexion-extension plane of motion without assuming or imposing a handle trajectory or centre of rotation. The subject's forearm was secured to the apparatus frame which was in turn bolted to the right hand side of a chair. The flexion-extension plane was defined as a plane pronated 10° from the sagittal as suggested by studies in free-moving hands (Palmer *et al.*, 1985). To move the handle, the subject had to develop sufficient wrist torque to lift a weight coupled to the handle via a pulley. The choice of weight (0, 2.2 or 4.5 kg) generated wrist torque magnitudes of 0, 1.25 and 2.5 N-m, respectively. The location and orientation of the handle were recorded using one linear and two angular position transducers with an accuracy of $\pm$ 0.35 mm and $\pm$ 0.63°, respectively. The apparatus, transducers and algorithm were validated by determining the trajectories, centres of rotation and radii of curvature of known test linkages with both fixed and moving centres of rotation. The assumption was made that the handle tracked the motion of the hand, as is accepted with instrumented spatial linkages (Chao, 1980). A personal computer was used to collect and analyze the position and orientation history of the handle and determine the location of the finite centre of rotation of the wrist in the apparatus reference frame using the planar rigid body method (Woltring *et al.*, 1985) for 100 points along the range of motion. An angular displacement of 8° between successive hand orientations was used as the angular step size. The finite radius of curvature was defined as the vector connecting the finite centre of rotation and the midpoint of the handle's translation during that 8° interval.

Subjects were instructed to isolate their motion to the wrist and develop the same grip force on the handle for all trials. Each of the ten subjects performed eight flexions at each torque level. To increase the confidence in the results, a final experiment was performed to determine the effect of a soft foam rubber interface cushioning between the handle and a calibration circular link.

RESULTS AND DISCUSSION

Figure 1 shows a typical handle trajectory and the trajectory of the finite centre of rotation in the apparatus coordinate system. Notice that, although the handle trajectory appears to be a smooth arc, the finite centre of rotation trajectory (centrode) exhibits distinct oscillations. It is apparent that the motion of the wrist finite centre of rotation produces variations in the radius of curvature. The oscillation amplitude of the radius of curvature was estimated via the residual range and residual standard deviation from a second order polynomial regression of radius of curvature vs. the flexion angle. Figure 2 shows the radius of curvature residuals for all trials of subject No. 1. The radius of curvature residual range and residual s.d. were calculated for every subject's trial, 230 in all. The average residual range and s.d. for every subject at every load were calculated. The residual range is a measure of the maximum amplitude of the radius of curvature oscillations about the best fit second order polynomial. The standard deviation of the residuals is a measure of how far from the best fit curve 68% of the radius of curvature values laid. From calibration, it was seen that the in the errors in radius of curvature residual range and residual standard deviation are influenced by radius of curvature magnitude, therefore, the mean subject residual range and s.d. were adjusted (normalized) by dividing by the mean radius of curvature for that subject at each load. This adjustment of the data minimized the effect of the experimental errors on the results. The adjusted mean subject residual range and s.d., for all subjects at all loads were thus obtained.

All values of the oscillations in the result were at least 300% greater than the values of the expected experimental error determined during the calibration. Therefore, the ranges of the oscillations seen in all subjects are not an artifact of the experimental or numerical methods used, but a product of rigid body motion of the handle as the flexion motion progresses.

As is apparent in Figure 2, the magnitude of the of radius of curvature oscillations increases with load, and a distinct pattern emerges at 2.5 N-m of torque. Furthermore, in most cases, when comparing several repetitions from different trials, the patterns become regular at high loads.

This leads to the question whether or not the motion of the finite centre of rotation of the wrist is truly load dependent. Repeated measures ANOVA of the adjusted residual range and adjusted residual s.d. of the radius of curvature were used to address this issue. The ANOVA results indicate that both the radius of curvature residual range and s.d were significantly different from each other at each load level with at least 99% confidence ($F[18,2]$, $p < 0.0004$ and $p < 0.0007$, respectively). The oscillations in the centre of rotation estimates for the cushioned link tests were not different for each load level ($f[6,2]$, $p < 0.9223$). This indicates that a soft tissue interface alone cannot be responsible for the finite center of rotation oscillations detected in the subjects, and that these phenomenæ are not an experimental artifact.

The Fisher protected least significant difference test is a more conservative analysis that tests for significance of differences in the mean subject scores between adjacent load levels (Howell, 1982). These results showed that, with 99% confidence, the 1.25 vs. 2.5 N-m scores and the No-load vs. 2.5 N-m scores are significantly different from each other. The No-load vs. 1.25 N-m scores are not significantly different from each other at this level of confidence.

Lastly, linear regressions between radius of curvature adjusted residual range and residual s.d. vs. load level were performed. These regressions yielded positive slopes with a 95% confidence. Therefore, we can advocate that the magnitude of the oscillations in the radius of curvature, and thus the motion of the finite centre of rotation of the wrist, increase with load.

This work may represent the first repeatable experimental evidence of a moving wrist centre of rotation and of the load dependence in wrist kinematics.

Previous kinematics studies of the wrist concluded that the movement of the hand during flexion-extension motion takes place about a small locus on the sagittal plane which can be considered as a point axis (Youm & Yoon, 1979;Hamas 1979; Linscheid 1986). However, the literature does not contain calculation of wrist finite centre of rotation locations using angular displacements smaller than 15° between successive hand orientations. The results presented here can, in fact, corroborate these findings when an angular step size larger than 15° is used with the data. In these cases, the oscillations in the radius of curvature magnitude disappear, yielding a finite centre of rotation that appears to remain fixed. It is important to mention that the results of these experiment were made possible by a new apparatus and method which yield position and orientation data accurate enough to calculate these kinematic parameters using angular step sizes significantly smaller than in previous studies.

The kinematic interpretation of these results is that the hand distal to the wrist alternates between periods of predominantly sliding and predominantly rotating throughout the flexion range of motion. When the radius of curvature is greatest (peaks in Figure 2), the hand has increased its proportion of sliding, conversely, when the radius of curvature is smallest (troughs in Figure 2), the hand has increased its proportion of rotation. These sliding/rotation stages of the flexion motion may be a result of the significant realignment of the carpal bones necessary to complete one flexion motion (Linscheid, 1986). Hence, the flexion motion of the hand about the wrist is not that of a pin joint, but rather a sequence of non-uniform orientation changes accompanied by some slippage as the carpal bones arrange themselves into different equilibrium configurations. The results of this study may be interpreted as the first functional detection of the complex internal mechanics of the carpus.

The load dependence of the wrist kinematics follows from the fact that muscular linear forces generate compressive joint forces as well as joint torques. High joint torques are accompanied by high compressive joint forces, and these joint forces in turn compress the synovial tissue in the wrist joint. This compression reduces the carpal interosseous distances, the intercarpal ligaments become lax and the friction coefficient between cartilage surfaces increases. These changes may modify intercarpal bone realignment. Therefore, we can expect flexion motion under load to be different from flexion motion under no load. The results presented indicate that this is the case: smaller radius of curvature oscillations (smooth motion) at low loads, and larger radius of curvature oscillations (more abrupt motion) at higher loads (see Figure 2).

Furthermore, the regularity and coincidence in the radius of curvature fluctuations at high torques between trials (see Figure 2) could mean the flexion motion of the wrist is composed of a specific sequence of intercarpal bone configurations.

The results reported here strongly suggest that the wrist joint flexion does not function like a pin joint, and that wrist kinematics depend on the magnitude of joint forces at the wrist. We postulate that wrist flexion consists of a sequence of carpal bone configurations, resulting in hand motion that alternates between sliding and rotation. By using this relationship between wrist kinematics and load, further development may lead to low cost methods of estimating joint integrity through task-oriented tests.

REFERENCES

Brumbaugh, R.B. *et al. J. Biomech. Eng., 104,176*-81, 1982.
Chao, E.Y.S. *J. Biomech.*, 13L, 989-1006 1980.
de Lange, A. *J Orthop. Res., 3*, 56-64, 1985.
Erdman, A.G., *et al. J. Biomech. Eng.*, 101, 124-133, 1979.
Hamas, R. S. *Orthopedics*, 2(3), 1979.
Howell, D.C. Statistical Methods for Psychology. Duxbury Press, 1982.
Linscheid, R.L. *Clin. Orthop. and Rel. Res.*, 202, 1986.
Palmer, A.K. J. *Hand Surg.*, 10A(1), 39-46, 1985.
Woltring, *et al. J. Biomech.*, 18, 379-389, 1985.
Youm, Y. & Yoon, Y.S. *J. Biomech.*, 12, 613-621, 1979.

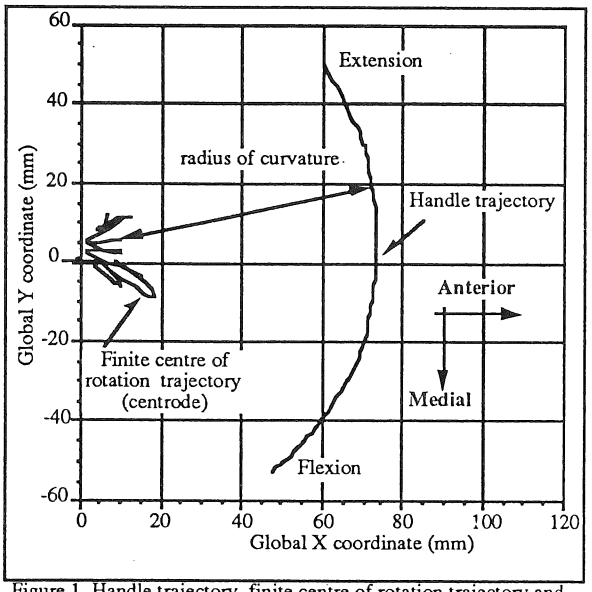

Figure 1. Handle trajectory, finite centre of rotation trajectory and sample radius of curvature shown in global space (Subject No. 1 lifting 4.5 kg).

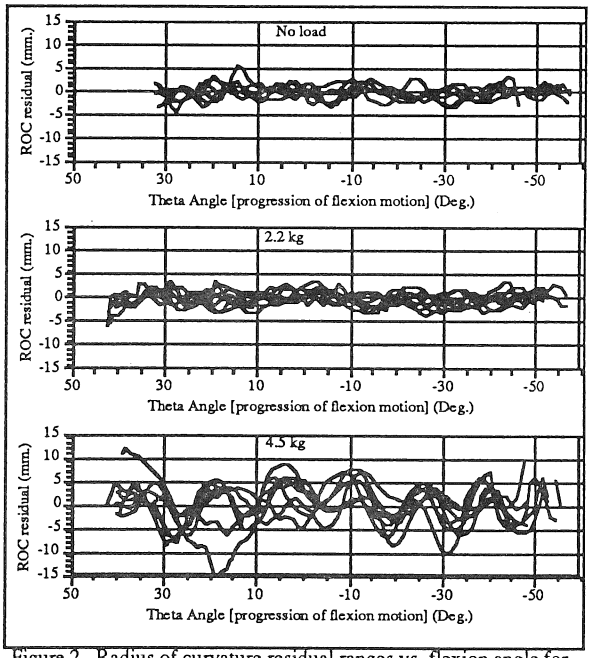

Figure 2. Radius of curvature residual ranges vs. flexion angle for three different sittings by subject No. 1. (ROC: radius of curvature magnitude).

ACKNOWLEDGMENTS

CIDA M.Sc. Scholarship, the Canadian National Research Council and David W. Risher for his helpful comments.

DEVELOPMENT OF A DYNAMOMETER FOR MEASURING DYNAMIC HAND FUNCTION

D. Pettit, R. Robertson, R. Cooper and J. Ster III

Human Engineering Laboratory, California State University, Sacramento

INTRODUCTION

Measurement of dynamic hand function is difficult due to the complex nature of finger and wrist motion for various forms of grasping maneuvers, particularly those commonly associated with the development of Carpal Tunnel Syndrome (CTS). The hand dynamometer was designed to simultaneously measure several components of hand function for controlled velocity movements, including wrist torque through full ranges of flexion-extension and adduction-abduction, wrist joint migration, and gripping force for a range of grip sizes. This device was designed in order to develop profiles of dynamic hand function for workers at risk for the development of CTS. A comparison of on-site hand motion requirements to dynamic hand function profiles will lead to recommendations for changes in tool design, job tasks, work stations and to demonstrate the need for "work hardening" programs. The present paper describes the design specifications of the dynamometer.

REVIEW AND THEORY

Assessment of the capabilities of the human hand for performing grasping and holding has generally involved a static measurement of hand grip forces with the hand held in a fixed position (Janda et al., 1987). Other studies have modeled the role of the digits in grasping cylindrical objects by analyzing the kinematics of the movement (Buchholz et al., 1992) or by describing the forces generated at each of the digit joints (Amis, 1987; Lee et al., 1991). Mathematical models of the hand have been developed for use in biomechanical and clinical studies (An et al., 1979). Wrist motion has been analyzed by describing the motion of the radio-carpal and intercarpal joints (Sarrafian et al., 1977; Youm et al., 1978). Control of wrist and finger positioning and motion has been described by investigating the activation patterns of the involved muscles (Radonjic et al., 1971). Few studies (Harris et al., 1989) have measured the dynamic capabilities of hand motion by measuring concurrent wrist torque and gripping forces for different speeds of movement throughout the full range of flexion-extension, adduction-abduction at the wrist joint.

In the work place, a number of tasks require that workers perform hand motions through large ranges of motion while firmly grasping a tool. In these situations, it has been shown (Armstrong et al., 1987) that workers are at risk for developing Carpal Tunnel Syndrome. An understanding of the capabilities of the human hand for producing these types of motion may be used to help redesign tools, work stations and job tasks. These redesign recommendations will be based on an understanding of the capabilities of workers for producing certain types of hand motion with the intent of reducing the incidence of CTS. The purpose of this study is to describe a device which has been developed to measure dynamic hand function.

PROCEDURES

The hand dynamometer was designed to allow several parameters to be measured simultaneously during controlled, constant wrist angular velocity. These include wrist torque, angular speed, wrist joint migration, wrist position and gripping force. These measurements can be made for full ranges of motion in the flexion-extension and adduction-abduction directions. Additionally, the diameter of the grip can be adjusted. Figure 1 illustrates the components of the device.

The dynamometer consists of a DC servo motor coupled to an instrumented torque shaft via a 20 to 1 worm gear reduction. Foil-type strain gages that are bonded to a narrowed section of the torque shaft allow measurement of applied torque. The shaft is aligned such that when the subject is strapped into the forearm restraining device, the wrist center is coincident with the shaft center. In this way, as the individual applies force against the handle assembly instantaneous torque can be measured. Speed of rotation is controlled by interfacing an optical encoder (aligned with the motor shaft) to the motor servo controller. Shaft speed is derived from the encoder signal which is frequency to voltage converted. The shaft position is read from a 1/2 degree resolution rotary potentiometer mounted to the torque shaft.

The handle assembly was designed to allow: 1) free rotation around the handle shaft with the axis coincident with the wrist joint center, 2) linear migration of the wrist during rotation, 3) changes in grip diameter, and 4) measurement of grip forces. Additionally, the shape of the gripping surfaces of the handle were modeled based on recommendations for tool shape (Armstrong et al., 1991). Specifically, grip forces are measured by strain gages mounted in a full bridge configuration to a portion of the handle assembly which was designed to act as a beam under loading. The entire handle assembly was allowed to linearly translate by coupling to a translation block. This block was outfitted with two pairs of linear bearings which ride along two parallel slider shafts. A linear potentiometer mounted to the translation block measured the motion perpendicular to the torque shaft (which is used to represent wrist joint migration). The grip portion of the handle assembly could be adjusted to allow 5 different grip diameters to be used from a minimum of 2 inches to a maximum of 4 inches.

The forearm restraint device (wrist cuff) was designed to strap the person into fixed positions of adduction-abduction for the flexion-extension tests. When the handle assembly was flipped 90 degrees, the forearm can be fixed for different positions of flexion-extension

while performing movements in the adduction-abduction direction.

Data acquisition was accomplished by interfacing a DT 2801 Data Translation A-D board to an IBM compatible computer. Software written in ASYST (Asyst Software Technologies, Inc.) was used to control the motor through the servo control board. After collection, data can be graphically displayed on the screen (for visual inspection) before storing as a permanent file on the hard disk for subsequent analysis.

RESULTS

The design of this device allows for the simultaneous measurement of several parameters of hand function. Each portion of the device has been shown to reliably record the appropriate data. The servo system adequately controls the angular velocity within a very small tolerance. The strain gages on the torque shaft and on the handle assembly record forces which are within expected ranges. The potentiometers recording the linear displacement of hand motion and recording shaft rotation delineate these motions within acceptable tolerance. This device measures the required parameters accurately and within small levels of tolerance.

DISCUSSION

A device for measuring dynamic hand function has been developed. Information related to simultaneous measures of wrist motion and torque and hand gripping force will allow an assessment of dynamic hand function capabilities to be made. The topology of the curve representing grip force, wrist position and wrist torque for different speeds of motion will allow profiles of individuals to be developed. This information will be used to make recommendations regarding safer tool design, job tasks, and work station configurations in industry.

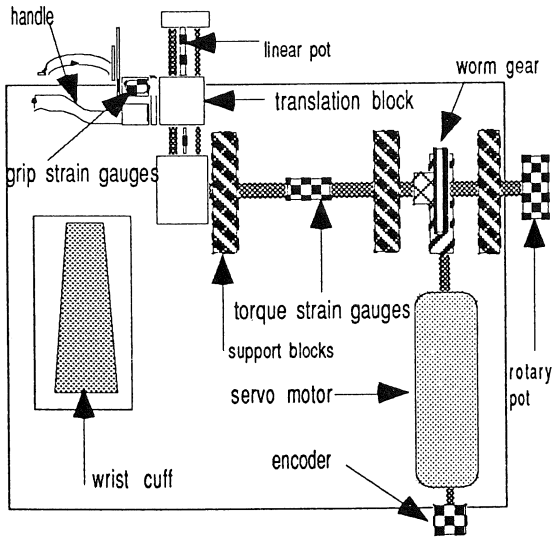

Figure 1. Top view of dynamometer assembly.

REFERENCES

Amis, A.A. *J. Biomed. Eng.*, **9**, 313-320, 1987.
An, K.N. et al. *J. Biomechanics*, **12**, 775-788, 1979.
Armstrong, T.J. et al. Clinical Concepts in Regional Musculoskeletal Illness, (pp.333-354), Grune and Stratton, 1987.
Armstrong et al. Occupational Biomechanics, (pp.420-422), John Wiley & Sons, Inc., 1991.
Buchholz, B. et al. *J. Biomechanics*, **25**(2), 149-162, 1992.
Harris et al. Proceedings of the 11th Annual International Conference of the IEEE Engineering in Medicine & Biology Society, Seattle, (pp.820-821), 1989.
Janda, D.H. et al. *J. Occup. Med.*, **29**, 569-571, 1987.
Lee, J.W. et al. *J. Biomed. Eng.*, **13**, 152-162, 1991.
Radonjic, D. et al. *Am J. Phys. Med.*, **50**(2), 57-71, 1971.
Sarrafian S.K. et al. *Clin. Orthop. Rel. Res.*, **126**, 153-159, 1977.
Youm, Y. et al. *J. Bone Joint Surg.*, **60-A**(4), 423-431, 1978.

ACKNOWLEDGMENTS

This project was supported in part by grants from the California State University System Wide Grant Program and the Rehabilitation Services Administration, U.S. Department of Education (H129E00005).

UPPER EXTREMITY

Poster

THE INTERACTION OF MUSCULAR FORCES DURING UNLOADED FINGER MOVEMENT: A FORWARD DYNAMIC MODEL

L. XIAO and R.P. WELLS

DEPARTMENT OF KINESIOLOGY , UNIVERSITY OF WATERLOO
WATERLOO, ON. CANADA N2L 3G1

INTRODUCTION

The finger is considered as a linkage system of intercalated bony systems balanced by muscle and tendon forces and joint constraints. The hand, as a mechanical structure, exhibits a high degree of complexity which has tended to lead to descriptive studied of small functional components, such as the lumbrical. The quantitative literature on the biomechanics of the hand, although relatively more recent, tends to exhibit the same characteristics. Although one needs to analyze and quantitatively describe each component of a complex system, the interaction of the component parts should not be overlooked. By measuring a number of variables, the biomechanist can determined how much of the behaviour is due to the joint configurations, inertial properties and the task constraints and how much of the behaviour is determined by neural control mechanism. Thus, understanding the mechanical nature of the system allow us to better interpret our findings when dealing with neural mechanism. The purpose of this paper is to develop a 3-dimensional forward dynamic model of human index finger to study the behaviour of the normal finger and can be used to examine the complex relationship between the active muscle force and the passive elasticities resident in the hand. Four segments and six muscles, flexor profundus and superficialis, extensor digitorum, lumbricalis, and the palmar and dorsal interossei are presented in the model. The pulley mechanism has been considered by setting the pulley in each interphalangeal joints, and the radius of the pulley is represented by the moment arm of each joint.

REVIEW

Many investigations of the biomechanics of the hand and analytical studies of tendon forces and joint torques in static hand position have been conducted. For example, Chao and An et al. (1988) using biplanar X-ray technique established a three-dimensional normative model of the hand based on the anatomical study of normal hand specimens. It can derive the tendon location and excursions under various functional configurations. But few investigations of dynamic charactistics of human hand have been found. Wells, et al (1984) presented a planar four segment model of index finger to examined the passive elastic force during unloaded finger movement. Buchner, et al. (1988) presented a kinematic and dynamic model of human finger to study finger movement dynamically. They described the so-called "bypass system" to indicate that not only the middle band is able to extend the distal phalanx, but also the lateral band bears a certain amounts of the load in both extension and flexion position of finger. Darling and Cole (1990) addressed that dynamic interaction torques that arise from the motion of adjacent finger segment influence the control of digit movement. They suggested that such torques are compensated by specific muscle activation patterns. Their results indicated that muscle action was necessary both to produce movement and to counterbalance the interaction torque arising because of the segmental linkage. Thus a muscle's contribution to movement production may be motion-dependent and not determinable from the static analysis that currently are used to describe finger muscle function.

APPROACH

The purpose of this paper is to develop a forward dynamic model of the human finger. The many ligamentous connections and constraints are explicitly included in the model. The forward solution approach allows for model validation by loading the tendons of cadaver hands, observing the finger behaviour, and comparing this behaviour to model predictions. A planar four segment model of the index finger was implemented as a deterministic mathematical model on HP UNIX system using ADAMS (Automatic Dynamic Analysis of Mechanical Systems, Mechanical Dynamics, Inc) which is a software package for simulating the force and motion behaviour in three dimensions. The ADAMS system can deal with the problem involved the rigid body and has the ability to simulate pulley mechanisms.

Brand, et al. (1975) proposed a pulley advancement at metacarpophalangeal joint of a finger and indicated that pulley increased the tendon excursion required to flex the joint, and thus, the mechanical advantage of this joint. In our model, we extended Brand's thought to set the pulley in each joints of the index finger for each muscle. Four segment and three joints (DIP, PIP, and MP joints) with up to ten pulleys on five muscles were modelled. The radius of pulleys were derived from the moment arm in Table 2. The system was assumed to be free of friction and the tendon was massless because we are interested in the tendon excursion of hand rather than the kinetic function of them and the tendon mass can be neglected comparing to the segments masses.

Table 1 gives the input phalanx parameter of the model taken from a number of sources. Moment arm and range of motion were taken from paper An, et al (1983), Micks, et al (1981) and Brand (1975). The segment's length was from Weightman and Amis (1982). Mass of segments were taken from Wells' unpublished data.

Table 1. The phalanx parameters of the model, Weightman and Amis (1982).

	mass (kg)	segment length
distal phalanx	0.006	20mm
middle phalanx	0.0075	29mm
proximal phalanx	0.018	46mm

FIG. 1 shows the model of the index finger. The global coordinate system was fixed at the metacarpal segment. Damper was added in each joint to simulate the effect of surrounding tissue and ligaments. Table 2 gives moment arm information for each joint.

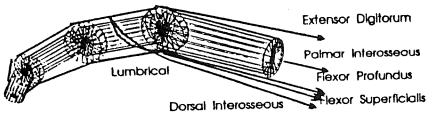

FIG. 1 The model of the index finger.

Table 2. Moment arm and range of motion of the model. Range of motion defined as the angle to create 1 Nm of moment.

	moment arm (mm)		range of motion
MP	FDP	13	-3 - 55 (degree)
	FDS	15	
	EC	12	
	RI	5.5	
	DI	8	
	LU	12	
PIP	FDP	9	17 - 91 (degree)
	FDS	7	
	EC	7	
DIP	FDP	5	5 - 45 (degree)
	EC	5	

RESULT

To simulate the extrinsic muscle contraction, a translation force was applied in each proximal part of muscle. The force function is step input: F(t)=10 N. The data of constraints on joint movement were taken from Brand (1985) and Micks and Reswick (1981). The MP and DIP constraints is given as :

$$m=-(A-A^*)^3*0.0006 Nmm/degree^3$$

and the PIP constrains is given as:

$$m=-(A-A^*)^2*0.0043 Nmm/degree^2$$

Given the force applied to each muscle separately, the final angle of three joints were listed in Table 3. The excursion of three joint angles under FDP force only was shown in FIG. 2.

DISCUSSION AND RECOMMENDATION

Table 3 shows the final equilibrium positions of the fingers under applied 10 N loads together with the positions reached under the same conditions in three cadaver hands (Wells' and Ranney, unpublished data). In general the model behaviour is similar to that described in the literature. However tension on EC produces unnatural PIP joint positions. Thus is likely related to the inadequate representation of the extensor expansion and lateral bands. Further extensions and uses of this model are planned. For example, if the step input force can be replaced by a series of the linear envelope EMG information, then the model can simulate the hand function in a real life manner. Hof, et al (1981,1987) have shown the EMG can be used as an active state input to an appropriate muscle model to estimate muscle force . Further 3-dimensional parameters can be added in this model to make the finger perform adduction-abduction movements. This model can also be developed to predict the grasp force when the hand holding an object. From these points of view, we believe this model is promising one to allow us to understand the complex relationship of fingers during prehension.

Table 3. Final joint angles in degree for 10 N force applied to different muscles. (Positive value represent flexion and negative value represent extension at the joint). Number in brackets represent unpublished cadaver joint angles under the same loads; Range of three hands.

	MP	PIP	DIP
FDP	56 (52-54)	50 (35-72)	55 (7-35)
FDS	63 (70-80)	60 (60-109)	-18 (0)
LUM	57 (70-80)	9 (0-12)	-16 (-5-0)
EC	-25 (-17-12)	-14 (20-40)	-25 (-8-5)
INT	52 (--)	8 (--)	-16 (--)

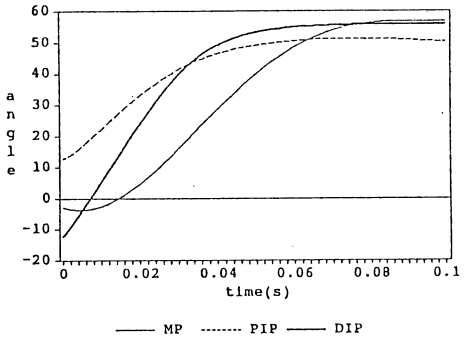

FIG.2 The joints angles under FDP force of 10 N.

REFERENCES

An, K.N. et al. (1983), J.Biomech. Vol. 16(6): 419-425.
Brand, P.W. et al. (1975), J.Bone & Joint Surg. 57-A(6): 779-784.
Brand, P.W. (1975), Clinical Biomech. of the Hand. C.V. Mosby.
Buchner, H.J. et al (1988), J.Biomech. Vol.21(6): 459-468.
Darling, W.G. et al. (1990), J. Neurophysiol. Vol.63(5): 1098-1108.
Micks and Reswick (1981), J. Hand Surg. 6(5): 462-267
Wells, R.P,et al. (1985), Biomech. Current Interdisciplinary Research, Martinus Nijhof Publishers: 743-748.

ACKNOWLEDGEMENTS

The authors would like to acknowledge the support of NSERC and Milad G.Ishac for technical assistance.

Load-Displacement Characteristics of the Scaphoid Ligament Complex In Vivo

J.J. Crisco, S.W. Wolfe, R. Brown
Departmentof Orthopaedics, Yale University School of Medicine, New Haven, CT

Purpose. Assessment of wrist instability in the absence of radiographic carpal malalignment is performed by isolating and manually displacing portions of the carpus. Increased carpal displacement, especially if symptomatic, is presumed to demonstrate ligamentous injury or disruption. The "scaphoid test" is an attempt to dorsally subluxate the scaphoid with a manual load applied at its tubercle (Watson, JBJS 68A:345, 1986). We developed an instrumented load-displacement device to determine if there is a correlation between the subjective assessment of a "scaphoid shift" and the mechanical properties of the scaphoid ligamentous complex.

Methods and Materials. Eleven wrists in six healthy volunteers, with no prior history of wrist injury or disease, were examined and tested. Clinical evaluation consisted of measurement of wrist range of motion, and performance of the scaphoid test by the senior author. The test was graded based on the degree of scaphoid subluxation. A grade of 0 indicated no palpable translation. A 1+ shift indicated generalized midcarpal displacement. A 2+ shift indicated dorsal subluxation of the scaphoid from the scaphoid fossa, with a palpable "clunk" as the force was relieved. For mechanical testing, the supinated forearm and wrist were strapped to the platform of the testing device. A second platform, situated over the wrist, included linear bearings which guided the vertical travel of a plastic tipped plunger. A dorsally directed load was applied to the scaphoid tubercle via the plunger. Load and displacement were simultaneously recorded by a load cell and displacement transducer. The computer audibly alerted the examiner when a maximum load of 40N had been applied. Five cycles are performed, and the data of the fifth cycle analyzed. The displacement at initiation of the fifth cycle was defined as a measure of laxity (mm). The maximum displacement (mm) was the displacement at 40N. The stiffness (N/mm) was the slope of the least squares fit to the load-displacement data.

Results. Laxity increased significantly, from 0.7 mm to 1.8mm (s.d. 0.6mm) in the four patients with a 2+ scaphoid shift ($p<0.02$, ANOVA, Fisher post-hoc). Maximum displacement increased and average stiffness decreased with scaphoid shift. For both measures the difference between grades 0 and 2+ was significant ($p<.02$) [Figures 1&2]. There was no significant correlation between wrist range of motion and scaphoid shift.

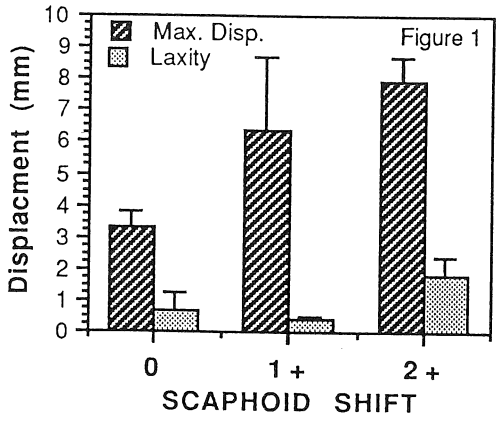

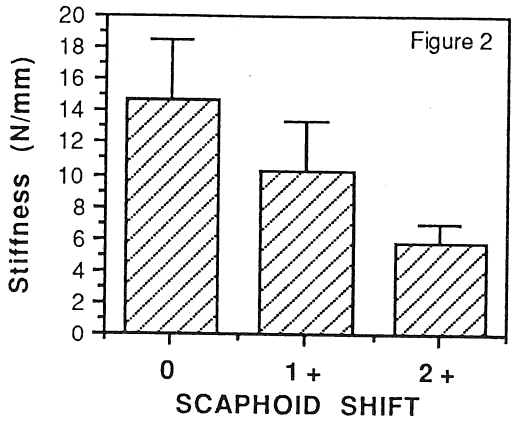

Conclusions. This study demonstrates a high correlation between the subjective clinical scaphoid test and the instrumented mechanical properties of the scaphoid ligamentous complex. Quantitative data is now being generated to describe the mechanical behavior of the normal and injured carpus.

THREE-DIMENSIONAL DYNAMIC ANALYSIS OF JOINT REACTION FORCES AND MOMENTS DURING WHEELCHAIR PROPULSION

M.M. Rodgers, S. Tummarakota*, J. Lieh*, and D.R. Schrag

Dayton Veterans Affairs Medical Center; Institute for Rehabilitation Research & Medicine,
*Department of Mechanical and Materials Engineering, Wright State University, Dayton, OH.

INTRODUCTION

Previous models of wheelchair propulsion have utilized two-dimensional analysis of the arm. The purpose of this study was to develop a three-dimensional (3D) dynamic model of the arm and hand to determine joint reaction forces and moments during wheelchair propulsion. The model incorporates the Newton-Euler method based on body coordinate systems; three rigid segments (hand, forearm, and upper arm) connected by the wrist, elbow and shoulder joints; and a recursive inverse dynamics approach. To test the model, a spinal cord injured male was videotaped during propulsion on a stationary, instrumented wheelchair positioned on a roller. Handrim force was monitored via strain gauges in the wheelchair handrim. Videotaped movements were analyzed using a computerized 3D motion analysis system. Results show that highest joint reaction forces occurred in the tangential direction at the wrist and shoulder joints. The shoulder flexor moment was the highest of the three joint moments. The model appears to provide 3D kinetic information which may help to analyze wheelchair designs and identify potential sites of injury in wheelchair users.

REVIEW AND THEORY

Chronic health problems due to long-term use of manual wheelchairs significantly impair the independence of wheelchair-dependent spinal cord injured individuals. Many of these health problems are musculoskeletal injuries related to the constant repetitive movements which occur with everyday wheelchair propulsion. A better understanding of wheelchair propulsion biomechanics is needed.

The few studies which have included descriptions of wheelchair propulsion biomechanics have analyzed only those movements occurring in one plane, neglecting the 3D aspects of the arm movements such as shoulder abduction [Cooper (1990), Sanderson *et al.* (1985)]. In addition, more recent models considered only the static case, and some utilized only the forearm and upper arm for the analysis [Ting *et al.* (1991), Veeger *et al.* (1991)]. Although these studies have provided important information, there is a need to develop a 3D dynamic model for the investigation of wheelchair propulsion biomechanics. The purpose of this study was to develop a 3D dynamic model for computing joint forces and moments during wheelchair propulsion.

PROCEDURES

The model was developed using the Newton-Euler method based on body coordinate systems. It incorporates three rigid segments (hand, forearm and upper arm) connected by the wrist, elbow and shoulder joints, respectively. The hand is modeled with two degrees of freedom (radial /ulnar deviation and flexion /extension), the forearm with one degree (flexion /extension) and the upper arm with two degrees (abduction /adduction and flexion /extension). The supination /pronation of the forearm and internal /external rotation of the upper arm were neglected. A body coordinate system, shown in Figure 1, is defined for each limb (hand, forearm, and upper arm). For this model, Euler angles with x-y-z rotation sequence (also known as Bryant angles) were adopted [Meirovitch (1970). The relative angular motion of one limb to the next limb is computed from the displacements of corresponding markers that are videotaped. These relative motions are used to obtain the transformation matrices. A symbolic method was adopted to assist in generating the equations of motion for each segment. The model can be used to compute the joint forces and moments based on input from experimental data. Input information includes linear displacements of markers and contact force (obtained from strain gauges) from the hand to the wheelchair handrim. The marker linear displacements are filtered (2nd order Butterworth) and differentiated to obtain velocities and accelerations. Contact force is transformed into hand coordinates and used as input to the hand equation. Computation of joint forces and moments of each limb is based on a recursive inverse dynamics approach.

Experimental data were obtained from a 38 year old male paraplegic (T10-L1 lesion level). Following informed consent procedures, physical characteristics were obtained and a test was performed using a wheelchair instrumented with strain gauges for measuring handrim force [Rodgers *et al.*(1989) which was positioned on rollers to enable stationary propulsion. Movement was videotaped using a three-dimensional motion analysis system (Peak Performance Technologies, Inc., Englewood, CO). Reflective markers were placed on the wheelchair hub, wheel rim, hip, shoulder, elbow, wrist (internal and external), and fifth metacarpophalangeal joint. These eight marker locations were computer digitized from videotape to provide 3D displacement data. Handrim force was monitored via computer.

RESULTS AND DISCUSSION

Example data are shown in Figure 2. Results show that highest joint reaction forces occurred in the tangential direction at the wrist (125 N) and shoulder (135 N) joints . Both the tangential and normal joint reaction forces at the wrist joint were very similar in pattern and magnitude to the handrim contact force. Tangential forces at the shoulder decreased at the middle of the contact phase. The shoulder flexor moment was the highest (70 N-m) of the joint moments.

The model appears to provide 3D kinetic data which may help to identify potential sites of injury. The findings suggest the wrist and shoulder joints in the test subject may be more susceptible to chronic injury related to the constant repetitive movements which occur with everyday wheelchair propulsion (e.g., overuse injuries). The use of these biomechanical techniques may provide a better understanding of those factors which relate to wheelchair user injuries so that they may be alleviated.

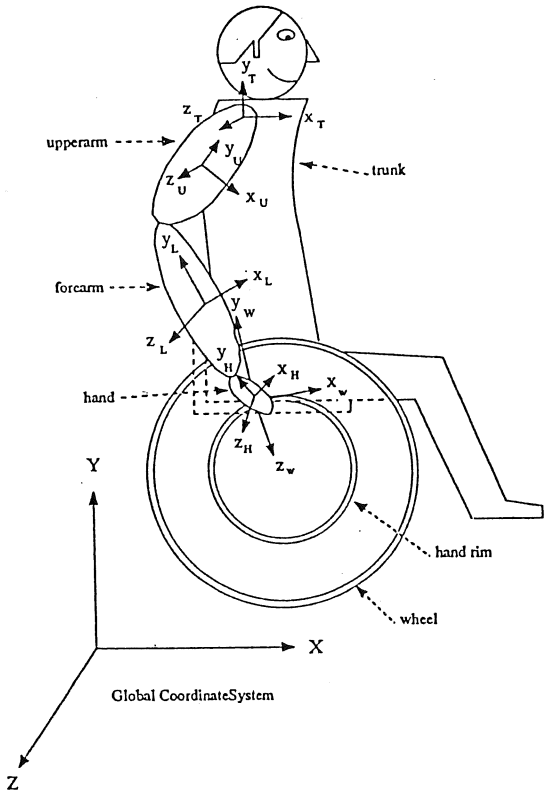

Figure 1. Coordinate systems of the wheelchair model.

REFERENCES

(1) Cooper R. *Adapt. Phys. Act. Quart.* 7:74-85, 1990.
(2) Sanderson, D.J. et al. *J Biom.*, 18:423-429, 1985.
(3) Ting, Y. et al. *Advances in Bioengineering*, 20:517-520, 1991.
(4) Veeger H. et al. *Proceedings, Human Propulsion Conference*, 1991.
(5) Meirovitch L. Methods of Analytical Dynamics, Prentice-Hall, 1970.
(6) Rodgers, M. et al. *Med. Sci. Sports Ex.* 21, 1989, S107.

ACKNOWLEDGEMENTS

Funding for this research was provided by the Research and Development Service of the U.S. Department of Veterans Affairs (#B90-87AP).

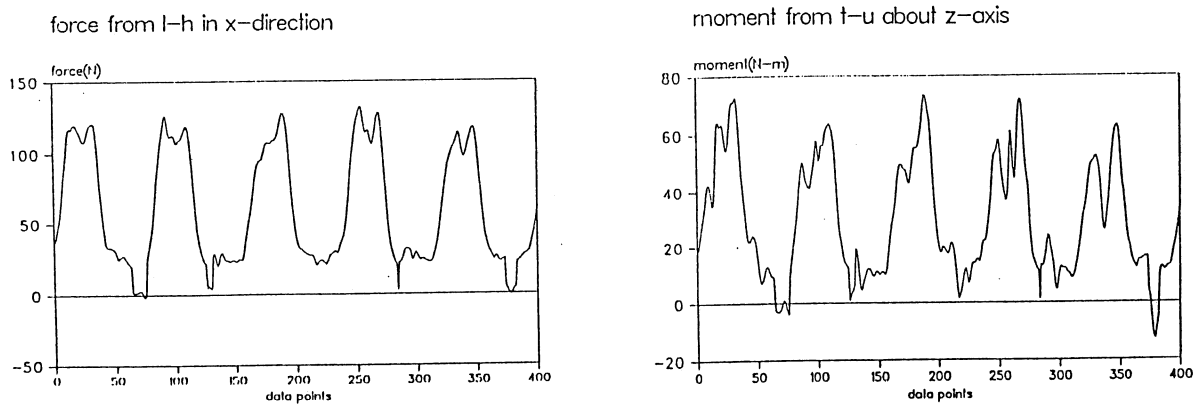

Figure 2. Example showing wrist joint reaction force (left) and shoulder joint moment data (right).

SHOULDER JOINT FORCES AND TORQUES IN WHEELCHAIR PROPULSION

G. Gehlsen, and R. Bahamonde

Director Biomechanics Laboratory, Ball State University
Assistant Professor of Biomechanics, Ball State University

INTRODUCTION

The handrim pushing action involved in propelling a wheelchair has been related to a high incidence of chronic shoulder and arm injuries, and is by far the least economical mode of transportation. Elderly individuals who depend on manual wheelchairs are required to use the relatively small upper body musculature for wheelchair locomotion. This places them at an immediate disadvantage because of the limited maximal oxygen uptake and power output capability for arm movement. Efficiency may be further reduced because of neuromuscular disorder as well as diminished muscular and cardiopulmonary fitness resulting from wheelchair confinement and sedentary lifestyle. Additionally, arm exercise appears to be inherently inefficient and stressful to the shoulder joint, cardiovascular system and pulmonary system. We hypothesized that simple adjustment to back of the chair and/or the seat of the chair could provide increase efficiency. Therefore, the purpose of this study was to determine shoulder joint forces and torques differences among variation in handrim size, seat height, and seat back distance.

REVIEW AND THEORY

Van Der Woulde et al (1988) found that the maximum level of wheelchair propulsion gross mechanical efficiency is 50 percent below the values for leg work. According to Glaser et al. (1980) the lack of wheelchair propulsion efficiency may be due to inefficient biomechanics and the relatively small upper body musculature. Glaser et al. (1980) also stated that the diameter of the handrim with respect to the diameter of the wheel can influence the efficiency of wheelchair locomotion because of alteration in muscle force-velocity relationships. Large diameter handrims provide for a low drive ratio because of the long lever length. Such high mechanical advantage handrims require less force to turn, but the stroking velocity must be higher for given wheelchair velocity. Conversely, smaller diameter handrims require more force to turn, but stroking velocity is lower for given wheelchair velocities.

A significant positive relationship between hand-handrim position and peak velocity was reported (Sanderson and Sommer, 1985). This relationship would tend to support the hypotheses that a forward lean of the trunk or a forward axis position of the trunk would allow an individual to apply maximum force further around the handrim, and thereby enhance force application. If a force is applied before or at the top of the handrim as reported by Van Der Woulde et al. (1988) and Sanderson and Sommer (1985), the trunk and chair receive a reaction force in the opposite direction (horizontal negative), which effectively reduces ground reaction forces. Sanderson and Sommer (1985) stated that the backward reaction force applied to the chair could be effectively reduced by increased forward lean and abdominal muscular strength. Van Der Woulde et al. (1988b), stated that a change in handrim diameter led to a change in the shoulder-to-rim distance. This according to Van Der Woulde et al. had an influence on the movement pattern and muscle mechanics in terms of length-force and force-velocity characteristics.

METHODOLOGY

Retired University faculty and staff members (10 males and 10 females) were recruited for participation in this study. The average age of the subjects was 67 yrs. None of the subjects had significant experience with wheelchair propulsion prior to the study. None of the subjects had any upper extremity injuries that currently interfered with daily functioning. A standard wheelchair (modified according to experimental requirements) was mounted on a roller. The roller was equipped with a tach-generator attached to the roller core and interfaced to a computer via an eight bit A/D converter (sampling rate 200 Hz). The front axis of the wheelchair was attached to a rigid frame.

The wheelchair was Modified for the study by adding crossbars to the frame and to permit changing of the seta position. Three rim sizes were used in the study: the normal (55 cm diameter, a medium sized (44 cm diameter) and a small sized (33 cm diameter) rim. Five seat heights were available, and were created by attaching wooden platforms of different height to the wheelchair frame. The available heights were 6 cm below standard height, standard height, and 2, 6, and 12 cm above standard height. Nine seat position were available 20, 15, and 5 cm anterior to the standard position, the standard position and 4, 10, 15, and 20 cm posterior to the standard position.

Two stationary Panasonic digital 500 shuttered video cameras were used to record the sagittal and frontal plane movements of the subjects . The recording rate was 30 HZ. A Zenith computer with a BCE Associated video controller circuit board was interfaced to the video playback system. A computer program designed by Peak Performance Technologies, Inc. was used to encode sequentially every frame of the tape with number on the audio track. When a frame was played back on the video playback system, the computer was able to detect which frame number was played: thus the time between any two given frames was determined with an accuracy of 1/60 of a second. Synchronization of film and computer data was accomplished by placing a light in the background of the filming area and interfaced to the computer. Each subject completed 15 trials of three to five pushes for each trial. The order of the trials was randomized to prevent fatigue effects.

The minimum torque needed to rotate the roller under different loads and rpm's was computed by a DC motor attached to the shaft of the roller. The amount of power produced by the motor is a function of the voltage generated times the current. Both of these parameters were measured under different loads and different rpm. The power generated by the motor was then converted to torque values. In order to compute the torque for any type of rpm, a logarithmic regression was fitted to the slopes of the Load vs Torque graphs. The load exerted on the roller was computed by first computing the location of the center of gravity of the subject relative to the wheelchair back wheel axis. Once the center of gravity position was determined the sum of the torques about the front support of the wheelchair was taken which enabled the determination of the load on the roller. The load exerted on the roller was determined for every instant of time analyzed, and was used to compute the torque needed to rotated the roller at a given angular velocity. The sum of the torques exerted on the roller was composed of two torques (frictional torque, and subject torque). The sum of the torques was calculated by taking the derivative of the angular momentum of the roller. It was assumed that the force exerted on the rim was tangential to the rim and that the subjects exerted a force throughout the pushing phase. The inverse dynamics approach as reported

by Andrews (1978) was used to calculate the joint forces and torques of the left arm. The left pushing arm was modeled as three-link kinetic chain made by the hand, forearm and the upper arm. The mass of the segments, as percentage of the total body mass and the location of the center of gravity of each segment were taken from Dempster's (1955) cadaver data. Moment of inertia values for the body segments were taken from Whitsett (1963) and personalized for each subject according to the procedure described by Dapena (1978).

The hand segment was assumed to be subjected to three forces and a proximal torque: the segment weight, a distal force exerted by the wheelchair rim and a force exerted by the forearm at the proximal joint (wrist). The forearm and upper arm segments were subjected to the force of their own weight acting at the center of gravity, plus a torque and force at the proximal and distal ends of the segments. The values for the joint torques and forces were first calculated in terms of an inertial reference frame attached to the ground, and later transformed to anatomically relevant reference frames attached to the joints of the left arm. At the shoulder, the X axis represent the internal/external rotation torques, the Y axis the flexion/extension torques, and the Z axis the abduction/adduction torques. At the elbow joint the X axis defined the pronation/supination torques, the Y axis the flexion/extension torques and the Z axis the varus/valgus torques.

RESULTS

The position of the mass center (center of gravity) relative to the wheelchair axis was determined. ANOVA indicated mass center significant differences ($p < .01$) between treatments for both seat height and seat back positions. There were no significant treatment effects between handrim variations.

Significant torque values were indicated. All handrim treatment mean values were found to be significantly ($p < .001$) different. ANOVA procedures indicated significant differences between shoulder joint internal rotation peak torque mean values. The torque patterns exhibited were very similar among the subjects. The main propulsion torque was shoulder joint flexion torque. The peak value for this torque occurred at the beginning of the propulsive phase, then decreased steadily until the end of the propulsive phase. In general, the subjects demonstrated a fairly constant abduction torque (Tz) throughout the propulsion phase. There was a small external rotation torque (Tx) present, usually having a larger value at the beginning of the propulsion phase and decreasing toward the end of propulsion.

As expected the handrim size produced changes in the shoulder joint torques values. There was a small increase in the torque values especially the abduction torque when the subjects used the medium size handrim. When the subjects used the small handrim there was a significant increase in all the torque values. With the smaller handrim the subjects exerted larger muscular torques in order to overcome the frictional torque of the roller and to accelerate the wheelchair.

No significant difference was indicated among seat height variation for the flexion and abduction peak torques values. However, there was a statistically significant difference between the - 6 external rotation peak torque mean value and all other seat height variations mean values.

No significant differences were indicated among the seat back independent variables. There was a great deal of variability in the magnitudes of the flexion torque patterns which may account for the lack of significant findings.

DISCUSSION

The results of the study indicated that the torques used in wheelchair propulsion are shoulder joint flexion (Ty), shoulder joint external rotation (Tx) and shoulder joint abduction (Tz). The main propulsive torque identified in this study was the shoulder joint flexion torque. This flexion torque was probably produced by the shoulder joint flexion musculature (pectoralis major and anterior deltoid). Brubaker's et al. (1981) EMG study confirms our findings. Brubaker et al. stated that the anterior deltoid exhibited distinct activity during the initial portion of the torque phase. The pectoralis major was most active during the entire torque phase. The shoulder joint flexion musculature appeared to be responsible for overcoming the frictional forces between the roller and the chair, and for producing the needed chair acceleration. In all subjects, the upper arm was maintained in an abducted position throughout the propulsive phase. The constant abduction torque present in all of the subjects may have been needed to stabilize the shoulder, and/or to prevent the upper arm hitting the wheelchair arm rests.

At the start of the propulsion phase the upper arm was in an internally rotated position followed by an external rotation movement. The external rotation torque (Tx) was presumably produced by external rotator muscles of the shoulder joint. The rim exerted a backward force on the hand, this force may have internally rotate the upper arm. In some subjects there was an increase in the external rotation torque which seemed to indicate that this torque may also be used to propel the wheelchair. Brubaker et al. (1981) states that a strong action of the infraspinatus muscle is needed to counter the internal rotation effect of the pectoralis major. The results of this study can support this internal rotation effect.

The results of this study clearly indicate that the larger rim size allowed the subjects to produce a greater amount of linear velocity with the minimum amount of toque. However, the statistical data for seat height and seat back indicated only a significant difference in external rotation peak torque mean values. The seat back and seat height variation data presented here may be due to adjustments made by the subjects in the elbow angle which allowed similar torque patterns. It is clear, however, that the load placed on the rollers was directly related to the magnitude of the torques produced. The subjects with larger masses had to exert larger muscular torques in order to overcome the frictional forces between the wheels and the rollers. The results of this study tend to support the position adjustment of a slightly higher (+2 cm) and a slightly forward seat back position. The forward seat back position may reduce the vertical force and thereby reduce frictional forces. In addition, the results of this study tend to suggest that an elevated position may allow a more comfortable shoulder joint position.

REFERENCES

Andrews, J.G. (1978). Biomechanical Analysis of Human Motion. Kinesiology IV. Washington, DC.:AAHPER.

Brubaker, C.E.,McLaurin,C.A., Gibson,J.D. & Soos T. (1981). Seat position and wheelchair performance. Wheelchair Mobility: A Summary of Activities at UVA REC During The period 1976-1981. University of Virginia, 12-21.

Dapena JA. (1978). A method to determine the angular momentum of a human body about three orthogonal axis passing through its center of gravity. Journal of Biomechanics, 17 (8) 533-59.

Dempster, W.T. (1955). Space requirements of the seated operator. WADC Technical report 55-159,Dayton OH: Wright Patterson Air Force Base.

Glaser, R.M.,Sawaka,M.N., Young, R.E., Suryaprasad, A.G.(1980). Applied physiology for wheelchair design. Journal of applied Physiology, Respiration, Exercise Physiology,48,41-44.

Sanderson, D.J.,& Sommer H.J. (1985). Kinematic features of wheelchair propulsion. Journal of Biomechanics, 16,423-429.

Van Der Woude, L.H.V.,Veeger, H.E., Rozendal, R.H., Van Ingen Schenau,G.J.,Rooth,F. & Van Nierop,P. (1988). Wheelchair racing:effects of rim diameter and speed on physiology and technique. Medicine and Science in Sports and Exercise, 20 (8), 492-500.

SPINE

Podium Session 19

MECHANICAL PROPERTIES OF MAMMALIAN INTERVERTEBRAL JOINTS

Julianna M. Gal,

Human Performance Laboratory, University of Calgary, Calgary, Alberta, Canada. T2N 1N4.

INTRODUCTION

The quantitative mechanical information required to understand the functional morphology of the mammalian spinal column is lacking. Therefore, dynamic sagittal bending moments were applied to lumbar intervertebral joints of monkeys, wallabies, jaguar, tigers and seal. Observed changes in intervertebral angle were modelled as negative exponential functions of specific bending moment. Model parameters reflected angular bending capacities and relative stiffness of the joints. Monkey and wallaby joints had greater flexion stiffnesses and greater flexion capacities than homologous tiger and jaguar joints. Seal joints were the most compliant in extension and flexion. Lesion experiments showed that ligamenta flava, and the intervertebral discs, were the most resistive structures for flexing monkey and wallaby, and jaguar and tiger joints respectively. Seal joint compliance is thought to be an adaptation to terrestrial locomotion. The enhancement of elastin- or collagen-containing intervertebral structures appears to be a size-related phenomenon, rather than one of posture, locomotor mode or taxonomy.

REVIEW AND THEORY

Due to the often puzzling nature of back pain, considerable research effort continues to be focused upon the mechanical behaviour of human intervertebral joints (White and Panjabi, 1990). Despite the wide variety of intervertebral size, morphology and mobility observed in other mammals, research efforts have been primarily anatomical (Slijper, 1946; Halpert et al, 1987). Smeathers (1981) conducted Euler buckling experiments with whole rabbit and goat lumbar spines, and further tensile and compressive tests with their intervertebral components. He was able to correlate their torsional and lateral bending stiffnesses to differences in vertebral bony morphology. Here, dynamic three-point sagittal bending and lesion experiments were performed with intervertebral joints from a variety of taxonomically-unrelated species of different sizes. Particular attention was paid to the roles of soft structural tissues in effecting joint resistances.

PROCEDURES

The lumbosacral column was dissected from monkeys, wallabies, tigers, a jaguar and a seal. Superficial axial musculature was removed. The columns were cut into specimens containing two complete intervertebral joints. A specimen was attached to the loadcell as shown in Fig.1a. It was forcibly bent by the action of the actuator and the three contact points. The load cell measured the bending resistance of the two joints. Sagittal x-rays were taken of the bent specimens at different stages in the loading cycle (see Fig.1b). Changes in intervertebral angle ($\Delta\theta_{iv}$) and applied specific bending moment (M/mass) were measured for each joint of each specimen, and modelled: $\Delta\theta_{iv}=A(1-e^{-B(M/mass)})$. Homologous joint flexion parameters were compared. Next, superspinous ligaments, interspinous muscles and ligaments, articular capsules and ligamenta flava were sequentially lesioned. The bending cycles were repeated and reductions in peak flexion forces were recorded. Mechanical and mathematical differences were correlated to differences in intervertebral joint anatomy.

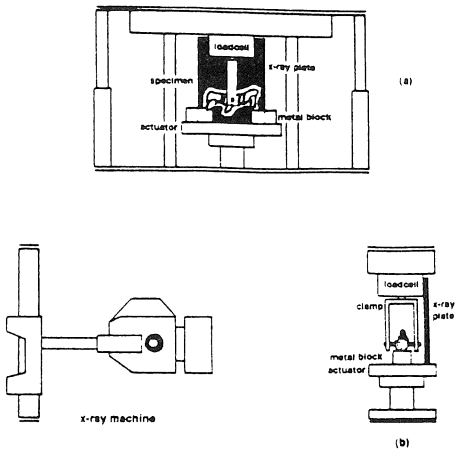

Fig.1 The experimental setup is shown from front (a) and side (b) views.

RESULTS

The negative exponential functions for flexing upper lumbar joints of seal, tiger/jaguar, wallaby and monkey are shown in Fig.2. The differences illustrated here were consistent for all homologous comparisons. Seal joints were the most compliant; monkey joints were the most stiff. Monkey and wallaby joints had greater flexion capacities than tiger/jaguar or seal joints. The results of lesioning the articular capsules and ligamenta flava are shown in Fig.3, for monkey and tiger joints in flexion. Complete inactivation of ligamenta flava and the articular capsules caused an almost total reduction in the peak flexion forces afforded by the monkey (and wallaby) joints. Little change was observed following lesion of homologous structures in the tiger (and jaguar) joints. Figure 4 depicts the deep intervertebral joint anatomy for monkey, wallaby, jaguar and seal. The monkey and wallaby joints have relatively prominent ligamenta flava. These contrast to the robust intervertebral discs of the jaguar (and tiger) joints. Seal joints were conspicuous for their almost total lack of soft structural tissue.

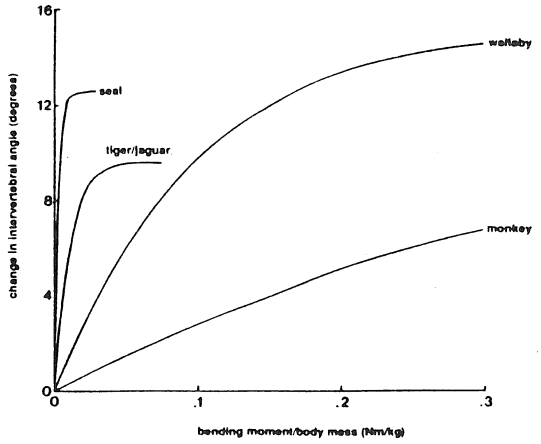

Fig.2. The functions are shown for the flexing joints.

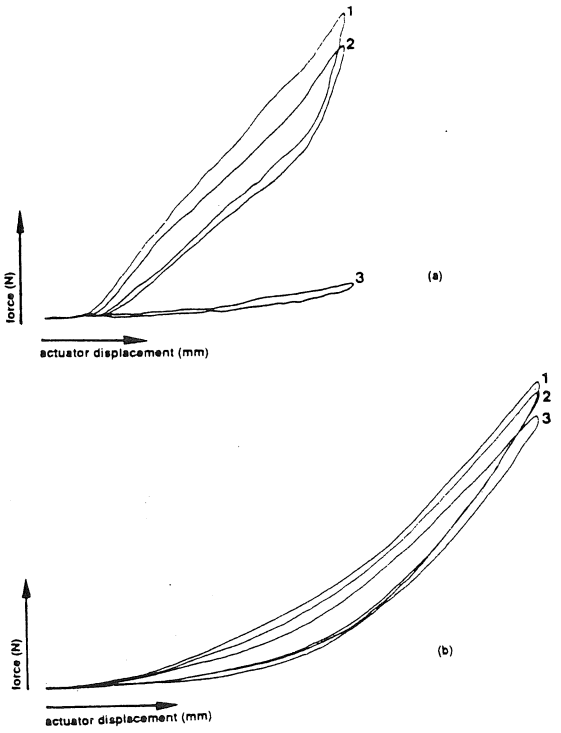

Fig.3. The results of lesioning the articular capsules and ligamenta flava are shown for monkey (a) and tiger (b) joints in flexion.

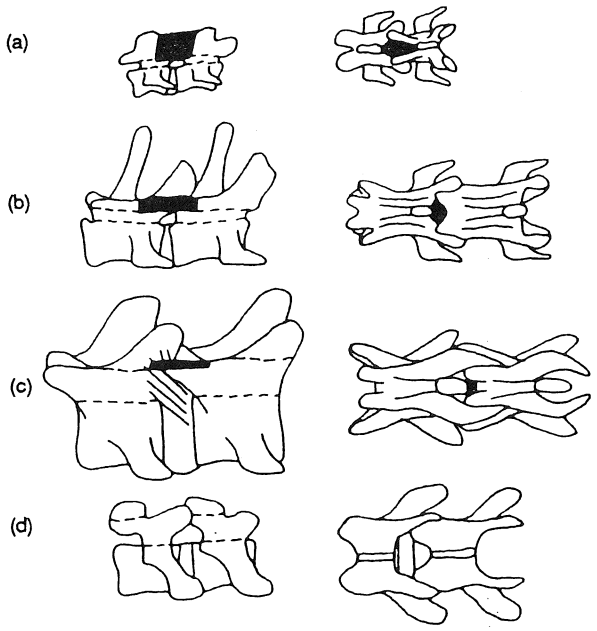

Fig.4. Joint anatomy is illustrated in sagittal and dorsal views for monkey, wallaby, jaguar and seal (a, b, c, and d respectively). Ligamenta flava are black.

DISCUSSION

True seals, like those individuals studied here, swim by lateral sweeps of their hindlimbs. Here, sagittal hypermobility may augment drag. True seals are clumsy on land. They progress by alternate periods of pelvic and pectoral girdle support. This would require considerable sagittal mobility. The marked sagittal compliance of the true seal lumbar column may be an adaptation to terrestrial locomotion for these effectively limbless mammals.

Two distinct mechanisms for resisting flexion moments have been demonstrated for terrestrial mammals. Like monkey and wallaby joints, rabbit intervertebral joints resist flexion moments primarily by tension in ligamenta flava (Smeathers, 1981). The tiger and jaguar joints, and goat and human lumbar joints (Smeathers, 1981; White and Panjabi, 1990, respectively) resist flexion moments by intervertebral disc properties. Clearly, similar mechanisms exist despite gross differences in taxonomy, posture and locomotor mode.

Ligamenta flava are elastin-containing structures. Intervertebral disc annuli consist primarily of collagen. Collagen is relatively stiffer than elastin in tension, but is much less extensible. It is suggested that as mammal size increases, collagenous intervertebral structures are enhanced to assume the supportive roles, because collagen has greater relative stiffness and strength than elastin. For smaller animals, joint mobility and support can be accomplished by the relatively robust ligamenta flava. However, since structural proteins are metabolically costly to synthesize and maintain, there may be shift in emphasis to the collagen-containing discs in order to minimize the amount of structural materials used. The problem of constructing a bendable collagenous intervertebral joint is solved by allowing the collagen fibres to be loaded initially in shear. This is consistent with the low stiffness measurements for the jaguar and tiger joints of this study. This scaling argument can be tested by conducting bending experiments with specimens from a taxonomically consistent group which varies considerably in size; ie. the cat family. It is a hypothesis that warrants further consideration.

REFERENCES

Halpert, A.P. et al. *J. Zool., Lond.*, **211**, 239-258, 1987.
Slijper, E.J. *Verh. Kon. Nederl. Akad. Wetensch. Amst. II*, **42:5**, 1-128, 1946.
Smeathers, J.E. A Mechanical Analysis of the Mammalian Lumbar Spine, Ph.D. Thesis, University of Reading, 1981.
White, A.A. and Panjabi, M.M. Clinical Biomechanics of the Spine. J.B. Lippincott Co. 1990.

ACKNOWLEDGEMENTS

This work represents part of the author's doctoral research. It was conducted at the University of Leeds, under the supervision of Prof R.McNeill Alexander. Dr Caroline Pond provided assistance in obtaining the animals. The author was funded by an NSERC PGS4 scholarship, and ORS and Tetley-Lupton awards.

Proceedings of NACOB II, The Second North American Congress on Biomechanics, Chicago, August 24th - 28th, 1992

HOW HUMAN VERTEBRAL BONE BREAKS

D.P. Fyhrie and M.B. Schaffler

Breech Research Laboratory, Bone and Joint Center
Henry Ford Hospital, Detroit MI 48202

INTRODUCTION: It has long been believed that cancellous bone is an optimally designed structure. This belief is based upon the discovery of the many features of its structure that make it beautifully suited for its role. Some of these are well known, such as the ability to adapt its mechanical properties to changed usage, to repair itself when broken, provide a protected space for the production of blood cells and to provide shape and flexible support to the articular surfaces of major joints. We have determined that, in addition to these well known properties, that the failure properties of vertebral cancellous bone also appear to be optimally designed. In the current study, we examined the microstructural bases of failure in trabecular bone after large strain loading and found that the material appears remarkably well designed to allow selected microstructural failures and simultaneously to maintain overall structural intergrity.

METHODS: Eight millimeter cubes of vertebral cancellous bone were cut from T12 and L1 human vertebrae obtained during routine autopsy. The specimens were cut so that the vertical axis coincided with the anatomical (infero-superior) axis of the vertebra. The specimens were frozen at -20C until mechanical testing. Using an INSTRON 8500 hydraulic testing system, the specimens were compressed in the infero-superior direction to 15% strain at either 15%/sec or 1%/sec. After loading the specimens were cut into two portions, one for low power examination of structural damage without sectioning using a stereo-microscope and the other for histological examination of microcracks. Specimens for histological evaluation were stained *en bloc* in basic fuchsin, which differentially stains microdamage in bone (Frost, 1960; Burr and Stafford, 1991); specimens were then embedded in plastic resin and 100 μm sections prepared. To date 8 of 100+ specimens have been loaded and analysed, with highly consistent results for each.

RESULTS: Low power examination of the damaged tissues showed several characteristic patterns of trabecular damage. Inspection of unsectioned vertical trabeculae virtually never revealed any damage. Transverse trabeculae, on the other hand, commonly showed marked damage in one of three patterns: 1) avulsed at the 'base' from connection to the vertical trabecula, 2) split (delaminated) along the axis of the transverse elements, or 3) broken in the middle. These types of damage are shown in Fig. 1. Despite the lack of externally visible damage in unsectioned vertical trabeculae, internally these elements commonly showed a cross-hatched pattern of cracks similar to that found in cortical bone damaged by compressive loads (Chamay 1970). Transverse trabeculae, on the other hand, commonly exhibited cracks parallel to the axis of the trabeculae, usually deep to the surface. All of these patterns of damage were exhibited in the specimens for both loading rates.

After compression to 15% strain, all of the tested cubes rebounded to 95% of their initial heights when unloaded (Fig. 2). This rebound is characteristic of a material that has retained structural integrity despite a reduction in stiffness due to damage.

DISCUSSION: The characteristic damage patterns of the vertical and transverse trabeculae clearly contribute to the ability of the bone to recover its initial height after compression to 15% strain. We hypothesize that both the ability to regain its height and the characteristic loss of stiffness of vertebral cancellous bone are due to the transverse elements breaking prior to the failure of the vertical elements.

The structure of vertebral bone is composed of relatively long vertical elements interconnected by shorter transverse elements. The transmission of stress through the tissue is by compression in the vertical elements, but by bending in the transverse elements. What is significant is that the vertical elements are typically less than 8 mm long. Therefore, in a compression test (or *in vivo*) the loads applied to the bone are not transmitted directly from one surface to another through compression of

continuous, single elements. The critical portion of the structure in terms of failure analysis are the transverse trabeculae. These elements transfer the load from one vertical trabecula to another. It is these elements which are the first to fail, and which, therefore, limit the maximum loading that the vertical elements must sustain, protecting them from fracture. This mechanism of shear release of dangerous levels of loading allows the structure to retain its structural integrity sufficiently to allow the rebound of the vertical trabeculae to nearly their initial positions.

An interesting observation is that the mechanisms of failure of the transverse trabeculae are similar to those of the branches of a tree broken down by too large a loading of snow. If the snow load on a tree branch becomes sufficiently large, the branch will avulse from the trunk or, more typically, green-stick fracture (delaminate) and bend down. In both mechanisms of failure, the tree trunk is protected from overload by the failure of the branch. Since the trunk is not broken, the tree can survive and grow new or heal delaminated branches. This protective mechanism of the "trunk" is also active in living human vertebral cancellous bone and we hypothesise that it is the primary structural mechanism protecting the tissue from catastrophic failure.

In summary, when very large (15%) strains are applied to vertebral bone specimens *in vitro* very few vertical trabeculae are broken. Virtually all of the broken trabeculae seen without sectioning are confined to the trabecular elements transverse to the direction of the applied load. More detailed microscopic examination of the trabeculae using differential staining for microdamage and thin sectioning shows that these transverse trabeculae are subject to damage by *delamination* and that the vertical elements are subject to *compression* damage. As a consequence of this unequal partitioning of structural damage between the vertical and transverse trabeculae, the structural integrity of the bone is not greatly compromised even though the apparent stiffness of the structure is reduced markedly by the damage. This retention of structural integrity has profound implications regarding the ability of damaged cancellous bone to regain much of its initial shape after damage and then to *heal* and regain complete mechanical and structural function.

REFERENCES:

Burr DB, Stafford T (1991): Validation of the bulk-staining technique to separate artifactual from in vivo fatigue microdamage, J Biomechanics, 18:189-200, 1985.

Chamay A (1970): Mechanical and morphological aspects of experimental overload and fatigue in bone. J Biomech, 3, 263-270, 1970.

Frost HM (1960): Presence of microscopic cracks in vivo in bone, Henry Ford Med Bulletin, 8:27-35, 1960.

Acknowledgments: The Whitaker Foundation and NIH AR40776.

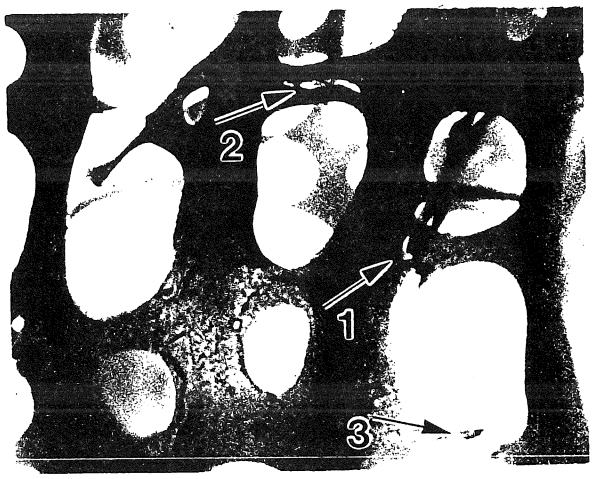

Fig. 1: Damage in transverse trabeculae.

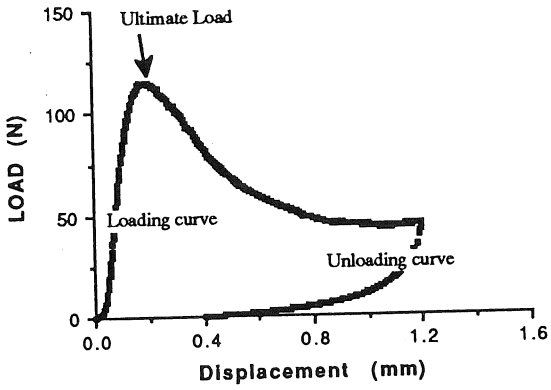

Fig. 2: Load-Displacement of bone specimen.

A MODEL TO STUDY DISC DEGENERATIVE PROCESS IN A MOTION SEGMENT

R.N.Natarajan, J.H.Ke, G.B.J.Andersson
Department of Orthopedic Surgery
Rush-Presbyterian St.Luke's Medical Center, Chicago

INTRODUCTION

The intervertebral disc is susceptible to ruptures and degenerative processes. Autopsy studies have shown that the formation of annular tears, dehydration of the nucleus pulposus and fissure formation in the cartilage end plate are the main early macroscopic features which characterize disc degeneration. Annular tears are classified into three types: radiating tears, circumferential tears and discrete peripheral tears. Radial tears and circumferential clefts occur in the areas of postero-lateral sector of the disc. In addition to fissures in the endplate, advanced age related changes in the disc often are associated with substantial structural disorganization producing endplates of varying irregularities, with reduced disc nutrition. The effect of these degenerative process on the disc mechanical performance is difficult to study by experimental techniques. The aim of the present study was to model the development of annular tears and endplate fractures and thus study propagation of these degenerative processes in a motion segment (MS).

METHOD

A 3D finite element model of a normal human lumbar spinal MS was used to study the failure initiation mechanism and damage accumulation. The model was developed from a serial CAT scan based on an L3-L4 disc body unit of a 41 years old woman. The failure was assumed to occur either in the annulus or in the endplate which were modelled as composite materials. The cancellous bone (Modulus E= 100 MPa) and cortical bone (Modulus E= 12 GPa) were assumed as isotropic. The annulus fibrosus consisted of 10 layers of fibrous materials with fibers inclined alternatively at both +29 and -29 degrees in a ground matrix. The orthotropic modulus property of the fibrous material along fiber direction varied from 66.23 MPa at the outermost layer of the annulus to 25.9 MPa at the innermost layer. The corresponding variation of modulus along a direction normal to the fibers was 4.94 MPa to 4.83 MPa. The endplate was assumed to posses a single layer having isotropic material property (Modulus E= 24 MPa). A finite element using a "thickness concept" (Panda 1980) was used to model several layers of fiber within one element. The nucleus was modelled by inviscid incompressible fluid elements (Bulk Modulus = 2.21 GPa).

An iterative method of solution was used to study the progression of the degeneration of the motion segment. It consisted of the following steps: Damage zone was identified by breakage of a fiber, failure of the matrix or fracture of the endplate. To locate the initial failure mode in a motion segment and the corresponding failure load, a finite element analysis was conducted on the entire segment under a unit applied compressive load. By analyzing the consequent stresses in the annulus along fiber and matrix directions as well as the maximum principal stress in the endplate and comparing it with their respective failure strength (Rolander et al., 1975 and Shirazi-Adl, 1989), it was possible to define "damage ratios" for each element. The maximum elemental damage ratio identified the location of initial damage as well as the corresponding failure initiation load. A second finite element analysis was conducted using the failure initiation load with modified elemental stiffness which took into account the initial failure. Elemental damage ratios were once again calculated and checked for enlargement of the damage zone. If the damage zone was enlarged, the applied load was kept constant and the analysis was repeated including the new zones of failure. Otherwise, the applied load was increased by a ratio of maximum elemental damage ratio and the analysis was continued. The analysis was terminated once the applied load reached a given value.

It is known that disc degeneration significantly alters the mechanical properties of the spinal unit. To include the degenerative process of the annulus and nucleus, at each iterative step, the elastic modulus values of un-damaged elements were modified by a factor which was assumed directly proportional to a ratio of current volume of intact motion segment to the total volume of the motion segment.

RESULTS

The accuracy of the finite element model was tested by subjecting the motion segment model to a compressive load of 400 Newtons. The finite element model predicted an axial compression of 0.5 mm which agreed very well with the published experimental results (Berkson et al. 1979). For the same applied compressive load and with an initial intradiscal pressure of 0.1 MPa, the model predicted an intradiscal pressure of 0.612 MPa. This value of the intradiscal pressure was very much within the range experimentally measured by Andersson et al. (1979) and Nachemson (1960). The bulge of the disc at it's mid-height varied from 0.12 mm at the anterior side to 0.213 mm on the posterior side in the model for an applied compressive load of 400 Newtons. These values, once again compared well with those experimentally measured by Berkson et al. (1979).

From the analysis of an intact motion segment it was found that the failure started first at the inferior endplate when the motion segment was subjected to a compressive stress of 3.9 MPa on the superior surface of the motion segment. The location of this initial failure of the endplate occurred at the junction of endplate and the annulus in the posterio-lateral quadrants. As the compressive load was increased, more and more of the endplate failed and the progression of this failure mode is shown in figure 1. As the applied load reached a value of 6.6 MPa, failure was initiated in the annulus as well. This failure started at a location near the inner surface of the annulus at a mid-cross-section of the disc in the same quadrants where the endplate failure had occurred already. With further increase in compressive load, failure progressed both in the endplate and in the annulus as shown in figure 1. All the endplate fissures and annulus failures were in the posterio-lateral quadrants of the inferior endplate.

DISCUSSION

The analyses showed that the failure in the motion segment starts at the endplate and not in the annulus. This conclusion is in agreement with those reported by Brickmann et al. (1988). Due to the compressive load, the nucleus intradiscal pressure increases which in turn produces bulging of the endplate. This deformation of the endplate produces high bending stresses in the endplate at the points where it is supported by the annulus. Thus the fracture of the endplate occurred at the junction of annulus and the endplate. The analyses also showed that the compressive load required to initiate failure in the annulus was about twice the magnitude that was required to start fracture in the endplate indicating that annular injuries may not be produced by this loading mode. The progression of the endplate fracture was found to accelerate with increasing load. These types of injuries therefore can be expected to more rapidly lead to mechanical fracture of the disc as a composite.

REFERENCES

Andersson GBJ et al., J Biomech., 12:453-458, 1979; Berkson MH et al., J Biomech Engg., 101:53-57, 1979

Brickmann P et al., Clinical Biomech.,Supp 1, 1988; Nachemson A, Acta Orthop Scand (Supp) 43:1-104, 1960

Panda S et al., Int. J Num Methods in Engg, 14:69, 1980; Rolander SD et al., Orthop Clin North Am 6:75-81, 1975; Shirazi-Adl, Spine 14:96-103, 1989

ACKNOWLEDGEMENTS

Bristol Meyers Excellence Award, NCSA Grant CUS910001N, UCR Grant ORA 91091523

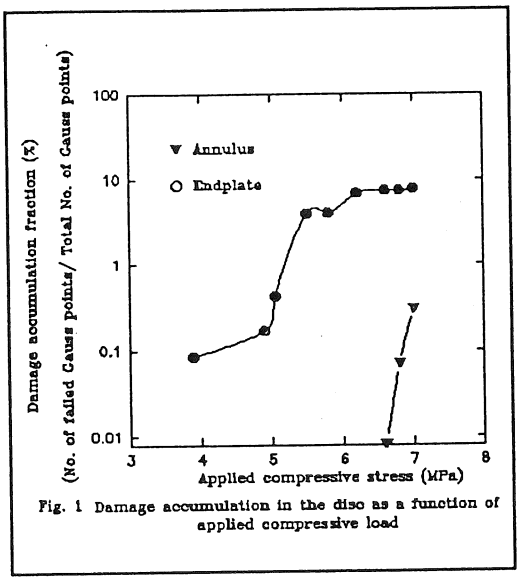

Fig. 1 Damage accumulation in the disc as a function of applied compressive load

Proceedings of NACOB II, The Second North American Congress on Biomechanics, Chicago, August 24th - 28th, 1992

DETAILED FE MODEL OF THORACOLUMBAR SPINE (T11-T12-L1) TO DETERMINE ROLE OF FACET ORIENTATION IN PRODUCING SPINAL INJURIES

L.G. Gilbertson, V.K. Goel, and A.G. Patwardhan*

Department Biomedical Engineering, University of Iowa, Iowa City, IA 52242

*V. A. Hospital, Hines, IL 60601

INTRODUCTION

A detailed three-dimensional finite element model of the thoracolumbar spine (T11-T12-L1), based on the geometry of a cadaveric spine specimen with material properties from the literature, was developed to study the role of facet orientation in producing fracture. Two different types of facet articulations between T11 and T12, lumbar- and thoracic-type, were simulated. The stresses in certain regions of the FE model transition vertebra (T12) were greater with an abrupt facet orientation transition compared to no transition. The von Mises stresses in the posterior regions of the cortical wall and the endplates of T12 increased 20% (superiorly) and 5 - 10% (inferiorly) under 1800N axial compressive loading when there was an abrupt facet orientation transition at T12. The "transition vertebra" between different regions of the spine may thus be more susceptible to fracture than adjacent vertebrae.

REVIEW AND THEORY

Anatomic differences in vertebral body shape, facet orientation, presence or absence of ribs, and shape/orientation of the transverse and spinous processes distinguish thoracic vertebrae from lumbar vertebrae. The thoraco-lumbar junction is a transition region between thoracic- and lumbar-type vertebrae, and it is also the site of the highest frequency of certain types of spinal injuries, including anterior compression fractures, burst fractures, and flexion rotation injuries. The role, if any, of the changing anatomy of the thoraco-lumbar spine in producing these injuries has been speculated upon in the literature, but has not been demonstrated experimentally or analytically. The goal of the current research described in this paper was to develop an analytic FE model of the thoracolumbar spine to study the effect of changes in geometry on spine fracture mechanics.

PROCEDURES

A cadaveric thoracolumbar spine specimen was dissected free of soft tissue except for the disc, embedded in clear plastic, and cut with a band saw into serial transverse cross-sections 5 mm thick. The sections were photographed to obtain the contours at each level upon which a finite element grid was drawn by hand. The grids were digitized using a computer to obtain the nodal coordinates for the FE model. These data were entered, together with the appropriate element connectivity, into the commercial FE analysis package ANSYS (Swanson Analysis Systems, Inc., Houston, PA). Eight-node 3-D isoparametric solid (brick) elements from the ANSYS element library were used to model the cortical shell and cancellous core of the vertebral bodies, and the posterior bony elements. Homogeneous and isotropic material properties were assumed from data in the literature. The anulus fibrosus was modeled as a composite of collagenous fibres embedded in a matrix of ground substance, using 3-D tension-only spar elements and 3-D brick elements, respectively. The nucleus pulposus was modeled using 3-D fluid elements. 3-D tension-only spar elements were also used to model the spinal ligaments (ALL,PLL,LF,TL,ISL,SSL) and facet joint capsular ligaments.

Finally, 3-D interface or "gap" elements were used to model the facet surfaces which can contact and slide relative to each other. The model was run first with the T11-T12 segment having thoracic-type facet articulation, and T12-L1 having lumbar-type facet articulation (i.e., abrupt facet orientation transition at T12). In this case, the superior facets of T12 faced mainly posteriorly and slightly laterally, while the L1 superior facets faced medially and posteriorly. Then, the model was changed: lumbar-type facet articulations were given to both the T11-T12 and T12-L1 segments, in effect eliminating the abrupt transition at T12. Axial compressive load was applied to the top surfaces of the half-model T11 vertebral body (90%) and superior facet (10%), while applying appropriate displacement constraints to the nodes on the inferior surface of L1 (and also the mid-sagittal plane, since a symmetric half-model was used). The stress output was examined to determine the effect of facet transition on the stress distribution in the vertebrae.

RESULTS

Under loading conditions equivalent to a spinal axial compression of 1800N, several regions of the T12 FE model vertebra showed an increase in stress associated with an abrupt facet transition at T12 (Figure 1). The von Mises stresses in the posterior regions of the cortical wall and the endplates of T12 increased approximately 20% (superiorly) and 5 - 10% (inferiorly) when there was an abrupt facet orientation transition at T12.

DISCUSSION

For the axial compressive loading conditions used in this study, the results indicate that the stress in certain regions of the transition vertebra (in this case, T12) is greater with an abrupt facet orientation transition compared to no transition. Elements of the T12 vertebral body located posteriorly in the endplates, and in the posterior cortical wall experienced an increase in von Mises stress. In burst fractures, failure frequently occurs in these regions. The FE model data support the hypothesis that changes in the facet orientation may alter the stress distribution in the vertebral body, producing stress patterns associated with spinal injury.

ACKNOWLEDGEMENTS

Work supported in part by a grant from NIH (AR32594-07) and a grant from V. A. Administration.

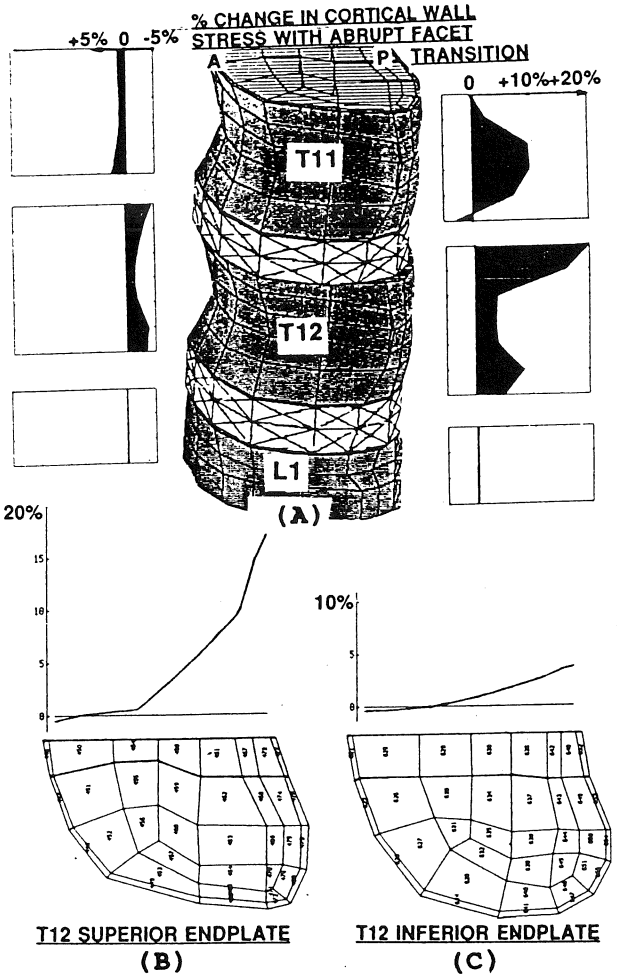

Figure 1. With abrupt facet transition at T12, von Mises stress increased in (A) cortical wall (posterior elements not shown here, for clarity), and in the (B) superior and (C) inferior endplates of T12.

A GEOMETRIC MODEL OF THE LUMBAR SPINE IN THE SAGITTAL PLANE

C. Sicard and M. Gagnon

Société de l'assurance automobile du Québec, Québec.
Département d'éducation physique, Université de Montréal, Montréal.

INTRODUCTION

The measurement of the geometric configuration of the spine in different postures is useful for studying ergonomics in the workplace, evolution of posture in maturing children, and also for diagnosing back pain. In the past, radiology has been the standard technique for obtaining this information; however, it involves high doses of radiation. Therefore, it is very desirable to develop a noninvasive technique for evaluating the geometric configuration of the spine.

The immediate goal of this research is to develop and validate a model for the reconstruction of the lumbar spine for all postures assumed in the sagittal plane. This model uses the skin profile and anthropometric data to determine the linear and angular positions of S1, T12 and each lumbar vertebra and to further evaluate the angular motions of the pelvis (S1) and the entire lumbar spine (L1/S1) as well as the intervertebral motions. This paper constitutes an important part of a more extensive study on the geometry of the lumbar spine (Sicard, 1991).

MATERIALS AND METHODS

Twenty-seven normal subjects took part in the study. The mean age was 23 yr (SD = 2 yr), the mean mass, 75.6 kg (SD = 9.2 kg) and the mean height, 1.76 m (SD = 0.06 m). These subjects were randomly divided into two groups, the first group (20) for the development of the model, and the second group (7) for its validation.

The subjects underwent two separate tests. Firstly, 12 anthropometric measurements were taken of the subject but only five of them were retained for this study. These were stature (ST), top-of-head to chin/neck intersection lenght (HCL), bicristal breadth (BB), umbilical skinfold (US) and subscapular skinfold (SS). Subsequently, a lateral radiograph was taken for each one of four postures (standing, extension, half-flexion and flexion). Thirteen radiopaque markers were placed over the skin in the middle of the back. They consisted of steel balls 5.5 mm in diameter that were inserted into rubber pieces glued to the skin. The first marker was placed over the spinous process of L5. Two other markers were placed under the first, and the others above it. The distance between any two markers was about 2 cm.

The lumbar radiographs were digitized on a digitizing table and the coordinates were fed into a computer. The coordinates on each film included the 13 markers on the skin, a series of two landmarks on the sacrum (S1), and five anatomic landmarks on each lumbar vertebra and T12. The coordinates of landmarks on the spine were processed to calculate the height of the lumbar spine. A local coordinate system was constructed on each vertebra to evaluate its linear and angular positions. Subsequently, a normalized coordinate system was constructed on the lumbar spine to evaluate its linear position ($X(Oc_{L5})$, $Y(Oc_{L5})$) and its angular position (Ψc) and to compute the indices of curvature (fc) (Figure 1).

GEOMETRIC MODEL

The model uses two input sources: five anthropometric measures and the coordinates of the skin markers. The model presents three important steps: normalization of skin profile, transformation of skin profile and reconstruction of lumbar spine.

The purpose of normalization was to provide a standard configuration by which different skin profiles could be compared between postures and individuals. In the first step, the mean change distance was computed between the skin markers in relation to the initial distance between markers in the standing posture (skin distraction). In the second step, the skin profile was mathematically described with parametric functions. The parameter was the summation of the distances between skin markers, and the function was a third degree polynomial equation. In the third step, seven segments with heights equivalent to those of the vertebrae were positioned along the parametric curve. The last step of the normalization process was to construct a coordinate system, on the parametric skin profile, using procedures similar to those described for the lumbar spine. This was used to evaluate the linear ($X(Os_{L5})$, $Y(Os_{L5})$) and angular (Ψs) positions of the the skin profile and to compute the indices of curvature (fs).

The purpose of the transformation process was to take into consideration the differences in indices of curvature, in orientation and the distance between the skin profile and the lumbar spine. This process involves three operations: deformation, rotation and translation of skin profile. Ten regression equations developed with the first group were used to predict these differences (Sicard, 1991).

Finally, the transformed skin profile was used for the reconstruction of the lumbar spine. A coordinate system was constructed on each segment. Subsequently, an anthropometric scaling technique was used to reconstruct each vertebra (Sicard, 1991).

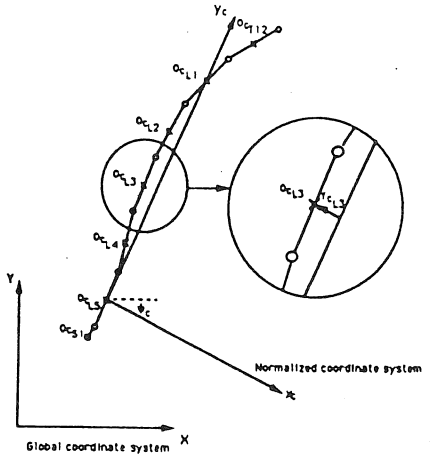

Figure 1. Illustration of a normalized coordinate system on the lumbar spine.

RESULTS

Table 1 presents the errors in the absolute linear and angular positions of the vertebrae. The mean error in the absolute linear position was relatively similar for all vertebrae. The most important part of this error was attributed to translation (1.63 ± 1.01 cm), an error that was systematic on each vertebra. When the effect of translation error was removed, the resulting error level decreased for all vertebrae (0.05 to 1.05 cm). The results showed that the error increased from the lower level (S1) to the upper level (T12).

The mean error in the absolute angular positions for all postures varied from 3.9 to 5.4 ° depending on the vertebral level (Table 1). The mean error was greater for L5 and T12. For all vertebrae, there was a strong correlation between the measured and estimated values of the absolute angular position (R varied between 0.95 and 0.99). As for the linear position, the mean error in the absolute angular position was greater for the extension posture.

Table 1: Mean error (M) and standard deviation (SD) on absolute linear and angular positions of vertebrae for all combined postures, and correlation (R) between estimated and mesured values of angular position.

	Linear position (cm)			Angular position (°)		
	N	M	SD	M	SD	R
S1	25	1.68	1.03	3.9	3.6	0.96*
L5	25	1.68	0.99	5.3	4.6	0.95*
L4	25	1.79	1.01	4.6	3.0	0.98*
L3	25	1.82	0.99	3.4	3.3	0.99*
L2	25	1.81	1.03	3.9	2.6	0.99*
L1	25	1.82	1.15	4.5	3.3	0.99*
T12	17	1.63	1.48	5.4	6.7	0.98*

N.B.: N represents the number of measurements on the seven subjects reserved for the validation
* Statiscally significant ($p \leq .05$)

The mean errors in the relative linear positions of the vertebrae were lower than the errors in the absolute linear positions (Table 2). These mean errors varied from 0.32 to 0.54 cm. The mean errors in the relative angular positions varied from 2.1 to 4.0 °. In general, the correlations between the measured and estimated values of the relative angular position were significant but smaller than those obtained for absolute angular positions.

The mean errors in the motion of the pelvis (S1) and the entire lumbar spine (L1/S1) were 12 ± 3 % and 14 ± 13 % respectively. On the other hand, the mean error to predict the intervertebral motions was acceptable for L4/L5 (13 ± 10 %) but not for the others segments (≥ 23 %).

DISCUSSION

The error analysis showed an important variation in the levels of error depending on the parameter that was estimated. For example, there was a decrease in accuracy levels observed between absolute angular positions, relative angular positions and angular displacement. This was expected since the absolute angular position was required to compute the relative angular position, which was in turn required to compute the angular displacement. There was a decrease in the level of accuracy at each step of the computing process. The validity of the model also depended on the vertebral level. In general, the errors in angular positions were greater for segments S1, L5 and T12. This was attributed to a lack of definition of these vertebrae on the radiographic images. In summary, the present model is judged valid for evaluating the absolute and relative angular positions of all vertebrae except for T12/L1. For angular displacements, the model is valid for evaluating the motion in flexion for the pelvis (S1) and the entire lumbar spine (L1/S1); however the model is not valid for the evaluation of intersegmental motions, except for L4/L5 in flexion.

Table 2: Mean error (M) and standard deviation (SD) on relative linear and angular positions of vertebrae for all combined postures, and correlation (R) between estimated and mesured values of angular position.

	Linear position (cm)			Angular position (°)		
	N	M	SD	M	SD	R
L5/S1	25	0.32	1.18	4.0	2.8	0.75*
L4/L5	25	0.54	0.45	3.1	2.5	0.88*
L3/L4	25	0.54	0.47	3.3	2.1	0.85*
L2/L3	25	0.46	0.33	2.1	1.4	0.90*
L1/L2	25	0.45	0.32	2.7	1.8	0.79*
T12/L1	17	0.32	0.41	3.1	3.6	0.33

N.B.: N represents the number of measurements on the seven subjects reserved for the validation
* Statiscally significant ($p \leq .05$)

The information obtained with the present model should be very useful when combined with models designed for the evaluation of spinal loadings for specific occupational tasks (Anderson et al., 1985; Gracovetsky et al., 1981; McGill and Norman, 1986). The current biomechanical models do not describe accurately the geometry of the lumbar spine during dynamic movements. This information is essential for an appreciation of the effect of the lumbar spinal curvature (kyphosis, lordosis) on spinal loading during manual materials handling. Our model contributes significant information on these geometric characteristics and its utilization should increase the validity of future studies to evaluate loadings on the lumbar spine.

REFERENCES

Anderson, C.K. et al. J. Biomech. 18, 571-584, 1985.
Gracovetsky, S. et al. Spine 6, 249-262, 1980.
McGill, S.M. and Norman, R.W. Spine 11, 666-678, 1986.
Sicard, C. Unpublished doctoral dissertation, Université de Montréal, Montréal, 1991.

ACKNOWLEDGMENTS

This research was supported by grants from the Institut de Recherche en Santé et en Sécurité au Travail du Québec (IRSST) and the Natural Sciences and Engineering Research Council of Canada (NSERC)

TWO AND THREE DIMENSIONAL ANALYSES IN THE FLEXURALLY LOADED CADAVERIC LUMBAR SPINE.

Droese K. Cusick J.F. Yoganandan N. Pintar F.
Department of Neurosurgery, Medical College of Wisconsin, Milwaukee WI
Department of Veteran Affairs Medical Center, Milwaukee WI

INTRODUCTION

Studies that identify and quantify motion of the spine at single or multiple levels, implement methods of measuring geometric relationships of features on the vertebrae. Depending upon the nature and the complexity of the loading and the method used to apply the load, the geometric relationships of the targeted features require three dimensions to describe the resulting inter- and intra-vertebral motions. Because the spine is a composite of various materials including bone, ligaments, intervertebral discs, and other soft tissues, the spine behaves anisotropically. As a result even simple loading can cause coupled motion in the spine. Coupled motion is the result of a single simple load but has the isotropic characteristics that would indicate more than one type of loading. A basic example of coupled motion is evident in the ends of a coil spring subjected to axial compressive loading. In addition to moving closer to each other, the ends also rotate relative to one another.

While three dimensional analysis is necessary to determine coupled motion even if the spine is subjected to a simple load, two dimensions may adequately describe the expected motion in the plane of the applied load. This study compares motion measurements in three dimensions with measurements taken using the same equipment in two dimensions. The entire lumbar spine (L1-L5) was used to compare the relative kinematics at the middle L2-L4 levels.

METHODS

The motion measuring system includes retroreflective targets, three video cameras, each connected to a separate video cassette recorder, a Video Processor (by Motion Analysis Corp. Santa Rosa CA.) which identifies light contrast and digitizes the border, and the ExpertVision software (also by Motion Analysis Corp.) which time collates the processed video views and defines each retroreflective target in three dimensional space sixty times a second.

The heads of straight pins were dipped in a retroreflective liquid (3M Inc.,Minneapolis, MN) and allowed to dry. The pins were inserted in osseous features of the vertebrae immediately prior to testing, which included four locations on each vertebral body, the lateral and medial facets, and the spinous processes. Ring lights (by Motion Analysis Corp.) mounted on the video cameras illuminate the targets to a greater intensity than the surrounding field, allowing the Video Processor to identify and outline the circular targets.

The fresh cadaver spines were bagged and kept at -25° C until ready for experimental use. After thawing, the distal end of the lumbar spine segment (L5) was prepared by threading 2 mm rods along the pedicles so that they cross in the vertebral body and emerge in the anterior. The prepared distal end was placed in a mold and poly-methyl-methacrylate (PMMA) poured so that L5 and half of L4 were submerged. The proximal end (L1) was similarly prepared with the threaded rods. Additionally, an 8 mm smooth rod was bent and inserted through the neural foramen, transversely passing through the spinal canal, and emerging through the contralateral neural foramen.

This "stirrup" supports the pedicles of L1 and simulates the prior capsular ligamentous attachments of L1 to T12. The proximal end of the segment was then cast in PMMA so that L1 and half of L2 were submerged.

The entire lumbar spine (L1 and L5) was included in the experimental model to retain the complete physiologic attachments of L2 and L4 on both the proximal and distal ends. While some fibers of the supraspinous ligament attach at each level, some fibers span more than one level. To achieve physiologic stress in the supraspinous ligament, the origins and the insertions of the ligament are left intact from L1 to L5.

Using an electronically controlled hydraulic piston (MTS Systems Corp,Minneapolis, MN) the spine was subjected to anteriorly eccentric, axially compressive loads of magnitudes up to 500 N. This type of loading produces flexion in the spine. A spherical contact plate was mounted at the superior end and located anterior to the specimen. The radius of the spherical contact plate matched the length of the specimen and was orientated with the convex side on the top. The load was applied using a ball transfer mounted on the end of the piston which contacted the spherical plate at 15 cm anterior to the Posterior Longitudinal Ligament. This loading fixture applies a flexion load to the spine while allowing multiple degrees of freedom to the specimen.

One video camera was located normal to the left lateral view. This camera provided the data for the two dimensional comparison. The other two cameras were placed in the same transverse plane but approximately plus and minus 45 degrees from the normal left lateral view. The two and three dimensional data were collected concurrently during testing. This removes the variability of time even at sixty frames per second.

RESULTS

The resulting inter-vertebral motion was three dimensional. In addition to the two dimensional flexural motion that was expected, there was a right lateral translation of the spine. The inter-vertebral motion of a vertebra was expressed relative to the adjacent inferior vertebra. The measurements therefore also represented distension in the posterior ligaments and the

compression of anterior components. The average magnitude of distension in the posterior ligaments was 3.5 mm and the average of the anterior compression was 1 mm.

The intra-vertebral motion was measured by relative motion of targets on the same vertebra. Two distinct motions were evident from the analysis.There was an anterior compression of the vertebral body and an extension at the pedicles which resulted in relative motion of the spinous process with the body as viewed laterally. The extension at the pedicles was measured as a change in angle between two lines. One line connected the targets at the posterior tip of the spinous process and the medial facet while the other line connected the targets at the superior and inferior of the anterior vertebral body. The maximum change in angle occurred typically at the peak of flexural loading, however was of a much shorter duration. The average magnitude of this angular displacement was approximately 1 degree.

When the measurements from two dimensions and three dimensions were compared, there was an average of 10% discrepancy between the two measurements. Projecting three dimensions onto the plane of expected motion results in the difference between the dimensional analyses.

DISCUSSION

Vertebrae are not rigid bodies. By measuring the relative motion of features on a single vertebrae intra-vertebral motion was measured. Although the inter-vertebral motion of the spine was measured, it was not possible to determine the stress in any ligaments from geometric analysis because of the statically indeterminate loading on the vertebrae as a result of numerous ligament attachments at each level. In addition to the indeterminate loading,the flexibility of the vertebrae preclude calculations of stress in the ligaments.

In the example of an entire lumbar column fixated at L1 and L5 subjected to a flexural load, the resulting motion can be measured in two dimensions and be accurate in describing the gross motion in that plane. The nature of the study may determine whether it is appropriate to use two dimensional analysis. A study that is intent on measuring flexural motion is suited for two dimensions, however a study designed to quantify strain in ligaments may be served best by three dimensions.

ACKNOWLEDGMENTS

This research was supported in part by the Department of Veteran Affairs Medical Research funds.

NETWORK MODELS FOR THE PREDICTION OF TORSO MUSCLE ACTIVATION DURING STATIC LOADING

M.A. Nussbaum

Center for Ergonomics, University of Michigan, Ann Arbor, MI 48109-2117

INTRODUCTION

As a technology undergoing rapidly increasing development and use, neural networks are also beginning to be used for biomechanical applications. Several advantageous properties of network models suggest they may be particularly suited to the solution of heretofore challenging problems. In this paper, a summary is presented of recent efforts towards developing network models which will predict torso muscle activity during static external loading.

External loading, especially during lifting, is known to be a significant risk factor in the development or exacerbation of a back injury. In a biomechanical analysis of the torso, it is crucial to obtain estimates of muscle forces because of the direct relationship between muscle forces and resultant spinal loads. While contemporary models have had relative success in determining forces, each has specific and possibly limiting weaknesses.

The feasibility of applying network models to muscle activity prediction is assessed by posing several questions: Can a network model be developed using available data; Are the networks of tractable size; Do the networks show a sufficient ability to generalize; and, Is the introduction of a new technology warranted by potentially superior performance relative to existing models. The results from initial experimentation suggest favorable responses to each.

REVIEW AND THEORY

In the present literature there are two main approaches to muscle force prediction. The first, which can be termed an empirical method, uses EMG to determine muscle forces for a specific activity (McGill *et al.*, 1986). While this method may allow for direct muscle force estimation, it is limited in its applicability to novel situations and validation can be difficult.

The second approach involves optimizing some assumed objective which is formulated in terms of muscle force. Through optimization, the indeterminate equations of static equilibrium are solvable. While optimization-based models have successfully modelled the torso musculature in certain scenarios (Hughes, 1991), they have generally failed in predicting co-contraction of ipsilateral muscles. In addition, any optimization model requires an assumed objective function; this assumption may or may not be related to an existing physiologic strategy.

Network models are proposed here as an alternative to the empirical and optimization methods. A neural network can have a variety of architectures or implementations depending on the data structures and intended applications. In the current work, muscle activations are predicted based on the magnitude of the external moment. Muscle activation is coded within the model as a percentage of maximum to allow for direct comparisons to normalized EMG (NEMG). Because of limitations on available data, only moment loading in the sagittal and frontal planes is considered. Similarly, only the activity of the following bilateral muscles is included: Erector Spinae (ES), Rectus Abdominis (RA), External Oblique (EO), and Latissimus Dorsi (LD).

PROCEDURES

The networks were constructed, trained, and tested using an available software package (McClelland *et al.*, 1989). All networks were three-layered, fully interconnected, feed-forward restricted, with sigmoid activation functions and linear output functions. The standard back-propagation algorithm was used to train each model.

The input layer of the model contained four units (nodes) corresponding to and receiving the magnitude of: flexion, extension, right lateral, and left lateral bending moments. The output layer contained eight units corresponding to the four pairs of torso muscles; the activation of the output layer was interpreted as muscle activation. A single hidden layer was also included with varying numbers of units.

The training and testing datasets were obtained from a previous experiment (Lavender *et al.*, 1992). The data contained normalized EMG collected from 10 subjects during a range of static horizontal plane loadings in an upright posture. By varying weights applied to a shoulder harness, five moment loads (10, 20, 30, 40, and 50 Nm) were applied in seven orientations. The loading directions were equispaced along the right side of the body from flexion through lateral bending and extension. The NEMG values were averaged over the 10 subjects to obtain a set of 35 load-NEMG patterns. Half of the patterns from this set were used for training and the remainder for validation.

RESULTS

A number of initial models were developed in order to evaluate the effects of certain parameters. An individual model was considered potentially useful if it first could be trained to replicate the training set of load-NEMG patterns within an error criterion corresponding to approximately 1%. Training typically required on the order of 10,000 learning cycles and about 2-3 hours on a personal microcomputer. The ability of a model to learn the testing pattern set to within the error criterion was

fairly insensitive to several model parameters including the learning rate.

The effects of varying the number of hidden units was evaluated. All models having between 5 and 20 hidden units were able to successfully learn the pattern set. When less than 5 hidden units were included, the model appeared unable to reduce the error with increased training. It is unclear whether a true error limit was reached. Since the decrement in error was exponentially reduced with increased training, an inordinate amount of time would have been required to continue training far enough to observe any reduction in error.

As noted above, the models were trained using a subset of the 35 patterns. The remaining patterns were used to validate the predictive ability of the networks. Three models were tested, containing 6, 8, and 10 hidden units. The untrained moment loads were input to the three models and the estimated muscle activations were linearly regressed versus the NEMG data. For the ES, RA, and EO muscles, all three models predicted activations with correlations (r^2) above 0.9. The left LD was predicted less accurately, (r^2=0.7) and the right LD was predicted relatively poorly (r^2=0.4-0.6). Comparison of the three networks showed that, with exception of the Latissimi, superior predictions were obtained with smaller numbers of hidden units.

Additions training cycles were performed on a single network model (10 hidden units). This model was trained to an error criterion half of that mentioned previously, which corresponded to average errors of about 1/2%. The additional training resulted in increased correlations except for the left ES which decreased slightly. The predictions of the Latissimi were substantially improved with the left LD increasing from r^2=0.75 to 0.9 and the right LD from r^2=0.55 to 0.8.

The predictive ability of an 8 hidden unit network was compared to that of a contemporary optimization model. The formulation (Crowninshield *et al.*, 1981; Hughes, 1991) solved for muscle forces by minimizing the sum of the cubed muscle intensities (force/area). Previous work had demonstrated that this objective enabled the most accurate predictions of muscle force over a wide variety of moment loads. Muscle force predictions were obtained using the optimization-based model for the same subset of moment loads used to test the network models. Correlations were obtained by linearly regressing the predicted forces with NEMG and are compared to the network model in Figure 1. For all muscles the network demonstrated superior predictive ability, and substantial differences can be seen for the right ES and both Latissimi.

DISCUSSION

These efforts were intended to assess whether network models can predict muscle activations during static loading. The results demonstrated that networks could be developed using existing data and that the required size is such that they can be implemented using standard algorithms on a personal computer. The insensitivity of the models to certain parameters as the learning rate may aid in limiting the scope of future surveys for an optimal model design.

Each of the three models so tested showed the ability to generalize from the training pattern sets. High correlations were observed between the predicted muscle activations and NEMG even through the network had not previously been exposed to the tested load-NEMG pairs. It was noted that smaller networks, containing fewer hidden units, generated better predictions. This is consistent with existing work suggesting that the maximal generalization potential is achieved when the number of hidden units is minimal yet sufficient to learn the required input-output transformation (Anshelevich *et al.*, 1989).

When compared with an effective optimization-based model, the network model was able to generate muscle activation predictions which were better correlated with EMG. This suggests that network models are a viable alternative to optimization. Furthermore, since networks are amenable to validation and have the ability to generalize to unprecedented input, they offer advantages not available through empirical models.

Future work will involve further evaluation of the effects of varying different model parameters. It is still unclear whether an 'ideal' model architecture exists and whether there is any consistency in the structure of trained models. Extension to 3-dimensional loading will be undertaken, although limitations of available experimental data may prevent full implementation.

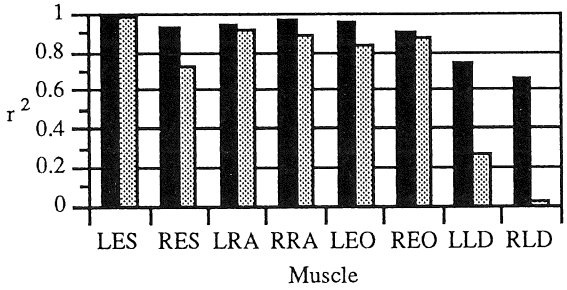

Figure 1. Comparison of r^2 values for a network model (dark bars) and an optimization based model (light bars).

REFERENCES

Anshelevich, V.V. et al. *Biol. Cybern.* **61**, 125-128, 1989.
Crowninshield, R.D. et al. *J. Biom.* **14**, 793-901, 1981.
Hughes, R.E. *PhD Thesis*, Univ. of Michigan, 1991.
Lavender, S. et al. *J. Orth. Res.* Accepted for Pub., 1992.
McClelland, J. et al. Explorations in Parallel Distributed Processing, MIT Press, 1989.
McGill, S. et al. *Spine*, **11**(7), 666-678, 1986.

ACKNOWLEDGMENTS

This work was partially supported by NIH Grant 1R01-AR39599, in cooperation with Rush Institute, Chicago, Ill., USA.

SPINE MODELS AND IMPLANTS

Poster

A COMPARISON OF TRUNK PERFORMANCE WITH AND WITHOUT FOOT SUPPORT WHILE IN THE SITTING POSTURE

O. Cartas, M. Davoodi and M. Nordin

Occupational and Industrial Orthopaedic Center (OIOC)
Hospital for Joint Diseases, New York
63 Downing Street, New York, NY 10014, U.S.A.

INTRODUCTION

Low back-pain (LBP) is a major cause of lost work days, the most costly claim in the workplace, and the most frequent cause of absenteeism beside the common cold Andersson (1981) and Gracovetsky (1991). Unsupported sitting, without leg stabilization, is common for window-washers, building restorers, external painters and construction workers.

REVIEW AND THEORY

The concentration has been on trunk muscle output from the standing position, focusing on those muscle groups that could be factors in LBP. Study parameters included EMG (Grieve and Pheasant, 1976), torque output (Troup and Chapman, 1969), motion parameters (Thorstensson and Carlson, 1985), fatigue analysis (Paniampour et al. 1988), and biomechanical models (Schultz et al. 1982). These studies do not correlate to the trunk muscle performance of seated person (Cartas, 1990). Practically, the trunk muscles are not an isolated musculature but part of the entire linked system of the human body. The proportion or mechanism of force transference from the lower body to upper body is not clearly understood at this time. The purpose of this study is to assess trunk strength in flexion and extension and rotation in the sitting position with feet supported and unsupported.

PROCEDURES

Twenty healthy male volunteers subjects between the ages of 20 and 38 with no history of LBP participated. Their mean (SD) age, height, and weight was 26.9 (6.7) years, 181.6 (6.8) cm, 78.6 (12.5) Kg, respectively. A triaxial dynamometer (Isotechnologies, Hillsborough, NC) with axes locked was used to test isometric trunk muscle performance in each of the two axes: sagittal (flexion/extension) and transverse (axial rotation). A seat was attached to the B200 to facilitate the testing. A battery-powered adjustable lift was used to adjust the hip-thigh and the knee angles to 90 degrees. Subjects were asked to perform maximum voluntary isometric contraction in the sitting posture for five seconds with one minute resting period between trial. The two axes were tested randomly and independently, first with feet supported and then with the lift removed and the feet allowed to hang freely. Two trials were taken for each test to ensure repeatability of maximum exertion. A paired t-test was performed to determine if any changes occur between the trials for supported versus unsupported posture and for direction of exertion. All statistical tests were made at the five percent level of significance.

RESULTS

Isometric: Flexion and Extension

Significance differences in isometric maximum and average torque output were found between supported versus trunk unsupported sitting positions. Trunk torque values in extension were found to be 10 percent higher with feet supported ($p < .0001$) than when feet were unsupported. Also in flexion, supported feet showed higher values than unsupported ($p < 0.0244$). Average isometric for flexion and extension torque shows the same pattern as maximum isometric torque for unsupported versus unsupported subjects.

Isometric: Rotation

In rotation, subjects produced higher torque output values with feet unsupported than when the feet were supported ($p < 0.001$). Rotation to the left was significantly greater ($p < 0.001$) in relation to rotation to the right in the supported position. Average rotation to the left showed greater values than rotation to the right. There was a coupling torque output in flexion/extension and lateral bending during the rotation movement. During flexion and extension, the torque motor output increased when the feet were unsupported. The maximum and average torque values were significantly higher for the supported versus unsupported position.

DISCUSSION

Other studies have distinguished between tests for trunk flexion and hip flexion (Langrana and Lee, 1984, Thorstensson, 1985) or have noted the importance and difficulty of keeping the hip isolated during trunk testing (Langrana and Lee 1984, Oddson and Thorstensson 1987). One of the objectives of this study was to explore whether the lower body does contribute to trunk muscle performance throughout the use of supported and unsupported sitting positions. It should be emphasized that this study did not seek to compare isolated trunk muscles acting with the assistance of the lower body, since there may be a lower body contribution in both positions. This study only examines the difference between sitting with the feet supported and unsupported. Isometric trunk torque output in a sitting posture is affected by foot support. In flexion and extension, the foot support increases the torque output of the trunk.
Torque produced during rotation was found to be higher during the left rotation than the right. There was a trend of increased torque produced in the supported position for main flexion/extension axis but not for the right rotation and lateral bending accessory axis.

REFERENCES

Andersson, B.G.J., Spine., 6,1, 53-60, 1981
Cartas, O., Thesis, New York University, 1990
Gracovetsky, S., J. Biomed. Eng., 8,7,217-223, 1985
Grieve, D.W., and Pheasant, S.T., J Bone Joint Surg, 35a, 3, 589-603, 1976
Parniampour et al. Spine., 13,9, 982-1002, 1988
Schultz et al. Spine., 15,9, 669-675, 1982
Thorstensson, A., and Carlson, H., Acta Physiol Scand, 125 309-321, 1985
Troup, J.D.G., and Chapman, A.E., J Biomech, 2, 49-62, 1969

MODEL OF MECHANICAL CONTROL OF GROWTH IN PROGRESSION OF IDIOPATHIC SCOLIOSIS

Ian A.F. Stokes

University of Vermont, Department of Orthopaedics and Rehabilitation, Burlington, VT 05405, USA.

INTRODUCTION

In order to investigate some of the questions surrounding scoliosis progression and growth, the 'Heuter-Volkmann' hypothesis of mechanically-mediated scoliosis progression was studied by means of a mathematical model which assumed a relationship between local growth rate and mechanical stress.

REVIEW AND THEORY

Growth in the vertebral body occurs in the cartilage of the end plates (Dickson & Deacon, 1987). Growth in these cartilages is influenced by biomechanical loading. Arkin (1949) and Roaf (1960) hypothesized that a "vicious circle" develops in the progression of scoliosis deformity. The concave side of a curve is subjected to greater compression load and this decelerates growth of the vertebral bodies compared with the convex side, according to the principles described by Heuter (1862) and Volkmann (1882). Roaf (1963) developed a rationale for the placement of staples on the vertebral bodies for treatment of scoliosis with varying degrees of kyphosis and lordosis. However, there are several unanswered questions about the scientific basis for this theory of scoliosis progression. For instance, the normal spinal curvatures (kyphosis and lordosis) in the sagittal plane are of similar magnitude to the curvature of scoliosis which is at risk to progress. Why do the normal kyphosis and lordosis not progress into hyperkyphosis and hyperlordosis?

Much of what is known about the interaction between mechanical forces and bone metabolism relates to the remodeling of mature bone, as opposed to the modeling of growing bone (Carter, 1987). One should distinguish between the effects of compression on longitudinal growth, torsion on rotational modeling, and bending on angular development. Strobino et al. (1952) placed springs across the tibial growth plates of calves, and it appeared that growth was relatively insensitive to compression forces of the order of body weight. Arkin and Katz (1956) reported a more sensitive response in growing rabbits, without evidence of a threshold level of load. They found elongation of limbs which were immobilized and relieved of weight-bearing. Tension forces applied across the growth plate produce a small acceleration of growth (Porter, 1978). It appears that growth cartilage placed under tension to accelerate growth requires fracture before significant growth acceleration occurs (Kenwright et al. 1990). However, Gooding and Neuhauser (1965) reported "tall vertebrae" in patients with paralysis and also in younger patients who had been treated surgically with posterior fusion of the spine. They argued that the relative unloading of the spine produced increased longitudinal growth.

PROCEDURES

The 'law' based on the work of Heuter (1862) and Volkmann (1882) was tested quantitatively in the model shown in Figure 1. In this model force is applied to a wedged motion segment. The stress distribution is assumed to be linearly distributed across the width of the endplates. The distribution of stress was calculated by assuming equilibrium of moments about the line joining the centers of the vertebral bodies.

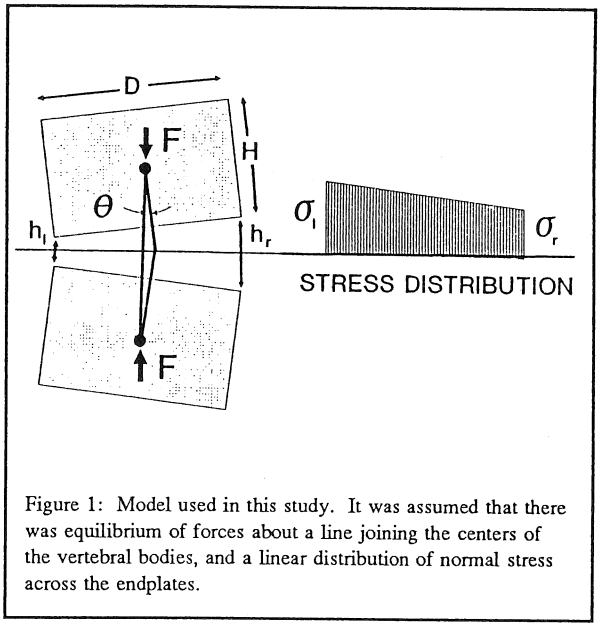

Figure 1: Model used in this study. It was assumed that there was equilibrium of forces about a line joining the centers of the vertebral bodies, and a linear distribution of normal stress across the endplates.

In the absence of published data giving a quantitative relationship between stress and growth rate, a linear relationship, without a threshold of response was used. It was then proposed that the growth strain ε is related to local stress σ and overall growth δG by the relationship previously used by Stokes and Laible (1990):

$$\varepsilon = \delta G(1 + \beta\sigma) \quad \text{where } \beta \text{ is an unknown constant.}$$

By assuming an overall growth δG of 10%, reduced by 1% by the average stress acting in the motion segment ($\delta G \beta \sigma_a$), the unknowns F and β could be eliminated from further consideration. The increase $\delta\Theta$ in wedging angle as a result of growth was then found to be

$$\delta\Theta = \frac{(\sigma_r h_r - \sigma_l h)}{(50D(\sigma_r + \sigma_l))} = \frac{(h_r - kh_l)}{50D(1+k)}$$

where k is a function of the geometry of the model.

RESULTS

This model failed to progress, in that the increase in 'wedging' was always two orders of magnitude less than the initial angulation. With an initial angulation of 1° in a motion segment, the increase in angle ($\delta\Theta$) was 0.01° after a 10% overall growth. Increasing the initial angulation to 10° only produced an additional angulation of 0.1° with growth. Increasing the load on the spine or increasing the sensitivity of growth to compressive stress simply decelerated the longitudinal spinal growth in the model, with minimal increase in the frontal plane curvature.

DISCUSSION

There is a lack of information about how mechanical factors interact with growth of the immature skeleton. Frost (1990) draws attention to the apparently inconsistent response of bone (as opposed to growth cartilage) to a mechanical compression. On one hand, a child with a malunion of a long bone which has resulted in a marked curvature will gradually remodel and straighten the diaphysis by a process through which tissue on the concave (compression) experiences apposition of bone, whereas the tension side experiences resorption. Conversely, the alignment of teeth can be altered by means of orthodontic braces in such a way that compressed bone resorbs while bone on the opposite side of the tooth socket (the tension side) advances. Clearly, there are complex processes underlying the modeling of immature bone. Biewener et al. (1986) found that ambient strain levels with ingrowing bones remain quite constant during the period of growth, but there were variations between different sites, indicating an underlying genetic control. Hall-Craggs & Lawrence (1969) rabbits, which had been stapled at one growth cartilage, produced accelerated growth at the growth cartilage at the other end of the bone. Cook et al. (1983) used a mathematical model to study progression of tibia vara. They found that for angulations greater than 10 degrees, the growth cartilage on the lateral side would experience tensile forces. This degree of angulation across several vertebrae would add up to a scoliosis with a large Cobb angle. From a mechanical point of view, the difference in the force transmission between the convex and concave side of an angular deformity must increase as the angulation of the deformity increases, and this may produce an effective threshold when rapid progression is to be expected. Development of the rotational deformity in the spine complicates this process further. The growth plates of long bones are also responsive to torsional loads (Arkin & Katz, 1956; Moreland, 1990), but the origin of such forces in the spine during scoliosis progression is not clear. As yet, the clinical observation (Lonstein & Carlson 1984) that the risk of progression of scoliosis is a combination both of curve magnitude and amount of residual growth cannot be explained quantitatively by mechanical principles.

REFERENCES

Arkin AM. J Bone Joint Surg 31A:519-528, 1949.
Arkin AM, Katz JF: *J. Bone Joint Surg.* 38A:1056-1076, 1956.
Biewener AA, et al. *Calcif. Tissue Int.* 39:390-395, 1986.
Carter DR: *J. Biomechanics* 20:1095-1109, 1987.
Cook SD *et al.* *J. Pediatr. Orthop.* 3:449-54, 1983.
Dickson RA, Deacon P: *J. Bone Joint Surg.*, 69B:690-692, 1987.
Frost HM: *Anat. Rec.*, 226(4):403-413, 1990.
Gooding CA, Neuhauser EBD: *Am. J. Roentgen., Radium Therapy & Nuclear Med.*, 93:388-394,1965.
Hall-Craggs ECB, Lawrence CA: *J. Bone Joint Surg.*, 51B:359-365, 1969.
Heuter C: *Virkows Archiv path. Anat. Physiol.*, 25:572-599, 1862.
Kenwright J. et al. *Clin Orthop.*, 250: 61-72, 1990.
Lonstein JE, Carlson JM: *J. Bone Joint Surg.*, 66A:1061-1071, 1984.
Moreland MS: *J. Bone Joint Surg.*, 62B:230-237, 1980.
Porter RW: *J. Bone Joint Surg.*, 60B:252-255, 1978.
Roaf R: *J. Bone & Joint Surg.*, 42B:40-59, 1960.
Roaf R: *J. Bone Joint Surg.*, 45B:637-651, 1963.
Stokes IAF, Laible JP: *J. Biomechanics,* 23(6):589-96, 1990.
Strobino LJ, et al. *Surg. Gyn. Obstet.*, 95:694-700, 1952.
Volkmann R: In: von Pitha und Billroth: Handbuch der allgemeinen und speciellen Chirurgie, Bd II, Teil II. Stuttgart: Ferdinand Enke, 1882.

ACKNOWLEDGEMENT

Supported in part by NIH R01 AR 40093.

THREE-DIMENSIONAL SIMULATIONS OF HARRINGTON DISTRACTION ROD FOR SCOLIOSIS SURGERY

Ian A.F. Stokes and Mack Gardner-Morse

Department of Orthopaedics and Rehabilitation, University of Vermont, Burlington, Vermont 05405, USA.

INTRODUCTION

A surgeon planning individualized surgical treatment of scoliosis deformity must decide which instrumentation to use and the vertebrae to which it will be applied, with little ability to predict the eventual outcome. The information which can be used in this decision-making process consists of clinical studies, laboratory testing of implants, animal testing and pre-operative studies of an individual patient. This paper is concerned with the possibility of using pre-operative simulations to augment this process.

REVIEW AND THEORY

Previous biomechanical models of scoliosis surgery have not been matched to the 3-D geometry of specific patients. Schultz *et al.* (1973) used a 3-D model which was adjusted to fit the frontal plane spinal deformity of six different patients with scoliosis to investigate the extent to which axial forces from Harrington rods might alter the spinal deformity. These simulations demonstrated a non-linear relationship between distraction force and correction of scoliosis, since the moment of the distraction force decreases as correction proceeds. They also predicted that distraction forces would produce little derotation of vertebrae. Vanderby *et al.* (1986) used a continuous beam model to study patients having surgery for scoliosis. They estimated intervertebral stiffness from the change in spinal shape. The solutions were sensitive to boundary conditions, but indicated that motion segments near the apex have flexibility similar to those more remote from the apex. Ghista *et al.* (1988) also used a two-dimensional model of a patient's spine to simulate variations on surgical procedure. They estimated the regional flexibility of each patient's spine *in vivo*, based on shape measurements before and after application of traction. Jayaraman *et al.* (1989) reported a 3-D analysis of an idealized scoliosis, with assumed force distributions representing four different procedures, from the point of view of maximizing correction.

This paper reports on finite element (FE) simulations of Harrington distraction rod (HDR) for scoliosis surgery. Although the effect of surgery on the frontal plane shape of the spine has been well described, its effect on the 3-D shape of the spine and ribcage and the mechanism of action are poorly understood. The objectives of this work are to develop and validate a model of the biomechanical behavior of the spine and ribcage to predict the effects of spinal surgery on scoliosis deformity. The purpose of this paper is to examine whether an elastic model based on individualized geometry and published flexibility properties of the spine and thorax can predict the changes in thoracic and spinal shape resulting from surgery using HDR.

PROCEDURES

Stereo radiography (Dansereau *et al.*, 1988) was used to reconstruct the shape of the spine and ribcage of six female adolescent patients before and after scoliosis surgery. The pre-operative measurements of the spine and ribcage were used to define the initial geometry of the finite element model. The pre-operative and post-operative measurements of the hook-rod attachments were used to determine the hook positions and the amount of rod elongation which was input to the FE model. The post-operative measurements of the spine and ribcage were used to validate the results of the FE model. Figure 1 shows the pre-operative PA and lateral views of the HDR model of patient 6.

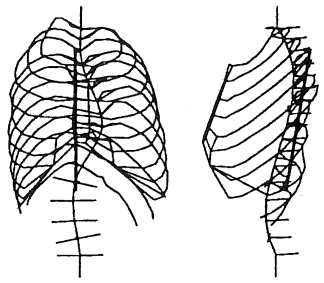

Figure 1 Pre-operative PA and lateral view (right side) of HDR model of patient 6. The geometry was obtained from stereo reconstruction. Straight lines represent finite elements. The thick lines represent the HDR and hooks.

Published flexibility data were incorporated into the FE models of the osseo-ligamentous components of the thorax and spine. This model, and its validation against published flexibility measurements was reported by Stokes *et al.* (1990). To investigate the dependence of the solution on the formulations of the spinal stiffness, the motion segments were represented by 'equivalent' beam elements (Gardner-Morse *et al.*, 1990) instead of stiffness matrices derived from experimental data. The 'equivalent' beams matched some experimental flexibilities, but omitted some of the 'coupling' terms.

To maintain the alignment of the head above the pelvis, and without axial rotation, model constraints (boundary conditions) were applied to the end vertebrae of the spine (C7 and the sacrum). The sacrum could rotate in flexion-extension and C7 could translate vertically and rotate in flexion-extension.

The linear elastic FE analyses were performed by a PC-based FE program (HyperSap, Algor Interactive Systems Inc., Pittsburgh, PA 15238).

Six female adolescent patients with idiopathic scoliosis who underwent HDR spinal fusion were studied. The six patients had an average pre-operative right thoracic Cobb angle of 45° and four of the six also had left lumbar curves with an average pre-operative Cobb angle of 44°.

The HDR was represented by up to three beams elements depending on its curvature. The hooks connected to the vertebrae by joints which allowed rotation about 2 of the 3 axes

of the hook. The lower hook was attached rigidly to the HDR but the upper hook was free to rotate around the rod.

Simulation of the surgical correction of scoliosis was done by applying hooks to the vertebrae selected for the actual surgery, and calculating the relative displacement of the hooks from the pre-operative and post-operative stereo x-ray reconstructions. This distraction was the input to the FE model, and was represented as a thermal expansion of the rod.

For the HDR simulations, the measured outputs of interest were the relative angulations and distance between the vertebrae to which the hooks were applied. See Figure 2.

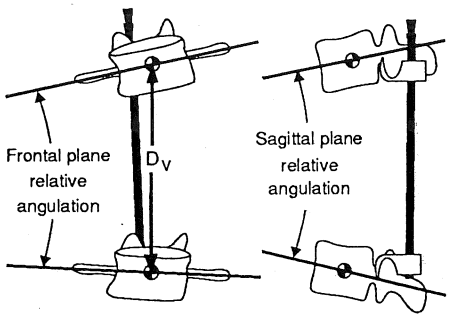

Figure 2 Definition of frontal and sagittal plane relative angulation and distance between vertebrae D_v. Changes in these measurements were used to characterize the spinal shape.

Because of the poor agreement in the sagittal plane outcomes, rigid offsets in the anterior (positive) and posterior (negative) direction relative to the vertebrae were applied to the motion segments as represented by the 'equivalent' beams in order to translate their shear centers. The amount of the rigid offset from the initial offset of zero was systematically varied in 10 mm increments from 10 to -30 mm to find the best agreement.

RESULTS

In the HDR simulations for 6 patients the amount of distraction was calculated from the measured changes in the distance between the hook sites (range 13-27 mm). Initial simulations underestimated the Cobb angle correction by an average 6%. The mean change in frontal plane relative angulation was 10° in both the simulations and stereo measurements. They underestimated the elongation of the spine (D_v) by 37% and predicted an average 13° increase in kyphosis while the actual measurements showed an average 10° decrease. The mean change in sagittal plane relative angulation increased by 11° while the measurements showed a 2° decrease. Agreement for both spinal elongation and sagittal curvature was improved in five cases when motion segments were represented in the models by beam elements with rigid offsets which displaced the beam posteriorly. In the sixth case (with the rod applied over a lordotic region) agreement was improved with the rigid offsets displaced anteriorly. Both measured and simulated changes in vertebral transverse plane rotations and in rib angulations were small. Removal of the ribcage had little effect except for an average 23% reduction in the force in the rod.

Full details of the HDR simulations are reported in a submitted manuscript (Stokes *et al.*, 1991)

DISCUSSION

Measured changes were documented by stereo x-rays several weeks apart and taken with the patients standing, whereas surgery was done with the patients anesthetized and supported on the operating table. There may also have been alterations in thoracic and spinal shape resulting from braces worn after surgery. The model simulates the acute elastic changes resulting from the surgical instrumentation alone. In principle, this could be resolved by intra-operative stereo x-rays. The elastic properties of tissues were taken from the literature, which mainly reports measurements of adult material. Direct measurement of the mechanical properties of the tissues of each patient pre-operatively was not possible. The passive stiffness of the spinal and trunk muscles may be important in the sagittal and transverse planes and these were not included in the simulations.

The initial HDR simulation did not agree well with measured changes in the sagittal plane. The best agreements resulted from changing the model representation of the flexibility behavior of the motion segments. The reason for the improvements in the HDR simulations after moving the 'equivalent' beam elements posteriorly is not clear. It may be that viscoelastic effects in the disc spaces occurred, and this was represented more accurately in our elastic approximation by a beam element placed posterior to the disc. The need to use different offsets for different patients (especially the different direction of the offset for the one patient with a rod spanning a lordotic segment) may reflect an inherent inaccuracy in attempting to represent the complex, nonlinear and time dependent behavior of motion segments by single elastic elements.

There was considerable variability of the predictions of the models for different patients, indicating that the results of surgery were sensitive to the individual pre-operative geometry, which also varies greatly. This emphases the need for individualized geometry in models intended to predict the outcome of surgery. Using 'equivalent' beams, which omitted certain coupling terms from the representation of the motion segments made little difference to the model behavior.

The HDR models showed that the published flexibilities of the spine fail to describe its behavior during surgery.

ACKNOWLEDGEMENT

Supported by NIH R01 AR 40093.

REFERENCES

Dansereau, J. et al. *J. Biomech.*, **21**, 893-901, 1988.
Gardner-Morse, M.G. et al. *J. Biomech. Eng.*, **112**, 481-483, 1990.
Ghista, D.N. et al. *J. Biomech.*, **21**, 77-88, 1988.
Jayaraman, G. et al. *J. Biomech.*, **22**, 427-438, 1989.
Schultz, A.B. et al. *J. Bone Joint Surg. [Am]*, **55**, 983-992, 1973.
Stokes, I.A.F. et al. *J. Orthop. Res.*, Submitted 1991.
Stokes, I.A.F. et al. *J. Biomech.*, **23**, 589-595, 1990.
Vanderby, R., Jr. et al. *J. Biomech. Eng.*, **108**, 312-316, 1986.

THREE-DIMENSIONAL SIMULATIONS OF COTREL-DUBOUSSET INSTRUMENTATION

Mack Gardner-Morse and Ian A.F. Stokes

Department of Orthopaedics and Rehabilitation, University of Vermont, Burlington, Vermont 05405, USA.

INTRODUCTION

For many years surgical instrumentation for treating scoliosis was intended primarily to apply distraction forces to the spine. Recently new options have become available with development of anterior instrumentation, sublaminar or spinous process wiring, a proliferation of possibilities provided by pedicle screw fixation to vertebrae and Cotrel-Dubousset instrumentation (CDI) (Dubousset and Cotrel, 1991). These developments in instrumentation designs provide new possibilities for application of complex combination of forces to the spine, as well as providing increased rigidity of the final construct. Although the effect of CDI has been described clinically, the biomechanics of CDI are not clearly understood. The purpose of this paper is to gain insight into the biomechanics of CDI on an idealized scoliosis model.

REVIEW AND THEORY

In the CDI procedure, curved rods are attached to the deformed spine by several hooks. The first rod (on the concave side of a scoliosis) is applied first, and a 'derotation' manoeuver is intended to rotate the spine from its predominant plane of curvature in the frontal plane (scoliosis) into the sagittal plane (normal kyphosis and lordosis). Thus the plane of the spine is rotated, but in order to derotate the vertebrae, which are generally rotated in the opposite direction into the concavity of a curve (Stokes et al., 1987) local 'derotation' in the opposite sense must be applied.

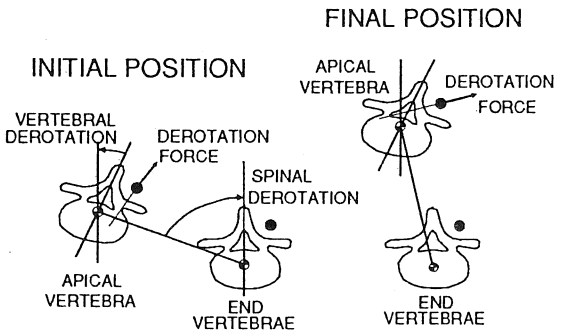

Figure 1 In the initial position, the derotation force has a moment about vertebra center tending to reduce apical vertebra local rotation. In the final position, the derotation force has a moment in the opposite direction.

In this study the 'derotation' step with subsequent locking of hooks to the rod in this multi-step procedure was simulated in order to determine the mechanics underlying this complex procedure. The paper reports on finite element (FE) simulations of CDI 'derotation' for an idealized single curve scoliosis.

PROCEDURES

The idealized geometry consisted of seven equally spaced vertebrae in the shape of a half sine wave with a 65° Cobb angle initial curvature in the frontal plane and straight (no kyphosis nor lordosis) in the sagittal plane.

The curved concave rod of the CDI was represented by beam elements (Figure 2). In the initial 'baseline' model the rod curvature was equal to that of the spine. Four hooks connected the rod to the vertebrae. Two hooks were connected to the end vertebrae and the two other hooks connected to the vertebrae on either side of the curve apex. The hooks were connected to the vertebrae by joints which allowed rotation about the lateral and posterior axes. The hooks were also free to rotate around the rod until the locking of the hooks to the rod after the rod was rotated 90°. The influence of rod curvature on the final geometry was investigated by increasing the lengths of either the end vertebrae hooks or the hooks on either side of the apical vertebra from 10 mm to 20 mm (Figure 2).

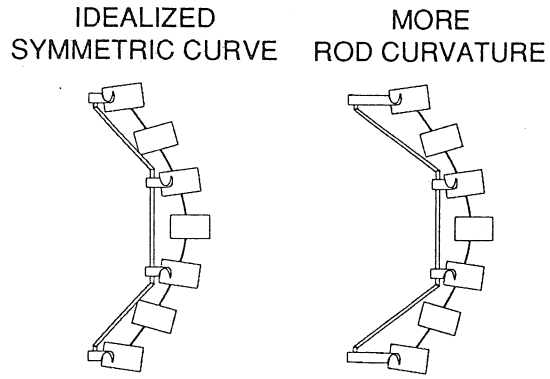

Figure 2 The finite element model geometry with a single idealized scoliosis curve with the concave side rod. Left: 'Baseline' model with equal curvature of the spine and rod. Right: Increased rod curvature by increasing end hook lengths.

Published flexibility data for motion segments were incorporated into the FE models using an 'equivalent' beam element representation (Gardner-Morse *et al.*, 1990). The 'equivalent' beam matched some experimental flexibilities, but omitted some of the 'coupling' terms. Based on Figure 1, the position of the 'equivalent' beam relative to the rod is important in determining both the magnitude and direction of the moment about the apical vertebra created by the 'derotation' force. The initial position suggests that a lateral offset of the spine would increase the apical vertebra 'derotation'. The final position suggests that a posterior offset of the spine would increase the apical vertebra 'derotation'. Therefore, the influence of 10 mm rigid offsets of the spine from its initial 'baseline' model position in the lateral and posterior directions were investigated.

To maintain the alignment of the curve, model constraints (boundary conditions) were applied to the end vertebrae of the curve. The end vertebrae could only rotate in flexion-extension and lateral bending and translate in the vertical direction. For symmetry in the model, the vertical translation was constrained at the apex (middle) vertebra. The rod was rotated by applying a moment about the vertical axis to the center of the rod. The nonlinear (large displacement) FE analysis was performed by a general purpose FE program (ANSYS, Swanson Analysis Systems, Inc., Houston, PA).

RESULTS

The simulated 'derotation' with hook lock-up after 90° of rod rotation in the 'baseline' model converted the initial 65° Cobb angle scoliosis curve into a 26° Cobb angle curve with a 61° kyphosis Cobb angle. The apical vertebra axial rotation increased by 12°. The spine rotation (defined as the rotation of the apex around the axis passing through the end vertebrae) was 60° for the 90° rod rotation (Figure 3).

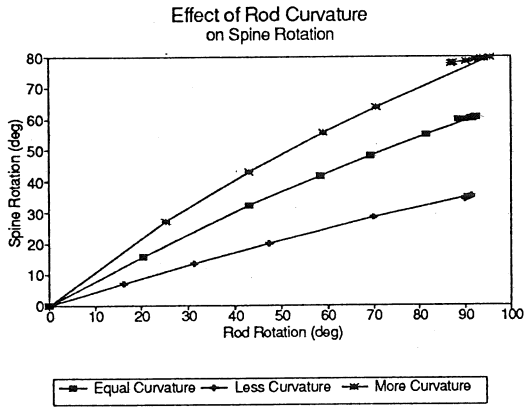

Figure 3 Spine rotation as a function of rod rotation with three different amounts of rod curvature.

Increased rod curvature increased the Cobb angle correction by 1° and increased the apical vertebra axial rotation by a 0.5°. The kyphosis Cobb angle increased to 80°. Reduced rod curvature produced a Cobb angle of only 53° Cobb angle with 38° kyphosis Cobb angle and 6° of apical vertebra axial rotation (Figures 3 and 4).

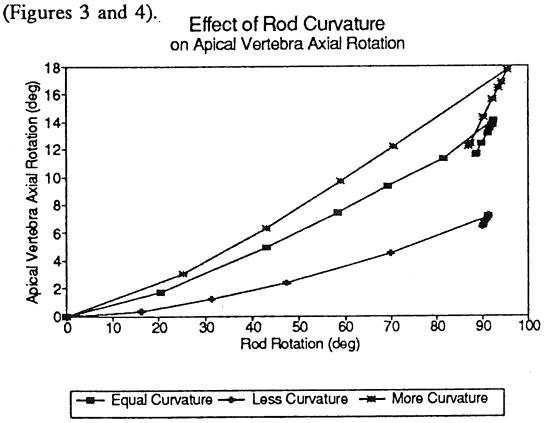

Figure 4 Apical vertebra axial rotation as a function of rod rotation with three different amounts of rod curvature.

There was a linear increase in the 'springback' after the locking of the hooks to the rod and in the applied moment necessary to achieve 90° of rod rotation with increased rod curvature.

The rigid lateral offset of the spine produced a 26° Cobb angle with a 63° kyphosis Cobb angle. The rigid posterior offset of the spine resulted in a 22° Cobb angle with a 59° kyphosis Cobb angle. The lateral offset model produced the same correction with a little more kyphosis than the 'baseline' model while the posterior offset model produced a little better correction with a little less kyphosis than the 'baseline' model. Both rigid offset models produced an apical vertebra axial rotation of 9° which is 3° less than the 'baseline' model. Both rigid offset models also produced a slight increase in the spine rotation relative to the 'baseline' model.

DISCUSSION

The model simulates the acute elastic changes resulting from the surgical instrumentation alone. The elastic properties of tissues were taken from the literature, which may not accurately reflect the *in vivo* properties of adolescent spines. The passive stiffness of the spinal and trunk muscles may be important in the sagittal and transverse planes and these were not included in the simulations.

The 'derotation' maneuver used in the CDI procedure is intended to address the three-dimensional deformity in scoliosis, by rotating the spine from a scoliosis curvature into a kyphosis. However, pre- and post-operative studies have shown that the local derotation of the apical vertebrae is quite small (Wood et al., 1991), as is that of the back surface asymmetry (Beaumont et al., 1989). The biomechanics of the CDI procedure is complicated because it can apply both distraction forces and lateral forces, and in the real surgery a second, convex side rod is applied.

This simulation study has demonstrated that the effects of the first rod on the transverse plane depends on the direction of the forces applied by the rod, in relationship to the relative positions of the vertebrae in the deformed region of the spine (Figure 1). This relationship changes continually during the 'derotation' maneuver and is dependent on the initial rod curvature.

REFERENCES

Beaumont, S.E. et al. *J. Bone Joint Surg. [Br]*, **71**, 153, 1989.
Dubousset, J. and Cotrel, Y. *Clin. Orthop.*, **264**, 103-110, 1991.
Gardner-Morse, M.G. et al. *J. Biomech. Eng.*, **112**, 481-483, 1990.
Stokes, I.A.F. et al. *J. Orthop. Res.*, **5**, 102-113, 1987.
Wood, K.B., et al. *Spine*, **16**, S404-S408, 1991.

ACKNOWLEDGEMENT

Supported by NIH R01 AR 40093. The authors thank Drs. David Aronson, M.D. and Jeffrey P. Laible, Ph.D. for their helpful discussions.

CASPAR CERVICAL SCREW PULL-OUT STRENGTH

Reinartz J. , Pintar F. , Yoganandan N. , Maiman D.
Department of Neurosurgery, Medical College of Wisconsin, Milwaukee WI
Department of Veteran Affairs Medical Center, Milwaukee WI

Introduction

Various fixation systems are frequently employed to impart stability to the anterior column of the cervical spine following tumor, trauma, and degenerative disease. One of these systems include Caspar plates, which are fixated to the anterior portion of the cervical vertebral bodies using Caspar bone screws, used in conjunction with bone fusion. While many retrospective clinical studies (1,2) and studies comparing Caspar instrumentation to posterior fixation devices (3,4) have been presented, biomechanical studies analyzing the effects of subcortical screw placement vs posterior cortical penetration of the screw have not been conducted. Since cortical penetration often carries a higher risk of morbidity and increased technical difficulty in placement (use of fluoroscopy), it is important to document the beneficial effects (if any) of such a procedure. Consequently, this initial research was performed to evaluate the biomechanics of the Caspar screw-plate instrumented cervical spine with and without penetration of the posterior cortex of the cervical vertebral body.

Methods

Cervical spines were removed from seven fresh human cadaveric specimens ranging in age from 60 to 78 years (mean = 68 ± 6 years), height from 160 to 188 cm (mean = 175.3 ± 10.7 cm), and weight from 41 to 100 kg (mean = 76.5 ± 22.9 kg). The specimens were selected to preclude previous trauma, cancer, bone disease, and marked degenerative changes through a review of medical records and radiography. The isolated cervical spines were wrapped in saline moistened towelettes, stored in double plastic bags, and kept deep frozen until use. The specimens were thawed for 12 - 24 hours at room temperature in a humidity controlled environment. Immediately prior to testing the individual vertebrae (C3 to T1) were isolated, geometrical dimensions (overall height, antero-posterior and lateral-lateral widths at superior, inferior, and mid-height) were obtained, and the specimens were mounted in polymethylmethacrylate, leaving the entire vertebral body exposed.

Caspar screws of appropriate lengths were inserted through a stainless steel U-shaped plate (same thickness as a Caspar plate) and screwed into the vertebral body approximately 1 cm lateral to midline. Two trials were attempted in each body while choice of level and cortical penetration (tip of screw subcortical or 2-3 mm of posterior cortical penetration) were randomly made. Placement of the screws were confirmed by conventional radiography. The screw was pulled out anteriorly (0.25 mm/sec) by an electrohydraulic testing device (MTS Corp, Minneapolis, MN) through attachment to the stainless steel plate. Force and deflection were measured at the point of the applied load.

Results and Discussion

Failure was defined as the point on the load deflection curve where increasing deflections are accompanied by a decrease in the applied force. The mode of failure typically was a clean axial pull-out with the remaining cancellous bone attached to the screw threads. Mean force and deflection at failure for subcortical screw placement was 375 ± 53 N and 1.3 ± 0.1 mm, respectively. With screws inserted 2-3 mm through the posterior cortex the mean force and deflection was 411 ± 71 N and 1.4 ± 0.2 mm. A typical force-deflection curve is shown in Figure 1. The differences observed in forces and deflections to failure with or without cortical penetration were not statistically significant. All statistics were based on an

The Sixteenth Annual Conference of the American Society of Biomechanics and
The Seventh Biennial Conference of the Canadian Society of Biomechanics/Société Canadienne de Biomécanique

unpaired t-test using a 95% confidence interval. Statistical analysis revealed no significant relationship between the level tested, load to failure, and the manner of screw placement.

Results of the present study clearly indicate no statistically significant differences between the biomechanical variables and suggest that it may be justified to place the screws subcortically when instrumenting the anterior cervical spine with Caspar plates. The finding that the failure deformations of the two procedures (subcortical and with posterior cortical penetration) are similar suggest that the fixation device is deformation sensitive with respect to screw pull-out. The resulting deformations approximate the distance between threads of the Caspar screw. The finding that differences in the forces to failure are not significant may be due to the relatively thin posterior cortical shell present in cervical vertebral bodies. It should however be emphasized that the present study was aimed the uniaxial pull-out strength biomechanics of the fixation device. Further studies are necessary to determine the effects of posterior cortical penetration under other relevant loading modes such as flexion-extension.

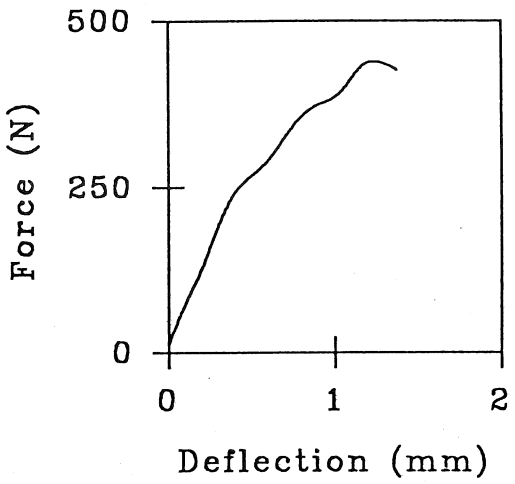

Figure 1 : Representative Force-deflection response.

References

1). Caspar W, Barbier DD, Klara PM: Anterior cervical fusion and Caspar plate stabilization for cervical trauma. **Neurosurgery 25**: 491-502, 1989.
2). Goffin J, Plets C, Van den Bergh R: Anterior cervical fusion and osteosynthetic stabilization according to Caspar: A prospective study of 41 patients with fractures and/or dislocations of the cervical spine. **Neurosurgery 25**: 865-871, 1989.
3). Sutterlin CE III, McAfee PC, Warden KE, Rey RM, Farey ID: A biomechanical evaluation of cervical spine stabilization methods in a bovine model. Static and cyclic loading. **Spine 13**: 795-802, 1988.
4). Coe JD, Warden KE, Sutterlin CE III, McAfee PC: Biomechanical evaluation of cervical spine stabilization methods in a human cadaveric model. **Spine 14**: 1122-1131, 1989.

Acknowledgment

This research was supported in part by the Department of Veterans Affairs Medical Reasearch Funds.

ROTATIONAL STIFFNESS OF A LUMBAR SPINAL PEDICLE SCREW/ROD SYSTEM

Frank A. Pintar, Karl W. Droese, Dennis J. Maiman, James Hollowell, N. Yoganandan

Department of Neurosurgery, Medical College of Wisconsin, and
Department of Veterans Affairs Medical Center, Milwaukee, WI 53295

INTRODUCTION

The use of spinal fixation devices has become more widespread over the past few years. The many choices of constructs and the relative paucity of biomechanical information comparing them leaves the spine surgeon with difficult decisions regarding efficacy in patient use. The ISOLA® pedicle screw with rods system is a relatively new construct with some advantages including ease of use, and the capability for transverse rod connections. The addition of the transverse rod connection is meant to increase the rotational stability of this spinal construct. This added rotational stability has yet to be fully quantified. Therefore the questions to be answered in the present study were as follows. What is the effect of the placement of one or two transverse rods on the rotational stability of the ISOLA® system? At what rod length does this effect have its greatest value? In other words, is there a critical length of rod that the placement of a transverse connector offers significant additional stability? How much stiffer is the placement of one transverse rod versus two?

METHODS

Since the fundamental questions to be answered by this investigation have only to do with the characteristics of the construct itself, pedicle screws were mounted in blocks of polymethylmethacrylate (PMMA) at angles to reproduce the configuration of placement in the human lumbar spine. The PMMA blocks with mounted screws were fixed to an electro-hydraulic multimotion actuator to apply axial rotation. The axis of rotation was placed to approximate lumbar vertebral rotation about the posterior longitudinal ligament. The ISOLA® rod system was mounted to the pedicle screws to test several different configurations. Rotation was applied to the construct in force control mode using a sine wave function. Twenty cycles up to ±15 Nm moment was applied, and the steady state response was used in the analysis. Configurations included longitudinal rod lengths from 4 cm to 18 cm, the addition of a single transverse rod at mid length, and the addition of two transverse rods placed close to the screws. For each of the above configurations, both medial and lateral placement of the longitudinal rods were tested.

RESULTS AND DISCUSSION

Rotation angles varied from 6° for 4 cm laterally placed rods to 17° for 18 cm medially placed rods with no transverse fixators. For any particular configuration rotation angle increased as the rod length increased. The effect of medial versus lateral placement of longitudinal rods showed the greatest differences when no transverse rods were mounted (20%). When transverse rods were used, medial placement of longitudinal rods resulted in higher rotation angles compared to lateral placement except for the 18 cm rod length. In other words, for greater rod lengths (18 cm) medial placement of longitudinal rods with transverse fixators offers a rotationally stiffer construct. For medial placement of longitudinal rods, the use of transverse fixators demonstrated a noticeable decrease in rotation angle for all rod lengths. However, the use of transverse fixators for laterally placed longitudinal rods had their greatest effect for the higher rod lengths (15 and 18 cm). The use of two transverse rods was never more than 6% stiffer than using one transverse rod.

In addition to measuring the variations in stiffness, identifying the components contributing to the flexibility of the construct is also important in understanding its behavior. The plot of longitudinal rod length versus degrees of rotation has a positive y-intercept. This contribution to the overall flexibility is due primarily to elastic deformation in the pedicle screws. Because it is independent of the instrumentation length the percent contribution of overall flexibility by the pedicle screws increases as the rod length becomes shorter. For a rod length of 6 cm, 60% of the total rotation is due to flexibility in the pedicle screws and connectors.

The question of when to use transverse fixators is dependent on the length of the rod and also if the longitudinal rods are medially or laterally placed. For medially placed rods, a single transverse connector will add significant rotational stiffness even for shorter rod lengths; for laterally placed longitudinal rods only the longer rod lengths need a transverse connector. Without transverse rods, lateral placement of longitudinal rods always results in a rotationally stiffer construct. The results of the present study offers quantitative information for the spine surgeon for using this construct in patients.

ACKNOWLEDGMENT This research was supported in part by the Department of Veterans Affairs Medical Center research funds.

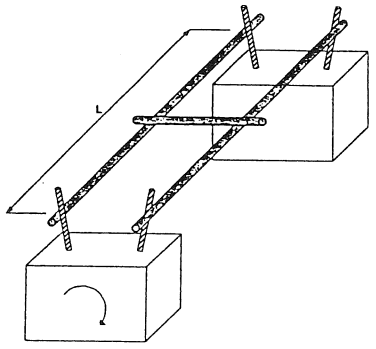

Proceedings of NACOB II, The Second North American Congress on Biomechanics, Chicago, August 24th - 28th, 1992

A THREE DIMENSIONAL MECHANICAL STUDY OF THE PSOAS MAJOR MUSCLE WITH RESPECT TO THE SPINE

P.L. Santaguida and S.M. McGill

Occupational Biomechanics Laboratories, Department of Kinesiology, University of Waterloo, Waterloo, Ontario, Canada, N2L-3G1

INTRODUCTION

The psoas major muscle is a large muscle affecting both the lumbar spine and hip joints. There is, however, limited detail regarding its morphology and its function with respect to the lumbar spine. Since electromyographic study of the muscle is restricted due to its location within the body, a computer model was developed to determine the biomechanical potential of this muscle. This mechanical model attempted to quantify, in three dimensions, the potential contribution of psoas major muscle in generating forces and moments during neutral, flexed and extended static spinal postures and at all lumbar levels.

REVIEW AND THEORY

While there are several hypotheses as to the role of the psoas major, (eg. stabilization of the lumbar spine and hip joints (Nachemson 1968, Crisco and Panjabi 1990), dominant hip flexor (Hamilton 1974), power source for bipedal ambulation (Gracovetsky 1986), controller of lumbar lordosis for challenging lumbar loads (Bogduk and Twomey 1987, Gracovetsky 1986) very little systematically collected data is available documenting the geometry of the psoas major from its origin to insertion and examining the mechanical implications.

PROCEDURES

This investigation is comprised of three parts; the first involved dissections of cadavers to collect morphological data of the psoas major muscle. In the second part, MRI scans (slices from T12 to the sacrum, 10 mm apart) were collected from 15 young male adults to measure invivo muscle cross-sectional areas (CSA) and moment arms. Moment arms were defined as the distance from the centroid of the disc to the centroid of the muscle CSA. All fifteen subjects were scanned in the supine position; this posture was defined as the neutral lordosis condition. Five of these subjects underwent additional scanning in two other spinal postures to obtain maximal lumbar flexion and extension as permitted by the size of the scanner and the comfort of the patient.

The third component of the study consisted of the development of a mechanical model of the lumbar spine (T12 to the sacrum) to assess the psoas major muscle line of action with respect to each vertebral level. The mechanical centres of rotation were located at the geometric centre of each lumbar intervertebral disc. A centroid line approach was used to determine the line of action of the psoas major muscle. Thus, straight lines from origin to insertion were not assumed, rather curves in the muscle were captured by centroid nodes. End-range flexion and extension was simulated using data from Pearcy and Tibrewal (1984). A force producing potential of 30 Nm per square centimeter was used in the model calculations.

RESULTS

Anatomical Dissections:
The cadaver dissections showed the psoas major muscle to be distinct from the iliopsoas muscle complex as it coursed to its insertion. The psoas major was observed to be tendinous at the bony pelvis (iliopubic eminence). In addition, a central tendon was observed to commence at approximately the L4/L5 level and on occasion at higher levels.

MRI Scans:
Several trends were noted in the muscle CSA and moment arms as a function of lumbar level. The muscle CSA increased in size reaching a maximum value at the L4/L5 lumbar level and decreasing in magnitude at the L5/S1 level. The lateral component of the moment arm increased from upper to lower lumbar levels reaching a maximum value at the L5/S1 centre. The anteroposterior component of the moment arm was located posteriorly from T12 to L3/L4 and then anterior from this point. Comparison of muscle CSA and moment arms for the three lordosis conditions (neutral, end-range flexion, end-range extension) showed no statistical difference ($p \geq 0.05$).

Mechanical Model:
Table A lists the forces and moments as a function of lumbar level for the right psoas major muscle. Note that 100% of neural activation level was assumed in all results. These calculations were made using MRI cross-sections corrected for scan plane obliquity and noting that the presence of the central tendon at the L5/S1 level transmits those forces produced by the L1 fascicle of the psoas major muscle.

Decomposition of the force unit vector suggests that the psoas major muscle varies (proportionally) its mechanical actions at some lumbar spine levels, but the dominant force at all lumbar levels is axial compression. In the symmetrical activation condition the compressive forces are additive reaching up to 1070 N at the L4/L5 level. Similarly, the A/P shear forces are additive reaching a peak value of 695 N at the L5/S1 level.

The dominant moment predicted by the model was ipsilateral side flexion at all lumbar levels (see table A). When examining the ability to create sagittal rotation (flexion/extension) about the various lumbar vertebrae, the

The Sixteenth Annual Conference of the American Society of Biomechanics and
The Seventh Biennial Conference of the Canadian Society of Biomechanics/Société Canadienne de Biomécanique

model shows that extension is created at the upper lumbar levels and flexion at the lower lumbar levels. In the symmetrical activation condition the muscle's dominant ability to create side flexion sums to zero, as does its small potential to create axial rotation. However, its ability to generate sagittal rotation is additive, showing a proportionally substantial increase at the L5/S1 centre of rotation.

The mechanical role of the psoas major does not appear to change as a function of lumbar lordosis (i.e. in the end-range flexed or extended postures).

DISCUSSION

The data presented in this study recognized the presence of a central tendon which can effectively transmit muscle forces from fibres that have inserted into the tendon above the L5/S1 level. In addition, the centroid nodes representing the line of action precluded a straight line of action representation.

Although the functional differences between spinal levels were predicted by the mechanical study, some speculation as to their possible importance and implications for lumbar spine modelling is warranted. Compression forces were found to be the largest force components generated by the psoas major. The total dominance of the compression component is not surprising at the middle lumbar levels which constitute the apex of the lordotic curve. The increased ability of the muscle to create anterior shear (decreasing the dominance of the compression vector component) at the L4/L5 and L5/S1 levels indicates that the psoas major muscle can counteract larger posterior shear forces at these levels. The posterior spine muscles (lower lumbar fascicles from the longissimus and iliocostalis muscles) also demonstrate an increasing ability to shear posteriorly (McGill and Norman 1987) at these levels.

In symmetrical activation, the compressive and anterior shear forces of psoas major from right and left body sides are additive. In contrast, only the moments occurring about the flexion/extension axis are cumulative in the symmetrical activation condition. It should be noted however, that the magnitude of the summed flexion/extension moments are very small in comparison to the individual muscle's potential to generate lateral bend and axial rotation and in comparison to other trunk muscles (McGill 1991). The fact that the left and right psoas major provide equal but opposite moments about both the lateral bend and axial rotation axes strongly suggests that the psoas major may function as a stabilizer of the lumbar spine. The analogy of guy wires (i.e.psoas major muscles) stabilizing the mast (i.e. the lumbar spine) aptly describes the symmetrical activation condition.

REFERENCES

Bogduk N and Twomey LT: CLINICAL ANATOMY OF THE LUMBAR SPINE. Churchill Livingstone, London, 1987.

Crisco JJ and Panjabi MM: Postural biomechanical Stability and Gross Muscular Architecture in the Spine. MULTIPLE MUSCLE SYSTEMS: BIOMECHANICS AND MOVEMENT ORGANIZATION. J. Winters and S. Woo editors. Springer-Verlag, New York, 1990.

Gracovetsky S.and Farfan H: The Optimum Spine. SPINE 11:543-573, 1986 (published but unreviewed manuscript).

Hamilton WJ (Ed): Textbook of HUMAN ANATOMY: Second Edition. Harper and Row, Baltimore, 1974.

McGill SM: Kinetic Potential of the Lumbar Trunk Musculature about Three Orthogonal Orthopaedic Axes in Extreme Postures. SPINE, 16:7: 809-815, 1991.

McGill SM and Norman RW: Effects of an Anatomically Detailed Erector Spinae model on L4/L5 Disc Compression and Shear. J BIOMECH, 20:6:591-600, 1987.

Nachemson A: The possible importance of the psoas muscle for stabilization of the lumbar spine. ACTA ORTHO SCAND 39:47-57,1968.

Pearcy MJ, and Tibrewal SB: Axial rotation and lateral bending in the normal lumbar spine measured by three dimensional radiography. SPINE 9:6:582-5587, 1984-b.

ACKNOWLEDGEMENTS

The authors wish to acknowledge A. Agur, department of Anatomy, University of Toronto, Drs. G. Froelich and J. Stevens, MRI Volume Investigations Laboratories, Toronto Western Hospital and to NSERC Canada for financial support.

TABLE A: The forces and moments generated by the RIGHT psoas major muscle about the relative lumbar axes. Lateral shear and coronal rotation (lateral bend) are (+) to the right body side. Axial Rotation (axial twist) to the right (i.e. spinous process moves towards the right) is (+). Sagittal rotation that is (+) indicates flexion and (-) indicates extension.

CENTRE OF	FORCES (N)			MOMENTS (Nm)		
ROTATION	AXIAL COMPRESSION	ANTERIOR SHEAR	LATERAL SHEAR	CORONAL ROTATION	SAGITTAL ROTATION	AXIAL ROTATION
L1/L2	109.74	3.89	20.30	3.46	0.39	-1.44
L2/L3	305.86	66.31	41.93	11.60	2.82	-2.23
L3/L4	460.88	82.25	57.04	20.24	3.91	-2.38
L4/L5	536.27	203.53	64.66	26.63	9.97	1.15
L5/S1	437.39	347.01	48.63	24.03	17.79	11.52

LOWER EXTREMITY LOADING

Podium Session 20

IN-VIVO DETERMINATION OF PATELLOFEMORAL JOINT CONTACT PRESSURES

J. Ronsky, W. Herzog * , T. Brown †, T. Leonard *.

Department of Mechanical Engineering, University of Calgary, Alberta.
* Faculty of Physical Education, University of Calgary, Alberta.
† Department of Orthopaedic Surgery, University of Iowa, Iowa.

INTRODUCTION

The onset and development of osteoarthritis (OA) and degenerative joint diseases are speculated to be associated with abnormal loading of joint articular surfaces. Although numerous studies investigating joint contact areas, contact forces and stress distributions have been performed in-vitro, direct in-vivo measurements of contact loads on intact joints have not been done. In this study, a methodology was developed to measure joint contact areas, contact pressures and relative movement of the articular surfaces under physiological loading conditions, in-vivo. The methodology was applied to an intact and an ACL transected cat patellofemoral joint. The results indicate a different contact area,a different contact pressure pattern and a greater range of patellar movement for the ACL transected compared to the intact joint.

REVIEW AND THEORY

Excessive stresses on the articulating surfaces of patellofemoral joints have been speculated as a mechanism initiating OA and other degenerative joint diseases (e.g. Insall et al., 1972). Surgical modifications of the knee joint stability and integrity in animals to produce variations in the contact stresses between the articulating surfaces have been used successfully to produce OA (e.g. McDevitt, 1977). However, relatively little information is available regarding the differences in biomechanical factors associated with these joint injury models. Comparison of in-vivo joint surface loading between normal and joint injury model animals has been primarily limited to external ground reaction force measurements (e.g. Visco et al., 1990). Direct measurements of articular joint contact loads in-vivo for both intact and surgically manipulated joints have not been performed. Consequently, the relationships between changes in joint loading associated with the joint injury model and the onset and pathogenesis of degenerative joint disease is not well understood.

We hypothesize that the onset and development of OA is associated with loading of joint articular surfaces. We expect that surgical interventions intended to produce OA will result in changes to external and muscle forces as well as imposing non-physiological contact between portions of the joint surfaces which would not articulate in the normal intact joint, creating abnormal stresses on the articulating joint surfaces. These abnormal stresses are expected to produce cartilage tissue adaptations, which can be quantified as changes in joint contact areas and pressures. The purpose of this study was twofold: firstly, to develop a methodology to directly measure patellofemoral joint contact loads in-vivo, and secondly to apply the methodology to determine the joint contact loads as a function of ACL condition (intact or transected), joint alignment and joint loading. This paper outlines the methodology developed and some preliminary results.

PROCEDURES

The methodology for in-vivo joint pressure measurements was developed on the cat patellofemoral joint. Details of the pressure measurement technique, specimen preparation and test protocol are outlined below.

Pressure Measurement Technique: The patellofemoral joint contact area and pressure measurements were obtained using Fuji Pressensor film (Fuji Photo Film, Ltd., C. Itoh and Co., New York, N.Y.) inserted between the articulating joint surfaces. The Pressensor film consists of two thin flexible sheets (combined thickness of 200 um), one containing dye-filled microcapsules (Sheet A) and the other containing a developer substance (Sheet C). Pressure applied to the sheets breaks the Sheet A dye capsules (according to the pressure magnitude) and is recorded as a red stain on the corresponding Sheet C. The density of the red stain varies non-linearly with the magnitude of the applied pressure. Medium range (10 MPa to 50 MPa) Fuji film sheets were sealed and fixed in position relative to each other by sandwiching them between a layer of thin adhesive film (Letracopy PF, Letraset Canada Ltd.). The Fuji film packet dimensions were 1.3 cm x 10 cm, with a thickness of 250 um. Calibration of the Fuji film packets was done by applying various load increments thoughout the film pressure range using a 4 mm flat circular indentor with an Instron 1122 testing machine. As Fuji film is temperature sensitive, the film calibration must be done at the specific in-vivo joint temperature. During calibration, the film was submerged in a water bath, which maintained a water temperature of 35.0 ± 0.1 C.

Specimen Preparation: For animal preparation, standard aneasthetization procedures were followed. Physiological joint loading was provided by stimulation of the quadriceps muscle group through the femoral nerve. A nerve cuff was inserted over the femoral nerve for this purpose. The articular surfaces of the joint were exposed through incisions in the medial and lateral retinaculum. The length of the incisions were sufficient to allow insertion of the Fuji film packet. To provide reference markings of the patellar orientation on the Fuji film, the patella was retracted anteriorly and 3 holes (diameter of 0.9 mm) were drilled through the patella, from the superior to the inferior aspect using a dentist drill. The 3 holes were located such that they would have minimal overlap with the contact regions, in the vicinity of the distal apex, the proximal medial border, and the proximal lateral border. The right cat hindlimb was fixed at three locations: the ilium near the anterior inferior iliac spine, the proximal tibia and the calcaneous. This arrangement produced a fixed knee flexion angle between the tibia and femur of 74 degrees. A digital thermometer was inserted into the joint incision. The temperature was maintained at 35.0 ± 1.0 C using an infrared heat lamp. Exposed tissues were continuously soaked in a warm saline solution to avoid drying and degeneration of the knee joint.

Test Protocol: Direct joint contact measurements were obtained for a given knee flexion angle, for a maximal tetanic contraction of the quadriceps muscle group. The Fuji film packets were inserted between the articulating surfaces of the joint by retracting the patella and pulling the the film through the joint space from lateral to medial side. Once the film packet was positioned, the patella was gently released. The nerve stimulation parameters were: excitation voltage of 2.0V, frequency of 100 Hz, pulse

duration of 0.1 ms, and stimulation duration of 1.5 - 3.0 s. Prior to muscle stimulation, the static position of the Fuji film with respect to the retropatellar surface was recorded by pressing blunt probes through the 3 patellar holes onto the Fuji film surface. The femoral nerve was stimulated, causing a maximal contraction of the quadriceps muscles. During the contraction, the probes were inserted and pressed against the film to provide dynamic reference marks of the retropatellar surface. Following the muscle stimulation, the patella was retracted again, and the film strip was repositioned for the next recording. The muscle was given a 2 minute recovery period between contractions. Ten recordings of the pressure were obtained. Only pressure stains which were assessed to be similar visually were accepted.

Variations in joint contact area and loads were introduced surgically by transecting the ACL. The hindlimb was positioned such that the ACL surgery could be performed without removing the limb from the fixture. This allowed a direct comparison between the results for the intact and surgically manipulated joint. The joint loading recordings were repeated as outlined for the intact joint.

The patellofemoral contact pressure recordings and calibration stains were digitally scanned and converted into high resolution pressure profiles using a modification of the method of Singerman et al. (1987). The spatial resolution for data analysis is 2300 pixels / mm^2. This method allows contact pressure data to be presented as contour plots, and provides evaluations of total contact area, mean contact stress, and peak local contact stress.

RESULTS

Contact pressure recordings were obtained for one cat patellofemoral joint at a given flexion angle of 74 degrees for the intact joint condition (Figure 1) and the ACL transected joint condition (Figure 2). For both ACL conditions, the contact region occured in the proximal third of the retropatellar surface. For the intact joint, the contact pressure was relatively evenly distributed in the distal region. However, in the proximal contact region, higher pressures occured laterally. Comparatively, the contact region for the ACL transected joint is larger than the intact joint. The contact pressure pattern for the ACL transected joint is also different than that for the intact joint. Higher contact pressures are located medially in the distal contact region and migrate laterally in the proximal contact region.

The patellar movement during muscular contraction is indicated by the relative position of the three reference marks between the static and dynamic conditions. The marks appear as small dark circles on the film. Comparison of the relative position between any pair of reference marks for the intact ACL indicates that the primary movement of the patella is translation, of approximately 1.5 mm (Figure 1). The movement direction is indicated by an arrow between the pair of distal markers. For the ACL transected joint, the dynamic movement of the patella was greater (Figure 2). The primary movement was also translation, of approximately 2.5 mm. A tendancy towards lateral rotation was also noted on 5 samples.

DISCUSSION

The preliminary results indicate that in-vivo joint contact areas and loading can be measured using Fuji Pressensor film. Although the quantitative results are currently being analyzed, qualitatively the contact areas and pressures can be recorded repeatably. With the use of the three reference markers, the methodology can also provide insight into patellar movements associated with each joint configuration and ACL condition. These results have important implications for use in OA injury models.

Changes in joint stability produced by the ACL transection resulted in changes in contact area, contact pressure and patellar movement patterns which were readably detectable with Fuji Pressensor film. With the given limb fixation, increased joint mobility associated with ACL transection would be manifested as increased movement of the femur and changes in joint loading. We speculate that the increase in contact area may be due to sliding of the joint surfaces during muscular contraction or by contact with regions of the articulating surfaces which would not usually contact under normal physiological conditions. The pronounced cat femoral condyle geometry combined with the magnitude and alignment of the quadriceps muscle force along the femoral sulcus are speculated to provide significant constraints to the patellar mediolateral range of motion. Additionally, these constraints will provide local regions of stress concentrations, which could promote degeneration of articular cartilage with repeated use.

The methodology presented here will be used to systematically evaluate joint contact loading profiles for a series of ACL transected joints which have been allowed different healing periods. The direct joint contact loading information provided by this method can provide valuable insights into the influence of various mechanical factors on the development of OA.

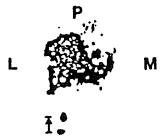

Figure 1: Pressure contact print for intact joint, arrow indicates direction of patellar movement. M = medial, L = lateral, P = proximal. (150% magnification).

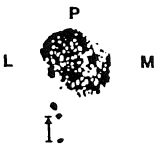

Figure 2: Pressure contact print for ACL transected joint, arrow indicates direction of patellar movement. M = medial, L = lateral, P = proximal. (150% magnification).

REFERENCES

Insall J. et al. Clin. Orthop. 88: 67-69, 1972.
McDevitt,C. et al. J. Bone Jt. Surg. 59: 24-35, 1977.
Singerman, R. et al. Exper. Mech. 27: 99-103, 1987.
Visco, D. et al. Transactions of the 36th Annual Meeting of the ORS, New Orleans, (p.559), 1990.

ACKNOWLEDGEMENTS

This study was supported by the Arthritis Society of Canada and the Alberta Heritage Foundation for Medical Research.

A Comprehensive Method of Complete Knee Kinematics and Three-dimensional Patellar Force Analysis

E.A. Giron, R.P. Mikosz, T.P. Andriacchi, G.A. Frey

Department of Orthopedic Surgery
Rush-Presbyterian St. Luke's Medical Center, Chicago, Illinois.

INTRODUCTION

The complex biomechanical relationship between tibiofemoral (TF) and patellofemoral (PF) kinematics (1) and their possible influence on retropatellar forces (RPF) requires that more comprehensive methods be used in cadaveric knee testing. Insufficient quantitative data exists on three-dimensional RPF. In-vitro measurements have been performed using an instrumented patellar replacement (2), however, there may be limitations on the size or style of prosthesis tested and it does not permit measurement of the intact knee. The purpose of this paper is to present on a method of simultaneous kinematic measurement and three-dimensional patellar force analysis in cadaveric knees.

METHODS

Seven fresh-frozen cadaver knees were dissected to expose the quadriceps and hamstring tendons. Care was taken not to disrupt the joint capsule or related ligaments. The knees were sized to fit in a custom designed loading fixture capable of controlled hamstring, quadriceps, and axial tibial compressive loading. Muscle force lines of action were directed along the anatomical axis of the femur. TF and PF kinematics were recorded using two six degree-of-freedom linkages (3) ($\pm$.5 deg., $\pm$.5 mm accuracy). The axes of displacement were similar to those described by van Kampen and Huiskes (1). Force in the patellar ligament was measured with a buckle transducer using the method reported previously (4) ($\pm$9 N. accuracy). The buckle-ligament unit was preconditioned based on the recommendations of Barry and Ahmed (5). The insertion site of the patellar ligament on the tibial tubercle relative to the tibial reference frame and ligament origin on the inferior patellar pole relative to the patellar reference frame were obtained from radiographs. TF and PF kinematic information were used to resolve the quadriceps and ligament force vectors in the patellar reference frame. Their vectorial sum was then represented as two components of shear and a compressive component. The direction of quadriceps pull relative to the patella deviated from the femoral axis subsequent to tendofemoral contact and was analyzed as such. A total load of approximately 340 N was applied. The intact knee was tested using a dominant quadriceps load (1H:2Q) and then a dominant hamstring load (2H:1Q). Full extension was taken as the initial reference position. Data were taken in 10 degree increments to a full displacement of 100 degrees of knee flexion. The RPF were reported as a percentage of the applied quadriceps force. Each knee was then fitted with a posterior cruciate retaining, relatively unconstraining TKR by an orthopedic surgeon using the required instrumentation. Soft-tissue releases were performed when necessary. The above test protocol was then repeated on the resurfaced knees.

RESULTS & DISCUSSION

Fig. 1 shows the M/L component of shear that the patella exerted on the femur for the intact knee. An initial increase in the lateral force component was

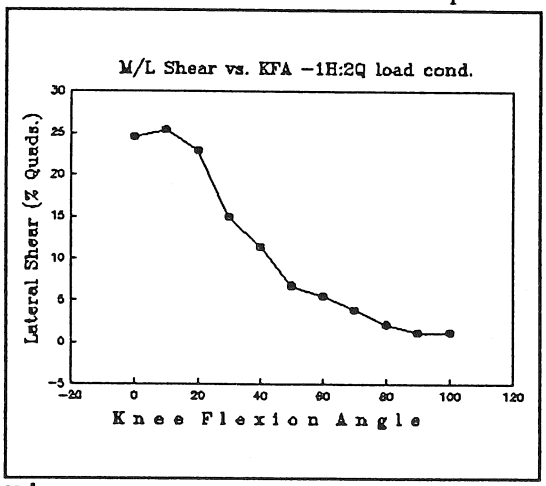

Figure 1

observed in the first 10 degrees of flexion. In the

first 10 degrees of flexion, tibial adduction and internal rotation occurred (fig. 2) which displaced the tibial tubercle medially. The patella also internally rotated slightly (fig. 3). These rotations would result in a medialization of M/L shear.

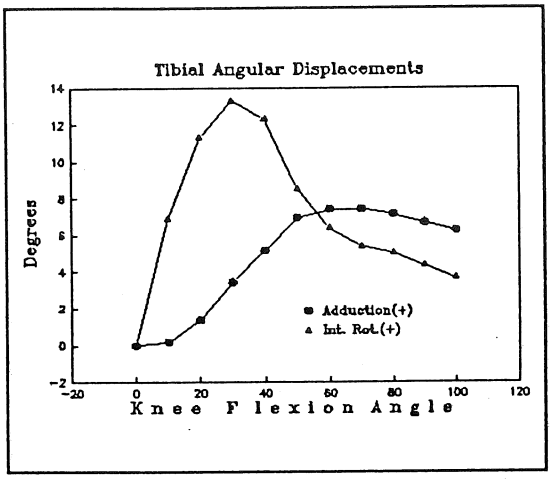

Figure 2

However, the observed increase in lateral shear can be explained by the concurrent medial patellar translation. Between ten and thirty degrees, tibial and patellar internal rotations along with tibial adduction continue but patellar M/L translation switches direction towards a lateral shift. This is

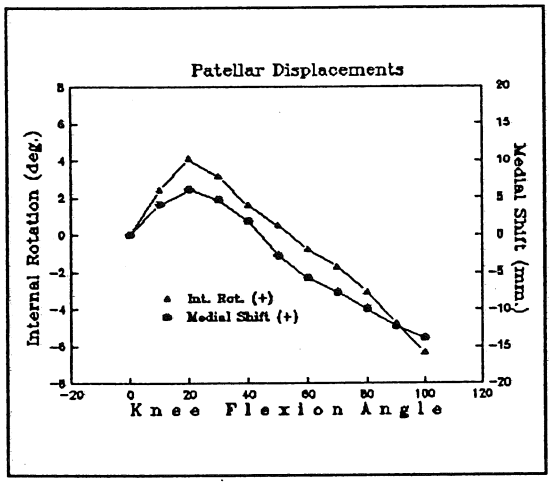

Figure 3

reflected in the rapidly decreasing magnitude of lateral shear. With continuing flexion, the frontal plane of the tibia deviates further from the frontal plane of the patella. As a result, the medializing or lateralizing effects of the tibial tubercle caused by tibial angular displacements become less pronounced. The patella continues to rotate externally which fails to increase the lateral shear. This is due to the small magnitudes of patellar rotation, and also to the significant lateral patellar shift which continues to reduce the lateral force component. The kinematic variability between specimens can vary substantially, especially with an imposed tibial torque (1) as was applied through hamstring tension. Similar kinematic and RPF interactions were observed for the implanted knees. The data demonstrates the complex biomechanical relationship between the RPF and knee kinematics.

REFERENCES

1. van Kampen, A. and Huiskes, R. *J Orthop Res*, 8:372-382, 1990.
2. Singerman, R. et al. *38th Ann Meet Orthop Res Soc*, Wash D.C., 1992.
3. Kinzel, G.L. et al. *J Biomech*, 5:93-105, 1972.
4. Huberti, H.H. et al. *J Orthop Res*, 2:49-54, 1984.
5. Barry D. and Ahmed, A.M. *J Biomech Eng*, 108:149-152, 1986.

ACKNOWLEDGEMENTS

Zimmer

Special thanks to Dr. B.M. Hillberry for his technical support concerning the spatial linkages.

THERMOELASTIC STRESS ANALYSIS OF THE HUMAN PATELLA: EFFECT OF BONE BLOCK REMOVAL AND PATELLAR PROSTHESIS

E.A. Friis[+], F.W. Cooke[+], D.A. McQueen[+¥] and C.E. Henning[¥*]

[+]Orthopaedic Research Institute, Inc., Wichita KS 67214
[¥]Dept. of Orthopedics, Division of Surgery, SFRMC, Wichita KS

INTRODUCTION

Reconstruction of the anterior cruciate ligament (ACL) with an autogenous graft from the central third of the patellar tendon with attached bone blocks from the patella and tibial tubercle is a relatively common surgical procedure. Various shapes of patellar bone blocks have been recommended for use in the graft. Fractures of the patella in ACL reconstructed knees under normal activity have been reported following excision of a large, trapezoidal patellar bone block. McCarroll (1983) The effect of the various patellar bone block defect shapes on patellar stresses was evaluated using thermoelastic stress analysis (TSA).
Complications of ACL injury often lead to degenerative changes in the knee that can lead to total knee joint replacement. This study also examined the effect of bone block removal with subsequent patellar prosthesis insertion on stresses in the patella. The TSA results are compared with previously reported finite element results.

REVIEW AND THEORY

Thermoelastic Stress Analysis (TSA) was used to experimentally measure patella surface stress. TSA utilizes the thermoelastic effect in materials to correlate small temperature changes of the specimen surface with the change in surface stress under cylic loading and adiabatic conditions. In TSA using the SPATE 9000 system, temperature changes of points on the cyclically loaded specimen surface are sequentially measured. For isotropic materials under cyclic loading and adiabatic conditions, the relationship between the reversible temperature change and the corresponding change in the first stress invariant is linear according the relationship

$$\Delta T = - K_m T \Delta I_1$$

where ΔT is the peak-to-peak change in temperature (which corresponds to the maximum and minimum loads), K_m is the thermoelastic constant of the material, T is the mean temperature of the structure, and ΔI_1 is the change in first stress invariant corresponding to the maximum and minimum loads applied .

Bone is anisotropic in both its mechanical and thermal properties. A thermoelastic coating was applied to the surface of the patellae to eliminate the effects of thermal anisotropy. This coating reflects patella surface strains in a manner similar to a strain gage. The first stress invariant in the coating was measured and related by the ratio of Young's moduli to the stress in the patella. The major criteria for the thermoelastic coating material selection were: 1. relatively strong thermoelastic response, 2. isotropic thermal and elastic properties, 3. ease of application, 4. fast curing, and 5. low thermal conductivity.

The purpose of this study was to determine the effect of bone block removal and prosthesis insertion on patellar stresses using TSA with a thermoelastic coating. These results are compared to a finite element analysis of the patella.

PROCEDURES

Several potential coating materials were selected and tested by TSA as a coating on a tensile specimen. A cyanoacrylate ester commonly used for bonding of strain gages was selected as the most suitable thermoelastic coating material for bone. The minimum coating thickness required such that the temperature response of the bone did not alter the temperature change at the surface of the coating was estimated to be 0.5 mm from a one-dimensional mathematical analysis using average reported values of thermal properties of bone and the polymer. TSA testing of a bone sample with varying coating thickness confirmed this analysis.

Nine pairs of fresh frozen cadaver knees between the ages of 35 and 80 years (average 54.6 ± 15.3) were prepared for testing by dissecting down to the joint capsule. The patella surface was exposed and defatted in a manner similar to the technique used in bone surface preparation for strain gages. The surface of the intact patella was coated with multiple layers of the cyanoacrylate polymer to build the minimum thickness required.

The knees were placed in a specially designed testing apparatus at 60° flexion. Sinusoidal loads of 0 to 267 N were applied to the patella by pulling the clamped quadriceps tendon at the appropriate Q-angle and quadriceps liftoff. A load cell was placed directly behind the quadriceps tendon clamp to provide the reference signal. Each intact patella anterior surface was scanned using the SPATE 9000 system (Ometron, Inc.) at a sensitivity of 200 mV and frequency of approximately 7 Hz. Subsequent patella surgical modifications were made according to a balanced block design. The surgical modifications performed and evaluated were: 1. intact

or no cut (INTACT); 2. boat-hull shaped bone block excised (BOAT CUT); 3. square shaped bone block excised (SQUARE CUT); 4. intact with patellar prosthesis inserted (INTACT BUTTON); 5. boat shaped bone block excised with patellar prosthesis inserted (BOAT BUTTON); 6. square bone block excised with patellar prosthesis inserted (SQUARE BUTTON). The patellar prostheses used in all tests were the Howmedica polyethylene PCA prosthesis. TSA stress calibration was done by determining the calibration constant of the coating material on a bone specimen under tension with identical sensitivity and frequency as in the patella analysis. A strain gage was placed adjacent to the region of bone with coating and the corresponding SPATE signal was correlated with the strain reading to yield the relationship between stress and SPATE output.

A 3-D finite element model of a typical patella was formed using 3211 8-node isoparametric solid elements. Friis, et al. (1991) A quadriceps load of 2400 N was applied. Modifications similar to the surgical bone block excisions done for TSA analysis were made on the patella FEA model. In addition, removal of a large trapezoidal shaped bone block was modeled. The first stress invariant on the anterior surface of each patella model was calculated and plotted in a manner similar to the TSA output.

RESULTS

Figure 1 shows the average values of maximum stress invariant at the superior region of the bone block cut as measured by TSA for all six surgical modification of the patellae. The maximum stress in the cut patellae was about 2.7 times the maximum stress in the intact patellae. There were no statistical differences between the stress measured in the boat cut and square cut patellae. The insertion of a polyethylene patellar prosthesis did not significantly affect the magnitude of the first strss invariant. These trends were similar for the stress invariant measured at other locations on the patellae. In a qualitative evaluation, it was of interest to note that general stress patterns in the intact patella with patellar prosthesis were shifted in a slightly superior direction.

The first stress invariant patterns obtained from FEA models were similar to the TSA stress patterns. Figure 2 shows the magnitudes of FEM calculated maximum first stress invariants in the intact, boat cut, square cut, and trapezoidal cut patella models at the proximal region of the cut. At the same applied load magnitude, the magnitude of I_1 for the intact patella model is comparable to that measured with TSA. The values of I_1 for the boat and square cut patellae did not compare as favorably with the FEA model, underestimating the magnitude of I_1 as compared to the average TSA results. This may be explained in part by the large standard deviation in the TSA data. Excision of the trapezoidal shaped bone block in the FEA model yielded much greater stresses in the patella than the other bone block shapes.

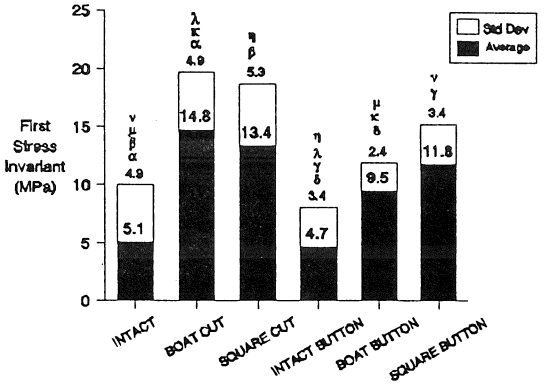

Figure 1. Maximum TSA measured tensile stress invariant at the superior region of the bone block cut. (Matching greek symbols indicate statistical differences at $p<0.05$)

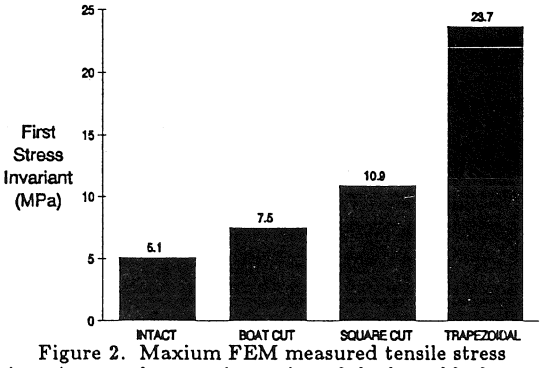

Figure 2. Maxium FEM measured tensile stress invariant at the superior region of the bone block cut. (Stress invariant magnitudes scaled down to reflect load magnitudes applied in TSA)

DISCUSSION

Thermoelastic stress analysis can be a useful tool in measuring full field stress invariants. Use of a thermoelastic coating increased the ease of calibration of the TSA signal and eliminated the effect of intra- and inter- specimen thermal property anisotropy.

REFERENCES

McCarroll, JR Am J Sports Med, 11(1):26-27, 1983.
Friis,EA et al. Trans 37th ORS, Anaheim (p. 575), 1991.

ACKNOWLEDGMENTS

The authors gratefully acknowledge the financial support of the Wesley Foundation for this work, Boeing Airplane Co. for use of their equipment, and Howmedica, Inc. for supplying prostheses and surgical jigs.
*Posthumous

HELICAL MOTION ANALYSIS OF THE ANKLE

N. Murphy, P. Allard and R. Aissaoui
Pediatric Research Center, Sainte-Justine Hospital, Montreal
Faculty of Physical Education, University of Montreal, Montreal

INTRODUCTION

This paper reports the helical motion for the talar bone at the ankle. More specifically, the degree of rotation about and amount of translation along a screw axis as well as the orientation and location of the axis at the ankle are defined. The results support the existance of helical motion. This confirms the need for a helical approach and analysis for accurate description of ankle kinematics.

REVIEW AND THEORY

The biomechanical function of the ankle is the foundation upon which prevention and treatment of foot injuries are based upon. The primary methods used to investigate and analyse the normal and pathological ankle are cinephotography and roentgenograms. These methods are mostly used in planar (2D) investigations. The absence of spatial (3D) research forestalls a complete understanding of the biomechanical function of the ankle (Areblad et al., 1990). Presently, most link segment representations and modelling of the foot and ankle consider the foot complex to be rigid, rotating about the ankle in 2D. The degree to which this actually corresponds to the rotation of the talar bone at the ankle remains undefined (Jahss, 1991). In this study, a stereophotogrammetric technique (Allard et al., 1987) was used to obtain 3D talar marker displacement data. This data was then used to define the helical motion of the talar bone at the ankle.

PROCEDURES

The experimental set-up consisted of four motorized still cameras, one mounted at each corner of a rectangular baseboard. At the center of the baseboard, a calibration object having 36 fiducial marks was used to calibrate the cameras and estimate the 3D reconstruction error (Murphy et al., 1991). The device removed, a fresh amputated human lower limb was fixed into position. Windows on the lateral side of the ankle were dissected to expose talar bone and malleolus tip surfaces. Three non-coplanar and one osseous marker were then embedded into the talar bone and malleolus, respectively. Stereophotographs of the markers were taken for five consecutive static positions during the motions of dorsiflexion and plantar flexion at the ankle. The movements were induced by a pulley and weight system attached to the primary muscle tendons. This procedure was used with four specimens. The 2D coordinates of the osseous marker displacements were obtained by manual hand digitization. The 3D coordinates were then reconstructed with the Direct Linear Transformation (DLT) technique (Marzan et al., 1975). With Rodriques' formula and the screw matrix (Beggs, 1966 and Bisshopp, 1969) programmed, the degree of rotation about and amount of translation of the talar bone along an ankle screw axis was calculated for each of the five consecutive positions. Additionally, the orientation with respect to the anatomical planes of the foot and location with respect to the lateral malleolus for the axes were calculated. Finally, to establish motion repeatability for the talar bone at the ankle, stereophotographs of the markers were taken for five consecutive static positions during five movements of dorsiflexion. The 3D pattern of motions were then compared.

RESULTS

The reconstruction error for the osseous marker 3D coordinates was estimated to be 0.36mm. For the five consecutive movements of dorsiflexion, talar bone motion was repeatabile. More specifically, the correlation coefficients obtained between the five patterns of motion were superior to 0.9. The helical motion of the talar bone about the ankle axis for the movements of dorsiflexion and plantar flexion are reported in Table 1.

Table 1. Total rotation and translation about the screw axis.

Specimen	Rotation (deg)	Translation (mm)
1	55.25	2.71
2	49.73	5.88
3	59.75	3.83
4	45.83	2.96

For the orientation and location of the screw axis, the mean and (standard deviation) for the five positions are reported in Tables 2, 3 and 4.

Table 2. Mean orientation with (standard deviation) for the screw axis with respect to the anatomical planes.

Specimen	In frontal plane wrt lat-med axis (deg)	In sagittal plane wrt pos-ant axis (deg)	In transv. plane wrt pos-ant axis (deg)
1	9.20 (7.23)	21.73 (15.80)	69.12 (1.18)
2	10.06 (1.85)	31.96 (9.20)	72.81 (8.23)
3	7.44 (1.26)	23.46 (5.14)	72.52 (6.38)
4	4.42 (2.76)	11.26 (7.74)	68.35 (2.08)

wrt - with respect to
transv - transverse
lat-med - lateromedial
pos-ant - posteroanterior

Table 3. Mean location with (standard deviation) for the screw axis with respect to the lateral malleolus.

Specimen	Distance inferior (mm)	Distance anterior (mm)
1	4.21 (0.98)	9.46 (4.67)
2	8.05 (1.88)	6.28 (2.15)
3	6.20 (2.28)	8.80 (4.47)
4	7.35 (2.26)	6.72 (3.54)

DISCUSSION

The results support that the pattern of motion for the talar bone at the ankle for movements of dorsiflexion and plantar flexion are repeatable. The values in Table 1. illustrate the presence of talar bone translation along the ankle axis. This confrms the presence of helical motion for the talar bone at the ankle. More specifically, for the combined four specimens, a mean rotation of 52.64 (6.12) degrees with a translation of 3.84 (1.44) mm was observed. The mean orientations (Table 2.) and locations (Table 3.) for the screw axis during the movements are within the ranges reported in the literature. It is important to note that, except for the mean orientation with respect to the posteroanterior axis in the sagittal plane for specimen 1, the variability of the screw axis during the movements is inferior to 10 degrees. Additionally, the variability in location of the screw axis during the movements is inferior to 5mm. For an accurate kinematic description of the ankle, a helical approached should be considered. Although that only four specimens were used to conduct this study, the results illustrate the presence of helical motion at the ankle.

REFERENCES

Areblad, M. et al. J. Biomech., 23, 933-940, 1990.
Allard, P. et al. Eng Med & Bio., Sept., 31-36, 1987.
Beggs, J.S. Adv. Mech., Macmilan, 1966.
Bisshopp, K.E. J. Eng. Ind., Feb., 179-185, 1969.
Jahss, M.H. Disorders of the FOOT and ANKLE. Medical and Surgical Management., Saunders, 385-599, 1991.
Marzan, G.T. et al. Symp. on Close-Range Photogram. Syst., 420-473, 1975.
Murphy, N. et al., J. Biomech., 24, 261, 1991.

TRANSLATIONAL AND ROTATIONAL JOINT POWER TERMS IN A SIX DEGREE-OF-FREEDOM MODEL OF THE ANKLE COMPLEX

Frank L. Buczek [1], Steven J. Stanhope [2], Thomas M. Kepple [2], & Karen Lohmann Siegel [2]

1. National Institute of Arthritis and Musculoskeletal and Skin Diseases
2. Biomechanics Laboratory, Department of Rehabilitation Medicine
National Institutes of Health (NIH), Bethesda, MD, USA

INTRODUCTION

Several projects currently underway at NIH are using joint powers (JPs) to describe normal gait or to quantify changes due to treatment in pathological gait. JP estimates must be reliable and consistent with the six degree-of-freedom (6 DOF) model used for inverse dynamics. Accordingly, JP calculations include translational terms not present in traditional models. Historically, two-dimensional link segment models have assumed that pin-joints exist between adjacent segments, allowing a single rotational degree of freedom. Here, the *translational* velocity of the assumed joint center (JC) is the same on each segment forming the joint. As a consequence, translational powers cancel across the joint, leaving only rotational powers as in:

$$JP = \mathbf{M} \cdot \omega_j \qquad (1)$$

where, $\mathbf{M}$ is the net joint reaction moment, and ω_j is the relative joint *angular* velocity.

In a 6 DOF joint model, 3 rotations and 3 translations are permitted. As implemented at NIH, an assumed "joint center" is determined from palpation during a static subject calibration trial. Following rigid body mechanics, velocities of the JC calculated for each segment during walking are typically unequal. The difference in velocities, ΔV, can arise due to actual joint translations, due to placement of the JC away from true axes of rotation, and due to measurement artifacts. Here, translational powers no longer cancel, requiring a more robust equation for JP:

$$JP = \mathbf{M}_d \cdot \omega_d + \mathbf{M}_p \cdot \omega_p + \mathbf{F}_d \cdot \mathbf{V}_d + \mathbf{F}_p \cdot \mathbf{V}_p \qquad (2)$$

where, $\mathbf{F}$ is a joint reaction force, $\mathbf{V}$ is a translational velocity of the JC, and subscripts d and p indicate distal and proximal segments. After appropriate substitutions:

$$JP = \mathbf{M} \cdot \omega_j + \mathbf{F} \cdot \Delta \mathbf{V} \qquad (3)$$

It can be shown that JP calculated using Equ.3 is independent of the point chosen for JC (including points along the helical axis). As such, the inclusion of $(\mathbf{F} \cdot \Delta \mathbf{V})$ provides reliability in JPs not available in pin-joint models. The purpose for this paper is to illustrate the importance of translational JP terms by comparing JP calculated for the ankle complex, including and excluding $(\mathbf{F} \cdot \Delta \mathbf{V})$.

METHODS

Five normal males were studied, with average age, height, and body mass equal to 37±6y, 181±8cm, and 73±7kg, respectively. Subjects walked at a velocity of 0.69 statures/s (±2.5%). Anthropometric data were collected for the estimation of body segment parameters. Kinematic data for one full stride were collected using a VICON system at 50Hz; ground reaction forces (GRF) were collected using two AMTI force plates at 200Hz. Three targets were fixed to the foot, with four each fixed to the shank, thigh, and pelvis. Anatomical landmarks were targeted for subject calibration. Kinematic and GRF data were low-pass filtered at 6 and 15 Hz, respectively. Using an in-house program for 6 DOF inverse dynamics, JPs for ankle complex rotation axes were calculated per Equs. 1 and 3. Intra-subject variability (N=5) was studied for one random subject. Inter-subject variability (N=25) was studied for JP normalized by body mass. A coefficient of variability (CV) was calculated for ensemble averages as the root mean square of standard deviations divided by the range in mean values. For each JP curve, bands of ±2 standard deviations (±2sd) were included. Where bands for Equ.1 did not overlap those for Equ.3, further statistical tests are planned.

RESULTS AND DISCUSSION

Figure 1 presents data for intra-subject variability, with panels 1a, 1b, and 1c representing JP for 3 rotational axes. (JPs as presented for these axes cannot be summed for total power at the joint; $(\mathbf{F} \cdot \Delta \mathbf{V})$ terms will be over-represented.) Panel 1a shows little difference between traditional and 6 DOF JPs for ankle dorsi/plantar flexion. Panel 1b shows differences in basic shape and in magnitudes for ankle complex in/eversion. Bands of ±2sd did not overlap in early stance and near heel rise (see circles on solid lines). Similar results are shown in panel 1c, foot ad/abduction. It is curious that JPs for corresponding circles in panels 1b and 1c are opposite in sign. The reason for this is under investigation. Figure 2 presents data for inter-subject variability, with results similar to Figure 1. It is concluded that translational power terms are important theoretically and practically in 6 DOF joint models.

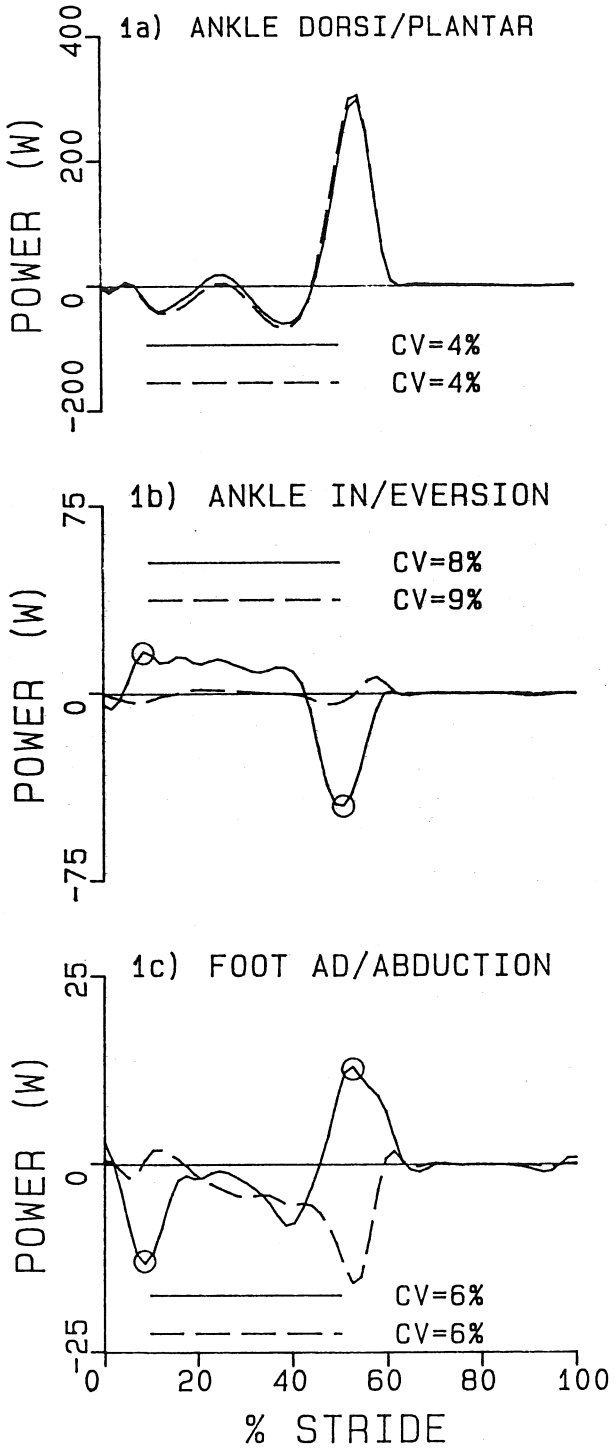

Figure 1. Intra-subject ensemble average joint powers (N=5) for the ankle complex. Solid lines indicate powers calculated by ($\mathbf{M}\cdot\omega j + \mathbf{F}\cdot\Delta V$); dashed lines by ($\mathbf{M}\cdot\omega j$). Circles indicate regions where ± 2 standard deviation bands did not overlap.

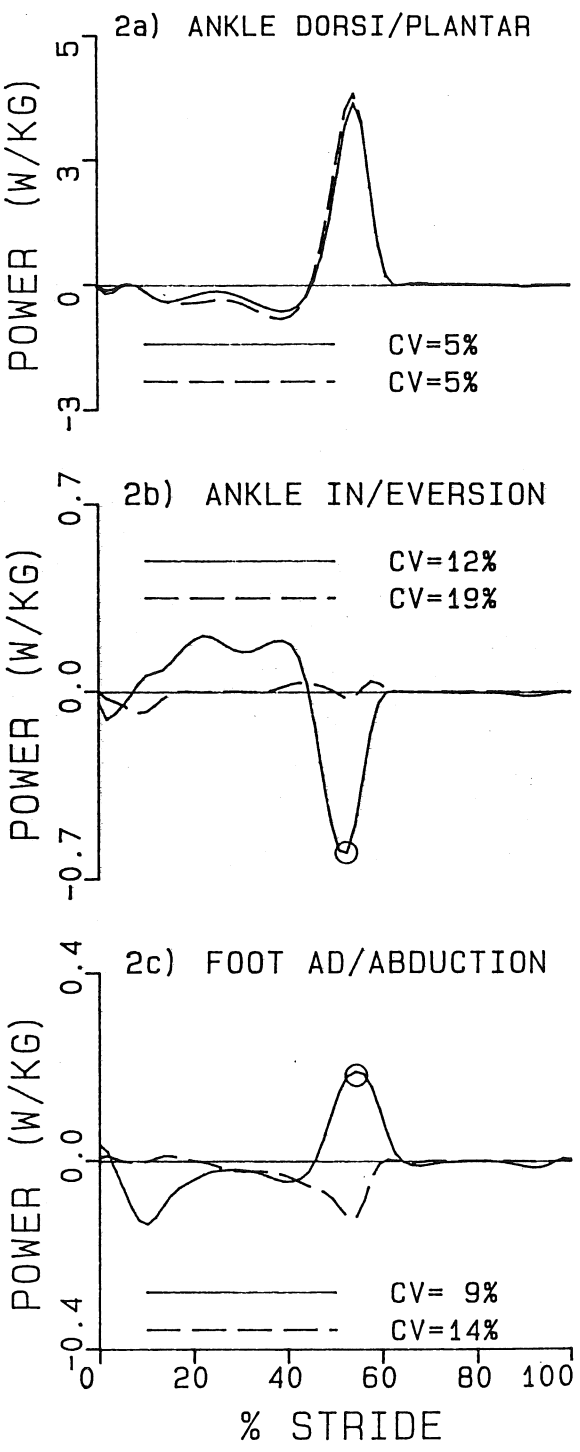

Figure 2. Inter-subject ensemble average joint powers (N=25) for the ankle complex. Solid lines indicate powers calculated by ($\mathbf{M}\cdot\omega j + \mathbf{F}\cdot\Delta V$); dashed lines by ($\mathbf{M}\cdot\omega j$). Circles indicate regions where ± 2 standard deviation bands did not overlap.

FUNCTION OF CAT PLANTARIS IN ANKLE EXTENSION AND DIGIT FLEXION: A QUANTITATIVE APPROACH

G. Brooks, W. Herzog†, T. Leonard, T. Allinger

†Human Performance Laboratory, The University of Calgary, Calgary, Canada.

INTRODUCTION

Force sharing among muscles has been explored as a method to study mechanisms underlying movement control and to determine forces acting on musculoskeletal structures. Direct force measurements on the cat triceps surae and plantaris muscles have frequently been used as an experimental solution to the muscle force sharing problem. Walmsley et al. (1978) pioneered these studies by measuring the force of the cat soleus and medial gastrocnemius muscles for a variety of movement conditions. Force measurements involving the cat plantaris muscle were performed by Abraham and Loeb (1985) and by Herzog and Leonard (1991). The plantaris muscle in the cat has a substantial size and, therefore, is assumed to play a major role in ankle extension in the cat.

REVIEW AND THEORY

Quantification of the contribution of the plantaris muscle to total ankle extensor moments is problematic due to the type and location of the plantaris insertion. The plantaris tendon wraps around the posterior aspect of the calcaneus and either side of the tendon is attached to the bone via heavy fascia. The middle portion of the tendon is not attached to the calcaneus and is continuous with the origin of the flexor digitorum brevis muscle on the plantar surface of the foot. Goslow et al. (1972) suggested that this anatomical arrangement of the plantaris insertion site may permit the plantaris to function in parallel with the triceps surae muscles in ankle extension, and to work in series with the flexor digitorum brevis (FDB) in digit flexion. Abraham and Loeb (1985) measured plantaris forces distal to the calcaneus on the FDB tendon in chronic cat preparations. Although the peculiarities of the plantaris insertion are discussed therein, all forces recorded on the FDB tendon were referred to as plantaris forces in the accompanying figures, thus implying a direct and in-series arrangement of these two muscles.

The roles of the cat plantaris in ankle extension and in digit flexion have been studied qualitatively (e.g. Goslow et al. 1972; Abraham and Loeb 1985). However, quantitative data establishing the transfer of force from the plantaris tendon proximal to the calcaneus onto the FDB tendon distal to the calcaneus are not available.

The purpose of this study was to provide quantitative insight into the transfer of force from the cat plantaris muscle across the calcaneus to the flexor digitorum brevis tendon, and vice versa, for varying ankle joint configurations and variable force levels. Quantitative knowledge of these relations may help to improve our understanding of the dual function of the cat plantaris muscle, and may serve in determining the force sharing properties of the plantaris with the triceps surae group.

PROCEDURES

Muscle force measurements were performed on the left hindlimb of three male cats weighing 40N on average. One "E"-shaped tendon force transducer as described by Walmsley et al. (1978) was placed on each the plantaris tendon (PLT) proximal to the calcaneus and the FDB tendon (distal to the calcaneus but proximal to the flexor digitorum brevis muscle). The cat was placed in an external fixation device which provided constant knee (90°) and metatarsophalangeal (180°) joint angles while ankle joint angles could be manipulated. Forces were recorded for stimulation of the plantaris as well as for passive pulling on the plantaris and FDB tendons, for varying ankle joint angles. Muscle temperature was maintained between 35 and 38° Celsius and the region of study was continuously kept moist using a warm saline solution throughout surgery and data collection. Force transducers were calibrated in a terminal experiment by detaching the most posterior part of the calcaneus from the foot and detaching the paw at the talocrural joint. This allowed FDB and PLT to hang freely, in linear fashion, allowing an in-series calibration of FDB and PLT transducers simultaneously. Known weights (5N-90N) were hung from the most distal portion of the tendon and a regression approach was used to find the best relation between force and tendon force transducer signals.

RESULTS

The results from all three animals were similar in the trends they demonstrated. Data presented in this section provide selected results from all three animals.

Figure 1 shows the peak forces measured at the PLT and FDB transducers as a function of ankle joint angle. The results were obtained from a single animal for stimulation of the PLT muscle alone; the FDB was denervated. Peak PLT forces depend strongly on the ankle joint angle. The FDB transducer shows some force at each joint configuration, indicating that there must be a transfer of PLT force to the FDB tendon, since the FDB is denervated. The ratio of PLT and FDB forces is less than 1.0 for ankle joint angles ranging from 60°-110°, close to 1.0 for an ankle joint angle of 120°, and for joint angles exceeding 120°, the ratio exceeds 1.0. This indicates an apparent dependence of the transfer of force from PLT to FDB on ankle joint angle. The relation between the PLT force and the FDB force was quantified using a linear regression approach and yielded a strong correlation between PLT and FDB forces at an ankle joint angle of 140° ($r^2 = 0.87$), and an almost perfect correlation at ankle joint angles of 70° and 110° ($r^2 = 0.99$ in both cases). Results of a series of passive pulls on the PLT tendon demonstrated trends similar to those found in the active experiments.

Although the stimulation of the FDB muscle alone was not successful, passive pulls on the FDB tendon provided some information regarding force transfer from the FDB over the calcaneus to the PLT tendon (Figure 2). The ratio of force transfer from FDB to PLT was less than the transfer from PLT to FDB in all animals and was ankle joint angle dependent. The ratio of force transferred decreased as the ankle joint angle increased. In fact, there was virtually no force transferred from the FDB to the PLT tendon at an ankle joint angle of 150°. (Figure 2b) Furthermore, the amount of force transferred to PLT was not linearly related to the force of pull on the FDB tendon and it appeared to

reach a specific maximal level that was related to the ankle joint angle. This maximum decreased as the ankle joint angle increased and was in the range of 26-27N for an ankle joint angle of 70° (figure 2a.), 8-9N for an ankle joint angle of 110°, and approaching 0-1N for an ankle joint angle of 150° (figure 2b.).

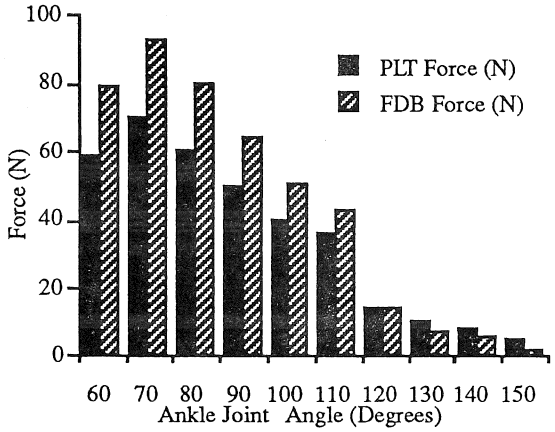

Figure 1. Peak plantaris (PLT) and flexor digitorum brevis (FDB) forces for active stimulation of the plantaris muscle at varying ankle joint angles and constant knee (90°) and metatarsophalangeal (180°) joint angles. Results shown were obtained from one animal.

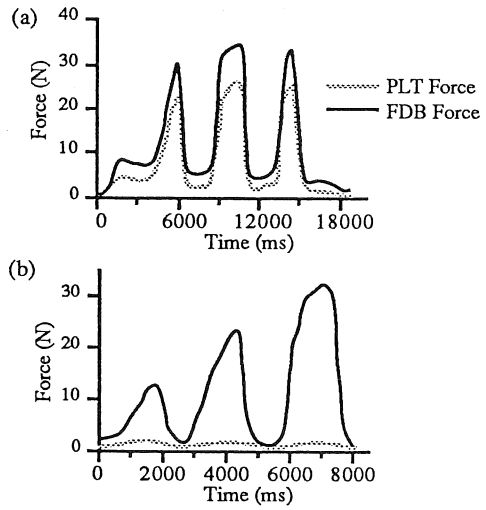

Figure 2. Force-time histories of plantaris (PLT) and flexor digitorum brevis (FDB) muscles during consecutive passive pulls on the flexor digitorum brevis tendon at ankle joint angles of 70° (a) and 150° (b). Results shown were obtained from one animal.

DISCUSSION

It appears that some force transfer from PLT to FDB is possible. This force transfer seems to be dependent on the ankle joint angle, dismissing the possibility of a direct and unique in-series arrangement as implied by Abraham and Loeb (1985) in their chronic measurments of plantaris forces on the FDB tendon.

The combination of the results found in both the active stimulation of the plantaris muscle and in the passive pulls suggests that the amount of force transfer from PLT to FDB decreases as the ankle joint angle increases. Thus, during cat locomotion, it would be expected that as the ankle joint angle increased throughout the stance phase, the effectiveness of PLT as a digit flexor would decrease thus possibly increasing its contribution to the ankle plantarflexion moment. This result agrees in principle with the suggsetion of Abraham and Loeb (1985) that the force exerted by PLT was distributed in time between digit flexion and ankle plantarflexion. Furthermore, the finding that some transfer of force may occur from FDB to PLT at ankle joint angles of up to 110° supports the suggestion by Abraham and Loeb (1985) that large length changes of PLT during the early part of the stance phase may be associated with passive dorsiflexion of the digits.

Goslow et al. (1972) suggested that the PLT functions in parallel with the triceps surae muscles in ankle extension and in-series with the FDB in digit flexion. This notion of a dual function of PLT as an ankle extensor and as a digit flexor is supported by the finding that a force transfer from PLT to FDB is possible and the degree of force transferred is dependent on the ankle joint angle.

The dual function of the plantaris has implications in the consideration of muscle load sharing between the triceps surae and plantaris muscles. This relevance is due to the fact that the plantaris could not achieve ankle extension and digit flexion independently. If, for example, 65% of the force exerted by plantaris at a certain instant in time is transmitted to the calcaneus via the partial plantar insertion, then this force would contribute to ankle extension but would not be available for digit flexion and vice versa. Thus, when considering the amount of force which plantaris contributes to a given ankle extensor moment, the force transferred to the metatarsophalangeal joint via the FDB tendon should also be considered. Furthermore, since the ratio of force transferred from the plantaris to the FDB appears to be ankle joint angle dependent, the ankle joint configuration must be taken into consideration in the determination of the contribution of the plantaris to the ankle extensor moment.

In conclusion, the results of this study demonstrate force transfers from PLT to FDB and vice versa. The ratio of force transferred was dependent on the ankle joint angle. The transfer of force from PLT to FDB was, in general, a direct linear relationship, however, the transfer of force from FDB to PLT was not linear and did not result in a unique functional relation. Thus, the FDB and PLT appear to interact in a complex way that depends on the mechanics of the partial calcaneus insertion of the PLT/FDB tendons.

REFERENCES

Abraham, L.D. et al. *Exp. Brain Res.*, 58, 580-593, 1985.
Goslow et al. *J. Morph.*, 137, 335-352, 1972.
Herzog and Leonard. *J. Biomechanics*, 24, 31-39, 1991.
Walmsley B. et al. *J. Neurophysiol.*,41, 1203-1216, 1978.

ACKNOWLEDGMENTS

This study was supported by an operating and a summer student grant from NSERC of Canada.

THE EFFECTS OF VARIOUS BACKPACK LOADS ON LOWER BODY JOINT TORQUES

Ki-Hoon Han, Everett Harman, Peter Frykman,
Michael Johnson, Franklin Russell and Michael Rosenstein

U.S. Army Research Institute of Environmental Medicine
Natick, MA 01760-5007, U.S.A.

INTRODUCTION

Despite the widespread and increasing use of wheeled vehicles for transport, carriage of loads on the back is still widely practiced, particularly in less technologically developed countries, in the military, and among recreational hikers. Increased understanding of the mechanics of load carriage can lead to injury reduction and enhanced performance through improvements in equipment, technique, personnel selection, and physical training.

REVIEW AND THEORY

Net torques produced by muscles about the major lower extremity joints have been calculated from films of subjects walking and force platform data (1,2,3). However, the effects of carrying loads on joint torques have not yet been reported. Our study was designed to assess the effects of carrying various loads on net joint torques about the ankle, knee and hip.

PROCEDURES

Sixteen normal, physically fit, adult males were filmed at 60 Hz from the right side with a Locam 16 mm movie camera as they carried backpacks loaded with 6, 20 and 47 kg across a force platform, in balanced order. Their walking speed was visually cued at 1.3 m/s using a specially designed device. Muscle EMG activity was monitored via electrodes on the quadriceps and gastrocnemius. The film images were rear-projected onto an Altek digitizer, where the major body joints as well as two points on the pack were hand digitized. After digital filtering, the film and force platform data were processed, using the link segment approach (4), to produce time histories of joint torques about the ankle, knee and hip.

RESULTS

Actual walking speed determined from the films was 1.34±.05 m/s, with no difference between loads. Figures 1, 2 and 3 respectively show net torque about the right ankle, knee and hip under each load condition as a function of percent of stride (0% and 100% = right foot heelstrike), where each point on each curve represents the mean of all subjects. Positive torque values indicate counterclockwise, and negative values clockwise torque exerted by the muscles on the body segment distal to the joint when the body is viewed from the right side.

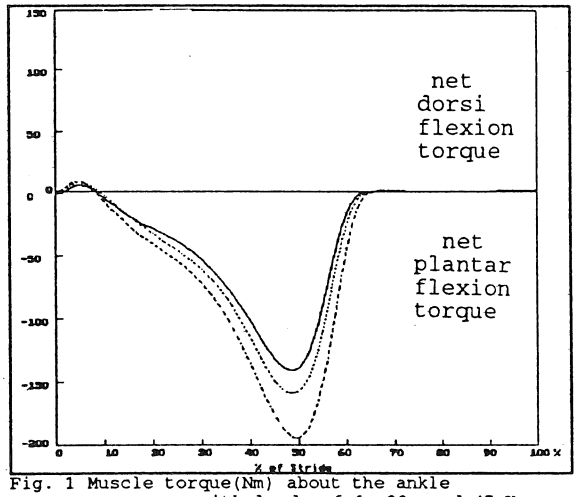

Fig. 1 Muscle torque(Nm) about the ankle with loads of 6, 20, and 47 Kg.
_____ = 6 kg ..... = 20 kg _ _ _ _ = 47 kg

Torques about all three joints clearly increased with load over most of the stride. For the ankle and knee, peak torque increased significantly ($p<.05$) with load, while for the hip, the effect of load on peak torque fell just short of significance.
Table 1 shows the percentage increases of body-plus-pack load and peak torques about the ankle, knee, and hip. It can be seen that for the ankle, peak torque increased less than the percent change in body-

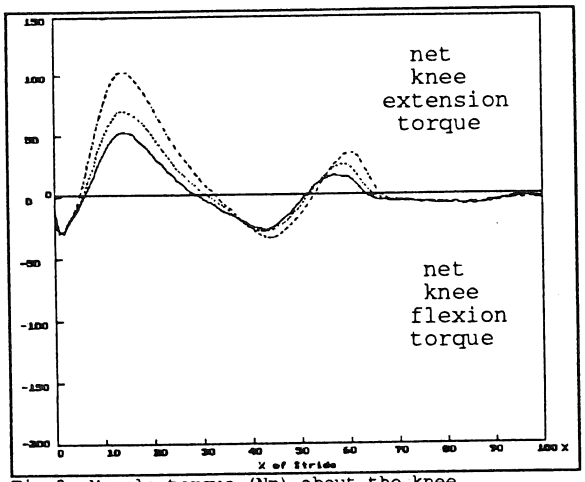

Fig.2 Muscle torque (Nm) about the knee with loads of 6, 20, and 47 Kg.
_____ = 6 kg ..... = 20 kg _ _ _ _ = 47 kg

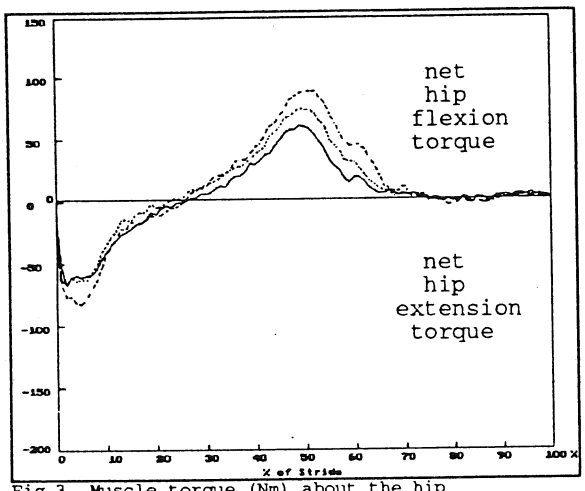

Fig.3 Muscle torque (Nm) about the hip with loads of 6, 20, and 47 Kg.
_____ = 6 kg ..... = 20 kg _ _ _ _ = 47 kg

plus-pack mass, while for the knee and hip, torque increased considerably more than the percent change in total load. As load increased from 6 to 47 kg, mean quadriceps EMG activity increased by 137% while mean gastrocnemius EMG activity increased by only 31%.

Timing of torque application about the ankle and hip didn't seem to be affected by load. However, at the knee, greater load appeared to be associated with later second peaks for both negative and positive torques.

Table I. Changes in body-plus-pack mass and peak torques from their values at the 6 kg load.

	change from value at 6 kg load			
pack mass (kg)	body plus pack mass	peak ankle torque	peak knee torque	peak hip torque
20	+16%	+11%	+31%	+35%
47	+49%	+37%	+104%	+107%

DISCUSSION

The finding that joint torques about the ankle, knee and hip were greater when heavier loads were carried was expected. However, the fact that the torques did not increase in proportion to body-plus-pack mass and that percentage increases were similar for the knee and hip but considerably less for the ankle indicates that carriage technique changed as load increased. The implication, corroborated in part by the EMG data, is that the burden of carrying a heavier load falls more upon the muscles that generate torque about the hip and knee than those that generate torque about the ankle. Further study will be required to identify the specific modifications in walking technique which alter the relative contribution of the different lower body muscle groups as load increases.

REFERENCES

1. Bresler, B. and J. Frankel. Transactions of the ASME, pp. 27-36, Jan. 1950.
2. Cavanagh, P. and R. Gregor. J. Biomechanics, 8:337-344, 1975.
3. Winter, D. and D. Robertson. Biological Cybernetics, 29:137-142, 1978.
4. Winter, D. Biomechanics of Human Movement, Wiley, NY, 1979.

MANUAL MATERIALS HANDLING

Podium Session 21

TRUNK MUSCLE ACTIVITY DURING AXIAL TWISTING MOTIONS

William S. Marras and Gary A. Mirka
The Ohio State University
Department of Industrial and Systems Engineering
Biodynamics Laboratory
1971 Neil Avenue
Columbus Ohio, 43210

This study investigated the activity of the trunk musculature during twisting trunk motions. The study is unique because twisting motions similar to those observed in the workplace were investigated in addition to upright standing twisting postures. The electromyographic (EMG) activity of ten trunk muscles and intra-abdominal pressure (IAP) were recorded from 12 subjects during twisting in different positions and at different velocities. The results show that there is far greater coactivation as well as specific functions associated with the muscles in non-upright twisting postures. These findings also provide information necessary to understand spine loading patterns during occupational twisting.

INTRODUCTION

Many epidemiologic investigations have identified trunk twisting or torsional motions on the job as a factor which increases the risk of suffering an occupationally-related low back disorder (LBD). However, few biomechanical studies have been performed that assess the behavior of the trunk's internal musculature. Such information is important in order to assess the nature of loading on the spine during work.

Limited numbers of biomechanical investigations of axial twisting appear in the literature. Pope et al (3) investigated the activity of the trunk musculature as ten subjects attempted to produce axial torques under static exertion conditions. They found that the external oblique muscle activity was proportional to the axial torque produced. There was also significant differences in muscle activity between the right and left erector spinae muscles. They also found that the antagonist muscle activity was much more substantial than expected.
Most biomechanical assessments have explored muscle behavior under static exertion conditions. The notable exception was McGill (2) who evaluated the EMG activity of six trunk muscles while subjects produced maximum voluntary isometric and isokinetic twisting exertions.
This study found lower EMG activity of the trunk muscles under the isokinetic conditions compared to the isometric conditions. McGill also found significant latissimus dorsi and erector spinae activity related to motion but not involved specifically in the generation of torque. Both Pope et al and McGill suggest that the increased coactivity may play a role in the control or stability of the trunk during twisting.

In both of these previous studies the trunks of subjects were rotated during upright standing. It is rare that this type of torsional load is applied to the trunk during work. Therefore, the purpose of the current study was to evaluate the role of the trunk musculature and IAP when trunk twisting occurs in postures other than the upright posture.

METHODS

Twelve college students served as subjects in this experiment. None had a history of low back disorder and each participated in a training session prior to the day of experimental testing.

A twisting reference frame (figure 1) was used to control isokinetic twisting velocity and position. The frame also measured trunk torque. The variables controlled in this experiment consisted of: 1) axial rotation position of the spine, 2) twisting torque exerted about this z-axis, 3) twisting velocity at three speeds, and 4) trunk position consisting of the combination of two posture related variables.

The normalized EMG of ten trunk muscles identifiable in a transverse cut through the trunk and IAP were the dependent measures of this study.

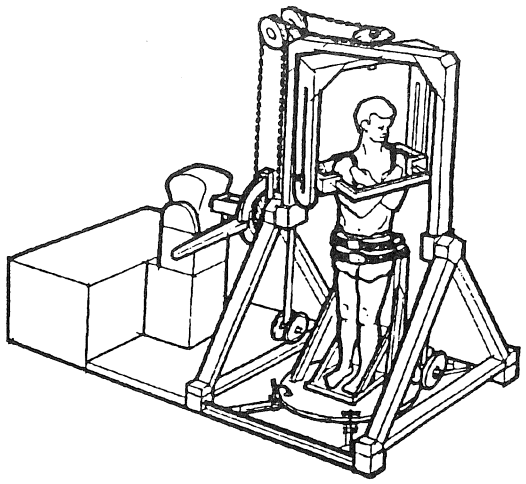

Figure 1. Twisting reference frame.

RESULTS AND DISCUSSION

All muscles were involved in changes of at least one of the experimental variables. It is interesting to note that both the external oblique and rectus abdominus muscle groups played a role in each of the individual experimental variables. Pope et al. (3) found similar results for the external oblique muscles. It is also interesting to note that changes in torque levels and twisting angle resulted in changes in activity of almost all muscles. Changes in twisting velocity resulted in muscle activity changes in all rectus abdominus and external obliques as well as the erector spinae and internal oblique muscles on the left side only. Significant interactions occurred within position and trunk angle conditions as well

as within torque and trunk angle conditions. All of these findings suggest that coactivation does increase during twisting motions and that the velocity of motion is a significant factor in determining muscle usage.

Intra-abdominal pressure was affected by three of the independent variables: twisting torque, twisting angle and trunk position. These results correspond well with earlier research which has shown IAP to be dependent on the trunk position and exerted torque (1). The levels of IAP were low as compared to those elicited during trunk extension exertions indicating that IAP may be performing a somewhat different task during twisting as compared to lifting. The effect of increasing the torque from 10 to 20 ft-lbs was to increase IAP by just over 50%.

Oblique Musculature

The line of action of the right external oblique and the left internal oblique suggest that they would be the primary muscles used to perform this task. This hypothesis is confirmed by the current data. Both were greatly affected by changes in twisting angle, twisting torque and twisting velocity. Increases due to increases in twisting torque from 10 to 20 ft-lbs of torque were on the order of 250%. Increasing the velocity from 0 to 20 deg/sec created increases in these muscles of 30% whereas moving from prerotated positions to fully twisted positions caused increases of approximately 275%. These trends are shown in figure 2.

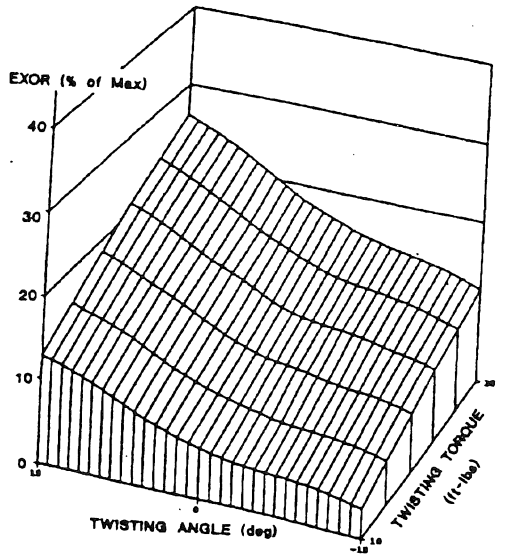

Figure 2. External Oblique activity.

Vertically Oriented Musculature

The muscles in this category are those muscles whose line of action when a subject is standing in a sagittally symmetric posture with no sagittal angle are for the most part oriented in the vertical direction. However, when the trunk is twisted, bent forward or bent to the side, the line of action of these muscles changes to a point where significant moments in the transverse plane can be generated. Therefore, it can not be assumed that these muscles are incapable of exerting twisting torques.

The two muscles in this category exhibiting significant muscle activities were the left erector spinae and the left rectus abdominus, but the role of these two muscles seems to much different. The erector spinae muscle exhibits significant responses to the twisting torque and the twisting angle. The left rectus abdominus on the other hand showed increased activity at twisting angles at the extremes of movement indicating that this muscle was acting as an antagonist muscle for the twisting task.

The right erector spinae muscle showed the opposite trends in muscle activity as compared to all of the other muscles of the trunk. While all other muscles showed significant decreases at the more complicated trunk postures this muscle showed significant increases in EMG activity indicating that it was the primary muscle for maintaining these postures. In addition it appears that it must act to maintain stability as the left erector spinae is adding to the twisting moment. Also, contrary to all the other muscles, the right erector spine had significant increases at the more prerotated postures. Presumably this results because the line of action of this muscle is such that prerotation does not indicate more passive muscle force. Therefore, in order to stabilize the trunk against all the increased passive muscle force exerted by the other muscles its activity must increase.

This study has shown that the muscles activate in unexpected complex manner during job related twisting.
This information could be used as input to EMG-assisted models of the spine to understanding how the spine is loaded during twisting.

REFERENCES

1. Marras WS and Mirka GA: J Orth Res, 8, 824-832, 1990
2. McGill, SM: J Orth Res, 9(1), 91-103, 1991
3. Pope MH et al.: J Orth Res, 4, 288-297, 1986

CAN FATIGUE COMPROMISE LIFTING SAFETY?

J.R. Potvin and R.W. Norman
Department of Kinesiology, University of Waterloo, Ontario.

INTRODUCTION

The purpose of this study was to determine whether fatigue, caused by repetitive lifting, increased the risk of damage to low back tissues by changing the demands on muscles, ligaments and other spinal structures. Eight subjects lifted during a 2 hour session and a short, intense 20 minute session. EMG was used to estimate the loading on trunk and leg muscles and external measures of spine kinematics were used to assess the passive extensor tissue demands continuously throughout each session. The most significant finding of this study was that some, but not all, subjects exhibited changes in lifting mechanics, in response to fatigue, which may have eventually put them at a higher risk of sustaining a low back injury.

REVIEW AND THEORY

Repetitive loading has been implicated in the progressive weakening of muscles, spinal ligaments, intervertebral discs and vertebrae to the point where they may be damaged by forces which do not exceed tissue tolerance limits for single load applications. In particular, increases in erector spinae forces will amplify this effect for the discs and vertebrae because they are loaded most heavily by the internal muscle forces.

Theoretically, fatigue may also precipitate changes in lifting mechanics and the subsequent partitioning of loads amongst spinal tissues. This may result in an acute or progressive overload of tissues not normally needed to perform the task. Extreme spine flexion has been shown to enhance the risk of annulus failure during repetitive compressive loading (Adams and Hutton, 1983a) and increase forces on the facets (Shirazi Adl, 1989). In addition, flexion will increase the forces on the interspinous and supraspinous ligaments making them more susceptible to injury (Adams and Hutton, 1983b) and undesirably increase the anterior shear forces on the discs (Potvin et al., 1991). The flexion may also increase the eccentrically mediated damage of the extensor muscles as they act at greater lengths (Armstrong et al., 1991).

An increase in force asymmetries from bilateral erector spinae muscles as well as coupled moments (lateral bending and/or axial twisting) have also been implicated as risk factors for intervertebral disc damage (Hickey and Hukins, 1980; Frymoyer and Gordon, 1989; Shirazi Adl, 1989). Also, a decrease in lumbar erector spinae forces reduces their shear support contributions and has been shown to result in an increase in anterior shear forces on the lumbar discs (Potvin et al., 1991). To date, little has been done to document the changes in lifting mechanics associated with fatigue so that potential implications for injury could be addressed.

PROCEDURES

Eight male subjects lifted repetitively in the sagittal plane. There was a 20 minute lifting session of relatively high intensity (8 lifts/minute, average load of 20 kg) and a longer session lasting 2 hours at a lower intensity (6 lifts/minute, average load of 18 kg). The subjects performed dynamic lifting movements with an unconstrained, hand held, inertial load. Each "lift" consisted of the subject taking the load from a table at waist height, lowering to the floor, then raising back up to the table.

It was critical to establish that each subject was fatigued before fatigue was used as a factor to explain the changes observed in the dynamic lifting mechanics. Neuromuscular and/or central fatigue were quantified intermittently throughout each session with strength measures and EMG statistics measured during submaximal, isometric contractions as well as a test of trunk extensor muscle endurance at the end of each session. These contractions were performed while subjects stood in a test apparatus which standardized posture and quantified extensor moment.

The theoretical mechanisms of low back injury discussed above were addressed with estimates of erector spinae muscle forces and extensor ligament utilization. Three dimensional spine kinematics were used to estimate lumbar joint rotations and interspinous and supraspinous ligament lengths. Bilateral lumbar and thoracic erector spinae forces were estimated from a combination of EMG and instantaneous muscle lengths and velocities over the whole duration of each session. In addition, bilateral vastus lateralis and external oblique EMG were monitored to reflect the demands on the lower limbs and antagonistic abdominals, respectively.

The 2 hour session was divided into 8 "trials" for each 15 minute interval and the 20 minute session was partitioned into four 5 minute trials. Statistics were performed with the mean and peak levels of estimated muscle forces, EMG, ligament lengths and the spine rotations about three axes for all the lifts in a trial. Ensemble average curves were generated to represent the average time-history of each variable for each trial.

RESULTS AND DISCUSSION

The fatigue assessment variables indicated extensor muscle fatigue for all subjects in the 2 hour sessions and for all but 2 subjects (7 and 8) in the 20 minute sessions. Therefore, in most cases, the changes in lifting mechanics which accompanied the tasks could be associated with the process of fatigue experienced by the subjects. For the group averages, both sessions exhibited similar changes in maximum moment, endurance time and EMG frequency and amplitude characteristics.

There were no variables which showed the same trend for all subjects in either session although there was a significant decrease in the group average of mean and peak vastus lateralis EMG in both sessions and a significant increase in peak spine flexion angle in the 20 minute session. These results indicated

a tendency for subjects to reduce the demands on the lower extremities and to flex the trunk more as they became fatigued.

All of the subjects exhibited a change in at least one of the variables hypothesized to be associated with injury during the lifting tasks. The observations of these changes are summarized for each subject/session in Table 1.

Table 1. A summary of the changes in lifting mechanics observed for each subject as they relate to hypothesized injury mechanisms. (* indicates significant change, ES - erector spinae).

Sess	Injury Mechanism Indicator	Subject							
		1	2	3	4	5	6	7	8
2 hr	↑ passive extensor loads	*	*			*	*		
	↑ flexion rotation	*	*			*	*		
	↑ erector spinae forces			*			*		*
	↑ ES asymmetries	*	*	*		*			
	↑ coupled moments	*							
	↓ ES shear support	*	*			*			
20 min	↑ passive extensor loads	*	*	*		*	*		
	↑ flexion rotation	*	*	*	*	*	*		
	↑ erector spinae forces			*		*		*	
	↑ ES asymmetries	*			*				
	↑ coupled moments								
	↓ ES shear support	*	*						

There were two subjects, in particular, who showed a progressively risky increase in the demands on low back tissues during both the long and short sessions as indicated by increased spine flexion and an increase in the asymmetry of bilateral erector spinae forces. An example of the lumbar and thoracic muscle forces is provided in Figure 1 (for the 2 hour session of subject 2) to demonstrate the progressive decrease in lumbar erector spinae forces in the middle portion of each lift. In this case the spine was approaching (then exceeding) the voluntary limits of flexion as the subject fatigued and the decrease in lumbar forces suggested that there was a progressive increase in the influence of a flexion-relaxation response as the passive extensor tissues began to bear a larger proportion of the extensor moment demands. Conversely, the thoracic forces were generally unaffected by the passive/active tradeoffs occurring in the lumbar region. This response to fatigue was present in both sessions for subjects 1 and 2.

For the reasons discussed previously, the increases in flexion observed for these two subjects are suspected to increase the risk of injury of the intervertebral discs, vertebrae, spinal ligaments and extensor muscles. The intervertebral discs may also be at a higher risk of injury because of the observed increases in asymmetrical erector spinae forces.

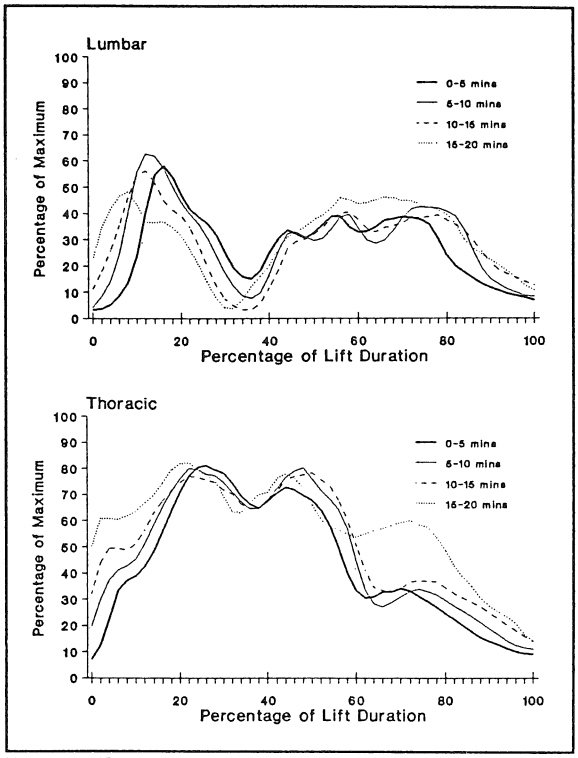

Figure 1. Ensemble average of lumbar and thoracic erector spinae forces for selected trials of subject 2's two hour session. (each trial is the average of approximately 70-80 lifts).

The differences observed between subjects and within sessions demonstrated the sensitivity of the data collection and analysis method to changes in lifting mechanics and tissue loading during long duration, repetitive lifting. Based on the findings of this analysis, it was concluded that individuals differed in their susceptibility to low back injuries during fatiguing dynamic lifting. Some subjects maintained consistent lifting mechanics, even in the presence of quantified trunk fatigue, while others responded by adopting mechanics which have been hypothesized to increase the risk of damaging the posterior ligaments, intervertebral discs, vertebral bodies and/or erector spinae muscles. Reasons for these individual differences remain to be studied.

REFERENCES

Adams, M. et al. *J. Bone Jt. Surg.*, 65:199-203, 1983a.
Adams, M. et al. *Spine*, 8:327-330, 1983b.
Armstrong, R. et al. *Sports Med.* 12:184-207, 1991.
New Perspectives on Low Back Pain, Frymoyer et al., 1989.
Hickey, D. et al. *Spine*, 5:106-115, 1980.
Potvin, J. et al. *Spine*, 16:1099-1107, 1991.
Shirazi Adl, A. *Spine*, 11:915-927, 1989.

BASE OF SUPPORT, TASK FRAGMENTATION AND LUMBAR SPINE LOADING DURING ASYMMETRICAL MATERIALS HANDLING

D. Gagnon[1] and M. Gagnon[2]

[1]Faculté d'éducation physique et sportive, Université de Sherbrooke, Québec, Canada, J1K 2R1.
[2]Département d'éducation physique, Université de Montréal, Québec, Canada, H3C 3J7.

INTRODUCTION

Motion dynamics and asymmetries are key factors in the prevention of injuries to the low back. This study was attempted to document how general motion alterations could change the loading on the lumbar spine during manual materials handling (MMH).

REVIEW AND THEORY

Asymmetrical MMH is predominant in the workplace (Drury et al., 1982) and is associated with higher risks of low back injury (Kelsey et al., 1984). The formulation of general motion principles for MMH may facilitate injury prevention. Such principles could involve stability, change of direction, task fragmentation, range of motion, etc. Asymmetrical MMH has not been approached from this perspective to our knowledge.

Two principles were explored in this study: stability and fragmentation. A reception-loading task was analyzed. It was hypothesized that for an asymmetrical reception-loading task (1) a decrease in the width of the base of support may increase the loading on the lumbar spine and (2) the insertion of a pause may reduce the loading on the lumbar spine.

PROCEDURES

Subjects. Five males (age: 22-39 years; mass: 68-87 kg; height: 1.71-1.88 m) volunteered to take part in the study. None of them had previous MMH experience or a medical history of spine injury.

Tasks. The subjects performed asymmetrical tasks involving the reception and loading of an 11.6 kg box. The box was received from the left side at the waist level and loaded on a shelf. The shelf was adjusted above shoulder level and oriented 90 degrees from the trajectory of the box.

Three task conditions were randomly administered to the subjects: (1) the wide base of support and continuous (WBC) condition, (2) the narrow base of support and continuous (NBC) condition and (3) the wide base of support and fragmented (WBF) condition. A similar feet position was selected for the WBC and WBF conditions by each subject. All the conditions were repeated for a total of 30 trials. This permitted comparisons between the WBC and NBC conditions (stability) and between the WBC and WBF conditions (fragmentation).

Data collection and analysis. Each trial was filmed by two synchronized Locam 16 mm cine-cameras. Each camera was paired with a large mirror to provide 4 views for 3D reconstruction. The spatial positions of 21 anatomical markers were computed by a DLT algorithm. Two AMTI force plates measured the external forces. Data were processed at 50 Hz.

A 3D dynamic model was used to compute the net loading at each anatomical joint (Gagnon, 1990). The net forces and moments were then used in a 3D articular model to estimate the compression and shear forces at the L5/S1 joint. The articular model was adapted from Schultz et al. (1981) and used a double linear optimization approach (Bean et al., 1988).

RESULTS AND DISCUSSION

Maximum net muscular moment and articular forces at the L5/S1 joint were selected for statistical analysis. Six of the 30 trials were rejected because of errors during the digitization process. Another trial was not entirely filmed. This decreased the number of complete cases available for inferential statistics from 10 to 5 and created unequal subject representation. It was thus decided to present exclusively descriptive statistics for all the available trials of each experimental condition.

The results for the maximal net muscular moment are presented in Table 1. The extension was always dominant, followed by positive bending and negative torsion. The results for the maximal articular forces (Table 2) showed that compression was 5 to 6 times larger than shear in all conditions. However, the compression values are

always below the NIOSH action limit (3430 N), except for a few cases of the NBC condition. Unfortunately, no such comparison was possible for the shear forces.

There seems to be no trend in the data to support differences between the experimental conditions. Consequently, as long as one stays within safe limits, the width of the base of support does not appear to be an issue for asymmetrical reception-loading tasks. The findings related to the inclusion of a pause to fragment a MMH task seem in opposition with the application of this same principle to patient handling task (Gagnon et al., 1987). Differences between the two types of activity involving the orientation of translation effort (mainly vertical for box handling vs only horizontal for patient handling) may explain this contradiction. More research may be needed to clarify the application of the fragmentation principle to MMH.

In conclusion, the two hypotheses of this study were rejected. Thus, the principle of stability is not playing a significant role in asymmetrical MMH and clarification of the principle of fragmentation may demand more research.

REFERENCES

Bean, J.C. et al. J. Biomech., 21(1), 59-66, 1988.
Drury, C.G. et al. Hum. Fac., 24(5), 553-65, 1982.
Gagnon, D. Ph.D. Thesis, Un. de Montréal, 1990.
Gagnon, D. et al. Pr. 13th ISB Cnf., 220-22, 1991.
Gagnon, M. et al. Ergon., 30(7), 1013-32, 1987.
Kelsey et al. J. of Orthop. Res., 2, 61-66, 1984.
NIOSH, Work Pract. Guide for Man. Lifting, 1981.
Schultz, A.B. et al. Spine, 6(1), 76-82, 1981.

ACKNOWLEDGEMENTS

Grants from Natural Science and Engineering Research Council of Canada, Institut de recherche en santé et sécurité du travail du Québec, Laurentian University Research Funds and Fonds de recherche de l'Université de Sherbrooke.

Table 1 Mean values (SD) for the maximal net muscular moment components (N.m) about the L5/S1 joint

Net Muscular Moment Component	Wide Base & Continuous (n=9)	Narrow Base & Continuous (n=7)	Wide Base & Fragmented (n=7)
Right Torsion	0(1)	0(0)	1(2)
Left Torsion	-22(9)	-20(8)	-32(6)
Extension	89(32)	85(43)	83(17)
Flexion	-2(3)	0(0)	-9(14)
Right Bending	53(24)	47(22)	30(2)
Left Bending	-16(11)	-10(12)	-7(10)
Resultant	106(26)	102(32)	89(18)

Table 2 Mean values (SD) for the maximal compression and shear forces (N) at the L5/S1 joint

Joint Force Component	Wide Base & Continuous (n=9)	Narrow Base & Continuous (n=7)	Wide Base & Fragmented (n=7)
Compression	2565(631)	2537(874)	2390(395)
Postero-Anterior Shear	-197(80)	-136(58)	-197(60)
Left-Right Shear	-382(179)	-340(205)	-555(95)
Resultant Shear	402(175)	374(181)	578(105)

PIVOTING WITH THE LOAD: AN ALTERNATIVE FOR PROTECTING THE BACK IN ASYMMETRICAL LIFTING

M. Gagnon[1], A. Plamondon[1] and D. Gravel[2]
[1]Département d'éducation physique, Université de Montréal and
[2]Ecole de réadaptation, Université de Montréal, Montréal, Québec

INTRODUCTION

The purpose of the study consisted of investigating three different lifting conditions, two of these combining flexion and twisting of the trunk (full twist and half twist techniques) and a third one consisting of pivoting with the load with minimization of trunk movements relative to pelvis. It was believed that pivoting could provide an alternative to protect the back in asymmetrical lifting. Nine subjects with limited experience were tested with two AMTI force plates and two Locam cameras coupled with two mirrors; dynamic 3D multi-segment models were constructed and the net muscular moments as well as the angular velocities of the trunk relative to pelvis were determined about the three orthogonal axes of the trunk in flexion/extension, lateral bending and twisting. The specific trunk/pelvis positions were expressed in a joint coordinate system with clinical significance (Grood et al., 1983). The results showed that pivoting required larger extension moments but considerably smaller twisting moments than the full twist and the half twist techniques and that these moments were exerted from a more suitable posture when pivoting. The presence of eccentric twisting moments with the twisting techniques may present some potential risks of injuries for the back. Pivoting presents a good compromise to avoid or minimize complex trunk postures and coupled motions.

REVIEW OF LITERATURE

A review of epidemiological data identifies physically heavy work and frequent bending and twisting as important factors in the process of low-back symptoms (Kelsey et al., 1984). In a survey conducted in 9 different industries, it was concluded that torso twisting occurred in 80% of the movements (Drury et al., 1989). In vitro and simulation studies have produced results which emphasize the strain supported by the soft tissues of the spine for forward bending coupled with torsion (Farfan et al., 1970; Adams et al., 1983; Sherazi-Adl, 1989). Moreover, in vivo studies have shown that such a posture was related to increased intradiscal pressure (Andersson, 1985), shear forces as well as compression forces (Mirka, 1988; Mital et al., 1986); it is also believed to affect muscular forces adversely (Kumar, 1980). Maximal efforts of trunk extension decrease with asymmetric trunk angle (Marras et al., 1989); however, the maximal muscular capability of trunk rotators increases for torsion efforts exerted in the direction opposite to the one assumed by the trunk (Gravel et al., 1992). These last results may explain why such postures are so often adopted by the workers in spite of the fact that the structures of the spine may not be adapted to support large exertions in these extreme postures; it may also explain why the management response to the problem consisting of training workers not to twist has failed. In this study, it was hypothesized that pivoting could be less stressful for the back when compared to twisting techniques.

PROCEDURES

Nine students in physical education with limited experience in manual materials handling for different jobs were used as subjects; their mean age was 23.2 yr, their mass, 75.7 kg and their height, 176 cm. The task consisted of moving a 16 kg load from a shelf placed at the subject's left, at a height of 68 cm from the force platform level and to bring it through a 90° position to the right on a shelf at a height of 80 cm. Three modes of lifting were used (Figure 1): the one where the trunk was flexed forward and twisted fully (feet facing the shelf of deposit), another one similar but with half twist (feet in an oblique position) and a third one where the subject was pivoting on his feet and facing the load at all times. The load was handled with an asymmetric and diagonal hand position.

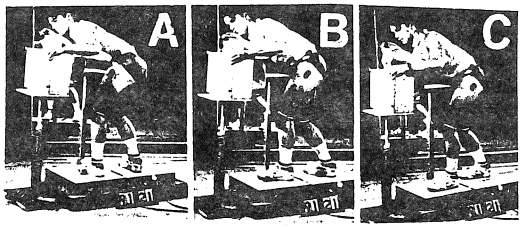

Fig. 1 A) Full twist; b) half twist; C) pivoting techniques.

The data were collected using two AMTI force plates, one under each foot, and two 16 mm Locam cameras which where synchronized at 100 Hz. Each camera was coupled to a large mirror. The 3D locations of the markers as well as the force data were obtained by the DLT procedures. The reconstruction RMS errors were 5.4 mm, 3.8 mm and 6.0 mm for x, y and z respectively.

A dynamic 3D multi-segment model was constructed and included 8 segments. The positions of the markers on each segment were filtered with a fourth-order zero-lag Butterworth filter using cut-off frequencies varying between 0.5 Hz for the markers on the feet and 3.0 Hz for the markers at the level of C7/T1. All data were collected at a frequency of 50 Hz. Finite-difference techniques were applied for the obtention of linear velocities and accelerations. A dynamic segmental analysis was performed on each segment, starting at the feet, to produce the net reactions and muscular moments. The external forces included the force plate data; the inertial forces and moments were obtained from the kinematics. For the present analysis the net muscular moments are reported about the three orthogonal orthoapedic axes on the trunk at L5/S1 to represent moments in flexion/extension, lateral bending and twisting. To understand the nature of muscular contractions, the angular velocities of the trunk relative to pelvis were obtained about the same axes as those in the trunk. To better comprehend specific trunk positions relative to the pelvis the approach described by Grood et al. (1983) was used where bending was about the floating axis.

Analyses of variance with repeated measures were applied to test the differences between the three lifting modes; a probability level of 0.05 was chosen.

RESULTS

The kinematics of the three modes of lifting were very similar for duration of motion, average and maximal load velocity and acceleration (not shown). The important differences in the kinematics were related to trunk orientation (Table 1), the pivoting technique being associated with smaller trunk flexion and twisting and the full twist technique, on the contrary, with larger trunk flexion and twisting.

Table 1 Means for kinematic and kinetic variables of the trunk/pelvis joint with three different modes of lifting (N=9).

Variables	Lifting techniques			
	Full twist	Half twist	Pivoting	Sign. level
Initial trunk flexion (°)	50	50	43	0.01
Initial trunk twisting (°)	26	18	15	0.01
Max. ext. moment (Nm)	202	217	229	0.00
Occurrence (%)	20	19	12	0.00
Trunk flexion (°)	47	46	40	0.04
Trunk left twisting(°)	23	17	14	0.00
Max. twist moment (Nm)	70	53	28	0.00
Occurrence (%)	26	20	84	0.00
Trunk flexion(°)	47	45	29	0.00
Trunk left twisting (°)	21	17	3	0.00

Pivoting required larger maximal extension moments than the full twist but these moments appeared to be exerted from a better trunk position with less flexion and twist; on the other hand, maximal twisting moments were considerably smaller when pivoting and they also occurred from a safer position with less trunk flexion and twist. The half twist technique classified between these techniques for most variables.

Typical curves are depicted for net muscular moments and joint velocities of trunk/pelvis for the full twist technique (Figures 2). They illustrate the concentric nature of trunk extensors: both moments and angular velocities are in extension excepted at the end of motion where the angular velocities go into flexion producing eccentric contractions; trunk twisting is shown to be eccentric with trunk moments exerted to the left when the trunk actually moves to the right due to the load, excepted at the end of motion when the trunk is seen to rotate to the left and the contraction becomes concentric; finally, the moments for lateral bending are more complex with concentric contractions to the left at the beginning, followed by concentric contractions to the right in the middle part of motion and eccentric contraction of the right flexors, at the end, to decelerate the motion. For the pivoting technique only the extensors were significant; the moments and velocities for the other muscular groups were rather small.

DISCUSSION

The techniques involving trunk twisting may present some risks for back injuries. First, even if trunk extension moments are smaller when applied from the twist techniques, it is known that trunk extensors are weaker when exerted with an asymmetric trunk angle; according to Marras et al. (1989) this moment decreased by approximately 8.5% of maximum for every 15° of asymmetry. This type of asymmetry is clearly present for the full twist technique but it also exists to a certain extent in the half twist and pivoting techniques.

Another point of importance to be emphasized is the fact that the twisting moments are considerably higher in the full twist technique and to a lesser extent in the half twist technique when compared to the pivoting technique. Moreover these moments are applied eccentrically. It is known that eccentric contractions do cause damage to muscle connective tissue (Abraham, 1977) and to the muscle fibers (Armstrong et al., 1983). McCully et al. (1986) reported several studies which demonstrate that the skeletal muscle is injured more severely by efforts exerted with eccentric contractions than those exerted isometrically or by concentric contractions. The EMG activities required to maintain a given mechanical tension are less under eccentric contractions; therefore, the tension produced is distributed over a smaller number of active fibers (Asmussen, E., 1953). This situation is reported to create uneven mechanical stresses and to predispose to physical damage (Newham et al., 1983).

In conclusion, it is apparent that manual handling tasks executed with coupled trunk motions involving flexion and twisting may expose the workers to spinal and muscular injuries. The pivoting task may be a potential solution which needs to be explored more deeply, specially in relation to floor/shoes design.

REFERENCES

Abraham, W.M. *Med. Sci. Sports*, 9, 11-26, 1977.
Adams, M.A. et al. *Spine*, 8, 327-330, 1983.
Andersson, G.B.J. *Ergonomics*, 28, 91-93, 1985.
Armstrong, R.B. et al. *J. Appl. Physiol.: Respirat. Environ. Exercise Physiol.*, 54, 80-93, 1983.
Asmussen, E. *Acta Physiol. Scand.*, 28, 364-382, 1953.
Drury, C.G. et al. *Ergonomics*, 32, 467-489, 1989.
Farfan, H.F. et al. *The Journal of Bone and Joint Surgery*, 52-A, 468-497, 1970.
Gravel, D. et al. *Eight meeting of ESB*, June, 1992 (submitted).
Grood, E.S. et al. *J. of Biomechanical Eng.*, 105, 136-144, 1983.
Kelsey, J.L. et al. *J. Orthop. Res.*, 2, 61-66, 1984.
Kumar, S. *Ergonomics*, 23, 987-993, 1980.
Marras, N.S. et al. *Human Factors*, 31, 667-677, 1989.
McCully, K.K. et al. *J. Appl. Physiol.*, 61, 293-299, 1986.
Mirka, G.A. *Proceedings of the Human Factors Society*, 32nd Annual Meeting, Santa Monica, 700-704, 1988.
Mital, A. et al. *Int. J. Indust. Ergon.*, 1, 91-101, 1986.
Sherazi-Adl, A. *Spine*, 14, 96-103, 1989.

Grants from NSERC and IRSST

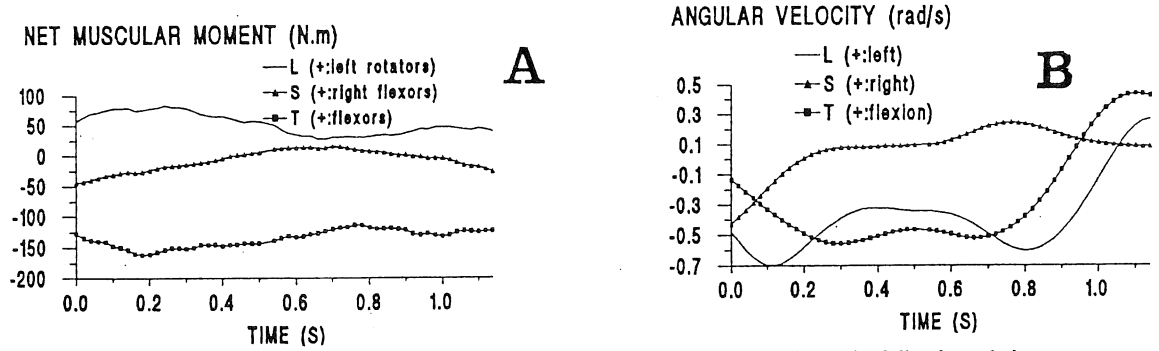

Fig. 2 A) Net muscular moments and B) relative angular velocities of trunk relative to pelvis for the full twist technique. (L: longitudinal; S: sagittal; T: transverse axes)

GENDER BIAS AND THE INCREMENTAL LIFTING MACHINE

J. Stevenson and D. Greenhorn

Ergonomics Research Group,
School of Physical and Health Education,
Queen's University, Kingston, Ontario, Canada, K7L 3N6

INTRODUCTION

The appropriateness of the Incremental Lifting Machine (ILM) for the assessment of female lifting capabilities was considered by analyzing gender differences in: (1) dynamic measures of displacement, velocity, force/acceleration, and power derived for an isoinertial lift; (2) regression equations developed to predict maximum mass on a box-lifting task; and (3) correlations between ILM test scores and scores obtained on maximal box-lifting tasks. It was concluded that the ILM did not provide a fair assessment of female lifting capabilities.

REVIEW AND THEORY

The entrance of North American females into many non-traditional civilian and military roles has produced a user population that is different from the male population for which many screening devices and working environments originally were designed (Celentano et al. 1984). These changing patterns of employment require that designers of screening tests and equipment give careful consideration to the capacities of women (Pheasant 1983) in order to ensure that females not be placed at an unfair disadvantage (Matzdorff 1987), as the use of male databases may be prejudicial to females achieving their full potential (Cox 1984).

In developing female databases to assess physical capabilities, it is particularly important that dynamic factors be taken into consideration, as evidence suggests that women may utilise their strength in different ways than men (Redgrove 1979). In the case of the ILM, which is commonly being used as a screening device for women and men alike, a technique has been developed by Stevenson et al. (1990) to quantify and analyze dynamic measures of an isoinertial lift. The purpose of the present study is to use this method to generate databases for both male and female lifters in order to analyze the appropriateness of the ILM for assessing female lifting capabilities.

PROCEDURES

Dynamic Analyses. A sample of 33 females and 99 males performed a maximum dynamic isoinertial lifting strength test on the ILM from a starting height of 0.34 m to a target height of 1.83 m using a constrained protocol. An Intertechnology Displacement/Velocity gauge attached to the ILM armature provided continuous dynamic data from which displacement, velocity, acceleration, force, and power profiles were determined. From these profiles, 37 lift parameters were derived to serve as a summary of the dynamic lift data. Means for each of these dynamic measures were calculated for both genders, and statistically compared using t-tests.

Regression Analyses. A maximal box-lifting task was completed by 25 female and 23 male participants from ground level to a platform 1.33 m high. Practice and starting weights were graded according to gender and body weight, and incremented by 2.5 kg for females and 5 kg for males to maximum. Participants also completed a maximal 1.80 m ILM test, for which dynamic measures were recorded, as previously described. Multiple regression equations for the male and female data were generated using the GENERAL LINEAR MODELS procedure.

Correlational Analyses. Two hundred and sixty nine participants (143 males and 126 females) completed a maximal isoinertial lifting test to 1.80 m on the ILM using a constrained protocol, as previously described. Participants then were divided into three samples for completion of a maximal box-lifting task, with each sample using one of the following task protocols: set style; free style; or ergonomically redesigned. Analysis of covariance was undertaken, and Pearson correlation coefficients were calculated between the logarithm of box-lifting scores and the logarithm of ILM scores.

RESULTS AND DISCUSSION

The quantitative dynamic data showed very clearly that successful completion of the 1.83 m isoinertial test required a very fast type of lifting action. Not only was the lifter required to overcome inertia in initiating upward acceleration of the load during a pulling phase of the lift, but he/she also had to generate enough velocity to allow momentum to assist during a wrist changeover manoeuvre, before completing the lift during a pushing phase. Since the rate of force development has been found to be greater for men than women (Anderson et al. 1979; Bell and Jacobs 1986), and since women in this study generated less than half the power generated by men, then it appears that the 1.83 m isoinertial test is designed to favour the rapid, powerful lifting motion of males.

Furthermore, since attainment of maximum force, power, velocity, and minimum force were found to occur at consistent anatomical landmarks (as shown in Figure 1), then specification of the same starting height for both males and females may have placed females at a disadvantage in three respects: (1) females, as a group, had shorter vertical distances over which to generate momentum during the crucial pulling phase; (2) females spent proportionately more time in the pushing phase and less time in the pulling phase than males; and (3) since gender differences in strength are more pronounced in the upper body than in the lower body (Laubach 1976), then those strength differences may have been amplified by having females perform lifts which relied more heavily on upper body strength than was the case for males. Hence, the resulting ILM scores may have underestimated female lifting potential.

Regression analyses revealed that ILM mass and associated dynamic parameters possessed much greater power for

predicting the lifting performance of males than females. Linear models generated by backward elimination procedures accounted for 66% of the variance in box-lifting scores for males, but only 33% of the variance for females. Also, marked differences in independent variables retained in these regression equations were observed between men and women, as has been noted by Yates et al. (1980) and Jacobs et al. (1988). It would appear that ILM mass and associated dynamic parameters alone served as inadequate predictors of female performance on a specified box-lifting task.

Modifications in box-lifting protocols from set style, to free style, to ergonomic redesign techniques were found to produce greater relative increases in maximum box-lifting scores for females than males (Figure 2). When masses lifted by females were expressed as percentages of those lifted by males, the resulting relationships were 51.3% for the constrained ILM protocol, 51.9% for the set style protocol, 56.4% for the free style protocol, and 63.8% for the protocol involving ergonomic redesign. Although differences in scores between genders remained statistically significant, it is evident that the lifting performance of females approached that of males as protocol constraints were reduced. Possible explanations include minimization of the need for upper body strength through ergonomic redesign of the testing area, and inappropriateness of the set style protocol for female lifting techniques.

When Pearson product-moment correlation coefficients between logarithmic scores on the box-lifting task and logarithmic scores on the 1.80 m ILM test were calculated (Table 1), disparate patterns in correlational changes were observed between males and females. While task-test correlations for the set style protocol were very similar for both genders, the protocol involving ergonomic redesign produced higher correlations for males, and much lower correlations for females. The implications of these findings are quite different, since both genders were able to lift significantly more mass as lifting constraints were removed. For males, the increased correlation between the ILM test and the ergonomically redesigned condition would suggest that male lifting capabilities were reflected reasonably well by ILM tests, in that correlation coefficients were highest for the maximum masses recorded on the box-lifting task. On the other hand, the tendency for female task-test correlations to decrease as lifting constraints were removed meant that the lowest correlations were calculated for the maximum masses lifted. Thus, the ILM test could not be considered to provide an accurate or fair assessment of the actual lifting capabilities of females.

REFERENCES

Anderson, C. et al. Medicine and Science in Sports, 11, 81-82, 1979.

Bell, D. and Jacobs, I. Medicine and Science in Sports, 18, 31-36, 1986.

Celentano, E. et al. Ergonomics, 27, 481-488, 1984.

Cox, S. Ergonomics, 27, 465-467, 1984.

Jacobs, I. et al. European Journal of Applied Physiology, 57, 146-153, 1988.

Laubach, L. Aviation, Space and Environmental Medicine, 47, 534-542, 1976.

Matzdorff, I. Work and Stress, 1, 293-297, 1987.

Pheasant, S. Applied Ergonomics, 14, 204-211, 1983.

Redgrove, J. Applied Ergonomics, 10, 215-223, 1979.

Stevenson, J. et al. Ergonomics, 33, 161-172, 1990.

Yates, J. et al. Ergonomics, 23, 37-47, 1983.

ACKNOWLEDGEMENT

This research was supported by funds provided by the Defence and Civil Institute of Environmental Medicine, Downsview, Ontario.

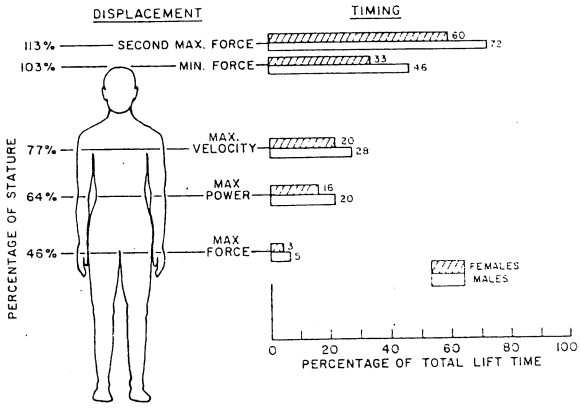

Figure 1. Displacement and timing parameters for 1.83 m isoinertial lift.

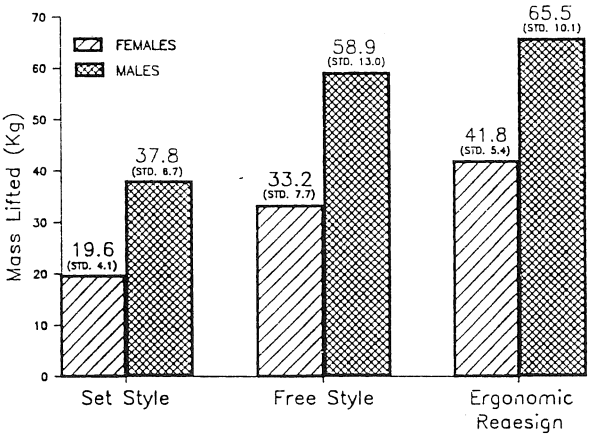

Figure 2. Maximal box-lifting task.

Table 1. Correlations between the logarithm of box-lifting scores and the logarithm of ILM scores.

	Correlation coefficients	
Variables	Males	Females
Maximal 1.80 m ILM lift		
vs Set Style	0.63***	0.65***
Free Style	0.62**	0.40*
Ergonomic Redesign	0.85**	0.23

* $p<0.05$; ** $p<0.01$; *** $p<0.001$.

MANUAL MATERIALS HANDLING

Poster

NORMALIZATION OF DYNAMIC TRUNK EXTENSOR EMG DURING STOOP LIFTING

V. Kippers and A.W. Parker

Department of Anatomy, The University of Queensland, Australia.
Department of Human Movement Sciences, The University of Wollongong, Australia.

INTRODUCTION

A static EMG study showed that the pattern of IEMG changes of four trunk extensor muscles, in a series of seven flexed-trunk postures, did not parallel the changes in trunk flexor moment. With 10 kg held in the hands there was a certain position of trunk flexion at which the erector spinae became electrically silent in all 10 adult male subjects. This also occurred in the hip extensor muscles of some subjects and may be related to the length-force properties of skeletal muscle. IEMG data from the series of static flexed-trunk postures were used to normalize the IEMG during dynamic trunk flexion/extension tasks performed by the same subjects. Mean normalized IEMG was greater during the concentric phase than the eccentric phase of the task. This can be explained by inertial effects and the velocity-force characteristics of skeletal muscle. Peak NIEMG occurred at different parts of the extension phase indicating differences between vertebral and hip contributions through the range of sagittal trunk motion.

REVIEW AND THEORY

Normalization of EMG most often involves relating the integrated EMG (IEMG) to the maximum level recorded during a maximal isometric voluntary contraction (Nemeth 1984; Jorgensen *et al.* 1985; McGill *et al.* 1986). Both maximum joint moment and IEMG are dependent on joint angle and therefore, so is the relationship between the two factors (Grieve *et al.* 1976; Schultz *et al.* 1985). This means that submaximal IEMG should be related to maximal IEMG in an equivalent joint position. During the stoop lift movement, a large range of trunk postures are adopted and there is normally a large change in IEMG activity throughout the movement (Floyd *et al.* 1955; Kippers *et al.* 1984). The purpose of this study was to demonstrate the patterns of dynamic IEMG during two phases of the stoop lift.

PROCEDURES

Ten young adult male subjects who had given their informed consent performed a stoop lift with a 10 kg mass held in the hands. The total movement time was eight seconds, consisting of two dynamic phases (trunk flexion and return extension) each lasting 3.2 s. The dynamic phases were separated by a 1.6 s period of static maintenance of peak trunk flexion. Surface electrodes were attached to the skin overlying four of the major trunk extensor muscles on the left side of the body; erector spinae, gluteus maximus, the long head of biceps femoris, and the medial hamstrings. The total range of trunk motion was divided into eight sectors, which were defined by the position of the wrist relative to the floor (wrist-floor distance, WFD). Immediately prior to the dynamic task, the static IEMG (expressed as the mean amplitude of the full-wave rectified signal, μV) in the middle of each sector was recorded with the same weight in the hands. Normalized IEMG (NIEMG) was expressed as the mean dynamic IEMG throughout the sector divided by the static calibration IEMG within the sector.

RESULTS

For erector spinae, there was generally an increase in IEMG from the erect position to a point of maximum activity at 0.8 m WFD and then an abrupt decrease at 0.6 m WFD to a level below that in the erect position. This low level was maintained through to 0.2 m WFD (Figure 1a) which was equivalent to a flexed-trunk posture in which the fingers were in contact with the floor. The patterns of activity of the other trunk extensor muscles were more variable. At one extreme there was a decrease in IEMG when the hamstring muscles were stretched towards the end of range of movement (Figure 1b) while in other individuals the IEMG tended to follow the pattern of hip joint moment caused by upper body weight and the load (Figure 1c).

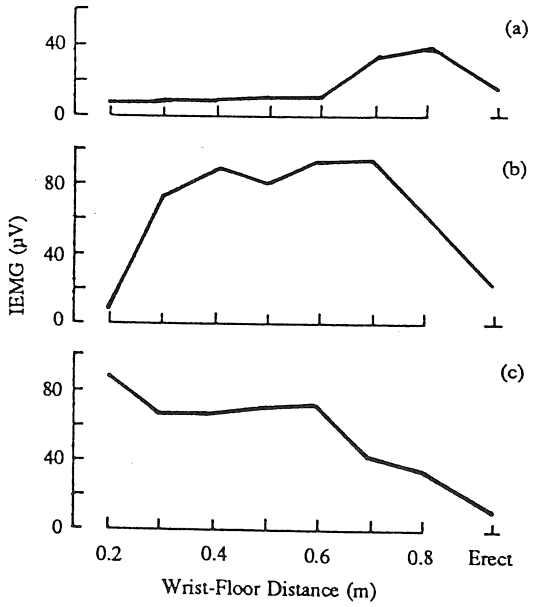

Figure 1. Mean IEMG of erector spinae (a) and IEMG of medial hamstrings for two individuals (b,c) at eight different flexed-trunk postures.

For each individual the pattern of dynamic IEMG was related to the pattern of static IEMG. For all muscles, NIEMG was less during the flexion phase when the trunk extensors acted eccentrically to control movement, than during the extension phase when the muscles contracted concentrically to produce trunk motion against the resistance of the combined weight of the upper body and external load (Figure 2). Throughout the eccentric phase, erector spinae NIEMG was greater than 1 (Figure 2a), while NIEMG of gluteus maximus was very close to 1 (Figure 2b). Dynamic hamstring NIEMG was often less than 1 (Figure 2c). Mean NIEMG for the hip extensors during the concentric phase was close to two, but it was four for erector spinae.

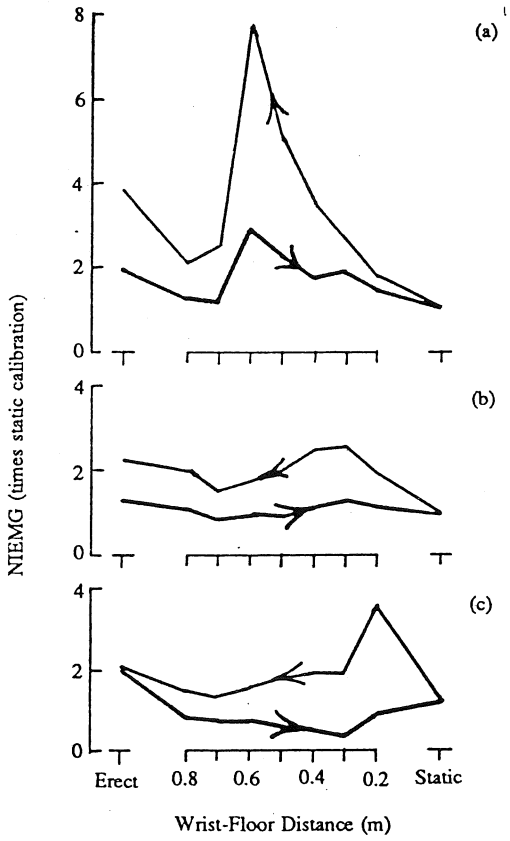

Figure 2. Relationships between trunk position and normalized IEMG of erector spinae (a), gluteus maximus (b), and long head of biceps femoris (c) during the two phases of dynamic trunk motion.

DISCUSSION

In the static flexed-trunk postures, the combination of low myoelectric activity of erector spinae with the requirement for large extensor moments emphasizes the complex relationship between the two factors. It has been hypothesized that the connective tissue associated with the back muscles and the postvertebral ligaments are able to support the vertebral column (Farfan 1975). This argument is based on the length-force properties of skeletal muscle (Evans *et al.* 1914), with an increased contribution from the associated passive connective tissue.

The process of normalization used in the present study allows a distinction to be made between the static and dynamic components of the observed EMG signal. Static IEMG patterns may be variable (Figures 1b, 1c) and patterns of direct dynamic EMG may reflect this variability. By normalizing to the static IEMG in similar postures the relative dynamic recruitment can be estimated. It was more of a calibration procedure in which the relationship between dynamic and static activation within small arcs of sagittal trunk motion could be quantified.

Through the ballistic part of trunk flexion, eccentric activity was sometimes less than the isometric in equivalent postures. However concentric activity levels were always comparatively high. The relative levels of activation can be related to both physiological and physical factors. Maximal eccentric forces are greater than concentric (Hill 1951), and so the same absolute force will be a smaller percentage of maximum during an eccentric muscular action. Also, the inertial effects of controlling motion of the weight during the flexion phase, and producing movement of the weight during extension may require different forces from the muscles.

It appeared from Figure 2 that reactivation of the hamstring muscles preceded the reactivation of erector spinae, which confirmed previous observations (Fischer *et al.* 1968; Okada 1970; Nemeth 1984). It has also been shown kinematically that hip extension precedes vertebral extension during a stoop-lift (Floyd *et al.* 1955; Davis *et al.* 1965; Kumar 1974).

REFERENCES

Davis, P. et al. *J. Anat.*, **99**, 13-26, 1965.
Evans, E. et al. *J. Physiol.*, **49**, 10-16, 1914.
Farfan, H. *Orthop. Clin. Nth Am.*, **6**, 135-144, 1975.
Fischer, F. et al. *Am. J. Phys. Med.*, **47**, 182-191, 1968.
Floyd, W. et al. *J. Physiol.*, **129**, 184-203, 1955.
Grieve, D. et al. *EMG Clin. Neurophysiol.*, **16**, 3-21, 1976.
Hill, A. *Lancet*, **261**, 947-951, 1951.
Kippers, V. et al. *Spine*, **9**, 740-745, 1984.
Kumar, S. *Ir. J. Med. Sci.*, **143**, 86-95, 1974.
McGill, S. et al. *Spine*, **11**, 666-678, 1986.
Nemeth, G. *Scand. J. Rehab. Med.*, **Suppl 10**, 4-35, 1984.
Okada, M. *J. Fac. Sci. Uni. Tokyo*, **8**, 311-336, 1970.
Schultz, A. et al. *J. Orthop. Res.*, **3**, 189-197, 1985.

OPTIMIZATION-BASED TORSO MUSCLE FORCE PREDICTION: ASYMMETRIC LOADING IN TWO FLEXED POSTURES

M.A. Nussbaum, S.A. Lavender, D.B. Chaffin, and G.B.J. Andersson

Center for Ergonomics, University of Michigan, Ann Arbor, MI 48109-2117
Dept. of Orthopaedic Surg., Rush Presbyterian-St. Lukes Medical Center, Chigago, IL 60612-3864

INTRODUCTION

Asymmetric loading of the torso is currently believed to be a potential risk factor in the etiology of low back injury. Muscle force prediction is a critical component of any biomechanical investigation of the physiological responses to asymmetric loads. Optimization techniques are a common means of predicting torso muscle forces relative to given external loading. These techniques have been well validated in cases of symmetric loading, and are beginning to be tested in cases of asymmetric loading in upright postures.

The present study is the first effort involving the application and evaluation of an optimization model of torso muscle activation when asymmetric loads are applied to a non-upright posture. The results demonstrate that, despite the additional complexity involved in modelling flexed postures, the optimization approach can nonetheless achieve reasonably accurate predictions of muscle forces. It is noted, however, that the results varying in accuracy for different muscles.

REVIEW AND THEORY

The prediction of torso muscle forces, assuming any reasonable level of complexity, is an ill-posed or indeterminate problem. Since there are more unknowns (forces) than equations (from static equilibrium), an infinite number of solutions typically exist. To resolve the indeterminacy, and specify a set of muscle forces which achieve static equilibrium, optimization techniques have been commonly employed.

In the present study, the objective function suggested by Crowninshield *et al.* (1981) is minimized. The function is based on the derivation that muscle endurance is maximized when the sum of the **n**-th power of muscle stresses is minimized. Here, **n** is set equal to 3, and the model is termed - sum of cubed intensities (SCI). Muscle forces are constrained to be ≥ 0 (act only in tension) or $\geq$ p (the force resulting from passive stretching of muscle elastic tissues), whichever is larger. Upper bounds on muscle forces are a function of a fixed maximal muscle intensity, physiological cross-sectional area, and the active force potential related to an assumed length-tension effect.

PROCEDURES

EMG data were obtained from a previous study involving nineteen male subjects. Loads were applied using weights connected to a shoulder harness while the pelvis was fixed, with the weights varied to obtain specific moment loads and moment directions about the L3/L4 interspace. Two moment magnitudes (20 and 40 Nm) in seven orientations (30 deg. increments about the right side) were applied in a plane normal to the long axis of the torso while the torso was flexed 30 and 60 degrees (Figure 1). One trial of each of the 28 loading combinations was presented in a randomized sequence.

The EMG data were collected using surface electrodes placed over 4 pairs of torso muscles: Erector Spinae (ES), Rectus Abdominis (RA), External Oblique (EO), and Latissimus Dorsi (LD). The raw EMGs were normalized using maximum values observed during static maximal voluntary exertions (flex, extend, and twist) in the appropriate trunk flexion. The normalized EMGs (NEMG) for each condition were averaged over the 19 subjects for comparison with model-based predictions.

ANALYSIS

Since the experimental loading occurred in non-upright postures, the muscle force prediction model could not be used simply based on applied moment loads and orientations. First, the additional moment generated by the weight of the upper body about L3/L4 was estimated using a 3-D static model. Second, both the muscle orientations and restorative moments resulting from muscle stretch were predicted using a geometric model of the torso (Nussbaum *et al.*, 1990). Third, the restorative moment resulting from spine flexion was estimated in the two postures using vertebral rotations determined by the geometric model and stiffness values obtained from the literature (Nachemson *et al.*, 1979; Miller *et al.*, 1986). The relative significance of the three types of moments (applied load, body weight, and passive restorative) can be seen in Table 1, recalling that the applied moments were 20 and 40 Nm.

Table 1. Mean External and Passive restorative moments in the two flexed postures used.

	Moment (Nm, + = flexion)		
Torso Flexion	Body Weight	Spine (passive)	Muscle (passive)
30 degrees	65	-7.9	-9.7
60 degrees	102	-45.0	-16.0

The muscle force prediction model was used to predict the active component of muscle force. The active component equilibrates the moment which remains when the applied moment is added to the body weight moment and spine and muscle restorative moments are subtracted.

RESULTS AND DISCUSSION

Linear regression of predicted muscle forces (normalized to maximum potential contractile force) versus NEMG was used to validate the predictive ability of the model. The resulting coefficients of simple determination (r^2) are shown in Table 2. The activity of the ES is predicted reasonable well bilaterally, while the remaining forces correlate poorly with observed EMG. The coefficients for the left and right RA and right EO are nonexistent because, for all loading conditions, zero force was predicted for these muscles.

The table also illustrates that, when regressions are performed separately on the 30 and 60 degree flexed postures, the correlations are generally superior versus the pooled case. This result supports the common hypothesis that the EMG-force response may differ between postures, and emphasizes the need to normalize EMGs using maximal values obtained from the same posture.

Table 2. Correlations between normalized muscle force and NEMG.

	r^2		
Muscle	Grouped	30-flex	60-flex
L-ES	0.814	0.856	0.871
R-ES	0.681	0.711	0.753
L-RA	-	-	-
R-RA	-	-	-
L-EO	0.065	0.105	0.134
R-EO	-	-	-
L-LD	0.510	0.007	0.822
R-LD	0.273	0.009	0.481

Previous investigation (Hughes, 1991) had suggested that the SCI model can successfully predict torso muscle activity during asymmetric loading. In contrast to that work, the present analysis considered loading in a non-upright posture. When the torso is deviated from the upright position, several additional factors must be accounted for, including the moments generated by external and internal sources. While the applied moments at a vertebral level are readily quantifiable, those resulting from body weight and passive tissue reactions less easily determined. Inaccuracies in the estimated moment loads may be a significant source of error in the muscle force predictions. As such, it is difficult to differentiate between errors implicit to the model and those resulting from poor input.

Interpretation of the non-existent regression coefficients requires reference to the original observed data. Because of the specific postures and applied moments, the torso always remained in a state of induced flexion. Even in the condition of 40 Nm of applied extension moment and 61 Nm of passive reactive moment, there was a net flexion due to the body weight moment of 102 Nm. Since the present model predicts zero antagonism, the RA muscles were never predicted to generate any force. A similar argument applies to the right EO since only right lateral bending moments were involved. In fact, these three muscles, were observed to have NEMGs which never exceeded 5%, so the predictions of zero force may indeed be warranted.

The left EO force failed to be successfully modeled. The NEMG values were consistently below 5%, with lateral bending moments resisted instead by differential ES contractions. The model, however, predicted substantial activation (~15%). Similarly, LD activity was observed to be minimal, yet predicted by the model to reach significant levels. Since the SCI model had been successful in modeling EO and LD forces during loading in upright postures (Nussbaum *et al.*, 1991), it is hypothesized that alternative muscle recruitment strategies are used in flexed postures. Specifically, the strategy for opposing lateral bending moments appeared to shift from the EO to recruiting the ES contralateral to the load.

In summary, the optimization-based muscle force prediction model demonstrated mixed performance when applied to asymmetric loading in flexed postures. Evidence for changing muscle recruitment strategies was observed, and the need for posture-specific EMG normalization is supported.

REFERENCES

Crowninshield, R.D. et al. *J. Biom.* **14**, 793-901, 1981.
Hughes, R.E. *PhD Thesis*, Univ. of Michigan, 1991.
Miller, J.A.A. et al. *J. Biom.*, **19**(1), 79-84, 1986.
Nachemson, A.L. et al. *Spine*, **4**(1), 1-8, 1979.
Nussbaum, M. et al. *Proc. ASB*, Miami, (145-146), 1990.
Nussbaum, M. et al. *Proc. ISB*, Perth, (559-560), 1991.

ACKNOWLEDGMENTS

This work was partially supported by NIH Grant 1R01-AR39599, in cooperation with Rush Institute, Chicago, Ill., USA.

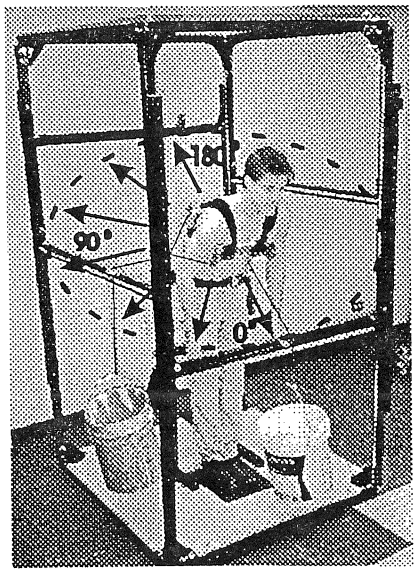

Figure 1. Illustration of subject loaded in a combination of flexion and right lateral bending in a 30-degree flexed posture.

QUANTIFICATION OF BACK MOTION IN RESPONSE TO ASYMMETRIC PLATFORM PERTURBATIONS

K. Ghosh *, M. Parnianpour *, W.S. Marras * and K. Barin **.

* Industrial & Systems Engineering Department,The Ohio State University, Columbus, OH.
** Department of Otolaryngology, The Ohio State University, Columbus, OH.

INTRODUCTION

Maintenance of the upright posture is a complex task involving the neural and musculo-skeletal systems. Falling is the most common cause of accidental death in the elderly [1]. It is suggested that lateral falls increase the risk of hip-fractures [6]. This study investigates the sway index and lumbar movement required to maintain balance in a simple weight-holding task for asymmetric platform movements.

REVIEW AND THEORY

Studies on the temporal patterns of muscle activation have shown that lumbar region is involved in the postural control mechanism [4]. The role of the ankle joint in compensating for sagittaly symmetric movements has been investigated [2,4]. However, the ankle does not have significant degrees of freedom in the coronal plane. Hence the ankle joint would seem to be less suitable for compensating for perturbations of the support surface in non-sagittal directions and this would lead to lumbar movement being required for balance maintenance. This study quantifies the motion of the low-back region and investigates the changes which occur in lumbar motion and in balance performance (sway index) as a result of support surface instability in asymmetric directions.

PROCEDURE

A modified version of the Balance System (Chattecx Co., Chattanooga, TN) was used to monitor the balance responses. The linear motor was replaced by a more powerful one (Maximum velocity 3.048 cm/s, amplitude 2.54 cm) while the angular motor (Maximum velocity 2.4 deg/s, amplitude 4 deg) was left unchanged. The Lumbar Motion Monitor (LMM) and custom software developed in the Biodynamics Lab was used in this experiment [5].

Eighteen healthy (with no prior history of back problems or balance disorders), male volunteers participated in the experiment. The subjects (mean age=25 years, SD=3.23 years) were exposed to three types of platform conditions: stable, linear translation and up-down (angular rotation) crossed with three conditions of asymmetry: 0,45 and 90 deg. Asymmetry was achieved by aligning the platform's axis of rotation with the ankles' axis of rotation (0 deg) and 45 and 90 deg to the ankles' axis with the midpoints of both axes aligned. The experimental design was randomized with restrictions on the randomization for the independent variable, asymmetry. The design counterbalanced the order of presentation of the asymmetry variable. Within a level of asymmetry the platform conditions were completely randomized. A description of the 10 independent variables used in this study are contained in the title of Table 1.

Subjects were fitted with the LMM and asked to step on the Balance System footplates (which were placed in one of the three asymmetric conditions specified earlier) holding a standard box weighing 20% of their body mass. This was done to increase the complexity of the balance task as well as to extrapolate the results to common MMH tasks in industry. The type of platform movement was unexpected for the subject.

A MANOVA was performed on the 10 independent variables followed by individual ANOVAs. Post-hoc (Tukey) tests were also performed on the significant (ANOVA) effects. The results of the MANOVA and ANOVA are shown in TABLE 1.

RESULTS

In general, ranges of motion, velocities and accelerations increased with asymmetry and with platform movement. Platform movement significantly affected more of the variables than the asymmetry of the perturbation (Table 1).

Figure 1(a) shows the interaction of the asymmetry and platform conditions for the sway index. The dispersion factor increases from the stable to the linear to the up-down condition, but this increase is much more dramatic in the 90 deg asymmetric condition. Figure 1(b) shows the same interaction for the sagittal peak acceleration. The main effect of asymmetry was not significant, however the main effect of platform was. The interaction effect was not significant.

DISCUSSION

Our results have shown that the involvement of the low-back increases even in a simple standing task with asymmetry of platform perturbation. Byl et al. [3] concluded that LBP patients demonstrated significantly greater postural sway and they used their hip and back as a fulcrum in contrast to healthy subjects who used their ankle. Our results indicate that lumbar region contributes significantly to instability compensation. Further research that quantifies balance performance in low-back patients and frequent fallers is needed. In the present study, no subject was close to employing the "stepping strategy" to maintain balance. Future studies should also consider the effect of stronger perturbations on healthy subjects.

Table 1. MANOVA and ANOVA p-value summary for asymmetry and platform effects. Only those effects significant at the .05 level have been included. (ASYM,asymmetry;PLAT,platform; DISP, dispersion; LROM, lateral range of motion; SROM, sagittal range of motion; TROM, transverse range of motion; LPV,lateral peak velocity; SPV, sagittal peak velocity; TPV, transverse peak velocity; LPA,lateral peak acceleration; SPA, sagittal peak acceleration; TPA, transverse peak acceleration).

INDEP. VARIABLE	MANOVA	ANOVA									
	.	DISP	LROM	SROM	TROM	LPV	SPV	TPV	LPA	SPA	TPA
ASYM	.0001	.0001		.0008					.0333		.0159
PLAT	.0001	.0001		.0038		.0001	.0001	.0101	.0080	.0020	
ASYM x PLAT	.0001	.0001									

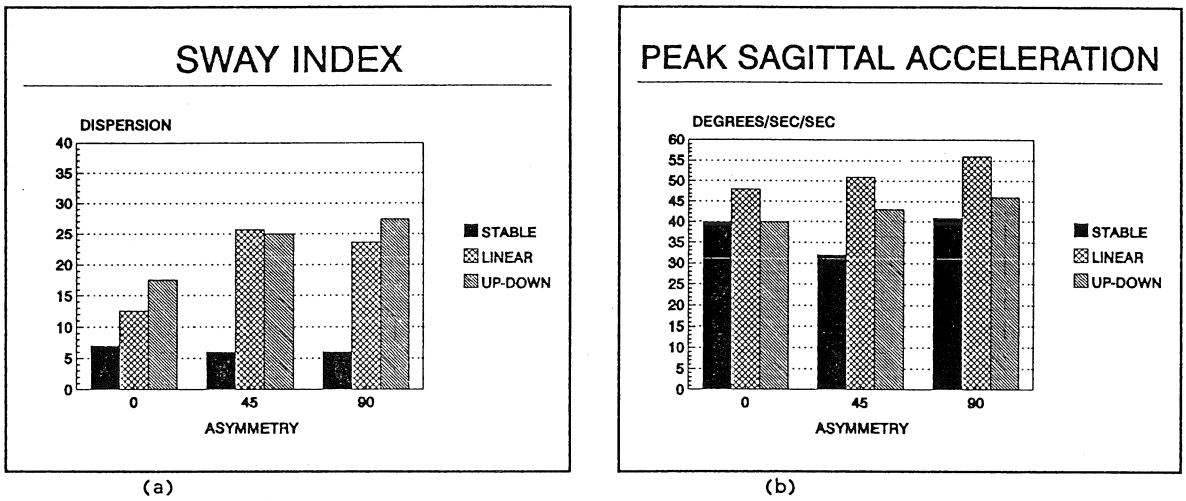

Figure 1. Interaction of the platform and asymmetry effects for (a) Sway index and (b) Sagittal peak acceleration.

REFERENCES

1) Bartlett SA et al.: On the classification of a geriatric subject as faller or nonfaller. Medicine and biology in Engineering and Computing, V 24, pp 219-222, 1986.

2) Barin K: Evaluation of a generalized model of human postural dynamics and control in the sagittal plane. Biol. Cyber. 61, pp 37-50, 1989.

3) Byl NN et al.: Variations in balance and body sway in middle-aged adults: Subjects with healthy backs compared with subjects with low-back dysfunction. Spine 16, pp 325- 329, 1991.

4) Keshner EA et al.: Neck, trunk and limb responses during postural perturbations in humans. Expt. Brain Res,V 71, pp 455-466, 1988.

5) Marras W.S. et al.: Accuracy of a three-dimensional lumbar motion monitor for recording dynamic trunk motion characteristics. International Journal of Industrial Ergonomics, 9, pp 75-87, 1992.

6) Robinovitch S.V. et al.: Prediction of femoral impact forces in falls on the hip. J of Biomech Eng. V 113, pp 366-374, 1991.

ACKNOWLEDGEMENTS

Partial funding for this project was provided by the Ohio Bureau of Worker's Compensation, Divison of Safety and Hygiene and the Bremer Foundation.

RELIABILITY AND VALIDITY OF THE KINEMATIC AND KINETIC MEASURES OF A LIFT SIMULATOR

P. Wright, M. Parnianpour, and W. Marras

Biodynamics Lab, Industrial & Systems Engineering Dept.,
The Ohio State University, Columbus, OH 43210.

The purpose of this experiment was to establish the validity and reliability the Lido Lift simulator. For research needs, it is crucial to have access to the time varying hand force and position during the lift. A data-acquisition system was used to independently collect the kinematic and kinetic signals according to a novel calibration protocol. All of the r-squared values of the linear regression analysis were above .999, indicating the validity of the device. Both repeatability of the signal within a day and their day to day reliability were very strong and significant. The evaluation of the isokinetic mode of testing resulted in models that predict the initial distance and time that the lift will be non-isokinetic. The position and force sensors of this device were proven valid and reliable.

INTRODUCTION

Comprehensive biomechanical modeling during manual material handling tasks requires integration of the force plate, multi-channel EMG, motion analysis system, and the hand (end effectors) forces. Lido Lift is a robotics based lift device (Loredan Biomedical Inc., Davis, CA) that simulates isometric, isokinetic, and isoinertial lifts. The purpose of this experiment was to establish the validity and reliability of the sensors of this system. The original software presents the data in summary tables or graphical display. The analog signals for the angle, length, and height of the Lido Lift's mechanical arm as well as the force at the end of the arm were collected for the validation purposes.

REVIEW AND THEORY

The quantification of trunk function has been viewed as a crucial elements of in the disability assessment and the rehabilitation process of low back pain patients. Clinical centers have not determined construct validity and accuracy of their measurements for the devices that they use. The test-retest reliability of maximum lifting capacity measured by the Lido Lift has been evaluated by Alpert et al, 1992. However, no study can be found to establish the validity and the reliability of the physical measurements of the sensors. In addition, to integrate the biological signal as described before requires simultaneous data collections. The purposes of this study are: 1) to develop a calibration protocol for kinematic and kinetic measurements of Lido Lift; and 2) to establish the validity and reliability of these measures.

PROCEDURES

The signals were correlated to physical measurements in the following manner. For the arm angle, the arc was traced by attaching a pen to the end of the arm and discrete points were marked while the voltage was recorded. The center of the arc and the corresponding degrees (+ 0.1 degrees) for each point were determined by graphical methods. For the arm length and box height, an anthropometer was used to measure the displacement to the nearest 0.5 mm. For the force at the end of the arm, known weights were used in two directions. The weights were hung from the end of the arm for the downward force and they were attached to a cable passing through an overhead pulley for the upward force. This was repeated for arm length and box height the next day to test for reliability. To determine the initial non-isokinetic portion of the lift, a maximum lift at five speeds (5,25,51,76,and 89 cm/s) was performed. The first derivative of the vertical distances of the box were computed. The velocity time histories showed an initial constant acceleration before the set velocities were achieved. Using this observation the predictive model for the non-isokinetic distance of each lift was developed.

RESULTS

Linear regression was performed to correlate voltages and physical measurements. See figure 1 for the equations of each line and their respective r-squared values. On the second day the procedure was repeated for arm length and box height. The voltages were used as input to the regression equations predicted values of length and height were determined. These predicted values were then compared to the physical measurements of the second day and the r squared values were 0.999636 and 0.999993, respectively. This part of the test was done to ensure day to day reliability of the signal and the validity of the linear equation transforming voltages into degrees, cm, and Newtons. A test for drift in the signal was performed as well, and no drift was found up to one hour. During isokinetic lift, the velocity of the box settled accurately to the set velocity, however, the settling time was a function of the final velocity. The non-isokinetic portion of the lift can be predicted based on Fig. 2.

DISCUSSION

This experiment showed the linearity of the Lido Lift signal for all four channels and showed that it was both valid reliable from day to day. The training at high speeds over short lifting distances may prove insignificant due to limitations shown in Fig. 2. The procedure developed for the calibration is short and allows the researcher or the clinicians to have an independent verification to the validity and the reliability of the data. The summary reports and the processed information based on the measurements can not be trusted unless the accuracy of the original measures are established.

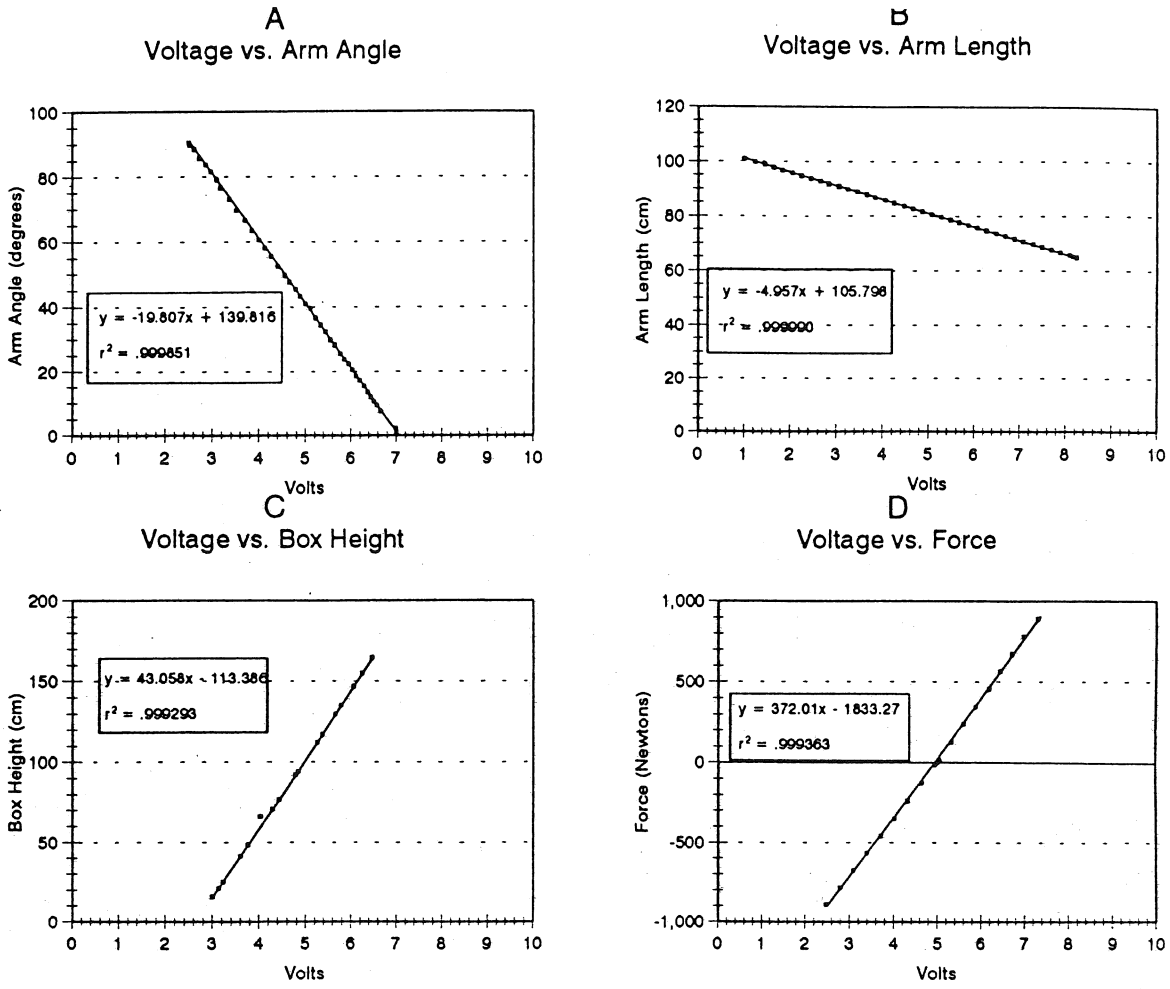

Figure 1. Regression equations for the box position and the force at the end of the Lido arm.

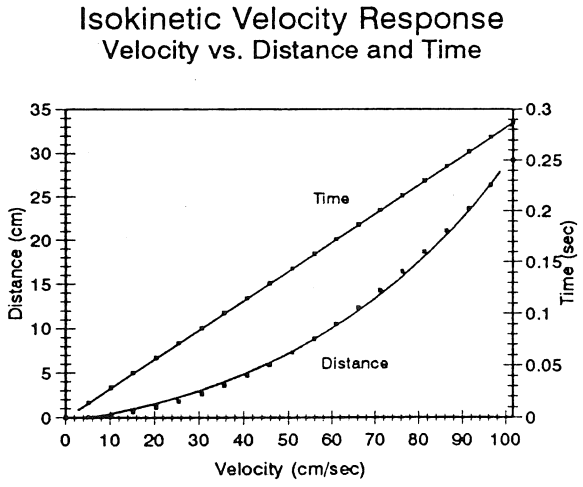

Figure 2. The initial non-isokinetic portion of the lift (distance and time) as a function of the set velocity of the lift.

ACKNOWLEDGEMENTS

Partial funding for this study was provided by the Ohio Bureau of Worker's Compensation, Division of Safety and Hygiene.

REFERENCES

Alpert J, Matheson L, Beam W, and Mooney V: The reliability and validity of two new tests of maximum lifting capacity. J Occup Rehab 1(1):13-29, 1992.

HOW MANY BITS OF DATA ARE NEEDED TO UNDERSTAND LIFTING DYNAMICS?

T. Morris, J. Trimble

Rehabilitation Research and Development Center
VA Hines Hospital, Hines, Illinois.

INTRODUCTION

The dynamics and kinematics of lifting have been described traditionally using high-dimensional models (McGill & Normand, 1986; Anderson et al., 1985). These models have provided insight into the relationships between intersegmental dynamics and joint torques (Schipplein, et al., 1990). However, they offer little insight into the motor control strategies that operate during lifting. This prompted us to search for methods for estimating lifting dynamics that provided information on lifting strategies.

REVIEW AND THEORY

We focused our search for a new methodology on variables that relate movement and posture. The importance of this relationship results form the fact that movement creates forces that destabilize posture. These forces must be compensated for by aligning the body's center of gravity (COG) and the location of the center of pressure located beneath the base of support (COP) (Frank and Earl, 1990).

Others have studied the relationship between COG and COP during quiescent standing, sit to stand maneuvers and standing isometric pulls (Lee et al., 1990; Pai and Rogers, 1990; Riley et al., 1991). In all cases, they found that the relationship was tightly controlled. This observation has prompted the idea that the COG-COP relationship may represent a dynamic constraint on the relationship between movement and posture. If so, then it might be used to estimate the kinetics of movement. We tested this hypothesis by using COG and COP to estimate intersegmental torques and disc compression forces during lifting.

PROCEDURES

Seven males and six females served as subjects. Their ages ranged from 21 to 35 years. All subjects gave their informed consent prior to participating in the study.

Body kinematics where obtained using a WATSMART™ motion analysis system with markers placed on the lateral malleolus, knee, hip, trunk, shoulder and wrist (Fig 1). All data were collected at 60 Hz. The motion data were filtered using a digital second-order Butterworth filter with a cutoff frequency of 5 Hz. The boundaries of each subject's feet were recorded to obtain a reference for COP. Segmental mass and inertial properties were estimated from Plagenhoff et al (1983). The resultant ground reaction force (GRF) acting through the COP was estimated using an AMTI 6 DOF force platform. The vertical reaction forces acting through the handles of the crate were recorded using strain gauges. The handle reaction forces were used to separate loaded and unloaded portions of the lift. The combined horizontal and vertical trajectory of the subject's COG and the load were estimated. The COP, GRF, and kinematic data were used with an inverse dynamic model to calculate the net muscular torques acting about each of the joints and the lumbosacral disc compression force (Frievalds et al., 1984; Schipplein et al., 1990). The disc compression force model was previously validated empirically (Jager and Luttmann, 1989).

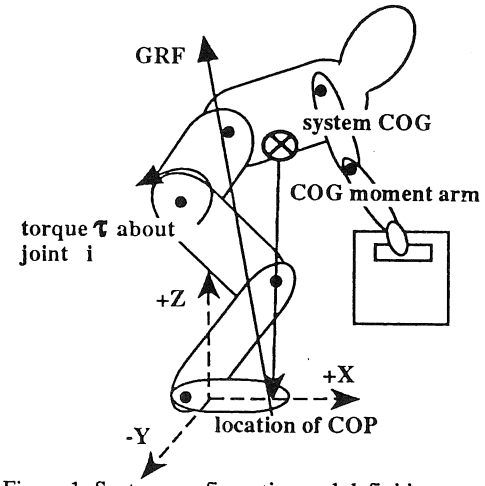

Figure 1. System configuration and definitions

Each subject was asked to lift a crate that was loaded with five weights that ranged from 60 to 216 N (13.5 to 48.5 lbs). The crate's dimensions were 30.5 by 30.5 by 28 cm (12 by 12 by 11 inches). Subjects were asked to lift the crate to knuckle height using whatever pace and technique they found most comfortable. Before the experimental trial, they were told to place their feet at a comfortable position relative to the load and allowed to practice the lift. For a given trial, the subjects were not told the load or allowed to practice the lift. They were told to lift the load at a comfortable pace for 30 seconds. Subjects were allowed to rest at least three minutes between trials.

RESULTS

Joint torques and disc compression forces were estimated using the following regression equations:

$$\tau_i = c_{1_i} \cdot COG_X + c_{2_i} \cdot COP_X + c_{3_i} \cdot COG_Z \qquad (1)$$

$$F_{disc} = d_1 \cdot COG_X + d_2 \cdot COP_X + d_3 \cdot COG_Z \qquad (2)$$

where F_{disc} is the disc compression force, τ_i is the net

muscular torque about joint i, and COG_Z and COG_X are the horizontal and vertical components of the COG and COP_X is the horizontal componenet of the COP.

The torques and forces in Equations 1 and 2 were expressed as percentages of maximum torque or force. COG_Z was scaled by the subject's height. COG_X and COP_X were expressed as a percentage of the distance from the static center of pressure relative to the toe or heel.

The coefficients for disc compression force for all subjects and all loads are shown in Figure 2. A comparative analysis of variance of the disc compression force predicted by the inverse dynamic model and equation 2 using the mean coefficient values (approximate centroid of the cluster in Figure 2) showed that the regression equations were highly correlated over all the subjects and weights ($r=0.80$ to $r=0.98$, $p<0.0001$). Figure 3 compares the disc compression force for one subject estimated with our model (thin line) and the inverse dynamic model (thick line). The arrows indicate 95% of the maximal COG height. The correlation between the two curves is remarkably high ($r=0.98$, $p<0.0001$ for the 60 N load and $r=0.96$, $p<0.0001$ for the 216 N load).

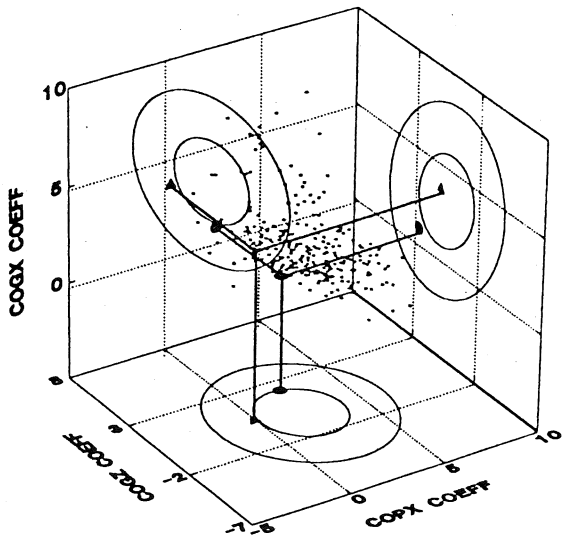

Figure 2. Pooled coefficients for each lift for all subjects and loads. Ellipsoids indicate 50% and 95% confidence limits. The circle (216 N) and triangle (60 N) show the coefficients for PW.

We also tested the model's validity by predicting the empirical vertical handle reaction forces. The predictions were in good agreement with those obtained empirically ($r = 0.91$, $p < 0.0001$).

DISCUSSION

Our data show clearly that disc compression forces during lifting can be accurately estimated using a simple model that is based on a hypothetical postural control strategy. We obtained similar results for torques at the hip, knee and ankle. This implies that intersegmental dynamics during lifting may be estimated using models that are considerably simpler than those used in the past. While our model may not be sufficient to reveal the entirety of cause and effect relationshipsduring lifting, it may be sufficient to explain the dynamics of many lift-related injuries. It also offers the unique possibility of estimating lifting dynamics using a force platform (Shimba, 1984) obviating the need for expensive and complicated motion analysis systems.

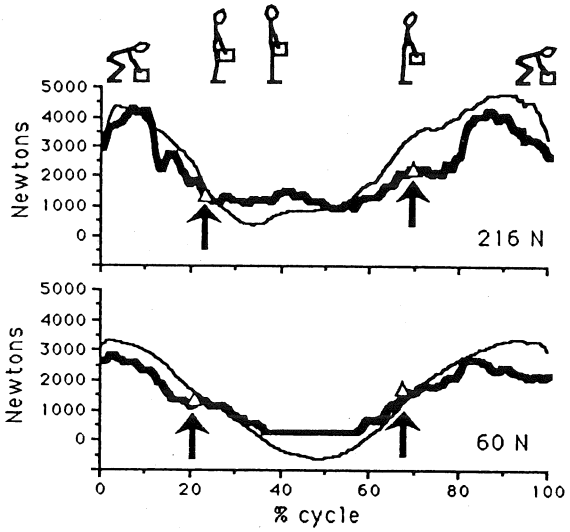

Figure 3. Estimated disc compression forces for subject PW

REFERENCES

Anderson, et al., J. Biomechanics, 18(8), 571-584,1985.
Frank, J.S. and Earl, M. Physical Therapy, 70(12), 855-863, 1990.
Frievalds, A. et al., J. Biomechanics, 17(4), 251-262, 1984.
Jager M. and Luttmann, A. Ergonomics, 32(1), 93-112, 1989
Lee, W.A., et al., Exp. Brain Res., 82, 304-314, 1990.
McGill, S.M. and Norman, R.W. Spine, 11(7), 666-678, 1986.
Michaels, C.F. et al,. In Press, 1992.
Pai, Y. and Rogers, M., Med. and Sci. in Sports and Exercise, 22(3), 378-384, 1990.
Plagenhoff , S. et al., Research Quarterly for Exercise and Sport, 54(2), 169-178, 1983.
Riley, P. O., et al., J. Biomechanics, 24(1), 77-85, 1991
Schipplein, O.D., et al. J. Biomechanics, 23(9), 907-912, 1990
Shimba, T, J. Biomechanics, 17(1), 53-60, 1984.

ACKNOWLEDGEMENTS

This research was supported by an award from the Rehabilitation R&D Service of the Dept. of Veterans Affairs (#B91-28AP).

PARASPINAL MUSCLE ACTIVATION DEFICITS AND CONCENTRIC-ECCENTRIC ISOKINETIC TRUNK EXTENSION PERFORMANCE

M.D. Grabiner and J. Kasprisin

Department of Biomedical Engineering & Applied Therapeutics
The Cleveland Clinic Foundation, Cleveland, Ohio, 44106

INTRODUCTION

The inability to normally fully activate skeletal muscle during voluntary maximum efforts are broadly associated with neural-inhibitory mechanisms. These mechanisms limit the external expression of muscle force, that is, they result in a muscle force deficit. Despite greater force output compared to maximum concentric contraction, maximum effort eccentric contraction are associated with an activation deficit, the origins of which remain unspecified. The present study describes the relationship between the isokinetic trunk extension eccentric-concentric force deficit and the associated parapsinal muscle activation deficit. It was expected that smaller eccentric activation deficits would be associated with increased eccentric force output relative to the concentric condition.

METHODS

Nine healthy, recreationally active male subjects performed maximum effort concentric and eccentric isokinetic trunk extension at 60, 90, and 120 deg/s. The trunk extensions were performed on a Kinetic Communicator (Chattecx Corp., Chattanooga, TN) isokinetic dynamometer. The range of motion was 60 degrees, thirty degrees on either side of the vertical trunk position (relative to the room coordinates) were measured. At each isokinetic speed, three levels of premotor trunk extension force were required to induce motion of the dynamometer- 0, 25, and 50 percent body weight.

Electromyographic were collected bilaterally from the paraspinal muscles using bipolar surface electrodes. The EMG and Kin-Com signals were digitized at 1 KHz and stored for postprocessing. For each trial, the isokinetic work and the parapsinal muscle activation, as measured by the rectified and integrated EMG value, from the middle third of the range of motion were extracted. The EMGs were expressed as a percentage of the values from the 60 deg/s, concentric contraction with zero precontraction condition. The trunk extension isokinetic work values were expressed as a percentage of the subject's body weight. A work and activation deficit index was calculated for both the isokinetic work and the muscle activation. The index was calculated as the difference between the values for the eccentric and the concentric conditions at each precontraction level. A positive index value results from the eccentric value being larger than the corresponding concentric value.

For each isokinetic speed, multiple regression was used to predict the isokinetic work index as a function of the muscle activation index, the quadratic representation of the activation index, and the precontraction level.

RESULTS

The regression analyses revealed that for each isokinetic speed tested, the equations expressing the isokinetic work index as a function of the activation index were statistically significant (all $p < 0.001$). The equation for the 60, 90, and 120 deg/s conditions, respectively, are as follows:

Work index = 98.22 + (76.51 * activation index)
-(0.71*isokinetic speed) + (0.68* preload)

was significant ($p<0.001$) and had an adjusted R^2 of 0.596. The standardized regression coefficients for the activation index, isokinetic speed, and preload were 0.70, -0.41, and 0.32 respectively. Parenthetically, an analysis of variance with repeated measures revealed that the effects of isokinetic speed and preload on the eccentric activation deficit were not significant ($p>0.05$).

DISCUSSION

The results demonstrate that as the eccentric activation deficit is reduced, the degree to which isokinetic work generated during maximum effort eccentric trunk extension can exceed that generated during maximum effort concentric trunk extension increases. The eccentric activation index was only moderately related to the maximum concentric isokinetic trunk extension strength. Thus, although decreasing the amplitude of the eccentric activation index results in an increase in eccentrically-generated trunk extension, the activation index may not be a function of the absolute strength of the muscle group as suggested by others (3). Insofar as (a) the eccentric activation index does appear to limit the eccentric muscle force that may be exerted and (b) eccentric muscle contraction has been associated with increased muscle strength and hypertrophy, further investigation of those factors influencing the eccentric activation index may be extremely relevant to physical training and rehabilitation.

REFERENCES

1. Garrett et al. New Perspectives on Low Back Pain, American Academy of Orthopaedic Surgeons, 1989
2. Neter J and Wasserman W: Applied Linear Statistical Models, R.D. Irwin, Inc., 1974
3. Hortobagyi T, Katch FI. Eur J Appl Physiol, 60:395-401, 1990

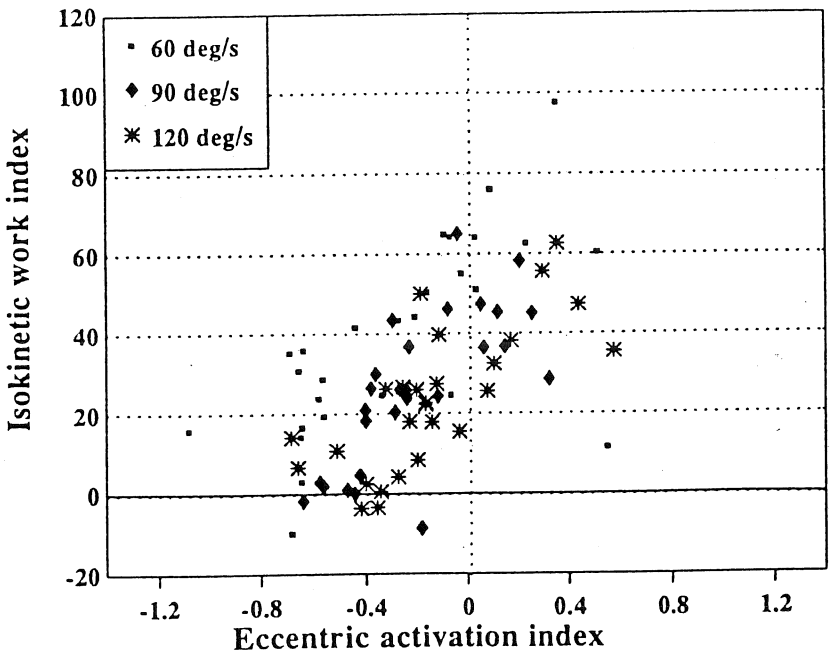

TRIAXIAL NET MUSCULAR MOMENTS AT THE L5/S1 JOINT WHEN LIFTING LOADS FROM DIFFERENT STARTING POSITIONS

A. Plamondon[1], M. Gagnon[1] and D. Gravel[2]
[1]Département d'éducation physique, Université de Montréal, Québec.
[2]Ecole de réadaptation, Université de Montréal, Québec.

INTRODUCTION

For many years manual materials handling (MMH) has been recognized as a major hazard to industrial workers. Combination of bending and twisting was identified as a possible cause of back injury in the workplace. The purpose of the present study was to estimate the influence of three different starting positions (90°, 45°, 0° at the left side of the subjects) on the triaxial net muscular moments at the L5/S1 joint during MMH. A dynamic three-dimensional (3D) multi-segment model was used to compute the twisting, extension/flexion and lateral bending net muscular moments at the L5/S1 joint. The moments generated at the L5/S1 joint for the three starting positions were approximately of the same magnitude and only little differences were observed between the conditions; however, the starting position at 90° remains more hazardous due to the larger degree of asymmetry of the trunk when the maximum net muscular moment is produced.

REVIEW AND THEORY

For many years manual materials handling (MMH) has been recognized as a major hazard to industrial workers (NIOSH, 1981). From epidemiological data, NIOSH (1981) cites studies revealing that 68% of the overexertion incidents involved lifting and 20% involved pushing and pulling objects. Chaffin(1974) showed that when the lifting tasks exceeded workers' strength capabilities, there was a greater probability of low back injuries. According to Marras and Mirka (1989), a strategy to minimize the risk of back injuries is to optimize the workplace so that the worker be using his back in positions where he is exerting a smaller portion of his available strength to perform the task. Usually, there is a high incidence of body twisting (trunk asymmetry) in the workplace (Drury et al.,1982). Frequent bending and twisting have been associated with an increased risk of low back pain. Hickey and Hukins (1980) found that twisting and bending may cause annular failure and protrusion of the intervertebral disc. Adams and Hutton (1981) indicated that a combination of flexion and lateral bending might be responsable for back injuries as it produces maximum streching of the posterolateral annulus.

Trunk strength measurement has been the focus of a large number of studies; however, studies about the resulting moments about L5/S1 when performing MMH are not common particularly when the tasks include body twisting. The knowledge of these moments is interesting because the strength to perform the task would be assessed in relation with the available strength of the worker and would provide a severity index of the task. The purpose of the present study was to estimate the influence of three different starting positions (90°,45°,0°) when performing a MMH task on the net muscular moments at the L5/S1 joint. A dynamic three-dimensional (3D) multi-segment model was used to compute the twisting, extension/flexion and lateral bending net muscular moments at the L5/S1 joint. It was hypothesized that different starting positions produce different net muscular moments at the L5/S1 joint.

PROCEDURES

Ten male students volunteered to participate in the study. Their average age was 23.4 yr (range: 19 to 30 yr), their mass, 74.4 kg (range: 63.2 to 86.3 kg) and their height, 1.75 m (range: 1.71 to 1.82 m). None of the subjects had previous medical history of low back pain or spine injury.

The task consisted of lifting a box (11.6 kg with dimensions of 23x35x24 cm^3) from a low table (22 cm above the force platforms) at three different locations, turning and placing the box on a maximum table (80 cm above the force platforms) at the right side of the subject. The three locations of the low table were at the left side of the subject (90°), directly in front of the subject (0°) and at an intermediate position between the two described positions (45°). Figure 1 illustrates the three starting conditions. One important condition was that the shoulders of the subject had to be parallel to the floor. The position of each foot was determined while the subject was standing in an anatomical position and the feet did not move during the tasks. The subjects adopted a diagonal manual grip and had to move the box in a diagonal trajectory.

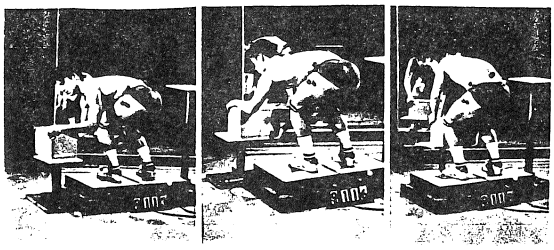

Figure 1. The three starting conditions for an asymmetrical lifting task.

Two 16 mm Locam cameras and two mirrors were used to collect the 3D positions of the anatomical markers on the subject. Twenty-four control points in a 2.2 m^3 volume were placed in the field of vision of both cameras and mirrors to establish a spatial co-ordinates reference frame. The external forces and their point of application were measured with two AMTI force platforms (one under each foot). The 3D loci of the anatomical landmarks (14 landmarks) were obtained with a DLT algorithm. The accuracy of the reconstruction was estimated around 5 mm with a maximal error of 10 mm. A fourth-order zero-phase Butterworth filter was used with an adjusted cut-off frequency for each marker and each axis. Cut-off values ranged from 0.5 Hz for the feet markers to 3 Hz for the trunk markers. The human body model consisted of 8 segments: feet (2), shanks(2), thighs(2), pelvis and trunk.

Linear velocity and linear acceleration of each body joint were computed by successive numerical differenciation procedures using the central-difference method. Angular velocities were determined by the method proposed by Berme et al (1987). Numerical differenciation was also used to calculate the angular accelerations. A 3D dynamic analysis was performed on each segment. First the free-body diagrams of the feet were drawn with all the forces and moments involved to determine the reaction forces and moments at the joint centres. The calculation proceeded sequentially upwards from the feet to L5/S1 joint through the shanks, thighs and pelvis.

A two-way analysis of variance with repeated measures was used to test statistical differences between the three tasks. Linear contrast were used to investigate the 'In-between effect'.

RESULTS AND DISCUSSION

The maximum net muscular moments for the three different starting positions were not generallly significant at the exception of the extension moment (table 1).

Table 1. Maximum net muscular moments (Nm) for the three starting positions (n=10)

	90°		45°		0°	
	M	SD	M	SD	M	SD
Left twisting	33	21	31	15	20	10
Left bending	21	13	37	35	25	15
Right twisting	9	8	8	7	7	6
Right bending	35	20	29	33	15	11
Extension	217	21	219*	25	228*	30

* Significantly different at P≤ .05

The maximum muscular moments varied between 20 and 33 Nm in left twisting, between 15 to 37 Nm in lateral bending (both directions) and between 217 and 228 Nm in extension. The maximum muscular moment in extension for the three tasks occurred at the beginning of the lift when concentric strength was required. The angle of flexion and the angular velocity (in extension) of the trunk were approximately the same for the three conditions around 67° and 30°/s respectively when the maximum muscular moment in extension occurred. However, the orientation of the trunk relative to the pelvis was significantly different for the three conditions. The twisting of the trunk to the left was 19°, 10° and 1° respectively for the 90°, 45° and 0° condition. According to Marras and Mirka (1989), trunk moment decreased by approximately 8.5% of maximum for every 15° of asymmetric trunk angle. Maximum trunk moment was observed at a trunk angle of 40° in a static exertion. With an angular velocity of 30°/s, a trunk angle of 40° with no asymmetry, trunk strength was at 65% of the maximum moment. If trunk asymmetry increased to 15°, trunk strength decreased by 5%. The results of this study show that the three starting positions do not have a large effect on the muscular moments. On the other hand, trunk position affects trunk strength in such a way that the risk of injury is probably greater in the starting position at 90° due to the larger degree of trunk asymmetry than at 45° or 0°. Moreover, the risk of injury at 90° is increased by the fact that twisting and bending may cause annular failure of the intervertebral disc (Hickey and Hukins, 1980).

The moment in extension imposed around the spine by the lifting tasks was around 220 Nm and it was always maximum than the other components by a factor of 5. Despite the asymmetrical nature of the tasks particularly for the starting position at 90°, the twisting and lateral bending moments were not really high. This could be attributed to the position of the shoulders (parallel to the ground) which minimizes twisting and bending efforts against gravity. According to Beimborn and Morrissey (1988) trunk extensors can generate the largest moment, followed in order by trunk flexors, trunk side benders, and trunk rotators. The problem to be solved remains the one of assessing the available strength of each muscular group and of examining if the moments imposed by the tasks do not reach the maximal muscular capacity of the trunk. The data available are not sufficient to assess the relative demand of the tasks in all directions. For instance, Marras and Mirka (1989) provided the regression coefficients for maximum moment production in extension. However, they do not mention if the effect of gravity was considered in the analysis. Parnianpour et al. (1991) measured the triaxial maximum isometric strength of normal subjects in all six possible directions; however, the effect of gravity, trunk asymmetry and trunk velocity were not considered which limits the use of their results in this study. More research is necessary to obtain the relative demand of a task.

In conclusion, the moments generated at the L5/S1 joint for the three starting positions were approximately the same magnitude and only little differences were observed between the conditions; however, the starting position at 90° remains more hazardous due to the larger degree of asymmetry of the trunk when the maximum net muscular moment is produced.

REFERENCES

Adams, M.A. and Hutton, W.C.*Spine*, 6(3),241-248,1981.
Berme, N. and Cappozo, A. Biomechanics of Human Movement: Applications in Rehabilitation, Sports and Ergonomics, Bertec Corporation, Worthington, Ohio, 1990.
Beimborn, D.S. and Morrissey, M.C.*Spine* 13(6), 655-660,1988.
Chaffin, D.B. *Journal of Occupational Medicine*, 21, 269-272
Drury, C.G. et al. *Human Factors,* 24(5), 553-565, 1982.
Hickey, D.S. and Hukins, D.W.L. *Spine*, 5(2),106-116,1980.
Marras, W.S. and Mirka, G.A. *Human Factors,* 31(6),667-677,1989.
NIOSH (National Institute for Occupational Health and Safety). A Work Practices Guide for Manual Lifting. Cincinnati, Ohio, Technical Report No 81-122, 1981.
Parnianpour, M. *International Journal of Industrial Ergonomics,* 8,279-287,1991.

GRANTS from IRSST and NSERC

BIOMECHANICAL COMPARISON OF FIXATION METHODS FOR THE PREVENTION OF PELVIC RING EXPANSION

Emmanuel M. Paul, Mark S. Vrahas, Scott C. Wilson and P. Dean Cummings
Department of Orthopaedic Surgery, M.S. Hershey Medical Center, Penn State, Hershey PA 17033 USA

INTRODUCTION: Several methods of fixation are commonly employed by orthopaedic surgeons to stabilize pelvic fractures. It is thought that these methods control intrapelvic bleeding by restricting radial expansion of the pelvis. To date no study has directly measured the circumferential stability of the pelvic ring obtained by these methods. We compared several constructs to determine which provided the most effective constraint.

METHODS: Three typical methods of internal fixation (I-III) and 3 representative methods of external fixation (IV-VI) were compared respectively: I) 2 pubic symphyseal plates with 2 sacroiliac screws, II) 2 pubic symphyseal plates alone, III) 2 sacroiliac screws alone, IV) Synthes rectangular frame, V) Orthofix frame, and VI) Slatis frame. Each of these devises are commercially available and were applied in a standard fashion. Four fresh frozen human cadaveric pelves were used, in which the pubic symphysis and one sacroiliac joint were disrupted to simulate an unstable fracture. Each device under test was applied to the pelvis and the fixation was assessed. A custom testing apparatus was devised which permitted uniform circumferential expansion from within the pelvic ring, thus loading the fixation device in a physiologic manner. This apparatus consisted of a sealed non-distensible bladder filled with water, mounted on a rigid frame. Two side ports allowed the system pressure to be monitored as the amount of water within the bladder was adjusted. The experimental construct was suspended from the frame with the pelvis encircling the bladder. The initial bladder volume was adjusted to zero the system pressure. The bladder volume was then sequentially increased to generate pressures up to 80 mm/Hg. Measurements of expander volume, expander pressure, and pelvic ring distraction were made. Circumferential stability was assessed by comparison of the pressure/volume curves. Failure of fixation was defined as the point at which the pressure/volume curve plateaued.

RESULTS: Predictably, fixation using 2 pubic symphyseal plates and 2 sacroiliac screws resulted in negligible distraction. Other methods required 1.7 to 2.3 times the volume to generate pressures of 10mm/Hg. Two anterior plates alone provided the least resistance to horizontal expansion; and in 2 of 4 pelves fixation failed at pressures less than 20mm/Hg. Two sacroiliac screws were somewhat more effective, but still less effective than all methods of external fixation. All 3 methods of external fixation were comparable.

DISCUSSION: Although internal fixation of the pelvis front and back provides the greatest circumferential stability, this technique requires considerable surgery and thus is impractical for emergent use. More limited forms of internal fixation may be used but offer minimal stability. External fixation significantly improves circumferential stability and is readily applied. Therefore, this method is preferable for the emergent control of intrapelvic bleeding.

IDENTIFICATION OF A GENERAL MECHANISM OF IMPACT ABSORPTION IN THE LOWER EXTREMITY

Paul DeVita, Tom Dolan, and William A. Skelly
Department of Physical Education, Southern Illinois University
Carbondale, Illinois 62901

INTRODUCTION

Joint torques at hip and knee along with EMG data for 6 lower limb muscles were analysed during airborne and floor contact phases of vertical landing, hopping and running for the purpose of identifying a general mechanism of impact absorption in the lower extremity. It was hypothesized these movements would have similar torque patterns during the period beginning shortly prior to and ending shortly after initial floor contact and the response in these measures to a change in landing stiffness would be similar in all movements. Results showed a general mechanism of impact absorption across movements which included hip extensor and knee flexor torques prior to floor contact and an increase in the magnitude of these torques as landing stiffness increased. EMG indicated that hamstrings may have a crucial role in setting these net torques in preparation for impact with the floor.

REVIEW AND THEORY

DeVita et al (1) showed subjects prepare for landing impacts from vertical falls by exerting hip extensor and knee flexor torques during the last 50 ms before floor contact and that landing stiffness was controlled by increasing these torques for stiffer landings. These results confirmed previous hypothesis that impact forces are modified by neuromuscular activity prior to floor contact (2) and showed stiffer landings are performed by changing relative tensions across the joints to produce changes in net torques and not by simply increasing muscle tensions on both sides of the joints. It was also observed that joint torques prior to impact and their response to increased stiffness were similar to torques during late swing phase in running and their response to increased running speed (4) which has been equated to stiffness (3). The similarity between the joint torques in landing and running led us to hypothesize a general mechanism of impact absorption and attenuation of impact forces for many types of impacts to the lower limb. The mechanism involves presetting hip extensor and knee flexor torques prior to impact with their magnitudes directly related to the desired landing stiffness. The purpose of the study was to test this hypothesis in 3 types of landings onto the lower extremities: landing from a vertical fall (single landing), landing during hopping (multiple landings) and landing during running.

PROCEDURES

Three males participated in this pilot study. Experimental setup included force platform (sampling at 1000 Hz), 16 mm cine camera (200 Hz) filming subjects' sagittal plane, EMG (1000 Hz) with surface electrodes on the gastrocnemius, semimembranosis, biceps femoris, rectus femoris, vastus lateralis, and gluteus maximus, and timing system to monitor running speed. Subjects performed soft and stiff landings from a vertical fall of 60 cm, soft and stiff hopping and slow (3.0 m/s) and fast (4.3 m/s) running. Soft and stiff landing and hopping had greater than and less than 90 degrees of knee flexion, respectively. Kinematic and ground reaction data were combined with inverse dynamics to evaluate lower extremity joint torques during airborne and floor contact phases. EMG data were rectified, and low pass filtered to produce linear envelops.

RESULTS AND DISCUSSION

Torque results (Fig 1) showed a stereotypical pattern during descent in preparation for floor contact. Prior to floor contact, hip extensor and knee flexor torques were observed in each movement and stiffness level except at the hip during soft hopping. Response to increased landing stiffness was consistent for all movements: magnitude of hip extensor and knee flexor torques increased in stiffer landings. Results for landing and running were consistent with previous work (1,4) and results from all movements showed that hip extensors produced more erect postures (less hip flexion) in preparation for stiffer landings. The larger hip extensor torque in stiff landings produced a greater rearward acceleration of the thigh which would cause knee extension. The increased knee flexor torque was therefore necessary to insure a flexed knee at impact. EMG showed greater activity in hamstrings during descent for stiff landings in all movements suggesting that appropriate force development in these muscles is critical for setting desired landing stiffness. After contact hip torque rapidly changed to flexor dominance in landing and hopping but remained extensor in running. Knee torques rapidly changed to extensor dominance in all movements.

REFERENCES

1 DeVita, P. et al. Med. Sci. Sports & Ex., 24, 108-115, 1992.
2 Lees, A. Eng. Med., 10, 204-211, 1981.
3 McMahon, T. et al. J. Appl. Physiol., 62, 2326-2337, 1987.
4 Simpson, K. et al. Int. J. Sport Biom., 6, 309-324, 1990.

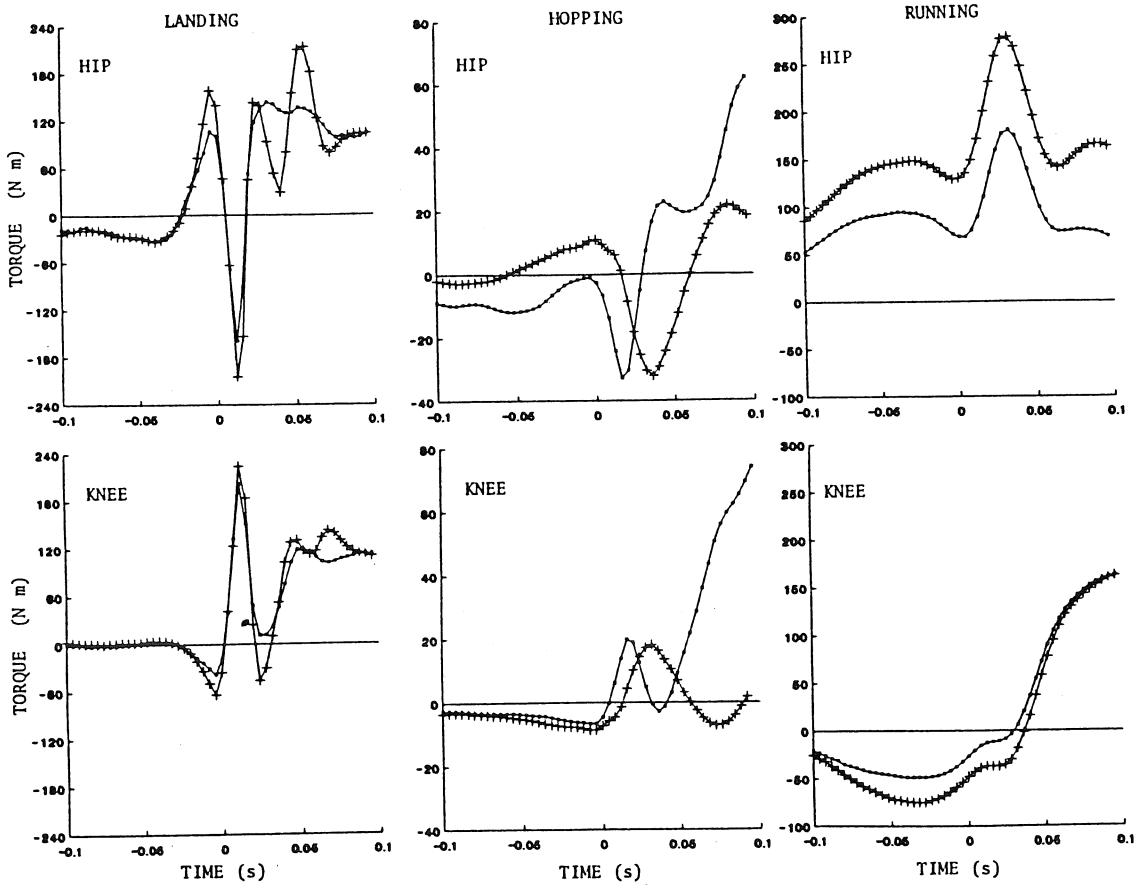

Fig. 1. Joint torques for 1 subject. Floor contact at time = 0 s. Positive values for extensor torques. Soft = dotted lines, stiff = + lines.

JUMPING AND LANDING

Podium Session 22

THE EFFECTS OF BILATERAL ASYMMETRY ON A MODEL OF THE COUNTER MOVEMENT JUMP

Jonathan I. Green,* Gary T. Yamaguchi* and John K. DeWitt†

***Department of Chemical, Bio, and Materials Engineering**
†Exercise and Sport Research Institute
Arizona State University, Tempe, Arizona 85287

INTRODUCTION

A model of the counter movement jump was developed to investigate the effects of bilateral asymmetry. The model contained seven degrees of freedom with three in each leg and one for the head, arms, and trunk (HAT). The dynamic equations of motion for the model were formulated using Kane's method. For this study, joint torques, rather than muscular forces, served as the inputs, while the outputs were the motion trajectories. A scheme of joint torques was compiled by trial and error to provide a bilaterally symmetric jump which matched the trajectories of experimental subjects. Asymmetries were then introduced to the model. These asymmetries caused large variations in the trajectories of the segments in comparison to the symmetric case. These results indicate that the modeled jumping task is extremely sensitive to asymmetries and bring into question the use of the bilateral symmetry assumption in future modeling studies.

REVIEW AND THEORY

Past investigations of the motion of jumping have centered upon the study of human subjects performing vertical jumps. In addition, mathematical modeling of the human musculoskeletal system has been a recent approach to the investigations (Bobbert *et al.*, 1990; Pandy *et al.*, 1990). These models have accurately represented the system such that the major characteristics of a jump are present in simulations. These models provide a noninvasive method where it is easy to change the parameters of the system in order to see the effects upon jumping performance (Pandy *et al.*, 1989; Pandy *et al.*, 1990).

One of the key assumptions made both in the collection of human data and modeling is that of bilateral symmetry (Hubley *et al.*, 1983; Pandy *et al.*, 1990). This assumption is certainly beneficial in that it simplifies the system to be modeled. The effects of asymmetry on vertical jumping are assessed in this study using a model which includes both legs as separate entities. The magnitude of these effects may be instrumental in questioning the use of the bilateral symmetry assumption in future modeling studies.

PROCEDURES

There are two distinct parts to the study. First, human subjects were observed in order to quantify a "normal" jump. Second, a model was developed in order to investigate the effects of slight asymmetries on jumping performance.

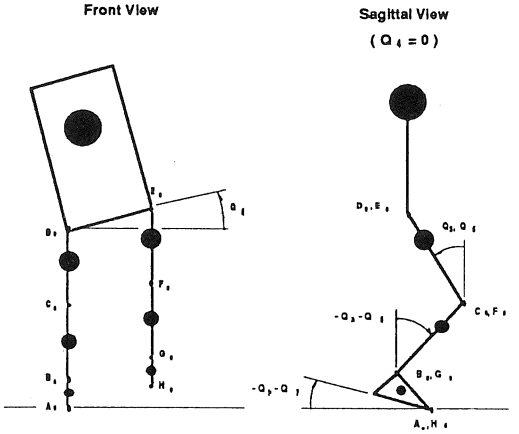

Figure 1. Schematic representation of the model

Three normal college age males (height 178 ± 4.5 cm and body mass 78.8 ± 2.4 kg) were chosen as subjects for these experiments. Each subject was asked to perform three two-legged counter movement jumps with five reflective markers on each side of his body at the hip, knee, ankle, heel, and fifth metatarsal. The marker coordinates were low-pass filtered, and this smoothed coordinate data was then used to provide foot, shank, and thigh angles. Both within-subject and between-subject averaging was accomplished.

The model developed, depicted in Fig. 1, consists of seven degrees of freedom (DOF), including three in each leg and one for the head, arms, and trunk (HAT). The three leg DOF all lie in the sagittal plane, while the DOF for the HAT is in the frontal plane. The actuators of the model are torques rather than muscles with three on each side corresponding to the ankles, knees, and hips. The dynamic equations of motion of the model were formulated using Kane's method and the symbolic manipulation program AUTOLEV (Schaechter *et al.*, 1987). Once the model was formulated, a scheme of joint torques was compiled by trial and error such that the angles of the model followed those obtained with the subjects as closely as possible. Asymmetries were then introduced to the model in four different ways: (1) moving the lateral position of the HAT CM, (2) increasing the mass of the entire leg , (3) differentially increasing joint torques, and (4) changing the time of torque application.

RESULTS

The foot, shank, and thigh angles of both the within-subject and between-subject data exhibit similar trends

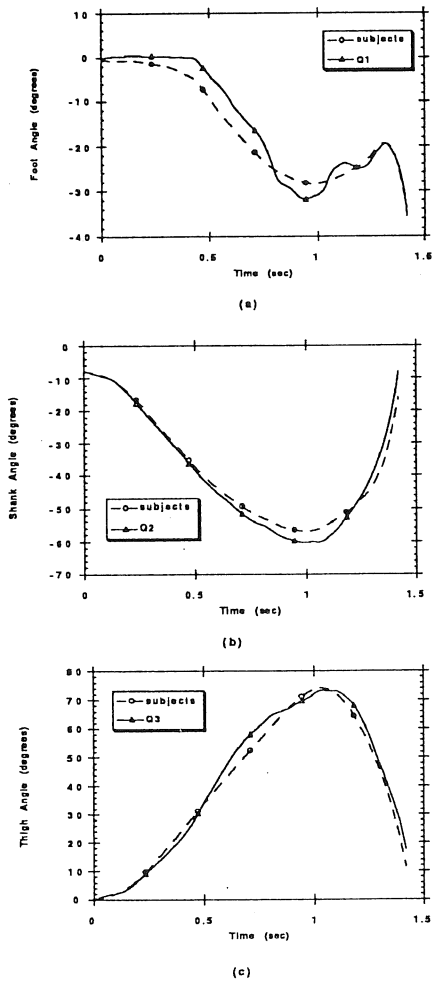

Figure 2. Angle trajectories for the (a) foot, (b) shank and (c) thigh for symmetric simulation

throughout the jump cycle. The time to 100% (takeoff) was computed to be 1.417 ± .231 sec. The height of the jumps was found to be 39.0 ± 3.7 cm. The angles of the foot, shank, and thigh are given in Fig. 2 for the average of the subject data along with the angles from the symmetric simulation. The general trends of all the experimental trajectories are followed in the simulation. The height of the simulated symmetric jump is 21.5 cm and the pelvic list is -2.514°.

As little as a 1% shift (0.86 mm) in the lateral position of the HAT CM greatly affects the jump. The shank and thigh farthest from the CM rotate upward more quickly than normal, while the foot falls more quickly. The same pattern is evident when the mass of one leg is increased and when a 1 msec time delay in the application of the joint torques is applied. A 1% increase in torque magnitude are of the opposite pattern where the affected side rotates upward too quickly. The height of the jump in all the asymmetric cases is decreased.

DISCUSSION

The time it took the subjects to complete the jump, 1.417 ± 0.231 sec, was longer than 0.4-0.5 and 0.5 sec respectively for Bosco *et al.* (1978) and Pandy *et al.* (1990). The height of the jump, 39.0 ± 3.7 cm, was less than the 41 ± 8 cm for Harman *et al.* (1990) who used a similar counter movement jump without arm motion. This increase in time and decrease in height can be attributed to the inability of the trunk to participate in a normal fashion. The height obtained in the symmetric simulation, 21.5 cm, was far less than that achieved by the actual subjects, 39.0 ± 3.7 cm. This can largely be attributed to the lack of ability of the model's HAT to move in the sagittal plane. Luhtanen *et al.* (1979) indicate that the trunk provides 10% of the jump height, which accounts for the lost height in our case.

Sensitivity to the introduced asymmetries is primarily due to the fact that the unaltered leg is essentially pushing up against less mass. Therefore, the extensor torques are too strong and result in a steep extension curve. Recall that the asymmetry of differential torque increase (case3) works in exactly the opposite fashion since the affected side is now stronger.

In summary, the magnitude of the effects of the asymmetries -- distance to the HAT CM, mass of the leg, torque magnitude increase, and torque timing delay -- cause considerable changes in the jump. In other words, the modeled jumping motion is highly sensitive to asymmetries. The results of this study make one question the use of the assumption of bilateral symmetry in future models of jumping. Past studies were effective in making conclusions about the general trends in jumping. However, future studies, particularly those interested in the intricacies of jumping, should explore the use of models with higher DOF so that the asymmetrical aspects of jumping are included.

REFERENCES

Bobbert, M. *et al. J. Biomechanics* **21**, 249-262, 1990.
Bosco, C. *et al. Eur. J. Appl. Physiol.* **41**, 275-284, 1979.
Harman, E. *et al. Med. Sci. Sports* **22**, 825-833, 1990.
Hubley, C. *et al. Eur. J. Appl. Physiol.* **50**, 247-254, 1983.
Luhtanen, P. *et al. Eur. J. Appl. Physiol.* **38**, 181-188, 1978.
Pandy, M. *et al. Proceedings of the 1989 ASME Winter Annual Meeting*, San Francisco, (pp. 59-63), 1989.
Pandy, M. *et al. J. Biomechanics* **23**, 1185-1198, 1990.
Schaechter, D. *et al.* AUTOLEV User's Manual: Version 2

ACKNOWLEDGEMENTS

We thank Daniel W. Moran for his assistance with the programming of the plotting and graphics subroutines. We also thank Philip E. Martin for allowing the use of his equipment and for his review of the paper.

THE CONTRIBUTION OF BELOW KNEE WOBBLING MASS TO THE ESTIMATION OF VERTICAL KNEE JOINT FORCES FOLLOWING IMPACT WITH THE GROUND

David Andrews, B.P.E. and James J. Dowling, PhD.
Department of Physical Education, McMaster University
Hamilton, Ontario, Canada.

INTRODUCTION

In human impact situations involving high peak accelerations, such as landing from a height onto one stiff leg, the wobbling mass (Gruber et. al,1987) of the support leg will accelerate relative to the rigid mass (bone), as indicated by the output of accelerometers mounted on the posterior wobbling tissue of the support leg, and on the tibia, respectively. Ground reaction forces (force platform) and leg accelerations, were used as input into rigid only and rigid and wobbling link segment models, to estimate vertical knee joint forces at impact. Mean peak vertical knee joint forces ranged in magnitude from 2.66 to 3.53 times body weight (BW) for the 5 and 10 cm drop heights respectively. A two-way (model type, and height) repeated measures ANOVA revealed no main effect for calculation method.

REVIEW OF THEORY

Studies by authors such as Radin et al., (1982) indicate that impact loading of musculoskeletal systems can lead to knee joint injury. The magnitudes of these potentially injurious knee joint forces transmitted between segments, can be achieved using a rigid link segment analysis if segment accelerations and ground reaction forces are known (Smith,1975). Rigid segment analyses however, do not take into account the independent motion of the wobbling mass which exists following impact. The purpose of this study then, was to determine whether vertical knee joint forces calculated using a rigid link segment model were effected by the introduction of a wobbling mass component.

PROCEDURES

Fifteen healthy subjects (8 male, 7 female) dropped vertically, landing on one leg (stiff knee), onto a force platform (AMTI), from heights of 5 and 10 cm. Accelerometers, 50g and 1000g (Durham Instruments) were cemented (Skin Bond Cement) to the wobbling mass on the posterior aspect of the support leg, and on the tibia respectively. Accelerometer and force plate data were sampled at 1000 Hz and then A/D converted (Northern Digital). Using accelerometer and force plate data, vertical knee joint forces were calculated for each subject using both rigid only and rigid and wobbling models of the leg. Equations [1] and [2] show how these calculations were made. Segment masses (wobbling=skin, muscle, fat and rigid=bone) were obtained from cadaver data (Clarys and Marfell-Jones, 1986). Statistical analysis of the reaction force data consisted of a two-

way repeated measures ANOVA, %RMS error, and correlation coefficients.

Rigid only:

$$R_Y = m_3 \cdot \ddot{x}_1 + m_3 \cdot g - F_Z \quad [1]$$

Rigid/wobbling:

$$R_Y = m_3 \cdot \ddot{x}_Y + m_1 \cdot g + m_2 \cdot g - F_Z \quad [2]$$

where:
R_Y = vertical knee joint force
F_Z = vertical ground reaction force
m_3 = total mass of leg
m_2 = mass of wobbling tissue
m_1 = mass of rigid tissue
$\ddot{x}_1$ = rigid mass acceleration
$\ddot{x}_Y$ = resultant acceleration of m_1 and m_2
g = gravity (9.81 m/s^2)

RESULTS AND DISCUSSION

Table 1 summarizes mean %RMS errors and correlation coefficients between vertical knee joint forces as calculated by both a rigid and a rigid and wobbling link segment model of the leg, for both drop heights (5 and 10 cm). Mean peak knee joint forces have also been included. Shown in Figure 1, are examples of exceptionally similar vertical knee joint forces resulting from impact, using both methods. Despite the fact that there were differences in the rigid and wobbling accelerations, for all subjects, peak vertical knee joint forces were virtually the same (as shown in Figure 1 for one subject), independent of the model used to calculate them. This was confirmed by a two-way repeated measures ANOVA which indicated no main effect for calculation method. Vertical knee joint forces (Equation [2]) were found to be sensitive to the large relative Fz values.

Table 1: Mean results for 15 subjects. (RR_Y = rigid only R_Y; RWR_Y = rigid and wobbling R_Y)

Height (cm)	Mean %RMS error±SD	Mean r value±SD	Mean RR_Y (BW)	Mean RWR_Y (BW)
5	19.8±6.8	.98±.015	2.657	2.643
10	21.1±6.0	.98±.013	3.529	3.520

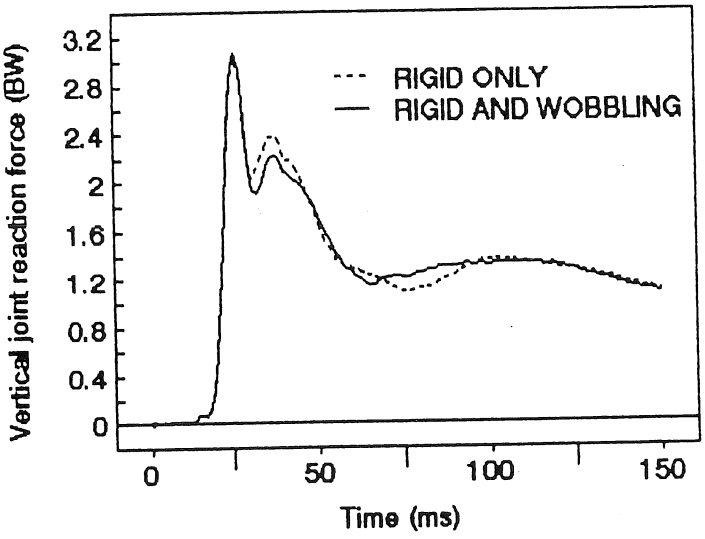

Figure 1: Typical vertical knee joint reaction forces.

REFERENCES

1. Clarys, J.P. et al., *Human Biology*, 58(5):761-769, 1986.
2. Gruber, K. et al., *Biomechanics X-B*, 1095-1099, 1987.
3. Radin, E.L. et al., *J. Biomechanics*, 15:487-492, 1982.
4. Smith, A.J. *J. Human Movmt. Studies*, 1:78-86, 1975.

MUSCLE ACTIVITY AND KINETICS DURING LANDINGS WITH REDUCED VERTICAL REACTION FORCES

by Dawn M.E. Irvine, Jill L. McNitt-Gray, Barry A. Munkasy,
Carolyn Barbieri, and Michelle D. Welch
Biomechanics Research Laboratory, Department of Exercise Sciences
University of Southern California, Los Angeles, CA 90089-0652, USA.

INTRODUCTION

Landing techniques favoring a greater than normal degree of lower extremity joint flexion (soft) have produced reductions in the peak magnitude of the vertical reaction forces (Lees, 1981; Ozguven & Berme, 1988) and net joint moments (McNitt-Gray et al., 1989; Devita & Skelly, 1992) experienced during landings. However, the consequences of these "softer" techniques on the large internal forces produced by the muscles controlling the joint motion has not been investigated. The purpose of this study is to quantify and compare the muscle activity and kinetics during landings between normal and softer than normal landings.

METHODS

Six healthy male collegiate gymnasts performed six drop landings using normal and softer than normal landing strategies. Self selected softer than normal landings produced reductions of peak vertical forces of 1-2 BW. Each landing was performed by stepping from a stationary platform positioned 0.72 meters above two gymnastics landing mats (12cm) fully supported by two force plates. The reaction forces acting at the mat-plate interface were quantified using the force plates (800Hz). Segment kinematics were recorded simultaneously using high speed video (200fps). The muscle activation patterns of seven lower extremity muscles, gluteus maximus (GM), Vastus Medialis (VM), Rectus Femoris (RF), Biceps Femoris (BF), Medial Gastrocnemius (MG), Semitendonosis (ST), and Tibialis Anterior (TA), prior to and during the landing were quantified using surface electromyography (1600Hz; Beckman Silver-Silver Chloride electrodes; Differential Amps, Data, Inc.). The reaction forces, kinematics and EMG were synchronized at the time of contact. Markers positioned on the body of the subjects were manually digitized using a video based data acquisition system (Peak Performance, Inc.). Each coordinate of the digitized body landmarks (Zatsiorsky & Solyanov, 1983) were digitally filtered independently using a second order Butterworth Filter (Saito & Yokai, 1983) with a cut-off frequency derived by the method of Jackson (1979). Net ankle, knee and hip moments were calculated using Newtonian mechanics (Nm/kg). Peak extensor moments were quantified and statistically compared within subject. The EMG signals were initially band pass filtered with cut off frequencies of 30-800Hz, then rectified (SNIP, 1988, Digital Dynamics, Inc.). EMG amplitude was normalized to the peak value observed during all trials (Yang & Winter, 1984). The interval of interest, identified as the impact phase of the landing was defined as the time of contact to the third peak in force. The average time to third peak in force was 120ms. The EMG signals were integrated during this impact phase (120ms) and statistically compared within subjects. The temporal characteristics and the relative adjustments of muscle activity and ankle, knee and hip kinetics during the landings were compared within subjects. The experimental design used to compare normal with softer than normal landings was an analysis of variance, one within factor , .05 level of significance (BMDP Statistical Software, Inc. 1988).

RESULTS AND DISCUSSION

On average, gymnasts were able to reduce the peak vertical force by 1-2 BW. However, peak extensor moments for the ankle, knee and hip were not significantly different. Relatively small reductions in peak reaction forces may explain the lack of significant differences in peak extensor moments. Consistent temporal characteristics in EMG for each subject were observed (figure 1 & 2) during normal and softer than normal landings. Of the 7 lower extremity muscles tested, only the VM was significantly different <.05, between normal and softer than normal conditions. The softer than normal landings tended to show less VM integrated EMG during the impact phase than the normal landings. For the remaining 6 muscles, an inconsistency in burst amplitude during the impact phase was observed. Further analysis of functional muscle group patterns however may produce significant results.

REFERENCES

Devita, P. et al. MSSE, 24 (1):108-115, 1992.
Ozguven, et al. J of Biomech. 21:1061-1066, 1988.
Gross, T.S., MSSE, 20:506-514, 1988.
Jackson, K.M., IEEE Trans. Bio Eng. 26:122-124, 1979.
Lees, A., Eng Med. 10:207-211, 1981.
McNitt-Gray, J.L. IJSB, 1991.
McNitt-Gray, J.L. et al. Proc of ASB, 1989.
Panzer, V.P., Doc. Dissert. U of Oregon, 1987.
Saito, S. et al., B Hlth Sports Sci, U of Tsukuba, 5:201-206, 1982.
Valiant, G.A. et al., Biomechanics VIII-A, 112-116, 1983.
Yang, J.F., Winter, D.A., Arch Phys Med Rehabil., 65:517:521, 1984.
Zatsiorsky, V. et al., Biomechanics VIII-B, 1152-1159, 1983.

Acknowledgements: USC Faculty Research and Innovation Fund, the US Olympic Committee and USC Biomechanics Research Team.

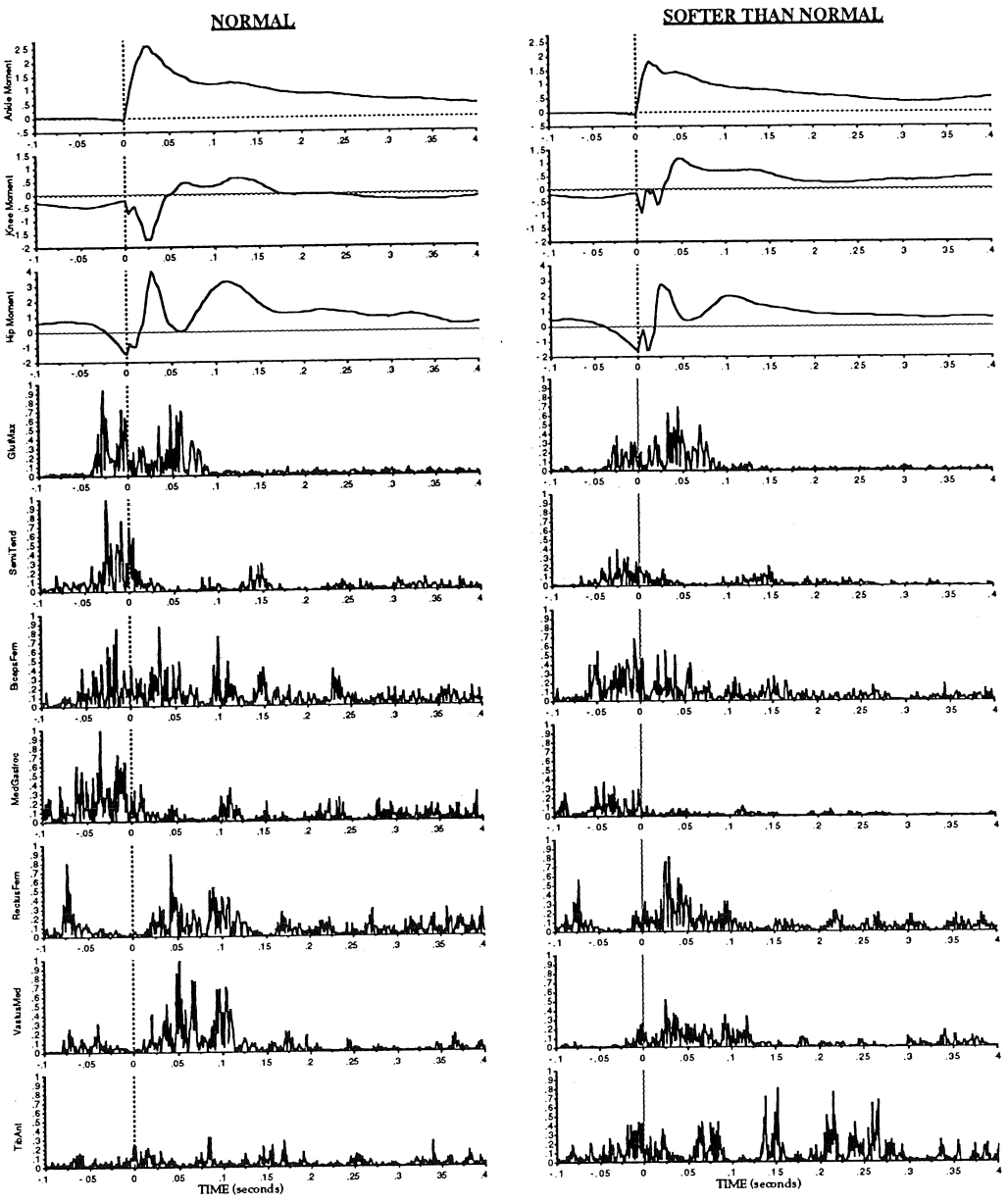

FIGURE 1. Ankle, knee and hip kinetics and rectified muscle activation patterns during a normal and softer than normal drop landing by a gymnast.

FACTORS INFLUENCING ANKLE AND KNEE SHEAR FORCE PARAMETERS DURING DANCE LANDINGS

K. J. Simpson & M. Pettit
Department of Exercise Science, University of Georgia, Athens, GA

INTRODUCTION

Knowledge of the magnitude and rate of loading shear forces during actual dance movements may be useful for understanding the influence of mechanical loading on the development of osteoarthritis or for designing prosthetics (1). Six female dancers performed 40 travelling jumps from various jump ranges. (JR). Analysis of the shear forces (SF) at the ankle (AJ) and knee joint (KJ) indicate that muscles act as an anti-shear mechanism at the AJ, but additively increase the instability at the KJ. When JR increases, the roles of the gastrocnemius-soleus complex at the AJ and the gastrocnemius at the KJ are minimal compared to joint reaction SFs and the quadriceps SFs. Furthermore, QuaF parameters are more closely associated with increased KJ SF parameters than KJ reaction forces.

REVIEW AND THEORY

Smith (1) noted the value of assessing the loads acting at the knee joint for designing prostheses that could withstand vigorous activity. The rate of loading shear forces (dF_{sf}/dt) is crucial to the understanding of the effect of forces on joint structures during activity. Therefore, the purpose of the study was to investigate the factors related to shear forces at the AJ and KJ generated during the landing phase of travelling jumps.

PROCEDURES

Six skilled female dancers performed 10 trials each at 30, 60, & 90% maximum JR at a consistent tempo. A fourth condition of trials consisted of a range between 35-100% maximum JR. A sagittal view of the right leg landing onto a force platform (500 Hz) was obtained using a high speed camera (100 fps). β, the patellar tendon angle (Fig. 1), and the quadriceps moment arm were interpolated from Nissell's (2) values using cubic splines. The moment arms for the other muscles were the calculated perpendicular distances to the line of action of the muscle. After deriving joint reaction and muscle forces from a Newtonian model, the SF components acting at the AJs and KJs were computed as follows (Fig. 1):

$$JRF1 = Fx1 * \cos\phi + Fy1 * \sin\phi \quad [1]$$

$$GaSoF = F_{gs} * \sin\Gamma \quad [2]$$

$$ASF = JRF1 + GaSoF \quad [3]$$

where JFR1 = the AJ reaction force, GaSoF = the gastrocnemius-soleus SF and ASF = the total SF acting at the ankle joint. Positive values imply that the foot is being sheared anteriorly relative to the tibia.

$$JRF2 = Fx2 * \cos\phi + Fy2 * \sin\phi \quad [4]$$

$$GasF = F_{gas} * \sin\Gamma \quad [5]$$

$$QuaF = F_{qua} * \sin\beta \quad [6]$$

$$KSF = JRF2 + GasF + KSF \quad [7]$$

where JRF2 = the KJ reaction force, GasF and QuaF are the SFs for the gastrocnemius and quadriceps, respectively, and KSF = total knee SF.

Maximum SF magnitudes and dF_{sf}/dt values and maximum values for angular kinematic parameters were generated. The Model Statistic (3) was used to assess ($p < .05$) the individual responses to increased JR. To determine the influence of various muscular, kinetic and kinematic biomechanical parameters on increased SFs, adjusted R^2 values were evaluated ($p < .05$).

RESULTS

The proportion of SF that an individual SF contributes to the maximum total joint SFs are shown in Table 1 and visually demonstrated in Figure 2. The JRF1 always demonstrated greater values than the opposing GaSoF, creating a negative resultant ankle SF. When the JR increased, the negative ASF increased even though GaSoF also increased. This was also true for the corresponding dF/dts. For the maximum KSF value, the GasF contributed minimally to the KSF, and the JRF2 contributed slightly less SF than the QuaF. However, during the initial landing phase, the JRF2 and QuaF contributed similarly to maximum KSF. Subjects demonstrated increased maximum magnitudes and dF_{sfmax}/dt for all knee SF parameters except for the rate of loading GasF.

The times to the maximum magnitude parameters generally decreased, although not all subjects and parameters demonstrated this trend. With increased JR, times to dF_{sfmax}/dt parameters fluctuated among subjects.

When JR increased, all subjects landed with the lower leg inclined more toward the horizontal and used greater knee flexion during the landing phase. Subjects displayed increased maximum flexion velocities and positive angular accelerations at the ankle and knee joints.

The R^2 analyses revealed that the maximum magnitude and dF_{sfmax}/dt, respectively, for ASF was more closely associated with JRF1 (.893 and .901) than the GaSoF (.046 and .082) values. For the KSF magnitudes and dF_{sfmax}/dt, the QuaF and KJRF parameters demonstrated R^2 values ranging from .663 to .923. In contrast, the contribution of the GasF to increased KSF values was less than 1% of the explained variance. The kinematic variables were less related. The maximum ankle and knee flexion velocities R^2s were greater (.330 to .523) than the negligible values for the tibial landing angle and minimum knee angle.

DISCUSSION

The SFs acting at the AJ demonstrate patterns similar to those reported by Scott and Winter (4) during the landing phase of running (4). A maximum ASF occuring within 25 ms of landing was observed by Skelly and DeVita (5) for stiff legged landing that was

barely discernible for these data even at the greatest JR. Because this movement required less vertical impact force than a stiff legged landing and the subjects are trained to flex the leg at landing, biomechanical differences in ASF patterns are expected. Because the JRF1 magnitudes are greater in the negative direction, the foot is being sheared in the negative direction. Increased ASFs, therefore, are highly related to increased JRF1s. The GaSoF, however, does provide SFs which minimize the resultant ankle SF. At the KJ, the GasF contribute very minimal SFs that oppose the QuaF and JRF2 forces. Joint reaction forces and QuaFs are the most important contributors to increased AJ and KJ SFs, respectively, which occur at greater JRs.

REFERENCES

1. Smith, AJ. Hum Movem Stud, 1:78-86, 1975.
2. Nissell R. Acta Orthop Scand Suppl, 56:216, 1985.
3. DeVita, P et al. Hum Movem Stud, 7:73-85, 1988.
4. Scott, S et al. Med Sci Sports Exerc. 22:357-369, 1990.
6. Skelly, WA et al. Proc 6th Bienn Conf. CSB, 59-60, 1990.

ACKNOWLEDGEMENTS

Partial funding was provided by the Univ. of Georgia Research Foundation. We thank Paul DeVita, Trish Shewokis and Lisa Kanter for their technical assistance.

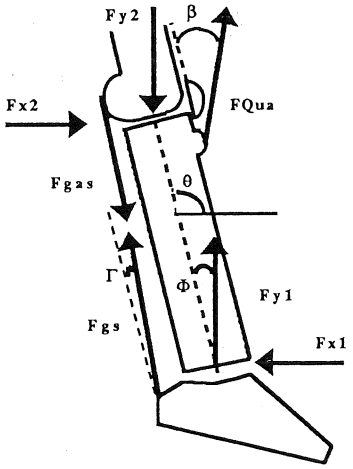

Figure 1. Free body diagram of leg. See text for details.

Table 1. Proportion of component SFs to maximum value of total SFs.

Shear Force Component	% of Total Joint SF Min.	Max.
At Ankle:		
JRF1	71.5	99.7
GaSoF	0.3	28.5
At Knee:		
JRF2	28.4	62.6
GasF	0.0	6.1
QuaF	33.4	71.2

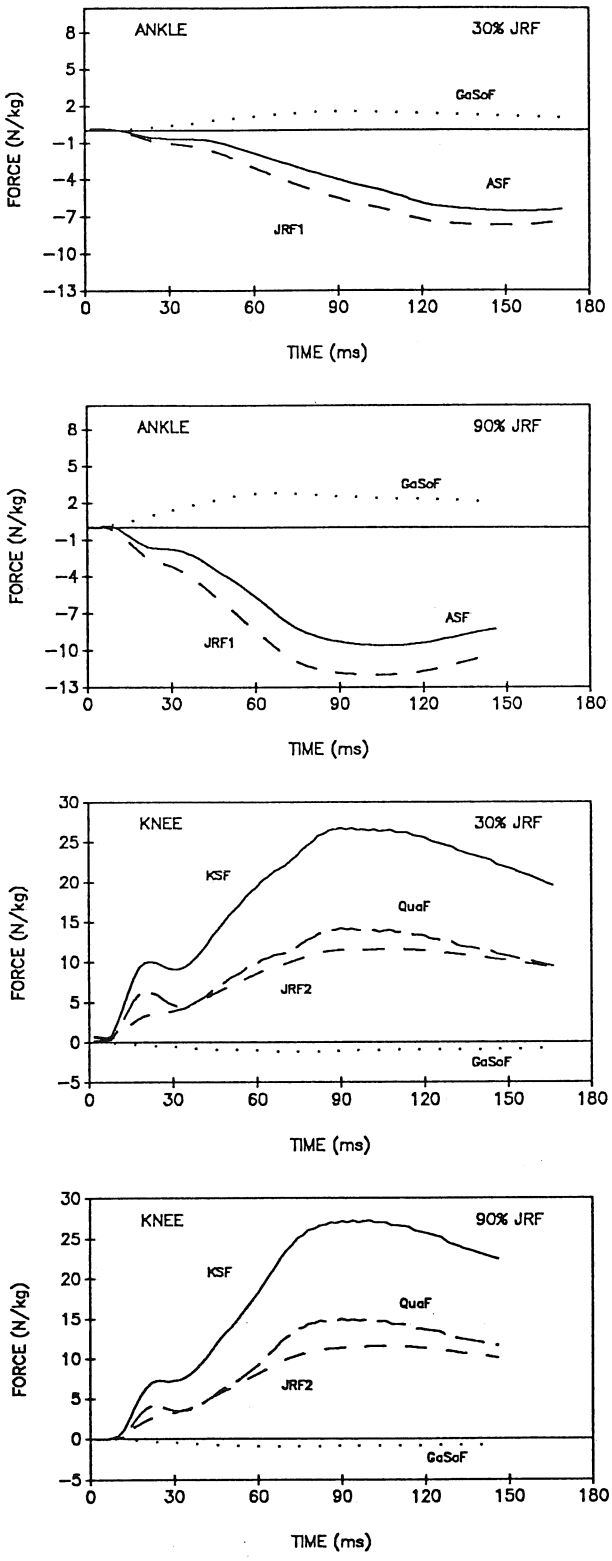

Figure 2. Ankle and knee shear forces for the 30% and 90% JR condition.

VARIABILITY OF TWO TYPES OF LANDINGS

J.S. Dufek*, T.R. Derrick# and B.T. Bates*

*Department of Exercise and Movement Science, University of Oregon, Eugene, Oregon 97403, USA.

#Department of Exercise Science, University of Massachusetts-Amherst, Amherst, Massachusetts 01003, USA.

INTRODUCTION

The impact phase of landing has been a topic of inquiry for numerous investigators. Various experimental paradigms have been incorporated to evaluate and describe the kinematics (McNitt-Gray, 1991) and kinetics (Dufek *et al.*, 1990) of landing during the passive loading phase while more recently, airborne and landing phase joint kinetics and energetics have been reported (DeVita *et al.*, 1992). Experimental control and performer variability inherent in the incorporated design is of concern with respect to statistical power and the ability to detect real performance differences.

REVIEW AND THEORY

Numerous sport/movement environments have been incorporated to investigate landing performance (Valiant *et al.*, 1985; Steele *et al.*, 1987; Ricard *et al.*, 1990; Dufek *et al.*, 1991) with few experimental results reported from non-simulated landing activities (Panzer *et al.*, 1988; Lafortune, 1985). The limitations presented to the researchers when attempting to obtain competitive or "game" landing data for biomechanical assessment are obvious.

Given the constraints of data collection facing the investigators in the competitive arena, a simulated environment is typically created in the laboratory. This approach to dynamic load assessment is not unique to landings, as it is typically embraced in gait-related evaluations that use a treadmill as well as numerous other sport studies. A unique question that does face landing investigators, however, is how to simulate the landing. One obvious method is to have subjects jump into the air in order to initiate a landing. It is, however, extremely difficult to achieve control using this procedure. Two common, more controllable methods that have appeared in the literature include suspension of the subject from an overhead apparatus allowing a vertical drop (Dufek *et al.*,1991; Mizrahi *et al.*, 1982; Smith, 1975) or positioning a raised platform from which the subject steps or jumps (DeVita *et al.*, 1992; McNitt-Gray, 1991; Dufek *et al.*, 1990). Any reduction in performer variability that can be obtained by selecting the appropriate methodology can maximize statistical power (Bates, 1989) and in turn provide a greater probability of identifying condition differences. In order to ascertain the inherent variability associated with each of these two common experimental methods, a comparative assessment of the techniques is necessary. The purpose of the study was to evaluate the variability associated with selected ground reaction force (GRF) characteristics of drop and step-off landing performances.

PROCEDURES

The drop condition (C1) was established with a horizontal bar suspended from the ceiling and appropriately adjusted for each subject such that the actual vertical displacement of the malleolus was 0.60 m plus the standing floor to malleolus height. An equal vertical displacement was created for the step-off condition (C2) by positioning a 0.60 m raised platform 0.25 m horizontally from the center of the landing target. The horizontal displacement was necessary but minimized in order to allow each subject to step off of the platform as opposed to jumping which would raise the center of gravity above 0.60 m. The drop was accomplished by suspending the subject from the properly adjusted overhead bar and subsequently performing a self-initiated release. The step-off was performed by first establishing a stable vertical standing position on the raised platform and then stepping off.

Five volunteer male recreational athletes (23-37 yrs) granted consent in accordance with the policies established by the University's Committee for the Protection of Human Subjects. All subjects performed drop and step-off landings onto a target dual force platform system (A.M.T.I., 1000 Hz) in alternating order for a total of 64 trials per subject. Right and left leg maximum forefoot (F1) and rearfoot (F2) vertical and braking (FB) and propulsive (FP) anterior-posterior (A-P) GRF values were evaluated for each subject-condition-trial. The first 25 trials per subject-condition were incorporated in the subsequent analysis.

RESULTS AND DISCUSSION

Symmetry was first assessed by using a Model Statistic within-subject statistical technique (Dufek *et al.*, 1991). Results identified 67.5% significant ($p<0.05$) differences

across subjects, with 16 right and 11 left leg dominant performances. A similar distribution of observed asymmetry between conditions (C1=14, C2=13) was observed, therefore, right and left leg data were averaged for each subject-condition-variable and these average force values were used for subsequent analyses.

The average F1, F2, FB and FP force values along with the respective coefficient of variation (CV) percentages are given in Table 1. These data clearly identify no one landing condition as being more or less variable than the other. Overall, 50% of the CV values were observed to be greater for each condition with mean values for all subject-variables within conditions being nearly equal for C1 (19.8%) and C2 (19.6%). Mean absolute variabilities were slightly greater for C1 (2.1 vs 1.9 N/kg) with similarly decreasing values for both conditions (F2, F1, FP, FB). The peak vertical GRF variability for individual subjects was greater for C1 (70%) while A-P variability was greater for C2 (60%). One subject (S2) exhibited consistently greater variability within a condition (C1) while two subjects (S1, S3) displayed greater A-P variability for C2. Overall, subject responses were differential.

These experimental results suggest a general trend toward increased variability during C1 for peak vertical GRF values. Conversely, greater variability for peak A-P forces was observed during C2. All individual subjects did not follow this trend and performance variability was nearly equally distributed suggesting that both methods of collecting data are equally satisfactory. Additionally, because mechanical loading is a function of both force magnitude and timing, it is suggested that temporal variability be similarly assessed in order to obtain a more complete picture of landing performance variability.

REFERENCES

Bates, B.T. *Jrl. Biomech.*, 22(8/9), 963-965, 1989.

DeVita, P. et al. *Med. Sci. Spt. Exerc.*, 24(1), 108-115, 1992.

Dufek, J.S. et al. *Med. Sci. Spt. Exerc.*, 23(9), 1062-1067, 1991.

Dufek, J.S. et al. *Med. Sci. Spt. Exerc.*, 22(3), 370-377, 1990.

Lafortune, M. *Spt. Sci. Med. Quart.*, 2(1), 2-4, 1985.

McNitt-Gray, J.L. *Intl. Jrl. Spt. Biomech.*, 7, 201-224, 1991.

Mizrahi, J. et al. *Eng. Med.*, 11(3), 141-147, 1982.

Panzer, V.P. et al. *Biomech. XI-B*, 727-735, 1988.

Ricard, M.D. et al. *Int. Jrl. Spt. Biomech.*, 6, 67-77, 1990.

Smith, A.J. *Jrl. Hum. Mvt. Studies*, 1, 78-86, 1975.

Steele, J.R. et al. *Jrl. Hum. Mvt. Studies*, 13, 399-410, 1987.

Valiant, G.A. et al. *Biomech. IX-B*, 117-122, 1985.

Table 1. Mean and standard deviation ground reaction force and coefficient of variation values

Sub	F1			F2			FB			FP		
	Mean	SD	CV	Mean	SD	CV	Mean	SD	CV	Mean	SD	CV
C1 (DROP)												
S1	19.0	(2.6)	13.9	27.1	(5.7)	21.0	6.1	(0.5)	8.9	7.3	(2.2)	29.9
S2	12.5	(1.2)	10.0	20.8	(3.4)	16.3	4.2	(0.9)	21.4	3.6	(1.1)	30.1
S3	12.5	(1.5)	12.4	22.0	(4.0)	18.4	4.6	(0.7)	16.3	4.6	(1.8)	40.2
S4	9.5	(1.4)	14.7	29.0	(5.7)	19.6	1.8	(0.1)	8.3	3.6	(1.5)	42.5
S5	14.8	(1.6)	10.8	33.7	(4.2)	12.6	5.9	(0.7)	11.8	4.9	(1.8)	37.4
Mean		1.7	12.4		4.6	17.6		0.6	13.3		1.7	36.0
C2 (STEP-OFF)												
S1	16.3	(1.6)	10.1	27.5	(4.2)	15.4	7.4	(0.9)	12.7	4.1	(2.0)	48.2
S2	14.5	(1.4)	9.6	22.5	(3.2)	14.2	7.4	(0.6)	8.8	3.9	(0.8)	21.5
S3	10.6	(1.0)	9.9	22.3	(4.6)	20.6	4.3	(0.5)	12.6	3.0	(1.2)	41.0
S4	7.8	(0.6)	7.0	30.6	(6.0)	19.7	1.8	(0.1)	8.3	2.2	(1.2)	54.5
S5	13.2	(2.2)	17.0	34.1	(3.5)	10.2	5.5	(0.8)	15.3	4.0	(1.4)	36.2
Mean		1.4	10.7		4.3	16.0		0.6	11.5		1.3	40.3

Note: Force values in N/kg; CV values in %; See text for abbreviations.

EFFECTS OF FATIGUE ON MECHANICAL AND MUSCULAR COMPONENTS OF PERFORMANCE DURING DROP LANDINGS

Roger James, Janet S. Dufek, and Barry T. Bates

Biomechanics/Sports Medicine Laboratory
University of Oregon
Eugene, Oregon 97403, USA

INTRODUCTION

Fatigue is a physiological constraint that could inhibit landing performance. Evaluation of the effects of fatigue on impact forces and muscle activity during landings could provide insight toward landing control mechanisms and injury prevention. Selected vertical ground reaction force (GRF) and integrated electromyographic (IEMG) variables were evaluated for drop landings during fatigue. Single subject ANOVA results indicated differential subject responses for all variables except the magnitude of the first maximum GRF value (F1) and the total amount of IEMG activity of the tibialis anterior muscle (TA) which increased and decreased ($p < 0.05$), respectively, for each subject. Results suggest different subject strategies for fatigue accommodation during landing.

REVIEW AND THEORY

The ability to control landing impact forces during repetitive dynamic airborne activities is believed important in the prevention of overuse injuries (Ricard et al., 1990; Steele et al., 1988). Previous researchers have documented the interactive responses of landing impact forces to manipulations of internal and external constraints (Bates et al. 1989; DeVita et al., 1992; Dufek et al., 1990; McNitt-Gray, 1991). Observed interactions between landing force magnitudes and performance constraints suggest the use of different neuromuscular control strategies for regulating landing forces.

Fatigue has been described as the progressive increase in effort and decrease in ability to produce force (Deschenes et al., 1989; Häkkinen et al., 1988; Vøllestad et al., 1988). Several mechanisms of fatigue have been identified (Åstrand et al., 1986; Deschenes et al., 1989; Vøllestad et al., 1988) and often function simultaneously at various levels to inhibit performance. Because of the importance of neuromuscular control in attenuating landing impact forces, fatigue that affects components of the neuromuscular system might influence the magnitude of the impact forces and, therefore, the possibility for injury. The purpose of the study was to examine the relationships between fatigue and landing performance. Specifically, the magnitude and temporal relationships of selected GRF variables and variations in the amount of electromyographic (EMG) activity of seven lower extremity muscles were evaluated during drop landings.

PROCEDURES

Prior to performing drop landing trials, five male volunteer subjects performed three trials of a maximum vertical counter-movement jump (MVJ) test to determine the criteria for assessing fatigue. The highest jump of the three trials was used as the MVJ criteria. Seven left lower extremity muscles of each subject were then instrumented with Beckman silver/silver-chloride EMG surface electrodes. The included muscles were the vastus lateralis (VL), vastus medialis (VM), rectus femoris (RF), biceps femoris (BF), semitendinosus (ST), gastrocnemius (GA), and tibialis anterior (TA).

Subjects performed two conditions of 30 hanging drop landing trials (60 cm) onto a dual AMTI force platform system (one foot per platform). The first condition (C1) consisted of normal drop landing trials with no imposed constraints. The second condition (C2) was performed under the influence of fatigue induced by a fatigue protocol (FP) which consisted of repeated maximum vertical jumps. Fatigue was defined as a five percent reduction in jumping performance during the FP compared to the MVJ criterion. Fatigue was assessed between each C2 trial to verify that jumping performance remained below 95% of maximum. If a subject's vertical jump performance (best of three jumps) between landing trials improved beyond the 95% criterion, the FP was repeated. Subjects performed drop landings within 30 s after fatigue assessment or the FP.

Left side vertical GRF values were obtained (1000 Hz) and evaluated during the impact phase of landing (200 ms post-contact). Four variables from each GRF curve were identified and compared between conditions. The selected GRF variables included the time (T1) and magnitude (F1) of the first maximum force and the time (T2) and magnitude (F2) of the second maximum force. All GRF magnitude values were normalized to body mass to permit between-subject comparisons. EMG data were obtained (1000 Hz) from each of the seven left lower extremity muscles. Total IEMG values (integrated from 150 ms pre-contact to 100 ms post-contact) were evaluated for each muscle during

the landing phase. Group and within-subject Repeated Measures ANOVAs were computed for between-condition comparisons.

RESULTS AND DISCUSSION

Results indicated no significant ($p < 0.05$) differences between conditions for the GRF or IEMG variables when data were collapsed across subjects. With acknowledgement to the limited statistical power ($n = 5$) these results are consistent with results reported by previous researchers when data are collapsed across subjects (Dufek, 1991; Bates et al., 1989; Dufek et al., 1990; Simpson et al., 1988). These non-significant group results suggest significant between-subject variability which can mask true between-condition differences (Bates et al., 1988; Dufek et al., 1991). Bates et al. (1988) suggested that a within-subject research design is a more effective method for analyzing impact force responses to variations in mechanical constraints during running.

The within-subject ANOVAs revealed a substantial number of significant ($p < 0.05$) between-condition comparisons but, the differences were inconsistent between subjects further supporting the hypothesis of significant between-subject variability. Directional changes for the GRF variables were more consistent than those for the IEMG variables. Within-subject analyses for the GRF variables revealed 65% of the subject-variable comparisons were significant ($p < 0.05$) with more increases (55%) than decreases (10%) for C2. F1 increased significantly ($p < 0.05$) for all subjects while F2 increased significantly ($p < 0.05$) for two subjects and exhibited no significant change for the other three subjects for C2. Even though the group results revealed no significant differences for the GRF magnitude values, it was hypothesized that given greater statistical power (larger sample size) the fatigue condition (C2) would have elicited a large enough treatment effect to overcome the within-subject variability. Within-subject analyses for IEMG variables revealed that 85% of the subject-variable comparisons were significant ($p < 0.05$) with fewer increases (26%) than decreases (59%) for C2. The observed values for the TA decreased ($p < 0.05$) for all five subjects for C2. The greater variability for the IEMG variable comparisons could relate directly to individual preferences in landing strategy. In order to more thoroughly evaluate differences in strategy, the kinematics of the landing phase should be examined. Significant relationships between the total amount of activity for a given muscle and observed changes in kinematic variables might indicate a shift from the control of one muscle (or muscle group) to another during fatigue. Concurrent variations in electromyographic and kinematic variables might reflect alterations in landing control strategies.

REFERENCES

Åstrand P. et al. Textbook of Work Physiology, McGraw-Hill, 1986.

Bates, B.T. et al. Biomechanics XI-B, (pp. 685-688), Free University Press, 1988.

Bates, B.T. et al. Proceedings of the XII International Congress of Biomechanics. Los Angeles, CA, (Abstract No. 58), 1989.

Deschenes, M.R. et al. *National Strength and Conditioning Assoc. J.*, 11(6), 41-44, 1989.

DeVita, P. et al. *Med. Sci. Sports Exerc.*, 24, 108-115, 1992.

Dufek, J.S. et al. *Med. Sci. Sports Exerc.*, 22, 370-377, 1990.

Dufek, J.S. et al. *Med. Sci. Sports Exerc.*, 23, 1062-1067, 1991.

Häkkinen, K. et al. *Electromyogr. clin. Neurophysiol*, 28, 79-87, 1988.

McNitt-Gray, J.L. Proceedings of the 15th Meeting of the American Society of Biomechanics. Tempe, AZ, (pp. 230-231), 1991.

Ricard, M.D. et al. *Int. J. Sport Biomech.*, 6, 67-77,1990.

Simpson, K.J. et al. Biomechanics XI-B (pp. 701-704), Free University Press, 1988.

Steele, J.R. et al. *Int. J. Sport Biomech.*, 4, 130-145, 1988.

Vøllestad et al. *Eur. J. Appl. Physiol.*, 57, 336- 347, 1988.

Table 1. Between-condition ANOVA results for GRF variables.

Subjects	T1	F1	T2	F2
S1	-	+	-	+
S2	+	+	+	*
S3	+	+	+	+
S4	*	+	*	*
S5	*	+	*	*

* Not significant ($p < 0.05$)
\+ Significant increase for C2
\- Significant decrease for C2

Table 2. Between-condition ANOVA results for IEMG variables.

Subjects	VL	VM	RF	BF	ST	GA	TA
S1	-	*	-	-	-	-	-
S2	-	+	+	+	-	*	-
S3	-	-	NA	-	-	-	-
S4	+	*	*	*	+	-	-
S5	+	+	+	-	-	+	-

* Not significant ($p < 0.05$)
\+ Significant increase for C2
\- Significant decrease for C2
NA Data not available

HUMAN PERFORMANCE

Poster

ASSESSMENT OF MOBILITY IN THE ELDERLY

J.A. Ashton-Miller, A.B. Schultz, N.B. Alexander[1] and J. Grenier

MEAM Biomechanics Research Laboratory and [1]Geriatric Medicine,
University of Michigan, Ann Arbor, MI 48109-2125

INTRODUCTION

Although mobility impairments become increasingly common with age, no consensus exists on how to assess mobility, the elements of mobility, or mobility impairments in the elderly. Widely-used subjective assessment instruments include questionaires and a battery of simple clinical tests devised by Tinetti, et al. (1986); there are however few comprehensive objective tests of mobility in widespread use. Thus the effect of natural aging on mobility is unknown.

METHODS

We developed a battery of simple "low-tech", yet objective, measures of five common ADL-like gait and transfer tasks: (1) 40' walk with a 180 deg. turn at the halfway point, (2) three stair ascent/descent, (3) sit-to-stand chair rise (4) supine-to-sit bed rise. The outcome measure was the total time taken to perform the task at a comfortable speed, and in some tests, the time for up to seven movement sub-phases. Test 3 was performed first without hands, then with hands. Timing measurements were made to the nearest msec using (a) infra-red beams at neck and head level, (b) seat, arm rest, pillow and foot switchpads, (c) contact plates, and (d) a microcomputer with 12 bit A/D. The fifth test, stepping-over-obstacles, separately reported (Chen et al. 1991), measured the slowing in gait speed in order to cross the obstacle safely, the foot clearance and placement relative to the obstacle using a Watsmart optoelectronic camera system. Test-retest reliability was assessed on two different days on three subjects.

We compared the performance of 36 healthy young adults (YA: mean (SD) age 20.9 (0.9) years) and 26 healthy old adults (OA: 71.2 (4.9) years) in the above mobility tests. All subjects were screened by a geriatrician to exclude strength, range-of-motion, non-correctable vision, neurological and cognitive deficits. Two similar, but separate groups of 24 YA and 24 OA performed the obstacle avoidance tests.

RESULTS

No statistically significant age effects were found in Tests 1 to 4 outcomes for these healthy subjects. The OA males and females completed Test 1 in 12.1 (3.1) and 13.0 (3.7) seconds, respectively, while the YA had corresponding values of 11.6 (1.3) and 11.8 (0.9) seconds. The female OA required 2.4 (1.5) sec for the 180 deg turn while the YA required 2.2 sec. For Test 2 YA and OA required 3.4 (.38) and 3.6 (.4) seconds, while corresponding values in Test 3 were 7.6 (1.32) and 7.5 (0.7) seconds, and in Test 4 were 2.2 (0.4) and 2.65 (0.7), respectively. Acceptable test-retest reliability, expressed as (mean intrasubject difference/mean value)*100 was found; it ranged from 2.6 to 9.4% across these tests.

DISCUSSION

Between the third and eighth decades, age is known to cause decrements in strength of approximately 30% and joint ranges-of-motion (ROM) of approximately 10%. However, the present study suggests that such deficits do not in themselves significantly affect the performance of the ADL-like gait and transfer tasks simulated by the five tests. The reason for this is that such tasks typically neither require large strengths or ROM. Interestingly, the obstacle test in which subjects perceived the potential risk for a fall, did show significant age effects: the OA had a significantly increased risk of obstacle contact with age, despite several differences suggesting increased conservatism on the part of the OA. The use of self-selected walking speeds has been validated as reliable in gait studies. We have extended that concept to other tasks. Both the test-retest results and the reasonable SD values support this use of the concept.

CONCLUSIONS

We conclude that timed measures of self-selected comfortable ADL activities may be reasonable measures of mobility in some tasks. Natural aging, up to the age of 72 years, does not degrade performance on many ADL tasks. When performance is degraded, factors other than the strength and joint ROM may play an important role in determining mobility.

REFERENCES

Chen, H. et al. **J Geront: Med Sci 46**: M196-203, 1991.
Tinetti, M. et al. **Am J Med 80**: 429-434, 1986.

MECHANICAL POWER RESPONSE OF OLD AND YOUNG ADULTS TO WALKING STRIDE LENGTH AND CADENCE MANIPULATION

P.E. Martin, A. Hreljac, T. Marsh, and D.E. Rothstein

Exercise and Sport Research Institute, Arizona State University, Tempe, AZ

INTRODUCTION

In an attempt to explain the higher walking aerobic demands commonly observed for the elderly, 30 old (O) and 30 young (Y) adults performed treadmill walking at 1.25 $m \cdot s^{-1}$ under five stride length/cadence (SL/C) combinations (preferred SL/C and SLs either increased or decreased from the preferred SL by 10 or 20% of leg length). Two descriptors of mechanical power ($W \cdot kg^{-1}$) and net aerobic demand ($ml \cdot kg^{-1} \cdot min^{-1}$) were quantified for each SL/C condition. Net aerobic demand was significantly higher (15%) for O. For both O and Y, aerobic demand was lowest for the preferred SL/C. External power was higher for Y than O, while segment power showed no age-related effect. These results demonstrated that the higher aerobic demands for O were not related to either: a) their use of less than optimal SL/Cs, or b) stride patterns that resulted in a higher total mechanical power. It is speculated that the higher aerobic demand of O is related to less efficient muscle force production.

REVIEW AND THEORY

Elderly adults exhibit higher aerobic demands to walk a given distance than young adults (Grimby & Söderholm, 1962; Larish *et al.*, 1988; Martin *et al.*, in press), but the reasons for this are not clear. Preferred walking speed, which is slower in the elderly, does not account for age-related differences in walking aerobic demand (Martin *et al.*, in press). Alexander (1984) and Zarrugh *et al.* (1974) have argued that one's basic gait pattern is highly related to economy, suggesting the possibility that preferred gait patterns of the elderly are less economical than those of young adults. For example, declines in muscle strength, bone strength, or flexibility may contribute to changes in walking mechanics that adversely affect economy. The purposes of this study were to determine: a) if the preferred walking patterns of young and old adults are their most economical, and b) whether mechanical power output helps to explain aerobic demand differences between young and old adults.

METHODS

Thirty old (O, $\bar{X}_{age}$ = 70.3±3.5 yrs, $\bar{X}_{mass}$ = 70.0±12.2 kg) and 30 young (Y, $\bar{X}_{age}$ = 23.7±3.1 yrs, $\bar{X}_{mass}$ = 66.2±12.0 kg) adults served as subjects. Participation was restricted to generally robust individuals who had no major orthopedic, neurologic, or cardiovascular disorders that might otherwise affect economy and gait mechanics. Following treadmill acclimation, each subject's preferred stride length/cadence combination (SL/C) for 1.25 $m \cdot s^{-1}$ walking was determined. Subjects subsequently completed trials under five randomly-ordered SL/C combinations: preferred SL/C and SLs either increased or decreased from the preferred SL by 10 or 20% of leg length (LL). Subjects coordinated foot contacts with the beat of an audible metronome in order to produce the desired SL/C combinations.

Net aerobic demand (gross $\dot{V}O_2$ minus a standing, pre-exercise $\dot{V}O_2$) was quantified during the last two minutes of five minute trials for each SL/C condition. A sagittal plane record of the subjects' walking patterns was recorded using 60 Hz videography at the end of each trial. A 14-segment model was used to compute two estimates of mechanical power. Coordinate data derived from the video records were digitally filtered prior to the computation of necessary velocity data. External mechanical power (based on center of mass kinematics) and segment or internal power (based on segment kinematics) were computed assuming energy exchange or transfer using well-known computation schemes (e.g., Pierrynowski *et al.*, 1980).

RESULTS

Net aerobic demand was significantly higher (15%) for O than Y. Similar U-shaped $\dot{V}O_2$-SL/C responses, however, were observed for O and Y (Figure 1). Lowest net aerobic demands for both O and Y were observed at the preferred SL/C. External power was significantly higher for Y

subjects and showed a tendency to increase with increasing SL (Figure 2). O and Y did not display significantly different segment powers, which declined for both groups with increasing SL (Figure 3).

DISCUSSION

Age-related walking economy differences were not associated with O utilizing less than optimal gait patterns as reflected by SL/C. While O adults typically reflect declines in muscle strength and joint range of motion (e.g., Larrson *et al.*, 1979), their preferred SL/C demanded the lowest aerobic demand. Thus, it is concluded that the O adults used patterns of gait that were as economical as possible given their physical and physiological limitations.

Mechanical power differences between O and Y also did not explain the higher aerobic demand of the O. Assuming that overall efficiency is similar for O and Y, the higher aerobic demand of the O should have been accompanied by higher mechanical power output. Results showed, however, that O displayed lower external power and similar segment power as Y. With a higher aerobic demand and similar or lower mechanical power output, the O reflected a poorer efficiency than the Y. Thus, it is concluded that the higher walking aerobic demand of O is not related to preferred gait mechanics, but rather appears to be related to less efficient force production by the muscles.

REFERENCES

Alexander, R.McN. *Amer. Sci.*, **72**, 348-355, 1984.

Grimby, G. & B. Söderholm. *Scand. J. Clin. Lab. Invest.*, **14**, 321-328, 1960.

Larish, D.D., *et al. Ann. N.Y. Acad. Sci.* **515**, 18-32, 1988.

Larsson, L., *et al. J. Appl. Physiol.*, **46**, 451-456, 1979.

Martin, P.E., *et al. J. Appl. Physiol*, in press.

Pierrynowski, M.R. *et al. Ergonomics*, **23**, 147-156, 1980.

Zarrugh, M.Y., *et al. Eur. J. Appl. Physiol.*, **33**, 293-306, 1974.

ACKNOWLEDGEMENTS

Supported by NIH grant AG07352.

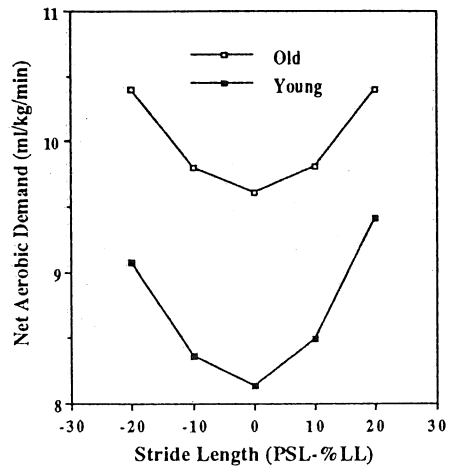

Figure 1. Net aerobic demand was significantly higher for O, but the most economical SL/C for both O and Y was the preferred condition.

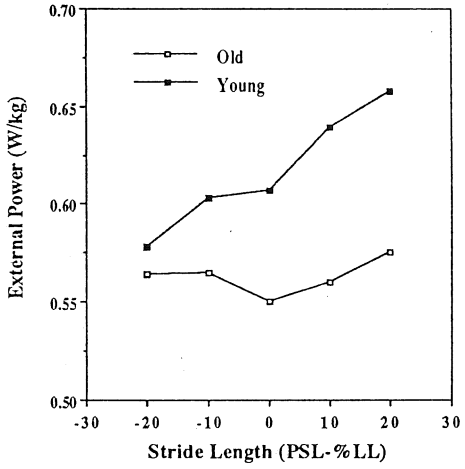

Figure 2. Y showed significantly higher external power than O.

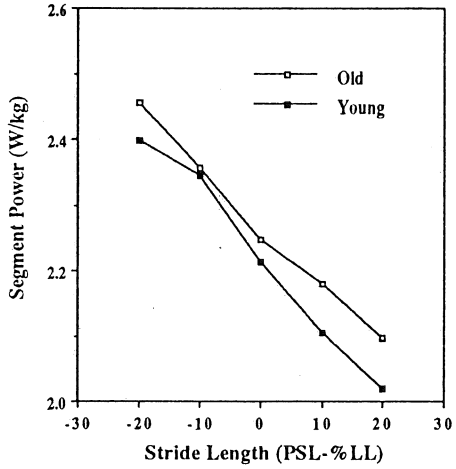

Figure 3. There were no significant differences between O and Y in segment power.

THE BILATERAL DEFICIT FOR STEP VERSUS RAMP MAXIMUM ISOMETRIC TORQUE GENERATION

Timothy J. Koh, Mark D. Grabiner and Carol A. Clough

Department of Biomedical Engineering and Applied Therapeutics
The Cleveland Clinic Foundation, Cleveland, OH 44196

INTRODUCTION

The maximum voluntary force produced by a muscle group during a unilateral task has been reported to be greater than that produced by the same muscle group when the corresponding contralateral muscle group is also required to generate maximum force. This phenomenon, called the bilateral deficit, has been attributed to a decreased recruitment of slow-twitch muscle fibers in pharmacological experiments (Secher et al., 1978), while physiological experiments have suggested a decreased recruitment of fast-twitch fibers (Vandervoort et al., 1984). Analysis of the power density spectrum of the associated EMG signal has not been suggestive either way (Schantz et al., 1989).

The purpose of the present study was to test hypotheses regarding the type of motor unit responsible for the bilateral deficit. The bilateral deficit was measured for a controlled, single-joint task in which maximum isometric knee extension torque was generated gradually (ramp condition) and as quickly as possible (step condition). The hypotheses of the study were formulated under the assumptions that (a) the ratio of force production of high threshold motor units (with fast-twitch muscle fibers) to low threshold motor units (with slow-twitch fibers) would be greater in the step versus the ramp condition, and (b) high threshold motor units would account for the fast rate of torque generation in the step condition. It then follows that if decreased recruitment of high threshold motor units is primarily responsible for the bilateral deficit, (a) the deficit should be larger in the step than in the ramp condition and (b) the rate of torque generation should be slower for bilateral tasks than for unilateral tasks in the step condition.

METHODS

Twelve healthy male subjects volunteered for participation in this study. None of the subjects performed maximal bilateral knee extensions regularly. All subjects were familiarized with the testing apparatus in a practice session.

Each subject was seated and secured on a dynamometer built to measure isometric knee extension torque. The trunk-thigh and knee joint angles were fixed at 100 and 60 degrees, respectively. Electromyographic (EMG) signals were recorded bilaterally from vastus lateralis and the hamstrings. Strain-gauge load cells were used to measure knee extension torque.

Each subject generated maximum knee extension torque unilaterally with each leg, and bilaterally, under ramp and step conditions. For the ramp condition, the subject was instructed to generate maximum torque gradually (in two to three seconds). For the step condition, the subject was instructed to generate maximum torque as quickly as possible. Three trials were performed for each task, and the trial which resulted in the maximum torque was used for analysis. At least thirty seconds rest was given between trials. No feedback was given to the subject during the experiment with respect to his performance.

Bilateral indices (Howard and Enoka, 1991) were calculated separately for the ramp and step conditions for torque (BI_T), rate of torque generation (BI_R), average-rectified vastus lateralis EMG (BI_E), and median frequency of the vastus lateralis EMG power density spectrum (BI_M). A BI greater than zero indicates that the bilateral values are greater than the unilateral values (bilateral facilitation), and a BI less than zero indicates that bilateral values are less than the unilateral values (bilateral deficit).

RESULTS

BI_T and BI_E were significantly less than zero ($p < 0.05$) for both the ramp and step conditions (Table 1). These results indicate a deficit in torque and EMG amplitude in the bilateral compared to the unilateral tasks. In addition, the BI_T for the step condition was significantly less than that for the ramp condition ($p < 0.05$), indicating a larger bilateral deficit for the step condition. BI_R was significantly less than zero ($p < 0.05$) for the step condition, indicating that the rate of torque generation was slower during the bilateral than the unilateral task. BI_M was not significantly different from zero for either the ramp or step condition ($p > 0.05$), suggesting that there was little, if any, difference between median frequency of the vastus lateralis EMG during unilateral and bilateral tasks. Hamstrings EMG data indicated that hamstrings cocontraction was not responsible for the deficits in bilateral versus unilateral tasks, or for the differences between step versus ramp conditions.

Table 1. Bilateral indices for ramp and step conditions

	BI_T (%)	BI_R (%)	BI_E (%)	BI_M (%)
Ramp	-17.0[1,2]	------	-14.6[1]	-3.6
	(7.4)	------	(15.9)	(12.8)
Step	-24.6[1,2]	-19.7[1]	-15.8[1]	-0.1
	(11.5)	(21.9)	(15.9)	(15.1)

Values are means and (standard deviations); n=12.
[1] Mean value significantly different from zero.
[2] Mean values significantly different from each other.

DISCUSSION

Fast-twitch muscle fibers are thought to dominate torque production during high-velocity isokinetic tasks (Coyle et al., 1979). It is reasonable to assume that the same occurs during rapid increases in isometric torque. In addition, there is evidence to suggest that high threshold motor units which may not remain active during ramp isometric conditions, may be active in step conditions (Enoka and Fuglevand, in press). The results of the present study showed that (a) the bilateral torque deficit was greater in the step versus the ramp condition, and (b) there was a bilateral deficit in the rate of torque generation in the step condition. These results suggest that decreased recruitment of high threshold motor units may be primarily responsible for the bilateral torque deficit. EMG amplitudes decreased in parallel with the relatively large reductions in torque from unilateral to bilateral tasks, suggesting a decrease (unilateral to bilateral) in neural drive to the vastus lateralis. BI_E did not show a parallel decrease with BI_T in comparisons between ramp and step conditions, perhaps because of the inherent variability in EMG signals (Howard and Enoka, 1991). As found previously (Schantz et al., 1989), EMG median frequencies did not prove useful for distinguishing motor unit activity between unilateral and bilateral tasks. In summary, the values for BI_T and BI_R suggest that decreased recruitment of high threshold motor units is primarily responsible for the bilateral torque deficit.

REFERENCES

Coyle et al. Med Sci Sports, 11, 12-15, 1979.
Enoka RM, Fuglevand AJ. In: Current Perspectives in Biomechanics, Human Kinetics, in press.
Howard JD, Enoka RM. J Appl Physiol, 70, 306-316, 1991.
Schantz PG et al. Acta Physiol Scand, 136, 185-192, 1989.
Secher NH et al. Acta Physiol Scand, 103, 456-462, 1978.
Vandervoort et al. J Appl Physiol, 56, 46-51, 1984.

RESISTANCE TRAINING AND FUNCTIONAL ELECTRICAL STIMULATION IN PREPARATION FOR STANDING AND WALKING IN COMPLETE SPINAL CORD INJURED PATIENTS

Marc Bélanger[1], Garry, D. Wheeler[2], Marguerite Wieler[1], David Reid[3], Tom Martin[4] and Richard B. Stein[1]

[1]Division of Neuroscience, [2]Rick Hansen Centre, [3]Department of Surgery and Glenn Sather Clinic, [4]Department of Physiotherapy, University of Alberta, Edmonton, Alberta, CANADA.

INTRODUCTION

Following spinal cord injury, there is a loss of muscle function which includes rapid atrophy of the muscle tissue and a decrease in muscle force. Concomitantly, there is a loss of bone mass (osteopenia) which progresses to a level where a fracture can occur even with minimal trauma such as spasms after the removal of a brace (Pilonchery et al. 1983). The deterioration of the muscular and skeletal systems during the initial injury stabilization period is often so severe that rehabilitation of muscle and bone strength must take place before weight bearing exercise begin. Hence, patients who are post-injury and have been immobilized for a long period of time cannot stand and/or walk safely without therapeutic interventions aimed at increasing muscular strength and endurance and bone mass.

Electrical stimulation can be used to enhance the size and function of the paralysed muscles as long as the motorneurons innervating the particular muscles remained intact following the injury. Functional electrical stimulation (FES), which produced static contractions of the unloaded extremities, has been shown to increase muscle strength (Kralj et al. 1980, Peckham et al., 1976). In contrast, Stein et al. (1992) reported that stimulation of the tibialis anterior muscle under unloaded conditions for up to 8 hr/day increased the fatigue resistance but had no effect on the strength or myosin-ATPase activity. Loading the extremities during FES-assisted contractions has also been demonstrated to be effective in increasing the strength and endurance of atrophied muscles (Kralj et al., 1980; 1989; Petrofsky et al., 1984). The most impressive results in strength gains have been obtained under progressive overload and gradual increases in training volume (Davis, 1990; Rodgers et al., 1991).

Loading of bone (i.e. weight bearing) and muscle contraction have also been shown to be important in preventing, decreasing or reversing osteopenia (for reviews see Bohnor et al., 1988; Snow-Harter et al., 1991). Although, FES appears relatively effective in increasing muscular strength, hence, mechanical stress and loading of bone, the attenuation or reversal of osteopenia in spinal cord injured patients has been largely unsuccessful. Leeds et al. (1990) reported no change in bone mineral density following 6 months of FES-assisted cycling training. Rogers et al. (1991) showed a decrease in the rate of bone loss in the proximal tibia following knee extension training, however, they were unable to demonstrate any reversal of osteopenia.

The purpose of the present investigation was to determine whether loading (resistance) has any effect on the strengthening of stimulated muscles in patients with complete spinal cord lesion. Another aspect of this study was to examine whether electrical stimulation under conditions of muscle and bone loading can slow or reverse osteopenia.

METHODOLOGY

Five complete paraplegics (3 C_{6-7}, a T_{3-4} and a T_6) were involved in this study. One of the inclusion criteria was that the quadriceps muscle could be stimulated without pain to the subject. Training consisted of identical amount of electrical stimulation to the quadriceps muscles bilaterally 5 days/week for a total of 24 weeks. The stimulation, which consisted of 300 μs pulses delivered at 20 Hz with a 5 s on/5 s off duty cycle, was applied with a commercially available isolated stimulator and multi-week electrodes. In order to determine the effect of loading, the stimulation of the quadriceps muscles was done with the subject seated in a hydraulic isokinetic leg extension/flexion device. A within subject contralateral limb design was used where one limb contracted against gravity (FES+no resistance - FESNR) while the other limb contracted against an isokinetic load supplied by the apparatus (FES+resistance - FESR). Subjects trained for 1 hour per day or until a fatigue criterion (less than 30° of extension from 90° in the unloaded limb) was met. The resistance on the loaded limb was increased when full extension could be produced for 15 minutes or more at a set load.

Limb girth and muscle strength measurements were done on a weekly basis. Limb girth was measured at 0, 5, 15 and 25 cm proximal to the superior patellar margin, but only the 15 cm data were used to determine gross changes in muscle bulk. Muscle strength was measured using a Cybex isodynamometer set at 30°/s. A correction for the effect of gravity was made. The test stimulation consisted of a train at 40 Hz lasting 2 s, repeated every 5 s for 4 minutes. The testing was done using gel and saline coated electrodes. The Dual Energy X-Ray Absorptiometry (DEXA) technique was used to quantify bone mass density (BMD) of the distal femur, proximal tibia and mid-tibia of both limbs at the 0, 3 and 6 months of the study. All data were expressed as a percentage of the initial measurement values (100%).

RESULTS AND DISCUSSION

Fig. 1 illustrates the changes in muscle girth measurements for the group of subjects. As can be seen, there was no change in the muscle bulk either in the FESNR or FESR limbs. Individually (not shown in Fig. 1), 2 subjects demonstrated an increase in girth on the FESR side which was significantly different ($p < 0.05$) from the FESNR limb which even showed a slight reduction. The lack of change in muscle girth may be attributed to a loss of adipose tissue which was not measured. The data from the study by Rodgers et al. (1991) also suggest a loss of subcutaneous adipose tissue, but because of some variability the changes in thigh skinfold thickness, thigh girth and mean body weight measurements were not significant.

In the limb with no resistance, there was a slight strength increase

of 4.1%/week (Fig.2). On the resisted side, the increase in strength was 1.5 times faster than that of the FESNR limb (6.0%/week). This difference was significant at the 0.05 level. Individually (not shown in Fig. 2), 3 of the 5 subjects showed a strength gain on the FESNR side while all 5 had an increase in strength on the FESR limb. Increases in strength have previously been shown with unloaded extremities (Peckham et al., 1976; Kralj et al., 1980; 1989) as well as following extremity loading programs (Rodgers et al., 1991). However, the results for this study suggest that one can increase the rate of strength gain by progressively loading the limb during the training.

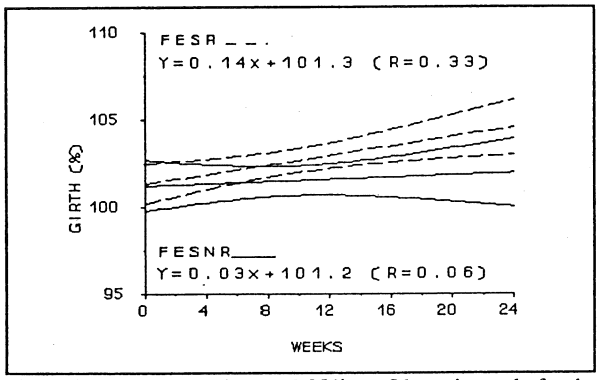

Figure 1. Linear regressions and 95% confidence intervals for the girth measurements of the FESNR (solid) and FESR (dashed) limbs at 15 cm proximal to the superior patellar margin. Values are expressed as a percentage of the initial values

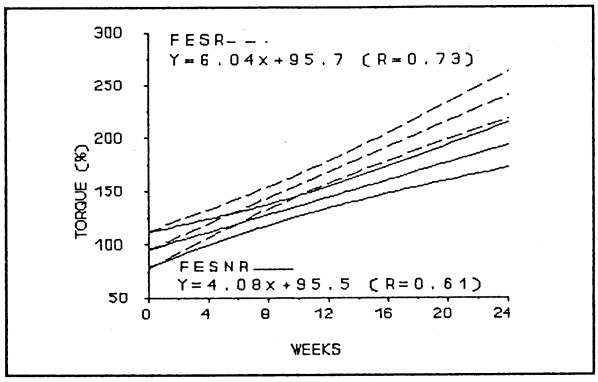

Figure 2. Strength measurements. (Format similar to Fig. 1).

Fig. 3 displays the changes in BMD for 3 subjects after 6 months of training. There was an increase in bone mass density in the distal femur and proximal tibia while there was little change in the mid tibia. Moreover, there does not appear to be much difference between the FESNR and FESR limbs. Although the number of subjects is small, the fact that all 3 subjects from whom data were collected showed an increase in BMD around the knee joint, is quite interesting. This is unlike previous studies which showed no change in bone mass following 6 months of cycling training (Leeds et al., 1990) or only a slight attenuation in the rate of osteopenia (Rodgers et al., 1991; Hangartner et al., 1991). The increase in BMD may be related to the intensity of training, for example, for a full session of training, subjects in the study by Rodgers et al. would complete about 120 contractions 3X/week whereas in the present study a total of about 720 contractions, 5X/week were performed.

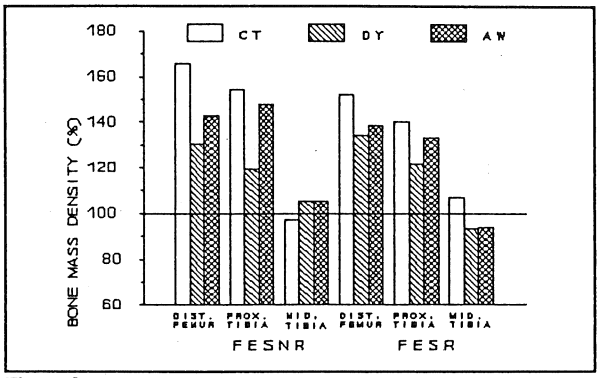

Figure 3. Bone mass density measurements for 3 subjects at the beginning (100% horizontal line) and end of the study (6 months).

REFERENCES

Bohnor et al., *Physiother. Can.*, **40**, 146-155, 1988.
Davis, G.M. *Physiology Update*, 1990.
Hangartner,T.N. et al. *Seventh Annual Spinal Cord Injury Research Symposium*, Edmonton, 1991.
Kralj et al. *Med. Prog. Technol.*, **7**, 3, 1980.
Kralj et al. Functional Electrical Stimulation: Standing and Walking After Spinal Cord Injury, (pp.17-35), CRC Press, 1989.
Leeds et al. *American Spinal Cord Assoc. Abstr.* Las Vegas, 1989
Peckham et al. *Clin. Orthop. Rel. Res.*, **114**, 326-334, 1976
Petrofsky et al. *Central Nervous System Trauma*, 1: 57-73, 1984.
Pilonchery et al. *Clin. Orthop. Rel. Res.*, **174**, 230-235, 1983
Rodgers, M.M. et al. *J.Rehab. Res. Dev.*, **26**, 19-26, 1991
Snow-Harter, C. et al. *Exercise Sports Sci. Rev.*, **19**, 351-388, 1991.
Stein, R.B. et al. *J. Appl. Physiol.*, **72**, ,1992

ACKNOWLEDGEMENTS

This work was supported by the Medical Research Council of Canada. Marc Bélanger was supported by the Fonds de la recherche en santé du Québec.

CONTRIBUTION OF HAMSTRINGS TO CRANK ACCELERATION IN ELECTRICAL STIMULATION-INDUCED LEG CYCLE ERGOMETRY: AN ANALYSIS BASED ON MUSCULOSKELETAL MODELS

L.M. Schutte, M.M. Rodgers*, R.M. Glaser* and F.E. Zajac

Mechanical Engineering Department, Stanford University and Rehabilitation R&D Center, VAMC, Palo Alto, CA
*Institute for Rehabilitation Research and Medicine, Wright State University, and VAMC, Dayton, OH

INTRODUCTION

The purpose of this study was to explore the function of the muscle groups used in electrical stimulation-induced leg cycle ergometry. Specifically, the effect of seat position on the ability of the hamstrings muscle group to produce force and accelerate the crank was considered. For this a model of the musculoskeletal system and its dynamic interaction with the ergometer was developed. This model predicts that the hamstrings produce a greater active force and are more effective at accelerating the crank when the seat is in a positioned closer to the crank. This prediction is supported by experimental data from a spinal cord injured paraplegic using electrical stimulation to pedal an ERGYS[1] leg cycle ergometer. When the seat was moved forward, the subject was able to achieve a higher cadence seven seconds after stimulation began.

REVIEW AND THEORY

The ability of a muscle to produce force depends on the length of the muscle-tendon actuator as well as on its shortening/lengthening velocity. The joint moment a muscle is capable of producing thus varies with angle of the joints that it crosses (Inman *et. al.* (1981)). Since different seat positions result in different amounts of knee and hip flexion while pedaling, it is expected that the forces that the knee and hip muscles can produce when stimulated would also vary with seat position.

Individual muscle forces act to accelerate not only the segments to which the muscle attaches but the other segments as well. (Zajac, *et al.* 1989). This is due to dynamic coupling among the limbs and the mechanical segments of the system being controlled. The angular acceleration induced by a particular muscle force on any joint, including the crank, can be calculated from the dynamic equations of motion of the system. The acceleration that a particular unit of muscle force is capable of producing depends upon the configuration of the system and, thus, also varies with the position of the seat.

MODEL

A model of pedaling on a cycling ergometer was developed. The ankle was assumed to be constrained, since this is the case with the ERGYS systems. The skeletal - ergometer linkage dynamics were modeled as a single degree of freedom linkage system composed of two planar four-bar linkages connected at the crank (Figure 1). All joints except for the knee were assumed to be simple pin joints. The knee, including the patella, were modeled as described by Yamaguchi *et al* (1989). The dynamic equation describing this system were generated with SD/FAST[2]

The hamstrings muscle group was modeled as three separate muscle-tendon actuators. These represent the uniarticular short head of biceps femoris and the biarticular long head. The biarticular semitendinosus and semimembranosus were lumped together to form the third actuator. The dynamics and force production capabilities of each actuator were modeled using a Hill - type model (Zajac *et al.* (1989). The geometry of the muscle attachment points and other muscle - tendon actuator parameters (i.e. tendon slack length and maximum isometric force) were modeled as described in Delp *et al.* (1990).

The one degree of freedom linkage model was used with a prescribed, constant 50 rpm crank velocity to calculate the kinematics of the other joints, and thus the kinematics of the hamstrings. The actuator was assumed to be stimulated by a 30Hz pulse-train that was either on or off depending on the crank angle. The assumed crank angles of hamstrings stimulation assumed are those used by the ERGYS (Schutte *et al.* (1992)). Since the objective was to assess the capabilities of the actuator, only maximal stimulation levels were modeled. The force produced by the pulse train was obtained by numerically integrating the actuator dynamics. This force was then used to calculate the contribution of the hamstrings to the acceleration of the crank.

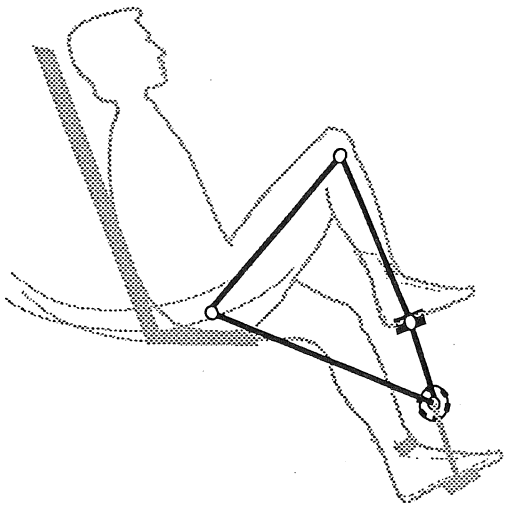

Figure 1. One side of the linkage model used to describe the interaction between the skeletal system and ergometer.

EXPERIMENTAL PROCEDURE

For comparison with the model predictions, the crank cadence of a spinal cord injured subject pedaling on the ERGYS leg cycle ergometer was measured in two different seat positions, normal and with the seat moved forward 24 cm. A video based motion analysis system[3] was used to make this measurement. Technician assistance was used to hand crank the ergometer and achieve an initial pedaling cadence of 50 rpm Stimulation of the hamstrings,

[1]ERGYS, Therapeutic Technologies, Inc. Tampa, FL.
[2]SD/FAST, Symbolic Dynamics: Mountain View, CA

[3]Peak Performance Technologies, Inc., Inglewood, CO.

as well as the gluteal and quadriceps muscle groups began at threshold levels and ramped up automatically with velocity feedback as the cadence dropped below 50 rpm . The same experiment was also done with no stimulation. In this case the cadence resulting from the passive limbs decreased from 50 rpm at a nearly constant rate. With stimulation, however, the pedaling cadence did not decrease as quickly and eventually began to increase. After seven seconds the cadence for the normal seat position case was almost 5 rpm slower than for the case with the seat moved forward. The trials were ordered such that the the normal position was tested prior to the forward case. Thus the difference is probably not due to muscle fatigue. Fatigue could, however, have caused the difference to be lower then it would have been otherwise.

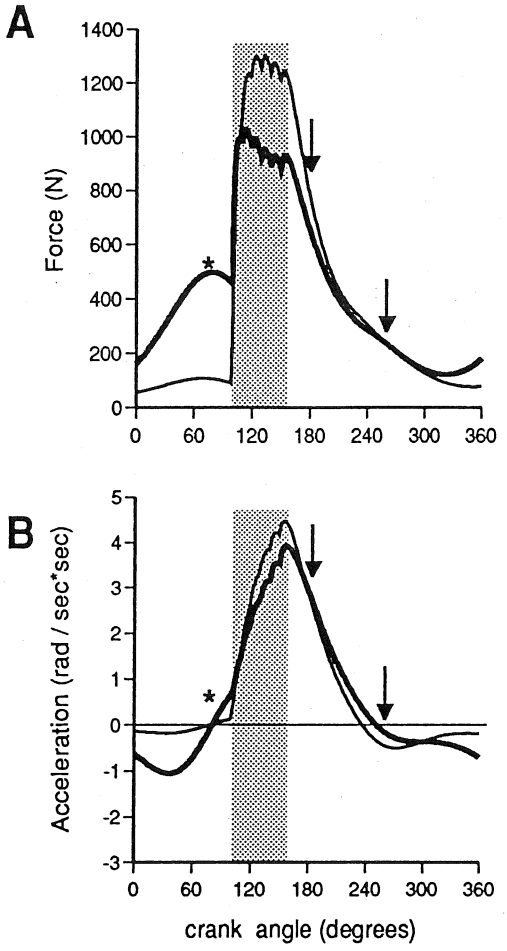

Figure 2. A. The total force developed in muscle-tendon actuators representing the hamstrings muscle group when pedaling at 50 rpm. The forces in the three modeled actuators was summed. The heavy curve corresponds to the seat in the normal position and the thin curve to the case where the seat is moved forward. The shaded region represents the crank angles where the muscle was stimulated. B. The acceleration of the crank resulting from the force produced by the three actuators. In both cases, 0 degrees is at the top of the crank cycle.

RESULTS AND DISCUSSION

The model predicts that the hamstrings muscles generate force even when not being stimulated (unshaded region in Figure 2). When the seat is moved forward, the knee and the hip are both flexed to a greater extent at all crank angles. The net effect of this is that the hamstrings muscle is stretched less. Thus, the force generated passively is greatly reduced. Also, the muscle is stimulated when it is at a shorter length. Since in both cases the muscle is operating on the descending region of its force - length curve, the effect of this is that the active force produced is greater when the seat is positioned closer to the crank.

The net acceleration produced by the hamstrings appears to be slightly greater when the seat is forward. The higher passive force of the actuator in the normal position results in a greater negative (backwards) crank acceleration. Similarly the higher active force generated in the forward case, results in a slightly greater forward acceleration. However, there is a region (between arrows in Figure 2) when the muscle is relaxing after cessation of stimulation, where, despite the higher active force, the crank acceleration is lower. Note also that the peak in the force generated when the muscle in not being stimulated (indicated by asterisk in Figure 2) occurs at approximately the same point in the crank cycle as when the direction of the acceleration reverses. This indicates that the passive force can generate a positive as well as a negative acceleration of the crank. If the muscle had not been stimulated, the acceleration resulting from the entirely passive muscle would have had positive and negative peaks of nearly equal magnitude.

These model predictions indicate that perhaps the increase in performance of the spinal cord injured subject on the ERGYS seen when the seat is moved forward can be attributed to the increased crank acceleration that the hamstrings muscles can produce in this position. Future work will show how the contributions of the other stimulated muscles, the gluteals and the quadriceps, are affected by this change in position.

REFERENCES

Delp, S.L. et al. IEEE Trans Biomed Eng, **37**, 757-767, 1990.

Inman, V.T. et al. Human Walking (pp. 95-100). Waverly Press, 1981.

Schutte, L.M. et al. *Proceedings of RESNA International '92*, Toronto, 1992.

Yamaguchi, G.T. et al. *J. Biomech*, **22**,1-10,1989.

Zajac, F.E. *CRC Critical Reviews in Biomechanical Engineering*, **17**, 359-411, 1989.

Zajac, F.E. et al. *Exercise and Sport Sciences Reviews*, **17**, 187-230, 1989.

ACKNOWLEDGMENTS

Funding for this research was provided by a NSF predoctoral Creativity in Engineering Award to L.M.S., the Rehabilitation Research and Development Service of the U.S. Department of Veterans Affairs, and NIH grant NS17662.

EFFECTS OF FATIGUING HEAVY RESISTANCE LOADING ON VOLUNTARY NEURAL ACTIVATION AND FORCE PRODUCTION IN MALES AND FEMALES

K. Häkkinen

Department of Biology of Physical Activity, University of Jyväskylä, Jyväskylä, Finland

INTRODUCTION

To examine effects of fatiguing heavy resistance loading on voluntary neural activation and force production ten male and nine female athletes loaded their leg extensor muscles by performing 10 sets in the squat-lift exercise by performing 10 repetitions in each set with the maximal load possible (about 70% of 1 RM in each set; 10 x 10 x 70%). Maximal voluntary neural activation (integrated EMG), maximal isometric bilateral force, force-time and relaxation-time curves of the leg extensor muscles were measured before, during and immediately after the exercise loading. The relative decrease of 47.1 ± 10.5 % ($p<0.001$) recorded in maximal force in males was significantly ($p<0.01$) greater than the decrease of 29.4 ± 13.8 % ($p<0.001$) recorded for females. Decreases were also observed in the maximal IEMGs of the exercised muscles both in males ($p<0.01$) and in females ($p<0.05$). The exercise loading led also to decreases in the force-time curve in males by 49.3 ± 11.5% ($p<0.001$) and in females by 32.4 ± 16.2% ($p<0.001$). The present findings suggest that strenuous heavy resistance loading may result in remarkable acute fatigue in the neuromuscular system observable not only by the decrease in muscle force characteristics but also by the decrease in the voluntary neural activation of the exercised muscles. In males neuromuscular fatique may be greater than in females.

REVIEW AND THEORY

Strenuous heavy resistance dynamic or isometric muscular work usually leads to momentary changes both in the maximal voluntary neural activation of the exercised muscles as well as in maximal strength of the muscles (Komi et al.1977; Viitasalo et al.1980; Häkkinen at al.1988). These types of strenuous heavy resistance exercise protocols utilized by athletes for their training purposes may also lead to acute changes in explosive strength observeable by the shifts in the shape of the isometric force-time curve of the exercised muscles (Komi et al. 1977; Häkkinen et al. 1988).

The sexual differences are very apparent in the amount of muscle mass and correspondingly in absolute maximal strength of the muscles. However, much less experimental information is available on acute fatiguing effects of strenuous heavy resistance exercise loading of the neuromuscular system in females in comparison to effects recorded from males (Clarke 1986; Häkkinen 1990). The purpose of the present study was therefore to examine effects of fatiguing heavy resistance loading on voluntary neural activation and force production characteristics of the muscles in males and females, when the relative loading intensity and the volume of the exercise were kept the same for both sexes.

PROCEDURES

The male subjects were ten adult strength athletes having a regular strength training background an average for 8 years. The female subjects were nine adult strength athletes with a similar type of background in strength training an average for 3 years. The subjects loaded their leg extensor muscles by performing 10 sets in the squat-lift exercise by performing 10 repetitions in each set with the maximal load possible (about 70 % of 1 RM; one repetition maximum). The recovery time between the sets was 3 minutes. The loads were adjusted during the course of the exercise due to fatigue so that each subject was able to perform 10 repetitions in each set (10 x 10 x 70%).

The measurements were performed before the exercise loading and after the third, sixth and the ninth set as well as immediately after the last set of the loading. Maximal voluntary force, force-time and relaxation-time curves of the leg extensor muscles were measured during the isometric bilateral contraction on a dynamometer (Komi 1973). Electromyographic activity was recorded from the vastus lateralis (VL) and vastus medialis (VM) muscles by surface electrodes and integrated to obtain maximum voluntary integrated EMG (IEMG) during the maximal force production as well as during the earlier phases of explosive force production of the same contraction to obtain the IEMG-time curve (Häkkinen et al. 1985). Blood samples for the determination of blood lactate were also taken during the course of the loading and determined using a lactate analyzer (Roche-640).

RESULTS

The loading resulted in great gradual decreases in maximal force in males by 47.1 ± 10.5 % (from 4258 ± 1061 N to 2220 ± 544 N; $p<0.001$) and in females by 29.4 ± 13.8 % (from 2445 ± 585 N to 1707 ± 426 N; $p<0.001$) (Fig. 1). The decrease in males was greater ($p<0.01$) than the decrease recorded for females. Significant decreases were observed also in the maximum IEMGs of the VM and VL muscles both in males ($p<0.001$ and 0.01) and in females ($p<0.05$) (Fig. 1). The relative decreases in the maximum IEMGs of the muscles were 44.4 ± 26.6 % and 32.2 ± 35.2 % for males and females, respectively. The loading led also to great decreases in explosive strength observable in the force-time curve both in males

($p<0.001$) and in females ($p<0.001$) (Fig. 2). The average decrease of 49.3 ± 11.5 % in explosive force recorded for males was greater ($p<0.05$) than that of 32.4 ± 16.2% recorded for females. In males great ($p<0.01$) decreases took place during the loading also in the voluntary explosive neural activation of the exercised muscles in the average IEMG-time curve, while the decreases in females were minor. The time of force relaxation lengthened ($p<0.05$) in both groups. The mean blood lactate concentration increased in males from 1.4 ± 0.3 mmol x l^{-1} to 15.0 ± 4.0 mmol x l^{-1} ($p<0.001$) and in females from 1.4 ± 0.5 mmol xl^{-1} to 6.0 ± 1.8 mmol x l^{-1} ($p<0.001$).

DISCUSSION

The present findings demonstrated that strenuous heavy resistance loading leads to remarkable acute fatigue in the neuromuscular system. Fatigue was observable not only by the decrease in maximal force but also by acute worsening both in explosive force production and relaxation characteristics of the exercised muscles. Accumulation of lactic acid inside the muscle with decreased pH level as well as depression in Ca^{2+} transport after exhaustive exercise may result in reduced contractile characteristics of the muscle. The great decrease observed in the maximal voluntary neural activation of the exercised muscles further indicates that considerable fatigue may have taken place also in the nervous system. Because no muscle biopsy sample were taken, it is difficult to consider, whether the difference between the male and female group in the magnitude of the decrease in maximal strength would in part result from the possible differences in the muscle fibre distribution of the groups (Thorstensson et al. 1976; Kroll et al. 1980; Häkkinen 1990). The difference in the duration of the training background between the present groups may have also contributed to the results obtained. One could also speculate that the lower testosterone level in females as compared to males could also imply lower level of "aggressiveness" during strenuous exercise leading therefore to smaller fatiguing effects in females than in males. The finding that the mean blood lactate concentration increased much more in males than in females may also in part support this suggestion. Nevertheless, the present results also suggest that this type of recording of neural activation and force characteristics of the exercised muscles could be useful in evaluation of the loading characteristics of various strength training sessions in order to optimize the contents of individual training sessions both for males and females.

REFERENCES

Clarke, D. Res. Quart. Exc. Sport 57, 144-149, 1986
Häkkinen, K. Sport Med. Health 457-462, 1990
Häkkinen, K. et al. Eur. J. Appl. Physiol. 57, 133-139, 1988
Häkkinen, K. et al. Acta. Physiol. Scand. 125, 573-585, 1985
Komi, P. et al. Acta Physiol. Scand. 100, 246-254, 1977
Komi, P. 3. Int. Sem. Ergom., Berlin, (pp. 173-176), 1973
Kroll, W. et al. Res. Quart. Exc. Sport 51, 323-333. 1980
Thorstensson, A. et al. Acta Physiol. Scand. 48, 318-322. 1976
Viitasalo, J. et al. Int. J. Sport Med 1, 185-190, 1980

ACKNOWLEDGMENTS

This study was supported in part by a grant from the Ministry of Education, Finland.

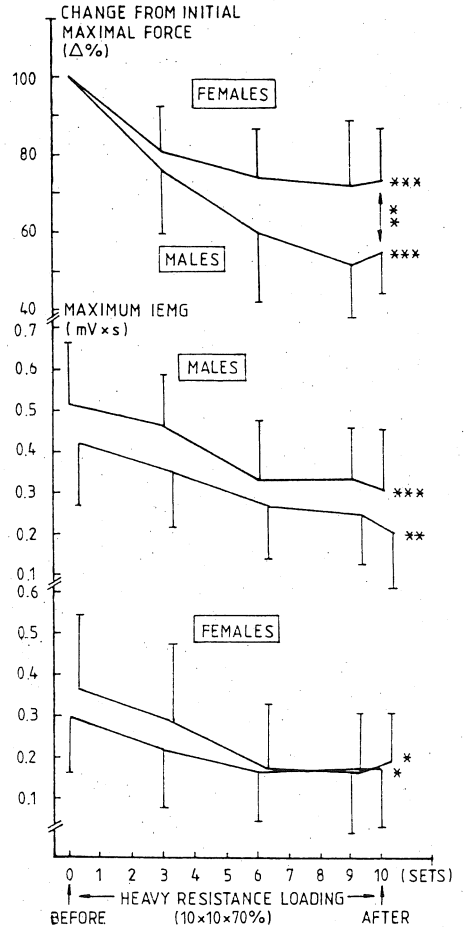

Fig. 1. Changes in maximal force and maximum IEMGs

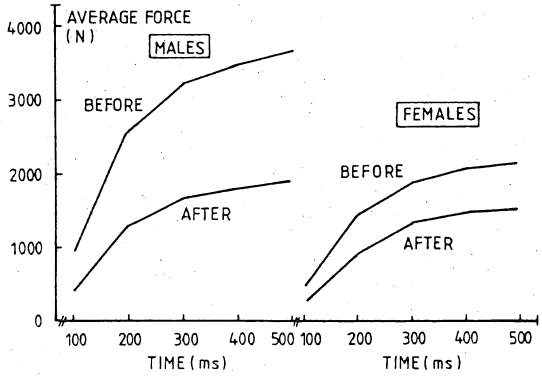

Fig. 2. Average force-time curves before and after the loading

EFFECT OF KNEE STABILIZATION ON HIP EXTENSION STRENGTH TESTING

D. Gravel, N. St-Denis, D. Bourbonnais and A.B. Arsenault

Rehabilitation Institute of Montreal, Québec
Ecole de Réadaptation, Université de Montréal, Québec

INTRODUCTION

Testing of hip extension strength is complicated by the presence of biarticular hamstring muscles. To generate a maximal hip extension moment, the distal insertions of hamstring muscles at the knee joint must be stable. However, in most studies evaluating hip extension strength, stabilization of the knee was not provided. Therefore, doubts concerning the validity of the reported results can be raised. Using a multi-articular dynamometer and EMG recordings, the effect of knee stabilization on hip extension strength was evaluated. The results show that maximal hip extension is not affected by the stabilization of the knee. In this condition, subjects generate a knee extension moment during hip testing. If no external knee fixation was used, co-contraction of knee extensors muscles stabilized the knee. The recruitment of the knee extensor muscles is associated with a decreasing activity of the hamstrings. However, hip extension strength is not affected. The small contribution of the hamstrings to hip extension moment probably explains this result.

REVIEW AND THEORY

The measurement of hip extension strength presents a specific problem related to the mechanical effect of the hamstrings at the knee. These biarticular muscles cross the knee and consequently have the potential to generate force at this joint during hip extension testing. Without the stabilization of the knee, the knee angle is not controlled and the contribution of the hamstring muscles to the hip extension moment is probably dependent on the strategy chosen by the subject. Therefore, some doubts may be raised about the results reported by authors that did not stabilize the knee during hip extension (Markhede et al., 1980; Németh et al., 1983; Cahalan et al., 1989).

A practical solution to this problem is to use an orthosis to stabilize the knee (Waters et al., 1974). In this manner, the hamstrings have a stable distal insertion and the full recruitment of these muscles is possible without any changes in muscle length. However, in preliminary testing, we observed that many subjects contracted the knee extensor muscles during hip extension testing. To further document this problem, we designed a study to test the hip extensor muscles using dynamometric and electromyographic (EMG) measures taken at both the hip and knee joints simultaneously.

The aim of the present study is to compare three methods of testing hip extensor strength. More specifically, the objectives are to: a) evaluate the effect of the stabilization of the knee, b) evaluate the influence of instructions to the subject and, c) describe the EMG activities of knee and hip extensor muscles during these methods of testing.

PROCEDURES

Sixteen subjects, 12 females and 8 males, participated in this study. They were all students in rehabilitation science and did not report any orthopedic or neurological problems. Their mean (±1SD) age, stature and body mass was 21.8 (±1.8) yr, 165 (±4) cm and 61.1 (±7.8) kg respectively.

The details of the static dynamometer used in the present study are described elsewhere (Bourbonnais et al., 1991). In this dynamometer, the distal parts of the thigh and leg are secured independently to multidirectional transducers mounted to an external rigid frame. Using segment link analysis, the muscular moments generated simultaneously at the hip and knee are computed in real time.

Hip extension strength was measured under three conditions (Fig. 1). Condition 1 was performed with the distal parts of thigh and leg attached to transducers (dark bands on Fig. 1) and an instruction was given to perform a hip extension effort. This condition was similar to having an orthosis stabilizing the knee joint. Condition 2 was similar to the first except that the subject received the instruction to simultaneously flex the knee during the hip effort. Inclusion of this condition was to ensure that full recruitment of hamstring muscles was achieved. In condition 3, the attachment at the distal part of the leg was removed. Condition 3 was added to analyze the effect of the distal fixation on hip extension strength and hamstring activation. Moreover, comparisons with results reported in the litterature will be possible because knee fixation is absent. Two other tests were performed to appreciate the relative involvement of knee extensors and flexors during the hip tests. These were a maximal knee extension (KE) and a maximal knee flexion (KF).

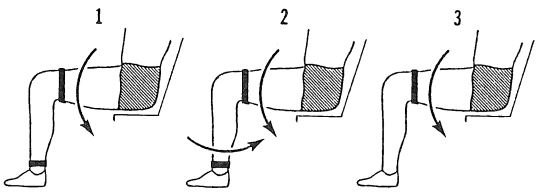

Figure 1. Hip testing conditions 1 to 3. Dark bands represent attachments of the transducers. Arrows indicate the requested efforts.

To standardize the instructions about the tasks to be performed, an illustration of the condition being evaluated was shown to the subjects just before each test (Fig. 1). The maximal strength was to be reached progressively in less that 5 s. Feedback concerning the hip extension moment was given in all hip testing conditions. Maximal values of three trials were averaged. The order of testing was balanced for conditions 1, 2, 3 and KF. KE was the last test since it was used only as a reference to estimate the involvement of the knee extensors.

EMG activities of the rectus femoris (RF), vastus lateralis (VL), gluteus maximus (GM) and biceps femoris (BF) muscles were recorded by surface electrodes. Bipolar derivations (spacing =

1.5 cm) were used with electrodes placed parallel to muscle fibers. The EMG signals were sampled at 1000 Hz and stored on disk for further processing. For each trial, filtered EMG were averaged over the 0.2 s preceding the maximal force. As for the moment, the mean of the three trials was calculated. The mean EMG of each muscle was then normalized to the maximal EMG recorded for this muscle in any condition including KF and KE.

One-way analysis of variance for repeated measures were performed to verify the significance of the differences between the hip testing conditions. Analysis were done for hip and knee moments as well as for the EMG data.

RESULTS

The maximal hip moments were not significantly different between hip testing conditions (Fig. 2). However, a knee extension moment was generated in condition 1 and, as expected, a knee flexion moment was observed in condition 2 (Fig. 3).

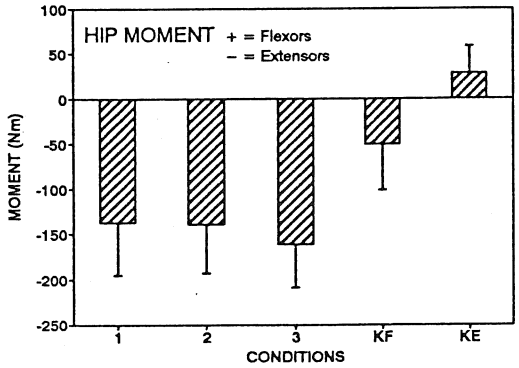

Figure 2. Hip moments generated in the hip testing conditions 1 to 3 and in knee flexion (KF) and extension (KE)

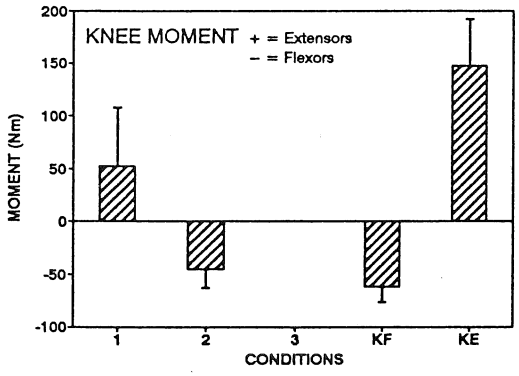

Figure 3. Knee moments generated in the hip testing conditions 1 to 3 and in knee flexion (KF) and extension (KE)

The EMG data confirm the dynamometric results. The GM activity was not significantly higher in condition 3 than in the other hip testing conditions. Significant higher activation of BF (Fig. 4) and VL (Fig. 5) were noted in conditions 2 and 1 respectively in comparison to the other conditions. No knee moment could be calculated in condition 3, but co-contractions of VL and BF muscles were observed.

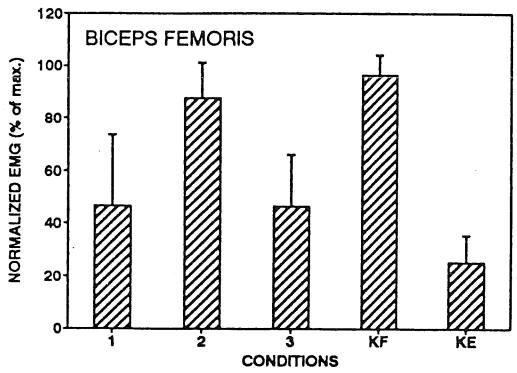

Figure 4. EMG of BF during the hip testing conditions 1 to 3 and the knee flexion (KF) and extension (KE)

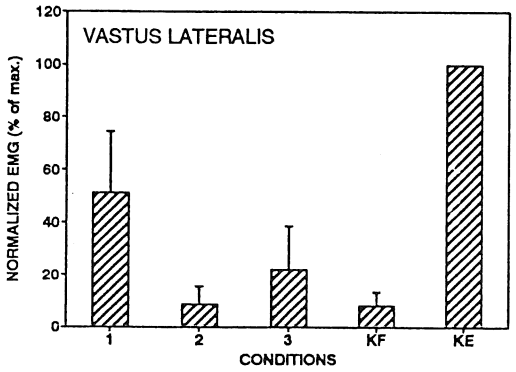

Figure 5. EMG of VL during the hip testing conditions 1 to 3 and the knee flexion (KF) and extension (KE)

DISCUSSION

The external knee fixation (condition 1) did not yield a significant change in the hip extension strength as subjects used the same muscular strategy as in condition 3 in which no fixation was provided. In both cases, subjects activated the knee extensors (Fig. 5) and decreased the recruitment of the biarticular hamstring muscles (Fig. 4). This decrease in the activation of hamstrings would diminish the maximal hip extension moment. To evaluate this effect, the contribution of hamstring muscles to the hip extension moment was estimated during the KF test (Fig 2). Full activation of BF in KF test corresponds to a hip extension moment of 50 Nm. Assuming a linear relationship between EMG and moment, the decrease of BF activity in condition 1 and 3 (about 50% of the maximal EMG recorded in KF) should give a difference of about 25 Nm in the maximal hip moment relative to condition 2. Since no statistical differences were observed, we concluded that the contribution of hamstrings to the hip extension is probably lower than estimated.

REFERENCES

Bourbonnais, D. et al. J. Biomech. (accepted for publication)
Cahalan, T.D. et al. Clin. Orthop. Rel. Res. 246, 136-145,
Markhede, G. et al. Scand. J. Rehabil Med. 12, 169-174, 1980
Németh, G. et al. Scand. J. Rehabil. Med. 15, 97-101, 1983
Waters, R.L. et al. J. Bone Joint Surg. 56-A, 1592-1597, 1974

ACKNOWLEDGMENTS

The authors wish to thank M. Goyette, eng., B. Brassard, D. Roy, and B. Lamarre for their help in this project. Granted by CAFIR (Université de Montréal) and FRSQ.

KNEE ANGLE AS A DETERMINANT OF LOWER LEG TREMOR

Jukka T. Viitasalo* and Jan Gajewski**
*** Research Institute for Olympic Sports, 40100 Jyväskylä, Finland**
**** Institute of Sport, Warsaw, Poland**

INTRODUCTION

The effects of knee joint angle (muscle length) and spring load stiffness on some parameters of lower leg tremor were studied among twelve male subjects using a piezoelectric accelerometer. The results showed knee angular position (length of knee extensors) to have a significant influence on the lower leg tremor parameters so that higher peak frequencies and lower tremor amplitude values were typical for the shorter knee extensor lengths . The frequency changes with knee angle were explained by the effect of changes in stiffness of a spring-mass system (knee extensor musculature) as a function of muscle length. It was suggested that tremor amplitude is mainly influenced by motor unit recruitment and firing characteristics.

REVIEW AND THEORY

Tremor in human limbs in pathological (e.g. Parkinsons´s disease) or in normal conditions has been a subject of scientific interests for over one hundred years (Schäfer, 1886). In spite of several investigations into human limb tremor, there continues to be uncertainty about its origin and nature as well as about effects of such biomechanical parameters as muscle length and load stiffness on it. The present study was designed to investigate the influence of knee joint angle (muscle length) on some parameters of lower leg tremor in isometric knee extensions performed against three various spring of different stiffness.

PROCEDURES

The subjects were twelve men ranging in age between 20 and 28 years , in body mass between 65 and 75 kg , and in body height between 1.70 and 1.90 m . The subjects had been biopsed (m. vastus lateralis) in our previous study (Viitasalo et al. 1991) in order to determine their muscle fiber distribution, the relative areas of the two fiber types and the percentage ratio of the area of fast twitch cells to that of the whole muscle tissue sample (CFT%, Viitasalo et al. 1980). CFT% values of the subjects participating in the present study ranged between 30% and 76%. Lower leg mass was determined according to volume which was measured by an immersion procedure.

Tremor was registered in the non-dominant lower leg using a piezoelectric accelerometer with the subject lying on his back on a dynamometer bench. After warming-up the subjects performed the following identical contractions for the 90°, 110 °and 130 ° knee angle positions with a five-minute recovery period in between changes of position: three maximal isometric knee extensions (MVC) at one-minute intervals against a rigid chain fixed firmly to the body of the dynamometer, a 20 s knee extension at the level of 50% MVC in turn against three springs of differing stiffness (at one-minute intervals). The horizontal position of the lower leg throughout data collection was ensured by a simultaneous change in hip and knee angles. In all the loading conditions the spring/chain was fixed via a strain gauge transducer and an metal cuff to the lower leg. The accelerometer was attached to the cuff in order to measure the vertical component of lower leg acceleration (tremor). The springs were attached to the dynamometer such that when the subject reached the desired level of contraction the lower leg was held during each registration in a horizontal position. The stiffness values of the springs were 935 N/m, 1090 N/m and 1524 N/m.

The power spectrum density function (PSD) for acceleration was estimated between 1 and 20 Hz. The following parameters were extracted from the tremor spectra : total power (the variance of the acceleration signal) of the low frequency (range 1 - 7 Hz) components (PTOT(1,7)), total power of the bandwith 7 to 20 Hz (PTOT(7,20)), PSD main peak value (PMAX) and frequency of the PSD main peak (FMAX).

RESULTS

The amplitude parameters (PTOT(1,7), PTOT(7,20), PMAX) of tremor were statistically significantly different for the three knee angles. The same trend was found for each spring so that the highest tremor acceleration variance was obtained for the 90° angle and the smallest value was observed for the 130° angle. These variables did not depend on spring stiffness.

The frequency of the PSD main peak (FMAX) was significantly dependent both on spring stiffness and knee angle as shown in Fig.1. The lowest FMAX values were found for the most compliant spring and for the 90 ° angle.

The correlation analysis did not reveal any statistically significant dependences between the tremor parameters and the background variables of body mass, lower leg mass and CFT%

DISCUSSION

The current results showed knee angular position to have a statistically significant influence on lower leg tremor parameters so that the higher peak frequencies and lower tremor amplitude values were typical of the shorter knee extensor lengths (greater knee angles). This can partly be explained as the effect of change in the stiffness of a spring-mass system (knee extensor musculature) brought about by a change in muscle length.

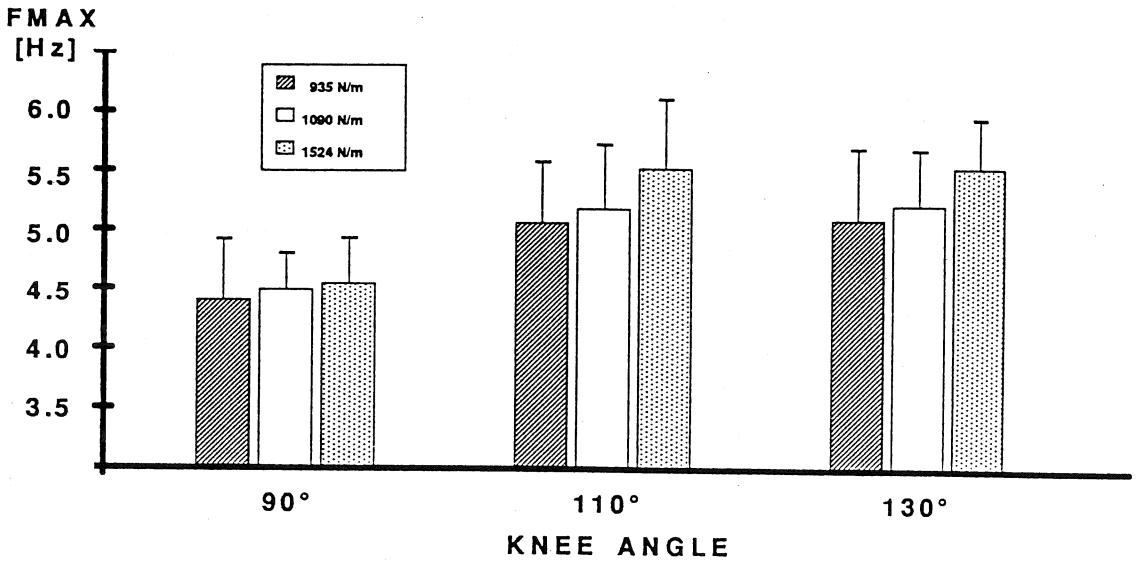

Figure 1. Mean FMAX values obtained for three knee angles and three springs.

Stiles (1980) suggested that tremor frequency parameters may vary with muscle tension. On the basis of the force - muscle length relationship (e.g. Kulig et al. 1984) the muscle tension of the knee extensor muscles against a constant load (weight of the lower leg + force output) must have been greater for the shorter as against the longer muscle lengths in the present study. Greater muscle tension (amount of acto-myosin bridges) means more stiffness in the musculature (e.g. Stiles, 1980) . From a purely mechanical point of view greater stiffness in a spring system means higher tremor frequencies. In accordance with the Stiles (1980) results the higher tremor frequency values in the present study were associated with the shorter muscle lengths .

The positive relation found between tremor frequency and the stiffness of the three springs used in the present study is in line with the explanation above and also in accordance with the results previously reported by e.g. Matthews et al. (1980) and Joyce et al. (1974) in which both intramuscular and external load stiffness were assumed to determine the tremor frequency characteristics.

Differences in muscle stiffness at different muscle lengths cannot, however, be used independently of any other assumptions as an explanation for tremor amplitude differences between the three knee angle positions found in the present study. Amplitude of acceleration, at resonance frequency, for a lightly damped visco-elastic system should increase with stiffness (at the same amplitude of disturbance). By contrast in the present experiment tremor amplitudes decreased when knee angle increased (muscle length decreased). Similarly the stiffness of the spring loads did not affect tremor amplitude as might be expected from a purely mechanical point of view. This suggests that the stiffness of either the intramuscular or external load as such is not the only variable which determine tremor amplitude. It may also be under the influence of such variables of the neuromuscular functioning as stretch reflex (Prochazka et al. 1988) and recruitment model of motor units (Christiakos et al. 1979; Windhorst et al. 1982).

REFERENCES

Christakos, C. et al. J. Biol. Cybern., 1,175-176, 1979.
Joyce, G. et al. J. Physiol., 240, 375-396, 1974.
Kulig, K. et al. Sport Sciences Reviews, 12, 417-466, 1984
Matthews, P. et al. J. Physiol., 302, 427-441, 1980.
Prochazka, A. et al. J. Physiol., 402, 421-442, 1988.
Schäfer, E. J. Physiol. 7, 111-117, 1886.
Stiles, R. J. Appl. Physiol., 40, 44-54, 1976.
Viitasalo, J. et al. Electromyogr. Clin. Neurophysiol., 20, 487-501, 1980.
Viitasalo, J. et al. Proceedings of the XIIIth International Congress on Biomechanics, Perth, (pp314-315),1991.
Windhorst, U. et al. Exp. Brain Res., 45, 417-427, 1982.

ACKNOWLEDGEMENTS

The study was supported by grant No 187/722/90, Ministry of Education, Finland. The Department of Biology of Physical Activity, University of Jyväskylä is acknowledged for laboratory and test equipment facilities.

MECHANICAL PROPERTIES OF SPASTIC MUSCLE IN HEMIPARETIC STROKE.

J.D. Given, J.P.A. Dewald, J.R. McGuire and W.Z. Rymer

Sensory Motor Performance Program, Rehabilitation Institute of Chicago, and Depts. of Rehab. Medicine & Physiology, Northwestern University Medical School, Chicago, IL.

INTRODUCTION

The primary goal of this study was to quantify joint impedance in spastic limbs and to identify the relative contributions from the passive and reflex components of spastic muscle in hemiparetic stroke subjects. Slow ramp stretches of the triceps brachii muscle were performed on spastic upper limbs (n=3) and compared with a normal control group (n=2). The passive elastic and viscous stiffness were estimated using the measured torque response to the ramp perturbation in the absence of any significant triceps EMG activity. A comparison of the hemiparetic and normal limbs revealed a significantly higher passive elastic stiffness in the hemiparetic limb.The increase in stiffness ranged from 20 to 80% of the averaged normal value which indicates that the passive stiffness is potentially a major contributor to the increased impedance behavior observed by the clinician. In the hemiparetic population, where the stretch reflex is more excitable, the reflex stiffness contribution was calculated by subtracting the estimated passive elastic stiffness contribution from the total torque. The resulting torque signal exhibited a non-linear transition representing the onset of the stretch reflex followed by a constant stiffness response. The stretch reflex elastic stiffness contribution to the total torque response was approximately 3-4 times greater than that of the passive elastic stiffness contribution in the hemiparetic limb.

REVIEW AND THEORY

Lance (1980) defines spasticity as a "motor disorder characterized by a velocity dependent increase in the tonic stretch reflexes ('muscle tone') with exaggerated tendon jerks, resulting from hyperexcitability of the stretch reflex, as one component of the upper motoneuron syndrome". Spastic hypertonia may be observed in patients who have suffered an hemiparetic stroke. Although hypertonia is readily discernible clinically, the severity of this clinical sign is not readily quantifiable, at least in any uniformly accepted way. As a consequence, the underlying mechanisms are not yet clearly understood, and a widely accepted quantitative definition of spasticity has yet to be achieved. In an effort to address this issue we chose to study the spastic muscle using controlled positional perturbation techniques. The obtained mechanical impedance of spastic muscle under passive conditions can be separated into two main components:1. passive tissue properties (tendon, connective tissue, passive muscle), 2. reflexive properties (reflexively mediated stiffness). When a muscle is active a third component often referred to as intrinsic (mediated by contractile elements) would be added to the total mechanical impedance of the muscle.

Under passive conditions the total mechanical resistance to a change in joint angle is the result of contributions from passive and reflexive properties of muscle. Thus the presence of increased stiffness cannot be automatically attributed to an enhanced stretch reflex stiffness. Observed increased resistance may be explained by a change in one or both of these properties. The premise of increased stiffness due to hyperactivity of the stretch reflex has gained wide support (e.g.. Herman *et al* (1973), Gottlieb *et al* (1978), Brober *et al* (1983), Rack *et al* (1984)) although no broadly acceptable validation, or explanation of the causes has been presented. In studies where separation of individual stiffness components has been attempted, Lee *et al* (1987) found comparable total stiffness in 11 of 15 hemiparetic test subjects for the affected and unaffected elbow flexors. Rymer and Powers (1989) found stretch reflex gains in spastic muscle comparable to normal muscle coupled, however, with a reduced threshold sensitivity to angular position. Sinkjaer *et al* (1991) also found no significant differences in the stretch reflex behavior for spastic and normal muscle but identified significant increases in the passive stiffness of spastic muscle. Such increases in passive stiffness we hypothesize to be due to a loss of contractile element in the spastic muscle due to the partial paralysis and a replacement by connective tissue. The disadvantage of the approach used by Sinkjaer *et al* (1991) is that it releys on single points for the estimates of passive and/or reflex stiffness. In this study we propose to address the issue of passive versus reflex contribution to total net torque in spastic versus normal muscle.

PROCEDURES

To address the issue of reflex versus passive contributions to the net stiffness in spastic muscle in a novel way, the elbow joints of three hemiparetic stroke and two normal subjects were subjected to positional perturbations in the form of variable speed slow ramps. The test subject was seated to one side of a computer controlled motor (using the Texas Instruments' TSM 320 Digital signal processor) and positioned with the shoulder in 10 degrees flexion and 80 degrees abduction. The subject's elbow rested in a shallow cup above the axis of the motor, and the wrist and hand casted and then attached with a U-bolt in a mid pro-supinated position to a lightweight beam coupled to the motor. Angular position and velocity were measured by a potentiometer and a tachometer, respectively, mounted on the motor shaft, and torque was measured by a torque meter mounted between the motor shaft and the beam. EMG activity in the biceps-brachialis (BB), brachioradialis (BRD), and lateral triceps (TRI) muscles were measured using surface electrodes . The subject's arm was positioned in 120 degrees of elbow extension (180 degrees is designated as full extension). The subject was instructed to relax completely and not to intervene. With the subject relaxed, which was determined by monitoring the triceps muscle EMG activity, the arm was flexed through an arc of one radian (57.3 degrees) at a constant angular velocity. The proper angular velocity (0.1, 0.25, 0.5, 1.0 or 1.25 radians/second) was chosen for each individual stroke subject based on the presence of stretch reflex response. Then the arm was stretched at that velocity for at least 20 times. Subsequently the elbow torque was fitted to a second order system comprising agonist and antagonist muscle subsystems with global parameters of elastic stiffness (K), viscous stiffness (B) and inertia (I). A second order angular mechanical system representation is described by the following equation:

$$I\ddot{\theta} + B\dot{\theta} + K\theta = T$$

where θ is angular position and T is the torque output of system.

Previous work at the elbow joint (Kirsch (1990)) and the ankle (Hunter and Kearney (1982), Weiss *et al* (1988)) has demonstrated that this model representation of the mechanical state of the joint is adequate and provides reliable and accurate estimation of the system's mechanical response to perturbations in position. Significant differences in system response behavior between the affected (spastic) and unaffected muscle states will be reflected by changes in the estimated global parameters K and B. Under the conditions of constant velocity, passive muscle and no stretch reflex response, the second order equation reduces to that of a straight line where the passive elastic stiffness K_p is the slope and the passive viscous stiffness

multiplied by the angular velocity is the intercept of the line. This approach provides statistically sound estimates of K_p and B_p based on a large number of data points. By using different velocities, the estimates were verified and the statistical significance improved. It was also possible to extract the contribution to the net torque signal originating in the reflex component. Using the data record where angular velocity is constant, but the stretch reflex onset has occurred, the stretch reflex component was estimated by simply subtracting the estimated elastic and viscous stiffness' contributions from the overall torque signal.

RESULTS AND DISCUSSION

The variable slow ramp protocol was applied by flexing the elbow of two normal and three hemiparetic stroke subjects. This resulted in an elongation of the triceps brachii muscle. Figure 1 is a representative example of the experimental data showing a comparison of torque and EMG between a normal and a spastic hemiparetic stroke subject. Note the obvious differences in torque magnitude over the range where the triceps EMG is at a resting level. Using the methods outlined, estimates of passive elastic and viscous stiffness K_p and B_p of the elbow joint were calculated for the hemiplegic and normal subjects. A significant difference in the estimated passive stiffness, K_p, between the normal and hemiplegic test subjects was observed (see table 1), which was not unexpected. However, the increase in stiffness ranged from 20 to 80% of the averaged normal value which indicates that the passive stiffness is potentially a major contributor to the increased impedance behavior observed by the clinician. Significant differences in passive elastic stiffness between the three hemiparetic subjects were observed consistent with our clinical assessments. Clinical spasticity scores indicated that hypertonicity in our test population ranged from moderate to severe. The viscous stiffness B_p did not change significantly between normals and hemiparetic stroke subjects studied to date.

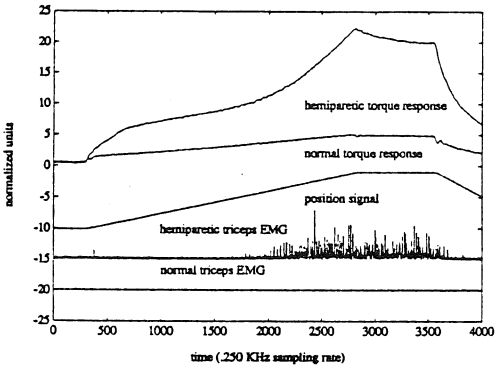

Figure 1: The measured normal and hemiparetic torque and triceps EMG responses to a slow ramp stretch of the elbow extensors.

After an identification of the passive contributions to the elbow torque, an analysis of the stretch reflex component was undertaken. The net torque signal was derived by subtracting the estimated passive elastic and viscous stiffness components from the total measured torque response. Until the onset of the stretch reflex, the net torque is zero indicating that the passive contributions have effectively been removed from the torque signal. The net stretch reflex torque response appears to be slightly nonlinear in the initial stage but approaches a linear response thereafter (see figure 1). An estimate of the elastic stiffness due to the stretch reflex is estimated by fitting a straight line to this data. The slope provides a rough estimate of K_{sr} (elastic stiffness due the stretch reflex, see table 1).

	N1	N2	H1	H2	H3
Kp $\pm 2 * \frac{std}{\sqrt{n}}$	0.0108 +/- 0.0014	0.01373 +/- 0.0014	0.02274 +/- 0.0005	0.02047 +/- 0.0017	0.01666 +/- 0.0006
Ksr $\pm 2 * \frac{std}{\sqrt{n}}$	———	———	0.10720 +/- 0.0051	0.06216 +/- 0.0346	———

Table 1: This table shows the passive elastic stiffness Kp and the stretch reflex elastic stiffness K_{sr} for two normals N1 & N2 and three stroke subjects H1,H2 & H3 (in order of decreasing hypertonicity). The passive viscous stiffness Bp and the stretch reflex viscous stiffness B_{sr} were not significantly different between normals and stroke subjects. Reflex stiffness in normals has not been estimated yet due to the inability of the mechanical system to produce rise times fast enough to elicit a stretch reflex response.

The estimated total torque, using both the estimated passive contributions and stretch reflex elastic stiffness contribution, had an average VAF (Variation Accounted For) value of 97.23% +/- 1.3% (95% confidence interval). The net torque signal with the passive and stretch reflex elastic stiffness components removed is essentially zero which implies the following:

(1) the viscous stiffness component due to the stretch reflex is negligible and the net effect of the stretch reflex is a rise in elastic stiffness of the elbow joint;
(2) stretch reflex and passive contributions are additive to yield the net torque response;
(3) the relative contributions of K_{sr} and K_p are significantly different and appear to be roughly a 3-4 to 1 ratio in the hemiplegic population, (although the statistical analysis has not yet been completed and no ratio is yet available for the normal population).

We believe that the augmentation in passive stiffness observed is due to an increase in connective tissue in the muscle resulting from a loss of muscle fiber.
The possibility of separating the components of joint impedance such as reflex and passive stiffness has important clinical implications. The effect of modalities such as electrical stimulation (Given *et al*, 1991) or the effects of range of motion exercises on the different components of joint impedance in the case of spasticity can now be studied in a quantitative fashion.

REFERENCES

Brober et al, *Scand. J. Rehab. Med.* 9 (suppl):108-117, 1983.
Given, J.et al, *Soc. Neurosci. Abstr.* 17:1033, 1991.
Gottlieb, G. et al, *J. Neurol. Neurosurg. Psychiatry* 41:32-39, 1978.
Herman, R. et al, *New developments in electromyography and clinical neurophysiology* 3:556-578, 1973.
Hunter I. and Kearney R., *J. Biomech.* 15:747-752, 1982.
Kirsch, R. *Ph.D. dissertation, Northwestern University,* 1990.
Lance J., Spasticity:Disorder motor control, *Yearbook Medical Publishers,* 1980.
Lee W. et al, *Exp. Neurol.* 98:317-335,1987.
Rack P. et al, *Brain* 107:637-654, 1984.
Rymer W. and Powers R. *Neurosurgery:* State of the art reviews 4:291-301,1989.
Sinkjaer et al, *J. of Neurophys.* 65:1402-1410, 1991.
Weiss et al, *J. Biomech.* 21:539-544, 1988.

THE INFLUENCE OF STATIC STRETCHING AND A 10-MINUTE WARM-UP RUN ON REFLEX FORCE DEVELOPMENT

Dieter Rosenbaum and Ewald M. Hennig

Sportmedizinisches Institut, Universität Essen, Essen, Germany

INTRODUCTION

Observing the athletic community, the value of preparatory exercises like stretching and warm-up appears undisputed. There is a wide variety of proposed consequences concentrating on two topics: injury prevention and performance enhancement. The present study compared the effects of two different modes of preparatory exercises on muscle activation characteristics as reflected by the reflex force development of the triceps surae. Specifically, the influence of 3 minutes of static stretching (SS) as well as warming up by 10 minutes of treadmill running (RUN) were investigated. The effects are to be discussed with respect to the above mentioned general objectives of prior exercises.

REVIEW AND THEORY

The acute aftereffects of 10 min of static stretching (SS) on motoneuron excitability and force development in Hoffmann reflexes have recently been investigated by Guissard *et al.* (1991). The authors reportedly found no changes in the contractile properties (maximal force and speed of movement) even though the range of motion was significantly increased. For the motoneuron excitability a depression was found during stetching but the effects did not last beyond the stretching manœuvre itself. The present study's main objective was to compare the changes in force development in tendon tap reflexes induced by static stretching alone and by a subsequent warm-up run.

PROCEDURES

Fifty male athletes with various sports background volunteered for participation and provided informed consent. Their mean (±SD) age was 25.1 (4.0) years, height was 181.9 (5.7) cm and weight was 76.1 (8.0) kg. In order to ensure comparability between the conditions, the data for each subject were collected in a single experimental session lasting approximately two hours.

Reflexes, explosive force developments, maximal contractions and flexibility measurements were performed under each of three experimental conditions executed in the following order:

PRE. Without any prior exercise or warm-up.
POS. Following 3 minutes of static stretching of the triceps surae.
POR. Following 10 minutes of treadmill running at a self-selected moderate speed.

Here, only the results for the reflex characteristics will be described and discussed.

During the experiments the subjects were seated on a specifically designed device in which the right leg was fixed with the knee and ankle at right angles (Fig. 1). The foot was supported on a rotating foot plate with the axis of rotation of the plate and the ankle aligned. Reflex force production was measured by a force transducer which connected the foot plate to the base plate of the whole set-up via a steel cord. Phasic stretch reflexes were elicited by mechanical percussion of the achilles tendon with a "reflex hammer": a U-curved bar was dropped from a predetermined height. hitting the achilles tendon with a constant force and at a location reproducible for each subject.

Flexibility was determined goniometrically by measuring the degree of dorsiflexion caused by a barbell pulling the footplate upwards with a torque of 32 Nm around the ankle joint.

Data were sampled for a period of 480 ms at a rate of 10 kHz. Some of the parameters extracted from the force signal are schematically shown below (Fig. 2). For all parameters, the mean values across the repetitive trials were computed for each subject and subsequently the means across all subjects were determined. For statistical analyses an ANOVA was used to determine the significance of differences between conditions.

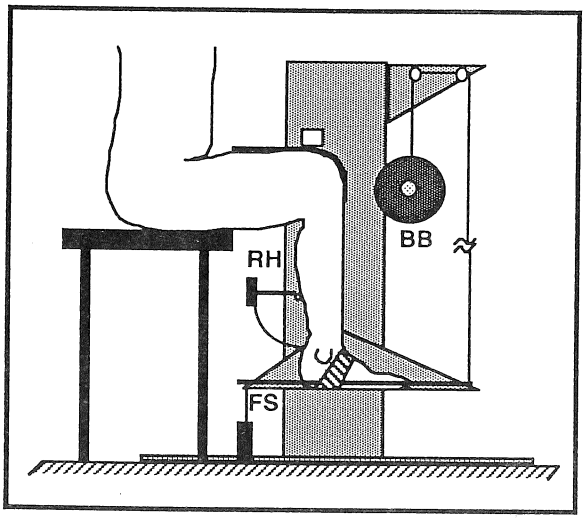

Figure 1. Experimental set-up for Achilles tendon tap reflexes (RH = reflex hammer, FS = force sensor, BB = barbell weight, only for flexibility measurements).

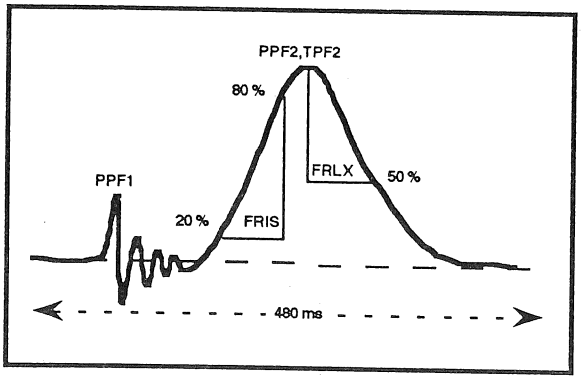

Figure 2 - Sample data and description of experimental parameters (see Table 1 for explanation).

RESULTS AND DISCUSSION

Looking at the results presented below (Table 1) one has to bear in mind that the values found in the post-running condition are a combined result of the stretching procedure and the warm-up run. The observed changes after RUN can, therefore, not solely be attributed to the effect of increased muscle temperature but may also be dependent on the lasting effect of the stretching regime. Nevertheless, it seemed more advantageous to investigate both treatments in a single session in order to allow for a direct comparability of the results within each subject.

The successful attainment of the different aims of two modes of preparatory exercise are reflected in the changes in skin temperature and flexibility (Table 2). No significant temperature changes could be detected after the stretching treatment. After running, the skin temperature was significantly raised by 1.7 °C ($P < 0.01$). The range of motion in dorsiflexion increased significantly after stretching from 30.2° to 31.1° ($P < 0.05$) and after running to 31.9° ($P < 0.01$). The observed improvement of 1.7° is comparable to that reported by Guissard *et al.* (1991) who gained 1.9° after ten minutes of SS.

The impulse induced in the achilles tendon by the reflex hammer is transferred via the footplate and can be deduced from the first force peak (PPF1). The transfer is influenced both by the stiffness of the triceps surae musculature and the properties of the total foot structure. A significant reduction of PPF1 by 9.1% ($P < 0.01$) was found following the stretching treatment of the triceps surae with no further decrease occurring after running.

One of the expected effects of stretching, the reduction of the stiffness of the musculo-tendinous unit, could be seen in this parameter. Since the reflex hammer had fallen from the same height it hit the achilles tendon with the same kinetic energy. This impact, however, was transferred with a lower peak force via the achilles tendon suggesting a more compliant tendon. These observations illustrate that after stretching the muscle and tendon are more pliable thus reducing the peak force resulting from an external impact. The decrease of the force peak and the force rise in events with passive or eccentric forces like ground contacts will also diminish the risk of injury. Thus, the muscle has to sustain less peak stress and will probably be less susceptible to strain injuries.

The reduced passive force component (PPF1) suggests that the degree of stretch and the stretch velocity sensed by the muscle spindles were also reduced. This would coincide with the significant 9% reduction in the maximum force of the reflex (PPF2) observed after SS and RUN ($P < 0.01$). Based on the results of the present study it cannot be determined whether the reduction of the force output of the reflex is solely or predominantly caused by changes in the mechanical properties of the connective tissue induced by the SS treatment. This effect might also be related to reduced alpha motoneuron excitability which was not investigated in the present study but has been reported elsewhere. Previous findings showed reduced alpha-motoneuron excitability following static stretching as seen in the H-reflex activity (Thigpen *et al.*, 1985) or active muscle contraction (Hutton, 1988). However, other studies found these effects only during static stretching (Guissard *et al.* 1988, 1991).

The overall shape of the force curve developed by the reflex activity appeared similar after the stretching treatment but, following the warm-up run, was changed towards a narrower and steeper shape. This altered appearance was reflected by significant changes in the time related force parameters. The time period (TPF2) needed to develop this peak force increased after the stretching by 6.9 ms ($P < 0.05$) and decreased after the running by 10.4 ms ($P < 0.01$) as compared to the unprepared state. The force development and relaxation were affected differently by the stretching and the running treatment. After stretching the force development rate (FRIS) decreased by 7.6% ($P < 0.01$), the half-relaxation rate (FRLX) by 5.3% (not significant). After the warm-up run, these parameters increased by 8.9% ($P < 0.01$) and 12.5% ($P < 0.01$), respectively, following running. Therefore, it is not surprising that the total impulse developed by the reflex activity (SFF) as determined by the area under the force curve was also reduced significantly after running by 11.8% ($P < 0.01$) whereas no significant difference was found after stretching.

These changes in the force development and relaxation rates after the warm-up run might be caused by improved metabolic and physiological mechanisms. Increased muscle and blood temperature had been shown to reduce intramuscular resistance to force development and improved oxygen dissociation mechanisms (Åstrand & Rodahl, 1977) which in turn can enhance the excitation-contraction coupling (Hortobagyi *et al.*, 1985; Hatcher & Luff, 1988).

Contrary to Guissard *et al.* (1991) the presented results suggest that static stretching alone may lead to impairments of the contractile properties like force production and relaxation. This might be due to the methodological differences in the reflex elicitation. The observed changes in reflex activity following warming-up by running appear to compensate the effects of static stretching. They indicate an improved reaction of the warmed-up muscles which appear to respond faster to a sudden event as modelled by the tendon tap. It has been shown for the wrist that the stretch reflex assists in the rapid return of the limb after mechanical displacement (Sinkjaer & Hayashi, 1989). Therefore, it seems legitimate to speculate that it is advantageous to respond quicker and stronger in situations where an unforeseen event might cause detrimental effects.

REFERENCES

Åstrand, P.-O. & K. Rodahl. Textbook of Work Physiology, 1986.

Guissard, N. et al. *Eur. J. Appl. Physiol.* **58**, 47-52, 1988.

Guissard, N. et al. *Proceedings of the 13th.International Congress on Biomechanics*, Perth, (pp. 264-265), 1991.

Hatcher, D. D. & A. R. Luff. *J. Appl. Physiol.* **64**, 502-510, 1988.

Hortobagyi, T.,et al. *Int. J. Sports Med.* **6**, 317-321, 1985.

Hutton, R. S. The Olympic book of Sports Medicine, (pp. 69-79), Dirix, Knuttgen and Tittel, 1988.

Sinkjaer, T. & R. Hayashi. *J. Biomechanics* **22**, 1133-1140, 1989.

Thigpen, L. K. et al. Biomechanics IX-A, (pp. 352-357) Winter, Norman, Wells, Hayes and Patla, 1985.

Table 1 Parameter Description and Mean Data (±COV); Δ1/Δ2 = Difference (in%) between PRE and POS/POR, (n = 50).

Parameter Abbreviation	Parameter Short Description	Units	PRE	POS		POR			Δ1	Δ2
TEMP	Skin temperature above the medial gestrocnemius	°C	**32.8** (2.0)	**32.9** (2.2)		**34.5** (1.7)	**		0.3	5.2
FLEX	Ankle Flexibility = dorsiflexion range of motion	°	**30.2** (7.1)	**31.1** (7.2)	*	**31.9** (7.0)	**		3.0	5.6
PPF1	Peak positive force 1 = tendon tap force	N	**29.8** (14.8)	**27.1** (14.4)	**	**27.0** (14.4)	**		-9.1	-9.4
PPF2	Peak positive force 2 = force maximum	N	**62.5** (26.4)	**59.7** (29.5)	*	**61.1** (26.0)			-4.5	-2.2
TPF2	Time from PPF1 to PPF2 = force development time	ms	**159.3** (9.7)	**166.2** (10.4)	*	**148.9** (9.3)	**	++	4.3	-6.5
FRIS	Force rise rate (between 20%-80% of PPF2)	N/s	**811.1** (29.7)	**749.3** (31.3)	**	**883.6** (28.8)	**	++	-7.6	8.9
FRLX	Half relaxation rate (between PPF2 and 50% of PPF2)	N/s	**366.1** (30.8)	**346.8** (33.0)		**411.7** (30.6)	**	++	-5.3	12.5
SFF	Force impulse = area under the force curve	Ns	**11.9** (25.2)	**11.8** (28.0)		**10.5** (25.7)	**	++	-0.9	-11.8

*/** Significantly different from PRE; $p<0.05$ / $p>0.01$; +/++ Significantly different from POS; $p<0.05$ / $p>0.01$.

INFLUENCE OF HIP AND KNEE JOINT ANGLES ON EXCITATION OF KNEE EXTENSOR MUSCLES

E. Hasler, J. Denoth*, A. Stacoff*, W. Herzog

Human Performance Laboratory, University of Calgary, Calgary, Alberta, Canada T2N 1N4
*Biomechanics Laboratory, ETH Zurich, Zurich, Switzerland

INTRODUCTION

Maximal isometric force of intact human skeletal muscles depends on muscular length and excitation. Effects of muscular length on maximal isometric force have been studied extensively, however the way how maximal excitation may vary as a function of muscular length (i.e. joint configuration) and therefore, may influence maximal force, has not been investigated systematically. The purpose of this study was to test if and how excitation of intact human knee extensor muscles is influenced by knee or hip joint configurations.

REVIEW AND THEORY

Excitation of human knee extensor muscles obtained during maximal, voluntary contractions has been found to decrease (Eloranta, 1989), remain constant (Lieb *et al.*, 1971) and increase (Basmajian *et al.*, 1985) towards full knee extension. Furthermore, it has been proposed that excitation of one-joint muscles during maximal voluntary contractions may be influenced by configurations of adjacent joints not crossed by the muscles of interest (Huijing *et al.*, 1987; Yamashita, 1988; Fujiwara *et al.*, 1975); however, force-length properties of intact human skeletal muscles have been derived assuming that excitation is independent of configurational changes in neighbouring joints (Herzog *et al.*, 1988). The contradictory results encountered in the literature motivated the present study.

PROCEDURES

Seven subjects performed 18 maximal isometric knee extension exercises on a strength testing machine. Six contractions were performed for each of three different knee joint angles (90°, 130°, 170°). For every knee joint angle, five different hip joint angles (90°, 112°, 135°, 157°, 180°) were tested. After the fifth contraction for one specific knee joint angle, the first contraction was repeated in order to assess possible effects of fatigue or training. Knee and hip joint angles of 180° correspond to full knee and hip extension, respectively.

Knee extensor moments and EMG measurements were synchronized and recorded for a period of 5 s. Muscular excitation from vastus lateralis (VL), vastus medialis (VM) and rectus femoris (RF) muscles was recorded using bipolar surface electrodes. EMG signals were full wave rectified and averaged. Data were analog-to-digital converted with a sampling frequency of 2000 Hz per channel. EMG data were normalized for each subject (a) with respect to the largest value independent of joint configurations and (b) with respect to the largest value at a given knee joint angle. Isometric EMG-force relations were assumed to be linear (Hof, 1984).

RESULTS

This study yielded two basic results. First, excitation of the one-joint knee extensor muscles (VL, VM) appeared to depend systematically on hip joint configuration, whereas excitation of the two-joint knee extensor RF was similar for different hip joint angles (fig 1).

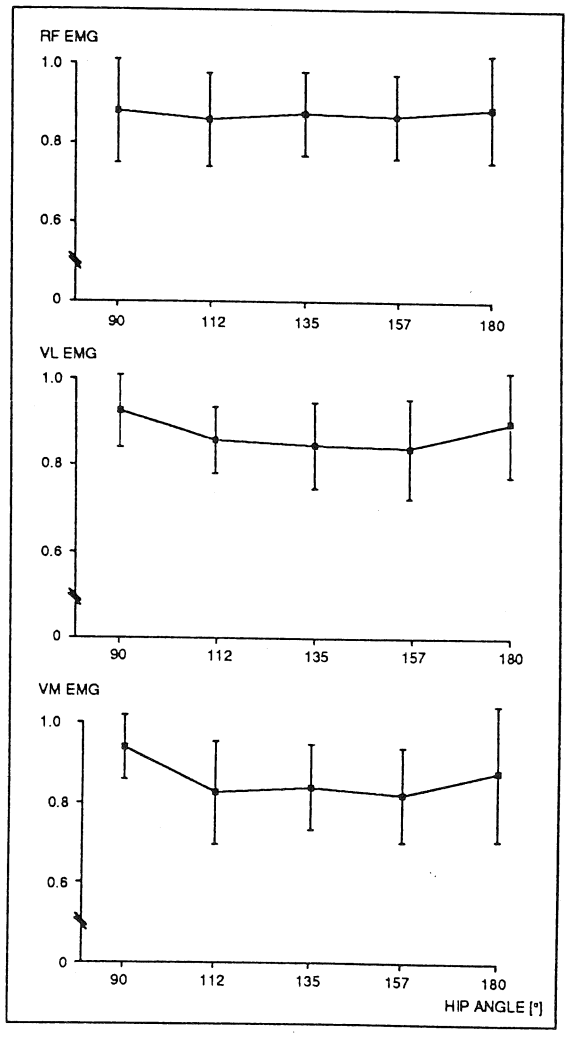

Figure 1. Normalized mean EMG's ± 1 SD for RF, VL, VM as a function of hip joint angles

Second, excitation of all knee extensor muscles tested was consistently higher at a knee joint angle of 170° than that at 130° (fig. 2).

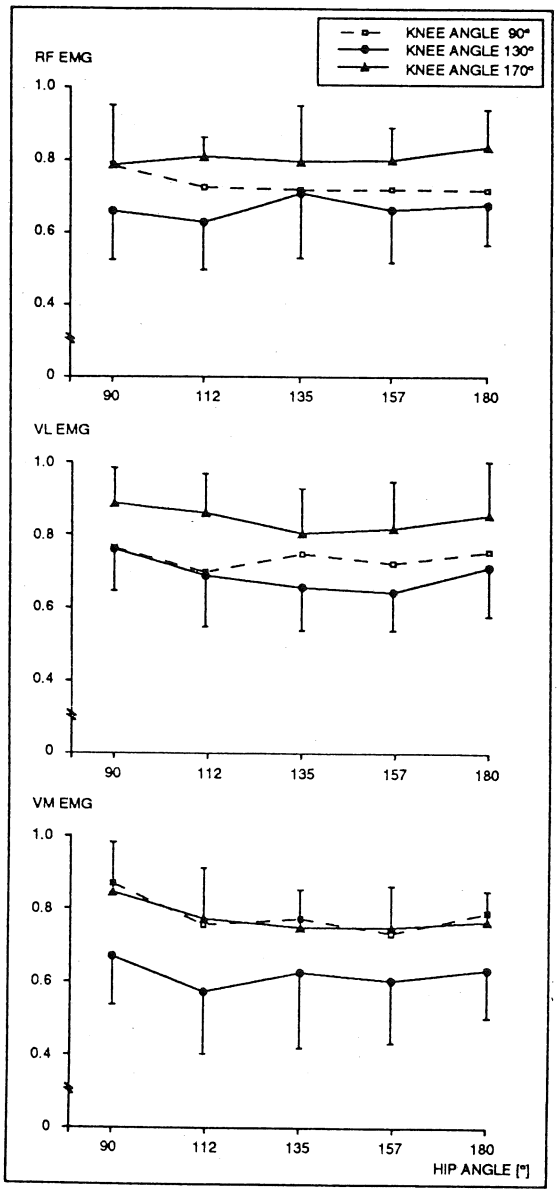

Figure 2. Normalized mean EMG's ± 1 SD for RF, VL and VM as a function of hip and knee joint angles.

DISCUSSION

Although VL and VM do not cross the hip joint, the results (fig. 1) indicate that excitation of these muscles is significantly higher at hip joint angles of 90° and 180° compared to the three intermediate hip joint angles. Interestingly, this does not appear to be the case for the RF muscle. Excitation values of the RF may be associated with recording artifacts, since the change in RF length induces movement of the muscle underneath the recording electrode. Nevertheless, there are no obvious neural mechanisms to explain the influence of varying hip joint angles on the excitation of the one-joint knee extensor muscles (VL, VM). Afferent innervation from Golgi tendon organs and muscle spindles are expected to be constant since the moments and lengths of the one-joint knee extensor muscles were nearly constant throughout the range of hip joint angles.

With respect to the second result, it has been shown that knee extensor muscles can only exert small forces near full knee extension due to the force-length properties of these muscles (Herzog *et al.*, 1991). The knee extensor muscles therefore are at a mechanical disadvantage near full knee extension compared to intermediate knee joint angles. Increased excitation of the knee extensor muscles near full knee extension as observed consistently here (fig, 2) may be a result of decreased inhibitory afferent innervation of the Golgi tendon organs. Therefore, the mechanical disadvantage of the muscles at short length may be partially compensated for by a neurophysiological control mechanism. However, this same mechanism can not explain why excitation values at a knee joint angle of 90° are higher than those at a knee joint angle of 130°. It is speculated that a complex interaction of sensory receptors and feedback loops could be responsible for the inconsistent excitation patterns between muscles within a synergistic group.

REFERENCES

Basmajian, J.V. et al., Muscles Alive. Their Functions Revealed by Electromyography, (p. 331), Williams and Wilkins, 1985.
Eloranta, V. *Electromyogr. clin. Neurophysiol.* 29:227-233, 1989.
Fujiwara, M. et al., *Am J Phys Med* 54:234-242, 1975.
Herzog, W. et al., *Eur J Physiol* 411:637-641, 1988.
Herzog, W. et al., *Med. Sci. Sports Exerc.* 23:108-114, 1991.
Hof, A.L. *Human Movement Science* 3:119-153, 1984.
Huijing, P.A. et al., *Biomechanics: Basic and applied research*, 667-672, 1987.
Lieb, J. et al., *J. Bone & Joint Surg.* 53-A:749-758, 1971.
Yamashita, N. *Eur J Appl Physiol* 58:274-277, 1988.

ACKNOWLEDGMENTS

This study was performed in the Biomechanics Laboratory, ETH Zurich, Switzerland, and supported by grants from ESK of Switzerland, Nationalfond of Switzerland and NSERC of Canada.

AUTHOR INDEX

Aissaoui, R. 501
Alexander, N.B. 557
Allard, P. 421, 501
Allinger, T. 81, 505
Amoroso, A.T. 249
Anderson, D. 29, 449
Andersson, G.B.J. 403, 467,525
Andres, R.O. 281
Andrews, B.P.E. 545
Andriacchi, T.P. 39, 41, 295, 313, 403, 411, 497
Anne, V. 363
Armstrong, T. 425
Arnaud, C.D. 129
Arsenault, A.B. 183, 569
Ashton-Miller, J.A. 557
Athanasiou, K.A. 119

Backus, S.I. 139
Bagchee, A. 155
Bahamonde, R.E. 343, 459
Baker, K.J. 361
Banes, A.J. 355
Banta, J.V. 315, 323
Baratz, M. 29, 441
Barbieri, C. 261, 547
Barden, J.M. 105
Barin, K. 527
Barnard, R. J. 33
Barr, A.E. 139
Barrach, H. 11
Barreto, P.M. 63
Bates, B.T. 243, 269, 275, 551, 553
Bechtold, J.E. 17
Bednarczyk, J.H. 429
Beekman Eden, K. 271
Belanger, M. 563
Bell, K.J. 315
Bell, G. D. 137
Benda, B. 417
Bennett, M.B. 227
Berme, N. 351
Berzins, A. 39
Beynnon, B. 117
Bhattacharya, A. 155
Bianco, P.T. 17
Biewener, A.A. 71
Bilodeau, M. 183
Binding, P. 327
Bishop, P.J. 205
Black, A.H. 245
Blackwell, J.R. 427
Blomstrom, G. 7
Bobet, J. 173
Boda, W.L. 161
Boucher, J.P. 329
Bourbonnai, D. 569
Bowsher, K.A. 319
Brand, R.A. 361
Broker, J.P. 211
Brooks, J.G. 407, 505
Brown, T.D. 43, 355, 361, 495
Brown, R. 455
Buchanan, T.S. 439
Buczek, F.L. 503
Burn, J. 111, 177, 189
Burr, D.B. 25
Bylski-Austrow, D.I. 133

Caldwell, G.E. 187
Callaghan, J.J. 43
Cann, C.E. 129
Caperna, T.J. 13
Carlton, L.G. 341
Carrier, D.R. 227
Carroll, N.C. 91
Cartas, O. 479
Caster, B.L. 275
Cavanagh, P.R. 151, 221, 279
Cerny, F.J. 215
Chaffin, D.B. 525
Chandler, J.M. 145
Chang, J. 71
Chang, H. 207
Chen, G. 179
Chertack, C.C. 313
Chew, Y.T. 47
Chiu, A. 321
Choi, N.Y. 9
Cholewicki, J. 179
Chou, L.S. 375
Chow, J.W. 159
Ciarelli, M.J. 37
Clark, C.R. 207
Clark, S. 317
Clough, C.A. 561
Cole, K.J. 443
Cole, G.K. 233
Cooke, T.D.V. 369
Cooke, F.W. 499
Cooper, R.A. 435, 449
Costigan, P.A. 369
Cotton, C. 97
Coulombe, V. 191
Crisco, J.J. 455
Crowe, A. 373
Cummings, J.F. 133
Cummings, P.D. 537
Cusick, J.F. 473

D'Agati, M. 265
Damiano, D.L. 319
Darling, W.G. 443
Dart, J.A. 349
Davis, B.L. 221
Davis, R.B. 315, 323
Davis, H.P. 243, 269
Davoodi, M. 479
Day, S. 175, 193
de la Berrera, E.J. 183
Delp, S.L. 91, 439
DeLuca, P.A. 315, 323
Dennerlein, J.T. 425
Denoth, J. 577
Derrick, T.R. 267, 551
DeVita, P. 539
Dewald, J.P.A. 573
DeWitt, J.K. 543
Dolan, T. 539
Dowling, J.J. 105, 195, 197, 545
Draganich, L.F. 375
Droese, K. 473, 489
Dufek, J.S. 275, 551, 553
Dumas, F. 299

Eastlund, D.T. 17
Eckhardt, R.B. 75
Egerton, V.R. 127
Ehrlich, M. 11
Elder, S.H. 43
Elliott, B. 51
Eng, T.J. 281
Eng, J.J. 419
Engsberg, J.R. 99, 235, 237, 321, 397, 401
Enoka, R.M. 63
Estabrooks, P.A. 235, 237

Fadale, P. 11
Fanghanel, J. 345, 347
Fazzalari, N.L. 357
Ferrell, M. 167
Feuerbach, J.W. 415
Fezio, J. 315
Fleming, B. 117
Fletcher, L. 149
Frank, J.S. 307
Frey, G.A. 497
Friis, E.A. 499
Frykman, P. 391, 507
Fuglevand, A.J. 63
Fujie, H. 7
Fung, T. 137
Fyhrie, D.P. 357, 465

Gabriel, D.A. 329
Gafney, D. 123
Gage, J.R. 291
Gagnon, D. 515
Gagnon, M. 431, 471, 515, 517, 535
Gajewski, J. 571
Gal, J.M. 463
Gardner-Morse, M. 483, 485
Gehlsen, G.M. 459
Ghosh, K. 527
Gilbertson, L.G. 207, 469
Giron, E.A. 39, 497
Giurintano, D.J. 445

Given, J.D. 573
Glaser, R.M. 565
Goel, V.K. 207, 469
Gouw, G.J. 379
Grabiner, M.D. 415, 533, 561
Gracovetsky, S.A. 379
Gravel, D. 517, 535, 569
Green, J.I. 399, 543
Greenhorn, D. 519
Gregor, R.J. 211
Grenier, J. 557
Griffin, S.R. 349
Grood, E.S. 133
Gross, T.S. 359
Guimaraes, A. 175, 185, 193
Guzelsu, N. 23

Hagel, B.E. 235, 237, 397
Hakkinen, A. 61
Hakkinen, K. 61, 567
Halloran, B.P. 129
Haman, F. 97
Hamill, J. 161, 213, 243, 267
Hamilton, J.J. 365
Hammond, M.E. 129
Han, K. 391, 507
Hanski, P. 395
Harder, J.A. 397
Harman, E. 391, 507
Harrigan, T.P. 365
Harry, J. 21
Hart, B.A. 349
Hasler, E. 577
Hatzitaki, V. 331
Hay, J.G. 57, 159
Hendrick, J.L. 167
Hennig, D.J. 249
Henning, E.M. 103, 163, 245, 247, 249, 251, 285, 575
Henning, C.E. 499
Herron, M. 441
Herzog, W. 81, 175, 327, 335, 185, 193, 407, 409, 495, 505, 577
Hickey, T. 45
Hickey, M. 403
Hintermeister, R.A. 213
Holden, J.P. 133
Hollister, A.M. 445
Hollowell, J. 489
Hong, D. 55
Hoshizaki, T.B. 329, 331, 333
Hreljac, A. 559
Hughes, M.A. 145
Huhtinen, J. 317, 395
Hulliger, M. 175, 185,193
Hurwitz, D.E. 313

Imbriglia, J. 29, 441
Irvine, D.M.E. 261, 547

Jacobs, D. 111, 177, 189
Jaeger, R.J. 147, 389
James, R. 553
Jamison, J.C. 187
Jennings, L. 51
Jensen, R.K. 65
Johnson, G.A. 9
Johnson, K.M. 107
Johnson, M. 391, 507
Johnson, R.J. 117
Judge, D.C. 11, 23

Kadaba, M.P. 111, 177, 189
Kamimura, M. 165
Kao, S. 169
Kashiwaguchi, S. 7
Kasprisin, J.E. 533
Ke, J.H. 467
Keessen, W. 373
Keir, P.J. 35
Kepple, T.M. 503
Kiefer, G.N. 321
Kim, H. 21
Kim, S. 223
Kippers, V. 523
Koh, T.J. 415, 561
Korvick, D.L. 133
Krebs, D.E. 417
Kubein-Meesenburg, D. 345, 347
Kuhn, J.L. 37

Lackner, J.R. 125
Ladd, K.A. 427
Ladin, Z. 265, 383
Laflamme, L.P. 253
Lafortune, M.A. 101, 103, 273
Lage, K.J. 405
Lake, M.J. 101
Lam, G. 29
Lambert, C.E. 101
Lamontagne, M. 85, 97, 191
Lankarani, H.M. 203
Lavender, S.A. 525
Lee, S. 187, 241
Lee, A.G. 397
Lee, C.N. 47
Leonard, T..R 407, 409, 495, 505
Leroux, M.A. 421
Li, J. 369
Lieh, J. 457
Lieu, Y.T. 341
Litsky, A. 45
Livesay, G.A. 7
Livingston, L.A. 77
Loebig, T. 441
Lohmann, K. 503
Loveland, M.E. 223
Low, H.T. 47
Lowe, R. 137
Lu, W. 205
Luchtenberg, D. 231
Luhtanen, P. 317, 395
Lynch, C.S. 195

Mackay, D. 45
MacKinnon, C.D. 419
Mahesh, M. 31
Maiman, D.J. 489
Maiman, D. 487
Maitland, M.E. 137, 409
Malapati, S. 203
Malkia, E. 317, 395
Malouin, F. 299
Manal, K. 333
Markze, M. 73
Marras, W.S. 511, 527, 529
Marsh, A.P. 255
Marsh, T. 559
Marshall, R. 51
Martin, B. 149
Martin, P.E. 255, 559
Martin, T. 563
Marzo, J.M. 139
Mason, D.J. 37
Matsumoto, D. 129
McCaw, S.T. 107
McConnell, S. 217
McFadyen, B.J. 387
McFarland, H.F. 153
McFaull, S. 85
McGill, S.M. 491
McGinnis, P. 167
McGuire, J.R. 573
McLean, S.P. 73
McLean, B 413
McMahon, P.J. 9
McNeil, M. 321
McNitt-Gray, J.L. 257, 259, 261, 547
McQueen, D.A. 499
Meglan, D. 351
Menon, R. 203
Mikosz, R.P. 411, 497
Milani, T.L. 285
Miller, J.A. 253
Miller, K. 283
Mirka, G.A. 511
Mitchell, L. 377
Mittlmeier, T.W.F. 113
Moon, J. 343
Moore, A. 179
Moran, D.W. 89, 399
Morlock, M.M. 113
Morris, T. 531
Mote, C.D. 425
Munkasy, B.A. 257, 547
Murphy, S.D. 95
Murphy, N. 501
Murray, W.M. 439

Nachbauer, W. 233
Nagerl, H. 345, 347
Naick, P.A. 25
Natarajan, R.N. 41, 467
Newell, K.M. 341
Newman, N. 379
Nichols, C. 117
Nigg, B. 233
Nohara, H. 165
Nordin, M. 479
Norman, R.W. 513
Nussbaum, M.A. 475, 525

O'Connor, B.J. 109

O'Connor, D.D. 281
Olney, S.J. 303, 369, 371
Orofino, T.A. 283
Orr, S. 179
Otis, J.C. 139
Ounpuu, S. 323

Pandy, M.G. 223
Panzer-Decius, V. 153
Park, H.S. 149
Parker, A.W. 523
Parker, P.A. 185
Parnianpour, M. 527, 529
Patla, A.E. 307, 337, 419
Patwardhan, A.G. 207, 469
Paul, E.M. 537
Pearsall, D.J. 77
Pedersen, D.R. 355
Pedotti, A. NA
Perry, S.D. 273
Pettit, D.J. 449
Pettit, M. 549
Phillips, S.J. 241
Pidaparti, R.M.V. 25, 363
Pierrynowski, M.R. 87
Pintar, F.A. 31, 201, 473, 487, 489
Plamondon, A. 517, 535
Ploeg, E.L. 99, 235, 237
Pope, M. 117
Potvin, J.R. 513
Prassas, S.G. 393

Ralston, J. 29
Ramakrishnan, H.K. 111
Rash, G. 53
Redfern, M.S. 377, 385
Reid, J.G. 77, 253
Reid, D. 563
Reinartz, J. 201, 487
Reinschmidt, C. 277
Rempel, D. 425
Renstrom, P. 117
Richards, C.L. 299
Riegger, C. 83
Riehle, H. 231
Rietdyk, S. 337
Riley, P.O. 67, 417
Ringwelski, D.A. 91
Rintala, P. 317
Roberts, E.M. 55
Robertson, D.G.E. 95, 105, 433
Rodgers, M.M. 457, 565
Rominger, A.W. 393
Ronsky, J.L. 495
Roozmon, P. 379
Rosenbaum, D. 575
Rosenstein, M 391, 507
Rothstein, D.E. 559
Rubin, C.T. 359
Russell, F. 391, 507
Russo, A. 97
Ryan, A. 45
Rymer, W.Z. 573

Salem, G.J. 33
Sances, A. 201
Sanchez, S.D. 129
Sanderson, D.J. 245, 247, 251, 429
Santaguida, P.L. 491
Sasken, H. 11
Schaffler, M.B. 357, 465
Schenck, R.C. 119
Schenkman, M. 67, 145
Schiereck, P. 373
Schipplein, O.D. 403
Schot, P.K. 349
Schrag, D.R. 457
Schram, E. 33
Schultz, A.B. 3, 557
Schumann, T. 377, 385
Schutte, L.M. 565
Sellens, R. 169
Shapiro, R. 53
Shiang, T.Y. 75, 279
Shiavi, R. 135
Sicard, C. 471
Simoneau, G.G. 151
Simpson, D.J. 321
Simpson, K.J. 549
Skelly, W.A. 539
Skrade, D. 201
Small, C.F. 447
Smith, A.W. 217
Smyth, G. 431
Sommer, H.J. 75
Song, S.M. 375
Spaeder, J. 29
Spriging, E. 51
Springer, M.J.N. 401
St-Denis, N. 569
Stacoff, A. 277, 577
Stanhope, S.J. 503
Stein, R.B. 173, 563
Stekewich, C. 117
Ster, J.F. 435, 449
Stergiou, N. 243, 269
Stevenson, J. 169, 519
Stewart, S. 137
Stokes, I.A.F. 481, 483, 485
Studenski, S.A. 145
Stussi, E. 277
Sumner, D.R. 19, 39, 41
Sun, H. 65
Swartz, S.M. 227

Takei, Y. 165
Thomas, S 217
Throckmorton, G.S. 27
Tramaglini, D.M. 9
Trimble, J. 531
Tummarakota, S. 457
Tupling, S.J. 87
Turner, C.H. 25, 363
Turner, T.M. 19

Ulbrecht, J.S. 151

Vail, G.R. 253
Valero-Cuevas, F.J. 447
Valiant, G.A. 103, 163, 271
Vanitchatchavan, P. 389
Vaughan, C.L. 319
Viitasalo, J.T. 571
Vossoughi, J. 13
Vrahas, M.S. 537

Walsh, W.R. 11, 21, 23
Wang, H. 371
Warren, R.F. 139
Washoo, L.A. 141
Weames, G.G. 433
Weiker, G.G. 415
Welch, M.D. 261
Welch, M 547
Wells, R.P. 35, 179, 453
Wenzel, T.E. 357
Whalen, R.T. 223
Wheeler, G.D. 563
White, S.C. 109, 215, 405
Whittle, M.W. 283
Wickiewsicz, T.L. 139
Wieler, M. 563
Wiggins, M. 11
Willke, T.L. 19
Wilson, S.C. 537
Wilson, C.R. 31
Winter, D.A. 289, 307, 419
Winterbottom, J.M. 207
Wisleder, D. 413
Wolfe, S.W. 455
Woloszko, J. 147
Woo, S.L.Y. 7,9
Wood-Dauphinee, S. 299
Wootten, M.E. 111, 177, 189
Wright, P. 529
Wu, G.E. 383
Wu, C.D. 411
Wyss, U.P. 369

Xiao, L. 453

Yack, H.J. 109, 141, 215, 405
Yamaguchi, G.T. 89, 399, 543
Yeadon, M. 225
Yingling, V.R. 215
Yoganandan, N. 31, 201, 473, 489
Yokoi, T. 259
Yu, B. 57

Zajac, F.E. 565
Zernicke, R.F. 33
Zhang, L.Q. 135
Zhang, Y.T. 175, 185, 193
Zimmerman, R. 17
Zoppi, A. 441

NACOB II: MEETING AT A GLANCE

TUESDAY AUGUST 25, 1992

	Ballroom VI	Ballroom VII	Ballroom V
8:00 a	**Welcome and Announcements**		
8:15 a	Keynote Address: A. Schultz Mobility Impairment in the Elderly: Challenges for Biomechanical Research		
9:45 a	Session 1 Soft Tissue		Session 2 Biomechanics of Throwing
11:00 a	Session 3 Development & Aging		Session 4 Anthropology
12:00 n	**Luncheon (on own)**		
1:25 p	ASB Young Scientist Award		
2:00 p	**ASB Symposium** Physiologic Adaptation to Microgravity: A Severe Hurdle to Extended Spaceflight?		
3:50 p	ASB Symposium (cont.)		
6:00 p	**Welcome Reception**		

WEDNESDAY AUGUST 26, 1992

	Ballroom VI	Ballroom VII	Ballroom V
9:00 a	Session 5 Knee Ligament Deficiency	Session 6 Posture	Session 7 Sport Biomechanics
11:00 a	**Interactive Poster Session** Odd Numbered Posters Rooms VIII - XX		
12:00 n	**Borelli Lecture and Luncheon** **Y.C. Fung**		
1:30 p	Interactive Poster Session Even Numbered Posters Rooms VIII - XX		
2:30 p	Session 8 Muscle Modelling	Session 9 Trauma and Impact	
4:00 p	Session 10 Energy Costs	Session 11 Microgravity & Airborne	Session 12 Running
5:30 p	**Student Reception and Meeting**		

THURSDAY AUGUST 27, 1992

	Ballroom VI	Ballroom VII	Ballroom V
8:30 a	**CSB/SCB: Locomotion VII** Clinical Gait and Balance Assessments: Millions of Bits of Data but Where is the Clinical Information?		
10:30 a	CSB/SCB: Locomotion VII (cont.)		
12:00 n	**Luncheon (on own)**		
1:30 p	Session 13 Non-Normal Gait	Session 14 Motor Control	Session 15 Bone Remodelling
3:30 p	Session 16 Normal Gait	Session 17 Ergonomics	Session 18 Upper Extremity
5:00 p	ASB AGM	CSB/SCB AGM	
7:00 p	**Dinner Cruise**		

FRIDAY AUGUST 28, 1992

	Ballroom VI	Ballroom VII	Ballroom V
8:15 a	Session 19 Spine		Session 20 Lower Extremity Loading
10:30 a	Session 21 Manual Materials Handling		Session 22 Jumping and Landing